CHROMATIC DEPENDENCE OF FIRST–ORDER OPTICAL PROPERTIES OF THE EYE

Tanya Evans

(Student number: 908905891)

A dissertation submitted to the Faculty of Health Sciences, University of Johannesburg, in fulfilment of the requirements for the degree of Magister Philosophiae in Optometry

Supervisor: Professor WF Harris

Johannesburg, 2015

DECLARATION

I declare that this dissertation is my own, unaided work. It is being submitted for the degree Magister Philosophiae in Optometry at the University of Johannesburg, Johannesburg. It has not been submitted before for any degree or examination in any other Technikon or University.

_____

(Signature of Candidate)

_____day of _____ 2015.

ABSTRACT

Many first-order optical properties depend on chromatic dispersion and, hence, on frequency of light. The purpose of this theoretical study is to investigate the dependence of first-order optical properties of model eyes on frequency. In this study we are purposefully not concerned with subjective measurements. Instead, definitions are obtained that are general for optical systems that have astigmatic and decentred elements, and then simplified for Gaussian systems.

In linear optics the transference is a matrix that is a complete representation of the effects of the system on a ray traversing it. Almost all of the familiar optical properties of the system can be obtained from the transference. From the transference **S** we obtain the four fundamental properties namely dilation **A**, disjugacy **B**, divergence **C** and divarication **D**, submatrices of **S**. Transferences are symplectic and do not define a linear space. Linear spaces are amenable to statistical analyses and therefore a number of mappings to linear spaces are investigated, including the Cayley and logarithmic mappings to Hamiltonian space and the four characteristic matrices. In each case, the individual entries of the transform are studied for their dependence on frequency and then the chromatic dependence relationship between the entries is compared graphically.

Four aspects of chromatic dependence of Gaussian systems are explored, namely the fundamental properties, derived properties, transverse and longitudinal chromatic aberration, and independent and dependent chromatic properties. Formulae are derived that apply to first-order optical systems in order to illustrate the chromatic dependence, chromatic difference or the chromatic magnification of each property. Numerical examples are given for the reduced eye and Le Grand's eye across the spectrum 430 to 750 THz.

Fundamental properties

The fundamental properties of the reduced and Le Grand's four surface eyes have a nearly perfectly straight-line dependence on frequency.

- Straight-line fits are obtained for the dependence of the fundamental properties on frequency. The resulting transference has a determinant of approximately 1 for every frequency.

- Straight-line fits in Hamiltonian space give a frequency-dependent transference with a determinant of exactly 1 for every frequency.
- Of the fundamental properties, only dilation *A* and divergence *C* are dependent on the refractive index upstream of the system. Disjugacy *B* and divarication *D* are independent of the medium upstream of the system.

Derived properties

Derived properties that are dependent on frequency are:

- Power, corneal-plane refractive compensation, exit-plane refractive compensation and front-vertex power have a straight-line dependence.
- Back-vertex power has a hyperbolic dependence.
- The cardinal and anti-cardinal points for Le Grand's eye, the anti-cardinal and focal points for the reduced eye and all the chromatic properties are dependent on frequency.

The incident and emergent principal and nodal points for the reduced eye are independent of frequency.

Chromatic aberration

Chromatic aberration is defined for linear systems, that is, for systems possibly with astigmatic and heterocentric elements such as the eye, using the classical optics definition as a departure point. The definition is then specialised for a Gaussian eye.

- Longitudinal chromatic aberration is defined as a 2×2 symmetric matrix for systems that have astigmatic elements. It depends on the longitudinal position of the object and simplifies to a scalar for Gaussian systems.
- Transverse chromatic aberration is defined as a 2×1 transverse vector for systems that have astigmatic or decentred elements. It depends on both the longitudinal and transverse position of the object point and simplifies to a scalar for Gaussian systems.

Independent and dependent chromatic properties

Chromatic properties of the system both independent of and dependent on the object or image and aperture positions are derived from the transference based on the definitions in the physiological optics literature.

Independent chromatic properties of the eye include chromatic difference in power, δF, chromatic difference in refractive compensation, δF_0 and chromatic difference in ametropia, δA.

Formulae are derived for the chromatic properties of the Gaussian eye for (i) distant objects and objects at a finite distance, (ii) image and object dependent properties and (iii) the special case of a pinhole held in front of the eye.

- Chromatic properties of the eye dependent on object and aperture position include chromatic difference in retinal position δy_{R}, retinal inclination δa_{R}, image size $\delta(\Delta y_{\mathrm{R}})$, image angular spread $\delta(\Delta a_{\mathrm{R}})$, retinal chromatic image size magnification M_{yR} and angular spread magnification M_{aR}. Chromatic properties of the eye dependent on image and aperture position include: chromatic difference in object position δy_{O}, inclination in object space δa_{O}, object size $\delta(\Delta y_{\mathrm{O}})$, object angular spread $\delta(\Delta a_{\mathrm{O}})$, chromatic object size magnification M_{yO} and object angular spread magnification M_{aO}. When the distance of the object from the eye is constant the dependence of the chromatic differences present as straight lines.
- The red and blue chief rays chosen to study the chromatic properties in image space are incident on the cornea a distance of some 5000 times the wavelength of the blue light apart.
- When the red and blue chief rays from two separated object points coincide at a point on the exit-plane, their emergent inclination is the same for the reduced eye but different for Le Grand's eye.

Though applied to model eyes one expects the results, particularly for Le Grand's eye, to give an idea of what happens in the case of real eyes, at least those close to emmetropia.

ACKNOWLEDGEMENT

To my husband and daughters, Gerard, Sarah and Megan who have supported me and put up with the long hours of absence and episodes of stress. Thank you!

To my parents who encouraged and supported me to study Optometry in the first place.

To my advisor, Professor WF Harris, who has encouraged me every step of the way. This study has been about the journey and not just the destination. Bill, thank you for allowing me to take the road less travelled, to explore anything and everything that interested us along the way. Thank you for your endless patience, reading, rereading and correcting each draft. And thank you for opening the door to the academic world and giving me the opportunities to attend and present my work at conferences.

The first year of this research was supported by a scholarship granted by the Medical Research Council of South Africa.

TABLE OF CONTENTS

1. EVANS T, Harris WF. Dependence of the transference of a reduced eye on frequency of light. *South African Optometrist* 2011 **70** 149-155.
2. Harris WF, EVANS T. Chromatic aberration in heterocentric astigmatic systems including the eye. *Optometry and Vision Science* 2012 **89** e37-e43.
3. Harris WF, van Gool RDHM, EVANS T. Line of sight of a heterocentric astigmatic eye. *Ophthalmic and Physiological Optics* 2013 **33** 57-66.
4. EVANS, T and Harris, WF. (2014) Dependence of the ray transference of model eyes on the frequency of light. *Proceedings: VII European / I World Meeting in Visual and Physiological Optics VPOptics 2014*. Wrocław University of Technology, Wrocław, 25-27 Aug 2014, ed by DR Iskander and HT Kasprzak. 74-77.
5. Harris WF, EVANS T and van Gool RDHM. (2014) Inner-product spaces for quantitative analysis of eyes and other optical systems. *Proceedings: VII European / I World Meeting in Visual and Physiological Optics*. Wrocław University of Technology, Wrocław, 25-27 Aug 2014, ed by DR Iskander and HT Kasprzak. 116-119.

PART I – INTRODUCTION

The objective of this study is to explore chromatic properties and other chromatic effects of the eye, particularly in the context of Gaussian optics. Numerous optical properties are investigated for their dependence on the frequency of light, specifically those optical properties that are relevant to Gaussian systems, that is, systems that are rotationally symmetric about a common optical axis (Guillemin and Sternberg, 1984:7).

1 INTRODUCTION

From Babylonia to Egypt and Nigeria and from Papua New Guinea to Mexico and Peru, human beings have been fascinated by the rainbow since the beginning of time (Lee and Fraser, 2001: 2-33). The phenomenon that creates the rainbow is chromatic dispersion, that is, the separation of white light into its spectral components or the variation of the refractive index with wavelength (Sharma, 2006: 45, 50; Le Grand, 1956: 9). Chromatic aberration, in turn, is defined by El Hage and Le Grand (1980:4) as "the influence of chromatic dispersion in the eye". That is to say, the white light entering the system is dispersed across the visible light spectrum and creates a rainbow effect as it exits the system or reaches an imaging surface such as the retina.

Chromatic aberration is quantified according to the classical (or physical) optics definition as the distance measured between the projections of the two focal points when light of two frequencies representing the two ends of the visible light spectrum are traced through the system. Measurements parallel to the longitudinal axis are defined as longitudinal chromatic aberration and measurements perpendicular to the longitudinal axis are defined as transverse chromatic aberration (Born and Wolf, 2002: 186-187). The definition is limited to systems that are Gaussian and distances that are unsigned.

In the literature of physiological optics many definitions exist. Longitudinal (or axial) chromatic aberration is defined in physiological optics as chromatic difference in power, refractive error, focus or ametropia (Atchison, Smith and Waterworth, 1993; Cooper and Pease, 1988; Rabbetts, 2007: 289-293; Thibos, Bradley, Still, Zhang and Howarth, 1990; Thibos, Bradley and, Zhang,

1991; Thibos, Ye, Zhang and Bradley, 1992; Wald and Griffin, 1947; Zhang, Thibos and Bradley, 1991). Transverse (or lateral) chromatic aberration is defined in physiological optics as chromatic difference in position or magnification (Rabbetts, 2007:289-293; Simonet and Campbell, 1990; Thibos *et al*, 1990, 1991, 1992; Zhang *et al*, 1991). Researchers have sought to define a relationship between longitudinal and transverse chromatic aberration and have succeeded for the reduced eye (Zhang *et al*, 1991) and for schematic eyes (Katz, 2002:261). The limitations of these definitions is that they are based on Gaussian schematic eyes, usually the reduced eye, and do not generalise to eyes with astigmatic or decentred elements. There is a risk of making assumptions or conclusions that pertain only to the reduced eye. We shall explore two such underlying implications in Chapter 7.

Gaussian optics has served as the foundation of optometry and the basis of visual optics and is a powerful tool (MacKenzie, 2004: 153-154). It is limited, however, in that it firstly assumes that all surfaces in the system are rotationally symmetric about an optical axis. Secondly, Gaussian optics relies on concepts such as principal points, nodal points, entrance- and exit-pupils which work well for Gaussian systems, but do not generalize well to astigmatic or heterocentric systems. However, the success of Gaussian optics in optometry and visual optics is evidence that the human eye is largely a first-order optical instrument (Le Grand, 1956:9; MacKenzie, 2004:3).

Linear optics is a method that fully accounts for all the aspects of first-order paraxial optics. The three-dimensional linear optics approach can account for elements that are astigmatic and decentred which traditional two-dimensional Gaussian techniques fall short of. Linear optics makes use of linear algebra and specifically a matrix, called here the ray transference **S**, that is, a complete representation of the effects of the system on a ray traversing it. Almost all of the familiar optical properties of the system can be calculated from the transference (Torre, 2005: 60). Linear optics can therefore describe the first-order behaviour of the eye as an optical instrument.

From the transference we obtain the four fundamental properties namely **A** dilation, **B** disjugacy, **C** divergence and **D** divarication. From these four

fundamental properties we can obtain a variety of seemingly unrelated derived properties such as power (Harris, 1997), refractive compensation (Harris, 1999a; Keating, 1988: 236), front- and back-vertex power (Keating, 1988: 236; Harris, 2010a), magnification, blur, image size and image position, (Harris, 2001a,b), cardinal points (Harris, 2010b, 2011a, b), Pascal's ring (Harris, 2011a) and locator lines (Harris, 2011b). This is by no means a comprehensive list of derived properties. By and large these properties have been studied under the assumption of a single reference wavelength. Of special interest is that the cardinal points, which form the basis of Gaussian ray-tracing optics, are derived properties. Similarly, power and refractive compensation are derived properties.

The transference that accounts for astigmatism is a 4×4 matrix with each of the four fundamental properties a 2×2 submatrix (Guillemin and Sternberg, 1984:26; Harris, 2010d). When elements that may be decentred or tilted are accounted for in the transference, we obtain an augmented transference that is of order 5×5 (Harris, 2004a, 2010d, 2012c). In contrast, when all the elements are stigmatic and rotationally symmetric about an optical axis, each of the four fundamental submatrices simplifies to a scalar matrix and we can reduce the transference to a 2×2 matrix. This can be thought of as representing the Gaussian subset of 4×4 and 5×5 transferences (Guillemin & Sternberg, 1984: 7-11, Harris, 2010d). Because the topic of chromatic dependence of the eye is broad it is necessary to limit the scope of the study. Except where it is necessary to use a 4×4 transference **S** or an augmented 5×5 transference **T** in order to gain insight into the nature and character of chromatic dependence of the eye, this study shall be limited to the Gaussian subset. However, most of the formulae obtained readily generalise to linear systems. Transferences are dealt with in more detail in Section 3.2.

Advantages are gained by limiting the scope of the study to the Gaussian subset. In particular, it becomes possible to display many of the dependencies on frequency in two- and three-dimensional space. However, the transference does not conform to the definition of a vector space (Anton and Rorres, 2005: 222; Harris, 2010d; 2007a, van Gool and Harris, 2005) although it is possible to map the symplectic transference to a Hamiltonian space in a number of ways.

Transformed transferences are Hamiltonian and therefore fulfil the definition of a vector space, allowing us to graphically map the dependency in a three-dimensional space. A 2×2 transformed transference has three independent entries which can be represented graphically (Harris, 2010d). On the other hand a 4×4 transformed transference has 10 and a 5×5 transformed transference has 14 independent entries requiring representation in 10- or 14-dimensional space (Harris, 2007a), a graphical impossibility. Insight is gained because many of the Gaussian derivations are simplified and can be represented graphically.

We have seen that there are many properties that can be derived from the transference. An objective of this dissertation is to study the dependence of the transference on frequency. The reasons why frequency is preferable to vacuum wavelength will be explored in Chapter 4. To understand the dependency of the optical system of the eye on frequency we explore a number of transformed transferences and characteristic matrices. The characteristic matrices are symmetric and therefore are amenable to mapping the relationships between the entries also in three-dimensional space. Because each of the entries of the characteristic matrices is a derived property, each of these derived properties will be explored independently and then in relationship to other entries of the four characteristic matrices. We therefore restrict the derived properties studied to power, corneal-plane refractive compensation, exit-plane compensation and front- and back-vertex power. These derived properties will be explored for both their dependence on frequency across the visible light spectrum and the chromatic difference between the values at the spectral end-points.

1.1 Purpose

The purpose of this dissertation is to study the chromatic dependence of the first-order optical properties of the eye. Specifically, we wish to explore the chromatic dependence of optical properties and other effects of the eye particularly in the context of Gaussian optics.

Many first-order optical properties are dependent on the effects of chromatic dispersion and hence on frequency of light. This study explores the effects of chromatic dispersion on a number of fundamental and derived

properties. The dependence of the transference, the transformed transferences, characteristic matrices and derived properties on the frequency of light are explored, including graphical representation. A formula is obtained for the linear dependence of the transference on the frequency of light.

A study of chromatic effects of the eye would be incomplete without including chromatic aberration. Chromatic aberration, based on the classical optics definition, is defined for systems in general, including systems with astigmatic and heterocentric elements. Chromatic properties, as defined in the physiological optics literature, are obtained from the transference. Numerical examples of chromatic aberration and all the chromatic properties are given.

1.2 Outline

1.2.1 Part II - Literature review

The literature review is divided into three chapters. In Chapter 2 the current definitions of chromatic aberration in both the classical and physiological optics literature are reviewed.

Chapter 3 outlines linear optics. While much of this chapter may be familiar to the reader, it is included in part for completeness but predominantly to form a basis for derivations in Part III. After placing linear optics within the much larger field of optics, a summary of linear optics of first-order systems is given. The four fundamental properties are defined and briefly explored. Only a small selection of derived properties can be accommodated in this study and the derivations of power, corneal-plane refractive compensation and front- and back-vertex power are given. Both the classical and physiological optics approaches to defining magnification are explored.

Cardinal points form the basis of Gaussian optics and can be derived from the transference (Harris, 2010b, f). We are interested in the dependence of the cardinal points on the frequency of light and therefore the derivations for cardinal points from the transference are given. Two novel methods to display relationships among the cardinal points of a system and changes or differences between the cardinal points of two systems will be given.

The transference is symplectic and does not define a vector space and, hence, does not allow conventional statistical analyses (Harris, 2010d). We therefore investigate a number of transforms, including the Cayley (Cardoso and Harris, 2007) and logarithmic transforms (Harris and Cardoso, 2006; Harris, 2004b, 2005, 2007a) and the four characteristic matrices (van Gool and Harris, 2005; Harris and van Gool, 2004), to seek a suitable vector space. The characteristic matrices form combinations of derived properties and are also symmetric. As a result, each characteristic matrix has three independent entries and can be represented graphically in three-dimensional space.

Chromatic aberration depends on the longitudinal and transverse position of the object. Because we wish to know where the conjugate image point is we turn our attention to vergence as an alternative to tracing a pencil of rays through the system. In the literature review, we define vergence and wavefronts relating to the system, from the transference, and the position of the image relative to the exit plane of the system.

Chapter 4 deals with a number of considerations that need to be taken into account for this study of chromatic dependence. Schematic eyes are by definition Gaussian eyes and two schematic eyes are singled out for inclusion in the study. The limits of the visible light spectrum that will be included in the study are defined. The advantages and disadvantages of studying the dependence of chromatic properties as a function of frequency or vacuum wavelength are discussed.

It is the refractive index of the medium that is dependent on frequency. There are a limited number of formulae available that define refractive index of the media of the eye as a function of wavelength or frequency. The refractive indices as a function of vacuum wavelength are given for the reduced eye, the four media of Le Grand's four-surface eye, air and water.

1.2.2 Part III– Definitions and derivations

The objective in Part III is, firstly, to define chromatic aberration for systems in general, including systems with astigmatic and heterocentric elements and secondly to derive equations from the transference for chromatic properties of

the system both independent of and dependent on the positions of the object and limiting aperture. The starting point for these derivations is the derived properties presented in Chapter 3. However, not all the necessary derived properties and definitions are available in the current literature and so in Chapter 5 we define those formulae that are needed to define chromatic properties. Chapter 5 therefore is a collection of seemingly unrelated derivations.

We start Chapter 5 by defining exit-plane compensation and revisiting magnification. The magnification, blur and ray state at the retina is defined for object points at a finite distance. Anti-cardinal points are added to the study of the cardinal points and these are extended beyond the formulae and relationships available in the current literature.

The transferences are calculated for the reduced eye and for Le Grand's eye for their intended reference frequency. Formulae for the transference as a function of refractive index are derived and given for both schematic eyes.

There are a number of formulae available that define Cayley's transform. In this section each of these transforms are dissected for their usefulness for our purposes and for the method and way that it maps to Hamiltonian space and back into the set of symplectic matrices. Only one Cayley transform fulfils the requirements and is chosen with reasons given. The Cayley transform simplifies for the reduced eye and the formula for the transformed transference of the reduced eye is given.

In Chapter 6 chromatic aberration is defined for systems in general and then specialised for the Gaussian subset. The point of departure is the classical optics definition. By first defining chromatic aberration using linear optics we gain insight into the nature of the longitudinal and transverse chromatic aberrations.

Chapter 7 defines the chromatic properties of the eye and of the eye dependent on the positions of the object or image and aperture. These chromatic properties are derived from the transference based on the definitions for chromatic aberration in physiological optics. Included are chromatic properties of the eye independent of object or image and aperture positions which include chromatic differences in power, refractive compensation and ametropia. The chromatic

properties of the system dependent on object and aperture positions include the chromatic difference in position, inclination, image size and angular spread and chromatic image size and angular spread magnifications. The formulae derived are specialised for Gaussian schematic eyes but apply to both the pupil and the pinhole.

1.2.3 Part IV – Findings and discussions

The three chapters in Part IV together comprise the results of this dissertation and in each case both the reduced eye and Le Grand's eye are studied.

In Chapter 8 the dependence of the fundamental properties on frequency is displayed graphically and discussed. Four scenarios are considered, namely with the refractive index of air equated to 1, with the refractive index of air as a function of frequency using Cauchy's formula and with the eye submerged in water. Cornu's formula for the refractive index of water as a function of frequency is used. Finally the dependence of the fundamental properties as functions of vacuum wavelength are given, with the refractive index of air equated to 1.

The dependence of the transformed transferences is studied for both the logarithmic and Cayley transforms. This includes the dependence on the individual entries as well as the three-dimensional graph of the three independent entries. A formula for the linear dependence of the fundamental properties on the frequency of light is derived. This forms an important finding in this dissertation.

Chapter 9 looks at the dependence of derived properties on the frequency of light. First, the dependence of the cardinal and anti-cardinal points are studied and displayed using the locator line diagram and Pascal's ring. Each of the derived properties is studied separately for its dependence on frequency and finally the dependence of the characteristic matrices on the frequency of light are displayed using three-dimensional graphs. Each entry is a derived property and the relationship between certain derived properties can be seen.

Chapter 10 gives details of the numerical and graphical results for both schematic eyes for all the derivations of chromatic aberration and chromatic properties of the eye both independent of and dependent on the object or image and aperture positions. Object points at distance and three near working distances

are illustrated. Both the naked eye with centred pupil and the eye with a decentred pinhole immediately in front of the eye are illustrated.

1.2.4 Part V - Conclusion

Chapter 11 concludes that the transference, the fundamental properties and almost all the derived properties included in the study are dependent on the frequency of light. Certain derived properties are observed to be independent of frequency when the reduced eye model is used, but are dependent when Le Grand's eye is used. Formulae for the longitudinal and transverse chromatic aberration of systems in general are derived. Formulae for the chromatic properties of the eye, according to the definitions in the physiological optics literature, are derived from the transference. An important formula for deriving the linear relationship of each of the fundamental properties in the transference is obtained.

2 Definitions and measurements of chromatic aberration

Introduction, historical perspective

Humans have been admiring the rainbow since the beginning of time and different cultures have ascribed to the rainbow much religious and mystical significance (Lee and Fraser, 2001: 2-33). Whether or not the Irish leprechaun really has hidden a pot of gold at the end of a rainbow remains to be discovered. However, chromatic dispersion and its effects have enchanted men and women for millennia and people still spend fortunes purchasing diamonds for their sparkly effects caused by chromatic dispersion. The earliest documented academic studies of colour vision and the rainbow date back to Aristotle, around 384-322 BCE (Aristotle, 1906: 55-63 ; 1928; Lee and Fraser, 2001: 102-114).

We now know that the rainbow represents a continuum of colours but it is Newton who receives the most credit for his study of "Opticks". He was by no means the first to study colour, nor to discover a technique to create chromatic dispersion, however he is credited with naming the colours in the visible light spectrum. He originally chose five colours and later changed this to seven because he felt that the central colours were "crowded" and he wished to "divide the image into parts more elegantly proportioned to one another". He then observed that "the parts of the image occupied by the colors were proportioned to a string divided so it would cause the individual degrees of the octave to sound". He appears to have been particularly pleased and encouraged by this connection between colour and music (Newton, c1670).

2.1 Chromatic dispersion

It is Newton (c1670) who is credited with the scientific proof of chromatic dispersion. During the period 1670 to 1672 he conducted a series of experiments in which he successfully split white light up into a continuum of colours through a prism. He defined seven colours and named them according to the familiar colours of the rainbow: red, orange, yellow, green, blue, indigo and violet. The colour Newton called blue, is more of a sea-green that we now refer to as cyan. The colour Newton referred to as indigo is today's perception of blue, and green

he compared to leek green (Newton, c1670; Hastings, 1901:42; Waldman, 2002: 193).

Chromatic dispersion is defined as the separation of white light into its spectral components or the variation of the refractive index with wavelength (Sharma, 2006: 45, 50; Le Grand, 1956: 9). Dispersion is quantified mathematically by various dispersion formulae for the refractive index of the medium as a function of wavelength or by the Abbe number, also known as the constringency or refractive efficiency (Keating, 2002: 443–445). The latter allows us to quantify and compare by means of a single number the dispersive property of one material with another material and is more commonly used for laboratory-type media, including spectacle lenses. On the other hand, the formulae for the refractive index of a medium as a function of wavelength allows us to calculate the refractive index of a medium for any chosen wavelength or frequency; this is the quantitative method that we will use in this dissertation. There are a number of such formulae available for many materials, such as spectacle lens materials, glass, water, air, *etc*. (Walther, 1995:115–117; Herzberger, 1959) but there are limited formulae available for the media of the eye (Rabbetts, 2007: 287-288; Sivak and Mandelman, 1982).

There are two methods of determining the formulae for the refractive index of the media of the eye as a function of wavelength. One is to measure the medium of an enucleated eye with a refractometer, which poses some problems, and the other is to measure experimentally the chromatic aberration present in a sample of (living) eyes and interpolate the formulae according to the results. Wald and Griffin (1947) made some measurements with a refractometer of the aqueous and vitreous humours of cattle. They could not obtain measurements of the cornea because it was too thin and made only a crude measurement of the lens, however the measurement was not reliable because the lens needed to be compressed and distorted in order to take the measurement. This was further compounded by the lens's gradient index (Emsley, 1950: 518-519). They concluded that the humours have refractive indices similar to distilled water and that the lens material has considerably higher dispersion than water. More recently, Sivak and Mandelman (1982) took measurements for the refractive index at four wavelengths using a

refractometer on a variety of vertebrates, including cow, pig, frog, chicken, rock bass, rat and cat, for the aqueous and vitreous humours, the cornea and the inner and outer periphery and inner and outer core of the lens. They also measured the refractive indices for the peripheral and core of the lens for the human eye. The data was fitted to a polynomial.

There are a number of dispersion formulae available for expressing the refractive index as a function of wavelength (or wavenumber or frequency) for a variety of media. Examples include the dispersion formulae of Schmidt, Cauchy, Sellmeier, Cornu, Hartmann, Ciddor and Herzberger (Koczorowski, 1990; Ciddor, 1996; Herzberger, 1959). The expressions usually take the form of a polynomial with the variable being wavelength and constants for various materials given in tables. Depending on the medium, factors that influence the refractive index include, where relevant, temperature, humidity, carbon-dioxide content, pressure and even contaminants such as air pollution, and are defined as constants (Le Grand, 1956: 12-13; Hodgman, 1959, Ciddor, 1996) or may be included as variables in the expression (Ciddor, 1996).

Le Grand (1956: 12-13) studied refractometry measurements from Kunst, Polack and Tagawa (done in 1895, 1923 and 1928, respectively) which he claimed were all in close agreement for the two humours, the cornea and the periphery and core of the crystalline lens. He then compiled a table of refractive indices for the four media of the eye (aqueous and vitreous humours, cornea and lens) for the wavelengths of five Fraunhofer lines (A, C, D, F and G) as well as the constants needed for Cornu's formula for these four media. Villegas, Carretero and Fimia (1996) presented formulae for the refractive index as a function of wavelength for these four media using Le Grand's table of refractive indices which they obtained by a polynomial fit. The formula and constants are given in Section 4.4.3.

Thibos, Ye, Zhang and Bradley (1992) took an alternative approach. Using least-squares and their own measurements they obtained constants for a better fit for Cornu's hyperbolic dispersion formula to the reduced eye. This formula will form a basis for calculations in this dissertation and will be discussed in greater detail in Section 4.4.2.

2.2 Chromatic aberration

As several authors have remarked (Thibos, Bradley, Still, Zhang and Howarth, 1990; Simonet and Campbell, 1990; Rabbetts, 2007:289) there is much confusion in the literature regarding the definition of longitudinal and transverse chromatic aberration. In part, this confusion arises because each of the classical and physiological optics approaches define chromatic aberration differently. For the purposes of clarity in this dissertation, the definition of chromatic aberration will be that based on the classical optics definition given in Section 2.2.1 below and generalized for all optical systems, including those with elements that may be astigmatic, tilted or decentred in Chapter 6. The definitions of chromatic aberration in the physiological optics literature, which are specialized for the eye, will be referred to as physiological chromatic properties or chromatic properties. These are defined in the literature in Section 2.3 below and defined from the transference for Gaussian eyes in Chapter 7.

Until now, chromatic aberrations and chromatic properties have been studied using ray tracing and reverse ray tracing techniques which involve the extensive use of cardinal points, in particular the nodal point. There appears to be no reference in the literature to chromatic aberrations and properties in astigmatic systems. An exhaustive search of the literature, including personal correspondence (Thibos, 2011), confirms this.

This literature review looks at how these concepts are defined and measured in the literature, and the limitations imposed by the definitions. The literature makes use of the terms object space and image space. By the classical definition adopted here, chromatic aberration is associated with image space. It is not (yet) possible to measure the chromatic aberration in an eye, so measurements are usually done in object space. Coincidence of the red and blue images is presumed on the retina and "dispersion" from separate red and blue objects is measured outside of the eye.

It is important to separate the classical definition of chromatic aberration from the ophthalmic and physiological optics definitions that attempt to measure the various chromatic properties in the eye, both experimentally, in object space and calculation-based, in image space. The classical definition defines transverse

and longitudinal chromatic aberration for all Gaussian systems. Rabbetts (2007: 289) differentiates between physiological and classical optics definitions, however, this distinction is not drawn in most of the literature referred to in this study. Furthermore, only the more recent literature draws a distinction between calculated and measured chromatic properties and distinguishes between object and image space in these definitions. The definitions in the ophthalmic and physiological optics literature define transverse chromatic properties in eyes which include chromatic difference in position and chromatic difference in magnification and longitudinal chromatic properties in eyes which include chromatic difference in power and chromatic difference in refractive compensation. It is the intention in this study to clearly define longitudinal and transverse chromatic aberration in general to include astigmatic, decentred and heterocentric optical systems.

2.2.1 Definition of chromatic aberration

Born and Wolf (2002:186-187) define the first-order chromatic aberrations for systems in general within the limits of Gaussian optics as the distances δz and δy between the projections of the two focus points for the two different wavelengths in the directions parallel and perpendicular to the optical axis as longitudinal and transverse chromatic aberration respectively. The distances are unsigned, as shown in Figure 2.2.1. One notes that the chromatic aberrations depend on the position of the object. The definition holds for optical systems with stigmatic elements. This definition is consistent with Keating (1988:429; 2002:442-443), Katz (2002: 258-261) and Sharma (2006: 250) and is the definition that forms the starting point for the general definition that will be used in this study which holds for astigmatic, decentred and heterocentric optical systems. This definition will be discussed in Chapter 6.

Figure 2.2.1 defines the longitudinal δz and transverse δy chromatic aberration of an arbitrary homocentric system S with stigmatic elements. System S has an entrance plane T_0 and exit plane T. None of the refracting elements of S is shown. T_0 and T do not coincide with a refracting surface. Z is the optical axis.

I_r and I_b are the red and blue images of object O, respectively. We introduce the symbols δ to denote a chromatic difference and Δ to denote a physical difference between two dimensions. The above definition applies to Gaussian systems in general. It is what we refer to here as the classical definition of chromatic aberration.

A number of longitudinal and transverse chromatic properties are defined that apply specifically to the eye or model eye. A review of the literature reveals that most approaches make use of stigmatic models and, in particular, the reduced eye (Simonet & Campbell, 1990; Thibos, 1987; Thibos, Bradley and Zhang, 1991, Thibos *et al*, 1992; Zhang, Thibos and Bradley, 1991). References to schematic eyes were found (Atchison, Smith and Waterworth 1993; Le Grand 1956: 13; Rabbetts, 2007: 291; Zhang, Thibos and Bradley, 1991) but are limited to systems with stigmatic elements. There appears to be no clear distinction between the definition of chromatic aberration and the measurement of the chromatic properties in the eye. Rabbetts (2007: 289-293) and Atchison and Smith (2000: 180-186) both state that there are two primary chromatic aberrations, namely longitudinal and transverse. Thibos, Bradley and Zhang (1991) argue that there are three primary forms of chromatic aberration, namely chromatic difference of focus, chromatic difference of magnification and chromatic difference of position.

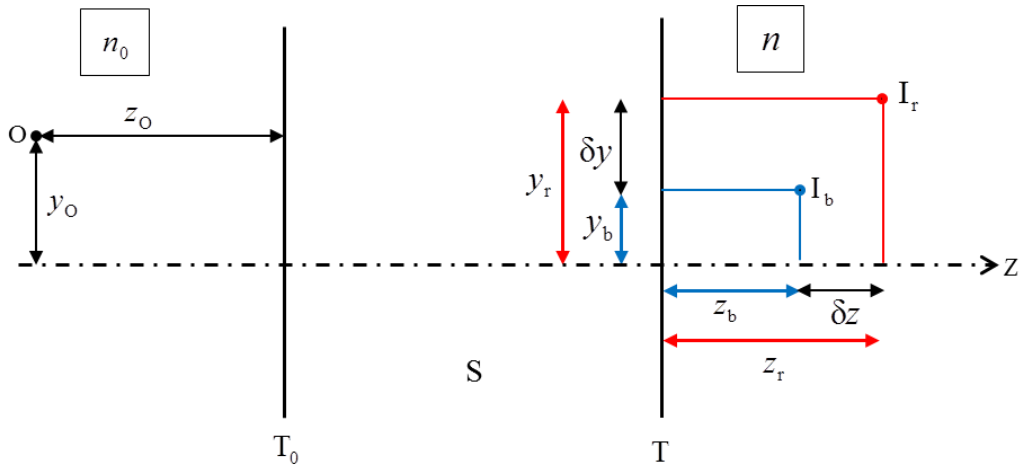

Figure 2.2.1 Longitudinal δz and transverse δy chromatic aberration of an arbitrary homocentric system with stigmatic elements. The system is drawn in the usual sense of a system such as the eye where $z_r > z_b$.

In Chapter 7 we will derive formulae for chromatic properties that are general for all Gaussian schematic eyes, regardless of the number of refracting surfaces. In Chapter 10 we will obtain numerical values for these derived formulae for chromatic aberration and chromatic properties for the reduced eye and Le Grand's four-surface eye.

2.3 Measurements of chromatic properties of the eye

Thibos, Bradley and Zhang (1991) emphasize that "chromatic aberration is the most important optical imperfection of the well corrected eye". The main differences in the definitions of longitudinal and transverse chromatic properties in the literature revolve around the use of reference points versus reference (or chief) rays and axes for the measurement and the units which are used. Some authors distinguish between image and object space, while others view them as the same thing (for example, Wald and Griffin, 1947).

Much work has been done to define a relationship between longitudinal and transverse chromatic aberration in the eye. Some authors (Simonet & Campbell, 1990) say there is no relationship, while others (Thibos *et al*, 1990, 1991; Zhang *et al*, 1991; Zhang, Bradley and Thibos, 1993) have derived formulae for a relationship. In Chapter 6, we show that longitudinal and transverse chromatic aberrations are fundamentally different (Harris and Evans, 2012).

2.3.1 Longitudinal chromatic properties

According to Rabbetts (2007: 289), longitudinal chromatic properties are defined in the physiological optics literature as the variation in focusing distance with wavelength. The literature defines two methods of measuring longitudinal chromatic properties of the eye, namely chromatic difference in refractive compensation and chromatic difference in power, each known by various names. Chromatic aberration is the distance measurement between the image points or object points created by two different wavelengths often measured as inverse units of distance (Wald and Griffin, 1947) and more commonly defined in object space as the difference in refractive compensation or object vergences required to provide clear imagery for two different wavelengths (Atchison, Smith and

Waterworth, 1993). Chromatic difference in power, or chromatic difference in focus (Wald & Griffin, 1947), is usually measured experimentally as chromatic difference in refractive error (Thibos *et al*, 1990, 1991; Wald & Griffin, 1947; Atchison, Smith and Waterworth 1993; Rabbetts, 2007).

Chromatic difference in refractive compensation is known as the chromatic difference in focus (Thibos, Bradley and Zhang, 1991; Atchison, Smith and Waterworth (1993)), chromatic difference in equivalent power (Atchison, Smith and Waterworth, 1993; Rabbetts, 2007:287-293), chromatic difference in power (Wald & Griffin, 1947), chromatic difference in refractive error (Thibos, Bradley and Zhang, 1991), chromatic difference in refraction (Rabbetts, 2007: 287-293), chromatic difference in ametropia (Atchison, Smith and Waterworth, 1993), axial chromatic aberration (Thibos, Bradley and Zhang, 1991; Wald & Griffin, 1947) or wavelength-dependent refractive error (Zhang, Thibos and Bradley, 1997).

Chromatic difference in power and chromatic difference in refractive compensation are not the same. Some authors use them interchangeably (Wald & Griffin, 1947), while others derive a linear relationship between them (Le Grand, 1956:14-16; Atchison, Smith and Waterworth, 1993; Thibos, Bradley and Zhang, 1991).

Chromatic difference in power

Thibos *et al* (1990) define the *ocular* longitudinal chromatic aberration in image space as "the distance between the image planes for different wavelengths" or "the variation of the eye's focusing power for different wavelengths", which is essentially the chromatic difference in power. Zhang, Thibos and Bradley (1991) define the chromatic difference in power as

$$\delta F = F_1 - F_2 = \frac{\delta n}{r} \qquad (2.3.1)$$

where δn is the difference between refractive indices of the medium for two wavelengths (λ_1 and λ_2) and r is the radius of curvature of the single refracting surface of the reduced eye. F_1 and F_2 are the powers of the same reduced eye for the two different wavelengths.

Chromatic difference in power is represented as longitudinal chromatic aberration (LCA) in Figure 2.3.1 for the reduced eye. The reduced eye has a single refracting surface, a longitudinal axis Z, which is also the achromatic axis and an optical axis, a nodal point N and a pupil or limiting aperture. The centre of curvature of the refracting surface coincides with the nodal point. The refractive index inside the reduced eye is *n* and before the reduced eye is n_0. Light from an object point O is refracted more for the short wavelength (shown in blue) than for the longer wavelength (shown in red). In Figure 2.3.1, the light with short wavelength creates a blue point focus I_b before the retinal plane and the light with the longer wavelength creates a red point focus I_r behind the retina. In Figure 2.3.1, the chromatic difference in power is shown as the distance between the image planes for different wavelengths, measured in units of inverse lengths.

Similarly, Rabbetts (2007: 290) defines chromatic difference in equivalent power (δF_e) as

$$\delta F_e = F_\lambda - F_o \qquad (2.3.2)$$

where F_λ is the equivalent power of the eye at a specified wavelength and F_o is the equivalent power of the eye at a reference wavelength.

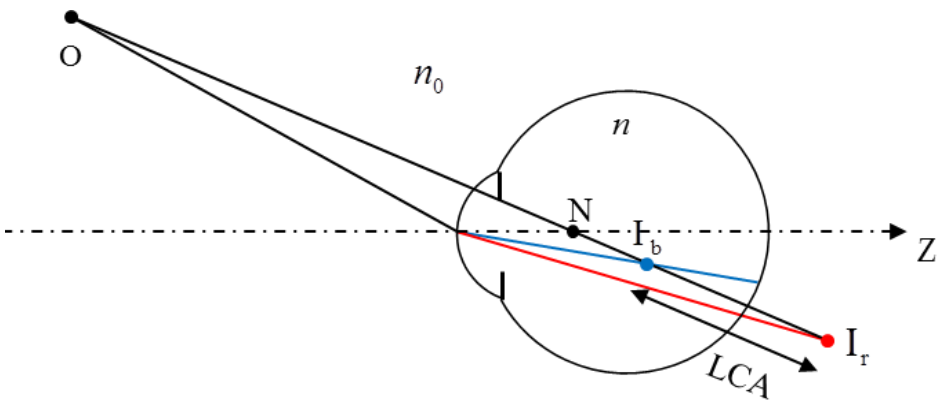

Figure 2.3.1 Chromatic difference in power shown as longitudinal chromatic aberration (LCA) for the reduced eye as the distance between the image planes for different wavelengths. (Figure adapted from Thibos *et al*, 1990.)

Chromatic difference in refractive compensation

Thibos *et al* (1990) define *ocular* longitudinal chromatic aberration in object space for the purposes of experimental study as the distance or dioptric interval between multiple object points of differing wavelengths that are positioned such that they focus simultaneously on the retina, thereby forming a single polychromatic image I shown in Figure 2.3.2. The dioptric interval is the difference in inverse distances from the refracting surface given by (Thibos *et al*, 1990)

$$\delta F_0 = \frac{1}{z_b} - \frac{1}{z_r} \qquad (2.3.3)$$

where δF_0 is the chromatic difference in refractive compensation, and z_r and z_b are the distances from the eye to the conjugate object points O_r and O_b respectively. The subscripts r and b represent red and blue, however, the exact wavelengths that they represent may differ from study to study. This effectively defines the chromatic difference in refractive compensation. Simply put, the chromatic difference in refractive compensation is the difference in power of the lens needed to compensate for the distance ametropia created by each wavelength (Thibos, Bradley and Zhang 1991). Rabbetts (2007: 290) defines chromatic difference in refraction as

$$\delta F_0 = F_{0\lambda} - F_{0o}$$

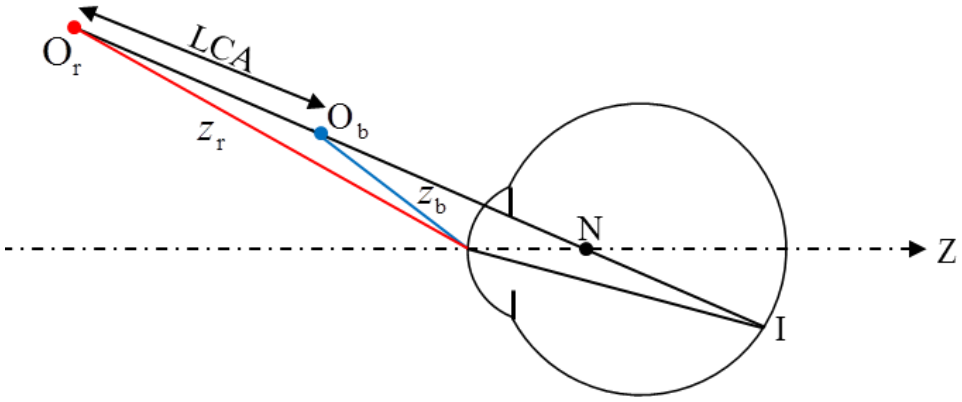

Figure 2.3.2 Chromatic difference in refractive compensation shown as longitudinal chromatic aberration (LCA) in the reduced eye, as the distance between the object planes for different wavelengths. (Figure adapted from Thibos *et al*, 1990).

where $F_{0\lambda}$ is the refraction of the eye at a specified wavelength and F_{0o} is the refraction of the eye at a reference wavelength. Furthermore, Rabbetts gives a relationship between chromatic difference in power and chromatic difference in refractive compensation for Gaussian schematic eyes as

$$\delta F_0 = -\delta F_e + \left(\frac{n_{\lambda v} - n_{ov}}{n_{ov}} \right) F_{0o}$$

where $n_{\lambda v}$ is the refractive index of the vitreous at a specified wavelength and n_{ov} is the refractive index of the vitreous at a reference wavelength.

Zhang, Thibos and Bradley (1991) and Thibos, Bradley and Zhang (1991) give the relationship between chromatic difference in power and chromatic difference in refractive compensation as

$$\delta F_0 = \frac{\delta n}{-n_D r} = \frac{\delta F}{-n_D} \qquad (2.3.4)$$

where n_D is the refractive index for the Fraunhofer line D ($\lambda_D = 589.3\,\text{nm}$) at which the reduced eye is emmetropic. λ_D is the reference wavelength for the reduced eye. All other symbols remain the same as already defined.

Experimental measurements

Wald and Griffin (1947) conducted an experiment using a spectral stigmatoscope with which they measured the *axial chromatic aberration* in dioptres as the refractive compensation required at each wavelength to bring the eye to the same power it possesses at the reference wavelength 578 nm.

Cooper and Pease (1988) conducted their experiment using a Badal optometer in order to measure wavelength in focus. Their aim was to establish which wavelength the eye preferred when accommodating on a near target. Their results are also expressed in dioptres for the refractive compensation required to focus light with a corresponding wavelength on the retina. They define this as longitudinal chromatic aberration.

Similarly, Thibos *et al* (1990) conducted an experiment using the Badal optometer as part of a larger experiment to find a relationship between longitudinal chromatic aberration (chromatic difference in refractive

compensation) and transverse chromatic aberration (chromatic difference in position).

Thibos *et al* (1992) conducted further experimental measurements using the two-colour Vernier method to measure the chromatic difference in refractive compensation. The aim of the set of experiments was to develop a reduced eye model that closely mimicked the real eye for chromatic aberration predictions. To this effect they developed the "chromatic eye" with three improvements over the reduced eye. Firstly, they refit Cornu's dispersion formula for the refractive index of the medium as a function of wavelength for the reduced eye to closely follow the experimental results. This formula will be discussed in Section 4.4.2. Secondly, they made the refracting surface aspherical (a prolate spheroid) to improve transverse chromatic aberration predictions. Finally, they included the pupil that Thibos (1987) previously introduced allowing for a reference axis and pupil centre to be defined.

Howarth and Bradley (1986) determined the chromatic difference in refractive compensation using a Badal optometer. The results showed that the Powell and Lewis achromatising lenses approximately corrected for the average longitudinal chromatic aberration. They also were able to conclude that individual differences in chromatic difference in refractive compensation are small, an important conclusion for this dissertation.

2.3.2 Transverse chromatic properties

According to Rabbetts (2007:289) when an off-axis polychromatic object point "produces laterally separated images on the retina due to dispersion … this is defined in the physiological optics literature as transverse chromatic aberration" and can also exist for an axial object point with a displaced artificial pupil. However, he states "in classical optics literature this is known as the transverse component of longitudinal chromatic aberration".

A number of terms and approaches are used to quantify transverse chromatic properties which are also referred to as lateral chromatic aberration, chromatic difference of magnification and chromatic difference of position. Zhang, Thibos and Bradley (1997) refer to *wavelength-dependent image*

magnification and *wavelength-dependent shifts in image position*, respectively, which they describe as *eccentricity-dependent transverse chromatic aberration*. Transverse chromatic aberration is defined either in image or object space and measured in object space. Measurements for transverse chromatic aberration are calculated either for an off axis object or a decentred pinhole.

Simonet and Campbell (1990) define transverse chromatic aberration as "the displacement of the image principal rays with wavelength". Certain definitions require that the chief ray should continue being projected to the retina or reference plane and the measurement taken as being from the centre of the projected blur patch to the centre of the second projected blur patch (e.g. Simonet & Campbell, 1990; Thibos, 1987; Thibos *et al*, 1990).

Thibos *et al* (1990) describe transverse chromatic aberration as the "variation in image position with wavelength". This creates a chromatic difference in position. The same mechanism will create a difference in image size called the chromatic difference in magnification. The chief ray from an object point is defined as the ray that traverses the centre of the pupil and therefore identifies the centre of the corresponding blur circle on the retina. The red and blue chief rays strike the retina at different positions, thereby defining the chromatic difference in position as the angle between the chief rays for different wavelengths, which Thibos *et al* (1990) define as transverse chromatic aberration. The chromatic difference in position depends on the pupil or pinhole position and the object location, which determines the incident inclination. The experimental variation of the position of the pinhole to control the position of the achromatic axis is referred to by Thibos *et al* (1990) as *induced* transverse chromatic aberration.

Thibos *et al* (1990) define the achromatic axis as the chief nodal ray; that is the ray that connects the centre of the pupil and the nodal point and which displays no transverse chromatic aberration. Typically, this would not intersect the fovea, however, when a pinhole is placed in front of the cornea, the achromatic axis can be manipulated to intersect the fovea. The nodal point is independent of wavelength (Thibos *et al*, 1990) for the reduced eye, however we will show in Section 9.1 that this is not strictly true of other schematic eyes or for eyes in general. According to Thibos *et al* (1990), the achromatic axis is important in

experimental situations because it represents the position where transverse chromatic aberration is null and thereby creates a link between theoretical and real eyes. They add that the achromatic axis can be manipulated experimentally, for example redirected to the fovea or other peripheral position, and therefore establishes a link between the optical theory and real eyes.

Chromatic difference in position

The chromatic difference in position is defined as the angular separation between the red and blue chief rays from a single object point in radians or minutes (Thibos *et al*, 1990, 1991). The chromatic difference in position is shown by angle *t* in Figure 2.3.3 (a), (b) and (c) (Thibos, 1987; Thibos *et al*, 1990). Thibos *et al* (1990) describe three approaches to defining and measuring chromatic difference in position: firstly in image space for a single object point, secondly in object space for the naked eye and finally also in object space, but manipulating the transverse position of the incident rays with a pinhole. These three approaches are shown in Figure 2.3.3 (a), (b) and (c).

According to Thibos (1987), Thibos *et al* (1990, 1991), the chromatic difference in position *t* will vary linearly with the angle of incidence of the chief rays, the angle of stimulus eccentricity, and the distance between the pupil centre and nodal point. *t* is also linearly related to the chromatic difference in refractive compensation (Thibos, Bradley and Zhang 1991). The transverse chromatic aberration depends on both the object location and the pupil location within the eye. The former will determine the angle of incidence of the selected rays while the latter will influence the position of the chief ray which is used in the calculations for transverse chromatic aberration.

For *induced* chromatic difference in position, Thibos *et al* (1990) conclude that each millimetre of displacement of the centre of the pinhole from the visual axis is approximately the same as 15 degrees of stimulus eccentricity. This means that, to first approximation, the two approaches to measuring chromatic difference in position in object space are directly proportional, with the constant of proportion being the displacement of the pinhole centre from the visual axis.

Thibos *et al* (1990) give the *transverse chromatic aberration*, shown in Figure 2.3.3(c), as

$$t = b - a = \frac{h}{z_b} - \frac{h}{z_r} = h\,\delta F_0 \qquad (2.3.5)$$

where the equation utilises the approximation of small angles. z_r and z_b are the distances from the red and blue object points respectively to the eye and *h* is the transverse displacement of the pinhole from the visual axis (in a reduced eye with a defined pupil and fovea).

Simonet and Campbell (1990) define *optical transverse chromatic aberration* "at the fovea as the difference for distinct wavelengths in the position of the centres of the images projected onto the retina". More specifically, the red chief ray is directed at the fovea and chromatic difference in position is measured as the angular difference in position of the blue chief ray relative to the fixed position of the red chief ray. The transverse chromatic aberration *t* is defined and measured experimentally in object space, consistent with *t* in Figure 2.3.3 (b), except that the red chief ray intercepts the fovea at the retina. They note that optical transverse chromatic aberration will have a vertical and horizontal component, but restrict their experimental measurements to only the horizontal component.

Simonet and Campbell (1990) also describe the relationship given by Equation 2.3.5 where *h* is the displacement in the entrance pupil of the rays with respect to the achromatic axis. δF_0 describes the slope of the relationship between transverse chromatic aberration *t* and displacement *h* in the entrance pupil. Simonet and Campbell make use of a Maxwellian view to direct the red and blue rays through the desired position in the pupil plane in contrast with Thibos *et al* (1990) who use a pinhole at the corneal plane.

Figure 2.3.3 illustrates the chromatic difference in position *t* for the reduced eye. Figure 2.3.3 (a) represents the chromatic difference in position in image space for the naked eye. Light from object point O is refracted at the single refracting surface. Light with a shorter wavelength (indicated in blue) is refracted more than light of a longer wavelength (indicated in red). *t* is measured as the angle between the blue and red light rays and represents the chromatic difference

in position. We can see that the red and blue rays each strike the retina at a different position, and that both images I_r and I_b are out of focus at the retina.

Figure 2.3.3 (b) represents the chromatic difference in position in object space for the naked eye. Light with a longer wavelength and originating from a red object point O_r along with light with a short wavelength originating from a blue object point O_b are refracted at the refracting surface and create a single, simultaneous image point I at the retina. In Figure 2.3.3 (b), the chromatic difference in position *t* is the angle between the red and blue rays in object space. Figure 2.3.3 (c) represents the chromatic difference in position in object space for the eye with artificial limiting aperture immediately in front of the refracting surface. The pinhole aperture allows us to choose the image point to arrive at the fovea F, making the line joining the object points O_r and O_b, the nodal point N and the fovea to be the visual axis. *a* is the angle between the red ray and the visual axis, *b* is the angle between the blue ray and the visual axis and *h* is the displacement of the pinhole from the visual axis. Similar to (b), the chromatic difference in position is the angle *t* between the red and blue rays in object space.

Thibos, Bradley and Zhang (1991) derived a relationship between chromatic difference in refractive compensation δF_0 and chromatic difference in position *t*. For chromatic difference in position for an off-axial object point the approximate equation is given as

$$t = z\,\delta F_0 \sin\varepsilon \qquad (2.3.6)$$

where *z* is the distance between the iris and the nodal point and ε is the eccentricity as shown in Figure 2.3.4 (a). For a displaced pinhole, Thibos, Bradley and Zhang (1991) define the approximate relationship as $t = h\,\delta F_0$. However the definition is subtly different from that as given in the Equation 2.3.5 by Thibos *et al* (1990). The definition in Equation 2.3.6 and its approximation are given as approximations and the angle *t* is subtended at the nodal point and shown in Figure 2.3.4 (a) and (b), whereas in Figure 2.3.3 (a), (b) and (c) the angle is subtended at the refracting surface. Comparing these two equations, Thibos, Bradley and Zhang (1991) also conclude that each millimetre of displacement of

an external pinhole or limiting aperture results in 15° of eccentricity for the naked eye.

Zhang, Thibos and Bradley (1997) schematically define *transverse chromatic aberration* as the angle subtended at the refracting surface, according to

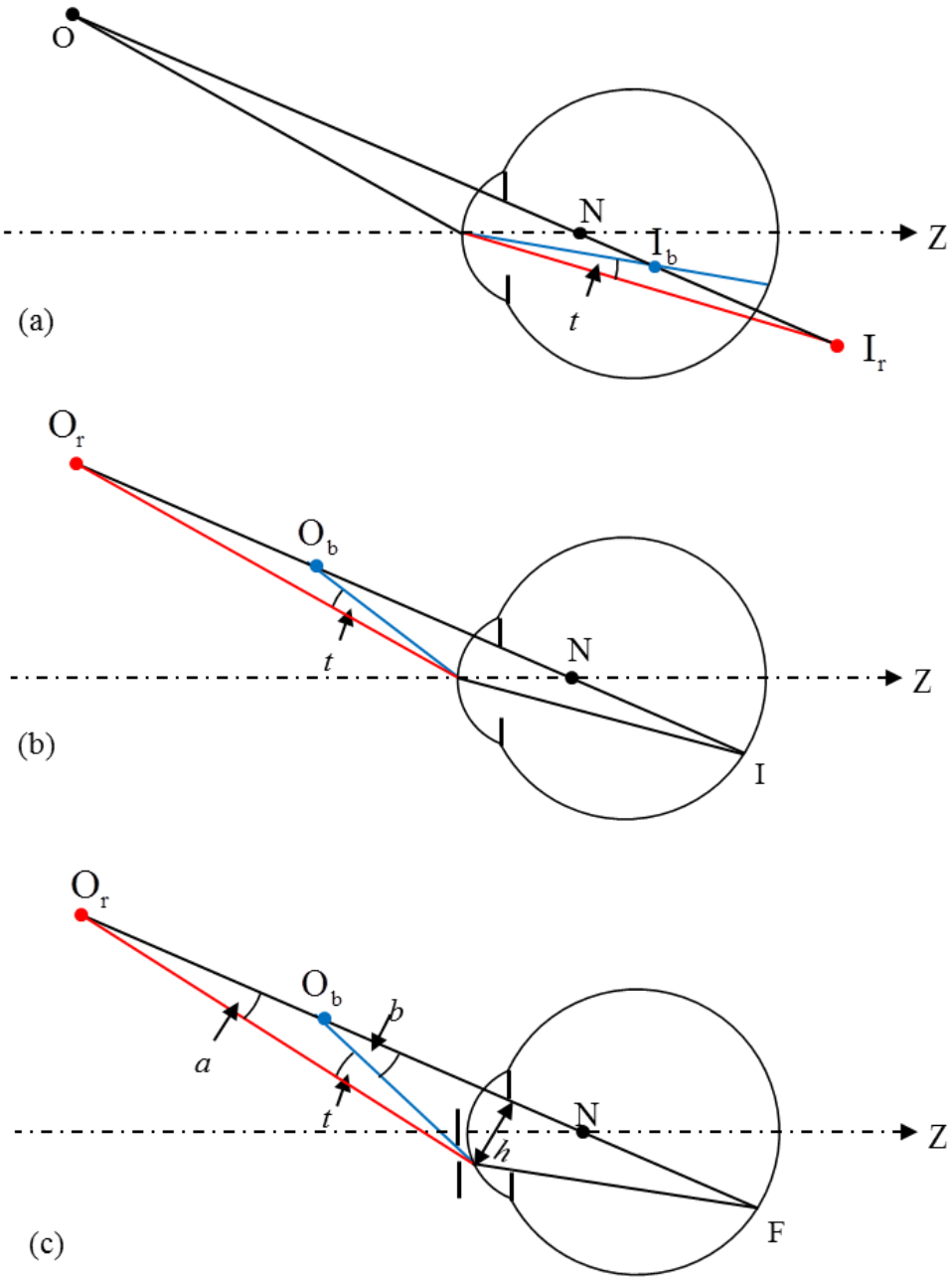

Figure 2.3.3 The chromatic difference in position *t* for the reduced eye. (a) The chromatic difference in position in image space for the naked eye. (b) The chromatic difference in position in object space for the naked eye. (c) The chromatic difference in position in object space for the eye with artificial limiting aperture immediately in front of the refracting surface. Figure not drawn to scale and adapted from Thibos *et al* (1990).

Figure 2.3.3 (a), however, they define *transverse chromatic aberration* algebraically as the angle subtended at the nodal point and shown in Figure 2.3.4. Zhang, Thibos and Bradley (1997) estimate that the angle subtended at the nodal point of the eye to be approximately 1.333 times larger than the angle subtended at the refracting surface.

Chromatic difference in magnification

The chromatic difference in magnification is defined as the magnification of the angle between the red and blue chief rays or difference in size between the centres of the red and blue retinal images as a percentage (Thibos, Bradley and Zhang, 1991; Zhang, Thibos and Bradley, 1991) or as a ratio (Rabbetts, 2007; Thibos, Bradley and Zhang, 1991) or seconds of arc (Simonet & Campbell, 1990),

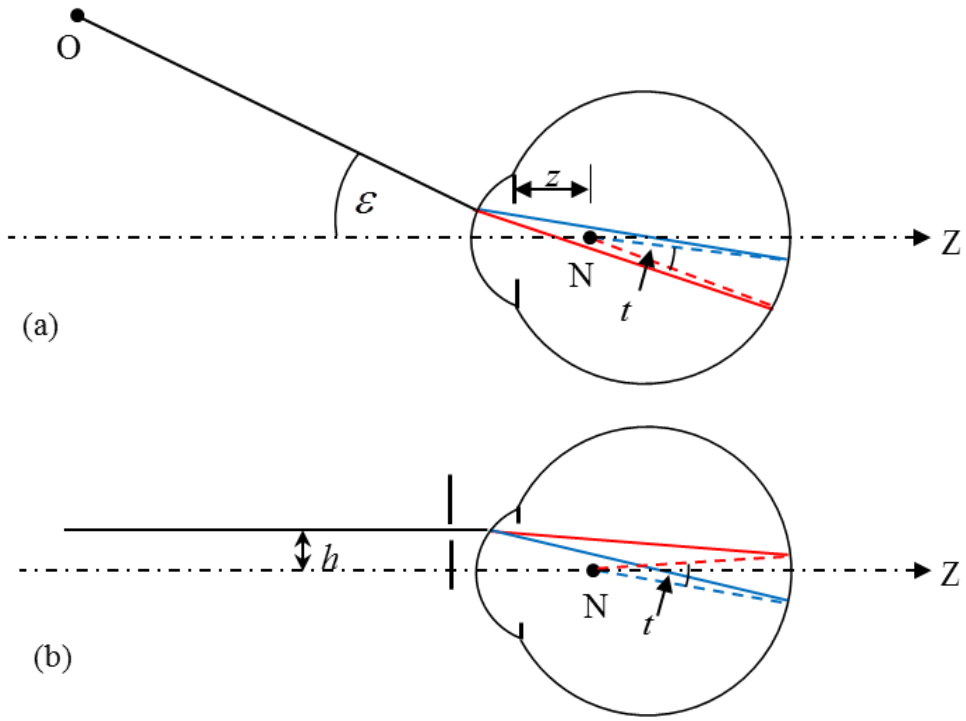

Figure 2.3.4 Chromatic difference in position *t* for the reduced eye in image space. (a) The ray arrives at the naked eye at eccentricity ε. *t* is the angle subtended at N by the intersections of the two rays with the retina. (b) A decentred pinhole aperture ensures that the ray arrives at the eye at some distance *h* from the achromatic axis. *t* is the angle subtended at N by the retinal intersections of the two rays. (Figure adapted from Thibos *et al*, 1991)

regardless of defocus. The chromatic difference in magnification is the variation in retinal image size with variation in wavelength (Thibos *et al*, 1990). One or both of the images for the two wavelengths used in the calculation will be out of focus (Thibos *et al*, 1990). Theoretically, chromatic difference in magnification can be calculated in both image and object space, however, because most of the experimental magnitudes measured are for chromatic difference in position, chromatic difference in magnification is usually calculated in image space.

Simonet and Campbell (1990) give the chromatic difference in magnification as

$$\delta M = y_r - y_b \tag{2.3.7}$$

where y_r and y_b are the red and blue image sizes at the retina, with the red image on the centre of the fovea F, regardless of defocus, and corresponding to object size y_O in seconds of arc. This is shown in Figure 2.3.5.

Chromatic difference in magnification is defined as an angular magnification given as

$$\delta M = \frac{t}{\varepsilon} \tag{2.3.8}$$

where *t* is the angle between the red and blue chief rays as given in Figure 2.3.3 (a) and ε is the eccentricity shown in Figure 2.3.4 (a) (Thibos, Bradley and Zhang, 1991; Zhang, Thibos and Bradley, 1991). Equation 2.3.8 gives the relationship between chromatic difference in position *t* and chromatic difference in magnification.

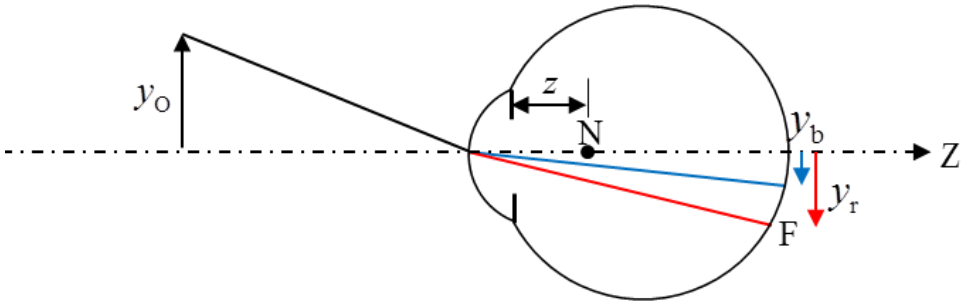

Figure 2.3.5 Chromatic difference in magnification is the difference between the image size for the two images created at the retina for two different chosen wavelengths, y_b and y_r, corresponding to object size y_O. y_r corresponds to F, the centre of the fovea.

Thibos, Bradley and Zhang (1991) and Zhang, Thibos and Bradley (1991) give the chromatic difference in magnification δM as

$$\delta M = z\,\delta F_0 \qquad (2.3.9)$$

where z is the distance between the pupil and the nodal point, shown in Figure 2.3.5. According to Thibos, Bradley and Zhang (1991), z is typically estimated at 0.4 cm, δF_0 is approximately 2 D and the chromatic difference in magnification is 0.8% across the visible light spectrum. Thibos, Bradley and Zhang (1991) conclude that chromatic difference in magnification is directly proportional to chromatic difference in refractive compensation and to the axial location of the entrance pupil relative to the nodal point. In the naked eye they find that this amounts to 0.8%, but by implication, the chromatic difference in magnification will increase when the limiting aperture is outside the eye, for example with a pinhole or optical instrument in front of the eye.

Of interest is the similarity between Equations 2.3.6 and 9. The chromatic difference in position is proportional to the sine of the eccentricity while the chromatic difference in magnification is independent of the eccentricity.

Experimental measurements

We recall that Thibos *et al* (1990) conducted an experiment as part of a larger experiment to find a relationship between *longitudinal chromatic aberration* (chromatic difference in refractive compensation) and *transverse chromatic aberration* (chromatic difference in position). They used a pinhole aperture to manipulate the angle of incidence of the foveal chief ray and measured the magnitude of the aberration as a function of pinhole displacement using a two-colour Vernier-alignment task.

Simonet and Campbell (1990) conducted experiments to measure *longitudinal chromatic aberration* (chromatic difference in refractive compensation) and *optical transverse chromatic aberration* (chromatic difference in position at the fovea). They made use of firstly, a dual Maxwellian view and vertical Vernier targets with the red target being the fixed target and the blue target being manipulated. This enabled them to take experimental measurements

of both *longitudinal chromatic aberration* and *transverse chromatic aberration*. They noted that the factors affecting the average and variability of *transverse chromatic aberration* include the value of angle α and any displacement of the pupil.

The experimental measurements of Thibos *et al* (1992) using the two-colour Vernier method also measured the induced chromatic difference in position in object space for pinhole positions. We recall that the aim of the set of experiments was to develop a reduced eye model that closely mimicked the real eye for chromatic aberration predictions. They developed the "chromatic eye" with three improvements over the reduced eye. The adaption that was most essential to measuring chromatic difference in position was the inclusion of a pupil that Thibos (1987) originally introduced allowing for a reference axis and pupil centre to be defined. Thibos *et al* (1992) show that the chromatic eye, by design, matches the experimental data almost exactly, enabling accurate prediction of chromatic difference in refractive compensation and position.

Zhang, Thibos and Bradley (1997) did a further experiment to compare the image sizes between the two eyes produced by an eccentric object point. The procedure measured interocular differences in image size produced stereoscopically and measured the amount of image magnification difference which are introduced by interocular differences in wavelength. They used the same procedure to compare firstly the naked eye and natural pupils, secondly, the naked eye with pinhole apertures in front of both eyes and measurements taken at three different vertex distances and finally while the subjects wore an achromatizing lens in front of the right eye. The achromatizing lenses compensate for wavelength-dependent refractive error, however, they exaggerate wavelength-dependent magnification by a factor of up to 7. In comparison, the artificial pupil at 20 mm vertex distance, showed the greatest increase in transverse chromatic aberration.

2.4 Summary

The assortment of terms and definitions is a source of confusion in the literature of chromatic aberration. For the purposes of this dissertation, we shall

differentiate between the classical optics definition of chromatic aberration and the ophthalmic and physiological optics definitions. We shall define first-order chromatic aberration according to the classical optics definition given by Born and Wolf (2002) and given in Section 2.2.1. This definition for longitudinal and transverse chromatic aberration is limited to Gaussian optics and in Chapter 6 we generalise this definition to include systems with astigmatic and heterocentric elements.

We shall distinguish between the definitions of ocular chromatic aberration found in the ophthalmic and physiological optics literature from the classical definition by referring to the former as ocular chromatic properties and to the latter as chromatic aberration. We shall distinguish between chromatic properties that are independent or dependent on object or image and aperture position. Independent chromatic properties include chromatic difference in power and chromatic difference in refractive compensation. Chromatic properties dependent on object or image and aperture positions include chromatic difference in position and chromatic difference in magnification. Chromatic properties in both image and object space will be examined.

In Chapter 7 we obtain formulae for calculating the chromatic properties in image and object space from the transference. The transference will enable us to calculate all of the chromatic properties of a compound Gaussian eye quickly and easily, and we will not have to restrict ourselves to the reduced eye.

The definitions in the literature consider the difference between wavelengths at two end-points of the visible light spectrum. While this is important, we shall, in Chapters 8 and 9, take a look at the dependence of the fundamental and derived properties of the transference on the frequency of light across the entire visible light spectrum.

3 BACKGROUND THEORY: OPTICS

First-order optics and the approximation of small angles are used throughout this study. Historically, the physiological optics approach to chromatic aberration has used ray tracing and cardinal points and for this reason, hence we take a brief look at this approach. However, the model of choice in this dissertation is linear optics; often simplified for Gaussian systems. Linear optics is a powerful tool in that it allows for surfaces that are astigmatic and tilted or decentred. The optical character of compound systems comprising multiple elements is represented by a single matrix, the transference. In linear and Gaussian optics, the transference is a complete representation of the first-order effects of an optical system on the ray traversing it (Torre, 2005: 60).

We start this chapter with a brief overview of the theories of light to ascertain where both linear and Gaussian optics are positioned in the field of optics. We then take a detailed look at linear optics, define the optical system, derive the transference of elementary and compound systems and show how it changes the state of the ray traversing the system. The fundamental properties of a system are defined. We see how the transference can be augmented to allow for tilt and decentration or simplified for a Gaussian system with only centred stigmatic elements.

In order to gain some insight into the fundamental properties, we take a look at four special systems. There are a number of familiar properties of optical systems that can be derived from the transference. We take a look at those that have implications for the study of chromatic properties of the eye. The derived properties that we will consider include power, compensating lenses, front- and back vertex power, magnification and cardinal points. There are many other properties that can be derived from the transference, however, we will limit this study to those just mentioned.

Because the transference is symplectic, there are a number of implications, for its mathematical manipulation. In particular there are limitations on the statistical analysis of the transference. To overcome this we turn to the literature to establish how to get around these limitations. It turns out that we can transform

the transference into an element of linear space which then allows quantitative analysis. Each of these transformed transferences will be studied in turn, and one in particular will be pivotal to the development, in Chapter 8, of a formula for the dependence of the transference on the frequency of light.

Finally, we look at how vergence and wavefronts are represented in linear and Gaussian optics. Of course, light is not a property of the system, but we are interested in the effect of the system on light. Because vergence is the basis for how we will be defining chromatic aberration in Chapter 6, we take a look at how vergence and wavefronts are defined in the linear optics literature.

3.1 Gaussian and Linear Optics

Gaussian and linear optics assume that rays are paraxial and therefore make use of the assumption of small angles and that the rays are close to the longitudinal axis. In the optics literature this is commonly referred to as either the Gaussian approximation or paraxial approximation. In the mathematics literature it is referred to as the first-order approximation; all quadratic (or higher-order) expressions in angles are ignored (Guillemin & Sternberg, 1984:5,23). The approximations $\sin\theta = \theta$, $\tan\theta = \theta$ and $\cos\theta = 1$ are used and Snell's law simplifies to $n_1 i_1 = n_2 i_2$ or $\imath_1 = \imath_2$ where $\imath = ni$. Both the ray tracing and matrix approaches in Gaussian optics make use of this assumption. In addition both Gaussian and linear optics assume that all media are homogenous and isotropic between refracting surfaces. This implies that rays are straight lines between refracting surfaces and geometrical aberrations are ignored (Guillemin & Sternberg, 1984:7).

3.1.1 Theories of light

In physics, as new theories supersede old ones, the older theory may still hold some relevance. It may be an approximation of the new theory or it may be valid in certain circumstances or a special case of the new theory (Guillemin & Sternberg, 1984:3). This is certainly true in optics in particular. Guillemin and Sternberg (1984:3-17, 37) describe the theories of light, a summary of which is presented below.

Quantum electrodynamics is the current theory of light and describes the interaction between light and charged particles, including its photo-electric effect and wavelike character of electro-magnetic radiation. *Maxwellian electrodynamics* is an approximation of quantum electrodynamics and ignores the quantum effects. It explains electricity, magnetism and electromagnetic radiation, including its source and propagation, but fails at the atomic or subatomic level.

Wave theory is mostly ascribed to Fresnel and is concerned with the propagation of light through various media. It includes diffraction, interference and polarization. It deals with certain wavelengths of light and ignores the emission of radiation.

Geometrical optics is an approximation of wave theory which ignores the wave character of light, diffraction, interference and polarization. *Geometrical optics* is valid for apertures of large dimension (when compared with the wavelength of light), provided one ignores what is happening in the vicinity of shadows and foci. Geometrical optics uses Snell's law ($n_1 \sin i_1 = n_2 \sin i_2$) without the approximation of small angles and the refractive indices of heterogeneous media may vary smoothly and sometimes rapidly. The deviations between linear and geometrical optics are known as geometrical or Seidel's (third-order) aberrations.

Linear optics is an approximation of geometrical optics which ignores Seidel's aberrations and uses the approximation of small angles. In linear optics a ray is defined in three-dimensional space at a fixed transverse plane for direction and position using four variables. A symplectic 4×4 matrix represents the system through which this ray will traverse. The trajectory of the light ray is traced as it passes through the various refracting and reflecting surfaces and homogenous gaps of the optical system. A coordinate system is introduced with a longitudinal axis Z and various transverse planes T, usually two. Because linear optics applies in three-dimensions, it accounts for all the effects of astigmatism. An augmented symplectic 5×5 matrix can account for the additional effects of tilted surfaces and decentred elements (Harris, 1994).

Gaussian optics is a special case of linear optics where all surfaces are rotationally symmetric about a central axis, hence the longitudinal axis Z

coincides with the optical axis. The rays studied are all coplanar, that is, they all lie on one plane, the reference plane. The transference simplifies to a 2×2 matrix and the vector representing the ray at a transverse plane is 2×1.

3.2 First-order optics

In this section we consider first-order optics, both Gaussian and linear, that will form the basis for the remaining chapters. It is not intended as a complete account of linear optics.

3.2.1 Definition of an optical system

An optical system is bound by two transverse planes, an entrance plane T_0 and an exit plane T, and has a longitudinal axis Z (see Figure 3.2.1). The entrance and exit planes can be chosen to be anywhere except at a refracting or reflecting surface. Usually the planes are taken to be immediately before or after a refracting or reflecting surface.

3.2.2 The state of the ray

The state of the ray at transverse plane T is defined as

$$\boldsymbol{\rho} = \begin{pmatrix} \mathbf{y} \\ \boldsymbol{\alpha} \end{pmatrix} \tag{3.2.1}$$

where

$$\boldsymbol{\alpha} = n\mathbf{a} \tag{3.2.2}$$

is the reduced inclination. (‘Reduced’ has the same sense as in ‘reduced to a common denominator’; it does not mean ‘made less’.) $\boldsymbol{\rho}$ is a 4×1 matrix consisting of two submatrices, $\mathbf{y}$ and $\boldsymbol{\alpha}$. $\mathbf{y}$ is a 2×1 matrix which represents a position vector with Cartesian coordinates y_1 and y_2:

$$\mathbf{y} = \begin{pmatrix} y_1 \\ y_2 \end{pmatrix}. \tag{3.2.3}$$

$\mathbf{a}$ is a 2×1 matrix that represents the inclination of the ray at T relative to Z. In terms of horizontal and vertical Cartesian coordinates

$$\mathbf{a} = \begin{pmatrix} a_1 \\ a_2 \end{pmatrix}. \tag{3.2.4}$$

In Figure 3.2.1 we distinguish between the incident ray state $\boldsymbol{\rho}_0$ at entrance plane T_0 and emergent ray state $\boldsymbol{\rho}$ at exit plane T.

3.2.3 The transference and fundamental properties

The transference **S** of an untilted, centred (homocentric) linear optical system is a 4×4 matrix often conveniently represented by (Guillemin and Sternberg, 1984: 26; Harris, 2010d)

$$\mathbf{S}=\begin{pmatrix}\mathbf{A} & \mathbf{B}\\ \mathbf{C} & \mathbf{D}\end{pmatrix} \tag{3.2.5}$$

where **A** the *dilation*, **B** the *disjugac*y, **C** the *divergence* and **D** the *divaricatio*n are the fundamental first-order optical properties of the system (Harris, 1999a; 2001c). Each of **A**, **B**, **C** and **D** is a 2×2 matrix.

The fundamental properties are strictly properties of the system itself and do not represent properties of anything else including light, vergence, image foci or object points (Harris, 1999b). A system may comprise a series of elementary systems, namely refracting surfaces and homogenous gaps between the entrance and exit planes.

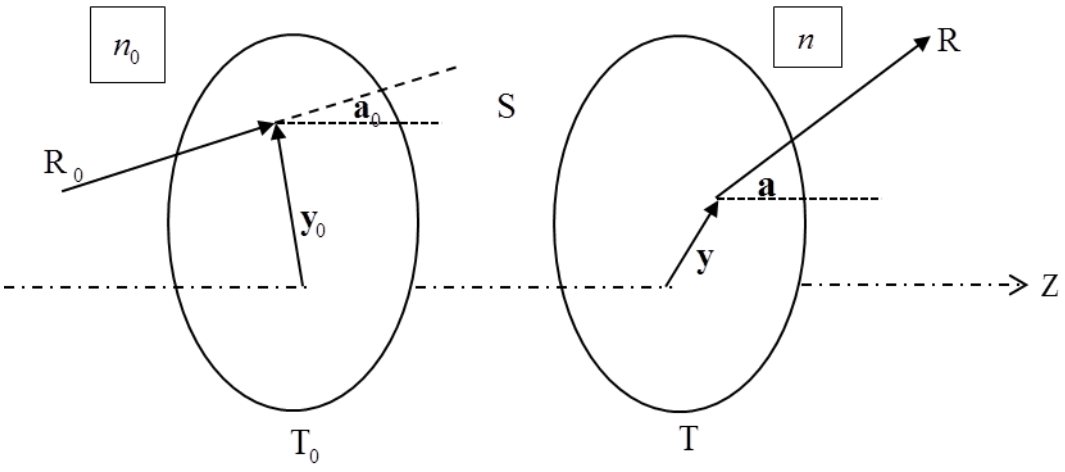

Figure 3.2.1 An optical system S is bound by an entrance plane T_0 and an exit plane T and has a longitudinal axis Z. A ray enters system S at T_0 with incident ray segment R_0 at transverse position $\mathbf{y}_0$ and inclination $\mathbf{a}_0$. The ray exits the system at T; the emergent ray segment R has position **y** and inclination **a**. The refractive index upstream of the system is n_0 and downstream it is *n*.

Let system S_1 have transference $\mathbf{S}_1$ and similarly for systems S_2, S_3, *etc*. Then the transference of the compound system $S_1S_2S_3...S_m$ made up of *m* juxtaposed optical systems is (Keating, 2002:325-345, Harris, 1994)

$$\mathbf{S} = \mathbf{S}_m ... \mathbf{S}_3 \mathbf{S}_2 \mathbf{S}_1 . \tag{3.2.6}$$

Multiplication is in reverse order.

The transference of a homogenous gap of width *z* and index *n* is (Guillemin and Sternberg, 1984: 9, 27)

$$\mathbf{S} = \begin{pmatrix} \mathbf{I} & \zeta\mathbf{I} \\ \mathbf{O} & \mathbf{I} \end{pmatrix} \tag{3.2.7}$$

where ζ is a scalar and is the reduced width defined by

$$\zeta = \frac{z}{n} . \tag{3.2.8}$$

I and **O** are the 2×2 identity and null matrices, respectively. The transference of a refracting surface or thin lens of power **F** (a symmetric matrix) is (Guillemin and Sternberg, 1984: 10, 27; Harris, 2010d; Keating, 1982)

$$\mathbf{S} = \begin{pmatrix} \mathbf{I} & \mathbf{O} \\ -\mathbf{F} & \mathbf{I} \end{pmatrix} . \tag{3.2.9}$$

3.2.4 The basic equation of a ray traversing a system

A ray traversing system S has its state at incidence $\boldsymbol{\rho}_0$ and emergence $\boldsymbol{\rho}$ related by

$$\mathbf{S}\boldsymbol{\rho}_0 = \boldsymbol{\rho} \tag{3.2.10}$$

an equation referred to as the basic equation of linear optics (Harris, 1999a,b).

Substituting from Equations 3.2.5, 1 and 2 into Equation 3.2.10 and multiplying out, we obtain two matrix equations for a system centred about an optical axis:

$$\mathbf{A}\mathbf{y}_0 + n_0\mathbf{B}\mathbf{a}_0 = \mathbf{y} \tag{3.2.11}$$

$$\mathbf{C}\mathbf{y}_0 + n_0\mathbf{D}\mathbf{a}_0 = n\mathbf{a} . \tag{3.2.12}$$

3.2.5 Symplecticity

The general linear group over the real numbers is denoted GL(n;$\mathbb{R}$) and is the group of all $n \times n$ invertible matrices with real entries. (We will restrict this dissertation to the set of real numbers). The general linear group is a matrix Lie group and is closed under matrix multiplication. The real symplectic group, denoted Sp(n;$\mathbb{R}$), is a subgroup of GL(n;$\mathbb{R}$) and is the set of all $2n \times 2n$ matrices (Hall, 2004:3-8).

By definition (Guillemin and Sternberg, 1984:26; Watkins, 2004; Hall, 2004:8), a $2n \times 2n$ matrix **S** is symplectic if it obeys the equation

$$\mathbf{S}^{\mathrm{T}}\mathbf{E}\mathbf{S} = \mathbf{E} \tag{3.2.13}$$

where

$$\mathbf{E} = \begin{pmatrix} \mathbf{O} & \mathbf{I} \\ -\mathbf{I} & \mathbf{O} \end{pmatrix} \tag{3.2.14}$$

and **I** and **O** are $n \times n$ identity and null matrices respectively and **E** is a $2n \times 2n$ matrix, sometimes known as the *symplectic unit matrix* (Torre, 2005: 11; Harris, 2010d). The superscript T represents the matrix transpose. In Gaussian optics $n = 1$ implying the simplest of optics, that on the reference plane, with the system being stigmatic, centred and 2-dimensional. In linear optics $n = 2$, giving us the simplest optical theory, that in 3-dimensions (Harris, 2010d).

Substituting from Equations 3.2.5 and 3.2.14 into Equation 3.2.13 and multiplying out we find

$$\begin{pmatrix} \mathbf{A} & \mathbf{B} \\ \mathbf{C} & \mathbf{D} \end{pmatrix}^{\mathrm{T}} \begin{pmatrix} \mathbf{O} & \mathbf{I} \\ -\mathbf{I} & \mathbf{O} \end{pmatrix} \begin{pmatrix} \mathbf{A} & \mathbf{B} \\ \mathbf{C} & \mathbf{D} \end{pmatrix} = \begin{pmatrix} \mathbf{O} & \mathbf{I} \\ -\mathbf{I} & \mathbf{O} \end{pmatrix} \tag{3.2.15}$$

$$\begin{pmatrix} \mathbf{A}^{\mathrm{T}}\mathbf{C} - \mathbf{C}^{\mathrm{T}}\mathbf{A} & \mathbf{A}^{\mathrm{T}}\mathbf{D} - \mathbf{C}^{\mathrm{T}}\mathbf{B} \\ \mathbf{B}^{\mathrm{T}}\mathbf{C} - \mathbf{D}^{\mathrm{T}}\mathbf{A} & \mathbf{B}^{\mathrm{T}}\mathbf{D} - \mathbf{D}^{\mathrm{T}}\mathbf{B} \end{pmatrix} = \begin{pmatrix} \mathbf{O} & \mathbf{I} \\ -\mathbf{I} & \mathbf{O} \end{pmatrix} \tag{3.2.16}$$

which gives the three distinct symplectic equations (Guillemin and Sternberg, 1984:26)

$$\mathbf{A}^{\mathrm{T}}\mathbf{C} - \mathbf{C}^{\mathrm{T}}\mathbf{A} = \mathbf{O}, \tag{3.2.17}$$

$$\mathbf{A}^{\mathrm{T}}\mathbf{D} - \mathbf{C}^{\mathrm{T}}\mathbf{B} = \mathbf{I} \tag{3.2.18}$$

and

$$\mathbf{B}^{\mathrm{T}}\mathbf{D} - \mathbf{D}^{\mathrm{T}}\mathbf{B} = \mathbf{O}. \tag{3.2.19}$$

For any 2×2 or 4×4 symplectic matrix there exists an optical system with that transference and any matrix that is not symplectic does not represent the transference of an optical system (Guillemin and Sternberg, 1984:23-27; Harris, 2004a, 2010d).

Manipulating Equation 3.2.18 and substituting the equality from either Equation 3.2.17 or 19 and the rule $(\mathbf{AB})^{\mathrm{T}} = \mathbf{B}^{\mathrm{T}}\mathbf{A}^{\mathrm{T}}$, one obtains four expressions, namely

$$\mathbf{A} - \mathbf{B}\mathbf{D}^{-1}\mathbf{C} = \mathbf{D}^{-\mathrm{T}}, \tag{3.2.20}$$

$$\mathbf{B} - \mathbf{A}\mathbf{C}^{-1}\mathbf{D} = -\mathbf{C}^{-\mathrm{T}}, \tag{3.2.21}$$

$$\mathbf{C} - \mathbf{D}\mathbf{B}^{-1}\mathbf{A} = -\mathbf{B}^{-\mathrm{T}}, \tag{3.2.22}$$

$$\mathbf{D} - \mathbf{C}\mathbf{A}^{-1}\mathbf{B} = \mathbf{A}^{-\mathrm{T}} \tag{3.2.23}$$

(Harris and van Gool, 2004; Harris, 2010d). The expression $\mathbf{A} - \mathbf{D}^{-\mathrm{T}}\mathbf{B}^{\mathrm{T}}\mathbf{C}$ is known as the Schur complement of **A** in **S** and similarly there are Schur complements of **B**, **C** and **D**. They have proven useful in visual optics and are particularly useful in simplifying complicated equations.

In a Gaussian system the three symplectic equations effectively reduce to the single equation

$$AD - CB = 1 \tag{3.2.24}$$

which is the equation for unit determinant. For a 2×2 matrix this is the only requirement for symplecticity (Guillemin & Sternberg, 1984:11, 15, 24) and any 2×2 matrix with determinant 1 is the transference of some optical system.

While the 4×4 transference of an optical system always has a unit determinant, the converse is not always true (Guillemin & Sternberg, 1984:23-24; Harris, 2010d). In order to test for symplecticity one needs to test whether the matrix obeys Equation 3.2.13, or, equivalently, whether it obeys all of Equations 3.2.17 to 19 (Harris, 2004a, 2010d).

All symplectic matrices have unit determinant (Bernstein, 2005:114; Hall, 2004:8,40). The implication of this is that because

$$\det(\mathbf{AB}) = \det\mathbf{A}\det\mathbf{B} \tag{3.2.25}$$

the product of all transferences will also have unit determinant (Bernstein, 2005:40-41; Anton and Rorres, 2005:104-105; Keating, 2002:330; Harris, 2010d)

and therefore all transferences are invertible. We note that the matrix in Equation 3.2.7 is symplectic and similarly the matrix in Equation 3.2.9 is symplectic provided **F** is symmetric (from Equation 3.2.17), which is true of refracting surfaces and thin lenses. While Harris and van Gool (2009) have considered the theoretical possibility of a thin lens of asymmetric power, it will not be considered here.

3.2.6 Augmented transferences and heterocentric systems

Up to this point, the optical systems described have been homocentric, that is all centred on a longitudinal axis Z, which is therefore an optical axis. Elements may have been stigmatic or astigmatic and represented by Gaussian 2×2 or linear 4×4 transferences respectively. We now briefly consider the effects of including elements that are tilted or decentred (heterocentric).

We define a 4×1 matrix (Harris, 1993)

$$\boldsymbol{\delta} = \begin{pmatrix} \mathbf{e} \\ \boldsymbol{\pi} \end{pmatrix}. \tag{3.2.26}$$

It accounts for all the effects of prism, tilt and decentration. The *transverse translation* **e** and *deflectance* $\boldsymbol{\pi}$ are each 2×1 submatrices of $\boldsymbol{\delta}$ and along with **A**, **B**, **C** and **D** are also fundamental first-order optical properties of the system (Harris 2010e). **e** has units of length and $\boldsymbol{\pi}$ is dimensionless. It is often convenient to think of $\boldsymbol{\pi}$ in radians.

In order to account for these effects we generalise Equation 3.2.10 to

$$\mathbf{S}\boldsymbol{\rho}_0 + \boldsymbol{\delta} = \boldsymbol{\rho}. \tag{3.2.27}$$

For a compound system consisting of *n* subsystems (Harris, 1993)

$$\mathbf{S}_n\left(...\left(\mathbf{S}_3\left(\mathbf{S}_2\boldsymbol{\delta}_1 + \boldsymbol{\delta}_2\right) + \boldsymbol{\delta}_3\right) + ...\right) + \boldsymbol{\delta}_n = \boldsymbol{\delta}. \tag{3.2.28}$$

Instead of Equation 3.2.28, Harris (1994) defines a 5×5 augmented transference **T**

$$\mathbf{T} = \begin{pmatrix} \mathbf{S} & \boldsymbol{\delta} \\ \mathbf{o}^{\mathrm{T}} & 1 \end{pmatrix} \tag{3.2.29}$$

where **o** is a 4×1 null matrix, the fifth row being a trivial row, and a 5×1 augmented ray state $\boldsymbol{\gamma}$

$$\boldsymbol{\gamma} = \begin{pmatrix} \boldsymbol{\rho} \\ 1 \end{pmatrix}. \tag{3.2.30}$$

The qualifier "augmented" will not be used repetitively and we will rely on the context to make clear whether the transference or ray state is augmented or not.

Equation 3.2.27 now generalises to

$$\mathbf{T}\boldsymbol{\gamma}_0 = \boldsymbol{\gamma} \tag{3.2.31}$$

which is simple and elegant like Equation 3.2.10 and encompasses all the detail of Equation 3.2.27. The proof is provided by Harris (1994). **T** is a matrix that represents all the first-order optical characteristics of the system, including homogenous spaces and astigmatic elements that may be tilted and decentred (heterocentric) or have prismatic effects (Harris, 2012c). Rewriting **T** with all six of its fundamental properties we have

$$\mathbf{T} = \begin{pmatrix} \mathbf{A} & \mathbf{B} & \mathbf{e} \\ \mathbf{C} & \mathbf{D} & \boldsymbol{\pi} \\ \mathbf{o}^{\mathrm{T}} & \mathbf{o}^{\mathrm{T}} & 1 \end{pmatrix}. \tag{3.2.32}$$

Each of **A**, **B**, **C** and **D** are 2×2 submatrices, **e**, $\boldsymbol{\pi}$ and **o** are 2×1 submatrices with **o** being a null vector. In particular, **T** represents the way the system will operate on the state of the ray traversing the system (Harris, 2001a). We note here that in order for a matrix to be symplectic it needs to be of the order $2n\times 2n$. **T** fails this requirement although it does have unit determinant. However, because submatrix **S** is symplectic one can call **T** an augmented symplectic matrix (Harris, 2010d, 2004a). Like symplectic matrices, augmented symplectic matrices remain closed under multiplication and are not closed under addition nor multiplication by a scalar.

Because of symplecticity and similarly to Equation 3.2.6 we can now obtain the transference for a compound heterocentric system (Harris, 1994):

$$\mathbf{T} = \mathbf{T}_m ... \mathbf{T}_3 \mathbf{T}_2 \mathbf{T}_1 . \tag{3.2.33}$$

Substituting from Equations 3.2.32 and 30 into Equation 3.2.31 and multiplying out, we now obtain the two matrix equations

$$\mathbf{A}\mathbf{y}_0 + \mathbf{B}\boldsymbol{\alpha}_0 + \mathbf{e} = \mathbf{y} \tag{3.2.34}$$

$$\mathbf{C}\mathbf{y}_0 + \mathbf{D}\boldsymbol{\alpha}_0 + \boldsymbol{\pi} = \boldsymbol{\alpha}. \tag{3.2.35}$$

3.2.7 Gaussian systems

We recall that a Gaussian system is defined where all surfaces are rotationally symmetric about a central axis. The longitudinal axis Z coincides with the optical axis creating an axis of symmetry. The implication is that all refracting surfaces are stigmatic and $\boldsymbol{\delta} = \mathbf{o}$. Specifically, each of the fundamental properties simplifies to a scalar matrix so that $\mathbf{A} = A\mathbf{I}$, $\mathbf{B} = B\mathbf{I}$, $\mathbf{C} = C\mathbf{I}$ and $\mathbf{D} = D\mathbf{I}$. Therefore, in a Gaussian system each of the fundamental properties reduces to a scalar and $\mathbf{S}$ to a 2×2 matrix. This is the equivalent to the study of the group Sl(2;$\mathbb{R}$); the group of 2×2 real matrices with determinant 1 (Guillemin and Sternberg, 1984:7-11).

In particular Equations 3.2.7 and 9 simplify to

$$\mathbf{S} = \begin{pmatrix} 1 & \zeta \\ 0 & 1 \end{pmatrix} \tag{3.2.36}$$

and

$$\mathbf{S} = \begin{pmatrix} 1 & 0 \\ -F & 1 \end{pmatrix} \tag{3.2.37}$$

respectively (Guillemin and Sternberg, 1984: 9-11). In general the transference simplifies to a 2×2 matrix represented by

$$\mathbf{S} = \begin{pmatrix} A & B \\ C & D \end{pmatrix} \tag{3.2.38}$$

and the 2×1 matrix representing the ray at a plane is

$$\boldsymbol{\rho} = \begin{pmatrix} y \\ na \end{pmatrix} \tag{3.2.39}$$

(Guillemin and Sternberg, 1984: 7-11). All the entries of $\mathbf{S}$ and $\boldsymbol{\rho}$ are scalars, as opposed to the non-scalar submatrices shown in Equations 3.2.5 and 1. Equations 3.2.34 and 35 reduce to

$$Ay_0 + n_0 Ba_0 = y \tag{3.2.40}$$

$$Cy_0 + n_0 Da_0 = na\,. \tag{3.2.41}$$

3.3 Fundamental properties

The fundamental properties are not usually encountered as such in optometry. Most of the properties that are encountered in optometry are derived properties. Certain derived properties need some additional information, such as length of the system, or its context, that is, the refractive indices upstream and downstream of the system (Harris, 2012c). Equations 3.2.34 and 35 are useful for these derivations, and are discussed in detail below.

In this section, an attempt is made to understand each of the fundamental properties of a Gaussian optical system. The fundamental properties are essentially mathematical and take on physical meanings only for particular situations. We use the transference for a Gaussian system defined in Equation 3.2.38 starting with Harris's (1999a) definition of ametropia. We then look at four special systems that result when each of the fundamental properties in turn is zero. Each of these situations results in interesting and familiar systems and relationships. Ultimately we can use this information to define systems that simplify the mathematics.

3.3.1 Ametropia

Harris (1999a) regards *A* in Equation 3.2.38 as representing ametropia. For a distant object all rays enter the eye parallel at some reduced inclination α_0. For $A = 0$ the eye is emmetropic and from Equation 3.3.1 below we see that all rays from a distant object point map to the same position *y* on the retina, a point focus. When $A \neq 0$ then the eye is ametropic, *A* represents a "squashing factor" where all rays entering the eye at different incident transverse positions map to respective positions on the retina. For an emmetropic eye, all rays with the same inclination will map to a single point on the retina. Positive values of *A* imply a hyperopic eye and negative values of *A* a myopic eye with the rays crossing over and inverting the direction of the position vector (Harris 1999b). There are exceptions to this rule (Harris, 1999b, 2007b).

3.3.2 Four special systems

We follow Harris' lead and start by looking at the four types of two-dimensional vector fields as obtained from the mathematical structure of the transference of a Gaussian system (Harris, 1996a). These are exit-plane focal systems where $A=0$, conjugate systems where $B=0$, afocal or telescopic systems where $C=0$ and entrance-plane focal systems where $D=0$.

Exit-plane focal systems ($A=0$)

We start with the exit-plane focal system shown in Figure 3.3.1. Equation 3.2.40 simplifies to

$$B\alpha_0 = y \tag{3.3.1}$$

when $A=0$. From Equation 3.3.1 we see that if all incident rays have the same reduced inclination then the emergent transverse position is the same for all the rays. This is shown in Figure 3.3.1. One can think of *B* as a sort of optical thickness, although it is not usually simply related to the actual length of a system. *B* therefore relates the emergent position through the system to the incident reduced inclination. Examples of an exit-plane focal system are an emmetropic eye, most schematic eyes and the compound system of an eye and distance compensating spectacle or contact lens in front of it.

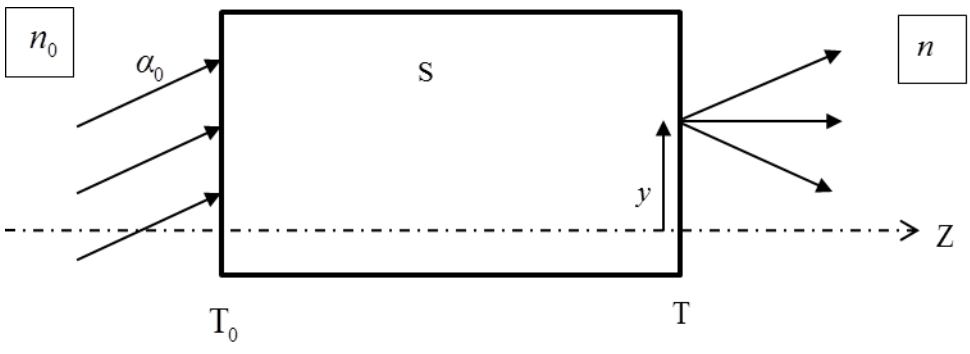

Figure 3.3.1 A Gaussian exit-plane focal system ($A=0$). All incident rays enter at the entrance plane T_0 with the same reduced inclination α_0. All emergent rays exit at T at the same transverse position *y*.

Conjugate systems *($B = 0$)*

Again, looking at Equation 3.2.40 we obtain

$$Ay_0 = y \tag{3.3.2}$$

when $B = 0$. This is shown in Figure 3.3.2. In a conjugate system the incident inclination plays no role and if all rays enter the system at point y_0 they will map to a conjugate point *y* on the exit plane. *A* is the transverse magnification. When we define a system to have the entrance plane at the object point and the exit plane at the image point, we have defined a conjugate system. This is an example of a system where, even though $B = 0$, the system itself does not usually have zero length. Conjugate systems are only defined for finite systems.

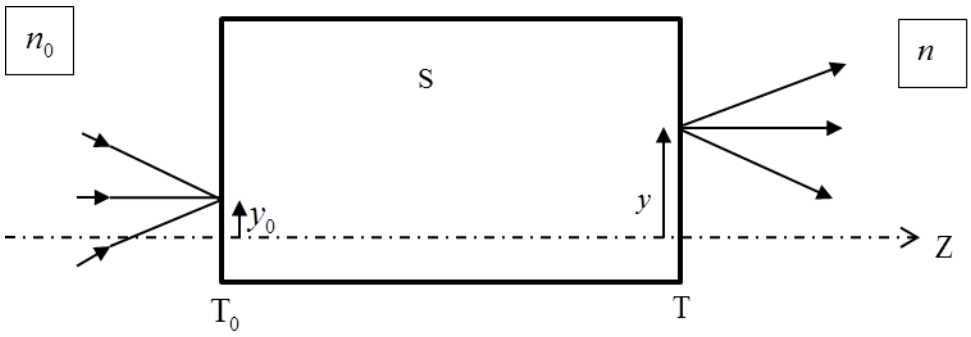

Figure 3.3.2 A conjugate system ($B = 0$). When all incident rays enter the system at the same transverse position y_0, they will exit at *y*. Points at y_0 and *y* are conjugate with each other.

Afocal systems *($C = 0$)*

Substituting $C = 0$ into Equation 3.2.41 we obtain

$$D\alpha_0 = \alpha \tag{3.3.3}$$

which is the formula for an afocal system such as a telescope used in low vision. It implies that for incident light, when all rays are parallel, the emerging light segments are also parallel to each other, but not necessarily parallel to the incident pencil, or to the longitudinal axis. This will be discussed in greater detail in Section 3.5.1. An afocal system is shown in Figure 3.3.3.

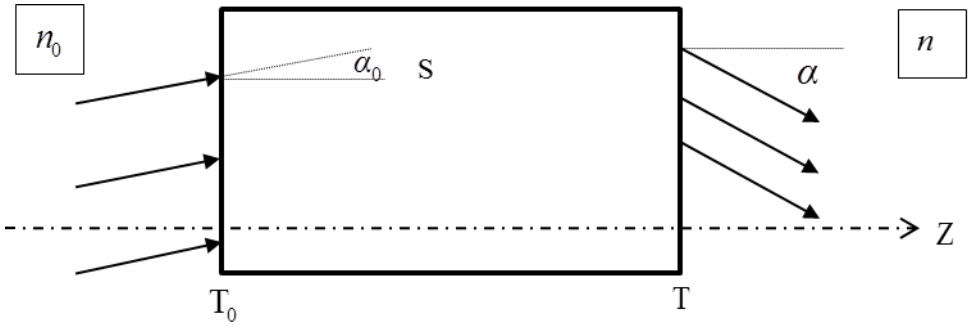

Figure 3.3.3 An afocal system ($C = 0$). If all incident rays are parallel to each other at reduced inclination α_0 then all emergent rays are parallel to each other at reduced inclination α.

Entrance-plane focal systems *($D = 0$)*

Finally, staying with Equation 3.2.41 but this time substituting $D = 0$, we obtain

$$Cy_0 = \alpha. \tag{3.3.4}$$

A point object at position y_0 on the entrance plane emits a pencil of light of zero vergence from the system at a reduced inclination of α. An entrance- plane focal system is shown in Figure 3.3.4. Examples include reversed emmetropic eyes and reversed ametropic eyes combined with the direct ophthalmoscope lens in ophthalmoscopy (Harris and van Gool, 2004).

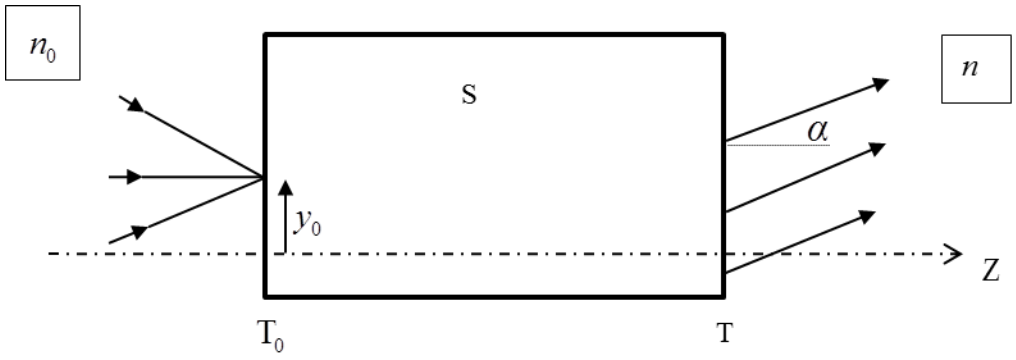

Figure 3.3.4 An entrance-plane focal system ($D = 0$). If all incident rays enter the system at the same position y_0 then they emerge parallel to each other with emergent reduced inclination α.

3.4 Derived properties

The fundamental properties of a first-order optical system can be obtained directly from the transference. In addition there are a number of first-order optical properties that can be derived from the transference. Certain of these derived properties are obtained from the transference alone, while others need input about the actual length of the system (e.g. Harris, 2009). Until now these properties have been studied under the assumption of a single reference wavelength.

The transference depends on its context, meaning the refractive indices upstream and downstream of the system. There are a number of derived properties that are of interest to this dissertation because they are dependent on frequency. These include the power of the system (Harris, 1997), magnification and blur (Harris, 2001a, b), compensatory systems such as entrance-plane refractive compensation (or neutralizing lens) (Harris, 1999a; Keating, 1988:236), front- and back-vertex power (Keating, 1988:236) and locations of the cardinal points (Harris, 2010d, 2011a,b). These derived properties are discussed in the rest of this chapter.

Additionally, in Chapter 6 this study derives formulae for longitudinal and transverse chromatic aberration from the transference and its context (Harris & Evans, 2012). In line with previous calculations done on Gaussian systems to quantify chromatic properties in the eye, in Chapter 7 this dissertation will derive equations from the transference for Gaussian systems for chromatic difference in power, refractive compensation, magnification and position. Other derived properties that will not form part of this dissertation are converter systems (Keating, Harris and van Gool, 2002), corneal patches and referred apertures (Harris, 2011c, 2012d, and a number of axes such as optical (Harris, 2009) visual (Harris, 2010c) and pupillary (Harris, 2013) axes and line of sight (Harris, van Gool and Evans, 2013). Achromatic axes have recently been defined from the transference for dichromatic light (Harris, 2012a, b).

Referred apertures, corneal patches and pinholes have significant relevance to current research being done on the intracorneal inlay, for example the AcuFocus Kamra corneal pinhole inlay. (Gatinel, 2010; Seyeddain, Riha, Hohensinn, Nix, Dexl and Grabner, 2010; Waring, 2010)). Two aspects are of

interest to this study. Firstly the chromatic properties resulting from positioning of the pinhole plane longitudinally within the cornea instead of the iridial plane and secondly, misplacement of the pinhole inlay during surgery in the transverse plane. The size of the pinhole and light entering the eye from around the inlay will also influence the chromatic properties in the eye. Thibos *et al* (1990) used a displaced pinhole to induce and measure transverse chromatic aberration experimentally. A misplaced pinhole results in a number of visual complaints, among which sensitivity to chromatic properties will be of special interest to this study.

3.4.1 Power

Power is well defined for refracting surfaces and thin lenses both as a power matrix and clinically as sphere / cylinder × axis. The power matrix is symmetric and has been derived by Fick (1972; 1973a; Blendowske, 2003) and Long (1976), apparently independently. Recently, we noted that the power matrix was being hinted at by Le Grand (1945: 326-327) and possibly by others before him. The equivalent power of a two surface thick lens system was defined by Keating (1981a, 1982, 2002: 343) who showed that the power matrix for such a system could be asymmetric, in which case it cannot be equivalent to a thin lens. Harris (1996a) derives a formula for the (equivalent) power for a system comprising three thin astigmatic lenses each separated by a gap.

Harris (1997) was the first to define power for optical systems in general. He defines power as

$$\mathbf{F} = -\mathbf{C}. \tag{3.4.1}$$

Power is therefore a first-order optical property derived from the transference of a system.

For Gaussian systems

$$\mathbf{C} = C\mathbf{I} \tag{3.4.2}$$

where **I** is an identity matrix. Hence for a Gaussian system we can write the power as

$$F = -C. \tag{3.4.3}$$

The eigenvalues of **F** are the two principal powers of an astigmatic system and the corresponding eigenvectors represent the directions of the two principal meridians (Keating, 1981a, b; Long, 1976; Harris, 2001c). Together the principal powers and meridians can be represented either by a power cross, or in principal meridional representation of power (Harris, 2000, 2001c). It is possible for a thick system, such as the eye, to have an asymmetric power, with corresponding non-orthogonal eigenvectors or meridians (Keating, 1981a, 1982). For any refracting surface or thin lens system, the power matrix is symmetric and the principal meridians therefore are orthogonal (Anton and Rorres, 2005: 381).

For thin systems equations were derived to convert from the clinical representation of power to the power matrix by Long (1976) and Fick (1972; Blendowske, 2003) and to revert back from the power matrix to clinical representation by Keating (1980) and Fick (1973b; Blendowske, 2003). Keating (1981b, 1997b) showed that the power matrix for a thick system comprising two or more astigmatic powers with nonaligned principal meridians will result in an asymmetric power matrix which corresponds to a power which has non-orthogonal meridians. Harris (2000, 2001c) developed conversion formulae to convert between principal meridional representation of power and matrices. This enables one to convert an asymmetric power matrix into power along two principal meridians which are not orthogonal.

3.4.2 Entrance-plane refractive compensation

We saw in Section 3.3.2 that an exit-plane focal system is defined by $A = 0$ (Harris, 1996a) which Harris (1999a) refers to as the "condition for emmetropia". The power of a thin lens juxtaposed immediately upstream to the system can be calculated in order to create such a system. Harris (1999a) refers to this as the "condition for compensation".

An example of an entrance-plane system is an emmetropic eye, or an ametropic eye compensated for distant viewing. Because of this, Harris (1999a) derives a formula for the power of the corneal-plane refractive compensation F_0. Making use of Equations 3.2.6, 37 and 38, we write the transference of the compound system of eye and compensating lens F_0 as

$$\begin{pmatrix} A_E & B_E \\ C_E & D_E \end{pmatrix}\begin{pmatrix} 1 & 0 \\ -F_0 & 1 \end{pmatrix}=\begin{pmatrix} A_E - B_E F_0 & \bullet \\ \bullet & \bullet \end{pmatrix} \tag{3.4.4}$$

where the dots represent values not needed here. Because this is an exit-plane focal system, we obtain

$$A_E - B_E F_0 = 0 \tag{3.4.5}$$

and solving we obtain the corneal-plane refractive compensation

$$F_0 = B_E^{-1} A_E . \tag{3.4.6}$$

Equation 3.4.6 shows that the corneal-plane refractive compensation depends on the dilation *A* and the disjugacy *B*. The divergence *C* (or power *F*) of the eye does not play a direct role, but does have an indirect role through the symplectic relations.

3.4.3 Front- and back-vertex power

Back-vertex power F_{bv}, shown in Figure 3.4.1(a), can be defined as either the vergence *L* leaving the system when incident rays are parallel or the reciprocal of the reduced emergent focal (or back-vertex) length (Keating, 2002:138-9, 145; Harris, 2010a). The definitions are equivalent. The front-vertex power F_{fv}, which is also called front neutralizing power F_{fn} and is shown in Figure 3.4.1(b), is defined as the negative of the incident vergence (L_0) (or power of the neutralizing effect of the system) in order for emerging rays to exit parallel (Keating, 2002: 138-9; Harris, 2010a). This is equivalent to the negative reciprocal of the incident reduced focal length.

The term power as it is used here is rather misleading. Vertex power is actually a measurement of vergence and as such the matrix is always symmetric (Keating, 1981a; Harris, 1996b). These vertex power formulae were originally derived by Keating (1981a, 1982) and the derivation was later simplified, using a different approach, by Harris (2010a). We take our lead from Harris (2010a), simplifying for Gaussian systems.

Derivation of back-vertex power

Comparing Figure 3.4.1 (a) and (c) we see that the thin postjuxtaposed lens of power F_{bn} compensates for the emergent vergence, such that the rays leave the system parallel and therefore we start with

$$F_{\text{bv}} = -F_{\text{bn}}. \tag{3.4.7}$$

We obtain F_{bn} from the transference of the compound system $\mathbf{S}$ made up of the transference of the system $\mathbf{S}_{\text{E}}$ followed by the transference of the thin lens $\mathbf{S}_{\text{b}}$ and then equating $C = 0$ for an afocal system, such that

$$\mathbf{S} = \mathbf{S}_{\text{b}}\mathbf{S}_{\text{E}} = \begin{pmatrix} 1 & 0 \\ -F_{\text{bn}} & 1 \end{pmatrix}\begin{pmatrix} A_{\text{E}} & B_{\text{E}} \\ C_{\text{E}} & D_{\text{E}} \end{pmatrix} = \begin{pmatrix} \bullet & \bullet \\ -F_{\text{bn}}A_{\text{E}} + C_{\text{E}} & \bullet \end{pmatrix}. \tag{3.4.8}$$

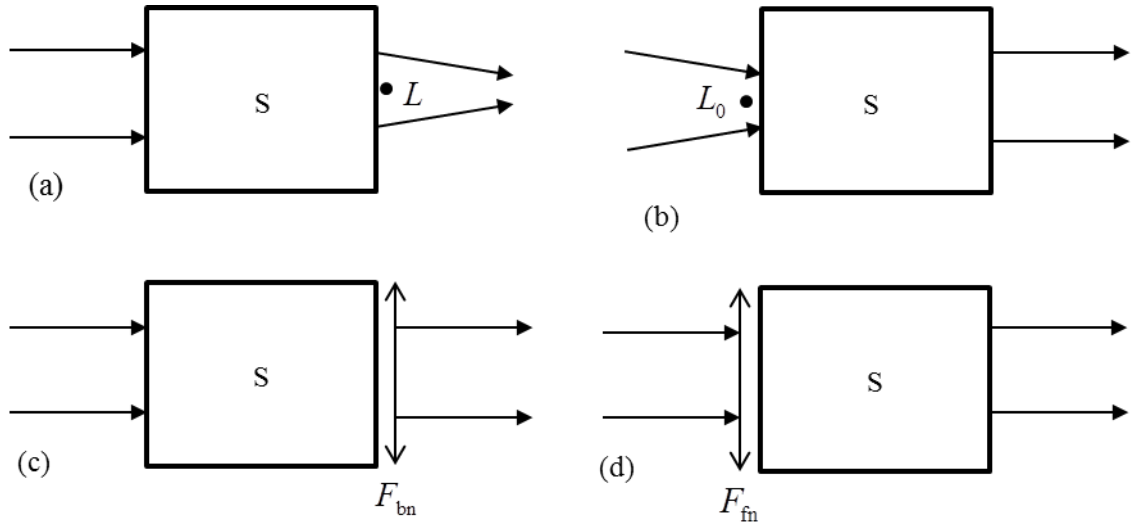

Figure 3.4.1 An optical system is shown as S. (a) Back-vertex power shown as emerging vergence L exiting the system when incident rays are parallel. (b) Front-vertex power, the negative of incident vergence shown as L_0 when the emerging rays are parallel. (c) A postjuxtaposed thin lens F_{bn} in combination with the system S creates an afocal compound system. (d) A prejuxtaposed thins lens F_{fn} creates an afocal system in combination with the system S.

therefore

$$-F_{\mathrm{bn}}A_{\mathrm{E}}+C_{\mathrm{E}}=0 \tag{3.4.9}$$

and

$$F_{\mathrm{bn}}=C_{\mathrm{E}}A_{\mathrm{E}}^{-1}. \tag{3.4.10}$$

Substituting Equation 3.4.10 into 3.4.7 we define back-vertex power as

$$F_{\mathrm{bv}}=-C_{\mathrm{E}}A_{\mathrm{E}}^{-1}. \tag{3.4.11}$$

Derivation of front-vertex power

Similarly to back-vertex power, Figures 3.4.1 (b) and (d) illustrate that the power of the thin neutralizing lens at the front-vertex of the system is the negative of the vergence at incidence onto the system

$$F_{\mathrm{fv}}=-F_{\mathrm{fn}} \tag{3.4.12}$$

The transference of the compound system $\mathbf{S}$ made up of the transferences of a thin lens $\mathbf{S}_{\mathrm{f}}$ followed by the system $\mathbf{S}_{\mathrm{E}}$ to create an afocal system is

$$\mathbf{S}=\mathbf{S}_{\mathrm{E}}\mathbf{S}_{\mathrm{f}}=\begin{pmatrix}A_{\mathrm{E}} & B_{\mathrm{E}}\\ C_{\mathrm{E}} & D_{\mathrm{E}}\end{pmatrix}\begin{pmatrix}1 & 0\\ -F_{\mathrm{fn}} & 1\end{pmatrix}=\begin{pmatrix}\bullet & \bullet\\ C_{\mathrm{E}}-D_{\mathrm{E}}F_{\mathrm{fn}} & \bullet\end{pmatrix}. \tag{3.4.13}$$

Equating $C=0$ for this afocal system

$$C_{\mathrm{E}}-D_{\mathrm{E}}F_{\mathrm{fn}}=0 \tag{3.4.14}$$

we calculate the power of F_{fn} as

$$F_{\mathrm{fn}}=D_{\mathrm{E}}^{-1}C_{\mathrm{E}}. \tag{3.4.15}$$

Substituting from Equation 3.4.12 into 3.4.15 we obtain the definition for front-vertex power

$$F_{\mathrm{fv}}=-D_{\mathrm{E}}^{-1}C_{\mathrm{E}}. \tag{3.4.16}$$

The derivations for front- and back-vertex power given above are from Harris (2010a). However, the typographical error in the original manuscript (a missing minus sign) for the equation for front-vertex power has been corrected here.

3.5 Magnification

Because a large proportion of the research on chromatic properties has focussed on chromatic difference of magnification and position (Atchison and Smith, 2002: 181-182; Rabbetts, 2007: 289-293; Thibos Bradley and Zhang, 1991), magnification and conjugation of points will be studied in more detail for its first-order effects. Three types of magnification are defined for conjugate Gaussian systems, namely transverse or lateral magnification, axial or longitudinal magnification and angular magnification (Meyer-Arendt, 1984:54; Keating, 2002: 56-62, 110, 154, 347-370; Smith and Atchison, 1997: 43-44, 71-72). We shall take a closer look at all three types in Gaussian systems.

3.5.1 Magnification of Gaussian systems

Transverse magnification

Transverse magnification is defined as

$$M_{\mathrm{t}} = \frac{y}{y_0} \tag{3.5.1}$$

as shown in Figure 3.5.1 (Emsley, 1950:33; Meyer-Arendt, 1984:54; Smith and Atchison, 1997:43; Keating, 2002:56, 110).

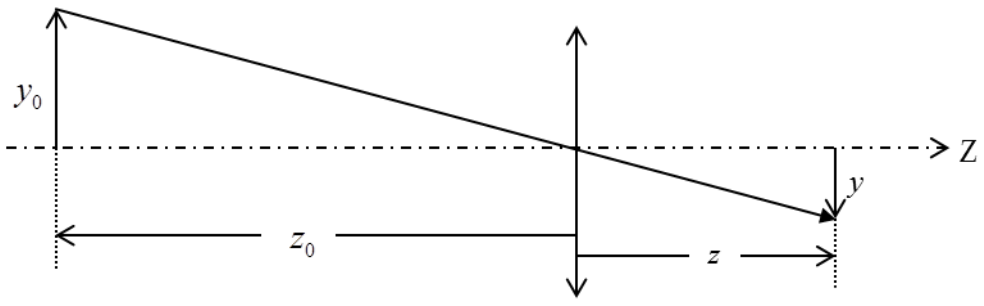

Figure 3.5.1 Transverse magnification of a thin system defined by Equation 3.5.1. y_0 is the height of the object at distance z_0 from the lens and *y* is the height of the image at a distance *z* from the lens.

Axial magnification

Axial magnification is defined by (Meyer-Arendt, 1984:56; Keating, 2002:154; Smith and Atchison, 1997:71-2)

$$M_z = \frac{\Delta z}{\Delta z_0} \tag{3.5.2}$$

where Δz_0 is the difference in axial length between the front and back of the object and Δz the corresponding axial length of the image. This is shown in Figure 3.5.2.

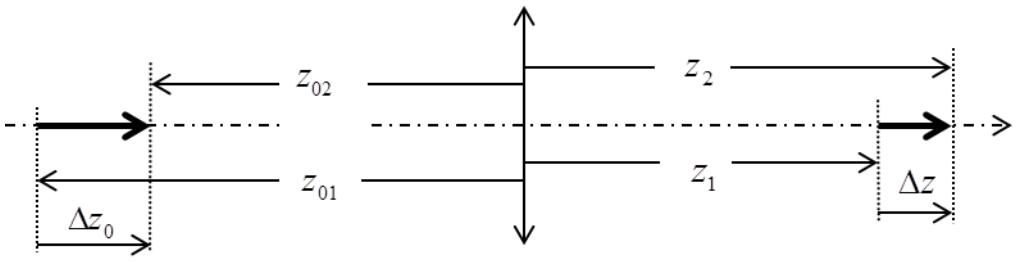

Figure 3.5.2 Axial magnification of a thin system. The two arrow bases (subscript 1) are conjugate and the two arrowhead apexes (2) of the object and image are conjugate. The axial magnification is the ratio of axial length of image to axial length of object.

Angular magnification

Angular magnification, commonly referred to as "magnifying power", is the most important type of magnification according to Meyer-Arendt (1984:57). This is the magnification that is used to define the magnifying power of afocal telescopes and binoculars and is typically denoted by an "×". It is defined as the ratio of the image's reduced inclination to the object's reduced inclination (Smith and Atchison, 1997:44, 69, 768). For axial objects this is defined as

$$M_\alpha = \frac{\alpha}{\alpha_0}. \tag{3.5.3}$$

where α is the reduced inclination as defined in Equation 3.2.2 and simplified for a Gaussian system.

In Figure 3.5.3 we see angular magnification created in two ways. In (a) the angular magnification is created by approach magnification. The system represents a reduced eye consisting of a refracting surface K and image surface R. An object of size y_{01} is positioned at a distance z_{01} from the reduced eye, creating

an image of size y_1 at R and an incident inclination of a_{01}. The object is now brought closer to the reduced eye by distance Δz_0, to a position at a distance z_{02}. The size of the object has not changed $(y_{01} = y_{02})$. However the size of the image has been magnified from y_1 to y_2 at R and the inclination has been magnified to a_{02}. Relative size magnification can be achieved by increasing the size of y_{01} to magnify incident inclination from a_{01} to a_{02} with corresponding image size increase at the image plane. In Figure 3.5.3(b) angular magnification is created by a thin lens. The system initially is the same as system 1 in (a) with incident inclination a_{01} (not redrawn in (b)). A lens F is added at a vertex distance z_v. We note that the object appears to be magnified to size y_i and the image at R has been magnified from y_1 to y_3 while the inclination has been magnified from a_{01} to a_{03}.

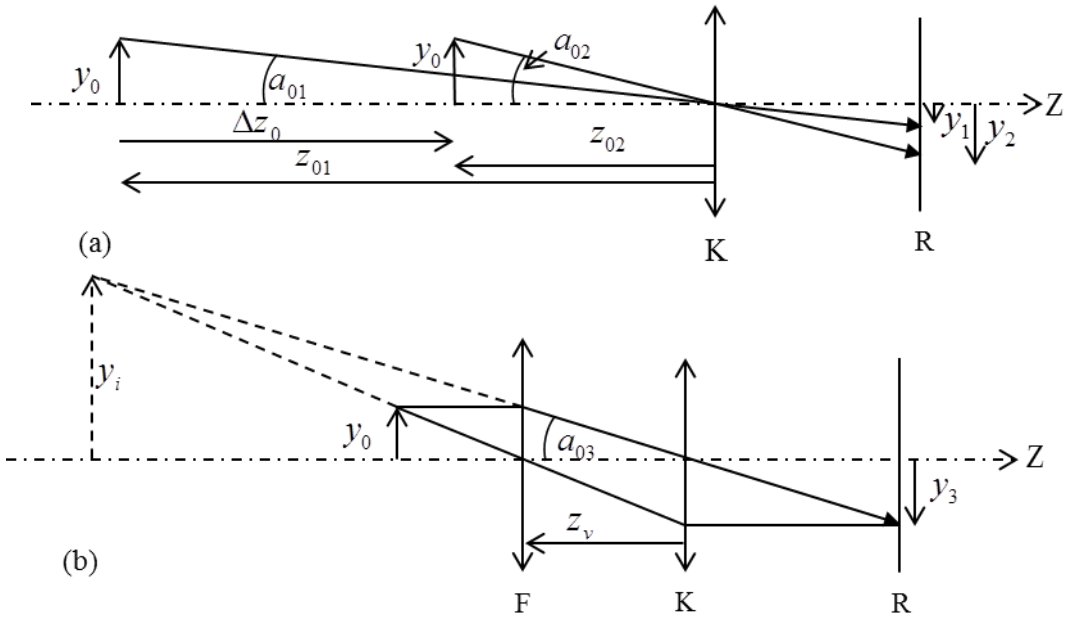

Figure 3.5.3 **(a)** Angular magnification created by approach magnification. The system represents a reduced eye consisting of a refracting surface K and image surface R. System 1 consists of object of size y_0 at position z_{01} creating an image of size y_1 at the retina. In system 2 the object has moved closer to the eye to position z_{02} to create a larger image of size y_2. **(b)** Angular magnification created by a thin lens. Diagrams are not to scale and angles have been exaggerated for clarity. All angles are within the paraxial limits. The diagrams are intended merely to demonstrate angular magnification and accommodation and ametropia have not been taken into account.

Relationships between the magnifications

The relationship between transverse and angular magnification is (Meyer-Arendt, 1984:60, Smith & Atchison, 1997:44, 382)

$$M_\alpha = \frac{1}{M_t}. \tag{3.5.4}$$

Keating (2002: 154) and Smith and Atchison (1997:383) derive the relationship

$$M_z = M_t^2. \tag{3.5.5}$$

between axial and transverse magnification.

3.5.2 Limitations of defining magnification in terms of conjugate object and image points

Defining magnification in terms of the longitudinal and transverse positions of the object and image points is simple and shows some very useful relationships between magnification as defined in Section 3.5.1 and the fundamental properties for conjugate and afocal systems as defined in Section 3.3.2. However, in physiological optics interest lies in what is happening to the image at the retina. If the image is not in focus on the retina then the approach of defining the magnification in terms of the object and image points (a conjugate system) will have limitations. This is further exacerbated when a single object point produces more than one image, such as the two line foci produced by an astigmatic system, or an infinity of coloured images resulting from chromatic dispersion.

If we bear in mind that in order to study the magnification of images on the retina, regardless of whether the images are in focus, or not, then we need to take a different tack on how we define magnification at the retina or exit plane. We now turn our attention to magnification of images at the retina.

3.5.3 Magnification, blur and the ray state at the retina

In physiological optics, magnification is calculated at the retina or image plane, regardless of the effects of blur. In order to do this we trace the chief ray from an object, through the centre of the pupil or a pinhole and do our calculations at the retina. In this section we wish to study and obtain the equations for

magnification at an image plane and will use this to derive formulae for the magnification of chromatic properties in Chapter 7.

We will be concentrating on the naked eye, or more specifically, model eyes, without any refractive or other compensation. We start by taking a look at systems where the object point is distant and then derive the formulae for systems where there is an object point at a finite distance in Chapter 5.

Systems with a distant object point

The system of a compound model eye is shown in Figure 3.5.4. It comprises two subsystems, divided by the pupillary plane T_P into anterior A and posterior B. An arbitrary ray is incident onto the cornea with ray state $\boldsymbol{\rho}_K$, it traverses the centre of the pupil with ray state $\boldsymbol{\rho}_P$ and emerges from the system at the retinal plane with emergent ray state $\boldsymbol{\rho}_R$. We want to solve for $\boldsymbol{\rho}_R$. We need α_K, the reduced inclination at the cornea, which will be the same for all rays incident on the system from a distant object. However, because we wish to trace the chief ray through the system we are interested in y_P, the centre of the pupil rather than y_K the transverse position of the ray at the cornea.

For the system shown in Figure 3.5.4, a transference is calculated for each of the sub-systems and for the eye itself. To differentiate the three transferences,

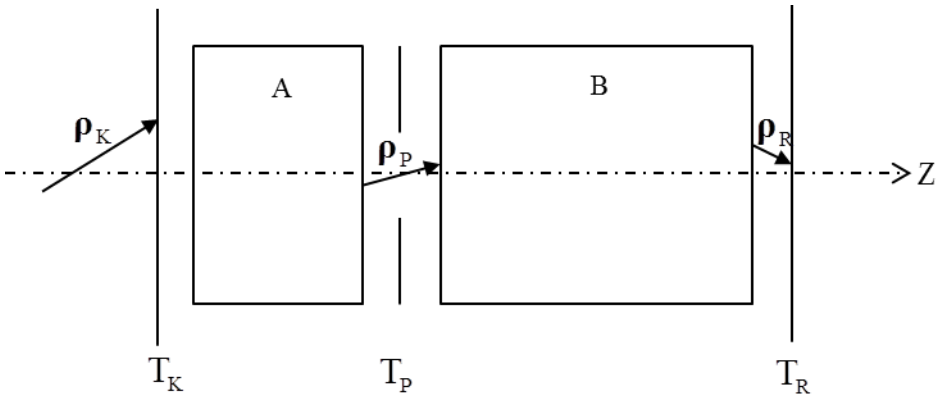

Figure 3.5.4 An exploded diagram of a compound model eye. The eye is defined by the entrance plane T_K immediately in front of the cornea, an exit plane T_R immediately in front of the retina and a longitudinal axis Z.

each of the fundamental properties is subscripted with either an A, B or E for anterior, posterior or eye, respectively. Similarly the state of the ray at the three positions is subscripted K, P or R for corneal plane, pupillary plane or retinal plane respectively. The corneal plane is immediately in front (upstream) of the tear layer, the pupillary plane immediately upstream of the crystalline lens, at the pupil and the retinal plane immediately in front (upstream) of the retina or image plane. The retina itself is not part of the optical system.

We calculate the transference of the eye as follows:

$$\begin{aligned}\mathbf{S}_{\mathrm{E}} &= \mathbf{S}_{\mathrm{B}}\mathbf{S}_{\mathrm{A}} = \begin{pmatrix} A_{\mathrm{B}} & B_{\mathrm{B}} \\ C_{\mathrm{B}} & D_{\mathrm{B}} \end{pmatrix}\begin{pmatrix} A_{\mathrm{A}} & B_{\mathrm{A}} \\ C_{\mathrm{A}} & D_{\mathrm{A}} \end{pmatrix} \\ &= \begin{pmatrix} A_{\mathrm{B}}A_{\mathrm{A}} + B_{\mathrm{B}}C_{\mathrm{A}} & A_{\mathrm{B}}B_{\mathrm{A}} + B_{\mathrm{B}}D_{\mathrm{A}} \\ C_{\mathrm{B}}A_{\mathrm{A}} + D_{\mathrm{B}}C_{\mathrm{A}} & C_{\mathrm{B}}B_{\mathrm{A}} + D_{\mathrm{B}}D_{\mathrm{A}} \end{pmatrix} = \begin{pmatrix} A_{\mathrm{E}} & B_{\mathrm{E}} \\ C_{\mathrm{E}} & D_{\mathrm{E}} \end{pmatrix}\end{aligned} \tag{3.5.6}$$

Harris (2001a) derived the following equations for the magnification, blur and ray state at the retina for a general naked eye

$$A_{\mathrm{E}}A_{\mathrm{A}}^{-1}y_{\mathrm{P}} + B_{\mathrm{B}}A_{\mathrm{A}}^{-1}\alpha_{\mathrm{K}} = y_{\mathrm{R}} \tag{3.5.7}$$

and

$$C_{\mathrm{E}}A_{\mathrm{A}}^{-1}y_{\mathrm{P}} + D_{\mathrm{B}}A_{\mathrm{A}}^{-1}\alpha_{\mathrm{K}} = \alpha_{\mathrm{R}}\,. \tag{3.5.8}$$

Interestingly, y_{P} is also a property of the eye, but not a fundamental property. The pupil centre is not necessarily fixed, but may shift slightly with dilation and

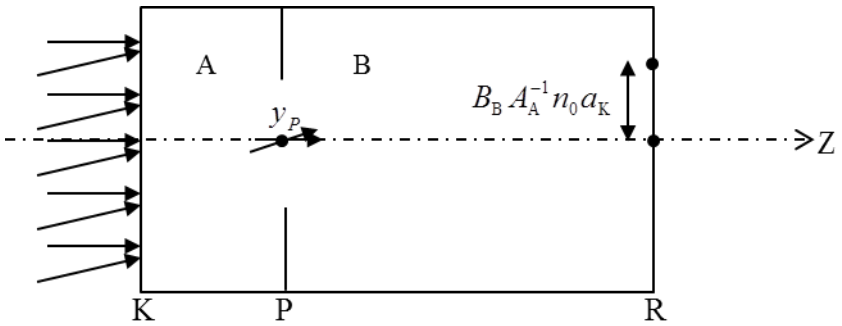

Figure 3.5.5 A simplified Gaussian model eye, divided by pupil P into anterior A and posterior B subsystems. Rays from infinity are incident onto the system initially parallel to the longitudinal axis, mapping the chief ray to a point on the retina on the longitudinal axis and then at an inclination that maps to a second point on the retina. $B_{\mathrm{B}}A_{\mathrm{A}}^{-1}n_0$ magnifies the incident inclination a_K to an image size as shown with the double-headed arrow.

constriction of the pupil (Wilson, Campbell and Simonet, 1992; Yang, Thompson and Burns, 2002).

In Figure 3.5.5 we can see how the magnification for a distant object is projected onto the retina of a Gaussian eye. An axial object of size a_K is magnified by $B_{\mathrm{B}}A_{\mathrm{A}}^{-1}n_0$ to obtain retinal image size y_{R}. Because we are working with the chief ray of a centred Gaussian system, $y_{\mathrm{P}} = 0$ and $A_{\mathrm{E}}A_{\mathrm{A}}^{-1}$ is negated.

The pupil size is defined as $p = y_{\mathrm{P2}} - y_{\mathrm{P1}}$, where y_{P1} and y_{P2} are the margins of the pupil. For a pencil of rays from a distant axial object point $(a_{\mathrm{K}} = 0)$ the size of the corresponding blur patch on the retina will be $A_{\mathrm{E}}A_{\mathrm{A}}^{-1}p = y_{\mathrm{R}}$. Hence, the size of the blur patch, corresponding to a single object point, is dependent on pupil size. The blur is not shown in Figure 3.5.5 because the size of the blur patch is dependent on the pupil size, which is outside the scope of the topic of this study.

Similarly, from Equation 3.5.9 we obtain the distant directional spread $C_{\mathrm{E}}A_{\mathrm{A}}^{-1}$ magnifying the pupil size and distant directional coefficient $D_{\mathrm{B}}A_{\mathrm{A}}^{-1}$ magnifying a_K to obtain the inclination(s) at the retina. From Equations 3.5.7 and 8, we have $(y_{\mathrm{R}} \quad \alpha_{\mathrm{R}})^{\mathrm{T}}$, the ray state at the retina. This will be discussed in greater detail in Section 5.2.

Systems with an object point at a finite distance

To calculate the magnification and blur at the retinal plane for a near system we take a different approach to Harris (2001b). We derive formulae for the magnification, blur and ray state at the retina for systems where the object point is at a finite distance in Section 5.2.2.

3.6 Cardinal points

There are two methods to trace the path of a ray through a system, the graphical method and the numerical method (Meyer-Arendt, 1984:52). The numerical method uses transferences (Section 3.2) and traces a ray from incidence onto a system, defining a ray of light by its inclination and position at incidence

onto a system, through a system and giving us the inclination and position of the ray as it exits the system.

The graphical method traces rays from an object point, through a system to a corresponding image point. Numerically one can apply Snell's law at each refracting surface and simple geometry rules across each homogenous gap (Meyer-Arendt, 1984:52). Methods of simplifying systems have been sought using cardinal points. Graphical ray tracing (Meyer-Arendt, 1984: 52-77) makes use of cardinal points and the approximation of small angles.

In Chapter 2 we saw how the definitions of chromatic aberration in the physiological optics literature make use of the cardinal points and paraxial ray tracing techniques. There are a number of interesting relationships between the cardinal points, all of which can be derived from the transference. Crucially, the positions of the cardinal points are dependent on the frequency of light. For this reason we wish to include cardinal points in this study. For completeness, we will start this section with a short overview of the use of cardinal points in ray tracing techniques followed by the derivation of the cardinal and anti-cardinal points from the transference. We will then take a look at two methods of visually displaying both the relationship of the points to each other in a system, but also changes to the points when that system undergoes a change, such as accommodation or the dependence on the frequency of light.

3.6.1 Ray tracing and cardinal points

We know that in order to simplify the graphical ray tracing through a system, the cardinal points are combined with three rays and a set of rules. We briefly revise the purpose of the cardinal points for completeness. Figure 3.6.1 shows a system with the incident and emergent principal planes in line with the incident and emergent principal points, P_0 and P respectively and likewise F_0 and F are the focal points. The system has the same refractive index upstream and downstream and therefore the nodal points are coincident with the principal points. Figure 3.6.1 shows that from an object point O, the focal ray (3) goes through F_0, refracts at the incident principal plane P_0 and emerges parallel to the optical axis Z. The parallel ray (1) travels from the object point O parallel to the optical axis

Z, refracts at the emergent principal plane P and then passes through the emergent focal point F. Finally the third ray is the chief ray (2) which passes through the centre of the lens or system. It goes to P_0 at its intersection with the optical axis, is translated along the optical axis and exits at P parallel to its incident inclination. All three rays are parallel to the optical axis between the two principal planes (Meyer-Arendt, 1984:53). The three rays intersect at the image I indicating that the object and image are conjugate. The focal ray and the parallel ray are what Keating (2002:44-46) refers to as "predictable rays" and the chief ray is a nodal ray. These in turn undergo refraction at the principal plane(s) and map to a conjugate image point. The three rays used in the ray tracing diagrams map a point on the object to a point on the image and do not represent the actual path of any rays.

For a thin system, all the refraction occurs at the plane of the refracting surface or lens, which is the single principal plane. In a compound system where the refractive indices upstream and downstream are the same, for example a thick lens in air, graphical ray-tracing uses the focal points, the principal planes and the chief ray, shown in Figure 3.6.1. The refraction appears to occur at the two principal planes.

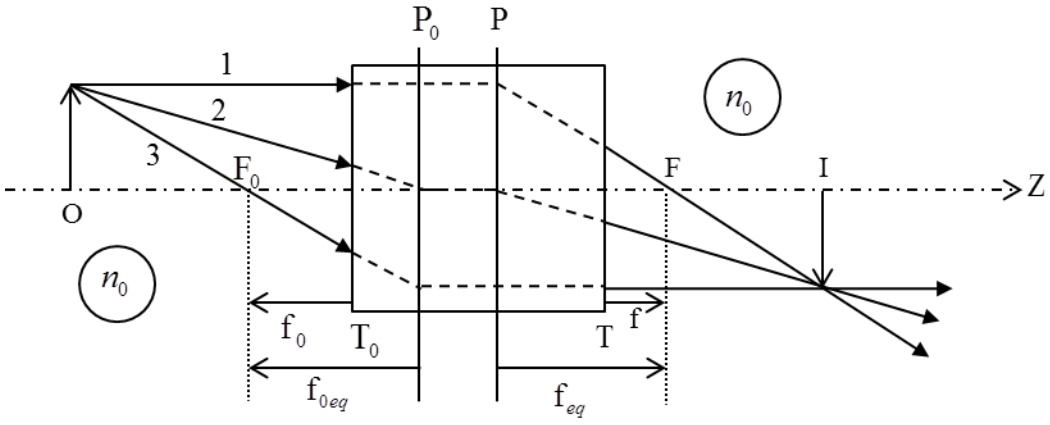

Figure 3.6.1 Diagram of a general Gaussian system with the same refractive index upstream and downstream of the system.

In a system where the refractive indices upstream and downstream of the system are the same the principal points and nodal points coincide. In systems where the indices of refraction are different upstream and downstream, such as the eye, then the principal and nodal points separate and all three pairs of cardinal points are needed for graphical ray-tracing (Figure 3.6.2). The focal and parallel rays are the same as in Figure 3.6.2. The chief ray can now clearly be seen as a nodal ray in Figure 3.6.2. Where the refractive indices are different upstream and downstream, the nodal points will move towards the side of the higher index. The nodal points are points where no refraction takes place (Meyer-Arendt, 1984:76).

We differentiate incident focal length f_0 as the distance from the entrance plane T_0 to the incident focal point F_0 from incident equivalent focal length f_{0eq} which is the distance from the incident principal plane P_0 to the incident focal point. In Figure 3.6.2 both f_0 and f_{0eq} have negative direction. Similarly the emergent focal length *f* is the distance from the exit plane T to the emergent focal point F compared to the emergent equivalent focal length f_{eq} which is from the emergent principal plane to the emergent focal point. In Figure 3.6.2 we can see that the *f* has a negative direction in contrast with f_{eq} which is positive.

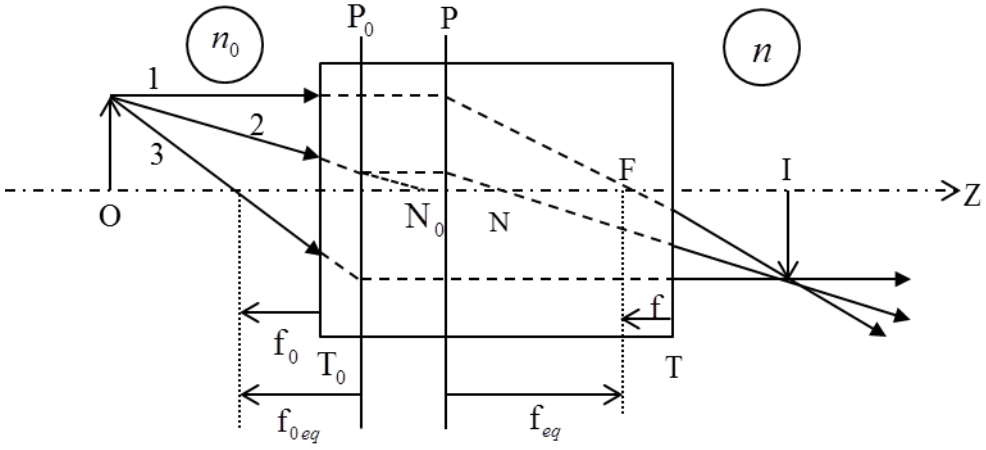

Figure 3.6.2 A diagram of a general Gaussian system with different refractive indices upstream n_0 and downstream *n*, resulting in the nodal points dissociating from the principal points.

3.6.2 Locations of the cardinal points obtained from the transference

The locations of the cardinal points can be derived from the transference. The positions of the incident cardinal points are measured from the entrance plane and for emergent cardinal points the positions are measured from the exit plane. The incident and emergent focal, principal and nodal points make up the six cardinal points for any optical system that are traditionally defined (Pascal, 1939; Smith, 1993,1995; Atchison and Smith, 2000: 7; Sharma, 2006: 168-171). The principal planes are not only conjugate, but have positive unit magnification (Smith and Atchison, 1997:56)

However there are other points, such as anti-nodal and anti-principal points (Katz, 2002: 143; Korsch, 1991: 48, 57; Hastings, 1901: 202) which all belong to a much larger set of special points (Harris, 2010b, 2010f). We refer to the set of anti-nodal and anti-principal points as the anti-cardinal points. Keating (2002: 63-64, 114-115, 308) refers to symmetry points as twice the equivalent focal length (both incident and emergent). An object at the incident symmetry plane will map to an image at the emergent symmetry plane with negative unit magnification (Keating, 2002:63-64, 114-115). Katz (2002: 143) refers to these same points as anti-principal points, giving a transverse magnification of –1 and similarly, the anti-nodal points result in an angular magnification of –1.

In order to show the relationships among cardinal points, Harris (2011b) developed a method of graphical construction of the locations of the cardinal points from the transference using locator lines. Pascal (1939, 1947, 1950a, b) developed a "Benzene ring" which Harris (2011a) elaborated on. Pascal's ring allows one to see the change in position of the six cardinal points with respect to each other when an optical system undergoes a change, such as that brought about by accommodation. Cardinal and anti-cardinal points derived from the transference, graphical construction and Pascal's ring will be explored in this section and Section 5.4.

Harris (2010b, f, 2011a, b) gives two equations, derived from the transference, which give us the locations of the incident and emergent cardinal and anti-cardinal points respectively. The equation for the locations of the incident points is given as

Table 3.6.1 Characteristics of the cardinal points of a general optical system.

Incident		Characteristic	Emergent	
Cardinal point	Symbol	X	Symbol	Cardinal point
Anti-nodal	$\overline{\mathrm{N}}_0$	$-n/n_0$	$\overline{\mathrm{N}}$	Anti-nodal
Anti-principal	$\overline{\mathrm{P}}_0$	-1	$\overline{\mathrm{P}}$	Anti-principal
Focal	F_0	0	—	—
Principal	P_0	1	P	Principal
Nodal	N_0	n/n_0	N	Nodal
—	—	∞	F	Focal

$$z_{\mathrm{Q0}} = n_0 \frac{D - X}{C} \tag{3.6.1}$$

where the subscript Q represents the respective point and the characteristic X is given in Table 3.6.1. The length z_{Q0} is measured from the entrance plane T_0. D and C are entries of the transferences of the system (Equation 3.2.38). Similarly, the locations of the emergent points are given by

$$z_{\mathrm{Q}} = -n \frac{A - \frac{1}{X}}{C} \tag{3.6.2}$$

where the length z_{Q} is measured from the exit plane T. n_0 is the refractive index upstream of the system and n the refractive index downstream of the system. X is the characteristic of any particular pair of special points. A and C are entries of the transference of the system. With the exception of the focal points, each emergent point is in conjugation with the corresponding incident point and can be seen to share the same value for X (Harris, 2010b, 2011a). The incident and emergent focal points are conjugates of infinity (Smith and Atchison, 1997: 72).

3.6.3 Relationships among the points

It is well known that there are a number of relationships among the cardinal points (Pascal, 1939, 1947,1950a, b; Smith and Atchison, 1997: 74-75). These are illustrated in Figure 3.6.3. Using Equations 3.6.1 and 2 and substituting the values for the characteristic X from Table 3.6.1, we can calculate the distances

for the position of each of the cardinal points. From there we can calculate and simplify the equalities between the points in terms of the fundamental properties and the addition of the refractive indices up- and downstream of the system and the length of the system *z*. The distances and equalities are shown in Figure 3.6.3.

Starting with the incident cardinal points and in the sequence given in Table 3.6.1 we find the distance from the entrance plane to the respective point is (Harris, 2010b)

$$z_{\bar{N}0} = C^{-1}(n_0 D + n), \tag{3.6.3}$$

$$z_{\bar{P}0} = n_0 C^{-1}(D + 1), \tag{3.6.4}$$

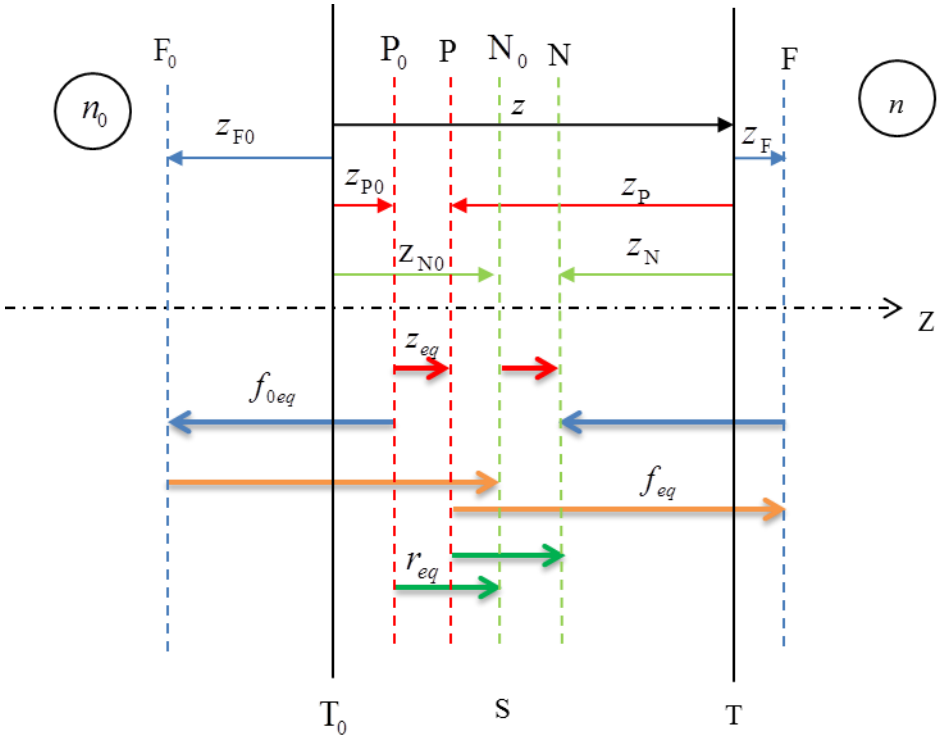

Figure 3.6.3 Cardinal points and their relationships and equalities. Gaussian system S of length *z* has an entrance plane T_0, an exit plane T and a longitudinal axis Z. Refractive index upstream n_0 is different from *n* downstream. All points are defined as being on the optical axis for a Gaussian system. Above the longitudinal axis, the distances from T_0 to the incident cardinal point and from T to the emergent cardinal point are shown with the thin arrows. All the symbols and subscripts are given in Table 3.6.1. Below the longitudinal axis the equalities are shown as follows: the equivalent length or "thickness" z_{eq} (red), incident equivalent focal length f_{0eq} (blue), emergent equivalent length f_{eq} (orange), and equivalent radius of curvature r_{eq} (green).

$$z_{\mathrm{F0}} = n_0 C^{-1} D = -n_0 F_{fv}^{-1}, \tag{3.6.5}$$

$$z_{\mathrm{P0}} = n_0 C^{-1}(D-1) = z_{\mathrm{F0}} - n_0 C^{-1} \tag{3.6.6}$$

and

$$z_{\mathrm{N0}} = C^{-1}(n_0 D - n) = z_{\mathrm{F0}} - nC^{-1}. \tag{3.6.7}$$

The distance of each emergent cardinal point, in the sequence given in the last two columns of Table 3.6.1, from the exit plane to the respective cardinal point is (Harris, 2010b)

$$z_{\bar{\mathrm{N}}} = -C^{-1}(nA - n_0), \tag{3.6.8}$$

$$z_{\bar{\mathrm{P}}} = -nC^{-1}(A+1), \tag{3.6.9}$$

$$z_{\mathrm{P}} = -nC^{-1}(A-1) = z_{\mathrm{F}} + nC^{-1}, \tag{3.6.10}$$

$$z_{N} = -C^{-1}(nA - n_0) = z_{\mathrm{F}} + n_0 C^{-1} \tag{3.6.11}$$

and

$$z_{\mathrm{F}} = -nC^{-1}A = nF_{bv}^{-1}. \tag{3.6.12}$$

These distances are all shown in Figure 3.6.3 above the optical axis Z. Harris (2010b) gives all these distances for linear systems; here they are specialized for Gaussian systems. F_{fv} and F_{bv} are the front- and back-vertex powers (Section 3.4.3).

Smith (1993) also developed a set of equations for the cardinal points in terms of the entries of the Gaussian transference, however his methodology is based on ray tracing. His matrix symbolism and arrangement of entries differs from that used in this dissertation so they have been adjusted to retain consistency. His equations are equivalent to those given by Harris above for incident focal and nodal points and emergent focal and principal points. His incident principal and emergent nodal point equations (Equations 3.6.7 and 11) are more complicated, but reduce under symplecticity to be the equivalent to those given above.

A summary of the equalities is given by Pascal (1939, 1947,1950a, b) for lengths only, without an indication of direction. The formulae are given by Harris (2011a) in terms of the entries of the Gaussian transference with the addition of direction. The incident equivalent focal length is the distance from P_0 to F_0

$$\mathrm{P_0F_0} = \mathrm{FN} = f_{0eq} = n_0 C^{-1} \tag{3.6.13}$$

and, similarly, the emergent equivalent focal length is

$$\mathrm{PF} = \mathrm{F_0N_0} = f_{eq} = -nC^{-1}. \tag{3.6.14}$$

Additional equalities are

$$\mathrm{P_0N_0} = \mathrm{PN} = r_{eq} = -(n - n_0)C^{-1}, \tag{3.6.15}$$

which Pascal (1950a) refers to as the "equivalent" radius, and

$$\mathrm{P_0P} = \mathrm{N_0N} = \mathrm{z}_{eq}, \tag{3.6.16}$$

which Pascal (1950a) refers to as the "thickness" (his quotation marks). Pascal (1950a) appears to have reservations about the terminology because he uses the terms "first" and "second" with quotation marks. He also refers to systems as being "thinner" or "thicker" (his quotation marks) according to variations in the equality given in Equation 3.6.16.

The equivalent focal lengths are directed from the principal plane to the respective focal point. Smith (1993) also gives the equalities for incident and emergent focal length, however his incident focal length formula is more involved, but can be simplified to that of Harris, given in Equation 3.6.13 above.

Harris (2010b) gives additional equalities which we specialize from linear optics:

$$z_{\mathrm{N0}} + z_{\bar{\mathrm{N}}0} = 2z_{\mathrm{F0}} = z_{\mathrm{P0}} + z_{\bar{\mathrm{P}}0}, \tag{3.6.17}$$

$$z_{\mathrm{N}} + z_{\bar{\mathrm{N}}} = 2z_{\mathrm{F}} = z_{\mathrm{P}} + z_{\bar{\mathrm{P}}} \tag{3.6.18}$$

and

$$z_{\mathrm{N0}} + z_{\mathrm{P}} = z_{\mathrm{F0}} + z_{\mathrm{F}} = z_{\mathrm{P0}} + z_{\mathrm{N}} \tag{3.6.19}$$

which show that the cardinal and anti-cardinal points are not independent.

The lengths and directions of each of the equalities between incident and emergent cardinal points are shown in Figure 3.6.3 above the optical axis (Z). Lengths are given as *z* with subscripts given in Table 3.6.1. Below the longitudinal axis, the thicker arrows denote the equalities.

3.6.4 Graphical construction and locator lines

Harris (2011b) developed a method to obtain the positions of the six cardinal points through graphical construction. Not only does this construction

make it easier to see the relationships among the points but also to observe the relationship as the points move when the system changes, for example due to accommodation or age.

Harris (2011b) rewrites Equation 3.6.1 as

$$X = \frac{-Cz_{Q0}}{n_0} + D \tag{3.6.20}$$

and Equation 3.6.2 as

$$\frac{1}{X} = \frac{Cz_{Q}}{n} + A. \tag{3.6.21}$$

and interprets them as straight lines. Harris (2011b) terms these two lines the *locator lines* because they can be used to find the locations of the cardinal points. With the additional knowledge of the refractive indices n_0 and n they can be obtained directly from the transference. They exist uniquely for any system.

The construction is superimposed over the system (Figure 3.6.4). The optical axis Z is horizontal. The X axis is superimposed over the entrance plane T_0

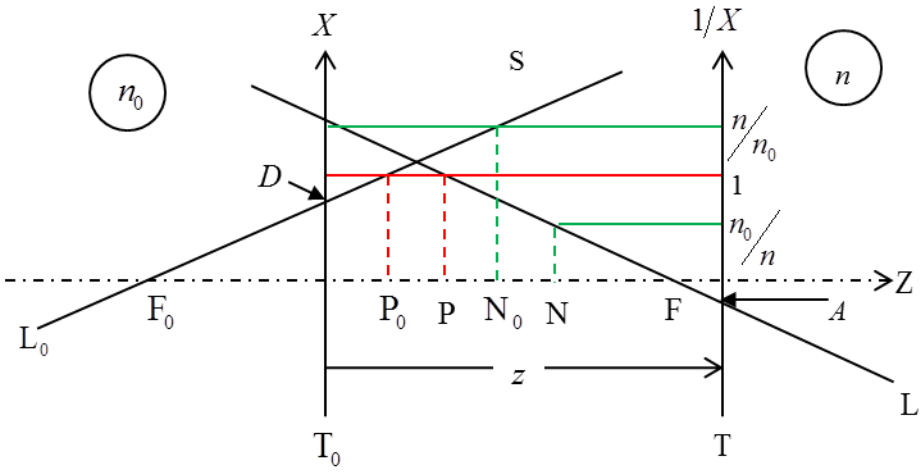

Figure 3.6.4 Graphical representation of a general optical system showing the locator lines for system S (not to scale). Line L_0 represents Equation 3.6.20 and line L Equation 3.6.21. Axis X is superimposed on entrance plane T_0 and axis $1/X$ on exit plane T. T is a distance z downstream from T_0. The focal points lie on the optical axis at intersection with the corresponding locator line. The principal points are shown in red and the nodal points in green. All symbols are described in Table 3.6.1. All incident points show intersection with the incident locator line and have subscript 0, while the emergent points intersect the emergent locator line L with no subscript.

and the $\frac{1}{X}$ axis is superimposed over the exit plane T with the origin at Z. T is a distance z downstream from T_0. The incident locator line L_0 has intersection $X = D$ in T_0 and slope $\frac{-C}{n_0}$ while emergent locator line L has intersection $\frac{1}{X} = A$ in T and slope $\frac{C}{n}$.

To find the location of the incident cardinal points along the optical axis, one draws a horizontal line at the value for the characteristic X in T_0 (Table 3.6.1) and where it intersects L_0 one constructs a vertical line. The intersection of the vertical line with Z locates the position of the corresponding incident cardinal point. Similarly, for the emergent cardinal points, one draws a horizontal line at the value of $\frac{1}{X}$ in T and constructs a vertical line at the intersection of the horizontal line with L. The intersection of the vertical line with Z locates the position of the corresponding emergent cardinal point.

3.6.5 Pascal's ring

Pascal (1939, 1947, 1950a, b) described a memory scheme in the shape of a benzene ring to remember the equalities between the six cardinal points, shown in Figure 3.6.5. He gives the equalities without any proof, his main purpose is to create a memory scheme to aid practitioners (Pascal, 1939). In successive articles

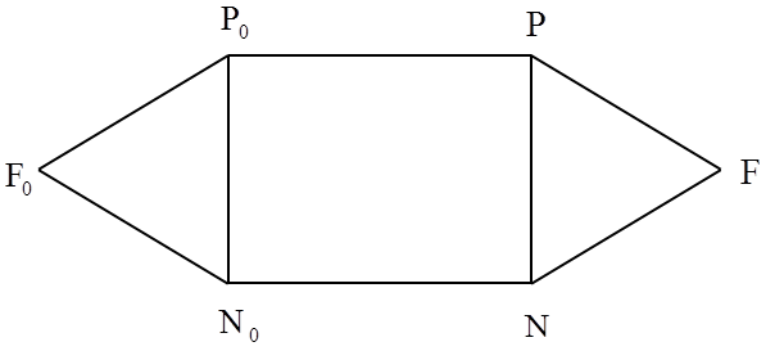

Figure 3.6.5 Pascal's ring, showing the equalities as distances among the cardinal points of a general system. From the diagram we can see that each of two sides that are parallel are equal in their distance apart in the system. Therefore we have four equalities $\mathrm{P_0P} = \mathrm{N_0N}$, $\mathrm{F_0P_0} = \mathrm{NF}$, $\mathrm{F_0N_0} = \mathrm{PF}$ and $\mathrm{P_0N_0} = \mathrm{PN}$.

he then uses the "benzene ring" to show how the points shift when a compensatory system is placed with its emergent principal point at the incident focal point of the system or eye (Pascal, 1950a), or how aphakia affects the ring (Pascal, 1947). Pascal states that "distances represented by opposite parallel lines are equal". He gives the four equalities $P_0P = N_0N$, $F_0P_0 = NF$, $F_0N_0 = PF$ and $P_0N_0 = PN$. In Pascal's initial article (1939) he placed less emphasis on the fourth equality, but later included it and stated that the distance $P_0N_0 = PN$ represents the "equivalent radius of the system" r_{eq} (1950a) which is the radius of a single refracting surface that can replace the system.

In an eye the principal and nodal points are located very close together and it is difficult to see, firstly, what the sequence of points is and, secondly, the shifts when the system undergoes some change such as refractive compensation or accommodation. In this way Pascal's ring is particularly useful in that it "magnifies" the changes in the relationships between the cardinal points when comparing more than one system. It is important to note that Pascal's ring is not drawn to scale but the sides represent a proportional change between two or more systems.

Harris (2011a) proved Pascal's equalities and further proposed that the equalities in the ring represent not just magnitude, but he gave the distances between the cardinal points direction as well. This ties up with the directions of the equalities given in Figure 3.6.3. In Figure 3.6.6, we see Pascal's ring again,

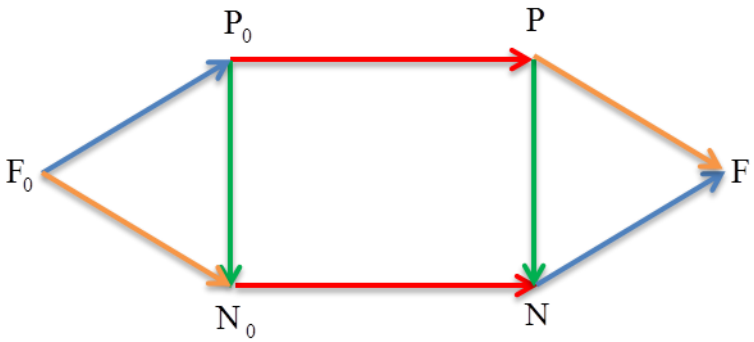

Figure 3.6.6 Pascal's ring showing equalities and their distances and directions among the cardinal points of a general system. Arrows that are the same colour are equal in length follow the same direction, consistent with Equations 3.6.13 to 16. All the directions have the sense of travelling from left to right, the same as light.

but this time with the equalities represented by distance and direction and using the same colour-coding that was given in Figure 3.6.3. The blue line represents the negative incident equivalent focal length.

3.7 The transformed transference

In Section 3.2.5 we saw that symplectic matrices ($\mathrm{Sp}(2n\times 2n;\mathbb{R})$) are closed under multiplication, inversion and transposition but are not closed under addition nor multiplication by a scalar. This creates a problem when we wish to calculate, for example, an average of symplectic matrices, including transferences in particular. In an effort to find an average eye, researchers have investigated a number of transformed transferences and characteristic matrices. These include the exponential-mean-log transference (Harris and Cardoso, 2006; Harris, 2004b, 2005, 2007, Mathebula, Rubin and Harris, 2007), metric geometric mean transference (Harris, 2008), Cayley transforms (Cardoso and Harris, 2007) and four characteristic matrices (van Gool and Harris, 2005; Harris and van Gool, 2004).

Our interest in these transformed transferences, for the purpose of this dissertation, lies not in calculating an average transference, but in the transformed matrix itself. Both the logarithm of a symplectic matrix and the Cayley transform are Hamiltonian and the characteristic matrices are symmetric. For $n=1$ this lends itself to being represented graphically in a three-dimensional space. The metric geometric mean has the limited scope of only calculating the mean of two transferences and therefore will not be explored further. We take a look at each of these transformations in the general sense.

3.7.1 The logarithmic transform

The exponential-mean-log-transference has proven to be particularly useful in calculating a meaningful average of an optical system. Mathebula, Rubin and Harris (2007) and Mathebula and Rubin (2011) have successfully used this method to calculate the mean of a number of readings of the cornea with allowance for thickness using the Pentacam, in a group of subjects. Consequently, Mathebula, Rubin and Harris (2007) and Mathebula and Rubin (2011) were able

to calculate the variance-covariance matrix in Hamiltonian space of the linear optical character of the cornea and the spread of the power of the cornea.

The Lie algebra is related to the matrix Lie group through the matrix exponential by passing information from the Lie algebra to the matrix Lie group. In particular, the Lie algebra defines a linear space, thereby making the Lie algebra not only simpler, but more understandable. To define the Lie algebra, let **G** be a matrix Lie group. The Lie algebra of **G**, denoted by $\mathfrak{g}$, is the set of all matrices **X** such that $e^{t\mathbf{X}}$ is in **G** for all real numbers *t*. If **X** is any $n \times n$ real matrix, then $e^{t\mathbf{X}}$ will be real and invertible. The Lie algebra of GL(n;$\mathbb{R}$) represented by the set of matrices **X** is real and denoted gl(n;$\mathbb{R}$) (Hall, 2004:27, 38-39).

The Lie algebra of the real symplectic group is denoted sp(n;$\mathbb{R}$) and is the space of $2n \times 2n$ real matrices. If **H** is any $2n \times 2n$ real matrix, then $e^{t\mathbf{H}}$ will be real and invertible. sp(n;$\mathbb{R}$) is a subset of gl(n;$\mathbb{R}$) and is therefore also a linear space, allowing one to do statistical analyses. We refer to the set of matrices $\mathfrak{h}$ that define the symplectic algebra as Hamiltonian matrices (Hall, 2004: 41).

In simpler terms, the principal matrix logarithm of a real symplectic matrix (belonging to Sp(n;$\mathbb{R}$)) results in a Hamiltonian matrix (belonging to sp(n;$\mathbb{R}$)) and the principal matrix exponential of a Hamiltonian matrix results in a symplectic matrix (Sanyal, 2001: 71; Bernstein, 2005: 88-89, 434; Dieci, 1996, 1998; Harris and Cardoso, 2006; Harris, 2005; Hall, 2004: 41). This relationship between symplectic and Hamiltonian matrices is referred to as the exponential map and the matrix logarithmic map (Sanyal, 2001: 72-73). Because the set of Hamiltonian matrices defines a linear space it is closed under matrix addition, multiplication by a scalar, transposition and the commutator operator (Dieci, 1996, 1998), they are amenable to the calculation of an average of any number of Hamiltonian matrices.

The exponential-mean-log-transference is defined as (Harris and Cardoso, 2006; Harris, 2004b, 2005, 2007)

$$\tilde{\mathbf{S}} := \exp\left(\frac{1}{N}\sum_{j=1}^{N}\mathrm{Log}\mathbf{S}_j\right). \qquad (3.7.1)$$

The principal matrix logarithm is calculated in Matlab® by using the command *logm* and the matrix exponential by using *expm*. (This is not the same as the command *log* which takes the logarithm of each entry in the matrix separately.)

In general

$$\mathbf{X} = \operatorname{Log} \mathbf{G} \tag{3.7.2}$$

where $e^{\mathbf{X}} = \mathbf{G}$ and $\mathbf{G} \in \mathbb{R}^{n \times n}$ provided **G** is invertible and has no negative real eigenvalues (Dieci, 1996, 1998). Any matrix that is invertible has at least one logarithm (Dieci, 1996), which for our purposes means that, because all transferences are invertible, they have at least one logarithm. Cardoso (2005) shows that the principal matrix logarithm of matrix **G** is an infinite series.

We represent the transformed transference by $\hat{\mathbf{S}}$. In terms of its entries we follow Harris's (2005) lead and write the transformed transference as

$$\hat{\mathbf{S}} = \begin{pmatrix} \hat{\mathbf{A}} & \hat{\mathbf{B}} \\ \hat{\mathbf{C}} & \hat{\mathbf{D}} \end{pmatrix} \tag{3.7.3}$$

where $\hat{\mathbf{S}}$ is Hamiltonian. However, our interest lies not in the average of transferences, but in the Hamiltonian space itself. A $2n \times 2n$ matrix **H** is Hamiltonian if (Bernstein, 2005: 85; Dieci, 1996, 1998; Fiori, 2011; Watkins, 2004; Hall, 2004:41)

$$\mathbf{H}^{\mathrm{T}}\mathbf{E} = \mathbf{E}^{\mathrm{T}}\mathbf{H} \tag{3.7.4}$$

where

$$\mathbf{E} = \begin{pmatrix} \mathbf{O} & \mathbf{I} \\ -\mathbf{I} & \mathbf{O} \end{pmatrix}. \tag{3.7.5}$$

It follows from Equations 3.7.3 to 5 that

$$\hat{\mathbf{A}} = -\hat{\mathbf{D}}^{\mathrm{T}} \tag{3.7.6}$$

and the $\hat{\mathbf{B}}$ and $\hat{\mathbf{C}}$ are both symmetric (Sanyal, 2001: 69; Dieci, 1996; Harris, 2007; Hall, 2004:41). Because $\hat{\mathbf{D}}$ is dependent on $\hat{\mathbf{A}}$ there are four independent entries between them and because $\hat{\mathbf{B}}$ and $\hat{\mathbf{C}}$ are symmetric they each have three independent entries, therefore $\hat{\mathbf{S}}$ has only ten independent entries (Harris, 2007a). However, our reservation with this transformed matrix is that each of the entries has a different unit. $\hat{\mathbf{A}}$ and $-\hat{\mathbf{D}}^{\mathrm{T}}$ are unitless, $\hat{\mathbf{B}}$ is in units of length and $\hat{\mathbf{C}}$ is in

units of inverse length. So while $\hat{\mathbf{S}}$ defines a linear space, it does not define an inner-product space.

For a Gaussian system Equation 3.7.3 simplifies to

$$\hat{\mathbf{S}} = \begin{pmatrix} \hat{A} & \hat{B} \\ \hat{C} & \hat{D} \end{pmatrix} \tag{3.7.7}$$

where each of the entries is a scalar and

$$\hat{A} = -\hat{D}. \tag{3.7.8}$$

The result is that for Gaussian systems $\hat{\mathbf{S}}$ has only three independent entries. This implies that we can create a three-dimensional graph of the relationship among the three entries. The chromatic properties on a Gaussian system will be shown in Chapter 8 and was shown as a nearly perfectly straight line for the reduced eye in an accompanying article (Evans and Harris, 2011).

3.7.2 The Cayley transform

Similar to the logarithmic transference, a Cayley transform maps a symplectic matrix (Sp(n;$\mathbb{R}$)) into a Hamiltonian matrix (sp(n;$\mathbb{R}$)). Cardoso and Harris (2007) introduced this and a few other transforms as alternative methods for mapping symplectic matrices into Hamiltonian matrices, and reversing the process in an effort to find other methods of calculating an average eye, or more generally, an average system. Cardoso and Harris (2007) note that one can construct an infinity of rational matrix functions that transform symplectic into Hamiltonian matrices. The one that plays an important role in several fields of mathematics and engineering (Cardoso and Harris, 2007; Fiori, 2011) and which we shall study is the Cayley transform. The Cayley mean is given by Cardoso and Harris (2007) as

$$\tilde{\mathbf{S}}_{\mathrm{C}} = \mathbb{C}^{-1}\left(\frac{1}{N} \sum_{j=1}^{N} \mathbb{C}\left(\mathbf{S}_j\right) \right) \tag{3.7.9}$$

where $\mathbb{C}(\mathbf{S})$ is the Cayley transform of $\mathbf{S}$ and $\mathbb{C}^{-1}$ represents the inverse Cayley transform.

In general, the Cayley transform is defined as (Bernstein, 2009: 208, 239; Sanyal, 2001: 72; Cardoso and Harris, 2007; Puzio, 2013)

$$\mathbf{B}=(\mathbf{A}-\mathbf{I})(\mathbf{A}+\mathbf{I})^{-1}=(\mathbf{A}+\mathbf{I})^{-1}(\mathbf{A}-\mathbf{I}) \tag{3.7.10}$$

and its inverse is defined as (Bernstein, 2009: 208; Sanyal, 2001: 72)

$$\mathbf{A}=(\mathbf{B}-\mathbf{I})(\mathbf{B}+\mathbf{I})^{-1}=(\mathbf{B}+\mathbf{I})^{-1}(\mathbf{B}-\mathbf{I}) \tag{3.7.11}$$

where **A** and **B** are $n\times n$ real matrices provided the respective inverses exist and **I** is the $n\times n$ identity matrix. From Equation 3.7.10 we can see that the factors of **B** are commutative. From Equations 3.7.10 and 11 we can see that the Cayley transform is its own functional inverse (Bernstein, 2009:208-209; Tsiotras, Junkins and Schaub, 1997; Sanyal, 2001: 72).

Others (Fiori, 2011; Golub and van Loan, 1996: 73; Puzio, 2013; Bernstein, 2009: 239) define the inverse as

$$\mathbf{A}=(\mathbf{I}+\mathbf{B})(\mathbf{I}-\mathbf{B})^{-1}=(\mathbf{I}-\mathbf{B})^{-1}(\mathbf{I}+\mathbf{B}) \tag{3.7.12}$$

where **A** and **B** are defined above, the factors of **A** are commutative and provided the respective inverses exist. This inverse is simple to derive from the Cayley transform given by Equation 3.7.10 and is given by Puzio (2013).

The Cayley transform is defined slightly differently by Tsiotras, Junkins and Schaub (1997), and Courant and Hilbert (1953: 536-7). Tsiotras, Junkins and Schaub (1997), Fallat and Tsatsomeros (2002), Hadjidimos and Tzoumas (2008, 2009) and Bernstein (2009: 208-209) define the Cayley transform as

$$\mathbf{C}=(\mathbf{I}-\mathbf{Q})(\mathbf{I}+\mathbf{Q})^{-1} \tag{3.7.13}$$

(or its commutative equivalent) where **C** and **Q** are $n\times n$ real matrices and exists provided $(\mathbf{I}+\mathbf{Q})$ is invertible. Fallat and Tsatsomeros (2002) and Hadjidimos and Tzoumas (2008, 2009) both define the Cayley transform for the set of $n\times n$ complex matrices, however, we will restrict this study to real matrices. Tsiotras, Junkins and Schaub (1997) give the inverse transformation as identical to itself. Solving Equation 3.7.13 for **Q** we obtain the same result. Fallat and Tsatsomeros (2002) and Courant and Hilbert (1953: 536-7) state that the order of factors may be reversed and $(\mathbf{I}-\mathbf{Q})$ commutes with $(\mathbf{I}+\mathbf{Q})^{-1}$.

For the set of matrices of the order $2n\times 2n$, **B** is a symplectic matrix as defined in Equation 3.7.10 and **A** is a Hamiltonian matrix as defined in Equation 3.7.11 by Bernstein, 2009: 208-209; Sanyal, 2001: 72 and in Equation 3.7.12 by Bernstein, 2009: 239 and Cardoso and Harris, 2007. Equation 3.7.13 is its own

functional inverse and so if **C** is symplectic, **Q** is the resultant Hamiltonian matrix and for the inverse, if **C** is Hamiltonian, **Q** is the resultant symplectic matrix.

In linear optics, because the Cayley transform of a transference is Hamiltonian, the units of the entries are the same as for a transference, that is, mixed units (Cardoso and Harris, 2007). Because of Equation 3.7.8, the Gaussian transformed transference has three independent entries, enabling us to create a three-dimensional graph of the Hamiltonian space represented by the Cayley Transform (Evans and Harris, 2011).

We mention in passing that Hamiltonian matrices fulfil the requirements for a vector space (Hall, 2004: 43; Anton and Rorres, 2005: 222) and therefore the mathematics of vector spaces can be applied to the three-dimensional (for $\mathbf{S}_{2\times2}$) , ten-dimensional (for $\mathbf{S}_{4\times4}$) and fourteen-dimensional (for $\mathbf{T}_{5\times5}$) spaces. Symplectic matrices on the other hand disobey the requirements for vector spaces and the rules of vector spaces cannot be meaningfully applied to symplectic matrices. The one-to-one mapping between the symplectic matrices and Hamiltonian spaces allows us to not be confined by the restrictions placed on symplectic systems. This is important to this dissertation and will be used to this effect in Section 8.2 to derive a formula for the dependence of the transference on the frequency of light.

3.7.3 The characteristic matrices

In an effort to find a set of matrices, related to the transference, that would offer a solution to quantitative analyses of the optical character of optical systems, Harris and van Gool (2004) turned to the four characteristic matrices. These are the point characteristic matrix **P**, the angle characteristic matrix **Q**, and the first and second mixed characteristic matrices, **M** and **N** respectively. According to Guillemin and Sternberg (1984:17, 35-37) the terminology point, angle and mixed characteristic was introduced by Hamilton, however, modern physics literature refers to them as the point and angle eikonals. Walther (1995:22, 238-241) refers to **P** as Hamilton's point characteristic and distinguishes between the point eikonal **P** and the angle eikonal **Q**. Arnaud (1970), discusses the point characteristic **P** and the ray matrix $\mathbf{S}$. The characteristic matrices are, in each case, defined for linear systems, however, we will concentrate on the application

to Gaussian systems. Harris and van Gool (2004) and van Gool and Harris (2005) apply the characteristic matrices to the 5×5 transference of the astigmatic heterocentric system, whereas Guillemin and Sternberg (1984: 35-36), Walther (1995:22, 238-241) and Arnaud (1970) apply the characteristic matrices to the 4×4 transference of the astigmatic homocentric system.

For any given Gaussian system S, the incident position y_0 and reduced inclination α_0 of the ray is mapped to the emergent position *y* and reduced inclination α by Equation 3.2.10. This equation pre-supposes that the incident state of the ray is known and that the emergent state of the ray is sought. Of course, if the opposite is true, that is if the emergent state of the ray is known, then it is a simple matter to calculate the incident state of the ray by

$$\boldsymbol{\rho}_0 = \mathbf{S}^{-1}\boldsymbol{\rho} \tag{3.7.14}$$

where $\mathbf{S}^{-1}$ is the matrix inverse of the transference. In both these situations, with regards to the state of the ray, there are two dependent and two independent variables.

However, Harris and van Gool (2004) point out that it is possible for other combinations of two dependent and two independent variables to exist. Each of the four characteristic matrices represents one of the four possible combinations of dependent and independent variables with respect to the incident and emergent positions and inclinations. In each case, the characteristic matrix functions as the operator on the chosen vector. The four operations are represented in Equations 3.7.15, 16, 18 and 19, below, as given by Harris and van Gool, (2004).

The point characteristic defines the incident and emergent inclinations when the positions are chosen:

$$\mathbf{P}\begin{pmatrix} y_0 \\ y \end{pmatrix} = \begin{pmatrix} -\alpha_0 \\ \alpha \end{pmatrix}. \tag{3.7.15}$$

Similarly the angle characteristic defines the incident and emergent positions when the reduced inclinations are known:

$$\mathbf{Q}\begin{pmatrix} -\alpha_0 \\ \alpha \end{pmatrix} = \begin{pmatrix} y_0 \\ y \end{pmatrix}. \tag{3.7.16}$$

As Harris and van Gool (2004) point out, from the above two equations it is obvious that

$$\mathbf{P} = \mathbf{Q}^{-1} \tag{3.7.17}$$

provided **Q** is non-singular. The derivations for **P** and **Q** make use of the Schur complements (Equations 3.2.20 to 23) (Harris, 2010d).

The first and second mixed characteristic matrices operate as follows:

$$\mathbf{M}\begin{pmatrix} y_0 \\ \alpha \end{pmatrix} = \begin{pmatrix} \alpha_0 \\ y \end{pmatrix} \tag{3.7.18}$$

and

$$\mathbf{N}\begin{pmatrix} \alpha_0 \\ y \end{pmatrix} = \begin{pmatrix} y_0 \\ \alpha \end{pmatrix}. \tag{3.7.19}$$

$$\mathbf{M} = \mathbf{N}^{-1} \tag{3.7.20}$$

provided **N** is non-singular.

Point characteristic

The point characteristic is defined for a Gaussian optical system as

$$\mathbf{P} = \begin{pmatrix} B^{-1}A & -B^{-1} \\ -B^{-1} & DB^{-1} \end{pmatrix} \tag{3.7.21}$$

provided $B \neq 0$. Difficulties can be anticipated as *B* approaches zero (van Gool and Harris, 2005), which should not pose a problem for any "reasonable" eye. This would be a problem for conjugate systems including thin systems, but for an eye or schematic eye $B \neq 0$. The matrix is symmetric and Harris and van Gool (2004) note that the minus sign in front of α_0 (Equation 3.7.15) is what creates the symmetry. Of particular interest is the first entry which is the refractive compensation (Equation 3.4.6) (Harris and van Gool, 2004; van Gool and Harris, 2005).

Angle characteristic

The angle characteristic **Q** is the inverse of **P**. From Equations 3.7.15 and 16 this appears obvious, however From Equations 3.7.21 and 22 this is not

immediately apparent, but is the result of symplecticity (Equation 3.2.24). **Q** is defined for a Gaussian optical system as

$$\mathbf{Q} = \begin{pmatrix} C^{-1}D & C^{-1} \\ C^{-1} & AC^{-1} \end{pmatrix} \tag{3.7.22}$$

provided $C \neq 0$. $C = 0$ defines an afocal system, which the eye is clearly not. The matrix is again symmetric, a consequence of the minus sign in front of the α_0 in Equation 3.7.16 (Harris and van Gool, 2004). Walther (1995:242) explores the advantage that for the angle eikonal it is easy to shift the entrance and exit planes. We can see this is possible from Equation 3.7.16.

First mixed characteristic

The first mixed characteristic is defined for a Gaussian system as

$$\mathbf{M} = \begin{pmatrix} -D^{-1}C & D^{-1} \\ D^{-1} & BD^{-1} \end{pmatrix} \tag{3.7.23}$$

provided $D \neq 0$, that is, provided the system is not entrance-plane focal.

Second mixed characteristic

The second mixed characteristic **N** is the inverse of **M** (Equation 3.7.20) which is easy to prove and is a result of symplecticity. **N** is defined for a Gaussian system as

$$\mathbf{N} = \begin{pmatrix} -A^{-1}B & A^{-1} \\ A^{-1} & CA^{-1} \end{pmatrix} \tag{3.7.24}$$

provided $A \neq 0$. In Section 3.3.1 we saw that *A* defines the ametropia of the system (Harris, 1999a). This is potentially a problem for eyes because $A = 0$ defines an emmetropic eye. Problems can be anticipated in eyes where *A* approaches zero (van Gool and Harris, 2005), which includes emmetropic eyes, compensated eyes and most schematic eyes.

It is the very issue of singularity of these characteristic matrices that implies that the choice of any two of y_0, y, α_0 or α does not necessarily fix the other two (Harris and van Gool, 2004). Existence and uniqueness create potential problems in the use of these characteristic matrices.

3.8 Vergence and wavefronts

Thus far in this chapter on linear optics and Gaussian systems, we have been studying the optics of systems with a strong emphasis on the transference and the properties of the system, both fundamental and derived. Vergence and wavefronts are not properties of a system, but rather our handle on light. Thus far we have considered the effect of the system on a single ray, quantified as a vector $\boldsymbol{\rho}$. We now turn our attention to the effect of the system on a pencil of light, quantified as a matrix **L**.

Vergence is merely the local reduced curvature of the wavefront. The wavefront is denoted as positive (converging) or negative (diverging). It also has a local inclination (Harris, 1996b).

3.8.1 Stigmatic vergence and wavefronts

The reduced vergence at entrance plane T_0 of system S is L_0. For an object O at a longitudinal distance z_O upstream of the entrance plane we have reduced vergence given as

$$L_0 = \frac{n_0}{z_\mathrm{O}}. \tag{3.8.1}$$

There are two special cases, when the object point is distant, $z_\mathrm{O} \to \infty$, we have $L_0 = 0\,\mathrm{D}$, and when the object point is at the entrance plane, $z_\mathrm{O} = 0\,\mathrm{m}$ and $L_0 \to \infty$.

3.8.2 Astigmatic vergence and wavefronts

In the presence of astigmatism the generalisation of the scalar reduced vergence *L* is the matrix reduced vergence **L** (Fick, 1973d; Keating, 1981a,b). **L** is a 2×2 symmetric matrix identical in mathematical character to the dioptric power matrix **F** of a thin system (Fick, 1972, 1973a, b ; Long, 1976). That is to say, for an astigmatic wavefront, the eigenvalues are the vergences (reduced principal curvatures) along the two principal meridians given by the eigenvectors (Keating, 1981a, b; Harris, 1996b). The vergence matrix **L** is always symmetric, even when it emerges from a thick astigmatic system with an asymmetric power matrix

(Keating, 1981a, b) and for which Harris (1996b) gives a proof, based on the symplecticity of the transference. The implication of this is that the two principal meridians are always orthogonal.

For a wavefront incident onto an astigmatic system from an object point O at longitudinal position z_{O} relative to T_0, Equation 3.8.1 generalizes to

$$\mathbf{L}_0 = \frac{n_0}{z_{\mathrm{O}}}\mathbf{I}\,. \tag{3.8.2}$$

For a distant object point $\mathbf{L}_0 = \mathbf{O}\,\mathrm{D}$.

3.8.3 The wavefront, its curvature and direction: distant object

For a distant object point, Harris (1996b) derives the equation for a wavefront at the optical axis as

$$z = \frac{\mathbf{y}^{\mathrm{T}}\mathbf{L}\mathbf{y}}{2n} - \frac{\mathbf{y}^{\mathrm{T}}\boldsymbol{\alpha}_{\times}}{n}\,. \tag{3.8.3}$$

This equation describes the geometry of the wavefront exiting the system and can be thought of as the sagitta at the optical axis of the wavefront as it exits the system.

$$\mathbf{L} = -\mathbf{C}\mathbf{A}^{-1} \tag{3.8.4}$$

is the reduced wavefront curvature and

$$\boldsymbol{\alpha}_{\times} = \mathbf{A}^{-\mathrm{T}}\boldsymbol{\alpha}_0 \tag{3.8.5}$$

is the reduced direction of the emergent wavefront at the optical axis. **y** is the transverse position of the ray at the exit plane. When the eigenvalues of **L** are distinct, the wavefront is astigmatic and when the eigenvalues are not distinct, the wavefront is a paraboloid of revolution (stigmatic). When **A** is singular, Equations 3.8.3 to 5 do not hold and the wavefront is not defined. The wavefront has reduced to a singularity and there is a focal point or line in the transverse plane.

3.8.4 Vergence emergent from a system: object at a finite distance

We now consider a system S with entrance plane T_0, exit plane T and longitudinal axis Z. The vergence incident onto the system at T_0 is $\mathbf{L}_0$. Harris (1996b) gives the vergence emergent from the system at exit plane T as

$$\mathbf{L} = \left(\mathbf{D}\mathbf{L}_0 - \mathbf{C}\right)\left(\mathbf{A} - \mathbf{B}\mathbf{L}_0\right)^{-1} \tag{3.8.6}$$

and the emergent direction of the wavefront as

$$\boldsymbol{\alpha}_{\times} = \left(\mathbf{A} - \mathbf{B}\mathbf{L}_0\right)^{-\mathrm{T}} \boldsymbol{\alpha}_{\times 0}\,. \tag{3.8.7}$$

$\boldsymbol{\alpha}_{\times 0}$ and $\boldsymbol{\alpha}_{\times}$ are the reduced inclinations of the rays at the optical axis incident and emergent to the system at the entrance and exit planes respectively.

3.8.5 Vergence across elementary systems

Homogenous gap

The transference of a homogenous gap of width *z* is given by Equation 3.2.7. Substituting into Equation 3.8.6 we obtain (Harris, 1996b)

$$\left(\mathbf{L}_0^{-1} - \zeta\,\mathbf{I}\right)^{-1} = \mathbf{L}\,, \tag{3.8.8}$$

the generalization of the equation for vergence across a homogenous gap.

Refracting surface

The transference of a thin system is given by Equation 3.2.9 with **F** symmetric. Both the power of a refracting surface and the power of a thin lens **F** are symmetric matrices. Substituting from Equation 3.2.9 into Equation 3.8.6 we obtain

$$\mathbf{L}_0 + \mathbf{F} = \mathbf{L}\,, \tag{3.8.9}$$

the generalization of Gauss' equation, first derived by Keating (1981a) and then by Harris (1996b).

3.8.6 Position of point or line foci

Calculations often require us to determine where focal points or lines are for a given object point. The calculation usually will give an answer as a distance, along the longitudinal axis, either upstream or downstream from the reference or image plane. For a stigmatic system this is simply obtained by solving

$$z = \frac{n}{L} \tag{3.8.10}$$

(from Equation 3.8.1). For an astigmatic wavefront one will obtain two orthogonal line foci (Keating, 1981b). The derivation for determining the longitudinal and transverse positions and orientations of the line foci will be given in Chapter 6.

3.9 Summary

This chapter has taken an in-depth look at linear and Gaussian optics and in particular the transference. We saw that we can calculate the effect that the system has on light by tracing either a single ray (Equation 3.2.31) or a pencil of light (Equation 3.8.6) through the optical system. Familiarly, these are the state of the ray vector or vergence, respectively. We took a look at the fundamental properties of an optical system as well as four special systems. We then spent some time studying a selection of derived properties of the optical system.

The derived properties that form part of this study include power, refractive compensation, front- and back-vertex power, magnification and the locations of the cardinal points. In addition two transformed transferences and four characteristic matrices are included as options for studying the dependence of the transference on the frequency of light and as vector spaces that allow statistical analysis.

This chapter is by no means a comprehensive account of Gaussian and linear optics and all derived properties. We have limited ourselves to a small selection of derived properties that are affected by the frequency of light in a Gaussian optical system. We also saw that not all the derived properties that we will need for our study of chromatic properties are available in the literature. Additional formulae will be derived in Chapter 5.

4 BACKGROUND THEORY: CONSIDERATIONS

The previous two chapters took a detailed looked, firstly, at how chromatic aberrations have been defined in classical and physiological optics and, secondly, at Gaussian and linear optics of systems. Chapter 3 gave a broad overview of linear optics in general, the fundamental properties and a selection of derived properties from the transference. We saw how we can trace either a single ray through a system, or the effect of a system on a pencil of rays in the section on vergence and wavefronts. However, there are a few additional considerations that need to be addressed.

Firstly, we take a look at schematic eyes. After a brief overview of the history of schematic eyes, we look at the classification of schematic eyes, from the simplest single-surface reduced eye to multi-surface schematic eyes that closely mimic a real eye. We then narrow our choice of eyes for this dissertation to two, that of the reduced eye, often used in previous studies on chromatic properties and Le Grand's four-surface schematic eye.

Secondly we take a look at the visible spectrum across which we will base our analyses. We define the frequencies we will highlight in tables and graphs in Part IV of this dissertation.

Thirdly, we consider the arguments for and against using frequency or wavelength in our treatment.

Finally, we take a look at the formulae available for the refractive index of a medium as a function of wavelength. We look at formulae for the refractive index of water, the medium of the reduced eye, the four media of Le Grand's model eye and air.

4.1 Schematic eyes

4.1.1 A short history of schematic eyes

Smith (1995) presents a comprehensive history of schematic eyes and this is discussed briefly, although we shall mention only the better known schematic eyes. For centuries the eye and the functions of the various structures within it

were misunderstood. The ancient Greeks and Arabs believed that light emanated from the lens inside the eye and caused a visual response when these light rays touched an object. This view prevailed till approximately 1000 AD when Ibn al-Haitham proposed that the light rays travelled from an object into the eye. However, it was not until the early sixteenth century that Leonardo da Vinci (*c*. 1500 AD) proposed that the lens was responsible for refracting the light.

Snell discovered the exact law of refraction in 1621 and published by Descartes in 1637. Scheiner was the first to attempt to measure the radius of curvature of the anterior corneal surface by the rather rudimentary method of comparing the size of reflection off the cornea with reflections from various sized marbles. Once the correct anatomical structure was understood, Christian Huygens proposed the first schematic eye in the seventeenth century.

Another two centuries went by before Young, in 1801, made more accurate measurements of the anterior refracting surface and anterior and posterior lenticular surfaces, the depth of the anterior chamber and the refractive indices of the humours and lens. As a result the first accurate schematic eye was attributed to Listing who described a three-surface schematic eye in 1851 (Emsley, 1950: 524). Emsley designed a reduced eye, based on certain parameters of the Gullstrand-Emsley eye, which is widely accepted (Emsley, 1950: 543-544).

According to Smith (1995) both the Gullstrand and the Le Grand schematic eyes enjoy reasonable popularity. In 1945, Le Grand (1945: 50-51) presented two schematic eyes, a full theoretical eye consisting of four surfaces and a simplified eye with a single cornea and a lens of zero thickness which too, was limited in its usefulness (Smith, 1995; Atchison and Smith, 2002: 45). Le Grand (1956: 9-27) did a number of calculations to determine the chromatic dispersion of each of the refractive indices. Because of the availability of refractive indices as a function of wavelength for all four media it is one of the theoretical model eyes to be used in this dissertation. This will be looked at in more detail in Section 4.4.3.

4.1.2 Classification of schematic eyes

According to Smith (1995) paraxial schematic eyes are classified into three classes, exact, simplified and reduced. Exact schematic eyes attempt to model a real eye as much as possible with a minimum of four spherical surfaces. Simplified schematic eyes reduce the number of surfaces to two or three. Reduced schematic eyes transfer all the refracting power to a single refracting surface or "cornea", usually resulting in a smaller radius of curvature and shortening of the axial length. Apart from the refractive index of the internal medium, none of the dimensions represent those of a real eye.

It is important to acknowledge the limitations of any model being studied. The limitations of paraxial schematic eyes are firstly that all surfaces are rotationally symmetrical, spherical and centred.

Secondly, it is assumed that the medium is homogenous and isotropic within each element. In a real eye the lens, in particular, is a gradient index lens. For these two reasons, the schematic eyes are poor predictors of monochromatic aberrations.

Thirdly, the eye is built from a combination of average parameters, each considered to be averages of many individual values. These average parameters are combined to represent an "average eye". It is important to note that this average eye is not an average of many eyes, but an eye created by a combination of average parameters (Rabbetts, 2007: 221-241; van Gool and Harris, 2005). This average eye is completely different to the average eye mentioned in Section 3.7 and sought by Harris, van Gool and Cardoso (Harris, 2004b, 2005, 2007; Harris and van Gool, 2004; van Gool and Harris, 2005; Harris and Cardoso, 2006; Cardoso and Harris, 2007; Harris, 2008). Individuals may vary significantly from these values. With the exception of the variations on the Bennett-Rabbetts eye, the schematic eyes are usually attempts to represent an emmetropic eye, based on a monochromatic reference wavelength which is usually yellow light.

Fourthly, the cornea is assumed to be spherical in shape, whereas a real cornea is aspherical (ellipsoid). Finally, the fovea is assumed to be on the optical axis and as a result the optical and visual axes coincide (Smith, 1995).

For completeness it is necessary to mention a newer class of schematic eyes, namely finite or wide angle schematic eyes. This class of model eyes attempts to overcome some of the limitations of the paraxial schematic eyes by including aspheric refracting surfaces, gradient index lenses, a curved retina and lack of surface alignment along a longitudinal axis (Smith, 1995; Atchison and Smith, 2002:39). A number of such eyes have been developed, mostly over the past forty years (Smith, 1995; Rabbetts, 2007:227-8). Of particular interest is the chromatic eye developed by Thibos *et al* (1992) with the express purpose of creating a reduced eye that mimics the effects of chromatic aberration found experimentally.

Paraxial schematic eyes are well suited to study numerous properties of the eye within Gaussian optics, including power, positions of the six cardinal points, pupil positions and sizes, retinal image size of small objects, magnifications and to a limited extent, the causes and effects of refractive errors and accommodation. Because the paraxial schematic eyes are Gaussian models, calculations are restricted to small image sizes and small pupils. The choice of eye will depend on the complexity of the subject being studied and level of accuracy desired. These model eyes are excellent models for calculations of chromatic aberrations. This is because the eye's media are composed mainly of water and the refractive indices vary little across eyes (Smith, 1995).

4.1.3 Emsley's reduced eye

The concept of the reduced eye was first proposed by Listing (Emsley, 1950: 543). The advantage of the reduced eye (see Figure 4.1.1) is its simplicity. The reduced eye has a single stigmatic refracting surface of radius of curvature *r* and a homogenous gap of length *z*. It implies that any ray intersecting the refracting surface orthogonally is an optical axis and therefore there is an infinity of optical axes. We choose one such ray as our longitudinal ray.

When designing the reduced eye, Emsley (1950: 523-544) based a number of parameters on the Gullstrand-Emsley schematic eye. He noted that the principal points of the schematic eye are very close together (0.3 mm apart) and he allowed these "to coalesce into a single intermediate point". He then reduced the schematic

eye into a single spherical refracting surface. Emsley wanted the focal points to coincide with those of the schematic eye. According to him, this fixed the power, radius of curvature and position of the single refracting surface all at once. He placed the vertex of the refracting surface at the principal point of the reduced eye, 5/3 mm behind that of the Gullstrand-Emsley schematic eye. The centre of the radius of curvature was placed at the single intermediate nodal point, giving a radius of curvature *r* of 50/9 mm (or 1/180 m). Because the eye is emmetropic, the length *z* of the eye is now 200/9 mm (or 1/45 m) and is also the emergent focal length. The incident focal length increases to 50/3 mm upstream of the refracting surface. He placed specific emphasis on the power 60 D and chose the refractive index in the reduced eye to be the same as that of water which, according to Emsley, is 4/3. He took the index of air to be 1 (Emsley, 1950: 525-527, 543-544; Bennett & Rabbetts, 1984: 18).

The reduced eye works well for calculating chromatic properties independent of object, image and aperture positions. In order to include chromatic properties dependent on object or image and aperture position, Thibos (1987) adapted the reduced eye by placing a pupil plane in line with that of the Gullstrand-Emsley schematic eye. This places the pupil 3.63 mm before the nodal point, or 1.926 mm behind the refracting surface. Thibos *et al* (1992) further adapted the reduced eye to enable calculations of chromatic properties to closely equate to those results found experimentally. They adapted the constants in Cornu's formula to match their experimental values and modified the corneal

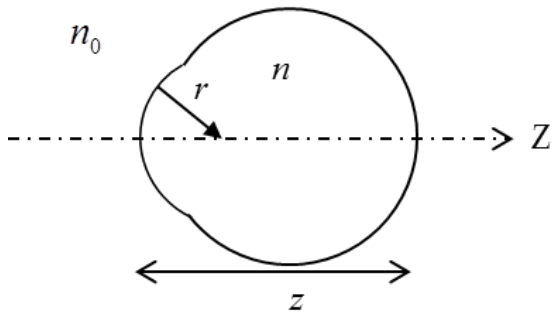

Figure 4.1.1 The reduced eye as a defined optical system. The length is *z*, with optical axis Z, the radius of curvature of the refracting surface is *r*, the refractive index outside the system is n_0 and inside the system is *n*.

profile to an ellipsoid. They refer to this reduced eye with three modifications as the "Chromatic eye". In this dissertation we will make use of a reduced eye with the same *r* and *z* as Emsley's eye and with an index *n* dependant on the frequency of light based on the modified formula proposed by Thibos *et al* (1992).

4.1.4 Le Grand's full theoretical eye

Le Grand proposed his two schematic eyes in 1945. Each schematic eye had an unaccommodated and accommodated version (Le Grand, 1945: 50-51, 1980: 65-67). This dissertation uses the unaccommodated full theoretical version which has four refracting surfaces. A schematic diagram of Le Grand's eye is shown in Figure 4.1.2. The dimensions of Le Grand's full theoretical unaccommodated eye are given in Table 4.1.1 (Le Grand, 1945:50). Subscripts used here are defined in Table 4.1.1 and Figure 4.1.2.

The dimensions given in Table 4.1.1 are limited to the radii of curvature of the refracting surfaces and the width of the gaps between them. The refractive indices in Table 4.1.1 are for a reference refractive index of 589 nm (Fraunhofer line D). At this reference refractive index, Le grand's schematic eye is emmetropic (Le Grand, 1956: 12-19).

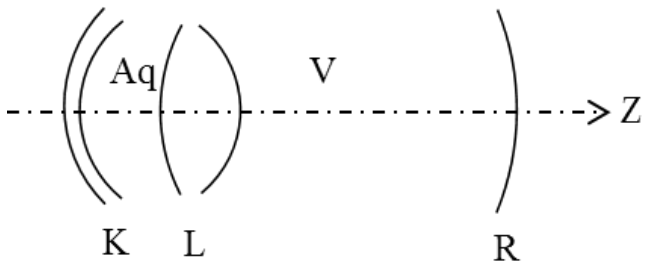

Figure 4.1.2 Le Grand's Complete Theoretical Eye, comprising four refracting surfaces and four homogenous gaps. The refracting surfaces are the anterior and posterior corneal surfaces (K1 and K2) and anterior and posterior lens surfaces (L1 and L2). The gaps are the thickness of the cornea (K), the depth of the anterior chamber (Aq), the thickness of the crystalline lens (L) and the depth of the posterior chamber (V). The optical axis Z is chosen to be centred with each of the stigmatic refracting surfaces, implying no deflectance or tilt in either system.

Table 4.1.1 The dimensions of Le Grand's full theoretical unaccommodated eye (Le Grand, 1945: 50).

Refracting surface or medium	Abbreviated subscript	Radius of curvature (mm)	Width (mm)	Refractive index
Corneal anterior surface	K1	7.8		
Cornea	K		0.55	1.3771
Corneal posterior surface	K2	6.5		
Anterior chamber	Aq		3.05	1.3374
Lens anterior surface	L1	10.2		
Lens	L		4.0	1.42
Lens posterior surface	L2	–6		
Posterior chamber	V		16.5965	1.336

4.2 Visible spectrum

The limits of the visible spectrum differ among studies and industries. The definition of the colour bands also differs (compare Sears, Zemansky and Young, 1987:827 and Keating: 2002: 475). For the purposes of this dissertation, we adopt the spectrum with frequencies between 430 and 750 THz (Sears, Zemansky and Young, 1987: 827) which represents vacuum wavelengths between 399.7 and 697.2 nm, approximately. This represents the range over which human spectral sensitivity ranges from 1 to 100% (Rabbetts, 2007: 287; Thibos *et al*, 1992; Le Grand, 1957: 7-8, 55-58, 71-73).

In Part IV wherever results are displayed graphically and where possible, six coloured reference points will be displayed. These six points represent an even spread across the chosen spectrum, with a gap of 64 THz between each reference point. The six colours are red, orange, yellow, green, blue and violet, and include the two spectral range end-points. The purpose is to create a consistent visual display that is comparable across all the results. The frequencies and corresponding calculated wavelengths of the six colours are detailed in Table 4.2.1. Frequency is given in THz $\left(\times 10^{12}\ \mathrm{s}^{-1}\right)$ and wavelength in nm $\left(\times 10^{-9}\ \mathrm{m}\right)$. The printed colours are not intended to be an exact replication of that particular frequency, but merely a key to the graph and the reference points.

Table 4.2.1 The frequencies and wavelengths of the six specified coloured reference points.

Colour	Frequency in THz	Vacuum wavelength in nm
Red	430	697.2
Orange	494	606.9
Yellow	558	537.3
Green	622	482.0
Blue	686	437.0
Violet	750	399.7

4.3 Frequency versus wavelength

Pease and Barbeito (1989) look at the relationship between frequency and wavelength for a number of studies involving chromatic aberration and conclude that results using frequency or wavenumber (the inverse of wavelength) are "nearly perfectly linear" in contrast to those using wavelength. They cite several reasons to support using frequency rather than wavelength, perhaps the most important being that frequency is independent of the medium whereas wavelength is not and that energy is directly proportional to frequency. Furthermore, we note from Cornu's hyperbolic formula for chromatic dispersion, that refractive index varies inversely with wavelength. These reasons make a compelling argument to study the dependence of properties on the frequency of light rather than on wavelength. Koczorowski (1990) and Rabbetts (2007:290, 292) both show this linear relationship graphically. Confirmation will be obtained in Chapter 8.

4.3.1 Frequency, wavelength and refractive index relationships

The fundamental relationship between frequency ν and vacuum wavelength λ_0 is given by

$$c_0 = \nu\lambda_0 \tag{4.3.1}$$

where light traveling in a vacuum has a speed $c_0 = 299\,792\,458\ \mathrm{m.s^{-1}}$ as defined by the 17th General Conference on Weights and Measures in November 1983. As light travels from one medium to another, the frequency remains the same whereas the wavelength and speed change.

In a particular medium light travels at speed $c < c_0$. The index of refraction in the medium is defined by

$$n = \frac{c_0}{c}. \tag{4.3.2}$$

Hence,

$$n = \frac{\lambda_0}{\lambda} \tag{4.3.3}$$

where λ is the wavelength in a medium.

According to Sears, Zemansky and Young (1987: 843) indices of refraction (for white light) are typically quoted for yellow light from a sodium lamp and with a wavelength of $\lambda = 589\,\text{nm}$, which is near the middle of the visible spectrum. The light emitted from this sodium lamp is inexpensive and nearly monochromatic. The refractive index of air for yellow light is approximately 1.0003 but is usually expressed as 1.

4.3.2 Frequency scale and linearity

Pease and Barbeito (1989) argue that the use of the frequency scale facilitates data analysis for the study of chromatic aberration. The linear nature of the frequency scale makes analysis simpler to compute and to understand.

4.4 Refractive index as a function of frequency for optical media and air

According to Rabbetts (2007: 287), "dispersion is the variation in refractive index of a medium with wavelength". The constringence or Abbe number is the reciprocal of dispersion (Sivak and Mandelman, 1982).

There are few formulae available that give the refractive index of a medium as a function of wavelength (Sivak and Mandelman, 1982; Rabbetts, 2007: 287). Cornu's formula gives the refractive index for water as a function of wavelength, includes three constants and has the form of Equation 4.4.1. This formula has formed the basis for a number of formulae used for the media of the four-surface eye and the reduced eye, with different values being given for the constants. Thibos *et al* (1992) based their formula on Cornu's formula, the constants being calculated from experimental data.

According to Le Grand (1956: 12), early results of the dispersion of the cornea, aqueous, lens and vitreous were obtained by Kunst in 1923. In 1923 Polack obtained Abbe numbers for the cornea, aqueous and lens, but had reservations about the value for the lens. These results were confirmed by Tagawa in 1928. Le Grand (1956: 11-13) considered Cornu's formula to be an adequate approximation for the humours of the eye within the visible spectrum. He calculated the constants by averaging the refractive indices of water and saline for a number of wavelengths. Based on Cornu's formula, and from Polack's experimental data, he was able to tabulate the refractive indices for the four media of his schematic eye for each of the Fraunhofer lines (A, C, D, F and G). Villegas, Carretero and Fimia (1996) extended Le Grand's tabulated results and obtained a polynomial fit of the refractive indices for the four media.

According to Koczorowski (1990) other formulae are available for calculating the dispersion of media such as those of Schmidt, Sellmeier, Hartman and Herzberger. However the constants in these formulae have not specifically been calculated for the media of the eye. Conrady's modification of Schmidt's formula is applicable to optical materials and Cauchy's formula is more suited to media with absorption in the shortwave part of the spectrum. Cauchy's and Sellmeier's formulae are rough approximations of each other while Cornu's, Hartmann's and Herzberg's formulae appear to have a heuristic rather than theoretical basis (Koczorowski, 1990).

More recently Sivak and Mandelman (1982) obtained mean refractive indices at four wavelengths of the ocular media of cow, pig, frog, chicken, rock bass, albino rat and cat using Abbe and Pulfrich refractometry. They also measured the human lens and obtained mean refractive indices and constringence values for the periphery and core for the four wavelengths. They concluded that the humours of the eyes are less dispersive than water, the cornea is more dispersive at short wavelengths and the lens is considerably more dispersive than water. According to Rabbetts (2007:288) Sivak and Mandelman's study is the only significant experimental study on the dispersion of human ocular media since Kunst and Polack.

Formulae for the refractive index of air also exist. The refractive index varies with air temperature, humidity, air pressure, carbon dioxide level and pollution. Cauchy's and Sellmeier's formulae specify standard levels for each of these factors (Hodgman, 1959: 2943). Lorentz's formula can accommodate humidity levels, however Ciddor's formula can account for each of these factors and calculate the refractive index for that situation (Ciddor, 1996).

4.4.1 Refractive index of water

Le Grand (1956: 11) bases his calculations of the refractive index of the eye on Cornu's formula, although it lacks a theoretical basis. He gives Cornu's formula as

$$n = n_{\infty} + \frac{\mathrm{K}}{\lambda - \Lambda} \tag{4.4.1}$$

where the three positive constants are given in Table 4.4.1. The three constants for pure water he based on Dorsey's work of 1940 and the constants for sea water, with salinity 37.4 parts per thousand, he based on Bein from 1935. The measurements were all done at 20°C. In Le Grand's table of measured versus calculated values, the refractive indices compare well across the visible spectrum for both pure water and saline water.

Table 4.4.1 The constants given by Le Grand (1956: 11) for Cornu's formula (Equation 4.4.1) for pure water and for sea water (salinity 37.4 parts per thousand) at temperature 20°C.

	Pure water	Sea water
n_{∞}	1.31848	1.32492
K	0.0066620 nm	0.0068153 nm
Λ	0.1292 nm	0.1333 nm

4.4.2 Refractive index of the reduced eye

Thibos *et al* (1992) represent the refractive index of the reduced eye as a function of wavelength as follows

$$n = a + \frac{b}{\lambda - c} \tag{4.4.2}$$

where $a = 1.320\,535$, $b = 4.685\,\text{nm}$ and $c = 214.102\,\text{nm}$. The formula is based on Cornu's formula for refractive index of water and constants were derived from clinical experimentation on real eyes. Using this formula Thibos *et al* (1992) showed that the refractive index of the body of the reduced eye changes more rapidly with wavelength than a reduced eye filled with water. The predictions for longitudinal chromatic aberration using this formula more closely approximate experimental data than Emsley's reduced eye filled with water.

4.4.3 Refractive indices of Le Grand's full theoretical eye

Le Grand (1956: 9-27) studied chromatic dispersion and chromatic aberration in detail. He too based his calculations on Cornu's formula. He published a table of refractive indices for the cornea, aqueous humour, lens and vitreous humour for five wavelengths represented by Fraunhofer lines A, C, D, F and G.

Villegas, Carretero and Fimia (1996) took Le Grand's table of refractive indices as a function of wavelength and, using a polynomial fit, expressed the data as formulae for refractive index as a function of wavelength. They then compared the results of their calculations from these formulae with those calculated using Emsley's reduced eye filled with water and with Thibos *et al*'s (1992) chromatic eye for chromatic difference in refractive compensation and chromatic difference of position. Because the chromatic eye was designed for the purpose of calculating chromatic properties, it is the best fit to the experimental data for chromatic difference in refractive error and chromatic difference in position. They concluded that the Le Grand eye is slightly underestimated for chromatic difference of refractive compensation but is approximately equivalent for chromatic difference of position. Because of these results, the Villegas, Carretero and Fimia (1996) formulae for Le Grand's eye is used in this study. The formula derived by Villegas, Carretero and Fimia (1996) are given as

$$n(\lambda) = a - b\lambda + c\lambda^2 - d\lambda^3 + e\lambda^4 \qquad (4.4.3)$$

and the constants are given in Table 4.4.2.

Table 4.4.2 The constants for use in Equation 4.4.3 to calculate the refractive index for each of the four media in Le Grand's eye from Villegas, Carretero and Fimia (1996).

	Units	Cornea	Aqueous humour	Lens	Vitreous humour
a	—	1.511 67	1.490 72	1.538 08	1.456 34
b	m^{-1}	0.000 636 054	0.000 805 138	0.000 448 268	0.000 561 861
c	m^{-2}	1.17×10^{-6}	1.68×10^{-6}	5.74×10^{-7}	1.02×10^{-6}
d	m^{-3}	1.01×10^{-9}	1.66×10^{-9}	2.61×10^{-10}	8.70×10^{-10}
e	m^{-4}	3.31×10^{-13}	6.31×10^{-13}	0	2.84×10^{-13}

4.4.4 Refractive index of air

The refractive index of air differs only very slightly from that of vacuum and for most optometric purposes one can write $n_0 = 1$. A number of equations, for example Cauchy's dispersion formula (Hodgson, 1959) and Ciddor's equations (Ciddor, 1996), are available for calculating the refractive index of air. Cauchy's formula is expressed in terms of wavelength whereas Ciddor's equations are expressed in terms of wavenumber. Cauchy's dispersion formula is

$$(n_0 - 1)10^7 = p + \frac{q}{\lambda^2} + \frac{t}{\lambda^4} \qquad (4.4.4)$$

where $p = 2\,726.43$, $q = 12.228\times10^6$ nm^2 and $t = 355.5\times10^9$ nm^4 for dry air at temperature 15°C, pressure 101 kPa and carbon dioxide content of 450 ppm. Ciddor's equations calculate the refractive index of air for variations in any of these values as well as air pollution density. This, however, would typically be of interest to the field of precise interferometry or geodetic surveying which requires an accuracy to a few parts in 10^8.

In the majority of cases we will use $n_0 = 1$ for the refractive index of air and for illustrative value one data set on the reduced and Le Grand's eyes will be shown using Cauchy's equation. A graph set will be shown comparing calculations using $n_0 = 1$ and Cauchy's formula.

4.5 Discussion

There are a number of schematic eyes available to the ophthalmic optics researcher, differing in the number and shape of refracting surfaces. Some

schematic eyes are available with a pupil or even a gradient index lens. However, because this dissertation focuses on the dependence of the first-order optical properties of the eye on frequency, we need to select schematic eyes for which the refractive indices of all media as a function of frequency (or wavelength) are known. For this reason we have selected the reduced eye and Le Grand's four-surface eye. The reduced eye forms an ideal basis because it is an excellent predictor of chromatic properties. However, the reduced eye is a very simple model and so we include Le Grand's four-surface eye which is somewhat more representative in structure. This point will become clearer later once we calculate the transferences of the two eyes.

The visible spectrum selected in numerical calculations in this dissertation is the range of frequencies from 400 THz to 700 THz. Frequency, rather than wavelength, is used in all calculations and graphical representations.

5 DERIVATIONS FOR BACKGROUND THEORY

In this chapter we derive formulae that will be needed for our study of chromatic dependence of first-order optical properties. As such Chapter 5 is made up of a random assortment of seemingly unrelated derivations. The equations that are presented in Chapter 3 and this chapter together will form the basis from which we will either study chromatic dependence directly or derive formulae for chromatic aberrations and quantifying of chromatic properties. While this chapter focusses on the eye as our system, we note that the formulae derived and figures presented are general for all Gaussian systems.

5.1 Exit-plane refractive compensation

As mentioned in Section 3.4.2 the derivation for exit-plane refractive compensation is not available in the literature. This is presumably because this derived property has no application to the eye. However it is defined here for systems in general. While this dissertation is primarily concentrating on the eye as a system, we include this derived property because it has a bearing on certain entries of the point characteristic **P**.

The exit-plane refractive compensation is the power of a thin lens juxtaposed immediately downstream to a general system so that the combined system becomes an entrance-plane focal system. Writing the transference of the combined system

$$\mathbf{S} = \mathbf{S}_{\mathrm{C}}\mathbf{S}_{\mathrm{S}} = \begin{pmatrix} 1 & 0 \\ -F_{\mathrm{C}} & 1 \end{pmatrix}\begin{pmatrix} A_{\mathrm{S}} & B_{\mathrm{S}} \\ C_{\mathrm{S}} & D_{\mathrm{S}} \end{pmatrix} = \begin{pmatrix} \bullet & \bullet \\ \bullet & -F_{\mathrm{C}}B_{\mathrm{S}} + D_{\mathrm{S}} \end{pmatrix} \tag{5.1.1}$$

and setting $D = 0$ for the exit-plane system

$$-F_{\mathrm{C}}B_{\mathrm{S}} + D_{\mathrm{S}} = 0 \tag{5.1.2}$$

we obtain the exit-plane refractive compensation for system S_{S}

$$F_{\mathrm{C}} = D_{\mathrm{S}}B_{\mathrm{S}}^{-1}. \tag{5.1.3}$$

This equation generalizes readily to linear systems.

5.2 Magnification

There is a relationship between the definition of magnification defined for a Gaussian system for conjugation of the object and image and the fundamental properties of the system's transference. Indeed, the relationship between transverse and angular magnification is to be found in the symplectic equation (Equation 3.2.24).

In Section 3.5.3 we saw how Harris (2001a) defined magnification, blur and the ray state at the retina for distant objects. We take a different approach to Harris (2001b) to define magnification, blur and the ray state at the retina for finite distances and these definitions are derived in Section 5.2.2.

The use of a pinhole immediately in front of the eye forms a large role in the experiments for chromatic properties of eyes, particularly chromatic properties dependent on object or image and aperture positions. For this reason we simplify this special situation for magnification of an object at a finite distance in Section 5.2.4.

5.2.1 Relationships between the types of magnification

In Section 3.3.2, we looked at the four special types of systems resulting from equating each of the fundamental properties in turn to zero. Then, in Section 3.5.1, we looked at the three types of magnification defined for Gaussian systems. We now observe that there are distinct similarities in the definitions between two of these systems. Transverse and angular magnification are related to the transference through their being defined in the same way as two of the special systems, that is the conjugate and afocal systems. Also, in a similar way to the relationship that we saw between these two magnifications in Section 3.5.1, the two types of magnification are inversely related to each other through the symplectic equation.

Transverse magnification

Where we have a conjugate system $B = 0$ such that an object at the entrance plane is positioned as height from the optical axis y_0, the point image

will form on the exit plane at position *y*. Equation 3.5.1 is the same as Equation 3.3.2 and *A* represents transverse magnification in a conjugate system. Therefore

$$A = M_{\mathrm{t}} \tag{5.2.1}$$

as long as $B = 0$. This equation is true for all Gaussian systems, both thin and thick, provided the object is at the entrance plane. Should the object be elsewhere, then *A* magnifies the ray height and Equation 5.2.1 does not apply.

Angular magnification

The equation for angular magnification, Equation 3.5.3 is the same equation as Equation 3.3.3. We can therefore state that

$$D = M_{\alpha}. \tag{5.2.2}$$

This is true of all afocal systems $C = 0$ and provided the object point is distant.

Relationships between the magnifications

Equation 3.5.4 gave us the relationship between angular and transverse magnification as the one being the inverse of the other. To confirm this, from the symplectic Equation 3.2.24, and substituting $B = 0$, we can see that

$$AD = 1. \tag{5.2.3}$$

The same is true if we substitute $C = 0$ into the symplectic equation. Substituting Equations 5.2.1 and 2 into Equation 5.2.3, we obtain Equation 3.5.4.

5.2.2 Summary of magnification, blur and ray state at the retina

Equations 3.5.7 and 8 define the magnification, blur and ray state at the retina. We recall that $\boldsymbol{\rho}_{\mathrm{R}} = \begin{pmatrix} y_{\mathrm{R}} & \alpha_{\mathrm{R}} \end{pmatrix}^{\mathrm{T}}$ defines the state of the ray at the retina. However, instead of α_{R} we are interested in the unreduced inclination at the retina a_{R}, and indeed elsewhere in the system. Therefore we define

$$\mathbf{r}_{\mathrm{R}} = \begin{pmatrix} y_{\mathrm{R}} \\ a_{\mathrm{R}} \end{pmatrix} \tag{5.2.4}$$

for the purposes of defining chromatic properties dependent on object and aperture positions. Equations 3.5.7 and 8 become

$$A_{\mathrm{E}} A_{\mathrm{A}}^{-1} y_{\mathrm{P}} + B_{\mathrm{B}} A_{\mathrm{A}}^{-1} n_0 a_{\mathrm{K}} = y_{\mathrm{R}} \tag{5.2.5}$$

and

$$n^{-1}C_{\mathrm{E}}A_{\mathrm{A}}^{-1}y_{\mathrm{P}} + n^{-1}D_{\mathrm{B}}A_{\mathrm{A}}^{-1}n_0 a_{\mathrm{K}} = a_{\mathrm{R}} \tag{5.2.6}$$

where n is the refractive index of the vitreous humour.

We write these two equations in the form

$$\mathbf{V}_{\mathrm{E}}\mathbf{v}_{\mathrm{E}} = \mathbf{r}_{\mathrm{R}} \tag{5.2.7}$$

where

$$\mathbf{V}_{\mathrm{E}} = \begin{pmatrix} W_{\mathrm{E}} & X_{\mathrm{E}} \\ Y_{\mathrm{E}} & Z_{\mathrm{E}} \end{pmatrix} = \begin{pmatrix} A_{\mathrm{E}}A_{\mathrm{A}}^{-1} & B_{\mathrm{B}}A_{\mathrm{A}}^{-1}n_0 \\ n^{-1}C_{\mathrm{E}}A_{\mathrm{A}}^{-1} & n^{-1}D_{\mathrm{B}}A_{\mathrm{A}}^{-1}n_0 \end{pmatrix}, \tag{5.2.8}$$

is the distance coefficient matrix and with subscript E for eye and

$$\mathbf{v}_{\mathrm{E}} = \begin{pmatrix} y_{\mathrm{P}} \\ a_{\mathrm{K}} \end{pmatrix}. \tag{5.2.9}$$

Harris (2001a) names each of the coefficients according to their characters and properties. W_{E} is the distance image blur coefficient, X_{E} is the distance image size coefficient, Y_{E} is the distance directional spread coefficient, and Z_{E} is the distance directional coefficient. While we have defined the coefficients slightly differently with regard to the refractive indices, the meaning conveyed is the same.

5.2.3 Magnification, blur and ray state at the retina for object points at finite distances

To calculate the magnification and blur at the retinal plane for a system where the object point is at a finite distance we take a different approach to Harris (2001b). We define the system of the eye, as shown in Figure 5.2.1, as having the entrance plane T_{K} immediately upstream of the tear layer on the cornea and the exit plane T_{R} immediately in front of the retina. The eye naturally divides into two subsystems at the plane of the pupil T_{P} which also acts as a limiting aperture. We divide our system, which represents the eye, into two subsystems, anterior, with subscript A and posterior, with subscript B. Immediately upstream of the eye is the homogenous gap of width $-z_{\mathrm{O}}$ measured from the corneal plane T_{K} to the object plane T_{O}, which represents the finite working distance. The object is

located at the entrance plane T_O and is positioned at a transverse distance of y_O with respect to the longitudinal axis Z.

We are interested in solving for the state of the ray $\boldsymbol{\rho}_R$ at the retina in terms of its transverse position in the pupil y_P and the transverse position of the object y_O, instead of the incident inclination of the ray at the cornea α_K which we used for the system with a distant object in Section 3.5.3. The advantage of defining the system this way is that we can either use the pupil as our partitioning plane or we can use any limiting aperture within an optical device through which the eye is looking, including a pinhole in front of the eye. The formulae we derive are general and we will show how they simplify further still when using a pinhole immediately in front of the eye. We noted earlier (Section 3.5.3) that the position of the centre of the pupil does vary slightly with changes in diameter, however, the use of a pinhole allows us to manipulate y_P to a much greater extent. In this case y_P is the distance from the longitudinal axis to the centre of the pinhole at the corneal-plane T_K. The near system and symbolism is introduced in Figure 5.2.1.

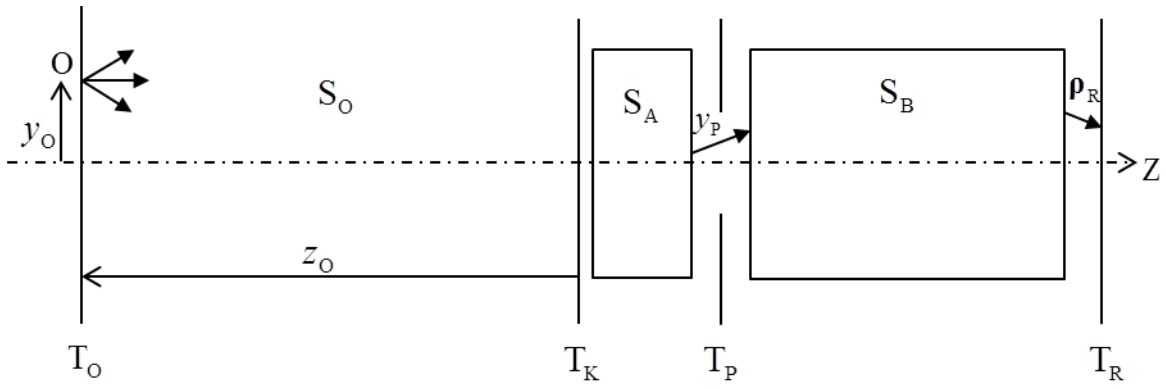

Figure 5.2.1 The Gaussian system of the eye S_E is partitioned into two subsystems by a pupillary plane T_P and consists of an anterior subsystem S_A and posterior subsystem S_B which are juxtaposed. The object plane is located at position $z_O < 0$ measured from the cornea. The width of S_O is $-z_O$.

The system of the eye S_E is made up of the anterior S_A and posterior S_B subsystems to obtain the transference:

$$\mathbf{S}_E = \mathbf{S}_B\mathbf{S}_A = \begin{pmatrix} A_B & B_B \\ C_B & D_B \end{pmatrix}\begin{pmatrix} A_A & B_A \\ C_A & D_A \end{pmatrix} = \begin{pmatrix} A_BA_A + B_BC_A & A_BB_A + B_BD_A \\ C_BA_A + D_BC_A & C_BB_A + D_BD_A \end{pmatrix} = \begin{pmatrix} A_E & B_E \\ C_E & D_E \end{pmatrix} \tag{5.2.10}$$

and for the compound systems of homogenous gap S_O upstream from the eye and either anterior subsystem S_A or eye S_E the transferences are:

$$\mathbf{S}_{OA} = \mathbf{S}_A\mathbf{S}_O = \begin{pmatrix} A_A & B_A \\ C_A & D_A \end{pmatrix}\begin{pmatrix} 1 & -\zeta_O \\ 0 & 1 \end{pmatrix} = \begin{pmatrix} A_A & -A_A\zeta_O + B_A \\ C_A & -C_A\zeta_O + D_A \end{pmatrix} = \begin{pmatrix} A_{OA} & B_{OA} \\ C_{OA} & D_{OA} \end{pmatrix}, \tag{5.2.11}$$

$$\mathbf{S}_{OE} = \mathbf{S}_B\mathbf{S}_{OA} = \begin{pmatrix} A_B & B_B \\ C_B & D_B \end{pmatrix}\begin{pmatrix} A_{OA} & B_{OA} \\ C_{OA} & D_{OA} \end{pmatrix}$$

$$= \begin{pmatrix} A_BA_{OA} + B_BC_{OA} & A_BB_{OA} + B_BD_{OA} \\ C_BA_{OA} + D_BC_{OA} & C_BB_{OA} + D_BD_{OA} \end{pmatrix} = \begin{pmatrix} A_{OE} & B_{OE} \\ C_{OE} & D_{OE} \end{pmatrix} \tag{5.2.12}$$

and

$$\mathbf{S}_{OE} = \mathbf{S}_E\mathbf{S}_O = \begin{pmatrix} A_E & B_E \\ C_E & D_E \end{pmatrix}\begin{pmatrix} 1 & -\zeta_O \\ 0 & 1 \end{pmatrix} = \begin{pmatrix} A_E & -A_E\zeta_O + B_E \\ C_E & -C_E\zeta_O + D_E \end{pmatrix} = \begin{pmatrix} A_{OE} & B_{OE} \\ C_{OE} & D_{OE} \end{pmatrix}. \tag{5.2.13}$$

A ray is traced from the object across the homogenous gap and through the anterior system to its ray state at the pupil to obtain

$$\mathbf{S}_{OA}\boldsymbol{\rho}_O = \boldsymbol{\rho}_P \tag{5.2.14}$$

and

$$A_{OA}y_O + B_{OA}\alpha_O = y_P \tag{5.2.15}$$

$$C_{OA}y_O + D_{OA}\,\alpha_O = \alpha_P. \tag{5.2.16}$$

Similarly from the pupillary plane to the retinal plane

$$\mathbf{S}_B\boldsymbol{\rho}_P = \boldsymbol{\rho}_R \tag{5.2.17}$$

and

$$A_By_P + B_B\alpha_P = y_R \tag{5.2.18}$$

$$C_By_P + D_B\alpha_P = \alpha_R. \tag{5.2.19}$$

Equation 5.2.15 is solved for α_O,

$$\alpha_{\mathrm{O}} = B_{\mathrm{OA}}^{-1} y_{\mathrm{P}} - B_{\mathrm{OA}}^{-1} A_{\mathrm{OA}} y_{\mathrm{O}} \tag{5.2.20}$$

and substituted into Equation 5.2.16 to obtain

$$\alpha_{\mathrm{P}} = C_{\mathrm{OA}} y_{\mathrm{O}} + D_{\mathrm{OA}} B_{\mathrm{OA}}^{-1} y_{\mathrm{P}} - D_{\mathrm{OA}} B_{\mathrm{OA}}^{-1} A_{\mathrm{OA}} y_{\mathrm{O}} . \tag{5.2.21}$$

From Equations 5.2.21 and 5.2.18 we obtain

$$y_{\mathrm{R}} = \left(A_{\mathrm{B}} + B_{\mathrm{B}} D_{\mathrm{OA}} B_{\mathrm{OA}}^{-1}\right) y_{\mathrm{P}} + \left(B_{\mathrm{B}} C_{\mathrm{OA}} - B_{\mathrm{B}} D_{\mathrm{OA}} B_{\mathrm{OA}}^{-1} A_{\mathrm{OA}}\right) y_{\mathrm{O}} .$$

Manipulating, we obtain

$$y_{\mathrm{R}} = \left(A_{\mathrm{B}} B_{\mathrm{OA}} + B_{\mathrm{B}} D_{\mathrm{OA}}\right) B_{\mathrm{OA}}^{-1} y_{\mathrm{P}} + B_{\mathrm{B}} \left(C_{\mathrm{OA}} - D_{\mathrm{OA}} B_{\mathrm{OA}}^{-1} A_{\mathrm{OA}}\right) y_{\mathrm{O}} .$$

From B_{OE}, Equation 5.2.12 and the third Schur complement (Equation 3.2.22) we obtain

$$y_{\mathrm{R}} = B_{\mathrm{OE}} B_{\mathrm{OA}}^{-1} y_{\mathrm{P}} - B_{\mathrm{B}} B_{\mathrm{OA}}^{-1} y_{\mathrm{O}} .$$

We make use here of the Schur compliment instead of the simpler unit determinant because of the generalisation we undertake in Section 5.2.5. Substituting equalities from Equations 5.2.11 and 13 into our equation we obtain

$$y_{\mathrm{R}} = \left(B_{\mathrm{E}} - A_{\mathrm{E}} \zeta_{\mathrm{O}}\right)\left(B_{\mathrm{A}} - A_{\mathrm{A}} \zeta_{\mathrm{O}}\right)^{-1} y_{\mathrm{P}} + B_{\mathrm{B}} \left(A_{\mathrm{A}} \zeta_{\mathrm{O}} - B_{\mathrm{A}}\right)^{-1} y_{\mathrm{O}} , \tag{5.2.22}$$

the transverse position of the ray at the retina.

Substituting from Equation 5.2.21 into Equation 5.2.19 to get rid of α_{P}, we obtain

$$\alpha_{\mathrm{R}} = \left(C_{\mathrm{B}} + D_{\mathrm{B}} D_{\mathrm{OA}} B_{\mathrm{OA}}^{-1}\right) y_{\mathrm{P}} + \left(D_{\mathrm{B}} C_{\mathrm{OA}} - D_{\mathrm{B}} D_{\mathrm{OA}} B_{\mathrm{OA}}^{-1} A_{\mathrm{A}}\right) y_{\mathrm{O}}$$

and manipulating,

$$\alpha_{\mathrm{R}} = \left(C_{\mathrm{B}} B_{\mathrm{OA}} + D_{\mathrm{B}} D_{\mathrm{OA}}\right) B_{\mathrm{OA}}^{-1} y_{\mathrm{P}} + D_{\mathrm{B}} \left(C_{\mathrm{OA}} - D_{\mathrm{OA}} B_{\mathrm{OA}}^{-1} A_{\mathrm{OA}}\right) y_{\mathrm{O}} .$$

From the equality for D_{OE} in Equation 5.2.12 and the third Schur complement (Equation 3.2.22) we obtain

$$\alpha_{\mathrm{R}} = D_{\mathrm{OE}} B_{\mathrm{OA}}^{-1} y_{\mathrm{P}} - D_{\mathrm{B}} B_{\mathrm{OA}}^{-1} y_{\mathrm{O}} .$$

Substituting equalities from Equation 5.2.11 and 13 into our equation we obtain

$$\alpha_{\mathrm{R}} = \left(D_{\mathrm{E}} - C_{\mathrm{E}} \zeta_{\mathrm{O}}\right)\left(B_{\mathrm{A}} - A_{\mathrm{A}} \zeta_{\mathrm{O}}\right)^{-1} y_{\mathrm{P}} + D_{\mathrm{B}} \left(A_{\mathrm{A}} \zeta_{\mathrm{O}} - B_{\mathrm{A}}\right)^{-1} y_{\mathrm{O}} , \tag{5.2.23}$$

the reduced inclination at the retina of the ray from the object. However, the unreduced inclination at the retina is required and so Equation 5.2.23 is rewritten

$$a_{\mathrm{R}} = \left(D_{\mathrm{E}} - C_{\mathrm{E}} \zeta_{\mathrm{O}}\right)\left(nB_{\mathrm{A}} - nA_{\mathrm{A}} \zeta_{\mathrm{O}}\right)^{-1} y_{\mathrm{P}} + D_{\mathrm{B}} \left(nA_{\mathrm{A}} \zeta_{\mathrm{O}} - nB_{\mathrm{A}}\right)^{-1} y_{\mathrm{O}} . \tag{5.2.24}$$

Equations 5.2.22 and 24 represent the physical (unreduced) state of the ray at the retinal plane for the ray from the object point at a finite working distance z_{O}. The equations are general and any ray could be chosen, including, for example, a chief ray or a marginal ray. This solution is summarized, in a similar layout to how we presented Harris's formulae in Equations 5.2.7 to 9, in terms of the system S_{OE} as defined in Equations 5.2.12 and 13 as

$$\mathbf{V}_{\mathrm{OE}}\mathbf{v}_{\mathrm{OE}} = \mathbf{r}_{\mathrm{R}} \tag{5.2.25}$$

where

$$\mathbf{V}_{\mathrm{OE}} = \begin{pmatrix} W_{\mathrm{OE}} & X_{\mathrm{OE}} \\ Y_{\mathrm{OE}} & Z_{\mathrm{OE}} \end{pmatrix} = \begin{pmatrix} \left(B_{\mathrm{E}} - A_{\mathrm{E}}\zeta_{\mathrm{O}}\right)\left(B_{\mathrm{A}} - A_{\mathrm{A}}\zeta_{\mathrm{O}}\right)^{-1} & B_{\mathrm{B}}\left(A_{\mathrm{A}}\zeta_{\mathrm{O}} - B_{\mathrm{A}}\right)^{-1} \\ \left(D_{\mathrm{E}} - C_{\mathrm{E}}\zeta_{\mathrm{O}}\right)\left(nB_{\mathrm{A}} - nA_{\mathrm{A}}\zeta_{\mathrm{O}}\right)^{-1} & D_{\mathrm{B}}\left(nA_{\mathrm{A}}\zeta_{\mathrm{O}} - nB_{\mathrm{A}}\right)^{-1} \end{pmatrix} \tag{5.2.26}$$

is the near coefficient matrix for system S_{OE} where the object point is at a finite working distance z_{O} from the eye, $\mathbf{r}_{\mathrm{R}}$ is defined by Equation 5.2.4 and

$$\mathbf{v}_{\mathrm{OE}} = \begin{pmatrix} y_{\mathrm{P}} \\ y_{\mathrm{O}} \end{pmatrix} \tag{5.2.27}$$

is an input vector for the system S_{OE}, from the object point at y_{O}, through the pupil at position y_{P}, to the retina. The entries in the top row of the near coefficient matrix $\mathbf{V}_{\mathrm{OE}}$ are unitless while the bottom row has units of inverse length. Multiplying Equation 5.2.25 out we obtain

$$W_{\mathrm{OE}}y_{\mathrm{P}} + X_{\mathrm{OE}}y_{\mathrm{O}} = y_{\mathrm{R}} \tag{5.2.28}$$

and

$$Y_{\mathrm{OE}}y_{\mathrm{P}} + Z_{\mathrm{OE}}y_{\mathrm{O}} = a_{\mathrm{R}}\,. \tag{5.2.29}$$

The near coefficient matrix exists provided $\left(B_{\mathrm{A}} - A_{\mathrm{A}}\zeta_{\mathrm{O}}\right)^{-1}$ exists. The coefficient matrix does not exist when $B_{\mathrm{A}} - A_{\mathrm{A}}\zeta_{\mathrm{O}} = 0$, which would imply that $B_{\mathrm{OA}} = 0$. In other words the coefficient matrix exists provided the object and iridial planes are not conjugate.

We note that the disjugacy B and divarication D appear to play a significant role in the magnification and blur of the system. Together the coefficient matrix $\mathbf{V}_{\mathrm{OE}}$ and input vector $\mathbf{v}_{\mathrm{OE}}$ define the position and unreduced

inclination of the pencil of rays at the retina for the system from an object at a finite distance. W_{OE} is the near image blur coefficient, X_{OE} is the near image size coefficient, Y_{OE} is the near directional spread coefficient, and Z_{OE} is the near directional coefficient.

Similar to our interpretation for distant objects, we can interpret Equation 5.2.28 for a system consisting of an eye and an object point at a finite distance upstream. If we wish to obtain the size Δy_R of the image at the exit plane corresponding to an object of size Δy_O for a Gaussian system, we follow the rays from the object through the same position through the pupil such that $y_{P1} = y_{P2}$ we obtain

$$y_{R2} - y_{R1} = W_{OE}(y_{P2} - y_{P1}) + X_{OE}(y_{O2} - y_{O1})$$

which simplifies to

$$\Delta y_R = X_{OE} \Delta y_O . \tag{5.2.30}$$

Equation 5.2.30 is linear in Δy_O and we consider the near image size coefficient, X_{OE} to be the transverse magnification of system S_{OE}.

For a single object point y_O, and a pupil of diameter Δy_P the size of the blur circle on the exit plane (from Equation 5.2.28) is

$$\Delta y_R = W_{OE} \Delta y_P . \tag{5.2.31}$$

The size of the blur circle is dependent on the size of the pupil and the near image blur coefficient W_{OE}. We can think of W_{OE} as a sort of blur-magnification.

One can interpret Equation 5.2.29 in a similar fashion for the angular spread of the rays at the retina Δa_R from an object of size Δy_O. For a Gaussian system, we follow the rays from the object through the same position in the pupil such that $y_{P1} = y_{P2}$ we obtain

$$\Delta a_R = Z_{OE} \Delta y_O \tag{5.2.32}$$

where Z_{OE} is the near directional coefficient. To obtain the angular spread of the blur across the retina produced from a single object point, we see that $\Delta y_O = 0$ and that the blur spread is a function of pupil size Δy_P

$$\Delta a_R = Y_{OE} \Delta y_P \tag{5.2.33}$$

where Y_{OE} is the near directional spread coefficient

The difference in inclinations of the rays reaching the retina has implications for the Stiles-Crawford effect (Smith and Atchison, 1997: 308; Atchison & Smith, 2000: 124-127; Stiles, 1939).

5.2.4 Eye with pinhole

Object at a finite distance

When a pinhole is held immediately in front of the cornea, the system and subsystems simplify. The plane of the pinhole is the partitioning plane, however, the system upstream of the pinhole is merely the homogenous gap of system S_O and the posterior system is that of the eye, S_E. The transference of the anterior subsystem S_A becomes the identity matrix and posterior subsystem S_B becomes S_E, the eye. The transverse position of the pinhole is the distance y_P from the optical axis and we assume that the pupil is sufficiently dilated to accommodate the chief ray through the pinhole. The near coefficient matrix $\mathbf{V}_{OE}$ therefore simplifies to

$$\mathbf{V}_{OE}^{P} = \begin{pmatrix} W_{OE}^{P} & X_{OE}^{P} \\ Y_{OE}^{P} & Z_{OE}^{P} \end{pmatrix} = \begin{pmatrix} A_E - B_E\zeta_O^{-1} & B_E\zeta_O^{-1} \\ n^{-1}\left(C_E - D_E\zeta_O^{-1}\right) & n^{-1}D_E\zeta_O^{-1} \end{pmatrix} \tag{5.2.34}$$

with the superscript P representing the specialisation for a pinhole in front of the eye. Equations 5.2.28 and 29 become

$$y_R = W_{OE}^{P} y_P + X_{OE}^{P} y_O \tag{5.2.35}$$

and

$$a_R = Y_{OE}^{P} y_P + Z_{OE}^{P} y_O . \tag{5.2.36}$$

Equations 5.2.28 and 29 still hold and are general for an eye with an object point at a finite distance, both with and without a pinhole. Equations 5.2.35 and 36 are the same as Equations 5.2.28 and 29 with the four coefficients merely simplifying, as shown in Equation 5.2.34, when a pinhole is placed in front of the eye. For this reason we shall refer to Equations 5.2.28 and 29 in all further discussions, and merely substitute from $\mathbf{V}_{OE}^{P}$ when appropriate.

Distant object

Similarly, for a distant object the coefficient matrix in Equation 5.2.8 simplifies to

$$\mathbf{V}_{\mathrm{E}}^{\mathrm{P}} = \begin{pmatrix} W_{\mathrm{E}}^{\mathrm{P}} & X_{\mathrm{E}}^{\mathrm{P}} \\ Y_{\mathrm{E}}^{\mathrm{P}} & Z_{\mathrm{E}}^{\mathrm{P}} \end{pmatrix} = \begin{pmatrix} A_{\mathrm{E}} & B_{\mathrm{E}} n_0 \\ n^{-1} C_{\mathrm{E}} & n^{-1} D_{\mathrm{E}} n_0 \end{pmatrix} \tag{5.2.37}$$

while Equation 5.2.9 remains unchanged. Equation 5.2.7 holds for the pinhole and the coefficients from Equation 5.2.37 may be substituted, when appropriate.

5.2.5 Generalizing to linear optics

In this section we have retained the order of multiplication and avoided division in an effort to allow the equations to generalize to linear optics for systems that have astigmatic elements. In Section 5.2.1 we can indeed generalize transverse and angular magnification to astigmatic systems. The equations in Sections 5.2.2 and 3 generalize, however we need to include a transpose which comes about from the symplectic equations (Equations 3.2.17 to 19) and the Schur compliments (Equations 3.2.20 to 23). We provide the linear generalizations below, the proofs following the format given in Section 5.2.3. Equation 5.2.8 becomes

$$\mathbf{V}_{\mathrm{E}} = \begin{pmatrix} \mathbf{W}_{\mathrm{E}} & \mathbf{X}_{\mathrm{E}} \\ \mathbf{Y}_{\mathrm{E}} & \mathbf{Z}_{\mathrm{E}} \end{pmatrix} = \begin{pmatrix} \mathbf{A}_{\mathrm{E}} \mathbf{A}_{\mathrm{A}}^{-1} & \mathbf{B}_{\mathrm{B}} \mathbf{A}_{\mathrm{A}}^{-\mathrm{T}} n_0 \\ n^{-1} \mathbf{C}_{\mathrm{E}} \mathbf{A}_{\mathrm{A}}^{-1} & n^{-1} \mathbf{D}_{\mathrm{B}} \mathbf{A}_{\mathrm{A}}^{-\mathrm{T}} n_0 \end{pmatrix} \tag{5.2.38}$$

and Equation 5.2.26 becomes

$$\mathbf{V}_{\mathrm{OE}} = \begin{pmatrix} \mathbf{W}_{\mathrm{OE}} & \mathbf{X}_{\mathrm{OE}} \\ \mathbf{Y}_{\mathrm{OE}} & \mathbf{Z}_{\mathrm{OE}} \end{pmatrix} = \begin{pmatrix} \left(\mathbf{B}_{\mathrm{E}} - \mathbf{A}_{\mathrm{E}} \zeta_{\mathrm{O}}\right)\left(\mathbf{B}_{\mathrm{A}} - \mathbf{A}_{\mathrm{A}} \zeta_{\mathrm{O}}\right)^{-1} & \mathbf{B}_{\mathrm{B}} \left(\mathbf{A}_{\mathrm{A}} \zeta_{\mathrm{O}} - \mathbf{B}_{\mathrm{A}}\right)^{-\mathrm{T}} \\ \left(\mathbf{D}_{\mathrm{E}} - \mathbf{C}_{\mathrm{E}} \zeta_{\mathrm{O}}\right)\left(n\mathbf{B}_{\mathrm{A}} - n\mathbf{A}_{\mathrm{A}} \zeta_{\mathrm{O}}\right)^{-1} & \mathbf{D}_{\mathrm{B}} \left(n\mathbf{A}_{\mathrm{A}} \zeta_{\mathrm{O}} - n\mathbf{B}_{\mathrm{A}}\right)^{-\mathrm{T}} \end{pmatrix}. \tag{5.2.39}$$

The transposes in the right-hand column of these two matrices fall away when we simplify for the situation of a pinhole in front of the eye and so the equations in Section 5.2.4 readily generalize to linear optics to include eyes with astigmatic elements.

5.3 Measurements in object space

From the literature review in Chapter 2, we saw how chromatic difference in position and chromatic difference in magnification are defined in physiological

optics. More specifically, we saw that when these measurements are taken experimentally, that the chromatic difference in object position occurs in object space and alignment is assumed at a position on the retina. Because such measurements are made in the clinical environment, we shall consider the scenario for finite distances only. Pinholes also feature often in such experiments.

The objective in this section is to derive formulae for the transverse position of an object point and the inclination of the ray incident onto the eye or pinhole when the position in the pupil or pinhole and the position at the retinal plane are known. Ultimately we keep the goal of deriving formulae for the chromatic difference in position or magnification in mind. These formulae will form the basis of the derivations for chromatic difference in position and magnification in Chapter 7.

5.3.1 Transverse position of an object point at a finite distance

We will start by deriving the formula for the transverse position of an object point at a finite distance upstream of the eye. We turn our attention to the system of the eye partitioned into anterior and posterior subsystems and object at finite distance upstream of the system illustrated in Figure 5.2.1 which we used in the previous section.

Because the system S_{OE} is the same as that described in Figure 5.2.1, with applicable subsystems S_{O}, S_{A}, S_{B} and combinations thereof, the equations that define S_{OE} and its subsystems, given by Equations 5.2.10 to 19, apply. Solving Equation 5.2.18 for α_{P} we obtain

$$\alpha_{\mathrm{P}} = B_{\mathrm{B}}^{-1} y_{\mathrm{R}} - B_{\mathrm{B}}^{-1} A_{\mathrm{B}} y_{\mathrm{P}} . \tag{5.3.1}$$

Substituting from Equation 5.2.21 into 5.3.1 and rearranging we obtain

$$\left(C_{\mathrm{OA}} - D_{\mathrm{OA}} B_{\mathrm{OA}}^{-1} A_{\mathrm{OA}}\right) y_{\mathrm{O}} = -\left(B_{\mathrm{B}}^{-1} A_{\mathrm{B}} + D_{\mathrm{OA}} B_{\mathrm{OA}}^{-1}\right) y_{\mathrm{P}} + B_{\mathrm{B}}^{-1} y_{\mathrm{R}} . \tag{5.3.2}$$

We make use of the third Schur compliment (Equation 3.2.22) and equalities in Equation 5.2.12 to simplify this equation to

$$-B_{\mathrm{OA}}^{-1} y_{\mathrm{O}} = -B_{\mathrm{B}}^{-1} B_{\mathrm{OE}} B_{\mathrm{OA}}^{-1} y_{\mathrm{P}} + B_{\mathrm{B}}^{-1} y_{\mathrm{R}} .$$

Hence

$$y_{\mathrm{O}} = B_{\mathrm{B}}^{-1} B_{\mathrm{OE}} y_{\mathrm{P}} - B_{\mathrm{OA}} B_{\mathrm{B}}^{-1} y_{\mathrm{R}} .$$

In terms of the distance of the object in front of the eye and the entries of the transferences of the eye, and anterior and posterior subsystems, this is

$$y_{\mathrm{O}} = B_{\mathrm{B}}^{-1}\left(B_{\mathrm{E}} - A_{\mathrm{E}}\zeta_{\mathrm{O}}\right)y_{\mathrm{P}} + \left(A_{\mathrm{A}}\zeta_{\mathrm{O}} - B_{\mathrm{A}}\right)B_{\mathrm{B}}^{-1}y_{\mathrm{R}}\,. \tag{5.3.3}$$

Equation 5.3.3 gives us the transverse position of the object point y_{O} at $\mathrm{T_O}$ of the ray through the pupil at transverse position y_{P} arriving at a position y_{R} on the retina.

Simplification when a pinhole is used

Similar to the scenario in Section 5.2.3, the transverse position of an object point at a finite distance in front of the eye simplifies when a pinhole is positioned immediately upstream of the corneal tear film. Equation 5.3.3 becomes

$$y_{\mathrm{O}} = \left(1 - B_{\mathrm{E}}^{-1}A_{\mathrm{E}}\zeta_{\mathrm{O}}\right)y_{\mathrm{P}} + \zeta_{\mathrm{O}}B_{\mathrm{E}}^{-1}y_{\mathrm{R}}\,. \tag{5.3.4}$$

5.3.2 Incident inclination measured in object space

We again turn our attention to Figure 5.2.1 and accompanying Equations 5.2.10 to 19. We wish to calculate the inclination in object space, a_{O} as a function of the ray, going through the pupil at y_{P} and reaching the retina at transverse position y_{R}. We solve Equation 5.2.15 for y_{O} to obtain

$$y_{\mathrm{O}} = A_{\mathrm{OA}}^{-1}y_{\mathrm{P}} - A_{\mathrm{OA}}^{-1}B_{\mathrm{OA}}\alpha_{\mathrm{O}} \tag{5.3.5}$$

which we substitute into Equation 5.2.16:

$$C_{\mathrm{OA}}A_{\mathrm{OA}}^{-1}y_{\mathrm{P}} - C_{\mathrm{OA}}A_{\mathrm{OA}}^{-1}B_{\mathrm{OA}}\alpha_{\mathrm{O}} + D_{\mathrm{OA}}\alpha_{\mathrm{O}} = \alpha_{\mathrm{P}}\,. \tag{5.3.6}$$

We now substitute from Equation 5.3.1 into Equation 5.3.6, simplify for A_{OA} and C_{OA} from Equation 5.2.11 and rearrange to obtain

$$\left(D_{\mathrm{OA}} - C_{\mathrm{OA}}A_{\mathrm{OA}}^{-1}B_{\mathrm{OA}}\right)\alpha_{\mathrm{O}} = -\left(B_{\mathrm{B}}^{-1}A_{\mathrm{B}} + C_{\mathrm{A}}A_{\mathrm{A}}^{-1}\right)y_{\mathrm{P}} + B_{\mathrm{B}}^{-1}y_{\mathrm{R}}\,. \tag{5.3.7}$$

Substituting the fourth Schur compliment (Equation 3.2.23) and equalities from Equations 5.2.10 into Equation 5.3.7 we obtain

$$A_{\mathrm{A}}^{-1}\alpha_{\mathrm{O}} = -B_{\mathrm{B}}^{-1}A_{\mathrm{E}}A_{\mathrm{A}}^{-1}y_{\mathrm{P}} + B_{\mathrm{B}}^{-1}y_{\mathrm{R}}$$

and, hence,

$$\alpha_{\mathrm{O}} = -B_{\mathrm{B}}^{-1}A_{\mathrm{E}}y_{\mathrm{P}} + A_{\mathrm{A}}B_{\mathrm{B}}^{-1}y_{\mathrm{R}}\,. \tag{5.3.8}$$

While there is an infinity of rays radiating from an object point, this equation singles out the reduced inclination of a single ray from an object point as a function of position in the pupil and at the retina. However, we need to calculate the equation for the unreduced inclination and so Equation 5.3.8 becomes

$$a_{\mathrm{O}} = -\left(n_0 B_{\mathrm{B}}\right)^{-1} A_{\mathrm{E}} y_{\mathrm{P}} + A_{\mathrm{A}} \left(B_{\mathrm{B}} n_0\right)^{-1} y_{\mathrm{R}} . \qquad (5.3.9)$$

Equation 5.3.9 gives the incident inclination of a ray, traversing a specific point in the pupil y_{P}, that will reach the retina at a predetermined transverse position y_{R}. The position through the pupil y_{P} may be chosen to be the chief ray where $y_{\mathrm{P}} = 0$; however the equation is general and any position can be chosen. For obvious reasons, the reduced working distance ζ_{O} and the transverse position y_{O} are both eliminated, implying that a_{O} is a more inclusive parameter to work with than the combination of y_{O} and ζ_{O}.

Simplification when a pinhole is used

The incident inclination from a finite object point to a position at the retina when a pinhole is placed immediately in front of the eye enables us to simplify Equation 5.3.9 to

$$a_{\mathrm{O}} = -\left(n_0 B_{\mathrm{E}}\right)^{-1} A_{\mathrm{E}} y_{\mathrm{P}} + \left(n_0 B_{\mathrm{E}}\right)^{-1} y_{\mathrm{R}} . \qquad (5.3.10)$$

Substituting from Equation 3.4.6 for the corneal-plane refractive compensation F_0 we see that the relationship in Equation 5.3.10 represents

$$a_{\mathrm{O}} = -n_0^{-1} F_0 y_{\mathrm{P}} + \left(n_0 B_{\mathrm{E}}\right)^{-1} y_{\mathrm{R}} . \qquad (5.3.11)$$

We mention in passing that for an emmetropic eye

$$a_{\mathrm{O}} = \left(n_0 B_{\mathrm{E}}\right)^{-1} y_{\mathrm{R}}$$

and the effect of the transverse position of the pinhole y_{P} in front of the emmetropic eye is nullified.

5.3.3 Summary of object space matrix equations with respect to position on the retina

Equations 5.3.3 and 9 are the two matrix equations that determine the incident transverse position and inclination that will result in the ray arriving at

the retina at a specific transverse position. Similarly to Section 3.5.3, we can summarise them as

$$\begin{pmatrix} B_{\mathrm{B}}^{-1}\left(B_{\mathrm{E}}-A_{\mathrm{E}}\zeta_{\mathrm{O}}\right) & \left(A_{\mathrm{A}}\zeta_{\mathrm{O}}-B_{\mathrm{A}}\right)B_{\mathrm{B}}^{-1} \\ -\left(n_0 B_{\mathrm{B}}\right)^{-1}A_{\mathrm{E}} & A_{\mathrm{A}}\left(B_{\mathrm{B}}n_0\right)^{-1} \end{pmatrix}\begin{pmatrix} y_{\mathrm{P}} \\ y_{\mathrm{R}} \end{pmatrix}=\begin{pmatrix} y_{\mathrm{O}} \\ a_{\mathrm{O}} \end{pmatrix} \tag{5.3.12}$$

which we shall abbreviate to

$$\mathbf{V}_{\mathrm{Oy}}\mathbf{v}_{\mathrm{Oy}}=\mathbf{r}_{\mathrm{O}} \tag{5.3.13}$$

where the subscript Oy indicates measurements that are made at a finite distance in front of the eye. $\mathbf{V}_{\mathrm{Oy}}$ is the coefficient matrix defined as

$$\mathbf{V}_{\mathrm{Oy}}=\begin{pmatrix} B_{\mathrm{B}}^{-1}\left(B_{\mathrm{E}}-A_{\mathrm{E}}\zeta_{\mathrm{O}}\right) & \left(A_{\mathrm{A}}\zeta_{\mathrm{O}}-B_{\mathrm{A}}\right)B_{\mathrm{B}}^{-1} \\ -\left(n_0 B_{\mathrm{B}}\right)^{-1}A_{\mathrm{E}} & A_{\mathrm{A}}\left(B_{\mathrm{B}}n_0\right)^{-1} \end{pmatrix}=\begin{pmatrix} W_{\mathrm{Oy}} & X_{\mathrm{Oy}} \\ Y_{\mathrm{Oy}} & Z_{\mathrm{Oy}} \end{pmatrix}, \tag{5.3.14}$$

$$\mathbf{v}_{\mathrm{Oy}}=\begin{pmatrix} y_{\mathrm{P}} \\ y_{\mathrm{R}} \end{pmatrix} \tag{5.3.15}$$

is the input vector and $\mathbf{r}_{\mathrm{O}}$ is the physical (unreduced) ray state at the object transverse plane T_{O} defined as

$$\mathbf{r}_{\mathrm{O}}=\begin{pmatrix} y_{\mathrm{O}} \\ a_{\mathrm{O}} \end{pmatrix}. \tag{5.3.16}$$

From Equation 5.3.12 we summarise Equations 5.3.3 and 9 as

$$y_{\mathrm{O}}=W_{\mathrm{Oy}}y_{\mathrm{P}}+X_{\mathrm{Oy}}y_{\mathrm{R}} \tag{5.3.17}$$

and

$$a_{\mathrm{O}}=Y_{\mathrm{Oy}}y_{\mathrm{P}}+Z_{\mathrm{Oy}}y_{\mathrm{R}}. \tag{5.3.18}$$

Simplification when pinhole is used

Similar to Section 5.2.4, we can summarise Equations 5.3.4 and 10 in the form given in Equation 5.3.14 for a system comprising an eye, given a specific position or inclination of an object point a finite distance upstream of the eye, to obtain the transverse position at the retina when a pinhole is held immediately in front of the corneal tear film. Equation 5.3.12 simplifies to

$$\begin{pmatrix} 1-B_{\mathrm{E}}^{-1}A_{\mathrm{E}}\zeta_{\mathrm{O}} & \zeta_{\mathrm{O}}B_{\mathrm{E}}^{-1} \\ -\left(n_0 B_{\mathrm{E}}\right)^{-1}A_{\mathrm{E}} & \left(n_0 B_{\mathrm{E}}\right)^{-1} \end{pmatrix}\begin{pmatrix} y_{\mathrm{P}} \\ y_{\mathrm{R}} \end{pmatrix}=\begin{pmatrix} y_{\mathrm{O}} \\ a_{\mathrm{O}} \end{pmatrix} \tag{5.3.19}$$

which we summarise as

$$\mathbf{V}_{\mathrm{Oy}}^{\mathrm{P}}\mathbf{v}_{\mathrm{Oy}} = \mathbf{r}_{\mathrm{O}} \tag{5.3.20}$$

and similar to Equation 5.2.34 the coefficient matrix in Equation 5.3.20 is given a superscript P to indicate the use of a pinhole immediately in front of the corneal tear film.

Comment on $\mathbf{V}_{\mathrm{Oy}}$ *and* $\mathbf{V}_{\mathrm{Oy}}^{\mathrm{P}}$

We need to consider for a moment the existence of $\mathbf{V}_{\mathrm{Oy}}$ and $\mathbf{V}_{\mathrm{Oy}}^{\mathrm{P}}$. We can see from Equation 5.3.12 that they exist provided $B_{\mathrm{B}} \neq 0$, or in the case of a pinhole in front of the eye (Equation 5.3.19), where $B_{\mathrm{E}} \neq 0$. The equations hold except in the unlikely situation in which the aperture and the retina are conjugate.

5.3.4 Summary of object space matrix equations with respect to inclination at the retina

When measurements are taken in object space and the corresponding images are perceived to be in alignment by the subject's eye, the physiological optics theory is that the two image points coincide on the retina. That is to say, the rays arrive at the retina at the same transverse position. In the literature review, there was no evidence of any theories that aligned the inclination at the retina from two object points, only the transverse position on the retina. Therefore we conclude that the derivations in object space with respect to transverse position at the retina are considered to be more important than those with respect to inclination at the retina.

Similar to the matrix equations derived in Section 5.3.3 which were obtained with respect to a position at the retinal plane, we can derive equations with respect to the inclination of a ray arriving at the retina. This has implications for the Stiles-Crawford effect. For completeness the summary of these formulae are given in Equations 5.3.21 and 22 below. It is quite possible for two rays of different frequency to arrive at the retina with the same inclination, but may or may not arrive at the same position. The exact implications of this are outside the scope of this dissertation.

The equation for the physical state of a ray $\mathbf{r}_{\mathrm{O}}$ at the object plane in order for that ray traversing the pupil at transverse position y_{P} to arrive at the retina with a certain emergent inclination a_{R} is

$$\begin{pmatrix} (D_{\mathrm{E}} - C_{\mathrm{E}}\zeta_{\mathrm{O}})D_{\mathrm{B}}^{-1} & n(A_{\mathrm{A}}\zeta_{\mathrm{O}} - B_{\mathrm{A}})D_{\mathrm{B}}^{-1} \\ -C_{\mathrm{E}}(D_{\mathrm{B}}n_0)^{-1} & nA_{\mathrm{A}}(D_{\mathrm{B}}n_0)^{-1} \end{pmatrix} \begin{pmatrix} y_{\mathrm{P}} \\ a_{\mathrm{R}} \end{pmatrix} = \begin{pmatrix} y_{\mathrm{O}} \\ a_{\mathrm{O}} \end{pmatrix} \tag{5.3.21}$$

or

$$\mathbf{V}_{\mathrm{Oa}}\mathbf{v}_{\mathrm{Oa}} = \mathbf{r}_{\mathrm{O}}. \tag{5.3.22}$$

Simplification when pinhole is used

Similar to Section 5.2.4 we can summarise for a system comprising an eye, given a specific position or inclination of an object point a finite distance upstream of the eye, to obtain the inclination at the retina when a pinhole is held immediately in front of the corneal tear film. Equation 5.3.21 simplifies to

$$\begin{pmatrix} (D_{\mathrm{E}} - C_{\mathrm{E}}\zeta_{\mathrm{O}})D_{\mathrm{E}}^{-1} & \zeta_{\mathrm{O}}D_{\mathrm{E}}^{-1}n \\ -C_{\mathrm{E}}(D_{\mathrm{E}}n_0)^{-1} & (D_{\mathrm{E}}n_0)^{-1}n \end{pmatrix} \begin{pmatrix} y_{\mathrm{P}} \\ a_{\mathrm{R}} \end{pmatrix} = \begin{pmatrix} y_{\mathrm{O}} \\ a_{\mathrm{O}} \end{pmatrix} \tag{5.3.23}$$

or

$$\mathbf{V}_{\mathrm{Oa}}^{\mathrm{P}}\mathbf{v}_{\mathrm{Oa}} = \mathbf{r}_{\mathrm{O}}. \tag{5.3.24}$$

Comment on $\mathbf{V}_{\mathrm{Oa}}$ *and* $\mathbf{V}_{\mathrm{Oa}}^{\mathrm{P}}$

The relationships derived in Equation 5.3.21 and 23 exist provided $D_B \neq 0$ or $D_E \neq 0$ in the case of a pinhole in front of the system. This would require the system to be entrance-plane focal which seems unlikely in a system comprising an eye and in most eyes D_B and D_E are close to 1.

5.3.5 Generalising to linear optics

The proofs provided in Section 5.3 involve the use of division and Schur compliments whilst at the same time ignoring the order of multiplication and the transpose. Therefore the results cannot be readily generalized to linear optics. However, the resultant generalised coefficient matrices are provided below, without detailed proofs. Equation 5.3.14 becomes

$$\mathbf{V}_{\mathrm{Oy}} = \begin{pmatrix} \left(\mathbf{B}_{\mathrm{A}} - \mathbf{A}_{\mathrm{A}}\zeta_{\mathrm{O}}\right)^{\mathrm{T}}\mathbf{B}_{\mathrm{B}}^{-1}\left(\mathbf{B}_{\mathrm{E}} - \mathbf{A}_{\mathrm{E}}\zeta_{\mathrm{O}}\right)\left(\mathbf{B}_{\mathrm{A}} - \mathbf{A}_{\mathrm{A}}\zeta_{\mathrm{O}}\right)^{-1} & \left(\mathbf{A}_{\mathrm{A}}\zeta_{\mathrm{O}} - \mathbf{B}_{\mathrm{A}}\right)^{\mathrm{T}}\mathbf{B}_{\mathrm{B}}^{-1} \\ -\mathbf{A}_{\mathrm{A}}^{\mathrm{T}}\left(n_0\mathbf{B}_{\mathrm{B}}\right)^{-1}\mathbf{A}_{\mathrm{E}}\mathbf{A}_{\mathrm{A}}^{-1} & \mathbf{A}_{\mathrm{A}}^{\mathrm{T}}\left(\mathbf{B}_{\mathrm{B}}n_0\right)^{-1} \end{pmatrix}$$

$$= \begin{pmatrix} \mathbf{W}_{\mathrm{Oy}} & \mathbf{X}_{\mathrm{Oy}} \\ \mathbf{Y}_{\mathrm{Oy}} & \mathbf{Z}_{\mathrm{Oy}} \end{pmatrix}. \qquad (5.3.25)$$

Equations 5.3.13, 15, 19 and 20 readily generalise to linear optics. Specifically, Equation 5.3.19 becomes

$$\begin{pmatrix} \mathbf{I} - \mathbf{B}_{\mathrm{E}}^{-1}\mathbf{A}_{\mathrm{E}}\zeta_{\mathrm{O}} & \zeta_{\mathrm{O}}\mathbf{B}_{\mathrm{E}}^{-1} \\ -\left(n_0\mathbf{B}_{\mathrm{E}}\right)^{-1}\mathbf{A}_{\mathrm{E}} & \left(n_0\mathbf{B}_{\mathrm{E}}\right)^{-1} \end{pmatrix}\begin{pmatrix} \mathbf{y}_{\mathrm{P}} \\ \mathbf{y}_{\mathrm{R}} \end{pmatrix} = \begin{pmatrix} \mathbf{y}_{\mathrm{O}} \\ \mathbf{a}_{\mathrm{O}} \end{pmatrix}. \qquad (5.3.26)$$

5.4 Cardinal points

The simplification made in ray tracing using the cardinal points relates the conjugal relationship between an object point and its image point but does not reveal what is actually happening inside the system. Linear optics makes no use of cardinal points for its calculations and is true paraxial ray tracing through the system.

5.4.1 Additional relationships among the points

In Section 3.6.3 we looked at the relationships among the cardinal points including the anti-cardinal points. We wish to extend these relationships and attempt to find simpler equations to represent the distances of the points from the entrance and exit plane and between the various points. The symbols used here are consistent with those introduced in Section 3.6.2 and Table 3.6.1.

Starting with the incident anti-cardinal points we find the equation for the distance from the entrance plane to the respective point can simplify further from the equalities given in Equations 3.6.3 and 4 to

$$z_{\bar{\mathrm{N}}0} = n_0C^{-1}D + nC^{-1} = z_{\mathrm{F}0} + nC^{-1}, \qquad (5.4.1)$$

$$z_{\bar{\mathrm{P}}0} = n_0C^{-1}D + n_0C^{-1} = z_{\mathrm{F}0} + n_0C^{-1} \qquad (5.4.2)$$

and similarly the equations for the distance of each emergent anti-cardinal point from the exit plane to the respective anti-cardinal point simplify from Equations 3.6.8 and 9 to

$$z_{\bar{\mathrm{N}}} = -nC^{-1}A - n_0C^{-1} = z_{\mathrm{F}} - n_0C^{-1} \qquad (5.4.3)$$

and

$$z_{\bar{\mathrm{P}}} = -nC^{-1}A - nC^{-1} = z_{\mathrm{F}} - nC^{-1}. \tag{5.4.4}$$

There are a number of relationships among the various cardinal and anti-cardinal points which are presented in summary in Equations 5.4.5 to 11 and corresponding to Figure 5.4.1. For completeness, we include the equalities given in Equations 3.6.13 to 16 and add additional equalities which include those that extend to the anti-cardinal points in Equations 5.4.5 to 8. We retain the symbolism introduced in Table 3.6.1. The equalities are illustrated in Figure 5.4.1 and the corresponding arrow colour is given in brackets for each. The incident equivalent focal length (blue) is therefore

$$f_{0eq} = \mathrm{P}_0\mathrm{F}_0 = \mathrm{FN} = \mathrm{F}_0\bar{\mathrm{P}}_0 = \bar{\mathrm{N}}\mathrm{F} = n_0C^{-1} \tag{5.4.5}$$

and similarly, the emergent equivalent focal length (orange) is

$$f_{eq} = \mathrm{PF} = \mathrm{F}_0\mathrm{N}_0 = \bar{\mathrm{N}}_0\mathrm{F}_0 = \mathrm{F}\bar{\mathrm{P}} = -nC^{-1}. \tag{5.4.6}$$

Pascal's (1950a, b) equalities for "equivalent" radius (green) and "thickness" (red) can be extended to

$$r_{eq} = \mathrm{P}_0\mathrm{N}_0 = \mathrm{PN} = \bar{\mathrm{N}}_0\bar{\mathrm{P}}_0 = \bar{\mathrm{N}}\bar{\mathrm{P}} = (n_0 - n)C^{-1} = f_{0eq} + f_{eq}, \tag{5.4.7}$$

and

$$\mathrm{z}_{eq} = \mathrm{P}_0\mathrm{P} = \mathrm{N}_0\mathrm{N} = z + z_{\mathrm{F}} - z_{\mathrm{F}0} + (n_0 + n)C^{-1} = z + z_{\mathrm{F}} - z_{\mathrm{F}0} + f_{0eq} - f_{eq} \tag{5.4.8}$$

respectively. We now derive some equalities involving the anti-cardinal points (violet)

$$\bar{\mathrm{P}}_0\bar{\mathrm{P}} = \bar{\mathrm{N}}_0\bar{\mathrm{N}} = z + z_{\mathrm{F}} - z_{\mathrm{F}0} - (n + n_0)C^{-1} = z + z_{\mathrm{F}} - z_{\mathrm{F}0} + f_{eq} - f_{0eq}. \tag{5.4.9}$$

From the above equalities we can also see (−2*blue)

$$\bar{\mathrm{P}}_0\mathrm{P}_0 = \mathrm{N}\bar{\mathrm{N}} = -2f_{0eq} \tag{5.4.10}$$

and (2*orange)

$$\bar{\mathrm{N}}_0\mathrm{N}_0 = \mathrm{P}\bar{\mathrm{P}} = 2f_{eq}. \tag{5.4.11}$$

For completeness and to compare to some of the above equalities we note that, while the incident to the emergent focal points (cyan) are not conjugate with each other, the distance from F_0 to F is

$$\mathrm{F}_0\mathrm{F} = z + z_{\mathrm{F}} - z_{\mathrm{F}0}. \tag{5.4.12}$$

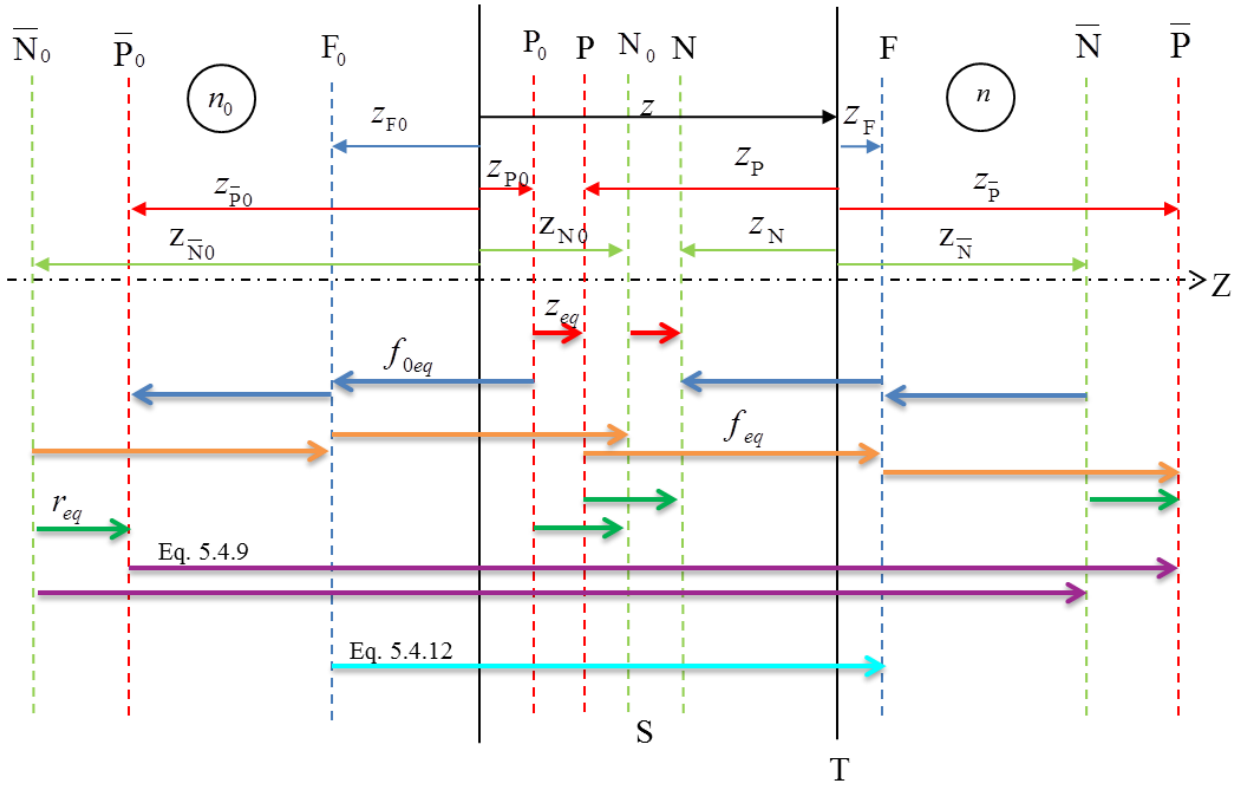

Figure 5.4.1 Cardinal points and their relationships and equalities. General Gaussian system S of length *z* has an entrance plane T_0, an exit plane T and a longitudinal axis Z. Refractive index upstream n_0 is different from *n* downstream. Points are defined as being on the optical axis for a Gaussian system. The distances from the entrance plane to the incident cardinal point and from the exit plane to the emergent cardinal point are shown in the section above the longitudinal axis, with the thin arrows. All the symbols and subscripts are given in Table 3.6.1. The equalities are shown below the longitudinal axis as follows: the equivalent "thickness" z_{eq} (red), incident equivalent focal length f_{0eq} (blue), emergent equivalent length f_{eq} (orange), equivalent radius of curvature r_{eq} (green), Equation 5.4.9 (violet) and Equation 5.4.12 (cyan). Equation 5.4.10 (blue) and 11 (orange) can also be seen from the diagram.

Symmetry points

In Section 3.6.2, we saw that Keating defines symmetry points as the case where lateral magnification is –1. This occurs when the object is at twice the incident equivalent focal length and the image is at twice the emergent equivalent focal length, which we can see from Equations 5.4.10 and 11, respectively. From Figure 5.4.1 this is quite clearly at the position of the incident and emergent anti-principal points.

In order to prove this statement, we need to prove that, firstly, the incident and emergent anti-principal planes are conjugate and secondly, the magnification is –1. We start by obtaining the transference of the compound system from $\overline{\mathrm{P}}_0$ to $\overline{\mathrm{P}}$ as follows

$$\mathbf{S}_{\overline{\mathrm{P}}}\mathbf{S}\mathbf{S}_{\overline{\mathrm{P}}_0} = \begin{pmatrix} 1 & \frac{z_{\overline{\mathrm{P}}}}{n} \\ 0 & 1 \end{pmatrix} \begin{pmatrix} A & B \\ C & D \end{pmatrix} \begin{pmatrix} 1 & \frac{-z_{\overline{\mathrm{P}}_0}}{n_0} \\ 0 & 1 \end{pmatrix}.$$

Substituting from Equations 3.6.4 and 9 we obtain

$$\mathbf{S}_{\overline{\mathrm{P}}}\mathbf{S}\mathbf{S}_{\overline{\mathrm{P}}_0} = \begin{pmatrix} 1 & -\frac{A+1}{C} \\ 0 & 1 \end{pmatrix} \begin{pmatrix} A & B \\ C & D \end{pmatrix} \begin{pmatrix} 1 & -\frac{D+1}{C} \\ 0 & 1 \end{pmatrix}.$$

Multiplying out and substituting from the symplectic equation (Equation 3.2.24) we obtain

$$\mathbf{S}_{\overline{\mathrm{P}}}\mathbf{S}\mathbf{S}_{\overline{\mathrm{P}}_0} = \begin{pmatrix} -1 & 0 \\ C & -1 \end{pmatrix}.$$

From the definition of a conjugate system (Section 3.3.2) we see that this compound system is conjugate and secondly from Equation 5.2.1 we can see that transverse magnification has negative unit magnification ($M_{\mathrm{t}} = A = -1$).

Conjugacy of the anti-nodal planes

Similarly, we can show that the transference of the compound system from the incident to emergent anti-nodal planes is

$$\mathbf{S}_{\overline{\mathrm{N}}}\mathbf{S}\mathbf{S}_{\overline{\mathrm{N}}_0} = \begin{pmatrix} -\frac{n_0}{n} & 0 \\ C & -\frac{n}{n_0} \end{pmatrix},$$

which confirms that the two planes are conjugate and the transverse magnification is $-\frac{n_0}{n}$.

The lengths and directions of each of the incident and emergent cardinal and anti-cardinal points are shown in Figure 5.4.1 in the section above the optical axis. Lengths are given as *z* with subscripts given in Table 3.6.1. Below the

longitudinal axis, the thicker arrows denote the equalities. From Figure 5.4.1, the equalities given in Equations 3.6.13 to 16 and 5.4.5 to 12 can be seen.

5.4.2 Graphical construction, locator lines and anti-cardinal points

In Section 3.6.4 we saw how to obtain the slope and position of the incident and emergent locator lines and to use these to obtain the six cardinal points. We now expand this method to obtain the positions of the four anti-cardinal points. To find the location of the incident anti-cardinal points along the optical axis, one draws a horizontal line at the value for the characteristic X in T_0 (from Table 3.6.1) and where it intersects the incident locator line L_0 one constructs a vertical line to intersect with Z which is the position of the respective incident anti-cardinal point. Similarly, for the emergent anti-cardinal points, one

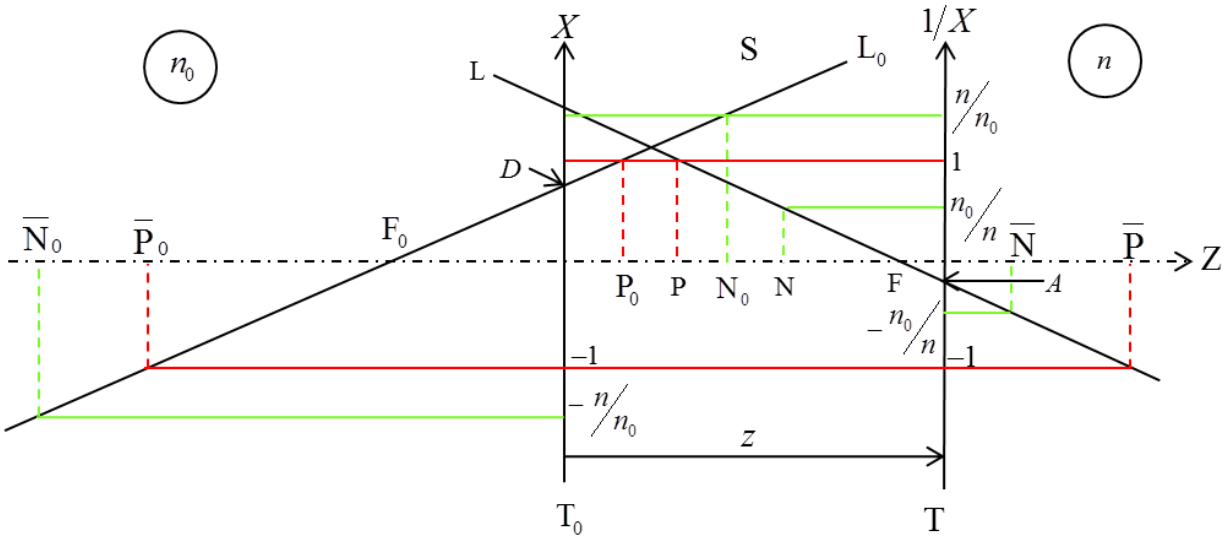

Figure 5.4.2 Graphical representation of a Gaussian optical system showing the locator lines for system S (not to scale). Line L_0 represents Equation 3.6.20 and line L Equation 3.6.21. Axis X is superimposed on entrance plane T_0 and axis $1/X$ on exit plane T, a distance z downstream from T_0. The focal points are on the optical axis Z at intersection with the corresponding locator line. The principal and anti-principal points are shown in red and the nodal and anti-nodal points in green. All symbols are described in Table 3.6.1. All incident points show intersection with the incident locator line and have subscript 0, while the emergent points intersect the emergent locator line L with no subscript.

draws a horizontal line for the value of $\frac{1}{X}$ in T and constructs a vertical line from the intersection with the emergent locator line L to Z.

From Figure 5.4.2 we note that the values of X and $1/X$ are positive for the cardinal points and negative for the anti-cardinal points. The construction is simple enough to be drawn by hand, however the scales on the axes have to be drawn accurately and for a system that includes an eye the scale on the vertical axis needs to be exaggerated. Numerical examples are given in Appendix 1.

5.4.3 Pascal's ring and anti-cardinal points

In Section 3.6.5 we saw how Pascal (1939, 1947, 1950a, b) described a memory scheme as an aid to memorizing the equalities between the six cardinal points. Harris (2011a) extended Pascal's ring and gave the equalities direction and gave proofs for the equalities. Here we extend Pascal's ring further to include the four anti-cardinal points.

In Figure 5.4.1 we see the relationships among the six cardinal points as well as the four anti-cardinal points. In Figure 5.4.3 we see Pascal's ring extended to include the equalities and relationships among the cardinal and anti-cardinal points. We retain Pascal's guideline that distances represented by parallel lines are equal.

The relationships among the cardinal and anti-cardinal points are illustrated in Figure 5.4.3. For example, the four blue arrows represent equal distances given by Equation 5.4.5 each representing $-f_{0eq}$. Equation 5.4.10 shows the equality $\overline{\mathrm{P}}_0\mathrm{P}_0 = \mathrm{N}\overline{\mathrm{N}} = -2f_{0eq}$ for two consecutive blue arrows. Similarly for the orange arrows and f_{eq}. The other colours represent red z_{eq}, green r_{eq} and violet the distance between incident and emergent anti-nodal or anti-principal points. This emphasises what can be seen in Figure 5.4.1. If we consider any one of the green arrows (r_{eq}), we can see that this is equivalent to an orange arrow (f_{eq}) minus a blue arrow ($-f_{0eq}$), which is given in Equation 5.4.7. One final example is to follow the violet arrow from which we can see that this makes up a combination of two orange, one red and two blue arrows. Any

such combination of equalities can be traced by following the arrows in Pascal's ring.

However the power of Pascal's ring lies not only in its use as a memory schema, but also in its ability to show changes in the positions of the points with respect to each other. Because Pascal's ring is not drawn to scale, the movements of the positions of the points are "magnified" and one is able to see how the changes to the system affect the locations of the points.

In order to gain a better understanding of the data, a number of familiar changes in the eye are demonstrated using the Bennett and Rabbetts schematic eye (Rabbetts, 2007: 225). These four numerical examples are given in Appendix 1. The example compares an emmetropic (relaxed) eye with a myopic eye and a hyperopic eye for changes in, firstly, axial length and, secondly, corneal curvature. The third example compares the emmetropic eye to changes due to accommodation and finally a young emmetropic eye is compared to its elderly counterpart. The first two changes are simple changes while the second two are compound changes. Refractive compensation does not form part of this study.

The purpose of the examples is to gain an understanding of the changes in the cardinal and anti-cardinal points arising because of various changes in a system, in particular, using the two models that we have just discussed, graphical construction and Pascal's ring. The examples should facilitate insight into the

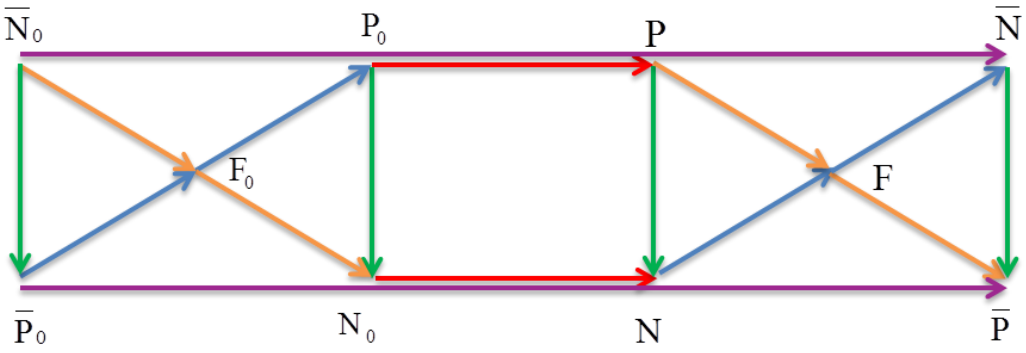

Figure 5.4.3 Pascal's ring showing the equalities and their directions and extended to include the anti-cardinal points. Arrows that are the same colour are equal in length and are either parallel or follow the same direction. The same colour-coding has been maintained as in Figure 5.4.1. Equations 5.4.5 to 12 give the equalities and formulae from the transference. The direction of the blue arrow has been reversed to represent $-f_{0eq}$.

changes in the cardinal points that occur in the eye due to change in the frequency of light, which will be examined in Section 9.1, using the two models.

5.5 Transferences of the two model eyes

The reduced eye is a simple eye and to derive its transference is a simple task because it is the product of only two elementary transferences. The transference of the reduced eye is then obtained using the parameters originally given by Emsley (Section 4.1.3), showing it to be emmetropic. However, we are interested in the dependence of the properties of the two model eyes on the frequency of light and so the transference of the reduced eye is derived as a function of the refractive index of the medium.

Le Grand's eye, on the other hand, is a four-surface eye and its transference is the product of eight elementary transferences. We therefore separate the derivation into anterior and posterior sub-systems, but deriving a single expression for the transference is impractical because the product does not simplify. Similarly, deriving a single expression for the transference for Le Grand's eye as a function of refractive index meets with the same difficulty; there are four media, each with a different refractive index. The transference is calculated for Le Grand's eye using his original parameters and refractive indices and is shown to be emmetropic.

5.5.1 The transference of the reduced eye

To calculate the transference for Emsley's reduced eye, one makes use of Equations 3.2.36 and 37 which we multiply in reverse to obtain the formula for the transference of the reduced eye

$$\mathbf{S}=\begin{pmatrix} 1-\dfrac{z}{n}\left(\dfrac{n-n_0}{r}\right) & \dfrac{z}{n} \\ \dfrac{n-n_0}{-r} & 1 \end{pmatrix}. \qquad (5.5.1)$$

We substitute the values for Emsley's reduced eye given in Section 4.1.3 to obtain the transference of the emmetropic reduced eye

$$\mathbf{S} = \begin{pmatrix} 0 & \frac{50}{3}\,\text{mm} \\ -0.060\,\text{kD} & 1 \end{pmatrix}. \qquad (5.5.2)$$

It is apparent that because $A = 0$ that this is an exit-plane focal system and that the eye is emmetropic with a power of 60 D. Furthermore it has a reduced length of 50/3 mm (or 1/60 m). Divarication *D* is 1 for a reduced eye.

5.5.2 The transference of the reduced eye as a function of refractive index

The variable affected by frequency of light is the refractive index *n*. We substitute the radius of curvature and length of Emsley's reduced eye into Equation 5.5.1 and simplify to obtain the transference for the reduced eye (Evans and Harris, 2011)

$$\mathbf{S} = \begin{pmatrix} \frac{4n_0}{n} - 3 & \frac{200}{9n}\,\text{mm} \\ -\frac{9}{50}(n - n_0)\,\text{kD} & 1 \end{pmatrix} \qquad (5.5.3)$$

where n_0 is the refractive index of air and *n* is the refractive index of the reduced eye. *n* is calculated using Equation 4.4.2. From Equation 5.5.3 we see that dilation *A*, disjugacy *B* and divergence *C* each depend on frequency. The refractive index of the surrounding medium n_0 has an effect only on *A* and *C*. The divarication *D* is constant and equals 1 for all reduced eyes.

5.5.3 The transference of Le Grand's eye

To obtain the transference of Le Grand's eye we substitute from Equations 3.2.36 and 37 as is appropriate and then multiplying in reverse according to Equation 3.2.6. We determine the transference for the anterior and posterior sub-systems and then the transference for the eye itself. The subscripts given correspond to those given in Figure 4.1.2 and Table 4.1.1. Starting with the anterior sub-system (A) we obtain

$$\mathbf{S}_{\text{A}} = \mathbf{S}_{\text{Aq}}\mathbf{S}_{\text{K2}}\mathbf{S}_{\text{K}}\mathbf{S}_{\text{K1}} \qquad (5.5.4)$$

and hence

$$\mathbf{S}_{\mathrm{A}} = \begin{pmatrix} 1 & \frac{z_{\mathrm{Aq}}}{n_{\mathrm{Aq}}} \\ 0 & 1 \end{pmatrix} \begin{pmatrix} 1 & 0 \\ \frac{n_{\mathrm{Aq}} - n_{\mathrm{K}}}{-r_{\mathrm{K2}}} & 1 \end{pmatrix} \begin{pmatrix} 1 & \frac{z_{\mathrm{K}}}{n_{\mathrm{K}}} \\ 0 & 1 \end{pmatrix} \begin{pmatrix} 1 & 0 \\ \frac{n_{\mathrm{K}} - n_0}{-r_{\mathrm{K1}}} & 1 \end{pmatrix}. \tag{5.5.5}$$

Similarly we derive the formula for the posterior sub-system (B)

$$\mathbf{S}_{\mathrm{B}} = \mathbf{S}_{\mathrm{V}}\mathbf{S}_{\mathrm{L2}}\mathbf{S}_{\mathrm{L}}\mathbf{S}_{\mathrm{L1}}, \tag{5.5.6}$$

and

$$\mathbf{S}_{\mathrm{B}} = \begin{pmatrix} 1 & \frac{z_{\mathrm{V}}}{n_{\mathrm{V}}} \\ 0 & 1 \end{pmatrix} \begin{pmatrix} 1 & 0 \\ \frac{n_{\mathrm{V}} - n_{\mathrm{L}}}{-r_{\mathrm{L2}}} & 1 \end{pmatrix} \begin{pmatrix} 1 & \frac{z_{\mathrm{L}}}{n_{\mathrm{L}}} \\ 0 & 1 \end{pmatrix} \begin{pmatrix} 1 & 0 \\ \frac{n_{\mathrm{L}} - n_{\mathrm{Aq}}}{-r_{\mathrm{L1}}} & 1 \end{pmatrix}. \tag{5.5.7}$$

We can now obtain the transference of Le Grand's eye as

$$\mathbf{S} = \mathbf{S}_{\mathrm{B}}\mathbf{S}_{\mathrm{A}}. \tag{5.5.8}$$

This can also be formulated in one step as

$$\mathbf{S} = \mathbf{S}_{\mathrm{V}}\mathbf{S}_{\mathrm{L2}}\mathbf{S}_{\mathrm{L}}\mathbf{S}_{\mathrm{L1}}\mathbf{S}_{\mathrm{Aq}}\mathbf{S}_{\mathrm{K2}}\mathbf{S}_{\mathrm{K}}\mathbf{S}_{\mathrm{K1}}. \tag{5.5.9}$$

This is the general transference of any four-surface schematic eye.

To calculate the transference for Le Grand's eye we substitute the values from Table 4.1.1 into Equation 5.5.9 and then multiplying out we obtain

$$\mathbf{S} = \begin{pmatrix} 0 & 16.6832\ \mathrm{mm} \\ -0.0599\ \mathrm{kD} & 0.9044 \end{pmatrix}. \tag{5.5.10}$$

That $A = 0$ implies an emmetropic eye. Its power is 59.9404D which is the same as given by Le Grand (1945: 48).

5.5.4 The transference of Le Grand's eye as a function of refractive index

Calculating the transference of the Le Grand eye as a function of refractive index is somewhat more complicated and does not simplify like Equation 5.5.3 for the reduced eye. Therefore the transference for each frequency needs to be calculated using Equation 5.5.9 each time.

5.5.5 The refractive indices of the reduced eye and Le Grand's eye for the six reference frequencies

The numerical values for the refractive indices of each of the media for the six reference points are given in tabular form for both the reduced and Le Grand's

Table 5.5.1 **S**ix reference colours, their frequencies υ, vacuum wavelengths λ, refractive indices for the reduced eye using Thibos *et al*'s equation (Equation 4.4.2) and refractive indices for the four media for the Le Grand eye using the Villegas *et al* equations (Equation 4.4.3).

			Refractive Index				
Colour	υ	λ	Thibos	Villegas *et al* equations			
	THz	nm	*et al*	Cornea	Aqueous	Lens	Vitreous
Red	430	697.2	1.3302	1.3729	1.3325	1.4161	1.3327
Orange	494	606.9	1.3325	1.3757	1.3354	1.4191	1.3351
Yellow	558	537.3	1.3350	1.3786	1.3382	1.4225	1.3376
Green	622	482.0	1.3380	1.3817	1.3411	1.4261	1.3404
Blue	686	437.0	1.3416	1.3849	1.3442	1.4300	1.3433
Violet	750	399.7	1.3458	1.3883	1.3474	1.4339	1.3464

eyes in Table 5.5.1. The frequencies and corresponding wavelengths are given for each of the six reference points.

5.6 The Cayley transformed transference for Gaussian systems

In Section 3.7.2 we were introduced to a number of versions of the Cayley transform. In order to choose the right one (or more) for our purposes, we need to be clear about what those purposes and subsequent requirements are. The Cayley transform was introduced as a method to obtain the average of a number of optical systems. The primary interest in the ophthalmic optics literature is its statistical usefulness. Our interest in this study is different; we wish to obtain a vector space to illustrate the dependence of the Gaussian eye on the frequency of light. Hamiltonian matrices belong to the Lie algebra $\mathsf{sp}(n;\mathbb{R})$ which defines a linear space, while symplectic matrices of the Lie group $\mathsf{Sp}(n;\mathbb{R})$ do not. The Cayley transform will allow us to graphically represent the dependence of the eye on the frequency of light.

Returning our attention to the different versions of the Cayley transform in the literature we need to narrow down our choice to the Cayley transform that applies to the symplectic Hamiltonian mapping. Sanyal (2001: 60, 70-71) states that the Cayley transform map relates to Hamiltonian and symplectic matrices the

same way that it relates skew-symmetric matrices to orthogonal matrices, with the exception that the Hamiltonian and symplectic matrices need to be of the order $2n \times 2n$. This implies that any of the Cayley transforms given in Equations 3.7.10 to 13 can be used as a mapping between the Lie group $\mathsf{Sp}(n;\mathbb{R})$ and its Lie algebra $\mathsf{sp}(n;\mathbb{R})$. However, we need to ensure that if we start with a transference **S** and map it into Hamiltonian space ($\hat{\mathbf{S}}$) and then back again, the symplectic matrix returned needs to be the same matrix as **S** that we started out with. We also wish to consider more favourably the Cayley transform that is most likely to exist for transferences of the eye. Finally, it is convenient, as Bernstein (2009:208-209), Tsiotras, Junkins and Schaub (1997) and Sanyal (2001: 72) suggest, that the Cayley transform be its own functional inverse.

Let us start with existence. For Equations 3.7.10, 11 and 13 the inverse exists where the inverse of $\mathbf{I}+\mathbf{S}$ exists. For Equation 3.7.12 the requirement is that the inverse of $\mathbf{I}-\mathbf{S}$ must exist, where **S** is the transference of a system. Because it is conceivable that a transference may be the identity matrix, or approach the identity matrix, we will exclude Equation 3.7.12 as potentially problematic. It is foreseeable that the inverse of $(\mathbf{I}+\mathbf{S})$ should exist for transferences of eyes. The requirement for the Cayley transform of a Hamiltonian matrix to exist is similar and requires that the inverse of $(\mathbf{I}+\hat{\mathbf{S}})$ exists where $\hat{\mathbf{S}}$ is a Hamiltonian matrix.

For each version of the Cayley transform given in Equations 3.7.10 to 13 there exists an inverse. In the case of Equations 3.7.10 and 11, we see that the Cayley transform is its own functional inverse. The same is claimed of Equation 3.7.13. However, let us take a closer look at Equations 3.7.10 and 13 and derive inverses for both of them.

From the definition of the Cayley transform, given in Equation 3.7.10, we derive the inverse transform. Starting with Equation 3.7.10 and changing the symbolism to that for the transference **S** and Hamiltonian transformed transference $\hat{\mathbf{S}}$ we have

$$\hat{\mathbf{S}} = (\mathbf{S}-\mathbf{I})(\mathbf{S}+\mathbf{I})^{-1}. \tag{5.6.1}$$

Solving for **S** we obtain

$$\mathbf{S} = \left(\mathbf{I} - \hat{\mathbf{S}}\right)^{-1}\left(\mathbf{I} + \hat{\mathbf{S}}\right) \tag{5.6.2}$$

which is the inverse given in Equation 3.7.12 and different from the one given in Equation 3.7.11. Similarly, the inverse of Equation 3.7.12 is 3.7.10.

Repeating this procedure to obtain the inverse of the Cayley transform given in Equation 3.7.13, we obtain

$$\hat{\mathbf{S}} = (\mathbf{I} - \mathbf{S})(\mathbf{I} + \mathbf{S})^{-1}. \tag{5.6.3}$$

Solving for **S** we obtain

$$\mathbf{S} = \left(\mathbf{I} + \hat{\mathbf{S}}\right)^{-1}\left(\mathbf{I} - \hat{\mathbf{S}}\right)$$

and because of commutativity,

$$\mathbf{S} = \left(\mathbf{I} - \hat{\mathbf{S}}\right)\left(\mathbf{I} + \hat{\mathbf{S}}\right)^{-1} \tag{5.6.4}$$

which is its own functional inverse.

Commutativity is simple to show. Multiplication shows the following to be true:

$$(\mathbf{I} + \mathbf{A})(\mathbf{I} - \mathbf{A}) = (\mathbf{I} - \mathbf{A})(\mathbf{I} + \mathbf{A}).$$

Hence

$$(\mathbf{I} - \mathbf{A})^{-1}(\mathbf{I} + \mathbf{A}) = (\mathbf{I} + \mathbf{A})(\mathbf{I} - \mathbf{A})^{-1}$$

provided the inverse exists. Hence $(\mathbf{I} - \mathbf{A})^{-1}$ and $\mathbf{I} + \mathbf{A}$ commute.

We return to the issue of which Cayley transform and inverse combination will return the original transference. All of the Cayley transforms given in Equations 3.7.10 to 13 can potentially be done by hand with just a handheld calculator for a Gaussian system. Retaining the symbolism above, we denote the 2×2 (symplectic) transference as **S** and the 2×2 (Hamiltonian) Cayley transformed transference as $\hat{\mathbf{S}}$. Starting with Equation 3.7.10 and expanding we get

$$\hat{\mathbf{S}} = \left(\begin{pmatrix} A & B \\ C & D \end{pmatrix} - \begin{pmatrix} 1 & 0 \\ 0 & 1 \end{pmatrix}\right)\left(\begin{pmatrix} A & B \\ C & D \end{pmatrix} + \begin{pmatrix} 1 & 0 \\ 0 & 1 \end{pmatrix}\right)^{-1}$$

simplifying and using the symplectic equation we obtain

$$\hat{\mathbf{S}} = \begin{pmatrix} A-D & 2B \\ 2C & D-A \end{pmatrix}\frac{1}{2+A+D} \tag{5.6.5}$$

or

$$\hat{\mathbf{S}} = \begin{pmatrix} A-D & 2B \\ 2C & D-A \end{pmatrix} \frac{1}{2+\mathrm{tr}\mathbf{S}} \tag{5.6.6}$$

giving us the Cayley transformed transference of a Gaussian system in terms of the fundamental properties of the Gaussian transference. This transformed transference exists provided $\mathrm{tr}\mathbf{S} \neq -2$, which is unlikely for a reasonable eye. It is, however, clearly a Hamiltonian matrix.

Similarly, we can simplify Equation 3.7.13 to obtain

$$\hat{\mathbf{S}} = \begin{pmatrix} A-D & 2B \\ 2C & D-A \end{pmatrix} \frac{-1}{2+\mathrm{tr}\mathbf{S}}, \tag{5.6.7}$$

the negative equivalent of Equation 5.6.6 and clearly also Hamiltonian.

Similarly, the Cayley transform given by Equation 3.7.12 simplifies for a Gaussian system to

$$\hat{\mathbf{S}} = \begin{pmatrix} A-D & 2B \\ 2C & D-A \end{pmatrix} \frac{1}{2-A-D} \tag{5.6.8}$$

or

$$\hat{\mathbf{S}} = \begin{pmatrix} A-D & 2B \\ 2C & D-A \end{pmatrix} \frac{1}{2-\mathrm{tr}\mathbf{S}} \tag{5.6.9}$$

which is also Hamiltonian. This transformed transference exists provided $\mathrm{tr}\mathbf{S} \neq 2$ which is a possibility. The entries within the matrix are the same for Equations 5.6.6, 7 and 9, but in each case they are multiplied by a different constant, giving different values for each of the three transformed transferences.

From Equations 5.6.6, 7 and 9 we see that the units are the same as for a transference and that the entries along the diagonal are the negative equivalent of each other as shown in Equation 3.7.8. This gives us three independent entries and enables us to create a three-dimensional graph of the Hamiltonian space represented by the Cayley Transform.

We derive an equation for the transference **S** as a function of the coefficients of the transformed transference $\hat{\mathbf{S}}$. We start with the definition of the inverse of the Cayley transform, given in Equation 3.7.12 and substitute the transformed coefficients into it from the Gaussian simplification of Equation 3.7.7,

$$\mathbf{S}=\left(\begin{pmatrix}1&0\\0&1\end{pmatrix}+\begin{pmatrix}\hat{A}&\hat{B}\\\hat{C}&\hat{D}\end{pmatrix}\right)\left(\begin{pmatrix}1&0\\0&1\end{pmatrix}-\begin{pmatrix}\hat{A}&\hat{B}\\\hat{C}&\hat{D}\end{pmatrix}\right)^{-1}$$

$$\mathbf{S}=\begin{pmatrix}1+\hat{A}-\hat{D}-\hat{A}\hat{D}+\hat{B}\hat{C} & 2\hat{B}\\ 2\hat{C} & \hat{C}\hat{B}+1+\hat{D}-\hat{A}-\hat{A}\hat{D}\end{pmatrix}\frac{1}{1-\hat{A}-\hat{D}+\hat{A}\hat{D}-\hat{C}\hat{B}}$$

and substituting the Gaussian simplification of Equation 3.7.8, $\hat{A}=-\hat{D}$ into this equation we can simplify further to obtain

$$\mathbf{S}=\begin{pmatrix}1+2\hat{A}-\hat{A}\hat{D}+\hat{B}\hat{C} & 2\hat{B}\\ 2\hat{C} & 1+2\hat{D}-\hat{A}\hat{D}+\hat{C}\hat{B}\end{pmatrix}\frac{1}{1+\hat{A}\hat{D}-\hat{C}\hat{B}}$$

$$\mathbf{S}=\frac{2}{1+\hat{A}\hat{D}-\hat{C}\hat{B}}\begin{pmatrix}\hat{A}+1 & \hat{B}\\ \hat{C} & \hat{D}+1\end{pmatrix}-\mathbf{I} \tag{5.6.10}$$

$$\mathbf{S}=\frac{2\left(\hat{\mathbf{S}}+\mathbf{I}\right)}{1+\det\hat{\mathbf{S}}}-\mathbf{I} \tag{5.6.11}$$

which is the equation for the transference in terms of the Cayley transformed transference.

Using the same methodology of substituting the entries from Equation 3.7.7 into the Cayley transform given by Equation 3.7.13, we obtain

$$\mathbf{S}=\frac{2\left(\mathbf{I}-\hat{\mathbf{S}}\right)}{1+\det\hat{\mathbf{S}}}-\mathbf{I} \tag{5.6.12}$$

for the transference in terms of the transformed transference for Equation 3.7.13.

Similarly Equations 3.7.10 and 11 simplify and we obtain

$$\mathbf{S}=\frac{2\left(\hat{\mathbf{S}}-\mathbf{I}\right)}{1+\det\hat{\mathbf{S}}}+\mathbf{I} \tag{5.6.13}$$

Which is the same regardless of whether we use the first or second equality, due to the commutativity of the Cayley transform.

We now have three formulae for the transformed transference in terms of the entries of the Gaussian transference and three formulae for the transference in terms of the entries of the transformed transference. We return to our initial requirement for the choice of Cayley transform and inverse Cayley transform; that is, that when a transference is transformed into Hamiltonian space and then the transformed transference is transformed back to a symplectic matrix, then the

same transference must be returned. To do this, we substitute Equation 5.6.7 into Equation 3.7.13 and obtain

$$\mathbf{S}=\begin{pmatrix} A & B \\ C & D \end{pmatrix},$$

the transference in its original values and with the original order. Similarly if we substitute Equation 5.6.12 into Equation 3.7.13 we obtain the transformed transference $\hat{\mathbf{S}}$ in its original values and with original order. This indicates to us that the Cayley transform given in Equation 3.7.13 is its own functional inverse and is the most suitable transform to use, along with the simplifications for Gaussian systems. We will use Equation 5.6.7 for mapping from the symplectic transference to the Hamiltonian matrix and Equation 5.6.12 to map from a Hamiltonian matrix back to its symplectic transference.

Let us consider, for completeness, other versions of the Cayley transform and respective functional inverses that meet our criteria for returning the transference in its original form when transformed into Hamiltonian space and then transformed back to a symplectic transference. If we consider the possibility of Equation 3.7.10 being its own functional inverse (given in Equation 3.7.11) then we should follow the same procedure we did above for Equation 3.7.13. However we find that the transformed transference maps back to

$$\mathbf{S}=\begin{pmatrix} -D & B \\ C & -A \end{pmatrix} \tag{5.6.14}$$

which is a symplectic matrix, but not the original transference. It is the negative inverse of the transference. Similarly the transformed transference maps back to

$$\hat{\mathbf{S}}=\begin{pmatrix} \hat{A} & \hat{B} \\ \hat{C} & \hat{D} \end{pmatrix}\frac{1}{\det\hat{\mathbf{S}}} \tag{5.6.15}$$

which is a Hamiltonian matrix, but not the original Hamiltonian matrix that was started with. We therefore can conclude that, for the 2×2 symplectic – Hamiltonian mapping, Equation 3.7.10 (and 11) is not its own functional inverse. However, we note that applying Equation 3.7.12 as an inverse to Equation 3.7.10 does return the original transference and will fulfil our requirements of returning a transference. However this option requires a different equation to map in each direction whereas Equation 3.7.13 is its own functional inverse and therefore only

one equation transforms a transference to a transformed transference and conversely the transformed transference maps to the original transference. It has the added requirement of having the inverse exist for the transferences of all reasonable eyes. Equation 3.7.13 can be considered more general and convenient and is therefore our Cayley transform of choice. Equation 3.7.13 is expressed in the notation used for transferences as

$$\hat{\mathbf{S}} = (\mathbf{I} - \mathbf{S})(\mathbf{I} + \mathbf{S})^{-1} \tag{5.6.16}$$

and

$$\mathbf{S} = (\mathbf{I} - \hat{\mathbf{S}})(\mathbf{I} + \hat{\mathbf{S}})^{-1}. \tag{5.6.17}$$

5.6.1 The Cayley transformed transference for the reduced eye

We are now in a position to obtain a formula for the transformed transference of the reduced eye as a function of frequency. In Section 5.5.2 we looked at the reduced eye as a function of the refractive index (*n*). Equation 5.5.3 gives the transference of the reduced eye with the refractive indices as the only unknowns. Equating the refractive index of air to be $n_0 = 1$, we substitute the values of A, B, C and D from Equation 5.5.3 into Equation 5.6.7 to obtain

$$\hat{\mathbf{S}} = \begin{pmatrix} n-1 & \dfrac{-100}{9}\,\text{mm} \\ \dfrac{9}{100}\left(n^2 - n\right)\text{kD} & 1-n \end{pmatrix}. \tag{5.6.18}$$

Equation 5.6.18 is the Cayley transformed transference for the reduced eye. The units are the same as for a transference. Of interest is that the refractive indices in $\hat{B}$ cancel out and $\hat{B}$ is a constant and coincidentally it is the negative inverse of the constant obtained in $\hat{C}$. $\hat{A}, \hat{C}$ and $\hat{D}$ are all functions of *n*.

5.6.2 The Cayley transformed transference for Le Grand's eye

Because of the problem we had in Section 5.5.4, that there are too many elementary transferences, we have the same restriction on deriving a transformed transference for Le Grand's eye as a function of refractive index.

5.7 Summary

This chapter provides us with a collection of derived properties of the Gaussian system from the transference, which along with the basis for linear optics and derivations in Chapter 3, brings to completeness the derivations we will need for this dissertation. We now have all the necessary formulae to define chromatic aberration in the eye using linear optics. We also are in a position to derive equations from the transference and the ray traversing the Gaussian system for the chromatic properties defined in the physiological optics literature as studied in Chapter 2.

The equations obtained in Sections 5.1 and 5.2 generalise to linear optics. In Section 5.3 the coefficient matrix defining the ray state in object space that maps to an image point at a selected position on the retina was given for astigmatic systems, although it did not generalise readily from Gaussian optics. Whilst Harris (2010b, e) gives formulae to obtain the position of cardinal points and structures for linear systems in general it is not obvious how the locator lines (Harris, 2011b) and Pascal's ring (Harris, 2011a) might generalize for linear systems. In Section 5.5, the transferences for the two model eyes belong clearly within the framework of Gaussian optics. So too, in Section 5.6, the derivations for the transformed Cayley transference in terms of the fundamental properties belong within the framework of Gaussian optics.

6 DEFINITIONS OF LONGITUDINAL AND TRANSVERSE CHROMATIC ABERRATION

In Chapter 2 we saw that many authors refer to chromatic difference of power, magnification, position or refractive error as chromatic aberration. Formulae to derive these properties from the transference of a Gaussian system will be derived in Chapter 7 to allow these definitions to be applied to more complex model eyes. However, there is a clear need for a general definition of chromatic aberration that makes allowance for astigmatic elements that may be tilted or decentred. This chapter defines chromatic aberration for Gaussian optical systems.

6.1 Defining chromatic aberration

To define longitudinal and transverse chromatic aberration we start with the classical definition, which is restricted to homocentric systems with stigmatic elements. However, we do so by defining chromatic aberration in general for systems with astigmatic and heterocentric elements and then simplifying for Gaussian systems.

6.1.1 Homocentric systems with stigmatic elements

In Section 2.2.1 and Figure 2.2.1 we saw how the first-order chromatic aberrations are defined within the limits of Gaussian optics as the distance between the projections of two focus points for two different wavelengths in the directions parallel and perpendicular to the optical axis as longitudinal and transverse chromatic aberration respectively. In this definition the distances between points are unsigned. The definition holds for optical systems with stigmatic elements. This definition is the starting point for the definition that will be used in this study.

In this study we use the definition by Harris and Evans (2012) and take the distances between image points to be signed. This is shown in Figure 6.1.1 where the longitudinal chromatic aberration δz and transverse chromatic aberration δy are shown in the positive sense as having direction from the red to the blue image

points, in addition to magnitude. In Figure 6.1.1, the object O corresponds to red and blue images $\mathrm{I_r}$ and $\mathrm{I_b}$ respectively.

Figure 6.1.1 shows the definitions of longitudinal and transverse chromatic aberration in Gaussian optics and represents the point of departure for the definition given by Harris and Evans (2012) for astigmatic heterocentric systems. It differs from Figure 2.2.1 in that it has signed distances. System S is Gaussian and consists of any number of centred refracting surfaces with stigmatic elements, but which are not shown. This implies that they are invariant under rotation about the common axis Z, which is therefore also the optical axis. S has entrance plane $\mathrm{T_0}$ and exit plane T and refractive indices n_0 upstream and n downstream of S. Object point O has longitudinal position z_O and transverse position y_O. In Figure 6.1.1 these positions are drawn such that $z_\mathrm{O} < 0$ and $y_\mathrm{O} > 0$.

The position of image point I depends on the frequency ν of light. For this purpose we look at two frequencies on opposite ends of the visible light spectrum, namely red ν_r and blue ν_b. The corresponding images for these two frequencies are red image $\mathrm{I_r}$ and blue image $\mathrm{I_b}$. The corresponding longitudinal positions are

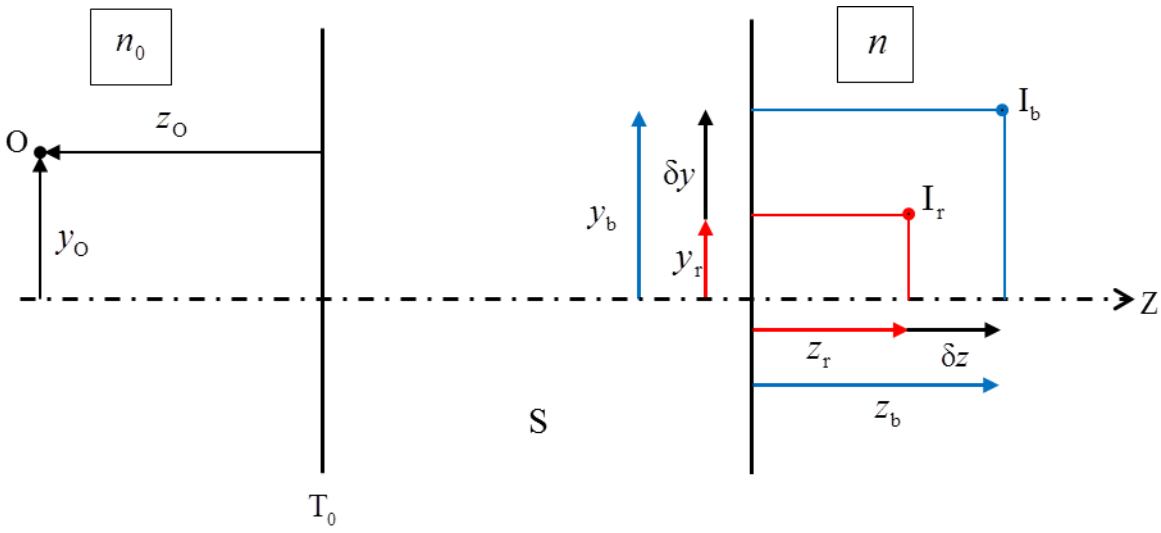

Figure 6.1.1 Longitudinal δz and transverse δy chromatic aberration in a homocentric system with stigmatic elements.

z_r and z_b and transverse positions y_r and y_b. In Figure 6.1.1, all image positions and directions are drawn in the positive sense, however, in a usual system such as the eye $z_r > z_b$.

Subscripts r and b will be used throughout this chapter. They denote two frequencies usually near opposite ends of the visible light spectrum, however, any two frequencies could be chosen. We call them 'red' and 'blue' for convenience. On the visible light spectrum, the blue is the higher frequency and the red is the lower frequency. Therefore the blue photons have a higher energy than the red photons which seems to suggest that we should subtract a lower energy from the higher energy. For this reason we chose to subtract red from blue in all chromatic aberration formulae. However, the formulae derived are general for any chosen frequencies. In Chapters 9 and 10 two frequencies are chosen for illustrative purposes.

We note that Figure 6.1.1 is a two-dimensional diagram and that the optical axis Z, object O and both the image points I_r and I_b lie in the same plane, that of the page. This is because system S is homocentric and has only stigmatic elements within it. Furthermore, a distinction is drawn between incident refractive indices n_{0r} and n_{0b} and emergent refractive indices n_r and n_b.

We define longitudinal (or axial) chromatic aberration as (Harris and Evans, 2012)

$$\delta z = z_b - z_r \tag{6.1.1}$$

and transverse (or lateral) chromatic aberration as

$$\delta y = y_b - y_r . \tag{6.1.2}$$

For convenience, the context of the system is implied when referring to the properties of a system. The chromatic aberration will also depend on the position of a point in object space, O. In Figure 6.1.1 this position is denoted by longitudinal position z_O and transverse position y_O.

For any system S, the chromatic aberration is not unique and usually there will exist an infinity of longitudinal and transverse chromatic aberrations. The chromatic aberration of a system is unique only when the object position is

specified. In other words, chromatic aberration depends on z_O and y_O. As will be shown, longitudinal chromatic aberration is dependent on z_O and transverse chromatic aberration on y_O. Chromatic aberration does not exist for the system in isolation. It is a measurement of a phenomenon of the images formed and for this reason is a property of the object point and the system.

From these definitions, longitudinal δz and transverse δy chromatic aberration are lengths measured orthogonally to each other and represented here by scalars. From Figure 6.1.1 one is tempted to draw an arrow from I_r to I_b, to represent chromatic aberration holistically as a vector with longitudinal and transverse chromatic aberration as components. However, when we make allowance for astigmatism one finds that the two aberrations are fundamentally different and cannot be combined into a single vector (Harris and Evans, 2012). We therefore refrain from representing chromatic aberration as a vector here as well.

6.1.2 Heterocentric systems with stigmatic elements

A heterocentric system is one in which the refracting elements are not all centred on a common optical axis. Elements may be decentred or tilted. We retain the stigmatic elements, however, the longitudinal axis is no longer an optical axis and we need to consider a three-dimensional representation as shown in Figure 6.1.2. In Figure 6.1.2, system S contains refracting surfaces which may be decentred. It may also contain prisms and surfaces which are tilted. Also shown in Figure 6.1.2 are the transverse planes containing the object point O at T_O, the red image I_r at T_r and the blue image I_b at T_b. The object O corresponds to red and blue images I_r and I_b respectively.

From Figure 6.1.2 it becomes clear that the definition of longitudinal chromatic aberration δz in the case of homocentric systems with stigmatic elements can be applied to heterocentric systems, Equation 6.1.1 remains unchanged and δz remains a scalar measurement of length between the red and blue transverse planes. Also from Figure 6.1.2, we can see that this is not the case

for transverse chromatic aberration $\delta\mathbf{y}$. Starting at the object plane T_O we see that the position of object point O is now defined as a vector

$$\mathbf{y}_O = \begin{pmatrix} y_{O1} \\ y_{O2} \end{pmatrix} \tag{6.1.3}$$

with horizontal and vertical components.

Similarly we note that the transverse positions of the red I_r and blue I_b image points are represented by $\mathbf{y}_r$ and $\mathbf{y}_b$ each with horizontal and vertical components. In order to obtain the transverse chromatic aberration, we project the red image point I_r onto the blue transverse plane T_b. The projection is along the longitudinal axis. $\Delta\mathbf{y}$ is represented as the vector from the red to the blue image points and defines transverse chromatic aberration as

$$\delta\mathbf{y} = \mathbf{y}_b - \mathbf{y}_r . \tag{6.1.4}$$

At this point we have transverse chromatic aberration, a vector, and longitudinal chromatic aberration, a scalar. Although one is a scalar and the other a vector, one is still tempted to combine them as a holistic concept of three components.

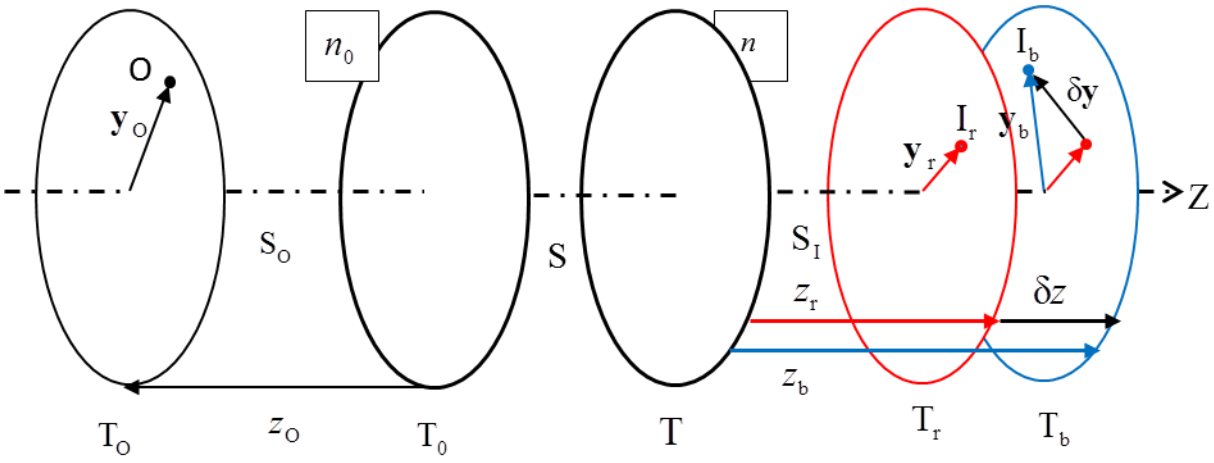

Figure 6.1.2 Longitudinal and transverse chromatic aberration in a heterocentric system with stigmatic elements.

6.1.3 Heterocentric astigmatic systems

We turn now to the general system in which elements may be decentred and astigmatic (Harris and Evans, 2012). System S consists of any number of elements which may be astigmatic, decentred, tilted or prismatic. The longitudinal axis Z is usually not an optical axis. In an astigmatic system image points $\mathrm{I_r}$ and $\mathrm{I_b}$ become fuzzy as shown in Figure 6.1.3. Each image point dissociates longitudinally into two orthogonal image lines and each fuzzy image becomes that of the interval of Sturm, which will be referred to simply as the image structure. The red and blue transverse image planes are no longer planes, but a fuzzy zone the width of the interval of Sturm and denoted by dotted lines in Figure 6.1.3. The system is drawn with the red and blue image zones separate, however, these may overlap. An additional problem arises when defining longitudinal chromatic aberration in that the orientations of the two sets of image lines may not match. That is to say, the first red image line may not be parallel to the first blue image line. There is a relative rotation that occurs between the red and then the blue image structures that must be considered. Additionally, the width of the interval of Sturm is not necessarily the same for each colour.

How now does one define longitudinal chromatic aberration? Intuitively one may wish to calculate a scalar distance between the two image structures by calculating the distance between the planes of the two circles of least confusion. However, the circle of least confusion is not an image point and this does not fully represent what is happening in the system. Each image structure is represented by a 2×2 symmetric vergence matrix and therefore a scalar distance does not make any sense. The definition needs to account for the fact that the two fuzzy image structures differ in position, orientation and degree of fuzziness. Therefore the definition needs to include at least three numbers to represent it completely.

The fuzzy image structure is a representation of light, so we turn our attention to vergence. In the absence of astigmatism the red pencil of light would have reduced vergence

$$L_{\mathrm{r}} = \frac{n_{\mathrm{r}}}{z_{\mathrm{r}}} \tag{6.1.5}$$

at exit plane T, where z_r is the longitudinal distance from exit plane T to transverse red image plane T_r, as shown in Figure 6.1.1. Hence

$$z_r = \frac{n_r}{L_r} \tag{6.1.6}$$

and similarly for the blue vergence and longitudinal distance. In the presence of astigmatism the generalisation of the scalar reduced vergence L is the reduced vergence $\mathbf{L}$, a symmetric matrix as defined in Section 3.8. The unit of vergence is reciprocal length. $\mathbf{L}_r$ is the reduced vergence at the exit plane T of system S of the red astigmatic pencil defined by object O and $\mathbf{L}_b$ is the same for the blue pencil.

From Equation 6.1.6, Harris and Evans (2012) generalize and define

$$\mathbf{Z} = \mathbf{L}^{-1} n . \tag{6.1.7}$$

$\mathbf{Z}$ is symmetric and has the unit length. Because the right-hand side of the equation is multiplied by n, $\mathbf{Z}$ represents the actual distance rather than the reduced distance. It can be regarded as the generalized position of the fuzzy image structure relative to the exit plane T.

Generalizing Equation 6.1.1, we see that

$$\delta\mathbf{Z} = \mathbf{Z}_b - \mathbf{Z}_r \tag{6.1.8}$$

represents the longitudinal chromatic aberration of a heterocentric astigmatic system S for object point O on the longitudinal axis. $\delta\mathbf{Z}$ characterises the longitudinal difference of the two fuzzy image points completely (Harris and Evans, 2012). By this definition longitudinal chromatic aberration becomes the 2×2 symmetric matrix $\delta\mathbf{Z}$ and can be characterised by three independent numbers.

From Equation 6.1.5, we see that the reduced vergence (both scalar L and matrix $\mathbf{L}$) is dependent on the longitudinal position z_O of object point O and system S and is independent of the transverse position y_O of O. Therefore, provided z_O of the object O and system S remain unchanged, decentration of the object point and elements of the system have no effect on the longitudinal positions and nature of the fuzzy image structures and we can take Equation 6.1.8 to be the definition of longitudinal chromatic aberration $\delta\mathbf{Z}$ of a heterocentric

astigmatic system for an object point at any specified position. The longitudinal chromatic aberration is more difficult to represent pictorially. In Figure 6.1.3 $\mathbf{Z}_r$ is shown as two red lines representing the two image line foci, orthogonal to each other. A line is drawn between them, parallel to the longitudinal axis. And similarly for the blue fuzzy image structure. The longitudinal chromatic aberration of system S for object O is $\delta\mathbf{Z}$. $\delta\mathbf{Z}$ is a 2×2 distance matrix and cannot be represented by a vector arrow on the diagram.

In contrast, the transverse chromatic aberration is the vector $\delta\mathbf{y}$, shown in Figure 6.1.3, from $\mathbf{y}_r$ to $\mathbf{y}_b$. Vectors $\mathbf{y}_r$ and $\mathbf{y}_b$ are drawn from the longitudinal axis Z to an axis, parallel to Z, between the two orthogonal image lines within the transverse plane for red and blue, respectively. It is not drawn to the circle of least confusion. The vector for $\mathbf{y}_r$ can be projected onto the blue image plane and the transverse chromatic aberration is vector $\delta\mathbf{y}$. The effect of decentring an object point and system elements is to cause transverse displacement of the fuzzy images I_r and I_b of object point O in the heterocentric astigmatic system S. Equation 6.1.4 defines the transverse chromatic aberration $\delta\mathbf{y}$ of S for O.

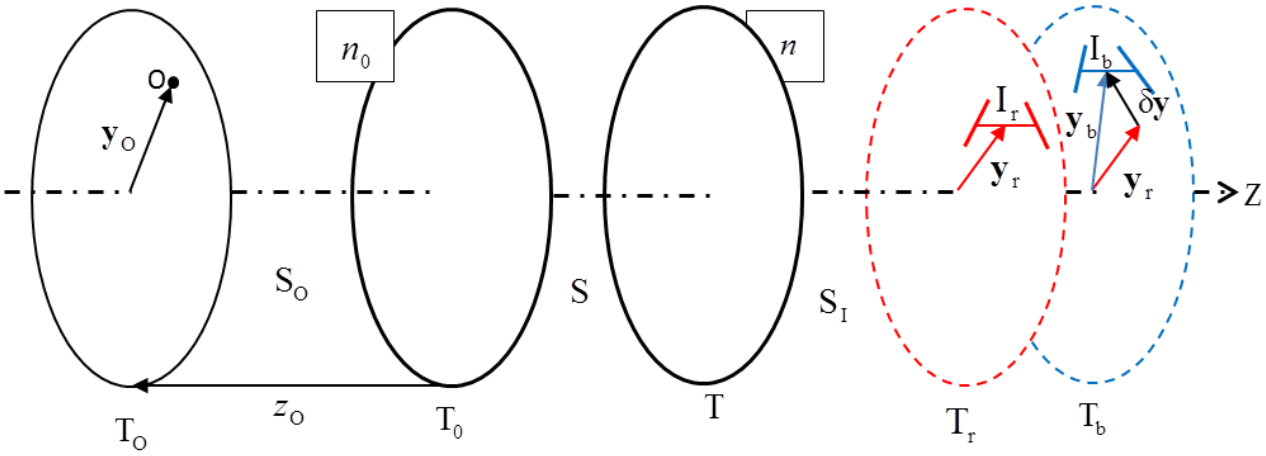

Figure 6.1.3 Longitudinal $\delta\mathbf{Z}$ and transverse $\delta\mathbf{y}$ chromatic aberration in a heterocentric system with astigmatic elements.

6.1.4 Chromatic aberration in general

Equations 6.1.4 and 8 are generalisations from Equations 6.1.2 and 1 to optical systems in general of the definitions for systems whose elements are stigmatic and centred on an optical axis. Equation 6.1.4 defines transverse chromatic aberration $\delta\mathbf{y}$ and Equation 6.1.8 longitudinal chromatic aberration $\delta\mathbf{Z}$ in general. $\delta\mathbf{y}$ is a two dimensional vector and $\delta\mathbf{Z}$ is a 2×2 symmetric matrix. The fact that transverse and longitudinal chromatic aberration are different in mathematical character shows that the two types of aberration are fundamentally different in nature and cannot be meaningfully combined into a single unified concept of chromatic aberration.

These general equations hold and indeed simplify for homocentric systems with stigmatic elements in particular. In such systems the transverse chromatic aberration $\delta\mathbf{y}$ becomes a scalar quantity δy and sketched in a single plane, that of the page. Δy is one component of $\delta\mathbf{y}$ with the other component being zero and perpendicular to the page. The longitudinal chromatic aberration $\delta\mathbf{Z}$ also becomes a scalar quantity represented as a scalar multiple of the identity matrix such that $\delta\mathbf{Z}=\mathbf{I}\delta z$, where $\mathbf{I}$ is the 2×2 identity matrix, and the image is a point. The image too is represented as simply in the plane of the page, as shown in Figure 6.1.1.

Equations 6.1.1 and 8 define longitudinal chromatic aberration and Equations 6.1.2 and 4 define transverse chromatic aberration in Gaussian and linear systems respectively. We now turn our attention to quantifying longitudinal and transverse chromatic aberration in Gaussian systems.

6.2 Quantifying chromatic aberration in Gaussian systems

In order to calculate the longitudinal and transverse chromatic aberration we need to consider the optical system which is represented by the system's ray transference, where the transference is a function of the frequency of light (Evans and Harris, 2011). This 2×2 transference was defined for a Gaussian system in Equation 3.2.38.

6.2.1 Vergence across a Gaussian system derived from the transference

The reduced vergence at an entrance plane T_0 of system S is L_0, given by Equation 3.8.1, for an object O at a longitudinal distance z_O from T_0. Following from this, the reduced vergence at the exit plane T of S for O is given by Equation 3.8.6 for light emerging from a linear system and which reduces to

$$L = (DL_0 - C)(A - BL_0)^{-1} \tag{6.2.1}$$

through a Gaussian system. Substituting Equation 3.8.1 into Equation 6.2.1 we find

$$L = \left(D\frac{n_0}{z_\mathrm{O}} - C \right)\left(A - B\frac{n_0}{z_\mathrm{O}} \right)^{-1} \tag{6.2.2}$$

or

$$L = \left(D - C\frac{z_\mathrm{O}}{n_0} \right)\left(A\frac{z_\mathrm{O}}{n_0} - B \right)^{-1}. \tag{6.2.3}$$

From Equations 6.2.2 and 3 we note that there are two special cases to consider. Firstly where $z_\mathrm{O} \to \infty$ Equation 6.2.2 simplifies to

$$L = -CA^{-1} \tag{6.2.4}$$

and where $z_\mathrm{O} = 0$ Equation 6.2.3 simplifies to

$$L = -DB^{-1}. \tag{6.2.5}$$

Equation 6.2.4 is the same as Equation 3.4.11 and represents the back-vertex power of the system. In order to calculate the red and blue vergences L_r and L_b at T, one can simply add the appropriate subscript to all the parameters of any of Equations 6.2.1 to 5, with the exception of z_O. Because the transference is a function of the frequency of light, a transference will need to be calculated for each of red and blue, $\mathbf{S}_\mathrm{r}$ and $\mathbf{S}_\mathrm{b}$, using the formulae discussed in Section 5.5.

6.2.2 Transference of a compound system: object at finite distance

We now look at the system more carefully to obtain the transference of not just system S, but of the compound system from the object plane to the image plane. From Figure 6.1.1 we see that the system upstream of system S is S_O and is

the homogenous gap of finite length $-z_{\mathrm{O}}$. The minus sign is needed because O is upstream of S.

The transference of a homogenous gap is defined by Equation 3.2.36 where ζ is the reduced distance defined in Equation 3.2.8. In the same way we consider the system $\mathrm{S_I}$, downstream of system S, of length *z*, from the exit plane T of system S, up to the plane of an image line $\mathrm{T_I}$, corresponding to object O, of an image point.

To obtain the transference of the compound system $\mathrm{S_C}$ we start with

$$\mathbf{S}_{\mathrm{C}} = \mathbf{S}_{\mathrm{I}}\mathbf{S}\mathbf{S}_{\mathrm{O}} \tag{6.2.6}$$

then substitute for the individual transferences,

$$\mathbf{S}_{\mathrm{C}} = \begin{pmatrix} 1 & \frac{z}{n} \\ 0 & 1 \end{pmatrix} \begin{pmatrix} A & B \\ C & D \end{pmatrix} \begin{pmatrix} 1 & \frac{-z_{\mathrm{O}}}{n_0} \\ 0 & 1 \end{pmatrix}. \tag{6.2.7}$$

Hence

$$\mathbf{S}_{\mathrm{C}} = \begin{pmatrix} A + C\frac{z}{n} & B + D\frac{z}{n} - \left(A + C\frac{z}{n}\right)\frac{z_{\mathrm{O}}}{n_0} \\ C & D - C\frac{z_{\mathrm{O}}}{n_0} \end{pmatrix}. \tag{6.2.8}$$

From Equation 3.2.40 and the top row of Equation 6.2.8, we see that a ray from object O at transverse position y_{O} on the entrance plane $\mathrm{T_O}$ arrives at the transverse image plane $\mathrm{T_I}$ with transverse position

$$y = \left(A + C\frac{z}{n}\right)y_{\mathrm{O}} + \left(B + D\frac{z}{n} - \left(A + C\frac{z}{n}\right)\frac{z_{\mathrm{O}}}{n_0}\right)n_0 a_{\mathrm{O}}. \tag{6.2.9}$$

From Section 3.3.2, we recognise this as a conjugate system and therefore we set $B + D\frac{z}{n} - \left(A + C\frac{z}{n}\right)\frac{z_{\mathrm{O}}}{n_0} = 0$, effectively nullifying any effect of a_{O}. Hence Equation 6.2.9 simplifies to

$$y = \left(A + C\frac{z}{n}\right)y_{\mathrm{O}}. \tag{6.2.10}$$

which gives us the transverse position of a point *y* at the image plane $\mathrm{T_I}$. Equation 6.2.10 can be written for red and blue image points which would then give y_b and y_r corresponding to an object point at a finite distance .

6.2.3 Transference of a compound system: distant object

We now define the transference of a compound system where the object point is at an infinite distance. Because $z_\mathrm{O} \to \infty$ we rather define our system as starting at $\mathrm{T_0}$ and make use of the incident inclination a_0 of the rays at entrance plane $\mathrm{T_0}$.

We therefore define our system as the compound system from $\mathrm{T_0}$ to $\mathrm{T_I}$, consisting of S and $\mathrm{S_I}$. The transference of $\mathrm{S_C}$ is

$$\mathbf{S}_\mathrm{C} = \mathbf{S}_\mathrm{I}\mathbf{S} \tag{6.2.11}$$

and, hence,

$$\mathbf{S}_\mathrm{C} = \begin{pmatrix} 1 & \frac{z}{n} \\ 0 & 1 \end{pmatrix} \begin{pmatrix} A & B \\ C & D \end{pmatrix} \tag{6.2.12}$$

or

$$\mathbf{S}_\mathrm{C} = \begin{pmatrix} A + C\frac{z}{n} & B + D\frac{z}{n} \\ C & D \end{pmatrix}. \tag{6.2.13}$$

Substituting from the top row of Equation 6.2.13 into Equation 3.2.40 we find that the ray will arrive in $\mathrm{T_I}$ at transverse position

$$y = \left(A + C\frac{z}{n} \right) y_\mathrm{O} + \left(B + D\frac{z}{n} \right) n_0 a_\mathrm{O} \tag{6.2.14}$$

and because the system is exit-plane focal, we have $A + C\frac{z}{n} = 0$ which nullifies any effect of y_O and therefore Equation 6.2.14 simplifies to

$$y = \left(B + D\frac{z}{n} \right) n_0 a_\mathrm{O}. \tag{6.2.15}$$

y is the transverse position on the image plane $\mathrm{T_I}$ corresponding to a point image for a system with an object at an infinite distance. Equation 6.2.15 can be written

for red and blue image points which would then give y_b and y_r for a distant object point.

6.2.4 Transverse chromatic aberration in a Gaussian system

The transverse chromatic aberration was defined in Equation 6.1.2 as $\delta y = y_b - y_r$ for Gaussian systems. Substituting from Equation 6.2.10 we obtain

$$\delta y = y_O\left[\left(A_b + C_b\frac{z_b}{n_b}\right) - \left(A_r + C_r\frac{z_r}{n_r}\right)\right]$$

$$\delta y = y_O\delta\left(A + C\frac{z}{n}\right) \tag{6.2.16}$$

similarly, for an object point at a finite distance and substituting from Equation 6.2.15 into Equation 6.1.2 we obtain

$$\delta y = a_O\delta\left(\left(B + D\frac{z}{n}\right)n_0\right) \tag{6.2.17}$$

for systems when the object point is distant ($z_O \to \infty$).

6.3 Calculation routines for longitudinal and transverse chromatic aberration

1. Calculate $\mathbf{S}_r$ and $\mathbf{S}_b$ the transferences of system S for red and blue light.
2. Calculate the reduced vergence *L* for each of red and blue light.
    i. For a finite object point O with longitudinal position z_O use Equation 6.2.3.
    ii. For a distant object where $z_O \to \infty$, use Equation 6.2.4.
3. Calculate the longitudinal position *z* of the image point for each frequency using Equation 6.1.6.

6.3.1 Calculation routine for longitudinal chromatic aberration

4. Calculate the longitudinal chromatic aberration δz from Equation 6.1.1.

6.3.2 Steps for calculating transverse chromatic aberration

- *For an object point at a finite distance of longitudinal position* z_O *upstream of the system:*

Following from steps 1, 2.i and 3.

4. For each of red and blue calculate $A + C\frac{z}{n}$.
5. Calculate $\delta\left(A + C\frac{z}{n}\right)$.
6. Calculate the transverse chromatic aberration δy using Equation 6.2.16.

- *For an object point at a distance where* $z_O \to \infty$ *upstream of the system:*

Following from steps 1, 2.ii and 3.

4. For each of red and blue calculate $\left(B + D\frac{z}{n}\right)n_0$.
5. Calculate $\delta\left(\left(B + D\frac{z}{n}\right)n_0\right)$.
6. Calculate the transverse chromatic aberration using Equation 6.2.17.

Numerical examples of longitudinal and transverse chromatic aberration for the reduced eye and Le Grand's eye are given in Section 10.1.

6.4 Comments on chromatic aberration

In this chapter we considered the definition for chromatic aberration. Firstly, we looked at the familiar definition given in the literature as the first order chromatic aberrations within the limits of Gaussian optics as the distance between the projections of two focus points for two different frequencies in the directions parallel and perpendicular to the optical axis as longitudinal and transverse chromatic aberration respectively and illustrated in Figure 6.1.1. From this figure it appears logical to draw an arrow between image points I_r and I_b, thereby representing both longitudinal and transverse chromatic aberration holistically as one vectorial chromatic aberration. This, however, would be incorrect. In order to understand why that is so we looked at the generalisation of this definition in heterocentric astigmatic systems and saw that the two aberrations have fundamentally different mathematical characters: longitudinal chromatic

aberration is represented by a 2×2 symmetric matrix $\delta\mathbf{Z}$ whereas transverse chromatic aberration is represented by a vector $\delta\mathbf{y}$. The fact that transverse and longitudinal chromatic aberration have different mathematical character shows that the two types of aberration are fundamentally different in nature and cannot be meaningfully combined into a single unified concept of chromatic aberration.

For any system S the chromatic aberrations are not unique and usually there will exist an infinity of longitudinal and transverse chromatic aberrations. The chromatic aberrations of a system are unique only when the object position is specified. In other words, chromatic aberration is dependent on z_{O} and y_{O}.

We noted that chromatic aberration does not exist for the system in isolation. It is a measurement of a phenomenon of the images formed and for this reason is a result of the system and the location of the object point. From Equations 6.1.1 and 6 and 6.2.2, 3 and 4, longitudinal chromatic aberration is dependent on longitudinal position z_{O} of the object point O and is independent of transverse position y_{O}. Transverse chromatic aberration is defined in Equation 6.1.2 and from Equations 6.2.16 and 17 we see that it is a linear function of the object's transverse position y_{O} in the case of the objects at finite distances and its direction a_{O} in the case of a distant object.

Chromatic aberrations are first-order phenomena and occur in the paraxial region. For this reason, Harris and Evans (2012) express reservations over the use of the word aberration in the context of chromatic aberrations.

The definitions and formulae given in this section are not specific to the eye, but are applicable to systems in general. When applying the definitions to the visual system one needs to be clear how the definitions are being used. Firstly, for an eye or a model eye the entrance plane would be immediately in front of the tear film and the exit plane immediately in front of the retina. Secondly, the position of the longitudinal axis needs to be specified. Thirdly, the location of the object point needs to be given. Finally, the two frequencies of light, ν_{r} and ν_{b}, need to be specified.

7 Quantifying chromatic properties

Longitudinal and transverse chromatic aberration was defined in general for Gaussian optical systems in Chapter 6. In Chapter 2 we reviewed the physiological optics definitions and experimental approaches to measure chromatic effects in the eye and calculate them in model eyes. Most of these approaches define chromatic differences in Gaussian model eyes, usually the reduced eye or modifications thereof. Measurements are done experimentally and calculated within the framework of Gaussian systems. In order to differentiate between the definitions defined in classical and physiological optics, the term "chromatic aberration" will be reserved for the definition given in Chapter 6 and the definitions given in the physiological optics, in this chapter, will be termed "chromatic properties of the eye".

In this section we consider chromatic properties of the eye in two categories: in Section 7.1 we define those that are properties of the eye alone, the independent chromatic properties of the eye, and in Section 7.2 we define the chromatic properties of the eye that are dependent on the object (or image) and aperture positions. Because these definitions are specific to eyes or model eyes, we deem the system of the eye to be from the entrance plane immediately in front of the cornea to the exit plane immediately in front of the retina.

For all the derivations that follow one needs to obtain two transferences, $\mathbf{S}_{\mathrm{r}}$, the transference for the red frequency and $\mathbf{S}_{\mathrm{b}}$, the transference for the blue frequency. In all the formulae below, the fundamental properties are taken from the two transferences with subscripts (or superscripts) r and b corresponding to the respective transference.

7.1 Independent chromatic properties of the eye

In Section 2.3.1 we saw that chromatic difference in power and chromatic difference in refractive compensation are usually categorised as longitudinal chromatic aberration which is in conflict with the definition for longitudinal chromatic aberration given in Chapter 6. In this section we will obtain formulae for the chromatic difference of power, refractive compensation and ametropia.

These chromatic properties of the eye are independent of the aperture, object and image, but depend on the frequencies chosen for red and blue.

7.1.1 Chromatic difference in power

Using Equation 3.4.3 we obtain the power F of the eye from the transference for a particular frequency of light. The chromatic difference in power is defined as

$$\delta F = F_{\mathrm{b}} - F_{\mathrm{r}} \tag{7.1.1}$$

and substituting from Equation 3.4.3 we obtain the chromatic difference in power from the transferences (Evans and Harris, 2011)

$$\delta F = -(C_{\mathrm{b}} - C_{\mathrm{r}})\,. \tag{7.1.2}$$

7.1.2 Chromatic difference in refractive compensation

We use Equation 3.4.6 to obtain the corneal-plane refractive compensation F_0 for an eye from the transference. The chromatic difference in refractive compensation is defined as

$$\delta F_0 = F_{0\mathrm{b}} - F_{0\mathrm{r}}\,. \tag{7.1.3}$$

Hence, from Equation 3.4.6 the chromatic difference in corneal-plane refractive compensation is (Evans & Harris, 2011)

$$\delta F_0 = B_{\mathrm{b}}^{-1} A_{\mathrm{b}} - B_{\mathrm{r}}^{-1} A_{\mathrm{r}}\,. \tag{7.1.4}$$

7.1.3 Chromatic difference in ametropia

The term ametropia is often used to refer to refractive compensation, however the term is used here as defined in Section 3.3.1.We read the ametropia A directly from the transference for each chosen frequency of light. The chromatic difference in ametropia across a specified spectrum of visible light is obtained directly from the transferences and therefore (Evans & Harris, 2011)

$$\delta A = A_{\mathrm{b}} - A_{\mathrm{r}}\,. \tag{7.1.5}$$

7.1.4 Chromatic properties for Emsley's reduced eye

In Section 4.1.3 we saw that the advantage of the reduced eye is its simplicity. It is a Gaussian system, has one refracting surface and there are only two refractive indices. We assume that Emsley's eye is in air and that $n_0 = 1$. What this implies is that we can derive very simple formulae for the chromatic difference of power, refractive compensation, and ametropia for the reduced eye. (Evans and Harris, 2011)

The parameter of the reduced eye that varies with frequency is the refractive index. We define the chromatic difference of refractive index for the reduced eye as

$$\delta n = n_{\mathrm{b}} - n_{\mathrm{r}}. \tag{7.1.6}$$

The refractive index for the reduced eye as a function of wavelength was given in Equation 4.4.2, from which we obtain (Evans & Harris, 2011)

$$\delta n = b\left(\frac{1}{\lambda_{\mathrm{b}} - c} - \frac{1}{\lambda_{\mathrm{r}} - c}\right) \tag{7.1.7}$$

where *b* and *c* are the constants given immediately after Equation 4.4.2. For the frequencies 430 THz and 750 THz, $\delta n = 0.015\,542$ for Emsley's reduced eye.

Chromatic difference in power for Emsley's reduced eye

From Equations 5.5.1 and 7.1.2 and the parameters for Emsley's reduced eye given in Section 4.1.3 for the radius of curvature *r* of the refracting surface and the length *z* of the reduced eye we obtain (Evans & Harris, 2011)

$$\delta F = (180\,\mathrm{D})\delta n, \tag{7.1.8}$$

the chromatic difference in power of Emsley's reduced eye, where δn is calculated according to Equation 7.1.7.

Chromatic difference in corneal-plane refractive compensation for Emsley's reduced eye

From Equations 5.5.1 and 7.1.4 and the parameters for the reduced eye given in Section 4.1.3 we obtain the chromatic difference in corneal-plane refractive compensation (Evans & Harris, 2011)

$$\delta F_0 = (-135\ \mathrm{D})\delta n\,. \tag{7.1.9}$$

Chromatic difference in ametropia for Emsley's reduced eye

From Equations 5.5.1 and Equation 7.1.5 and the parameters for the reduced eye we obtain the chromatic difference in ametropia (Evans & Harris, 2011)

$$\delta A = 4\left(\frac{1}{n_{\mathrm{b}}} - \frac{1}{n_{\mathrm{r}}}\right). \tag{7.1.10}$$

The formulae, given in Equations 7.1.7 to 10, are specific to the reduced eye and make use of the parameters of Emsley's reduced eye in the form of rational numbers. They are not general, but emphasise the simplicity of the reduced eye. Equations 7.1.7 to 10 enable us to very quickly obtain the chromatic difference in refractive index, power, refractive compensation or ametropia for any two chosen frequencies.

Generalizing to linear optics

Equations 7.1.1 to 5 readily generalize to linear systems. Equations 7.1.8 to 10 pertain to the reduced eye which is a Gaussian system.

7.2 Chromatic properties of the eye dependent on object and aperture positions

In Section 2.3.2 we saw that the two chromatic properties usually defined as transverse chromatic aberration are chromatic difference in position and chromatic difference in magnification. They are measured in object space and calculated in both image and object space for model eyes. Our purpose in this section is to derive formulae from the transference for the chromatic properties that are dependent on object and aperture positions for Gaussian eyes.

When we derive formulae for chromatic properties dependent on object and aperture positions we are interested in what is happening at the retina, that is, in image space. If we take into account that the light rays of different frequencies focus at different longitudinal positions, systems where the object and image are in conjugation, such as those discussed in Sections 3.3.2 and 3.5.1, are seldom

useful. Instead, we trace the chief ray from an object point projected onto the retina to locate the image position and magnification at the retinal plane and ignore the amount of blur at the retina. Chromatic difference in position is a commonly used term in the literature and is defined, in Section 2.3.2, as the difference in angular spread or difference in inclination of the red and blue reference rays in either image or object space. We will look at the chromatic difference in transverse position in both image δy_{R} and object space δy_{O} and the chromatic difference in inclination, again in both image δa_{R} and object space δa_{O}.

Unlike the independent chromatic properties of the eye, the chromatic properties discussed in this section are functions of the state of the rays at the retina. Changes in the position of object point and changes to the position of the limiting aperture will influence the state of the rays at the retina.

A ray incident onto the eye undergoes chromatic dispersion and reaches the retina resembling a little rainbow dispersed across the retina (Thibos *et al*, 1991). We concentrate on the two frequencies chosen for the particular study, usually representing the end points of the visual spectrum (as chosen for any specific study) and calculate the difference in position between them. Figure 7.2.1 shows the chromatic difference in position δy_{R} of the blue and red rays at the retina.

We retain the generality of the formulae by including the refractive index of the medium upstream of the eye as dependent on frequency. This is applicable, for example, for an eye submerged in water. Furthermore, equations are written such that they can, as far as possible, generalise to linear optics for centred systems with astigmatic elements. Where equations do not readily generalise, the general linear equation is provided.

7.2.1 Chromatic difference in coefficient matrices

In Section 5.2.2 we defined the distant coefficient matrix $\mathbf{V}_{\mathrm{E}}$. The matrix coefficients $\mathbf{V}_{\mathrm{E}}$ and $\mathbf{V}_{\mathrm{OE}}$ for eyes and either a distant or finite distance object point respectively are dependent on frequency and therefore there will be a blue

and a red matrix coefficient for each object distance. We now define the chromatic difference in distance coefficient matrices

$$\delta\mathbf{V}_{\mathrm{E}} = \mathbf{V}_{\mathrm{E}}^{\mathrm{b}} - \mathbf{V}_{\mathrm{E}}^{\mathrm{r}} = \begin{pmatrix} \delta W_{\mathrm{E}} & \delta X_{\mathrm{E}} \\ \delta Y_{\mathrm{E}} & \delta Z_{\mathrm{E}} \end{pmatrix} \tag{7.2.1}$$

where δW_{E} is the chromatic difference in distance image blur coefficient, δX_{E} is the chromatic difference in distance image size coefficient, δY_{E} is the chromatic difference in distance directional spread coefficient and δZ_{E} is the chromatic difference in distance directional coefficient.

Similarly, we can define the chromatic difference in near coefficient matrices $\delta\mathbf{V}_{\mathrm{OE}}$ and each of the respective simplifications for when a pinhole is in front of the eye, namely $\delta\mathbf{V}_{\mathrm{E}}^{\mathrm{P}}$ and $\delta\mathbf{V}_{\mathrm{OE}}^{\mathrm{P}}$. Also, we can define the chromatic difference in object space coefficient matrix with respect to position at the retina $\delta\mathbf{V}_{\mathrm{Oy}}$ and with respect to the inclination at the retina $\delta\mathbf{V}_{\mathrm{Oa}}$ and the simplifications when a pinhole is used, $\delta\mathbf{V}_{\mathrm{Oy}}^{\mathrm{P}}$ and $\delta\mathbf{V}_{\mathrm{Oa}}^{\mathrm{P}}$.

7.2.2 Chromatic difference in image positions at the retina

In Figure 7.2.1 we see a pencil of rays of inclination a_{K} incident onto the eye at the entrance plane T_{K}. We choose to follow only one ray from this pencil. For convenience, we choose the chief ray, however any ray could be chosen, for example a marginal ray. Because of dispersion we will have a chief ray for each frequency of which we choose to follow the red and blue chief rays. Because refraction and dispersion start at the entrance plane, but the limiting aperture T_{P} is downstream of the entrance plane, there will be a different incident ray for each frequency. In other words $y_{\mathrm{K}}^{\mathrm{b}} \neq y_{\mathrm{K}}^{\mathrm{r}}$. Similarly, the inclination of the red and blue chief rays will be different through the centre of the pupil, that is, $a_{\mathrm{P}}^{\mathrm{b}} \neq a_{\mathrm{P}}^{\mathrm{r}}$. The red and blue chief rays are shown in Figure 7.2.1 to illustrate this.

We start with Equations 5.2.7 to 9 for an eye and distant object point and Equations 5.2.25 to 27 for an eye and an object point at a finite distance in order to obtain the position and inclination of the ray at the retina.

We define the chromatic difference in position at the retina as

$$\delta y_{\mathrm{R}} = y_{\mathrm{R}}^{\mathrm{b}} - y_{\mathrm{R}}^{\mathrm{r}}. \tag{7.2.2}$$

Substituting from Equations 5.2.5 and 8 into this equation we obtain

$$\delta y_{\mathrm{R}} = W_{\mathrm{E}}^{\mathrm{b}} y_{\mathrm{P}} - W_{\mathrm{E}}^{\mathrm{r}} y_{\mathrm{P}} + X_{\mathrm{E}}^{\mathrm{b}} a_{\mathrm{K}} - X_{\mathrm{E}}^{\mathrm{r}} a_{\mathrm{K}}$$

which we rewrite as

$$\delta y_{\mathrm{R}} = (\delta W_{\mathrm{E}}) y_{\mathrm{P}} + (\delta X_{\mathrm{E}}) a_{\mathrm{K}} \tag{7.2.3}$$

where δW_{E} is the chromatic difference in the distance image blur coefficients and δX_{E} is the chromatic difference in the distance image size coefficients as defined in Equation 7.2.1. The incident pencil of rays has inclination a_{K} and both the red and blue rays go through the same position in the pupil, that is $y_{\mathrm{P}}^{\mathrm{r}} = y_{\mathrm{P}}^{\mathrm{b}}$. Similarly, from Equation 5.2.28, for eyes with an object point at a finite distance we obtain

$$\delta y_{\mathrm{R}} = (\delta W_{\mathrm{OE}}) y_{\mathrm{P}} + (\delta X_{\mathrm{OE}}) y_{\mathrm{O}}. \tag{7.2.4}$$

If the model eye has its pupil centred on the optical axis, then tracing the chief rays such that $y_{\mathrm{P}} = 0$, Equations 7.2.3 and 4 simplify to

$$\delta y_{\mathrm{R}} = (\delta X_{\mathrm{E}}) a_{\mathrm{K}} \tag{7.2.5}$$

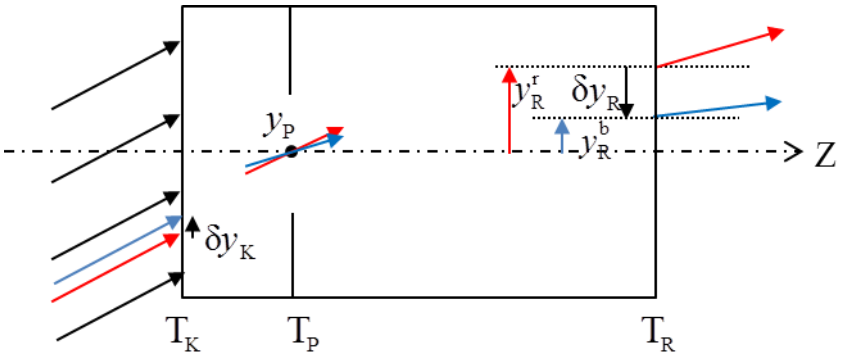

Figure 7.2.1 Chromatic difference in image position is shown as δy_{R}. Rays, all with the same incident inclination a_{K}, enter the eye and traverse a selected position through the pupil, y_{P} and are traced to the retina. The chief ray is illustrated and represents the centre of the blur circle at the retina. At the retina the two rays representing the blue and red light are shown. Chromatic difference in image position is the difference in position on the retina of these two rays, δy_{R}. The red and blue chief rays will follow different paths as illustrated. All measurements are taken at the respective transverse plane. Inclinations and positions are exaggerated for clarity.
for a distant object point and

$$\delta y_{\mathrm{R}} = \left(\delta X_{\mathrm{OE}}\right) y_{\mathrm{O}} \tag{7.2.6}$$

for an object point at a finite distance. Equations 7.2.5 and 6 are both linear equations. From this we can see that the chromatic difference in position for an eye has a linear dependence on incident inclination for distant objects and on object position for finite objects.

We consider distant objects first. In Equation 7.2.5 δX_{E} is a constant for that eye and represents a magnification by the eye. The chromatic difference in position is then linearly dependent on the inclination of the incident light. In Section 5.2.2 we defined the system (subscript E) for the distant object scenario as consisting of just the eye while in Section 5.2.3 we define the system for the near object scenario (subscript OE) to include the eye and working distance. Similarly, at near δX_{OE} represents a constant, provided z_{O} remains unchanged. While the actual value of δX_{OE} will be different to δX_{E} this eye too shows us that chromatic difference in position is linearly dependent on the position of the object. Because z_{O} is incorporated into the coefficient matrix $\delta \mathbf{V}_{\mathrm{OE}}$, δX_{OE} will vary with any change in z_{O}. This will be shown for a selection of numerical examples in Chapter 10.

Let us look at Equations 7.2.5 and 6 in terms of the entries of the transferences. Substituting from Equation 5.2.8 and 5.2.26 into Equations 7.2.5 and 6 respectively, we obtain

$$\delta y_{\mathrm{R}} = \left(\delta \frac{B_{\mathrm{B}} n_0}{A_{\mathrm{A}}}\right) a_{\mathrm{K}} \tag{7.2.7}$$

for a distance object and

$$\delta y_{\mathrm{R}} = \left(\delta \frac{B_{\mathrm{B}}}{A_{\mathrm{A}} \zeta_{\mathrm{O}} - B_{\mathrm{A}}}\right) y_{\mathrm{O}} \tag{7.2.8}$$

for an object at a finite distance before S_{E}. These give us the chromatic difference in transverse position at the retina δy_{R}, firstly with a distant object and secondly with an object at a finite distance, in terms of the fundamental properties of the Gaussian model eye.

An underlying implication

Chromatic dispersion starts as the light enters the first refracting surface, that is, the cornea. However, we then follow only the chief ray, defined by y_{P}. This implies that the blue and red rays that traverse the pupil centre are not originating from the same ray incident on the cornea, but rather two incident rays, both with the same inclination, incident at different positions onto the cornea, as illustrated in Figure 7.2.1. This difference in position is probably rather small, but nonetheless worth noting. Starting with Equations 3.2.40 and 3.5.7 we can derive the formulae for δy_{K}, the chromatic difference in position of the two chief rays at the entrance plane to be

$$\delta y_{\mathrm{K}} = \left[\delta\left(\frac{n_0}{A_{\mathrm{E}}}\left(\frac{B_{\mathrm{B}}}{A_{\mathrm{A}}} - B_{\mathrm{E}}\right)\right)\right]a_{\mathrm{K}} + \left[\delta\left(\frac{1}{A_{\mathrm{A}}}\right)\right]y_{\mathrm{P}} \tag{7.2.9}$$

for a distant object and

$$\delta y_{\mathrm{K}} = \left(\delta\frac{B_{\mathrm{A}}}{B_{\mathrm{OA}}}\right)y_{\mathrm{O}} + \left(\delta\frac{\zeta_{\mathrm{O}}}{B_{\mathrm{OA}}}\right)y_{\mathrm{P}} \tag{7.2.10}$$

for an object point at a finite distance from the eye.

Use of pinhole

We return to Equations 7.2.3 and 4 and consider the clinical scenario where a pinhole is held immediately in front of the eye. The limiting aperture is no longer centred on the optical axis and the chromatic difference in position increases in magnitude with increasing decentration of the pinhole and the object. The entries of $\mathbf{V}_{\mathrm{E}}$ and $\mathbf{V}_{\mathrm{OE}}$, given by Equations 5.2.8 and 26, simplify for the pinhole in front of the eye and therefore Equations 7.2.3 and 4 become

$$\delta y_{\mathrm{R}} = \left(\delta W_{\mathrm{E}}^{\mathrm{P}}\right)y_{\mathrm{P}} + \left(\delta X_{\mathrm{E}}^{\mathrm{P}}\right)a_{\mathrm{K}} \tag{7.2.11}$$

and

$$\delta y_{\mathrm{R}} = \left(\delta W_{\mathrm{OE}}^{\mathrm{P}}\right)y_{\mathrm{P}} + \left(\delta X_{\mathrm{OE}}^{\mathrm{P}}\right)y_{\mathrm{O}} \tag{7.2.12}$$

where the coefficients for $\mathbf{V}_{\mathrm{E}}^{\mathrm{P}}$ and $\mathbf{V}_{\mathrm{OE}}^{\mathrm{P}}$ are given in Equations 5.2.37 and 5.2.34 respectively. In terms of the entries of the transferences Equations 7.2.11 and 12 simplify to become

$$\delta y_{\mathrm{R}} = (\delta A_{\mathrm{E}})y_{\mathrm{P}} + (\delta(B_{\mathrm{E}} n_0))a_{\mathrm{K}} \tag{7.2.13}$$

and

$$\delta y_{\mathrm{R}} = (\delta(A_{\mathrm{E}} - B_{\mathrm{E}}\zeta_{\mathrm{O}}^{-1}))y_{\mathrm{P}} + (\delta(B_{\mathrm{E}}\zeta_{\mathrm{O}}^{-1}))y_{\mathrm{O}}. \tag{7.2.14}$$

Equations 7.2.11 and 12 are the specialised versions of Equations 7.2.3 and 4 which indicate substitution of the coefficients from $\mathbf{V}_{\mathrm{E}}^{\mathrm{P}}$ and $\mathbf{V}_{\mathrm{OE}}^{\mathrm{P}}$ respectively for the special situation of a pinhole placed in front of the eye. The conclusions that we can draw from the four equations are similar: the chromatic difference in position will increase in magnitude firstly for distant objects with the increase in incident inclination, secondly, for object points at a finite distance with increase in transverse displacement of the object point from the axis and finally with increased transverse displacement of the pinhole or position of the ray through the pupil from the optical axis. These conclusions are consistent with the findings in the literature, discussed in Chapter 2.

7.2.3 Chromatic difference in inclination at the retina

In Section 7.2.2 we defined, quite literally, the chromatic difference in image position at the retina. However, in Chapter 2 it was shown that a number of studies treat the chromatic difference in image position as the difference in inclination between the red and blue dispersed rays from a single object point. Here we define chromatic difference in inclination at the retina as the difference in emergent inclination of the two coloured reference rays, dispersed by the eye, from a particular object point, that is to say δa_{R}. This definition is general and defined with centred astigmatic eyes in mind. In an astigmatic eye the nodal structure is not a point and in a multi-surface eye the nodal structure differs in position with frequency and is unlikely to make a pivotal point. Similarly, the entrance pupil is merely an image of the pupil viewed through the cornea. The first refracting surface is a fixed physical structure (with an infinity of optical axes) but is not suitable because the rays do not necessarily coincide at this point. The definition, therefore, measures the difference in inclination of the emergent chromatic rays without concern for where or even if these two rays intersect.

We define the chromatic difference of inclination at the retina as

$$\delta a_{\mathrm{R}} = a_{\mathrm{R}}^{\mathrm{b}} - a_{\mathrm{R}}^{\mathrm{r}} \tag{7.2.15}$$

where $a_{\mathrm{R}}^{\mathrm{b}}$ and $a_{\mathrm{R}}^{\mathrm{r}}$ are the (unreduced) inclinations of the blue and red chief rays at the retina. From Equations 5.2.7 and 29 we obtain the difference in emergent reduced inclination from an eye

$$\delta a_{\mathrm{R}} = (\delta Y_{\mathrm{E}}) y_{\mathrm{P}} + (\delta Z_{\mathrm{E}}) a_{\mathrm{K}} \tag{7.2.16}$$

for a distant object point and

$$\delta a_{\mathrm{R}} = (\delta Y_{\mathrm{OE}}) y_{\mathrm{P}} + (\delta Z_{\mathrm{OE}}) y_{\mathrm{O}} \tag{7.2.17}$$

for a finite-distance object point. For model eyes with a centred pupil this simplifies to

$$\delta a_{\mathrm{R}} = (\delta Z_{\mathrm{E}}) a_{\mathrm{K}} \tag{7.2.18}$$

and

$$\delta a_{\mathrm{R}} = (\delta Z_{\mathrm{OE}}) y_{\mathrm{O}} \tag{7.2.19}$$

for distant and finite object points respectively. Equation 7.2.18, solved for δZ_{E}, resembles Equation 2.3.8 which Thibos, Bradley and Zhang (1991) and Zhang, Thibos and Bradley (1991) define as the chromatic difference in magnification.

The Gaussian eye and a distant object point are shown in Figure 7.2.2. This is an extension of Figure 7.2.1 and the paths of the rays at emergence at the retinal plane are shown. The point where they intersect is unimportant and may, for example, be upstream from the lens which implies that the diagram does not show the actual ray path but merely a projection of the rays inside the eye. In Gaussian eyes, we can envision an intersection, however this may not coincide with the optical axis and is also not necessarily going to intersect with the pupil centre, a refracting surface or any of the cardinal points. This is shown in Figure 7.2.2. It will depend on the complexity of the schematic eye being modelled.

For a Gaussian eye, the red and blue non-parallel rays intersect at some position in the plane of the eye to create a chromatic difference in inclination. However, it is foreseeable that in a three-dimensional linear system with heterocentric astigmatic elements that the red and blue rays are skew rays that may not intersect. It is possible that they may swirl past each other and never coincide. Investigating this is, however, outside the scope of this dissertation.

Use of a pinhole

Let us consider the situation where there is a pinhole held immediately before the corneal plane. Equations 7.2.16 and 17 still hold, however we substitute the relevant coefficients from $\delta\mathbf{V}_{\mathrm{E}}^{\mathrm{P}}$ and $\delta\mathbf{V}_{\mathrm{OE}}^{\mathrm{P}}$ instead of $\delta\mathbf{V}_{\mathrm{E}}$ and $\delta\mathbf{V}_{\mathrm{OE}}$. Two simplifications we will consider are when the light originates firstly from a distant object point and parallel to the optical axis that is $a_{\mathrm{K}}=0$ and secondly from an axial object point, where $y_{\mathrm{O}}=0$. Equations 7.2.16 and 17 simplify to

$$\delta a_{\mathrm{R}}=\left(\delta Y_{\mathrm{E}}^{\mathrm{P}}\right)y_{\mathrm{P}} \tag{7.2.20}$$

and

$$\delta a_{\mathrm{R}}=\left(\delta Y_{\mathrm{OE}}^{\mathrm{P}}\right)y_{\mathrm{P}} \tag{7.2.21}$$

respectively. $Y_{\mathrm{E}}^{\mathrm{P}}$ and $Y_{\mathrm{OE}}^{\mathrm{P}}$ are defined by Equations 5.2.37 and 34. In terms of the entries of the transference, Equations 7.2.20 and 21 simplify to

$$\delta a_{\mathrm{R}}=\left(\delta\left(C_{\mathrm{E}}n^{-1}\right)\right)y_{\mathrm{P}}$$

and

$$\delta a_{\mathrm{R}}=\left(\delta\left(n^{-1}\left(C_{\mathrm{E}}-D_{\mathrm{E}}\zeta_{\mathrm{O}}^{-1}\right)\right)\right)y_{\mathrm{P}},$$

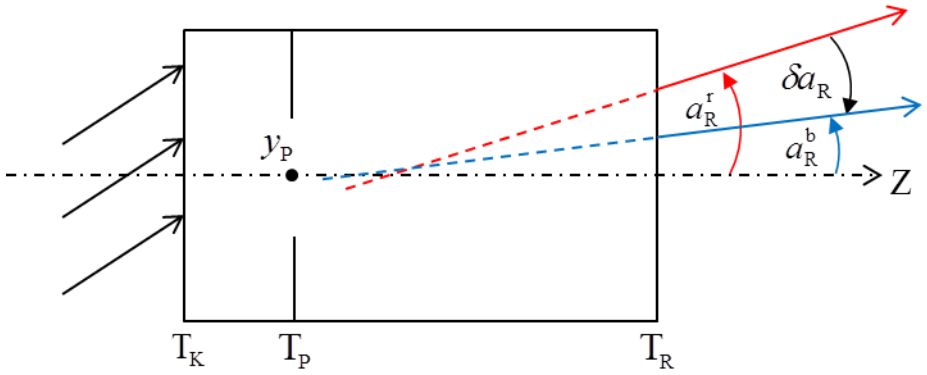

Figure 7.2.2 A Gaussian eye and a pencil of rays from a distant object showing chromatic difference in inclination between the two dispersed rays. The pivotal point is the where the projection of the two rays intersect to create an angle. It may or may not coincide with any reference structure, including the longitudinal axis. Inclinations in the diagram are exaggerated for clarity.

respectively. These are both linear equations showing that, when a pinhole is held immediately in front of the eye, the chromatic difference in inclination at the retina is dependent on the position of the pinhole from the optical axis.

Now from Equations 7.2.16 and 17 we can see that chromatic properties increase with increased transverse displacement of the object point from the optical axis and also with increased transverse displacement of the pinhole from the optical axis. This is consistent with conclusions discussed in Chapter 2.

In summary

Equations 7.2.3 and 16 can be summarised as

$$\delta\mathbf{V}_{\mathrm{E}}\mathbf{v}_{\mathrm{E}} = \delta\mathbf{r}_{\mathrm{R}} \tag{7.2.22}$$

where $\delta\mathbf{V}_{\mathrm{E}}$ is defined by Equation 7.2.1, $\mathbf{v}_{\mathrm{E}}$ by Equation 5.2.9 and $\delta\mathbf{r}_{\mathrm{R}}$ as

$$\delta\mathbf{r}_{\mathrm{R}} = \begin{pmatrix} \delta y_{\mathrm{R}} \\ \delta a_{\mathrm{R}} \end{pmatrix} \tag{7.2.23}$$

giving us δy_{R} the chromatic difference in transverse image position at the retina and δa_{R} chromatic difference in inclination at the retina for a distant object.

Similarly, we can summarise Equations 7.2.4 and 17 as

$$\delta\mathbf{V}_{\mathrm{OE}}\mathbf{v}_{\mathrm{OE}} = \delta\mathbf{r}_{\mathrm{R}} \tag{7.2.24}$$

where $\delta\mathbf{V}_{\mathrm{OE}}$ is defined in Section 7.2.1, $\mathbf{v}_{\mathrm{OE}}$ by Equation 5.2.27 and $\delta\mathbf{r}_{\mathrm{R}}$ by Equation 7.2.23.

In the same way, we can summarise δy_{R} and δa_{R} using a pinhole in front of the eye as

$$\delta\mathbf{V}_{\mathrm{E}}^{\mathrm{P}}\mathbf{v}_{\mathrm{E}} = \delta\mathbf{r}_{\mathrm{R}} \tag{7.2.25}$$

for a distant object and for an object point at a finite distance from the eye as

$$\delta\mathbf{V}_{\mathrm{OE}}^{\mathrm{P}}\mathbf{v}_{\mathrm{OE}} = \delta\mathbf{r}_{\mathrm{R}}\,. \tag{7.2.26}$$

Generalizing to linear optics

The chromatic difference in transverse image position at the retina (Equations 7.2.2 to 6), the chromatic difference in inclination at the retina (Equations 7.2.15 to 19) and their summary (Equations 7.2.22 to 24) readily generalize to linear optics, provided one substitutes from Equations 5.2.38 and 39 when obtaining the chromatic difference in coefficient matrices (Equation 7.2.1). The equations for the scenario when a pinhole is placed immediately in front of the eye for chromatic difference in transverse image position at the retina

(Equations 7.2.11 to 14), the chromatic difference in inclination at the retina (Equations 7.2.20 to 21) and the summary (Equations 7.2.25 and 26) also readily generalize to linear optics. The equations for the underlying implication of chromatic difference in corneal position when the rays originate from the same object point can be rewritten to be general as

$$\delta\mathbf{y}_{\mathrm{K}} = \delta\left(\mathbf{A}_{\mathrm{E}}^{-1}\left(\mathbf{X}_{\mathrm{E}} - n_0\mathbf{B}_{\mathrm{E}}\right)\right)\mathbf{a}_{\mathrm{K}} + \delta\left(\mathbf{A}_{\mathrm{E}}^{-1}\mathbf{W}_{\mathrm{E}}\right)\mathbf{y}_{\mathrm{P}}$$

for a distant object and

$$\delta\mathbf{y}_{\mathrm{K}} = \delta\left(\left(\zeta_{\mathrm{O}}\mathbf{A}_{\mathrm{E}} + n_{\mathrm{O}}^{-1}\mathbf{X}_{\mathrm{E}} - \mathbf{B}_{\mathrm{E}}\right)^{-1}\left(n_{\mathrm{O}}^{-1}\mathbf{X}_{\mathrm{E}} - \mathbf{B}_{\mathrm{E}}\right)\right)\mathbf{y}_{\mathrm{O}} + \delta\left(\left(\zeta_{\mathrm{O}}\mathbf{A}_{\mathrm{E}} + n_{\mathrm{O}}^{-1}\mathbf{X}_{\mathrm{E}} - \mathbf{B}_{\mathrm{E}}\right)^{-1}\left(\zeta_{\mathrm{O}}\mathbf{W}_{\mathrm{E}}\right)\right)\mathbf{y}_{\mathrm{P}}$$

for an object at a finite distance where $\mathbf{X}_{\mathrm{E}}$ and $\mathbf{W}_{\mathrm{E}}$ are given in Equation 5.2.38.

7.3 Chromatic properties of the eye dependent on object size or angular spread

The terminology used in the literature is *chromatic difference in magnification.* Let us start by trying to understand what this term means. Magnification was defined in Section 3.5.1 as a ratio of either the image to object size or the ratio of image's reduced inclination to the object's reduced inclination. In Sections 3.5.3 and 5.2 the magnification is defined for specific circumstances in terms of coefficients, which are also ratios. What meaning, then, can we give to a difference between ratios?

In Chapter 2 we saw that there are a number of different approaches to defining chromatic difference in magnification. Simonet and Campbell (1990) define chromatic difference in magnification as the difference in image sizes at the retina (Equation 2.3.7), but the measurement is given in seconds of arc. Similarly, we firstly define the chromatic difference in image size at the retina, and, secondly, we obtain the chromatic difference in angular spread across the retina.

Thibos, Bradley and Zhang (1991) and Zhang, Thibos and Bradley (1991) define chromatic difference in magnification as the ratio of the difference in angle between the red and blue chief rays to the angle of eccentricity subtended by the object point (Equation 2.3.8). However, is this a difference in magnification or the magnification of differences? They give their resultant chromatic difference in magnification as a percentage. Similarly, we take this definition of magnification

and compare both the magnification of image sizes and the magnification of angular spread between the blue and red images. We will see that the issue of blur is not ignored, but rather is nullified by the definition.

7.3.1 Chromatic difference in image size

In order to obtain the chromatic difference in image size $\delta(\Delta y_{\mathrm{R}})$ we first need to calculate the size of each of the blue and red images from Equation 5.2.5 and then calculate the difference in size between them. For a distant object, the size of the blue image will be

$$\Delta y_{\mathrm{R}}^{\mathrm{b}} = W_{\mathrm{E}}^{\mathrm{b}} y_{\mathrm{P2}} - W_{\mathrm{E}}^{\mathrm{b}} y_{\mathrm{P1}} + X_{\mathrm{E}}^{\mathrm{b}} a_{\mathrm{K2}} - X_{\mathrm{E}}^{\mathrm{b}} a_{\mathrm{K1}}. \tag{7.3.1}$$

The position in the pupil or pinhole is the same for both rays, that is $y_{\mathrm{P1}} = y_{\mathrm{P2}}$ and therefore this simplifies to

$$\Delta y_{\mathrm{R}}^{\mathrm{b}} = X_{\mathrm{E}}^{\mathrm{b}} \Delta a_{\mathrm{K}} \tag{7.3.2}$$

and similarly for the red image. The angle subtended by the distant object is

$$\Delta a_{\mathrm{K}} = a_{\mathrm{K2}} - a_{\mathrm{K1}}. \tag{7.3.3}$$

The chromatic difference in image size is

$$\delta(\Delta y_{\mathrm{R}}) = \Delta y_{\mathrm{R}}^{\mathrm{b}} - \Delta y_{\mathrm{R}}^{\mathrm{r}} = X_{\mathrm{E}}^{\mathrm{b}} \Delta a_{\mathrm{K}} - X_{\mathrm{E}}^{\mathrm{r}} \Delta a_{\mathrm{K}} = (\delta X_{\mathrm{E}})(\Delta a_{\mathrm{K}}) \tag{7.3.4}$$

where $\Delta y_{\mathrm{R}}^{\mathrm{b}}$ is the size of the blue image at the retina and likewise $\Delta y_{\mathrm{R}}^{\mathrm{r}}$ is the size of the red image at the retina, as indicated in Figure 7.3.1. We use the symbolisms Δ to represent a size (difference in position) or angle subtended (difference in inclination) and δ to represent a chromatic difference in, for example, position, size, inclination or angular spread.

The size of the blue image at the retina from an object at a finite distance is

$$\Delta y_{\mathrm{R}}^{\mathrm{b}} = W_{\mathrm{OE}}^{\mathrm{b}} y_{\mathrm{P2}} - W_{\mathrm{OE}}^{\mathrm{b}} y_{\mathrm{P1}} + X_{\mathrm{OE}}^{\mathrm{b}} y_{\mathrm{O2}} - X_{\mathrm{OE}}^{\mathrm{b}} y_{\mathrm{O1}} \tag{7.3.5}$$

but

$$y_{\mathrm{P1}} = y_{\mathrm{P2}} \tag{7.3.6}$$

therefore

$$\Delta y_{\mathrm{R}}^{\mathrm{b}} = X_{\mathrm{OE}}^{\mathrm{b}} \Delta y_{\mathrm{O}}. \tag{7.3.7}$$

and similarly for the size of the red image at the retina. X^{b}_{OE} is the near image size coefficient and represents a magnification of the object to the blue image. It is similar to Equation 3.5.1 which represents a transverse magnification. For near the chromatic difference in image size will be

$$\delta(\Delta y_R) = \Delta y^{b}_{R} - \Delta y^{r}_{R} = X^{b}_{OE}\Delta y_O - X^{r}_{OE}\Delta y_O = (\delta X_{OE})(\Delta y_O) \qquad (7.3.8)$$

where Δy_O is the length of the object at the object plane T_O.

The result indicates that δX_E, the chromatic difference in distance image size coefficients and δX_{OE}, the chromatic difference in near image size coefficients, represent constants and therefore the actual size of the image will depend on the size of the object (for distant objects this is represented by the change in incident inclination of the rays) and not on any transverse displacement of the pupil (or pinhole). We can conclude that δX_E and δX_{OE} represent a chromatic difference in image size magnification by the system of either a distant

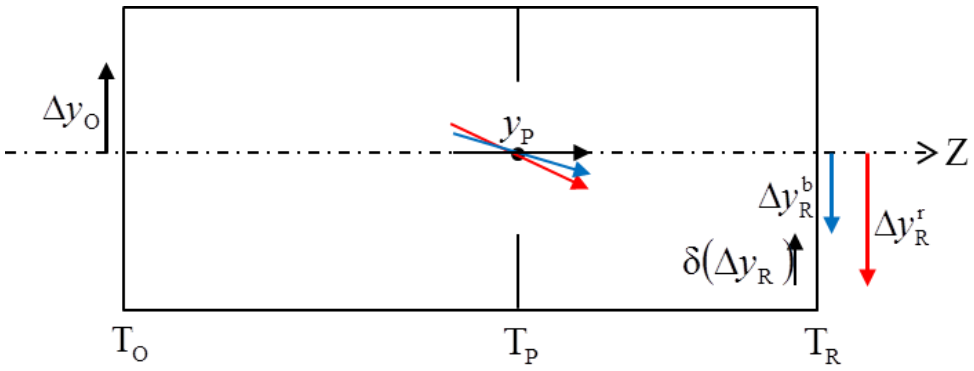

Figure 7.3.1 Chromatic difference in image size $\delta(\Delta y_R)$ in a Gaussian system S_{OE} with the object at a finite distance from the eye S_E. The size of the object is shown at the entrance plane as Δy_O. Rays from the two endpoints of the object enter the eye and are illustrated traversing the pupil, but don't necessarily have to traverse the pupil centre. The two rays are dispersed through the eye and result in a blue and a red image at the retina. One or both images may be blurred, however it is their size magnification that we are interested in. The chromatic difference in magnification is shown as the difference in size of the two coloured images. The figure is drawn for the simpler situation of an axial based object. All objects and images are measured at the respective transverse planes, and are drawn separately for clarity.

or near object. Figure 7.3.1 shows chromatic difference in image size for near for a Gaussian system and axial object, however, it is not necessary for an object to be axial, Equations 7.3.4 and 8 apply to non-axial objects of size Δy_{O}.

7.3.2 Chromatic difference in angular spread at the retina

The chromatic difference in angular spread at the retina $\delta(\Delta a_{\mathrm{R}})$ is obtained in a similar way to the chromatic difference in image size. From Equation 5.2.6 we can define the angular spread of the blue image on the retina as

$$\Delta a_{\mathrm{R}}^{\mathrm{b}} = Y_{\mathrm{E}}^{\mathrm{b}} y_{\mathrm{P2}} - Y_{\mathrm{E}}^{\mathrm{b}} y_{\mathrm{P1}} + Z_{\mathrm{E}}^{\mathrm{b}} a_{\mathrm{K2}} - Z_{\mathrm{E}}^{\mathrm{b}} a_{\mathrm{K1}}. \tag{7.3.9}$$

Equation 7.3.6 applies and so Equation 7.3.9 simplifies to

$$\Delta a_{\mathrm{R}}^{\mathrm{b}} = Z_{\mathrm{E}}^{\mathrm{b}} \Delta a_{\mathrm{K}} \tag{7.3.10}$$

and similarly for the angular spread of the red image across the retina. $Z_{\mathrm{E}}^{\mathrm{b}}$ is the distance directional coefficient and represents a magnification of the angular spread of the incident rays to the blue emergent rays. For an axial object, Equation 7.3.10 is similar to Equation 3.5.3, the angular magnification of image to object. To calculate the chromatic difference in angular spread between the red and blue images across the retina from an object with angular spread of Δa_{K}, we obtain

$$\delta(\Delta a_{\mathrm{R}}) = \Delta a_{\mathrm{R}}^{\mathrm{b}} - \Delta a_{\mathrm{R}}^{\mathrm{r}} = Z_{\mathrm{E}}^{\mathrm{b}} \Delta a_{\mathrm{K}} - Z_{\mathrm{E}}^{\mathrm{r}} \Delta a_{\mathrm{K}} = (\delta Z_{\mathrm{E}})(\Delta a_{\mathrm{K}}). \tag{7.3.11}$$

Similarly, the chromatic difference in angular spread for an object with size Δy_{O} at a finite distance is

$$\delta(\Delta a_{\mathrm{R}}) = (\delta Z_{\mathrm{OE}})(\Delta y_{\mathrm{O}}). \tag{7.3.12}$$

δZ_{E} is the chromatic difference in distance directional coefficient and δZ_{OE} is the chromatic difference in near directional coefficient, both being constants for any particular chosen system. Equations 7.3.11 and 12 are linear equations with δZ_{E} and δZ_{OE} representing the slope. δZ_{E} magnifies the incident angular spread from the object and, likewise, δZ_{OE} magnifies the object size to obtain the $\delta(\Delta a_{\mathrm{R}})$.

The angular spread Δa_{R} is the difference in inclination of the two rays that subtend the end-points of an image on the retina, that is $\Delta a_{\mathrm{R}} = a_{\mathrm{R2}} - a_{\mathrm{R1}}$. The pivotal point where these two rays (a_{R1} and a_{R2}) meet is not necessarily

represented by a cardinal point, the longitudinal axis or a physical structure. The red and blue images have different sizes and will subtend different Δa_{R}. The pivotal points for the red and blue images will not necessarily coincide. This is a different definition to that defined in the literature by angle *t* in Figures 2.3.3 and 4, however, it does represent the actual rays and as such has implications for the Stiles-Crawford effect.

Chromatic difference in image size and angular spread with a pinhole

We can obtain the chromatic difference in image size and angular spread at the retina when a pinhole is placed immediately in front of the eye using Equations 7.3.4, 8, 11 and 12, and replacing the coefficients with the respective coefficients from $\mathbf{V}_{\mathrm{E}}^{\mathrm{P}}$ (Equation 5.2.37) and $\mathbf{V}_{\mathrm{OE}}^{\mathrm{P}}$ (Equation 5.2.34). The effect of placing a pinhole immediately in front of the eye has the effect of moving the limiting aperture longitudinally. However, the effect of any transverse displacement of the pinhole is nullified, as shown by Equation 7.3.6.

In summary

Equations 7.3.4 and 11 can be summarized as

$$\delta\mathbf{V}_{\mathrm{E}}\Delta\mathbf{v}_{\mathrm{E}} = \delta\Delta\mathbf{r}_{\mathrm{R}} \tag{7.3.13}$$

where $\delta\mathbf{V}_{\mathrm{E}}$ is the chromatic difference in coefficient matrix given in Equation 7.2.1,

$$\Delta\mathbf{v}_{\mathrm{E}} = \begin{pmatrix} \Delta y_{\mathrm{P}} \\ \Delta a_{\mathrm{K}} \end{pmatrix} \tag{7.3.14}$$

where $\Delta y_{\mathrm{P}} = 0$ and Δa_{K} is the angular spread indicating the distant object size, and

$$\delta\Delta\mathbf{r}_{\mathrm{R}} = \delta\begin{pmatrix} \Delta y_{\mathrm{R}} \\ \Delta a_{\mathrm{R}} \end{pmatrix} \tag{7.3.15}$$

is the chromatic difference in image sizes $\delta\Delta y_{\mathrm{R}}$ or chromatic difference in angular spread $\delta\Delta a_{\mathrm{R}}$ at the retina.

Similarly, we summarize Equations 7.3.8 and 12 as

$$\delta\mathbf{V}_{\mathrm{OE}}\Delta\mathbf{v}_{\mathrm{OE}} = \delta\Delta\mathbf{r}_{\mathrm{R}} \tag{7.3.16}$$

where

$$\Delta\mathbf{v}_{\mathrm{OE}} = \begin{pmatrix} \Delta y_{\mathrm{P}} \\ \Delta y_{\mathrm{O}} \end{pmatrix}, \tag{7.3.17}$$

$\Delta y_{\mathrm{P}} = 0$ and Δy_{O} is the object size. When placing a pinhole immediately in front of the eye, we substitute $\delta\mathbf{V}_{\mathrm{E}}^{\mathrm{P}}$ for $\delta\mathbf{V}_{\mathrm{E}}$ and $\delta\mathbf{V}_{\mathrm{OE}}^{\mathrm{P}}$ for $\delta\mathbf{V}_{\mathrm{OE}}$ in Equations 7.3.13 and 16 respectively.

Generalizing to linear optics

The chromatic difference in image size (Equations 7.3.1 to 8) and the chromatic difference in angular spread (Equations 7.3.9 to 12) as well as the respective summary (Equations 7.3.13 to 17) readily generalize to linear optics, provided one substitutes from Equations 5.2.38 and 39 when obtaining the chromatic difference in coefficient matrices (Equation 7.2.1).

7.3.3 Retinal chromatic image size magnification

In this section we adopt the method described by Thibos *et al* (1991) and Zhang *et al* (1991) of defining chromatic difference in magnification (Equation 2.3.8) as a ratio. We first investigate the retinal chromatic image size magnification and then the retinal chromatic angular spread magnification. The retinal chromatic image size magnification is defined as the magnification of the size of the red image to obtain the size of the blue image at the retina as

$$M_{\mathrm{yR}}\ \Delta y_{\mathrm{R}}^{\mathrm{r}} = \Delta y_{\mathrm{R}}^{\mathrm{b}} \tag{7.3.18}$$

where $\Delta y_{\mathrm{R}}^{\mathrm{b}}$ and $\Delta y_{\mathrm{R}}^{\mathrm{r}}$ are the blue and red retinal image sizes defined by Equation 7.3.2. Substituting from Equation 7.3.2 into 7.3.18 we obtain

$$M_{\mathrm{yR}} X_{\mathrm{E}}^{\mathrm{r}} \Delta a_{\mathrm{K}} = X_{\mathrm{E}}^{\mathrm{b}} \Delta a_{\mathrm{K}}$$

which simplifies to

$$M_{\mathrm{yR}} X_{\mathrm{E}}^{\mathrm{r}} = X_{\mathrm{E}}^{\mathrm{b}} \tag{7.3.19}$$

for a distant object. Substituting from Equation 7.3.7 into 7.3.18 we obtain

$$M_{\mathrm{yR}} X_{\mathrm{OE}}^{\mathrm{r}} \Delta y_{\mathrm{O}} = X_{\mathrm{OE}}^{\mathrm{b}} \Delta y_{\mathrm{O}}$$

which simplifies to

$$M_{\mathrm{yR}} X^{\mathrm{r}}_{\mathrm{OE}} = X^{\mathrm{b}}_{\mathrm{OE}} \tag{7.3.20}$$

for an object at a finite distance. Taking the magnification a step further, we can substitute the elements of the transferences, as defined in Equations 5.2.8 and 26 into 7.3.19 and 20 to obtain

$$M_{\mathrm{yR}} B^{\mathrm{r}}_{\mathrm{B}} A^{\mathrm{b}}_{\mathrm{A}} n^{\mathrm{r}}_0 = B^{\mathrm{b}}_{\mathrm{B}} A^{\mathrm{r}}_{\mathrm{A}} n^{\mathrm{b}}_0 \tag{7.3.21}$$

and

$$M_{\mathrm{yR}} B^{\mathrm{r}}_{\mathrm{B}} \left(A^{\mathrm{b}}_{\mathrm{A}} \zeta^{\mathrm{b}}_{\mathrm{O}} - B^{\mathrm{b}}_{\mathrm{A}} \right) = B^{\mathrm{b}}_{\mathrm{B}} \left(A^{\mathrm{r}}_{\mathrm{A}} \zeta^{\mathrm{r}}_{\mathrm{O}} - B^{\mathrm{r}}_{\mathrm{A}} \right) \tag{7.3.22}$$

respectively. From Equations 7.3.19 to 22 we can conclude that the retinal chromatic size magnification will be a fixed ratio for the system and does not depend on object size or transverse position.

7.3.4 Retinal chromatic angular spread magnification

The second approach to retinal chromatic magnifications makes use of the angular spread, obtaining the magnification of the red to blue angular spreads of the emergent chief rays reaching the retina from an object. We therefore define the retinal chromatic angular spread magnification as

$$M_{a\mathrm{R}} \Delta a^{\mathrm{r}}_{\mathrm{R}} = \Delta a^{\mathrm{b}}_{\mathrm{R}} \tag{7.3.23}$$

where $\Delta a^{\mathrm{b}}_{\mathrm{R}}$ and $\Delta a^{\mathrm{r}}_{\mathrm{R}}$ are the angular spread across the retina for the blue and red images. We define the blue angular spread at the retina, $\Delta a^{\mathrm{b}}_{\mathrm{R}}$ as

$$\Delta a^{\mathrm{b}}_{\mathrm{R}} = Y^{\mathrm{b}}_{\mathrm{E}} y_{\mathrm{P2}} - Y^{\mathrm{b}}_{\mathrm{E}} y_{\mathrm{P1}} + Z^{\mathrm{b}}_{\mathrm{E}} a_{\mathrm{K2}} - Z^{\mathrm{b}}_{\mathrm{E}} a_{\mathrm{K1}} \tag{7.3.24}$$

however, the two rays traverse the same position through the pupil and therefore

$$\Delta a^{\mathrm{b}}_{\mathrm{R}} = Z^{\mathrm{b}}_{\mathrm{E}} \Delta a_{\mathrm{K}} \tag{7.3.25}$$

and similarly for the angular spread of the red image at the retina. The angular spread of a blue image at the retina from an object at a finite distance is

$$\Delta a^{\mathrm{b}}_{\mathrm{R}} = Z^{\mathrm{b}}_{\mathrm{OE}} \Delta y_{\mathrm{O}} . \tag{7.3.26}$$

Substituting from Equations 7.3.25 and 26 in turn into Equation 7.3.23 we obtain

$$M_{a\mathrm{R}} Z^{\mathrm{r}}_{\mathrm{E}} \Delta a_{\mathrm{K}} = Z^{\mathrm{b}}_{\mathrm{E}} \Delta a_{\mathrm{K}}$$

which simplifies to

$$M_{a\mathrm{R}} Z^{\mathrm{r}}_{\mathrm{E}} = Z^{\mathrm{b}}_{\mathrm{E}} \tag{7.3.27}$$

for a distant object and

$$M_{aR} Z^{r}_{OE} \Delta y_O = Z^{b}_{OE} \Delta y_O$$

which in turn simplifies to

$$M_{aR} Z^{r}_{OE} = Z^{b}_{OE} \tag{7.3.28}$$

for an object at a finite distance, respectively. We now substitute from Equations 5.2.8 and 26 into the above equations respectively to obtain

$$M_{aR} D^{r}_{B} A^{b}_{A} n^{r}_{0} n^{b} = D^{b}_{B} A^{r}_{A} n^{b}_{0} n^{r} \tag{7.3.29}$$

for distance objects and

$$M_{aR} D^{r}_{B} \left(A^{b}_{A} \zeta^{b}_{O} - B^{b}_{A} \right) n^{b} = D^{b}_{B} \left(A^{r}_{A} \zeta^{r}_{O} - B^{r}_{A} \right) n^{r} \tag{7.3.30}$$

for objects at a finite distance. Again we can conclude that the retinal chromatic angular spread magnification is not dependent on the object's size or transverse position.

Comparing Equation 7.3.21 to 7.3.29 and 7.3.22 to 7.3.30 we see that the only variable that is different in the two pairs of equations is the ratio $\frac{B^{b}_{B}}{B^{r}_{B}}$ for retinal chromatic size magnification versus $\frac{D^{b}_{B} n^{r}}{D^{r}_{B} n^{b}}$ for the retinal chromatic angular spread magnification. We will do numerical examples in Chapter 10 to see how these ratios affect our ultimate result.

Retinal chromatic magnifications with a pinhole

We have seen that, when comparing image sizes of the red and blue images on the retina, the effect of transverse displacement of a pinhole y_P in front of the eye is nullified, however, the effect of displacing the longitudinal position of the limiting aperture will have an effect on the coefficients and hence on the magnifications. For each of Equations 7.3.19, 20, 27 and 28, we replace the respective coefficient with those from $\mathbf{V}^{P}_{E}$ (Equation 5.2.37) and $\mathbf{V}^{P}_{OE}$ (Equation 5.2.34), the distance and near coefficient matrices for a Gaussian eye with a pinhole immediately in front of it.

Generalizing to linear optics

The Equations in Section 7.3 have been written and derived such that they readily generalize to linear optics. The proof is beyond the scope of this dissertation.

7.4 Chromatic properties of the eye dependent on image and aperture positions

The derivations in Sections 7.2 and 3 apply in image space. However, experimental measurements and analyses are done in object space. In Section 2.3.2 we learnt that experiments make use of a target at a finite distance, a Vernier scale to measure the induced chromatic effect and a pinhole or Maxwellian view which controls and varies the position of the ray entering the eye (Thibos *et al*, 1990, 1992; Simonet and Campbell, 1990). The pinhole has the added benefit of eliminating any refractive compensation needed without the use of spectacle lenses which could add chromatic properties to the experiment (Thibos *et al*, 1990).

7.4.1 Chromatic difference in object position

Consider an eye and two coloured object points at different positions in object space. The two objects appear to be lined up on the retina as shown in Figure 7.4.1 where $y_{\mathrm{R}}^{\mathrm{b}} = y_{\mathrm{R}}^{\mathrm{r}}$. The superimposed points may or may not be at the fovea, and the emergent inclination need not be the same for the red and blue rays. Because such experiments are conducted in the clinical environment, we shall derive formulae for the near scenario only.

From Figure 7.4.1 we can see that while there are two object points of different frequencies at positions $y_{\mathrm{O}}^{\mathrm{b}}$ and $y_{\mathrm{O}}^{\mathrm{r}}$, we have a common transverse position through the pupil y_{P} for the chosen ray path for each frequency. The two rays arrive at a common point on the retina y_{R} where it should appear to the eye as being one object point; that is the two image points of differing frequencies are superimposed.

We wish to obtain the chromatic distance between the two object points, δy_{O}. From Equation 5.3.17 we obtain

$$\delta y_{\mathrm{O}} = \left(\delta W_{\mathrm{Oy}}\right) y_{\mathrm{P}} + \left(\delta X_{\mathrm{Oy}}\right) y_{\mathrm{R}} \tag{7.4.1}$$

where

$$\delta y_{\mathrm{O}} = y_{\mathrm{O}}^{\mathrm{b}} - y_{\mathrm{O}}^{\mathrm{r}} \tag{7.4.2}$$

is the distance between the red and blue object points at the object plane. δW_{Oy} is the chromatic difference in near object blur coefficient and δX_{Oy} is the chromatic difference in near object size coefficient, both with respect to the position of the image at the retina. Equation 7.4.1 gives us the chromatic difference in position for two object points of different frequencies in object space. This is comparable to the clinical or experimental scenario described in Section 2.3.2. It is a simple matter to choose the position of the fovea as y_{R}, where applicable. For the scenario where there is no pinhole and the pupil is centred on the optical axis such that $y_{\mathrm{P}} = 0$, we obtain the linear relationship

$$\delta y_{\mathrm{O}} = \left(\delta X_{\mathrm{Oy}}\right) y_{\mathrm{R}}. \tag{7.4.3}$$

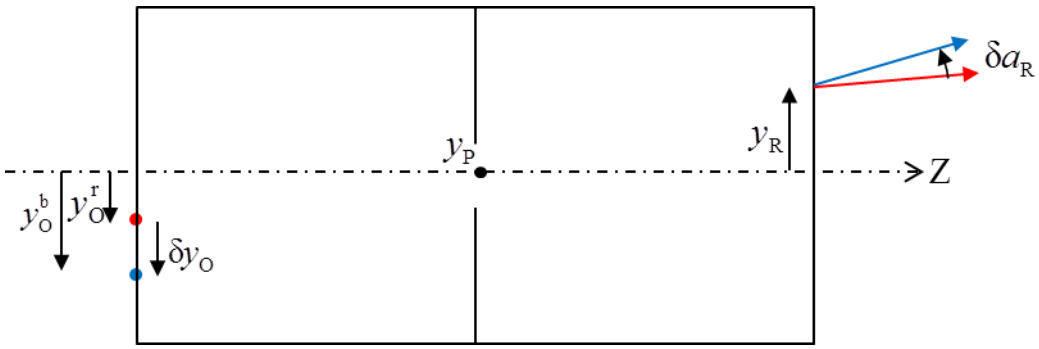

Figure 7.4.1 Chromatic difference in object position. A Gaussian system S_{OE} at near. The object consists of two separated point targets of different frequencies and at different transverse positions. The emergent rays coincide positionally at the retinal plane. The figure is general and the dividing plane may represent either a pupil or a pinhole. All measurements are taken at the respective transverse planes, but these are separated in the diagram for clarity.

For two chosen frequencies and a set working distance, δX_{Oy} will be a constant representing a magnification. Any increase in the magnitude of y_{R} will result in an increase in the separation of the red and blue object points δy_{O}. When fixation is set at the fovea it is possible to obtain the position of the fovea, $y_{\mathrm{R}} = \delta y_{\mathrm{O}} / \left(\delta X_{\mathrm{Oy}}\right)$ (from Equation 7.4.3), for a centred pupil.

Including the use of a pinhole

On the other hand, the preferred experimental procedure is to place a pinhole in front of the eye, immediately in front of the entrance plane or corneal plane and keep the position of the image on the retina constant. Equation 7.4.1 still applies, except that we can substitute the coefficients from the simpler $\delta \mathbf{V}_{\mathrm{Oy}}^{\mathrm{P}}$ such that

$$\delta y_{\mathrm{O}} = \left(\delta W_{\mathrm{Oy}}^{\mathrm{P}}\right) y_{\mathrm{P}} + \left(\delta X_{\mathrm{Oy}}^{\mathrm{P}}\right) y_{\mathrm{R}} . \tag{7.4.4}$$

Substituting from Equation 5.3.19 and then from Equation 3.4.6 we obtain

$$\delta y_{\mathrm{O}} = \left(\delta\left(1 - B_{\mathrm{E}}^{-1} A_{\mathrm{E}} \zeta_{\mathrm{O}}\right)\right) y_{\mathrm{P}} + \left(\delta\left(B_{\mathrm{E}}^{-1} \zeta_{\mathrm{O}}\right)\right) y_{\mathrm{R}} = \left(\delta\left(1 - F_0 \zeta_{\mathrm{O}}\right)\right) y_{\mathrm{P}} + \left(\delta\left(B_{\mathrm{E}}^{-1} \zeta_{\mathrm{O}}\right)\right) y_{\mathrm{R}} \tag{7.4.5}$$

where F_0 is the refractive compensation for the eye at the specified frequency.

For a model eye the fovea coincides with the optical axis at $y_{\mathrm{R}} = 0$ simplifying Equations 7.4.4 and 5 even further. However, the fovea is usually not on the optical axis, but does represent a constant for y_{R}. This means that Equation 7.4.4 is the equation for a straight line with $\left(\delta X_{\mathrm{Oy}}^{\mathrm{P}}\right) y_{\mathrm{R}}$ being a constant and $\left(\delta W_{\mathrm{Oy}}^{\mathrm{P}}\right)$ giving the slope of the straight line. From Equation 7.4.5 we can see that the separation of the two object points is directly proportional to the displacement of the pinhole from the optical axis and the constant of proportionality is related to the chromatic difference in refractive compensation and working distance.

7.4.2 Chromatic difference in inclination in object space

We again turn our attention to Figure 7.4.1, to obtain the chromatic difference in inclination in object space of each of the red and blue chief rays that will ultimately both reach the retina at the same point. When the aperture plane is

that of the pinhole, then these two rays will meet and create a point of intersection at the centre of the pinhole. However, when the aperture plane is the eye's pupil, then the rays will undergo refraction before reaching the pupil and, in Gaussian optics, the straight line projections of the two rays will meet at some other point, which may or may not be on the optical axis.

Figure 2.3.3(b) shows the definition of chromatic difference in position as the angle *t* between the incident chief rays for the blue and red targets. With this in mind we will derive equations to solve for δa_{O}.

In order to obtain the angle between the red and blue chief rays from a red and a blue object point, respectively, on the object plane which coincide at a single point on the retina we can obtain, from Equation 5.3.18, an equation for chromatic difference in inclination in object space

$$\delta a_{\mathrm{O}} = \left(\delta Y_{\mathrm{Oy}}\right) y_{\mathrm{P}} + \left(\delta Z_{\mathrm{Oy}}\right) y_{\mathrm{R}} . \qquad (7.4.6)$$

For a model eye with a centred pupil and no pinhole, we can equate $y_{\mathrm{P}} = 0$ and Equation 7.4.6 simplifies to

$$\delta a_{\mathrm{O}} = \left(\delta Z_{\mathrm{Oy}}\right) y_{\mathrm{R}} \qquad (7.4.7)$$

from which we can see the linear relationship that the angle between the two rays of differing frequencies increases with increasing transverse position on the retinal plane from the optical axis.

Including the use of a pinhole

In Section 2.3.2 we saw that the angular difference between the two incident rays which vary with displacement of a pinhole from the optical axis and create a single image at the retina is referred to by Thibos *et al* (1990) as induced transverse chromatic aberration. This is specifically achieved by the use of a pinhole immediately in front of the eye and held at varying transverse distances from the model eye's optical axis, that is, where y_{P} is not necessarily zero. Equation 7.4.6 is general and still applies, with substitution of the coefficients from $\delta \mathbf{V}_{\mathrm{Oy}}^{\mathrm{P}}$ for the pinhole situation. For simplicity, we again allow the retinal image to coincide with the eye's longitudinal axis, that is at $y_{\mathrm{R}} = 0$. This is

consistent with the assumption that in model eyes the fovea coincides with the optical axis. Equation 7.4.6 therefore simplifies to

$$\delta a_{\mathrm{O}} = \left(\delta Y_{\mathrm{Oy}}^{\mathrm{P}}\right) y_{\mathrm{P}}. \tag{7.4.8}$$

Substituting from Equations 5.3.19 and 3.4.6 we obtain

$$\delta a_{\mathrm{O}} = \left(\delta\left(-\left(n_0 B_{\mathrm{E}}\right)^{-1} A_{\mathrm{E}}\right)\right) y_{\mathrm{P}} = \left(\delta\left(-n_0^{-1} F_0\right)\right) y_{\mathrm{P}}. \tag{7.4.9}$$

Unsurprising, this equation, like Equation 7.4.7, gives us a linear relationship between the angular spread from the red to the blue object points at incidence onto the pinhole, the chromatic difference in refractive compensation and the displacement of the pinhole from the optical axis. It resembles Equation 2.3.5 which Thibos *et al* (1990) define as induced transverse chromatic aberration.

Simonet and Campbell (1990) also describe a relationship resembling Equations 2.3.5 and 7.4.9 to measure the transverse chromatic aberration, however, in their equation *h* is defined at the pupillary plane whereas Thibos *et al* (1990) and Equation 7.4.9 are defined for a pinhole at the corneal plane. However, $\delta Y_{\mathrm{Oy}}^{\mathrm{P}} \neq \delta Y_{\mathrm{Oy}}$ which may explain the discrepancy in results described by Simonet and Campbell between their indirect derivation (using Equation 2.3.5) and direct measurements (obtained experimentally) and defined by Equation 7.4.6. Exploring this further is beyond the scope of this dissertation.

In summary

Equations 7.4.1 and 6 can be summarized as

$$\delta\mathbf{V}_{\mathrm{Oy}}\mathbf{v}_{\mathrm{Oy}} = \delta\mathbf{r}_{\mathrm{O}} \tag{7.4.10}$$

where $\delta\mathbf{V}_{\mathrm{Oy}}$ is defined in Section 7.2.1, $\mathbf{v}_{\mathrm{Oy}}$ is given by Equation 5.3.15 and

$$\delta\mathbf{r}_{\mathrm{O}} = \begin{pmatrix} \delta y_{\mathrm{O}} \\ \delta a_{\mathrm{O}} \end{pmatrix}. \tag{7.4.11}$$

δy_{O} defines the chromatic difference in transverse object position and δa_{O} is the chromatic difference in inclination in object space.

Similarly the scenario of placing a pinhole immediately in front of the eye can be summarized as

$$\delta\mathbf{V}_{\mathrm{Oy}}^{\mathrm{P}}\mathbf{v}_{\mathrm{Oy}} = \delta\mathbf{r}_{\mathrm{O}} \tag{7.4.12}$$

where $\delta\mathbf{V}_{\mathrm{Oy}}^{\mathrm{P}}$ is defined by Equation 5.3.19.

From Equations 7.4.10 and 12 we can see that chromatic difference in position and inclination in object space is a function of both transverse displacement of the retinal image from the optical axis and transverse displacement of the pinhole from the optical axis.

An underlying implication

We return to the experimental setup with the pinhole as the limiting aperture and underlying assumptions as shown in Figure 7.4.1. The experiments theorise that the two different chromatic images are superimposed at the retina and perceived as one. This implies $y_{\mathrm{R}}^{\mathrm{b}} = y_{\mathrm{R}}^{\mathrm{r}}$. However, it is quite possible that the inclination at the retina of the two chromatic rays is not the same. This has implications for the Stiles-Crawford effect. We derive an equation to obtain the chromatic difference in inclination of these two rays at the retina, δa_{R}. The red and blue chief rays are traversing the pupil through the same position. We therefore start at the plane of the aperture. From Equation 5.2.18 and 19 and equating for α_{P}, simplifying, solving for a_{R} and then taking the chromatic difference we obtain

$$\delta a_{\mathrm{R}} = \left(\delta\left(-nB_{\mathrm{B}}\right)^{-1}\right)y_{\mathrm{P}} + \left(\delta\left(D_{\mathrm{B}}\left(B_{\mathrm{B}}n\right)^{-1}\right)\right)y_{\mathrm{R}} \qquad (7.4.13)$$

which is the chromatic difference in inclination at the retina when two rays from separated objects of differing frequencies are superimposed at the retina.

Generalizing to linear optics

Equations 7.4.1 to 12 readily generalize to linear optics provided we substitute from Equation 5.3.25 for $\mathbf{V}_{\mathrm{Oy}}$ and from Equation 5.3.26 for $\mathbf{V}_{\mathrm{Oy}}^{\mathrm{P}}$. For Equation 7.4.13 we need to include a transpose to obtain

$$\delta\mathbf{a}_{\mathrm{R}} = \left(\delta\left(-n\mathbf{B}_{\mathrm{B}}^{\mathrm{T}}\right)^{-1}\right)\mathbf{y}_{\mathrm{P}} + \left(\delta\left(\mathbf{D}_{\mathrm{B}}\left(\mathbf{B}_{\mathrm{B}}n\right)^{-1}\right)\right)\mathbf{y}_{\mathrm{R}}\,. \qquad (7.4.14)$$

7.5 Chromatic properties of the eye dependent on object size or angular spread

In Section 2.3.2 we saw that experiments are designed to measure chromatic difference in position of a red and a blue object point in object space. When working in object space experimentally, we are working with single red and blue object points rather than objects with size, according to the current literature. Chromatic difference in image size and angular spread are calculated in image space using ray tracing based on the experimental data for objects with size. It is conceivable that an experiment could be devised to compare the sizes of a red and a blue object to appear to be the same size in image space.

7.5.1 Chromatic difference in object size

The approach to obtaining the chromatic difference in object size is similar to that for the retinal chromatic difference in image size. Substituting from Equation 5.3.17, the size of the blue object is

$$\Delta y_{\mathrm{O}}^{\mathrm{b}} = W_{\mathrm{Oy}}^{\mathrm{b}} y_{\mathrm{P2}}^{\mathrm{b}} - W_{\mathrm{Oy}}^{\mathrm{b}} y_{\mathrm{P1}}^{\mathrm{b}} + X_{\mathrm{Oy}}^{\mathrm{b}} y_{\mathrm{R2}}^{\mathrm{b}} - X_{\mathrm{Oy}}^{\mathrm{b}} y_{\mathrm{R1}}^{\mathrm{b}} \tag{7.5.1}$$

where the blue rays all go through the same position in the pupil such that

$$y_{\mathrm{P2}}^{\mathrm{b}} = y_{\mathrm{P1}}^{\mathrm{b}}. \tag{7.5.2}$$

Equation 7.5.1 simplifies to obtain

$$\Delta y_{\mathrm{O}}^{\mathrm{b}} = X_{\mathrm{Oy}}^{\mathrm{b}} \left(\Delta y_{\mathrm{R}}^{\mathrm{b}} \right), \tag{7.5.3}$$

the blue object size, where

$$\Delta y_{\mathrm{R}}^{\mathrm{b}} = y_{\mathrm{R2}}^{\mathrm{b}} - y_{\mathrm{R1}}^{\mathrm{b}} \tag{7.5.4}$$

is the size of the blue image at the retina. The size of the red object is obtained in a similar fashion. The chromatic difference in object size is obtained when the red and blue images at the retina appear to have the same size, such that

$$\Delta y_{\mathrm{R}}^{\mathrm{b}} = \Delta y_{\mathrm{R}}^{\mathrm{r}}. \tag{7.5.5}$$

The chromatic difference in object size is

$$\delta\left(\Delta y_{\mathrm{O}}\right) = \Delta y_{\mathrm{O}}^{\mathrm{b}} - \Delta y_{\mathrm{O}}^{\mathrm{r}} = X_{\mathrm{Oy}}^{\mathrm{b}} \left(\Delta y_{\mathrm{R}}^{\mathrm{b}} \right) - X_{\mathrm{Oy}}^{\mathrm{r}} \left(\Delta y_{\mathrm{R}}^{\mathrm{r}} \right) = \delta X_{\mathrm{Oy}} \left(\Delta y_{\mathrm{R}} \right) \tag{7.5.6}$$

where δX_{Oy} is described in Section 7.2.1

7.5.2 Chromatic difference in object angular spread

The angular spread of the blue object $\Delta a_{\mathrm{O}}^{\mathrm{b}}$ is obtained from Equation 5.3.18 to be

$$\Delta a_{\mathrm{O}}^{\mathrm{b}} = Y_{\mathrm{Oy}}^{\mathrm{b}} y_{\mathrm{P2}}^{\mathrm{b}} - Y_{\mathrm{Oy}}^{\mathrm{b}} y_{\mathrm{P1}}^{\mathrm{b}} + Z_{\mathrm{Oy}}^{\mathrm{b}} y_{\mathrm{R2}}^{\mathrm{b}} - Z_{\mathrm{Oy}}^{\mathrm{b}} y_{\mathrm{R1}}^{\mathrm{b}}. \tag{7.5.7}$$

Equation 7.5.2 applies and so Equation 7.5.7 simplifies to obtain the angular spread from the blue object,

$$\Delta a_{\mathrm{O}}^{\mathrm{b}} = Z_{\mathrm{Oy}}^{\mathrm{b}} \left(\Delta y_{\mathrm{R}}^{\mathrm{b}} \right) \tag{7.5.8}$$

where the size of the blue retinal image $\Delta y_{\mathrm{R}}^{\mathrm{b}}$ is defined by Equation 7.5.4. Similarly, we obtain the red object angular spread. The chromatic difference in object angular spread is

$$\delta\left(\Delta a_{\mathrm{O}}\right) = \Delta a_{\mathrm{O}}^{\mathrm{b}} - \Delta a_{\mathrm{O}}^{\mathrm{r}} = Z_{\mathrm{Oy}}^{\mathrm{b}} \left(\Delta y_{\mathrm{R}}^{\mathrm{b}} \right) - Z_{\mathrm{Oy}}^{\mathrm{r}} \left(\Delta y_{\mathrm{R}}^{\mathrm{r}} \right) = \delta Z_{\mathrm{Oy}} \left(\Delta y_{\mathrm{R}} \right) \tag{7.5.9}$$

where δX_{Oy} is described in Section 7.2.1.

Summary of chromatic differences in object space

Equations 7.5.6 and 9 can be summarized as

$$\delta \mathbf{V}_{\mathrm{Oy}} \, \Delta \mathbf{v}_{\mathrm{Oy}} = \delta\left(\Delta \mathbf{r}_{\mathrm{O}}\right) \tag{7.5.10}$$

where $\delta \mathbf{V}_{\mathrm{Oy}}$ is described in Section 7.2.1,

$$\delta\left(\Delta \mathbf{r}_{\mathrm{O}}\right) = \delta \begin{pmatrix} \Delta y_{\mathrm{O}} \\ \Delta a_{\mathrm{O}} \end{pmatrix} \tag{7.5.11}$$

is the chromatic difference in object size and angular spread vector and

$$\Delta \mathbf{v}_{\mathrm{Oy}} = \begin{pmatrix} \Delta y_{\mathrm{P}} \\ \Delta y_{\mathrm{R}} \end{pmatrix} \tag{7.5.12}$$

where $\Delta y_{\mathrm{P}} = 0$.

7.5.3 Chromatic object size magnification

Similar to Section 7.3.3, we can obtain the magnification of the size of the red to blue objects when the red and blue images appear to have the same size to the subject. We define the chromatic object size magnification as

$$M_{\mathrm{yO}} \, \Delta y_{\mathrm{O}}^{\mathrm{r}} = \Delta y_{\mathrm{O}}^{\mathrm{b}}. \tag{7.5.13}$$

Substituting from Equation 7.5.3 for the blue and red object sizes we obtain

$$M_{\mathrm{yO}} X^{\mathrm{r}}_{\mathrm{Oy}}\left(\Delta y^{\mathrm{r}}_{\mathrm{R}}\right) = X^{\mathrm{b}}_{\mathrm{Oy}}\left(\Delta y^{\mathrm{b}}_{\mathrm{R}}\right). \tag{7.5.14}$$

The red and blue images at the retina are the same size and so Equation 7.5.5 applies and Equation 7.5.14 simplifies to

$$M_{\mathrm{yO}} X^{\mathrm{r}}_{\mathrm{Oy}} = X^{\mathrm{b}}_{\mathrm{Oy}}. \tag{7.5.15}$$

7.5.4 Chromatic object angular spread magnification

The magnification of the angular spread of the red to blue incident rays, from the red and blue objects is defined as

$$M_{\mathrm{aO}}\ \Delta a^{\mathrm{r}}_{\mathrm{O}} = \Delta a^{\mathrm{b}}_{\mathrm{O}}. \tag{7.5.16}$$

Substituting from Equation 7.5.8 we obtain

$$M_{\mathrm{aO}}\ Z^{\mathrm{r}}_{\mathrm{Oy}}\left(\Delta y^{\mathrm{r}}_{\mathrm{R}}\right) = Z^{\mathrm{b}}_{\mathrm{Oy}}\left(\Delta y^{\mathrm{b}}_{\mathrm{R}}\right) \tag{7.5.17}$$

and because of Equation 7.5.5 this simplifies to

$$M_{\mathrm{aO}}\ Z^{\mathrm{r}}_{\mathrm{Oy}} = Z^{\mathrm{b}}_{\mathrm{Oy}}. \tag{7.5.18}$$

Including the use of a pinhole

We can see from Equations 7.5.6 and 9 that the transverse position of the rays through the pupil is nullified. When a pinhole is placed immediately in front of the eye its transverse displacement will have no effect on the chromatic difference in object size or angular spread or the chromatic object size or angular spread magnifications, however, the longitudinal displacement of bringing the limiting aperture forward will have an effect. The coefficients in Equations 7.5.6, 9, 15 and 18 are replaced with those from $\mathbf{V}^{\mathrm{P}}_{\mathrm{Oy}}$ (Equation 5.3.19).

Generalizing to linear optics

The equations in Section 7.5 have all been written and derived such that they readily generalized to linear optics. The proofs are beyond the scope of this dissertation.

7.6 Comment on the use of the corneal pinhole inlay

In this section the use of the pinhole is implied in the experimental sense. However, the Acufocus Kamra corneal inlay is an intrastromal pinhole that is placed in the cornea at a depth of $170\,\mu\text{m}$ (Seyeddain, Riha, Hohensinn, Nix, Dexl and Grabner, 2010). The pinhole inlay is 3.8 mm in diameter and has a pinhole in its centre of 1.6 mm in diameter. Its effect is similar to that of moving the limiting aperture from the pupil to the corneal plane. Surgeons and researchers go to great lengths to ensure that the transverse placement of the pinhole inlay is correct, so as to avoid induced aberrations. Research is ongoing into establishing where the correct position is to place the inlay. According to Tabernero and Artal (2011), just a 0.5 mm transverse offset can significantly reduce the retinal image quality and overall vision. Numerical examples in Chapter 10 will illustrate the effect of a misplaced inlay is on the object and aperture-dependent chromatic properties at the retina.

7.7 Summary of equations for chromatic properties

Table 7.7.1 Summary of the independent chromatic properties of the eye. The equation is given as a definition and in terms of the entries of the transferences.

Independent Chromatic Properties		
Chromatic property	**Equation**	**Eq. no.**
Chromatic difference in power	$\delta F = F_{\text{b}} - F_{\text{r}} = -\left(C_{\text{b}} - C_{\text{r}}\right)$	7.1.1 & 2
Chromatic difference in refractive compensation	$\delta F_0 = F_{0\text{b}} - F_{0\text{r}} = \dfrac{A_{\text{b}}}{B_{\text{b}}} - \dfrac{A_{\text{r}}}{B_{\text{r}}}$	7.1.3 & 4
Chromatic difference in ametropia	$\delta A = A_{\text{b}} - A_{\text{r}}$	7.1.5

Table 7.7.2 Summary of the chromatic properties of the eye dependent on object and aperture positions. The table is in a set of four sections each giving the equations for an object at distance and a finite distance. The final column gives the equation number for the respective equations. Only the general derivations are given.

Dependent Chromatic Properties			
Chromatic property	**Equation at distance**	**Equation for finite distance**	**Eq. no.**
Coefficient matrix	$\mathbf{V}_{\mathrm{E}}=\begin{pmatrix} W_{\mathrm{E}} & X_{\mathrm{E}} \\ Y_{\mathrm{E}} & Z_{\mathrm{E}} \end{pmatrix}$ $=\begin{pmatrix} A_{\mathrm{E}}A_{\mathrm{A}}^{-1} & B_{\mathrm{B}}A_{\mathrm{A}}^{-1}n_0 \\ n^{-1}C_{\mathrm{E}}A_{\mathrm{A}}^{-1} & n^{-1}D_{\mathrm{B}}A_{\mathrm{A}}^{-1}n_0 \end{pmatrix}$	$\mathbf{V}_{\mathrm{OE}}=\begin{pmatrix} W_{\mathrm{OE}} & X_{\mathrm{OE}} \\ Y_{\mathrm{OE}} & Z_{\mathrm{OE}} \end{pmatrix}$ $=\begin{pmatrix} (B_{\mathrm{E}}-A_{\mathrm{E}}\zeta_{\mathrm{O}})(B_{\mathrm{A}}-A_{\mathrm{A}}\zeta_{\mathrm{O}})^{-1} & B_{\mathrm{B}}(A_{\mathrm{A}}\zeta_{\mathrm{O}}-B_{\mathrm{A}})^{-1} \\ (D_{\mathrm{E}}-C_{\mathrm{E}}\zeta_{\mathrm{O}})(nB_{\mathrm{A}}-A_{\mathrm{A}}\zeta_{\mathrm{O}})^{-1} & D_{\mathrm{B}}(A_{\mathrm{A}}\zeta_{\mathrm{O}}-nB_{\mathrm{A}})^{-1} \end{pmatrix}$	5.2.8 & 5.2.26
Chromatic difference in image position and inclination at the retina			
Chromatic difference in image position	$\delta y_{\mathrm{R}}=(\delta W_{\mathrm{E}})y_{\mathrm{P}}+(\delta X_{\mathrm{E}})a_{\mathrm{K}}$	$\delta y_{\mathrm{R}}=(\delta W_{\mathrm{OE}})y_{\mathrm{P}}+(\delta X_{\mathrm{OE}})y_{\mathrm{O}}$	7.2.3 & 4
Chromatic difference in inclination	$\delta a_{\mathrm{R}}=(\delta Y_{\mathrm{E}})y_{\mathrm{P}}+(\delta Z_{\mathrm{E}})a_{\mathrm{K}}$	$\delta a_{\mathrm{R}}=(\delta Y_{\mathrm{OE}})y_{\mathrm{P}}+(\delta Z_{\mathrm{OE}})y_{\mathrm{O}}$	7.2.16 & 17
Chromatic difference in image size and angular spread at the retina			
Chromatic difference in image size	$\delta(\Delta y_{\mathrm{R}})=(\delta X_{\mathrm{E}})(\Delta a_{\mathrm{K}})$	$\delta(\Delta y_{\mathrm{R}})=(\delta X_{\mathrm{OE}})(\Delta y_{\mathrm{O}})$	7.3.4 & 8
Chromatic difference in image angular spread	$\delta(\Delta a_{\mathrm{R}})=(\delta Z_{\mathrm{E}})(\Delta a_{\mathrm{K}})$	$\delta(\Delta a_{\mathrm{R}})=(\delta Z_{\mathrm{OE}})(\Delta y_{\mathrm{O}})$	7.3.11 & 12
Chromatic magnification			
Retinal chromatic image size magnification	$M_{\mathrm{yR}}X_{\mathrm{E}}^{\mathrm{r}}=X_{\mathrm{E}}^{\mathrm{b}}$	$M_{\mathrm{yR}}X_{\mathrm{OE}}^{\mathrm{r}}=X_{\mathrm{OE}}^{\mathrm{b}}$	7.3.19 & 20
Retinal chromatic angular spread magnification	$M_{\mathrm{aR}}Z_{\mathrm{E}}^{\mathrm{r}}=Z_{\mathrm{E}}^{\mathrm{b}}$	$M_{\mathrm{aR}}Z_{\mathrm{OE}}^{\mathrm{r}}=Z_{\mathrm{OE}}^{\mathrm{b}}$	7.3.27 & 28

Table 7.7.3 Summary of the chromatic properties of the eye dependent on image and aperture positions. The table gives the equations for an object at a finite distance. The final column gives the equation number for the respective equations. Only the general derivations are given.

Chromatic Properties in Object Space	**-for finite distances-**	
Coefficient matrix	$\mathbf{V}_{\mathrm{Oy}} = \begin{pmatrix} W_{\mathrm{Oy}} & X_{\mathrm{Oy}} \\ Y_{\mathrm{Oy}} & Z_{\mathrm{Oy}} \end{pmatrix} = \begin{pmatrix} B_{\mathrm{B}}^{-1}\left(B_{\mathrm{E}} - A_{\mathrm{E}}\zeta_{\mathrm{O}}\right) & \left(A_{\mathrm{A}}\zeta_{\mathrm{O}} - B_{\mathrm{A}}\right)B_{\mathrm{B}}^{-1} \\ -\left(n_0 B_{\mathrm{B}}\right)^{-1} A_{\mathrm{E}} & A_{\mathrm{A}}\left(B_{\mathrm{B}} n_0\right)^{-1} \end{pmatrix}$	5.3.14
Chromatic difference in object position	$\delta y_{\mathrm{O}} = \left(\delta W_{\mathrm{Oy}}\right) y_{\mathrm{P}} + \left(\delta X_{\mathrm{Oy}}\right) y_{\mathrm{R}}$	7.4.1
Chromatic difference in inclination in object space	$\delta a_{\mathrm{O}} = \left(\delta Y_{\mathrm{Oy}}\right) y_{\mathrm{P}} + \left(\delta Z_{\mathrm{Oy}}\right) y_{\mathrm{R}}$	7.4.6
Chromatic difference in object size	$\delta\left(\Delta y_{\mathrm{O}}\right) = \delta X_{\mathrm{Oy}}\left(\Delta y_{\mathrm{R}}\right)$	7.5.6
Chromatic difference in object angular spread	$\delta\left(\Delta a_{\mathrm{O}}\right) = \delta Z_{\mathrm{Oy}}\left(\Delta y_{\mathrm{R}}\right)$	7.5.9
Chromatic object size magnification	$M_{\mathrm{yO}} X_{\mathrm{Oy}}^{\mathrm{r}} = X_{\mathrm{Oy}}^{\mathrm{b}}$	7.5.15
Chromatic object angular spread magnification	$M_{\mathrm{aO}} Z_{\mathrm{Oy}}^{\mathrm{r}} = Z_{\mathrm{Oy}}^{\mathrm{b}}$	7.5.18

Table 7.7.4 Summary of the coefficient matrices for an eye with a pinhole immediately in front of the eye for either an object at distance or an object at a finite distance.

Coefficient matrices for an eye with pinhole		
Equation at distance	**Equation for finite distance**	**Eq. no.**
$\mathbf{V}_{\mathrm{E}}^{\mathrm{P}} = \begin{pmatrix} W_{\mathrm{E}}^{\mathrm{P}} & X_{\mathrm{E}}^{\mathrm{P}} \\ Y_{\mathrm{E}}^{\mathrm{P}} & Z_{\mathrm{E}}^{\mathrm{P}} \end{pmatrix} = \begin{pmatrix} A_{\mathrm{E}} & B_{\mathrm{E}} n_0 \\ n^{-1} C_{\mathrm{E}} & n^{-1} D_{\mathrm{E}} n_0 \end{pmatrix}$	$\mathbf{V}_{\mathrm{OE}}^{\mathrm{P}} = \begin{pmatrix} W_{\mathrm{OE}}^{\mathrm{P}} & X_{\mathrm{OE}}^{\mathrm{P}} \\ Y_{\mathrm{OE}}^{\mathrm{P}} & Z_{\mathrm{OE}}^{\mathrm{P}} \end{pmatrix} = \begin{pmatrix} A_{\mathrm{E}} - B_{\mathrm{E}}\zeta_{\mathrm{O}}^{-1} & B_{\mathrm{E}}\zeta_{\mathrm{O}}^{-1} \\ n^{-1}\left(C_{\mathrm{E}} - D_{\mathrm{E}}\zeta_{\mathrm{O}}^{-1}\right) & n^{-1} D_{\mathrm{E}}\zeta_{\mathrm{O}}^{-1} \end{pmatrix}$	5.2.37 & 34
—	$\mathbf{V}_{\mathrm{Oy}}^{\mathrm{P}} = \begin{pmatrix} W_{\mathrm{Oy}}^{\mathrm{P}} & X_{\mathrm{Oy}}^{\mathrm{P}} \\ Y_{\mathrm{Oy}}^{\mathrm{P}} & Z_{\mathrm{Oy}}^{\mathrm{P}} \end{pmatrix} = \begin{pmatrix} 1 - B_{\mathrm{E}}^{-1} A_{\mathrm{E}}\zeta_{\mathrm{O}} & B_{\mathrm{E}}^{-1}\zeta_{\mathrm{O}} \\ -\left(n_0 B_{\mathrm{E}}\right)^{-1} A_{\mathrm{E}} & \left(n_0 B_{\mathrm{E}}\right)^{-1} \end{pmatrix}$	5.3.19

Table 7.7.5 Summary of the equations for the chromatic difference in corneal position of the two chief rays, for a single object point either at distance or at a finite distance and for the chromatic difference in inclination of two chief rays that emerge at the same position on the retina, from two separated object points at a finite distance.

Underlying implications			
Chromatic difference in corneal position	$\delta y_{\mathrm{K}} = \left[\delta\left(\frac{n_0}{A_{\mathrm{E}}}\left(\frac{B_{\mathrm{B}}}{A_{\mathrm{A}}} - B_{\mathrm{E}}\right)\right)\right] a_{\mathrm{K}} + \left[\delta\left(\frac{1}{A_{\mathrm{A}}}\right)\right] y_{\mathrm{P}}$	$\delta y_{\mathrm{K}} = \left(\delta\frac{B_{\mathrm{A}}}{B_{\mathrm{OA}}}\right) y_{\mathrm{O}} - \left(\delta\frac{\zeta_{\mathrm{O}}}{B_{\mathrm{OA}}}\right) y_{\mathrm{P}}$	7.2.9 & 10
Chromatic difference in inclination at retina	—	$\delta a_{\mathrm{R}} = \left(\delta\left(-nB_{\mathrm{B}}\right)^{-1}\right) y_{\mathrm{P}} - \left(\delta\left(D_{\mathrm{B}}\left(B_{\mathrm{B}}n\right)^{-1}\right)\right) y_{\mathrm{R}}$	7.4.13

7.8 Discussion

In this section we unpacked and derived equations to enable us to calculate chromatic properties from the transferences. Contrary to the definition of chromatic aberration in Chapter 6 which distinguished between longitudinal and transverse chromatic aberration, chromatic properties are categorised as firstly those chromatic properties that are independent of object, image and aperture positions and secondly the chromatic properties of the eye that are dependent on the object (or image) and aperture positions.

The derivations of the chromatic properties have in certain instances confirmed what we intuitively suspected and in other instances gave us new insight into the definitions. We saw that the independent chromatic properties of the eye are derived from the fundamental properties of the red and blue transferences alone and are not the direct property of light, nor object and image positions. The result is that one obtains, as a result, a single value for each of chromatic difference in power, refractive compensation and ametropia for the eye.

In contrast, the derivations for chromatic properties of the eye and object and aperture positions are dependent on light, relying on ray tracing, and therefore vary with changes in both longitudinal and transverse object position and longitudinal and transverse aperture position. We derived formulae for chromatic

difference in position, firstly for chromatic difference in transverse image position and secondly for chromatic difference in inclination at the retina.

An interesting underlying implication is that even when one chooses a pencil of rays, all having the same incident inclination, and then selects the chief ray through the centre of the pupil, that there is a red ray and blue ray at incidence, separated at the cornea by a distance δy_K. The two rays reaching the retina do not originate from the exact same multi-chromatic ray.

After taking a close look at chromatic difference in magnification we determined that what is being measured in the literature is not a chromatic difference but rather a chromatic magnification. Nonetheless, we derived equations for chromatic difference in image size on the retina and chromatic difference in angular spread which turn out to be independent of transverse displacement of the pupil or pinhole. More appropriately, we derived formulae for the chromatic image size magnification and chromatic image angular spread magnification.

Finally, we take a look at the experimental situation where two coloured object points are positioned a distance apart such that the two coloured images are superimposed at the same point on the retina. We were able to derive equations for the chromatic difference in object position and chromatic difference in object inclination of these two coloured object points.

The underlying implication of the experimental situation is that while the red and blue rays reach the retina at the same position, there is a difference in inclination between these two rays upon reaching the retina. This has possible implications for the Stiles-Crawford effect, but further investigation is beyond the scope of this dissertation.

It is conceivable that an experiment could be set up to compare the sizes of a red and a blue object to appear to be the same size to the subject. The chromatic difference in object size and object angular spread were defined in object space. The chromatic object size magnification and chromatic object angular spread magnification were defined in object space.

All the derivations for the dependent chromatic properties of the eye are amenable to placing a pinhole immediately in front of the eye. In each case the general equations still hold and the coefficients simplify.

8 Chromatic dependence of the transference and transformed transferences on frequency

In this chapter the dependence of each of the four fundamental properties of two model eyes is calculated as a function of frequency with the refractive index of air assumed constant. We then compare the effect on the fundamental properties of the two model eyes when the refractive index of air is treated as a function of frequency. For comparison, the dependence of the fundamental properties on wavelength is displayed graphically. Finally, we consider the two model eyes submerged in water.

The four fundamental properties, each dependent on the frequency of light, are displayed graphically and turn out to be very nearly linear. A linear equation for each fundamental property as a function of frequency is obtained. It turns out that one can utilise this equation to obtain the transference as an approximate function of frequency.

We then turn our attention to the two transformed transferences that were introduced in Section 3.7.1 and 2. These are displayed graphically as a function of frequency using three-dimensional graphs. This enables us to study the fundamental and derived properties, their relationships to each other and their dependence on frequency.

Each of the entries of the transformed transference also displays a nearly linear dependence on the frequency of light. These transformed spaces allow us to derive a formula for a transference, necessarily symplectic, as a function of frequency.

8.1 Transference as a function of frequency

The transference and its fundamental properties are dependent on the frequency of light. In order to study this we first equate the refractive index of air to 1, the usual assumption in optometry. For illustrative purposes, we then examine the effect on the fundamental properties of treating the refractive index of air as a function of frequency. We use Cauchy's formula for that purpose. For comparison, we also consider the dependence of the transference on wavelength.

Finally, we take a look at the more unusual situation of the eye submerged in water.

Each of the graphs in this section shows four sub-graphs, one for each of the fundamental properties as a function of frequency, across the spectrum from 430 to 750 THz. Two graphs in Section 8.1.3 will be in terms of wavelength, but across the same spectrum and with the same six coloured reference points. For the graphs, values are calculated for every 1 THz, that is for 321 points across the spectrum. However, in the tables only the values for the six reference points are given.

We make use of the SI units and prefixes for time, picosecond (ps) which is 10^{-12} s, and its inverse, the derived unit for frequency, teraHertz (THz) which is 10^{12} s^{-1}.

8.1.1 The transference as a function of frequency with $n_0 = 1$

The reduced eye

The transferences of the reduced eye as a function of the frequency of light are given for the six reference frequencies in Table 8.1.1 with the refractive index of air (n_0) equated to 1. The transferences for the reduced eye as a function of frequency are calculated according to Equation 5.5.1 with $n_0 = 1$ and the refractive index *n* calculated according to Equation 4.4.2. The disjugacy *B* is given in millimetres (mm) and the divergence *C* in corresponding units, kilodioptres ($\mathrm{kD} = \mathrm{mm}^{-1}$).

Figure 8.1.1 represents each of the fundamental properties of the reduced eye as a function of frequency. The six coloured reference points described in Section 4.2 are shown by means of coloured diamonds. The coloured diamonds represent five equally spaced intervals (64 THz) of frequency.

In Figure 8.1.1, the axis scales have been chosen to exaggerate curvature. The range of the scale for each sub-graph indicates the chromatic difference in each fundamental property. The dilation *A* ranges from 0.0070 to -0.0277 which represents a chromatic difference in ametropia of –0.0347. The chromatic

Table 8.1.1 Transferences of the reduced eye and Le Grand's eye for six reference frequencies ν (in THz), calculated with $n_0 = 1$.

Colour	ν	Reduced eye	Le Grand's eye
Red	430	$\begin{pmatrix} 0.0070 & 16.7055\,\text{mm} \\ -0.0594\,\text{kD} & 1 \end{pmatrix}$	$\begin{pmatrix} 0.0078 & 16.7276\,\text{mm} \\ -0.0594\,\text{kD} & 0.9044 \end{pmatrix}$
Orange	494	$\begin{pmatrix} 0.0020 & 16.6775\,\text{mm} \\ -0.0598\,\text{kD} & 1 \end{pmatrix}$	$\begin{pmatrix} 0.0024 & 16.6912\,\text{mm} \\ -0.0598\,\text{kD} & 0.9041 \end{pmatrix}$
Yellow	558	$\begin{pmatrix} -0.0038 & 16.6455\,\text{mm} \\ -0.0603\,\text{kD} & 1 \end{pmatrix}$	$\begin{pmatrix} -0.0037 & 16.6494\,\text{mm} \\ -0.0603\,\text{kD} & 0.9034 \end{pmatrix}$
Green	622	$\begin{pmatrix} -0.0105 & 16.6082\,\text{mm} \\ -0.0608\,\text{kD} & 1 \end{pmatrix}$	$\begin{pmatrix} -0.0102 & 16.6029\,\text{mm} \\ -0.0608\,\text{kD} & 0.9026 \end{pmatrix}$
Blue	686	$\begin{pmatrix} -0.0184 & 16.5646\,\text{mm} \\ -0.0615\,\text{kD} & 1 \end{pmatrix}$	$\begin{pmatrix} -0.0170 & 16.5545\,\text{mm} \\ -0.0613\,\text{kD} & 0.9018 \end{pmatrix}$
Violet	750	$\begin{pmatrix} -0.0277 & 16.5126\,\text{mm} \\ -0.0622\,\text{kD} & 1 \end{pmatrix}$	$\begin{pmatrix} -0.0237 & 16.5065\,\text{mm} \\ -0.0619\,\text{kD} & 0.9011 \end{pmatrix}$

difference for disjugacy B is –0.1929 mm and for divergence C it is $-0.0028\,\text{kD}$, or –2.7975 D. For divarication D the chromatic difference is zero.

In Figure 8.1.1, the dashed lines represent the least squares straight line fitted to the data for the reduced eye. Each of A, B and C present as curves in each sub-graph. D is a straight line at 1 as required by Equation 5.5.1. Because the curves in the sub-graphs of Figure 8.1.1 are nearly straight lines, Equations 8.1.1 to 4 below can be thought of as approximations of the dependence of each fundamental property on frequency. The equations for the four dashed straight lines are

$$A = \left(-1.0691\times10^{-4}\,\text{ps}\right)\nu + 0.05494 \tag{8.1.1}$$

$$B = \left(-5.9394\times10^{-4}\,\text{mm ps}\right)\nu + 16.9719\,\text{mm} \tag{8.1.2}$$

$$C = \left(-8.6047\times10^{-6}\,\text{kD ps}\right)\nu - 0.05558\,\text{kD} \tag{8.1.3}$$

$$D = 1 \tag{8.1.4}$$

where ν is measured in THz and the units of each constant is given. The set of equations can be reconstituted into a transference such that

$$\mathbf{S} = \begin{pmatrix} a_1 & b_1 \\ c_1 & d_1 \end{pmatrix} \nu + \begin{pmatrix} a_2 & b_2 \\ c_2 & d_2 \end{pmatrix} \tag{8.1.5}$$

where the constants for the reduced eye are given in Table 8.1.2.

The set of four equations given for the straight line of each fundamental property is an approximation of the value of each fundamental property for any particular frequency. Strictly speaking, because of symplecticity, it is not correct to determine **S** by obtaining expressions for the fundamental properties independently as done in Equation 8.1.5. However, det**S** has a mean of 1.000 024 and a standard deviation of 4.0×10^{-5} across the spectrum which would seem to be sufficiently close to the required 1 for most purposes. We will explore this further in Section 8.2 when we look at mapping transformations into Hamiltonian space.

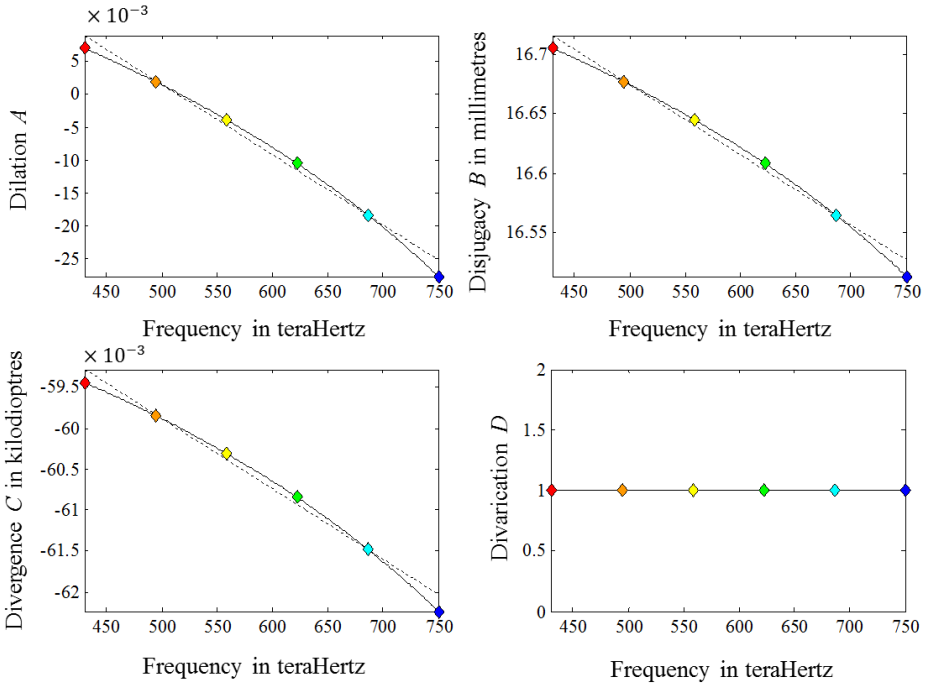

Figure 8.1.1 Fundamental properties of the reduced eye as functions of frequency ν. The refractive index of air is equated to 1. The four sub-graphs are for dilation *A*, disjugacy *B*, divergence *C* and divarication *D*. The six coloured diamonds represent the frequencies listed in Table 4.2.1, red, orange, yellow, green, blue and violet and are evenly spread at 64 THz apart. The dashed lines represent the least squares straight line. Each of *A*, *B* and *C* present as curves, while *D* is a horizontal straight line at 1.

Table 8.1.2 The constants for the reduced eye in air for Equation 8.1.5. The units are picoseconds (ps), millimetres (mm) and kilodioptres (kD).

$a_1 = -1.0691\times10^{-4}$ ps	$a_2 = 0.05494$
$b_1 = -5.9394\times10^{-4}$ mm ps	$b_2 = 16.9719$ mm
$c_1 = -8.6047\times10^{-6}$ kD ps	$c_2 = -0.05558$ kD
$d_1 = 0$ ps	$d_2 = 1$

Le Grand's eye

Similarly we look at the fundamental optical properties for Le Grand's four-surface eye. The transferences were calculated according to Equations 5.5.4 to 8 and the refractive indices given by Equation 4.4.3 with constants listed in Table 4.4.2. The transferences for the six coloured reference frequencies are given in Table 8.1.1.

The range along the vertical axis for each fundamental property shows the range along the spectrum, or chromatic difference. The chromatic difference of dilation or ametropia is –0.0315. The chromatic difference of disjugacy is

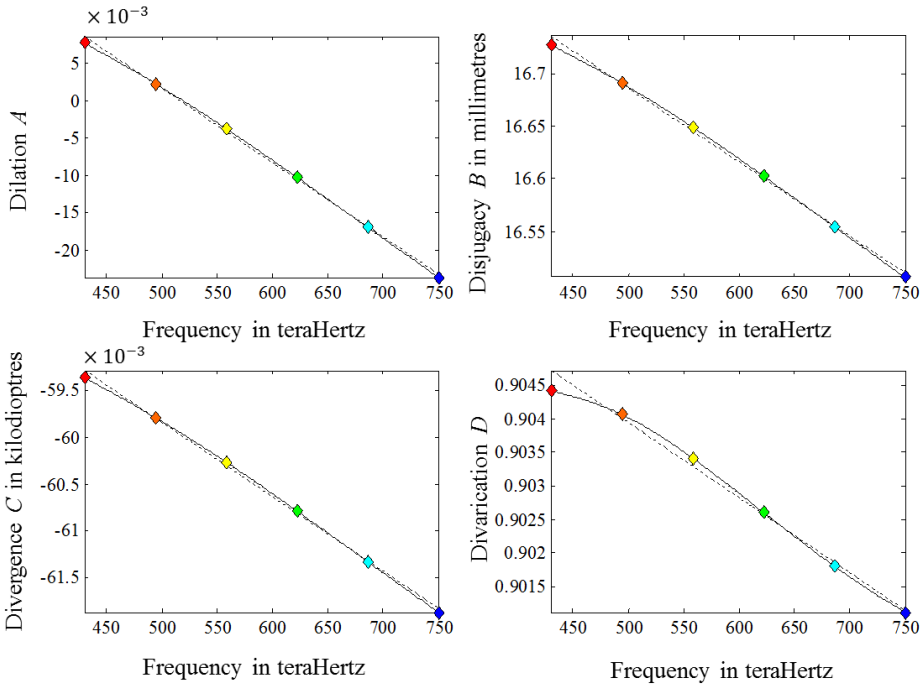

Figure 8.1.2 Fundamental properties of Le Grand's eye as a function of frequency ν. $n_0 = 1$.

Table 8.1.3 The constants for Le Grand's eye in air for Equation 8.1.5.

$a_1 = -0.9973\times10^{-4}$ ps	$a_2 = 0.05156$
$b_1 = -7.0345\times10^{-4}$ mm ps	$b_2 = 17.0382$ mm
$c_1 = -7.9756\times10^{-6}$ kD ps	$c_2 = -0.05581$ kD
$d_1 = -1.1515\times10^{-5}$ ps	$d_2 = 0.9095$

-0.2211 mm and for divergence it is –0.0025 kD or –2.5158 D. The chromatic difference of divarication is –0.0033 which is a very small range from 0.9044 to 0.9011.

From Figure 8.1.2 we can see that the curve is nearly linear. Because of this linearity, the dependence of the four fundamental properties of Le Grand's eye on the frequency of light can be approximated by Equation 8.1.5. The constants for Le Grand's eye for Equation 8.1.5 are given in Table 8.1.3. In contrast to Figure 8.1.1 *D* is no longer a horizontal straight line at 1 but is close to a straight line at $D = 0.9$, approximately.

Table 8.1.4 gives examples of transferences calculated by means of Equation 8.1.5 and constants given in Tables 8.1.2 and 3. Obtaining the approximate transference **S** for each frequency in the spectrum for Le Grand's eye from Equation 8.1.5, the average value for det**S** is $0.999\,35$ and the standard deviation is 3.5×10^{-5}. As for the reduced eye, this is probably sufficiently close to 1 for most purposes.

Comparison of the two model eyes

The graphs of the fundamental properties versus frequency for the reduced eye and Le Grand's eye, are superimposed in Figure 8.1.3. By means of Figure 8.1.3 we can compare the fundamental properties of the reduced eye (in blue) and Le Grand eye (in black). The six reference points are included and are circular for the reduced eye and diamond shaped for the Le Grand eye. For the dilation *A*, disjugacy *B* and divergence *C* we see that the dependence of each fundamental property on frequency is similar for the two model eyes. They are closest in the central part of the spectrum. The divarication *D*, constant at 1 for the reduced eye,

Table 8.1.4 Transferences of the reduced eye and Le Grand's eye for the six reference frequencies (in THz), calculated by means of Equation 8.1.5 and the constants in Tables 8.1.2 and 3 with $n_0 = 1$.

Colour	ν	Reduced eye	Le Grand's eye
Red	430	$\begin{pmatrix} 0.008656 & 16.7148\text{ mm} \\ -0.05930\text{ kD} & 1 \end{pmatrix}$	$\begin{pmatrix} 0.008457 & 16.7336\text{ mm} \\ -0.05930\text{ kD} & 0.9046 \end{pmatrix}$
Orange	494	$\begin{pmatrix} 0.001760 & 16.6764\text{ mm} \\ -0.05986\text{ kD} & 1 \end{pmatrix}$	$\begin{pmatrix} 0.002117 & 16.6890\text{ mm} \\ -0.05981\text{ kD} & 0.9039 \end{pmatrix}$
Yellow	558	$\begin{pmatrix} -0.005135 & 16.6381\text{ mm} \\ -0.06042\text{ kD} & 1 \end{pmatrix}$	$\begin{pmatrix} -0.004223 & 16.6443\text{ mm} \\ -0.06031\text{ kD} & 0.9032 \end{pmatrix}$
Green	622	$\begin{pmatrix} -0.01203 & 16.5998\text{ mm} \\ -0.06097\text{ kD} & 1 \end{pmatrix}$	$\begin{pmatrix} -0.01056 & 16.5997\text{ mm} \\ -0.06082\text{ kD} & 0.9026 \end{pmatrix}$
Blue	686	$\begin{pmatrix} -0.01893 & 16.5615\text{ mm} \\ -0.06153\text{ kD} & 1 \end{pmatrix}$	$\begin{pmatrix} -0.01690 & 16.5551\text{ mm} \\ -0.06133\text{ kD} & 0.9019 \end{pmatrix}$
Violet	750	$\begin{pmatrix} -0.02582 & 16.5232\text{ mm} \\ -0.06208\text{ kD} & 1 \end{pmatrix}$	$\begin{pmatrix} -0.02324 & 16.5104\text{ mm} \\ -0.06183\text{ kD} & 0.9012 \end{pmatrix}$

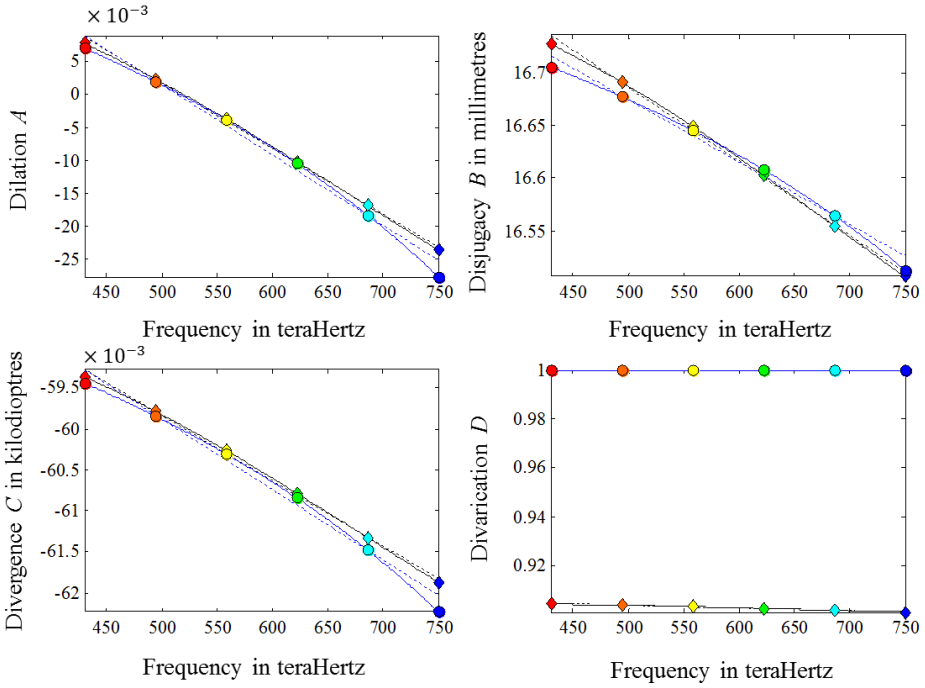

Figure 8.1.3 Fundamental properties of the reduced eye (blue line and circles) and Le Grand's eye (black line and diamonds) versus frequency ν superimposed. The least squares straight lines are also shown.

becomes weakly dependent on frequency at about 0.9 for Le Grand's eye. It is also interesting to note that the curves for Le Grand's eye more closely approximate straight lines than do the curves for the reduced eye.

8.1.2 Transference as a function of frequency using Cauchy's formula for the refractive index of air

For most purposes the index of refraction of air n_0 is taken as 1. Here we examine the effects on the transferences of allowing n_0 to depend on frequency according to Cauchy's dispersion formula (Equation 4.4.4). The effects are shown in Figures 8.1.4 and 5 for the reduced and Le Grand's eyes respectively. The blue line is for n_0 according to Cauchy's formula and the black line is for $n_0 = 1$. The transferences for the six reference frequencies, with n_0 calculated by means of Cauchy's formula, are given in Table 8.1.6 for the reduced and Le Grand's eyes.

The reduced eye

From Equation 5.5.1 for the reduced eye we see that n_0 has no effect on the disjugacy *B* and the divarication *D*. The only fundamental properties that are affected are the dilation *A* and the divergence *C*. This can also be seen in Figure 8.1.4. The effect of setting n_0 equal to 1, and not allowing for dependence of n_0 on ν, is to decrease *A* by about $0.000\,83$ and *C* by about $0.000\,05$ kD across the spectrum. The effect, therefore, would appear to be negligible and the use of $n_0 = 1$ justifiable.

Least-square straight lines fitted to the curves in Figure 8.1.4 lead to the approximate expression for transference **S** in terms of ν given by Equation 8.1.5 with constants given in Table 8.1.5.

Table 8.1.5 Constants for the expressions in Equation 8.1.5 for dilation *A* and divergence *C* for the reduced eye where n_0 is given by Cauchy's formula.

$a_1 = -1.0688 \times 10^{-4}$ ps	$a_2 = 0.05575$
$c_1 = -8.6012 \times 10^{-6}$ kD ps	$c_2 = -0.05553$ kD

Table 8.1.6 Transferences for the reduced eye and Le Grand's eye for the six reference frequencies in THz, calculated for n_0 given by Cauchy's formula.

Colour	ν	Reduced eye	Le Grand's eye
Red	430	$\begin{pmatrix} 0.0078 & 16.7055\text{ mm} \\ -0.0594\text{ kD} & 1 \end{pmatrix}$	$\begin{pmatrix} 0.0084 & 16.7276\text{ mm} \\ -0.0593\text{ kD} & 0.9044 \end{pmatrix}$
Orange	494	$\begin{pmatrix} 0.0028 & 16.6775\text{ mm} \\ -0.0598\text{ kD} & 1 \end{pmatrix}$	$\begin{pmatrix} 0.0029 & 16.6912\text{ mm} \\ -0.0598\text{ kD} & 0.9041 \end{pmatrix}$
Yellow	558	$\begin{pmatrix} -0.0030 & 16.6455\text{ mm} \\ -0.0603\text{ kD} & 1 \end{pmatrix}$	$\begin{pmatrix} -0.0031 & 16.6494\text{ mm} \\ -0.0602\text{ kD} & 0.9034 \end{pmatrix}$
Green	622	$\begin{pmatrix} -0.0097 & 16.6082\text{ mm} \\ -0.0608\text{ kD} & 1 \end{pmatrix}$	$\begin{pmatrix} -0.0096 & 16.6029\text{ mm} \\ -0.0608\text{ kD} & 0.9026 \end{pmatrix}$
Blue	686	$\begin{pmatrix} -0.0175 & 16.5646\text{ mm} \\ -0.0615\text{ kD} & 1 \end{pmatrix}$	$\begin{pmatrix} -0.0164 & 16.5545\text{ mm} \\ -0.0613\text{ kD} & 0.9018 \end{pmatrix}$
Violet	750	$\begin{pmatrix} -0.0269 & 16.5126\text{ mm} \\ -0.0622\text{ kD} & 1 \end{pmatrix}$	$\begin{pmatrix} -0.0231 & 16.5065\text{mm} \\ -0.0618\text{ kD} & 0.9011 \end{pmatrix}$

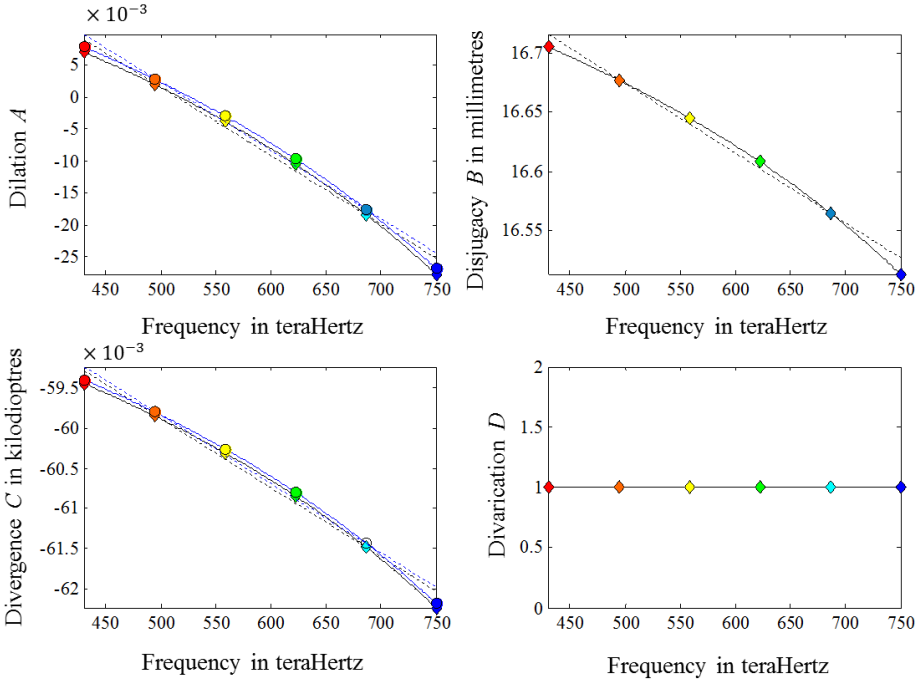

Figure 8.1.4 Fundamental properties of the reduced eye as functions of frequency. The black lines and diamond shaped reference points are for $n_0 = 1$ and the blue lines and circular reference points for n_0 given by Cauchy's formula. For B and D the curves coincide.

Le Grand's eye

Figure 8.1.5 shows the fundamental properties of Le Grand's eye as functions of frequency. The black line is calculated with $n_0 = 1$ and the blue line is calculated with n_0 as a function of frequency according to Cauchy's dispersion formula given by Equation 4.4.4. The results are similar to those in Figure 8.1.4 for the reduced eye in that only the dilation *A* and divergence *C* are affected.

To see why only *A* and *C* are affected by using Cauchy's formula for n_0, let us examine the effect of the refractive index of the surrounding medium on Le Grand's eye. From Equations 5.5.5 and 7 we observe that the only elementary transference containing n_0 is $\mathbf{S}_{\mathrm{K1}}$. The meaning of the subscripts is given in Table 4.1.1. Let us write the transference of the eye as

$$\mathbf{S} = \mathbf{S}_{\mathrm{R}}\mathbf{S}_{\mathrm{K1}} \tag{8.1.6}$$

where

$$\mathbf{S}_{\mathrm{R}} = \mathbf{S}_{\mathrm{V}}\mathbf{S}_{\mathrm{L2}}\mathbf{S}_{\mathrm{L}}\mathbf{S}_{\mathrm{L1}}\mathbf{S}_{\mathrm{Aq}}\mathbf{S}_{\mathrm{K2}}\mathbf{S}_{\mathrm{K}}. \tag{8.1.7}$$

We now substitute for $\mathbf{S}_{\mathrm{K1}}$ from Equation 5.5.5 to obtain

$$\mathbf{S} = \begin{pmatrix} A_{\mathrm{R}} & \mathrm{B}_{\mathrm{R}} \\ C_{\mathrm{R}} & D_{\mathrm{R}} \end{pmatrix} \begin{pmatrix} 1 & 0 \\ \dfrac{n_{\mathrm{K}} - n_0}{-r_{\mathrm{K1}}} & 1 \end{pmatrix} = \begin{pmatrix} A_{\mathrm{R}} - \mathrm{B}_{\mathrm{R}}\left(\dfrac{n_{\mathrm{K}} - n_0}{r_{\mathrm{K1}}}\right) & \mathrm{B}_{\mathrm{R}} \\ C_{\mathrm{R}}\left(\dfrac{n_{\mathrm{K}} - n_0}{-r_{\mathrm{K1}}}\right) & D_{\mathrm{R}} \end{pmatrix} \tag{8.1.8}$$

which shows that, for Le Grand's eye, the only fundamental properties affected by n_0 are the dilation *A* and divergence *C*.

In Figure 8.1.5 the lines for $n_0 = 1$ and for n_0 calculated according to Cauchy's formula, are very close together and appear to be approximately parallel in sub-graphs *A* and *C*. Sub-graphs *B* and *D* are indeed superimposed, as implied by Equation 8.1.8. The formulae for the least-squares straight lines for Le Grand's eye shown in Figure 8.1.5 for *A* and *C* using Cauchy's formula for n_0 as functions of frequency can be obtained from Equation 8.1.5 with the constants given in Table 8.1.7 and transferences given in Table 8.1.6. Comparing the straight lines for $n_0 = 1$ with the straight lines using Cauchy's dispersion formula we observe

Table 8.1.7 The constants for dilation *A* and divergence *C* for Le Grand's eye for the straight line equations in Equation 8.1.5 where the refractive index is calculated according to Cauchy's formula.

$a_1 = -0.9969 \times 10^{-4}$ ps	$a_2 = 0.05214$
$c_1 = -7.9733 \times 10^{-6}$ kD ps	$c_2 = -0.05582$ kD

that the two straight lines (a_1 and c_1) are very nearly parallel and the in positions (a_2 and c_2) change slightly.

Table 8.1.8 shows the difference between the two lines for both model eyes for each of the six reference frequencies. The mean and standard deviation are calculated for every 1 THz across the spectrum. Visual inspection of both Table 8.1.8 and Figure 8.1.5 indicates that the two curves for *A* and *C* are very nearly parallel and are very close together. Because the lines are nearly parallel, any chromatic difference calculations will be negligibly influenced by the choice of refractive index for air.

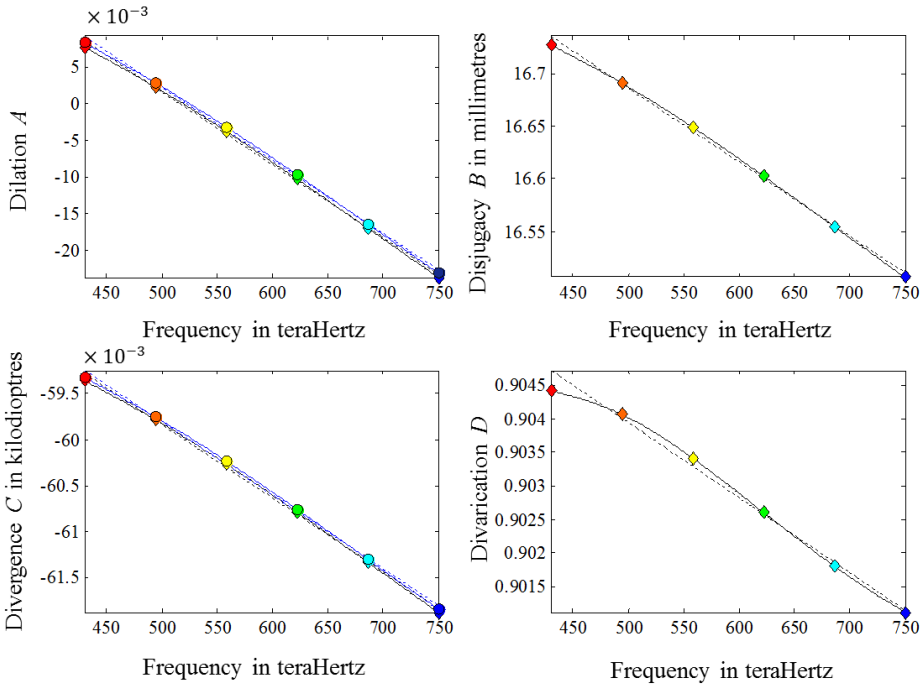

Figure 8.1.5 Fundamental properties of Le Grand's eye as functions of frequency. The black line and diamond shaped reference points are for $n_0 = 1$ and the blue line and circular reference points are for n_0 calculated by means of Cauchy's formula. The two lines for *B* and *D* are superimposed. For *A* and *C* the blue line is displaced upwards.

Table 8.1.8 The differences in each of the fundamental properties between the transference calculated using $n_0 = 1$ and using n_0 according to Cauchy's formula. The numbers indicate the difference (vertical distance) from the black to the blue line in the graphs in Figures 8.1.4 and 5. The mean and standard deviation are obtained for 321 frequencies across the visible spectrum.

Colour	ν in THz	Reduced eye				Le Grand eye			
		ΔA	ΔB in mm	ΔC in kD	ΔD	ΔA	ΔB in mm	ΔC in kD	ΔD
		$\times 10^{-3}$		$\times 10^{-3}$		$\times 10^{-3}$		$\times 10^{-3}$	
Red	430	0.8279	0	0.04956	0	0.5904	0	0.03192	0
Orange	494	0.8293	0	0.04972	0	0.5911	0	0.03202	0
Yellow	558	0.8309	0	0.04992	0	0.5920	0	0.03212	0
Green	622	0.8328	0	0.05015	0	0.5930	0	0.03224	0
Blue	686	0.8350	0	0.05041	0	0.5944	0	0.03238	0
Violet	750	0.8374	0	0.05071	0	0.5962	0	0.03255	0
Mean:		0.8321	0	0.05006	0	0.5927	0	0.03220	0
Standard deviation:		0.002775	0	0.000334	0	0.001629	0	0.01778	0

Discussion

Here we have examined whether the dispersive effect of air plays a significant role in the overall dispersion through the system ultimately reaching the exit plane, or retina. Figures 8.1.4 and 5 compare the eye in air, firstly, with $n_0 = 1$ and secondly, with the refractive index as a function of frequency calculated using Cauchy's formula. The disjugacy *B* and divarication *D* are not affected. Only the dilation *A* and divergence *C* are affected.

Table 8.1.8 shows the difference in each of the fundamental properties when the transference is calculated using $n_0 = 1$ and when using Cauchy's formula. The standard deviation shows how close to being parallel the two lines are and therefore gives an indication of the effect of dispersion, while the mean indicates how accurate the constant for n_0 is and the difference between the two lines. From the graphs and numerical values of the tables in this section, we conclude that because the two lines in each graph are very nearly parallel, the

amount of dispersion occurring in air is insignificant and the refractive index of air can be taken to be 1.

8.1.3 Dependence of the fundamental properties on vacuum wavelength

The fundamental properties of the reduced eye and Le Grand's eye as functions of vacuum wavelength λ are represented in Figures 8.1.6 and 7, respectively. In each graph the visible spectrum used is the same as used throughout this dissertation, that is, frequency from 430 to 750 THz, except that it is converted to vacuum wavelength using Equation 4.3.1 and given in Table 4.2.1. Figures 8.1.6 and 7 depart considerably more from straight lines than the corresponding figures (Figures 8.1.1 and 2) in terms of frequency ν.

The reduced eye

When we compare to the fundamental properties of the reduced eye as a function of vacuum wavelength (Figure 8.1.6) to frequency (Figure 8.1.1), we see that, as expected, the divarication *D* is a constant of 1, but that the other three properties are significantly more curved.

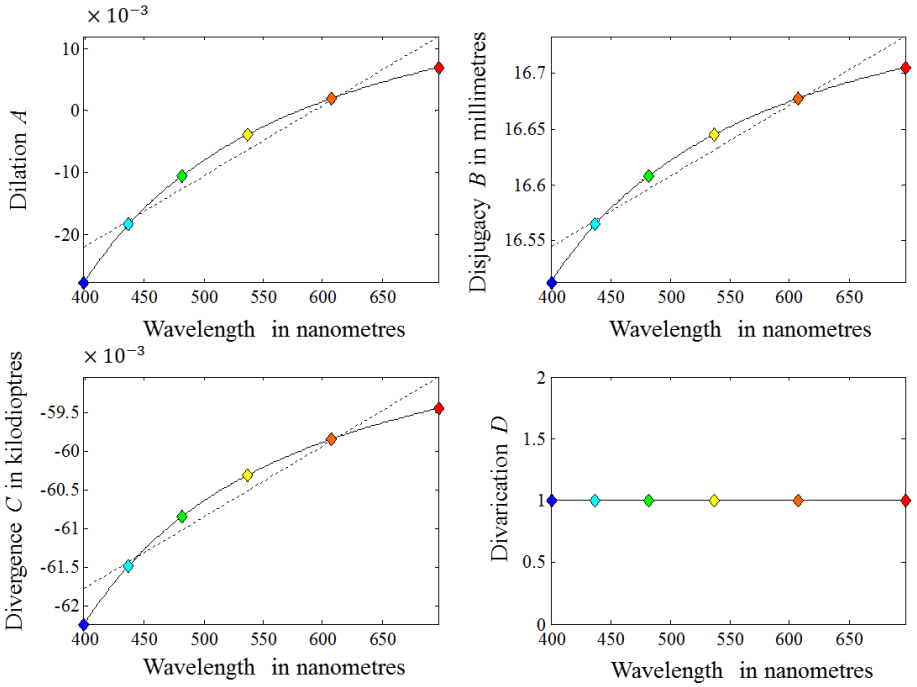

Figure 8.1.6 Fundamental properties of the reduced eye as functions of vacuum wavelength λ with $n_0 = 1$.

Le Grand's eye

Figure 8.1.7, shows the fundamental properties of Le Grand's eye as functions of vacuum wavelength λ. Again the curves depart more from straight lines than for the fundamental properties as functions of frequency ν. The four-surface eye of Le Grand shows less curvature than the single-surface reduced eye, with the exception of the divarication *D*.

Comparing the transferences of the reduced eye and Le Grand's eye

Figure 8.1.8 plots the results of Figures 8.1.6 and 7 together. The behaviour of the fundamental properties versus vacuum wavelength λ is similar for the reduced and Le Grand's eyes, especially in the central region of the spectrum. For both model eyes, the curves of the fundamental properties versus frequency ν are closer to straight lines than the corresponding curves for vacuum wavelength. This provides additional justification for using frequency instead of the more commonly-used wavelength.

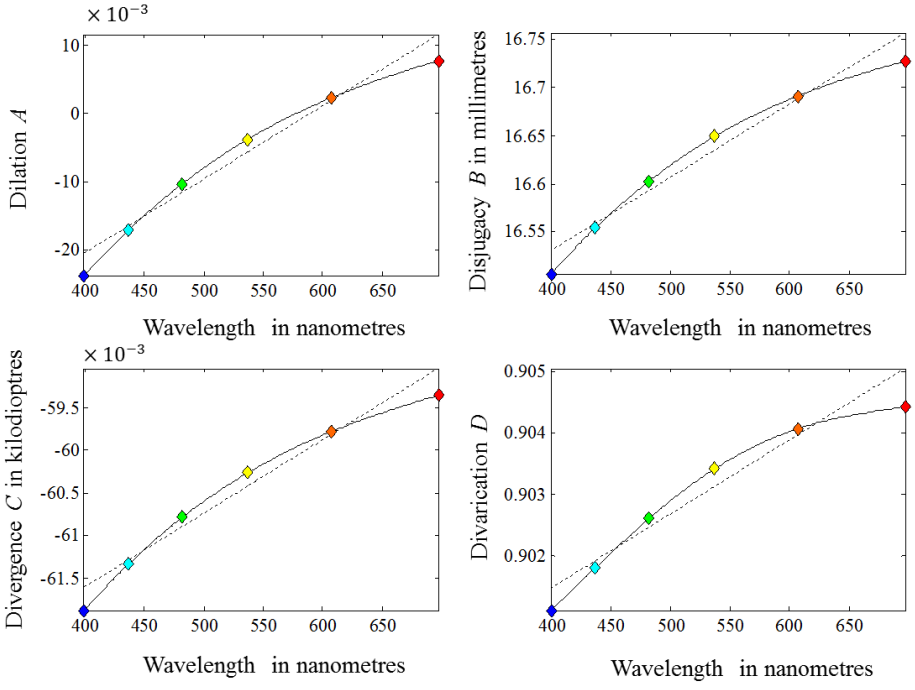

Figure 8.1.7 Fundamental properties of Le Grand's eye as a function of vacuum wavelength λ with $n_0 = 1$. The wavelengths of the six reference points are given in Table 4.2.1. Compared with the graphs for the fundamental properties as functions of frequency, these curves further depart from straight lines.

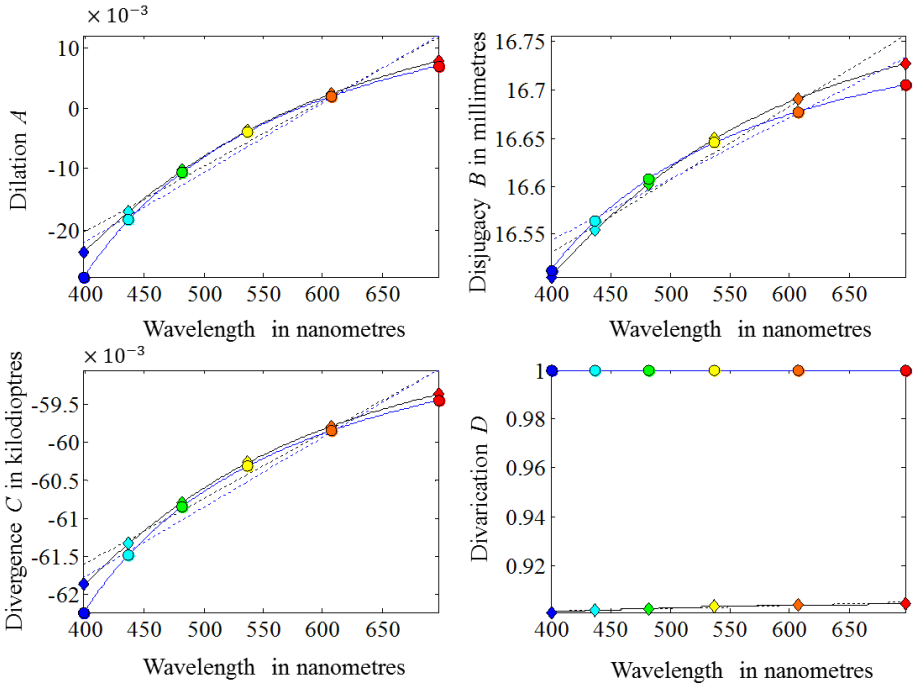

Figure 8.1.8 Dependence of the four fundamental properties of the reduced eye (blue line with circles) and Le Grand's eye (black line with diamonds) on vacuum wavelength.

8.1.4 Transference of the eye submerged in water as a function of frequency with Cornu's formula used for the refractive index of water

The formulae for the dependence of the transference of the reduced eye (Equation 5.5.3) and Le Grand's eye (Equations 5.5.5, 7 and 8) on the refractive indices and hence on the frequency of light include the possibility of n_0 also being dependent on frequency, including media other than air. In Section 8.1.1 we studied the two model eyes in air with the refractive index of air taken as 1. In Section 8.1.2 we compared the effect of the refractive index of air treated as a function of frequency. However, Equations 5.5.1 and 5.5.4 to 9 will hold for the eye in any medium. As an example of the model eye in a medium other than air, we calculate the effect on the fundamental properties of each model eye if the eye is submerged in water. Figure 8.1.9 allows comparison of the fundamental properties of the reduced eye (blue line and circles) and Le Grand's eye (black line and diamonds) as functions of frequency ν when the eye is submerged in water.

In Figure 8.1.9, the refractive index of water is calculated according to Cornu's formula, given as Equation 4.4.1. It is shown in Section 8.1.2 that the

refractive index of the medium upstream of any eye only affects the dilation *A* and divergence *C*. When the eyes are submerged in water the effect on *A* and *C* is still close to straight lines for each model eye; however there is a clear difference in position of the curves of the reduced and Le Grand's eyes. We recall that in Figure 8.1.3 we compared the graphs for the reduced eye and Le Grand's eye on the same set of sub-graphs and that the lines for the eyes were similar, often touching or running parallel. In Figure 8.1.9 we see that this is less so. The lines are similar in slope, but differ in position for *A* and *C* when the eyes are submerged in water.

The constants for the least-squares straight lines for *A* and *C* (Equation 8.1.5) for the reduced and Le Grand's eyes are given in Table 8.1.9. The curves for disjugacy *B* and divarication *C* are the same as in Figures 8.1.1 and 2. We saw from Equations 5.5.1 and 8.1.8 that only *A* and *C* are affected by the change in refractive index upstream of the system.

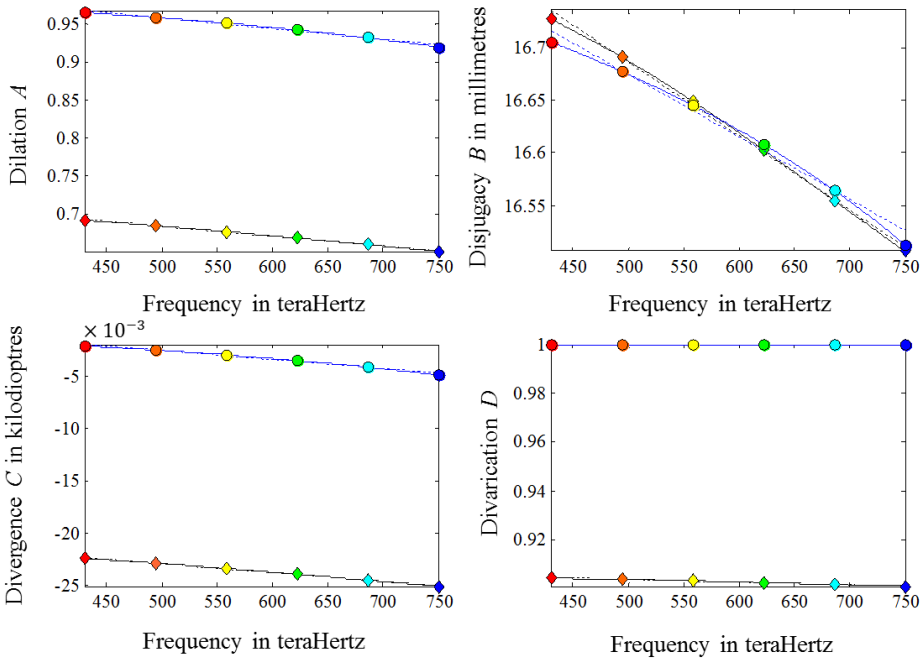

Figure 8.1.9 Dependence of the fundamental properties of the reduced eye (blue line and circles) and Le Grand's eye (black line and diamonds) on frequency ν when the eye is submerged in water. The disjugacy *B* and divarication *D* are, unsurprisingly, the same as for the eyes in air, or any other medium, however the dilation *A* and divergence *C* differ considerably, not only between the two eyes, but also from the eye in air.

Table 8.1.9 Constants for Equation 8.1.5 for *A* and *C* for the reduced and Le Grand's eyes submerged in water. The refractive index of water is calculated using Cornu's formula (Equation 4.4.1).

The Reduced Eye	
$a_1 = -1.4089\times10^{-4}$ ps	$a_2 = 1.0279$
$c_1 = -8.6007\times10^{-6}$ kD ps	$c_2 = 1.7475\times10^{-3}$ kD
Le Grand's Eye	
$a_1 = -1.2838\times10^{-4}$ ps	$a_2 = 0.7472$
$c_1 = -8.4280\times10^{-6}$ kD ps	$c_2 = -0.01871$ kD

Table 8.1.10 The transferences for the reduced eye and for Le Grand's eye submerged in water for the six reference frequencies (in THz), calculated equating the refractive index of water according to Cornu's formula (Equation 4.4.1).

Colour	ν	Reduced eye	Le Grand's eye
Red	430	$\begin{pmatrix} 0.9647 & 16.7055\text{ mm} \\ -0.002114\text{ kD} & 1 \end{pmatrix}$	$\begin{pmatrix} 0.6908 & 16.7276\text{ mm} \\ -0.02243\text{ kD} & 0.9044 \end{pmatrix}$
Orange	494	$\begin{pmatrix} 0.9581 & 16.6775\text{ mm} \\ -0.002515\text{ kD} & 1 \end{pmatrix}$	$\begin{pmatrix} 0.6840 & 16.6912\text{ mm} \\ -0.02287\text{ kD} & 0.9041 \end{pmatrix}$
Yellow	558	$\begin{pmatrix} 0.9504 & 16.6455\text{ mm} \\ -0.002977\text{ kD} & 1 \end{pmatrix}$	$\begin{pmatrix} 0.6761 & 16.6494\text{ mm} \\ -0.02337\text{ kD} & 0.9034 \end{pmatrix}$
Green	622	$\begin{pmatrix} 0.9416 & 16.6082\text{ mm} \\ -0.003515\text{ kD} & 1 \end{pmatrix}$	$\begin{pmatrix} 0.6677 & 16.6029\text{ mm} \\ -0.02393\text{ kD} & 0.9026 \end{pmatrix}$
Blue	686	$\begin{pmatrix} 0.9313 & 16.5646\text{ mm} \\ -0.004150\text{ kD} & 1 \end{pmatrix}$	$\begin{pmatrix} 0.6590 & 16.5545\text{ mm} \\ -0.02451\text{ kD} & 0.9018 \end{pmatrix}$
Violet	750	$\begin{pmatrix} 0.9189 & 16.5126\text{ mm} \\ -0.004910\text{ kD} & 1 \end{pmatrix}$	$\begin{pmatrix} 0.6503 & 16.5065\text{ mm} \\ -0.02508\text{ kD} & 0.9011 \end{pmatrix}$

Constants a_2 and c_2 (Table 8.1.9) for *A* and *C* for the two model eyes are very different, confirming the difference in the vertical position shown in Figure 8.1.9. The slopes (a_1 and c_1) are similar to those for the model eyes in air (Tables 8.1.2 and 3). The transferences for the six reference frequencies for the two eyes submerged in water are given in Table 8.1.10.

Submerging the eye in water has the effect of increasing *A* and *C*. Because the power of the system is the negative of the divergence (Equation 3.4.3), submerging the eye in water has the well-known effect of decreasing and, hence, partly neutralising the power of the eye.

8.1.5 Discussion

In conclusion, we saw how the fundamental properties of the reduced and Le Grand model eyes depend on the frequency of light. We compared the two model eyes in air when the refractive index is equated to the constant of 1 and when it is given by Cauchy's formula and saw firstly, that only the dilation *A* and divergence *C* are affected by the refractive index of the surrounding media, and secondly, that the effect is small and affects the vertical position of the graph. This provides justification for using $n_0 = 1$, as is often done in practice.

We then studied the fundamental properties as a function of vacuum wavelength. We observed that the curves depart further from straight lines than do those with frequency ν as independent variable. We conclude, in addition to the reasons discussed in Section 4.3, that it is preferable to study chromatic properties as functions of ν rather than λ.

Finally we considered the effect on the fundamental properties when the model eyes are submerged in water. Again, only the dilation *A* and divergence *C* are affected. There were two noticeable differences in the graphs. Firstly, in Figure 8.1.9, the curves for *A* and *C* differ in vertical position, but the slopes are similar. Secondly, when we compare the respective model eye (Figure 8.1.9) to the same eye in air (Figure 8.1.3) for *A* and *C*, we again see a significant change in position of the curve, but a similar slope. We know that the effect of submerging any eye in water is to tend to neutralise the refractive effect of the corneal surface. As a result the power *F* is decreased and, hence, the divergence *C* is increased. The ametropia *A* is increased and consequently, because of Equation 3.4.6, there is a need for an increased power of the refractive compensation F_0.

In this section we have seen that the fundamental properties of the two model eyes are dependent on frequency. The dependence curves for the fundamental properties of the two model eyes were roughly similar but differed

due to the underlying differences in design of the two eyes. The dependence is very nearly linear and we obtained a linear expression for the dependence of each fundamental property on frequency. When these expressions are used, the estimated transference is approximately symplectic.

8.2 The transformed transferences

In Section 3.7, we introduced transformed transferences and characteristic matrices. Transformed transferences are members of Hamiltonian space whereas each characteristic matrix represents a combination of derived properties of the system. In this section we look at transformed transferences and then examine characteristic matrices in Chapter 9.

Here we consider the logarithmic and Cayley transforms introduced in Section 3.7, both of which are Hamiltonian. Our interest in these transformed transferences, for the purpose of this dissertation, lies not in calculating an average transference (as done elsewhere; Harris, 2004b; 2005; Harris and Cardoso, 2006) but rather is two-fold. Firstly we wish to study the nature of the transformed matrix itself and how it depends on the frequency of light. An advantage is that, for a Gaussian system, one can represent a transference in three-dimensional linear space. Secondly, we utilise the mathematical properties of the Hamiltonian and symplectic matrices to obtain a formula for transferences as functions of frequency. The advantage is that the transferences one obtains are strictly symplectic which contrasts with the transferences obtained above (Equation 8.1.5) which are approximately symplectic.

In Section 5.6 we saw that the Cayley transform can be represented as a simple equation (Equations 5.6.6, 7 and 9) as a function of the entries of the transference. In contrast, a logarithmic transform makes use of an infinite series (Cardoso, 2005) therefore, because of its simple form, the Cayley transform gives greater insight. For this reason we spend some time unpacking the Cayley transform in Section 8.2.1. We take a brief look at the logarithmic transform in Section 8.2.2

8.2.1 The Cayley transformed transference

The Cayley transform is defined by Equation 3.7.13, and simplified for Gaussian systems to Equation 5.6.7. We use the caret (^) to denote transformed qualities. For example $\hat{\mathbf{S}}$ is the transformed **S** and $\hat{A}$ is the transformed *A*. Hamiltonian matrices are defined by Equation 3.7.4 and the resulting equality given by Equation 3.7.6. For a Gaussian system this simplifies to

$$\hat{A} = -\hat{D}. \tag{8.2.1}$$

Hence there are only three independent variables, $\hat{A}$, (or $\hat{D}$), $\hat{B}$ and $\hat{C}$, and therefore $\hat{\mathbf{S}}$ can be plotted on a three-dimensional graph. We recall that the Cayley transform of a symplectic matrix is Hamiltonian and, therefore, Equation 8.2.1 applies to a Gaussian system.

We now consider the dependence of the Cayley transformed transference $\hat{\mathbf{S}}$ on the frequency ν of light. The dependence of the individual entries is shown in Figures 8.2.1 and 4 for the reduced eye and Le Grand's eyes respectively. The relationship between the three independent entries of the transformed transference can be shown on a three-dimensional graph. This is shown in Figure 8.2.3 for the reduced eye and Figure 8.2.6 for Le Grand's eye. The six reference frequencies, as defined in Table 4.2.1, are used to define the frequency at six points, evenly spaced at every 64 THz.

Because Hamiltonian matrices define a vector space we are able to represent the transformed transference, dependent on ν, in the space. The meaning of each axis in Hamiltonian space is outside the scope of this dissertation. The Hamiltonian spaces generated by the logarithmic and Cayley transforms differ. Equation 5.6.7 begins to give some interpretation of what Hamiltonian space represents. We recall that there is an infinity of transforms between symplectic and Hamiltonian matrices; in this study we consider just two, the logarithmic transform (Equation 3.7.2) and the Cayley transform defined by Equation 3.7.13.

We now take a closer look at the formulae derived in Section 5.6. Firstly, Equation 5.6.7 is the formula for the transformed transference as a function of the fundamental properties of the system. This equation gives us some insight into the

meaning of the three independent entries of the Cayley transformed transference. We see that the transformed transference is multiplied by a constant that includes only the entries on the diagonal, that is, *A* and *D*. Within the matrix, the diagonal entries are the difference between the diagonal entries of the transference, while the two off-diagonal entries are the same as for the transference, each multiplied by 2. This gives us a transformed transference that is an interesting mix of the fundamental properties.

The reduced eye

Equation 5.6.18 gives the transformed transference for the reduced eye. Because we have worked with rational numbers all along, we find some interesting simplifications and the transformed transference for the reduced eye turns out to be a simple matrix dependent on the refractive index and therefore on the frequency of light. $\hat{B}$ turns out to be a constant because the refractive indices cancel out. The result of this Cayley transformed transference for the reduced eye is shown graphically for each entry of the matrix in Figure 8.2.1 as functions of frequency.

In Figure 8.2.1 the dashed red straight lines obtained using the least squares method represent the entries of the Cayley transformed transference as functions of frequency. These three straight line equations are represented as a matrix in Equation 8.2.3, with constants given in Table 8.2.1 for the reduced eye. Calculating a matrix from Equation 8.2.3 for any particular frequency results in a Hamiltonian matrix. This in turn, using the Cayley transform, Equation 8.2.2, maps to a transference. Equations 8.2.2 and 3 together give us the formula for the approximation of the transference for the reduced eye as a function of frequency. The equation to map the transference from the transformed transference (originally given in Equation 5.6.12) is

$$\mathbf{S} = \frac{2\left(\mathbf{I} - \hat{\mathbf{S}}\right)}{1 + \det \hat{\mathbf{S}}} - \mathbf{I} \tag{8.2.2}$$

where

$$\hat{\mathbf{S}} = \begin{pmatrix} \hat{a}_1 & \hat{b}_1 \\ \hat{c}_1 & -\hat{a}_1 \end{pmatrix} v + \begin{pmatrix} \hat{a}_2 & \hat{b}_2 \\ \hat{c}_2 & -\hat{a}_2 \end{pmatrix}. \tag{8.2.3}$$

Table 8.2.1 The constants for the reduced eye in air for Equation 8.2.3. The units are picoseconds (ps), millimetres (mm) and kilodioptres (kD).

$\hat{a}_1 = 4.7804\times10^{-5}$ ps	$\hat{a}_2 = 0.3088$
$\hat{b}_1 = 0$ mm ps	$\hat{b}_2 = -11.1111$ mm
$\hat{c}_1 = 7.2055\times10^{-6}$ kD ps	$\hat{c}_2 = 3.6298\times10^{-2}$ kD

Frequency (ν) is in teraHertz $(10^{12}\ \mathrm{s}^{-1})$ and the constants for Equation 8.2.3 are given in Table 8.2.1 for the reduced eye in air.

Equations 8.2.3 and 2 hold for any Gaussian eye, however, because of the changes in structure, that is, the exact parameters of the refracting surfaces, number of refracting surfaces, width of homogenous gaps and formulae of the refractive indices of the media, we can expect different constants for each model eye. Using the methodology above, it is simple for MATLAB® to generate the constants for any Gaussian eye coded into the Matfile.

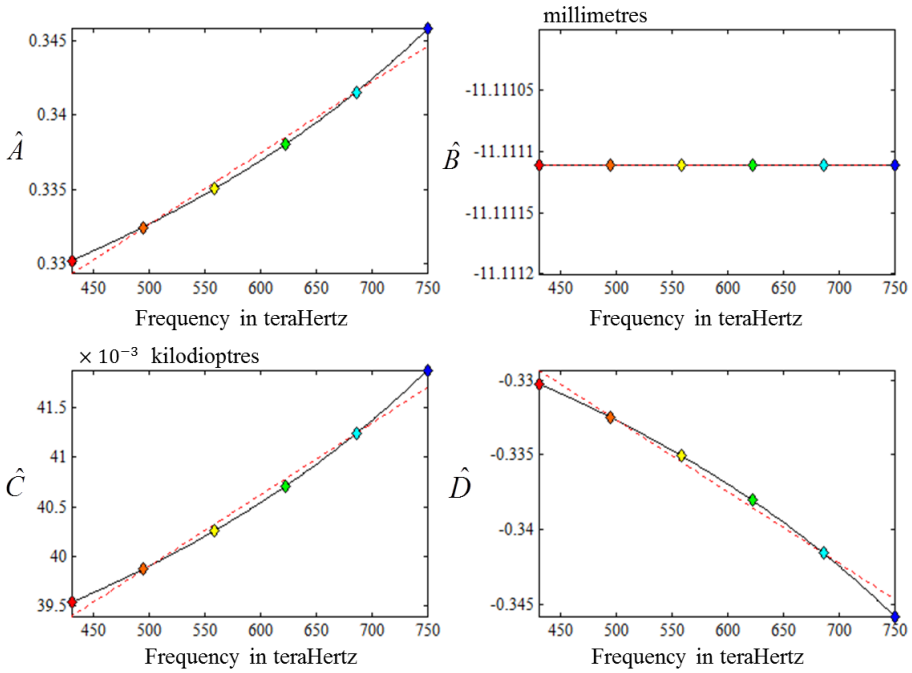

Figure 8.2.1 Entries of the Cayley transformed transference for the reduced eye as functions of frequency. The solid lines represent the entries as functions of frequency and the red dashed lines the fitted least squares straight lines.

The transferences of the reduced eye, obtained using Equations 8.2.2 and 3 are all symplectic matrices to the level of the accuracy of MATLAB®. The graphs for the fundamental properties of the reduced eye in air as a function of frequency are given in Figure 8.2.2. The solid black lines with coloured diamond shaped reference points represent the actual transference of the reduced eye dependent on frequency, and are the same curved lines we saw in Figure 8.1.1. The red lines represent the lines obtained using Equations 8.2.2 and 3 with constants given in Table 8.2.1. The dashed lines representing the least squares straight lines from Figure 8.1.1 are superimposed with the red lines for dilation *A*, disjugacy *B* and divergence *C* and with the black line for divarication *D* and are therefore suppressed to unclutter the figure. Where previously the dashed straight lines created from the least squares of the fundamental properties did not produce transferences that were exactly symplectic, we now have the red lines for each of the fundamental properties representing symplectic transferences. In Hamiltonian space, these red lines are the straight lines produced from the least squares formulation of the entries of the transformed transferences shown by the dashed red lines in Figure 8.2.1.

The relationship between the three independent entries of the Cayley transformed transference for the reduced eye where $n_0 = 1$ are plotted on a three-dimensional graph showing how these properties change with frequency. In Figure 8.2.3, we see how the relationship is a straight line. From Equation 8.2.3 and Table 8.2.1 we have

$\hat{A} = \hat{a}_1 \nu + \hat{a}_2$,

$\hat{B} = \hat{b}_2$

and

$\hat{C} = \hat{c}_1 \nu + \hat{c}_2$.

Manipulating, we obtain

$$\hat{C} = \frac{\hat{c}_1}{\hat{a}_1} \hat{A} + \frac{\hat{a}_1 \hat{c}_2 - \hat{c}_1 \hat{a}_2}{\hat{a}_1},$$

the equation of a straight line.

The derivation of Equation 8.2.2 and the graphs in this section give us some insight into the Hamiltonian space. We have utilised the properties of the Hamiltonian space to derive approximate equations for a transference of the reduced eye as a function of any chosen frequency of light, that is symplectic with determinant exactly 1. Furthermore, Equation 8.2.3 has the advantage of having less constants – six instead of the eight needed for Equation 8.1.5.

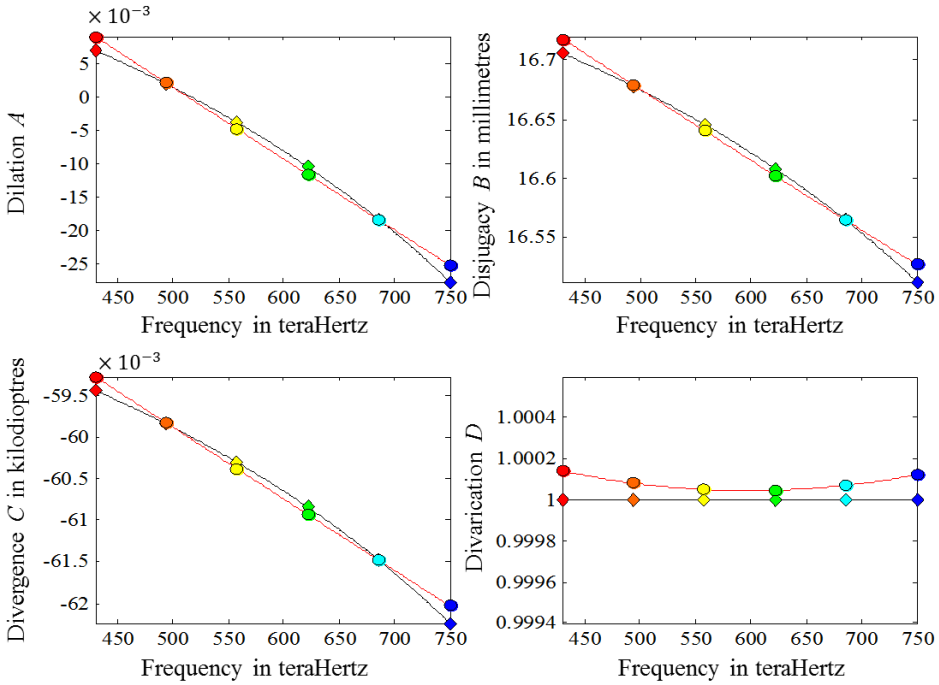

Figure 8.2.2 Fundamental properties of the transference of the reduced eye as functions of frequency. The black lines and diamond reference points represent the dependence as shown in Figure 8.1.1 while the red lines represent the dependence of the reduced eye on frequency according to the formulae and constants given in Equations 8.2.2 and 3 and Table 8.2.1. The least squares straight lines (shown with black dashed lines in Figure 8.1.1) appear superimposed with the red lines for dilation *A*, disjugacy *B* and divergence *C* and have been suppressed.

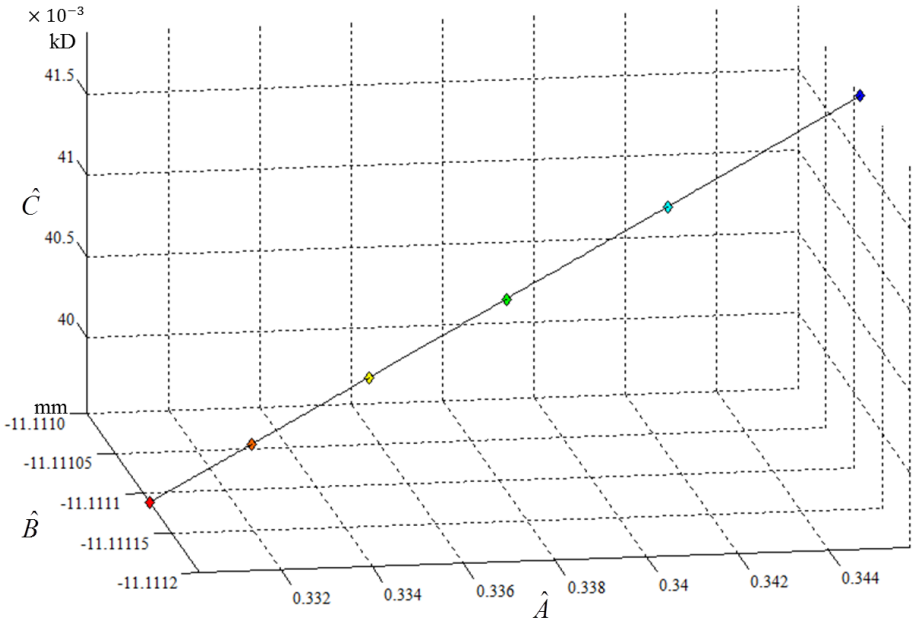

Figure 8.2.3 Three-dimensional graph of the Cayley transformed transference of the reduced eye with $n_0 = 1$ showing change with frequency. The azimuth is -9° and elevation 23°.

Le Grand's eye

In Figure 8.2.4 the individual entries of the Cayley transformed transference for the Le Grand eye are graphed as a function of frequency and in Figure 8.2.6 the three independent entries are graphed in three-dimensions.

If we compare the graphs for the dependence of the transformed transference on the frequency of light for Le Grand's eye (Figure 8.2.4) to that of the reduced eye (Figure 8.2.1) we see strong similarities for $\hat{A}$, $\hat{C}$ and $\hat{D}$, however Le Grand's eye has a curve for $\hat{B}$ whereas the reduced eye has a straight line. However, the scale along the vertical-axis for $\hat{B}$ for Le Grand's eye, indicates that the chromatic difference is small (0.01485 mm) and that the solid lines representing the transformed transference as a function of frequency are very near to linear for each entry.

Similar to the reduced eye, the equations for the dashed red straight lines in Figure 8.2.4 are obtainable using MATLAB®, giving us the constants for Le Grand's eye and given in Table 8.2.2. These constants are substituted into

Table 8.2.2 The constants for Equation 8.2.3 for Le Grand's eye in air.

$\hat{a}_1 = 4.2626\times10^{-5}$ ps	$\hat{a}_2 = 0.2892$
$\hat{b}_1 = 4.6331\times10^{-5}$ mm ps	$\hat{b}_2 = -11.5087$ mm
$\hat{c}_1 = 7.1114\times10^{-6}$ kD ps	$\hat{c}_2 = 3.7630\times10^{-2}$ kD

Equation 8.2.3 to obtain the Cayley transformed transference for each frequency and then into Equation 8.2.2 to obtain the transference for the frequency. The matrix obtained from Equation 8.2.3, by definition, is Hamiltonian and in turn, when transformed using the Cayley transform (Equation 8.2.2), maps to a symplectic matrix. Checking this for every frequency in the visible light spectrum we find that every transference obtained this way has unit determinant and is indeed symplectic.

Equations 8.2.2 and 3 represent a linear approximation to obtain the transference as a function of the frequency of light for any chosen frequency in the visible spectrum. In addition, the calculation can be done with a handheld

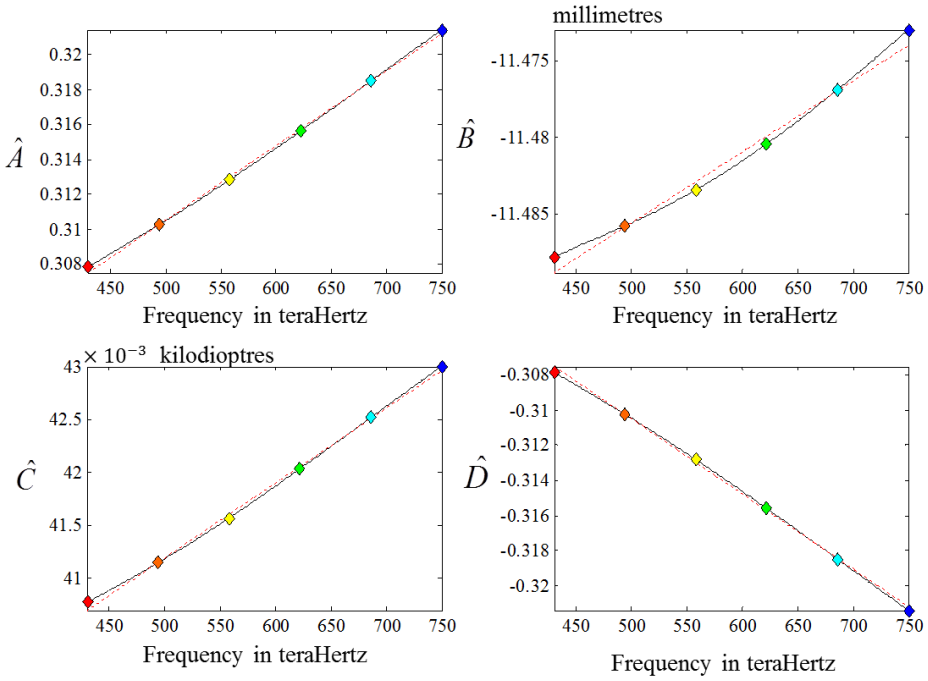

Figure 8.2.4 The entries of the Cayley transformed transference as a function of frequency for the Le Grand eye. The red dashed lines represent the least-squares straight lines for each entry in Hamiltonian space.

calculator in two steps, compared to the far lengthier process of obtaining a refractive index for each medium and then multiplying eight transferences to obtain a transference for the Le Grand eye for a chosen frequency, such as that used to produce the curves in Figure 8.1.2. Deriving the formulae for the transforms enables us to gain some insight into the transformed space and fundamental properties.

The fundamental properties of the transferences for Le Grand's eye obtained from Equations 8.2.3 and 2 are plotted in red in Figure 8.2.5 as functions of the frequency of light. For comparative purposes, we include the lines for the transferences obtained in Figure 8.1.2 in black.

In order to gain some insight into the relationship between the entries of the transformed transference, we plot the Cayley transformed transference for each frequency on a three-dimensional graph in Hamiltonian space. This is shown in Figure 8.2.6, firstly with the azimuth and elevation oriented in order to maximise any curvature along the line plotted and secondly oriented so as to attempt to look along the blue line and superimpose the six coloured diamonds to establish if there is any curvature present on the line. The straight line produced by Equation 8.2.3 is given in red in Figure 8.2.6(a). For the reduced eye we deduced that the line was straight, however, for the Le Grand eye, we see in Figure 8.2.6(b) that there is a small amount of curvature present.

The relationship between each of the fundamental properties and its dependence on frequency of light is nearly linear and similarly the relationship between the entries of the transformed transference and its dependence on the frequency of light are also nearly linear. This applies to both the reduced and Le Grand model eyes. This is in part due to the nature of the frequency of light and the eye being approximately a ball of water. We know from Section 4.3, that the refractive index of water, according to Cornu's equation, is approximately proportional to frequency. The chromatic aberration of the eye is due to the chromatic dispersion of the ocular media, which are mostly water and does not differ much between individuals (Smith, 1995).

Because of the linear relationships, the Cayley transform has enabled us to derive a set of linear equations for the dependence of each of the fundamental

properties on the frequency of light that gives a good approximation of the transference as a function of the frequency of light and given by Equations 8.2.2 and 3. Because we have derived simple equations in terms of the fundamental properties or entries of the transformed transference we have been able to gain some insight into the relationship of the fundamental properties and Hamiltonian space. The numerical transformed transferences for the Cayley transforms of the reduced and Le Grand's eyes, obtained using Equations 8.2.3 and 2, are given in Table 8.2.3.

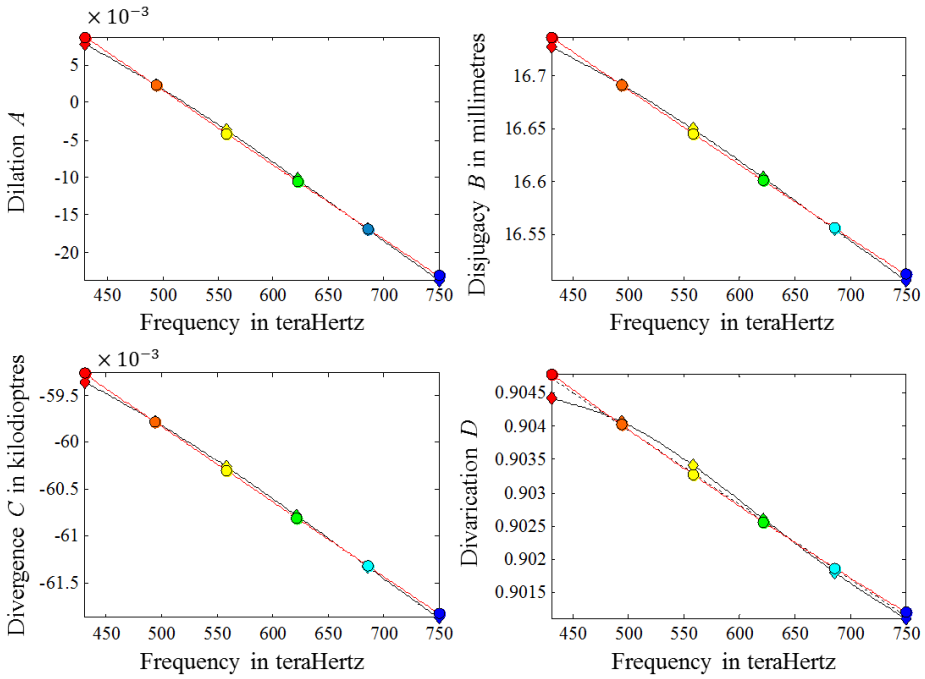

Figure 8.2.5 Fundamental properties of Le Grand's eye as a function of frequency of light. The solid black lines and diamond reference points represent the dependence as shown in Figure 8.1.2 while the red lines represent the dependence of Le Grand's eye on frequency according to the formula and constants given in Equation 8.2.2 and 3 and Table 8.2.2. The least squares straight lines (shown with black dashed lines in Figure 8.1.2) appear superimposed with the red lines for dilation *A*, disjugacy *B* and divergence *C* and have been suppressed. The dashed black least squares line for divarication *D* is shown and can be seen to be very close to the red line.

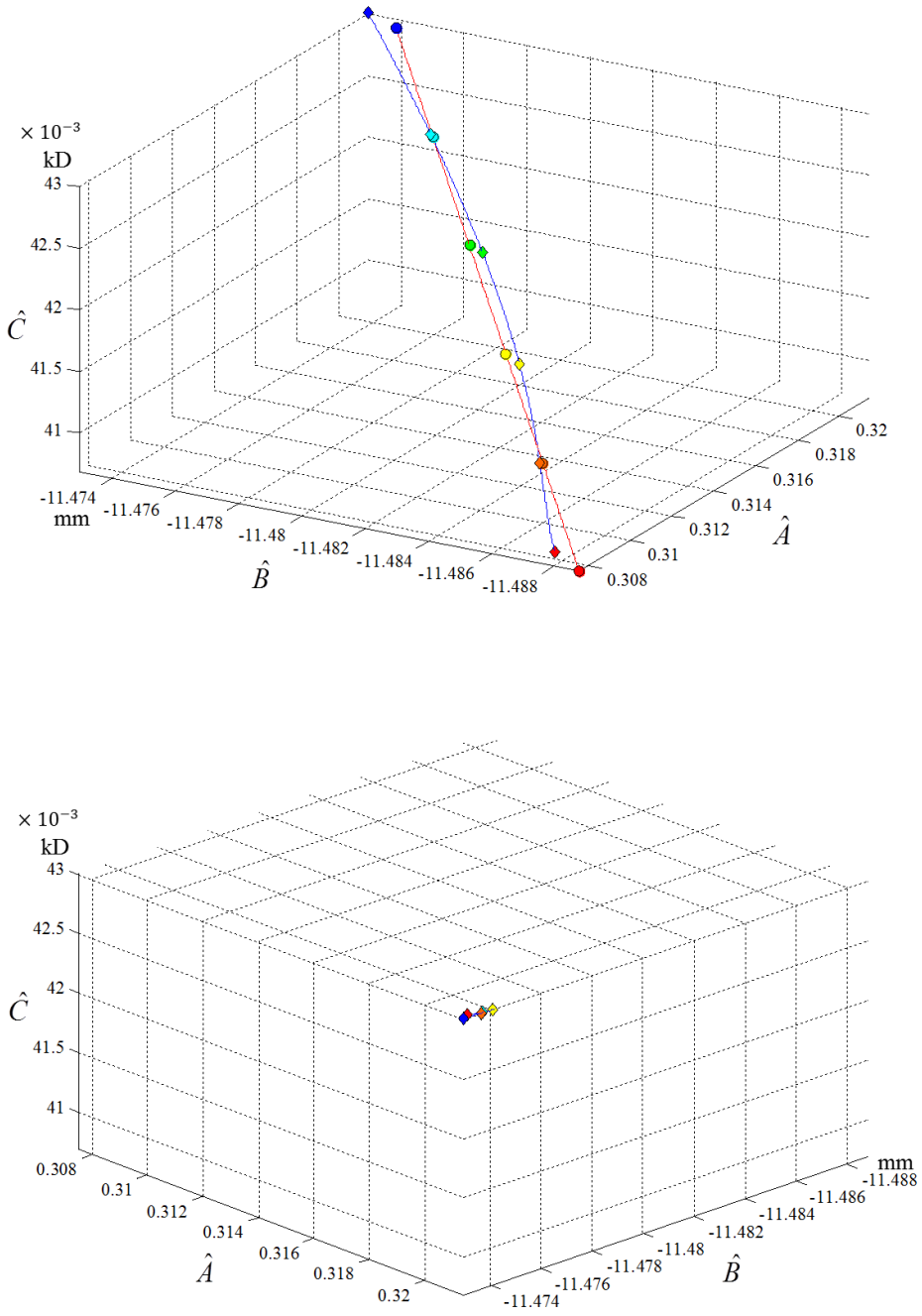

Figure 8.2.6 Three-dimensional graph of the Hamiltonian space of the Cayley transformed transference of Le Grand's eye showing change with frequency with $n_0 = 1$. In **(a)** the azimuth (-60°) and elevation (35°) show a gentle curve along the blue line with diamond markers, representing the transformed transference. The red straight line with circular markers represents the least squares straight line given by Equation 8.2.3. In **(b)** the azimuth (-46.5°) and elevation (-36°) are oriented so as to line up the red and blue diamonds. It is clear from the position of the remaining diamonds that the line is not completely straight, However, in this position the red line creates a single point, but has been suppressed to unclutter the figure.

Table 8.2.3 The numerical values for the Cayley transformed transferences for the six reference frequencies in THz for the reduced and Le Grand's eyes obtained using Equations 8.2.3 and 2 and constants from Tables 8.2.1 and 2.

ν	Colour	Reduced eye	Le Grand's eye
430	Red	$\begin{pmatrix} 0.3302 & -11.1111\,\text{mm} \\ 0.0395\,\text{kD} & -0.3302 \end{pmatrix}$	$\begin{pmatrix} 0.3079 & -11.4878\,\text{mm} \\ 0.0408\,\text{kD} & -0.3079 \end{pmatrix}$
494	Orange	$\begin{pmatrix} 0.3325 & -11.1111\,\text{mm} \\ 0.0399\,\text{kD} & -0.3325 \end{pmatrix}$	$\begin{pmatrix} 0.3102 & -11.4858\,\text{mm} \\ 0.0411\,\text{kD} & -0.3102 \end{pmatrix}$
558	Yellow	$\begin{pmatrix} 0.3350 & -11.1111\,\text{mm} \\ 0.0403\,\text{kD} & -0.3350 \end{pmatrix}$	$\begin{pmatrix} 0.3128 & -11.4834\,\text{mm} \\ 0.0416\,\text{kD} & -0.3128 \end{pmatrix}$
622	Green	$\begin{pmatrix} 0.3380 & -11.1111\,\text{mm} \\ 0.0407\,\text{kD} & -0.3380 \end{pmatrix}$	$\begin{pmatrix} 0.3156 & -11.4804\,\text{mm} \\ 0.0420\,\text{kD} & -0.3156 \end{pmatrix}$
686	Blue	$\begin{pmatrix} 0.3416 & -11.1111\,\text{mm} \\ 0.0412\,\text{kD} & -0.3416 \end{pmatrix}$	$\begin{pmatrix} 0.3185 & -11.4769\,\text{mm} \\ 0.0425\,\text{kD} & -0.3185 \end{pmatrix}$
750	Violet	$\begin{pmatrix} 0.3458 & -11.1111\,\text{mm} \\ 0.0419\,\text{kD} & -0.3458 \end{pmatrix}$	$\begin{pmatrix} 0.3214 & -11.4730\,\text{mm} \\ 0.0430\,\text{kD} & -0.3214 \end{pmatrix}$

8.2.2 The logarithmic-transformed transference

The logarithm of the transference was introduced in Section 3.7.1 and defined by Equation 3.7.2. We denote the transforms, as for Cayley transforms, by means of a caret (^).

The dependence of the logarithmic transformed transference on frequency of light is similar to the Cayley transformed transference in that the logarithmic transformed transference is Hamiltonian and there are three independent entries which show the dependence on frequency of light. The units are the same as the Cayley transformed transference. The dependence of the individual entries of the transformed transference as a function of frequency is given in Figures 8.2.7 and 9 for the reduced and Le Grand's eyes respectively. The relationship represented by Equation 8.2.1 is clear in the graph. The relationship between the dependencies of the three independent entries on the frequency of light on a three-dimensional graph is shown in Figure 8.2.8 for the reduced eye and Figure 8.2.10 for Le Grand's eye.

Table 8.2.4 gives the numerical values of the transformed transferences for six reference frequencies for each of the reduced and Le Grand's eyes with $n_0 = 1$. From the numerical values in the table and the lines in each of the figures, we see that, while the Cayley transform and the logarithmic transform are both Hamiltonian, they each define very different regions within the three-dimensional spaces.

The constants in Equation 8.2.3 for the least-squares straight lines in Figures 8.2.7 and 9 for the logarithmic transform of the reduced eye and Le Grand's eye are given in Table 8.2.5. Using them we obtain a transference dependent on frequency.

From Section 3.7.1 we define the transference **S** obtained from the logarithmic transform $\hat{\mathbf{S}}$ as

$$\mathbf{S} = \exp \hat{\mathbf{S}} \tag{8.2.4}$$

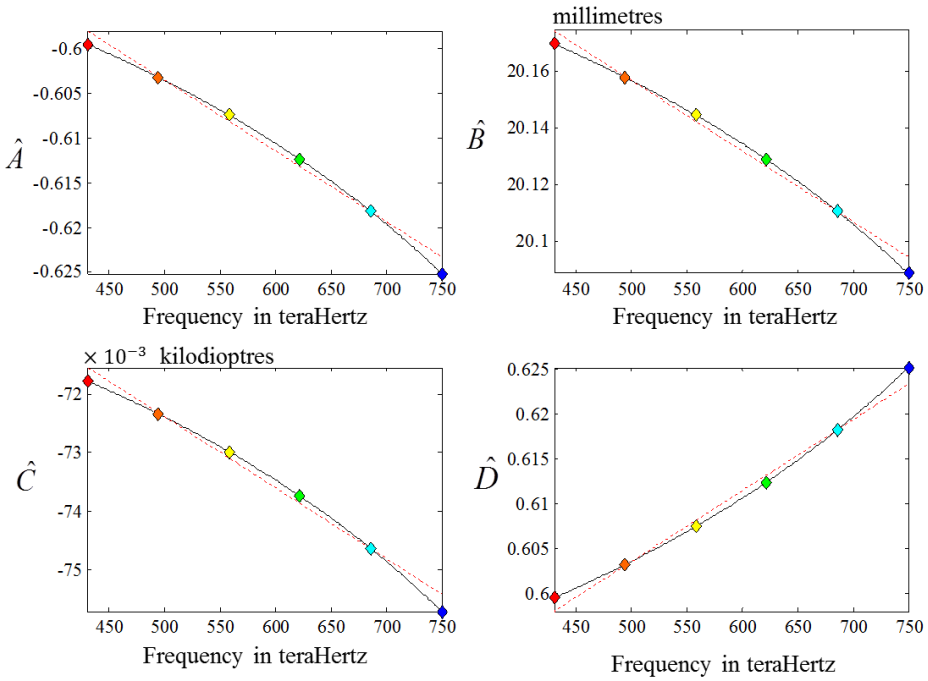

Figure 8.2.7 The entries of the logarithmic transformed transference of the reduced eye as a function of frequency. $\hat{A}$ and $\hat{D}$ are unitless and $\hat{A} = -\hat{D}$, while $\hat{B}$ is in millimetres and $\hat{C}$ is in units of kilodioptres. The red dashed lines represent the least-squares straight line for each entry.

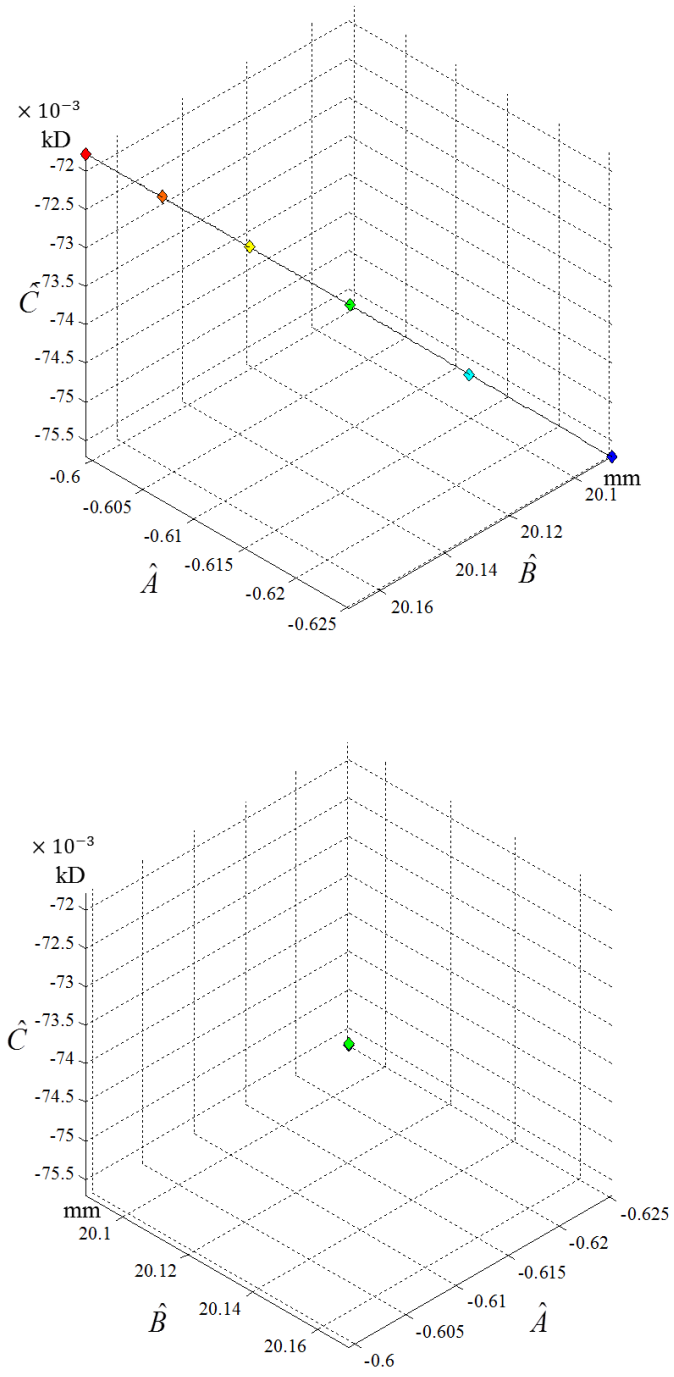

Figure 8.2.8 Three-dimensional graph of the logarithmic transformed transference of the reduced eye showing change with frequency. In **(a)** we see the graph with the azimuth 225° and elevation 35.2° oriented so as to exaggerate any possible curvature. In **(b)** the azimuth 135° and elevation 35.2° are oriented so that we are looking along the line and the coloured diamonds are superimposed on each other showing that the line is straight.

Table 8.2.4 Logarithmic transformed transferences $\hat{\mathbf{S}}$ for six reference frequencies (in THz) for the reduced and Le Grand's eyes.

ν	Colour	Reduced eye	Le Grand's eye
430	Red	$\begin{pmatrix} -0.5995 & 20.1696\text{ mm} \\ -0.0718\text{ kD} & 0.5995 \end{pmatrix}$	$\begin{pmatrix} -0.5527 & 20.6232\text{ mm} \\ -0.0732\text{ kD} & 0.5527 \end{pmatrix}$
494	Orange	$\begin{pmatrix} -0.6032 & 20.1579\text{ mm} \\ -0.0723\text{ kD} & 0.6032 \end{pmatrix}$	$\begin{pmatrix} -0.5566 & 20.6052\text{ mm} \\ -0.0738\text{ kD} & 0.5566 \end{pmatrix}$
558	Yellow	$\begin{pmatrix} -0.6074 & 20.1444\text{ mm} \\ -0.0730\text{ kD} & 0.6074 \end{pmatrix}$	$\begin{pmatrix} -0.5608 & 20.5845\text{ mm} \\ -0.0745\text{ kD} & 0.5608 \end{pmatrix}$
622	Green	$\begin{pmatrix} -0.6124 & 20.1288\text{ mm} \\ -0.0737\text{ kD} & 0.6124 \end{pmatrix}$	$\begin{pmatrix} -0.5652 & 20.5610\text{ mm} \\ -0.0753\text{ kD} & 0.5652 \end{pmatrix}$
686	Blue	$\begin{pmatrix} -0.6182 & 20.1105\text{ mm} \\ -0.0746\text{ kD} & 0.6182 \end{pmatrix}$	$\begin{pmatrix} -0.5699 & 20.5360\text{ mm} \\ -0.0761\text{ kD} & 0.5699 \end{pmatrix}$
750	Violet	$\begin{pmatrix} -0.6252 & 20.0886\text{ mm} \\ -0.0757\text{ kD} & 0.6252 \end{pmatrix}$	$\begin{pmatrix} -0.5746 & 20.5107\text{ mm} \\ -0.0769\text{ kD} & 0.5746 \end{pmatrix}$

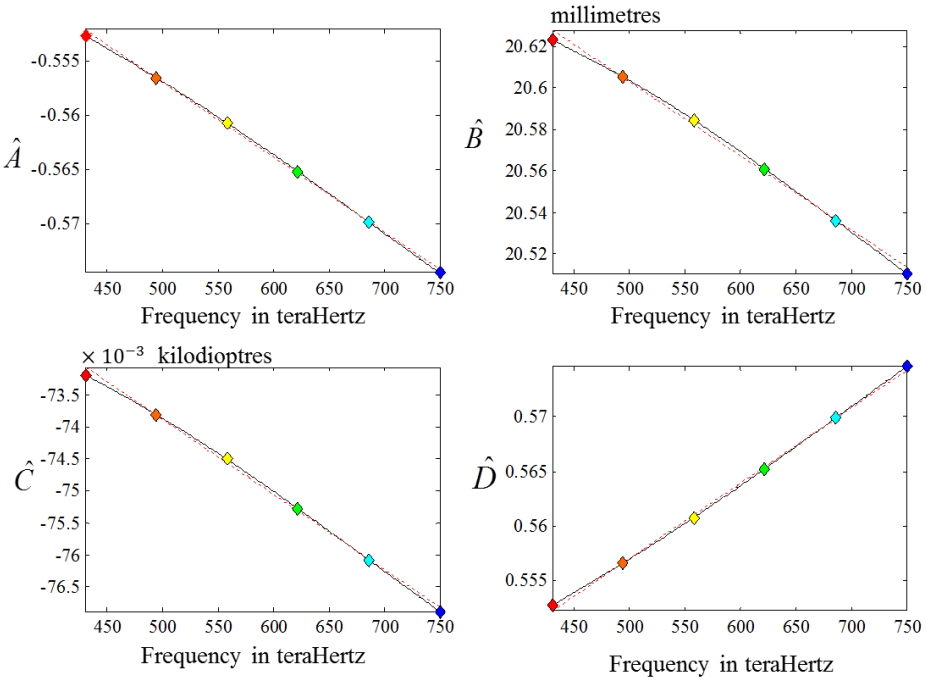

Figure 8.2.9 Entries of the logarithmic transformed transference of Le Grand's eye showing change with frequency. The curves for each entry of the transformed transference are almost linear. The red dashed lines represent the least-squares straight line.

Table 8.2.5 The constants for Equation 8.2.3 for the logarithmic transformed transference $\hat{\mathbf{S}}$ as a function of the frequency of light for the reduced eye and Le Grand's eye.

The Reduced Eye	
$\hat{a}_1 = -7.9053\times10^{-5}$ ps	$\hat{a}_2 = -0.5640$
$\hat{b}_1 = -2.4909\times10^{-4}$ mm ps	$\hat{b}_2 = 20.2813$ mm
$\hat{c}_1 = -1.2145\times10^{-5}$ kD ps	$\hat{c}_2 = -6.6312\times10^{-2}$ kD
Le Grand's Eye	
$\hat{a}_1 = -6.8870\times10^{-5}$ ps	$\hat{a}_2 = -0.5226$
$\hat{b}_1 = -3.5673\times10^{-4}$ mm ps	$\hat{b}_2 = 20.7813$ mm
$\hat{c}_1 = -1.1743\times10^{-5}$ kD ps	$\hat{c}_2 = -6.8009\times10^{-2}$ kD

and substituting from Equation 8.2.3 into this equation we obtain

$$\mathbf{S} = \exp\left(\begin{pmatrix} \hat{a}_1 & \hat{b}_1 \\ \hat{c}_1 & -\hat{a}_1 \end{pmatrix} v + \begin{pmatrix} \hat{a}_2 & \hat{b}_2 \\ \hat{c}_2 & -\hat{a}_2 \end{pmatrix}\right) \tag{8.2.5}$$

the equation for the transference as an approximate dependence on any chosen frequency of light, and which is symplectic. Equation 8.2.5 needs an appropriate software programme such as MATLAB® to execute the principal matrix exponent (*expm*).

The relationship between the three independent entries of the logarithmic transformed transference for Le Grand's eye as a function of frequency is shown by the blue line and diamond markers in Figure 8.2.10(a). By comparison, the red line and circular markers show the relationship obtained from Equation 8.2.5, also for Le Grand's eye. When the blue line is oriented so as to look along the line in Figure 8.2.10 (b), we see that the line is very slightly curved. The red line is straight and is suppressed to unclutter the figure.

In Figures 8.2.11 and 12 the black line with diamonds indicates the dependence of the fundamental properties as functions of frequency and matches the curves in Figures 8.1.1 and 2 for the two model eyes. The red line with circles shows the approximate dependence of the fundamental properties on frequency as calculated using Equation 8.2.5.

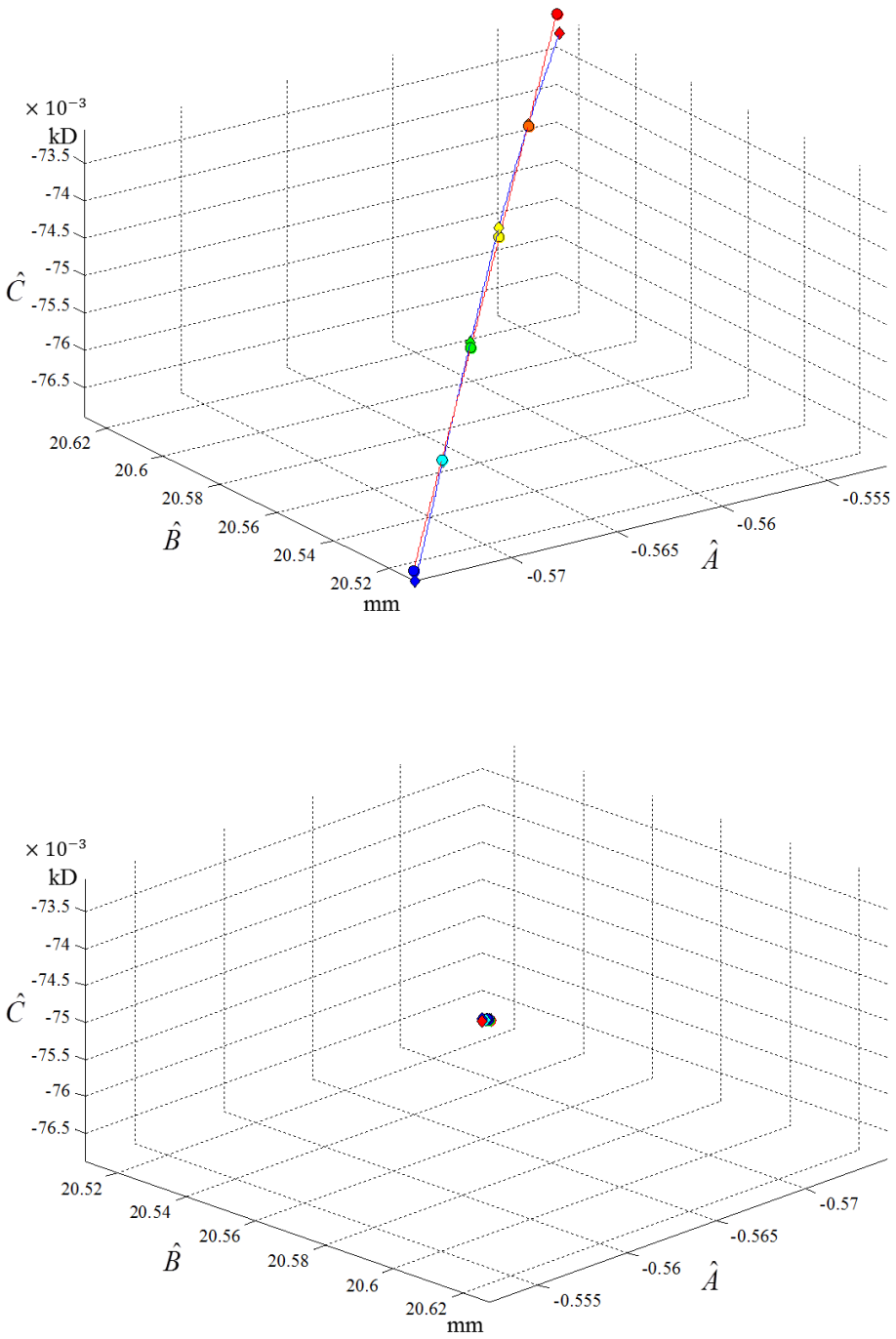

Figure 8.2.10 Three-dimensional graph of the Hamiltonian space of the logarithmic transformed transference of Le Grand's eye showing change with frequency. In **(a)** the azimuth (325°) and elevation (35°) are oriented so as to exaggerate the very slight curve in the line. The blue line and diamond markers show the transformed transference and the red line and circular markers indicate the approximate transformed transference according to Equation 8.2.5. In **(b)** the azimuth (134.5°) and elevation (35.5°) are oriented so as to attempt to line up the coloured diamonds and look along the blue line. This is not completely possible and we note a very slight curvature to the line.

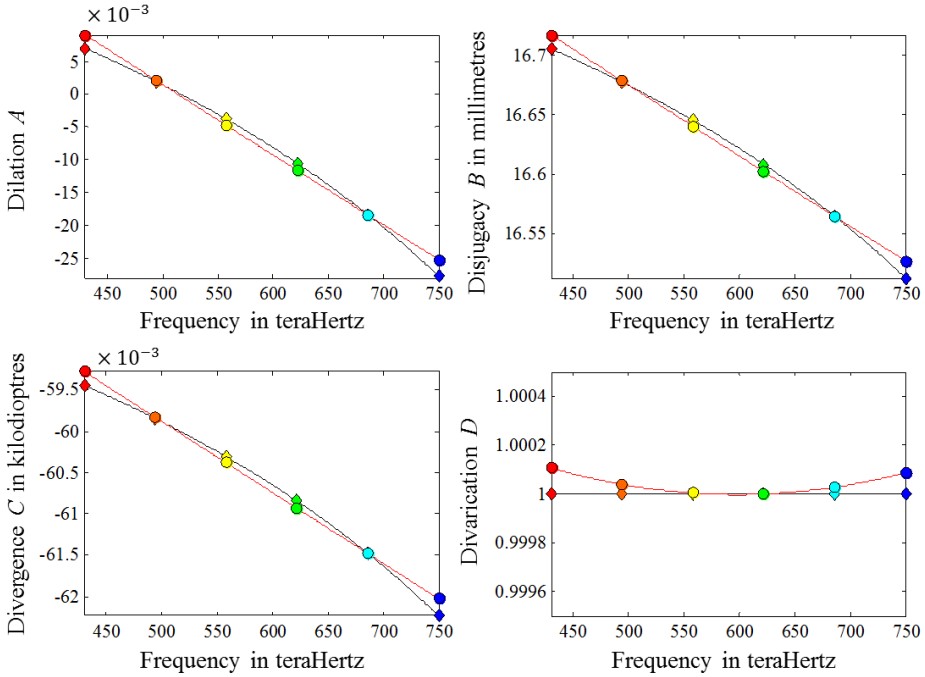

Figure 8.2.11 Fundamental properties of the reduced eye as functions of frequency. The black line and diamond reference points show the transference as an exact function of frequency and the red lines and circular reference points show the approximate transference calculated from the exponential of the linear dependence of the logarithmic transformed transference (Equation 8.2.5). The dashed straight lines seen in Figure 8.1.1 are superimposed on the red lines for dilation *A*, disjugacy *B* and divergence *C* and have been supressed. For divarication *D* it is the straight line at 1.

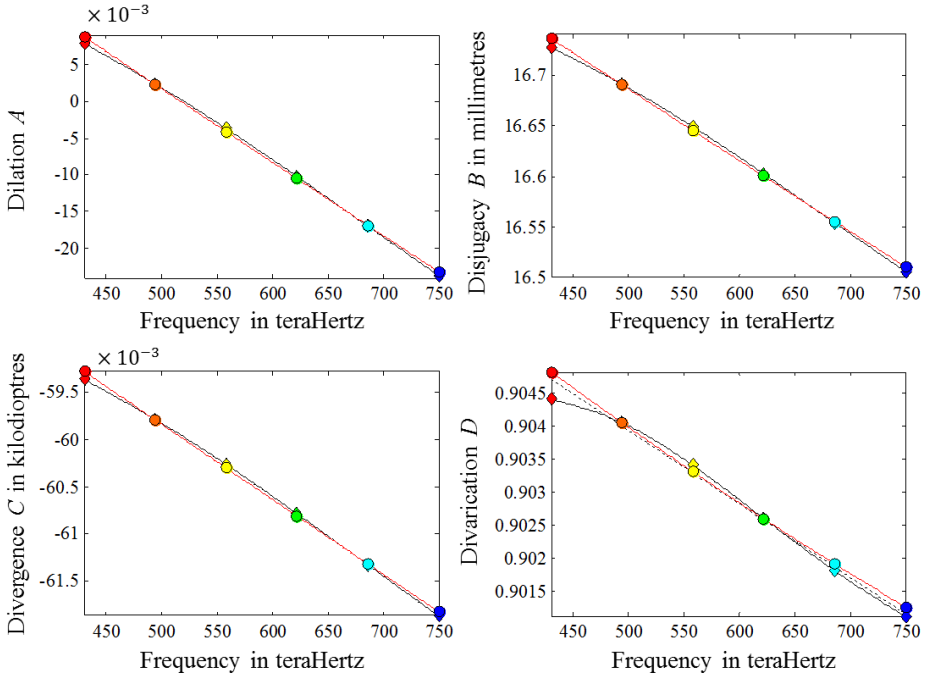

Figure 8.2.12 The fundamental properties of Le Grand's eye as functions of frequency.

The transference for any chosen frequency of light, obtained using the linear approximation given in Equation 8.2.5 and constants in Table 8.2.5 has unit determinant and is symplectic

8.3 Discussion

This chapter has looked at the dependence of the transference on the frequency of light. In Section 8.1, we saw that this relationship for each of the fundamental properties is very close to linear. We obtained an equation for each fundamental property using the least squares method for the straight line, Equation 8.1.5 (shown by a black dashed straight line on each sub-graph). Once combined, the fundamental properties for any particular frequency create an estimated transference whose determinant is approximately 1.

In Section 8.2, we looked at the transformed transference in Hamiltonian vector space. In particular we considered the Cayley and the logarithmic transforms. Because the 2×2 Hamiltonian matrix has three independent entries we were able to visualise the relationship between the entries in three-dimensional vector space. For the reduced eye the relationship is linear and for Le Grand's eye it is nearly perfectly linear. However, when the entries of the transference or transformed transference are looked at independently, Le Grand's eye appears to be closer to linear.

We looked at the dependence of the individual entries of the transformed transference $\hat{\mathbf{S}}$ on the frequency of light and noted, similar to the fundamental properties of the transference **S**, that the entries of $\hat{\mathbf{S}}$ are nearly linear. We obtained equations for the least-squares straight line for each of the three independent entries of the Cayley transformed transference (Equation 8.2.3). When transformed back to a symplectic matrix using Equation 8.2.2, it turns out that we have a matrix for every frequency with a determinant of exactly 1. These two equations are significant because we now have a formula for the straight line approximation giving us the dependence of the fundamental properties and hence the Gaussian transference which is symplectic and therefore the transference of an optical system. The constants are given for Equation 8.2.3 for the reduced eye (Table 8.2.1) and Le Grand's eye (Table 8.2.2).

The formula for the linear dependence of the transference on the frequency of light is based on the Cayley transform. This allows us to create simple equations that are possible to calculate using a handheld calculator. We also derived constants for Equation 8.2.3 for the straight lines of the logarithmic transformed transferences (Table 8.2.5), however Equation 8.2.4 shows that to transform this equation from Hamiltonian space to a symplectic matrix would require the principal matrix exponential which requires sophisticated software such as MATLAB®. Because of this, the Cayley transform gives greater insight.

9 Chromatic dependence of derived properties

Sections 3.4 and 5.1 looked at some familiar optical properties derived from the transference, including power, entrance- and exit-plane refractive compensation, and front- and back-vertex power. Then, Sections 3.6 and 5.4 looked at the cardinal and anti-cardinal points and ways to represent the relationships among the points using graphical construction and Pascal's ring. The distances from the system to the points are also properties of the system that can be derived from the transference. Here we study the dependence of these derived properties on frequency.

Section 3.7.3 introduced the four characteristic matrices. These transformed transferences are not Hamiltonian matrices, but each in its own right creates a vector space enabling us to do certain calculations in these vector spaces. However, unlike the Cayley and Logarithmic transformed transferences, the point **P** and angle **Q** characteristics are dimensionally uniform. Because each characteristic matrix is symmetric in Gaussian optics, it comprises three independent entries which can be graphed in three-dimensions. The dependence of the entries of each of the four characteristic matrices on the frequency of light will be graphed in Section 9.3 below.

9.1 Cardinal and anti-cardinal points

Sections 3.6 and 5.4 looked at the cardinal and anti-cardinal points of systems in general. We now look at how the frequency of light affects the positions and spread of the various points in the reduced and Le Grand's eyes. We start by obtaining the incident and emergent cardinal and anti-cardinal points for the six reference frequencies for each eye. These are given in Tables 9.1.1 to 4. We include the chromatic difference in positions, mean and standard deviation for each cardinal and anti-cardinal point in the tables. The chromatic difference in positions is calculated as

$$\delta z_Q = z_Q^{\mathrm{b}} - z_Q^{\mathrm{r}} \tag{9.1.1}$$

where Q represents any of the cardinal or anti-cardinal points and b and r represent the blue and red frequencies respectively. Longitudinal positions, *z*, are

Table 9.1.1 The positions of the incident cardinal points of the reduced eye for the six reference points, the chromatic difference in positions, mean and standard deviation across the spectrum 430 to 750 THz. Longitudinal positions *z* are relative to entrance plane T_0 and subscripts are defined in Table 3.6.1.

Colour	Freq THz	$z_{\overline{N}0}$ mm	$z_{\overline{P}0}$ mm	z_{F0} mm	z_{P0} mm	z_{N0} mm
Red	430	–39.2018	–33.6463	–16.8231	0	5.5556
Orange	494	–38.9761	–33.4206	–16.7103	0	5.5556
Yellow	558	–38.7198	–33.1643	–16.5821	0	5.5556
Green	622	–38.4263	–32.8708	–16.4354	0	5.5556
Blue	686	–38.0868	–32.5312	–16.2656	0	5.5556
Violet	750	–37.6895	–32.1340	–16.0670	0	5.5556
Chromatic difference		1.5123	1.5123	0.7562	0	0
Mean		–38.5343	–32.9788	–16.4894	0	5.5556
Standard deviation		0.4343	0.4343	0.2172	0	0

Table 9.1.2 Positions of the emergent cardinal and anti-cardinal points of the reduced eye as a function of frequency for the six reference points. The longitudinal positions *z* are given in millimetres from the exit plane T which is 22.2222 mm downstream of the entrance plane. The chromatic difference in position between the red and blue emergent points, the mean and standard deviation across the spectrum are given. Subscripts are defined in Table 3.6.1.

Colour	ν THz	z_P mm	z_N mm	z_F mm	$z_{\overline{N}}$ mm	$z_{\overline{P}}$ mm
Red	430	–22.2222	–16.6667	0.1565	16.9796	22.5352
Orange	494	–22.2222	–16.6667	0.0436	16.7539	22.3095
Yellow	558	–22.2222	–16.6667	–0.0845	16.4976	22.0532
Green	622	–22.2222	–16.6667	–0.2313	16.2041	21.7596
Blue	686	–22.2222	–16.6667	–0.4011	15.8646	21.4201
Violet	750	–22.2222	–16.6667	–0.5997	15.4673	21.0229
Chromatic difference		0	0	–0.7562	–1.5123	–1.5123
Mean		–22.2222	–16.6667	–0.1773	16.3121	21.8676
Standard deviation		0	0	0.2172	0.4343	0.4343

relative to the corresponding transverse plane. Consistent with Section 4.2 the frequency of red is taken to be 430 THz and blue to be

Table 9.1.3 The positions of the incident cardinal and anti-cardinal points of Le Grand's eye as a function of frequency for six reference frequencies. Positions are relative to the entrance plane.

Colour	Freq THz	$z_{\overline{\mathrm{N}}0}$ mm	$z_{\overline{\mathrm{P}}0}$ mm	$z_{\mathrm{F}0}$ mm	$z_{\mathrm{P}0}$ mm	$z_{\mathrm{N}0}$ mm
Red	430	–37.6878	–32.0833	–15.2365	1.6103	7.2148
Orange	494	–37.4540	–31.8489	–15.1221	1.6048	7.2098
Yellow	558	–37.1882	–31.5854	–14.8489	1.6028	7.2056
Green	622	–36.9000	–31.3001	–14.8489	1.6022	7.2022
Blue	686	–36.6078	–31.0094	–14.7042	1.6010	7.1994
Violet	750	–36.3241	–30.7255	–14.5637	1.5637	7.1967
Chromatic difference		1.3638	1.3578	0.6728	–0.0122	–0.0182
Mean		–37.0320	–31.4304	–14.9137	1.6029	7.2045
Standard deviation		0.4032	0.4006	0.1990	0.0027	0.0052

Table 9.1.4 Positions of the emergent cardinal and anti-cardinal points for Le Grand's eye as a function of frequency for six reference frequencies. The distances are relative to the exit plane, which is 24.1965 mm downstream from the entrance plane.

Colour	Freq THz	z_{P} mm	z_{N} mm	z_{F} mm	$z_{\overline{\mathrm{N}}}$ mm	$z_{\overline{\mathrm{P}}}$ mm
Red	430	–22.2758	–16.6712	0.1756	17.0223	22.6269
Orange	494	–22.2793	–16.6742	0.0526	16.7795	22.3845
Yellow	558	–22.2788	–16.6760	–0.0819	16.5122	22.1150
Green	622	–22.2765	–16.6765	–0.2254	16.2258	21.8258
Blue	686	–22.2750	–16.6766	–0.3714	15.9338	21.5322
Violet	750	–22.2754	–16.6766	–0.3714	15.9338	21.5322
Chromatic difference		0.0004	–0.0056	–0.6906	–1.3756	–1.38105
Mean		–22.2771	–16.6755	–0.1588	16.3578	21.9594
Standard deviation		0.0017	0.0015	0.2028	0.4044	0.4070

750 THz, the end-points of the spectrum. The mean and standard deviation are calculated across the spectrum from 430 to 750 THz at every 1 THz.

The reduced eye

Tables 9.1.1 and 2 show that the incident P_0 and emergent P principal points of the reduced eye both coincide with the entrance plane (or cornea) T_0 and the incident N_0 and emergent N nodal points both coincide with each other at the centre of curvature which is 5.5556 mm downstream of the entrance plane. This implies that P_0, P, N_0 and N are independent of frequency in the reduced eye and remain single point structures. On the other hand, the incident F_0 and emergent F and anti-cardinal points $\overline{P}_0$, $\overline{P}$, $\overline{N}_0$ and $\overline{N}$ depend on frequency and are therefore not point structures, but spread out like little rainbows into fuzzy zones rather than points. Furthermore, the magnitude of the chromatic difference in position of each of the anti-cardinal points is the same for the reduced eye, that is, $\left|\delta z_{\overline{Q}}\right| = 1.5123\,\text{mm}$.

Le Grand's eye

Tables 9.1.3 and 4 show that all ten of the cardinal and anti-cardinal points for Le Grand's eye depend on frequency and each is a fuzzy zone like a little rainbow. This is represented by both the chromatic difference and standard deviation. Because the points are mathematical concepts they will not actually be visible as a rainbow, with the exception of F. The statistical data at the bottom of each table shows that the fuzzy spread is greater for the anti-cardinal points than for the cardinal points. The P_0's and P's demonstrate the least spread, with the fuzzy spread increasing with each point as it moves further away from the P_0's and P's.

9.1.1 Graphical construction

The data given in Tables 9.1.1 to 4 is displayed visually using graphical construction as introduced in Sections 3.6.4 and 5.4.2. For this we construct the locator lines and points for the red and blue transferences for each of the reduced and Le Grand's eyes. In order to prevent the graph from being too cluttered, only the locator lines for the transferences representing the red (430 THz) and blue (750 THz) frequencies will be displayed. The positions of the ten cardinal and anti-cardinal points are shown.

Graphical construction of the reduced eye

Figure 9.1.1 shows the graphical construction for the reduced eye showing the locator lines for the red and blue transferences and the ten cardinal and anti-cardinal points. In Figure 9.1.1 the black horizontal line represents the optical axis Z, positioned at $X = 0$. The two vertical black lines represent the entrance plane T_0 at $z = 0$ and the exit plane T a distance z downstream from T_0 at $z = \frac{200}{9}\,\mathrm{mm}$, which is the length of the reduced eye. The locator lines L_0 and L for the reduced eye are drawn in red (430 THz) and blue (750 THz). From Section 3.6.4, the slope of the incident locator lines L_0 is given by $\frac{-C}{n_0}$. For the reduced eye in air, the refractive index of air is constant, 1, however, we know that C depends on frequency, and therefore the slope of L_0 also varies with frequency. The slope of the emergent locator line L is given by $\frac{C}{n}$. Both C and n depend on frequency and hence so does the slope of L. The slope of the blue locator line is steeper in magnitude than that of the red line for both L_0 and L.

In Figure 9.1.1 F_0 and F are positioned at the point of intersection between the respective locator line L_0 and L and the optical axis Z. The F_0's show that the blue F_0 is closer to the eye than the red F_0. More applicably, for F, the blue F is before the exit-plane T or retina and the red F is behind the retina. While the result is not surprising, the locator lines visibly illustrate this.

Locator line diagrams were described in Section 3.6.2. In Figure 9.1.1 horizontal lines are drawn in green at $X=1$ and $X=-1$ and vertical lines extended to the longitudinal axis for P_0 and P in green for the red points and cyan for the blue points. P_0 and P are coincident with T_0 for the reduced eye and only the cyan line is visible in the diagram. The red and blue anti-principal points $\overline{P}_0$ and $\overline{P}$ are distinct. P_0 and P simplify as follows: for z_{P0} for the reduced eye $D=1$ (from Equation 5.5.1), regardless of frequency. Substituting $D=1$ and $X=1$ for P_0 from Table 3.6.1 into Equation 3.6.1, it simplifies to 0 making z_{P0} coincident with the entrance plane for all frequencies. For z_P, by substituting $X=1$ and A and C from Equation 5.5.1 into Equation 3.6.2, z_P simplifies to $-z$. Because z is the length of the reduced eye, P is also coincident with T_0 for all frequencies. This is illustrated in Figure 9.1.1 where all four locator lines cross at the entrance-plane at both $X=1$ and $\frac{1}{X}=1$, shown by the uppermost green horizontal line.

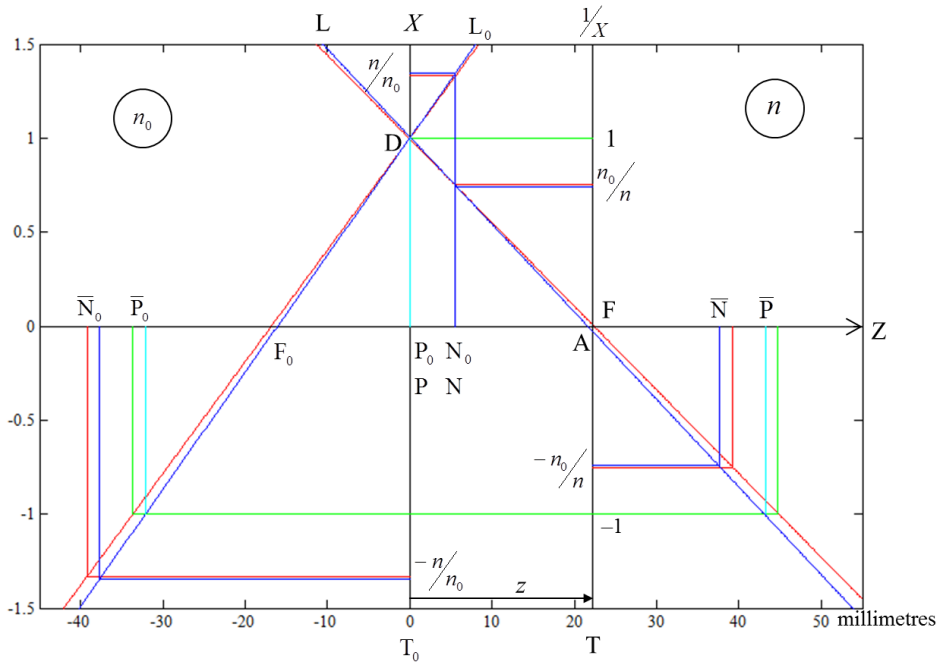

Figure 9.1.1 The graphical construction for the reduced eye showing the locator lines for the red and blue transferences and the ten cardinal and anti-cardinal points.

The nodal and anti-nodal points are indicated in Figure 9.1.1 with horizontal lines at $\pm\frac{n}{n_0}$ for N_0 and $\overline{\mathrm{N}}_0$ and $\pm\frac{n_0}{n}$ for N and $\overline{\mathrm{N}}$ in red and blue respectively. Because the indices depend on frequency, we obtain different positions for the red and blue horizontal lines. In turn vertical lines are extended to indicate the position of the nodal points on the longitudinal axis. For the reduced eye N_0 and N coincide, however $\overline{\mathrm{N}}_0$ and $\overline{\mathrm{N}}$ are distinct. The coincidence of N_0 and N is found in Equation 5.5.1; substituting *C*, *D* and *X* into Equation 3.6.1, z_{N0} simplifies to *r*, the radius of curvature of the corneal refracting surface. Therefore z_{N0} is independent of refractive indices, n_0 and *n*, and, hence, frequency ν. This is seen in Figure 9.1.1 by the single blue line dropping to the position for N_0. Similarly, substituting for *X*, and *A* and *C* from Equation 5.5.1 into Equation 3.6.2 and simplifying, we obtain the position for N as $z_{\mathrm{N}} = r - z$ with respect to T. This places N at position *r* with respect to T_0 for all frequencies. N is therefore independent of frequency and coincident with N_0.

Simplifications of anti-cardinal points for the reduced eye

We now turn our attention to the anti-cardinal points of the reduced eye, starting with $\overline{\mathrm{P}}_0$ and $\overline{\mathrm{P}}$. We know that the horizontal line to find the position of the points on the locator lines needs to be drawn at $X = -1$, shown by the lower green horizontal line in Figure 9.1.1. From the figure and from Equations 5.5.1 and 3.6.1 and 2, we see that $\overline{\mathrm{P}}_0$ and $\overline{\mathrm{P}}$ depend on frequency. Similarly, $\overline{\mathrm{N}}_0$ and $\overline{\mathrm{N}}$ are also dependent on frequency. $\overline{\mathrm{N}}_0$ and $\overline{\mathrm{N}}$ for the reduced eye are equidistant from the entrance-plane, albeit in opposite directions. From Tables 9.1.1 and 2 we see that each of the anti-cardinal points is equidistant between the red and blue positions (chromatic difference); this is shown algebraically for $\overline{\mathrm{P}}_0$, $\overline{\mathrm{P}}$, $\overline{\mathrm{N}}_0$ and $\overline{\mathrm{N}}$ below.

Most of the simplifications that occur for the reduced eye above and in Figure 9.1.1 stem from the transference and the fact that $D = 1$ for all

transferences of the reduced eye, regardless of the frequency. Let us look at this in more detail. Firstly, $\overline{\mathrm{N}}_0$ and $\overline{\mathrm{N}}$ are equidistant from T_0, in opposite directions. Starting with Equation 3.6.3, we substitute the values for *C* and *D* from Equation 5.5.1 and $n_0 = 1$ to obtain

$$z_{\overline{\mathrm{N}}0} = -\frac{n+1}{n-1}r \tag{9.1.2}$$

for the position of $\overline{\mathrm{N}}_0$ of the reduced eye and

$$z_{\overline{\mathrm{N}}} = \frac{n+1}{n-1}r - z \tag{9.1.3}$$

for the position of $\overline{\mathrm{N}}$ of the reduced eye. Because the emergent points are defined as the distance from the exit-plane, we expect that the incident and emergent formulae will differ by the length of the reduced eye, *z*. From Equations 9.1.2 and 3, we see that $\overline{\mathrm{N}}_0$ and $\overline{\mathrm{N}}$ are equidistant from T_0, $\overline{\mathrm{N}}_0$ being upstream and $\overline{\mathrm{N}}$ downstream of T_0.

Similar equations derived for $\overline{\mathrm{P}}_0$ and $\overline{\mathrm{P}}$, from T_0 and T respectively, turn out to be

$$z_{\overline{\mathrm{P}}0} = \frac{-2r}{n-1} \tag{9.1.4}$$

for the distance of $\overline{\mathrm{P}}_0$ from T_0, and

$$z_{\overline{\mathrm{P}}} = \frac{2nr}{n-1} - z \tag{9.1.5}$$

for the distance of $\overline{\mathrm{P}}$ from T. These are clearly not equidistant from T_0 and confirms what we deduce from Figure 9.1.1.

Secondly, we examine the result in Tables 9.1.1 and 2 that the magnitude of the distance between the red and blue anti-cardinal points in the reduced eye is the same for all four anti-cardinal points. Starting with the chromatic difference between points defined in Equation 9.1.1 and substituting in turn the equations derived for each of the anti-cardinal points in Equations 9.1.2 to 5, we obtain the chromatic difference in position of $\overline{\mathrm{P}}_0$

$$\delta z_{\overline{\mathrm{P}}0} = z^b_{\overline{\mathrm{P}}0} - z^r_{\overline{\mathrm{P}}0} = \frac{2r(n_b - n_r)}{(n_b - 1)(n_r - 1)}. \tag{9.1.6}$$

The equation for $\delta z_{\bar{N}0}$, the chromatic difference in distance between the red and blue $\bar{N}_0$'s is equal to Equation 9.1.6. The chromatic difference in position of $\bar{P}$ and $\bar{N}$ are equal in magnitude, but the negative of the incident equation. That is to say

$$\delta z_{\bar{N}0} = \delta z_{\bar{P}0} = -\delta z_{\bar{N}} = -\delta z_{\bar{P}}. \qquad (9.1.7)$$

The negative value found in the chromatic difference of the emergent anti-cardinal points indicates that the positions of the red and blue anti-cardinal points are switched compared to the incident points. The equalities derived in Equations 9.1.2 to 7 only apply to the reduced eye and cannot be generalised to other eyes.

We conclude that while the reduced eye is well suited to the study of most chromatic properties, it is not suitable for studying cardinal points and, in particular, not suitable for studying the dependence of the cardinal points on frequency.

Graphical construction of Le Grand's eye

Let's us, therefore, consider a more complex Gaussian eye, that of Le Grand's four-surface eye. From Table 8.1.1 and Section 8.1.1 we already know that all four fundamental properties depend on the frequency of the light traversing the system. Figure 9.1.2 shows the graphical construction of the locator lines for Le grand's eye for the red (430 THz) and blue (750 THz) frequencies.

The optical axis Z, entrance-plane T_0 and exit-plane T are the same as in Figure 9.1.1. It is apparent that Le Grand's eye does not simplify to the extent that the reduced eye does. We start with the incident locator lines L_0, the slope of which, from the equation for the slope given above and from Figure 9.1.2, depend on frequency. The slope of L_0 is 0.05936 kD for the red line and 0.06187 kD for the blue line. Unsurprisingly, the intersection of L_0 with Z shows that the blue F_0 is in closer proximity to the eye than the red F_0. L_0 intersects the entrance-plane at position *D*. From the transferences listed in Table 8.1.1 we know that the entries for *D* depend on frequency and therefore the two L_0s cross T_0 at different

positions. The values for *D* are, however, very close and it is difficult to see the separation on Figure 9.1.2. The red and blue L_0 s cross at

$$z_{Q0} = \frac{D_b - D_r}{C_b - C_r} \tag{9.1.8}$$

which is 1.32 mm downstream of T_0.

The emergent locator lines L intersect T at *A*. From Section 3.3.1, we know that a positive value for *A* implies hyperopia and a negative value, myopia. This is visible in Figure 9.1.2, where the red L indicates a positive value for *A* and intersects Z behind T or the retina and the blue L shows a negative value for *A* and intersects Z with F before the retina. The red and blue L's intersect at position

$$z_Q = \frac{A_b - A_r}{\frac{C_r}{n_r} - \frac{C_b}{n_b}} \tag{9.1.9}$$

which is –22.4474 mm from T, or 1.7491 mm from T_0. The position of intersection of the incident red and blue L_0 's does not coincide with the same for L's, nor does either intersection coincide with the position of either P_0 's or P's. The slopes of the L's are –0.04454 kD for the red line and –0.04596 kD for the

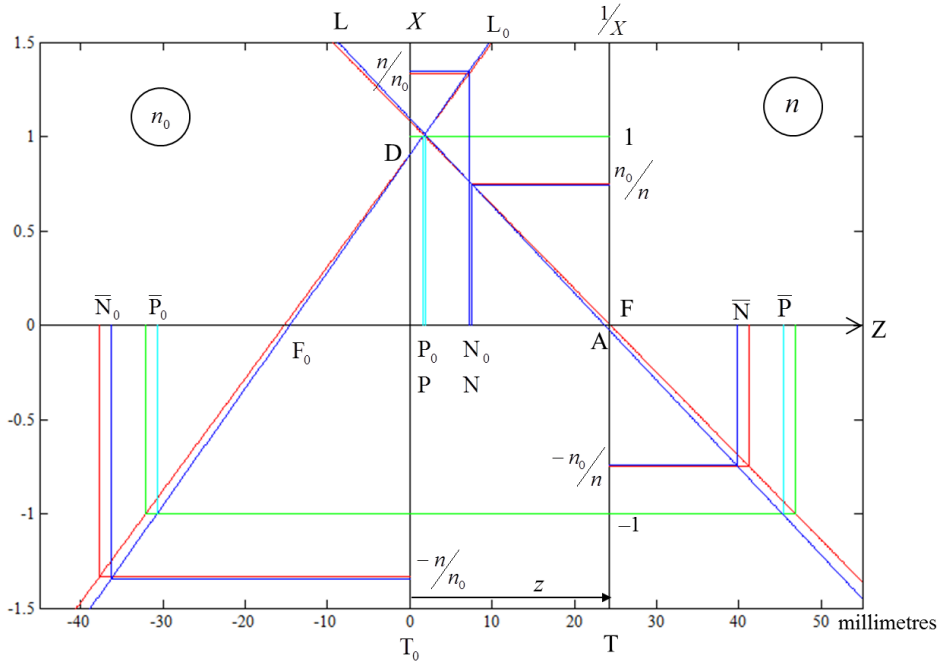

Figure 9.1.2 The graphical construction for Le Grand's eye showing the locator lines for the red and blue transferences and the ten cardinal and anti-cardinal points.

blue line. Because the difference in slope of the L_0's and L's is so slight, it is difficult to distinguish the point of intersection of the red and blue lines in Figure 9.1.2.

In Figure 9.1.2 the principal and anti-principal horizontal lines are drawn in green at 1 or –1 respectively and vertical lines extended to Z in green for the red points and cyan for the blue points. The P_0's and P's are separate, and do not coincide with T_0. The red and blue P_0's and P's are also distinct, but too close to be discernible in the diagram. The cyan lines appear superimposed over the green lines and from the diagram it appears that each of P_0 and P is the same for the red and blue lines. However, if we look at the values given in Tables 9.1.3 and 4, we see that the red and blue transferences have different values for the P_0's and P's and therefore the P_0's and P's depend on frequency. The $\overline{P}_0$'s and $\overline{P}$'s are distinct.

In Figure 9.1.2 the nodal and anti-nodal points are indicated with horizontal lines at $\pm\frac{n}{n_0}$ at N_0 and $\overline{N}_0$ and $\pm\frac{n_0}{n}$ for N and $\overline{N}$ in red and blue respectively. Because the indices depend on frequency, we obtain different positions for the horizontal lines. For Le Grand's eye the N_0's and N's are distinct and the red and blue points are also distinct, but too close to be distinguishable in the diagram. For clarity, we see from Tables 9.1.3 and 4 that the red and blue N_0's and N's are distinct and therefore the N_0's and N's depend on frequency, implying that the N_0's and N's are not points, but rather fuzzy nodal zones. The $\overline{N}_0$'s and $\overline{N}$'s are distinct for red and blue.

Unlike the reduced eye, the chromatic difference in position between each of the four anti-cardinal points for Le Grand's eye is different for all four points.

Summary

We have illustrated how the principal and nodal points for the reduced eye are independent of frequency and that P_0 and P are positioned at the entrance plane while N_0 and N are positioned at the centre of curvature of the single

refracting surface. For the reduced eye, F_0, F and the anti-cardinal points depend on frequency and the chromatic difference in distance between the red and blue position of each of the anti-cardinal points is the same, but the sequence is different for incidence and emergence.

On the other hand, for the four-surface Le Grand eye, all six cardinal and four anti-cardinal points depend on frequency and are distinct from each other, implying that these cardinal points are not points but fuzzy zones.

9.1.2 Pascal's ring

In the previous section, we looked at the positions and changes among the various cardinal and anti-cardinal points. Tables 9.1.1 to 4 gave numerical values and we were able to see which points were dependent on frequency. The graphical constructions given in Figure 9.1.1 for the reduced eye and Figure 9.1.2 for Le Grand's eye showed the relationships between the positions of the points, however, certain points are so close together as to be indiscernible in the figures. Pascal's ring was introduced in Section 3.6.5 and expanded on in Section 5.4.3 and while the ring is not drawn to scale, it does show the relationships among the points and the directions of the changes. Pascal's ring emphasises which points are dependent, or, in the case of the reduced eye, independent, of frequency.

Pascal's ring for the reduced eye

Pascal's ring for the reduced eye as a function of frequency is shown in Figure 9.1.3. For clarity, we compare the rings for only the red and blue cardinal points. From the graphical construction of the reduced eye in Figure 9.1.1, there is no separation of principal planes nor nodal points and so for Pascal's ring the central square fuses to become a single vertical line. As expected, the blue focal points are both closer to the eye than the red focal points and this is represented in Pascal's ring. When we consider the Pascal's ring in Figure 9.1.3 and the extended Pascal's ring in Figure 9.1.4 we see that, for the reduced eye, the blue ring contracts towards the principal-nodal line. The width, between the focal points, is narrower for the blue than for the red ring structure. The vertical height of both red and blue structures is equal.

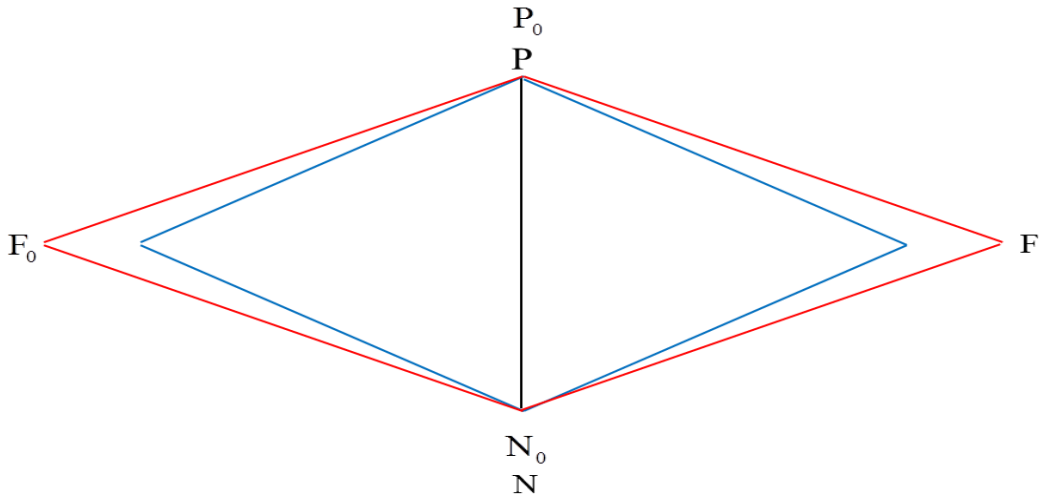

Figure 9.1.3 Pascal's ring for the reduced eye for the red and blue cardinal points. The vertical black line is common to both frequencies.

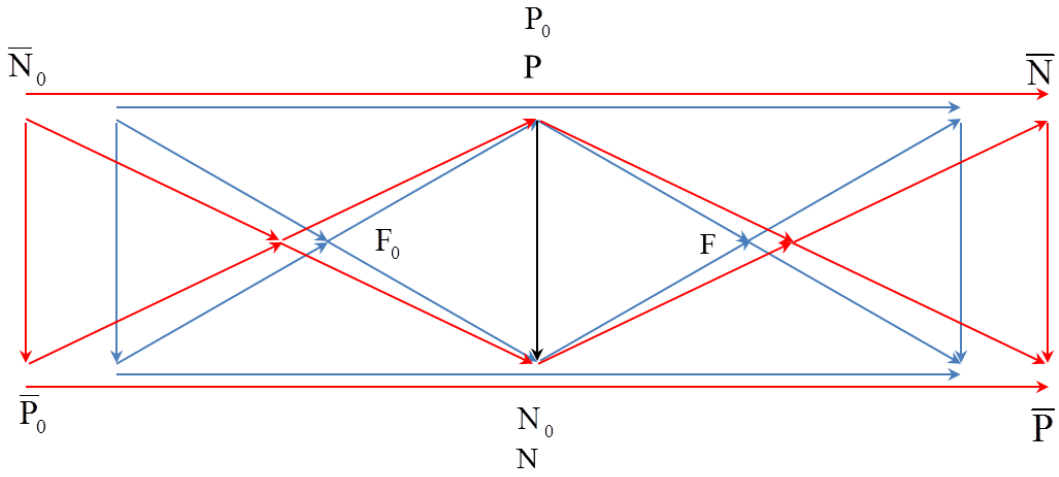

Figure 9.1.4 Extended Pascal's ring for the reduced eye showing the addition of anti-cardinal points and directions of all relationships.

Pascal's ring for Le Grand's eye

The reduced eye has both advantages and disadvantages that come hand in hand with the simplest model eye available. In order to highlight some of the disadvantages of the simplification, let us take a look at Pascal's ring for the four-surface Le Grand eye. Pascal's ring is shown in Figure 9.1.5 and the extended Pascal's ring in Figure 9.1.6.

Pascal's ring is shown in Figure 9.1.5 for Le Grand's eye for the set of six cardinal points for the red and blue frequencies derived from the transferences. The blue ring is narrower than the red ring for the distance between F_0 and F, which matches what we found in the graphical construction in Figure 9.1.2. The blue inner square is wider and shorter than the red inner square. This width

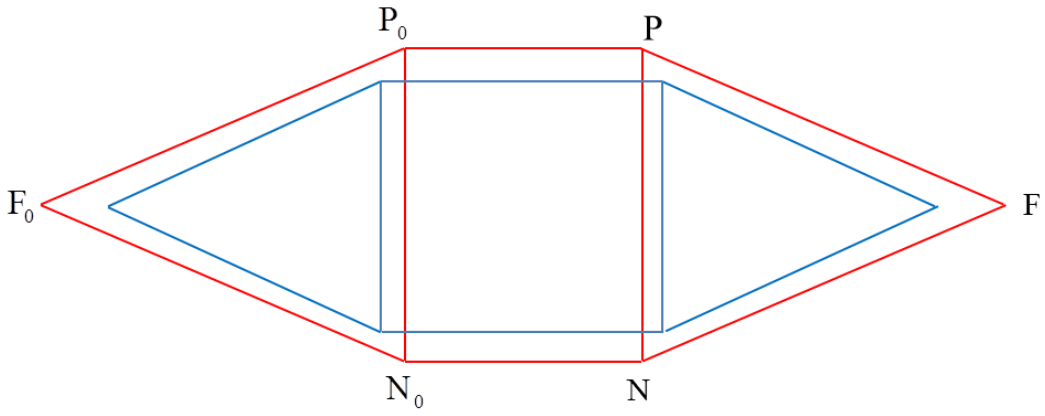

Figure 9.1.5 Pascal's ring for Le Grand's eye showing rings for the red and blue frequencies.

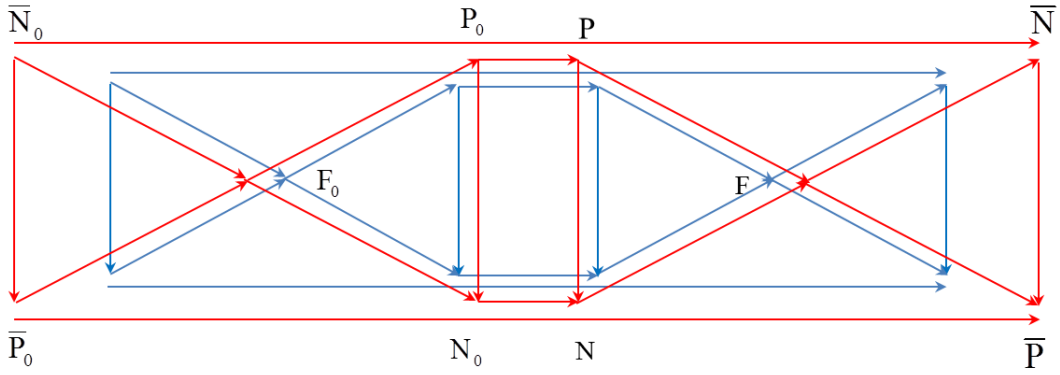

Figure 9.1.6 Extended Pascal's ring of Le Grand's eye for red and blue frequencies, showing the cardinal and anti-cardinal points and the directions of the relationships.

represents the distance between P_0 and P, which Pascal called the "thickness" (Pascal, 1950a), and also between N_0 and N. While the difference is too small to be evident in the graphical construction, from Tables 9.1.3 and 4 we calculate the width of the square to be 0.3230 mm for the blue "thickness" and 0.3105 mm for the red. This represents a chromatic difference of 0.0126 mm between the red and blue "thicknesses". The height of the square represents the distance between P_0 and N_0 or between P and N. The blue P and N are positioned closer together than the red P and N. From Tables 9.1.3 and 4 we calculate the distance from P to N to be 5.5986 mm for blue and 5.6046 mm for red. This represents a chromatic difference of -0.0060 mm which is not discernible in Figure 9.1.2.

The equivalent incident focal length f_{0eq} is represented by the distance from P_0 to F_0 and is equal to the distance from F to N. For the blue f_{0eq} this is a distance of $-16.1618\,\text{mm}$ and for the red f_{0eq} this is $-16.8468\,\text{mm}$, giving us a chromatic difference of $0.6850\,\text{mm}$. f_{eq} is the length from P to F and is equal to the length from F_0 to N_0. This is a distance of 21.7604 mm for the blue f_{eq} and 22.4513 mm for the red f_{eq}, giving us a chromatic difference of –0.6910 mm. These are very small differences and not obvious from Figure 9.1.2, but do indicate that the positions of, and relationships among the cardinal points of Le Grand's eye are all dependent on frequency. When we compare f_{0eq} and f_{eq} it becomes obvious why we cannot draw Pascal's ring to scale. The distortion created by the unequal f_{0eq} and f_{eq} would create a shape that resembles a lightning bolt at best, or one that would not join up at all.

In Figure 9.1.6 we observe that the blue extended Pascal's ring appears to be contracted compared to the red ring. It becomes obvious that, despite the rings not being drawn to scale, the chromatic difference in position of the anti-cardinal points is greater than the same for the cardinal points.

Conclusion

From Pascal's ring we see which points depend on frequency and which are independent of frequency. The reduced eye clearly shows that the principal and nodal points are independent of frequency, but that the focal points and the anti-cardinal points do depend on frequency. Pascal's ring for Le Grand's eye shows clearly that all six cardinal and four anti-cardinal points do depend on frequency. In addition the ring shows the direction of chromatic differences of each point.

9.2 Derived properties as a function of frequency

In Sections 3.4 and 5.1 we looked at a selection of derived properties, including power, entrance- and exit-plane refractive compensation and front- and back-vertex power. For each of these derived properties, we graph its dependence on the frequency of light. Although certain derived properties, such as exit-plane refractive compensation, apply to systems in general and have little application to the eye, we will include them because they have application to the characteristic matrices that will be discussed in Section 9.3.

9.2.1 Power

Power of a system is the simplest derived property, given by Equation 3.4.3. From the simplicity of the definition, we see that the dependence will be similar to that in Section 8.1.1 for each of the *C* sub-graphs. We therefore look at the dependence of power on the frequency of light only briefly.

Figure 9.2.1 shows the dependence of power of the system on the frequency of light for the reduced eye (blue with circles) and Le Grand's eye (black with diamonds). The curves represent the actual values calculated from the transference as a function of frequency and the dotted-dashed lines represent the power approximated from the linear dependence on the frequency of light (Equations 8.2.2 and 3).

The numerical values for the powers at the six reference points are given in Table 9.2.1. In addition the chromatic difference in power is given for the actual and approximate power values, represented by the dashed lines in Figure

Table 9.2.1 The power of the reduced and Le Grand's eyes at six reference frequencies, and their comparative values according to the formula for the symplectic straight line dependence on the frequency of light derived in the previous chapter (Equations 8.2.2 and 3).

Frequency THz	Colour	Reduced eye		Le Grand's eye	
		Actual D	Approximate D	Actual D	Approximate D
430	Red	59.4419	59.2756	59.3586	59.2736
494	Orange	59.8434	59.8299	59.7841	59.7877
558	Yellow	60.3058	60.6825	60.2625	60.2999
622	Green	60.8444	60.9335	60.7860	60.8104
686	Blue	61.4794	61.4828	61.3301	61.3192
750	Violet	62.2394	62.0304	61.8744	61.8263
Chromatic difference in power		2.7975	2.7548	2.5158	2.5526

9.2.1, for the reduced and Le Grand eyes. The values in the column labelled "approximate" have been obtained using Equations 8.2.2 and 3.

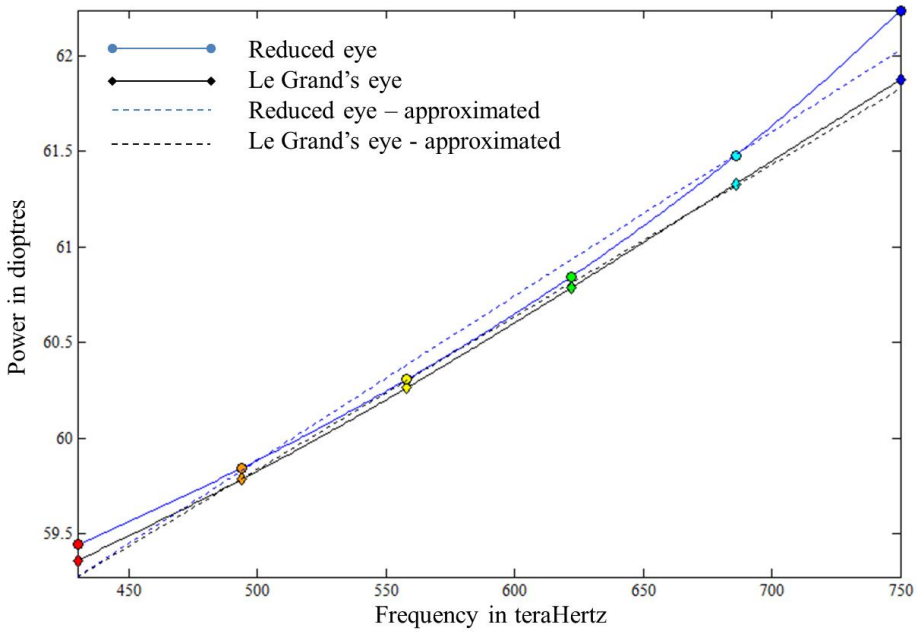

Figure 9.2.1 The dependence of power of the model eyes on the frequency of light. The corresponding dot-dashed lines in blue and black respectively show the straight line relationship according to Equations 8.2.2 and 3.

The values for the actual and approximate powers given in Table 9.2.1 compare well. Additionally, the values for chromatic difference in power compare favourably to published values (Section 2.3.1). These vary according to the frequencies chosen for red and blue ends of the spectrum.

9.2.2 Corneal-plane and exit-plane refractive compensation

The formulae for entrance-plane and exit-plane refractive compensation are given by Equations 3.4.6 and 5.1.3 respectively. While both of these formulae are general for all systems, entrance-plane refractive compensation for an eye is the equivalent of corneal-plane refractive compensation, however, exit-plane refractive compensation is not of conventional optometric interest. However, because the formula is related to the fourth entry for the point characteristic matrix, we will include exit-plane refractive compensation in our discussion. The dependence of the entrance- and exit-plane refractive compensations on frequency are shown in Figures 9.2.2 and 3, respectively.

Figure 9.2.2 shows that the corneal-plane refractive compensation is similar for the reduced and Le Grand's eyes. The reduced eye shows a more curved dependence than Le Grand's eye, which reflects the underlying structure of the two model eyes and the formulae for the refractive indices of the media. The values obtained using the actual transferences dependent on frequency are very similar to the approximated values obtained using the linear symplectic calculated transferences. The values for six reference frequencies are given in Table 9.2.2 for the refractive compensation of the two eyes and compared with the values obtained using Equations 8.2.2 and 3.

The exit-plane refractive compensation in Figure 9.2.3 shows almost six dioptres difference between the lines for the two eyes while the chromatic difference between the red and blue frequencies is far less for each eye compared with the corneal-plane refractive compensation. The dotted-dashed straight line is almost indistinguishable from the solid curved line for Le Grand's eye. From Table 9.2.3 we see that the chromatic difference in exit-plane refractive compensation is 0.69 D for the reduced eye and 0.52 D for Le Grand's eye.

Table 9.2.2 The entrance-plane refractive compensation of the reduced and Le Grand's eyes at six reference frequencies, and their comparative values according to the formula for the symplectic straight line dependence on the frequency of light derived in the previous chapter (Equations 8.2.2 and 3).

Frequency THz	Colour	Reduced eye		Le Grand's eye	
		Actual D	Approximate D	Actual D	Approximate D
430	Red	0.4185	0.5412	0.4674	0.5250
494	Orange	0.1175	0.1264	0.1412	0.1387
558	Yellow	–0.2294	–0.2876	–0.2216	–0.2470
622	Green	–0.6333	–0.7007	–1.6155	–0.6322
686	Blue	–1.1095	–1.1130	–1.0243	–1.0169
750	Violet	–1.6796	–1.5245	–1.4338	–1.4009
Chromatic difference in entrance-plane refractive compensation		–2.0981	–2.0657	–1.9013	–1.9260

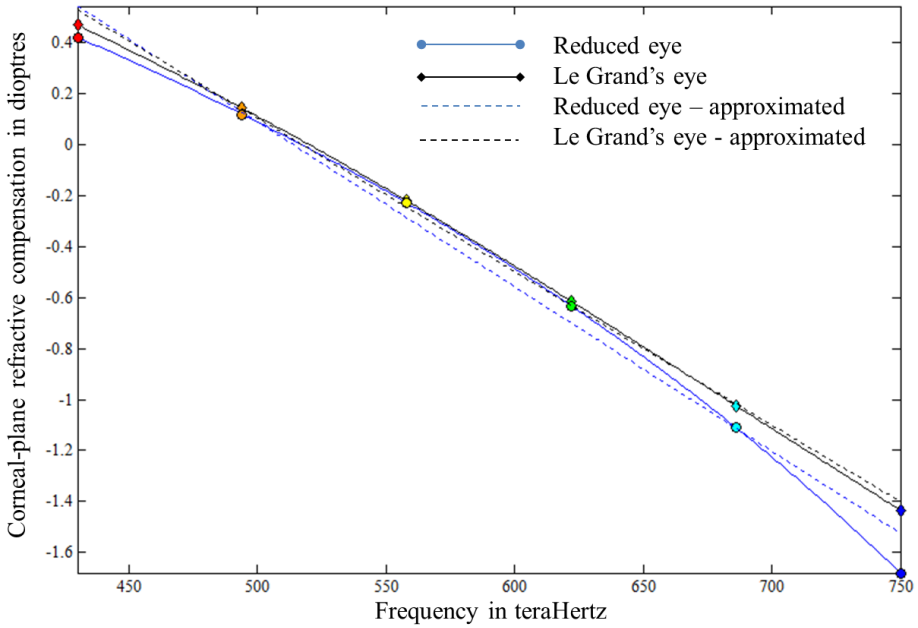

Figure 9.2.2 The dependence of the entrance-plane refractive compensation of the reduced and Le Grand's eyes on the frequency of light. The entrance-plane refractive compensation approximated from Equations 8.2.2 and 3 for the linear symplectic dependence transference is indicated by the straight dotted-dashed lines in corresponding colours.

Table 9.2.3 The exit-plane refractive compensation of the reduced and Le Grand model eyes at the six reference frequencies, and their comparative values according to the formula for the symplectic straight line dependence on the frequency of light derived in the previous chapter (Equations 8.2.2 and 3).

Frequency THz	Colour	Reduced eye		Le Grand's eye	
		Actual D	Approximate D	Actual D	Approximate D
430	Red	59.8605	59.8253	54.0673	54.05699
494	Orange	59.9608	59.9612	54.1638	54.1624
558	Yellow	60.0765	60.0980	54.2611	54.2658
622	Green	60.2111	60.2355	54.3644	54.3699
686	Blue	60.3698	60.3739	54.4751	54.4749
750	Violet	60.5599	60.5131	54.5920	54.5807
Chromatic difference in exit-plane refractive compensation		0.6994	0.6878	0.5247	0.5208

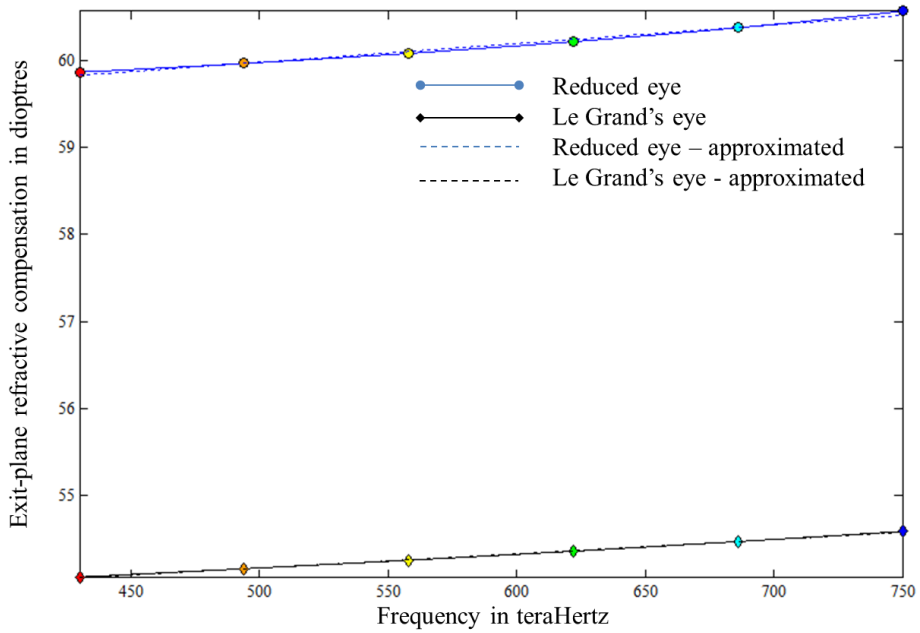

Figure 9.2.3 The dependence of the exit-plane refractive compensation of the reduced eye and Le Grand's eye on the frequency of light. The approximate exit-plane refractive compensation obtained from Equations 8.2.2 and 3 for the linear symplectic dependence transference is indicated by the straight dotted-dashed lines in corresponding colours.

9.2.3 Front- and back-vertex power

The formulae for front- and back-vertex power of systems in general, derived from the transference, were given in Equations 3.4.16 and 11, respectively. From the definition, back-vertex power measures the vergence at emergence from the system when incident vergence is zero. For an eye, including a model eye, this measures the vergence at the retinal-plane. Because light focuses at or close to the retina, we expect the back-vertex power to approach infinity. This is seen in Figure 9.2.4. The formula for back-vertex power is found in the first entry of the first mixed characteristic matrix **M** (Equation 3.7.23).

In Figure 9.2.4 we see the vergence initially increasing rapidly as we move from the red markers to the orange markers and asymptotes to infinity. The back-vertex power between 430 and 517 THz is positive. The vertical lines indicate a jump from infinity to minus infinity and show the frequency at which each eye forms a focal point (image). This is 517 THz for the reduced eye and 520THz for Le Grand's eye. The vergence then, again increasing as we move from yellow through green and blue to violet, asymptotes from minus infinity and eventually asymptotes to the zero dioptre vergence line in the ultra-violet range. The back-vertex powers of six reference frequencies are given in Table 9.2.4 for the two model eyes, compared with the values obtained using Equations 8.2.2 and 3.

Front-vertex-power defines the vergence at the entrance plane required for light to emerge with zero vergence. This is plausible for systems in general, but makes little sense for the eye. It may have an application for the reversed eye, however this is beyond the scope of this dissertation. Nonetheless, because the formula for front-vertex power is the negative of the fourth entry of the second mixed characteristic matrix **N** (Equation 3.7.24) we shall include it here. The dependence of the front-vertex power on frequency is shown in Figure 9.2.5. The dependence is very nearly linear for the two model eyes.

From Table 9.2.5 and Figure 9.2.5 we see that there is approximately a 6 D difference between the two model eyes. The chromatic difference in front-vertex power is 2.80 D for the reduced eye and 3.09 D for Le Grand's eye.

Table 9.2.4 Back-vertex power of the reduced and Le Grand's model eyes for six coloured reference points. The columns are separated into actual values and those approximated using Equations 8.2.2 and 3.

Frequency THz	Colour	Reduced eye		Le Grand's eye	
		Actual D	Approximate D	Actual D	Approximate D
430	Red	8 501	6 551	7 591	6 745
494	Orange	30 548	28 382	25 373	25 824
558	Yellow	–15 795	–12 618	–16 336	–14 664
622	Green	–5 786	–5 238	–5 948	–5 794
686	Blue	–3 345	–3 335	–3 617	–3 642
750	Violet	–2 244	–2 462	–2 614	–2 673

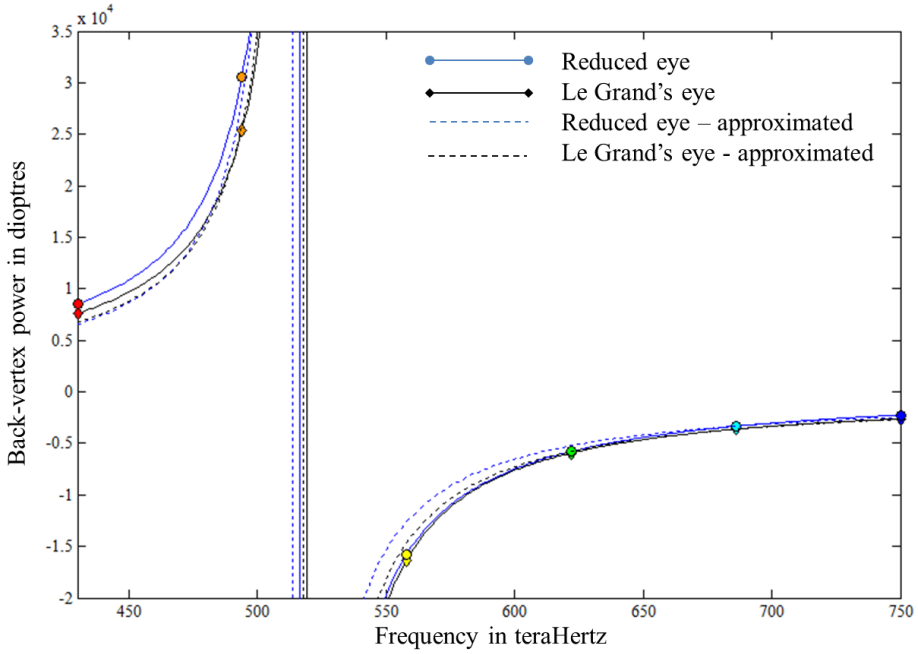

Figure 9.2.4 Back-vertex power of the two model eyes as a function of frequency. The corresponding dashed lines are approximated according to Equations 8.2.2 and 3 for the linear relationship of the transference's dependency on frequency. The vertical axis has been restricted to [–20 000 D 35 000 D] in order to include all six reference points and to discern the individual curves, which approach ± infinity dioptres.

Table 9.2.5 Front-vertex power of the reduced and Le Grand's model eyes for the six coloured reference points. Chromatic difference of front-vertex power is given. The columns are separated into actual values and those approximated using Equations 8.2.2 and 3.

Frequency THz	Colour	Reduced eye		Le Grand's eye	
		Actual D	Approximate D	Actual D	Approximate D
430	Red	59.4419	59.2671	65.6319	65.5111
494	Orange	59.8434	59.8250	66.1284	66.1355
558	Yellow	60.3058	60.0380	66.7053	66.7570
622	Green	60.8444	60.9031	67.3450	67.3755
686	Blue	61.4794	61.1478	68.0077	67.9910
750	Violet	62.2394	62.2023	68.6638	68.6035
Chromatic difference in front-vertex power		2.7975	2.7556	3.0320	3.0924

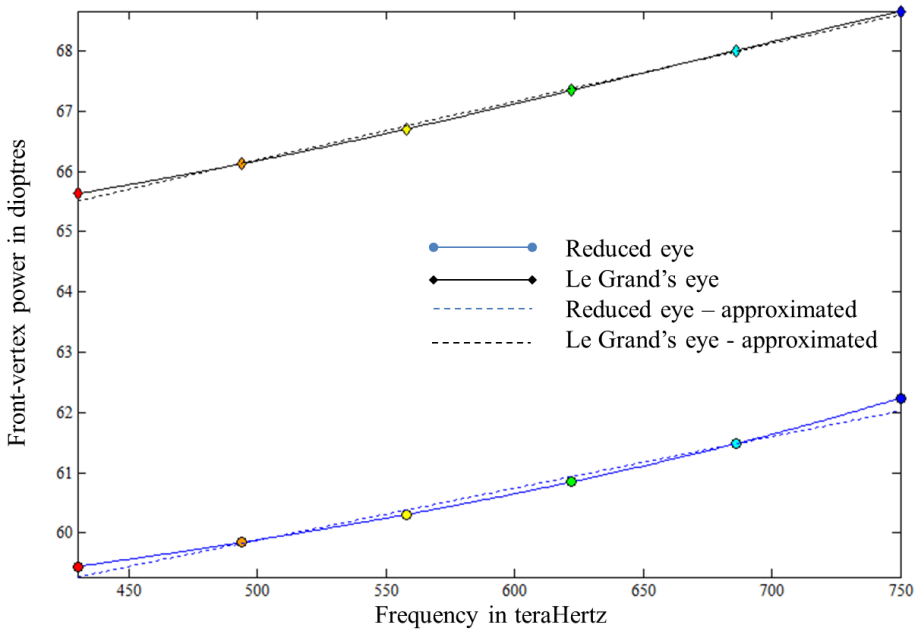

Figure 9.2.5 Front-vertex power of the two model eyes as a function of frequency. The solid lines represent the actual values from the transference while the dotted-dashed lines are approximated from the linearly transformed transferences according to Equation 8.2.2.

9.3 Characteristic matrices

The four characteristic matrices were introduced in Section 3.7.3; they are symmetric and represent familiar derived properties in relationship to each other. Our interest lies in the fact that each of the characteristic matrices is symmetric and therefore can be represented in a three-dimensional vector space. Of these characteristic matrices, the point characteristic **P** and the angle characteristic **Q** appear to be the most promising for our objective because they each have the same units throughout. **P** has units of inverse length and **Q** units of length. It is the uniformity of units of the point- and angle-characteristics that holds appeal for our purposes. **M** and **N** each have mixed units, however there are some interesting relationships among the entries of each of the four characteristic matrices and many of the familiar properties of systems.

Equations 3.7.15, 16, 18 and 19 give the four characteristic matrices in terms of varying combinations of incident or emergent transverse positions or reduced inclinations. In each case, two knowns map to two unknowns. Then the entries of the four characteristic matrices are defined in terms of the fundamental properties of the Gaussian transference in Equations 3.7.21, 22, 23 and 24.

What becomes apparent in Section 3.7.3 is that for each characteristic matrix there are issues of singularity that limit the usefulness of each matrix for particular situations. It further implies that the choice of any two of y_0, y, α_0 or α does not necessarily fix the other two (Harris and van Gool, 2004).

9.3.1 Point characteristic

As is apparent from Equation 3.7.21, the point characteristic exists provided the disjugacy is not zero, or does not approach zero. This would be problematic in a conjugate or thin system, however we foresee no problem in a model eye. As pointed out in Section 3.7.3, the first entry represents the corneal-plane refractive compensation (F_0) given by Equation 3.4.6 and the second and third entries are the negative inverse of disjugacy ($-B^{-1}$). The fourth entry is the exit-plane refractive compensation (F_C) of the system (Equation 5.1.3). This is of interest for systems in general, but apparently holds little practical meaning for the

Table 9.3.1 The point characteristic matrices **P** for the reduced and Le Grand's eyes for six reference frequencies.

Frequency		Point characteristic **P** in dioptres	
THz	Colour	Reduced eye	Le Grand's eye
430	Red	$\begin{pmatrix} 0.4185 & -59.8605 \\ -59.8605 & 59.8605 \end{pmatrix}$	$\begin{pmatrix} 0.4674 & -59.7814 \\ -59.7814 & 54.0673 \end{pmatrix}$
494	Orange	$\begin{pmatrix} 0.1175 & -59.9608 \\ -59.9608 & 59.9608 \end{pmatrix}$	$\begin{pmatrix} 0.1412 & -59.9117 \\ -59.9117 & 54.1638 \end{pmatrix}$
558	Yellow	$\begin{pmatrix} -0.2294 & -60.0765 \\ -60.0765 & 60.0765 \end{pmatrix}$	$\begin{pmatrix} -0.2216 & -60.0623 \\ -60.0623 & 54.2611 \end{pmatrix}$
622	Green	$\begin{pmatrix} -0.6333 & -60.2111 \\ -60.2111 & 60.2111 \end{pmatrix}$	$\begin{pmatrix} -0.6155 & -60.2304 \\ -60.2304 & 54.3644 \end{pmatrix}$
686	Blue	$\begin{pmatrix} -1.1095 & -60.3698 \\ -60.3698 & 60.3698 \end{pmatrix}$	$\begin{pmatrix} -1.0243 & -60.4064 \\ -60.4064 & 54.4751 \end{pmatrix}$
750	Violet	$\begin{pmatrix} -1.6796 & -60.5599 \\ -60.5599 & 60.5599 \end{pmatrix}$	$\begin{pmatrix} -1.4338 & -60.5824 \\ -60.5824 & 54.5920 \end{pmatrix}$

eye. The divergence of the system does not play a role. We summarise the entries of the point characteristic matrix as

$$\mathbf{P} = \begin{pmatrix} F_0 & -\mathrm{B}^{-1} \\ -\mathrm{B}^{-1} & F_\mathrm{C} \end{pmatrix}.$$

The entrance- and exit-plane refractive compensation, dependent on frequency, was shown for the two model eyes in Figures 9.2.2 and 3. The dependence of B on frequency is shown in Figure 8.1.3. The dependence of $-B^{-1}$ resembles a nearly straight line, similar to that shown in Figure 8.1.3. The chromatic difference in $-B^{-1}$ is –0.6994 D and –0.8010 D for the reduced and Le Grand's eyes, respectively. In Figure 9.3.1, we represent the point characteristic of the reduced eye in a three-dimensional vector space. The axes are labelled according to the derived property that each represents and the units are dioptres. Unsurprisingly the relationship is perfectly linear and is seen when the azimuth and elevation are oriented such that all the diamonds line up behind each other perfectly. We note that the coloured reference points, which are evenly spread at

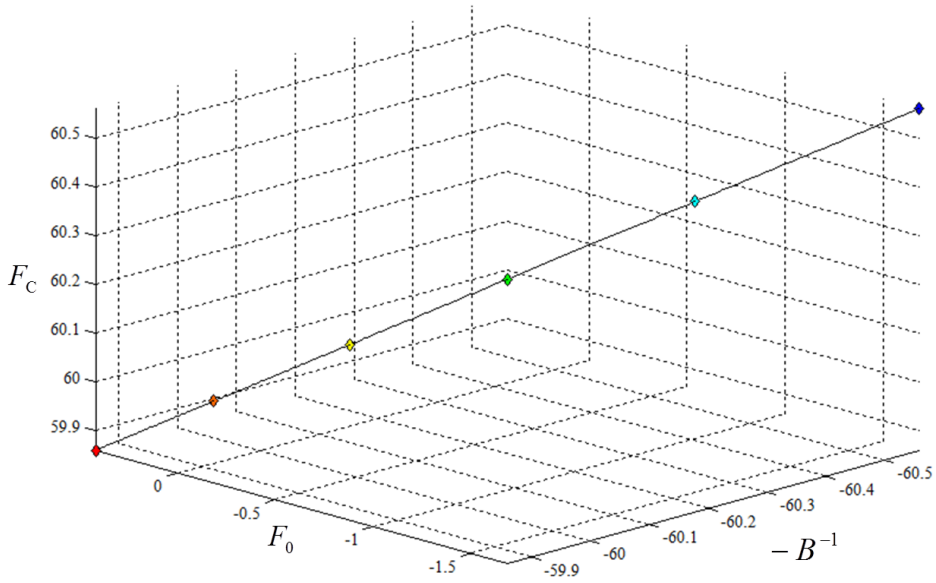

Figure 9.3.1 The three independent entries of **P** the point characteristic for the reduced eye. Units are dioptres.

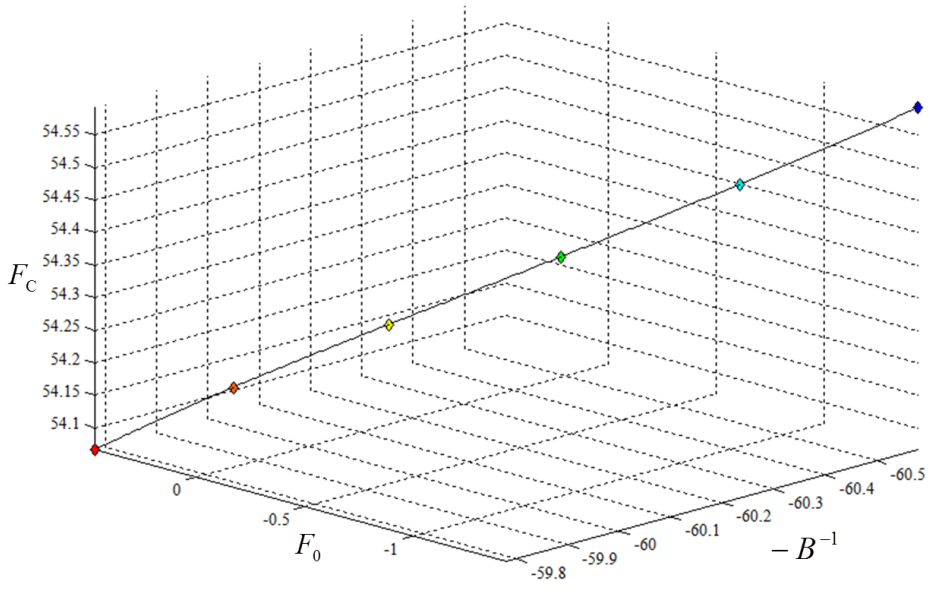

Figure 9.3.2 The three independent entries of **P** the point characteristic as a function of frequency for the Le Grand eye. The line is slightly curved. Units are dioptres.

The three independent entries of **P** for Le Grand's eye are illustrated in every 64 THz, appear to be closer together on the red end of the spectrum compared to the blue end of the spectrum. Figure 9.3.2 and show a slightly curved line. The point characteristic matrices of the two model eyes are given in Table 9.3.1 for six reference frequencies.

9.3.2 Angle characteristic

The angle characteristic **Q** (Equation 3.7.22) exists provided the divergence *C* is not zero. This would be a problem for an afocal system; however this poses no problem for an eye or model eye. Of interest is the relationship of the diagonal elements to the negative inverse of front- (F_{fv}) and back-vertex power (F_{bv}), as given in Equations 3.4.16 and 11. The dependencies of F_{fv} and F_{bv} on frequency are displayed graphically in Figures 9.2.4 and 5. Also related, are the incident (z_{F0}) and emergent focal lengths (z_{F}) (Equations 3.6.5 and 12). The relationships of the focal lengths to the system were discussed in Sections 3.6 and 5.4 and their dependence on frequency displayed graphically in Section 9.1. However all the entries are in units of length and, similar to **P**, make the axes comparable once graphed.

Down the diagonal, the first entry is $-F_{\mathrm{fv}}^{-1}$ and the last entry is $-F_{\mathrm{bv}}^{-1}$. There is also a relationship between the first entry and incident focal length in that

$$C^{-1}D = \frac{1}{n_0} z_{\mathrm{F0}} \tag{9.3.1}$$

and between the fourth entry and the emergent focal length as

$$C^{-1}A = -\frac{1}{n} z_{\mathrm{F}}. \tag{9.3.2}$$

The off-diagonal entries represent the inverse of divergence and are related to the incident and emergent equivalent focal lengths as

$$\frac{1}{C} = \frac{1}{n_0} f_{0eq} = -\frac{1}{n} f_{eq}. \tag{9.3.3}$$

These relationships can be summarised as

$$\mathbf{Q} = \begin{pmatrix} -F_{\mathrm{fv}}^{-1} & n_0^{-1} f_{0\mathrm{eq}} \\ -\mathrm{n}^{-1} f_{\mathrm{eq}} & -F_{\mathrm{bv}}^{-1} \end{pmatrix}$$

or

$$\mathbf{Q} = \begin{pmatrix} n_0^{-1} z_{\mathrm{F0}} & n_0^{-1} f_{0\mathrm{eq}} \\ -\mathrm{n}^{-1} f_{\mathrm{eq}} & -n^{-1} z_{\mathrm{F}} \end{pmatrix}.$$

We saw from Section 9.1 that all of these focal lengths depend on the frequency of light. These relationships are shown in Figure 9.3.3 for the reduced eye and Figure 9.3.4 for Le Grand's eye as a function of frequency. Unsurprisingly, the relationships, as for **P**, form a straight line for the reduced eye and a nearly straight line for Le Grand's eye. **Q** is given for six reference frequencies in Table 9.3.2.

As per the point characteristic, the relationships among the independent entries of **Q** is linear. Furthermore, the spacing between the six reference frequencies is more spread out at the blue end of the spectrum. While the differences between the red and blue angle characteristic matrices are similar for the two model eyes, the actual positions are slightly different. This can be seen by comparing the numerical values in the angle characteristic matrices given in Table 9.3.2.

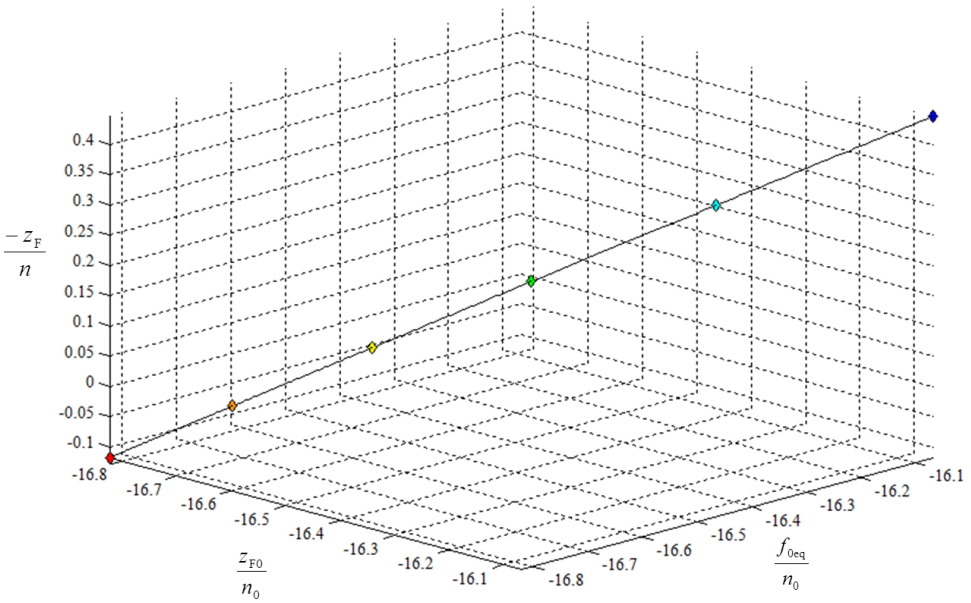

Figure 9.3.3 The angle characteristic **Q** of the reduced eye. Units are millimetres.

Table 9.3.2 The angle characteristic matrices **Q** for the six reference frequencies for the reduced eye and Le Grand's eye.

Frequency		Angle characteristic **Q** in millimetres	
THz	Colour	Reduced eye	Le Grand's eye
430	Red	$\begin{pmatrix} -16.8231 & -16.8231 \\ -16.8231 & -0.1176 \end{pmatrix}$	$\begin{pmatrix} -15.2365 & -16.8468 \\ -16.8468 & -0.1317 \end{pmatrix}$
494	Orange	$\begin{pmatrix} -16.7103 & -16.7103 \\ -16.7103 & -0.0327 \end{pmatrix}$	$\begin{pmatrix} -15.1221 & -16.7269 \\ -16.7269 & -0.03941 \end{pmatrix}$
558	Yellow	$\begin{pmatrix} -16.5821 & -16.5821 \\ -16.5821 & 0.0633 \end{pmatrix}$	$\begin{pmatrix} -14.9913 & -16.5941 \\ -16.5941 & 0.0612 \end{pmatrix}$
622	Green	$\begin{pmatrix} -16.4354 & -16.4354 \\ -16.4354 & 0.1729 \end{pmatrix}$	$\begin{pmatrix} -14.8489 & -16.4511 \\ -16.4511 & 0.1681 \end{pmatrix}$
686	Blue	$\begin{pmatrix} -16.2656 & -16.2656 \\ -16.2656 & 0.2989 \end{pmatrix}$	$\begin{pmatrix} -14.7042 & -16.3052 \\ -16.3052 & 0.2765 \end{pmatrix}$
750	Violet	$\begin{pmatrix} -16.0670 & -16.0670 \\ -16.0670 & 0.4456 \end{pmatrix}$	$\begin{pmatrix} -14.5637 & -16.1618 \\ -16.1618 & 0.3825 \end{pmatrix}$

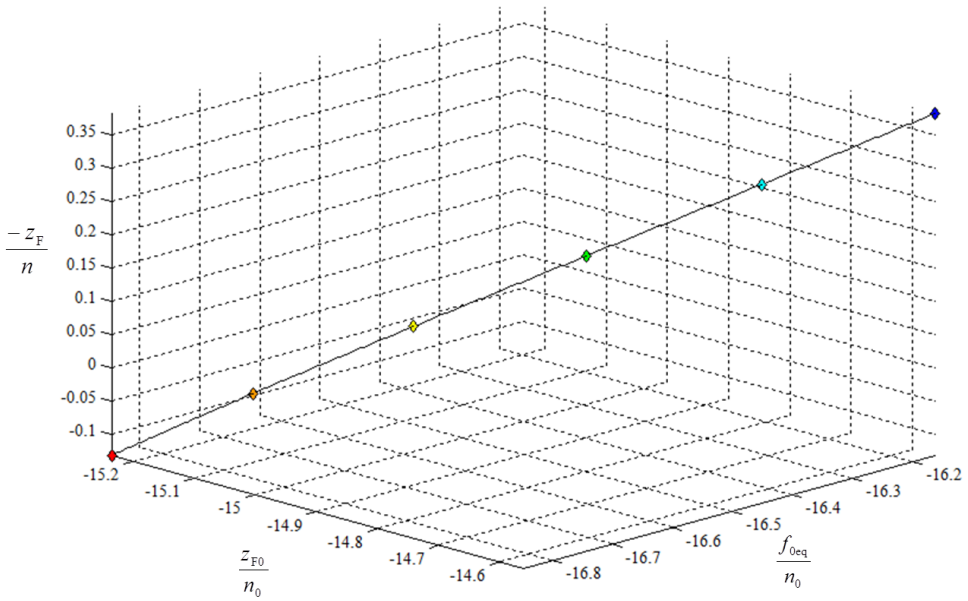

Figure 9.3.4 Angle characteristic **Q** for Le Grand's eye. The units are millimetres.

9.3.3 First mixed characteristic

The first mixed characteristic **M** (Equation 3.7.23) exists provided $D \neq 0$. The entries of **M** is summarised as

$$\mathbf{M} = \begin{pmatrix} F_{\text{fv}} & D^{-1} \\ D^{-1} & F_{\text{C}}^{-1} \end{pmatrix}.$$

The dependence of front-vertex power F_{fv} on the frequency of light was shown in Figure 9.2.5 and the same for exit-plane refractive compensation F_{C} in Figure 9.2.3. From Equation 5.5.1 we see that for a reduced eye $D = 1$, regardless of the frequency ν and for multi-surface eyes D is usually close to 1, but does vary weakly with ν. For systems in general, D will have different values.

In Figures 9.3.5 and 6 we represent **M** on a three-dimensional graph for the reduced eye and Le Grand's eye. For the reduced eye we see that the line is perfectly straight, however Le Grand's eye produces a visible S-shaped curve. F_{fv} has a chromatic difference of 2.7974 D for the reduced eye and 3.0320 D for Le Grand's eye.

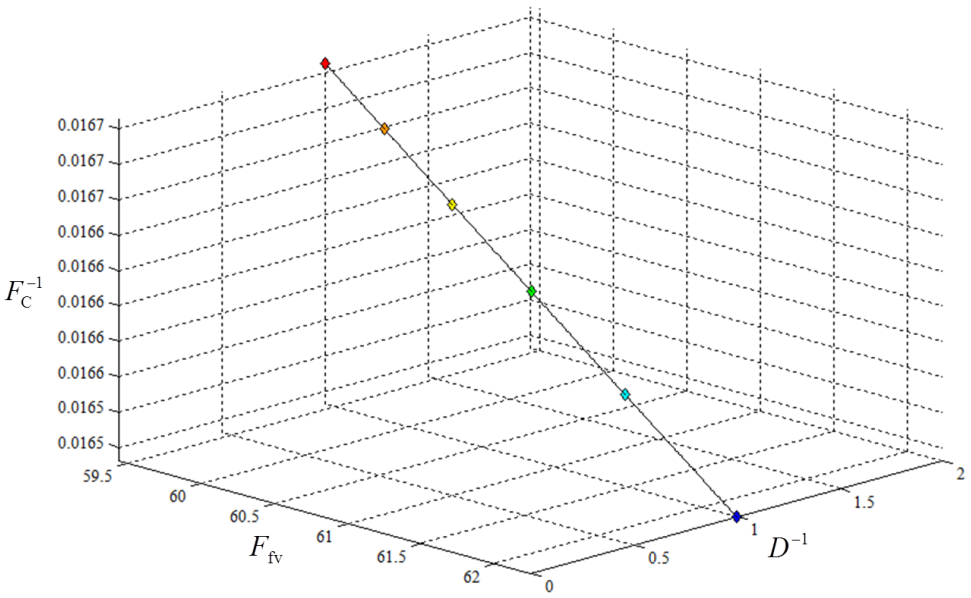

Figure 9.3.5 The first mixed characteristic **M** of the reduced eye. The vertical axis represents F_{C}^{-1} in meters, the middle axis represents F_{fv}, the front vertex power, in dioptres and the right-hand axis represents D^{-1}, which is 1 for all frequencies.

Table 9.3.3 The First mixed characteristic matrix **M** for the six reference frequencies for the reduced eye and Le Grand's eye.

Frequency		First mixed characteristic **M**	
THz	Colour	Reduced eye	Le Grand's eye
430	Red	$\begin{pmatrix} 59.4419\ \text{D} & 1 \\ 1 & 0.01671\ \text{m} \end{pmatrix}$	$\begin{pmatrix} 65.6319\ \text{D} & 1.1057 \\ 1.1057 & 0.01850\ \text{m} \end{pmatrix}$
494	Orange	$\begin{pmatrix} 59.8434\ \text{D} & 1 \\ 1 & 0.01668\ \text{m} \end{pmatrix}$	$\begin{pmatrix} 66.1284\ \text{D} & 1.1061 \\ 1.1061 & 0.01846\ \text{m} \end{pmatrix}$
558	Yellow	$\begin{pmatrix} 60.3058\ \text{D} & 1 \\ 1 & 0.01665\ \text{m} \end{pmatrix}$	$\begin{pmatrix} 66.7053\ \text{D} & 1.1069 \\ 1.1069 & 0.016843\ \text{m} \end{pmatrix}$
622	Green	$\begin{pmatrix} 60.8444\ \text{D} & 1 \\ 1 & 0.01661\ \text{m} \end{pmatrix}$	$\begin{pmatrix} 67.3450\ \text{D} & 1.1079 \\ 1.1079 & 0.01840\ \text{m} \end{pmatrix}$
686	Blue	$\begin{pmatrix} 61.4794\ \text{D} & 1 \\ 1 & 0.01657\ \text{m} \end{pmatrix}$	$\begin{pmatrix} 68.0077\ \text{D} & 1.1089 \\ 1.1089 & 0.01836\ \text{m} \end{pmatrix}$
750	Violet	$\begin{pmatrix} 62.2319\ \text{D} & 1 \\ 1 & 0.01651\ \text{m} \end{pmatrix}$	$\begin{pmatrix} 68.6638\ \text{D} & 1.1097 \\ 11097 & 0.01832\ \text{m} \end{pmatrix}$

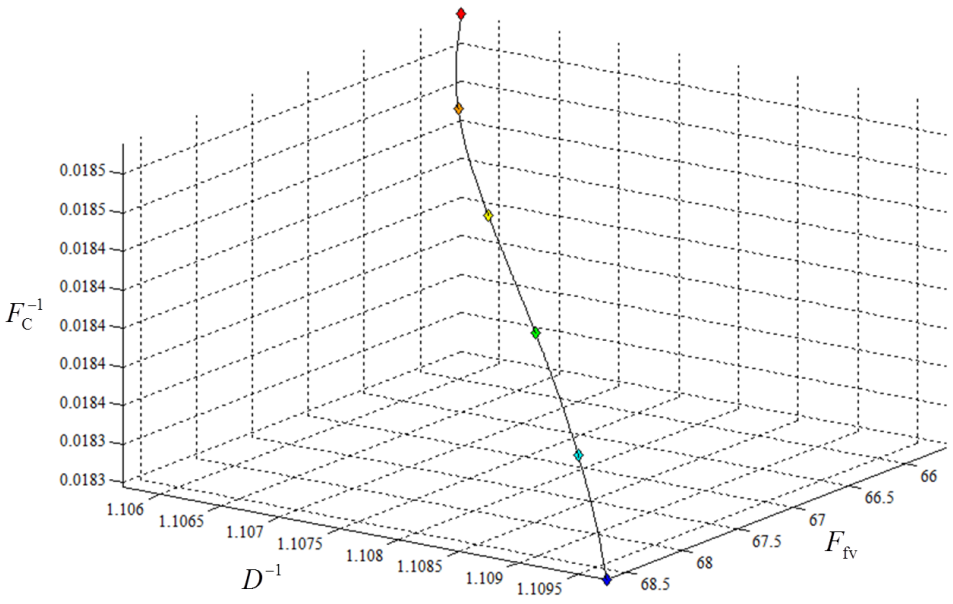

Figure 9.3.6 The first mixed characteristic **M** of the Le Grand eye. The vertical axis represents F_C^{-1} in meters, the right-hand axis represents F_{fv} in dioptres and the middle axis represents D^{-1}.

9.3.4 Second mixed characteristic

The second mixed characteristic **N** (Equation 3.7.24) exists provided the dilation *A* is not zero. For the model eye as a function of frequency, we see *A* approaching zero as we reach the reference frequency, usually in the yellow band, the exact frequency will differ for each model eye and is given in Section 9.2.3 for the reduced eye and Le Grand's eye. It is also dependent on n_0. The problems arising when *A* approaches zero are seen in Figure 9.2.4 where the back-vertex power is graphed as a function of frequency. We see that where *A* approaches zero, back-vertex power approaches infinity, indicating a focal point (or image point) on the exit plane or retina and the curves of the graph extend off the scale.

The entries of **N** are summarised as

$$\mathbf{N} = \begin{pmatrix} -F_0^{-1} & A^{-1} \\ A^{-1} & -F_{\text{bv}} \end{pmatrix}.$$

The dependence of entrance-plane refractive compensation F_0 (Equation 3.4.6) on frequency is shown in Figure 9.2.2 and similarly for back-vertex power F_{bv} (Equation 3.4.11) in Figure 9.2.4. Figures 9.3.7 and 8 show **N** for the reduced eye and Le Grand's eye are graphed, respectively.

We anticipated a problem in calculating **N** for eyes where $A = 0$ or where *A* approaches 0. The axes limits were adjusted to include the orange (494 THz) and yellow (558 THz) points and ignore the values at infinity. The result is that all six reference points are distinct, however, they are no longer sequenced according to their frequencies and instead the sequence is orange, red, then violet, blue, green and yellow. The line does not stop at orange or yellow, but continues to infinity or negative infinity. With infinity (or emmetropia) lying between 494 and 558 THz we conclude that the model eyes' reference frequencies for emmetropia lie between these two frequencies.

Table 9.3.4 The second mixed characteristic matrices **N** for the six reference frequencies for the reduced eye and Le Grand's eye.

Frequency		Second mixed characteristic **N**	
THz	Colour	Reduced eye	Le Grand's eye
430	Red	$\begin{pmatrix} -2.3892\ \text{m} & 143.0200 \\ 143.0200 & -8501.3857\ \text{D} \end{pmatrix}$	$\begin{pmatrix} -2.1393\ \text{m} & 127.8910 \\ 127.8910 & -7591.4352\ \text{D} \end{pmatrix}$
494	Orange	$\begin{pmatrix} -8.5134\ \text{m} & 510.4690 \\ 510.4690 & -30548.1908\ \text{D} \end{pmatrix}$	$\begin{pmatrix} -7.0841\ \text{m} & 424.4182 \\ 424.4182 & -25373.4668\ \text{D} \end{pmatrix}$
558	Yellow	$\begin{pmatrix} 4.3596\ \text{m} & -261.9085 \\ -261.9085 & 15794.6100\ \text{D} \end{pmatrix}$	$\begin{pmatrix} 4.5133\ \text{m} & -271.0772 \\ -271.0772 & 16335.78153\ \text{D} \end{pmatrix}$
622	Green	$\begin{pmatrix} 1.5791\ \text{m} & -95.0799 \\ -95.0799 & 5785.0746\ \text{D} \end{pmatrix}$	$\begin{pmatrix} 1.6246\ \text{m} & -97.8500 \\ -97.8500 & 5947.9146\ \text{D} \end{pmatrix}$
686	Blue	$\begin{pmatrix} 0.9013\ \text{m} & -54.4098 \\ -54.4098 & 3345.0822\ \text{D} \end{pmatrix}$	$\begin{pmatrix} 0.9763\ \text{m} & -58.9759 \\ -58.9759 & 3616.9941\ \text{D} \end{pmatrix}$
750	Violet	$\begin{pmatrix} 0.5954\ \text{m} & -36.0568 \\ -36.0568 & 2244.1573\ \text{D} \end{pmatrix}$	$\begin{pmatrix} 0.6974\ \text{m} & -42.2520 \\ -42.2520 & 2614.3169\ \text{D} \end{pmatrix}$

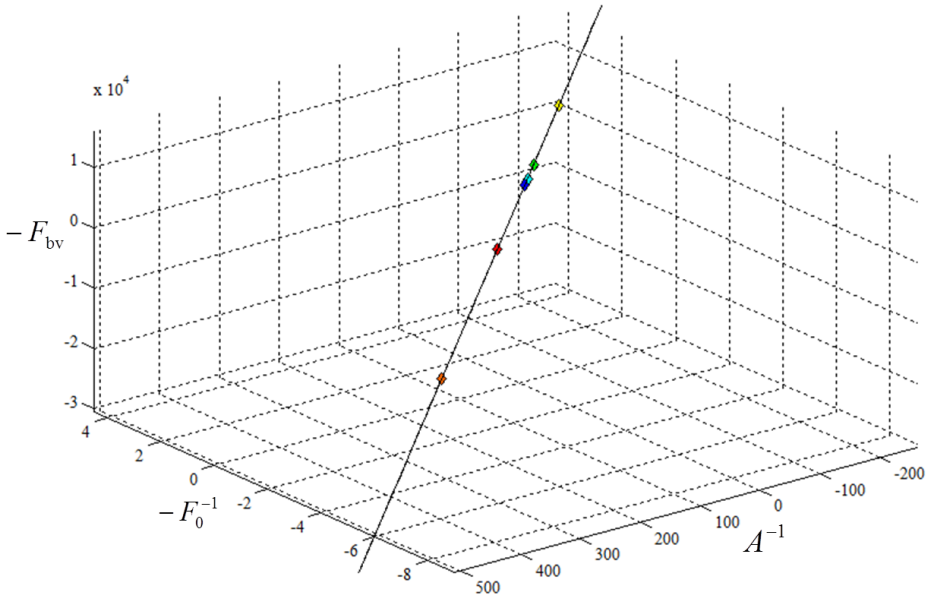

Figure 9.3.7 The second mixed characteristic **N** of the reduced eye. The sequence of the coloured reference points is not in order of frequency.

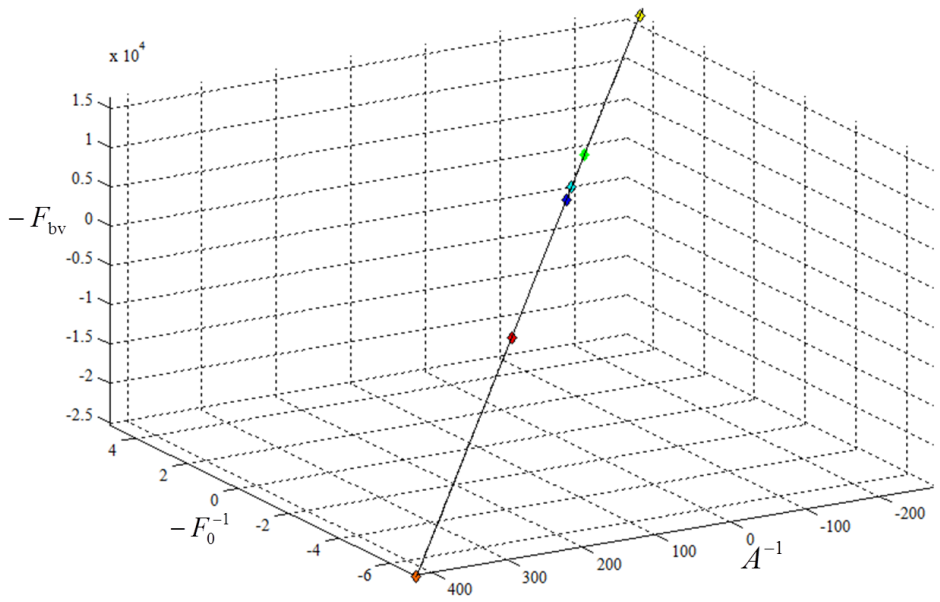

Figure 9.3.8 The second mixed characteristic **N** of Le Grand's eye.

9.4 Discussion

In this chapter we looked at the cardinal and anti-cardinal points of the reduced and Le Grand's eyes and used graphical construction and Pascal's ring methods in an effort to better understand how the cardinal and anti-cardinal points are affected by the frequency of light.

The reduced eye showed that the incident and emergent principal and nodal points are independent of the frequency of light and are not distinct for incidence and emergence. The locations of the focal points and four anti-cardinal points depend on frequency. Interesting relationships arose because of the simplicity of the reduced eye. Firstly, the incident and emergent anti-nodal point pairs are equidistant from the entrance-plane for each frequency, but in opposite directions. Secondly, each of the red and blue pairs of anti-cardinal points are equidistant between the red and blue positions, however the incident anti-cardinal points have the red upstream of the blue points and the emergent anti-cardinal points have the red points downstream of the blue points.

From Le Grand's eye we conclude that the locations of all ten cardinal and anti-cardinal points depend on the frequency of light and their positions are

distinct. In summary, the incident or emergent blue point is always positioned closer to its corresponding entrance- or exit-plane than its paired red point. The frequency-dependent cardinal and anti-cardinal points are more like fuzzy zones than actual points.

We then looked at a selection of optical properties derived from the transference. In particular, we considered power of the system, entrance- and exit-plane refractive compensation and front- and back-vertex power, all of which depend on the frequency of light.

Finally, we explored the characteristic matrices using three-dimensional graphs. Each characteristic matrix has three independent entries which are related in some way to the derived properties and therefore allow us to see the relationships among these properties in three-dimensional space. For the reduced eye all the relationships are linear while for Le Grand's eye the relationships appear nearly perfectly linear for **P**, **Q** and **N**, but has an S-shaped curve for **M**.

10 Numerical examples of chromatic aberration and chromatic properties

The aim of this chapter is to examine the equations derived in Chapters 6 and 7 numerically. The transferences of the reduced and Le Grand's eyes for the red and blue frequencies were given in Table 8.1.1, with $n_0 = 1$ for all frequencies.

In Gaussian systems longitudinal and transverse chromatic aberration are defined by Equations 6.1.1 and 2. Chromatic aberration depends on the longitudinal and transverse position of the object (z_O and y_O) corresponding to longitudinal and transverse image positions (z and y). For a distant object point, the position of the object is defined by its inclination a_O.

In Chapter 7 two categories of chromatic properties of an eye were defined; those independent of and those dependent on the object or image and aperture positions. Three independent chromatic properties of an eye were defined, namely chromatic difference in power δF, refractive compensation δF_0 and ametropia δA.

The chromatic properties of the eye dependent on object and aperture positions depend on both the eye and the longitudinal and transverse object (a_K or z_O and y_O) and aperture (y_P) positions. Chromatic difference in position is defined by chromatic difference in transverse image position at the retina, δy_R and chromatic difference in inclination at the retina, δa_R. Chromatic difference in magnification is defined by the chromatic difference in image size $\delta(\Delta y_R)$ or chromatic difference in angular spread $\delta(\Delta a_R)$. Retinal chromatic size magnification M_{yR} and retinal chromatic angular spread magnification M_{aR} are also defined.

The chromatic properties of the system dependent on image (y_R) and aperture (y_P) positions in object space mimic the experimental situation. The chromatic difference in transverse object position δy_O, chromatic difference in

inclination δa_{O}, chromatic difference in object size $\delta(\Delta y_{\mathrm{O}})$, chromatic difference in angular spread $\delta(\Delta a_{\mathrm{O}})$, chromatic object size ratio M_{yO} and chromatic object angular spread ratio M_{aO} are included.

The chromatic aberration and object or image and aperture-dependent chromatic properties for the two model eyes are illustrated numerically by means of a selection of parameters. Specifically, the numerical examples include a distant object and an object at three illustrative finite distances measured from the entrance plane, namely $z_{\mathrm{O}} = -3$ m, –2 m and –0.5 m. For distant objects, the inclination from an object will be illustrated for $a_{\mathrm{K}} = 0.1$ (radian) and for objects at finite distances, an object of $y_{\mathrm{O}} = 200$ mm in size will be used in the examples. According to the situation, the fovea may be assumed to be centred on the optical axis, or offset $y_{\mathrm{R}} = 1.46$ mm to approximate a visio-optical angle (angle alpha) of 5°.

Finally, we look at the two underlying implications derived in Chapter 7 and resulting from the simplifications that occur when basing chromatic studies on the reduced eye and the use of chief rays.

10.1 Chromatic aberration

In Chapter 6 chromatic aberration was defined for homocentric systems with stigmatic elements, that is, for Gaussian systems in general. It was shown that chromatic aberration is not a property of the system alone, but on the system and the location of the object point.

10.1.1 Longitudinal chromatic aberration

Le Grand's eye

The steps for calculating longitudinal chromatic aberration were given in Section 6.3.1. Equation 6.2.4 defines the vergence exiting the system when incident vergence is from a distant object. For Le Grand's eye the red and blue emergent vergences are

$$L_r = 7.5914 \text{ kD} \qquad (10.1.1)$$

and

$$L_b = -2.6143 \text{ kD} \tag{10.1.2}$$

respectively. Hence from Equation 6.1.6 one obtains

$$z_r = 0.1756 \text{ mm} \tag{10.1.3}$$

and

$$z_b = -0.5150 \text{ mm}, \tag{10.1.4}$$

the positions of red and blue image points from the exit plane. The longitudinal chromatic aberration is (Equation 6.1.1),

$$\delta z = -0.6906 \text{ mm}. \tag{10.1.5}$$

The signed distance of the longitudinal chromatic aberration is from red to blue, and therefore, the direction of δz is from behind the retina to in front of the retina.

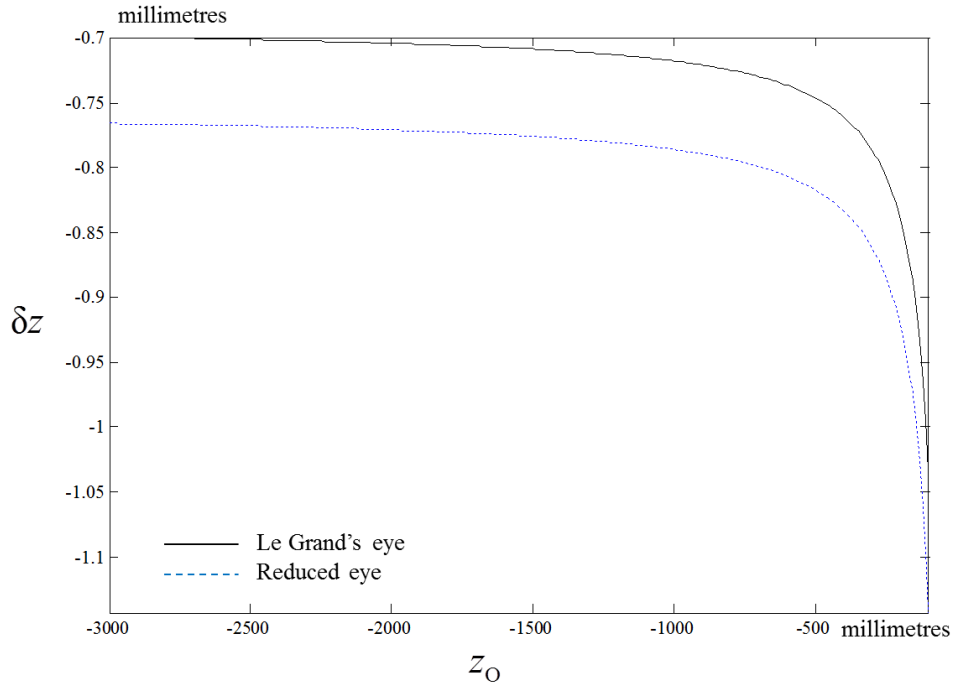

Figure 10.1.1 The longitudinal chromatic aberration δz as a function of object distance z_O for Le Grand's eye in black and the reduced eye in blue. z_O is measured from the cornea to the object point.

Table 10.1.1 Summary, for Le Grand's eye, of the red and blue wavefront vergences (L), image distances (z) from the retina and longitudinal chromatic aberration (δz) at object distances (z_O) of –3, –2 and –0.5 m.

z_O	–3 m	–2 m	–0.5 m
L_r	4.4089 kD	3.6400 kD	1.3943 kD
L_b	–3.3896 kD	–3.9849 kD	6.4280 kD
z_r	0.3023 mm	0.3661 mm	0.9558 mm
z_b	–0.3972 mm	–0.3379 mm	0.2095 mm
δz	–0.6995 mm	–0.7040 mm	–0.7463 mm

Equation 6.2.3 defines the vergence emerging from a system when incident vergence originates from a finite object, as a function of the distance of the object in front of the system (in millimetres). For red vergence this becomes

$$L_r = \frac{0.9044 + 0.05936 z_O}{0.007819 z_O - 16.7276} \tag{10.1.6}$$

and for blue vergence it is

$$L_b = \frac{0.9011 + 0.06187 z_O}{-0.02367 z_O - 16.5065}. \tag{10.1.7}$$

The red and blue emergent vergence L, image distances z and longitudinal chromatic aberration δz for the three illustrative object distances z_O are summarized in Table 10.1.1. From Table 10.1.1 and Figure 10.1.1 we see that as an object approaches the eye, so the magnitude of the longitudinal chromatic aberration increases.

The reduced eye

For the reduced eye we summarize the results for δz in Table 10.1.2. We see from Table 10.1.2 and Figure 10.1.1 that the magnitude of δz increases as the object approaches the eye. The summary in Table 10.1.2 and Figure 10.1.1 both emphasise that as the object point approaches the eye, so the magnitude of the δz increases. From Figure 10.1.1 we see that the changes in δz are similar for the

Table 10.1.2 Summary, for the reduced eye, of the red and blue wavefront vergences (L), image distances from the retina (z) and longitudinal chromatic aberration (δz) at object distances (z_O) distant, –3, –2 and –0.5 m.

z_O	Distant	–3 m	–2 m	–0.5 m
L_r	8.5014 kD	4.7059 kD	3.8412 kD	1.4217 kD
L_b	–2.2442 kD	–2.7848 kD	–3.1698 kD	11.3848 kD
z_r	0.1565 mm	0.2827 mm	0.3463 mm	0.9356 mm
z_b	–0.5997 mm	–0.4833 mm	–0.4246 mm	0.1182 mm
δz	–0.7562 mm	–0.7659 mm	–0.7709 mm	–0.8174 mm

two model eyes, but the magnitude of δz is greater for the reduced eye (blue line) than for Le Grand's eye (black line).

10.1.2 Transverse chromatic aberration

Le Grand's eye

The steps to calculate transverse chromatic aberration (δy) are given in Section 6.3.2. The first three steps have already been calculated above for longitudinal chromatic aberration. δy is dependent on a_O or a combination of z_O and y_O. Starting with a distant object, we continue with step 4 and Equation 6.2.17. Substituting from the red and blue transferences $\mathbf{S}_r$ and $\mathbf{S}_b$ (Table 8.1.1) and from Section 10.1.1 for z_r and z_b (Equations 10.1.3 and 4) we obtain

$$\delta y = a_O(-0.6850 \text{ mm}) \tag{10.1.8}$$

a linear relationship. For the purposes of illustrating δy of a distant object, we substitute $a_O = 0.1$ into Equation 10.1.8 to obtain $\delta y = -0.06850$ mm and the red image point is located superior to the blue image point.

For an object point at a finite distance the position of the object is determined by z_O and y_O. For illustrative purposes, we use the three distances for z_O, and $y_O = 200$ mm as described above. Continuing with step 4 of Section 6.3.2

Table 10.1.3 Summary, for Le Grand's eye, of the transverse chromatic aberration (δy) at working distances of –3, –2 and –0.5 m for an object position (y_O) 200 mm above the longitudinal axis.

z_O	–3 m	–2 m	–0.5 m
δy	0.04614 mm	0.06958 mm	0.2918 mm

to calculate δy for an object at a finite distance and substituting into Equation 6.2.16 we obtain

$$\delta y = y_O(-0.03149 - 0.04595\ \text{kD}\ z_b + 0.04454\ \text{kD}\ z_r) \qquad (10.1.9)$$

as a function of y_O and the respective red z_r and blue z_b image positions, which are, in turn, dependent on z_O and given in Table 10.1.1. The numerical results for δy are given in Table 10.1.3. The dependence of δy on y_O for any chosen z_O will be linear.

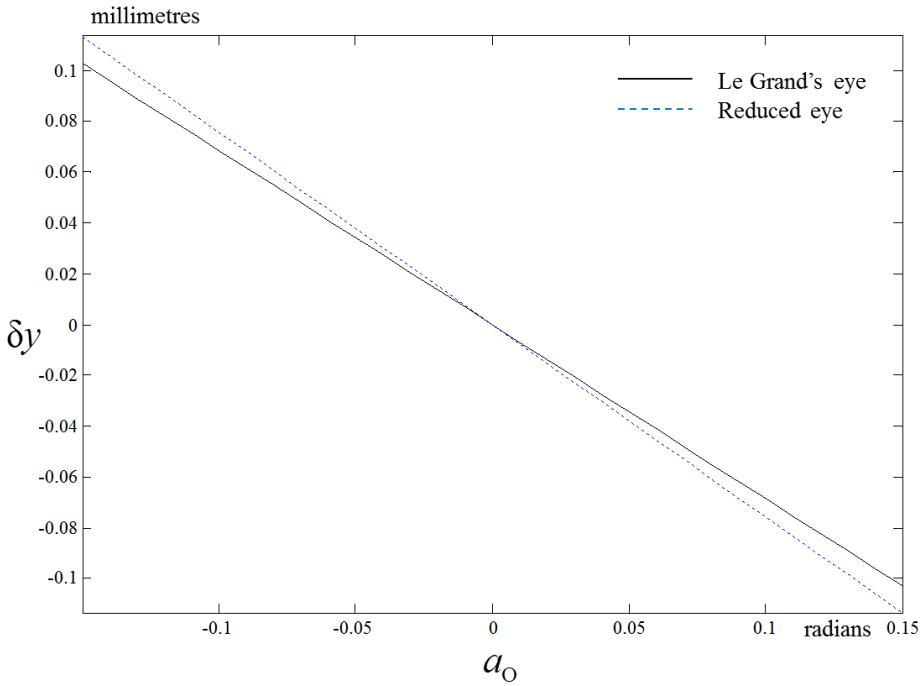

Figure 10.1.2 The dependence of the transverse chromatic aberration δy on the incident inclination a_O for a distant object for Le Grand's eye in black and the reduced eye in blue.

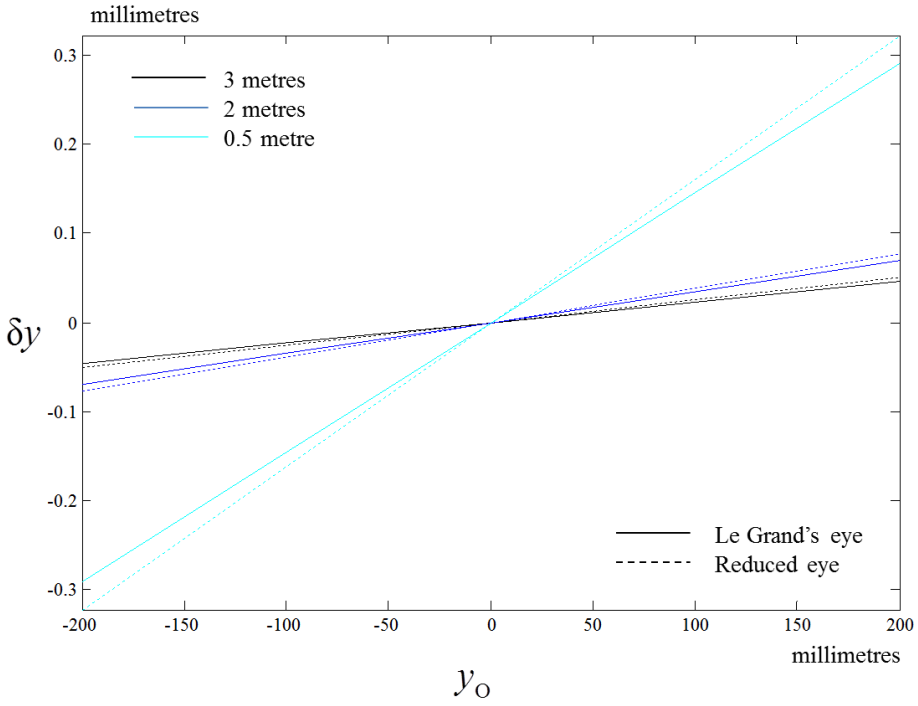

Figure 10.1.3 The transverse chromatic aberration (δy) of Le Grand's eye (solid lines) and the reduced eye (dashed lines) for three longitudinal distances (z_O) as a function of transverse object position y_O. The coloured lines represent the distance of the object from the eye with black being at –3 m, blue at –2 m and cyan at –0.5 m.

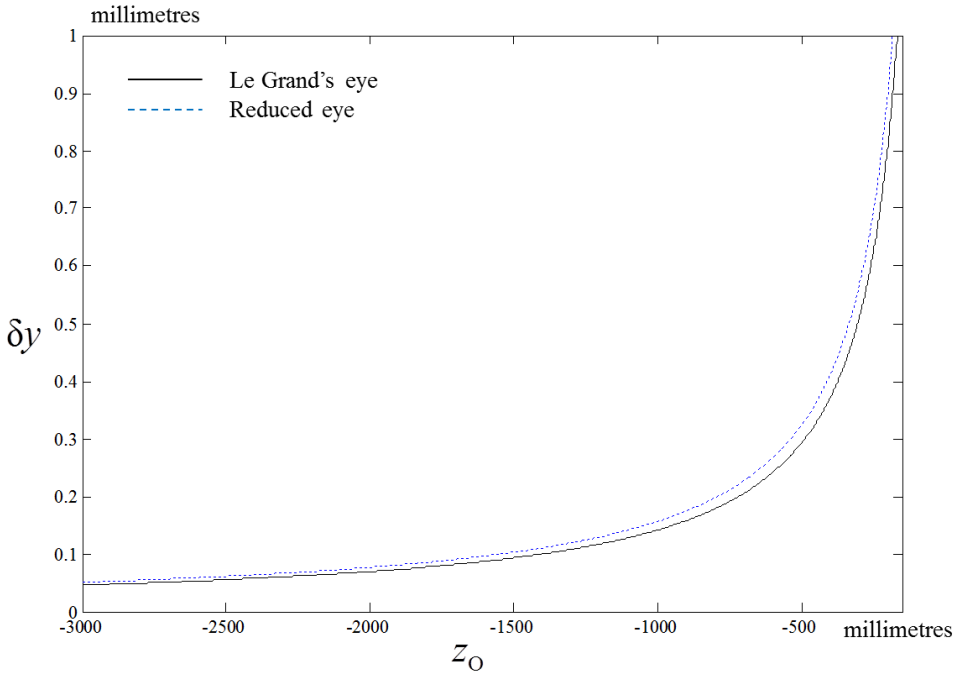

Figure 10.1.4 The transverse chromatic aberration (δy) of Le Grand's eye (black line) and the reduced eye (blue line) as a function of change in z_O for an object at $y_O = 200\,\text{mm}$.

Table 10.1.4 Summary, for the reduced eye, of the transverse chromatic aberration (δy) for a distant object with incident inclination of $a_O = 0.1$ and for an object at finite object distances (z_O) of –3, –2 and –0.5 m with the object at $y_O = 200\,\text{mm}$ above the longitudinal axis.

z_O	Distance	–3 m	–2 m	–0.5 m
δy	–0.07562 mm	0.05097 mm	0.07687 mm	0.3234 mm

The results are unsurprising, as the object approaches the eye, so the incident inclination increases in magnitude. To gain a better understanding, we show the effect of changes in y_O at the three illustrative positions of z_O in Figure 10.1.3. Figure 10.1.4 shows δy as a function of z_O when the object remains at $y_O = 200\,\text{mm}$ above the longitudinal axis.

The reduced eye

Similarly, we obtain the values for δy for the reduced eye for a distant object point and for an object at –3, –2 and –0.5 m from the eye at a distance of 200 mm above the longitudinal axis. The results are summarized in Table 10.1.4.

The conclusion of the effect of transverse chromatic aberration in the reduced eye is similar to that for Le Grand's eye. The relationship between δy and a_O (distant objects) or y_O (objects at a finite distance) at any particular working distance z_O is linear, however $|\delta y|$ for the reduced eye is slightly greater than that for Le Grand's eye.

10.2 Independent chromatic properties of the eye

The chromatic properties of the eye (alone) are defined as functions of the fundamental properties (or derivations thereof) of the red and blue transferences ($\mathbf{S}_r$ and $\mathbf{S}_b$). They are not directly dependent on light and therefore also not on object and image points. The three independent chromatic properties of the eye were defined in Section 7.1 as the chromatic difference in power, δF (Equation 7.1.2), chromatic difference in refractive compensation, δF_0 (Equation 7.1.4) and chromatic difference in ametropia, δA (Equation 7.1.5). The values for the

Table 10.2.1 Independent chromatic properties of Le Grand's and the reduced eyes.

Chromatic difference in:	Le Grand's eye	Reduced eye
Power (δF)	2.5158 D	2.7975 D
Refractive compensation (δF_0)	–1.9013 D	–2.0981 D
Ametropia (δA)	–0.03149	–0.03473

chromatic properties for Le Grand's and the reduced eye are given in Table 10.2.1.

For both model eyes, δF is more than a half dioptre greater in magnitude than δF_0 and therefore the two definitions cannot be interchanged. Also apparent is that the magnitude of all three independent chromatic properties is greater for the reduced eye than for Le grand's eye.

The chromatic difference in refractive compensation has been the subject of numerous experimental measurements and the consensus is that there is very little variation between studies and between subjects (Howarth and Bradley, 1986; Cooper and Pease, 1988; Simonet and Campbell, 1990; Atchison, Smith and Waterworth, 1993; Wald and Griffin, 1947; Bennett and Rabbetts, 2007:292-3; Atchison and Smith, 2000: 184-5). Adjusting for the different wavelengths chosen for each study, the results in Table 10.2.1 compare well to experimental studies.

10.3 Chromatic properties of the eye dependent on object and aperture positions

The chromatic properties dependent on object and aperture positions were defined in Chapter 7. Sections 7.2 and 3 looked at the object and aperture-dependent chromatic properties in image space and Sections 7.4 and 5 looked at the image and aperture-dependent chromatic properties in object space. Definitions for the chromatic properties in image space (subscript R) were derived for both distant objects and objects at finite distances. The definitions for chromatic properties in object space (subscript O) were limited to finite distances to mimic the experimental or clinical situation where these properties are present.

Table 10.3.1 The red and blue coefficient matrices for Le Grand's eye for distant objects, $\mathbf{V}_{\mathrm{E}}$ and objects at the finite distances of –3, –2 and –0.5 m from the eye, $\mathbf{V}_{\mathrm{OE}}$.

		Red	Blue
$\mathbf{V}_{\mathrm{E}}$	Distant	$\begin{pmatrix} 0.008832 & 16.7038\ \mathrm{mm} \\ -0.05031\ \mathrm{kD} & 0.8142 \end{pmatrix}$	$\begin{pmatrix} -0.02685 & 16.5780\ \mathrm{mm} \\ -0.05213\ \mathrm{kD} & 0.8082 \end{pmatrix}$
$\mathbf{V}_{\mathrm{OE}}$	–3 m	$\begin{pmatrix} 0.01511 & -0.005562 \\ -0.05000\ \mathrm{kD} & -0.0002711\ \mathrm{kD} \end{pmatrix}$	$\begin{pmatrix} -0.02059 & -0.005520 \\ -0.05182\ \mathrm{kD} & -0.0002691\ \mathrm{kD} \end{pmatrix}$
$\mathbf{V}_{\mathrm{OE}}$	–2 m	$\begin{pmatrix} 0.01825 & -0.008339 \\ -0.04984\ \mathrm{kD} & -0.0004065\ \mathrm{kD} \end{pmatrix}$	$\begin{pmatrix} -0.01746 & -0.008276 \\ -0.05167\ \mathrm{kD} & -0.0004035\ \mathrm{kD} \end{pmatrix}$
$\mathbf{V}_{\mathrm{OE}}$	–0.5 m	$\begin{pmatrix} 0.04634 & -0.03321 \\ -0.04848\ \mathrm{kD} & -0.001619\ \mathrm{kD} \end{pmatrix}$	$\begin{pmatrix} 0.01054 & -0.03296 \\ -0.05031\ \mathrm{kD} & -0.001607\ \mathrm{kD} \end{pmatrix}$

Table 10.3.2 The red and blue coefficient matrices for the reduced eye for distant objects, $\mathbf{V}_{\mathrm{E}}$ and objects at the finite distances of –3, –2 and –0.5 m from the eye, $\mathbf{V}_{\mathrm{OE}}$.

		Red	Blue
$\mathbf{V}_{\mathrm{E}}$	Distant	$\begin{pmatrix} 0.007650 & 16.6944\ \mathrm{mm} \\ -0.04889\ \mathrm{kD} & 0.8225 \end{pmatrix}$	$\begin{pmatrix} -0.03045 & 16.5562\ \mathrm{mm} \\ -0.05077\ \mathrm{kD} & 0.8157 \end{pmatrix}$
$\mathbf{V}_{\mathrm{OE}}$	–3 m	$\begin{pmatrix} 0.01374 & -0.005562 \\ -0.04859\ \mathrm{kD} & -0.0002740\ \mathrm{kD} \end{pmatrix}$	$\begin{pmatrix} -0.02439 & -0.005516 \\ -0.05047\ \mathrm{kD} & -0.0002718\ \mathrm{kD} \end{pmatrix}$
$\mathbf{V}_{\mathrm{OE}}$	–2 m	$\begin{pmatrix} 0.01678 & -0.008341 \\ -0.04844\ \mathrm{kD} & -0.0004109\ \mathrm{kD} \end{pmatrix}$	$\begin{pmatrix} -0.02137 & -0.008272 \\ -0.05032\ \mathrm{kD} & -0.0004075\ \mathrm{kD} \end{pmatrix}$
$\mathbf{V}_{\mathrm{OE}}$	–0.5 m	$\begin{pmatrix} 0.04407 & -0.03328 \\ -0.04710\ \mathrm{kD} & -0.001640\ \mathrm{kD} \end{pmatrix}$	$\begin{pmatrix} 0.005790 & -0.03301 \\ -0.04898\ \mathrm{kD} & -0.001626\ \mathrm{kD} \end{pmatrix}$

The derivations for chromatic properties dependent on object and aperture positions in image space are all based on the coefficient matrices for distant objects $\mathbf{V}_{\mathrm{E}}$ (Equation 5.2.8) and for objects at a finite distance $\mathbf{V}_{\mathrm{OE}}$ (Equation 5.2.26), both given in the summary in Table 7.7.2. $\mathbf{V}_{\mathrm{OE}}$ is a function of the distance of the object point in front of the eye, z_{O}. Consistent with the three illustrative distances used throughout this chapter, $\mathbf{V}_{\mathrm{OE}}$ is calculated at each

Table 10.3.3 The chromatic difference in red and blue coefficient matrices for Le Grand's and the reduced eye for distant objects, $\delta\mathbf{V}_{\mathrm{E}}$ and objects at the finite distances of –3, –2 and –0.5 m from the eye, $\delta\mathbf{V}_{\mathrm{OE}}$.

		Le Grand's eye	Reduced eye
$\delta\mathbf{V}_{\mathrm{E}}$	Distant	$\begin{pmatrix} -0.03568 & -0.1258\ \mathrm{mm} \\ -0.001822\ \mathrm{kD} & -0.006011 \end{pmatrix}$	$\begin{pmatrix} -0.03810 & -0.1383\ \mathrm{mm} \\ -0.001877\ \mathrm{kD} & -0.006813 \end{pmatrix}$
$\delta\mathbf{V}_{\mathrm{OE}}$	–3 m	$\begin{pmatrix} -0.03570 & 4.1853\times10^{-5} \\ -0.001823\ \mathrm{kD} & 1.9998\times10^{-6}\ \mathrm{kD} \end{pmatrix}$	$\begin{pmatrix} -0.03813 & 4.6047\times10^{-5} \\ -0.001878\ \mathrm{kD} & 2.2687\times10^{-6}\ \mathrm{kD} \end{pmatrix}$
$\delta\mathbf{V}_{\mathrm{OE}}$	–2 m	$\begin{pmatrix} -0.03571 & 6.2720\times10^{-5} \\ -0.001823\ \mathrm{kD} & 2.9968\times10^{-6}\ \mathrm{kD} \end{pmatrix}$	$\begin{pmatrix} -0.03814 & 6.9034\times10^{-5} \\ -0.001879\ \mathrm{kD} & 3.4013\times10^{-6}\ \mathrm{kD} \end{pmatrix}$
$\delta\mathbf{V}_{\mathrm{OE}}$	–0.5 m	$\begin{pmatrix} -0.03580 & 2.4873\times10^{-4} \\ -0.001828\ \mathrm{kD} & 1.1883\times10^{-5}\ \mathrm{kD} \end{pmatrix}$	$\begin{pmatrix} -0.03828 & 2.7484\times10^{-4} \\ -0.001886\ \mathrm{kD} & 1.3541\times10^{-5}\ \mathrm{kD} \end{pmatrix}$

distance for red and blue frequencies. These are summarized for Le Grand's eye in Table 10.3.1 and for the reduced eye in Table 10.3.2. The chromatic difference in coefficient matrices for distant objects $\delta\mathbf{V}_{\mathrm{E}}$ and objects at a finite distance $\delta\mathbf{V}_{\mathrm{OE}}$ as defined by Equation 7.2.1 are given in Table 10.3.3 for both model eyes.

10.3.1 Chromatic difference in transverse image positions at the retina

Le Grand's eye

The chromatic difference in transverse image positions at the retina, δy_{R} is defined by Equation 7.2.3 for an object at distance. Substituting the values from the entries of $\delta\mathbf{V}_{\mathrm{E}}$ we obtain the relationship for δy_{R} for a distant object, given in the first line of Table 10.3.4. From this relationship one can see that δy_{R} is dependent on any decentration of the pupil y_{P} and the incident inclination of the pencil of rays from a distant object, a_{K}. For a centred Gaussian model eye ($y_{\mathrm{P}} = 0$) the relationship simplifies to $\delta y_{\mathrm{R}} = (-0.1258\,\mathrm{mm})\,a_{\mathrm{K}}$. This is illustrated in Figure 7.2.1 and the results shown graphically in Figure 10.3.1. For the illustrative inclination of $a_{\mathrm{K}} = 0.1$ radians we obtain $\delta y_{\mathrm{R}} = -0.01258\,\mathrm{mm}$.

Similarly, we substitute the values from $\delta\mathbf{V}_{\mathrm{OE}}$, given in Table 10.3.3, for the three illustrative object distances z_{O} into Equation 7.2.4 to obtain relationships for the three illustrative finite working distances for Le Grand's eye, summarised in Table 10.3.4. Unsurprisingly, the closer the object is to the eye, so δy_{R} increases, which is seen in Figure 10.3.2

We now substitute the illustrative value of $y_{\mathrm{O}} = 200\,\mathrm{mm}$ for the displacement of the object point from the longitudinal axis at each z_{O} and we obtain δy_{R}, in Table 10.3.4. As expected, from these numerical examples and Figure 10.3.2, we can see that the magnitude of δy_{R} increases as the object approaches the eye for an off-axial object point.

The reduced eye

The results and conclusions for δy_{R} for the reduced eye are similar to Le Grand's eye. The constants for the reduced eye for Equations 7.2.3 and 4 are given in Table 10.3.5.

From Figures 10.3.1 and 2, we see that δy_{R} for the centred reduced eye is slightly greater in magnitude across object points at all distances than for Le

Table 10.3.4 The chromatic difference in image position at the retina, δy_R for Le Grand's eye. The illustrative example is for the centred reduced eye with $a_K = 0.1$ for the distant object point and $y_O = 200$ mm for the three finite distance object points.

Chromatic difference in image position		Illustrative example
Distant object	$\delta y_R = (-0.03568) y_P + (-0.1258\ \text{mm})\, a_K$	$\delta y_R = -0.01258$ mm
–3 m	$\delta y_R = (-0.03570) y_P + (4.1853\times10^{-5}) y_O$	$\delta y_R = 0.008371$ mm
–2 m	$\delta y_R = (-0.03571) y_P + (6.2720\times10^{-5}) y_O$	$\delta y_R = 0.01254$ mm
–0.5m	$\delta y_R = (-0.03580) y_P + (2.4873\times10^{-4}) y_O$	$\delta y_R = 0.04975$ mm

Grand's eye. The reason for this is revealed in Table 10.3.3 where we see that δX_E and δX_{OE} are greater in magnitude for the reduced eye than for Le Grand's eye. Comparing Equations 5.2.8 and 26, we can determine that the discrepancies lie in the underlying structural differences in the two model eyes, that is, number of refracting surfaces and their positions relative to the pupil or limiting aperture.

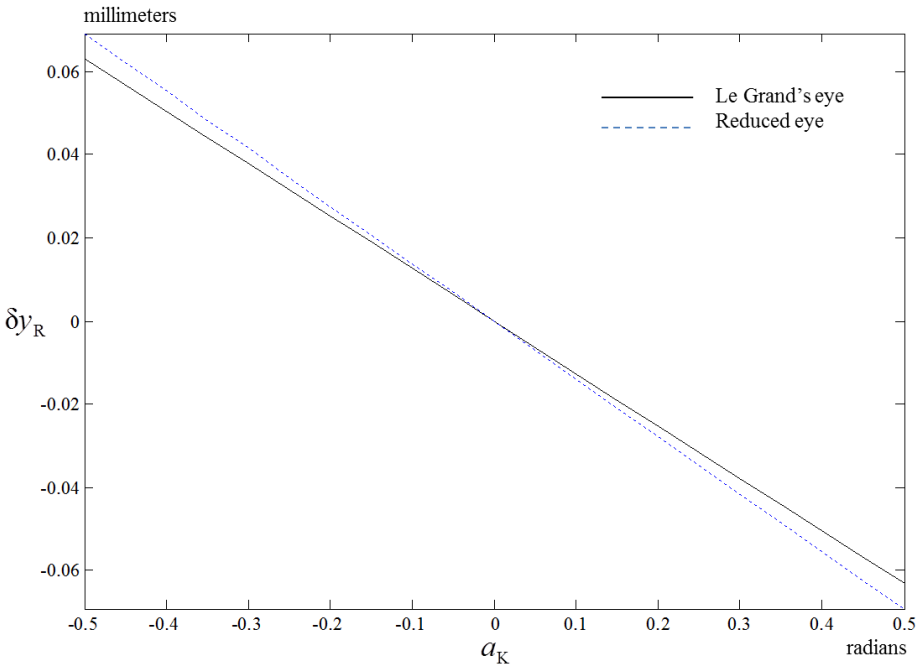

Figure 10.3.1 The chromatic difference in transverse image position at the retina δy_R as a function of incident inclination a_K for Le Grand's eye (solid black line) and reduced eye (dashed blue line) for a distant object point.

Table 10.3.5 The chromatic difference in image position at the retina, δy_{R} for the reduced eye. The illustrative example is for the centred reduced eye with $a_{\mathrm{K}} = 0.1$ for the distant object point and $y_{\mathrm{O}} = 200$ mm for the three finite distance object points.

Chromatic difference in image position		Illustrative example
Distant object	$\delta y_{\mathrm{R}} = (-0.03810) y_{\mathrm{P}} + (-0.1383\ \mathrm{mm}) a_{\mathrm{K}}$	$\delta y_{\mathrm{R}} = -0.01383$ mm
–3 m	$\delta y_{\mathrm{R}} = (-0.03813) y_{\mathrm{P}} + (4.6047 \times 10^{-5}) y_{\mathrm{O}}$	$\delta y_{\mathrm{R}} = 0.009209$ mm
–2 m	$\delta y_{\mathrm{R}} = (-0.03814) y_{\mathrm{P}} + (6.9034 \times 10^{-5}) y_{\mathrm{O}}$	$\delta y_{\mathrm{R}} = 0.01381$ mm
–0.5m	$\delta y_{\mathrm{R}} = (-0.03828) y_{\mathrm{P}} + (2.7484 \times 10^{-4}) y_{\mathrm{O}}$	$\delta y_{\mathrm{R}} = 0.05497$ mm

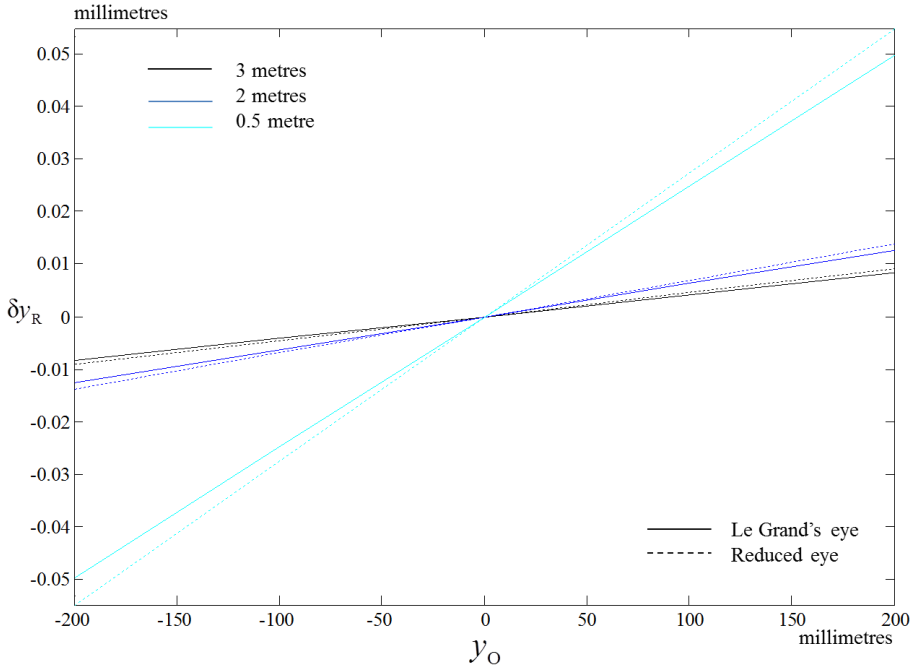

Figure 10.3.2 The chromatic difference in image position at the retina, δy_{R} as a function of transverse displacement of the object point from the longitudinal axis, y_{O} at the three illustrative distances, –3, –2 and –0.5 m for Le Grand's eye (solid lines) and the reduced eye (dashed line).

10.3.2 Chromatic difference in inclination at the retina

Le Grand's eye

Perhaps more insight can be gained from the chromatic difference in inclination at the retina, δa_{R}. Starting with a distant object and substituting from $\delta\mathbf{V}_{\mathrm{E}}$ for Le Grand's eye in Table 10.3.3 into Equation 7.2.16 we obtain a relationship for δa_{R} for a distant object point. This is summarised in Table 10.3.6 and shown in Figure 10.3.3, with the magnitude of a_{K} being magnified slightly more for the reduced eye than for Le Grand's eye.

Similarly, we substitute the respective entries of $\delta\mathbf{V}_{\mathrm{OE}}$ in Table 10.3.3 for the three illustrative z_{O}s in front of the eye into Equation 7.2.17 to obtain relationships at three working distances and summarised in Table 10.3.6. The relationships between δa_{R} and y_{O} are illustrated graphically in Figure 10.3.4.

The illustrative values obtained from Equations 7.2.16 and 17 are summarised in Table 10.3.6. As the object approaches the eye, so the magnitude of the emergent angular spread between the red and blue chief rays increases, as expected. δa_{R} is measured as the emergent inclination from the red ray to the emergent blue ray at the retina. For illustrative purposes, the chief ray has been chosen as $y_{\mathrm{P}} = 0\,\mathrm{mm}$.

The reduced eye

The results and conclusions for δa_{R} for the reduced eye are similar to Le Grand's eye, however the values vary slightly. From Figure 10.3.4, one can see that the magnitude of δa_{R} is consistently slightly greater in magnitude for the reduced eye than for Le Grand's eye. The illustrated values for δa_{R} for the centred reduced eye for a distant object with $a_{\mathrm{K}} = 0.1$ or for an object placed at $y_{\mathrm{O}} = 200\,\mathrm{mm}$ are summarised in Table 10.3.7.

Table 10.3.6 The chromatic difference in inclination at the retina δa_{R} for Le Grand's eye. The illustrative example is for a centred reduced eye and $a_{\mathrm{K}} = 0.1$ for a distant object point or $y_{\mathrm{O}} = 200\ \mathrm{mm}$ for an object point at the three finite distances. δa_{R} is given in radians.

	Chromatic difference in inclination at the retina	Illustrative example
Distant object	$\delta a_{\mathrm{R}} = (-0.001822\ \mathrm{kD})y_{\mathrm{P}} + (-0.006011)a_{\mathrm{K}}$	-6.0110×10^{-4}
–3 m	$\delta a_{\mathrm{R}} = (-0.001823\ \mathrm{kD})y_{\mathrm{P}} + (1.9998\times10^{-6}\ \mathrm{kD})y_{\mathrm{O}}$	3.9996×10^{-4}
–2 m	$\delta a_{\mathrm{R}} = (-0.001823\ \mathrm{kD})y_{\mathrm{P}} + (2.9968\times10^{-6}\ \mathrm{kD})y_{\mathrm{O}}$	5.9936×10^{-4}
–0.5m	$\delta a_{\mathrm{R}} = (-0.001828\ \mathrm{kD})y_{\mathrm{P}} + (1.1883\times10^{-5}\ \mathrm{kD})y_{\mathrm{O}}$	2.3767×10^{-3}

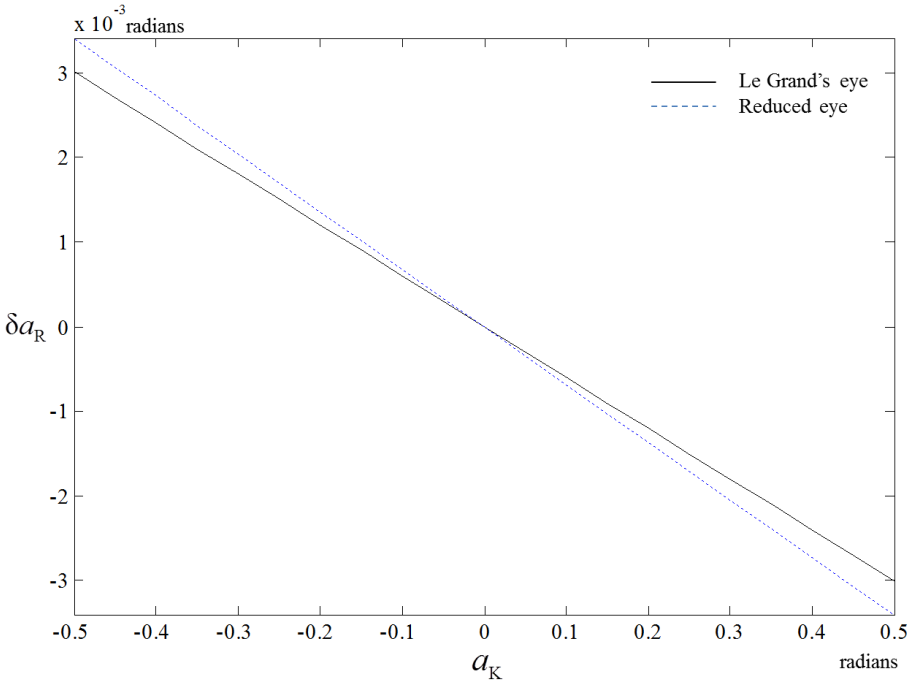

Figure 10.3.3 The chromatic difference in inclination at the retina δa_{R} as a function of incident inclination a_{K} for Le Grand's eye (black line) and the reduced eye (blue line).

Table 10.3.7 The chromatic difference in inclination at the retina δa_{R} for the reduced eye. The illustrative example is for a centred reduced eye and $a_{\mathrm{K}} = 0.1$ for a distant object point or $y_{\mathrm{O}} = 200\ \mathrm{mm}$ for an object point at the three finite distances.

	Chromatic difference in inclination at the retina	Illustrative example
Distant object	$\delta a_{\mathrm{R}} = (-0.001877\ \mathrm{kD})\, y_{\mathrm{P}} + (-0.006813)\, a_{\mathrm{K}}$	-6.8133×10^{-4}
–3 m	$\delta a_{\mathrm{R}} = (-0.001878\ \mathrm{kD})\, y_{\mathrm{P}} + (2.2687\times10^{-6}\ \mathrm{kD})\, y_{\mathrm{O}}$	4.5374×10^{-4}
–2 m	$\delta a_{\mathrm{R}} = (-0.001879\ \mathrm{kD})\, y_{\mathrm{P}} + (3.4013\times10^{-6}\ \mathrm{kD})\, y_{\mathrm{O}}$	6.8025×10^{-4}
–0.5m	$\delta a_{\mathrm{R}} = (-0.001886\ \mathrm{kD})\, y_{\mathrm{P}} + (1.3541\times10^{-5}\ \mathrm{kD})\, y_{\mathrm{O}}$	0.002708

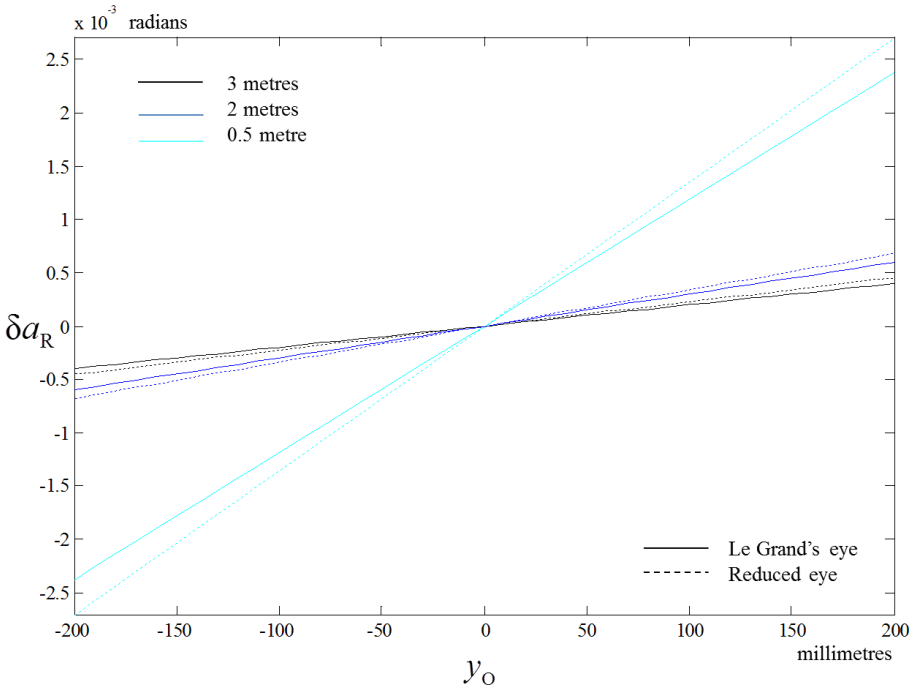

Figure 10.3.4 The chromatic difference in inclination at the retina δa_{R} as a function of transverse displacement of the object point from the longitudinal axis y_{O} at the three illustrative distances of –3, –2 and –0.5m from the eye for Le Grand's eye (solid lines) and the reduced eye (dashed lines).

10.3.3 Chromatic difference in image size

Le Grand's eye

Section 7.3.1 showed that the chromatic difference in image size, $\delta(\Delta y_{\mathrm{R}})$ simplified to a linear relationship between the object and image sizes (Δy_{R}). The size of a distant object is defined by the difference in incident inclination (Δa_{K}) or angular spread and at a finite distance z_{O}, by the object size (Δy_{O}). Substituting the relevant entry from $\delta\mathbf{V}_{\mathrm{E}}$ for Le Grand's eye given in Table 10.3.3 into Equation 7.3.4 for a distant object and from $\delta\mathbf{V}_{\mathrm{OE}}$ in Table 10.3.3 into Equation 7.3.8 we obtain relationships for $\delta(\Delta y_{\mathrm{R}})$ for Le Grand's eye.

For $\delta(\Delta y_{\mathrm{R}})$, the pupil position is nullified (Section 7.3.1) and therefore we obtain the same values as for δy_{R} when the system is assumed to be centred. Therefore the numerical examples for the two model eyes are not repeated. The graphical relationship for a distant object of size $\Delta a_{\mathrm{K}} = 0.1$ will be identical to that shown in Figure 10.3.1 and Figure 10.3.2 for the object of size $\Delta y_{\mathrm{O}} = 200\ \mathrm{mm}$ at finite distances.

The reduced eye

The linear relationships for $\delta(\Delta y_{\mathrm{R}})$ of the reduced eye are summarized in Table 10.3.8. The conclusions drawn are similar to those for Le Grand's eye.

Table 10.3.8 The Chromatic difference in image size at the retina $\delta(\Delta y_{\mathrm{R}})$ for Le Grand's and the reduced eyes.

	Le Grand's eye	Reduced eye
Distant object	$\delta(\Delta y_{\mathrm{R}}) = (-0.1258\ \mathrm{mm})\,\Delta a_{\mathrm{K}}$	$\delta(\Delta y_{\mathrm{R}}) = (-0.1383\ \mathrm{mm})\,\Delta a_{\mathrm{K}}$
–3 m	$\delta(\Delta y_{\mathrm{R}}) = (4.1853\times10^{-5})\,\Delta y_{\mathrm{O}}$	$\delta(\Delta y_{\mathrm{R}}) = (4.6047\times10^{-5})\,\Delta y_{\mathrm{O}}$
–2 m	$\delta(\Delta y_{\mathrm{R}}) = (6.2720\times10^{-5})\,\Delta y_{\mathrm{O}}$	$\delta(\Delta y_{\mathrm{R}}) = (6.9034\times10^{-5})\,\Delta y_{\mathrm{O}}$
–0.5m	$\delta(\Delta y_{\mathrm{R}}) = (2.4873\times10^{-4})\,\Delta y_{\mathrm{O}}$	$\delta(\Delta y_{\mathrm{R}}) = (2.7484\times10^{-4})\,\Delta y_{\mathrm{O}}$

10.3.4 Chromatic difference in angular spread at the retina

Le Grand's eye

Equation 7.3.11 defines the chromatic difference in angular spread across the retina, $\delta(\Delta a_{\mathrm{R}})$, as a linear relationship with the angular spread of the incident rays directed from a distant object. For Le Grand's eye this relationship is given in Table 10.3.9. Equation 7.3.12 defines $\delta(\Delta a_{\mathrm{R}})$ as a linear relationship with the object size Δy_{O} for an object at a finite distance. The values for the $\delta(\Delta a_{\mathrm{R}})$ at the three illustrative distances are given in Table 10.3.9.

Table 10.3.9 The chromatic difference in angular spread across the retina $\delta(\Delta a_{\mathrm{R}})$ for Le Grand's and the reduced eyes.

	Le Grand's eye	Reduced eye
Distant object	$\delta(\Delta a_{\mathrm{R}}) = -0.006011\,\Delta a_{\mathrm{K}}$	$\delta(\Delta a_{\mathrm{R}}) = -0.006813\,\Delta a_{\mathrm{K}}$
–3 m	$\delta(\Delta a_{\mathrm{R}}) = (1.9998\times10^{-6})\,\Delta y_{\mathrm{O}}$	$\delta(\Delta a_{\mathrm{R}}) = (2.2687\times10^{-6})\,\Delta y_{\mathrm{O}}$
–2 m	$\delta(\Delta a_{\mathrm{R}}) = (2.9968\times10^{-6})\,\Delta y_{\mathrm{O}}$	$\delta(\Delta a_{\mathrm{R}}) = (3.4013\times10^{-6})\,\Delta y_{\mathrm{O}}$
–0.5m	$\delta(\Delta a_{\mathrm{R}}) = (1.1883\times10^{-5})\,\Delta y_{\mathrm{O}}$	$\delta(\Delta a_{\mathrm{R}}) = (1.3541\times10^{-5})\,\Delta y_{\mathrm{O}}$

The Reduced eye

The values for the chromatic difference in angular spread across the retina are given in Table 10.3.9 for the reduced eye.

10.3.5 Retinal chromatic magnification

Le Grand's eye

In Sections 7.3.3 and 4 formulae for the retinal chromatic image size magnification M_{yR} and retinal chromatic angular spread magnification $M_{a\mathrm{R}}$ were obtained. These are chromatic magnifications and not chromatic differences and give a magnification of the red compared to the blue image size or angular spread at the retina. The magnification is dependent on the longitudinal distance of the object in front of the eye z_{O}, however, we expect these magnifications to be similar in value. Substituting the relevant values from the red and blue coefficient

matrices $\mathbf{V}_{\mathrm{E}}$ in Table 10.3.1 into Equation 7.3.19 we obtain M_{yR} for a distant object, where $n_0 = 1$ for both the red and blue incident light in air, given in Table 10.3.10. To obtain the retinal chromatic image size magnification for the three illustrative finite object distances in front of Le Grand's eye, we substitute the entries of the red and blue near coefficient matrices $\mathbf{V}_{\mathrm{OE}}$ from Table 10.3.1 into Equation 7.3.20 to obtain the M_{yR} for objects at the three illustrative distances in front of the eye, summarised in Table 10.3.10.

Similarly the retinal chromatic angular spread ratios $M_{a\mathrm{R}}$ are obtained by substituting the relevant entries of $\mathbf{V}_{\mathrm{E}}$ and $\mathbf{V}_{\mathrm{OE}}$ into Equations 7.3.27 and 28. The values are also summarised in Table 10.3.10.

The chromatic magnification of image sizes is 0.75% for distant objects and objects at a finite distance, with the red image being slightly larger than the blue image, which is very much in line with the calculated values in the literature (Thibos *et al*, 1991; Rabbetts, 2007: 291). Similarly, the retinal chromatic angular spread ratio is 0.74% for the objects at a finite distance in front of Le Grand's eye, implying that the red near directional spread is greater than the blue near directional spread.

The reduced eye

The numerical results for the reduced eye are given in Table 10.3.11. Table 10.3.11 indicates that for the reduced eye the retinal chromatic image size magnification is 0.83% regardless of the distance that the object is in front of the reduced eye. The distance and near image size coefficients X_{E} and X_{OE} are greater for red than blue. The retinal chromatic angular spread ratio is also 0.83% and the distance of the object in front of the reduced eye z_{O} plays very little part. The distance and near directional coefficients Z_{E} and Z_{OE} are greater for red than for blue. The object distance plays a negligibly small role.

These results are comparable to those in the literature. Zhang *et al* (1991) and Thibos *et al* (1991) give the magnification calculated using Equation 2.3.9.

Table 10.3.10 The retinal chromatic image size and angular spread magnifications for Le Grand's eye.

Retinal chromatic:	image size ratio	angular spread ratio
Distant object	$M_{yR} = 0.9925$	$M_{aR} = 0.9926$
–3 m	$M_{yR} = 0.9925$	$M_{aR} = 0.9926$
–2 m	$M_{yR} = 0.9925$	$M_{aR} = 0.9926$
–0.5m	$M_{yR} = 0.9925$	$M_{aR} = 0.9927$

Table 10.3.11 The retinal chromatic image size and angular spread magnifications for the reduced eye.

Retinal chromatic:	image size ratio	angular spread ratio
Distant object	$M_{yR} = 0.9917$	$M_{aR} = 0.9917$
–3 m	$M_{yR} = 0.9917$	$M_{aR} = 0.9917$
–2 m	$M_{yR} = 0.9917$	$M_{aR} = 0.9917$
–0.5m	$M_{yR} = 0.9917$	$M_{aR} = 0.9917$

Adjusting for the differences in wavelengths, the results obtained using Equations 7.3.19 and 27 compare well for all the examples given by Zhang *et al*. The same is true when a pinhole is held at a vertex distance of 15 mm and the retinal chromatic image size magnification increases to 4.3% for the reduced eye and 4.1% for Le Grand's eye.

10.4 Chromatic properties dependent on object and aperture positions in an eye – with a pinhole

In Section 5.2.4 we saw that when we introduce a pinhole immediately in front of the eye, Figures 3.5.4 and 5.1.1 simplify; the posterior system S_B is now the eye and the anterior system simplifies to the identity matrix. The coefficient matrix for an object at distance becomes simpler, given by $\mathbf{V}_E^P$ in Equation 5.2.37 and for an object at a finite distance in front of the eye, $\mathbf{V}_{OE}^P$ is given by Equation

5.2.34. The coefficient matrices for Le Grand's and the reduced eye with a pinhole immediately in front are given in Tables 10.4.1 and 2 and the chromatic difference in coefficient matrices with a pinhole in Table 10.4.3.

The methodology for each of the transverse chromatic properties was worked through step by step in Section 10.3. Therefore, in this section, the results are simply given in tabular form and the results discussed, without repeating the methodology.

Table 10.4.1 The red and blue coefficient matrices for Le Grand's eye with a pinhole immediately in front (superscript P) for distant objects (subscript E) and objects at the finite distances of –3, –2 and –0.5 m from the eye (subscript OE).

		Red	Blue
$\mathbf{V}_{\mathrm{E}}^{\mathrm{P}}$	Distant	$\begin{pmatrix} 0.007819 & 16.7276\ \mathrm{mm} \\ -0.04454\ \mathrm{kD} & 0.6786 \end{pmatrix}$	$\begin{pmatrix} -0.02367 & 16.5065\ \mathrm{mm} \\ -0.04596\ \mathrm{kD} & 0.6693 \end{pmatrix}$
$\mathbf{V}_{\mathrm{OE}}^{\mathrm{P}}$	–3 m	$\begin{pmatrix} 0.01340 & -0.005576 \\ -0.04431\ \mathrm{kD} & -2.2622\times10^{-4}\ \mathrm{kD} \end{pmatrix}$	$\begin{pmatrix} -0.01817 & -0.005502 \\ -0.04573\ \mathrm{kD} & -2.2309\times10^{-4}\ \mathrm{kD} \end{pmatrix}$
$\mathbf{V}_{\mathrm{OE}}^{\mathrm{P}}$	–2 m	$\begin{pmatrix} 0.01618 & -0.008364 \\ -0.04420\ \mathrm{kD} & -3.3932\times10^{-4}\ \mathrm{kD} \end{pmatrix}$	$\begin{pmatrix} -0.01541 & -0.008253 \\ -0.04562\ \mathrm{kD} & -3.3464\times10^{-4}\ \mathrm{kD} \end{pmatrix}$
$\mathbf{V}_{\mathrm{OE}}^{\mathrm{P}}$	–0.5 m	$\begin{pmatrix} 0.04127 & -0.03346 \\ -0.04318\ \mathrm{kD} & -1.3573\times10^{-3}\ \mathrm{kD} \end{pmatrix}$	$\begin{pmatrix} 0.009345 & -0.03301 \\ -0.04462\ \mathrm{kD} & -1.3386\times10^{-3}\ \mathrm{kD} \end{pmatrix}$

Table 10.4.2 The red and blue coefficient matrices for the reduced eye with a pinhole immediately in front for distant objects and objects at the finite distances of –3, –2 and –0.5 m.

		Red	Blue
$\mathbf{V}_{\mathrm{E}}^{\mathrm{P}}$	Distant	$\begin{pmatrix} 0.006992 & 16.7055\ \mathrm{mm} \\ -0.04469\ \mathrm{kD} & 0.7517 \end{pmatrix}$	$\begin{pmatrix} -0.02773 & 16.5126\ \mathrm{mm} \\ -0.04625\ \mathrm{kD} & 0.7431 \end{pmatrix}$
$\mathbf{V}_{\mathrm{OE}}^{\mathrm{P}}$	–3 m	$\begin{pmatrix} 0.01256 & -0.005569 \\ -0.04443\ \mathrm{kD} & -2.5058\times10^{-4}\ \mathrm{kD} \end{pmatrix}$	$\begin{pmatrix} -0.02223 & -0.005514 \\ -0.04600\ \mathrm{kD} & -2.4769\times10^{-4}\ \mathrm{kD} \end{pmatrix}$
$\mathbf{V}_{\mathrm{OE}}^{\mathrm{P}}$	–2 m	$\begin{pmatrix} 0.01534 & -0.008353 \\ -0.04431\ \mathrm{kD} & -3.7587\times10^{-4}\ \mathrm{kD} \end{pmatrix}$	$\begin{pmatrix} -0.01948 & -0.008256 \\ -0.04588\ \mathrm{kD} & -3.7153\times10^{-4}\ \mathrm{kD} \end{pmatrix}$
$\mathbf{V}_{\mathrm{OE}}^{\mathrm{P}}$	–0.5 m	$\begin{pmatrix} 0.04040 & -0.03341 \\ -0.04318\ \mathrm{kD} & -1.5035\times10^{-3}\ \mathrm{kD} \end{pmatrix}$	$\begin{pmatrix} 0.005291 & -0.03303 \\ -0.04476\ \mathrm{kD} & -1.4861\times10^{-3}\ \mathrm{kD} \end{pmatrix}$

Table 10.4.3 The chromatic difference between red and blue coefficient matrices for Le Grand's and the reduced eye with a pinhole immediately in front for distant objects and objects at the finite distances of –3, –2 and –0.5 m from the eye.

		Le Grand's eye	Reduced eye
$\delta\mathbf{V}_{\mathrm{E}}^{\mathrm{P}}$	Distant	$\begin{pmatrix} -0.03149 & -0.2212\ \mathrm{mm} \\ -0.001414\ \mathrm{kD} & -9.3691\times10^{-3} \end{pmatrix}$	$\begin{pmatrix} -0.03473 & -0.1929\ \mathrm{mm} \\ -0.001563\ \mathrm{kD} & -0.008682 \end{pmatrix}$
$\delta\mathbf{V}_{\mathrm{OE}}^{\mathrm{P}}$	–3 m	$\begin{pmatrix} -0.03156 & 7.3721\times10^{-5} \\ -0.00417\ \mathrm{kD} & 3.1230\times10^{-6}\ \mathrm{kD} \end{pmatrix}$	$\begin{pmatrix} -0.03479 & 6.4307\times10^{-5} \\ -0.001566\ \mathrm{kD} & 2.8938\times10^{-6}\ \mathrm{kD} \end{pmatrix}$
$\delta\mathbf{V}_{\mathrm{OE}}^{\mathrm{P}}$	–2 m	$\begin{pmatrix} -0.03160 & 1.1058\times10^{-4} \\ -0.001419\ \mathrm{kD} & 4.6845\times10^{-6}\ \mathrm{kD} \end{pmatrix}$	$\begin{pmatrix} -0.03482 & 9.6461\times10^{-5} \\ -0.001567\ \mathrm{kD} & 4.3408\times10^{-6}\ \mathrm{kD} \end{pmatrix}$
$\delta\mathbf{V}_{\mathrm{OE}}^{\mathrm{P}}$	–0.5 m	$\begin{pmatrix} -0.03193 & 4.4233\times10^{-4} \\ -0.001433\ \mathrm{kD} & 1.8738\times10^{-5}\ \mathrm{kD} \end{pmatrix}$	$\begin{pmatrix} -0.03511 & 3.8584\times10^{-4} \\ -0.001580\ \mathrm{kD} & 1.7363\times10^{-5}\ \mathrm{kD} \end{pmatrix}$

10.4.1 Chromatic difference in transverse image positions and inclinations at the retina with pinhole in front of the eye

The chromatic difference in transverse image positions δy_{R} (Equations 7.2.11 and 12) and inclinations δa_{R} (Equations 7.2.20 and 21) at the retina when a pinhole is immediately in front of the eye is given in Table 10.4.4 for Le Grand's eye and Table 10.4.5 for the reduced eye.

To generate numerical examples for the chromatic difference in transverse image positions δy_{R} and inclinations δa_{R} at the retina, we assume that the object is on the longitudinal axis; that is to say $a_{\mathrm{K}} = 0$ or $y_{\mathrm{O}} = 0$. Furthermore, an eye that is cyclopleged will allow for 4 mm of pinhole decentration and we therefore equate $y_{\mathrm{P}} = 4\ \mathrm{mm}$. The values are summarized in Table 10.4.6.

Inspecting the results, in each case there is a very small difference resulting from the change in longitudinal position of the object point from the eye. Additionally, the results obtained for the two eyes are distinct for both δy_{R} and δa_{R}. This is emphasized in Figures 10.4.1 and 2 which give δy_{R} and δa_{R} as a function of transverse displacement of the pinhole y_{P} held immediately in front of the eye.

Table 10.4.4 The chromatic difference in transverse image positions δy_{R} and inclinations δa_{R} at the retina when a pinhole is immediately in front of Le Grand's eye.

	Chromatic difference in transverse image positions	Chromatic difference in inclinations at the retina
Distant	$\delta y_{\mathrm{R}} = (-0.03149) y_{\mathrm{P}} + (-0.2212\ \mathrm{mm}) a_{\mathrm{K}}$	$\delta a_{\mathrm{R}} = (-0.001413\ \mathrm{kD}) y_{\mathrm{P}} + (-0.009369) a_{\mathrm{K}}$
–3 m	$\delta y_{\mathrm{R}} = (-0.03156) y_{\mathrm{P}} + (7.3721\times10^{-5}) y_{\mathrm{O}}$	$\delta a_{\mathrm{R}} = (-0.001417\ \mathrm{kD}) y_{\mathrm{P}} + (3.1230\times10^{-6}\ \mathrm{kD}) y_{\mathrm{O}}$
–2 m	$\delta y_{\mathrm{R}} = (-0.03160) y_{\mathrm{P}} + (1.1058\times10^{-4}) y_{\mathrm{O}}$	$\delta a_{\mathrm{R}} = (-0.001419\ \mathrm{kD}) y_{\mathrm{P}} + (4.6845\times10^{-6}\ \mathrm{kD}) y_{\mathrm{O}}$
–0.5 m	$\delta y_{\mathrm{R}} = (-0.03193) y_{\mathrm{P}} + (4.4233\times10^{-4}) y_{\mathrm{O}}$	$\delta a_{\mathrm{R}} = (-0.001433\ \mathrm{kD}) y_{\mathrm{P}} + (1.8738\times10^{-5}\ \mathrm{kD}) y_{\mathrm{O}}$

Table 10.4.5 The chromatic difference in transverse image positions δy_{R} and inclinations δa_{R} at the retina when a pinhole is immediately in front of the reduced eye.

	Chromatic difference in transverse image positions	Chromatic difference in inclinations at the retina
Distant	$\delta y_{\mathrm{R}} = (-0.03473) y_{\mathrm{P}} + (-0.1929\ \mathrm{mm}) a_{\mathrm{K}}$	$\delta a_{\mathrm{R}} = (-0.001563\ \mathrm{kD}) y_{\mathrm{P}} + (-0.008682) a_{\mathrm{K}}$
–3 m	$\delta y_{\mathrm{R}} = (-0.03479) y_{\mathrm{P}} + (6.4307\times10^{-5}) y_{\mathrm{O}}$	$\delta a_{\mathrm{R}} = (-0.001566\ \mathrm{kD}) y_{\mathrm{P}} + (2.8938\times10^{-6}\ \mathrm{kD}) y_{\mathrm{O}}$
–2 m	$\delta y_{\mathrm{R}} = (-0.03482) y_{\mathrm{P}} + (9.6461\times10^{-5}) y_{\mathrm{O}}$	$\delta a_{\mathrm{R}} = (-0.001567\ \mathrm{kD}) y_{\mathrm{P}} + (4.3408\times10^{-6}\ \mathrm{kD}) y_{\mathrm{O}}$
–0.5 m	$\delta y_{\mathrm{R}} = (-0.03511) y_{\mathrm{P}} + (3.8584\times10^{-4}) y_{\mathrm{O}}$	$\delta a_{\mathrm{R}} = (-0.001580\ \mathrm{kD}) y_{\mathrm{P}} + (1.7363\times10^{-5}\ \mathrm{kD}) y_{\mathrm{O}}$

Table 10.4.6 The values for the chromatic difference in transverse image positions δy_{R} and inclinations δa_{R} at the retina for Le Grand's eye and the reduced eye. The object is on the longitudinal axis and the pinhole in front of the cyclopleged eye is displaced 4 mm from the optical axis.

	Chromatic difference in transverse image positions δy_{R}		Chromatic difference in inclinations δa_{R}	
	Le Grand	Reduced eye	Le Grand	Reduced eye
Distant	–0.1259 mm	–0.1389 mm	–0.005657	–0.006251
–3 m	–0.1262 mm	–0.1392 mm	–0.005670	–0.006262
–2 m	–0.1264 mm	–0.1393 mm	–0.005676	–0.006268
–0.5 m	–0.1277 mm	–0.1404 mm	–0.005732	–0.006320

The relationship obtained for the chromatic difference in inclination at the retina using a pinhole compares well with the theoretically calculated values given by Thibos *et al* (1991).

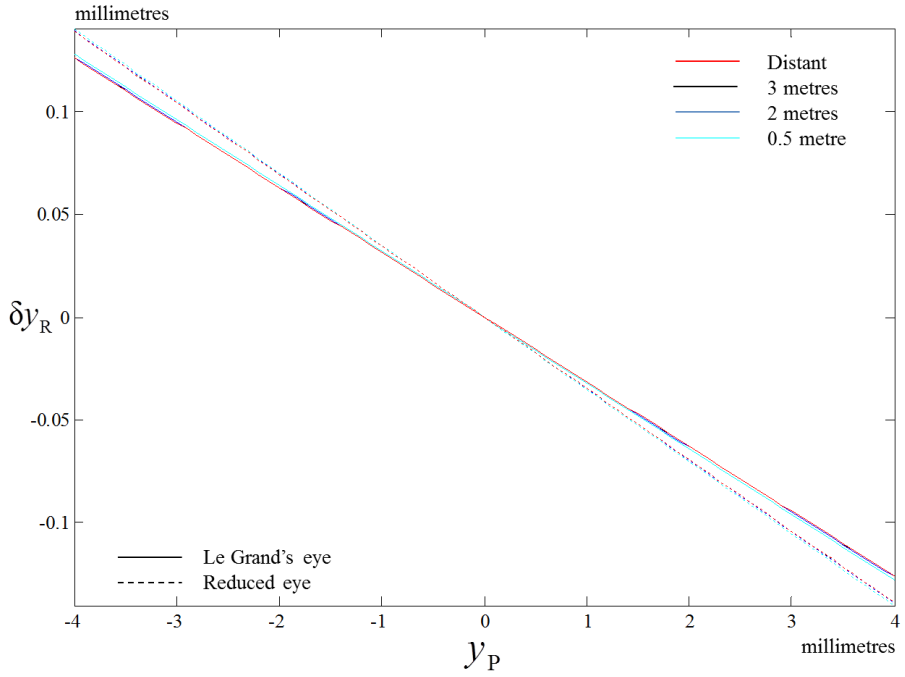

Figure 10.4.1 Chromatic difference in transverse image positions δy_R as a function of displacement of a pinhole y_P immediately in front of the eye. The red, black, blue and cyan lines appear to be superimposed for both the Le Grand and reduced eyes.

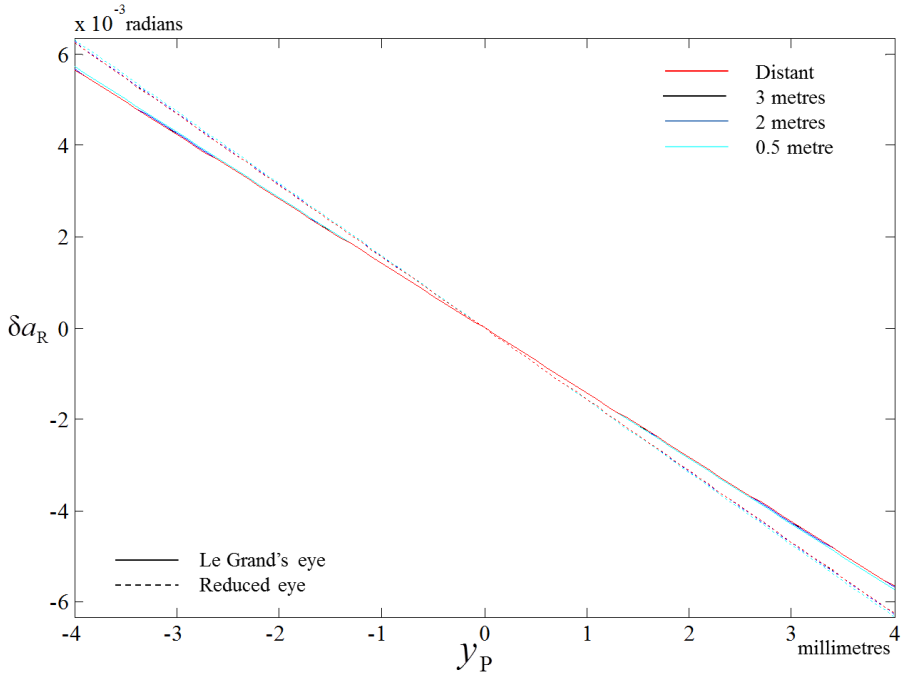

Figure 10.4.2 Chromatic difference in retinal inclinations δa_R as a function of pinhole displacement y_P in front of the eye. The red, black, blue and cyan solid lines representing Le Grand's eye appear to be superimposed and similarly, the red, black, blue and cyan dashed lines representing the reduced eye also appear superimposed.

10.4.2 Chromatic difference in image size, angular spread and chromatic magnifications: with a pinhole

The equations that define the chromatic difference in image size (Equations 7.3.4 and 8), chromatic difference in angular spread (Equations 7.3.11 and 12), retinal chromatic image size magnification (Equations 7.3.19 and 20) and retinal chromatic angular spread magnification (Equations 7.3.27 and 28) are each independent of transverse displacement in the pupil or pinhole planes. However, the longitudinal displacement of the aperture from the plane of the pupil to the plane of the pinhole immediately in front of the cornea will have an effect.

Chromatic difference in image size and angular spread – with a pinhole

The chromatic difference in image size $\delta(\Delta y_{\mathrm{R}})$ when a pinhole is placed immediately in front of the eye is summarized in Tables 10.4.7 and 8 for the two model eyes. It is obvious from Tables 10.4.7 and 8 that the chromatic difference in image sizes and angular spread $\delta(\Delta a_{\mathrm{R}})$ at the retina are all linear equations dependent on the object size.

$\delta(\Delta a_{\mathrm{R}})$ has been defined differently in this study to those definitions in the literature. We saw in Section 2.3.2 that the definitions in the literature differ by the position of the pivotal point used to measure the chromatic difference in angular spread at the retina (for example nodal point, entrance pupil, refracting surface or "cornea"), with adjustments included in the formulae for such differences in choice of pivotal point. In contrast, this study defines the actual difference in the ray inclinations at the retina. For Gaussian eyes these rays will intersect on the Gaussian plane but in astigmatic heterocentric eyes the two rays may not intersect. When comparing the results in this study for the two model eyes to the results in the literature, the results appear similar for the naked centred eye. However, it is when the pinhole is placed away from the eye that the difference in the definitions becomes apparent. This is because the actual point of intersection moves further upstream from those used in the literature. This is an important discrepancy to note. The equations for $\delta(\Delta a_{\mathrm{R}})$ suggest that the chromatic difference in ray inclinations at the retina have implications for the Stiles-Crawford effects that previous definitions have not highlighted.

Table 10.4.7 The chromatic difference in image sizes $\delta(\Delta y_{\mathrm{R}})$ and angular spread $\delta(\Delta a_{\mathrm{R}})$ at the retina when a pinhole is immediately in front of Le Grand's eye.

	Chromatic difference in image sizes at the retina	Chromatic difference in angular spread at the retina
Distant	$\delta(\Delta y_{\mathrm{R}}) = (-0.2212\ \mathrm{mm})\,\Delta a_{\mathrm{K}}$	$\delta(\Delta a_{\mathrm{R}}) = (-0.009369)\,\Delta a_{\mathrm{K}}$
–3 m	$\delta(\Delta y_{\mathrm{R}}) = (7.3721\times10^{-5})\,\Delta y_{\mathrm{O}}$	$\delta(\Delta a_{\mathrm{R}}) = (3.1230\times10^{-6}\ \mathrm{kD})\,\Delta y_{\mathrm{O}}$
–2 m	$\delta(\Delta y_{\mathrm{R}}) = (1.1058\times10^{-4})\,\Delta y_{\mathrm{O}}$	$\delta(\Delta a_{\mathrm{R}}) = (4.6845\times10^{-6}\ \mathrm{kD})\,\Delta y_{\mathrm{O}}$
–0.5 m	$\delta(\Delta y_{\mathrm{R}}) = (4.4233\times10^{-4})\,\Delta y_{\mathrm{O}}$	$\delta(\Delta a_{\mathrm{R}}) = (1.8738\times10^{-5}\ \mathrm{kD})\,\Delta y_{\mathrm{O}}$

Table 10.4.8 The chromatic difference in image size $\delta(\Delta y_{\mathrm{R}})$ and angular spread $\delta(\Delta a_{\mathrm{R}})$ at the retina when a pinhole is immediately in front of the reduced eye.

	Chromatic difference in image sizes at the retina	Chromatic difference in angular spread at the retina
Distant	$\delta(\Delta y_{\mathrm{R}}) = (-0.1929\ \mathrm{mm})\,\Delta a_{\mathrm{K}}$	$\delta(\Delta a_{\mathrm{R}}) = (-0.008682)\,\Delta a_{\mathrm{K}}$
–3 m	$\delta(\Delta y_{\mathrm{R}}) = (6.4307\times10^{-5})\,\Delta y_{\mathrm{O}}$	$\delta(\Delta a_{\mathrm{R}}) = (2.8938\times10^{-6}\ \mathrm{kD})\,\Delta y_{\mathrm{O}}$
–2 m	$\delta(\Delta y_{\mathrm{R}}) = (9.6461\times10^{-5})\,\Delta y_{\mathrm{O}}$	$\delta(\Delta a_{\mathrm{R}}) = (4.3408\times10^{-6}\ \mathrm{kD})\,\Delta y_{\mathrm{O}}$
–0.5 m	$\delta(\Delta y_{\mathrm{R}}) = (3.8584\times10^{-4})\,\Delta y_{\mathrm{O}}$	$\delta(\Delta a_{\mathrm{R}}) = (1.7363\times10^{-5}\ \mathrm{kD})\,\Delta y_{\mathrm{O}}$

Chromatic image size and angular spread magnifications - with a pinhole

The effect of replacing the pupil with a pinhole has a magnifying effect. We substitute from the respective red and blue coefficient matrices $\mathbf{V}_{\mathrm{E}}^{\mathrm{P}}$ and $\mathbf{V}_{\mathrm{OE}}^{\mathrm{P}}$ in Tables 10.4.1 and 2 into Equations 7.3.19, 20, 27 and 28. For Le Grand's eye with a pinhole the retinal chromatic image size magnification is $M_{\mathrm{yR}}^{\mathrm{P}} = 0.9868$ and the retinal chromatic angular spread magnification is $M_{\mathrm{aR}}^{\mathrm{P}} = 0.9862$ for all four illustrative distances. For the reduced eye with a pinhole the retinal chromatic image size magnification, $M_{\mathrm{yR}}^{\mathrm{P}}$ and the retinal chromatic angular spread magnification, $M_{\mathrm{aR}}^{\mathrm{P}}$ are both 0.9885 for all four illustrative distances. This equates to magnifications ranging between 1.1 and 1.4%, and compares well to the values given by Zhang *et al* (1991). These values represent an increased magnification over the naked model eyes.

10.4.3 AcuFocus Kamra corneal pinhole inlay

The AcuFocus Kamra corneal inlay was discussed in Section 7.6 and consists of an intrastromal pinhole inlay. The examples in Section 10.4 have illustrated what the effect of the corneal pinhole inlay are on the visual system. Only the chromatic difference in image position and image inclination are directly dependent on the transverse displacement of the pinhole. A misplaced pinhole inlay of only 0.5 mm can have a significant detrimental effect on the vision of the eye (Tabernero and Artal, 2011).

All the chromatic differences and chromatic magnifications in image space indirectly depend on the longitudinal shift in position of the limiting aperture from the pupillary plane to the corneal plane. Comparison of the equations in Table 10.3.9 with those in Tables 10.4.7 and 8, shows that $\delta(\Delta a_{\mathrm{R}})$ increases when a pinhole is placed at the corneal plane and that this effect is greater for Le Grand's eye than for the reduced eye. When $M_{\mathrm{yR}}^{\mathrm{P}}$ and $M_{\mathrm{aR}}^{\mathrm{P}}$ are compared with M_{yR} and M_{aR} in Tables 10.3.10 and 11 we see that both $M_{\mathrm{yR}}^{\mathrm{P}}$ and $M_{\mathrm{aR}}^{\mathrm{P}}$ increase when a pinhole is placed at the corneal plane and that these chromatic magnification effects are greater in Le Grand's eye than the reduced eye. Additionally, the results for $M_{\mathrm{yR}}^{\mathrm{P}}$ and $M_{\mathrm{aR}}^{\mathrm{P}}$ indicate that the chromatic magnification effects are greater for the retinal inclination than for retinal position. The increase in chromatic magnification will have implications for eyes that have an AcuFocus Kamra corneal pinhole inlay, something that is raised as a concern by Tabernero and Artal (2011).

The corneal pinhole inlay has an outer diameter of 3.8 mm (Seyeddain *et al*, 2010; Tabernero and Artal, 2011). Even with the best centration, a normal pupil, without pharmacological intervention, can dilate wider than the inlay. If we imagine a pencil of rays from an object point, then the effect of rays entering the eye as a full ring around the outer diameter of the inlay will be to create a rainbow-type arc forming a full circle on the retina. For a distant axial object point this will create a chromatic difference in position δy_{R} of $-0.1197\,\mathrm{mm}$ for Le Grand's eye. The red ring will be positioned outer-most and the blue ring will be

the inner-ring. The rainbow-ring will not necessarily be in focus and will be positioned in the peripheral retina.

The rainbow that we see in the sky is part of a full circular-arc, the lower part of which is hidden from view below the horizon. However, the shape of the rainbow is not a bow, but rather a cone shape, the apex of the cone being positioned at the viewer's eye (Lee and Fraser, 2001: 112-113, 322). In effect, the rainbow-ring created in the eye by the outer edge of the pinhole inlay is an image at the retina of a cone of light, with each frequency creating its own cone. The apexes of the cones are unlikely to coincide and the angle between the red and the blue cones is represented by the chromatic difference in image inclination δa_{R} and is -5.3694×10^{-3} (radians) for Le Grand's eye.

10.5 Chromatic properties of the eye dependent on image and aperture positions in object space

Chromatic properties of the eye dependent on image and aperture positions in object space mimic the set-up created in the experimental environment. They differ from the object and aperture dependent chromatic properties of the eye in image space in that the red and blue image points are directed at the same point on the retina and the chromatic separation occurs in object space. The Vernier distance between the red and blue object points is measured when the two points appear to coincide to the subject. Because the use of a pinhole to manipulate and induce transverse chromatic effects features strongly experimentally, we shall include the pinhole alternative in this section. Additionally, because experimental set-ups are conducted at finite distances the study of image- and aperture-dependent chromatic properties in object space shall be limited to finite distances.

The coefficient matrix for the chromatic properties in object space for objects at finite distances ($\mathbf{V}_{\mathrm{Oy}}$) was defined for the eye by Equation 5.3.14 and with a pinhole in front of the eye ($\mathbf{V}^{\mathrm{p}}_{\mathrm{Oy}}$) by Equation 5.3.19. Only the top row is dependent on the longitudinal distance of the object in front of the eye, z_{O}, while the bottom row is independent of object distance in front of the eye. This implies

Table 10.5.1 The red and blue coefficient matrices $\mathbf{V}_{\mathrm{Oy}}$ for image and aperture dependent chromatic properties in object space for Le Grand's eye for objects at the finite distances of 3, 2 and 0.5 metres.

		Red	Blue
$\mathbf{V}_{\mathrm{Oy}}$	–3 m	$\begin{pmatrix} 2.7172 & -179.7819 \\ -5.2871\times10^{-4}\ \mathrm{kD} & 0.05987\ \mathrm{kD} \end{pmatrix}$	$\begin{pmatrix} -3.7289 & -181.1450 \\ 1.6195\times10^{-3}\ \mathrm{kD} & 0.06032\ \mathrm{kD} \end{pmatrix}$
$\mathbf{V}_{\mathrm{Oy}}$	–2 m	$\begin{pmatrix} 2.1885 & -119.9154 \\ -5.2871\times10^{-4}\ \mathrm{kD} & 0.05987\ \mathrm{kD} \end{pmatrix}$	$\begin{pmatrix} -2.1095 & -120.8241 \\ 1.6195\times10^{-3}\ \mathrm{kD} & 0.06032\ \mathrm{kD} \end{pmatrix}$
$\mathbf{V}_{\mathrm{Oy}}$	–0.5 m	$\begin{pmatrix} 1.3954 & -30.1155 \\ -5.2871\times10^{-4}\ \mathrm{kD} & 0.05987\ \mathrm{kD} \end{pmatrix}$	$\begin{pmatrix} 0.3197 & -30.3428 \\ 1.6195\times10^{-3}\ \mathrm{kD} & 0.06032\ \mathrm{kD} \end{pmatrix}$

Table 10.5.2 The red and blue coefficient matrices for image and aperture dependent chromatic properties in object space for the reduced eye for objects at the finite distances of 3, 2 and 0.5 metres.

		Red	Blue
$\mathbf{V}_{\mathrm{Oy}}$	–3 m	$\begin{pmatrix} 2.4696 & -179.7954 \\ -4.5825\times10^{-4}\ \mathrm{kD} & 0.05990\ \mathrm{kD} \end{pmatrix}$	$\begin{pmatrix} -4.4219 & -181.2964 \\ 1.8389\times10^{-3}\ \mathrm{kD} & 0.06040\ \mathrm{kD} \end{pmatrix}$
$\mathbf{V}_{\mathrm{Oy}}$	–2 m	$\begin{pmatrix} 2.0114 & -119.8953 \\ -4.5825\times10^{-4}\ \mathrm{kD} & 0.05990\ \mathrm{kD} \end{pmatrix}$	$\begin{pmatrix} -2.5829 & -120.8959 \\ 1.8389\times10^{-3}\ \mathrm{kD} & 0.06040\ \mathrm{kD} \end{pmatrix}$
$\mathbf{V}_{\mathrm{Oy}}$	–0.5 m	$\begin{pmatrix} 1.3240 & -30.0450 \\ -4.5825\times10^{-4}\ \mathrm{kD} & 0.05990\ \mathrm{kD} \end{pmatrix}$	$\begin{pmatrix} 0.1754 & -30.2951 \\ 1.8389\times10^{-3}\ \mathrm{kD} & 0.06040\ \mathrm{kD} \end{pmatrix}$

Table 10.5.3 The chromatic difference in coefficient matrices for image and aperture dependent chromatic properties in object space for Le Grand's and the reduced eye for objects at the finite distances of 3, 2 and 0.5 metres.

		Le Grand's eye	Reduced eye
$\delta\mathbf{V}_{\mathrm{Oy}}$	–3 m	$\begin{pmatrix} -6.4461 & -1.3630 \\ 2.1482\times10^{-3}\ \mathrm{kD} & 4.5429\times10^{-4}\ \mathrm{kD} \end{pmatrix}$	$\begin{pmatrix} -6.8915 & -1.5010 \\ 2.2972\times10^{-3}\ \mathrm{kD} & 5.0032\times10^{-4}\ \mathrm{kD} \end{pmatrix}$
$\delta\mathbf{V}_{\mathrm{Oy}}$	–2 m	$\begin{pmatrix} -4.2980 & -0.9087 \\ 2.1482\times10^{-3}\ \mathrm{kD} & 4.5429\times10^{-4}\ \mathrm{kD} \end{pmatrix}$	$\begin{pmatrix} -4.5943 & -1.0006 \\ 2.2972\times10^{-3}\ \mathrm{kD} & 5.0032\times10^{-4}\ \mathrm{kD} \end{pmatrix}$
$\delta\mathbf{V}_{\mathrm{Oy}}$	–0.5 m	$\begin{pmatrix} -1.0757 & -0.2273 \\ 2.1482\times10^{-3}\ \mathrm{kD} & 4.5429\times10^{-4}\ \mathrm{kD} \end{pmatrix}$	$\begin{pmatrix} -1.1486 & -0.2502 \\ 2.2972\times10^{-3}\ \mathrm{kD} & 5.0032\times10^{-4}\ \mathrm{kD} \end{pmatrix}$

that the chromatic difference in inclination, δa_{O} (Equation 7.4.6) will be independent of z_{O}.

The red and blue coefficient matrices, $\mathbf{V}_{\mathrm{Oy}}$ for Le Grand's eye are given in Table 10.5.1 and for the reduced eye in Table 10.5.2. The chromatic difference in coefficient matrices $\delta\mathbf{V}_{\mathrm{Oy}}$ is given in Table 10.5.3 for both eyes.

10.5.1 Chromatic difference in object position

The chromatic difference in object position δy_{O} measures the difference in the transverse position from the red object point to the blue object point when the two coloured image points are superimposed on the retina and appear to the subject as a single dichromatic image. The position on the retina y_{R} can be manipulated and may be on the fovea, or some chosen point in the peripheral retina. For model eyes, the fovea is often assumed to be coincidental with the optical axis, thus nullifying the visio-optical angle (angle alpha).

We substitute the relevant entries from $\delta\mathbf{V}_{\mathrm{Oy}}$ in Table 10.5.3 into Equation 7.4.1 to obtain δy_{O} for three illustrative distances of the object from Le Grand's eye. These are given in Table 10.5.4. If we assume that the pupil is centred on the longitudinal axis, then δy_{O} is dependent on the position chosen for the image point to reach the retina, y_{R}. If this is the fovea, then δy_{O} is dependent on the visio-optical angle, the angle between the visual and optical axes (Atchison and Smith, 2000: 30-35; Rabbetts, 2007: 234-235). Because the fovea is static, one obtains a single value for the chosen longitudinal object distance in front of the eye.

If, for example, we assume that the eye is centred $y_{\mathrm{P}} = 0\,\mathrm{mm}$ and that the fovea is 5° from the optical axis, then this equates to an approximate distance of 1.46 mm at the retina for a model eye. Substituting these two illustrative values into the equations in Table 10.5.4, we obtain a chromatic difference in object position, summarized for Le Grand's eye in the right-hand column of Table 10.5.4 and for the reduced eye, the equations and numerical illustrative values are summarized in Table 10.5.5 .

Table 10.5.4 The equations for the chromatic difference in object position δy_O for Le Grand's eye for objects at the finite distances of –3, –2 and –0.5 m. The illustrative values are for a centred reduced eye with transverse retinal displacement of 1.46 mm.

	Chromatic difference in object position	Illustrative values
–3 m	$\delta y_O = (-6.4462)y_P + (-1.3630)y_R$	–1.9900 mm
–2 m	$\delta y_O = (-4.2980)y_P + (-0.9087)y_R$	–1.3267 mm
–0.5 m	$\delta y_O = (-1.0757)y_P + (-0.2273)y_R$	–0.3318 mm

Table 10.5.5 The equations for the chromatic difference in object position δy_O for the reduced eye for objects at the finite distances of –3, –2 and –0.5 m. The illustrative values are for a centred reduced eye with transverse retinal displacement of 1.46 mm.

	Chromatic difference in object position	Illustrative values
–3 m	$\delta y_O = (-6.8915)y_P + (-1.5010)y_R$	–2.1914 mm
–2 m	$\delta y_O = (-4.5943)y_P + (-1.0006)y_R$	–1.4609 mm
–0.5 m	$\delta y_O = (-1.1486)y_P + (-0.02502)y_R$	–0.3652 mm

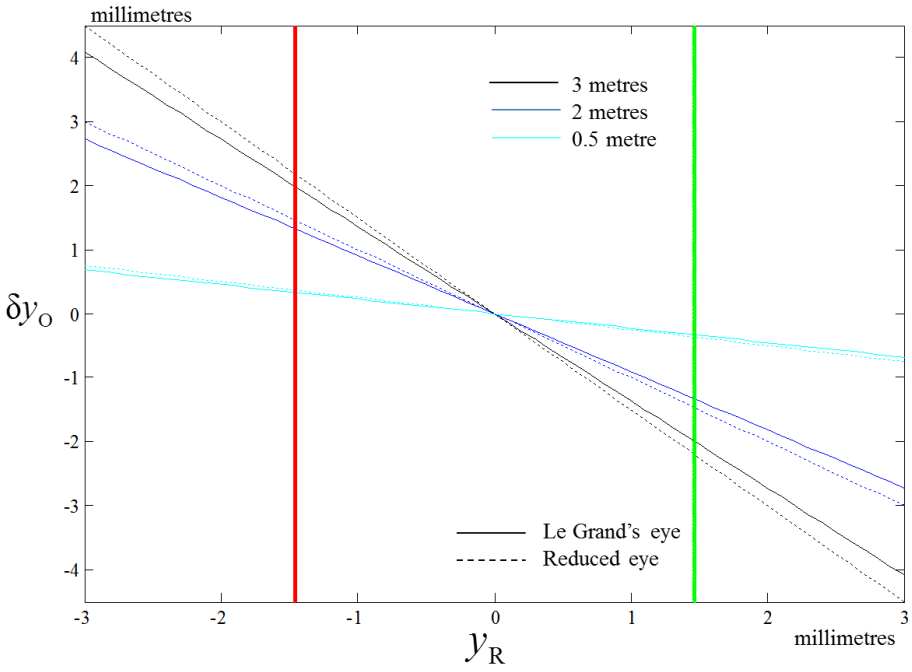

Figure 10.5.1 Chromatic difference in object position δy_O is shown for illustrative working distances of –3 m, –2 m and –0.5 m from the eye. The red and blue images are superimposed at the retina at a chosen position, y_R, with foveal positions shown by the red and green vertical lines for the right and left eyes, respectively.

The chromatic difference in object position δy_O is the Vernier separation from the red object point to the blue object point at illustrative working distances of –3 m, –2 m and –0.5 m. This is indicated in Figure 10.5.1. The red and blue images are superimposed at the retina at a chosen position, y_R. In Figure 10.5.1, the red vertical line indicates the foveal position of the right eye $y_R = -1.46$ mm and the green line indicates the foveal position of the left eye $y_R = 1.46$ mm.

10.5.2 Chromatic difference in inclination in object space

The chromatic difference in inclination in object space δa_O is the angle subtended by the incident rays from the red and blue object points which, after both traversing the same position through the pupil, both reach the retina at the same position so as to appear superimposed to the viewer. The chromatic difference in inclination in object space δa_O utilises the bottom row of $\mathbf{V}_{Oy}$ which

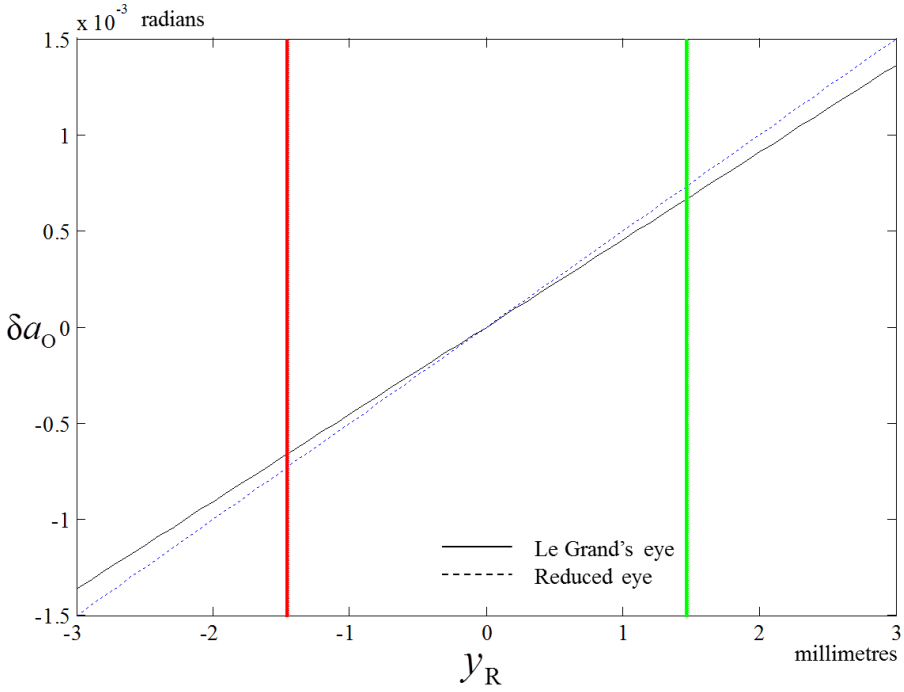

Figure 10.5.2 Chromatic difference in inclination in object space δa_O for Le Grand's eye and the reduced eye as a function of retinal position. δa_O is independent of working distance.

is independent of z_{O}. Substituting the relevant entries from $\mathbf{V}_{\mathrm{Oy}}$ into Equation 7.4.6 we obtain

$$\delta a_{\mathrm{O}} = \left(2.1482\times10^{-3}\ \mathrm{kD}\right) y_{\mathrm{P}} + \left(4.5429\times10^{-4}\ \mathrm{kD}\right) y_{\mathrm{R}} \qquad (10.5.1)$$

for Le Grand's eye and

$$\delta a_{\mathrm{O}} = \left(2.2972\times10^{-3}\ \mathrm{kD}\right) y_{\mathrm{P}} + \left(5.0032\times10^{-4}\ \mathrm{kD}\right) y_{\mathrm{R}} \qquad (10.5.2)$$

for the reduced eye. If we substitute the illustrative values of $y_{\mathrm{P}} = 0$ for a centred system and $y_{\mathrm{R}} = 1.46\ \mathrm{mm}$ for the position of the fovea, then we obtain a chromatic difference in inclination in object space of $\delta a_{\mathrm{O}} = 6.6327\times10^{-4}$ for Le Grand's eye and 7.3047×10^{-4} for the reduced eye.

Figure 10.5.2 illustrates the relationship of δa_{O} as a function of position of the rays reaching the retina. The red vertical line indicates the position of the fovea of the right eye, and the green line indicates the position of the left fovea in schematic eyes that have a 5º visio-optical angle.

10.5.3 Chromatic difference in object size

The results for the chromatic difference in object size $\delta\left(\Delta y_{\mathrm{O}}\right)$ are similar to those in Section 10.5.1 and are given in Table 10.5.6. The relationships are all linear. One can think of the δX_{Oy} as having a magnifying effect on the image size to obtain the chromatic difference in object size.

Table 10.5.6 Chromatic difference in object size for Le Grand's eye and the reduced eye for the three illustrative working distances.

	Le Grand's eye	Reduced eye
–3 m	$\delta(\Delta y_{\mathrm{O}}) = -1.3630\,\Delta y_{\mathrm{R}}$	$\delta(\Delta y_{\mathrm{O}}) = -1.5010\,\Delta y_{\mathrm{R}}$
–2 m	$\delta(\Delta y_{\mathrm{O}}) = -0.9087\,\Delta y_{\mathrm{R}}$	$\delta(\Delta y_{\mathrm{O}}) = -1.0006\,\Delta y_{\mathrm{R}}$
–0.5 m	$\delta(\Delta y_{\mathrm{O}}) = -0.2273\,\Delta y_{\mathrm{R}}$	$\delta(\Delta y_{\mathrm{O}}) = -0.2502\,\Delta y_{\mathrm{R}}$

10.5.4 Chromatic difference in object angular spread

The numerical results for chromatic difference in object angular spread $\delta(\Delta a_{\mathrm{O}})$ are similar to those in Section 10.5.2 for the illustrative examples and are therefore given in Table 10.5.7. Again, the relationships are all linear and because δZ_{Oy} is independent of working distance, we obtain one relationship for each of Le Grand's and the reduced eyes.

Table 10.5.7 Chromatic difference in object angular spread for Le Grand's eye and the reduced eye for the three illustrative working distances.

Le Grand's eye	Reduced eye
$\delta(\Delta a_{\mathrm{O}}) = (4.5429\times10^{-4}\ \mathrm{kD})\,\Delta y_{\mathrm{R}}$	$\delta(\Delta a_{\mathrm{O}}) = (5.0032\times10^{-4}\ \mathrm{kD})\,\Delta y_{\mathrm{R}}$

10.5.5 Chromatic magnification in object space

Le Grand's eye

The chromatic object size magnification M_{yO} (Equation 7.5.15) defines the magnification of the size of the red to blue objects. M_{yO} is 1.0076 for objects at –3 and –2 m and 1.0075 for an object at –0.5m from the eye. The chromatic object angular spread magnification M_{aO} (Equation 7.5.18) defines the magnification of the angular spread subtended by the red object to the angular spread of the blue object where both images appear to be the same size at the retina and is 1.0076. Because the bottom row of $\mathbf{V}_{\mathrm{aO}}$ is independent of z_{O}, M_{aO} is independent of object distance. These both equate to 0.75% magnification where the blue object is larger than the red object. That is $\Delta y_{\mathrm{O}}^{\mathrm{b}} > \Delta y_{\mathrm{O}}^{\mathrm{r}}$ from Equation 7.5.13 and $\Delta a_{\mathrm{O}}^{\mathrm{b}} > \Delta a_{\mathrm{O}}^{\mathrm{r}}$ from Equation 7.5.16.

The reduced eye

For the reduced eye, M_{yO} is 1.0083 for all three illustrative distances and M_{aO} is 1.0084. These equate to 0.83% and 0.84% with the blue object larger than the red object.

10.6 Chromatic properties of the eye dependent on image and aperture positions in object space: with a pinhole

Experimental measurements in object space, as seen in Chapter 2, include the effect of placing a pinhole immediately in front of the eye. The coefficient matrix, $\mathbf{V}_{\mathrm{Oy}}^{\mathrm{P}}$ simplifies to Equation 5.3.19 and is given in Tables 10.6.1 and 2 for Le Grand's eye and the reduced eye respectively. The chromatic difference of the coefficient matrices $\delta\mathbf{V}_{\mathrm{Oy}}^{\mathrm{P}}$ is summarised in Table 10.6.3.

10.6.1 Chromatic difference in object positions: with a pinhole

The chromatic difference in object positions δy_{O} is dependent on image y_{R} and aperture positions y_{P}. The effect of change in aperture position on δy_{O} is direct with respect to y_{P} and indirect in that the longitudinal displacement from the pupil to the corneal plane is incorporated in $\mathbf{V}_{\mathrm{Oy}}^{\mathrm{P}}$. Because the coefficient matrices for the eye with the pinhole $\mathbf{V}_{\mathrm{Oy}}^{\mathrm{P}}$ and measurements in object space are derived from the coefficient matrix for the chromatic properties in object space $\mathbf{V}_{\mathrm{Oy}}$, the bottom row is again independent of z_{O}. The equations for δy_{O} for the three illustrative distances of the object in front of the eye are given in Tables 10.6.4 and 5 for Le Grand's eye and the reduced eye respectively. In the right-hand column of each table is the illustrative value calculated by a 4mm displacement of the pinhole immediately in front of the cyclopleged eye $\left(y_{\mathrm{P}} = 4\ \mathrm{mm}\right)$ and assuming that the image points are both directed at the same point on the retina. The illustrative values are given for an eye with, firstly, the fovea centred on the longitudinal axis $y_{\mathrm{R}} = 0\ \mathrm{mm}$ and, secondly, with the fovea positioned at 1.46 mm to approximate a visio-optical angle of 5°.

Table 10.6.1 The red and blue coefficient matrices for chromatic properties of Le Grand's eye in object space dependent on image and aperture positions for objects at the finite distances of 3, 2 and 0.5 metres, with a pinhole placed immediately in front of the eye.

		Red	Blue
$\mathbf{V}^{\mathrm{P}}_{\mathrm{Oy}}$	–3 m	$\begin{pmatrix} 2.4023 & -179.3441 \\ -4.6744\times10^{-4}\ \mathrm{kD} & 0.05978\ \mathrm{kD} \end{pmatrix}$	$\begin{pmatrix} -3.3015 & -181.7471 \\ 1.4338\times10^{-3}\ \mathrm{kD} & 0.06058\ \mathrm{kD} \end{pmatrix}$
$\mathbf{V}^{\mathrm{P}}_{\mathrm{Oy}}$	–2 m	$\begin{pmatrix} 1.9349 & -119.5628 \\ -4.6744\times10^{-4}\ \mathrm{kD} & 0.05978\ \mathrm{kD} \end{pmatrix}$	$\begin{pmatrix} -1.8677 & -121.1647 \\ 1.4338\times10^{-3}\ \mathrm{kD} & 0.06058\ \mathrm{kD} \end{pmatrix}$
$\mathbf{V}^{\mathrm{P}}_{\mathrm{Oy}}$	–0.5 m	$\begin{pmatrix} 1.2337 & -29.89072 \\ -4.6744\times10^{-4}\ \mathrm{kD} & 0.05978\ \mathrm{kD} \end{pmatrix}$	$\begin{pmatrix} 0.2831 & -30.2912 \\ 1.4338\times10^{-3}\ \mathrm{kD} & 0.06058\ \mathrm{kD} \end{pmatrix}$

Table 10.6.2 The red and blue coefficient matrices for chromatic properties of the reduced eye in object space dependent on image and aperture positions for objects at the finite distances of 3, 2 and 0.5 metres, with a pinhole placed immediately in front of the eye.

		Red	Blue
$\mathbf{V}^{\mathrm{P}}_{\mathrm{Oy}}$	–3 m	$\begin{pmatrix} 2.2556 & -179.5815 \\ -4.1855\times10^{-4}\ \mathrm{kD} & 0.05986\ \mathrm{kD} \end{pmatrix}$	$\begin{pmatrix} -4.0387 & -181.6796 \\ 1.6796\times10^{-3}\ \mathrm{kD} & 0.06056\ \mathrm{kD} \end{pmatrix}$
$\mathbf{V}^{\mathrm{P}}_{\mathrm{Oy}}$	–2 m	$\begin{pmatrix} 1.8371 & -119.7210 \\ -4.1855\times10^{-4}\ \mathrm{kD} & 0.05986\ \mathrm{kD} \end{pmatrix}$	$\begin{pmatrix} -2.3591 & -121.1197 \\ 1.6796\times10^{-3}\ \mathrm{kD} & 0.06056\ \mathrm{kD} \end{pmatrix}$
$\mathbf{V}^{\mathrm{P}}_{\mathrm{Oy}}$	–0.5 m	$\begin{pmatrix} 1.2093 & -29.9302 \\ -4.1855\times10^{-4}\ \mathrm{kD} & 0.05986\ \mathrm{kD} \end{pmatrix}$	$\begin{pmatrix} 0.1602 & -30.2799 \\ 1.6796\times10^{-3}\ \mathrm{kD} & 0.06056\ \mathrm{kD} \end{pmatrix}$

Table 10.6.3 The chromatic difference in coefficient matrices for chromatic properties of the eye in object space dependent on image and aperture positions for Le Grand's and the reduced eye for objects at the finite distances of 3, 2 and 0.5 metres, with a pinhole placed immediately in front of the eye.

		Le Grand's eye	Reduced eye
$\delta\mathbf{V}^{\mathrm{P}}_{\mathrm{Oy}}$	–3 m	$\begin{pmatrix} -5.7038 & -2.4030 \\ 1.9013\times10^{-3}\ \mathrm{kD} & 8.0099\times10^{-4}\ \mathrm{kD} \end{pmatrix}$	$\begin{pmatrix} -6.2943 & -2.0981 \\ 2.0981\times10^{-3}\ \mathrm{kD} & 6.9937\times10^{-4}\ \mathrm{kD} \end{pmatrix}$
$\delta\mathbf{V}^{\mathrm{P}}_{\mathrm{Oy}}$	–2 m	$\begin{pmatrix} -3.8025 & -1.6020 \\ 1.9013\times10^{-3}\ \mathrm{kD} & 8.0099\times10^{-4}\ \mathrm{kD} \end{pmatrix}$	$\begin{pmatrix} -4.1962 & -1.3987 \\ 2.0981\times10^{-3}\ \mathrm{kD} & 6.9937\times10^{-4}\ \mathrm{kD} \end{pmatrix}$
$\delta\mathbf{V}^{\mathrm{P}}_{\mathrm{Oy}}$	–0.5 m	$\begin{pmatrix} -0.9506 & -0.4005 \\ 1.9013\times10^{-3}\ \mathrm{kD} & 8.0099\times10^{-4}\ \mathrm{kD} \end{pmatrix}$	$\begin{pmatrix} -1.0491 & -0.3497 \\ 2.0981\times10^{-3}\ \mathrm{kD} & 6.9937\times10^{-4}\ \mathrm{kD} \end{pmatrix}$

Table 10.6.4 The equations for the chromatic difference in object position δy_O for Le Grand's eye for objects at the finite distances of –3, –2 and –0.5 m from the eye and pinhole displaced by $y_P = 4$ mm.

	Chromatic difference in object position	Illustrative values	
		$y_R = 0$ mm	$y_R = 1.46$ mm
–3 m	$\delta y_O = (-5.7038)y_P + (-2.4030)y_R$	–22.8153 mm	–26.3236 mm
–2 m	$\delta y_O = (-3.8025)y_P + (-1.6020)y_R$	–15.2102 mm	–17.5491 mm
–0.5 m	$\delta y_O = (-0.9506)y_P + (-0.4005)y_R$	–3.8025 mm	–4.3873 mm

Table 10.6.5 The equations for δy_O for the reduced eye for objects at the finite distances of –3, –2 and –0.5 m from the eye. The illustrative values are for an eye with $y_P = 4$ mm and $y_R = 0$ mm or $y_R = 1.46$ mm.

	Chromatic difference in object position	Illustrative values	
		$y_R = 0$ mm	$y_R = 1.46$ mm
–3 m	$\delta y_O = (-6.2943)y_P + (-2.0981)y_R$	–25.1773 mm	–28.2406 mm
–2 m	$\delta y_O = (-4.1962)y_P + (-1.3987)y_R$	–16.7849 mm	–18.8271 mm
–0.5 m	$\delta y_O = (-1.0491)y_P + (-0.3497)y_R$	–4.1962 mm	–4.7068 mm

Figure 10.6.1 gives δy_O as a function of pinhole displacement at the corneal plane for the three illustrative distances from the eye. The image is superimpose on the retina at $y_R = 0$ mm. Not only does δy_O increase as the object points move further away from the eye, but the magnitudes of the illustrative values using a pinhole are greater than those for the eye without the pinhole, given in Section 10.5.1.

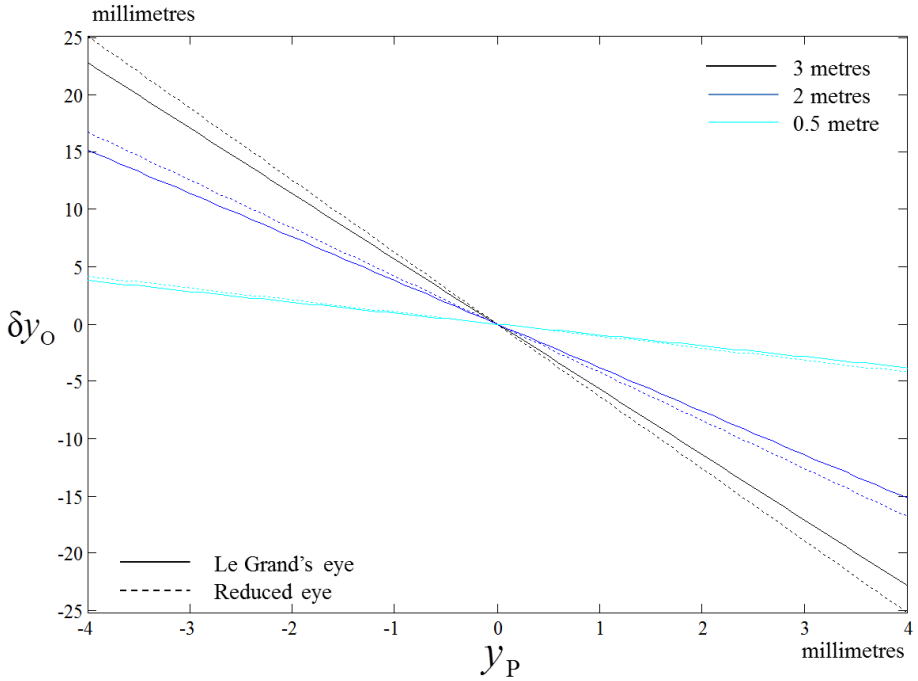

Figure 10.6.1 Chromatic difference in object positions δy_O between the red and blue object points as a function of transverse displacement of the pinhole y_P at three illustrative object distances from the eye, –3 m in black, –2 m in blue and –0.5 m in cyan.

10.6.2 Chromatic difference in inclination in object space: with a pinhole

The chromatic difference in inclination in object space δa_O is dependent on image and aperture positions. δa_O is independent of z_O and therefore we obtain one equation for each model eye. The chromatic difference in inclination in object space is

$$\delta a_O = \left(1.9013\times10^{-3}\ \text{kD}\right)y_P + \left(8.0099\times10^{-4}\ \text{kD}\right)y_R \qquad (10.6.1)$$

for Le Grand's eye and

$$\delta a_O = \left(2.0981\times10^{-3}\ \text{kD}\right)y_P + \left(6.9937\times10^{-4}\ \text{kD}\right)y_R \qquad (10.6.2)$$

for the reduced eye. For the illustrative situation of $y_P = 4\,\text{mm}$ combined with firstly $y_R = 0\,\text{mm}$, then $y_R = 1.46\,\text{mm}$, the chromatic difference in inclination in object space is 7.6051×10^{-3} and 8.7745×10^{-3} respectively for Le Grand's eye and 8.3924×10^{-3} and 9.4135×10^{-3} respectively for the reduced eye. From Equations 10.6.1 and 2 we can see that δa_O is linearly dependent on y_P. For any particular constant distance of the object points from the eye, y_P is "magnified"

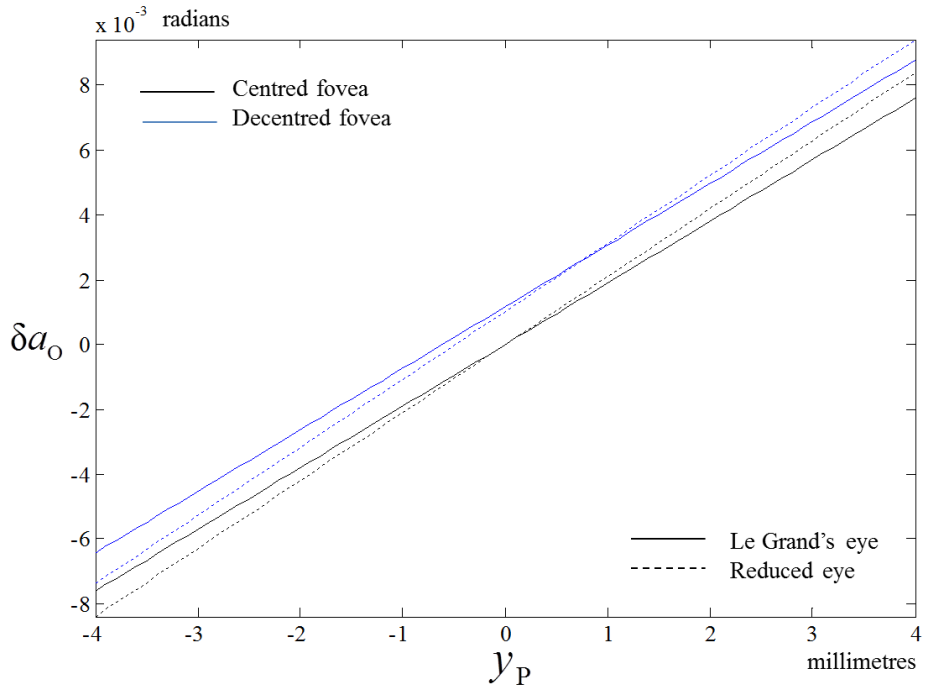

Figure10.6.2 The chromatic difference in inclination in object space δa_{O} as a function of transverse pinhole displacement y_{P} for Le Grand's eye (solid lines) and the reduced eye (dashed lines). The black lines represent the variation in inclination when the fovea is centred on the optical axis $y_{\mathrm{R}} = 0$ and the blue lines represent the fovea some 1.46 mm from the optical axis; that is at $y_{\mathrm{R}} = 1.46\ \mathrm{mm}$ (left eye).

by a constant, δY_{Oy}, the chromatic difference in the near directional spread coefficient and the slope of the line in Figure 10.6.2. If the red and blue image points are superimposed on the fovea, that is to say $y_{\mathrm{R}} = 1.46\ \mathrm{mm}$, then this will merely add a fixed value to the chromatic difference in object inclination which will still vary by y_{P}. This is illustrated graphically in Figure 10.6.2 by the blue lines. Similarly, any point in the peripheral retina can be chosen such that $y_{\mathrm{R}} \neq 0$.

10.6.3 Chromatic difference in object size: with a pinhole

From Equation 7.5.6, we can see that when a pinhole is placed in front of the eye the effect of any transverse displacement is nullified. The only change will be that created by the longitudinal displacement of the pinhole, that is, from the plane of the pupil to the plane immediately in front of the cornea. The effect of

Table 10.6.6 The chromatic difference in object size for the three illustrative distances for Le Grand's eye and the Reduced eye.

	Le Grand's eye	Reduced eye
–3 m	$\delta(\Delta y_{\mathrm{O}}) = -2.4030\ \Delta y_{\mathrm{R}}$	$\delta(\Delta y_{\mathrm{O}}) = -2.0981\ \Delta y_{\mathrm{R}}$
–2 m	$\delta(\Delta y_{\mathrm{O}}) = -1.6020\ \Delta y_{\mathrm{R}}$	$\delta(\Delta y_{\mathrm{O}}) = -1.3987\ \Delta y_{\mathrm{R}}$
–0.5 m	$\delta(\Delta y_{\mathrm{O}}) = -0.4005\ \Delta y_{\mathrm{R}}$	$\delta(\Delta y_{\mathrm{O}}) = -0.3497\ \Delta y_{\mathrm{R}}$

$\delta X_{\mathrm{Oy}}^{\mathrm{P}}$ is to magnify the image size Δy_{R} to obtain the chromatic difference in object size. This is summarized in Table 10.6.6 for the three working distances.

10.6.4 Chromatic difference in object angular spread: with a pinhole

From Equation 7.5.9 we can see that the chromatic difference in object angular spread is also independent of any transverse displacement of the pinhole y_{P}, and the magnification $\delta Z_{\mathrm{Oy}}^{\mathrm{P}}$ differs from δZ_{Oy} for the chromatic difference in object inclination $\delta(\Delta a_{\mathrm{O}})$ due to the longitudinal displacement of the limiting aperture from the pupil to the pinhole plane. Additionally, the bottom row of $\mathbf{V}_{\mathrm{Oy}}^{\mathrm{P}}$ is independent of z_{O} and therefore the chromatic difference in object angular spread $\delta(\Delta a_{\mathrm{O}})$ with a pinhole is also independent of the distance of the object from the eye. $\delta(\Delta a_{\mathrm{O}})$ is given in Table 10.6.7 for the two schematic eyes. When we compare the values for $\delta Z_{\mathrm{Oy}}^{\mathrm{P}}$ in Table 10.6.7 to those for δZ_{Oy} in Table 10.5.7, we see that introducing a pinhole immediately in front of the eye has a magnifying effect. This is more pronounced in Le Grand's eye than for the reduced eye.

Table 10.6.7 The chromatic difference in angular spread for Le Grand's eye and the reduced eye.

Le Grand's eye	Reduced eye
$\delta(\Delta a_{\mathrm{O}}) = (8.0099\times10^{-4}\ \mathrm{kD})\Delta y_{\mathrm{R}}$	$\delta(\Delta a_{\mathrm{O}}) = (6.9937\times10^{-4}\ \mathrm{kD})\Delta y_{\mathrm{R}}$

10.6.5 Chromatic object magnification: with a pinhole

Chromatic object size magnification

In Section 7.5.3 we obtained the chromatic object size magnification M_{yO} (Equation 7.5.15). When a pinhole is placed immediately in front of the eye, we substitute values for $X_{\mathrm{Oy}}^{\mathrm{P}}$ instead of X_{Oy} into Equation 7.5.15. Both M_{yO} and hence $M_{\mathrm{yO}}^{\mathrm{P}}$ are independent of the transverse position of the pinhole, and $M_{\mathrm{yO}}^{\mathrm{P}}$ is influenced only by the longitudinal displacement of the limiting aperture. For Le Grand's eye $M_{\mathrm{yO}}^{\mathrm{P}}$ is 1.0134 and for the reduced eye $M_{\mathrm{yO}}^{\mathrm{P}}$ is 1.0117. Comparing this to the results obtained without the pinhole, the chromatic magnification has increased from 0.75% to 1.3% and 1.2% respectively, nearly double.

Chromatic object angular spread magnification

The chromatic object angular spread magnification with a pinhole immediately in front of the eye $M_{\mathrm{aO}}^{\mathrm{P}}$ is obtained from Equation 7.5.18, substituting values for $Z_{\mathrm{Oy}}^{\mathrm{P}}$. $M_{\mathrm{aO}}^{\mathrm{P}}$, like M_{aO} is independent of any transverse displacement of the pinhole and any magnification is obtained by placing the pinhole in front of the eye, effectively moving the limiting aperture form the pupillary plane to the corneal plane. For Le Grand's eye $M_{\mathrm{aO}}^{\mathrm{P}}$ is 1.0134 and for the reduced eye we have 1.0117, exactly the same results as for $M_{\mathrm{yO}}^{\mathrm{P}}$. The blue object is larger than the red object, that is, $\Delta y_{\mathrm{O}}^{\mathrm{b}} > \Delta y_{\mathrm{O}}^{\mathrm{r}}$ from Equation 7.5.13 and $\Delta a_{\mathrm{O}}^{\mathrm{b}} > \Delta a_{\mathrm{O}}^{\mathrm{r}}$ from Equation 7.5.16.

10.7 Underlying implications

There are two underlying implications which do not appear to be addressed in the literature. Firstly, a chromatic difference in incident position occurs when measuring chromatic difference in position at the retina. The effect is null when a pinhole is introduced in front of the eye. Secondly, there is a chromatic difference in inclination at the retina when measuring the chromatic difference in object positions or inclinations. This effect is null for the reduced

eye. The effects are small and only apparent in eyes with more than one refracting surface and hence, real eyes.

10.7.1 Chromatic difference in incident position

In Section 7.2.2 we defined chromatic difference in image positions at the retina when a pencil of rays is incident at the cornea with inclination a_{K}. We noted that while the red and blue rays both traverse the same transverse position through the pupil, y_{P}, this does not necessarily mean that the red and blue rays originate from the same dichromatic ray that is incident on the eye or cornea. Instead, there are separate red and blue rays, each with incident inclination a_{K} which are refracted and traced through the same position through the limiting aperture y_{P}. This is illustrated in Figure 7.2.1 where we see separate red and blue rays intersecting the cornea, separated by distance δy_{K} and then traversing the pupil through the same point, but with different inclinations.

Equation 7.2.9 enables us to calculate the chromatic difference in corneal position δy_{K}, incident onto the eye, of the red and blue rays from a distance object and Equation 7.2.10 likewise calculates the chromatic difference in incident position δy_{K} for rays originating from an object at a finite distance. Substituting from the red and blue transferences for the anterior and posterior subsystems and the transference for the eye, we obtain a relationship for Le Grand's eye, given in Table 10.7.1. The chromatic difference of incident position δy_{K} is given as an illustrative example for a centred model eye $y_{\mathrm{P}} = 0$ with incident inclination of $a_{\mathrm{K}} = 0.1$, in Table 10.7.1. $\delta y_{\mathrm{K}} = 0.02061\,\mathrm{mm}$ represents a distance of more than 5 000 times the wavelength of the blue ray or almost 3 000 times the wavelength of the red ray.

For the reduced eye with a pupil the equivalent equation for the chromatic difference of incident position δy_{K} for a distant object is given as a relationship in Table 10.7.2. The illustrative value for the reduced eye is also given in Table 10.7.2 for an example where $y_{\mathrm{P}} = 0$ and $a_{\mathrm{K}} = 0.1$.

Table 10.7.1 The chromatic difference in incident position for Le Grand's eye for an object point positioned –3 m, –2 m and –0.5 m from the eye and illustrated with $y_{\mathrm{O}} = 200\ \mathrm{mm}$ and $y_{\mathrm{P}} = 0\ \mathrm{mm}$.

Distance from eye	Chromatic difference in incident position	Illustrative value
Distant object	$\delta y_K = (0.02061\ \mathrm{mm})a_{\mathrm{K}} + 0.004887\, y_{\mathrm{P}}$	0.002061 mm
–3 m	$\delta y_K = -6.8576\times10^{-6}\, y_{\mathrm{O}} - 0.004890\, y_{\mathrm{P}}$	–0.001372 mm
–2 m	$\delta y_K = -1.0276\times10^{-5}\, y_{\mathrm{O}} - 0.004891\, y_{\mathrm{P}}$	–0.002055 mm
–0.5 m	$\delta y_K = -4.0733\times10^{-5}\, y_{\mathrm{O}} - 0.004904\, y_{\mathrm{P}}$	–0.008147 mm

Table 10.7.2 The chromatic difference in incident position for the reduced eye for an object point positioned –3 m, –2 m and –0.5 m from the eye and illustrated with $y_{\mathrm{O}} = 200\ \mathrm{mm}$ and $y_{\mathrm{P}} = 0\ \mathrm{mm}$.

Distance from eye	Chromatic difference in incident position	Illustrative value
Distant object	$\delta y_K = (0.01312\ \mathrm{mm})a_{\mathrm{K}} + 0.003614\, y_{\mathrm{P}}$	0.001312 mm
–3 m	$\delta y_K = -4.3685\times10^{-6}\, y_{\mathrm{O}} - 0.003617\, y_{\mathrm{P}}$	-8.7370×10^{-4} mm
–2 m	$\delta y_K = -6.5493\times10^{-6}\, y_{\mathrm{O}} - 0.003618\, y_{\mathrm{P}}$	–0.001310 mm
–0.5 m	$\delta y_K = -2.6074\times10^{-5}\, y_{\mathrm{O}} - 0.003631\, y_{\mathrm{P}}$	–0.005215mm

For an object at a finite distance, we summarize the three illustrative distances of the object from the eye in Table 10.7.1 for Le Grand's eye and Table 10.7.2 for the reduced eye. The illustrative values are given for an object point that is placed $y_{\mathrm{O}} = 200\ \mathrm{mm}$ above the longitudinal axis and assuming that the eye is centred.

Chromatic difference in incident position with pinhole

When a pinhole is placed in front of the eye the chief ray is the ray traversing the centre of the pinhole, which is placed immediately in front of the eye. Equations 7.2.9 and 10 both simplify to $\delta y_K = (0\ \mathrm{mm})$ and, as expected, there is no chromatic difference in incident position present when a pinhole is placed in front of either model eye.

10.7.2 Chromatic difference in emergent inclination from object space

Equation 7.4.13 was derived to calculate the chromatic difference in inclination of the two rays that traverse, from separated object points through the same position in the pupil or pinhole and arrive at the retina at the same position, that is to say $y_{\mathrm{R}}^{\mathrm{r}} = y_{\mathrm{R}}^{\mathrm{b}}$. For convenience, the chief rays are usually chosen. However, Equation 7.4.13 shows that the two rays are refracted differently and do indeed follow different paths through the system. Although the red and blue rays, by definition, are chosen to both traverse the same position through the aperture, they may not necessarily traverse through this aperture with the same inclination and will not arrive at the retina with the same inclination. This is illustrated in Figure 7.4.1 and has implications for the Stiles-Crawford effects. For Le Grand's eye, the chromatic difference in inclination at the retina will be

$$\delta a_{\mathrm{R}} = \left(-8.2635\times10^{-5}\ \mathrm{kD}\right)y_{\mathrm{P}} + \left(7.3139\times10^{-6}\ \mathrm{kD}\right)y_{\mathrm{R}} \qquad (10.7.1)$$

which is independent of the distance of the object in front of the eye. For a centred model eye ($y_{\mathrm{P}} = 0\ \mathrm{mm}$) with the fovea $y_{\mathrm{R}} = 1.46\ \mathrm{mm}$ from the optical axis, this is a chromatic difference in inclination at the fovea of $\delta a_{\mathrm{R}} = 1.0678\times10^{-5}$. When a pinhole is placed in front of the eye, Equation 7.4.13 becomes

$$\delta a_{\mathrm{R}} = \left(-1.3746\times10^{-4}\ \mathrm{kD}\right)y_{\mathrm{P}} + \left(-2.4013\times10^{-5}\ \mathrm{kD}\right)y_{\mathrm{R}}. \qquad (10.7.2)$$

For a pinhole in front of the cyclopleged Le Grand model eye with transverse displacement of $y_{\mathrm{P}} = 4\ \mathrm{mm}$, the chromatic difference in inclination at the optical axis ($y_{\mathrm{R}} = 0\ \mathrm{mm}$) is $\delta a_{\mathrm{R}} = -5.4984\times10^{-4}$ and at the fovea ($y_{\mathrm{R}} = 1.46\ \mathrm{mm}$) it increases in magnitude to $\delta a_{\mathrm{R}} = -5.8490\times10^{-4}$. However, we note that the direction changes when a pinhole is introduced. When light traverses the pupil, the blue and red rays appear as shown in Figure 7.4.1, however, when a pinhole is introduced the red and blue are swopped. This too has implications for the Stiles-Crawford effects.

The reduced eye, being a much simplified model, has no refractive elements posterior of the "pupil" and therefore Equation 7.4.13 simplifies to

$$\delta a_{\mathrm{R}} = \left(0\ \mathrm{kD}\right)y_{\mathrm{P}} + \left(0\ \mathrm{kD}\right)y_{\mathrm{R}} \qquad (10.7.3)$$

and the reduced eye has zero chromatic difference in inclination at the retina. The same result occurs when a pinhole is placed in front of the reduced eye.

10.8 Summary of dependent chromatic properties

In Sections 10.3 to 10.6 we explored the chromatic properties of Le Grand's and the reduced eye dependent on object or image and aperture position, both with and without a pinhole, for an object at a selection of working distances. All these examples can quickly become overwhelming and confusing, however, it soon becomes clear that all the chromatic difference relationships are linear in nature. The two model eyes tell the same story, however, the slope of the straight line is slightly different each time.

The distant object situation is described in terms of the incident inclination a_{K} however the objects at a finite working distance are described in terms of object position, directly by the object's transverse position y_{O} and indirectly by incorporating the working distance z_{O} into the coefficient matrices, $\mathbf{V}_{\mathrm{OE}}$, $\mathbf{V}_{\mathrm{OE}}^{\mathrm{P}}$, $\mathbf{V}_{\mathrm{yO}}$ and $\mathbf{V}_{\mathrm{yO}}^{\mathrm{P}}$. The combination of y_{O} and z_{O} to describe the object position can be summarily described by the incident inclination a_{K}. The relationship can be simply obtained by $\mathbf{S}_{\mathrm{O}}\boldsymbol{\rho}_{\mathrm{O}} = \boldsymbol{\rho}_{\mathrm{K}}$. Multiplying this out

$$\begin{pmatrix} 1 & -\zeta_{\mathrm{O}} \\ 0 & 1 \end{pmatrix}\begin{pmatrix} y_{\mathrm{O}} \\ \alpha_{\mathrm{O}} \end{pmatrix} = \begin{pmatrix} y_{\mathrm{K}} \\ \alpha_{\mathrm{K}} \end{pmatrix}$$

to obtain

$$\begin{pmatrix} y_{\mathrm{O}} - \zeta_{\mathrm{O}}\alpha_{\mathrm{O}} \\ \alpha_{\mathrm{O}} \end{pmatrix} = \begin{pmatrix} y_{\mathrm{K}} \\ \alpha_{\mathrm{K}} \end{pmatrix}$$

and solving for a_{K} we obtain

$$a_{\mathrm{K}} = \frac{y_{\mathrm{K}} - y_{\mathrm{O}}}{-z_{\mathrm{O}}}. \qquad (10.8.1)$$

From Equation 10.8.1 we can look at the distant object situation and draw conclusions that are general for all systems.

Below we summarise the chromatic properties that are dependent on object or image and apertures position. We divide this summary into three sections, firstly the chromatic difference in image position, inclination, size and angular spread, secondly the chromatic difference in object position, inclination, size and angular spread and finally the chromatic magnifications. For the chromatic differences in image and object space, the two eyes only differ in the

magnitude of the slope and so we will narrow the summary down to only Le Grand's eye.

10.8.1 Chromatic differences in image space

Chromatic difference in image position and inclination

The chromatic difference in image positions δy_{R} and inclinations δa_{R} were summarised by Equation 7.2.22. Substituting for $\delta\mathbf{V}_{\mathrm{E}}$ from Table 10.3.3 into Equation 7.2.22, we obtain

$$\begin{pmatrix} -0.03568 & -0.1258\ \mathrm{mm} \\ -0.001822\ \mathrm{kD} & -0.006011 \end{pmatrix}\begin{pmatrix} y_{\mathrm{P}} \\ a_{\mathrm{K}} \end{pmatrix}=\begin{pmatrix} \delta y_{\mathrm{R}} \\ \delta a_{\mathrm{R}} \end{pmatrix}. \tag{10.8.2}$$

This summarises Figures 10.3.1 and 3, which are very similar. Assuming a centred eye ($y_{\mathrm{P}}=0$), both δy_{R} and δa_{R} have a linear relationship with a_{K} with a negative slope. A decentred pupil will merely add a constant value to δy_{R} and δa_{R}, but the slope will not change.

When a pinhole is placed immediately in front of Le Grand's eye the values in $\delta\mathbf{V}_{\mathrm{E}}$ change due to the longitudinal displacement of the limiting aperture. Equation 10.8.2 becomes

$$\begin{pmatrix} -0.03149 & -0.2212\ \mathrm{mm} \\ -0.001414\ \mathrm{kD} & -9.3691\times10^{-3} \end{pmatrix}\begin{pmatrix} y_{\mathrm{P}} \\ a_{\mathrm{K}} \end{pmatrix}=\begin{pmatrix} \delta y_{\mathrm{R}} \\ \delta a_{\mathrm{R}} \end{pmatrix}. \tag{10.8.3}$$

From Equation 10.8.3 we can see that any increase in incident inclination when a pinhole is placed in front of the eye will magnify the δy_{R} and δa_{R} more than for the naked eye and any transverse movement of the pinhole will very slightly increase the effect on the δy_{R} and δa_{R}. However, the magnitude of y_{P} is potentially far greater for a pinhole than for a pupil. This can be seen in Figures 10.4.1 and 2 where it is evident that the working distance has very little effect for an axial object. The effect of adding a pinhole at the corneal plane is to potentially increase δy_{R} and δa_{R}. This has implications for the AcuFocus Kamra corneal pinhole inlay.

Chromatic difference in image size and angular spread

The chromatic difference in image size $\delta(\Delta y_{\mathrm{R}})$ and angular spread $\delta(\Delta a_{\mathrm{R}})$ were summarised by Equation 7.3.13. Substituting for $\delta\mathbf{V}_{\mathrm{E}}$ from Table 10.3.3 into Equation 7.3.13, we obtain

$$\begin{pmatrix} -0.03568 & -0.1258\ \mathrm{mm} \\ -0.001822\ \mathrm{kD} & -0.006011 \end{pmatrix}\begin{pmatrix} 0 \\ \Delta a_{\mathrm{K}} \end{pmatrix} = \delta\begin{pmatrix} \Delta y_{\mathrm{R}} \\ \Delta a_{\mathrm{R}} \end{pmatrix} \tag{10.8.4}$$

which is very similar to Equation 10.8.2. $\delta(\Delta y_{\mathrm{R}})$ and $\delta(\Delta a_{\mathrm{R}})$ are independent of pupil (or pinhole) position. The relationships are linear, Δa_{K} is magnified by δX_{E} or δZ_{E} to obtain $\delta(\Delta y_{\mathrm{R}})$ and $\delta(\Delta a_{\mathrm{R}})$ respectively.

For a pinhole in front of the eye we obtain

$$\begin{pmatrix} -0.03149 & -0.2212\ \mathrm{mm} \\ -0.001414\ \mathrm{kD} & -9.3691\times10^{-3} \end{pmatrix}\begin{pmatrix} 0 \\ \Delta a_{\mathrm{K}} \end{pmatrix} = \delta\begin{pmatrix} \Delta y_{\mathrm{R}} \\ \Delta a_{\mathrm{R}} \end{pmatrix} \tag{10.8.5}$$

and while the transverse displacement of the pinhole will have no effect on $\delta(\Delta y_{\mathrm{R}})$ and $\delta(\Delta a_{\mathrm{R}})$, the longitudinal change in position of the limiting aperture will create a magnified effect of $\delta(\Delta y_{\mathrm{R}})$ and $\delta(\Delta a_{\mathrm{R}})$, as can be seen by the increase in magnitude of $\delta X_{\mathrm{E}}^{\mathrm{P}}$ and $\delta Z_{\mathrm{E}}^{\mathrm{P}}$ from δX_{E} and δZ_{E} respectively.

10.8.2 Chromatic difference in object space

Chromatic difference in object position and inclination

The object space scenario was derived to mimic the experimental situation and as a result has been limited to finite working distances. The chromatic difference in object position δy_{O} and inclination δa_{O} is summarised by Equation 7.4.10. Substituting for $\delta\mathbf{V}_{\mathrm{Oy}}$ at $z_{\mathrm{O}} = -3\ \mathrm{m}$ from Table 10.5.3 for Le Grand's eye into Equation 7.4.10 we obtain

$$\begin{pmatrix} -6.4461 & -1.3630 \\ 2.1482\times10^{-3}\ \mathrm{kD} & 4.5429\times10^{-4}\ \mathrm{kD} \end{pmatrix}\begin{pmatrix} y_{\mathrm{P}} \\ y_{\mathrm{R}} \end{pmatrix} = \begin{pmatrix} \delta y_{\mathrm{O}} \\ \delta a_{\mathrm{O}} \end{pmatrix}. \tag{10.8.6}$$

Equation 10.8.6 summarises Figures 10.5.1 and 2; the peripheral retina experiences greater magnitudes of chromatic difference in position or inclination than the posterior pole. From Figure 7.4.1 it is easy to see that δy_{O} and δa_{O} will have opposite signs. We recall from Equation 5.3.14 that the bottom row of $\delta\mathbf{V}_{\mathrm{Oy}}$

is independent of working distance z_{O}, making δa_{O} easier to compare across studies.

With a pinhole and substituting $\delta\mathbf{V}_{\mathrm{Oy}}^{\mathrm{P}}$ at $z_{\mathrm{O}} = -3\,\mathrm{m}$ from Table 10.6.3, Equation 7.4.12 becomes

$$\begin{pmatrix} -5.7038 & -2.4030 \\ 1.9013\times10^{-3}\ \mathrm{kD} & 8.0099\times10^{-4}\ \mathrm{kD} \end{pmatrix}\begin{pmatrix} y_{\mathrm{P}} \\ y_{\mathrm{R}} \end{pmatrix} = \begin{pmatrix} \delta y_{\mathrm{O}} \\ \delta a_{\mathrm{O}} \end{pmatrix} \tag{10.8.7}$$

which summarises Figures 10.6.1 and 2. We draw similar conclusions to the image space situation; δy_{O} and δa_{O} will increase in magnitude with an increase in transverse pinhole displacement or with distance at the retina from the posterior pole.

Chromatic difference in object size and angular spread

The chromatic difference in object size $\delta(\Delta y_{\mathrm{O}})$ and angular spread $\delta(\Delta a_{\mathrm{O}})$ is summarised by Equation 7.5.10. Substituting $\delta\mathbf{V}_{\mathrm{Oy}}$ at $z_{\mathrm{O}} = -3\,\mathrm{m}$ from Table 10.5.3 into Equation 7.5.10 we obtain

$$\begin{pmatrix} -6.4461 & -1.3630 \\ 2.1482\times10^{-3}\ \mathrm{kD} & 4.5429\times10^{-4}\ \mathrm{kD} \end{pmatrix}\begin{pmatrix} 0 \\ \Delta y_{\mathrm{R}} \end{pmatrix} = \delta\begin{pmatrix} \Delta y_{\mathrm{O}} \\ \Delta a_{\mathrm{O}} \end{pmatrix} \tag{10.8.8}$$

which, as expected, resembles Equation 10.8.6. Similar to δa_{O}, $\delta(\Delta a_{\mathrm{O}})$ is independent of z_{O}. $\delta(\Delta y_{\mathrm{O}})$ and $\delta(\Delta a_{\mathrm{O}})$ are independent of any pupil decentration y_{P}. It is obvious from Equation 10.8.8 that the relationship between $\delta(\Delta y_{\mathrm{O}})$ or $\delta(\Delta a_{\mathrm{O}})$ and retinal image size Δy_{R} is linear.

Placing a pinhole immediately in front of Le Grand's eye merely changes the values of $\delta\mathbf{V}_{\mathrm{Oy}}$ to those of $\delta\mathbf{V}_{\mathrm{Oy}}^{\mathrm{P}}$ so that Equation 10.8.8 becomes

$$\begin{pmatrix} -5.7038 & -2.4030 \\ 1.9013\times10^{-3}\ \mathrm{kD} & 8.0099\times10^{-4}\ \mathrm{kD} \end{pmatrix}\begin{pmatrix} 0 \\ \Delta y_{\mathrm{R}} \end{pmatrix} = \delta\begin{pmatrix} \Delta y_{\mathrm{O}} \\ \Delta a_{\mathrm{O}} \end{pmatrix} \tag{10.8.9}$$

from which we can see that moving the plane of the limiting aperture from the pupillary plane to immediately in front of the cornea will have a magnifying effect on $\delta(\Delta y_{\mathrm{O}})$ and $\delta(\Delta a_{\mathrm{O}})$, by almost double.

10.8.3 Chromatic magnifications

Obtaining a summarised relationship for the chromatic magnifications is messy and one cannot easily obtain a neat and tidy relationship like those for the chromatic differences (Equations 7.2.22, 7.3.13, 7.4.10 and 7.5.10). However, it is apparent that the influence of working distance on chromatic magnifications is so small as to be ignored. Therefore the magnifications are summarised in Table 10.8.1. We recall that chromatic magnification is independent of transverse pupil or pinhole displacement, but placing a pinhole in front of the eye does have a magnifying effect on the chromatic magnification due to the longitudinal placement of the limiting aperture.

As expected, we see from Table 10.8.1 that in image space the red image is larger than the blue image, or subtends a greater angular spread while in object space the blue object is larger than the red object, or subtends a larger angular spread. It is clear that moving the limiting aperture from the pupillary plane to the cornea increases the chromatic magnification, a result that has implications for the AcuFocus Kamra corneal pinhole inlay.

Table 10.8.1 Chromatic magnifications of Le Grand's eye and the reduced eye, firstly as the naked eye followed by placing a pinhole immediately in front of the eye. The percentages in the last column are included as a guide for comparative purposes only and represent the mean of chromatic magnifications for each eye.

	M_{yR}	M_{aR}	M_{yO}	M_{aO}	as %
Le Grand's eye	0.9925	0.9926	1.0076	1.0076	0.76%
– with pinhole	0.9868	0.9862	1.0134	1.0134	1.34%
Reduced eye	0.9917	0.9917	1.0083	1.0084	0.83%
– with pinhole	0.9885	0.9885	1.0117	1.0117	1.16%

10.9 Summary of dependencies

Nearly all the chromatic effects discussed in this chapter are dependent on up to three different variables, as summarised in Table 10.9.1. In particular the summary highlights which chromatic properties are dependent or independent of object distance z_{O} from the eye. Chromatic aberration, independent chromatic properties and chromatic difference in image size and angular spread are all

Table 10.9.1 Summary of the dependence of the chromatic effects on variable parameters. In particular, chromatic aberrations or properties that are dependent on working distance are indicated by ∘ and those independent of working distance are indicated by •. The dependencies are separated into those with an object at distance and those with an object at a finite distance. Dependencies given in a matrix represent the entries of the respective chromatic difference in coefficients. Additional dependencies are also given.

			Distant object		Finite distance		Eq. no.
			z_O	Additional	z_O	Additional	
Chromatic Aberration							
	Longitudinal	δz	•		∘		6.1.1
	Transverse	δy	•	a_K	∘	y_O	6.1.2
Chromatic Properties							
Independent	δF		•		•		7.1.1
Independent	δF_0		•		•		7.1.3
Independent	δA		•		•		7.1.5
Dependent on object and aperture positions	$\delta \mathbf{V}_E \mathbf{v}_E = \delta \mathbf{r}_R$	$\delta \begin{pmatrix} y_R \\ a_R \end{pmatrix}$	$\begin{pmatrix} • & • \\ • & • \end{pmatrix}$	$\begin{pmatrix} y_P \\ a_K \end{pmatrix}$			7.2.22
Dependent on object and aperture positions	$\delta \mathbf{V}_{OE} \mathbf{v}_{OE} = \delta \mathbf{r}_R$	$\delta \begin{pmatrix} y_R \\ a_R \end{pmatrix}$			$\begin{pmatrix} ∘ & ∘ \\ ∘ & ∘ \end{pmatrix}$	$\begin{pmatrix} y_P \\ y_O \end{pmatrix}$	7.2.24
Dependent on object and aperture positions	$\delta \mathbf{V}_E \Delta \mathbf{v}_E = \delta \Delta \mathbf{r}_R$	$\delta \begin{pmatrix} \Delta y_R \\ \Delta a_R \end{pmatrix}$	$\begin{pmatrix} • & • \\ • & • \end{pmatrix}$	$\begin{pmatrix} • \\ \Delta a_K \end{pmatrix}$			7.3.13
Dependent on object and aperture positions	$\delta \mathbf{V}_{OE} \Delta \mathbf{v}_{OE} = \delta \Delta \mathbf{r}_R$	$\delta \begin{pmatrix} \Delta y_R \\ \Delta a_R \end{pmatrix}$			$\begin{pmatrix} ∘ & ∘ \\ ∘ & ∘ \end{pmatrix}$	$\begin{pmatrix} • \\ \Delta y_O \end{pmatrix}$	7.3.16
Dependent on object and aperture positions	M_{yR}		•		∘		7.3.19 & 20
Dependent on object and aperture positions	M_{aR}		•		∘		7.3.27 & 28
Dependent on image and aperture positions	$\delta \mathbf{V}_{Oy} \mathbf{v}_{Oy} = \delta \mathbf{r}_O$	$\delta \begin{pmatrix} y_O \\ a_O \end{pmatrix}$			$\begin{pmatrix} ∘ & ∘ \\ • & • \end{pmatrix}$	$\begin{pmatrix} y_P \\ y_R \end{pmatrix}$	7.4.10
Dependent on image and aperture positions	$\delta \mathbf{V}_{Oy} \Delta \mathbf{v}_{Oy} = \delta(\Delta \mathbf{r}_O)$	$\delta \begin{pmatrix} \Delta y_O \\ \Delta a_O \end{pmatrix}$			$\begin{pmatrix} ∘ & ∘ \\ • & • \end{pmatrix}$	$\begin{pmatrix} • \\ \Delta y_R \end{pmatrix}$	7.5.10
Dependent on image and aperture positions	M_{yO}				∘		7.5.15
Dependent on image and aperture positions	M_{aO}				•		7.5.18

independent of transverse pupil or pinhole position, y_P. Chromatic aberration is dependent on the conjugate system of object and image positions while the dependent chromatic difference properties depend on object position(s) and position of the centre of the blurred image(s) on the retina. The chromatic

differences in image space are dependent on y_O while those in object space are dependent on y_R. The chromatic magnification for an object at a finite distance is weakly dependent on the working distance and on not on the transverse object and image positions.

10.10 Discussion

The chromatic effects have been explored in this chapter by means of a number of numerical illustrative examples. Two schematic eyes were used in the examples, Le Grand's and the reduced eyes. Where applicable object points were explored at four distances from the eye, that is, for a distant object with $a_K = 0.1$ and at finite distances with of –3, –2 and –0.5m from the eye, each time with $y_O = 0.2$ m. The examples in object space required an image on the retina, and these examples included the three finite distances for the objects from the eye and the image at either $y_R = 0$ mm or $y_R = 1.46$ mm which approximates the position of the fovea at a visio-optical angle of 5º.

From Figure 10.1.1 we saw that the magnitude of δz increases as the object approaches the eye. The relationship is true for both Le Grand's eye and the reduced eye, although the magnitude is generally greater for the reduced eye The magnitude of δy increases as the incident inclination a_O increases, as can be seen from Figures 10.1.2 and 3.

The object or image and aperture-dependent chromatic properties are defined either in image space or object space and each in turn is explored for the naked eye and the eye with a pinhole aperture immediately in front of the eye. The dependence of each of the dependent chromatic properties is summarised in Table 10.9.1.

Finally, two underlying implications arising from the literature are examined. When a pencil of rays is incident on the eye and the red and blue chief rays are traced through the pupil, the incident red and blue rays are distinctly separate by more than 3000 times their wavelength and cannot be assumed to originate from a single dichromatic ray. Furthermore, in the experimental set-up where the red and blue objects are separated in object space and the images are

superimposed at the same position on the retina, the red and blue rays reaching the retina for Le Grand's eye have different inclinations, which may have implications for the Stiles-Crawford effects or other physiological stimulus-response mechanisms that are beyond the scope of this dissertation. The simplified design of the reduced eye nullifies this measurement.

The Stiles-Crawford effects describe the directional sensitivity of the cones. The Stiles-Crawford effects show that the cones are far more sensitive to light that strikes the retina head-on than to light which enters obliquely. The first Stiles-Crawford effect describes how oblique rays appear disproportionately less bright than rays that strike the retina head-on while the second describes that monochromatic rays of different wavelengths appear to have altered hue and saturation when striking the retina obliquely compared to rays striking head-on. The obliquely striking rays produce a different ratio of responses in the three types of cones to a ray that enters head-on. Both Stiles-Crawford effects are produced by directional sensitivity of the cones and may affect object or image and aperture-dependent chromatic properties. (Stiles and Crawford, 1933; Stiles, 1939; Lakshminarayanan, 2009; Westheimer, 2008.)

The chromatic aberrations and object or image and aperture-dependent chromatic properties depend on the transverse and longitudinal position of the object point. The object, image and aperture-dependent chromatic properties are additionally dependent on the longitudinal and transverse displacement of the pupil or pinhole aperture, making their understanding and relationships more complex. The chromatic difference in power, refractive compensation and ametropia are properties of the system alone and are independent of object, image and aperture positions. The object, image and aperture-dependent chromatic properties are defined specially for the eye, while chromatic aberration is defined for systems in general, making chromatic aberration a more general definition.

PART V – CONCLUSION

11 Concluding discussion

11.1 Introduction

We return to the oldest example of chromatic dispersion known to man, the rainbow. We know that the colours are created by chromatic dispersion, but why does the rainbow form a bow shape? The answer lies in the symmetry of the raindrops. Indeed, it is not a bow, but a cone. The bow that we perceive is part of a full circle and the apex of the cone is at the viewer's eye. Each colour forms its own cone, with the red cone outermost and each colour (or frequency) sitting inside the previous cone, with violet being inner-most (Lee and Fraser, 2001:112-113). But this is what is happening in object space.

What happens when an eye looks at a multi-chromatic object point? Is this comparable to the rainbow? Raindrops are spherical and so is the eye. However, in a raindrop as the light enters it is refracted and dispersed, then the light is reflected internally and finally exits the raindrop whilst being refracted and dispersed some more. The rainbow is created by an infinity of rays from the sun being dispersed, refracted and reflected by an infinity of raindrops. In the eye, the light enters and is imaged on the retina after undergoing refraction and dispersion by the eye's structures. (The structure of the eye prevents the light rays from following the same path as they would in a raindrop). So while rainbows and chromatic effects in the eye are both caused by chromatic dispersion, there is a distinct difference between a rainbow and an eye.

11.2 Findings and conclusions

This study is about "The Chromatic Dependence of First-order Optical Properties of the Eye". We saw, in Chapter 3, that the first-order optical properties of the eye can be divided into fundamental properties and derived properties. Therefore the dependence of each of the fundamental properties on frequency and on wavelength is studied. To better understand the relationship between the fundamental properties and their dependence on frequency, we transform the

transference into Hamiltonian space, study the dependence in this linear space and transform the straight line relationships back to a symplectic transference.

Fundamental properties

The chromatic dependence of each of the fundamental properties of the transferences for both the reduced eye and Le Grand's eye as a function of frequency is found to be very nearly linear (Figures 8.1.3). A formula is derived which gives the linear dependence of the transference on the frequency of light. It is given by Equation 8.1.5 where ν is the frequency of light and the constants are given in Tables 8.1.2 and 3 for the reduced eye and Le Grand's eye, respectively. The result of substituting the values into Equation 8.1.5 for any chosen frequency is a transference that is very nearly symplectic with a mean determinant of approximately 1.

When studying the dependence of the fundamental properties on wavelength, the dependence loses it linearity and one cannot derive an equation such as Equation 8.1.5 as a linear function of wavelength with nearly the same level of accuracy (Figure 8.1.8). This confirms what Pease and Barbeito (1989) state, that the linear function of the frequency scale make analysis simpler to compute and understand.

When calculating the refractive index of air as a function of frequency, we see that, firstly, only the dilation (*A*) and divergence (*C*) are affected and that the change in the curve is so slight and so uniform as to be disregarded and the refractive index of air can be equated to 1 (Figures 8.1.4 and 5). Similarly, when the eyes are submerged in water and the dependence of water on the frequency of light is calculated using Cornu's formula, only the dilation and divergence are affected (Figures 8.1.9).

The dependence of each of the entries of the Cayley-transformed transference is graphed as a function of frequency and found to be very nearly linear for both eyes (Figures 8.2.1 and 4). When the three independent entries are graphed on a three-dimensional graph as a function of frequency, we obtain a straight line for the reduced eye and a gently curved line for Le Grand's eye (Figures 8.2.3 and 6). Because of the resultant linearity of each of the entries, a

formula is derived which results in a transference that gives a linear dependence on frequency (Figures 8.2.2 and 5). This is given by Equation 8.2.3 for the Cayley-transformed transference and substituting it into Equation 8.2.2, we obtain the transference with the constants given in Tables 8.2.1 and 2 for the reduced eye and Le Grand's eye in air, respectively. The advantage of Equation 8.2.3 over Equation 8.1.5 is that Equation 8.2.3 has fewer constants and more importantly, is more accurate. Equation 8.2.3 and 2 result in a symplectic transference with a mean determinant of exactly 1 for any chosen frequency.

Similarly, the dependence of the entries of the logarithmic-transformed transference is graphed as a function of frequency and unsurprisingly found to be very nearly linear for both model eyes (Figures 8.2.7 and 9). However, the region that the transformed transference occupies within the Hamiltonian space is different for the Cayley-transformed transference compared to the logarithmic-transformed transference (Figures 8.2.8 and 10). The formula for deriving the transference from the logarithmic-transformed transference as a linear function of frequency is given by Equation 8.2.5 where the constants are given in Table 8.2.5 for the two model eyes (Figures 8.2.11 and 12). The accuracy given by this derivation is similar to that for the Cayley-transformed transference but because of the simplicity of Equation 8.2.2, this is the preferred method.

Derived properties

Next we study the chromatic dependence of a number of derived properties, including cardinal points. Because a relationship between specific derived properties is given by the characteristic matrices, each of these derived properties is studied for its dependence on frequency (Figures 9.2.1 to 5) and the relationship between the entries of each of the symmetric characteristic matrices is displayed as three-dimensional graphs (Figures 9.3.1 to 10). The purpose is two-fold; firstly we wish to understand the dependence of each first-order optical property of the eye on the frequency of light and secondly, we wish to gain a deeper understanding the different linear spaces.

Four characteristic matrices are introduced, each being symmetric and each entry representing a derived property. Five derived properties are of

particular interest and are illustrated graphically for their dependence on the frequency of light. Power F (Equation 3.4.3), entrance- and exit-plane refractive compensation F_0 and F_C (Equations 3.4.6 and 5.1.3) and front-vertex power F_{fv} (Equation 3.4.16) each show a very nearly linear relationship to the frequency of light. Back-vertex power F_{bv}, given by Equation 3.4.11 is representative of vergence at the exit-plane and has a hyperbolic relationship; clearly illustrating which frequency is in focus at the retina. The four characteristic matrices given in Section 3.7.3 represent a linear space and therefore the three independent entries of each characteristic matrix is graphed on a 3-dimensional graph. For the point **P**, angle **Q** and first mixed **M** characteristic matrices the relationship is linear for the reduced eye and nearly linear for Le Grand's eye. The second mixed characteristic matrix **N**, expectedly, was problematic because of the division by *A*, the dilation, which approaches zero for an emmetropic eye.

The dependence of the cardinal and anti-cardinal points on the frequency of light is explored for the two model eyes. For the reduced eye a number of points simplified and we find that the incident and emergent principal and nodal points are independent of frequency. The incident and emergent focal points, anti-principal and anti-nodal points are all dependent on frequency. The chromatic difference between the four red and blue anti-cardinal points all have the same magnitude, the emergent anti-cardinal points having opposite direction to the incident anti-cardinal points (Figures 9.1.1, 3 and 4).

In contrast, for Le Grand's eye we find that all six of the cardinal points and all four of the anti-cardinal points are dependent on frequency and that there is no relationship to the magnitude of the chromatic difference between any of the cardinal or anti-cardinal points (Figures 9.1.2, 5 and 6). This emphasises that while the reduced eye is a convenient simplification, one should be cautious of making conclusions based on the dimensions and mathematics of the reduced eye.

Chromatic aberration and chromatic properties

A study of the chromatic dependence of the first-order optical properties of an eye would be incomplete without a detailed study of chromatic aberration. There are two approaches to defining chromatic aberration, the classical optics

and physiological optics approaches. Both definitions are defined in the literature for Gaussian systems or eyes. In this dissertation we define chromatic aberration for systems in general, that is, systems that may include astigmatic and decentred or tilted elements. Additionally, we define chromatic properties, in line with the physiological optics approach, also generalised for systems with astigmatic elements.

In Gaussian optics longitudinal chromatic aberration is defined as $\delta z = z_{\mathrm{b}} - z_{\mathrm{r}}$, the signed distance from the red image plane to the blue image plane. In an astigmatic system, this is the generalized distance defined as $\delta\mathbf{Z} = \mathbf{Z}_{\mathrm{b}} - \mathbf{Z}_{\mathrm{r}}$ from a matrix representing the red image structure to a matrix representing the blue image structure; each of the red and blue image structures consisting of two orthogonal image line foci, separated by an interval of Sturm. Transverse chromatic aberration is defined as the transverse vector $\delta\mathbf{y} = \mathbf{y}_{\mathrm{b}} - \mathbf{y}_{\mathrm{r}}$, from the transverse position of the red to the blue image structures. In Gaussian optics, it would seem that one could regard longitudinal and transverse chromatic aberration as components of a unified chromatic aberration vector. In linear optics, however, because of their fundamentally different characters (transverse chromatic aberration is a vector and longitudinal chromatic aberration is a matrix) this would not seem possible. Recent research suggests that it may be possible to represent the relationship as a five-dimensional inner-product space (Harris, Evans and van Gool; 2014), however, this is beyond the scope of this dissertation.

The numerical examples give some insight into chromatic aberration, which, because it is based on vergence, is dependent on the object position. Longitudinal chromatic aberration is dependent on the longitudinal object position and transverse chromatic aberration is dependent on both the longitudinal and transverse object position. Longitudinal chromatic aberration increases in magnitude as the object approaches the eye (Figure 10.1.1). Transverse chromatic aberration has a linear dependence on transverse displacement of an object point from the optical axis (Figure 10.1.2 and 3). As the incident inclination increases in magnitude, so the transverse chromatic aberration increases in magnitude (Figure 10.1.4).

The independent chromatic properties of the eye are not dependent on light and therefore not on the object and image positions. They are properties of the system alone and are derived from the fundamental properties of the system. This implies that one will have a single number for each of the definitions with no graph to illustrate any dependence on frequency. The independent chromatic properties of the eye include chromatic difference in power δF, refractive compensation δF_0 and ametropia δA, with derivations obtained from the transference. The results are summarized in Table 10.2.1. Of course, the frequencies chosen for 'red' and 'blue' will influence the results.

Equations are obtained from the transference for the chromatic properties of the eye dependent on the object or image and aperture position. In image space, the chromatic properties dependent on the object and aperture position, derived from the transference, are chromatic difference in transverse image position δy_{R} and inclination at the retina δa_{R}. The chromatic difference in magnification is a misnomer and so we define chromatic difference in image size $\delta(\Delta y_{\mathrm{R}})$ and angular spread $\delta(\Delta a_{\mathrm{R}})$ at the retina. Magnification is a comparative, unitless measure and not defined by a difference. Therefore chromatic magnifications for image size M_{yR} and angular spread M_{aR} are defined and derived from the transference. These formulae allow us to calculate the chromatic properties at the imaging plane, that is to say what is happening in the eye, at the retina. Because the chromatic difference derivations are not dependent on the position of the nodal point or other structures, they measure actual distances and changes in inclination.

Experimental measurements take place in object space and for this reason derivations for chromatic difference in transverse object position δy_{O}, inclination δa_{O}, object size $\delta(\Delta y_{\mathrm{O}})$, object angular spread $\delta(\Delta a_{\mathrm{O}})$, chromatic object size magnification M_{yO} and chromatic object angular spread magnification M_{aO} are included that account for chromatic differences and magnifications in object space. In an experimental situation one manipulates and takes measurements in object space whilst controlling what is happening at the retinal plane. These

equations allow us to compare our theoretical numerical results with published results obtained experimentally, and were found to compare well.

The equations for chromatic properties dependent on object or image and aperture position simplify to account for the effects of introducing a pinhole in front of the eye. δy_{R}, δa_{R}, δy_{O} and δa_{O} are directly dependent on y_{P}, the transverse displacement of the pinhole. However, the longitudinal shift in position of the limiting aperture from the pupillary plane to upstream of the cornea has a magnifying effect and therefore all the chromatic differences and chromatic magnifications are affected by this change. This has implications for both the Stiles-Crawford effect and for the AcuFocus Kamra corneal pinhole inlay.

Table 11.1.1 attempts to simplify the many variations and permutations of the dependent chromatic properties by indicating which variables each chromatic property is dependent on. Any parameter marked ○ has a linear relationship with the chromatic property, that is, magnified by a constant. Where indicated by □, this constant will have its slope affected by the distance of the object in front of the eye. The chromatic properties are symbolized as chromatic difference in transverse image position δy_{R}, inclination δa_{R}, image size $\delta(\Delta y_{\mathrm{R}})$, angular spread $\delta(\Delta a_{\mathrm{R}})$ retinal chromatic image size magnification M_{yR}, retinal chromatic angular spread magnification M_{aR}, chromatic difference in object position δy_{O}, inclination δa_{O}, object size $\delta(\Delta y_{\mathrm{O}})$, object angular spread $\delta(\Delta a_{\mathrm{O}})$, size magnification M_{yO} and object angular spread magnification M_{aO} in object space.

Table 11.1.1 Summary of chromatic properties and their dependencies. Variables marked ○ have a linear dependence on the respective variable. Objects at finite distance which have the slope of the linear dependence affected by the distance of the object in front of the eye are marked □. The table remains unchanged when a pinhole is introduced immediately in front of the eye. Chromatic properties in object space are defined for finite object distances only.

		Distant object		Object at finite distance			
		a_K	y_P	z_O	y_O	y_P	y_R
Image space	δy_R	○	○	□	○	○	
	δa_R	○	○	□	○	○	
	$\delta(\Delta y_R)$	○		□	○		
	$\delta(\Delta a_R)$	○		□	○		
	M_{yR}			□			
	M_{aR}			□			
Object space	δy_O	—		□		○	○
	δa_O	—				○	○
	$\delta(\Delta y_O)$	—		□			○
	$\delta(\Delta a_O)$	—					○
	M_{yO}	—		□			
	M_{aO}	—					

11.3 Limitations in the scope of this dissertation

At the outset it was clear that studying "the chromatic dependence of *all* first-order optical properties of the eye" would have far too large a scope for a Masters dissertation and so a conscious decision was made to limit the scope of the study to firstly Gaussian systems, whilst keeping all derivations as general as possible, and secondly to limit the derived properties to those applicable to the characteristic matrices and appropriate for Gaussian systems. This is a long dissertation and there are numerous topics and derived properties that have been omitted. In particular there are a number of derived properties that would be more appropriately studied as linear systems for their chromatic dependence such as all the axes of the eye. There were a number of issues that were raised during the

study which fell outside the scope of this dissertation, but which warrant further studies. Indeed, this study may give some insight into some of these issues.

There is a need for a complete set of formulae for the refractive indices as a function of frequency for all the media of the eye. The formula used for the refractive index of the reduced eye is based on relatively recent experimental data and is therefore considered to reflect the real eye fairly accurately for most of the properties studied. The refractive indices for Le Grand's eye differed from those for the reduced eye and are based on a combination of refractometer readings and experimental data. More recent refractometer readings are incomplete for the human eye. While these formulae form the basis of all the numerical examples in this dissertation, the derivations based on these formulae are sufficiently general so as to accommodate new formulae that may be available in the future.

In Section 8.2 we made use of the transformed transference. This mapping between the symplectic group and Hamiltonian space enabled us to develop an equation for the straight line dependence of the fundamental properties as a function of frequency and resulting in a symplectic transference with determinant exactly equal to 1. However, what meaning can be given to the entries of the Hamiltonian matrix. What region in the Hamiltonian space would be representative of eyes? Equation 5.6.7 may give us some insight into the meaning of the three-dimensional Hamiltonian space obtained using the Cayley transform and what region within this space is occupied by Gaussian eyes? Would it subsequently be possible to gain insight into what region of the ten-dimensional Hamiltonian space would be representative of real eyes with astigmatic surfaces?

In Gaussian optics it is tempting to represent the longitudinal and transverse chromatic aberration as a single combined chromatic aberration by obtaining a vector from the red to the blue image point. However, in linear optics the longitudinal chromatic aberration is represented by a matrix and the transverse chromatic aberration is a vector and combining the two into a unified chromatic aberration seems improbable. However, recent research indicates that this might be possible using a five-dimensional inner-product space (Harris, Evans and van Gool; 2014). The definition of inner-product space is based on the point and angle

characteristic matrices. How the two are related is beyond the scope of this dissertation and is the topic of further investigation at a later stage.

The definition for chromatic aberration includes astigmatic systems, however, this was not explored further; the scope of the dissertation being purposefully restricted to Gaussian systems. The chromatic properties too were defined for Gaussian systems. Where possible these definitions were generalized to linear optics for astigmatic systems without proof or being explored further. This creates an opportunity for further study of the chromatic properties for systems with astigmatic elements. Indeed, the two eyes studied are not only Gaussian, but emmetropic at a reference frequency. Additional studies into the chromatic properties of myopic, hyperopic, astigmatic, accommodating or even aging eye could be undertaken.

Many of the findings for the chromatic properties have implications for Stiles-Crawford effect. This needs to be explored in more detail.

The chromatic properties dependent on object and aperture position present the formulae necessary to obtain the chromatic properties induced by the placement of a pinhole immediately in front of the eye, or indeed, embedded in the corneal stroma. Further studies need to be done to explore the impact of these findings on the corneal pinhole inlay, such as the Kamra® by AcuFocus.

11.4 Summary of findings

1. The fundamental properties of the reduced and Le Grand's four surface eyes have a nearly perfectly linear dependence on frequency.
2. A formula is derived that gives the linear dependence of the fundamental properties of the transference.
3. Derivations are given for the chromatic aberration of systems in general, including systems with astigmatic and heterocentric elements, such as the eye, and particulated for the Gaussian eye.
4. Longitudinal chromatic aberration depends on the longitudinal position of the object and transverse chromatic aberration is dependent on both the longitudinal and transverse position of the object point.

5. Only the dilation and divergence are dependent on the refractive index upstream of the system. Disjugacy and divarication are independent of the medium upstream of the system.
6. Independent chromatic properties of the eye include:
    - Chromatic difference in power, δF .
    - Chromatic difference in refractive compensation, δF_0 .
    - Chromatic difference in ametropia, δA.
7. A set of formulae is derived for the chromatic properties of the Gaussian eye for
    - Objects at distance and at a finite distance.
    - Image and object space.
    - The special case of a pinhole held immediately in front of the eye.

    Chromatic properties of the eye dependent on object and aperture position include:
    - Chromatic difference in transverse image positions, δy_{R} .
    - Chromatic difference in inclination at the retina, δa_{R} .
    - Chromatic difference in image size, $\delta(\Delta y_{\mathrm{R}})$.
    - Chromatic difference in angular spread at retina, $\delta(\Delta a_{\mathrm{R}})$.
    - Chromatic image size magnification, M_{yR}.
    - Retinal chromatic angular spread magnification, M_{aR} .

    Chromatic properties of the eye dependent on image and aperture position include:
    - Chromatic difference in object position, δy_{O} .
    - Chromatic difference in object inclination, δa_{O} .
    - Chromatic difference in object size, $\delta(\Delta y_{\mathrm{O}})$.
    - Chromatic difference in object angular spread, $\delta(\Delta a_{\mathrm{O}})$.
    - Chromatic object size magnification, M_{yO}.
    - Chromatic object angular spread magnification, M_{aO} .

8. The red and blue chief rays chosen to study the chromatic properties in image space are incident on the entrance-plane of the system a distance of some 5000 times the wavelength of the blue light apart. When the red and blue chief rays from two separated object points coincide at a point on the exit-plane, their emergent inclination is the same for the reduced eye but different for Le Grand's eye.
9. Chromatic aberration and chromatic properties are dependent on:
    - Object position (longitudinal and transverse position, or incident inclination).
    - Frequencies chosen for 'red' and 'blue'.
    - Choice of schematic eye.
    - Formulae used for calculating the refractive indices of the media as a function of frequency.
    - Dependent chromatic properties can additionally be manipulated by introducing a pinhole in front of the eye.
10. Derived properties that are dependent on frequency are:
    - Power (linear).
    - Corneal-plane refractive compensation (linear).
    - Exit-plane refractive compensation (linear).
    - Back-vertex power (hyperbolic).
    - Front-vertex power (linear).
    - All the cardinal and anti-cardinal points for Le Grand's eye.
    - The anti-cardinal and focal points for the reduced eye.
    - All the chromatic properties. When the object distance remains stationary the dependence is linear.
11. The incident and emergent principal and nodal points are independent of frequency for the reduced eye.

11.5 Concluding summary

This dissertation studies the chromatic dependence of first-order optical properties of the eye, investigating both the fundamental and derived properties of the eye as a function of frequency. An equation is obtained that gives the linear dependency of each of the fundamental properties of the model eyes as a function of frequency, giving a transference that is truly symplectic with determinant equal to 1 (Evans and Harris, 2014).

Chromatic aberration is defined for systems in general, that is systems with elements that may be astigmatic and decentred, including the eye. Longitudinal chromatic aberration is defined by a 2×2 matrix and is dependent on the longitudinal position of the object point. Transverse chromatic aberration is defined by a 2×1 vector and is dependent on both the longitudinal and transverse position of the object point (Harris and Evans, 2012).

Chromatic properties are defined as those independent of and those dependent on the image or object and aperture positions. The definitions are derived for the subset of Gaussian eyes, however, the set of equations for astigmatic eyes is provided.

A selection of derived properties including power, corneal-plane and exit-plane refractive compensation, front- and back-vertex power and the cardinal points is investigated for their dependence on frequency. With the exception of the principal and nodal points of the reduced eye, all points investigated are dependent on frequency. The derived properties are related to each other through the characteristic matrices, which each define a linear space.

The transference, being a symplectic matrix, does not define a linear space, but can be mapped to Hamiltonian space which does define a linear space. Two mappings are investigated, namely the Cayley transform and the exponential-logarithmic mapping. The linear dependence of the entries of the Hamiltonian matrix on frequency is obtained. Graphs show the linear dependence on frequency of the individual entries as well as the three-dimensional linear space.

While understanding the meaning of Hamiltonian space and the region occupied by the eye is in its infancy, this study has given us insight into this linear

space. In particular, the Cayley transform derived from the fundamental properties (Equation 5.6.7) can potentially give us a deeper insight into this linear space.

This dissertation has opened the door to the study of the chromatic dependence of the first-order optical properties of the eye. A number of first-order optical properties, both fundamental and derived, have been investigated for their dependence on frequency. All the numerical examples have been purposefully limited to Gaussian eyes to allow insight into the dependence on frequency and chosen variables like object position and pinholes. We have a set of formulae that are not restricted to the reduced, or even schematic eyes. The stage is now set to generalise to systems and eyes with astigmatic and heterocentric elements.

S Afr Optom 2011 **70**(4) 149-155

Dependence of the transference of a reduced eye on frequency of light*

T Evans and WF Harris

Department of Optometry, University of Johannesburg, PO Box 524, Auckland Park, 2006 South Africa

<tevans@uj.ac.za>
<wharris@uj.ac.za>

Received 7 July 2011; revised version accepted 25 October 2011

Abstract

In Gaussian optics the transference is a matrix that is a complete representation of the effects of the system on a ray traversing it. Almost all of the familiar optical properties of the system, such as refractive error and power of the system, can be calculated from the transference. Because of the central importance of the transference it is useful to have some idea of how it depends on the frequency of light. This paper examines the simplest model eye, the reduced eye. The dependence of the transference is calculated in terms of both frequency and wavelength of light and both dependencies are displayed graphically. The principal matrix logarithms are also calculated and displayed graphically. Chromatic difference in refractive compensation, power and ametropia are obtained for the reduced eye from the transferences. (*S Afr Optom* 2011 **70**(4) 149-155)

Key Words: Transference, frequency, wavelength, Emsley's reduced eye, transformed transference, chromatic difference in: refractive compensation, power and ametropia.

Introduction

A transference is a matrix that represents the linear optical properties of an optical system, such as the eye. In Gaussian optics the transference is a complete representation of the effects of the system on a ray traversing it. Most of the optical properties of the system, such as refractive compensation[1], back- and front-vertex power[2], locations of the cardinal points[3, 4] and power of the system[5] can be calculated from the system's transference. Because of the central importance of the transference it is useful to have some idea of how it depends on the frequency of the light traversing it. We take a look at the simplest model eye, the reduced eye.

The dependence of the fundamental first-order properties, calculated in terms of both frequency and wavelength of light, will be represented graphically across the visible light spectrum. Further, the dependence of the transformed transference will be represented graphically. Formulae for the calculation of chromatic difference in corneal-plane refractive-compensation of the reduced eye and chromatic difference in power and ametropia are derived.

Emsley's reduced eye

The advantage of the reduced eye (see Figure 1) is its simplicity. The reduced eye has a single stigmatic refracting surface of radius of curvature r and a homogenous gap of length z. Emsley[6] designed his reduced eye to match certain measurements of the Gullstrand-Emsley schematic eye. He placed specific emphasis on the power of 60 D and chose the refractive index in the reduced eye to be the same as that of water, namely 4/3. He took the index of air to be 1. These numbers imply a radius of curvature r of 50/9 mm (or 1/180 m) and a length z of 200/9 mm (or 1/45

*Based on research towards a higher degree by T Evans under the guidance of Professor WF Harris.

m)[6, 7]. In this paper we will make use of a reduced eye with the same r and z as Emsley's eye and with an index n dependant on the frequency of light.

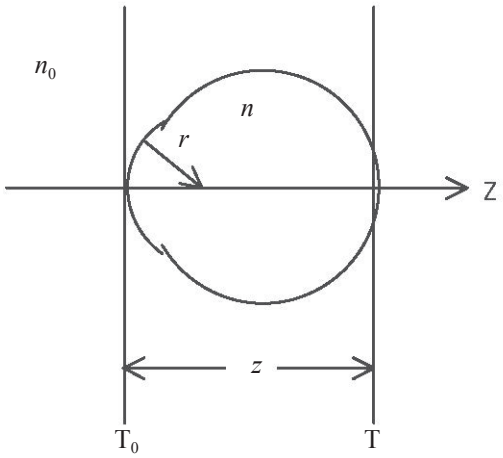

Figure 1. The reduced eye as a defined optical system. The length is z, the radius of curvature of the refracting surface is r, the refractive index outside the system is n_0 and inside the system is n. The optical system has a longitudinal axis, Z and is bound by an entrance plane T_0 immediately in front of the refracting surface and an exit plane T immediately in front of the retinal surface.

Linear optics

An optical system is bound by an entrance plane T_0 and an exit plane T and has a longitudinal axis Z. The transference **T** of a stigmatic, untilted, centred Gaussian optical system is represented by[8]

$$\mathbf{T} = \begin{pmatrix} A & B \\ C & D \end{pmatrix} \tag{1}$$

where A the dilation, B the disjugacy, C the divergence and D the divarication are the fundamental first-order optical properties of the system[1, 8, 9]. The power F is given simply by[5, 8]

$$F = -C\,. \tag{2}$$

When the system is an eye the dilation A can be considered to be the ametropia[8] of the eye. In particular when the eye is emmetropic

$$A = 0\,. \tag{3}$$

The corneal-plane refractive compensation is given by[1, 8]

$$F_0 = B^{-1}A\,. \tag{4}$$

The transferences of the two elementary optical systems[10, 11] are

$$\mathbf{T}_\xi = \begin{pmatrix} 1 & \dfrac{z}{n} \\ 0 & 1 \end{pmatrix} \tag{5}$$

for a homogenous gap and

$$\mathbf{T}_K = \begin{pmatrix} 1 & 0 \\ -\dfrac{n-n_0}{r} & 1 \end{pmatrix} \tag{6}$$

for a refracting surface. To calculate the transference of the reduced eye one multiplies in reverse[12] as follows

$$\mathbf{T} = \mathbf{T}_\xi \mathbf{T}_K\,. \tag{7}$$

Substituting Equations 5 and 6 into Equation 7 and multiplying one obtains

$$\mathbf{T} = \begin{pmatrix} 1-\dfrac{z}{n}\left(\dfrac{n-n_0}{r}\right) & \dfrac{z}{n} \\ -\dfrac{n-n_0}{r} & 1 \end{pmatrix}. \tag{8}$$

Substituting the values for Emsley's reduced eye into Equation 8 one obtains

$$\mathbf{T} = \begin{pmatrix} 0 & \dfrac{50}{3}\ \text{mm} \\ -0.060\ \text{kD} & 1 \end{pmatrix}. \tag{9}$$

It is immediately apparent from Equations 3 and 9 that the eye is emmetropic and has a power of 60 D.

Frequency or wavelength?

The fundamental relationship between frequency (ν) and vacuum wavelength (λ) is given by

$$c_0 = \nu\lambda \tag{10}$$

where light traveling in a vacuum has a speed c_0=299 792 458 m.s^{-1} as defined by the 17th General Conference on Weights and Measures in November 1983. Pease and Barbeito[13] look at the relationship between frequency and wavelength for a number of studies involving chromatic aberration and conclude that results using frequency or wavenumber (the inverse of wavelength) are "nearly perfectly linear"[13, 14] in contrast to those using wavelength. They cite several reasons to support using frequency rather than wavelength (perhaps the most important being that frequency is independent of the medium whereas wavelength is not). These reasons make a compelling argument to study

the dependence of the transference on the frequency of light rather than its dependence on wavelength. We will compare the dependence of the transference on both frequency and wavelength.

Visible light colour spectrum

The spectrum with wavelengths in vacuum is between 400 and 700 nm and represents the range over which human spectral sensitivity varies between 1 and 100%.[14-16] This represents frequencies between 428.3 THz and 749.5 THz, approximately. Six coloured reference points are shown on each of the graphs below. The four colours red-orange, yellow, green and blue represent the peak vacuum wavelengths where each colour is considered "pure"[17] while the deep-red and violet-blue represent the spectral range end-points. The frequencies and wavelengths of the six colours are detailed in Table 1.

Transference as a function of refractive index

The transference of the reduced eye in Equation 8 shows that the variable affected by different frequencies of light is the refractive index n. Entering the radius of curvature and length of Emsley's reduced eye we obtain its transference as a function of the refractive indices:

$$\mathbf{T} = \begin{pmatrix} \dfrac{4n_0}{n} - 3 & \dfrac{200}{9n}\ \text{mm} \\ -\dfrac{9}{50}(n - n_0)\ \text{kD} & 1 \end{pmatrix}. \qquad (11)$$

Refractive index of the Reduced Eye

Thibos *et al*[15] represent the refractive index of the reduced eye as a function of wavelength as follows

$$n = a + \frac{b}{\lambda - c} \qquad (12)$$

where a=1.320535, b=4.685 nm and c=214.102 nm. The formula is based on Cornu's formula for refractive index of water and constants were derived from clinical experimentation on real eyes. Using this formula, Thibos *et al*[15] showed that the refractive index of the body of the reduced eye changes more rapidly with wavelength than a reduced eye filled with water. The predictions for longitudinal chromatic aberration using this formula more closely approximate experimental data than Emsley's reduced eye filled with water. The refractive indices for our six reference points were calculated using Equation 12 and are given in Table 1.

Refractive index of air

The refractive index of air differs only very slightly from that of a vacuum and for most optometric calculations one can put n_0=1. A number of equations, for example Cauchy's dispersion formula[18] and Ciddor's equations[19], are available for calculating the refractive index of air. Cauchy's formula is expressed in terms of wavelength whereas Ciddor's equations are expressed in terms of wavenumber. Cauchy's dispersion formula[18] is

$$(n_0 - 1)10^7 = p + \frac{q}{\lambda^2} + \frac{t}{\lambda^4} \qquad (13)$$

Table 1. The colours of the six reference points and their frequencies, vacuum wavelengths, refractive indices for the reduced eye, ametropias, powers for the reduced eye and refractive compensations are provided. The last row shows the chromatic difference across the spectrum 428.3 to 749.5 THz.

Colour	Frequency in THz	Vacuum wavelength in nm	Refractive index	Ametropia	Power of reduced eye in dioptres	Refractive compensation in dioptres
Deep red	428.27	700	1.3302	0.0071	59.4318	0.4261
Red	475.86	630	1.3318	0.0035	59.7240	0.2070
Yellow	516.88	580	1.3333	0.0000	60.0010	0.0008
Green	576.52	520	1.3359	−0.0057	60.4531	−0.3398
Blue	631.14	475	1.3385	−0.0116	60.9286	−0.6964
Violet-blue	749.48	400	1.3457	−0.0277	62.2327	−1.6745
Chromatic difference in:			Δn = 0.0156	ΔA = −0.0348	ΔF = 2.8008	ΔF_0 = −2.1006

where p=2726.43, q=12.288×10^{6}nm^2 and t=355.5×10^9 nm^4 for dry air at temperature 15°C and pressure 101 kPa.

When Cauchy's dispersion formula is used for n_0 one obtains results that differ insignificantly from those for n_0=1. In particular for dilation the difference is less than 0.00083 across the entire visible light spectrum. For divergence this difference is 0.05 D. This results in a very slight upward shift in the graphs for *A* and *C* in Figure 2, however, the curvatures are unaffected.

Calculation shows that the reduced eye is emmetropic at the frequency 517 THz (580 nm, yellow) when we use n_0=1 but is emmetropic at the frequency 526 THz (570 nm, yellow-green) when the refractive index of air is calculated using Cauchy's formula.

Graphical representation of the fundamental properties

The properties are calculated for frequencies according to Equation 11 with n_0=1 and *n* given by Equation 12. The results of the calculations of each of the fundamental first-order optical properties are given in the accompanying graphs. Figure 2 represents each of the fundamental properties as functions of frequency of light and Figure 3 as functions of wavelength. The six coloured reference points are shown by means of coloured diamonds. The small black dots on Figure 2 represent 10 equally spaced intervals of frequency of approximately 32.1 THz and the crosses on Figure 3 represent 10 equally spaced intervals of 30 nm wavelength.

We note that in Figure 2 the dots are more evenly spaced than the crosses in Figure 3. The dashed line represents the slope of the curve calculated using the least squares method. Each of *A*, *B* and *C* present as curves in both sets of graphs. *D* is a straight line at 1 as required by Equation 11. The curves are closer to straight lines in Figure 2 than in Figure 3; this provides some justification for preferring to think in terms of frequency rather than wavelength of light.

The transferences at the extremes of the visible spectrum (428.3 THz or 700 nm and 749.5 THz or 400 nm), are

$$\mathbf{T}_{428.3\,\mathrm{THz}} = \begin{pmatrix} 0.0071 & 16.7062\ \mathrm{mm} \\ -0.0594\ \mathrm{kD} & 1 \end{pmatrix} \qquad (14)$$

$$\mathbf{T}_{749.5\,\mathrm{THz}} = \begin{pmatrix} -0.0277 & 16.5130\ \mathrm{mm} \\ -0.0622\ \mathrm{kD} & 1 \end{pmatrix}. \qquad (15)$$

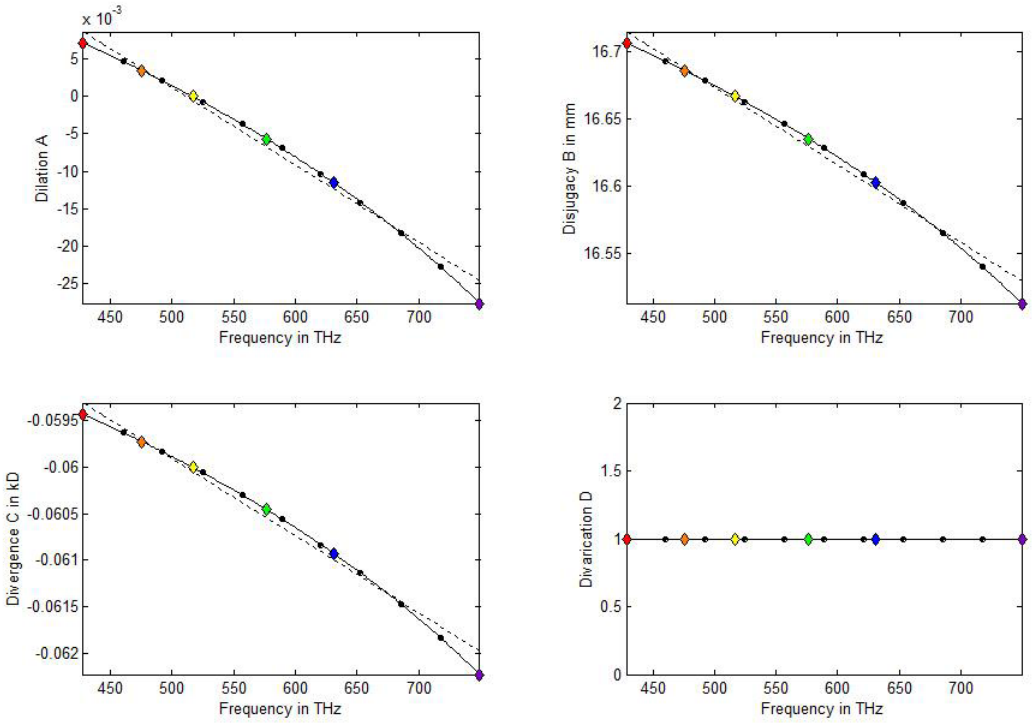

Figure 2. Sub-graphs A, B, C and D represent the four fundamental optical properties of the reduced eye as a function of frequency of light. The six coloured diamonds indicate six reference points as indicated in Table 1. The small black dots represent 10 equal intervals of 32.1 THz each. Each of *A*, *B* and *C* present as curves, while *D* is a horizontal straight line at 1.

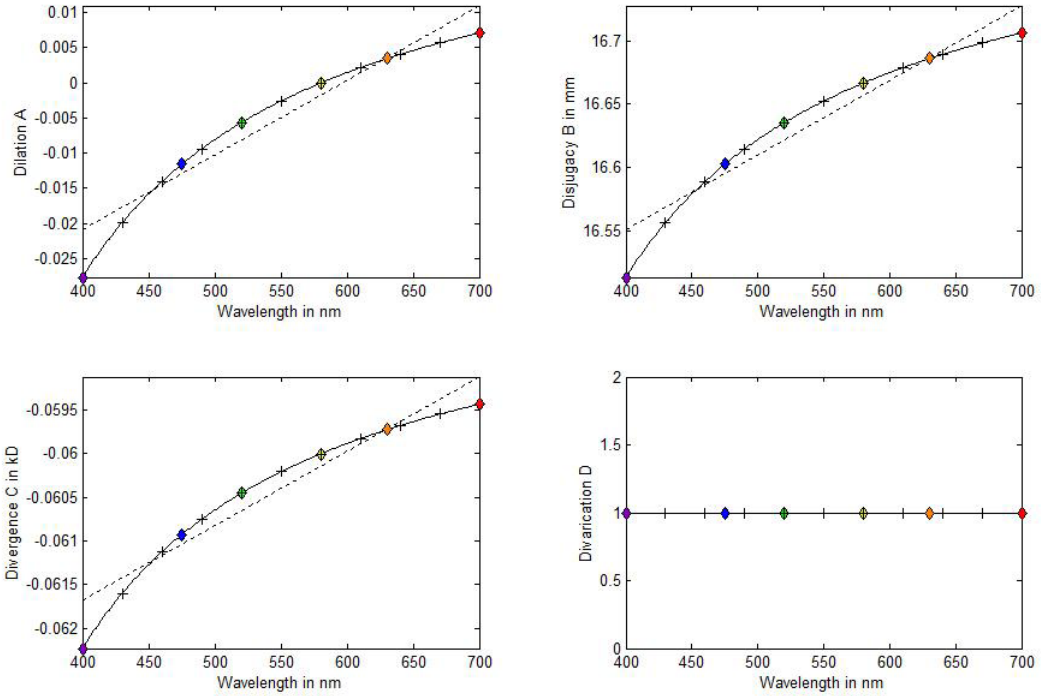

Figure 3. The four fundamental properties of the reduced eye as a function of wavelength. The black crosses represent 10 equal intervals of 30 nm each.

The transformed transference

By taking the principal matrix logarithm we convert each transference T into a Hamiltonian matrix[8, 20]. We represent the transformed matrix[8] by $\hat{\mathbf{T}}$. Thus

$$\hat{\mathbf{T}} = \mathrm{Log}\mathbf{T}. \tag{16}$$

In MATLAB the function used is *logm*. In terms of its entries we write the transformed transference[8] as

$$\hat{\mathbf{T}} = \begin{pmatrix} \hat{A} & \hat{B} \\ \hat{C} & \hat{D} \end{pmatrix}. \tag{17}$$

Because $\hat{\mathbf{T}}$ is Hamiltonian[20],

$$\hat{A} = -\hat{D}. \tag{18}$$

$\hat{\mathbf{T}}$ therefore has only three independent entries. This creates a 3-dimensional vector space which can be plotted on a 3-dimensional graph as done in Figure 4. In the figure $\hat{A}, \hat{B}$ and $\hat{C}$ are along three orthogonal axes, where $\hat{A}$ (and $\hat{D}$) are unitless, $\hat{B}$ is in millimetres and $\hat{C}$ is in kilodioptres. The result is close to a straight line. The small black dots represent 20 equally spaced intervals of frequency of 16.1 THz.

Transforming Equations 14 and 15, we find

$$\hat{\mathbf{T}}_{428.3\,\mathrm{THz}} = \begin{pmatrix} -0.5994 & 20.1699\ \mathrm{mm} \\ -0.0718\ \mathrm{kD} & 0.5994 \end{pmatrix} \tag{19}$$

$$\hat{\mathbf{T}}_{749.5\,\mathrm{THz}} = \begin{pmatrix} -0.6251 & 20.0888\ \mathrm{mm} \\ -0.0757\ \mathrm{kD} & 0.06251 \end{pmatrix}. \tag{20}$$

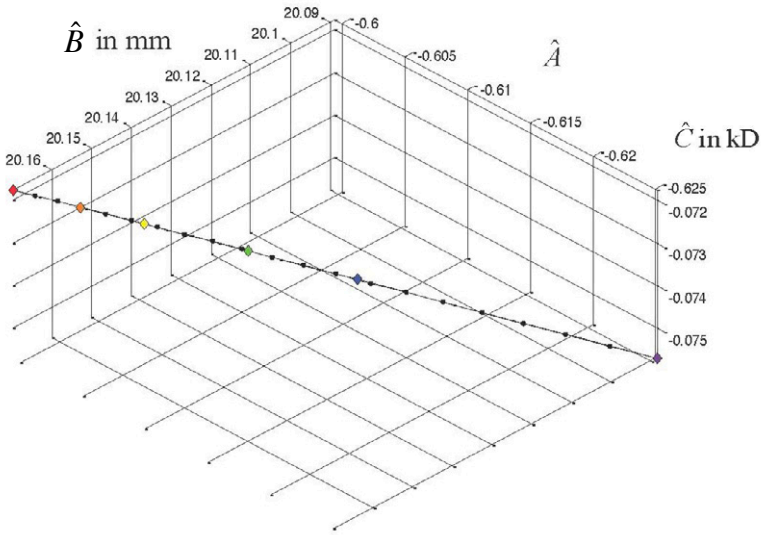

Figure 4. The transformed transference of the reduced eye in Hamiltonian space. The three axes represent $\hat{A}$, $\hat{B}$ and $\hat{C}$. The black dots represent frequencies spaced at intervals of 16.06 THz. The six diamonds represent the six coloured reference points. (The azimuth of 45° and elevation of 125° were chosen to exaggerate any possible curvature.)

Some Derived Properties

We obtain here some derived properties of the reduced eye that are directly and simply obtainable from the transference. Using Equation 2 we calculate the power F of the reduced eye for a particular frequency of light and using Equation 4 we calculate the corneal-plane refractive compensation F_0 for the frequency. We read the ametropia A directly from the transference for the chosen frequency of light. Of greater interest is the chromatic difference in refractive compensation ΔF_0 (known by various terms including longitudinal chromatic aberration[21], chromatic difference of refractive error[21], chromatic difference in refraction[14], and axial chromatic aberration[21]), chromatic difference in power (also known as chromatic difference of equivalent power[14]) and chromatic difference in ametropia across a specified spectrum of visible light to be studied.

Each of these derived properties in chromatic difference between two frequencies or wavelengths can be calculated in two ways: either directly from the two transferences or using the equations below. Equations 21, 23, 24 and 26 are general equations while Equations 22, 25 and 27 apply to the reduced eye.

To calculate the chromatic difference in corneal-plane refractive compensation across a specified spectrum we take values from the two transferences (Equation 1) and substitute them into Equation 4 as follows:

$$\Delta F_0 = B_2^{-1}A_2 - B_1^{-1}A_1 \quad . \tag{21}$$

Now substituting from Equation 8 and also substituting the values for z and r for the reduced eye, we find

$$\Delta F_0 = (-135\ \mathrm{D})\Delta n \tag{22}$$

where Δn simplifies to

$$\Delta n = b\left(\frac{1}{\lambda_2 - c} - \frac{1}{\lambda_1 - c}\right) \tag{23}$$

and b and c are the same constants as for Equation 12.

To calculate chromatic difference in power we similarly take values from the transferences and substitute them into Equation 2 as follows

$$\Delta F = -(C_2 - C_1) \tag{24}$$

and substituting from Equation 8 and then substituting the value for r for the reduced eye we find

$$\Delta F = (180\ \mathrm{D})\Delta n \quad . \tag{25}$$

The chromatic difference in ametropia is derived directly from the transferences and therefore

$$\Delta A = A_2 - A_1 \, . \tag{26}$$

Substituting values for z and r we obtain

$$\Delta A = 4\left(\frac{1}{n_2} - \frac{1}{n_1}\right) \tag{27}$$

where n_1 and n_2 are calculated from Equation 12.

The chromatic difference in corneal-plane refractive compensation of the reduced eye was calculated across the visible light spectrum 428.3 to 749.5 THz and is −2.1006 D (see Table 1). The chromatic difference in power is 2.8 D. The chromatic difference in ametropia is −0.0348.

Conclusion

The transference of the reduced eye depends on the frequency of light. The accuracy of the calculations depends on the formula used to calculate the refractive index as a function of either frequency of light or wavelength. In this article we have used Equation 12.

Results are displayed graphically for the transferences both as a function of frequency and as a function of wavelength. Divarication D is constant while ametropia A, disjugacy B and divergence C exhibit curved lines. The graph for the transformed transference in Hamiltonian space is approximately a straight line.

Chromatic difference in refractive compensation, chromatic difference in power and chromatic difference in ametropia are calculated directly from the transference for the reduced eye.

Acknowledgements

We thank RD van Gool for continued discussions. WF Harris acknowledges support from the National Research Foundation. All calculations and graphs were done using MATLAB.

References

1. Harris WF. Magnification, blur, and ray state at the retina for the general eye with and without a general optical instrument in front of it. 1. Distant objects. *Optom Vis Sci* 2001 **78** 888-900.
2. Harris WF. Back- and front-vertex powers of astigmatic systems. *Optom Vis Sci* 2010 **87** 70-72.
3. Harris WF. Graphical construction of cardinal points from the transference. *S Afr Optom* 2011 **70** 3-13.

4. Harris WF. Pascal's ring, cardinal points, and refractive compensation. *Vision Res* 2011 **51** 1679-1685.
5. Harris WF. Dioptric power: its nature and its representation in three- and four-dimensional space. *Optom Vis Sci* 1997 **74** 349-366.
6. Emsley HH. *Visual Optics*. London: Hatton Press Ltd, 1950 pp 525-527, 543-544.
7. Bennett AG, Rabbetts RB. *Clinical Visual Optics*. London: Butterworth. 1984; p 18.
8. Harris WF. The log-transference and an average Gaussian eye. *S Afr Optom* 2005 **64** 84-88.
9. Harris WF. The four fundamental properties of Gaussian optical systems including the eye. *S Afr Optom* 1999 **58** 69-79.
10. Harris WF. General approach to the sensitivity of the optics of an eye to change in elementary parameters with application to the Gaussian optics of a reduced eye. *S Afr Optom* 2009 **68** 166-174.
11. Harris WF. Symplecticity and relationships among the fundamental properties in linear optics. *S Afr Optom* 2010 **69** 3-13.
12. Harris WF. Stigmatic optical systems. *Optom Vis Sci* 2004 **81** 947-952.
13. Pease PL, Barbeito R. Axial chromatic aberration of the human eye: frequency or wavelength? *Ophthal Physiol Opt* 1989 **9** 215-217.
14. Rabbetts RB. *Bennett and Rabbetts' Clinical Visual Optics*, 4th Ed. Edinburgh: Butterworth Heineman Elsevier, 2007 pp 287-293.
15. Thibos LN, Ye M, Zhang X, Bradley A. The chromatic eye: a new reduced-eye model of ocular chromatic aberration in humans. *Appl Opt* 1992 **31** 3594-3600.
16. Le Grand Y. Light, *Colour and Vision*. Chapman and Hall, London; 1957 pp 72-73.
17. Meyer-Arendt JR. *Introduction to Classical and Modern Optics*. New Jersey: Prentice Hall, 1995 p 5.
18. Hodgson CD. *Handbook of Chemistry and Physics*. Chemical Rubber Publishing Co, Cleveland, 1959 p 2943.
19. Ciddor PE. Refractive index of air: new equations for the visible and near infrared. *Appl Opt* 1996 **35** 1566-1573.
20. Harris WF. Quantitative analysis of transformed ray transferences of optical systems in space of augmented Hamiltonian matrices. *S Afr Optom* 2007 **66** 62-67.
21. Thibos LN, Bradley A, Zhang X. Effect of ocular chromatic aberration on monocular visual performance. *Optom Vis Sci* 1991 **68** 599-607.

APPENDIX to Harris WF & Evans T Chromatic Aberration in Heterocentric Astigmatic Systems Including the Eye Optom Vis Sci 2012;89

The theory is illustrated here for a model eye with four tilted astigmatic refracting surfaces. The optical system is the visual optical system of the eye from immediately in front of the cornea to immediately in front of the retina. The curvatures, tilts, and separations are listed in Table A1. K1 and K2 are the first and second surfaces of the cornea and L1 and L2 are the first and second surfaces of the lens of the eye. K1 has principal meridians at 180° and 90°; the radii of curvature along them are 6.5 and 8 mm respectively. The horizontal and vertical components of tilt of K1 are 0.06 and -0.05 (radians) respectively; the right side of the cornea would be tilted away from and the top towards an observer looking at the eye. We use the equations for refractive index of the cornea, aqueous, lens, and vitreous published by Villegas, Carretero, and Fimia[1]. The index in front of the eye is $n_0 = 1$. We use the vacuum wavelengths 656.3 nm for red and 486.1 nm for blue respectively that have been used by others[2]. In order to show small differences we retain more digits than may be physically meaningful.

TABLE A1.

Principal radii of curvature, separation, and tilt of surfaces of the model eye used in the numerical example.

Surface	Principal radii mm{degr}mm	Separation mm	Tilt
K1	$6.5\{180\}8$		$(0.06 \quad -0.05)^{\mathrm{T}}$
		0.5	
K2	$5.8\{20\}7.2$		$(0.04 \quad 0.06)^{\mathrm{T}}$
		3	
L1	$10.2\{100\}8.7$		$(-0.07 \quad 0.1)^{\mathrm{T}}$
		4	
L2	$-4.5\{70\}-6.5$		$(-0.05 \quad -0.03)^{\mathrm{T}}$
		16.5	

The transferences calculated by the method described elsewhere[3] for red and blue light turn out to be

$$\mathbf{T}_\mathrm{r} = \begin{pmatrix} -0.1513 & -0.0134 & 16.5690 & -0.1292 & -0.3134 \\ -0.0121 & -0.0125 & -0.1290 & 16.3221 & 0.1936 \\ -0.0686 & -0.0012 & 0.9046 & -0.0104 & -0.0176 \\ -0.0011 & -0.0619 & -0.0103 & 0.8840 & 0.0084 \\ 0 & 0 & 0 & 0 & 1 \end{pmatrix} \qquad \text{(A1)}$$

and

$$\mathbf{T}_\mathrm{b} = \begin{pmatrix} -0.1687 & -0.0136 & 16.4641 & -0.1309 & -0.3185 \\ -0.0123 & -0.0279 & -0.1307 & 16.2137 & 0.1957 \\ -0.0700 & -0.0012 & 0.9030 & -0.0106 & -0.0179 \\ -0.0011 & -0.0632 & -0.0105 & 0.8820 & 0.0086 \\ 0 & 0 & 0 & 0 & 1 \end{pmatrix} \qquad \text{(A2)}$$

Entries in the last three columns of the first two rows are in millimetres; entries in the first two columns of the third and fourth rows are in kilodiopters.

Distant Object Point

Consider a distant object point O in a vertical plane containing longitudinal axis Z. Rays from O arrive at the model eye with inclination $\mathbf{a}_\mathrm{O} = \begin{pmatrix} 0 \\ -0.05 \end{pmatrix}$ relative to Z. Details of the calculation are summarized in Table A2. For example, the red blurred image has a near vertical line (it is at about $94.90°$) 2.9567 mm in front of the retina; the other line is 0.2455 mm in front of the retina. (The blue image has a line at $94.87°$, not quite the same as for the red image.) The longitudinal chromatic aberration is $\Delta\mathbf{Z}$ as listed. Its principal structure is -0.3235 mm along $96.96°$ and -0.2884 mm. The horizontal and vertical components of the transverse chromatic aberration are -0.0008 mm and 0.0160 mm respectively.

It may also be of interest to calculate the chromatic difference of refractive compensation for the eye. The refractive compensation is given by[4] $\mathbf{F}_0 = \mathbf{B}^{-1}\mathbf{A}$, a dioptric power matrix. We obtain it from the transferences (Eqs. A1 and A2). In conventional spherocylindrical terms the results are $-0.6958\ -8.5194\times 95.50$ and $-1.6481\ -8.6850\times 95.59$ for red and blue light respectively. The chromatic difference of refractive compensation turns out to be

TABLE A2.

Longitudinal $\Delta\mathbf{Z}$ and transverse $\Delta\mathbf{y}$ chromatic aberration of a model heterocentric astigmatic eye and a distant object point with $\mathbf{a}_O = \begin{pmatrix} 0 \\ -0.05 \end{pmatrix}$.

	red	**blue**
$\mathbf{L}$ (kD) (Eq.11)	$\begin{pmatrix} -0.4874 & 0.4236 \\ 0.4236 & -5.3960 \end{pmatrix}$	$\begin{pmatrix} -0.4270 & 0.1643 \\ 0.1643 & -2.3414 \end{pmatrix}$
$\mathbf{Z}$ (mm) (Eq.4)	$\begin{pmatrix} -2.9369 & -0.2306 \\ -0.2306 & -0.2653 \end{pmatrix}$	$\begin{pmatrix} -3.2258 & -0.2263 \\ -0.2263 & -0.5882 \end{pmatrix}$
z_- (mm)	-2.9567	-3.2451
z_+ (mm)	-0.2455	-0.5960
$\mathbf{v}_+$	$\begin{pmatrix} 0.0853 \\ -0.9964 \end{pmatrix}$	$\begin{pmatrix} 0.0849 \\ -0.9964 \end{pmatrix}$
$\mathbf{V}$ (mm) (Eq. 26)	$\begin{pmatrix} -2.2021 & -0.1729 \\ -0.1729 & -0.1989 \end{pmatrix}$	$\begin{pmatrix} -2.4070 & -0.1689 \\ -0.1689 & -0.4389 \end{pmatrix}$
$(\mathbf{B}+\mathbf{VD})n_0$ (mm)	$\begin{pmatrix} 14.5787 & -0.2592 \\ -0.2833 & 16.1480 \end{pmatrix}$	$\begin{pmatrix} 14.2923 & -0.2545 \\ -0.2785 & 15.8283 \end{pmatrix}$
$\mathbf{e}+\mathbf{V}\boldsymbol{\pi}$ (mm)	$\begin{pmatrix} -0.2762 \\ 0.1950 \end{pmatrix}$	$\begin{pmatrix} -0.2767 \\ 0.1950 \end{pmatrix}$
	$\Delta((\mathbf{B}+\mathbf{VD})n_0) = \begin{pmatrix} -0.2864 & 0.0047 \\ 0.0048 & -0.3197 \end{pmatrix}$ mm	
	$\Delta(\mathbf{e}+\mathbf{V}\boldsymbol{\pi}) = \begin{pmatrix} -0.0006 \\ 0.0000 \end{pmatrix}$ mm	
	$\Delta\mathbf{Z} = \begin{pmatrix} -0.2889 & 0.0042 \\ 0.0042 & -0.3230 \end{pmatrix}$ mm (Eq. 5)	
	$\Delta\mathbf{y} = \begin{pmatrix} -0.0008 \\ 0.0160 \end{pmatrix}$ mm (Eq. 29)	

$\Delta\mathbf{F}_0 = \mathbf{F}_{0b} - \mathbf{F}_{0r} = \begin{pmatrix} -1.1136 & -0.0298 \\ -0.0298 & -0.9565 \end{pmatrix}$ D which is $-0.9510 \quad -0.1680 \times 100.37$ as a spherocylindrical power. It follows from the definitions that there is no simple relationship between chromatic difference of refractive compensation and longitudinal chromatic aberration for a distant object point.

Near Object Point

Table A3 lists the details for the model eye and object point O 400 mm in front of the eye and with transverse position $\mathbf{y}_O = \begin{pmatrix} -30 \\ 30 \end{pmatrix}$ mm relative to longitudinal axis Z. For an observer looking at the eye along Z, with O between the observer and the eye, O is up and to the left. The principal structure of the longitudinal chromatic aberration is -0.3555 mm along $97.25°$ and -0.3139 mm. The principal longitudinal chromatic aberrations are slightly larger in magnitude compared with those for the distant object and the principal meridians have undergone a small anticlockwise rotation. The horizontal and vertical components of the transverse chromatic aberration are -0.0238 mm and 0.0262 mm.

REFERENCES

1. Villegas ER, Carretero L, Fimia A. Le Grand eye for the study of ocular chromatic aberration. Ophthal Physiol Opt 1996; 16: 528-31.
2. Powell I. Lenses for correcting chromatic aberration of the eye. Appl Opt 1981; 20: 4152-5.
3. Harris WF. Transferences of heterocentric astigmatic catadioptric systems including Purkinje systems. Optom Vis Sci 2010; 87: 778-86.
4. Harris WF. A unified paraxial approach to astigmatic optics. Optom Vis Sci 1999; 76: 480-99.

TABLE A3.

Longitudinal $\Delta\mathbf{Z}$ and transverse $\Delta\mathbf{y}$ chromatic aberration of a model heterocentric astigmatic eye and object point with $z_O = -400$ mm and $\mathbf{y}_O = \begin{pmatrix} -30 \\ 30 \end{pmatrix}$ mm.

	red	**blue**
$\mathbf{L}$ (kD) (Eq. 10)	$\begin{pmatrix} -0.5773 & -0.2359 \\ -0.2359 & 1.9984 \end{pmatrix}$	$\begin{pmatrix} -0.4875 & -0.4410 \\ -0.4410 & 4.3566 \end{pmatrix}$
$\mathbf{Z}$ (mm) (Eq. 4)	$\begin{pmatrix} -2.2038 & -0.2601 \\ -0.2601 & 0.6367 \end{pmatrix}$	$\begin{pmatrix} -2.5184 & -0.2549 \\ -0.2549 & 0.2818 \end{pmatrix}$
z_- (mm)	-2.2275	-2.5414
z_+ (mm)	0.6603	0.3048
$\mathbf{v}_+$	$\begin{pmatrix} 0.0904 \\ -0.9959 \end{pmatrix}$	$\begin{pmatrix} 0.0899 \\ -0.9959 \end{pmatrix}$
$\mathbf{V}$ (mm) (Eq. 26)	$\begin{pmatrix} -1.6524 & -0.1950 \\ -0.1950 & 0.4774 \end{pmatrix}$	$\begin{pmatrix} -1.8792 & -0.1902 \\ -0.1902 & 0.2103 \end{pmatrix}$
$\mathbf{A}+\mathbf{VC}$	$\begin{pmatrix} -0.0377 & 0.0007 \\ 0.0008 & -0.0419 \end{pmatrix}$	$\begin{pmatrix} -0.0369 & 0.0007 \\ 0.0008 & -0.0410 \end{pmatrix}$
$\mathbf{e}+\mathbf{V\pi}$ (mm)	$\begin{pmatrix} -0.2860 \\ 0.2011 \end{pmatrix}$	$\begin{pmatrix} -0.2864 \\ 0.2009 \end{pmatrix}$
	$\Delta(\mathbf{A}+\mathbf{VC}) = \begin{pmatrix} 0.0008 & -0.0000 \\ -0.0000 & 0.0009 \end{pmatrix}$	
	$\Delta(\mathbf{e}+\mathbf{V\pi}) = \begin{pmatrix} -0.0004 \\ -0.0001 \end{pmatrix}$ mm	
	$\Delta\mathbf{Z} = \begin{pmatrix} -0.3145 & 0.0052 \\ 0.0052 & -0.3548 \end{pmatrix}$ mm (Eq. 5)	
	$\Delta\mathbf{y} = \begin{pmatrix} -0.0238 \\ 0.0262 \end{pmatrix}$ mm (Eq. 28)	

1040-5488/12/8911-e37/0 VOL. 89, NO. 11, PP. e37–e43
OPTOMETRY AND VISION SCIENCE

TECHNICAL REPORT

Chromatic Aberration in Heterocentric Astigmatic Systems Including the Eye

William F. Harris* and Tanya Evans†

ABSTRACT

Purpose. There is inconsistency in the literature in the definitions of longitudinal and transverse chromatic aberration, and there appear to be no definitions that make allowance for astigmatism and heterocentricity. The purpose is to propose definitions of longitudinal and transverse chromatic aberration that hold for systems which, like the typical eye, may be heterocentric and astigmatic and to develop the associated optics.

Methods. Common definitions of longitudinal and transverse chromatic aberration based on Gaussian optics are generalized naturally in terms of linear optics to accommodate heterocentricity and astigmatism.

Conclusions. The definitions offered here apply to systems in general, including the visual optical system of the eye, and hold for homocentric stigmatic systems in particular. Care is advocated in the use of the terms longitudinal and transverse chromatic aberration.

(Optom Vis Sci 2012;89:e37–e43)

Key Words: longitudinal chromatic aberration, transverse chromatic aberration, astigmatism, heterocentricity, transference, fundamental properties

Definitions in the literature[1–6] of first-order chromatic aberration treat the optical system in question as homocentric and as having refracting elements that are stigmatic. There appear to be no published definitions of longitudinal and transverse chromatic aberration in systems that are heterocentric and astigmatic. The lack of definitions would seem unfortunate in view of the fact that heterocentricity and astigmatism are features of the typical eye. It might also suggest that such definitions may not be easy to come by. This note has the limited objective of proposing definitions and developing the linear optics of longitudinal and transverse chromatic aberration of systems that may be heterocentric and astigmatic. The definitions are natural generalizations of familiar definitions in Gaussian optics. They hold for systems in general and apply to the eye in particular, and they allow one to explore the effects of changes to the eye including those that accompany accommodation and refractive surgery for example.

There is inconsistency in the optometric literature over the use of the term chromatic aberration, particularly, perhaps, in the more clinically oriented literature. This does not facilitate communication within the discipline and between optometry and other disciplines. Greater care needs to be taken over terminology; usage should be as consistent as possible with that of the broader scientific community, and distinct concepts should be assigned distinct names. (We take up these points at the end of this note.) In keeping with these thoughts we take our point of departure to be a definition of chromatic aberration used commonly in the literature of both general optics and optometry.[1–3]

HOMOCENTRIC SYSTEMS WITH STIGMATIC ELEMENTS

Fig. 1 illustrates definitions[1–3] of longitudinal and transverse chromatic aberration. The definitions are in terms of Gaussian optics. System S consists of refracting elements invariant under rotation about, and centered on, a common axis Z, the optical axis of S. None of its refracting surfaces is shown. S has entrance plane T_0 and exit plane T, both transverse to axis Z. The indices of refraction are n_0 and n upstream and downstream, respectively, of S. Object point O has longitudinal position z_O and transverse position y_O. Fig. 1 is drawn with $y_O > 0$ and $z_O < 0$. The location of the image point I depends on the frequency ν of light involved. Consider two particular frequencies ν_r and ν_b. It will be convenient to refer to the light as red and blue, respectively. The red and blue images of O are represented in Fig. 1 as I_r and I_b,

*PhD, FAAO
†BOptom
Department of Optometry, University of Johannesburg, Johannesburg, South Africa.

Supplemental digital content is available for this article. Direct URL citations appear in the printed text and are provided in the HTML and PDF versions of this article on the journal's Web site (*www.optvissci.com*).

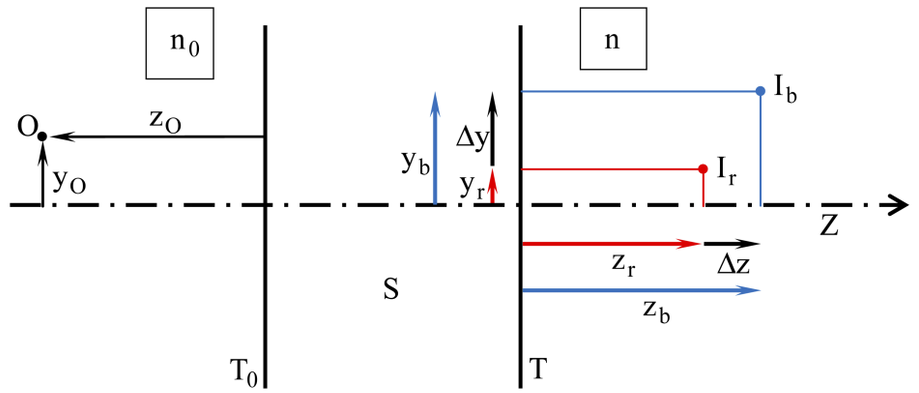

FIGURE 1.

Chromatic aberration in Gaussian optics. S is an optical system with entrance and exit planes T_0 and T, respectively. Z is the optical axis. Corresponding to an object point O are red and blue image points I_r and I_b. By definition, the longitudinal chromatic aberration of S for O is the signed length Δz. The transverse chromatic aberration of S for O is the signed length Δy. Usually $z_r > z_b$ and not as shown here.

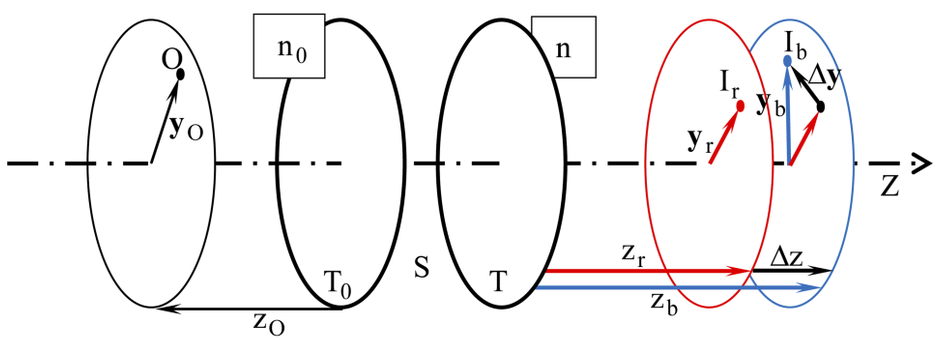

FIGURE 2.

Longitudinal chromatic aberration Δz (a scalar) and transverse chromatic aberration Δy (a vector) of heterocentric stigmatic system S for object point O. Longitudinal axis Z is not an optical axis.

respectively, with longitudinal z_r and z_b and transverse y_r and y_b positions, all being positive in the figure. We need to distinguish the incident n_{0r} and n_{0b} and emergent n_r and n_b indices corresponding to frequencies ν_r and ν_b. By definition

$$\Delta z = z_b - z_r \tag{1}$$

and

$$\Delta y = y_b - y_r \tag{2}$$

are the *longitudinal* (or *axial)* and *transverse* (or *lateral) chromatic aberrations,* respectively.

We note that longitudinal and transverse chromatic aberrations do not depend on the properties of system S alone; they depend on the properties of system S and the property of object point O. Most properties of a system depend on the context or environment of the system, that is, the indices n_0 and n. For convenience, we take reference to properties of a system to imply the context as well. The property of object point O is its position in space. In Fig. 1, it is represented by its longitudinal and transverse positions z_O and y_O. It follows that for a given system S, the chromatic aberration is not unique. There is usually an infinity of longitudinal and transverse chromatic aberrations. The chromatic aberration of the system becomes unique when the location of the object point is specified.

By these definitions, both longitudinal Δz and transverse Δy chromatic aberrations are lengths measured orthogonally and represented by scalars. One is tempted, therefore, to regard the two chromatic aberrations as Cartesian components of a vectorial chromatic aberration and to insert an arrow from I_r to I_b to represent it in Fig. 1. We could then treat chromatic aberration holistically and not have to write separate equations for the two components. We shall find below, however, that the two aspects are fundamentally different and cannot meaningfully be combined in this way.

HETEROCENTRIC SYSTEMS WITH STIGMATIC ELEMENTS

A two-dimensional drawing, like that of Fig. 1, suffices for representing chromatic aberration in the case of homocentric systems free of astigmatism because optical axis Z, object point O, and images I_r and I_b all lie in a common plane; that plane becomes the plane of the paper. However, when homocentricity is relaxed, this is usually no longer the case. In general, for heterocentric systems with stigmatic elements, we need a three-dimensional representation like that attempted in Fig. 2. In Fig. 2, system S contains refracting elements that may be mutually decentered. S may contain prisms and tilted surfaces. Z is no longer an optical axis but merely a longitudinal axis.

It is apparent that the definition for longitudinal chromatic aberration Δz in the case of homocentric systems with stigmatic elements (Eq. 1) can be generalized to heterocentric systems unchanged. This is not the case for transverse chromatic aberration however. Transverse chromatic aberration becomes a two-component vector $\Delta\mathbf{y}$ defined by

$$\Delta\mathbf{y} = \mathbf{y}_b - \mathbf{y}_r \tag{3}$$

where $\mathbf{y}_r$ and $\mathbf{y}_b$ are the transverse position vectors of images I_r and I_b. Transverse chromatic aberration $\Delta\mathbf{y}$ can be decomposed into horizontal and vertical components in the transverse plane if desired.

One still needs to resist any temptation to lump longitudinal and transverse chromatic aberration into a single concept of chromatic aberration that could be represented by an arrow (not shown) in Fig. 2 from I_r to I_b.

HETEROCENTRIC ASTIGMATIC SYSTEMS

We now relax the requirement that the elements of system S of Fig. 2 be stigmatic; the elements of S may be heterocentric and astigmatic. Each image point, I_r and I_b, in Fig. 2 becomes blurred in Fig. 3. One can think of each image point as dissociating longitudinally into a pair of orthogonal image lines. The structure becomes that of the familiar interval of Sturm, its nature and location being dependent on the frequency of the light. We need to allow for the fact that the orientations of the image lines usually do not match; that is, the first image line of the red blurred image is usually not parallel to the first image line of the blue blurred image. How now do we define longitudinal and transverse chromatic aberration?

Let us first consider chromatic aberration in a system with astigmatic elements that are centered on Z. Z then is an optical axis. Suppose, further, that object point O lies on Z. Red image I_r is then centered on Z, and its associated line segments intersect Z. The same holds for blue image I_b. Evidently, there is no transverse chromatic aberration. What chromatic aberration there is longitudinal. But how do we define it? The definition should surely account for the fact that the two blurred images may differ not only in longitudinal position but also in the nature and degree of blur. In other words, longitudinal chromatic aberration would need at least three numbers for its complete quantitative representation.

The images themselves do not suggest an obvious answer. Instead, we shift focus to the pencils of light containing them. In the absence of astigmatism, the red pencil would have reduced vergence $L_r = n_r/z_r$ in exit plane T where z_r is the longitudinal position of the image point relative to T. Turning the equation around, we obtain $z_r = n_r/L_r$. In the presence of astigmatism, the generalization of the scalar reduced vergence L is the matrix reduced vergence $\mathbf{L}$ introduced by Fick[7,8] and, independently, by Keating.[9] $\mathbf{L}$ is a 2×2 symmetric matrix[10] identical in mathematical character to the dioptric power matrix $\mathbf{F}$ described by Fick[7,8] and Long[11] if not by others before them. Its entries have the units of reciprocal length and so can be in diopters. $\mathbf{L}_r$ is the reduced vergence at exit plane T of system S of the red astigmatic pencil defined by O, and $\mathbf{L}_b$ is the same but for the blue pencil.

We define

$$\mathbf{Z} = \mathbf{L}^{-1}\mathrm{n}. \tag{4}$$

$\mathbf{Z}$ is symmetric and has the units of length and can be regarded as a generalized position of the blurred image relative to exit plane T. The eigenvalues of $\mathbf{Z}$ give the longitudinal positions of the image lines, and the eigenvectors define their orientations. (Eigenvalues and eigenvectors are treated in standard texts in linear algebra and have been applied in this context in several articles.[9–11]) (For the moment, we assume that $\mathbf{L}^{-1}$ exists and return to the issue of nonexistence later.) Let the eigenvalues of $\mathbf{Z}$ be z_- and z_+ where $z_- \leq z_+$ and let the corresponding normalized eigenvectors be $\mathbf{v}_-$ and $\mathbf{v}_+$. Then, the first image line has longitudinal position z_- relative to exit plane T and is parallel to the complementary eigenvector $\mathbf{v}_+$, and the second image line has longitudinal position z_+ and is parallel to $\mathbf{v}_-$.

Eq. 1 suggests the definition

$$\Delta\mathbf{Z} = \mathbf{Z}_b - \mathbf{Z}_r \tag{5}$$

for the longitudinal chromatic aberration of a homocentric astigmatic system S for object point O on the optical axis. There is no

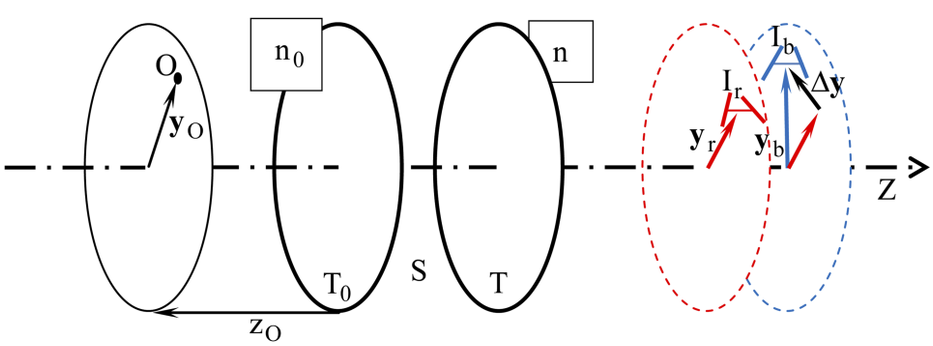

FIGURE 3.

Chromatic aberration of a system S with heterocentric astigmatic elements. Corresponding to object point O are blurred images I_r and I_b, each of which has a pair of longitudinally separated orthogonal image lines shown here by means of short line segments connected by a line segment parallel to Z. Longitudinal chromatic aberration is defined by Eq. 5 in terms of the reduced vergence of light at emergence from S at T. Transverse chromatic aberration is the vector $\Delta\mathbf{y}$. If Z is an optical axis and O is on Z then $\Delta\mathbf{y} = \mathbf{o}$ and I_r and I_b are centered on Z.

transverse chromatic aberration. $\Delta\mathbf{Z}$ characterizes the longitudinal difference of the two images completely. By this definition, longitudinal chromatic aberration becomes the 2×2 symmetric matrix $\Delta\mathbf{Z}$ and, as such, can be characterized by three independent numbers. However, we need to examine it further.

Now reduced vergence (either as scalar L or as matrix $\mathbf{L}$) depends on the relative longitudinal positions of object point and refracting elements and is independent of relative transverse positions. Thus, provided relative longitudinal positions are maintained, decentering the object point and elements of the system has no effect on the longitudinal positions and natures of the blurred images including the longitudinal positions and orientations of the image lines. It follows, therefore, that we can relax the requirement that O and the centers of the elements of S be on axis Z and take Eq. 5 to be the definition of the longitudinal chromatic aberration $\Delta\mathbf{Z}$ of a heterocentric astigmatic system for an object point anywhere.

Because $\Delta\mathbf{Z}$ is 2×2 and symmetric, longitudinal chromatic aberration has two orthogonal principal meridians. They are the meridians within which the longitudinal chromatic aberration is a maximum and a minimum. The maximum and minimum values are the *principal longitudinal chromatic aberrations*. They are the eigenvalues of $\Delta\mathbf{Z}$, and the corresponding principal meridians are the corresponding eigenvectors.

The only effect of relative decentration of object point and system elements is to cause transverse displacement $\mathbf{y}_r$ and $\mathbf{y}_b$ of blurred images I_r and I_b of object point O in heterocentric astigmatic system S. Then, Eq. 3 defines the transverse chromatic difference $\Delta\mathbf{y}$ of the images. We, therefore, call $\Delta\mathbf{y}$ the transverse chromatic aberration of system S for object point O.

CHROMATIC ABERRATION IN GENERAL

Eqs. 3 and 5 represent the generalizations to optical systems in general of the definitions (Eq. 1 and 2) for systems whose refracting elements are all stigmatic and centered on an optical axis. Eq. 3 defines $\Delta\mathbf{y}$ transverse and Eq. 5 $\Delta\mathbf{Z}$ longitudinal chromatic aberration in general; the first is a two-dimensional vector, and the second is a 2×2 symmetric matrix. The essential difference in mathematical character between transverse and longitudinal chromatic aberration highlights the fact that the two types of aberration are fundamentally different in nature and cannot meaningfully be combined into a single unified concept of chromatic aberration.

All this holds in particular for systems whose elements are stigmatic and homocentric. However, in a context in which only such systems are under discussion $\Delta\mathbf{y}$ and $\Delta\mathbf{Z}$ can be reduced to the scalar quantities Δy and Δz and sketched in one plane as in Fig. 1. Then, Δy is one component of $\Delta\mathbf{y}$, the other being zero and perpendicular to the plane of the paper, and Δz is the scalar coefficient in the scalar matrix $\Delta Z = \mathbf{I}\Delta z$, $\mathbf{I}$ being an identity matrix.

QUANTIFYING CHROMATIC ABERRATION

Having defined them, and given the makeup of an optical system, how do we calculate longitudinal and transverse chromatic aberration? Here, we derive general formulae in linear optics. The key is the system's ray transference, which is a function of the frequency of light.[12] For systems that may be heterocentric and astigmatic, the transference is the 5×5 matrix[13,14]

$$\mathbf{T} = \begin{pmatrix} \mathbf{A} & \mathbf{B} & \mathbf{e} \\ \mathbf{C} & \mathbf{D} & \boldsymbol{\pi} \\ \mathbf{o}^{\mathrm{T}} & \mathbf{o}^{\mathrm{T}} & 1 \end{pmatrix}. \quad (6)$$

$\mathbf{A}$, $\mathbf{B}$, $\mathbf{C}$, and $\mathbf{D}$ are 2×2 and $\mathbf{e}$ and $\boldsymbol{\pi}$ are 2×1 submatrices. They are the fundamental properties of the system. $\mathbf{o}^{\mathrm{T}}$ is the matrix transpose of the 2×1 null matrix $\mathbf{o}$. The fifth row of $\mathbf{T}$ is the trivial (0 0 0 0 1). $\mathbf{e}$ and $\boldsymbol{\pi}$ account for the effects of tilt and decentration; each is null if the longitudinal axis is an optical axis.[15]

Longitudinal Chromatic Aberration

If the reduced vergence is $\mathbf{L}_0$ at entrance plane T_0 of system S, then the reduced vergence is[10,16]

$$\mathbf{L} = (\mathbf{D}\mathbf{L}_0 - \mathbf{C})(\mathbf{A} - \mathbf{B}\mathbf{L}_0)^{-1} \quad (7)$$

at the exit plane T of S. For an object point O at longitudinal position z_O relative to T_0

$$\mathbf{L}_0 = \mathbf{I}n_0/z_O. \quad (8)$$

Hence

$$\mathbf{L} = (\mathbf{D}n_0/z_O - \mathbf{C})(\mathbf{A} - \mathbf{B}n_0/z_O)^{-1} \quad (9)$$

or

$$\mathbf{L} = (\mathbf{D} - \mathbf{C}z_O/n_0)(\mathbf{A}z_O/n_0 - \mathbf{B})^{-1} \quad (10)$$

with two special cases,

$$\mathbf{L} = -\mathbf{C}\mathbf{A}^{-1} \quad (11)$$

for $z_O \to \infty$ and

$$\mathbf{L} = -\mathbf{D}\mathbf{B}^{-1} \quad (12)$$

for $z_O = 0$. (Eq. 11 represents the back-vertex power of system S.[17]) Adding subscripts to all the parameters in these equations (except z_O) gives expressions for the red and blue reduced vergences $\mathbf{L}_r$ and $\mathbf{L}_b$ at exit plane T. Substitution into Eq. 5 then gives the longitudinal chromatic aberration $\Delta\mathbf{Z}$ for system S and object point O.

Transverse Chromatic Aberration

Perhaps surprisingly, the problem of calculating the transverse chromatic aberration is more challenging. We first examine object points at finite distances.

Consider the compound system from the transverse plane of O to the transverse plane containing an image line of a blurred image. Let the longitudinal position of the plane of the image line be z relative to exit plane T of system S. The compound system's transference is obtained by multiplying the transferences of the components in reverse order in the usual way.[14] Its top block row turns out to be

$$\left(\mathbf{A} + \mathbf{C}z/n \quad \mathbf{B} + \mathbf{D}z/n \quad -(\mathbf{A} + \mathbf{C}z/n)z_O/n_0 \quad \mathbf{e} + \boldsymbol{\pi}z/n\right). \quad (13)$$

Combining this with the equation for the transverse position at emergence (Eq. 14 of a previous article[14]), we see that a ray of

inclination $\mathbf{a}_O$ at object point O arrives at the transverse plane of the image line with transverse position

$$\mathbf{y} = (\mathbf{A} + \mathbf{C}z/n)\mathbf{y}_O + \Big(\mathbf{B} + \mathbf{D}z/n - (\mathbf{A} + \mathbf{C}z/n)z_O/n_0\Big)n_0\mathbf{a}_O + \mathbf{e} + \boldsymbol{\pi}z/n. \quad (14)$$

In particular for the ray parallel to longitudinal axis Z at O

$$\mathbf{y} = (\mathbf{A} + \mathbf{C}z/n)\mathbf{y}_O + \mathbf{e} + \boldsymbol{\pi}z/n. \quad (15)$$

We write this as

$$\mathbf{y} = \mathbf{A}\mathbf{y}_O + (\mathbf{C}\mathbf{y}_O + \boldsymbol{\pi})z/n + \mathbf{e}. \quad (16)$$

The first image line goes through the point given by Eq. 16 with $z = z_-$ and is parallel to $\mathbf{v}_+$. Hence, we can write a parametric equation for the first image line as

$$\mathbf{y}_- = \mathbf{v}_+k_- + \mathbf{A}\mathbf{y}_O + (\mathbf{C}\mathbf{y}_O + \boldsymbol{\pi})z_-/n + \mathbf{e} \quad (17)$$

for all real scalars k_-. Interchanging the plus and minus signs gives the equation of the second image line. But $\mathbf{v}_+$ is orthogonal to $\mathbf{v}_-$ so we can write the equation for the second image line as

$$\mathbf{y}_+ = \mathbf{E}\mathbf{v}_+k_+ + \mathbf{A}\mathbf{y}_O + (\mathbf{C}\mathbf{y}_O + \boldsymbol{\pi})z_+/n + \mathbf{e} \quad (18)$$

where $\mathbf{E} = \begin{pmatrix} 0 & 1 \\ -1 & 0 \end{pmatrix}$. Subtracting Eq. 17 from Eq. 18 we obtain

$$\mathbf{y}_+ - \mathbf{y}_- = (\mathbf{E}k_+ - \mathbf{I}k_-)\mathbf{v}_+ + \mathbf{c} \quad (19)$$

where

$$\mathbf{c} = (\mathbf{C}\mathbf{y}_O + \boldsymbol{\pi})(z_+ - z_-)/n. \quad (20)$$

Now $\mathbf{y}_+ - \mathbf{y}_-$ is the longitudinal projection of a vector from a point on the first image line to a point on the second. We make this vector parallel to Z, i.e., $\mathbf{y}_+ - \mathbf{y}_- = \mathbf{o}$. Then, in terms of the components of $\mathbf{v}_+$ and $\mathbf{c}$, Eq. 19 becomes

$$\begin{pmatrix} k_- & -k_+ \\ k_+ & k_- \end{pmatrix}\begin{pmatrix} v_{+1} \\ v_{+2} \end{pmatrix} = \begin{pmatrix} c_1 \\ c_2 \end{pmatrix}. \quad (21)$$

Multiplying out, rearranging, and reassembling into matrices we obtain

$$\begin{pmatrix} v_{+2} & -v_{+1} \\ v_{+1} & v_{+2} \end{pmatrix}\begin{pmatrix} k_+ \\ k_- \end{pmatrix} = \begin{pmatrix} -c_1 \\ c_2 \end{pmatrix}. \quad (22)$$

Because $\mathbf{v}_+$ is a unit vector, the 2×2 matrix on the left has unit determinant. Hence

$$\begin{pmatrix} k_+ \\ k_- \end{pmatrix} = \begin{pmatrix} v_{+2} & v_{+1} \\ -v_{+2} & v_{+2} \end{pmatrix}\begin{pmatrix} -c_1 \\ c_2 \end{pmatrix} \quad (23)$$

from which we obtain

$$k_- = \mathbf{v}_+^T\mathbf{c} \quad (24)$$

in particular. Substituting from Eq. 24 into Eq. 17 and rearranging one finds that the transverse position of the image is

$$\mathbf{y} = (\mathbf{A} + \mathbf{V}\mathbf{C})\mathbf{y}_O + \mathbf{e} + \mathbf{V}\boldsymbol{\pi} \quad (25)$$

where $\mathbf{V}$ is the matrix

$$\mathbf{V} = \Big(\mathbf{v}_+\,\mathbf{v}_+^T(z_+ - z_-) + \mathbf{I}z_-\Big)/n. \quad (26)$$

For a distant object point we take the compound system to be system S and the homogeneous gap between S and an image line and apply a similar method to that used above for an object point at a finite distance. We find that, for a distant object point O, the transverse position of the image turns out to be

$$\mathbf{y} = (\mathbf{B} + \mathbf{V}\mathbf{D})n_0\mathbf{a}_O + \mathbf{e} + \mathbf{V}\boldsymbol{\pi} \quad (27)$$

where $\mathbf{a}_O$ is the inclination of the rays from O.

Eqs. 25 to 27 can be written for the red and blue blurred images. Eq. 27 then gives $\mathbf{y}_b$ and $\mathbf{y}_r$ for distant object points and Eq. 25 gives them otherwise. Hence, from Eq. 3, we obtain the transverse chromatic aberration

$$\Delta\mathbf{y} = \Delta(\mathbf{A} + \mathbf{V}\mathbf{C})\mathbf{y}_O + \Delta(\mathbf{e} + \mathbf{V}\boldsymbol{\pi}) \quad (28)$$

for an object point at a finite distance and

$$\Delta\mathbf{y} = \Delta\Big((\mathbf{B} + \mathbf{V}\mathbf{D})n_O\Big)\mathbf{a}_O + \Delta(\mathbf{e} + \mathbf{V}\boldsymbol{\pi}) \quad (29)$$

for a distant object point.

The calculation fails when the reduced vergence $\mathbf{L}$ of either the blue or red light is singular, that is, when an image line is at infinity. However, such cases seem of little practical interest and we consider them no further.

Systems with Stigmatic Elements

In particular, if every element of the system is stigmatic, then $\mathbf{A}$, $\mathbf{B}$, $\mathbf{C}$, and $\mathbf{D}$ are all scalar matrices; that is, $\mathbf{A} = \mathbf{I}A$ where A is a scalar, and similarly for the other three 2×2 fundamental properties. The reduced vergence at emergence is also a scalar matrix, $\mathbf{L} = \mathbf{I}L$, and so is $\mathbf{Z}$ (Eq. 4), $\mathbf{Z} = \mathbf{I}Z$. The eigenvalues of $\mathbf{Z}$ are not distinct: $z_- = z_+ = Z$ is simply the longitudinal position of the image point relative to exit plane T. The longitudinal chromatic aberration is $\Delta\mathbf{Z} = \mathbf{I}\Delta Z$ where ΔZ is the longitudinal position of the blue image point relative to the longitudinal position of the red image point. Eq. 26 reduces to $\mathbf{V} = \mathbf{I}Z/n$ and, finally, Eqs. 28 and 29 become

$$\Delta\mathbf{y} = \Delta(A + ZC/n)\mathbf{y}_O + \Delta(\mathbf{e} + Z\boldsymbol{\pi}/n) \quad (30)$$

and

$$\Delta\mathbf{y} = \Delta\Big((B + ZD/n)n_0\Big)\mathbf{a}_O + \Delta(\mathbf{e} + Z\boldsymbol{\pi}/n). \quad (31)$$

Summary of the Routine for Calculating Longitudinal and Transverse Chromatic Aberration

Suppose we know the transferences of a system S for blue and red light. We can then calculate the longitudinal and transverse chromatic aberrations of the system for a finite object point O with longitudinal position z_O and transverse position $\mathbf{y}_O$. We proceed as follows. We use Eqs. 9 or 10 to determine the reduced vergence $\mathbf{L}$ of blue light from O leaving S. Eq. 4 then gives the generalized longitudinal position $\mathbf{Z}$ of the blue image. We repeat for the red image. The longitudinal chromatic aberration is then $\Delta\mathbf{Z}$ given by Eq. 5. For $\mathbf{Z}$, for blue light, we obtain the eigenvalues z_- and z_+ and the corresponding normalized eigenvectors $\mathbf{v}_-$ and $\mathbf{v}_+$. Eq. 26 gives $\mathbf{V}$. Hence one determines $\mathbf{A} + \mathbf{V}\mathbf{C}$ and $\mathbf{e} + \mathbf{V}\boldsymbol{\pi}$ for the blue light. This is repeated for red light. $\Delta(\mathbf{A} + \mathbf{V}\mathbf{C})$ is calculated by subtraction (blue minus red) and similarly for $\Delta(\mathbf{e} + \mathbf{V}\boldsymbol{\pi})$.

Finally, the transverse chromatic aberration $\Delta\mathbf{y}$ is given by Eq. 28.

If object point O is distant then we need the inclination $\mathbf{a}_O$. The calculation is the same as for a finite object point except that the vergence $\mathbf{L}$ is obtained via Eq. 11, $(\mathbf{B} + \mathbf{VD})n_0$ replaces $\mathbf{A} + \mathbf{VC}$, and Eq. 29 is used instead of Eq. 28.

The Appendix illustrates the calculations for a heterocentric astigmatic model eye with four refracting surfaces (available at http://links.lww.com/OPX/A107).

CONCLUSIONS

For systems with homocentric stigmatic refracting elements definitions of chromatic aberration differ from author to author. Several authors have remarked on the inconsistency and confusion.[18–20] We believe there is a need for authors to take greater care to define terms in general but particularly in the context of chromatic aberration.

Here, we have offered definitions that are natural generalizations of the familiar concepts[1–6] in Gaussian optics; they hold for the special case of systems with homocentric stigmatic elements, and they hold for systems, like the eye, with elements that are heterocentric and astigmatic. We have also derived expressions for longitudinal and transverse chromatic aberration in terms of the fundamental properties of the optical system.

For general systems, which may be heterocentric and astigmatic, we have defined longitudinal chromatic aberration to be the 2×2 symmetric matrix $\Delta\mathbf{Z}$ given by Eq. 5. It depends on the longitudinal position z_O of the object point O but is independent of the transverse position $\mathbf{y}_O$. Its eigenvectors are principal meridians of longitudinal chromatic aberration, and its eigenvalues are the principal longitudinal chromatic aberrations along them.

The transverse chromatic aberration $\Delta\mathbf{y}$, a vector defined by Eq. 3, can be calculated by means of Eqs. 28 or 29. In general, it is an affine function of the object's transverse position $\mathbf{y}_O$ (Eq. 28) in the case of objects at finite distances or of its direction, in effect $\mathbf{a}_O$, (Eq. 29) in the case of distant objects. If the refracting elements of the system are all centered on longitudinal axis Z, then Z is an optical axis, and because $\mathbf{e}$ and $\boldsymbol{\pi}$ are both null,[15] the constant term $\Delta(\mathbf{e} + \mathbf{V}\boldsymbol{\pi})$ in those equations vanishes, and the transverse chromatic aberration becomes linear in $\mathbf{y}_O$ or $\mathbf{a}_O$.

It may be worth mentioning that the principal meridians of the red and blue pencils, leaving the optical system, need not match. This is why one cannot, in general, simply calculate longitudinal chromatic aberration separately in two orthogonal principal meridians. Nevertheless, preliminary calculations (such as those in the Appendix) suggest that, for many practical purposes, it may well be sufficiently accurate to do so.

If the system in question is composed of stigmatic elements arranged homocentrically, then the definitions here reduce to the familiar definitions[1–6] of chromatic aberration in Gaussian optics. This special case has been treated above. We note, however, that stigmatic systems exist with astigmatic elements.[21,22] For them, the special case does not apply, although their longitudinal chromatic aberration $\Delta\mathbf{Z}$ is a scalar matrix.

We are not entirely comfortable with the word aberration in the terms longitudinal and transverse chromatic aberration. It suggests an optical concept beyond first order, whereas here, and in most cases in the literature, the concept is one in first-order optics. However, until a more suitable term is suggested, we believe longitudinal and transverse chromatic aberration be reserved for the concepts defined here.

The definitions proposed here are not specific to the eye. The retina, in particular, is not mentioned in the definitions. When applied to the eye, as to any other system, it is important to be unambiguous about how the definitions are being used. First, it should be clear what the system is whose chromatic aberration is being defined; in particular, the entrance and exit planes T_0 and T should be defined. For the visual optical system of the eye that would most likely have T_0 immediately in front of the tear film on the cornea and T immediately in front of the retina. Second, the location of longitudinal axis Z should be specified in some way. Third, the location of the object point relative to Z should be given. Finally, the two frequencies ν_r and ν_b of the light should be given or understood.

In his or her introduction to optometry, the beginning student often learns to refract with the interval of Sturm and its relation to the retina in mind. What is clear from the analysis here is that there is such an interval for each frequency, that they differ longitudinally and transversely by the longitudinal and transverse chromatic aberration, and that, from a knowledge of the structure of the eye, we are now able to calculate these differences. (A somewhat different perspective on what underlies the routine of refraction is presented elsewhere.[23])

It would seem that the familiar concepts of longitudinal and transverse chromatic aberration, as defined in Gaussian optics,[1–6] are probably less directly useful in the clinical context which may be why a variety of concepts related to them has been devised for use in practice. Confusion arises, however, because many of these concepts are called by the same names. They should, we believe, be assigned suitable distinguishing designations. Our generalization of the concepts in Gaussian optics to allow for heterocentricity and astigmatism may also be of less direct use in the clinical environment. Nevertheless, it has its place in optometric didactics and in the broader understanding of the optics of vision. Furthermore, the theory provides tools for exploring the effects of changes to the eye that accompany accommodation and refractive surgery for example.

APPENDIX

The appendix is available online at http://links.lww.com/OPX/A107.

ACKNOWLEDGMENTS

We thank L. N. Thibos and R. D. van Gool for continuing discussions. WFH gratefully acknowledges a grant from the National Research Foundation of South Africa. TE, a graduate student working with him, acknowledges support from the Medical Research Council of South Africa.

Received January 15, 2012; accepted July 2, 2012.

REFERENCES

1. Born M, Wolf E. Principles of Optics: Electromagnetic Theory of Propagation, Interference and Diffraction of Light, 7th (expanded) ed. Cambridge, UK: Cambridge University Press; 2002.

2. Sharma KK. Optics: Principles and Applications. Amsterdam, The Netherlands: Academic Press; 2006.
3. Smith G, Atchison DA. The Eye and Visual Optical Instruments. Cambridge, UK: Cambridge University Press; 1997.
4. Hofstetter HW, Griffin JR, Berman MS, Everson RW. Dictionary of Visual Science and Related Clinical Terms, 5th ed. Boston, MA: Butterworth-Heinemann; 2000.
5. Millodot M, Laby DM. Dictionary of Ophthalmology. Oxford, UK: Butterworth-Heinemann; 2002.
6. Millodot M. Dictionary of Optometry and Visual Science, 7th ed. Edinburgh, UK: Butterworth-Heinemann Elsevier; 2009.
7. Fick HH. Fortschrittliche Rechnungsarten in der Augenoptik. Der Augenoptiker 1973;(20):55–61.
8. Blendowske R. Hans-Heinrich Fick: early contributions to the theory of astigmatic systems. S Afr Optom 2003;62:105–10.
9. Keating MP. A system matrix for astigmatic optical systems: part I. Introduction and dioptric power relations. Am J Optom Physiol Opt 1981;58:810–9.
10. Harris WF. Wavefronts and their propagation in astigmatic optical systems. Optom Vis Sci 1996;73:606–12.
11. Long WF. A matrix formalism for decentration problems. Am J Optom Physiol Opt 1976;53:27–33.
12. Evans T, Harris WF. Dependence of the transference of a reduced eye on frequency of light. S Afr Optom 2011;70:149–55.
13. Harris WF. Paraxial ray tracing through noncoaxial astigmatic optical systems, and a 5 × 5 augmented system matrix. Optom Vis Sci 1994;71:282–5.
14. Harris WF. Transferences of heterocentric astigmatic catadioptric systems including Purkinje systems. Optom Vis Sci 2010;87:778–86.
15. Harris WF. Optical axes of eyes and other optical systems. Optom Vis Sci 2009;86:537–41.
16. Harris WF. Dioptric power: its nature and its representation in three- and four-dimensional space. Optom Vis Sci 1997;74:349–66.
17. Harris WF. Back- and front-vertex powers of astigmatic systems. Optom Vis Sci 2010;87:70–2.
18. Thibos LN, Bradley A, Still DL, Zhang X, Howarth PA. Theory and measurement of ocular chromatic aberration. Vision Res 1990;30:33–49.
19. Simonet P, Campbell MC. The optical transverse chromatic aberration on the fovea of the human eye. Vision Res 1990;30:187–206.
20. Rabbetts RB. Bennett and Rabbett's Clinical Visual Optics, 4th ed. Edinburgh, UK: Butterworth-Heinemann-Elsevier; 2007.
21. Harris WF. Stigmatic optical systems. Optom Vis Sci 2004;81: 947–52.
22. Harris WF. Proper and improper stigmatic optical systems. Optom Vis Sci 2004;81:953–9.
23. Harris WF. Subjective refraction: the mechanism underlying the routine. Ophthalmic Physiol Opt 2007;27:594–602.

William F. Harris
Department of Optometry,
University of Johannesburg
APK Campus, PO Box 524,
Auckland Park, Johannesburg 2006
South Africa
e-mail: wharris@uj.ac.za

OPO OPHTHALMIC & PHYSIOLOGICAL OPTICS
THE JOURNAL OF THE COLLEGE OF OPTOMETRISTS

Ophthalmic & Physiological Optics ISSN 0275-5408

Line of sight of a heterocentric astigmatic eye

William F Harris, Radboud DHM van Gool and Tanya Evans

Department of Optometry, University of Johannesburg, Johannesburg, South Africa

Citation information: Harris WF, van Gool RDHM & Evans T. Line of sight of a heterocentric astigmatic eye. *Ophthalmic Physiol Opt* 2013, **33**, 57–66. doi: 10.1111/opo.12007

Keywords: astigmatism, corneal sighting centre, heterocentricity, line of sight, sighting axis, transference

Correspondence: William F Harris
E-mail address: wharris@uj.ac.za

Received: 17 July 2012; Accepted: 7 November 2012

Abstract

Background: The line of sight and the corneal sighting centre are important references for clinical work in optometry and ophthalmology. Their locations are not fixed but may vary with displacement of the pupil and other changes in the eye.
Purpose: To derive equations for the dependence of the locations on properties of an eye which may be heterocentric and astigmatic.
Methods: The optical model used is linear optics. It allows for the refracting surfaces of the eye to be astigmatic and tilted or decentred. Because the approach is general it applies not only to the natural eye but also to a pseudophakic eye and to the compound system of eye and any optical instrument in front of it. The analysis begins with the line of sight defined in terms of the foveal chief ray.
Results: Equations are derived for the position and inclination of the line of sight at incidence onto the eye. They allow one to locate the line of sight and corneal sighting centre given the structure (curvatures, tilts, spacings of refracting surfaces) of the eye. The results can be generalized in several ways including application in the case of extra-foveal fixation and when there is a lens or other optical instrument in front of the eye. The calculation is illustrated in the Appendix for a model eye with four separated, astigmatic and tilted refracting surfaces.
Conclusions: The equations allow routine calculation of the line of sight for an eye of known structure and of the eye combined with an optical device such as a spectacle lens. They also allow exploration of the dependence of the line of sight on the location of the centre of the pupil and on other properties in the eye. There is a dependence of the line of sight on the frequency (or vacuum wavelength) of light but this may not be of clinical significance.

Introduction

Among the several axes defined for the eye the line of sight has been described as 'the most important axis from the point of view of visual function, including refraction procedures'.[1] However the line of sight is not fixed for any eye because the centre of the pupil can vary.[1–3] Indeed displacement of the pupil centre is but one of many changes, inside and outside the eye, that may alter the line of sight. Actually, even for a fixed eye, there is strictly no unique line of sight but one for each frequency or vacuum wavelength of light. (These statements will be justified below.) However, how significant are these effects? Despite the importance of the concept the literature seems to have no clear answers. Our purpose here is to develop a framework for finding answers. More particularly we shall make use of the powerful methodology of linear optics to derive an equation for the line of sight as a function of properties of the eye with or without an optical device in front of it.

The methodology used in this note is the same as that used in several recent papers[4–10] to which the reader is referred for more details than are given here. The equations derived below allow one to examine the sensitivity of the line of sight to displacement of the centre of the pupil, to accommodation, to decentration of an intraocular lens, to frequency and so on. Linear optics and the concept of the ray transference allow one to approach the problem in a very general manner; we are not limited to particular models of the eye and can handle eyes with multiple, separated, decentred and nonaligned astigmatic elements. Further-

more, although we shall talk of the eye, the generality of the approach means that the results also apply to compound systems consisting of eye and optical instrument (lens, telescope, etc.) in front of it.

Definition of the line of sight

Like many others[11–16] Alpern[17] defines the line of sight as the line joining the fixation point and the centre of the entrance pupil. It is a line in object space, that is, outside the eye. Implicit in the definitions is that the index of refraction of the medium (usually air but it may be water for example) in object space is uniform and isotropic and, hence, that the line of sight is a straight line. The general direction of the light into the eye assigns it a positive sense. We shall regard the line of sight as infinite; in other words it is the directed straight line segment from fixation point to centre of entrance pupil extended to infinity in both positive and negative senses. It remains a line in object space and allows for the possibility of real and virtual object points. (We shall not consider virtual objects explicitly.)

We mention in passing that the International Organization for Standardization (ISO) defines the line of sight in terms of the entrance and exit pupils and the centre of the fovea.[18] ISO call it the *visual axis* although in the forthcoming edition of the Standard the name has been changed to *line of sight* (personal communication from R. B. Rabbetts).

If the cornea is astigmatic then, strictly speaking, the centre of the entrance pupil is not well defined. The image of the centre of the (actual) pupil in the cornea is not a point but a blurred region consisting of a pair of separated orthogonal lines in the familiar interval of Sturm. The effect is usually sufficiently small to be of no consequence in the clinical environment but it does present problems in optical analyses. Regardless of the degree of astigmatism the problems are overcome if the line of sight is defined in terms of the foveal chief ray[17,19] (the ray through the centres of the pupil and the fovea) instead of the entrance pupil. The Optical Society of America (OSA) defines the line of sight as the foveal chief ray itself.[19] On the other hand, for Alpern the line of sight is that part of the foveal chief ray which can be specified in object space[17]; this has more in common with the definition in terms of entrance pupil. Accordingly, for the purposes of this paper we take the line of sight to be the infinite straight line defined by the portion of the foveal chief ray in object space, that is, the portion incident onto the eye.

The location of the line of sight can be defined by specifying a single point and a direction. A convenient point is the intersection of the line with the first surface of the cornea, the *corneal sighting centre* in Mandell's[20] terminology. Accordingly our primary objective will be to find formulae for the location of the corneal sighting centre and the direction of the line of sight in terms of properties of the eye which can be calculated from knowledge of the structure of the eye.

Locating the line of sight

Figure 1 is a schematic representation of an eye and its line of sight. The only physical structure of the eye actually shown in the figure is the iris (grey). The hole in the iris, not necessarily circular, is the pupil. The pupil lies in transverse plane T_P. Z is a reference longitudinal axis relative to which transverse positions and inclinations are measured. T_K is a transverse plane immediately anterior to the tear film on the cornea and T_R a transverse plane immediately anterior to the retina. The medium immediately anterior to T_K has index of refraction n_0; the indices in the pupil and immediately anterior to the retina are n_P and n_R respectively. The visual optical system of the eye is from T_K to T_R; we represent it as optical system S. T_P partitions S into subsystems S_A and S_B. We call S_A the anterior portion of the eye or simply the anterior eye and similarly for S_B, the posterior portion. Properties of S_A are identified by means of subscript A and similarly for S_B. We call S the eye or the whole eye; properties of S have no subscripts.

In *Figure 1* point P represents the centre of the pupil and point R the centre of the fovea. By definition the foveal chief ray intersects centres P and R; three of its segments are shown, an incident segment, a segment through the pupil and a segment arriving at the fovea. K is the corneal sighting centre. By definition the infinite straight line defined by the incident segment is the line of sight LL.

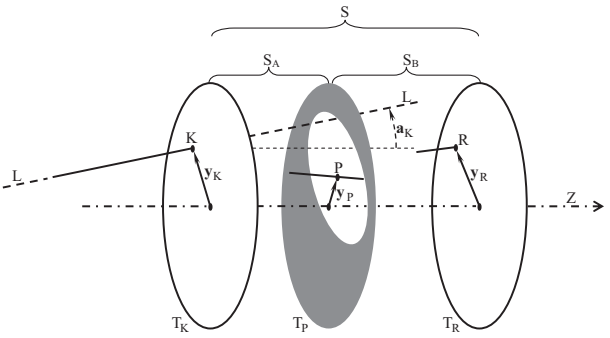

Figure 1. The line of sight or sighting axis LL and the corneal K, pupillary P and retinal R sighting centres (P and R usually being the centres of the pupil and fovea). S is the visual optical system of an eye; it extends from entrance plane T_K, immediately anterior to the corneal tear film, to the exit plane T_R, immediately in front of the retina. The iris and pupil are the only structures of the eye shown explicitly; they define plane T_P which partitions the eye into anterior S_A and posterior S_B portions. Z is the longitudinal axis relative to which transverse positions and inclinations are measured. Three segments of the foveal chief ray or sighting ray are shown: incident onto S at K, in the pupil through P and emergent from S_B at R.

Relative to longitudinal axis Z points K, P and R have transverse positions represented by the vectors $\mathbf{y}_K$, $\mathbf{y}_P$ and $\mathbf{y}_R$ respectively. Each vector is represented by a 2×1 matrix whose top and bottom entries are Cartesian components which we may regard as its horizontal and vertical components respectively; they are in length units.

The line of sight has transverse position $\mathbf{y}_K$ at T_K and inclination $\mathbf{a}_K$. Like $\mathbf{y}_K$, $\mathbf{a}_K$ is 2×1 and its components are the horizontal and vertical components of the inclination; they are in radians and, hence, unitless. $\mathbf{y}_K$ characterizes the location of the corneal sighting centre completely and $\mathbf{y}_K$ and $\mathbf{a}_K$ together completely characterize the line of sight LL. Our objective is to obtain expressions for $\mathbf{y}_K$ and $\mathbf{a}_K$ in terms of other properties of the eye, properties that can be calculated from curvatures, tilts and spacings of refracting elements in the eye and of refractive indices of the media between them.

We represent the inclination of the foveal chief ray at P in the pupil and at R on the retina as $\mathbf{a}_P$ and $\mathbf{a}_R$ respectively. We now apply the basic equations of linear optics across the whole eye (Equations 7, 8 of a previous paper[7] for example). This gives a pair of simultaneous matrix equations in terms of the transverse positions $\mathbf{y}_K$ and $\mathbf{y}_R$ and inclinations $\mathbf{a}_K$ and $\mathbf{a}_R$ of the foveal chief ray at incidence onto the cornea and at the retina:

$$\mathbf{A}\mathbf{y}_K + n_0\mathbf{B}\mathbf{a}_K + \mathbf{e} = \mathbf{y}_R \tag{1}$$

and

$$\mathbf{C}\mathbf{y}_K + n_0\mathbf{D}\mathbf{a}_K + \boldsymbol{\pi} = n_R\mathbf{a}_R. \tag{2}$$

A, **B**, **C**, **D** are 2×2 matrices and **e** and $\boldsymbol{\pi}$ 2×1 matrices; they are submatrices of the ray transference **T** (5×5) of the eye S and represent its fundamental optical properties. **A**, **B** and **e** form the first or top block-row of **T** and **C**, **D** and $\boldsymbol{\pi}$ the second block-row. It is apparent from Equation 1 that **A** is unitless and **B** and **e** have length units and from equation 2 that **C** has reciprocal length units (dioptres, for example) and **D** and $\boldsymbol{\pi}$ no units. Equation 1 written across S_A, the anterior eye, becomes

$$\mathbf{A}_A\mathbf{y}_K + n_0\mathbf{B}_A\mathbf{a}_K + \mathbf{e}_A = \mathbf{y}_P \tag{3}$$

where $\mathbf{A}_A$, $\mathbf{B}_A$ and $\mathbf{e}_A$ are fundamental properties of S_A.

Equations 1 and 3 can be combined into the single matrix equation

$$\mathbf{Q}\begin{pmatrix}\mathbf{y}_K\\ \mathbf{a}_K\end{pmatrix} = \begin{pmatrix}\mathbf{y}_R - \mathbf{e}\\ \mathbf{y}_P - \mathbf{e}_A\end{pmatrix} \tag{4}$$

where $\begin{pmatrix}\mathbf{y}_K\\ \mathbf{a}_K\end{pmatrix}$ is a 4×1 matrix which we call the *incident location* of the line of sight and

$$\mathbf{Q} = \begin{pmatrix}\mathbf{A} & n_0\mathbf{B}\\ \mathbf{A}_A & n_0\mathbf{B}_A\end{pmatrix} \tag{5}$$

is a 4×4 matrix whose top block-row is a property of the whole eye S and whose bottom block-row is a property of the anterior eye S_A. We refer to **Q** as the *coefficient matrix*. The top block-row of the 4×1 matrix on the right of Equation 4 is a property of the whole eye, including the location of the centre of the fovea $\mathbf{y}_R$, and the bottom block-row is a property of the anterior eye including the centre of the pupil $\mathbf{y}_P$.

A line of sight necessarily satisfies Equation 4. Equation 4 is an example of a linear equation, a standard equation in linear algebra. Depending on the coefficient matrix and the matrix on the right of the equation it may have no solution for $\begin{pmatrix}\mathbf{y}_K\\ \mathbf{a}_K\end{pmatrix}$, a unique solution or an infinity of solutions. The conditions on existence and uniqueness, and the set of all solutions when there is more than one solution, have been presented elsewhere.[7,21]

One expects a ray through P and R to be unique. Hence one expects there to be a unique line of sight. Mathematically this means that **Q** should be nonsingular, that is, its determinant should not be zero, in which case one can solve Equation 4 to give the unique solution

$$\begin{pmatrix}\mathbf{y}_K\\ \mathbf{a}_K\end{pmatrix} = \mathbf{Q}^{-1}\begin{pmatrix}\mathbf{y}_R - \mathbf{e}\\ \mathbf{y}_P - \mathbf{e}_A\end{pmatrix}. \tag{6}$$

An exception occurs when P and R happen to be conjugate points; there are then an infinity of lines of sight. It is hard to imagine a situation in which there is no line of sight. It seems safe to disregard such exceptions and take Equation 6 to be the unique solution for the line of sight of an eye. Should they occur, however, one would need to turn to the conditions and expressions presented before.[7,21] We consider them no further here.

We conclude that Equation 6 locates the line of sight in terms of the properties of the eye (represented by **Q**, **e** and $\mathbf{e}_A$) including the locations of the centres of the pupil and fovea $\mathbf{y}_P$ and $\mathbf{y}_R$. It gives the transverse position $\mathbf{y}_K$ and inclination $\mathbf{a}_K$ of the line of sight at incidence onto the cornea, that is, at the corneal sighting centre. For reference below we note from Equation 6 that the incident location $\begin{pmatrix}\mathbf{y}_K\\ \mathbf{a}_K\end{pmatrix}$ of the line of sight is linear in the matrix $\begin{pmatrix}\mathbf{y}_R - \mathbf{e}\\ \mathbf{y}_P - \mathbf{e}_A\end{pmatrix}$.

Because it is a straight line the line of sight intersects the retina in the point with transverse position

$$\mathbf{y}_{KR} = \mathbf{y}_K + z\mathbf{a}_K. \quad (7)$$

z is the length of the eye. This point on the retina provides another way of visualizing the line of sight. It is the transverse position of the image of the centre of the fovea for an observer looking along the line of sight.

Rearranging Equation 2 and substituting from Equation 6 we obtain

$$\mathbf{a}_R = (\,\mathbf{C} \quad n_0\mathbf{D}\,)\mathbf{Q}^{-1}\begin{pmatrix}\mathbf{y}_R - \mathbf{e}\\ \mathbf{y}_P - \mathbf{e}_A\end{pmatrix}/n_R + \boldsymbol{\pi}/n_R, \quad (8)$$

the inclination, relative to longitudinal axis Z, of the foveal chief ray at the fovea explicitly in terms of properties of the eye.

The use of Equations 6, 7 and 8 is illustrated in the Appendix where the line of sight is determined for a model eye with four separated, astigmatic and tilted refracting surfaces. The calculation is performed for two frequencies of light.

Sensitivity to changes in the eye

Coefficient matrix **Q**, defined by Equation 5, depends on fundamental properties **A** and **B** of the whole eye and of the anterior portion of the eye. These fundamental properties in turn depend on curvatures and separations of the refracting surfaces in the eye but they are independent of tilts or decentrations of those surfaces.[8] Thus **Q** is usually affected by changes in curvatures and spacings of the refracting surfaces but not by changes in tilt or decentration. Fundamental property **e**, however, is usually altered by changes in curvatures, spacings, tilts and decentrations. This means that changes in transverse position of the centres of the pupil and fovea, $\mathbf{y}_P$ and $\mathbf{y}_R$, and changes in tilt and decentration of the refracting surfaces in the eye change $\begin{pmatrix}\mathbf{y}_R - \mathbf{e}\\ \mathbf{y}_P - \mathbf{e}_A\end{pmatrix}$ without changing **Q**; the incident location of the line of sight is, therefore, linear in such changes. Relatively simple explicit equations are easily obtained as illustrated below for changes in $\mathbf{y}_P$ and $\mathbf{y}_R$.

Because changes in curvatures and spacings of refracting surfaces may change **Q**, **e** and $\mathbf{e}_A$ one expects from Equation 6 that the sensitivity of the line of sight to such changes should be much more complicated. By making use of the fact that properties **A**, **B** and **e** of a system are particular affine functions of curvatures and spacings of the refracting surfaces[8] one could, if desired, obtain explicit equations for the sensitivity to changes in curvature and separation of refracting surfaces in the eye. However because such equations are probably very messy, differ for each surface and gap and depend on the particular model eye chosen it seems unwarranted to attempt to do so here. Furthermore they are probably of little interest because the change in the line of sight can be determined simply by applying Equation 6 twice, once before and once after a change. (This is illustrated in the Appendix for changes in curvature of the first and third surfaces of the four-surface model eye and in the distance between the second and third surfaces.)

Alternative approaches

Equation 6 represents a direct and relatively simple routine for locating the line of sight of an eye of known optical structure. It is unlikely to present problems in most applications of interest. However it displays little information on relationships and gives little insight. There are a number of different approaches which lead to equations which do not have those disadvantages. Each of these other approaches, however, brings with it additional problems concerning singularity and possible associated computational difficulties. We outline some of them here.

From Equation 1 one can write

$$\mathbf{a}_K = \mathbf{B}^{-1}(\mathbf{y}_R - \mathbf{e} - \mathbf{A}\mathbf{y}_K)/n_0. \quad (9)$$

Substitution into Equation 3 gives an equation in $\mathbf{y}_K$ which can be solved to give

$$\mathbf{y}_K = (\mathbf{A}_A - \mathbf{B}_A\mathbf{F}_0)^{-1}\big(\mathbf{y}_P - \mathbf{B}_A\mathbf{B}^{-1}(\mathbf{y}_R - \mathbf{e}) - \mathbf{e}_A\big), \quad (10)$$

the transverse position of the corneal sighting centre relative to longitudinal axis Z. Here

$$\mathbf{F}_0 = \mathbf{B}^{-1}\mathbf{A} \quad (11)$$

is the corneal-plane refractive compensation of the eye.[22] Equation 9 holds under the assumption that fundamental property **B** of the eye is nonsingular; Equation 10 holds under the assumption that both **B** and $\mathbf{A}_A - \mathbf{B}_A\mathbf{F}_0$ are nonsingular. Substitution from Equation 10 into Equation 9 gives an explicit equation for the inclination $\mathbf{a}_K$ of the line of sight. Together $\mathbf{y}_K$ and $\mathbf{a}_K$ locate the line of sight completely relative to longitudinal axis Z.

We could also find the line of sight by solving Equation 1 for $\mathbf{y}_K$, substituting into Equation 3 and, hence, obtaining expressions for $\mathbf{y}_K$ and $\mathbf{a}_K$. The first step in that approach assumes that **A** is nonsingular. **A** is strictly a measure of the ametropia of the eye[22]; it is singular whenever a distant object point maps to a point (emmetropia) or a line (simple astigmatism or what we might call semi-emmetropia) on the retina. Equations for the line of sight obtained this way would fail, therefore, for such eyes at

least. Furthermore one would anticipate computational problems and uncertainty for eyes that are close to these conditions if not for others.

Yet more equations can be obtained for the line of sight if one begins by solving Equation 3 for $\mathbf{y}_K$ or $\mathbf{a}_K$ and substituting into Equation 1.

Although these equations have limitations arising out of possible singularity they may all have their uses for particular applications. For example suppose the centre of the pupil undergoes a transverse displacement $\Delta\mathbf{y}_P$. Then it follows from Equation 10 that the corneal sighting centre is displaced by

$$\Delta\mathbf{y}_K = (\mathbf{A}_A - \mathbf{B}_A\mathbf{F}_0)^{-1}\Delta\mathbf{y}_P. \qquad (12)$$

Equation 12 shows explicitly that change in the location of the corneal sighting centre, and the incident position of the line of sight, is linear in the transverse displacement of the centre of the pupil, the proportionality matrix being the property $(\mathbf{A}_A - \mathbf{B}_A\mathbf{F}_0)^{-1}$ of the eye. According to Equation 9 transverse displacement of the centre of the pupil has no effect on the inclination of the line of sight. On the other hand both the inclination and the incident position of the line of sight are dependent on the location of the centre of the fovea; from Equations 9 and 10 we obtain a transverse shift in incident position

$$\Delta\mathbf{y}_K = -(\mathbf{A}_A - \mathbf{B}_A\mathbf{F}_0)^{-1}\mathbf{B}_A\mathbf{B}^{-1}\Delta\mathbf{y}_R \qquad (13)$$

and change in inclination

$$\Delta\mathbf{a}_K = \mathbf{B}^{-1}\left(\mathbf{I} + \left(\mathbf{B}\mathbf{B}_A^{-1}\mathbf{A}_A\mathbf{A}^{-1} - \mathbf{I}\right)^{-1}\right)\Delta\mathbf{y}_R/n_0 \qquad (14)$$

of the line of sight corresponding to a transverse displacement $\Delta\mathbf{y}_R$ of the centre of the fovea. (We are not implying that the fovea actually shifts; we could, for example, be comparing the lines of sight of two model eyes identical except for the locations of the centres of their foveas.) $\mathbf{I}$ represents the identity matrix. Both dependences are linear.

The proportionality matrices in Equations 12 to 14 are calculated for the model eye in the Appendix.

In effect Equations 9, 10 and 12–14 all represent special cases of the linearity in $\begin{pmatrix}\mathbf{y}_R - \mathbf{e}\\ \mathbf{y}_P - \mathbf{e}_A\end{pmatrix}$ represented by Equation 6 and discussed above under the heading **Sensitivity to changes in the eye**.

Chromatic dependence

Equation 6 expresses the location of the line of sight in terms of the fundamental properties (more particularly the top block-row fundamental properties) of the whole eye and the anterior eye. However, the fundamental properties are dependent on the frequency of light.[23] Hence we expect there to be a line of sight for each frequency. One can define a chromatic difference for lines of sight by

$$\Delta\begin{pmatrix}\mathbf{y}_K\\ \mathbf{a}_K\end{pmatrix} = \begin{pmatrix}\mathbf{y}_K\\ \mathbf{a}_K\end{pmatrix}^b - \begin{pmatrix}\mathbf{y}_K\\ \mathbf{a}_K\end{pmatrix}^r \qquad (15)$$

where the superscripts b and r denote light of two specified frequencies. In the numerical example in the Appendix the corneal sighting centres for red and blue light are more than two wavelengths apart and the inclinations of the lines of sight differ by a little more than 0.001 radians. These differences are small and may be of little clinical significance.

Generalizations

Although we have talked here of the eye and the centres of the pupil and fovea there is nothing in the mathematics that limits application to the eye as such or that requires the points in the pupil and fovea to be their centres. This means that the results described above can be generalized. We outline three generalizations.

The results apply equally well, for example, to a compound system of eye and lens or other optical instrument in front of the eye. In the analysis above system S then becomes the compound system, and, instead of being immediately anterior to the tear film on the cornea, transverse plane T_K is now immediately anterior to the first surface of the optical instrument. T_R, immediately in front of the retina, is unchanged. T_P is unchanged at the plane of the pupil unless an aperture in the optical instrument becomes the limiting aperture of the compound system in which case T_P is at that limiting aperture. As above, system S_A is from T_K to T_P and S_B is from T_P to T_R. $\mathbf{y}_R$ remains the position vector relative to longitudinal axis Z of the centre of the fovea on the retina. $\mathbf{y}_P$ remains the centre of the pupil or becomes the centre of the limiting aperture if the pupil is not the limiting aperture. The line of sight for the compound system is located by Equation 6 in which $\mathbf{a}_K$ is its inclination at incidence onto the instrument and $\mathbf{y}_K$ is its transverse position on the first surface of the instrument. Instead of being the corneal sighting centre $\mathbf{y}_K$ becomes the sighting centre as it were on the front of the instrument. In the case of a thin spectacle lens $\mathbf{y}_K$ locates the visual point on the lens with respect to longitudinal axis Z. It can also be obtained directly from Equation 10.

In the case of extra-foveal fixation one can interpret $\mathbf{y}_R$ as the transverse position of the centre of visual attention on the retina. The results above then can be applied in physiological and pathological conditions in which fixation is not centred on the centre of the fovea.

There may be circumstances in which one wishes to interpret $\mathbf{y}_P$ as the transverse position relative to Z of a point in the pupil other than the centre. We have in mind here the Stiles-Crawford effect[24] and Tscherning's comment[15] that 'In sighting … the image of the point fixed … has nothing to do with the centre of the pupil'. Or the pupil may be irregular in shape with a centre not easy to define.[3] A line of sight could be located using the results above if $\mathbf{y}_P$ were known.

Concluding remarks

Equation 6 represents the central result of this paper; it locates the line of sight of an eye (natural or pseudophakic) in terms of properties of the eye. It does so by giving the transverse position $\mathbf{y}_K$ at incidence onto the eye and the inclination $\mathbf{a}_K$ of the line of sight, both being relative to longitudinal axis Z. Coefficient matrix $\mathbf{Q}$ in Equation 6 is defined by Equation 5 and depends on the top block-rows of the transferences of the whole eye and the anterior portion of the eye. The transferences can be determined from knowledge of the structure of the eye. (The use of the equations is illustrated in the Appendix for a particular heterocentric astigmatic eye.)

The usual definition of line of sight in terms of the entrance pupil may suggest that the line of sight of an eye depends on the location of the centre of the entrance pupil and is independent of other structures. The analysis here shows that in fact it may vary with change of any structure in the eye; in particular one expects it to vary with accommodation.

Strictly there is a line of sight for each frequency of light. Whether the differences between them are of any significance remains to be seen.

Although we refer here to the eye, with some appropriate reinterpretations (described under **Generalizations**), the analysis has much broader application. It can be applied, for example, to the compound system of eye and any optical instrument in front of the eye. $\mathbf{y}_K$ and $\mathbf{a}_K$, then, given by Equation 6, represent the transverse position and inclination of the line of sight relative to Z at incidence onto the anterior surface of the instrument.

The analysis can also accommodate physiological and pathological conditions in which fixation is not foveal or phenomena such as the Stiles-Crawford effect in which it may be appropriate to use a point in the pupil other than the centre. In situations such as these it seems appropriate to extend Mandell's terminology[20] (corneal sighting centre) to other surfaces. Hence we have *retinal sighting centre*, for example, whose location is given by $\mathbf{y}_R$. Usually it is the centre of the fovea but it is elsewhere in extra-foveal fixation. Similarly $\mathbf{y}_P$ locates the *pupillary sighting centre* which may usually be taken as the centre of the pupil but could be elsewhere. The visual point on a thin spectacle lens would be the *spectacle sighting centre*.

The line of sight was defined above in terms of the foveal chief ray but, when the retinal or pupillary sighting centres are not the centres of the fovea or pupil, then the ray in terms of which the line of sight is defined is not the foveal chief ray. In general one might refer to the ray through the pupillary and retinal sighting centres as the *sighting ray*. Usually one would expect the sighting ray to be the foveal chief ray.

It is possible for Equation 6 for the line of sight to fail. This occurs when matrix $\mathbf{Q}$ is singular. We do not expect that to happen in the case of eyes but it is conceivable when the eye is a component of a compound system. In such cases, depending on the nature of $\mathbf{Q}$ and the matrix on the right of Equation 4, there may be no line of sight or multiple lines of sight. Equation 4 is standard in linear algebra. Conditions of existence and uniqueness of solutions are presented elsewhere.[7,21] When there are multiple solutions the equation for all solutions is also given in those papers.

Alternative equations for the line of sight can be obtained. Examples include Equations 9 and 10. Some give additional insight into relationships and may be useful but all have potential problems associated with singularity.

The equations here allow one to explore the effects of changes both inside and outside the eye, for example when a spectacle lens is placed in front of the eye or there is accommodation or shift in location of the centre of the pupil. The location of the pupil centre, if regarded as the pupillary sighting centre, is represented explicitly as $\mathbf{y}_P$ in Equation 6 and accommodation changes at least the top-block row of $\mathbf{Q}$ in that equation.

The nature of Equation 6 suggests a complicated dependence of the line of sight on changes of curvature and spacings of refracting surfaces within the eye. However, tilts and decentrations of refracting surfaces and the locations of the centres of the pupil and fovea (or pupillary and retinal sighting centres) are exceptional in that changes in them produce linear changes in the line of sight. If there are no other changes Equation 9 shows that a transverse shift of the centre of the pupil has no effect on the inclination of the line of sight; its effect on the incident position of the line of sight is linear (Equation 12). For the model eye treated in the Appendix the corneal sighting centre undergoes a shift approximately 13% larger than the pupillary sighting centre and approximately in the same direction. Equations 13 and 14 show that the incident transverse position and inclination of the line of sight are both linearly sensitive to position of the retinal sighting centre. The sensitivities are calculated for the model eye in the Appendix.

The Appendix also illustrates application of Equation 6 to determine the effect on the line of sight of other particular changes within the eye, including changes of curvature of the first and third surfaces of the eye and separation between the

second and third surfaces. In most of these cases the effects are small and, perhaps, of little significance in many applications. They depend, however, on the particular model eye chosen for the analysis and should not necessarily be regarded as representative of eyes in general. Nevertheless the numbers do suggest that accommodation and other changes in the eye are less significant than displacement of the centre of the pupil. It is also evident that change in curvature, tilt or decentration of the first surface of the eye causes no shift in position of the corneal sighting centre.

The line of sight is based on the incident segment of the sighting ray, the segment external to the eye. However, the Stiles-Crawford phenomenon[24] and what Bradley and Thibos[25] describe as the retina's 'inherent optical axis' suggest that there might be merit in also defining an axis based on the segment of the sighting ray at the retina. We would then distinguish between the *incident* or *external* line of sight of an eye (what we have simply been calling the line of sight) and the eye's *retinal* line of sight. The latter would be the infinite straight line containing the segment of the sighting ray at the retina. The retinal line of sight is located by Equation 8 which gives its inclination, its transverse position at the retina, of course, being the retinal sighting centre.

Ordinarily a lens or other instrument placed in front of a fixed eye changes the incident line of sight but not the retinal line of sight. It is only if an aperture in the instrument becomes limiting that both incident and retinal lines of sight may change.

One expects the pupillary sighting centre to be the centre of the pupil but it may be elsewhere in the pupil. If the structure of the anterior part of the eye and the location of the line of sight are known then the location of the pupillary sighting centre can be calculated by means of Equation 3.

The entrance pupil of an eye is in object space. Thus the traditional definition of line of sight in terms of point of fixation (in object space) and entrance pupil (also in object space) might, at first sight, give the impression that the line of sight of an eye is more a property of object space and less a property of the eye. The equations developed here stress the fact that the line of sight of an eye is a property of the eye alone. In particular it does not depend on a fixation point. Indeed the line of sight exists even if there is no fixation point (in the dark for example). The only provisos are that the index of refraction immediately in front of the eye does not change and that the pupil remains the limiting aperture. (The line of sight changes, for example, if an eye in air submerges in water or a pinhole aperture is placed in front of the eye.) We can think of the eye as having a pointer attached to it at the cornea along the line of sight and directed forward. The act of fixating a point object involves turning the eye so that the pointer points at the object in question.

Line of sight is a term not unique to optometry, ophthalmology and vision science. It is common in several fields, cosmology[26] being but one example. In such fields, in contrast to the term we have been using, the term does not necessarily imply an eye at all. The line of sight is simply a ray from some object in question. If one wishes to see the object then one needs to bring the line of sight of an eye, or of each eye, into coincidence locally with a line of sight of the object. Again 'eye' here may also be interpreted 'compound system of eye and instrument in front of it'.

Partly because two such distinct concepts have the same name we have reservations about the term 'line of sight' for the property of the eye. Implicit in the traditional definition is that the line is straight, but lines are not necessarily straight. 'Axis' seems more appropriate than 'line'; it better suggests a straight line and is more in keeping with the names of other axes of the eye including optical axis, visual axis and achromatic axis. 'Sighting axis' seems a possible alternative to 'line of sight'. An eye would then have corneal, pupillary and retinal sighting centres, a sighting ray and a sighting axis. To see a distant object one would need to turn the eye to bring its sighting axis into coincidence with a line of sight of the object.

We have used here the powerful methodology of linear optics to obtain explicit equations for the location of the line of sight in the case of an eye with multiple separated refracting surfaces that may be heterocentric, tilted and astigmatic. All that is required beyond refractive indices and axial separations is the paraxial geometry of each refracting surface. As with the simpler optical model, Gaussian optics, we need to keep in mind, however, that the theory is paraxial and that accuracy declines with increasing distances and inclinations relative to the longitudinal axis. For greater accuracy we would need to turn to geometrical optics but then we would need the whole geometry of every surface (which we seldom have) and we would usually have to be satisfied with numerical computation. The explicit equations obtained here are, we assert, the best obtainable.

Traditionally the line of sight is defined in terms of the entrance pupil. But, strictly speaking, an entrance pupil is not well defined if the eye has an astigmatic cornea; its centre, as any other point in it, is blurred out as an interval of Sturm. Although this effect may be negligible for clinical purposes it presents a problem for optical analyses including the analysis presented here. By making use of the actual pupil instead the entrance pupil, as one does when defining the line in terms of the foveal chief ray, one avoids the problem. The clinician, however, does not have the luxury of access to the pupil and has to be satisfied with the entrance pupil. Nevertheless, for most purposes, there is no conflict between the two definitions; the clinician and the theoretician are talking about the same thing and merely approaching it with the particular tools that each has at his or her disposal.

Acknowledgements

WF Harris gratefully acknowledges a grant from the National Research Foundation of South Africa. T Evans, a graduate student working with him, acknowledges support from the Medical Research Council of South Africa. We thank Ronald B Rabbetts for helpful comments and Margaret McGovern (Librarian, College of Optometrists, UK) and Kay Hévey (Editorial Assistant, *Optician*) for help with references.

References

1. Atchison DA & Smith G. Optics of the Human Eye. Butterworth-Heinemann: Oxford, 2000; pp. 31–36.
2. Yang Y, Thompson K & Burns SA. Pupil location under mesopic, photopic, and pharmacologically dilated conditions. *Invest Ophthalmol Vis Sci* 2002; 43: 2508–2512.
3. Wyatt HJ. The form of the human pupil. *Vis Res* 1995; 14: 2021–2036.
4. Harris WF. Nodes and nodal points and lines in eyes and other optical systems. *Ophthalmic Physiol Opt* 2010; 30: 24–42.
5. Harris WF. Visual axes in eyes that may be astigmatic and have decentred elements. *Ophthalmic Physiol Opt* 2010; 30: 204–207.
6. Harris WF. Aperture referral in heterocentric astigmatic systems. *Ophthalmic Physiol Opt* 2011; 31: 603–614.
7. Harris WF. Achromatic axes and their linear optics. *Vis Res* 2012; 58: 1–9.
8. Harris WF. Dependence of optical properties of heterocentric astigmatic systems on internal elements, with application to the human eye. *Trans Roy Soc S Afr* 2012; 67: 11–16.
9. Harris WF & Evans T. Chromatic aberration in heterocentric astigmatic systems including the eye. *Optom Vis Sci* 2012; 89: e37–e43.
10. Harris WF. Chief nodal axes of a heterocentric astigmatic eye and the Thibos-Bradley achromatic axis. *Vis Res* 2012; 73: 40–45.
11. Millodot M & Laby DM. Dictionary of Ophthalmology. Butterworth-Heinemann: Oxford, 2002; p. 163.
12. Hofstetter HW, Griffin JR, Berman MS & Everson RW. Dictionary of Visual Science and Related Clinical Terms, 5th edn. Butterworth-Heinemann: Boston, 2000; p. 306.
13. Millodot M. Dictionary of Optometry and Visual Science, 7th edn. Butterworth-Heinemann-Elsevier: Edinburgh, 2009; p. 208.
14. Stidwill D & Fletcher R. Normal Binocular Vision: Theory, Investigation and Practical Aspects. Wiley-Blackwell: Oxford, 2011; p. 4.
15. Tscherning MHE. Physiologic Optics, 2nd edn. The Keystone: Philadelphia, PA, 1904; p. 74.
16. Le Grand Y & El Hage SG. Physiological Optics. Springer-Verlag: Berlin, 1980; p. 72.
17. Alpern M. Specification of the direction of regard. In: Muscular Mechanisms. Vol. 3 of The Eye, (Davson H, editor), 2nd edn, Academic Press: New York, 1969; pp. 5–12.
18. International Organization for Standardization. Ophthalmic Optics Spectacle Lenses Vocabulary, International Standard ISO 13666. ISO: Geneva, 1998; p. 13.
19. Applegate RA, Thibos LN, Bradley A *et al.* Reference axis selection: subcommittee report of the OSA working group to establish standards for measurement and reporting of optical aberrations of the eye. *J Refract Surg* 2000; 16: S656–S658.
20. Mandell RB. Locating the corneal sighting center in videokeratography. *J Refract Surg* 1995; 11: 253–258.
21. Harris WF. Optical axes of eyes and other optical systems. *Optom Vis Sci* 2009; 86: 537–541.
22. Harris WF. A unified paraxial approach to astigmatic optics. *Optom Vis Sci* 1999; 76: 480–499.
23. Evans T & Harris WF. Dependence of the transference of a reduced eye on frequency of light. *S Afr Optom* 2011; 70: 149–155.
24. Stiles WS & Crawford BH. The luminous efficiency of rays entering the eye pupil at different points. *Proc Roy Soc* 1933; 112: 428–450.
25. Bradley A & Thibos LN. Modelling off-axis vision. I: The optical effects of decentering visual targets or the eye's entrance pupil. In: Vision Models for Target Detection and Recognition (E Peli, editor), World Scientific: Singapore, 1995; pp. 313–337.
26. Eggleton P. Evolutionary Processes in Binary and Multiple Stars. Cambridge University Press: Cambridge, 2006; pp. 3, 6, 10, etc.
27. Villegas ER, Carretero L & Fimia A. Le Grand eye for the study of ocular chromatic aberration. *Ophthalmic Physiol Opt* 1996; 16: 528–531.

Appendix

We illustrate application of the theory by locating the line of sight, including the corneal sighting centre, for a particular ametropic heterocentric astigmatic model eye. We also illustrate the effect on the line of sight of changes in frequency of light, transverse position of the centres of the pupil and fovea, curvature of the third and first refracting surfaces and separation of the second and third surfaces.

The model eye has four separated astigmatic and tilted refracting surfaces the details of which are listed in *Table 1*. The principal radii of curvature of the first surface of the cornea (K1) are 5.8 mm along the horizontal and 7 mm along the vertical and the surface has tilts 0.06 in the horizontal (from in front of the eye the right of the surface would appear pushed away relative to the left) and −0.05 in the vertical (the bottom of the surface would appear pushed away relative to the top) all measured at the reference axis Z. The tilts are in radians or, equivalently, no units. The curvatures and tilts of the second surface of the cornea (K2) and the first (L1) and second (L2) surfaces of the lens of the eye should be interpreted similarly. The

Table 1. Principal radii of curvature, separation, and tilt of surfaces (K1 and K2 of the cornea and L1 and L2 of the lens) of the model eye used in the numerical example

Surface	Principal radii, mm{degr}mm	Separation, mm	Tilt
K1	5.8{180} 7		$(0.06\ -0.05)^{\mathrm{T}}$
		0.5	
K2	5{10}6.2		$(0.04\ \ 0.06)^{\mathrm{T}}$
		4	
L1	4.1{20}5		$(-0.07\ 0.1)^{\mathrm{T}}$
		4	
L2	−5{70}−6.2		$(-0.05\ -0.03)^{\mathrm{T}}$
		16	

separation between K1 and K2 is 0.5 mm. The expressions for refractive index as a function of vacuum wavelength published by Villegas *et al.*[27] have been used.

The principal meridians of the refracting surfaces are not aligned. The eye is in air; hence we set $n_0 = 1$. The eye's length is $z = 24.5$ mm. We suppose the centre of the pupil is located 1 mm to the left of axis Z. Hence, taking it to be the pupillary sighting centre, we set $\mathbf{y}_{\mathrm{P}} = \begin{pmatrix} -1 \\ 0 \end{pmatrix}\mathrm{mm}$.

We also suppose that the retinal sighting centre is located 1 mm from Z in the 45° direction. It may be at the centre of the fovea but this makes no difference to the calculation. Thus $\mathbf{y}_{\mathrm{R}} = \begin{pmatrix} \cos 45^\circ \\ \sin 45^\circ \end{pmatrix}\mathrm{mm}$.

The calculation is done for light of frequencies corresponding to the vacuum wavelengths 486.1 ('blue') and 656.3 ('red') nm; the results are summarized in Table 2. **A** is the top left 2 × 2 submatrix of the transference, **B** the top middle 2 × 2 matrix and **e** the top right 2 × 1 submatrix. Below **A**, **B** and **e** in the transference are **C**, **D** and $\boldsymbol{\pi}$ respectively. The coefficient matrices **Q** were calculated using Equation 5. Their determinants turn out to be approximately 205 and 202 mm^2 for red and blue respectively which confirms that the lines of sight exist uniquely and that Equation 6 gives their transverse positions $\mathbf{y}_{\mathrm{K}}$ and inclinations $\mathbf{a}_{\mathrm{K}}$ at incidence on to the eye. The red and blue corneal sighting centres are about 1.3 mm left and 0.2 mm below longitudinal axis Z. The lines of sight slope up and to the right into the eye at about 0.04 radians (4 prism dioptres) away from axis Z. The chromatic difference for the eye of the red and blue lines of sight is (Equation 15)

$$\Delta\begin{pmatrix} \mathbf{y}_{\mathrm{K}} \\ \mathbf{a}_{\mathrm{K}} \end{pmatrix} = \begin{pmatrix} 0.001335\,\mathrm{mm} \\ -0.000432\,\mathrm{nm} \\ -0.00101 \\ -0.00016 \end{pmatrix}.$$

Thus the red and blue corneal sighting centres are a few wavelengths apart. The lines of sight intersect the retina in the point represented by $\mathbf{y}_{\mathrm{KR}}$ calculated by means of Equation 7. The blue and red sighting rays arrive at the retina with inclination $\mathbf{a}_{\mathrm{R}}$ given by Equation 8; here they are identical up to a few tens of microradians.

The last row in *Table 2* lists the proportionality matrix $(\mathbf{A}_{\mathrm{A}} - \mathbf{B}_{\mathrm{A}}\mathbf{F}_0)^{-1}$ of Equation 12. It differs only slightly for red and blue light and is close to the scalar matrix 1.13**I**. In other words a transverse shift of the centre of the pupil causes a shift of the line of sight, and hence of the corneal sighting centre, that is approximately 13% larger in magnitude and in approximately the same transverse direction.

The proportionality matrices in Equations 13 and 14 also turn out to be close to identity matrices, −0.24**I** and $0.057\mathbf{I}\ \mathrm{mm}^{-1}$ respectively. Thus a shift of the retinal sighting centre causes a shift in the corneal sighting centre that is about a quarter in magnitude but in approximately the opposite direction and it causes the inclination of line of sight to change by about 5.7 prism dioptres or 3.3 degrees per millimetre in approximately the same direction.

Repeating the calculation using Equation 6 but with the principal powers of the third surface of the model eye each increased by 1 D we obtain a change in incident location of the line of sight by about $\begin{pmatrix} 0.0033717\,\mathrm{mm} \\ 0.0000003\,\mathrm{mm} \\ -0.0008066 \\ -0.0000008 \end{pmatrix}$. Thus the corneal sighting centre has been shifted by roughly 3 μm approximately to the right and the inclination of the line of sight has increased by about 0.05 degrees approximately to the left.

If instead 1 D is added to each principal power of the first surface Equation 6 shows that the change in incident location of the line of sight is $\begin{pmatrix} 0\ \mathrm{mm} \\ 0\ \mathrm{mm} \\ -0.0012896 \\ -0.0001956 \end{pmatrix}$. Thus the corneal sighting centre is not moved, as is to be expected, while the inclination of the line of sight increases by about 0.08 degrees approximately to the left.

Increasing the distance between the second and third surfaces (the depth of the anterior chamber) by 1 mm the incident location of the line of sight changes by $\begin{pmatrix} -0.0640562\,\mathrm{mm} \\ -0.0437903\,\mathrm{mm} \\ -0.0036075 \\ -0.0020368 \end{pmatrix}$, that is, the incident position shifts about 0.08 mm in the 214-degree direction (left and down) and the incident inclination increases by about 0.24 degrees in the 209-degree direction.

Many of these numbers may well be negligibly small for most purposes. The degree to which they are representative of eyes, however, remains to be examined.

Table 2. Locating the lines of sight for red and blue light for the heterocentic astigmatic model eye defined in Table 1. Lengths are in millimetres and reciprocal lengths in kilodioptres

	Red	**Blue**
Transference of S	$\begin{pmatrix} -0.3718 & -0.0183 & 16.2363 & -0.1309 & -0.3073 \\ -0.0169 & -0.2012 & -0.1303 & 16.1841 & 0.1944 \\ -0.0811 & -0.0014 & 0.8522 & -0.0100 & -0.0165 \\ -0.0013 & -0.0723 & -0.0100 & 0.8459 & 0.0076 \\ 0 & 0 & 0 & 0 & 1 \end{pmatrix}$	$\begin{pmatrix} -0.3914 & -0.0186 & 16.1246 & -0.1321 & -0.3121 \\ -0.0171 & -0.2185 & -0.1315 & 16.0708 & 0.1964 \\ -0.0826 & -0.0014 & 0.8500 & -0.0102 & -0.0168 \\ -0.0013 & -0.0737 & -0.0101 & 0.8435 & 0.0077 \\ 0 & 0 & 0 & 0 & 1 \end{pmatrix}$
Top block-row of the transference of S_A	$\begin{pmatrix} 0.8066 & 0.0008 & 3.3717 & 0.0003 & -0.0708 \\ 0.0008 & 0.8396 & 0.0003 & 3.3701 & 0.0703 \end{pmatrix}$	$\begin{pmatrix} 0.8035 & 0.0008 & 3.3538 & 0.0003 & -0.0719 \\ 0.0008 & 0.8370 & 0.0003 & 3.3522 & 0.0712 \end{pmatrix}$
$\mathbf{Q}$	$\begin{pmatrix} -0.3718 & -0.0183 & 16.2363 & -0.1309 \\ -0.0169 & -0.2012 & -0.1303 & 16.1841 \\ 0.8066 & 0.0008 & 3.3717 & 0.0003 \\ 0.0008 & 0.8396 & 0.0003 & 3.3701 \end{pmatrix}$	$\begin{pmatrix} -0.3914 & -0.0186 & 16.1246 & -0.1321 \\ -0.0171 & -0.2185 & -0.1315 & 16.0708 \\ 0.8035 & 0.0008 & 3.3538 & 0.0003 \\ 0.0008 & 0.8370 & 0.0003 & 3.3522 \end{pmatrix}$
$\begin{pmatrix} \mathbf{y}_R - \mathbf{e} \\ \mathbf{y}_P - \mathbf{e}_A \end{pmatrix}$	$\begin{pmatrix} 1.0144 \\ 0.5127 \\ -0.9292 \\ -0.0703 \end{pmatrix}$	$\begin{pmatrix} 1.0192 \\ 0.5107 \\ -0.9281 \\ -0.0712 \end{pmatrix}$
$\mathbf{y}_K$	$\begin{pmatrix} -1.2896 \\ -0.1956 \end{pmatrix}$	$\begin{pmatrix} -1.2882 \\ -0.1960 \end{pmatrix}$
$\mathbf{a}_K$	$\begin{pmatrix} 0.0330 \\ 0.0282 \end{pmatrix}$	$\begin{pmatrix} 0.0319 \\ 0.0280 \end{pmatrix}$
$\mathbf{y}_{KR}$	$\begin{pmatrix} -0.4821 \\ 0.4944 \end{pmatrix}$	$\begin{pmatrix} -0.5056 \\ 0.4901 \end{pmatrix}$
$\mathbf{a}_R$	$\begin{pmatrix} 0.08712 \\ 0.03518 \end{pmatrix}$	$\begin{pmatrix} 0.08715 \\ 0.03518 \end{pmatrix}$
$(\mathbf{A}_A - \mathbf{B}_A\mathbf{F}_0)^{-1}$	$\begin{pmatrix} 1.1315 & -0.0063 \\ -0.0063 & 1.1345 \end{pmatrix}$	$\begin{pmatrix} 1.1301 & -0.0064 \\ -0.0064 & 1.1331 \end{pmatrix}$

Dependence of the ray transference of model eyes on the frequency of light

Tanya Evans* and William F Harris
Department of Optometry, University of Johannesburg, Johannesburg, South Africa
*Corresponding author: tevans@uj.ac.za

The transference defines the first-order character of an optical system; almost all the system's optical properties can be calculated from it. It is useful, therefore, to have some idea of how it depends on the frequency of light. We examine the dependence for two Gaussian eyes. It turns out to be nearly linear for all four fundamental properties. The result is an equation for the dependence of the transference on frequency which is almost symplectic. We also transform the transference into Hamiltonian space, obtain equations for the least-squares straight line for the three independent transformed properties and map them back to the group of transferences. The result is an equation for the dependence of the transference on frequency which is exactly symplectic and therefore representative of an optical system. The results may approximate those of real eyes and give estimates of the dependence of almost all optical properties on frequency.

Keywords: ray transference; frequency; symplecticity

Introduction

The ray transference is of central importance in linear optics. Nearly all the familiar optical properties of an eye such as power, refractive compensation, magnification and cardinal points can be derived from the transference. It is therefore useful to have some idea of how it depends on the frequency of light. In this presentation we examine the dependence of the transference of the reduced eye [1] and Le Grand's four-surface schematic eye [2] on frequency with the objective of obtaining an equation for the dependence. Consequently, the dependence of the eye's optical properties on frequency, as well as their chromatic difference between two frequencies, can be obtained from the frequency-dependent transference. This forms part of a much larger study. Many of these chromatic properties can be generalised to astigmatic heterocentric eyes.

Method

The underlying method used here is that of first-order optics. We make use of the ray transference which is a complete representation of the first-order effects of an optical system on the rays traversing it [3]. We represent the transference as

$$\mathbf{S} = \begin{pmatrix} A & B \\ C & D \end{pmatrix} \tag{1}$$

where A the dilation, B the disjugacy, C the divergence and D the divarication are the four fundamental properties of the Gaussian system [4].

Being a member of the symplectic group, the transference has unit determinant [4, 5]. Symplectic matrices are closed under multiplication, inversion and transposition but are not closed under

addition nor multiplication by a scalar [4, 5]. This creates problems when doing quantitative analyses on sets of transferences [5]. To overcome this limitation, we make use of the mapping from the symplectic group to the set of Hamiltonian matrices. The set of all Hamiltonian matrices defines a linear (vector) space and is therefore closed under matrix addition and multiplication by a scalar, [4, 5]. This makes the set of Hamiltonian matrices suitable for quantitative analysis including conventional statistical analysis. We explore two mappings. Firstly, the principal matrix logarithm of a symplectic matrix is a Hamiltonian matrix and inversely the matrix exponential of a Hamiltonian matrix is a symplectic matrix. Secondly, the Cayley transform, being its own functional inverse, provides a mapping between symplectic and Hamiltonian matrices. The Cayley transform is defined as [6]

$$\hat{\mathbf{S}} = (\mathbf{I} - \mathbf{S})(\mathbf{I} + \mathbf{S})^{-1} \tag{2}$$

where the caret (^) denotes the Hamiltonian transformed transference.

We are interested in the dependence of the transference on the frequency of light across the visible spectrum, 430 to 750 THz ($\times 10^{12}\mathrm{s}^{-1}$). Frequency is independent of the medium whereas wavelength is not and energy is proportional to frequency, good reasons for studying the dependence of properties on the frequency of light rather than on wavelength [7]. When obtaining the transference, it is the refractive index that is dependent on frequency. We make use of the formula for the refractive index as a function of wavelength developed for the chromatic eye [8] and the formulae for the refractive indices as functions of wavelength for the cornea, aqueous, lens and vitreous developed by Villegas *et al.* [9] based on the polynomial fit of Le Grand's findings [10] for the four-surface schematic eye. Both sets of equations are based on experimental findings. The refractive index of air is approximated by $n_0 = 1$. The transferences were calculated as described elsewhere [11].

Results

In Figure 1 the dependence of the transference on the frequency of light is shown for the reduced eye (blue) and Le Grand's eye (black) and is very nearly linear for each of the fundamental properties. The dashed straight lines shown in the figure are obtained using the least-squares method. The formula for the straight lines as a function of frequency (v) is given by

$$\mathbf{S} = \begin{pmatrix} a_1 & b_1 \\ c_1 & d_1 \end{pmatrix} v + \begin{pmatrix} a_2 & b_2 \\ c_2 & d_2 \end{pmatrix} \tag{3}$$

with constants given in Table 1 for the reduced and Le Grand's eyes. This gives us a good approximation for the transference of a Gaussian eye as a function of frequency.

Transforming the frequency-dependent transferences into Hamiltonian matrices, we are able to obtain the least-squares straight line for each of the three independent entries in Hamiltonian space, which we map back to symplectic matrices. This allows us to obtain an expression for the dependence of the transference on the frequency of light which is exactly symplectic. The least-squares straight line in Hamiltonian space is

$$\hat{\mathbf{S}} = \begin{pmatrix} \hat{a}_1 & \hat{b}_1 \\ \hat{c}_1 & -\hat{a}_1 \end{pmatrix} v + \begin{pmatrix} \hat{a}_2 & \hat{b}_2 \\ \hat{c}_2 & -\hat{a}_2 \end{pmatrix} \tag{4}$$

with the constants for the reduced and Le Grand's eyes given in Table 2 for the Cayley transform and Table 3 for the logarithmic transform. To obtain the transference as a function of frequency one

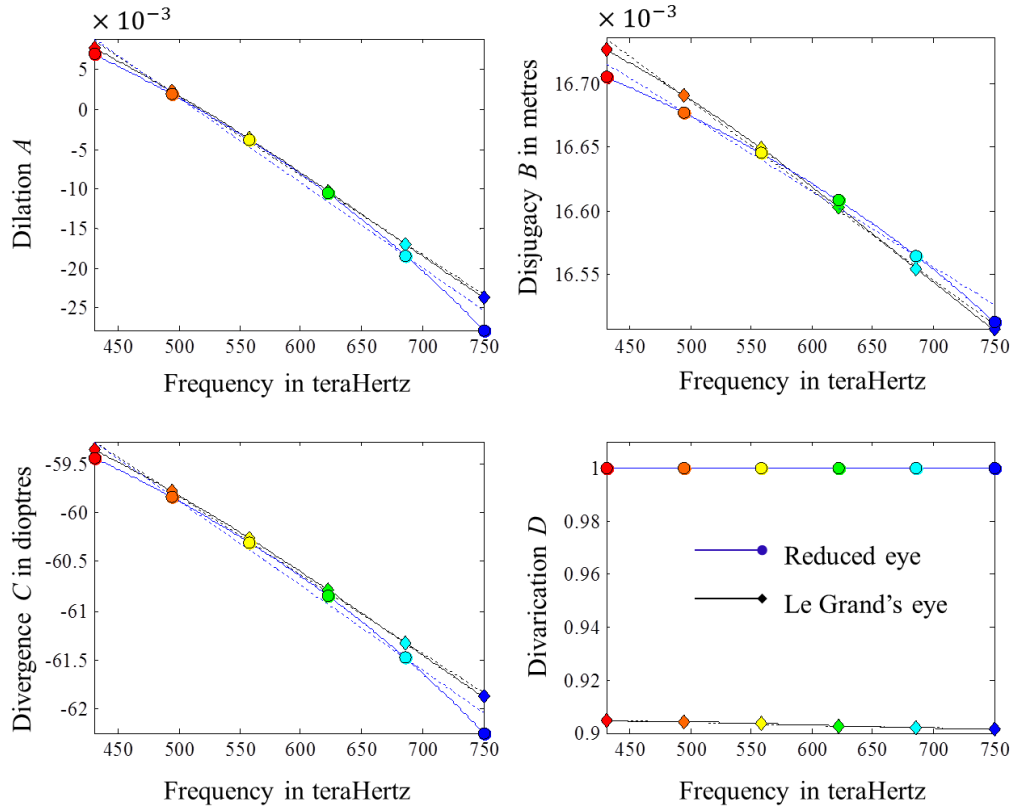

Figure 1. The fundamental properties of the reduced and Le Grand's eyes as functions of frequency. The least squares straight lines (Equation 3) are shown with dashed lines. The coloured markers represent equal spacings of 64 THz ($\times 10^{12}$ s^{-1}) and approximate the colours represented at each frequency.

Table 1. Constants for Equation 3, the units being picoseconds ($\times 10^{-12}$ s), metres and dioptres (m^{-1}).

Reduced eye		Le Grand's eye	
$a_1 = -1.069\times10^{-4}$ ps	$a_2 = 0.0549$	$a_1 = -0.997\times10^{-4}$ ps	$a_2 = 0.0516$
$b_1 = -5.939\times10^{-7}$ m ps	$b_2 = 16.972\times10^{-3}$ m	$b_1 = -7.034\times10^{-7}$ m ps	$b_2 = 17.038\times10^{-3}$ m
$c_1 = -8.605\times10^{-3}$ D ps	$c_2 = -55.579$ D	$c_1 = -7.975\times10^{-3}$ D ps	$c_2 = -55.849$ D
$d_1 = 0$ ps	$d_2 = 1$	$d_1 = -1.115\times10^{-5}$ ps	$d_2 = 0.910$

Table 2. Constants for Equation 4 for the Cayley transform.

Reduced eye		Le Grand's eye	
$\hat{a}_1 = 4.780\times10^{-5}$ ps	$\hat{a}_2 = 0.309$	$\hat{a}_1 = 4.263\times10^{-5}$ ps	$\hat{a}_2 = 0.289$
$\hat{b}_1 = 0$ m ps	$\hat{b}_2 = -11.111\times10^{-3}$ m	$\hat{b}_1 = 4.633\times10^{-8}$ m ps	$\hat{b}_2 = -11.509\times10^{-3}$ m
$\hat{c}_1 = 7.206\times10^{-3}$ D ps	$\hat{c}_2 = 36.298$ D	$\hat{c}_1 = 7.111\times10^{-3}$ D ps	$\hat{c}_2 = 37.630$ D

Table 3. Constants for Equation 4 for the logarithmic transform.

Reduced eye		Le Grand's eye	
$\hat{a}_1 = -7.905\times10^{-5}$ ps	$\hat{a}_2 = -0.564$	$\hat{a}_1 = -6.887\times10^{-5}$ ps	$\hat{a}_2 = -0.523$
$\hat{b}_1 = -2.491\times10^{-7}$ m ps	$\hat{b}_2 = 20.281\times10^{-3}$ m	$\hat{b}_1 = -3.567\times10^{-7}$ m ps	$\hat{b}_2 = 20.781\times10^{-3}$ m
$\hat{c}_1 = -12.145\times10^{-3}$ D ps	$\hat{c}_2 = -66.312$ D	$\hat{c}_1 = -11.743\times10^{-3}$ D ps	$\hat{c}_2 = -68.009$ D

needs to map the transformed transference back to its respective transference using either the Cayley transform (Equation 2) or the matrix exponential. The frequency-dependent transference is easy to obtain using pencil and paper and either the Cayley transform of Equation 2 or, easier still,

$$\mathbf{S} = \frac{2\left(\mathbf{I} - \hat{\mathbf{S}}\right)}{1 + \det \hat{\mathbf{S}}} - \mathbf{I}. \qquad (5)$$

On the other hand, the logarithmic transform requires the use of sophisticated matrix software.

Conclusion

The four fundamental properties of a Gaussian eye are shown to have a very nearly linear dependence on frequency. An equation is obtained for the least-squares straight line dependence of the fundamental properties on frequency, the estimated transference is almost symplectic. A transference, that is, a matrix which is exactly symplectic, is obtained by fitting a straight line in Hamiltonian space, giving the dependence of the transference of a Gaussian eye on the frequency of light across the visible spectrum. These equations allow one to write approximate equations for the dependence of almost all the optical properties of the eye, both fundamental and derived, on frequency.

Acknowledgements

This work is based on research by TE towards a higher degree under the guidance of WFH who gratefully acknowledges support from the National Research Foundation of South Africa.

References

[1] Emsley HH. *Visual Optics.* 4th ed. London: Hatton Press Ltd. 1950; 523-544.

[2] Le Grand Y. *Optique Physiologique. Tome Premier, le Dioptrique de l'Œil et sa Correction*. Paris: Revue d'optique. 1945; 50-51.

[3] Torre, A. Linear Ray and Wave Optics in Phase Space. Amsterdam: Elsevier. 2005; 60.

[4] Harris WF. The log-transference and an average Gaussian eye. *S. Afr. Optom.* 2005; **64**: 84-88.

[5] Harris WF. Symplecticity and relationships among the fundamental properties in linear optics. *S. Afr. Optom.* 2010; **69**: 3-13.

[6] Bernstein DS. *Matrix Mathematics. Theory, Facts, and Formulas.* 2nd ed. Princeton: Princeton University Press. 2009; 208-9, 238-9.

[7] Pease PL, Barbeito R. Axial chromatic aberration of the human eye: frequency or wavelength? *Ophthal. Physiol. Opt.*1989; **9**: 215-217.

[8] Thibos LN, Ye M, Zhang X, Bradley A. The chromatic eye: a new reduced-eye model of ocular chromatic aberration in humans. *Appl. Opt*. 1992; **31**: 3594-3600.

[9] Villegas ER, Carretero L, Fimia A. Le Grand eye for the study of ocular chromatic aberration. *Ophthal. Physiol. Opt*. 1996; **16**: 528-531.

[10] Le Grand Y. *Optique Physiologique. Tome Troisième, L'espace Visuel*. Paris: Revue d'optique. 1956; 9-27.

[11] Guillemin V, Sternberg S. *Symplectic Techniques in Physics.* Cambridge: Cambridge University Press. 1984; 9-27.

Inner-product spaces for quantitative analysis of eyes and other optical systems

William F Harris*, Tanya Evans and Radboud D van Gool
Department of Optometry, University of Johannesburg, Johannesburg, South Africa
*Corresponding author: wharris@uj.ac.za

Because dioptric power matrices of thin systems constitute a (three-dimensional) inner-product space it is possible to define distances and angles in the space and so do quantitative analyses on dioptric power for thin systems. That includes astigmatic corneal powers and refractive errors. The purpose of this paper is to generalize to thick systems. The paper begins with the ray transference of a system. Two 10-dimensional inner-product spaces are devised for the holistic quantitative analysis of the linear optical character of optical systems. One is based on the point characteristic and the other on the angle characteristic; the first has distances with the physical dimension L^{-1} and the second with the physical dimension L. A numerical example calculates the locations, distances from the origin and angles subtended at the origin in the 10-dimensional space for two arbitrary astigmatic eyes.

Keywords: ray transference; inner-product space; linear optics; astigmatism

Introduction

The optical character of a thin system in linear optics can be represented by a symmetric 2×2 matrix **F**, the symmetric dioptric power matrix. The set of all such powers defines a three-dimensional linear (or vector) space, symmetric dioptric power space [1]. Because the matrix has uniform physical dimensionality [2] (each entry has the dimension L^{-1} and is usually measured in dioptres) one can define an inner-product on the space and the space becomes an inner-product space. Because symmetric dioptric power space is an inner-product space we have been able to define distances, angles, orthonormal axes, confidence ellipsoids, *etc.* in the space. This has provided the basis for the quantitative analysis we have done on powers including refractive errors and corneal powers (*e.g.* [3]).

For some years we have sought to extend this type of analysis to thick systems like the eye (*e.g.* [4]). In linear optics the optical character of a system that may be thick or thin is completely characterized by the ray transference (a real 4×4 matrix)

$$\mathbf{S}=\begin{pmatrix}\mathbf{A} & \mathbf{B}\\ \mathbf{C} & \mathbf{D}\end{pmatrix} \tag{1}$$

of the system [5]. In strong contrast to the set of symmetric dioptric powers the set of transferences is neither a linear space nor does it have uniform dimensionality. There is, therefore, no inner-product space that would provide a basis for holistic quantitative analysis of the optical character of thick systems like the eye. The purpose of this paper is to show how inner-product spaces can in

fact be constructed for general optical systems.

Method

The method is based on the transference. The transference **S** (Equation 1) obeys the equation [5]

$$\mathbf{S}^{\mathrm{T}}\mathbf{E}\mathbf{S} = \mathbf{E} \tag{2}$$

where

$$\mathbf{E} = \begin{pmatrix} \mathbf{O} & \mathbf{I} \\ -\mathbf{I} & \mathbf{O} \end{pmatrix} \tag{3}$$

and **I** and **O** are identity and null matrices respectively. Such matrices are called *symplectic* [6]. **A**, **B**, **C** and **D** are 2×2 submatrices of **S** and represent the *fundamental* (linear) optical properties of the system [7]. **B** has the physical dimension L and **C** the physical dimension L^{-1}; the other two fundamental properties are dimensionless. Other optical properties of the system can be obtained from the fundamental properties; for example the power of the system is given by [7]

$$\mathbf{F} = -\mathbf{C} \tag{4}$$

and, for eyes, the corneal-plane refractive compensation (or refractive error) is given by [7]

$$\mathbf{F}_0 = \mathbf{B}^{-1}\mathbf{A}\,. \tag{5}$$

Two matrices related to the transference are the *point characteristic*

$$\mathbf{P} = \begin{pmatrix} \mathbf{B}^{-1}\mathbf{A} & -\mathbf{B}^{-1} \\ -\mathbf{B}^{-\mathrm{T}} & \mathbf{D}\mathbf{B}^{-1} \end{pmatrix} = \begin{pmatrix} \mathbf{U} & \mathbf{V} \\ \mathbf{V}^{\mathrm{T}} & \mathbf{W} \end{pmatrix} \tag{6}$$

and the *angle characteristic*

$$\mathbf{Q} = \begin{pmatrix} \mathbf{C}^{-1}\mathbf{D} & \mathbf{C}^{-1} \\ \mathbf{C}^{-\mathrm{T}} & \mathbf{A}\mathbf{C}^{-1} \end{pmatrix} = \begin{pmatrix} \mathbf{X} & \mathbf{Y} \\ \mathbf{Y}^{\mathrm{T}} & \mathbf{Z} \end{pmatrix}. \tag{7}$$

Elsewhere [8] we use these matrices to calculate average systems.

Results

From **P** and **Q** we construct the 2×6 matrices

$$\mathbf{G} = \begin{pmatrix} \mathbf{U} & \mathbf{V} & \mathbf{W} \end{pmatrix} \tag{8}$$

and

$$\mathbf{H} = \begin{pmatrix} \mathbf{X} & \mathbf{Y} & \mathbf{Z} \end{pmatrix}. \tag{9}$$

It is a consequence of symplecticity (Equation 2) that **U**, **W**, **X** and **Z** are symmetric; **V** and **Y** are general. (Properties of symplectic matrices are summarised elsewhere [9]). The set of all matrices **G** is a linear space and **G** has uniform physical dimensionality (L^{-1}). Similarly matrices **H** define a dimensionally uniform (dimension L) vector space.

G can be expanded as

$$\begin{aligned}\mathbf{G} = {} & U_{\mathbf{I}}(\mathbf{I} \quad \mathbf{O} \quad \mathbf{O}) + U_{\mathbf{J}}(\mathbf{J} \quad \mathbf{O} \quad \mathbf{O}) + U_{\mathbf{K}}(\mathbf{K} \quad \mathbf{O} \quad \mathbf{O}) \\ & + V_{\mathbf{I}}(\mathbf{O} \quad \mathbf{I} \quad \mathbf{O}) + V_{\mathbf{J}}(\mathbf{O} \quad \mathbf{J} \quad \mathbf{O}) + V_{\mathbf{K}}(\mathbf{O} \quad \mathbf{K} \quad \mathbf{O}) + V_{\mathbf{L}}(\mathbf{O} \quad \mathbf{L} \quad \mathbf{O}) \\ & + W_{\mathbf{I}}(\mathbf{O} \quad \mathbf{O} \quad \mathbf{I}) + W_{\mathbf{J}}(\mathbf{O} \quad \mathbf{O} \quad \mathbf{J}) + W_{\mathbf{K}}(\mathbf{O} \quad \mathbf{O} \quad \mathbf{K})\end{aligned} \tag{10}$$

where $\mathbf{J} = \begin{pmatrix} 1 & 0 \\ 0 & -1 \end{pmatrix}$, $\mathbf{K} = \begin{pmatrix} 0 & 1 \\ 1 & 0 \end{pmatrix}$, $\mathbf{L} = \begin{pmatrix} 0 & 1 \\ -1 & 0 \end{pmatrix}$. Also

$$V_{\mathbf{I}} = (v_{11} + v_{22})/2 \qquad V_{\mathbf{J}} = (v_{11} - v_{22})/2 \qquad V_{\mathbf{K}} = (v_{12} + v_{21})/2 \qquad V_{\mathbf{L}} = (v_{12} - v_{21})/2 \tag{11}$$

and similarly for $U_{\mathbf{I}}$ and the other coefficients in Equation 10. We define the coordinate vector

$$\mathbf{g} = (U_{\mathbf{I}} \quad U_{\mathbf{J}} \quad U_{\mathbf{K}} \quad V_{\mathbf{I}} \quad V_{\mathbf{J}} \quad V_{\mathbf{K}} \quad V_{\mathbf{L}} \quad W_{\mathbf{I}} \quad W_{\mathbf{J}} \quad W_{\mathbf{K}})^{\mathrm{T}} \tag{12}$$

relative to the basis

$$\beta = \{(\mathbf{I} \quad \mathbf{O} \quad \mathbf{O}), (\mathbf{J} \quad \mathbf{O} \quad \mathbf{O}), (\mathbf{K} \quad \mathbf{O} \quad \mathbf{O}), \cdots, (\mathbf{O} \quad \mathbf{O} \quad \mathbf{K})\}. \tag{13}$$

Consider two optical systems 1 and 2. Their coordinate vectors are $\mathbf{g}_1$ and $\mathbf{g}_2$. Now we define the inner product of $\mathbf{g}_1$ and $\mathbf{g}_2$ by

$$\langle \mathbf{g}_1, \mathbf{g}_2 \rangle = \mathbf{g}_1^{\mathrm{T}} \mathbf{g}_2. \tag{14}$$

Consequently we have distances (magnitudes) g and angles θ in the space defined by

$$g = \sqrt{\mathbf{g}^{\mathrm{T}} \mathbf{g}} \tag{15}$$

and

$$\cos\theta = \frac{\mathbf{g}_1^{\mathrm{T}} \mathbf{g}_2}{g_1 g_2} \tag{16}$$

respectively.

Thus we have a 10-dimensional inner-product space for quantitative analysis of optical systems in linear optics for which **B** is nonsingular. One can think of distances in the space as powers (*e.g.* dioptres).

For matrices of the form **H** (Equation 9) one can follow a similar approach. It leads to a second 10-dimensional inner-product space. It applies for optical systems for which **C** is nonsingular and distances in the space are lengths (*e.g.* metres).

We illustrate the theory using two optical systems whose transferences have been presented before [8]:

$$\mathbf{S}_1 = \begin{pmatrix} -0.2066 & -0.0031 & 0.0200 & 0.0000 \\ -0.0031 & -0.2240 & 0.0000 & 0.0200 \\ -58.8160 & -0.0853 & 0.8569 & 0.0017 \\ -0.0841 & -59.5090 & 0.0017 & 0.8599 \end{pmatrix}$$

and

$$\mathbf{S}_2 = \begin{pmatrix} -0.1641 & 0.0060 & 0.0197 & 0.0000 \\ 0.0060 & -0.1399 & 0.0000 & 0.0197 \\ -57.9190 & 0.3455 & 0.8670 & 0.0024 \\ 0.3415 & -56.9734 & 0.0024 & 0.8637 \end{pmatrix},$$

the units being dioptres and metres. The coordinate vectors (Equation 12) turn out to be

$$\mathbf{g}_1 = \begin{pmatrix} -10.7650 & 0.4350 & -0.1550 & -50.0000 & 0 & 0 & 0 & 42.9200 & -0.0750 & 0.0850 \end{pmatrix}^{\mathrm{T}} \text{ D}$$

and

$$\mathbf{g}_2 = \begin{pmatrix} -7.7157 & -0.6142 & 0.3046 & -50.7614 & 0 & 0 & 0 & 43.9264 & 0.0838 & 0.1218 \end{pmatrix}^{\mathrm{T}} \text{ D}.$$

These vectors locate the two optical systems relative to the origins of the space. Their distances from the origin are $g_1 = 66.77$ D and $g_2 = 67.57$ D respectively and they subtend an angle $\theta = 2.90°$ at the origin.

Conclusion

We have here constructed two inner-product spaces for the linear optical characters of optical systems. One is based on the point characteristic and the other on the angle characteristic. Both spaces can be used for eyes because they have nonsingular **B** and **C**. We now have the machinery for holistic quantitative analysis of optical systems in general and eyes in particular.

Acknowledgements

WFH gratefully acknowledges support from the National Research Foundation of South Africa.

References

[1] Harris WF. Representation of dioptric power in Euclidean 3-space. *Ophthal. Physiol. Opt.* 1991; **11**: 130-136

[2] Hart GW. Multidimensional Analysis: Algebras and Systems for Science and Engineering. New York: Springer. 1995; 66.

[3] Harris WF. Reduction of artefact in scatter plots of spherocylindrical data. *Ophthal. Physiol. Opt.* 2005; **25**: 13-17.

[4] Harris WF, Cardoso JR. The exponential-mean-log-transference as a possible representation of the optical character of an average eye. *Ophthal. Physiol. Opt.* 2006; **26**: 380-383.

[5] Torre A. Linear Ray and Wave Optics in Phase Space. Amsterdam: Elsevier. 2005; 60, 155.

[6] Guillemin V, Sternberg S. Symplectic Techniques in Physics. Cambridge: Cambridge University Press. 1984; 23 *et seq*.

[7] Harris WF. Dioptric power: its nature and its representation in three- and four-dimensional space. *Optom. Vis. Sci*. 1997; **74**: 349-366.

[8] van Gool R D, Harris WF. The concept of the average eye. *S. Afr. Optom.* 2005; **64**: 38-43.

[9] Harris WF. Symplecticity and relationships among the fundamental properties in linear optics. *S. Afr. Optom.* 2010; **69**: 3-13.

APPENDIX A LIST OF SYMBOLS

Symbol	Meaning	Ch	Sym-bol	Sub-script	Super script
A	Anterior	3		•	
A, **A**	Dilation (scalar, 2×2)	3, 1	•		
a	Angle between visual axis and red chief ray	2	•		
a, **a**	Inclination of the ray relative to Z (scalar, 2×1)	3	•		
Aq	Aqueous / anterior camber	4	•	•	
aO	Of inclinations from two object points	7		•	
aR	Of angular spread at the retina	7		•	
$\hat{A}$, $\hat{B}$, $\hat{C}$, $\hat{D}$, $\hat{\mathbf{A}}$, $\hat{\mathbf{B}}$, $\hat{\mathbf{C}}$, $\hat{\mathbf{D}}$	Entries of the transformed transference $\hat{\mathbf{S}}$ (scalar, 2×2)	3	•		
B	Posterior	3		•	
B, **B**	Disjugacy (scalar, 2×2)	3, 1	•		
b	Angle between visual axis and blue chief ray	2	•		
b	Blue	2		•	•
bv	Back-vertex	3		•	
C	Exit-plane compensation system	5		•	
C	Compound system	6		•	
C, **C**	Divergence (scalar, 2×2)	3, 1	•		
$\mathcal{C}(\mathbf{S})$	The Cayley transform	3	•		
c	Speed of light	4	•		
D	Dioptres	4	•		
D	Fraunhofer line D ($\lambda_D = 589.3\,\text{nm}$)	2		•	
D, **D**	Divarication (scalar, 2×2)	1	•		
det	Determinant	3	•		
E	Eye (with distant object)	3		•	
E	The symplectic unit matrix	3	•		
e	Equivalent	2		•	
e	Euler's number	3	•		
e	Transverse translation (2×1)	3	•		
eq	Equivalent (measured from principal plane)	3		•	
F	Fovea	2	•		
F	Focal point	3	•	•	
F, **F**	Power (scalar, 2×2)	2, 3	•		
f	Focal length (measured from transverse plane T)	3	•		
fn	Front-neutralising	3		•	
fv	Front-vertex	3		•	
G	A matrix Lie Group	3	•		
GL	General linear group	3	•		
$\mathfrak{g}$	The Lie algebra of **G**	3	•		
gl	The Lie algebra of GL	3	•		
H	Hamiltonian matrix	3	•		
H	The symplectic Lie group	3	•		

Symbol	Meaning	Ch	Sym-bol	Sub-script	Super script
h	Transverse displacement of pinhole from visual axis or displacement in entrance pupil of rays with respect to achromatic axis	2	•		
$\mathfrak{h}$	The set of Hamiltonian matrices, the symplectic algebra of **H**	3	•		
I	Image	2	•	•	
I	Identity matrix	3	•		
i	Angle between normal to the surface and the ray	3	•		
K	Cornea (refracting surface)	3	•	•	
K1	Corneal anterior surface	4	•	•	
K2	Corneal posterior surface	4	•	•	
kD	Kilodioptres	5	•		
kPa	KiloPascal	4	•		
L	Lens	4	•	•	
L	Locator line	3	•		
L, **L**	Vergence (scalar, 2×2); reduced wavefront curvature	3	•		
L1	Lens anterior surface	4	•	•	
L2	Lens posterior surface	4	•	•	
M	Magnification	2	•		
M	First mixed characteristic	3	•		
mm	Millimetres	4	•		
N	Nodal point	2, 3	•	•	
$\overline{\text{N}}$	Anti-nodal point	3	•	•	
N	Second mixed characteristic	3	•		
n	Refractive index	2	•		
$n\times n$ or n	Size of a square matrix	3	•		
nm	Nanometres $\left(\times10^{-9}\text{ m}\right)$	4	•		
O	Object or subsystem from object to first surface of eye; Object point or in object space	2, 3	•	•	
O	Null matrix	3	•		
o	Reference	2		•	
o	Null matrix (2×1 or 4×1)	3	•		
OA	Super-system from object, including anterior subsystem	5		•	
Oa	Measurements of inclination made at a finite distance in front of the eye	5		•	
OE	Super-system from object, including eye	5		•	
Oy	In object space, with respect to y, transverse position,				
Oy	Measurements of distance made at a finite distance in front of the eye	5		•	
P	Principal point	3	•	•	
$\overline{\text{P}}$	Anti-principal point	3	•	•	
P	Pupillary	3		•	
P	Pinhole	5			•
P	Point characteristic	3	•		
ppm	Parts per million	4	•		

Symbol	Meaning	Ch	Sym-bol	Sub-script	Super script
ps	Picosecond (10^{-12} s)	8	•		
Q	A cardinal point	3		•	
Q	Angle characteristic	3	•		
R	Retina (imaging surface) or in image space	3	•	•	
R	Ray	3	•		
$\mathbb{R}$	Set of real numbers	3	•		
r	Red	2		•	•
r	Radius of curvature	2	•		
r	State of the ray with unreduced inclination (2×1)	5	•		
S	General system	3, 5	•	•	
S	Transference (4×4 or 2×2)	3	•		
$\hat{\mathbf{S}}$	The transformed transference	3	•		
Sl(2;$\mathbb{R}$)	The group of 2×2 real matrices with determinant 1	3	•		
Sp	Symplectic group (Lie group)	3	•		
sp	Lie algebra (set of Hamiltonian matrices)	3	•		
T	Transverse plane	2	•		
T	Matrix transpose	3			•
T	Augmented transference (5×5)	3	•		
THz	Terahertz $(\times10^{12}\ \mathrm{s}^{-1})$	4	•		
t	Transverse (magnification)	3		•	
t	Transverse chromatic aberration	2	•		
t	All real numbers	3	•		•
tr	Trace	5	•		
V	Vitreous/ Posterior chamber	4	•	•	
V	Coefficient matrix	5	•		
v	Vitreous	2		•	
v	Input vector	5	•		
W, **W**	Image blur coefficient (scalar, 2×2)	5	•		
X, **X**	Image size coefficient (scalar, 2×2)	5	•		
X	Characteristic	3	•		
X	Set of all real matrices	3	•		
Y, **Y**	Directional spread coefficient (scalar, 2×2)	5	•		
y	Transverse position (scalar)	2, 3	•		
y	Transverse position (2×1)	3	•		
yO	Of size or separation distance of the object(s)	7		•	
yR	Of size at the retina	7		•	
Z	Longitudinal axis	2	•		
Z, **Z**	Directional coefficient (scalar, 2×2)	5	•		
Z	Generalised distance (2×2)				
z	Longitudinal position or gap, measured from a transverse plane T	3	•		
z	Axial (magnification)	3		•	
∞	Infinity	3	•		
0	Associated with incidence or upstream	2		•	
(No subscript)	Associated with emergence or downstream	2		•	
α, **α**	Reduced inclination (scalar, 2×1)	3	•		

Symbol	Meaning	Ch	Sym-bol	Sub-script	Super script
α	Angular (magnification)	3		•	
Δ	Physical difference	2	•		
δ	Chromatic difference	2	•		
$\boldsymbol{\delta}$	System vector accounting for prism and decentration of elements of the system (4×1)	3	•		
ε	Eccentricity	2	•		
$\boldsymbol{\gamma}$	Augmented ray state (5×1)	3	•		
$\imath$	Reduced angle between ray and normal	3	•		
λ	Wavelength	2	•		
ν	Frequency	4	•		
$\boldsymbol{\pi}$	Deflectance (2×1)	3	•		
$\boldsymbol{\rho}$	State of the ray at a transverse plane T (4×1 or 2×1)	3	•		
ζ	Reduced distance	3	•		
F_{bv}	Back-vertex power	3	•		
F_C	Exit-plane compensation	5	•		
F_{fv}	Front-vertex power	3	•		
F_0	Refractive compensation	3	•		
M_{aO}	Chromatic object angular spread magnification	7	•		
M_{aR}	Retinal chromatic angular spread magnification	7	•		
M_{yO}	Chromatic object size magnification	7	•		
M_{yR}	Retinal chromatic size magnification	7	•		
c_0	Speed of light in a vacuum	4	•		
n_∞, K, Λ	Constants in Cornu's formula	4	•		
δA	Chromatic difference in ametropia	7	•		
δF	Chromatic difference in power	7	•		
δF_0	Chromatic difference in refractive compensation	7	•		
δa_{O}	Chromatic difference in inclination in object space	7	•		
$\delta(\Delta a_{\mathrm{O}})$	Chromatic difference in object angular spread	7	•		
δa_{R}	Chromatic difference in inclination at the retina	7	•		
$\delta(\Delta a_{\mathrm{R}})$	Chromatic difference in angular spread at the retina	7	•		
δy	Transverse chromatic aberration (scalar)	6	•		
δy_{K}	Chromatic difference in corneal position	7	•		
δy_{O}	Chromatic difference in object position	7	•		
$\delta(\Delta y_{\mathrm{O}})$	Chromatic difference in object size	7	•		
δy_{R}	Chromatic difference in image position	7	•		
$\delta(\Delta y_{\mathrm{R}})$	Chromatic difference in image size	7	•		
δz	Longitudinal chromatic aberration (scalar)	6	•		
δy, $\delta\mathbf{y}$	Transverse chromatic aberration (scalar, 2×1)	6	•		
δz, $\delta\mathbf{Z}$	Longitudinal chromatic aberration (scalar, 2×2)	6	•		
λ_0	Vacuum wavelength	4	•		

APPENDIX B LIST OF FIGURES

APPENDIX C LIST OF TABLES

APPENDIX D PUBLICATIONS

1. EVANS T, Harris WF. Dependence of the transference of a reduced eye on frequency of light. *South African Optometrist* 2011 **70** 149-155.

2. Harris WF, EVANS T. Chromatic aberration in heterocentric astigmatic systems including the eye. *Optometry and Vision Science* 2012 **89** e37-e43.

3. Harris WF, van Gool RDHM, EVANS T. Line of sight of a heterocentric astigmatic eye. *Ophthalmic and Physiological Optics* 2013 **33** 57-66.

4. EVANS, T and Harris, WF. (2014) Dependence of the ray transference of model eyes on the frequency of light. *Proceedings: VII European / I World Meeting in Visual and Physiological Optics VPOptics 2014*. Wrocław University of Technology, Wrocław, 25-27 Aug 2014, ed by DR Iskander and HT Kasprzak. 74-77.

5. Harris WF, EVANS T and van Gool RDHM. (2014) Inner-product spaces for quantitative analysis of eyes and other optical systems. *Proceedings: VII European / I World Meeting in Visual and Physiological Optics*. Wrocław University of Technology, Wrocław, 25-27 Aug 2014, ed by DR Iskander and HT Kasprzak. 116-119.

PART II – LITERATURE REVIEW

In the literature review of the chromatic dependence of the first-order optical properties of the eye we consider three aspects, firstly chromatic aberrations, secondly first-order optical properties, both fundamental and derived, and finally the eye as a Gaussian optical system. For this reason, the literature review is divided into three chapters, each chapter dealing with these three aspects of this dissertation in turn.

In Chapter 2 we take a look at chromatic dispersion which is the basis for chromatic aberration, and how chromatic dispersion is measured for the media of the eye. We then take an in-depth look at the current definitions of chromatic aberration in both the classical and ophthalmic optics literature.

In Chapter 3 we look at the background theory of linear optics. In particular we are interested in Gaussian systems. The transference defines the fundamental properties of the eye and this enables one to trace the state of a ray through a system. A selection of derived properties that are of interest to this study of chromatic effects in the eye will be looked at. Because magnification, cardinal points and vergence form a pivotal role in chromatic aberration studies, we take a close look at how these are defined in the linear optics literature. Finally we take a look at the transformed transference and how this enables us to represent the transference in a three-dimensional space.

Chapter 4 is the final chapter of the literature review and looks at a number of considerations that are needed for this study. Firstly we take a look at the schematic eyes that are available in the literature, choosing Emsley's reduced eye and Le Grand's four-surface eye to base the numerical examples on. Secondly, the visible light spectrum that shall be used in this study is defined. Next, we consider the reasons for using frequency rather than wavelength. Finally, we look at the formulae for the refractive index of the various media as a function of frequency and wavelength.

PART III - DEFINITIONS AND DERIVATIONS

This study of the chromatic dependence of the first-order optical properties of the eye relies mostly on linear optics of systems in general. The background theory of Gaussian and linear optics needed for this study was summarized in Chapter 3. There are, however, formulae that we will need for this dissertation that have not been published in the literature which are derived in Part III.

In Chapter 5 we take a look at derivations for systems and rays that are needed as background equations that are not available in the literature. The chapter consists of an assortment of properties, derived from the transference, that are needed in Chapters 6 and 7. In particular, we shall revisit derived properties, magnification, cardinal points and Cayley's transform. Formulae are derived for the reduced and Le Grand's eyes as a function of refractive index and hence frequency.

In Chapter 6 longitudinal and transverse chromatic aberration are defined for systems in general and then simplified for the Gaussian model eye. The basis of the definition is the classical optics definition of chromatic aberration given in Section 2.2 which is generalized to systems that include astigmatic and decentred elements (Harris and Evans, 2012).

In Chapter 7 a number of formulae for quantifying chromatic properties are derived from the transference. The bases for these derivations are the physiological optics' definitions of the chromatic properties as defined in the literature in Section 2.3. Numerous formulae for chromatic properties both independent of and dependent on the object or image and aperture positions, each with a variety of alternatives, are summarized in tables at the end of the chapter.

Part III concentrates on Gaussian optics and linear optics of systems in general. All the formulae in this part, consisting of three chapters, are derived from the transference with special interest in the effect of frequency on the transference. The properties derived in these three chapters are done so specifically to illustrate and emphasise the effect of frequency on systems in general and the eye. Numerical examples, represented graphically and in tabular form, will be given in Part IV based on the derivations given in Part III.

PART IV – FINDINGS AND DISCUSSIONS

Because of the central importance of the transference it is useful to have some idea of how it depends on the frequency of light. In this part we examine the dependence of the transference of the reduced eye and Le Grand's four-surface schematic eye on frequency for several chromatic properties.

The considerations discussed in Chapter 4 will be applied or explored in the three chapters that make up this part. We will use the refractive index formula for the chromatic eye, developed by Thibos *et al* (1992), to calculate the refractive index of the reduced eye (Section 4.4.2) and the formula of Villegas, Carretero and Fimia (1996) for the refractive indices of Le Grand's complete theoretical eye given by Equation 4.4.3. As discussed in Section 4.2, the visible light spectrum, between the frequencies of 430 and 750 THz and will be used.

In Chapter 8 we examine the dependence of the fundamental properties of the model eyes on the frequency of light. The effect of the refractive index of air as a function of frequency is considered. Also studied are the dependence of the transference on vacuum wavelength and on frequency when the eye is submerged in water. The two transformed transferences will be calculated and displayed graphically both in terms of their individual entries and as three-dimensional graphs. These three-dimensional graphs show how the entries of the Hamiltonian matrix are related and begin to give us some insight into the meaning of Hamiltonian space.

In Chapter 9, various derived properties will be studied as a function of frequency. The effect of frequency on the cardinal points will be calculated and displayed using graphical construction and Pascal's ring methods. The formulae for both the derived properties and the cardinal points were given in Chapter 3 and further formulae derived in Chapter 5. The dependence of the four characteristic matrices on the frequency of light will be studied and the relationships among various derived properties will be explored.

Finally in Chapter 10, chromatic aberration will be calculated numerically and displayed according to changes in the object position. In Chapter 7 we derived the formulae for a variety of chromatic difference properties. These will be

calculated in both object and image space for the two model eyes. Numerical examples are given for all of the chromatic properties given by the equations summarized in Sections 7.4 and 5.

The numerical examples in Chapter 10 and the cardinal points examples in Section 9.1 show the difference between the two end points of the chosen spectrum and do not give us any insight into the dependence of the system on frequency across the visible light spectrum. In contrast to this, the numerical examples of the two model eyes in Chapter 8 and Sections 9.2 and 3 show us the dependence of the system on frequency across the spectrum. Firstly the fundamental properties of the transference, then the entries of the Hamiltonian matrix and finally the derived properties and the characteristic matrices are all studied to understand the dependence of each on the frequencies of light.

REFERENCES

Anton, H and Rorres, C. (2005). *Elementary Linear Algebra. Applications Version*. 9th ed. New Jersey: John Wiley & Sons, Inc.

Aristotle. (1906). *De Sensu and De Memoria*. Text and Translation with Introductory Comment by Ross, GRT. Cambridge: Cambridge University Press.

Aristotle. (1928). *Meteorologica*. Book 3, sections 4 and 5. The works of Aristotle, translated into English, Ross, WD (Ed). Available from: http://etext.lib.virginia.edu/etcbin/toccer-new2?id=AriMete.xml&images=images/modeng&data=/texts/english/modeng/parsed&tag=public&part=3&division=div2 Accessed 24 June 2013.

Arnaud, JA. (1970). Nonorthogonal optical waveguides and resonators. *The Bell System Technical Journal*, **49**: 2311-2348.

Atchison, DA, Smith, G and Waterworth, MD. (1993). Theoretical effect of refractive error and accommodation on longitudinal chromatic aberration of the human eye. *Optometry and Vision Science*, **70**: 716-722.

Atchison, DA and Smith, G. (2000). *Optics of the Human Eye*. Oxford: Butterworth-Heinemann.

Bennett, AG and Rabbetts, RB. (1989). Letter to the Editor (on proposals for new reduced and schematic eyes). *Ophthalmic and Physiological Optics*, **9**: 228-230.

Bernstein, DS. (2005). *Matrix Mathematics. Theory, Facts, and Formulas with Application to Linear Systems Theory*. Princeton: Princeton University Press.

Bernstein, DS. (2009). *Matrix Mathematics. Theory, Facts, and Formulas*. 2nd ed. Princeton: Princeton University Press.

Blendowske, R. (2003). Hans-Heinrich Fick: Early contributions to the theory of astigmatic systems. *South African Optometrist*, **62**: 105-110.

Born, M and Wolf, E. (2002). *Principles of Optics. Electromagnetic Theory of Propagation, Interference and Diffraction of Light.* 7th ed. Cambridge: Cambridge University Press.

Cardoso, JR. (2005). An explicit formula for the matrix logarithm. *South African Optometrist*, **64**: 80-83.

Cardoso, JR and Harris, WF. (2007). Transformations of ray transferences of optical systems to augmented Hamiltonian matrices and the problem of the average system. *South African Optometrist*, **66**: 56-61.

Cayley, A. (1846). Sur quelques propriétés des déterminants gauches. [On some properties of left determinants]. *Journal für die reine und angewandte Mathematik (Crelle).* **32**: 119-123. From The Collected Mathematical Papers of Arthur Cayley, Volume I: 332-336. Cambridge University Press (1897). Obtained from: http://quod.lib.umich.edu/u/umhistmath/abs3153.0001.001/349?didno=ABS3153.0001.001;page=root;rgn=full+text;size=100;view=image Accessed 27 June 2013.

Ciddor, PE. (1996). Refractive index of air: new equations for the visible and near infrared. *Applied Optics*, **35**: 1566-1573.

Cooper, DP and Pease, PL. (1988). Longitudinal chromatic aberration of the human eye and wavelength in focus. *American Journal of Optometry and Physiological Optics*, **65**: 99-107.

Courant, R and Hilbert, D. (1953). *Methods of mathematical physics, Volume I*. New York: Interscience Publishers, Inc.

Dieci, L. (1996). Considerations on computing real logarithms of matrices, Hamiltonian logarithms, and skew-symmetric logarithms. *Linear Algebra and its Applications*, **244**: 35-54.

Dieci, L. (1998). Real Hamiltonian logarithm of a symplectic matrix. *Linear Algebra and its Applications*, **281**: 227-246.

El Hage, SG and Le Grand, Y. (1980). *Physiological Optics*. Berlin: Springer-Verlag.

Emsley, HH. (1950). *Visual Optics*. 4th ed. London: Hatton Press Ltd.

Evans, T and Harris, WF. (2011). Dependence of the transference of a reduced eye on frequency of light. *South African Optometrist*, **70**: 149-155.

EVANS, T and Harris, WF. (2014) Dependence of the ray transference of model eyes on the frequency of light. *Proceedings: VII European / I World Meeting in Visual and Physiological Optics VPOptics 2014*. Wrocław University of Technology, Wrocław, 25-27 Aug 2014, ed by DR Iskander and HT Kasprzak. 74-77.

Fallat, SM and Tsatsomeros MJ. (2002). On the Cayley transform of positivity classes of matrices, *The Electronic Journal of Linear Algebra*, **9**: 190-196.

Fick, HH. (1972). Fortschrittliche Rechnungsarten in der Augenoptik [Progressive calculation methods in optometry]. *Der Augenoptiker*, **12/1972**: 60-63.

Fick, HH. (1973a). Fortschrittliche Rechnungsarten in der Augenoptik [Progressive calculation methods in optometry]. *Der Augenoptiker*, **2/1973**: 45-49.

Fick, HH. (1973b). Fortschrittliche Rechnungsarten in der Augenoptik [Progressive calculation methods in optometry]. *Der Augenoptiker*, **4/1973**: 39-43.

Fick, HH. (1973c). Fortschrittliche Rechnungsarten in der Augenoptik [Progressive calculation methods in optometry]. *Der Augenoptiker*, **10/1973**: 55-61.

Fiori, S. (2011). Solving minimal-distance problems over the manifold of real-symplectic matrices. *Society for Industrial and Applied Mathematics: Journal on Matrix Analysis and Applications*, **32**: 938-968.

Gatinel, D. (2010). Personal communications in preparation for Tshukudu Conference.

Golub, GH and van Loan, CF. (1996). *Matrix Computations*. 3rd ed. Baltimore: The Johns Hopkins University Press.

Guillemin, V and Sternberg, S. (1984). *Symplectic Techniques in Physics*. Cambridge: Cambridge University Press.

Hadjidimos, A and Tzoumas, M. (2008). The principle of extrapolation and the Cayley transform. *Linear Algebra and its Applications*, **429**: 2464-2480.

Hadjidimos, A and Tzoumas, M. (2009). On the optimal complex extrapolation of the complex Cayley transform. *Linear Algebra and its Applications*, **430**: 619-632.

Hall. BC. (2004). Lie Groups, Lie Algebras, and Representations. An Elementary Introduction. New York: Springer.

Harris, WF. (1993). Astigmatic optical systems with separated and prismatic or noncoaxial elements: system matrices and system vectors. *Optometry and Vision Science*, **70**: 545-551.

Harris, WF. (1994). Paraxial ray tracing through noncoaxial astigmatic optical system, and a 5×5 augmented system matrix. *Optometry and Vision Science*, **71**: 282-285.

Harris, WF. (1996a). Ray vector fields, prismatic effect, and thick astigmatic optical systems. *Optometry and Vision Science*, **73**: 418-423.

Harris, WF. (1996b). Wavefronts and their propagation in astigmatic optical systems. *Optometry and Vision Science*, **73**: 606-612.

Harris, WF. (1997). Dioptric power: its nature and its representation in three- and four-dimensional space. *Optometry and Vision Science*, **74**: 349-366.

Harris, WF. (1999a). A unified paraxial approach to astigmatic optics. *Optometry and Vision Science*, **76**: 480-499.

Harris, WF. (1999b). The four fundamental properties of Gaussian optical systems including the eye. *South African Optometrist*, **58**:69-79.

Harris, WF. (2000). Interconverting the matrix and principal-meridional representations of dioptric power and reduced vergence. *Ophthalmic and Physiological Optics*, **20**: 494-500.

Harris, WF. (2001a). Magnification, blur, and the ray state at the retina for the general eye with and without a general optical instrument in front of it: 1. Distant objects. *Optometry and Vision Science*, **78**: 888-900.

Harris, WF. (2001b). Magnification, blur, and ray state at the retina for the general eye with and without a general optical instrument in front of it: 2. Near objects. *Optometry and Vision Science,* **78:** 901-905.

Harris, WF. (2001c). Interconverting the matrix and principal meridional representations of dioptric power in general including powers with nonorthogonal and complex meridians. *Ophthalmic and Physiological Optics*, **21**: 247-252.

Harris, WF. (2002). Symplecticity in visual optics. *South African Optometrist*, **61**: 97-100.

Harris, WF. (2004a). Realizability of optical systems of given linear optical character. *Optometry and Vision Science*, **81**: 807-809.

Harris, WF. (2004b). The average eye. *Ophthalmic and Physiological Optics*, **24**: 580-585.

Harris, WF. (2005). The log-transference and an average Gaussian eye. *South African Optometrist*, **64**: 84-88.

Harris, WF. (2007a). Quantitative analysis of transformed ray transferences of optical systems in a space of augmented Hamiltonian matrices. *South African Optometrist*, **66**: 62-67.

Harris, WF. (2007b). Subjective refraction: the mechanism underlying the routine. *Ophthalmic and Physiological Optics*, **27**: 594-602.

Harris, WF. (2008). The geometric mean transference and the problem if the average eye. *South African Optometrist*, **67**: 48-55.

Harris, WF. (2009). Optical axes of eyes and other optical systems. *Optometry and Vision Science*, **86**: 537-541.

Harris, WF. (2010a). Back- and front-vertex powers of astigmatic systems. *Optometry and Vision Science*, **87**: 70-72.

Harris, WF. (2010b). Cardinal points and generalizations. *Ophthalmic and Physiological Optics*, **30**: 391-401.

Harris, WF. (2010c). Visual axes in eyes that may be astigmatic and have decentred elements. *Ophthalmic and Physiological Optics*, **30**: 204-204.

Harris, WF. (2010d). Symplecticity and relationships among the fundamental properties in linear optics. *South African Optometrist*, **69**: 3-13.

Harris, WF. (2010e). Nodes and nodal points and lines in eyes and other optical systems. *Ophthalmic and Physiological Optics*, **30**: 24-42.

Harris, WF. (2010f). Special rays and structures in general optical systems: generalized magnifications associated with the fundamental properties. *South African Optometrist*, **69**: 51-57.

Harris, WF. (2011a). Pascal's ring, cardinal points, and refractive compensation. *Vision Research*, **51**: 1679-1685.

Harris, WF. (2011b). Graphical construction of cardinal points from the transference. *South African Optometrist*, **70**: 3-13.

Harris, WF. (2011c). Effective corneal patch of an astigmatic heterocentric eye. *Ophthalmic and Physiological Optics*, **31**: 79-90.

Harris, WF. (2012a). Achromatic axes and their linear optics. *Vision Research*, **58**: 1-9.

Harris, WF. (2012b). Chief nodal axes of a heterocentric astigmatic eye and the Thibos-Bradley achromatic axis. *Vision Research*, **73**: 40-45.

Harris, WF. (2012c). Dependence of optical properties of heterocentric astigmatic systems on internal elements, with application to the human eye. *Transactions of the Royal Society of South Africa*, **67**: 11-16.

Harris, WF. (2012d). Aperture referral in dioptric systems with stigmatic elements. *South African Optometrist*, **71**: 3-11.

Harris, WF. (2013a). Pupillary axis of a heterocentric astigmatic eye. *South African Optometrist*, **72**: 3-10.

Harris, WF. (2013b). Yves Le Grand on matrices in optics with. vision: Translation and critical analysis, *South African Optometrist*, **72**: 145-166.

Harris, WF and Cardoso, JR. (2006). The exponential-mean-log-transference as a possible representation of the optical character of an average eye. *Ophthalmic and Physiological Optics*, **26**: 380-383.

Harris, WF and Evans, T. (2012). Chromatic aberration in heterocentric astigmatic systems including the eye. *Optometry and Vision Science*, **89**: e37-e43.

Harris WF, EVANS T and van Gool RDHM. (2014) Inner-product spaces for quantitative analysis of eyes and other optical systems. *Proceedings: VII European / I World Meeting in Visual and Physiological Optics*. Wrocław University of Technology, Wrocław, 25-27 Aug 2014, ed by DR Iskander and HT Kasprzak. 116-119.

Harris, WF and van Gool, RD. (2001). Comparing optical systems, and the concept of the converter system. *Optometry and Vision Science*, **78**: 825-830.

Harris, WF and van Gool, RD. (2004). First-order characteristic matrices of optical systems. *South African Optometrist*, **63**: 142-146.

Harris, WF and van Gool, RD. (2009). Thin lenses of asymmetric power. *South African Optometrist*, **68**: 52-60.

Harris, WF, van Gool, RDHM and Evans T. (2013). Line of sight of a heterocentric astigmatic eye. *Ophthalmic and Physiological Optics*, **33**: 57-66.

Hastings, CS. (1901*). Light; A Consideration of the More Familiar Phenomena of Optics*. New York: Charles Scribner's Sons.

Herzberger, M. (1959). Colour correction in optical systems and a new dispersion formula. *Optica Acta*, **6**: 197-215.

Hodgman, CD (Editor). (1959). *Handbook of Chemistry and Physics*. Cleveland: Chemical Rubber Publishing Co.

Howarth, PA and Bradley, A. (1986). The longitudinal chromatic aberration of the human eye, and its correction. *Vision Research*, **26**: 361-366.

Katz, M. (2002). *Introduction to Geometrical Optics*. Singapore: World Scientific Publishing Co.

Keating, MP. (1980). An easier method to obtain the sphere, cylinder, and axis from an off-axis dioptric power matrix. *American Journal of Optometry and Physiological Optics*, **57**: 734-737.

Keating, MP. (1981a). A system matrix for astigmatic optical systems: I. Introduction and dioptric power relations. *American Journal of Optometry and Physiological Optics*, **58**: 810-819.

Keating, MP. (1981b). A system matrix for astigmatic optical systems: II. Corrected systems including an astigmatic eye. *American Journal of Optometry and Physiological Optics*, **58**: 919-929.

Keating, MP. (1982). Advantages of a block matrix formulation for an astigmatic system. *American Journal of Optometry and Physiological Optics*, **59**: 851-857.

Keating, MP. (1988). *Geometric, Physical, and Visual Optics*. Boston: Butterworth-Heinemann.

Keating, MP. (1997a). Equivalent dioptric power asymmetry relations for thick astigmatic systems. *Optometry and Vision Science*, **74**: 388-392.

Keating, MP. (1997b). Asymmetric dioptric power matrices and corresponding thick lenses. *Optometry and Vision Science*, **74**: 393-396.

Keating, MP. (2002). *Geometric, Physical, and Visual Optics*. 2nd ed. Boston: Butterworth-Heinemann.

Keating, MP, Harris, WF and van Gool, RD. (2002b). Relation between anterior and posterior converter systems. *Optometry and Vision Science*, **79**: 459-461.

Koczorowski, P. (1990). Axial chromatic aberration: linear or power function of wavenumber? *Ophthalmic and Physiological Optics*, **10**: 405-408.

Korsch, D. (1991). *Reflective Optics*. Boston: Academic Press.

Lakshminarayanan, V. (2009). Introduction. *Journal of Modern Optics*, **56**: 2159-2163.

Lee, RL and Fraser, AB. (2001). *The Rainbow Bridge: Rainbows in Art, Myth and Science.* Bellingham: The Pennsylvania State University Press.

Le Grand, Y. (1945). *Optique Physiologique. Tome Premier, le Dioptrique de l'Œil et sa Correction* [Physiological optics. First volume, dioptrics of the eye and its correction]. Paris: Revue d'optique.

Le Grand, Y. (1956). *Optique Physiologique. Tome Troisième, L'espace Visuel* [Physiological optics. Third volume, Visual space]. Paris: Revue d'optique.

Le Grand Y. (1957). *Light, Colour and Vision*. Translated from French by Hunt, RWG, Walsh, JWT and Hunt, FRW. London: Chapman & Hall Ltd.

Long, WF. (1976). A matrix formulation for decentration problems. *American Journal of Optometry and Physiological Optics*, **53**: 27-33.

MacKenzie, GE. (2004). *Linear Optics of the Pseudophakic Eye*. Doctoral thesis. Johannesburg: Rand Afrikaans University.

Mathebula, SD, Rubin, A and Harris, WF. (2007). Quantitative analysis in Hamiltonian space of the transformed ray transferences of a cornea. *South African Optometrist*, **66**: 68-76.

Mathebula, SD and Rubin, A. (2011). Application of optical transferences for ray tracing through the human cornea. *South African Optometrist*, **70**: 156-167.

Meyer-Arendt, JR. (1984). *Introduction to Classical and Modern Optics.* 2nd ed. New-Jersey: Prentice-Hall, Inc.

Newton, I. (1670-1672). *Optica*, Part II, Lecture 11. In *The Optical Papers of Isaac Newton, Volume 1: The Optical Lectures 1670-1672* (1984). Edited by Shapiro, AE. Cambridge: Cambridge University Press.

Pascal, JI. (1939). A memory scheme for the cardinal points. *Archives of Ophthalmology*, **22**: 448-449.

Pascal, JI. (1947). Cardinal points in aphakia. *Archives of Ophthalmology*, **37**: 83-84.

Pascal, JI. (1950a). Role of the cardinal points in the correction of ametropia. *Eye, Ear, Nose and Throat Monthly*, **29**: 24-28.

Pascal, JI. (1950b). The cardinal points in corrected ametropia. *British Journal of Ophthalmology*, **34**: 261-264.

Pease, PL and Barbeito, R. (1989). Axial chromatic aberration of the human eye: frequency or wavelength? *Ophthalmic and Physiological Optics*, **9**: 215-217.

Puzio, RS. (2013). Cayley's parameterization of orthogonal matrices. Available from: http://planetmath.org/cayleysparameterizationoforthogonalmatrices (Accessed 22 June 2013).

Rabbetts, RB. (2007). *Bennett & Rabbetts' Clinical Visual Optics*. 4th ed. London: Butterworth-Heinemann-Elsevier.

Sears, FW, Zemansky, MW and Young, HD. (1987). *University Physics*. 7th ed. Reading, Massachusetts: Addison-Wesley Publishing Company.

Seyeddain, O, Riha, W, Hohensinn, M, Nix, G, Dexl, AK and Grabner, G. (2010). Refractive surgical correction of presbyopia with the AcuFocus small aperture corneal inlay: two-year follow-up. *The Journal of Refractive Surgery*, **26**: 707-715.

Sharma, KK. (2006). *Optics. Principles and Applications*. Boston: Elsevier.

Simonet, P and Campbell, MCW. (1990). The optical transverse chromatic aberration on the fovea of the human eye. *Vision Research*, **30**: 187-206.

Sivak, JG and Mandelman, T. (1982). Chromatic dispersion of the ocular media. *Vision Research*, **22**: 997-1003.

Smith, G. (1993). Calculation of the cardinal points of an optical system. *Ophthalmic and Physiological Optics*, **13**: 327-332.

Smith, G. (1995). Schematic eyes: history, description and applications. *Clinical and Experimental Optometry*, **78**: 176-189.

Smith, G and Atchison, DA. (1997). *The Eye and Visual Optical Instruments*. Cambridge: Cambridge University Press.

Stiles, WS and Crawford, BH. (1933). The luminous efficiency of rays entering the eye pupil at different points. *Proceedings of the Royal Society of London, Series B*, **112**: 428-450.

Stiles, WS. (1939). The directional sensitivity of the retina and the spectral sensitivities of the rods and cones. *Proceedings of the Royal Society of London, Series B*, **127**: 64-105.

Sunyal, AK. (2001). *Geometrical Transformations in Higher Dimensional Euclidean Spaces.* Masters dissertation. College Station: Texas A & M University.

Tabernero, J and Artal P. (2011). Optical modelling of a corneal inlay in real eyes to increase depth of focus: Optimum centration and residual focus. *Journal of Cataract and Refractive Surgery*, **38**: 270-277.

Thibos, LN. (1987). Calculation of the influence of lateral chromatic aberration on image quality across the visual field. *Journal of the Optical Society of America*, **4**: 1673-1680.

Thibos, LN. (2011). Personal communication to Harris, WF, 7 December 2011.

Thibos, LN, Bradley, A, Still, DL, Zhang, X and Howarth, PA. (1990). Theory and measurement of ocular chromatic aberration. *Vision Research*, **30**: 33-49.

Thibos, LN, Bradley, A and Zhang, X. (1991). Effect of ocular chromatic aberration on monocular visual performance. *Optometry and Vision Science*, **68**: 599-607.

Thibos, LN, Ye, M, Zhang, X and Bradley, A. (1992). The chromatic eye: a new reduced-eye model of ocular chromatic aberration in humans. *Applied Optics*, **31**: 3594-3600.

Torre, A. (2005). *Linear Ray and Wave Optics in Phase Space*. Amsterdam: Elsevier.

Tscherning, M. (1904). *Physiologic Optics: Dioptrics of the Eye, Functions of the Retina, Ocular Movements and Binocular Vision*. Translated from French by Weiland, C. 2nd ed. Philedelphia: The Keystone.

Tsiotras, P, Junkins, JL and Schaub, H. (1997). Higher order Cayley transforms with applications to attitude representations. *Journal of Guidance, Control, and Dynamics*, **20**: 528-536.

Van Gool, RD and Harris, WF. (2005). The concept of the average eye. *South African Optometrist*, **64**: 38-43.

Villegas, ER, Carretero, L and Fimia, A. (1996). Le Grand eye for the study of ocular chromatic aberration. *Ophthalmic and Physiological Optics*, **16**: 528-531.

von Helmholtz, H. (1909). *Treatise on Physiological Optics, Volume I*. Translated from the German (2005): Southall, JPC (ed), New York: Dover Phoenix Editions Inc. (Original work published in 1909; Original translation published in 1924).

Wald, G and Griffin, DR. (1947). The change in refractive power of the human eye in dim and bright light. *Journal of the Optical Society of America*, **37**: 321-336.

Waldman, G. (2002). *Introduction to Light: The Physics of Light, Vision, and Color*. New York: Dover Publications Inc.

Walther, A. (1995). *The Ray and Wave Theory of Lenses*. Cambridge: Cambridge University Press.

Waring, GO. (2010). Corneal inlay uses pinhole effect. *Ophthalmology Times*, 35(7). Available from: http://ophthalmologytimes.modernmedicine.com/ophthalmologytimes/news/modernmedicine/modern-medicine-feature-articles/corneal-inlay-uses-pinhole-e (Accessed on: 8 June 2013.)

Watkins, DS. (2004). On Hamiltonian and symplectic Lanczos processes. *Linear Algebra and its Applications*, **385**: 24-45.

Westheimer. G. (2008). Directional sensitivity of the retina: 75 years of Stiles-Crawford effect. *Proceedings of the Royal Society B*, **275**: 2777-2786.

Wilson, MA, Campbell, MCW and Simonet, P. (1992). Change of pupil centration with change of illumination and pupil size. *Optometry and Vision Science*, **69**: 129-136.

Yang, Y, Thompson, K and Burns, SA. (2002). Pupil location under mesopic, photopic and pharmacologically dilated conditions. *Investigative Ophthalmology and Visual Science*, **43**: 2508-2512.

Zhang, X, Bradley, A and Thibos, LN. (1993). Experimental determination of the chromatic difference of magnification of the human eye and the location of the anterior nodal point. *Journal of the Optical Society of America A*, **10**: 213-220.

Zhang, X, Thibos, LN and Bradley, A. (1991). Relation between the chromatic difference of refraction and the chromatic difference of magnification for the reduced eye. *Optometry and Vision Science*, **68**: 456-458.

Zhang, X, Thibos, LN and Bradley, A. (1997). Wavelength-dependent magnification and polychromatic image quality in eyes corrected for longitudinal chromatic aberration. *Optometry and Vision Science*, **74**: 563-569.

CHROMATIC DEPENDENCE OF FIRST–ORDER OPTICAL PROPERTIES OF THE EYE

Tanya Evans

(Student number: 908905891)

A dissertation submitted to the Faculty of Health Sciences, University of Johannesburg, in fulfilment of the requirements for the degree of Magister Philosophiae in Optometry

Supervisor: Professor WF Harris

Johannesburg, 2015

DECLARATION

I declare that this dissertation is my own, unaided work. It is being submitted for the degree Magister Philosophiae in Optometry at the University of Johannesburg, Johannesburg. It has not been submitted before for any degree or examination in any other Technikon or University.

_____

(Signature of Candidate)

_____day of _____ 2015.

ABSTRACT

Many first-order optical properties depend on chromatic dispersion and, hence, on frequency of light. The purpose of this theoretical study is to investigate the dependence of first-order optical properties of model eyes on frequency. In this study we are purposefully not concerned with subjective measurements. Instead, definitions are obtained that are general for optical systems that have astigmatic and decentred elements, and then simplified for Gaussian systems.

In linear optics the transference is a matrix that is a complete representation of the effects of the system on a ray traversing it. Almost all of the familiar optical properties of the system can be obtained from the transference. From the transference **S** we obtain the four fundamental properties namely dilation **A**, disjugacy **B**, divergence **C** and divarication **D**, submatrices of **S**. Transferences are symplectic and do not define a linear space. Linear spaces are amenable to statistical analyses and therefore a number of mappings to linear spaces are investigated, including the Cayley and logarithmic mappings to Hamiltonian space and the four characteristic matrices. In each case, the individual entries of the transform are studied for their dependence on frequency and then the chromatic dependence relationship between the entries is compared graphically.

Four aspects of chromatic dependence of Gaussian systems are explored, namely the fundamental properties, derived properties, transverse and longitudinal chromatic aberration, and independent and dependent chromatic properties. Formulae are derived that apply to first-order optical systems in order to illustrate the chromatic dependence, chromatic difference or the chromatic magnification of each property. Numerical examples are given for the reduced eye and Le Grand's eye across the spectrum 430 to 750 THz.

Fundamental properties

The fundamental properties of the reduced and Le Grand's four surface eyes have a nearly perfectly straight-line dependence on frequency.

- Straight-line fits are obtained for the dependence of the fundamental properties on frequency. The resulting transference has a determinant of approximately 1 for every frequency.

- Straight-line fits in Hamiltonian space give a frequency-dependent transference with a determinant of exactly 1 for every frequency.
- Of the fundamental properties, only dilation *A* and divergence *C* are dependent on the refractive index upstream of the system. Disjugacy *B* and divarication *D* are independent of the medium upstream of the system.

Derived properties

Derived properties that are dependent on frequency are:

- Power, corneal-plane refractive compensation, exit-plane refractive compensation and front-vertex power have a straight-line dependence.
- Back-vertex power has a hyperbolic dependence.
- The cardinal and anti-cardinal points for Le Grand's eye, the anti-cardinal and focal points for the reduced eye and all the chromatic properties are dependent on frequency.

The incident and emergent principal and nodal points for the reduced eye are independent of frequency.

Chromatic aberration

Chromatic aberration is defined for linear systems, that is, for systems possibly with astigmatic and heterocentric elements such as the eye, using the classical optics definition as a departure point. The definition is then specialised for a Gaussian eye.

- Longitudinal chromatic aberration is defined as a 2×2 symmetric matrix for systems that have astigmatic elements. It depends on the longitudinal position of the object and simplifies to a scalar for Gaussian systems.
- Transverse chromatic aberration is defined as a 2×1 transverse vector for systems that have astigmatic or decentred elements. It depends on both the longitudinal and transverse position of the object point and simplifies to a scalar for Gaussian systems.

Independent and dependent chromatic properties

Chromatic properties of the system both independent of and dependent on the object or image and aperture positions are derived from the transference based on the definitions in the physiological optics literature.

Independent chromatic properties of the eye include chromatic difference in power, δF, chromatic difference in refractive compensation, δF_0 and chromatic difference in ametropia, δA.

Formulae are derived for the chromatic properties of the Gaussian eye for (i) distant objects and objects at a finite distance, (ii) image and object dependent properties and (iii) the special case of a pinhole held in front of the eye.

- Chromatic properties of the eye dependent on object and aperture position include chromatic difference in retinal position δy_{R}, retinal inclination δa_{R}, image size $\delta(\Delta y_{\mathrm{R}})$, image angular spread $\delta(\Delta a_{\mathrm{R}})$, retinal chromatic image size magnification M_{yR} and angular spread magnification M_{aR}. Chromatic properties of the eye dependent on image and aperture position include: chromatic difference in object position δy_{O}, inclination in object space δa_{O}, object size $\delta(\Delta y_{\mathrm{O}})$, object angular spread $\delta(\Delta a_{\mathrm{O}})$, chromatic object size magnification M_{yO} and object angular spread magnification M_{aO}. When the distance of the object from the eye is constant the dependence of the chromatic differences present as straight lines.
- The red and blue chief rays chosen to study the chromatic properties in image space are incident on the cornea a distance of some 5000 times the wavelength of the blue light apart.
- When the red and blue chief rays from two separated object points coincide at a point on the exit-plane, their emergent inclination is the same for the reduced eye but different for Le Grand's eye.

Though applied to model eyes one expects the results, particularly for Le Grand's eye, to give an idea of what happens in the case of real eyes, at least those close to emmetropia.

ACKNOWLEDGEMENT

To my husband and daughters, Gerard, Sarah and Megan who have supported me and put up with the long hours of absence and episodes of stress. Thank you!

To my parents who encouraged and supported me to study Optometry in the first place.

To my advisor, Professor WF Harris, who has encouraged me every step of the way. This study has been about the journey and not just the destination. Bill, thank you for allowing me to take the road less travelled, to explore anything and everything that interested us along the way. Thank you for your endless patience, reading, rereading and correcting each draft. And thank you for opening the door to the academic world and giving me the opportunities to attend and present my work at conferences.

The first year of this research was supported by a scholarship granted by the Medical Research Council of South Africa.

TABLE OF CONTENTS

1. EVANS T, Harris WF. Dependence of the transference of a reduced eye on frequency of light. *South African Optometrist* 2011 **70** 149-155.
2. Harris WF, EVANS T. Chromatic aberration in heterocentric astigmatic systems including the eye. *Optometry and Vision Science* 2012 **89** e37-e43.
3. Harris WF, van Gool RDHM, EVANS T. Line of sight of a heterocentric astigmatic eye. *Ophthalmic and Physiological Optics* 2013 **33** 57-66.
4. EVANS, T and Harris, WF. (2014) Dependence of the ray transference of model eyes on the frequency of light. *Proceedings: VII European / I World Meeting in Visual and Physiological Optics VPOptics 2014*. Wrocław University of Technology, Wrocław, 25-27 Aug 2014, ed by DR Iskander and HT Kasprzak. 74-77.
5. Harris WF, EVANS T and van Gool RDHM. (2014) Inner-product spaces for quantitative analysis of eyes and other optical systems. *Proceedings: VII European / I World Meeting in Visual and Physiological Optics*. Wrocław University of Technology, Wrocław, 25-27 Aug 2014, ed by DR Iskander and HT Kasprzak. 116-119.

PART I – INTRODUCTION

The objective of this study is to explore chromatic properties and other chromatic effects of the eye, particularly in the context of Gaussian optics. Numerous optical properties are investigated for their dependence on the frequency of light, specifically those optical properties that are relevant to Gaussian systems, that is, systems that are rotationally symmetric about a common optical axis (Guillemin and Sternberg, 1984:7).

1 INTRODUCTION

From Babylonia to Egypt and Nigeria and from Papua New Guinea to Mexico and Peru, human beings have been fascinated by the rainbow since the beginning of time (Lee and Fraser, 2001: 2-33). The phenomenon that creates the rainbow is chromatic dispersion, that is, the separation of white light into its spectral components or the variation of the refractive index with wavelength (Sharma, 2006: 45, 50; Le Grand, 1956: 9). Chromatic aberration, in turn, is defined by El Hage and Le Grand (1980:4) as "the influence of chromatic dispersion in the eye". That is to say, the white light entering the system is dispersed across the visible light spectrum and creates a rainbow effect as it exits the system or reaches an imaging surface such as the retina.

Chromatic aberration is quantified according to the classical (or physical) optics definition as the distance measured between the projections of the two focal points when light of two frequencies representing the two ends of the visible light spectrum are traced through the system. Measurements parallel to the longitudinal axis are defined as longitudinal chromatic aberration and measurements perpendicular to the longitudinal axis are defined as transverse chromatic aberration (Born and Wolf, 2002: 186-187). The definition is limited to systems that are Gaussian and distances that are unsigned.

In the literature of physiological optics many definitions exist. Longitudinal (or axial) chromatic aberration is defined in physiological optics as chromatic difference in power, refractive error, focus or ametropia (Atchison, Smith and Waterworth, 1993; Cooper and Pease, 1988; Rabbetts, 2007: 289-293; Thibos, Bradley, Still, Zhang and Howarth, 1990; Thibos, Bradley and, Zhang,

1991; Thibos, Ye, Zhang and Bradley, 1992; Wald and Griffin, 1947; Zhang, Thibos and Bradley, 1991). Transverse (or lateral) chromatic aberration is defined in physiological optics as chromatic difference in position or magnification (Rabbetts, 2007:289-293; Simonet and Campbell, 1990; Thibos *et al*, 1990, 1991, 1992; Zhang *et al*, 1991). Researchers have sought to define a relationship between longitudinal and transverse chromatic aberration and have succeeded for the reduced eye (Zhang *et al*, 1991) and for schematic eyes (Katz, 2002:261). The limitations of these definitions is that they are based on Gaussian schematic eyes, usually the reduced eye, and do not generalise to eyes with astigmatic or decentred elements. There is a risk of making assumptions or conclusions that pertain only to the reduced eye. We shall explore two such underlying implications in Chapter 7.

Gaussian optics has served as the foundation of optometry and the basis of visual optics and is a powerful tool (MacKenzie, 2004: 153-154). It is limited, however, in that it firstly assumes that all surfaces in the system are rotationally symmetric about an optical axis. Secondly, Gaussian optics relies on concepts such as principal points, nodal points, entrance- and exit-pupils which work well for Gaussian systems, but do not generalize well to astigmatic or heterocentric systems. However, the success of Gaussian optics in optometry and visual optics is evidence that the human eye is largely a first-order optical instrument (Le Grand, 1956:9; MacKenzie, 2004:3).

Linear optics is a method that fully accounts for all the aspects of first-order paraxial optics. The three-dimensional linear optics approach can account for elements that are astigmatic and decentred which traditional two-dimensional Gaussian techniques fall short of. Linear optics makes use of linear algebra and specifically a matrix, called here the ray transference **S**, that is, a complete representation of the effects of the system on a ray traversing it. Almost all of the familiar optical properties of the system can be calculated from the transference (Torre, 2005: 60). Linear optics can therefore describe the first-order behaviour of the eye as an optical instrument.

From the transference we obtain the four fundamental properties namely **A** dilation, **B** disjugacy, **C** divergence and **D** divarication. From these four

fundamental properties we can obtain a variety of seemingly unrelated derived properties such as power (Harris, 1997), refractive compensation (Harris, 1999a; Keating, 1988: 236), front- and back-vertex power (Keating, 1988: 236; Harris, 2010a), magnification, blur, image size and image position, (Harris, 2001a,b), cardinal points (Harris, 2010b, 2011a, b), Pascal's ring (Harris, 2011a) and locator lines (Harris, 2011b). This is by no means a comprehensive list of derived properties. By and large these properties have been studied under the assumption of a single reference wavelength. Of special interest is that the cardinal points, which form the basis of Gaussian ray-tracing optics, are derived properties. Similarly, power and refractive compensation are derived properties.

The transference that accounts for astigmatism is a 4×4 matrix with each of the four fundamental properties a 2×2 submatrix (Guillemin and Sternberg, 1984:26; Harris, 2010d). When elements that may be decentred or tilted are accounted for in the transference, we obtain an augmented transference that is of order 5×5 (Harris, 2004a, 2010d, 2012c). In contrast, when all the elements are stigmatic and rotationally symmetric about an optical axis, each of the four fundamental submatrices simplifies to a scalar matrix and we can reduce the transference to a 2×2 matrix. This can be thought of as representing the Gaussian subset of 4×4 and 5×5 transferences (Guillemin & Sternberg, 1984: 7-11, Harris, 2010d). Because the topic of chromatic dependence of the eye is broad it is necessary to limit the scope of the study. Except where it is necessary to use a 4×4 transference **S** or an augmented 5×5 transference **T** in order to gain insight into the nature and character of chromatic dependence of the eye, this study shall be limited to the Gaussian subset. However, most of the formulae obtained readily generalise to linear systems. Transferences are dealt with in more detail in Section 3.2.

Advantages are gained by limiting the scope of the study to the Gaussian subset. In particular, it becomes possible to display many of the dependencies on frequency in two- and three-dimensional space. However, the transference does not conform to the definition of a vector space (Anton and Rorres, 2005: 222; Harris, 2010d; 2007a, van Gool and Harris, 2005) although it is possible to map the symplectic transference to a Hamiltonian space in a number of ways.

Transformed transferences are Hamiltonian and therefore fulfil the definition of a vector space, allowing us to graphically map the dependency in a three-dimensional space. A 2×2 transformed transference has three independent entries which can be represented graphically (Harris, 2010d). On the other hand a 4×4 transformed transference has 10 and a 5×5 transformed transference has 14 independent entries requiring representation in 10- or 14-dimensional space (Harris, 2007a), a graphical impossibility. Insight is gained because many of the Gaussian derivations are simplified and can be represented graphically.

We have seen that there are many properties that can be derived from the transference. An objective of this dissertation is to study the dependence of the transference on frequency. The reasons why frequency is preferable to vacuum wavelength will be explored in Chapter 4. To understand the dependency of the optical system of the eye on frequency we explore a number of transformed transferences and characteristic matrices. The characteristic matrices are symmetric and therefore are amenable to mapping the relationships between the entries also in three-dimensional space. Because each of the entries of the characteristic matrices is a derived property, each of these derived properties will be explored independently and then in relationship to other entries of the four characteristic matrices. We therefore restrict the derived properties studied to power, corneal-plane refractive compensation, exit-plane compensation and front- and back-vertex power. These derived properties will be explored for both their dependence on frequency across the visible light spectrum and the chromatic difference between the values at the spectral end-points.

1.1 Purpose

The purpose of this dissertation is to study the chromatic dependence of the first-order optical properties of the eye. Specifically, we wish to explore the chromatic dependence of optical properties and other effects of the eye particularly in the context of Gaussian optics.

Many first-order optical properties are dependent on the effects of chromatic dispersion and hence on frequency of light. This study explores the effects of chromatic dispersion on a number of fundamental and derived

properties. The dependence of the transference, the transformed transferences, characteristic matrices and derived properties on the frequency of light are explored, including graphical representation. A formula is obtained for the linear dependence of the transference on the frequency of light.

A study of chromatic effects of the eye would be incomplete without including chromatic aberration. Chromatic aberration, based on the classical optics definition, is defined for systems in general, including systems with astigmatic and heterocentric elements. Chromatic properties, as defined in the physiological optics literature, are obtained from the transference. Numerical examples of chromatic aberration and all the chromatic properties are given.

1.2 Outline

1.2.1 Part II - Literature review

The literature review is divided into three chapters. In Chapter 2 the current definitions of chromatic aberration in both the classical and physiological optics literature are reviewed.

Chapter 3 outlines linear optics. While much of this chapter may be familiar to the reader, it is included in part for completeness but predominantly to form a basis for derivations in Part III. After placing linear optics within the much larger field of optics, a summary of linear optics of first-order systems is given. The four fundamental properties are defined and briefly explored. Only a small selection of derived properties can be accommodated in this study and the derivations of power, corneal-plane refractive compensation and front- and back-vertex power are given. Both the classical and physiological optics approaches to defining magnification are explored.

Cardinal points form the basis of Gaussian optics and can be derived from the transference (Harris, 2010b, f). We are interested in the dependence of the cardinal points on the frequency of light and therefore the derivations for cardinal points from the transference are given. Two novel methods to display relationships among the cardinal points of a system and changes or differences between the cardinal points of two systems will be given.

The transference is symplectic and does not define a vector space and, hence, does not allow conventional statistical analyses (Harris, 2010d). We therefore investigate a number of transforms, including the Cayley (Cardoso and Harris, 2007) and logarithmic transforms (Harris and Cardoso, 2006; Harris, 2004b, 2005, 2007a) and the four characteristic matrices (van Gool and Harris, 2005; Harris and van Gool, 2004), to seek a suitable vector space. The characteristic matrices form combinations of derived properties and are also symmetric. As a result, each characteristic matrix has three independent entries and can be represented graphically in three-dimensional space.

Chromatic aberration depends on the longitudinal and transverse position of the object. Because we wish to know where the conjugate image point is we turn our attention to vergence as an alternative to tracing a pencil of rays through the system. In the literature review, we define vergence and wavefronts relating to the system, from the transference, and the position of the image relative to the exit plane of the system.

Chapter 4 deals with a number of considerations that need to be taken into account for this study of chromatic dependence. Schematic eyes are by definition Gaussian eyes and two schematic eyes are singled out for inclusion in the study. The limits of the visible light spectrum that will be included in the study are defined. The advantages and disadvantages of studying the dependence of chromatic properties as a function of frequency or vacuum wavelength are discussed.

It is the refractive index of the medium that is dependent on frequency. There are a limited number of formulae available that define refractive index of the media of the eye as a function of wavelength or frequency. The refractive indices as a function of vacuum wavelength are given for the reduced eye, the four media of Le Grand's four-surface eye, air and water.

1.2.2 Part III– Definitions and derivations

The objective in Part III is, firstly, to define chromatic aberration for systems in general, including systems with astigmatic and heterocentric elements and secondly to derive equations from the transference for chromatic properties of

the system both independent of and dependent on the positions of the object and limiting aperture. The starting point for these derivations is the derived properties presented in Chapter 3. However, not all the necessary derived properties and definitions are available in the current literature and so in Chapter 5 we define those formulae that are needed to define chromatic properties. Chapter 5 therefore is a collection of seemingly unrelated derivations.

We start Chapter 5 by defining exit-plane compensation and revisiting magnification. The magnification, blur and ray state at the retina is defined for object points at a finite distance. Anti-cardinal points are added to the study of the cardinal points and these are extended beyond the formulae and relationships available in the current literature.

The transferences are calculated for the reduced eye and for Le Grand's eye for their intended reference frequency. Formulae for the transference as a function of refractive index are derived and given for both schematic eyes.

There are a number of formulae available that define Cayley's transform. In this section each of these transforms are dissected for their usefulness for our purposes and for the method and way that it maps to Hamiltonian space and back into the set of symplectic matrices. Only one Cayley transform fulfils the requirements and is chosen with reasons given. The Cayley transform simplifies for the reduced eye and the formula for the transformed transference of the reduced eye is given.

In Chapter 6 chromatic aberration is defined for systems in general and then specialised for the Gaussian subset. The point of departure is the classical optics definition. By first defining chromatic aberration using linear optics we gain insight into the nature of the longitudinal and transverse chromatic aberrations.

Chapter 7 defines the chromatic properties of the eye and of the eye dependent on the positions of the object or image and aperture. These chromatic properties are derived from the transference based on the definitions for chromatic aberration in physiological optics. Included are chromatic properties of the eye independent of object or image and aperture positions which include chromatic differences in power, refractive compensation and ametropia. The chromatic

properties of the system dependent on object and aperture positions include the chromatic difference in position, inclination, image size and angular spread and chromatic image size and angular spread magnifications. The formulae derived are specialised for Gaussian schematic eyes but apply to both the pupil and the pinhole.

1.2.3 Part IV – Findings and discussions

The three chapters in Part IV together comprise the results of this dissertation and in each case both the reduced eye and Le Grand's eye are studied.

In Chapter 8 the dependence of the fundamental properties on frequency is displayed graphically and discussed. Four scenarios are considered, namely with the refractive index of air equated to 1, with the refractive index of air as a function of frequency using Cauchy's formula and with the eye submerged in water. Cornu's formula for the refractive index of water as a function of frequency is used. Finally the dependence of the fundamental properties as functions of vacuum wavelength are given, with the refractive index of air equated to 1.

The dependence of the transformed transferences is studied for both the logarithmic and Cayley transforms. This includes the dependence on the individual entries as well as the three-dimensional graph of the three independent entries. A formula for the linear dependence of the fundamental properties on the frequency of light is derived. This forms an important finding in this dissertation.

Chapter 9 looks at the dependence of derived properties on the frequency of light. First, the dependence of the cardinal and anti-cardinal points are studied and displayed using the locator line diagram and Pascal's ring. Each of the derived properties is studied separately for its dependence on frequency and finally the dependence of the characteristic matrices on the frequency of light are displayed using three-dimensional graphs. Each entry is a derived property and the relationship between certain derived properties can be seen.

Chapter 10 gives details of the numerical and graphical results for both schematic eyes for all the derivations of chromatic aberration and chromatic properties of the eye both independent of and dependent on the object or image and aperture positions. Object points at distance and three near working distances

are illustrated. Both the naked eye with centred pupil and the eye with a decentred pinhole immediately in front of the eye are illustrated.

1.2.4 Part V - Conclusion

Chapter 11 concludes that the transference, the fundamental properties and almost all the derived properties included in the study are dependent on the frequency of light. Certain derived properties are observed to be independent of frequency when the reduced eye model is used, but are dependent when Le Grand's eye is used. Formulae for the longitudinal and transverse chromatic aberration of systems in general are derived. Formulae for the chromatic properties of the eye, according to the definitions in the physiological optics literature, are derived from the transference. An important formula for deriving the linear relationship of each of the fundamental properties in the transference is obtained.

2 Definitions and measurements of chromatic aberration

Introduction, historical perspective

Humans have been admiring the rainbow since the beginning of time and different cultures have ascribed to the rainbow much religious and mystical significance (Lee and Fraser, 2001: 2-33). Whether or not the Irish leprechaun really has hidden a pot of gold at the end of a rainbow remains to be discovered. However, chromatic dispersion and its effects have enchanted men and women for millennia and people still spend fortunes purchasing diamonds for their sparkly effects caused by chromatic dispersion. The earliest documented academic studies of colour vision and the rainbow date back to Aristotle, around 384-322 BCE (Aristotle, 1906: 55-63 ; 1928; Lee and Fraser, 2001: 102-114).

We now know that the rainbow represents a continuum of colours but it is Newton who receives the most credit for his study of "Opticks". He was by no means the first to study colour, nor to discover a technique to create chromatic dispersion, however he is credited with naming the colours in the visible light spectrum. He originally chose five colours and later changed this to seven because he felt that the central colours were "crowded" and he wished to "divide the image into parts more elegantly proportioned to one another". He then observed that "the parts of the image occupied by the colors were proportioned to a string divided so it would cause the individual degrees of the octave to sound". He appears to have been particularly pleased and encouraged by this connection between colour and music (Newton, c1670).

2.1 Chromatic dispersion

It is Newton (c1670) who is credited with the scientific proof of chromatic dispersion. During the period 1670 to 1672 he conducted a series of experiments in which he successfully split white light up into a continuum of colours through a prism. He defined seven colours and named them according to the familiar colours of the rainbow: red, orange, yellow, green, blue, indigo and violet. The colour Newton called blue, is more of a sea-green that we now refer to as cyan. The colour Newton referred to as indigo is today's perception of blue, and green

he compared to leek green (Newton, c1670; Hastings, 1901:42; Waldman, 2002: 193).

Chromatic dispersion is defined as the separation of white light into its spectral components or the variation of the refractive index with wavelength (Sharma, 2006: 45, 50; Le Grand, 1956: 9). Dispersion is quantified mathematically by various dispersion formulae for the refractive index of the medium as a function of wavelength or by the Abbe number, also known as the constringency or refractive efficiency (Keating, 2002: 443–445). The latter allows us to quantify and compare by means of a single number the dispersive property of one material with another material and is more commonly used for laboratory-type media, including spectacle lenses. On the other hand, the formulae for the refractive index of a medium as a function of wavelength allows us to calculate the refractive index of a medium for any chosen wavelength or frequency; this is the quantitative method that we will use in this dissertation. There are a number of such formulae available for many materials, such as spectacle lens materials, glass, water, air, *etc*. (Walther, 1995:115–117; Herzberger, 1959) but there are limited formulae available for the media of the eye (Rabbetts, 2007: 287-288; Sivak and Mandelman, 1982).

There are two methods of determining the formulae for the refractive index of the media of the eye as a function of wavelength. One is to measure the medium of an enucleated eye with a refractometer, which poses some problems, and the other is to measure experimentally the chromatic aberration present in a sample of (living) eyes and interpolate the formulae according to the results. Wald and Griffin (1947) made some measurements with a refractometer of the aqueous and vitreous humours of cattle. They could not obtain measurements of the cornea because it was too thin and made only a crude measurement of the lens, however the measurement was not reliable because the lens needed to be compressed and distorted in order to take the measurement. This was further compounded by the lens's gradient index (Emsley, 1950: 518-519). They concluded that the humours have refractive indices similar to distilled water and that the lens material has considerably higher dispersion than water. More recently, Sivak and Mandelman (1982) took measurements for the refractive index at four wavelengths using a

refractometer on a variety of vertebrates, including cow, pig, frog, chicken, rock bass, rat and cat, for the aqueous and vitreous humours, the cornea and the inner and outer periphery and inner and outer core of the lens. They also measured the refractive indices for the peripheral and core of the lens for the human eye. The data was fitted to a polynomial.

There are a number of dispersion formulae available for expressing the refractive index as a function of wavelength (or wavenumber or frequency) for a variety of media. Examples include the dispersion formulae of Schmidt, Cauchy, Sellmeier, Cornu, Hartmann, Ciddor and Herzberger (Koczorowski, 1990; Ciddor, 1996; Herzberger, 1959). The expressions usually take the form of a polynomial with the variable being wavelength and constants for various materials given in tables. Depending on the medium, factors that influence the refractive index include, where relevant, temperature, humidity, carbon-dioxide content, pressure and even contaminants such as air pollution, and are defined as constants (Le Grand, 1956: 12-13; Hodgman, 1959, Ciddor, 1996) or may be included as variables in the expression (Ciddor, 1996).

Le Grand (1956: 12-13) studied refractometry measurements from Kunst, Polack and Tagawa (done in 1895, 1923 and 1928, respectively) which he claimed were all in close agreement for the two humours, the cornea and the periphery and core of the crystalline lens. He then compiled a table of refractive indices for the four media of the eye (aqueous and vitreous humours, cornea and lens) for the wavelengths of five Fraunhofer lines (A, C, D, F and G) as well as the constants needed for Cornu's formula for these four media. Villegas, Carretero and Fimia (1996) presented formulae for the refractive index as a function of wavelength for these four media using Le Grand's table of refractive indices which they obtained by a polynomial fit. The formula and constants are given in Section 4.4.3.

Thibos, Ye, Zhang and Bradley (1992) took an alternative approach. Using least-squares and their own measurements they obtained constants for a better fit for Cornu's hyperbolic dispersion formula to the reduced eye. This formula will form a basis for calculations in this dissertation and will be discussed in greater detail in Section 4.4.2.

2.2 Chromatic aberration

As several authors have remarked (Thibos, Bradley, Still, Zhang and Howarth, 1990; Simonet and Campbell, 1990; Rabbetts, 2007:289) there is much confusion in the literature regarding the definition of longitudinal and transverse chromatic aberration. In part, this confusion arises because each of the classical and physiological optics approaches define chromatic aberration differently. For the purposes of clarity in this dissertation, the definition of chromatic aberration will be that based on the classical optics definition given in Section 2.2.1 below and generalized for all optical systems, including those with elements that may be astigmatic, tilted or decentred in Chapter 6. The definitions of chromatic aberration in the physiological optics literature, which are specialized for the eye, will be referred to as physiological chromatic properties or chromatic properties. These are defined in the literature in Section 2.3 below and defined from the transference for Gaussian eyes in Chapter 7.

Until now, chromatic aberrations and chromatic properties have been studied using ray tracing and reverse ray tracing techniques which involve the extensive use of cardinal points, in particular the nodal point. There appears to be no reference in the literature to chromatic aberrations and properties in astigmatic systems. An exhaustive search of the literature, including personal correspondence (Thibos, 2011), confirms this.

This literature review looks at how these concepts are defined and measured in the literature, and the limitations imposed by the definitions. The literature makes use of the terms object space and image space. By the classical definition adopted here, chromatic aberration is associated with image space. It is not (yet) possible to measure the chromatic aberration in an eye, so measurements are usually done in object space. Coincidence of the red and blue images is presumed on the retina and "dispersion" from separate red and blue objects is measured outside of the eye.

It is important to separate the classical definition of chromatic aberration from the ophthalmic and physiological optics definitions that attempt to measure the various chromatic properties in the eye, both experimentally, in object space and calculation-based, in image space. The classical definition defines transverse

and longitudinal chromatic aberration for all Gaussian systems. Rabbetts (2007: 289) differentiates between physiological and classical optics definitions, however, this distinction is not drawn in most of the literature referred to in this study. Furthermore, only the more recent literature draws a distinction between calculated and measured chromatic properties and distinguishes between object and image space in these definitions. The definitions in the ophthalmic and physiological optics literature define transverse chromatic properties in eyes which include chromatic difference in position and chromatic difference in magnification and longitudinal chromatic properties in eyes which include chromatic difference in power and chromatic difference in refractive compensation. It is the intention in this study to clearly define longitudinal and transverse chromatic aberration in general to include astigmatic, decentred and heterocentric optical systems.

2.2.1 Definition of chromatic aberration

Born and Wolf (2002:186-187) define the first-order chromatic aberrations for systems in general within the limits of Gaussian optics as the distances δz and δy between the projections of the two focus points for the two different wavelengths in the directions parallel and perpendicular to the optical axis as longitudinal and transverse chromatic aberration respectively. The distances are unsigned, as shown in Figure 2.2.1. One notes that the chromatic aberrations depend on the position of the object. The definition holds for optical systems with stigmatic elements. This definition is consistent with Keating (1988:429; 2002:442-443), Katz (2002: 258-261) and Sharma (2006: 250) and is the definition that forms the starting point for the general definition that will be used in this study which holds for astigmatic, decentred and heterocentric optical systems. This definition will be discussed in Chapter 6.

Figure 2.2.1 defines the longitudinal δz and transverse δy chromatic aberration of an arbitrary homocentric system S with stigmatic elements. System S has an entrance plane T_0 and exit plane T. None of the refracting elements of S is shown. T_0 and T do not coincide with a refracting surface. Z is the optical axis.

I_r and I_b are the red and blue images of object O, respectively. We introduce the symbols δ to denote a chromatic difference and Δ to denote a physical difference between two dimensions. The above definition applies to Gaussian systems in general. It is what we refer to here as the classical definition of chromatic aberration.

A number of longitudinal and transverse chromatic properties are defined that apply specifically to the eye or model eye. A review of the literature reveals that most approaches make use of stigmatic models and, in particular, the reduced eye (Simonet & Campbell, 1990; Thibos, 1987; Thibos, Bradley and Zhang, 1991, Thibos *et al*, 1992; Zhang, Thibos and Bradley, 1991). References to schematic eyes were found (Atchison, Smith and Waterworth 1993; Le Grand 1956: 13; Rabbetts, 2007: 291; Zhang, Thibos and Bradley, 1991) but are limited to systems with stigmatic elements. There appears to be no clear distinction between the definition of chromatic aberration and the measurement of the chromatic properties in the eye. Rabbetts (2007: 289-293) and Atchison and Smith (2000: 180-186) both state that there are two primary chromatic aberrations, namely longitudinal and transverse. Thibos, Bradley and Zhang (1991) argue that there are three primary forms of chromatic aberration, namely chromatic difference of focus, chromatic difference of magnification and chromatic difference of position.

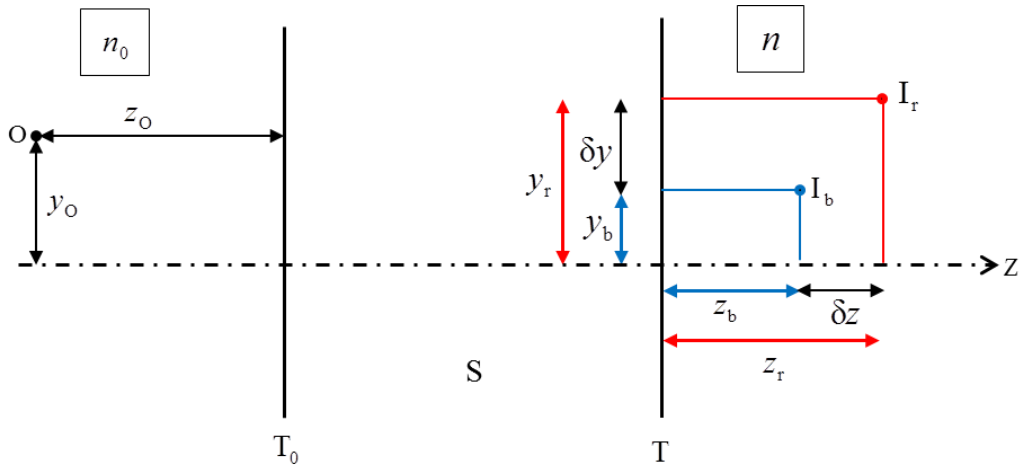

Figure 2.2.1 Longitudinal δz and transverse δy chromatic aberration of an arbitrary homocentric system with stigmatic elements. The system is drawn in the usual sense of a system such as the eye where $z_r > z_b$.

In Chapter 7 we will derive formulae for chromatic properties that are general for all Gaussian schematic eyes, regardless of the number of refracting surfaces. In Chapter 10 we will obtain numerical values for these derived formulae for chromatic aberration and chromatic properties for the reduced eye and Le Grand's four-surface eye.

2.3 Measurements of chromatic properties of the eye

Thibos, Bradley and Zhang (1991) emphasize that "chromatic aberration is the most important optical imperfection of the well corrected eye". The main differences in the definitions of longitudinal and transverse chromatic properties in the literature revolve around the use of reference points versus reference (or chief) rays and axes for the measurement and the units which are used. Some authors distinguish between image and object space, while others view them as the same thing (for example, Wald and Griffin, 1947).

Much work has been done to define a relationship between longitudinal and transverse chromatic aberration in the eye. Some authors (Simonet & Campbell, 1990) say there is no relationship, while others (Thibos *et al*, 1990, 1991; Zhang *et al*, 1991; Zhang, Bradley and Thibos, 1993) have derived formulae for a relationship. In Chapter 6, we show that longitudinal and transverse chromatic aberrations are fundamentally different (Harris and Evans, 2012).

2.3.1 Longitudinal chromatic properties

According to Rabbetts (2007: 289), longitudinal chromatic properties are defined in the physiological optics literature as the variation in focusing distance with wavelength. The literature defines two methods of measuring longitudinal chromatic properties of the eye, namely chromatic difference in refractive compensation and chromatic difference in power, each known by various names. Chromatic aberration is the distance measurement between the image points or object points created by two different wavelengths often measured as inverse units of distance (Wald and Griffin, 1947) and more commonly defined in object space as the difference in refractive compensation or object vergences required to provide clear imagery for two different wavelengths (Atchison, Smith and

Waterworth, 1993). Chromatic difference in power, or chromatic difference in focus (Wald & Griffin, 1947), is usually measured experimentally as chromatic difference in refractive error (Thibos *et al*, 1990, 1991; Wald & Griffin, 1947; Atchison, Smith and Waterworth 1993; Rabbetts, 2007).

Chromatic difference in refractive compensation is known as the chromatic difference in focus (Thibos, Bradley and Zhang, 1991; Atchison, Smith and Waterworth (1993)), chromatic difference in equivalent power (Atchison, Smith and Waterworth, 1993; Rabbetts, 2007:287-293), chromatic difference in power (Wald & Griffin, 1947), chromatic difference in refractive error (Thibos, Bradley and Zhang, 1991), chromatic difference in refraction (Rabbetts, 2007: 287-293), chromatic difference in ametropia (Atchison, Smith and Waterworth, 1993), axial chromatic aberration (Thibos, Bradley and Zhang, 1991; Wald & Griffin, 1947) or wavelength-dependent refractive error (Zhang, Thibos and Bradley, 1997).

Chromatic difference in power and chromatic difference in refractive compensation are not the same. Some authors use them interchangeably (Wald & Griffin, 1947), while others derive a linear relationship between them (Le Grand, 1956:14-16; Atchison, Smith and Waterworth, 1993; Thibos, Bradley and Zhang, 1991).

Chromatic difference in power

Thibos *et al* (1990) define the *ocular* longitudinal chromatic aberration in image space as "the distance between the image planes for different wavelengths" or "the variation of the eye's focusing power for different wavelengths", which is essentially the chromatic difference in power. Zhang, Thibos and Bradley (1991) define the chromatic difference in power as

$$\delta F = F_1 - F_2 = \frac{\delta n}{r} \qquad (2.3.1)$$

where δn is the difference between refractive indices of the medium for two wavelengths (λ_1 and λ_2) and r is the radius of curvature of the single refracting surface of the reduced eye. F_1 and F_2 are the powers of the same reduced eye for the two different wavelengths.

Chromatic difference in power is represented as longitudinal chromatic aberration (LCA) in Figure 2.3.1 for the reduced eye. The reduced eye has a single refracting surface, a longitudinal axis Z, which is also the achromatic axis and an optical axis, a nodal point N and a pupil or limiting aperture. The centre of curvature of the refracting surface coincides with the nodal point. The refractive index inside the reduced eye is *n* and before the reduced eye is n_0. Light from an object point O is refracted more for the short wavelength (shown in blue) than for the longer wavelength (shown in red). In Figure 2.3.1, the light with short wavelength creates a blue point focus I_b before the retinal plane and the light with the longer wavelength creates a red point focus I_r behind the retina. In Figure 2.3.1, the chromatic difference in power is shown as the distance between the image planes for different wavelengths, measured in units of inverse lengths.

Similarly, Rabbetts (2007: 290) defines chromatic difference in equivalent power (δF_e) as

$$\delta F_e = F_\lambda - F_o \qquad (2.3.2)$$

where F_λ is the equivalent power of the eye at a specified wavelength and F_o is the equivalent power of the eye at a reference wavelength.

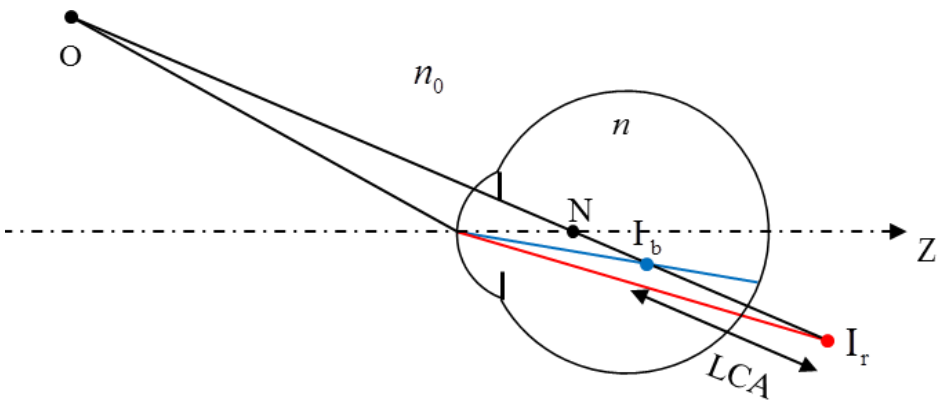

Figure 2.3.1 Chromatic difference in power shown as longitudinal chromatic aberration (LCA) for the reduced eye as the distance between the image planes for different wavelengths. (Figure adapted from Thibos *et al*, 1990.)

Chromatic difference in refractive compensation

Thibos *et al* (1990) define *ocular* longitudinal chromatic aberration in object space for the purposes of experimental study as the distance or dioptric interval between multiple object points of differing wavelengths that are positioned such that they focus simultaneously on the retina, thereby forming a single polychromatic image I shown in Figure 2.3.2. The dioptric interval is the difference in inverse distances from the refracting surface given by (Thibos *et al*, 1990)

$$\delta F_0 = \frac{1}{z_b} - \frac{1}{z_r} \qquad (2.3.3)$$

where δF_0 is the chromatic difference in refractive compensation, and z_r and z_b are the distances from the eye to the conjugate object points O_r and O_b respectively. The subscripts r and b represent red and blue, however, the exact wavelengths that they represent may differ from study to study. This effectively defines the chromatic difference in refractive compensation. Simply put, the chromatic difference in refractive compensation is the difference in power of the lens needed to compensate for the distance ametropia created by each wavelength (Thibos, Bradley and Zhang 1991). Rabbetts (2007: 290) defines chromatic difference in refraction as

$$\delta F_0 = F_{0\lambda} - F_{0o}$$

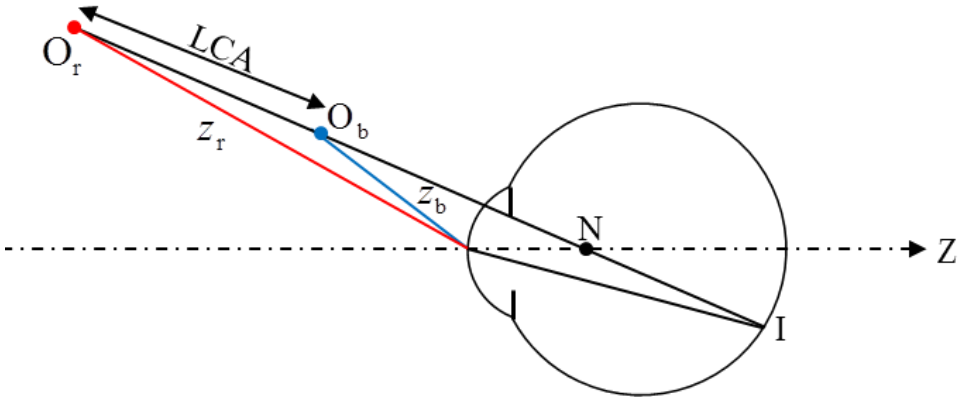

Figure 2.3.2 Chromatic difference in refractive compensation shown as longitudinal chromatic aberration (LCA) in the reduced eye, as the distance between the object planes for different wavelengths. (Figure adapted from Thibos *et al*, 1990).

where $F_{0\lambda}$ is the refraction of the eye at a specified wavelength and F_{0o} is the refraction of the eye at a reference wavelength. Furthermore, Rabbetts gives a relationship between chromatic difference in power and chromatic difference in refractive compensation for Gaussian schematic eyes as

$$\delta F_0 = -\delta F_e + \left(\frac{n_{\lambda v} - n_{ov}}{n_{ov}} \right) F_{0o}$$

where $n_{\lambda v}$ is the refractive index of the vitreous at a specified wavelength and n_{ov} is the refractive index of the vitreous at a reference wavelength.

Zhang, Thibos and Bradley (1991) and Thibos, Bradley and Zhang (1991) give the relationship between chromatic difference in power and chromatic difference in refractive compensation as

$$\delta F_0 = \frac{\delta n}{-n_D r} = \frac{\delta F}{-n_D} \qquad (2.3.4)$$

where n_D is the refractive index for the Fraunhofer line D ($\lambda_D = 589.3\,\text{nm}$) at which the reduced eye is emmetropic. λ_D is the reference wavelength for the reduced eye. All other symbols remain the same as already defined.

Experimental measurements

Wald and Griffin (1947) conducted an experiment using a spectral stigmatoscope with which they measured the *axial chromatic aberration* in dioptres as the refractive compensation required at each wavelength to bring the eye to the same power it possesses at the reference wavelength 578 nm.

Cooper and Pease (1988) conducted their experiment using a Badal optometer in order to measure wavelength in focus. Their aim was to establish which wavelength the eye preferred when accommodating on a near target. Their results are also expressed in dioptres for the refractive compensation required to focus light with a corresponding wavelength on the retina. They define this as longitudinal chromatic aberration.

Similarly, Thibos *et al* (1990) conducted an experiment using the Badal optometer as part of a larger experiment to find a relationship between longitudinal chromatic aberration (chromatic difference in refractive

compensation) and transverse chromatic aberration (chromatic difference in position).

Thibos *et al* (1992) conducted further experimental measurements using the two-colour Vernier method to measure the chromatic difference in refractive compensation. The aim of the set of experiments was to develop a reduced eye model that closely mimicked the real eye for chromatic aberration predictions. To this effect they developed the "chromatic eye" with three improvements over the reduced eye. Firstly, they refit Cornu's dispersion formula for the refractive index of the medium as a function of wavelength for the reduced eye to closely follow the experimental results. This formula will be discussed in Section 4.4.2. Secondly, they made the refracting surface aspherical (a prolate spheroid) to improve transverse chromatic aberration predictions. Finally, they included the pupil that Thibos (1987) previously introduced allowing for a reference axis and pupil centre to be defined.

Howarth and Bradley (1986) determined the chromatic difference in refractive compensation using a Badal optometer. The results showed that the Powell and Lewis achromatising lenses approximately corrected for the average longitudinal chromatic aberration. They also were able to conclude that individual differences in chromatic difference in refractive compensation are small, an important conclusion for this dissertation.

2.3.2 Transverse chromatic properties

According to Rabbetts (2007:289) when an off-axis polychromatic object point "produces laterally separated images on the retina due to dispersion … this is defined in the physiological optics literature as transverse chromatic aberration" and can also exist for an axial object point with a displaced artificial pupil. However, he states "in classical optics literature this is known as the transverse component of longitudinal chromatic aberration".

A number of terms and approaches are used to quantify transverse chromatic properties which are also referred to as lateral chromatic aberration, chromatic difference of magnification and chromatic difference of position. Zhang, Thibos and Bradley (1997) refer to *wavelength-dependent image*

magnification and *wavelength-dependent shifts in image position*, respectively, which they describe as *eccentricity-dependent transverse chromatic aberration*. Transverse chromatic aberration is defined either in image or object space and measured in object space. Measurements for transverse chromatic aberration are calculated either for an off axis object or a decentred pinhole.

Simonet and Campbell (1990) define transverse chromatic aberration as "the displacement of the image principal rays with wavelength". Certain definitions require that the chief ray should continue being projected to the retina or reference plane and the measurement taken as being from the centre of the projected blur patch to the centre of the second projected blur patch (e.g. Simonet & Campbell, 1990; Thibos, 1987; Thibos *et al*, 1990).

Thibos *et al* (1990) describe transverse chromatic aberration as the "variation in image position with wavelength". This creates a chromatic difference in position. The same mechanism will create a difference in image size called the chromatic difference in magnification. The chief ray from an object point is defined as the ray that traverses the centre of the pupil and therefore identifies the centre of the corresponding blur circle on the retina. The red and blue chief rays strike the retina at different positions, thereby defining the chromatic difference in position as the angle between the chief rays for different wavelengths, which Thibos *et al* (1990) define as transverse chromatic aberration. The chromatic difference in position depends on the pupil or pinhole position and the object location, which determines the incident inclination. The experimental variation of the position of the pinhole to control the position of the achromatic axis is referred to by Thibos *et al* (1990) as *induced* transverse chromatic aberration.

Thibos *et al* (1990) define the achromatic axis as the chief nodal ray; that is the ray that connects the centre of the pupil and the nodal point and which displays no transverse chromatic aberration. Typically, this would not intersect the fovea, however, when a pinhole is placed in front of the cornea, the achromatic axis can be manipulated to intersect the fovea. The nodal point is independent of wavelength (Thibos *et al*, 1990) for the reduced eye, however we will show in Section 9.1 that this is not strictly true of other schematic eyes or for eyes in general. According to Thibos *et al* (1990), the achromatic axis is important in

experimental situations because it represents the position where transverse chromatic aberration is null and thereby creates a link between theoretical and real eyes. They add that the achromatic axis can be manipulated experimentally, for example redirected to the fovea or other peripheral position, and therefore establishes a link between the optical theory and real eyes.

Chromatic difference in position

The chromatic difference in position is defined as the angular separation between the red and blue chief rays from a single object point in radians or minutes (Thibos *et al*, 1990, 1991). The chromatic difference in position is shown by angle *t* in Figure 2.3.3 (a), (b) and (c) (Thibos, 1987; Thibos *et al*, 1990). Thibos *et al* (1990) describe three approaches to defining and measuring chromatic difference in position: firstly in image space for a single object point, secondly in object space for the naked eye and finally also in object space, but manipulating the transverse position of the incident rays with a pinhole. These three approaches are shown in Figure 2.3.3 (a), (b) and (c).

According to Thibos (1987), Thibos *et al* (1990, 1991), the chromatic difference in position *t* will vary linearly with the angle of incidence of the chief rays, the angle of stimulus eccentricity, and the distance between the pupil centre and nodal point. *t* is also linearly related to the chromatic difference in refractive compensation (Thibos, Bradley and Zhang 1991). The transverse chromatic aberration depends on both the object location and the pupil location within the eye. The former will determine the angle of incidence of the selected rays while the latter will influence the position of the chief ray which is used in the calculations for transverse chromatic aberration.

For *induced* chromatic difference in position, Thibos *et al* (1990) conclude that each millimetre of displacement of the centre of the pinhole from the visual axis is approximately the same as 15 degrees of stimulus eccentricity. This means that, to first approximation, the two approaches to measuring chromatic difference in position in object space are directly proportional, with the constant of proportion being the displacement of the pinhole centre from the visual axis.

Thibos *et al* (1990) give the *transverse chromatic aberration*, shown in Figure 2.3.3(c), as

$$t = b - a = \frac{h}{z_b} - \frac{h}{z_r} = h\,\delta F_0 \qquad (2.3.5)$$

where the equation utilises the approximation of small angles. z_r and z_b are the distances from the red and blue object points respectively to the eye and *h* is the transverse displacement of the pinhole from the visual axis (in a reduced eye with a defined pupil and fovea).

Simonet and Campbell (1990) define *optical transverse chromatic aberration* "at the fovea as the difference for distinct wavelengths in the position of the centres of the images projected onto the retina". More specifically, the red chief ray is directed at the fovea and chromatic difference in position is measured as the angular difference in position of the blue chief ray relative to the fixed position of the red chief ray. The transverse chromatic aberration *t* is defined and measured experimentally in object space, consistent with *t* in Figure 2.3.3 (b), except that the red chief ray intercepts the fovea at the retina. They note that optical transverse chromatic aberration will have a vertical and horizontal component, but restrict their experimental measurements to only the horizontal component.

Simonet and Campbell (1990) also describe the relationship given by Equation 2.3.5 where *h* is the displacement in the entrance pupil of the rays with respect to the achromatic axis. δF_0 describes the slope of the relationship between transverse chromatic aberration *t* and displacement *h* in the entrance pupil. Simonet and Campbell make use of a Maxwellian view to direct the red and blue rays through the desired position in the pupil plane in contrast with Thibos *et al* (1990) who use a pinhole at the corneal plane.

Figure 2.3.3 illustrates the chromatic difference in position *t* for the reduced eye. Figure 2.3.3 (a) represents the chromatic difference in position in image space for the naked eye. Light from object point O is refracted at the single refracting surface. Light with a shorter wavelength (indicated in blue) is refracted more than light of a longer wavelength (indicated in red). *t* is measured as the angle between the blue and red light rays and represents the chromatic difference

in position. We can see that the red and blue rays each strike the retina at a different position, and that both images I_r and I_b are out of focus at the retina.

Figure 2.3.3 (b) represents the chromatic difference in position in object space for the naked eye. Light with a longer wavelength and originating from a red object point O_r along with light with a short wavelength originating from a blue object point O_b are refracted at the refracting surface and create a single, simultaneous image point I at the retina. In Figure 2.3.3 (b), the chromatic difference in position *t* is the angle between the red and blue rays in object space. Figure 2.3.3 (c) represents the chromatic difference in position in object space for the eye with artificial limiting aperture immediately in front of the refracting surface. The pinhole aperture allows us to choose the image point to arrive at the fovea F, making the line joining the object points O_r and O_b, the nodal point N and the fovea to be the visual axis. *a* is the angle between the red ray and the visual axis, *b* is the angle between the blue ray and the visual axis and *h* is the displacement of the pinhole from the visual axis. Similar to (b), the chromatic difference in position is the angle *t* between the red and blue rays in object space.

Thibos, Bradley and Zhang (1991) derived a relationship between chromatic difference in refractive compensation δF_0 and chromatic difference in position *t*. For chromatic difference in position for an off-axial object point the approximate equation is given as

$$t = z\,\delta F_0 \sin\varepsilon \qquad (2.3.6)$$

where *z* is the distance between the iris and the nodal point and ε is the eccentricity as shown in Figure 2.3.4 (a). For a displaced pinhole, Thibos, Bradley and Zhang (1991) define the approximate relationship as $t = h\,\delta F_0$. However the definition is subtly different from that as given in the Equation 2.3.5 by Thibos *et al* (1990). The definition in Equation 2.3.6 and its approximation are given as approximations and the angle *t* is subtended at the nodal point and shown in Figure 2.3.4 (a) and (b), whereas in Figure 2.3.3 (a), (b) and (c) the angle is subtended at the refracting surface. Comparing these two equations, Thibos, Bradley and Zhang (1991) also conclude that each millimetre of displacement of

an external pinhole or limiting aperture results in 15° of eccentricity for the naked eye.

Zhang, Thibos and Bradley (1997) schematically define *transverse chromatic aberration* as the angle subtended at the refracting surface, according to

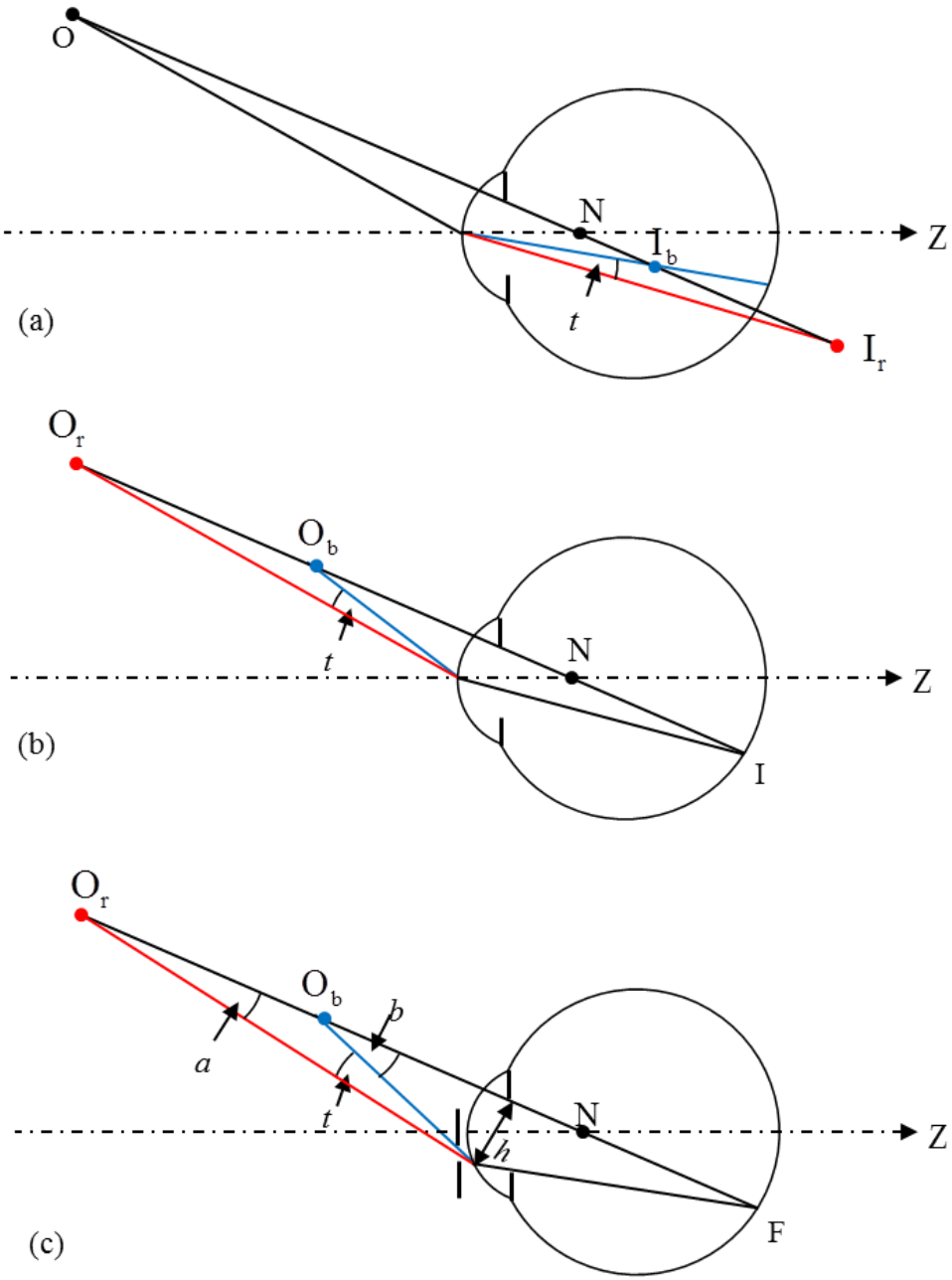

Figure 2.3.3 The chromatic difference in position *t* for the reduced eye. (a) The chromatic difference in position in image space for the naked eye. (b) The chromatic difference in position in object space for the naked eye. (c) The chromatic difference in position in object space for the eye with artificial limiting aperture immediately in front of the refracting surface. Figure not drawn to scale and adapted from Thibos *et al* (1990).

Figure 2.3.3 (a), however, they define *transverse chromatic aberration* algebraically as the angle subtended at the nodal point and shown in Figure 2.3.4. Zhang, Thibos and Bradley (1997) estimate that the angle subtended at the nodal point of the eye to be approximately 1.333 times larger than the angle subtended at the refracting surface.

Chromatic difference in magnification

The chromatic difference in magnification is defined as the magnification of the angle between the red and blue chief rays or difference in size between the centres of the red and blue retinal images as a percentage (Thibos, Bradley and Zhang, 1991; Zhang, Thibos and Bradley, 1991) or as a ratio (Rabbetts, 2007; Thibos, Bradley and Zhang, 1991) or seconds of arc (Simonet & Campbell, 1990),

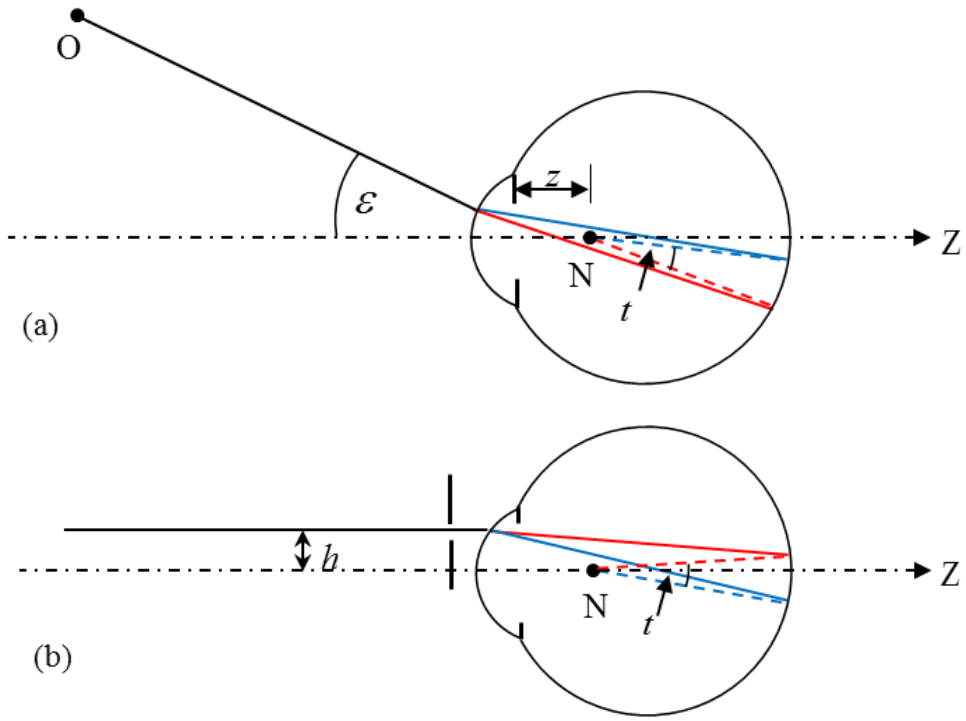

Figure 2.3.4 Chromatic difference in position *t* for the reduced eye in image space. (a) The ray arrives at the naked eye at eccentricity ε. *t* is the angle subtended at N by the intersections of the two rays with the retina. (b) A decentred pinhole aperture ensures that the ray arrives at the eye at some distance *h* from the achromatic axis. *t* is the angle subtended at N by the retinal intersections of the two rays. (Figure adapted from Thibos *et al*, 1991)

regardless of defocus. The chromatic difference in magnification is the variation in retinal image size with variation in wavelength (Thibos *et al*, 1990). One or both of the images for the two wavelengths used in the calculation will be out of focus (Thibos *et al*, 1990). Theoretically, chromatic difference in magnification can be calculated in both image and object space, however, because most of the experimental magnitudes measured are for chromatic difference in position, chromatic difference in magnification is usually calculated in image space.

Simonet and Campbell (1990) give the chromatic difference in magnification as

$$\delta M = y_r - y_b \tag{2.3.7}$$

where y_r and y_b are the red and blue image sizes at the retina, with the red image on the centre of the fovea F, regardless of defocus, and corresponding to object size y_O in seconds of arc. This is shown in Figure 2.3.5.

Chromatic difference in magnification is defined as an angular magnification given as

$$\delta M = \frac{t}{\varepsilon} \tag{2.3.8}$$

where *t* is the angle between the red and blue chief rays as given in Figure 2.3.3 (a) and ε is the eccentricity shown in Figure 2.3.4 (a) (Thibos, Bradley and Zhang, 1991; Zhang, Thibos and Bradley, 1991). Equation 2.3.8 gives the relationship between chromatic difference in position *t* and chromatic difference in magnification.

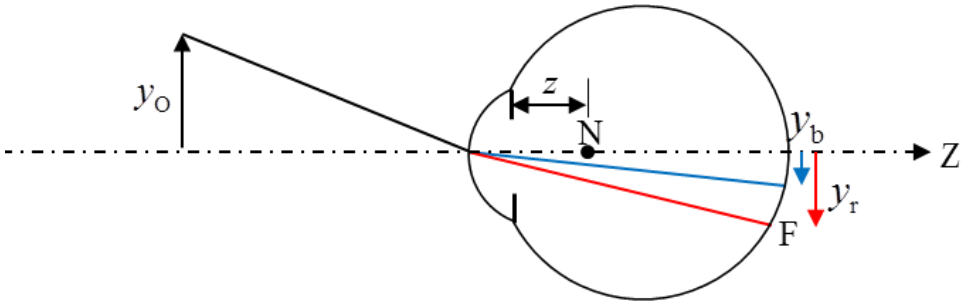

Figure 2.3.5 Chromatic difference in magnification is the difference between the image size for the two images created at the retina for two different chosen wavelengths, y_b and y_r, corresponding to object size y_O. y_r corresponds to F, the centre of the fovea.

Thibos, Bradley and Zhang (1991) and Zhang, Thibos and Bradley (1991) give the chromatic difference in magnification δM as

$$\delta M = z\,\delta F_0 \qquad (2.3.9)$$

where z is the distance between the pupil and the nodal point, shown in Figure 2.3.5. According to Thibos, Bradley and Zhang (1991), z is typically estimated at 0.4 cm, δF_0 is approximately 2 D and the chromatic difference in magnification is 0.8% across the visible light spectrum. Thibos, Bradley and Zhang (1991) conclude that chromatic difference in magnification is directly proportional to chromatic difference in refractive compensation and to the axial location of the entrance pupil relative to the nodal point. In the naked eye they find that this amounts to 0.8%, but by implication, the chromatic difference in magnification will increase when the limiting aperture is outside the eye, for example with a pinhole or optical instrument in front of the eye.

Of interest is the similarity between Equations 2.3.6 and 9. The chromatic difference in position is proportional to the sine of the eccentricity while the chromatic difference in magnification is independent of the eccentricity.

Experimental measurements

We recall that Thibos *et al* (1990) conducted an experiment as part of a larger experiment to find a relationship between *longitudinal chromatic aberration* (chromatic difference in refractive compensation) and *transverse chromatic aberration* (chromatic difference in position). They used a pinhole aperture to manipulate the angle of incidence of the foveal chief ray and measured the magnitude of the aberration as a function of pinhole displacement using a two-colour Vernier-alignment task.

Simonet and Campbell (1990) conducted experiments to measure *longitudinal chromatic aberration* (chromatic difference in refractive compensation) and *optical transverse chromatic aberration* (chromatic difference in position at the fovea). They made use of firstly, a dual Maxwellian view and vertical Vernier targets with the red target being the fixed target and the blue target being manipulated. This enabled them to take experimental measurements

of both *longitudinal chromatic aberration* and *transverse chromatic aberration*. They noted that the factors affecting the average and variability of *transverse chromatic aberration* include the value of angle α and any displacement of the pupil.

The experimental measurements of Thibos *et al* (1992) using the two-colour Vernier method also measured the induced chromatic difference in position in object space for pinhole positions. We recall that the aim of the set of experiments was to develop a reduced eye model that closely mimicked the real eye for chromatic aberration predictions. They developed the "chromatic eye" with three improvements over the reduced eye. The adaption that was most essential to measuring chromatic difference in position was the inclusion of a pupil that Thibos (1987) originally introduced allowing for a reference axis and pupil centre to be defined. Thibos *et al* (1992) show that the chromatic eye, by design, matches the experimental data almost exactly, enabling accurate prediction of chromatic difference in refractive compensation and position.

Zhang, Thibos and Bradley (1997) did a further experiment to compare the image sizes between the two eyes produced by an eccentric object point. The procedure measured interocular differences in image size produced stereoscopically and measured the amount of image magnification difference which are introduced by interocular differences in wavelength. They used the same procedure to compare firstly the naked eye and natural pupils, secondly, the naked eye with pinhole apertures in front of both eyes and measurements taken at three different vertex distances and finally while the subjects wore an achromatizing lens in front of the right eye. The achromatizing lenses compensate for wavelength-dependent refractive error, however, they exaggerate wavelength-dependent magnification by a factor of up to 7. In comparison, the artificial pupil at 20 mm vertex distance, showed the greatest increase in transverse chromatic aberration.

2.4 Summary

The assortment of terms and definitions is a source of confusion in the literature of chromatic aberration. For the purposes of this dissertation, we shall

differentiate between the classical optics definition of chromatic aberration and the ophthalmic and physiological optics definitions. We shall define first-order chromatic aberration according to the classical optics definition given by Born and Wolf (2002) and given in Section 2.2.1. This definition for longitudinal and transverse chromatic aberration is limited to Gaussian optics and in Chapter 6 we generalise this definition to include systems with astigmatic and heterocentric elements.

We shall distinguish between the definitions of ocular chromatic aberration found in the ophthalmic and physiological optics literature from the classical definition by referring to the former as ocular chromatic properties and to the latter as chromatic aberration. We shall distinguish between chromatic properties that are independent or dependent on object or image and aperture position. Independent chromatic properties include chromatic difference in power and chromatic difference in refractive compensation. Chromatic properties dependent on object or image and aperture positions include chromatic difference in position and chromatic difference in magnification. Chromatic properties in both image and object space will be examined.

In Chapter 7 we obtain formulae for calculating the chromatic properties in image and object space from the transference. The transference will enable us to calculate all of the chromatic properties of a compound Gaussian eye quickly and easily, and we will not have to restrict ourselves to the reduced eye.

The definitions in the literature consider the difference between wavelengths at two end-points of the visible light spectrum. While this is important, we shall, in Chapters 8 and 9, take a look at the dependence of the fundamental and derived properties of the transference on the frequency of light across the entire visible light spectrum.

3 BACKGROUND THEORY: OPTICS

First-order optics and the approximation of small angles are used throughout this study. Historically, the physiological optics approach to chromatic aberration has used ray tracing and cardinal points and for this reason, hence we take a brief look at this approach. However, the model of choice in this dissertation is linear optics; often simplified for Gaussian systems. Linear optics is a powerful tool in that it allows for surfaces that are astigmatic and tilted or decentred. The optical character of compound systems comprising multiple elements is represented by a single matrix, the transference. In linear and Gaussian optics, the transference is a complete representation of the first-order effects of an optical system on the ray traversing it (Torre, 2005: 60).

We start this chapter with a brief overview of the theories of light to ascertain where both linear and Gaussian optics are positioned in the field of optics. We then take a detailed look at linear optics, define the optical system, derive the transference of elementary and compound systems and show how it changes the state of the ray traversing the system. The fundamental properties of a system are defined. We see how the transference can be augmented to allow for tilt and decentration or simplified for a Gaussian system with only centred stigmatic elements.

In order to gain some insight into the fundamental properties, we take a look at four special systems. There are a number of familiar properties of optical systems that can be derived from the transference. We take a look at those that have implications for the study of chromatic properties of the eye. The derived properties that we will consider include power, compensating lenses, front- and back vertex power, magnification and cardinal points. There are many other properties that can be derived from the transference, however, we will limit this study to those just mentioned.

Because the transference is symplectic, there are a number of implications, for its mathematical manipulation. In particular there are limitations on the statistical analysis of the transference. To overcome this we turn to the literature to establish how to get around these limitations. It turns out that we can transform

the transference into an element of linear space which then allows quantitative analysis. Each of these transformed transferences will be studied in turn, and one in particular will be pivotal to the development, in Chapter 8, of a formula for the dependence of the transference on the frequency of light.

Finally, we look at how vergence and wavefronts are represented in linear and Gaussian optics. Of course, light is not a property of the system, but we are interested in the effect of the system on light. Because vergence is the basis for how we will be defining chromatic aberration in Chapter 6, we take a look at how vergence and wavefronts are defined in the linear optics literature.

3.1 Gaussian and Linear Optics

Gaussian and linear optics assume that rays are paraxial and therefore make use of the assumption of small angles and that the rays are close to the longitudinal axis. In the optics literature this is commonly referred to as either the Gaussian approximation or paraxial approximation. In the mathematics literature it is referred to as the first-order approximation; all quadratic (or higher-order) expressions in angles are ignored (Guillemin & Sternberg, 1984:5,23). The approximations $\sin\theta = \theta$, $\tan\theta = \theta$ and $\cos\theta = 1$ are used and Snell's law simplifies to $n_1 i_1 = n_2 i_2$ or $\imath_1 = \imath_2$ where $\imath = ni$. Both the ray tracing and matrix approaches in Gaussian optics make use of this assumption. In addition both Gaussian and linear optics assume that all media are homogenous and isotropic between refracting surfaces. This implies that rays are straight lines between refracting surfaces and geometrical aberrations are ignored (Guillemin & Sternberg, 1984:7).

3.1.1 Theories of light

In physics, as new theories supersede old ones, the older theory may still hold some relevance. It may be an approximation of the new theory or it may be valid in certain circumstances or a special case of the new theory (Guillemin & Sternberg, 1984:3). This is certainly true in optics in particular. Guillemin and Sternberg (1984:3-17, 37) describe the theories of light, a summary of which is presented below.

Quantum electrodynamics is the current theory of light and describes the interaction between light and charged particles, including its photo-electric effect and wavelike character of electro-magnetic radiation. *Maxwellian electrodynamics* is an approximation of quantum electrodynamics and ignores the quantum effects. It explains electricity, magnetism and electromagnetic radiation, including its source and propagation, but fails at the atomic or subatomic level.

Wave theory is mostly ascribed to Fresnel and is concerned with the propagation of light through various media. It includes diffraction, interference and polarization. It deals with certain wavelengths of light and ignores the emission of radiation.

Geometrical optics is an approximation of wave theory which ignores the wave character of light, diffraction, interference and polarization. *Geometrical optics* is valid for apertures of large dimension (when compared with the wavelength of light), provided one ignores what is happening in the vicinity of shadows and foci. Geometrical optics uses Snell's law ($n_1 \sin i_1 = n_2 \sin i_2$) without the approximation of small angles and the refractive indices of heterogeneous media may vary smoothly and sometimes rapidly. The deviations between linear and geometrical optics are known as geometrical or Seidel's (third-order) aberrations.

Linear optics is an approximation of geometrical optics which ignores Seidel's aberrations and uses the approximation of small angles. In linear optics a ray is defined in three-dimensional space at a fixed transverse plane for direction and position using four variables. A symplectic 4×4 matrix represents the system through which this ray will traverse. The trajectory of the light ray is traced as it passes through the various refracting and reflecting surfaces and homogenous gaps of the optical system. A coordinate system is introduced with a longitudinal axis Z and various transverse planes T, usually two. Because linear optics applies in three-dimensions, it accounts for all the effects of astigmatism. An augmented symplectic 5×5 matrix can account for the additional effects of tilted surfaces and decentred elements (Harris, 1994).

Gaussian optics is a special case of linear optics where all surfaces are rotationally symmetric about a central axis, hence the longitudinal axis Z

coincides with the optical axis. The rays studied are all coplanar, that is, they all lie on one plane, the reference plane. The transference simplifies to a 2×2 matrix and the vector representing the ray at a transverse plane is 2×1.

3.2 First-order optics

In this section we consider first-order optics, both Gaussian and linear, that will form the basis for the remaining chapters. It is not intended as a complete account of linear optics.

3.2.1 Definition of an optical system

An optical system is bound by two transverse planes, an entrance plane T_0 and an exit plane T, and has a longitudinal axis Z (see Figure 3.2.1). The entrance and exit planes can be chosen to be anywhere except at a refracting or reflecting surface. Usually the planes are taken to be immediately before or after a refracting or reflecting surface.

3.2.2 The state of the ray

The state of the ray at transverse plane T is defined as

$$\boldsymbol{\rho} = \begin{pmatrix} \mathbf{y} \\ \boldsymbol{\alpha} \end{pmatrix} \tag{3.2.1}$$

where

$$\boldsymbol{\alpha} = n\mathbf{a} \tag{3.2.2}$$

is the reduced inclination. (‘Reduced’ has the same sense as in ‘reduced to a common denominator’; it does not mean ‘made less’.) $\boldsymbol{\rho}$ is a 4×1 matrix consisting of two submatrices, $\mathbf{y}$ and $\boldsymbol{\alpha}$. $\mathbf{y}$ is a 2×1 matrix which represents a position vector with Cartesian coordinates y_1 and y_2:

$$\mathbf{y} = \begin{pmatrix} y_1 \\ y_2 \end{pmatrix}. \tag{3.2.3}$$

$\mathbf{a}$ is a 2×1 matrix that represents the inclination of the ray at T relative to Z. In terms of horizontal and vertical Cartesian coordinates

$$\mathbf{a} = \begin{pmatrix} a_1 \\ a_2 \end{pmatrix}. \tag{3.2.4}$$

In Figure 3.2.1 we distinguish between the incident ray state $\boldsymbol{\rho}_0$ at entrance plane T_0 and emergent ray state $\boldsymbol{\rho}$ at exit plane T.

3.2.3 The transference and fundamental properties

The transference **S** of an untilted, centred (homocentric) linear optical system is a 4×4 matrix often conveniently represented by (Guillemin and Sternberg, 1984: 26; Harris, 2010d)

$$\mathbf{S}=\begin{pmatrix}\mathbf{A} & \mathbf{B}\\ \mathbf{C} & \mathbf{D}\end{pmatrix} \tag{3.2.5}$$

where **A** the *dilation*, **B** the *disjugac*y, **C** the *divergence* and **D** the *divaricatio*n are the fundamental first-order optical properties of the system (Harris, 1999a; 2001c). Each of **A**, **B**, **C** and **D** is a 2×2 matrix.

The fundamental properties are strictly properties of the system itself and do not represent properties of anything else including light, vergence, image foci or object points (Harris, 1999b). A system may comprise a series of elementary systems, namely refracting surfaces and homogenous gaps between the entrance and exit planes.

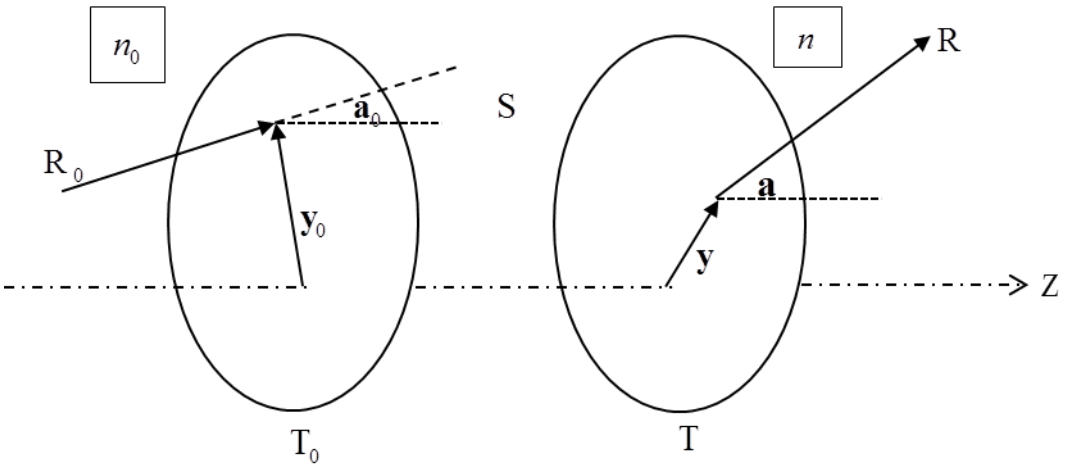

Figure 3.2.1 An optical system S is bound by an entrance plane T_0 and an exit plane T and has a longitudinal axis Z. A ray enters system S at T_0 with incident ray segment R_0 at transverse position $\mathbf{y}_0$ and inclination $\mathbf{a}_0$. The ray exits the system at T; the emergent ray segment R has position **y** and inclination **a**. The refractive index upstream of the system is n_0 and downstream it is *n*.

Let system S_1 have transference $\mathbf{S}_1$ and similarly for systems S_2, S_3, *etc*. Then the transference of the compound system $S_1S_2S_3...S_m$ made up of *m* juxtaposed optical systems is (Keating, 2002:325-345, Harris, 1994)

$$\mathbf{S} = \mathbf{S}_m ... \mathbf{S}_3 \mathbf{S}_2 \mathbf{S}_1 . \tag{3.2.6}$$

Multiplication is in reverse order.

The transference of a homogenous gap of width *z* and index *n* is (Guillemin and Sternberg, 1984: 9, 27)

$$\mathbf{S} = \begin{pmatrix} \mathbf{I} & \zeta\mathbf{I} \\ \mathbf{O} & \mathbf{I} \end{pmatrix} \tag{3.2.7}$$

where ζ is a scalar and is the reduced width defined by

$$\zeta = \frac{z}{n} . \tag{3.2.8}$$

I and **O** are the 2×2 identity and null matrices, respectively. The transference of a refracting surface or thin lens of power **F** (a symmetric matrix) is (Guillemin and Sternberg, 1984: 10, 27; Harris, 2010d; Keating, 1982)

$$\mathbf{S} = \begin{pmatrix} \mathbf{I} & \mathbf{O} \\ -\mathbf{F} & \mathbf{I} \end{pmatrix} . \tag{3.2.9}$$

3.2.4 The basic equation of a ray traversing a system

A ray traversing system S has its state at incidence $\boldsymbol{\rho}_0$ and emergence $\boldsymbol{\rho}$ related by

$$\mathbf{S}\boldsymbol{\rho}_0 = \boldsymbol{\rho} \tag{3.2.10}$$

an equation referred to as the basic equation of linear optics (Harris, 1999a,b).

Substituting from Equations 3.2.5, 1 and 2 into Equation 3.2.10 and multiplying out, we obtain two matrix equations for a system centred about an optical axis:

$$\mathbf{A}\mathbf{y}_0 + n_0\mathbf{B}\mathbf{a}_0 = \mathbf{y} \tag{3.2.11}$$

$$\mathbf{C}\mathbf{y}_0 + n_0\mathbf{D}\mathbf{a}_0 = n\mathbf{a} . \tag{3.2.12}$$

3.2.5 Symplecticity

The general linear group over the real numbers is denoted GL(n;$\mathbb{R}$) and is the group of all $n \times n$ invertible matrices with real entries. (We will restrict this dissertation to the set of real numbers). The general linear group is a matrix Lie group and is closed under matrix multiplication. The real symplectic group, denoted Sp(n;$\mathbb{R}$), is a subgroup of GL(n;$\mathbb{R}$) and is the set of all $2n \times 2n$ matrices (Hall, 2004:3-8).

By definition (Guillemin and Sternberg, 1984:26; Watkins, 2004; Hall, 2004:8), a $2n \times 2n$ matrix **S** is symplectic if it obeys the equation

$$\mathbf{S}^{\mathrm{T}}\mathbf{E}\mathbf{S} = \mathbf{E} \tag{3.2.13}$$

where

$$\mathbf{E} = \begin{pmatrix} \mathbf{O} & \mathbf{I} \\ -\mathbf{I} & \mathbf{O} \end{pmatrix} \tag{3.2.14}$$

and **I** and **O** are $n \times n$ identity and null matrices respectively and **E** is a $2n \times 2n$ matrix, sometimes known as the *symplectic unit matrix* (Torre, 2005: 11; Harris, 2010d). The superscript T represents the matrix transpose. In Gaussian optics $n = 1$ implying the simplest of optics, that on the reference plane, with the system being stigmatic, centred and 2-dimensional. In linear optics $n = 2$, giving us the simplest optical theory, that in 3-dimensions (Harris, 2010d).

Substituting from Equations 3.2.5 and 3.2.14 into Equation 3.2.13 and multiplying out we find

$$\begin{pmatrix} \mathbf{A} & \mathbf{B} \\ \mathbf{C} & \mathbf{D} \end{pmatrix}^{\mathrm{T}} \begin{pmatrix} \mathbf{O} & \mathbf{I} \\ -\mathbf{I} & \mathbf{O} \end{pmatrix} \begin{pmatrix} \mathbf{A} & \mathbf{B} \\ \mathbf{C} & \mathbf{D} \end{pmatrix} = \begin{pmatrix} \mathbf{O} & \mathbf{I} \\ -\mathbf{I} & \mathbf{O} \end{pmatrix} \tag{3.2.15}$$

$$\begin{pmatrix} \mathbf{A}^{\mathrm{T}}\mathbf{C} - \mathbf{C}^{\mathrm{T}}\mathbf{A} & \mathbf{A}^{\mathrm{T}}\mathbf{D} - \mathbf{C}^{\mathrm{T}}\mathbf{B} \\ \mathbf{B}^{\mathrm{T}}\mathbf{C} - \mathbf{D}^{\mathrm{T}}\mathbf{A} & \mathbf{B}^{\mathrm{T}}\mathbf{D} - \mathbf{D}^{\mathrm{T}}\mathbf{B} \end{pmatrix} = \begin{pmatrix} \mathbf{O} & \mathbf{I} \\ -\mathbf{I} & \mathbf{O} \end{pmatrix} \tag{3.2.16}$$

which gives the three distinct symplectic equations (Guillemin and Sternberg, 1984:26)

$$\mathbf{A}^{\mathrm{T}}\mathbf{C} - \mathbf{C}^{\mathrm{T}}\mathbf{A} = \mathbf{O}, \tag{3.2.17}$$

$$\mathbf{A}^{\mathrm{T}}\mathbf{D} - \mathbf{C}^{\mathrm{T}}\mathbf{B} = \mathbf{I} \tag{3.2.18}$$

and

$$\mathbf{B}^{\mathrm{T}}\mathbf{D} - \mathbf{D}^{\mathrm{T}}\mathbf{B} = \mathbf{O}. \tag{3.2.19}$$

For any 2×2 or 4×4 symplectic matrix there exists an optical system with that transference and any matrix that is not symplectic does not represent the transference of an optical system (Guillemin and Sternberg, 1984:23-27; Harris, 2004a, 2010d).

Manipulating Equation 3.2.18 and substituting the equality from either Equation 3.2.17 or 19 and the rule $(\mathbf{AB})^{\mathrm{T}} = \mathbf{B}^{\mathrm{T}}\mathbf{A}^{\mathrm{T}}$, one obtains four expressions, namely

$$\mathbf{A} - \mathbf{B}\mathbf{D}^{-1}\mathbf{C} = \mathbf{D}^{-\mathrm{T}}, \tag{3.2.20}$$

$$\mathbf{B} - \mathbf{A}\mathbf{C}^{-1}\mathbf{D} = -\mathbf{C}^{-\mathrm{T}}, \tag{3.2.21}$$

$$\mathbf{C} - \mathbf{D}\mathbf{B}^{-1}\mathbf{A} = -\mathbf{B}^{-\mathrm{T}}, \tag{3.2.22}$$

$$\mathbf{D} - \mathbf{C}\mathbf{A}^{-1}\mathbf{B} = \mathbf{A}^{-\mathrm{T}} \tag{3.2.23}$$

(Harris and van Gool, 2004; Harris, 2010d). The expression $\mathbf{A} - \mathbf{D}^{-\mathrm{T}}\mathbf{B}^{\mathrm{T}}\mathbf{C}$ is known as the Schur complement of **A** in **S** and similarly there are Schur complements of **B**, **C** and **D**. They have proven useful in visual optics and are particularly useful in simplifying complicated equations.

In a Gaussian system the three symplectic equations effectively reduce to the single equation

$$AD - CB = 1 \tag{3.2.24}$$

which is the equation for unit determinant. For a 2×2 matrix this is the only requirement for symplecticity (Guillemin & Sternberg, 1984:11, 15, 24) and any 2×2 matrix with determinant 1 is the transference of some optical system.

While the 4×4 transference of an optical system always has a unit determinant, the converse is not always true (Guillemin & Sternberg, 1984:23-24; Harris, 2010d). In order to test for symplecticity one needs to test whether the matrix obeys Equation 3.2.13, or, equivalently, whether it obeys all of Equations 3.2.17 to 19 (Harris, 2004a, 2010d).

All symplectic matrices have unit determinant (Bernstein, 2005:114; Hall, 2004:8,40). The implication of this is that because

$$\det(\mathbf{AB}) = \det\mathbf{A}\det\mathbf{B} \tag{3.2.25}$$

the product of all transferences will also have unit determinant (Bernstein, 2005:40-41; Anton and Rorres, 2005:104-105; Keating, 2002:330; Harris, 2010d)

and therefore all transferences are invertible. We note that the matrix in Equation 3.2.7 is symplectic and similarly the matrix in Equation 3.2.9 is symplectic provided **F** is symmetric (from Equation 3.2.17), which is true of refracting surfaces and thin lenses. While Harris and van Gool (2009) have considered the theoretical possibility of a thin lens of asymmetric power, it will not be considered here.

3.2.6 Augmented transferences and heterocentric systems

Up to this point, the optical systems described have been homocentric, that is all centred on a longitudinal axis Z, which is therefore an optical axis. Elements may have been stigmatic or astigmatic and represented by Gaussian 2×2 or linear 4×4 transferences respectively. We now briefly consider the effects of including elements that are tilted or decentred (heterocentric).

We define a 4×1 matrix (Harris, 1993)

$$\boldsymbol{\delta} = \begin{pmatrix} \mathbf{e} \\ \boldsymbol{\pi} \end{pmatrix}. \tag{3.2.26}$$

It accounts for all the effects of prism, tilt and decentration. The *transverse translation* **e** and *deflectance* $\boldsymbol{\pi}$ are each 2×1 submatrices of $\boldsymbol{\delta}$ and along with **A**, **B**, **C** and **D** are also fundamental first-order optical properties of the system (Harris 2010e). **e** has units of length and $\boldsymbol{\pi}$ is dimensionless. It is often convenient to think of $\boldsymbol{\pi}$ in radians.

In order to account for these effects we generalise Equation 3.2.10 to

$$\mathbf{S}\boldsymbol{\rho}_0 + \boldsymbol{\delta} = \boldsymbol{\rho}. \tag{3.2.27}$$

For a compound system consisting of *n* subsystems (Harris, 1993)

$$\mathbf{S}_n\left(...\left(\mathbf{S}_3\left(\mathbf{S}_2\boldsymbol{\delta}_1 + \boldsymbol{\delta}_2\right) + \boldsymbol{\delta}_3\right) + ...\right) + \boldsymbol{\delta}_n = \boldsymbol{\delta}. \tag{3.2.28}$$

Instead of Equation 3.2.28, Harris (1994) defines a 5×5 augmented transference **T**

$$\mathbf{T} = \begin{pmatrix} \mathbf{S} & \boldsymbol{\delta} \\ \mathbf{o}^{\mathrm{T}} & 1 \end{pmatrix} \tag{3.2.29}$$

where **o** is a 4×1 null matrix, the fifth row being a trivial row, and a 5×1 augmented ray state $\boldsymbol{\gamma}$

$$\boldsymbol{\gamma} = \begin{pmatrix} \boldsymbol{\rho} \\ 1 \end{pmatrix}. \tag{3.2.30}$$

The qualifier "augmented" will not be used repetitively and we will rely on the context to make clear whether the transference or ray state is augmented or not.

Equation 3.2.27 now generalises to

$$\mathbf{T}\boldsymbol{\gamma}_0 = \boldsymbol{\gamma} \tag{3.2.31}$$

which is simple and elegant like Equation 3.2.10 and encompasses all the detail of Equation 3.2.27. The proof is provided by Harris (1994). **T** is a matrix that represents all the first-order optical characteristics of the system, including homogenous spaces and astigmatic elements that may be tilted and decentred (heterocentric) or have prismatic effects (Harris, 2012c). Rewriting **T** with all six of its fundamental properties we have

$$\mathbf{T} = \begin{pmatrix} \mathbf{A} & \mathbf{B} & \mathbf{e} \\ \mathbf{C} & \mathbf{D} & \boldsymbol{\pi} \\ \mathbf{o}^{\mathrm{T}} & \mathbf{o}^{\mathrm{T}} & 1 \end{pmatrix}. \tag{3.2.32}$$

Each of **A**, **B**, **C** and **D** are 2×2 submatrices, **e**, $\boldsymbol{\pi}$ and **o** are 2×1 submatrices with **o** being a null vector. In particular, **T** represents the way the system will operate on the state of the ray traversing the system (Harris, 2001a). We note here that in order for a matrix to be symplectic it needs to be of the order $2n\times 2n$. **T** fails this requirement although it does have unit determinant. However, because submatrix **S** is symplectic one can call **T** an augmented symplectic matrix (Harris, 2010d, 2004a). Like symplectic matrices, augmented symplectic matrices remain closed under multiplication and are not closed under addition nor multiplication by a scalar.

Because of symplecticity and similarly to Equation 3.2.6 we can now obtain the transference for a compound heterocentric system (Harris, 1994):

$$\mathbf{T} = \mathbf{T}_m ... \mathbf{T}_3 \mathbf{T}_2 \mathbf{T}_1 . \tag{3.2.33}$$

Substituting from Equations 3.2.32 and 30 into Equation 3.2.31 and multiplying out, we now obtain the two matrix equations

$$\mathbf{A}\mathbf{y}_0 + \mathbf{B}\boldsymbol{\alpha}_0 + \mathbf{e} = \mathbf{y} \tag{3.2.34}$$

$$\mathbf{C}\mathbf{y}_0 + \mathbf{D}\boldsymbol{\alpha}_0 + \boldsymbol{\pi} = \boldsymbol{\alpha}. \tag{3.2.35}$$

3.2.7 Gaussian systems

We recall that a Gaussian system is defined where all surfaces are rotationally symmetric about a central axis. The longitudinal axis Z coincides with the optical axis creating an axis of symmetry. The implication is that all refracting surfaces are stigmatic and $\boldsymbol{\delta} = \mathbf{o}$. Specifically, each of the fundamental properties simplifies to a scalar matrix so that $\mathbf{A} = A\mathbf{I}$, $\mathbf{B} = B\mathbf{I}$, $\mathbf{C} = C\mathbf{I}$ and $\mathbf{D} = D\mathbf{I}$. Therefore, in a Gaussian system each of the fundamental properties reduces to a scalar and $\mathbf{S}$ to a 2×2 matrix. This is the equivalent to the study of the group Sl(2;$\mathbb{R}$); the group of 2×2 real matrices with determinant 1 (Guillemin and Sternberg, 1984:7-11).

In particular Equations 3.2.7 and 9 simplify to

$$\mathbf{S} = \begin{pmatrix} 1 & \zeta \\ 0 & 1 \end{pmatrix} \tag{3.2.36}$$

and

$$\mathbf{S} = \begin{pmatrix} 1 & 0 \\ -F & 1 \end{pmatrix} \tag{3.2.37}$$

respectively (Guillemin and Sternberg, 1984: 9-11). In general the transference simplifies to a 2×2 matrix represented by

$$\mathbf{S} = \begin{pmatrix} A & B \\ C & D \end{pmatrix} \tag{3.2.38}$$

and the 2×1 matrix representing the ray at a plane is

$$\boldsymbol{\rho} = \begin{pmatrix} y \\ na \end{pmatrix} \tag{3.2.39}$$

(Guillemin and Sternberg, 1984: 7-11). All the entries of $\mathbf{S}$ and $\boldsymbol{\rho}$ are scalars, as opposed to the non-scalar submatrices shown in Equations 3.2.5 and 1. Equations 3.2.34 and 35 reduce to

$$Ay_0 + n_0 Ba_0 = y \tag{3.2.40}$$

$$Cy_0 + n_0 Da_0 = na\,. \tag{3.2.41}$$

3.3 Fundamental properties

The fundamental properties are not usually encountered as such in optometry. Most of the properties that are encountered in optometry are derived properties. Certain derived properties need some additional information, such as length of the system, or its context, that is, the refractive indices upstream and downstream of the system (Harris, 2012c). Equations 3.2.34 and 35 are useful for these derivations, and are discussed in detail below.

In this section, an attempt is made to understand each of the fundamental properties of a Gaussian optical system. The fundamental properties are essentially mathematical and take on physical meanings only for particular situations. We use the transference for a Gaussian system defined in Equation 3.2.38 starting with Harris's (1999a) definition of ametropia. We then look at four special systems that result when each of the fundamental properties in turn is zero. Each of these situations results in interesting and familiar systems and relationships. Ultimately we can use this information to define systems that simplify the mathematics.

3.3.1 Ametropia

Harris (1999a) regards *A* in Equation 3.2.38 as representing ametropia. For a distant object all rays enter the eye parallel at some reduced inclination α_0. For $A = 0$ the eye is emmetropic and from Equation 3.3.1 below we see that all rays from a distant object point map to the same position *y* on the retina, a point focus. When $A \neq 0$ then the eye is ametropic, *A* represents a "squashing factor" where all rays entering the eye at different incident transverse positions map to respective positions on the retina. For an emmetropic eye, all rays with the same inclination will map to a single point on the retina. Positive values of *A* imply a hyperopic eye and negative values of *A* a myopic eye with the rays crossing over and inverting the direction of the position vector (Harris 1999b). There are exceptions to this rule (Harris, 1999b, 2007b).

3.3.2 Four special systems

We follow Harris' lead and start by looking at the four types of two-dimensional vector fields as obtained from the mathematical structure of the transference of a Gaussian system (Harris, 1996a). These are exit-plane focal systems where $A = 0$, conjugate systems where $B = 0$, afocal or telescopic systems where $C = 0$ and entrance-plane focal systems where $D = 0$.

Exit-plane focal systems ($A = 0$)

We start with the exit-plane focal system shown in Figure 3.3.1. Equation 3.2.40 simplifies to

$$B\alpha_0 = y \tag{3.3.1}$$

when $A = 0$. From Equation 3.3.1 we see that if all incident rays have the same reduced inclination then the emergent transverse position is the same for all the rays. This is shown in Figure 3.3.1. One can think of *B* as a sort of optical thickness, although it is not usually simply related to the actual length of a system. *B* therefore relates the emergent position through the system to the incident reduced inclination. Examples of an exit-plane focal system are an emmetropic eye, most schematic eyes and the compound system of an eye and distance compensating spectacle or contact lens in front of it.

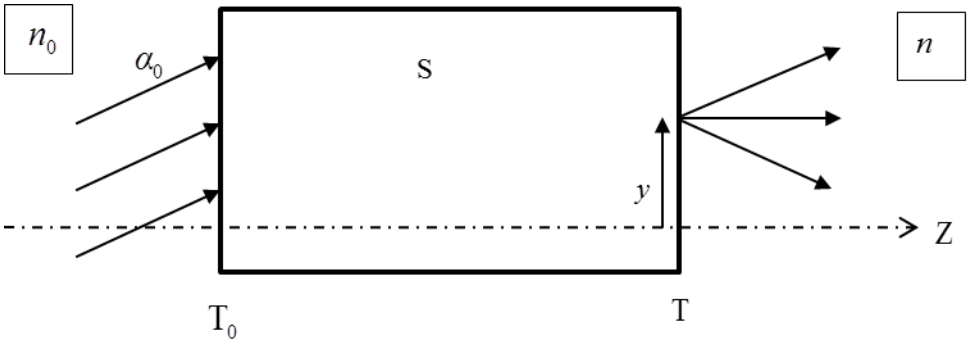

Figure 3.3.1 A Gaussian exit-plane focal system ($A = 0$). All incident rays enter at the entrance plane T_0 with the same reduced inclination α_0. All emergent rays exit at T at the same transverse position *y*.

Conjugate systems *($B = 0$)*

Again, looking at Equation 3.2.40 we obtain

$$Ay_0 = y \tag{3.3.2}$$

when $B = 0$. This is shown in Figure 3.3.2. In a conjugate system the incident inclination plays no role and if all rays enter the system at point y_0 they will map to a conjugate point *y* on the exit plane. *A* is the transverse magnification. When we define a system to have the entrance plane at the object point and the exit plane at the image point, we have defined a conjugate system. This is an example of a system where, even though $B = 0$, the system itself does not usually have zero length. Conjugate systems are only defined for finite systems.

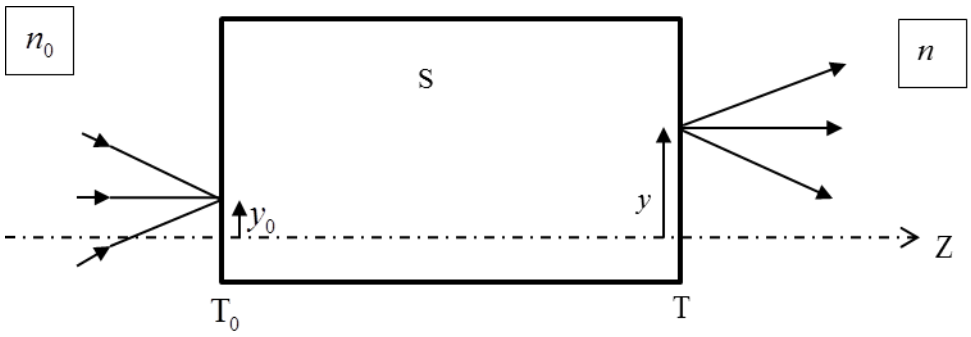

Figure 3.3.2 A conjugate system ($B = 0$). When all incident rays enter the system at the same transverse position y_0, they will exit at *y*. Points at y_0 and *y* are conjugate with each other.

Afocal systems *($C = 0$)*

Substituting $C = 0$ into Equation 3.2.41 we obtain

$$D\alpha_0 = \alpha \tag{3.3.3}$$

which is the formula for an afocal system such as a telescope used in low vision. It implies that for incident light, when all rays are parallel, the emerging light segments are also parallel to each other, but not necessarily parallel to the incident pencil, or to the longitudinal axis. This will be discussed in greater detail in Section 3.5.1. An afocal system is shown in Figure 3.3.3.

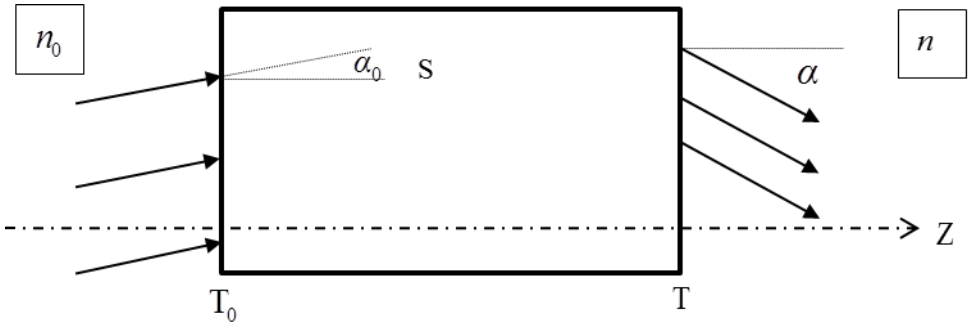

Figure 3.3.3 An afocal system ($C = 0$). If all incident rays are parallel to each other at reduced inclination α_0 then all emergent rays are parallel to each other at reduced inclination α.

Entrance-plane focal systems *($D = 0$)*

Finally, staying with Equation 3.2.41 but this time substituting $D = 0$, we obtain

$$Cy_0 = \alpha. \tag{3.3.4}$$

A point object at position y_0 on the entrance plane emits a pencil of light of zero vergence from the system at a reduced inclination of α. An entrance- plane focal system is shown in Figure 3.3.4. Examples include reversed emmetropic eyes and reversed ametropic eyes combined with the direct ophthalmoscope lens in ophthalmoscopy (Harris and van Gool, 2004).

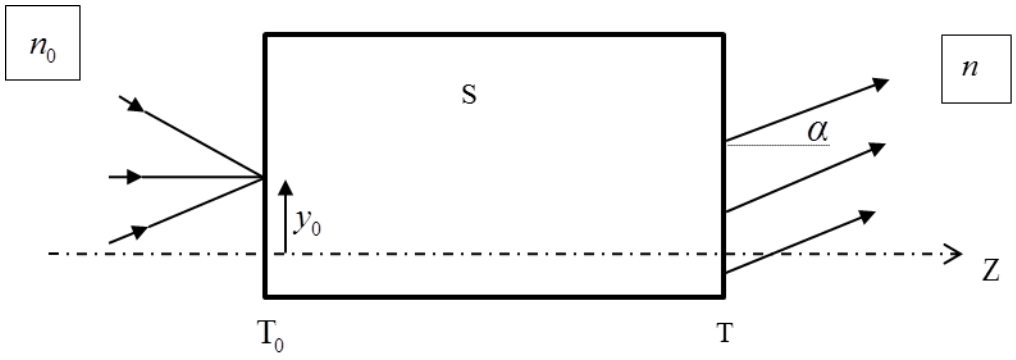

Figure 3.3.4 An entrance-plane focal system ($D = 0$). If all incident rays enter the system at the same position y_0 then they emerge parallel to each other with emergent reduced inclination α.

3.4 Derived properties

The fundamental properties of a first-order optical system can be obtained directly from the transference. In addition there are a number of first-order optical properties that can be derived from the transference. Certain of these derived properties are obtained from the transference alone, while others need input about the actual length of the system (e.g. Harris, 2009). Until now these properties have been studied under the assumption of a single reference wavelength.

The transference depends on its context, meaning the refractive indices upstream and downstream of the system. There are a number of derived properties that are of interest to this dissertation because they are dependent on frequency. These include the power of the system (Harris, 1997), magnification and blur (Harris, 2001a, b), compensatory systems such as entrance-plane refractive compensation (or neutralizing lens) (Harris, 1999a; Keating, 1988:236), front- and back-vertex power (Keating, 1988:236) and locations of the cardinal points (Harris, 2010d, 2011a,b). These derived properties are discussed in the rest of this chapter.

Additionally, in Chapter 6 this study derives formulae for longitudinal and transverse chromatic aberration from the transference and its context (Harris & Evans, 2012). In line with previous calculations done on Gaussian systems to quantify chromatic properties in the eye, in Chapter 7 this dissertation will derive equations from the transference for Gaussian systems for chromatic difference in power, refractive compensation, magnification and position. Other derived properties that will not form part of this dissertation are converter systems (Keating, Harris and van Gool, 2002), corneal patches and referred apertures (Harris, 2011c, 2012d, and a number of axes such as optical (Harris, 2009) visual (Harris, 2010c) and pupillary (Harris, 2013) axes and line of sight (Harris, van Gool and Evans, 2013). Achromatic axes have recently been defined from the transference for dichromatic light (Harris, 2012a, b).

Referred apertures, corneal patches and pinholes have significant relevance to current research being done on the intracorneal inlay, for example the AcuFocus Kamra corneal pinhole inlay. (Gatinel, 2010; Seyeddain, Riha, Hohensinn, Nix, Dexl and Grabner, 2010; Waring, 2010)). Two aspects are of

interest to this study. Firstly the chromatic properties resulting from positioning of the pinhole plane longitudinally within the cornea instead of the iridial plane and secondly, misplacement of the pinhole inlay during surgery in the transverse plane. The size of the pinhole and light entering the eye from around the inlay will also influence the chromatic properties in the eye. Thibos *et al* (1990) used a displaced pinhole to induce and measure transverse chromatic aberration experimentally. A misplaced pinhole results in a number of visual complaints, among which sensitivity to chromatic properties will be of special interest to this study.

3.4.1 Power

Power is well defined for refracting surfaces and thin lenses both as a power matrix and clinically as sphere / cylinder × axis. The power matrix is symmetric and has been derived by Fick (1972; 1973a; Blendowske, 2003) and Long (1976), apparently independently. Recently, we noted that the power matrix was being hinted at by Le Grand (1945: 326-327) and possibly by others before him. The equivalent power of a two surface thick lens system was defined by Keating (1981a, 1982, 2002: 343) who showed that the power matrix for such a system could be asymmetric, in which case it cannot be equivalent to a thin lens. Harris (1996a) derives a formula for the (equivalent) power for a system comprising three thin astigmatic lenses each separated by a gap.

Harris (1997) was the first to define power for optical systems in general. He defines power as

$$\mathbf{F} = -\mathbf{C}. \tag{3.4.1}$$

Power is therefore a first-order optical property derived from the transference of a system.

For Gaussian systems

$$\mathbf{C} = C\mathbf{I} \tag{3.4.2}$$

where **I** is an identity matrix. Hence for a Gaussian system we can write the power as

$$F = -C. \tag{3.4.3}$$

The eigenvalues of **F** are the two principal powers of an astigmatic system and the corresponding eigenvectors represent the directions of the two principal meridians (Keating, 1981a, b; Long, 1976; Harris, 2001c). Together the principal powers and meridians can be represented either by a power cross, or in principal meridional representation of power (Harris, 2000, 2001c). It is possible for a thick system, such as the eye, to have an asymmetric power, with corresponding non-orthogonal eigenvectors or meridians (Keating, 1981a, 1982). For any refracting surface or thin lens system, the power matrix is symmetric and the principal meridians therefore are orthogonal (Anton and Rorres, 2005: 381).

For thin systems equations were derived to convert from the clinical representation of power to the power matrix by Long (1976) and Fick (1972; Blendowske, 2003) and to revert back from the power matrix to clinical representation by Keating (1980) and Fick (1973b; Blendowske, 2003). Keating (1981b, 1997b) showed that the power matrix for a thick system comprising two or more astigmatic powers with nonaligned principal meridians will result in an asymmetric power matrix which corresponds to a power which has non-orthogonal meridians. Harris (2000, 2001c) developed conversion formulae to convert between principal meridional representation of power and matrices. This enables one to convert an asymmetric power matrix into power along two principal meridians which are not orthogonal.

3.4.2 Entrance-plane refractive compensation

We saw in Section 3.3.2 that an exit-plane focal system is defined by $A = 0$ (Harris, 1996a) which Harris (1999a) refers to as the "condition for emmetropia". The power of a thin lens juxtaposed immediately upstream to the system can be calculated in order to create such a system. Harris (1999a) refers to this as the "condition for compensation".

An example of an entrance-plane system is an emmetropic eye, or an ametropic eye compensated for distant viewing. Because of this, Harris (1999a) derives a formula for the power of the corneal-plane refractive compensation F_0. Making use of Equations 3.2.6, 37 and 38, we write the transference of the compound system of eye and compensating lens F_0 as

$$\begin{pmatrix} A_E & B_E \\ C_E & D_E \end{pmatrix}\begin{pmatrix} 1 & 0 \\ -F_0 & 1 \end{pmatrix}=\begin{pmatrix} A_E - B_E F_0 & \bullet \\ \bullet & \bullet \end{pmatrix} \tag{3.4.4}$$

where the dots represent values not needed here. Because this is an exit-plane focal system, we obtain

$$A_E - B_E F_0 = 0 \tag{3.4.5}$$

and solving we obtain the corneal-plane refractive compensation

$$F_0 = B_E^{-1} A_E . \tag{3.4.6}$$

Equation 3.4.6 shows that the corneal-plane refractive compensation depends on the dilation *A* and the disjugacy *B*. The divergence *C* (or power *F*) of the eye does not play a direct role, but does have an indirect role through the symplectic relations.

3.4.3 Front- and back-vertex power

Back-vertex power F_{bv}, shown in Figure 3.4.1(a), can be defined as either the vergence *L* leaving the system when incident rays are parallel or the reciprocal of the reduced emergent focal (or back-vertex) length (Keating, 2002:138-9, 145; Harris, 2010a). The definitions are equivalent. The front-vertex power F_{fv}, which is also called front neutralizing power F_{fn} and is shown in Figure 3.4.1(b), is defined as the negative of the incident vergence (L_0) (or power of the neutralizing effect of the system) in order for emerging rays to exit parallel (Keating, 2002: 138-9; Harris, 2010a). This is equivalent to the negative reciprocal of the incident reduced focal length.

The term power as it is used here is rather misleading. Vertex power is actually a measurement of vergence and as such the matrix is always symmetric (Keating, 1981a; Harris, 1996b). These vertex power formulae were originally derived by Keating (1981a, 1982) and the derivation was later simplified, using a different approach, by Harris (2010a). We take our lead from Harris (2010a), simplifying for Gaussian systems.

Derivation of back-vertex power

Comparing Figure 3.4.1 (a) and (c) we see that the thin postjuxtaposed lens of power F_{bn} compensates for the emergent vergence, such that the rays leave the system parallel and therefore we start with

$$F_{\text{bv}} = -F_{\text{bn}}. \tag{3.4.7}$$

We obtain F_{bn} from the transference of the compound system $\mathbf{S}$ made up of the transference of the system $\mathbf{S}_{\text{E}}$ followed by the transference of the thin lens $\mathbf{S}_{\text{b}}$ and then equating $C = 0$ for an afocal system, such that

$$\mathbf{S} = \mathbf{S}_{\text{b}}\mathbf{S}_{\text{E}} = \begin{pmatrix} 1 & 0 \\ -F_{\text{bn}} & 1 \end{pmatrix}\begin{pmatrix} A_{\text{E}} & B_{\text{E}} \\ C_{\text{E}} & D_{\text{E}} \end{pmatrix} = \begin{pmatrix} \bullet & \bullet \\ -F_{\text{bn}}A_{\text{E}} + C_{\text{E}} & \bullet \end{pmatrix}. \tag{3.4.8}$$

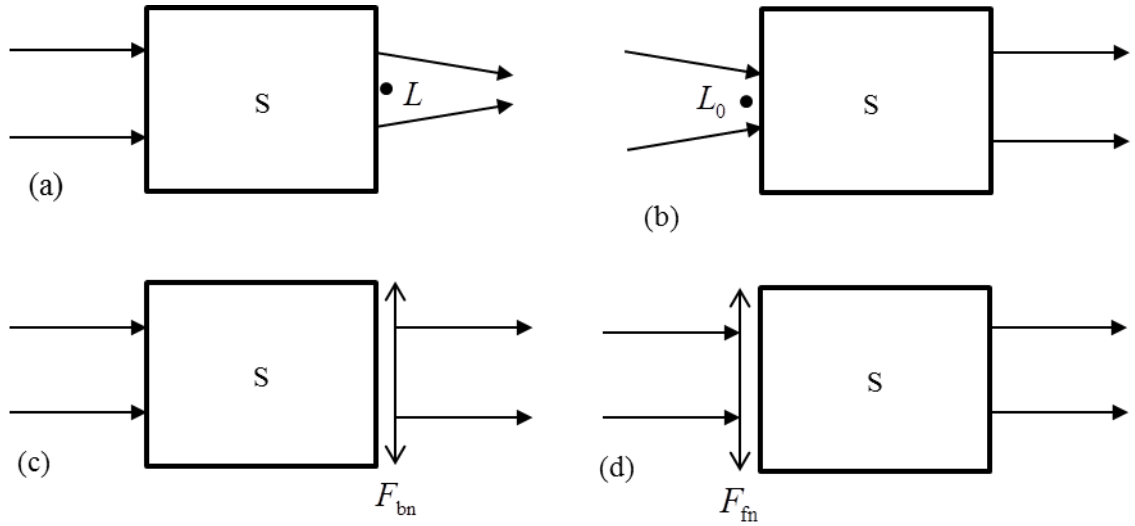

Figure 3.4.1 An optical system is shown as S. (a) Back-vertex power shown as emerging vergence L exiting the system when incident rays are parallel. (b) Front-vertex power, the negative of incident vergence shown as L_0 when the emerging rays are parallel. (c) A postjuxtaposed thin lens F_{bn} in combination with the system S creates an afocal compound system. (d) A prejuxtaposed thins lens F_{fn} creates an afocal system in combination with the system S.

therefore

$$-F_{\mathrm{bn}}A_{\mathrm{E}}+C_{\mathrm{E}}=0 \tag{3.4.9}$$

and

$$F_{\mathrm{bn}}=C_{\mathrm{E}}A_{\mathrm{E}}^{-1}. \tag{3.4.10}$$

Substituting Equation 3.4.10 into 3.4.7 we define back-vertex power as

$$F_{\mathrm{bv}}=-C_{\mathrm{E}}A_{\mathrm{E}}^{-1}. \tag{3.4.11}$$

Derivation of front-vertex power

Similarly to back-vertex power, Figures 3.4.1 (b) and (d) illustrate that the power of the thin neutralizing lens at the front-vertex of the system is the negative of the vergence at incidence onto the system

$$F_{\mathrm{fv}}=-F_{\mathrm{fn}} \tag{3.4.12}$$

The transference of the compound system $\mathbf{S}$ made up of the transferences of a thin lens $\mathbf{S}_{\mathrm{f}}$ followed by the system $\mathbf{S}_{\mathrm{E}}$ to create an afocal system is

$$\mathbf{S}=\mathbf{S}_{\mathrm{E}}\mathbf{S}_{\mathrm{f}}=\begin{pmatrix}A_{\mathrm{E}} & B_{\mathrm{E}}\\ C_{\mathrm{E}} & D_{\mathrm{E}}\end{pmatrix}\begin{pmatrix}1 & 0\\ -F_{\mathrm{fn}} & 1\end{pmatrix}=\begin{pmatrix}\bullet & \bullet\\ C_{\mathrm{E}}-D_{\mathrm{E}}F_{\mathrm{fn}} & \bullet\end{pmatrix}. \tag{3.4.13}$$

Equating $C=0$ for this afocal system

$$C_{\mathrm{E}}-D_{\mathrm{E}}F_{\mathrm{fn}}=0 \tag{3.4.14}$$

we calculate the power of F_{fn} as

$$F_{\mathrm{fn}}=D_{\mathrm{E}}^{-1}C_{\mathrm{E}}. \tag{3.4.15}$$

Substituting from Equation 3.4.12 into 3.4.15 we obtain the definition for front-vertex power

$$F_{\mathrm{fv}}=-D_{\mathrm{E}}^{-1}C_{\mathrm{E}}. \tag{3.4.16}$$

The derivations for front- and back-vertex power given above are from Harris (2010a). However, the typographical error in the original manuscript (a missing minus sign) for the equation for front-vertex power has been corrected here.

3.5 Magnification

Because a large proportion of the research on chromatic properties has focussed on chromatic difference of magnification and position (Atchison and Smith, 2002: 181-182; Rabbetts, 2007: 289-293; Thibos Bradley and Zhang, 1991), magnification and conjugation of points will be studied in more detail for its first-order effects. Three types of magnification are defined for conjugate Gaussian systems, namely transverse or lateral magnification, axial or longitudinal magnification and angular magnification (Meyer-Arendt, 1984:54; Keating, 2002: 56-62, 110, 154, 347-370; Smith and Atchison, 1997: 43-44, 71-72). We shall take a closer look at all three types in Gaussian systems.

3.5.1 Magnification of Gaussian systems

Transverse magnification

Transverse magnification is defined as

$$M_{\mathrm{t}} = \frac{y}{y_0} \tag{3.5.1}$$

as shown in Figure 3.5.1 (Emsley, 1950:33; Meyer-Arendt, 1984:54; Smith and Atchison, 1997:43; Keating, 2002:56, 110).

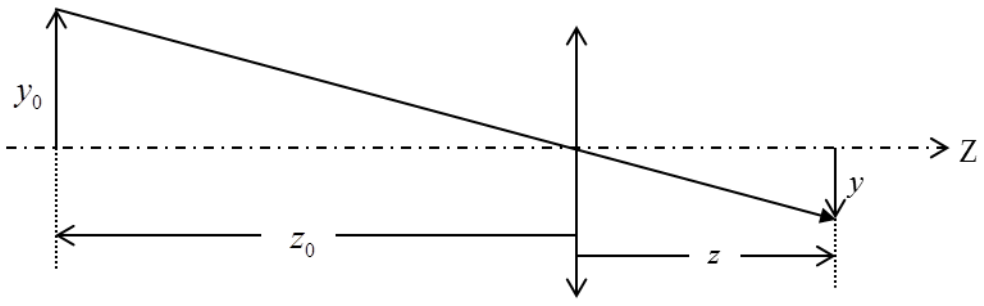

Figure 3.5.1 Transverse magnification of a thin system defined by Equation 3.5.1. y_0 is the height of the object at distance z_0 from the lens and *y* is the height of the image at a distance *z* from the lens.

Axial magnification

Axial magnification is defined by (Meyer-Arendt, 1984:56; Keating, 2002:154; Smith and Atchison, 1997:71-2)

$$M_z = \frac{\Delta z}{\Delta z_0} \tag{3.5.2}$$

where Δz_0 is the difference in axial length between the front and back of the object and Δz the corresponding axial length of the image. This is shown in Figure 3.5.2.

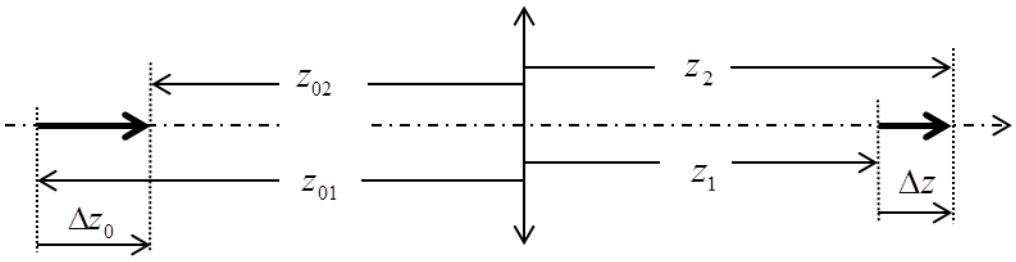

Figure 3.5.2 Axial magnification of a thin system. The two arrow bases (subscript 1) are conjugate and the two arrowhead apexes (2) of the object and image are conjugate. The axial magnification is the ratio of axial length of image to axial length of object.

Angular magnification

Angular magnification, commonly referred to as "magnifying power", is the most important type of magnification according to Meyer-Arendt (1984:57). This is the magnification that is used to define the magnifying power of afocal telescopes and binoculars and is typically denoted by an "×". It is defined as the ratio of the image's reduced inclination to the object's reduced inclination (Smith and Atchison, 1997:44, 69, 768). For axial objects this is defined as

$$M_\alpha = \frac{\alpha}{\alpha_0}. \tag{3.5.3}$$

where α is the reduced inclination as defined in Equation 3.2.2 and simplified for a Gaussian system.

In Figure 3.5.3 we see angular magnification created in two ways. In (a) the angular magnification is created by approach magnification. The system represents a reduced eye consisting of a refracting surface K and image surface R. An object of size y_{01} is positioned at a distance z_{01} from the reduced eye, creating

an image of size y_1 at R and an incident inclination of a_{01}. The object is now brought closer to the reduced eye by distance Δz_0, to a position at a distance z_{02}. The size of the object has not changed $(y_{01} = y_{02})$. However the size of the image has been magnified from y_1 to y_2 at R and the inclination has been magnified to a_{02}. Relative size magnification can be achieved by increasing the size of y_{01} to magnify incident inclination from a_{01} to a_{02} with corresponding image size increase at the image plane. In Figure 3.5.3(b) angular magnification is created by a thin lens. The system initially is the same as system 1 in (a) with incident inclination a_{01} (not redrawn in (b)). A lens F is added at a vertex distance z_v. We note that the object appears to be magnified to size y_i and the image at R has been magnified from y_1 to y_3 while the inclination has been magnified from a_{01} to a_{03}.

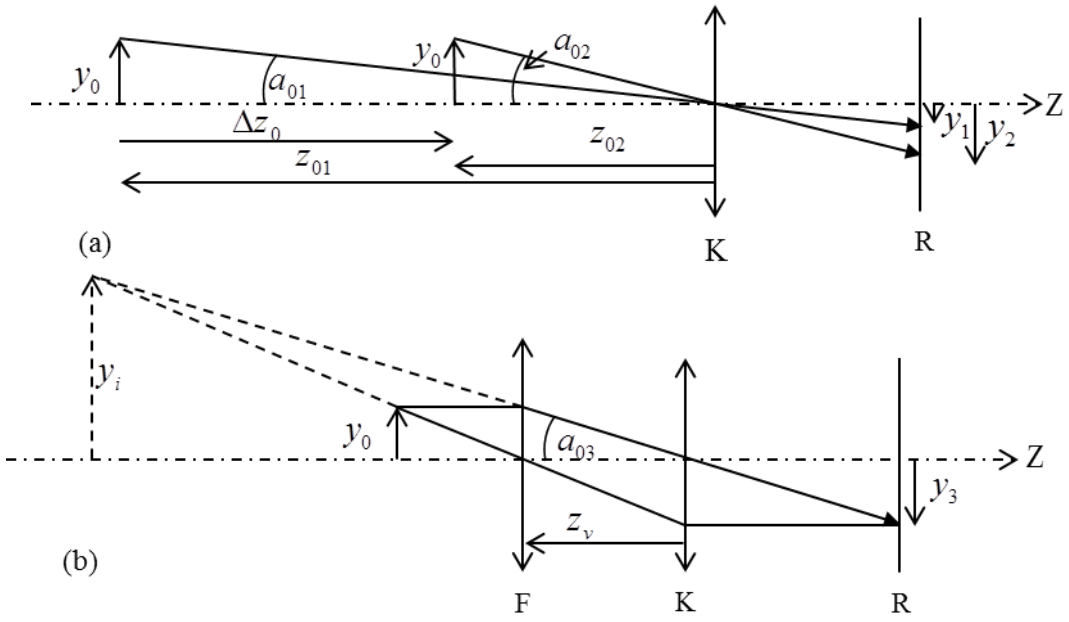

Figure 3.5.3 **(a)** Angular magnification created by approach magnification. The system represents a reduced eye consisting of a refracting surface K and image surface R. System 1 consists of object of size y_0 at position z_{01} creating an image of size y_1 at the retina. In system 2 the object has moved closer to the eye to position z_{02} to create a larger image of size y_2. **(b)** Angular magnification created by a thin lens. Diagrams are not to scale and angles have been exaggerated for clarity. All angles are within the paraxial limits. The diagrams are intended merely to demonstrate angular magnification and accommodation and ametropia have not been taken into account.

Relationships between the magnifications

The relationship between transverse and angular magnification is (Meyer-Arendt, 1984:60, Smith & Atchison, 1997:44, 382)

$$M_\alpha = \frac{1}{M_t}. \tag{3.5.4}$$

Keating (2002: 154) and Smith and Atchison (1997:383) derive the relationship

$$M_z = M_t^2. \tag{3.5.5}$$

between axial and transverse magnification.

3.5.2 Limitations of defining magnification in terms of conjugate object and image points

Defining magnification in terms of the longitudinal and transverse positions of the object and image points is simple and shows some very useful relationships between magnification as defined in Section 3.5.1 and the fundamental properties for conjugate and afocal systems as defined in Section 3.3.2. However, in physiological optics interest lies in what is happening to the image at the retina. If the image is not in focus on the retina then the approach of defining the magnification in terms of the object and image points (a conjugate system) will have limitations. This is further exacerbated when a single object point produces more than one image, such as the two line foci produced by an astigmatic system, or an infinity of coloured images resulting from chromatic dispersion.

If we bear in mind that in order to study the magnification of images on the retina, regardless of whether the images are in focus, or not, then we need to take a different tack on how we define magnification at the retina or exit plane. We now turn our attention to magnification of images at the retina.

3.5.3 Magnification, blur and the ray state at the retina

In physiological optics, magnification is calculated at the retina or image plane, regardless of the effects of blur. In order to do this we trace the chief ray from an object, through the centre of the pupil or a pinhole and do our calculations at the retina. In this section we wish to study and obtain the equations for

magnification at an image plane and will use this to derive formulae for the magnification of chromatic properties in Chapter 7.

We will be concentrating on the naked eye, or more specifically, model eyes, without any refractive or other compensation. We start by taking a look at systems where the object point is distant and then derive the formulae for systems where there is an object point at a finite distance in Chapter 5.

Systems with a distant object point

The system of a compound model eye is shown in Figure 3.5.4. It comprises two subsystems, divided by the pupillary plane T_P into anterior A and posterior B. An arbitrary ray is incident onto the cornea with ray state $\boldsymbol{\rho}_K$, it traverses the centre of the pupil with ray state $\boldsymbol{\rho}_P$ and emerges from the system at the retinal plane with emergent ray state $\boldsymbol{\rho}_R$. We want to solve for $\boldsymbol{\rho}_R$. We need α_K, the reduced inclination at the cornea, which will be the same for all rays incident on the system from a distant object. However, because we wish to trace the chief ray through the system we are interested in y_P, the centre of the pupil rather than y_K the transverse position of the ray at the cornea.

For the system shown in Figure 3.5.4, a transference is calculated for each of the sub-systems and for the eye itself. To differentiate the three transferences,

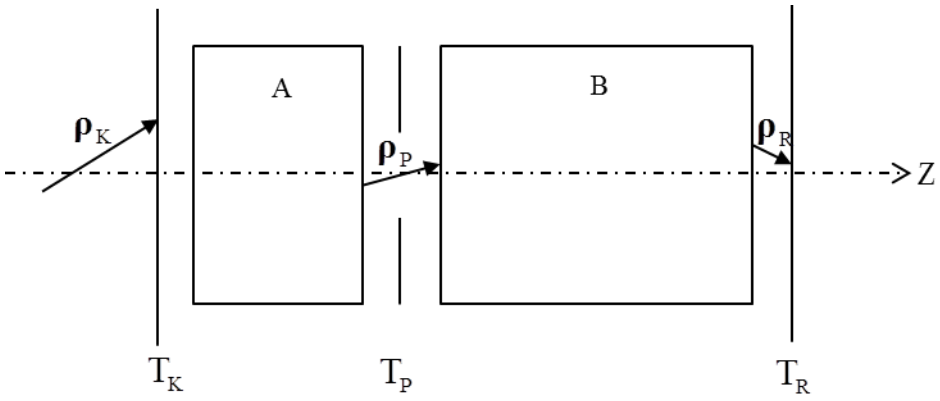

Figure 3.5.4 An exploded diagram of a compound model eye. The eye is defined by the entrance plane T_K immediately in front of the cornea, an exit plane T_R immediately in front of the retina and a longitudinal axis Z.

each of the fundamental properties is subscripted with either an A, B or E for anterior, posterior or eye, respectively. Similarly the state of the ray at the three positions is subscripted K, P or R for corneal plane, pupillary plane or retinal plane respectively. The corneal plane is immediately in front (upstream) of the tear layer, the pupillary plane immediately upstream of the crystalline lens, at the pupil and the retinal plane immediately in front (upstream) of the retina or image plane. The retina itself is not part of the optical system.

We calculate the transference of the eye as follows:

$$\begin{aligned}\mathbf{S}_{\mathrm{E}} &= \mathbf{S}_{\mathrm{B}}\mathbf{S}_{\mathrm{A}} = \begin{pmatrix} A_{\mathrm{B}} & B_{\mathrm{B}} \\ C_{\mathrm{B}} & D_{\mathrm{B}} \end{pmatrix}\begin{pmatrix} A_{\mathrm{A}} & B_{\mathrm{A}} \\ C_{\mathrm{A}} & D_{\mathrm{A}} \end{pmatrix} \\ &= \begin{pmatrix} A_{\mathrm{B}}A_{\mathrm{A}} + B_{\mathrm{B}}C_{\mathrm{A}} & A_{\mathrm{B}}B_{\mathrm{A}} + B_{\mathrm{B}}D_{\mathrm{A}} \\ C_{\mathrm{B}}A_{\mathrm{A}} + D_{\mathrm{B}}C_{\mathrm{A}} & C_{\mathrm{B}}B_{\mathrm{A}} + D_{\mathrm{B}}D_{\mathrm{A}} \end{pmatrix} = \begin{pmatrix} A_{\mathrm{E}} & B_{\mathrm{E}} \\ C_{\mathrm{E}} & D_{\mathrm{E}} \end{pmatrix}\end{aligned} \tag{3.5.6}$$

Harris (2001a) derived the following equations for the magnification, blur and ray state at the retina for a general naked eye

$$A_{\mathrm{E}}A_{\mathrm{A}}^{-1}y_{\mathrm{P}} + B_{\mathrm{B}}A_{\mathrm{A}}^{-1}\alpha_{\mathrm{K}} = y_{\mathrm{R}} \tag{3.5.7}$$

and

$$C_{\mathrm{E}}A_{\mathrm{A}}^{-1}y_{\mathrm{P}} + D_{\mathrm{B}}A_{\mathrm{A}}^{-1}\alpha_{\mathrm{K}} = \alpha_{\mathrm{R}}\,. \tag{3.5.8}$$

Interestingly, y_{P} is also a property of the eye, but not a fundamental property. The pupil centre is not necessarily fixed, but may shift slightly with dilation and

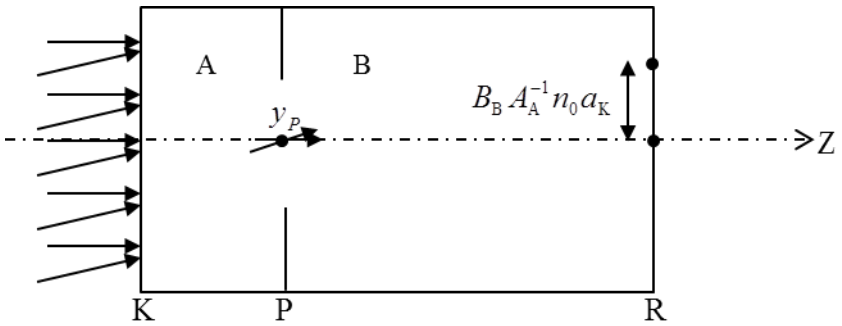

Figure 3.5.5 A simplified Gaussian model eye, divided by pupil P into anterior A and posterior B subsystems. Rays from infinity are incident onto the system initially parallel to the longitudinal axis, mapping the chief ray to a point on the retina on the longitudinal axis and then at an inclination that maps to a second point on the retina. $B_{\mathrm{B}}A_{\mathrm{A}}^{-1}n_0$ magnifies the incident inclination a_K to an image size as shown with the double-headed arrow.

constriction of the pupil (Wilson, Campbell and Simonet, 1992; Yang, Thompson and Burns, 2002).

In Figure 3.5.5 we can see how the magnification for a distant object is projected onto the retina of a Gaussian eye. An axial object of size a_K is magnified by $B_{\mathrm{B}}A_{\mathrm{A}}^{-1}n_0$ to obtain retinal image size y_{R}. Because we are working with the chief ray of a centred Gaussian system, $y_{\mathrm{P}} = 0$ and $A_{\mathrm{E}}A_{\mathrm{A}}^{-1}$ is negated.

The pupil size is defined as $p = y_{\mathrm{P2}} - y_{\mathrm{P1}}$, where y_{P1} and y_{P2} are the margins of the pupil. For a pencil of rays from a distant axial object point $(a_{\mathrm{K}} = 0)$ the size of the corresponding blur patch on the retina will be $A_{\mathrm{E}}A_{\mathrm{A}}^{-1}p = y_{\mathrm{R}}$. Hence, the size of the blur patch, corresponding to a single object point, is dependent on pupil size. The blur is not shown in Figure 3.5.5 because the size of the blur patch is dependent on the pupil size, which is outside the scope of the topic of this study.

Similarly, from Equation 3.5.9 we obtain the distant directional spread $C_{\mathrm{E}}A_{\mathrm{A}}^{-1}$ magnifying the pupil size and distant directional coefficient $D_{\mathrm{B}}A_{\mathrm{A}}^{-1}$ magnifying a_K to obtain the inclination(s) at the retina. From Equations 3.5.7 and 8, we have $(y_{\mathrm{R}} \quad \alpha_{\mathrm{R}})^{\mathrm{T}}$, the ray state at the retina. This will be discussed in greater detail in Section 5.2.

Systems with an object point at a finite distance

To calculate the magnification and blur at the retinal plane for a near system we take a different approach to Harris (2001b). We derive formulae for the magnification, blur and ray state at the retina for systems where the object point is at a finite distance in Section 5.2.2.

3.6 Cardinal points

There are two methods to trace the path of a ray through a system, the graphical method and the numerical method (Meyer-Arendt, 1984:52). The numerical method uses transferences (Section 3.2) and traces a ray from incidence onto a system, defining a ray of light by its inclination and position at incidence

onto a system, through a system and giving us the inclination and position of the ray as it exits the system.

The graphical method traces rays from an object point, through a system to a corresponding image point. Numerically one can apply Snell's law at each refracting surface and simple geometry rules across each homogenous gap (Meyer-Arendt, 1984:52). Methods of simplifying systems have been sought using cardinal points. Graphical ray tracing (Meyer-Arendt, 1984: 52-77) makes use of cardinal points and the approximation of small angles.

In Chapter 2 we saw how the definitions of chromatic aberration in the physiological optics literature make use of the cardinal points and paraxial ray tracing techniques. There are a number of interesting relationships between the cardinal points, all of which can be derived from the transference. Crucially, the positions of the cardinal points are dependent on the frequency of light. For this reason we wish to include cardinal points in this study. For completeness, we will start this section with a short overview of the use of cardinal points in ray tracing techniques followed by the derivation of the cardinal and anti-cardinal points from the transference. We will then take a look at two methods of visually displaying both the relationship of the points to each other in a system, but also changes to the points when that system undergoes a change, such as accommodation or the dependence on the frequency of light.

3.6.1 Ray tracing and cardinal points

We know that in order to simplify the graphical ray tracing through a system, the cardinal points are combined with three rays and a set of rules. We briefly revise the purpose of the cardinal points for completeness. Figure 3.6.1 shows a system with the incident and emergent principal planes in line with the incident and emergent principal points, P_0 and P respectively and likewise F_0 and F are the focal points. The system has the same refractive index upstream and downstream and therefore the nodal points are coincident with the principal points. Figure 3.6.1 shows that from an object point O, the focal ray (3) goes through F_0, refracts at the incident principal plane P_0 and emerges parallel to the optical axis Z. The parallel ray (1) travels from the object point O parallel to the optical axis

Z, refracts at the emergent principal plane P and then passes through the emergent focal point F. Finally the third ray is the chief ray (2) which passes through the centre of the lens or system. It goes to P_0 at its intersection with the optical axis, is translated along the optical axis and exits at P parallel to its incident inclination. All three rays are parallel to the optical axis between the two principal planes (Meyer-Arendt, 1984:53). The three rays intersect at the image I indicating that the object and image are conjugate. The focal ray and the parallel ray are what Keating (2002:44-46) refers to as "predictable rays" and the chief ray is a nodal ray. These in turn undergo refraction at the principal plane(s) and map to a conjugate image point. The three rays used in the ray tracing diagrams map a point on the object to a point on the image and do not represent the actual path of any rays.

For a thin system, all the refraction occurs at the plane of the refracting surface or lens, which is the single principal plane. In a compound system where the refractive indices upstream and downstream are the same, for example a thick lens in air, graphical ray-tracing uses the focal points, the principal planes and the chief ray, shown in Figure 3.6.1. The refraction appears to occur at the two principal planes.

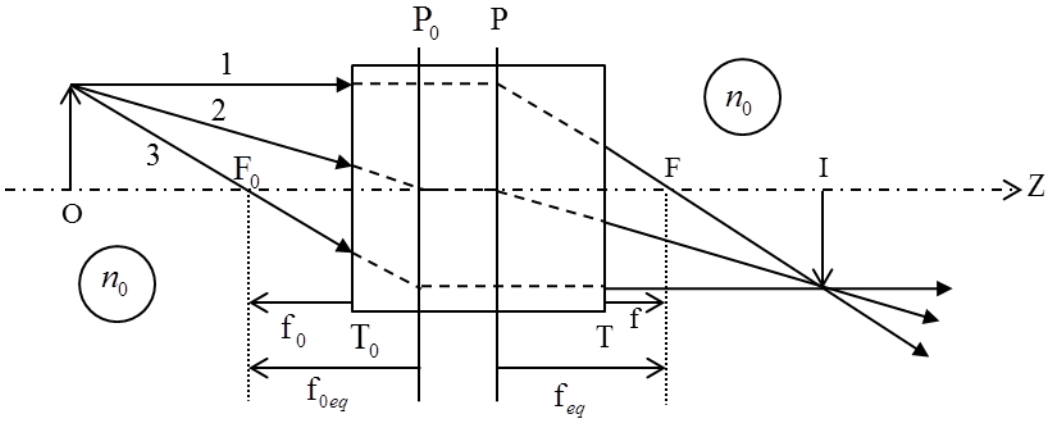

Figure 3.6.1 Diagram of a general Gaussian system with the same refractive index upstream and downstream of the system.

In a system where the refractive indices upstream and downstream of the system are the same the principal points and nodal points coincide. In systems where the indices of refraction are different upstream and downstream, such as the eye, then the principal and nodal points separate and all three pairs of cardinal points are needed for graphical ray-tracing (Figure 3.6.2). The focal and parallel rays are the same as in Figure 3.6.2. The chief ray can now clearly be seen as a nodal ray in Figure 3.6.2. Where the refractive indices are different upstream and downstream, the nodal points will move towards the side of the higher index. The nodal points are points where no refraction takes place (Meyer-Arendt, 1984:76).

We differentiate incident focal length f_0 as the distance from the entrance plane T_0 to the incident focal point F_0 from incident equivalent focal length f_{0eq} which is the distance from the incident principal plane P_0 to the incident focal point. In Figure 3.6.2 both f_0 and f_{0eq} have negative direction. Similarly the emergent focal length *f* is the distance from the exit plane T to the emergent focal point F compared to the emergent equivalent focal length f_{eq} which is from the emergent principal plane to the emergent focal point. In Figure 3.6.2 we can see that the *f* has a negative direction in contrast with f_{eq} which is positive.

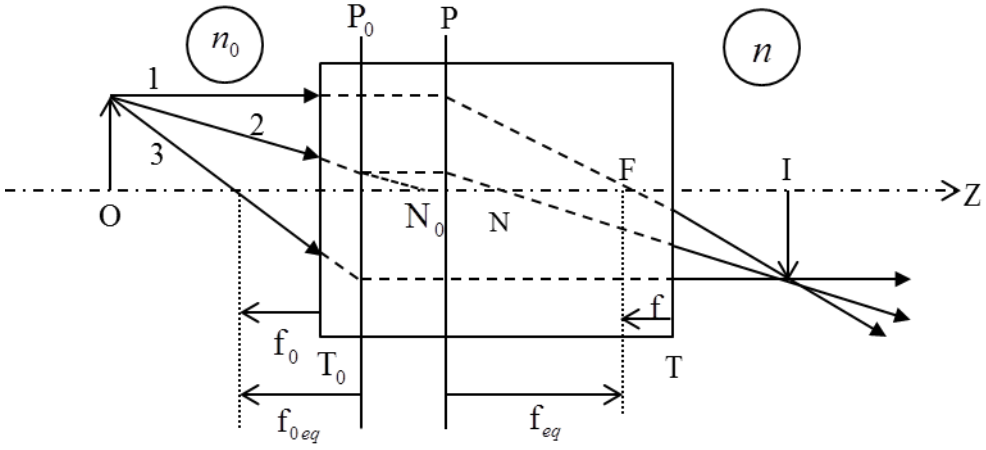

Figure 3.6.2 A diagram of a general Gaussian system with different refractive indices upstream n_0 and downstream *n*, resulting in the nodal points dissociating from the principal points.

3.6.2 Locations of the cardinal points obtained from the transference

The locations of the cardinal points can be derived from the transference. The positions of the incident cardinal points are measured from the entrance plane and for emergent cardinal points the positions are measured from the exit plane. The incident and emergent focal, principal and nodal points make up the six cardinal points for any optical system that are traditionally defined (Pascal, 1939; Smith, 1993,1995; Atchison and Smith, 2000: 7; Sharma, 2006: 168-171). The principal planes are not only conjugate, but have positive unit magnification (Smith and Atchison, 1997:56)

However there are other points, such as anti-nodal and anti-principal points (Katz, 2002: 143; Korsch, 1991: 48, 57; Hastings, 1901: 202) which all belong to a much larger set of special points (Harris, 2010b, 2010f). We refer to the set of anti-nodal and anti-principal points as the anti-cardinal points. Keating (2002: 63-64, 114-115, 308) refers to symmetry points as twice the equivalent focal length (both incident and emergent). An object at the incident symmetry plane will map to an image at the emergent symmetry plane with negative unit magnification (Keating, 2002:63-64, 114-115). Katz (2002: 143) refers to these same points as anti-principal points, giving a transverse magnification of –1 and similarly, the anti-nodal points result in an angular magnification of –1.

In order to show the relationships among cardinal points, Harris (2011b) developed a method of graphical construction of the locations of the cardinal points from the transference using locator lines. Pascal (1939, 1947, 1950a, b) developed a "Benzene ring" which Harris (2011a) elaborated on. Pascal's ring allows one to see the change in position of the six cardinal points with respect to each other when an optical system undergoes a change, such as that brought about by accommodation. Cardinal and anti-cardinal points derived from the transference, graphical construction and Pascal's ring will be explored in this section and Section 5.4.

Harris (2010b, f, 2011a, b) gives two equations, derived from the transference, which give us the locations of the incident and emergent cardinal and anti-cardinal points respectively. The equation for the locations of the incident points is given as

Table 3.6.1 Characteristics of the cardinal points of a general optical system.

Incident		Characteristic	Emergent	
Cardinal point	Symbol	X	Symbol	Cardinal point
Anti-nodal	$\overline{\mathrm{N}}_0$	$-n/n_0$	$\overline{\mathrm{N}}$	Anti-nodal
Anti-principal	$\overline{\mathrm{P}}_0$	-1	$\overline{\mathrm{P}}$	Anti-principal
Focal	F_0	0	—	—
Principal	P_0	1	P	Principal
Nodal	N_0	n/n_0	N	Nodal
—	—	∞	F	Focal

$$z_{\mathrm{Q0}} = n_0 \frac{D - X}{C} \tag{3.6.1}$$

where the subscript Q represents the respective point and the characteristic X is given in Table 3.6.1. The length z_{Q0} is measured from the entrance plane T_0. D and C are entries of the transferences of the system (Equation 3.2.38). Similarly, the locations of the emergent points are given by

$$z_{\mathrm{Q}} = -n \frac{A - \frac{1}{X}}{C} \tag{3.6.2}$$

where the length z_{Q} is measured from the exit plane T. n_0 is the refractive index upstream of the system and n the refractive index downstream of the system. X is the characteristic of any particular pair of special points. A and C are entries of the transference of the system. With the exception of the focal points, each emergent point is in conjugation with the corresponding incident point and can be seen to share the same value for X (Harris, 2010b, 2011a). The incident and emergent focal points are conjugates of infinity (Smith and Atchison, 1997: 72).

3.6.3 Relationships among the points

It is well known that there are a number of relationships among the cardinal points (Pascal, 1939, 1947,1950a, b; Smith and Atchison, 1997: 74-75). These are illustrated in Figure 3.6.3. Using Equations 3.6.1 and 2 and substituting the values for the characteristic X from Table 3.6.1, we can calculate the distances

for the position of each of the cardinal points. From there we can calculate and simplify the equalities between the points in terms of the fundamental properties and the addition of the refractive indices up- and downstream of the system and the length of the system *z*. The distances and equalities are shown in Figure 3.6.3.

Starting with the incident cardinal points and in the sequence given in Table 3.6.1 we find the distance from the entrance plane to the respective point is (Harris, 2010b)

$$z_{\bar{N}0} = C^{-1}(n_0 D + n), \tag{3.6.3}$$

$$z_{\bar{P}0} = n_0 C^{-1}(D + 1), \tag{3.6.4}$$

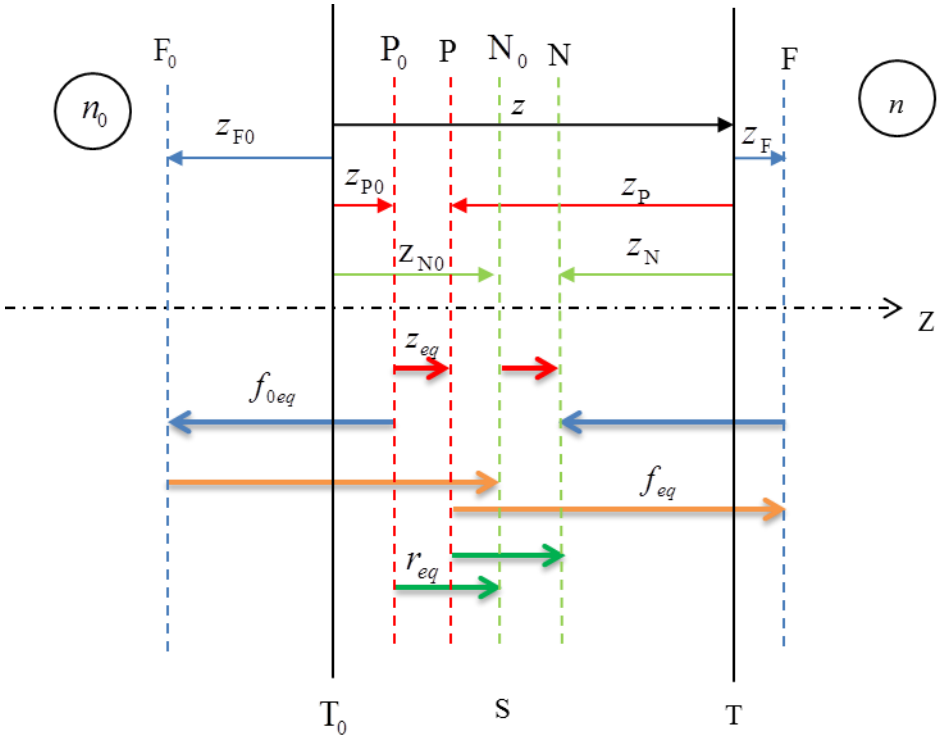

Figure 3.6.3 Cardinal points and their relationships and equalities. Gaussian system S of length *z* has an entrance plane T_0, an exit plane T and a longitudinal axis Z. Refractive index upstream n_0 is different from *n* downstream. All points are defined as being on the optical axis for a Gaussian system. Above the longitudinal axis, the distances from T_0 to the incident cardinal point and from T to the emergent cardinal point are shown with the thin arrows. All the symbols and subscripts are given in Table 3.6.1. Below the longitudinal axis the equalities are shown as follows: the equivalent length or "thickness" z_{eq} (red), incident equivalent focal length f_{0eq} (blue), emergent equivalent length f_{eq} (orange), and equivalent radius of curvature r_{eq} (green).

$$z_{\mathrm{F0}} = n_0 C^{-1} D = -n_0 F_{fv}^{-1}, \tag{3.6.5}$$

$$z_{\mathrm{P0}} = n_0 C^{-1}(D-1) = z_{\mathrm{F0}} - n_0 C^{-1} \tag{3.6.6}$$

and

$$z_{\mathrm{N0}} = C^{-1}(n_0 D - n) = z_{\mathrm{F0}} - nC^{-1}. \tag{3.6.7}$$

The distance of each emergent cardinal point, in the sequence given in the last two columns of Table 3.6.1, from the exit plane to the respective cardinal point is (Harris, 2010b)

$$z_{\bar{\mathrm{N}}} = -C^{-1}(nA - n_0), \tag{3.6.8}$$

$$z_{\bar{\mathrm{P}}} = -nC^{-1}(A+1), \tag{3.6.9}$$

$$z_{\mathrm{P}} = -nC^{-1}(A-1) = z_{\mathrm{F}} + nC^{-1}, \tag{3.6.10}$$

$$z_{N} = -C^{-1}(nA - n_0) = z_{\mathrm{F}} + n_0 C^{-1} \tag{3.6.11}$$

and

$$z_{\mathrm{F}} = -nC^{-1}A = nF_{bv}^{-1}. \tag{3.6.12}$$

These distances are all shown in Figure 3.6.3 above the optical axis Z. Harris (2010b) gives all these distances for linear systems; here they are specialized for Gaussian systems. F_{fv} and F_{bv} are the front- and back-vertex powers (Section 3.4.3).

Smith (1993) also developed a set of equations for the cardinal points in terms of the entries of the Gaussian transference, however his methodology is based on ray tracing. His matrix symbolism and arrangement of entries differs from that used in this dissertation so they have been adjusted to retain consistency. His equations are equivalent to those given by Harris above for incident focal and nodal points and emergent focal and principal points. His incident principal and emergent nodal point equations (Equations 3.6.7 and 11) are more complicated, but reduce under symplecticity to be the equivalent to those given above.

A summary of the equalities is given by Pascal (1939, 1947,1950a, b) for lengths only, without an indication of direction. The formulae are given by Harris (2011a) in terms of the entries of the Gaussian transference with the addition of direction. The incident equivalent focal length is the distance from P_0 to F_0

$$\mathrm{P_0F_0} = \mathrm{FN} = f_{0eq} = n_0 C^{-1} \tag{3.6.13}$$

and, similarly, the emergent equivalent focal length is

$$\mathrm{PF} = \mathrm{F_0N_0} = f_{eq} = -nC^{-1}. \tag{3.6.14}$$

Additional equalities are

$$\mathrm{P_0N_0} = \mathrm{PN} = r_{eq} = -(n - n_0)C^{-1}, \tag{3.6.15}$$

which Pascal (1950a) refers to as the "equivalent" radius, and

$$\mathrm{P_0P} = \mathrm{N_0N} = \mathrm{z}_{eq}, \tag{3.6.16}$$

which Pascal (1950a) refers to as the "thickness" (his quotation marks). Pascal (1950a) appears to have reservations about the terminology because he uses the terms "first" and "second" with quotation marks. He also refers to systems as being "thinner" or "thicker" (his quotation marks) according to variations in the equality given in Equation 3.6.16.

The equivalent focal lengths are directed from the principal plane to the respective focal point. Smith (1993) also gives the equalities for incident and emergent focal length, however his incident focal length formula is more involved, but can be simplified to that of Harris, given in Equation 3.6.13 above.

Harris (2010b) gives additional equalities which we specialize from linear optics:

$$z_{\mathrm{N0}} + z_{\bar{\mathrm{N}}0} = 2z_{\mathrm{F0}} = z_{\mathrm{P0}} + z_{\bar{\mathrm{P}}0}, \tag{3.6.17}$$

$$z_{\mathrm{N}} + z_{\bar{\mathrm{N}}} = 2z_{\mathrm{F}} = z_{\mathrm{P}} + z_{\bar{\mathrm{P}}} \tag{3.6.18}$$

and

$$z_{\mathrm{N0}} + z_{\mathrm{P}} = z_{\mathrm{F0}} + z_{\mathrm{F}} = z_{\mathrm{P0}} + z_{\mathrm{N}} \tag{3.6.19}$$

which show that the cardinal and anti-cardinal points are not independent.

The lengths and directions of each of the equalities between incident and emergent cardinal points are shown in Figure 3.6.3 above the optical axis (Z). Lengths are given as *z* with subscripts given in Table 3.6.1. Below the longitudinal axis, the thicker arrows denote the equalities.

3.6.4 Graphical construction and locator lines

Harris (2011b) developed a method to obtain the positions of the six cardinal points through graphical construction. Not only does this construction

make it easier to see the relationships among the points but also to observe the relationship as the points move when the system changes, for example due to accommodation or age.

Harris (2011b) rewrites Equation 3.6.1 as

$$X = \frac{-Cz_{Q0}}{n_0} + D \tag{3.6.20}$$

and Equation 3.6.2 as

$$\frac{1}{X} = \frac{Cz_{Q}}{n} + A. \tag{3.6.21}$$

and interprets them as straight lines. Harris (2011b) terms these two lines the *locator lines* because they can be used to find the locations of the cardinal points. With the additional knowledge of the refractive indices n_0 and n they can be obtained directly from the transference. They exist uniquely for any system.

The construction is superimposed over the system (Figure 3.6.4). The optical axis Z is horizontal. The X axis is superimposed over the entrance plane T_0

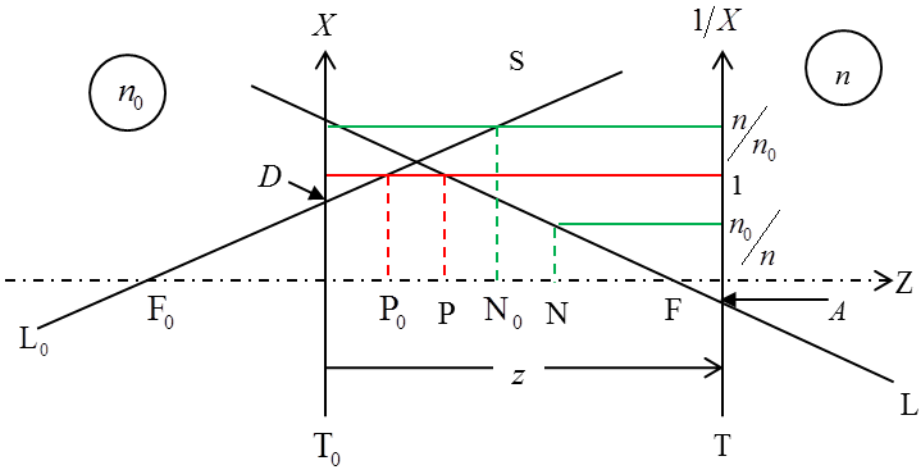

Figure 3.6.4 Graphical representation of a general optical system showing the locator lines for system S (not to scale). Line L_0 represents Equation 3.6.20 and line L Equation 3.6.21. Axis X is superimposed on entrance plane T_0 and axis $1/X$ on exit plane T. T is a distance z downstream from T_0. The focal points lie on the optical axis at intersection with the corresponding locator line. The principal points are shown in red and the nodal points in green. All symbols are described in Table 3.6.1. All incident points show intersection with the incident locator line and have subscript 0, while the emergent points intersect the emergent locator line L with no subscript.

and the $\frac{1}{X}$ axis is superimposed over the exit plane T with the origin at Z. T is a distance z downstream from T_0. The incident locator line L_0 has intersection $X = D$ in T_0 and slope $\frac{-C}{n_0}$ while emergent locator line L has intersection $\frac{1}{X} = A$ in T and slope $\frac{C}{n}$.

To find the location of the incident cardinal points along the optical axis, one draws a horizontal line at the value for the characteristic X in T_0 (Table 3.6.1) and where it intersects L_0 one constructs a vertical line. The intersection of the vertical line with Z locates the position of the corresponding incident cardinal point. Similarly, for the emergent cardinal points, one draws a horizontal line at the value of $\frac{1}{X}$ in T and constructs a vertical line at the intersection of the horizontal line with L. The intersection of the vertical line with Z locates the position of the corresponding emergent cardinal point.

3.6.5 Pascal's ring

Pascal (1939, 1947, 1950a, b) described a memory scheme in the shape of a benzene ring to remember the equalities between the six cardinal points, shown in Figure 3.6.5. He gives the equalities without any proof, his main purpose is to create a memory scheme to aid practitioners (Pascal, 1939). In successive articles

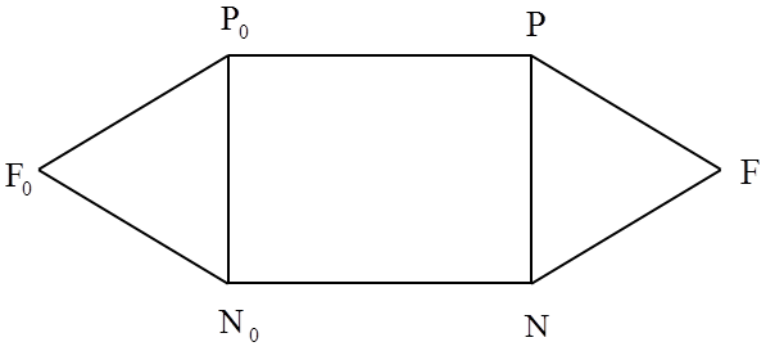

Figure 3.6.5 Pascal's ring, showing the equalities as distances among the cardinal points of a general system. From the diagram we can see that each of two sides that are parallel are equal in their distance apart in the system. Therefore we have four equalities $\mathrm{P_0P} = \mathrm{N_0N}$, $\mathrm{F_0P_0} = \mathrm{NF}$, $\mathrm{F_0N_0} = \mathrm{PF}$ and $\mathrm{P_0N_0} = \mathrm{PN}$.

he then uses the "benzene ring" to show how the points shift when a compensatory system is placed with its emergent principal point at the incident focal point of the system or eye (Pascal, 1950a), or how aphakia affects the ring (Pascal, 1947). Pascal states that "distances represented by opposite parallel lines are equal". He gives the four equalities $P_0P = N_0N$, $F_0P_0 = NF$, $F_0N_0 = PF$ and $P_0N_0 = PN$. In Pascal's initial article (1939) he placed less emphasis on the fourth equality, but later included it and stated that the distance $P_0N_0 = PN$ represents the "equivalent radius of the system" r_{eq} (1950a) which is the radius of a single refracting surface that can replace the system.

In an eye the principal and nodal points are located very close together and it is difficult to see, firstly, what the sequence of points is and, secondly, the shifts when the system undergoes some change such as refractive compensation or accommodation. In this way Pascal's ring is particularly useful in that it "magnifies" the changes in the relationships between the cardinal points when comparing more than one system. It is important to note that Pascal's ring is not drawn to scale but the sides represent a proportional change between two or more systems.

Harris (2011a) proved Pascal's equalities and further proposed that the equalities in the ring represent not just magnitude, but he gave the distances between the cardinal points direction as well. This ties up with the directions of the equalities given in Figure 3.6.3. In Figure 3.6.6, we see Pascal's ring again,

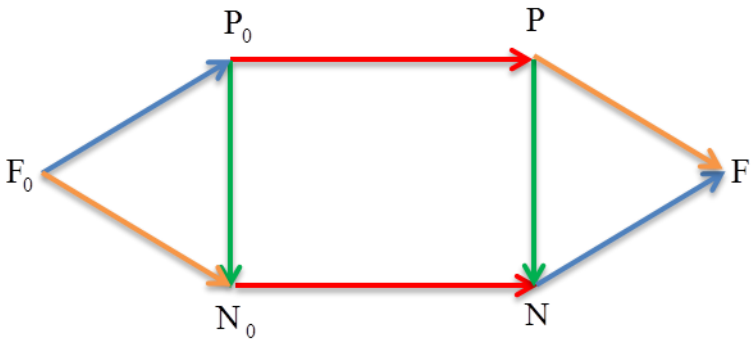

Figure 3.6.6 Pascal's ring showing equalities and their distances and directions among the cardinal points of a general system. Arrows that are the same colour are equal in length follow the same direction, consistent with Equations 3.6.13 to 16. All the directions have the sense of travelling from left to right, the same as light.

but this time with the equalities represented by distance and direction and using the same colour-coding that was given in Figure 3.6.3. The blue line represents the negative incident equivalent focal length.

3.7 The transformed transference

In Section 3.2.5 we saw that symplectic matrices ($\mathrm{Sp}(2n\times 2n;\mathbb{R})$) are closed under multiplication, inversion and transposition but are not closed under addition nor multiplication by a scalar. This creates a problem when we wish to calculate, for example, an average of symplectic matrices, including transferences in particular. In an effort to find an average eye, researchers have investigated a number of transformed transferences and characteristic matrices. These include the exponential-mean-log transference (Harris and Cardoso, 2006; Harris, 2004b, 2005, 2007, Mathebula, Rubin and Harris, 2007), metric geometric mean transference (Harris, 2008), Cayley transforms (Cardoso and Harris, 2007) and four characteristic matrices (van Gool and Harris, 2005; Harris and van Gool, 2004).

Our interest in these transformed transferences, for the purpose of this dissertation, lies not in calculating an average transference, but in the transformed matrix itself. Both the logarithm of a symplectic matrix and the Cayley transform are Hamiltonian and the characteristic matrices are symmetric. For $n=1$ this lends itself to being represented graphically in a three-dimensional space. The metric geometric mean has the limited scope of only calculating the mean of two transferences and therefore will not be explored further. We take a look at each of these transformations in the general sense.

3.7.1 The logarithmic transform

The exponential-mean-log-transference has proven to be particularly useful in calculating a meaningful average of an optical system. Mathebula, Rubin and Harris (2007) and Mathebula and Rubin (2011) have successfully used this method to calculate the mean of a number of readings of the cornea with allowance for thickness using the Pentacam, in a group of subjects. Consequently, Mathebula, Rubin and Harris (2007) and Mathebula and Rubin (2011) were able

to calculate the variance-covariance matrix in Hamiltonian space of the linear optical character of the cornea and the spread of the power of the cornea.

The Lie algebra is related to the matrix Lie group through the matrix exponential by passing information from the Lie algebra to the matrix Lie group. In particular, the Lie algebra defines a linear space, thereby making the Lie algebra not only simpler, but more understandable. To define the Lie algebra, let **G** be a matrix Lie group. The Lie algebra of **G**, denoted by $\mathfrak{g}$, is the set of all matrices **X** such that $e^{t\mathbf{X}}$ is in **G** for all real numbers *t*. If **X** is any $n \times n$ real matrix, then $e^{t\mathbf{X}}$ will be real and invertible. The Lie algebra of GL(n;$\mathbb{R}$) represented by the set of matrices **X** is real and denoted gl(n;$\mathbb{R}$) (Hall, 2004:27, 38-39).

The Lie algebra of the real symplectic group is denoted sp(n;$\mathbb{R}$) and is the space of $2n \times 2n$ real matrices. If **H** is any $2n \times 2n$ real matrix, then $e^{t\mathbf{H}}$ will be real and invertible. sp(n;$\mathbb{R}$) is a subset of gl(n;$\mathbb{R}$) and is therefore also a linear space, allowing one to do statistical analyses. We refer to the set of matrices $\mathfrak{h}$ that define the symplectic algebra as Hamiltonian matrices (Hall, 2004: 41).

In simpler terms, the principal matrix logarithm of a real symplectic matrix (belonging to Sp(n;$\mathbb{R}$)) results in a Hamiltonian matrix (belonging to sp(n;$\mathbb{R}$)) and the principal matrix exponential of a Hamiltonian matrix results in a symplectic matrix (Sanyal, 2001: 71; Bernstein, 2005: 88-89, 434; Dieci, 1996, 1998; Harris and Cardoso, 2006; Harris, 2005; Hall, 2004: 41). This relationship between symplectic and Hamiltonian matrices is referred to as the exponential map and the matrix logarithmic map (Sanyal, 2001: 72-73). Because the set of Hamiltonian matrices defines a linear space it is closed under matrix addition, multiplication by a scalar, transposition and the commutator operator (Dieci, 1996, 1998), they are amenable to the calculation of an average of any number of Hamiltonian matrices.

The exponential-mean-log-transference is defined as (Harris and Cardoso, 2006; Harris, 2004b, 2005, 2007)

$$\tilde{\mathbf{S}} := \exp\left(\frac{1}{N}\sum_{j=1}^{N}\mathrm{Log}\mathbf{S}_j\right). \qquad (3.7.1)$$

The principal matrix logarithm is calculated in Matlab® by using the command *logm* and the matrix exponential by using *expm*. (This is not the same as the command *log* which takes the logarithm of each entry in the matrix separately.)

In general

$$\mathbf{X} = \operatorname{Log} \mathbf{G} \tag{3.7.2}$$

where $e^{\mathbf{X}} = \mathbf{G}$ and $\mathbf{G} \in \mathbb{R}^{n \times n}$ provided **G** is invertible and has no negative real eigenvalues (Dieci, 1996, 1998). Any matrix that is invertible has at least one logarithm (Dieci, 1996), which for our purposes means that, because all transferences are invertible, they have at least one logarithm. Cardoso (2005) shows that the principal matrix logarithm of matrix **G** is an infinite series.

We represent the transformed transference by $\hat{\mathbf{S}}$. In terms of its entries we follow Harris's (2005) lead and write the transformed transference as

$$\hat{\mathbf{S}} = \begin{pmatrix} \hat{\mathbf{A}} & \hat{\mathbf{B}} \\ \hat{\mathbf{C}} & \hat{\mathbf{D}} \end{pmatrix} \tag{3.7.3}$$

where $\hat{\mathbf{S}}$ is Hamiltonian. However, our interest lies not in the average of transferences, but in the Hamiltonian space itself. A $2n \times 2n$ matrix **H** is Hamiltonian if (Bernstein, 2005: 85; Dieci, 1996, 1998; Fiori, 2011; Watkins, 2004; Hall, 2004:41)

$$\mathbf{H}^{\mathrm{T}}\mathbf{E} = \mathbf{E}^{\mathrm{T}}\mathbf{H} \tag{3.7.4}$$

where

$$\mathbf{E} = \begin{pmatrix} \mathbf{O} & \mathbf{I} \\ -\mathbf{I} & \mathbf{O} \end{pmatrix}. \tag{3.7.5}$$

It follows from Equations 3.7.3 to 5 that

$$\hat{\mathbf{A}} = -\hat{\mathbf{D}}^{\mathrm{T}} \tag{3.7.6}$$

and the $\hat{\mathbf{B}}$ and $\hat{\mathbf{C}}$ are both symmetric (Sanyal, 2001: 69; Dieci, 1996; Harris, 2007; Hall, 2004:41). Because $\hat{\mathbf{D}}$ is dependent on $\hat{\mathbf{A}}$ there are four independent entries between them and because $\hat{\mathbf{B}}$ and $\hat{\mathbf{C}}$ are symmetric they each have three independent entries, therefore $\hat{\mathbf{S}}$ has only ten independent entries (Harris, 2007a). However, our reservation with this transformed matrix is that each of the entries has a different unit. $\hat{\mathbf{A}}$ and $-\hat{\mathbf{D}}^{\mathrm{T}}$ are unitless, $\hat{\mathbf{B}}$ is in units of length and $\hat{\mathbf{C}}$ is in

units of inverse length. So while $\hat{\mathbf{S}}$ defines a linear space, it does not define an inner-product space.

For a Gaussian system Equation 3.7.3 simplifies to

$$\hat{\mathbf{S}} = \begin{pmatrix} \hat{A} & \hat{B} \\ \hat{C} & \hat{D} \end{pmatrix} \tag{3.7.7}$$

where each of the entries is a scalar and

$$\hat{A} = -\hat{D}. \tag{3.7.8}$$

The result is that for Gaussian systems $\hat{\mathbf{S}}$ has only three independent entries. This implies that we can create a three-dimensional graph of the relationship among the three entries. The chromatic properties on a Gaussian system will be shown in Chapter 8 and was shown as a nearly perfectly straight line for the reduced eye in an accompanying article (Evans and Harris, 2011).

3.7.2 The Cayley transform

Similar to the logarithmic transference, a Cayley transform maps a symplectic matrix (Sp(n;$\mathbb{R}$)) into a Hamiltonian matrix (sp(n;$\mathbb{R}$)). Cardoso and Harris (2007) introduced this and a few other transforms as alternative methods for mapping symplectic matrices into Hamiltonian matrices, and reversing the process in an effort to find other methods of calculating an average eye, or more generally, an average system. Cardoso and Harris (2007) note that one can construct an infinity of rational matrix functions that transform symplectic into Hamiltonian matrices. The one that plays an important role in several fields of mathematics and engineering (Cardoso and Harris, 2007; Fiori, 2011) and which we shall study is the Cayley transform. The Cayley mean is given by Cardoso and Harris (2007) as

$$\tilde{\mathbf{S}}_{\mathrm{C}} = \mathbb{C}^{-1}\left(\frac{1}{N} \sum_{j=1}^{N} \mathbb{C}\left(\mathbf{S}_j\right) \right) \tag{3.7.9}$$

where $\mathbb{C}(\mathbf{S})$ is the Cayley transform of $\mathbf{S}$ and $\mathbb{C}^{-1}$ represents the inverse Cayley transform.

In general, the Cayley transform is defined as (Bernstein, 2009: 208, 239; Sanyal, 2001: 72; Cardoso and Harris, 2007; Puzio, 2013)

$$\mathbf{B}=(\mathbf{A}-\mathbf{I})(\mathbf{A}+\mathbf{I})^{-1}=(\mathbf{A}+\mathbf{I})^{-1}(\mathbf{A}-\mathbf{I}) \tag{3.7.10}$$

and its inverse is defined as (Bernstein, 2009: 208; Sanyal, 2001: 72)

$$\mathbf{A}=(\mathbf{B}-\mathbf{I})(\mathbf{B}+\mathbf{I})^{-1}=(\mathbf{B}+\mathbf{I})^{-1}(\mathbf{B}-\mathbf{I}) \tag{3.7.11}$$

where **A** and **B** are $n\times n$ real matrices provided the respective inverses exist and **I** is the $n\times n$ identity matrix. From Equation 3.7.10 we can see that the factors of **B** are commutative. From Equations 3.7.10 and 11 we can see that the Cayley transform is its own functional inverse (Bernstein, 2009:208-209; Tsiotras, Junkins and Schaub, 1997; Sanyal, 2001: 72).

Others (Fiori, 2011; Golub and van Loan, 1996: 73; Puzio, 2013; Bernstein, 2009: 239) define the inverse as

$$\mathbf{A}=(\mathbf{I}+\mathbf{B})(\mathbf{I}-\mathbf{B})^{-1}=(\mathbf{I}-\mathbf{B})^{-1}(\mathbf{I}+\mathbf{B}) \tag{3.7.12}$$

where **A** and **B** are defined above, the factors of **A** are commutative and provided the respective inverses exist. This inverse is simple to derive from the Cayley transform given by Equation 3.7.10 and is given by Puzio (2013).

The Cayley transform is defined slightly differently by Tsiotras, Junkins and Schaub (1997), and Courant and Hilbert (1953: 536-7). Tsiotras, Junkins and Schaub (1997), Fallat and Tsatsomeros (2002), Hadjidimos and Tzoumas (2008, 2009) and Bernstein (2009: 208-209) define the Cayley transform as

$$\mathbf{C}=(\mathbf{I}-\mathbf{Q})(\mathbf{I}+\mathbf{Q})^{-1} \tag{3.7.13}$$

(or its commutative equivalent) where **C** and **Q** are $n\times n$ real matrices and exists provided $(\mathbf{I}+\mathbf{Q})$ is invertible. Fallat and Tsatsomeros (2002) and Hadjidimos and Tzoumas (2008, 2009) both define the Cayley transform for the set of $n\times n$ complex matrices, however, we will restrict this study to real matrices. Tsiotras, Junkins and Schaub (1997) give the inverse transformation as identical to itself. Solving Equation 3.7.13 for **Q** we obtain the same result. Fallat and Tsatsomeros (2002) and Courant and Hilbert (1953: 536-7) state that the order of factors may be reversed and $(\mathbf{I}-\mathbf{Q})$ commutes with $(\mathbf{I}+\mathbf{Q})^{-1}$.

For the set of matrices of the order $2n\times 2n$, **B** is a symplectic matrix as defined in Equation 3.7.10 and **A** is a Hamiltonian matrix as defined in Equation 3.7.11 by Bernstein, 2009: 208-209; Sanyal, 2001: 72 and in Equation 3.7.12 by Bernstein, 2009: 239 and Cardoso and Harris, 2007. Equation 3.7.13 is its own

functional inverse and so if **C** is symplectic, **Q** is the resultant Hamiltonian matrix and for the inverse, if **C** is Hamiltonian, **Q** is the resultant symplectic matrix.

In linear optics, because the Cayley transform of a transference is Hamiltonian, the units of the entries are the same as for a transference, that is, mixed units (Cardoso and Harris, 2007). Because of Equation 3.7.8, the Gaussian transformed transference has three independent entries, enabling us to create a three-dimensional graph of the Hamiltonian space represented by the Cayley Transform (Evans and Harris, 2011).

We mention in passing that Hamiltonian matrices fulfil the requirements for a vector space (Hall, 2004: 43; Anton and Rorres, 2005: 222) and therefore the mathematics of vector spaces can be applied to the three-dimensional (for $\mathbf{S}_{2\times2}$) , ten-dimensional (for $\mathbf{S}_{4\times4}$) and fourteen-dimensional (for $\mathbf{T}_{5\times5}$) spaces. Symplectic matrices on the other hand disobey the requirements for vector spaces and the rules of vector spaces cannot be meaningfully applied to symplectic matrices. The one-to-one mapping between the symplectic matrices and Hamiltonian spaces allows us to not be confined by the restrictions placed on symplectic systems. This is important to this dissertation and will be used to this effect in Section 8.2 to derive a formula for the dependence of the transference on the frequency of light.

3.7.3 The characteristic matrices

In an effort to find a set of matrices, related to the transference, that would offer a solution to quantitative analyses of the optical character of optical systems, Harris and van Gool (2004) turned to the four characteristic matrices. These are the point characteristic matrix **P**, the angle characteristic matrix **Q**, and the first and second mixed characteristic matrices, **M** and **N** respectively. According to Guillemin and Sternberg (1984:17, 35-37) the terminology point, angle and mixed characteristic was introduced by Hamilton, however, modern physics literature refers to them as the point and angle eikonals. Walther (1995:22, 238-241) refers to **P** as Hamilton's point characteristic and distinguishes between the point eikonal **P** and the angle eikonal **Q**. Arnaud (1970), discusses the point characteristic **P** and the ray matrix $\mathbf{S}$. The characteristic matrices are, in each case, defined for linear systems, however, we will concentrate on the application

to Gaussian systems. Harris and van Gool (2004) and van Gool and Harris (2005) apply the characteristic matrices to the 5×5 transference of the astigmatic heterocentric system, whereas Guillemin and Sternberg (1984: 35-36), Walther (1995:22, 238-241) and Arnaud (1970) apply the characteristic matrices to the 4×4 transference of the astigmatic homocentric system.

For any given Gaussian system S, the incident position y_0 and reduced inclination α_0 of the ray is mapped to the emergent position *y* and reduced inclination α by Equation 3.2.10. This equation pre-supposes that the incident state of the ray is known and that the emergent state of the ray is sought. Of course, if the opposite is true, that is if the emergent state of the ray is known, then it is a simple matter to calculate the incident state of the ray by

$$\boldsymbol{\rho}_0 = \mathbf{S}^{-1}\boldsymbol{\rho} \tag{3.7.14}$$

where $\mathbf{S}^{-1}$ is the matrix inverse of the transference. In both these situations, with regards to the state of the ray, there are two dependent and two independent variables.

However, Harris and van Gool (2004) point out that it is possible for other combinations of two dependent and two independent variables to exist. Each of the four characteristic matrices represents one of the four possible combinations of dependent and independent variables with respect to the incident and emergent positions and inclinations. In each case, the characteristic matrix functions as the operator on the chosen vector. The four operations are represented in Equations 3.7.15, 16, 18 and 19, below, as given by Harris and van Gool, (2004).

The point characteristic defines the incident and emergent inclinations when the positions are chosen:

$$\mathbf{P}\begin{pmatrix} y_0 \\ y \end{pmatrix} = \begin{pmatrix} -\alpha_0 \\ \alpha \end{pmatrix}. \tag{3.7.15}$$

Similarly the angle characteristic defines the incident and emergent positions when the reduced inclinations are known:

$$\mathbf{Q}\begin{pmatrix} -\alpha_0 \\ \alpha \end{pmatrix} = \begin{pmatrix} y_0 \\ y \end{pmatrix}. \tag{3.7.16}$$

As Harris and van Gool (2004) point out, from the above two equations it is obvious that

$$\mathbf{P} = \mathbf{Q}^{-1} \tag{3.7.17}$$

provided **Q** is non-singular. The derivations for **P** and **Q** make use of the Schur complements (Equations 3.2.20 to 23) (Harris, 2010d).

The first and second mixed characteristic matrices operate as follows:

$$\mathbf{M}\begin{pmatrix} y_0 \\ \alpha \end{pmatrix} = \begin{pmatrix} \alpha_0 \\ y \end{pmatrix} \tag{3.7.18}$$

and

$$\mathbf{N}\begin{pmatrix} \alpha_0 \\ y \end{pmatrix} = \begin{pmatrix} y_0 \\ \alpha \end{pmatrix}. \tag{3.7.19}$$

$$\mathbf{M} = \mathbf{N}^{-1} \tag{3.7.20}$$

provided **N** is non-singular.

Point characteristic

The point characteristic is defined for a Gaussian optical system as

$$\mathbf{P} = \begin{pmatrix} B^{-1}A & -B^{-1} \\ -B^{-1} & DB^{-1} \end{pmatrix} \tag{3.7.21}$$

provided $B \neq 0$. Difficulties can be anticipated as *B* approaches zero (van Gool and Harris, 2005), which should not pose a problem for any "reasonable" eye. This would be a problem for conjugate systems including thin systems, but for an eye or schematic eye $B \neq 0$. The matrix is symmetric and Harris and van Gool (2004) note that the minus sign in front of α_0 (Equation 3.7.15) is what creates the symmetry. Of particular interest is the first entry which is the refractive compensation (Equation 3.4.6) (Harris and van Gool, 2004; van Gool and Harris, 2005).

Angle characteristic

The angle characteristic **Q** is the inverse of **P**. From Equations 3.7.15 and 16 this appears obvious, however From Equations 3.7.21 and 22 this is not

immediately apparent, but is the result of symplecticity (Equation 3.2.24). **Q** is defined for a Gaussian optical system as

$$\mathbf{Q} = \begin{pmatrix} C^{-1}D & C^{-1} \\ C^{-1} & AC^{-1} \end{pmatrix} \tag{3.7.22}$$

provided $C \neq 0$. $C = 0$ defines an afocal system, which the eye is clearly not. The matrix is again symmetric, a consequence of the minus sign in front of the α_0 in Equation 3.7.16 (Harris and van Gool, 2004). Walther (1995:242) explores the advantage that for the angle eikonal it is easy to shift the entrance and exit planes. We can see this is possible from Equation 3.7.16.

First mixed characteristic

The first mixed characteristic is defined for a Gaussian system as

$$\mathbf{M} = \begin{pmatrix} -D^{-1}C & D^{-1} \\ D^{-1} & BD^{-1} \end{pmatrix} \tag{3.7.23}$$

provided $D \neq 0$, that is, provided the system is not entrance-plane focal.

Second mixed characteristic

The second mixed characteristic **N** is the inverse of **M** (Equation 3.7.20) which is easy to prove and is a result of symplecticity. **N** is defined for a Gaussian system as

$$\mathbf{N} = \begin{pmatrix} -A^{-1}B & A^{-1} \\ A^{-1} & CA^{-1} \end{pmatrix} \tag{3.7.24}$$

provided $A \neq 0$. In Section 3.3.1 we saw that *A* defines the ametropia of the system (Harris, 1999a). This is potentially a problem for eyes because $A = 0$ defines an emmetropic eye. Problems can be anticipated in eyes where *A* approaches zero (van Gool and Harris, 2005), which includes emmetropic eyes, compensated eyes and most schematic eyes.

It is the very issue of singularity of these characteristic matrices that implies that the choice of any two of y_0, y, α_0 or α does not necessarily fix the other two (Harris and van Gool, 2004). Existence and uniqueness create potential problems in the use of these characteristic matrices.

3.8 Vergence and wavefronts

Thus far in this chapter on linear optics and Gaussian systems, we have been studying the optics of systems with a strong emphasis on the transference and the properties of the system, both fundamental and derived. Vergence and wavefronts are not properties of a system, but rather our handle on light. Thus far we have considered the effect of the system on a single ray, quantified as a vector $\boldsymbol{\rho}$. We now turn our attention to the effect of the system on a pencil of light, quantified as a matrix **L**.

Vergence is merely the local reduced curvature of the wavefront. The wavefront is denoted as positive (converging) or negative (diverging). It also has a local inclination (Harris, 1996b).

3.8.1 Stigmatic vergence and wavefronts

The reduced vergence at entrance plane T_0 of system S is L_0. For an object O at a longitudinal distance z_O upstream of the entrance plane we have reduced vergence given as

$$L_0 = \frac{n_0}{z_\mathrm{O}}. \tag{3.8.1}$$

There are two special cases, when the object point is distant, $z_\mathrm{O} \to \infty$, we have $L_0 = 0\,\mathrm{D}$, and when the object point is at the entrance plane, $z_\mathrm{O} = 0\,\mathrm{m}$ and $L_0 \to \infty$.

3.8.2 Astigmatic vergence and wavefronts

In the presence of astigmatism the generalisation of the scalar reduced vergence *L* is the matrix reduced vergence **L** (Fick, 1973d; Keating, 1981a,b). **L** is a 2×2 symmetric matrix identical in mathematical character to the dioptric power matrix **F** of a thin system (Fick, 1972, 1973a, b ; Long, 1976). That is to say, for an astigmatic wavefront, the eigenvalues are the vergences (reduced principal curvatures) along the two principal meridians given by the eigenvectors (Keating, 1981a, b; Harris, 1996b). The vergence matrix **L** is always symmetric, even when it emerges from a thick astigmatic system with an asymmetric power matrix

(Keating, 1981a, b) and for which Harris (1996b) gives a proof, based on the symplecticity of the transference. The implication of this is that the two principal meridians are always orthogonal.

For a wavefront incident onto an astigmatic system from an object point O at longitudinal position z_{O} relative to T_0, Equation 3.8.1 generalizes to

$$\mathbf{L}_0 = \frac{n_0}{z_{\mathrm{O}}}\mathbf{I}\,. \tag{3.8.2}$$

For a distant object point $\mathbf{L}_0 = \mathbf{O}\,\mathrm{D}$.

3.8.3 The wavefront, its curvature and direction: distant object

For a distant object point, Harris (1996b) derives the equation for a wavefront at the optical axis as

$$z = \frac{\mathbf{y}^{\mathrm{T}}\mathbf{L}\mathbf{y}}{2n} - \frac{\mathbf{y}^{\mathrm{T}}\boldsymbol{\alpha}_{\times}}{n}\,. \tag{3.8.3}$$

This equation describes the geometry of the wavefront exiting the system and can be thought of as the sagitta at the optical axis of the wavefront as it exits the system.

$$\mathbf{L} = -\mathbf{C}\mathbf{A}^{-1} \tag{3.8.4}$$

is the reduced wavefront curvature and

$$\boldsymbol{\alpha}_{\times} = \mathbf{A}^{-\mathrm{T}}\boldsymbol{\alpha}_0 \tag{3.8.5}$$

is the reduced direction of the emergent wavefront at the optical axis. **y** is the transverse position of the ray at the exit plane. When the eigenvalues of **L** are distinct, the wavefront is astigmatic and when the eigenvalues are not distinct, the wavefront is a paraboloid of revolution (stigmatic). When **A** is singular, Equations 3.8.3 to 5 do not hold and the wavefront is not defined. The wavefront has reduced to a singularity and there is a focal point or line in the transverse plane.

3.8.4 Vergence emergent from a system: object at a finite distance

We now consider a system S with entrance plane T_0, exit plane T and longitudinal axis Z. The vergence incident onto the system at T_0 is $\mathbf{L}_0$. Harris (1996b) gives the vergence emergent from the system at exit plane T as

$$\mathbf{L} = \left(\mathbf{D}\mathbf{L}_0 - \mathbf{C}\right)\left(\mathbf{A} - \mathbf{B}\mathbf{L}_0\right)^{-1} \tag{3.8.6}$$

and the emergent direction of the wavefront as

$$\boldsymbol{\alpha}_{\times} = \left(\mathbf{A} - \mathbf{B}\mathbf{L}_0\right)^{-\mathrm{T}} \boldsymbol{\alpha}_{\times 0}\,. \tag{3.8.7}$$

$\boldsymbol{\alpha}_{\times 0}$ and $\boldsymbol{\alpha}_{\times}$ are the reduced inclinations of the rays at the optical axis incident and emergent to the system at the entrance and exit planes respectively.

3.8.5 Vergence across elementary systems

Homogenous gap

The transference of a homogenous gap of width *z* is given by Equation 3.2.7. Substituting into Equation 3.8.6 we obtain (Harris, 1996b)

$$\left(\mathbf{L}_0^{-1} - \zeta\,\mathbf{I}\right)^{-1} = \mathbf{L}\,, \tag{3.8.8}$$

the generalization of the equation for vergence across a homogenous gap.

Refracting surface

The transference of a thin system is given by Equation 3.2.9 with **F** symmetric. Both the power of a refracting surface and the power of a thin lens **F** are symmetric matrices. Substituting from Equation 3.2.9 into Equation 3.8.6 we obtain

$$\mathbf{L}_0 + \mathbf{F} = \mathbf{L}\,, \tag{3.8.9}$$

the generalization of Gauss' equation, first derived by Keating (1981a) and then by Harris (1996b).

3.8.6 Position of point or line foci

Calculations often require us to determine where focal points or lines are for a given object point. The calculation usually will give an answer as a distance, along the longitudinal axis, either upstream or downstream from the reference or image plane. For a stigmatic system this is simply obtained by solving

$$z = \frac{n}{L} \tag{3.8.10}$$

(from Equation 3.8.1). For an astigmatic wavefront one will obtain two orthogonal line foci (Keating, 1981b). The derivation for determining the longitudinal and transverse positions and orientations of the line foci will be given in Chapter 6.

3.9 Summary

This chapter has taken an in-depth look at linear and Gaussian optics and in particular the transference. We saw that we can calculate the effect that the system has on light by tracing either a single ray (Equation 3.2.31) or a pencil of light (Equation 3.8.6) through the optical system. Familiarly, these are the state of the ray vector or vergence, respectively. We took a look at the fundamental properties of an optical system as well as four special systems. We then spent some time studying a selection of derived properties of the optical system.

The derived properties that form part of this study include power, refractive compensation, front- and back-vertex power, magnification and the locations of the cardinal points. In addition two transformed transferences and four characteristic matrices are included as options for studying the dependence of the transference on the frequency of light and as vector spaces that allow statistical analysis.

This chapter is by no means a comprehensive account of Gaussian and linear optics and all derived properties. We have limited ourselves to a small selection of derived properties that are affected by the frequency of light in a Gaussian optical system. We also saw that not all the derived properties that we will need for our study of chromatic properties are available in the literature. Additional formulae will be derived in Chapter 5.

4 BACKGROUND THEORY: CONSIDERATIONS

The previous two chapters took a detailed looked, firstly, at how chromatic aberrations have been defined in classical and physiological optics and, secondly, at Gaussian and linear optics of systems. Chapter 3 gave a broad overview of linear optics in general, the fundamental properties and a selection of derived properties from the transference. We saw how we can trace either a single ray through a system, or the effect of a system on a pencil of rays in the section on vergence and wavefronts. However, there are a few additional considerations that need to be addressed.

Firstly, we take a look at schematic eyes. After a brief overview of the history of schematic eyes, we look at the classification of schematic eyes, from the simplest single-surface reduced eye to multi-surface schematic eyes that closely mimic a real eye. We then narrow our choice of eyes for this dissertation to two, that of the reduced eye, often used in previous studies on chromatic properties and Le Grand's four-surface schematic eye.

Secondly we take a look at the visible spectrum across which we will base our analyses. We define the frequencies we will highlight in tables and graphs in Part IV of this dissertation.

Thirdly, we consider the arguments for and against using frequency or wavelength in our treatment.

Finally, we take a look at the formulae available for the refractive index of a medium as a function of wavelength. We look at formulae for the refractive index of water, the medium of the reduced eye, the four media of Le Grand's model eye and air.

4.1 Schematic eyes

4.1.1 A short history of schematic eyes

Smith (1995) presents a comprehensive history of schematic eyes and this is discussed briefly, although we shall mention only the better known schematic eyes. For centuries the eye and the functions of the various structures within it

were misunderstood. The ancient Greeks and Arabs believed that light emanated from the lens inside the eye and caused a visual response when these light rays touched an object. This view prevailed till approximately 1000 AD when Ibn al-Haitham proposed that the light rays travelled from an object into the eye. However, it was not until the early sixteenth century that Leonardo da Vinci (*c*. 1500 AD) proposed that the lens was responsible for refracting the light.

Snell discovered the exact law of refraction in 1621 and published by Descartes in 1637. Scheiner was the first to attempt to measure the radius of curvature of the anterior corneal surface by the rather rudimentary method of comparing the size of reflection off the cornea with reflections from various sized marbles. Once the correct anatomical structure was understood, Christian Huygens proposed the first schematic eye in the seventeenth century.

Another two centuries went by before Young, in 1801, made more accurate measurements of the anterior refracting surface and anterior and posterior lenticular surfaces, the depth of the anterior chamber and the refractive indices of the humours and lens. As a result the first accurate schematic eye was attributed to Listing who described a three-surface schematic eye in 1851 (Emsley, 1950: 524). Emsley designed a reduced eye, based on certain parameters of the Gullstrand-Emsley eye, which is widely accepted (Emsley, 1950: 543-544).

According to Smith (1995) both the Gullstrand and the Le Grand schematic eyes enjoy reasonable popularity. In 1945, Le Grand (1945: 50-51) presented two schematic eyes, a full theoretical eye consisting of four surfaces and a simplified eye with a single cornea and a lens of zero thickness which too, was limited in its usefulness (Smith, 1995; Atchison and Smith, 2002: 45). Le Grand (1956: 9-27) did a number of calculations to determine the chromatic dispersion of each of the refractive indices. Because of the availability of refractive indices as a function of wavelength for all four media it is one of the theoretical model eyes to be used in this dissertation. This will be looked at in more detail in Section 4.4.3.

4.1.2 Classification of schematic eyes

According to Smith (1995) paraxial schematic eyes are classified into three classes, exact, simplified and reduced. Exact schematic eyes attempt to model a real eye as much as possible with a minimum of four spherical surfaces. Simplified schematic eyes reduce the number of surfaces to two or three. Reduced schematic eyes transfer all the refracting power to a single refracting surface or "cornea", usually resulting in a smaller radius of curvature and shortening of the axial length. Apart from the refractive index of the internal medium, none of the dimensions represent those of a real eye.

It is important to acknowledge the limitations of any model being studied. The limitations of paraxial schematic eyes are firstly that all surfaces are rotationally symmetrical, spherical and centred.

Secondly, it is assumed that the medium is homogenous and isotropic within each element. In a real eye the lens, in particular, is a gradient index lens. For these two reasons, the schematic eyes are poor predictors of monochromatic aberrations.

Thirdly, the eye is built from a combination of average parameters, each considered to be averages of many individual values. These average parameters are combined to represent an "average eye". It is important to note that this average eye is not an average of many eyes, but an eye created by a combination of average parameters (Rabbetts, 2007: 221-241; van Gool and Harris, 2005). This average eye is completely different to the average eye mentioned in Section 3.7 and sought by Harris, van Gool and Cardoso (Harris, 2004b, 2005, 2007; Harris and van Gool, 2004; van Gool and Harris, 2005; Harris and Cardoso, 2006; Cardoso and Harris, 2007; Harris, 2008). Individuals may vary significantly from these values. With the exception of the variations on the Bennett-Rabbetts eye, the schematic eyes are usually attempts to represent an emmetropic eye, based on a monochromatic reference wavelength which is usually yellow light.

Fourthly, the cornea is assumed to be spherical in shape, whereas a real cornea is aspherical (ellipsoid). Finally, the fovea is assumed to be on the optical axis and as a result the optical and visual axes coincide (Smith, 1995).

For completeness it is necessary to mention a newer class of schematic eyes, namely finite or wide angle schematic eyes. This class of model eyes attempts to overcome some of the limitations of the paraxial schematic eyes by including aspheric refracting surfaces, gradient index lenses, a curved retina and lack of surface alignment along a longitudinal axis (Smith, 1995; Atchison and Smith, 2002:39). A number of such eyes have been developed, mostly over the past forty years (Smith, 1995; Rabbetts, 2007:227-8). Of particular interest is the chromatic eye developed by Thibos *et al* (1992) with the express purpose of creating a reduced eye that mimics the effects of chromatic aberration found experimentally.

Paraxial schematic eyes are well suited to study numerous properties of the eye within Gaussian optics, including power, positions of the six cardinal points, pupil positions and sizes, retinal image size of small objects, magnifications and to a limited extent, the causes and effects of refractive errors and accommodation. Because the paraxial schematic eyes are Gaussian models, calculations are restricted to small image sizes and small pupils. The choice of eye will depend on the complexity of the subject being studied and level of accuracy desired. These model eyes are excellent models for calculations of chromatic aberrations. This is because the eye's media are composed mainly of water and the refractive indices vary little across eyes (Smith, 1995).

4.1.3 Emsley's reduced eye

The concept of the reduced eye was first proposed by Listing (Emsley, 1950: 543). The advantage of the reduced eye (see Figure 4.1.1) is its simplicity. The reduced eye has a single stigmatic refracting surface of radius of curvature *r* and a homogenous gap of length *z*. It implies that any ray intersecting the refracting surface orthogonally is an optical axis and therefore there is an infinity of optical axes. We choose one such ray as our longitudinal ray.

When designing the reduced eye, Emsley (1950: 523-544) based a number of parameters on the Gullstrand-Emsley schematic eye. He noted that the principal points of the schematic eye are very close together (0.3 mm apart) and he allowed these "to coalesce into a single intermediate point". He then reduced the schematic

eye into a single spherical refracting surface. Emsley wanted the focal points to coincide with those of the schematic eye. According to him, this fixed the power, radius of curvature and position of the single refracting surface all at once. He placed the vertex of the refracting surface at the principal point of the reduced eye, 5/3 mm behind that of the Gullstrand-Emsley schematic eye. The centre of the radius of curvature was placed at the single intermediate nodal point, giving a radius of curvature *r* of 50/9 mm (or 1/180 m). Because the eye is emmetropic, the length *z* of the eye is now 200/9 mm (or 1/45 m) and is also the emergent focal length. The incident focal length increases to 50/3 mm upstream of the refracting surface. He placed specific emphasis on the power 60 D and chose the refractive index in the reduced eye to be the same as that of water which, according to Emsley, is 4/3. He took the index of air to be 1 (Emsley, 1950: 525-527, 543-544; Bennett & Rabbetts, 1984: 18).

The reduced eye works well for calculating chromatic properties independent of object, image and aperture positions. In order to include chromatic properties dependent on object or image and aperture position, Thibos (1987) adapted the reduced eye by placing a pupil plane in line with that of the Gullstrand-Emsley schematic eye. This places the pupil 3.63 mm before the nodal point, or 1.926 mm behind the refracting surface. Thibos *et al* (1992) further adapted the reduced eye to enable calculations of chromatic properties to closely equate to those results found experimentally. They adapted the constants in Cornu's formula to match their experimental values and modified the corneal

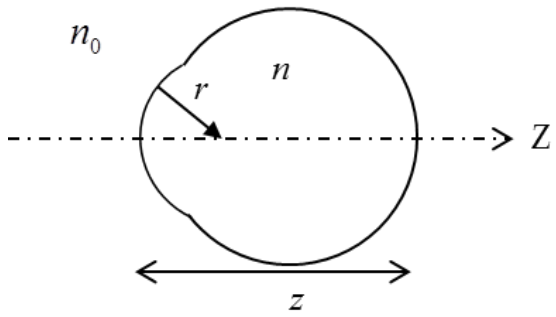

Figure 4.1.1 The reduced eye as a defined optical system. The length is *z*, with optical axis Z, the radius of curvature of the refracting surface is *r*, the refractive index outside the system is n_0 and inside the system is *n*.

profile to an ellipsoid. They refer to this reduced eye with three modifications as the "Chromatic eye". In this dissertation we will make use of a reduced eye with the same *r* and *z* as Emsley's eye and with an index *n* dependant on the frequency of light based on the modified formula proposed by Thibos *et al* (1992).

4.1.4 Le Grand's full theoretical eye

Le Grand proposed his two schematic eyes in 1945. Each schematic eye had an unaccommodated and accommodated version (Le Grand, 1945: 50-51, 1980: 65-67). This dissertation uses the unaccommodated full theoretical version which has four refracting surfaces. A schematic diagram of Le Grand's eye is shown in Figure 4.1.2. The dimensions of Le Grand's full theoretical unaccommodated eye are given in Table 4.1.1 (Le Grand, 1945:50). Subscripts used here are defined in Table 4.1.1 and Figure 4.1.2.

The dimensions given in Table 4.1.1 are limited to the radii of curvature of the refracting surfaces and the width of the gaps between them. The refractive indices in Table 4.1.1 are for a reference refractive index of 589 nm (Fraunhofer line D). At this reference refractive index, Le grand's schematic eye is emmetropic (Le Grand, 1956: 12-19).

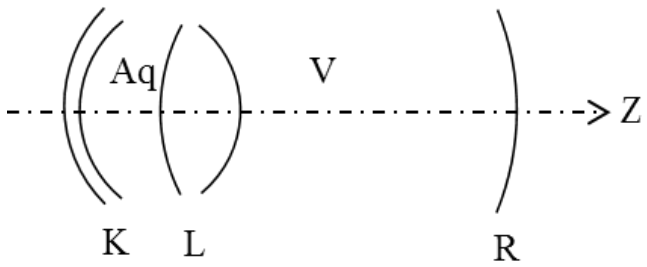

Figure 4.1.2 Le Grand's Complete Theoretical Eye, comprising four refracting surfaces and four homogenous gaps. The refracting surfaces are the anterior and posterior corneal surfaces (K1 and K2) and anterior and posterior lens surfaces (L1 and L2). The gaps are the thickness of the cornea (K), the depth of the anterior chamber (Aq), the thickness of the crystalline lens (L) and the depth of the posterior chamber (V). The optical axis Z is chosen to be centred with each of the stigmatic refracting surfaces, implying no deflectance or tilt in either system.

Table 4.1.1 The dimensions of Le Grand's full theoretical unaccommodated eye (Le Grand, 1945: 50).

Refracting surface or medium	Abbreviated subscript	Radius of curvature (mm)	Width (mm)	Refractive index
Corneal anterior surface	K1	7.8		
Cornea	K		0.55	1.3771
Corneal posterior surface	K2	6.5		
Anterior chamber	Aq		3.05	1.3374
Lens anterior surface	L1	10.2		
Lens	L		4.0	1.42
Lens posterior surface	L2	–6		
Posterior chamber	V		16.5965	1.336

4.2 Visible spectrum

The limits of the visible spectrum differ among studies and industries. The definition of the colour bands also differs (compare Sears, Zemansky and Young, 1987:827 and Keating: 2002: 475). For the purposes of this dissertation, we adopt the spectrum with frequencies between 430 and 750 THz (Sears, Zemansky and Young, 1987: 827) which represents vacuum wavelengths between 399.7 and 697.2 nm, approximately. This represents the range over which human spectral sensitivity ranges from 1 to 100% (Rabbetts, 2007: 287; Thibos *et al*, 1992; Le Grand, 1957: 7-8, 55-58, 71-73).

In Part IV wherever results are displayed graphically and where possible, six coloured reference points will be displayed. These six points represent an even spread across the chosen spectrum, with a gap of 64 THz between each reference point. The six colours are red, orange, yellow, green, blue and violet, and include the two spectral range end-points. The purpose is to create a consistent visual display that is comparable across all the results. The frequencies and corresponding calculated wavelengths of the six colours are detailed in Table 4.2.1. Frequency is given in THz $\left(\times 10^{12}\ \mathrm{s}^{-1}\right)$ and wavelength in nm $\left(\times 10^{-9}\ \mathrm{m}\right)$. The printed colours are not intended to be an exact replication of that particular frequency, but merely a key to the graph and the reference points.

Table 4.2.1 The frequencies and wavelengths of the six specified coloured reference points.

Colour	Frequency in THz	Vacuum wavelength in nm
Red	430	697.2
Orange	494	606.9
Yellow	558	537.3
Green	622	482.0
Blue	686	437.0
Violet	750	399.7

4.3 Frequency versus wavelength

Pease and Barbeito (1989) look at the relationship between frequency and wavelength for a number of studies involving chromatic aberration and conclude that results using frequency or wavenumber (the inverse of wavelength) are "nearly perfectly linear" in contrast to those using wavelength. They cite several reasons to support using frequency rather than wavelength, perhaps the most important being that frequency is independent of the medium whereas wavelength is not and that energy is directly proportional to frequency. Furthermore, we note from Cornu's hyperbolic formula for chromatic dispersion, that refractive index varies inversely with wavelength. These reasons make a compelling argument to study the dependence of properties on the frequency of light rather than on wavelength. Koczorowski (1990) and Rabbetts (2007:290, 292) both show this linear relationship graphically. Confirmation will be obtained in Chapter 8.

4.3.1 Frequency, wavelength and refractive index relationships

The fundamental relationship between frequency ν and vacuum wavelength λ_0 is given by

$$c_0 = \nu\lambda_0 \tag{4.3.1}$$

where light traveling in a vacuum has a speed $c_0 = 299\,792\,458\ \mathrm{m.s^{-1}}$ as defined by the 17th General Conference on Weights and Measures in November 1983. As light travels from one medium to another, the frequency remains the same whereas the wavelength and speed change.

In a particular medium light travels at speed $c < c_0$. The index of refraction in the medium is defined by

$$n = \frac{c_0}{c}. \tag{4.3.2}$$

Hence,

$$n = \frac{\lambda_0}{\lambda} \tag{4.3.3}$$

where λ is the wavelength in a medium.

According to Sears, Zemansky and Young (1987: 843) indices of refraction (for white light) are typically quoted for yellow light from a sodium lamp and with a wavelength of $\lambda = 589\,\text{nm}$, which is near the middle of the visible spectrum. The light emitted from this sodium lamp is inexpensive and nearly monochromatic. The refractive index of air for yellow light is approximately 1.0003 but is usually expressed as 1.

4.3.2 Frequency scale and linearity

Pease and Barbeito (1989) argue that the use of the frequency scale facilitates data analysis for the study of chromatic aberration. The linear nature of the frequency scale makes analysis simpler to compute and to understand.

4.4 Refractive index as a function of frequency for optical media and air

According to Rabbetts (2007: 287), "dispersion is the variation in refractive index of a medium with wavelength". The constringence or Abbe number is the reciprocal of dispersion (Sivak and Mandelman, 1982).

There are few formulae available that give the refractive index of a medium as a function of wavelength (Sivak and Mandelman, 1982; Rabbetts, 2007: 287). Cornu's formula gives the refractive index for water as a function of wavelength, includes three constants and has the form of Equation 4.4.1. This formula has formed the basis for a number of formulae used for the media of the four-surface eye and the reduced eye, with different values being given for the constants. Thibos *et al* (1992) based their formula on Cornu's formula, the constants being calculated from experimental data.

According to Le Grand (1956: 12), early results of the dispersion of the cornea, aqueous, lens and vitreous were obtained by Kunst in 1923. In 1923 Polack obtained Abbe numbers for the cornea, aqueous and lens, but had reservations about the value for the lens. These results were confirmed by Tagawa in 1928. Le Grand (1956: 11-13) considered Cornu's formula to be an adequate approximation for the humours of the eye within the visible spectrum. He calculated the constants by averaging the refractive indices of water and saline for a number of wavelengths. Based on Cornu's formula, and from Polack's experimental data, he was able to tabulate the refractive indices for the four media of his schematic eye for each of the Fraunhofer lines (A, C, D, F and G). Villegas, Carretero and Fimia (1996) extended Le Grand's tabulated results and obtained a polynomial fit of the refractive indices for the four media.

According to Koczorowski (1990) other formulae are available for calculating the dispersion of media such as those of Schmidt, Sellmeier, Hartman and Herzberger. However the constants in these formulae have not specifically been calculated for the media of the eye. Conrady's modification of Schmidt's formula is applicable to optical materials and Cauchy's formula is more suited to media with absorption in the shortwave part of the spectrum. Cauchy's and Sellmeier's formulae are rough approximations of each other while Cornu's, Hartmann's and Herzberg's formulae appear to have a heuristic rather than theoretical basis (Koczorowski, 1990).

More recently Sivak and Mandelman (1982) obtained mean refractive indices at four wavelengths of the ocular media of cow, pig, frog, chicken, rock bass, albino rat and cat using Abbe and Pulfrich refractometry. They also measured the human lens and obtained mean refractive indices and constringence values for the periphery and core for the four wavelengths. They concluded that the humours of the eyes are less dispersive than water, the cornea is more dispersive at short wavelengths and the lens is considerably more dispersive than water. According to Rabbetts (2007:288) Sivak and Mandelman's study is the only significant experimental study on the dispersion of human ocular media since Kunst and Polack.

Formulae for the refractive index of air also exist. The refractive index varies with air temperature, humidity, air pressure, carbon dioxide level and pollution. Cauchy's and Sellmeier's formulae specify standard levels for each of these factors (Hodgman, 1959: 2943). Lorentz's formula can accommodate humidity levels, however Ciddor's formula can account for each of these factors and calculate the refractive index for that situation (Ciddor, 1996).

4.4.1 Refractive index of water

Le Grand (1956: 11) bases his calculations of the refractive index of the eye on Cornu's formula, although it lacks a theoretical basis. He gives Cornu's formula as

$$n = n_{\infty} + \frac{\mathrm{K}}{\lambda - \Lambda} \tag{4.4.1}$$

where the three positive constants are given in Table 4.4.1. The three constants for pure water he based on Dorsey's work of 1940 and the constants for sea water, with salinity 37.4 parts per thousand, he based on Bein from 1935. The measurements were all done at 20°C. In Le Grand's table of measured versus calculated values, the refractive indices compare well across the visible spectrum for both pure water and saline water.

Table 4.4.1 The constants given by Le Grand (1956: 11) for Cornu's formula (Equation 4.4.1) for pure water and for sea water (salinity 37.4 parts per thousand) at temperature 20°C.

	Pure water	Sea water
n_{∞}	1.31848	1.32492
K	0.0066620 nm	0.0068153 nm
Λ	0.1292 nm	0.1333 nm

4.4.2 Refractive index of the reduced eye

Thibos *et al* (1992) represent the refractive index of the reduced eye as a function of wavelength as follows

$$n = a + \frac{b}{\lambda - c} \tag{4.4.2}$$

where $a = 1.320\,535$, $b = 4.685\,\text{nm}$ and $c = 214.102\,\text{nm}$. The formula is based on Cornu's formula for refractive index of water and constants were derived from clinical experimentation on real eyes. Using this formula Thibos *et al* (1992) showed that the refractive index of the body of the reduced eye changes more rapidly with wavelength than a reduced eye filled with water. The predictions for longitudinal chromatic aberration using this formula more closely approximate experimental data than Emsley's reduced eye filled with water.

4.4.3 Refractive indices of Le Grand's full theoretical eye

Le Grand (1956: 9-27) studied chromatic dispersion and chromatic aberration in detail. He too based his calculations on Cornu's formula. He published a table of refractive indices for the cornea, aqueous humour, lens and vitreous humour for five wavelengths represented by Fraunhofer lines A, C, D, F and G.

Villegas, Carretero and Fimia (1996) took Le Grand's table of refractive indices as a function of wavelength and, using a polynomial fit, expressed the data as formulae for refractive index as a function of wavelength. They then compared the results of their calculations from these formulae with those calculated using Emsley's reduced eye filled with water and with Thibos *et al*'s (1992) chromatic eye for chromatic difference in refractive compensation and chromatic difference of position. Because the chromatic eye was designed for the purpose of calculating chromatic properties, it is the best fit to the experimental data for chromatic difference in refractive error and chromatic difference in position. They concluded that the Le Grand eye is slightly underestimated for chromatic difference of refractive compensation but is approximately equivalent for chromatic difference of position. Because of these results, the Villegas, Carretero and Fimia (1996) formulae for Le Grand's eye is used in this study. The formula derived by Villegas, Carretero and Fimia (1996) are given as

$$n(\lambda) = a - b\lambda + c\lambda^2 - d\lambda^3 + e\lambda^4 \qquad (4.4.3)$$

and the constants are given in Table 4.4.2.

Table 4.4.2 The constants for use in Equation 4.4.3 to calculate the refractive index for each of the four media in Le Grand's eye from Villegas, Carretero and Fimia (1996).

	Units	Cornea	Aqueous humour	Lens	Vitreous humour
a	—	1.511 67	1.490 72	1.538 08	1.456 34
b	m^{-1}	0.000 636 054	0.000 805 138	0.000 448 268	0.000 561 861
c	m^{-2}	1.17×10^{-6}	1.68×10^{-6}	5.74×10^{-7}	1.02×10^{-6}
d	m^{-3}	1.01×10^{-9}	1.66×10^{-9}	2.61×10^{-10}	8.70×10^{-10}
e	m^{-4}	3.31×10^{-13}	6.31×10^{-13}	0	2.84×10^{-13}

4.4.4 Refractive index of air

The refractive index of air differs only very slightly from that of vacuum and for most optometric purposes one can write $n_0 = 1$. A number of equations, for example Cauchy's dispersion formula (Hodgson, 1959) and Ciddor's equations (Ciddor, 1996), are available for calculating the refractive index of air. Cauchy's formula is expressed in terms of wavelength whereas Ciddor's equations are expressed in terms of wavenumber. Cauchy's dispersion formula is

$$(n_0 - 1)10^7 = p + \frac{q}{\lambda^2} + \frac{t}{\lambda^4} \qquad (4.4.4)$$

where $p = 2\,726.43$, $q = 12.228\times10^6$ nm^2 and $t = 355.5\times10^9$ nm^4 for dry air at temperature 15°C, pressure 101 kPa and carbon dioxide content of 450 ppm. Ciddor's equations calculate the refractive index of air for variations in any of these values as well as air pollution density. This, however, would typically be of interest to the field of precise interferometry or geodetic surveying which requires an accuracy to a few parts in 10^8.

In the majority of cases we will use $n_0 = 1$ for the refractive index of air and for illustrative value one data set on the reduced and Le Grand's eyes will be shown using Cauchy's equation. A graph set will be shown comparing calculations using $n_0 = 1$ and Cauchy's formula.

4.5 Discussion

There are a number of schematic eyes available to the ophthalmic optics researcher, differing in the number and shape of refracting surfaces. Some

schematic eyes are available with a pupil or even a gradient index lens. However, because this dissertation focuses on the dependence of the first-order optical properties of the eye on frequency, we need to select schematic eyes for which the refractive indices of all media as a function of frequency (or wavelength) are known. For this reason we have selected the reduced eye and Le Grand's four-surface eye. The reduced eye forms an ideal basis because it is an excellent predictor of chromatic properties. However, the reduced eye is a very simple model and so we include Le Grand's four-surface eye which is somewhat more representative in structure. This point will become clearer later once we calculate the transferences of the two eyes.

The visible spectrum selected in numerical calculations in this dissertation is the range of frequencies from 400 THz to 700 THz. Frequency, rather than wavelength, is used in all calculations and graphical representations.

5 DERIVATIONS FOR BACKGROUND THEORY

In this chapter we derive formulae that will be needed for our study of chromatic dependence of first-order optical properties. As such Chapter 5 is made up of a random assortment of seemingly unrelated derivations. The equations that are presented in Chapter 3 and this chapter together will form the basis from which we will either study chromatic dependence directly or derive formulae for chromatic aberrations and quantifying of chromatic properties. While this chapter focusses on the eye as our system, we note that the formulae derived and figures presented are general for all Gaussian systems.

5.1 Exit-plane refractive compensation

As mentioned in Section 3.4.2 the derivation for exit-plane refractive compensation is not available in the literature. This is presumably because this derived property has no application to the eye. However it is defined here for systems in general. While this dissertation is primarily concentrating on the eye as a system, we include this derived property because it has a bearing on certain entries of the point characteristic **P**.

The exit-plane refractive compensation is the power of a thin lens juxtaposed immediately downstream to a general system so that the combined system becomes an entrance-plane focal system. Writing the transference of the combined system

$$\mathbf{S} = \mathbf{S}_{\mathrm{C}}\mathbf{S}_{\mathrm{S}} = \begin{pmatrix} 1 & 0 \\ -F_{\mathrm{C}} & 1 \end{pmatrix}\begin{pmatrix} A_{\mathrm{S}} & B_{\mathrm{S}} \\ C_{\mathrm{S}} & D_{\mathrm{S}} \end{pmatrix} = \begin{pmatrix} \bullet & \bullet \\ \bullet & -F_{\mathrm{C}}B_{\mathrm{S}} + D_{\mathrm{S}} \end{pmatrix} \tag{5.1.1}$$

and setting $D = 0$ for the exit-plane system

$$-F_{\mathrm{C}}B_{\mathrm{S}} + D_{\mathrm{S}} = 0 \tag{5.1.2}$$

we obtain the exit-plane refractive compensation for system S_{S}

$$F_{\mathrm{C}} = D_{\mathrm{S}}B_{\mathrm{S}}^{-1}. \tag{5.1.3}$$

This equation generalizes readily to linear systems.

5.2 Magnification

There is a relationship between the definition of magnification defined for a Gaussian system for conjugation of the object and image and the fundamental properties of the system's transference. Indeed, the relationship between transverse and angular magnification is to be found in the symplectic equation (Equation 3.2.24).

In Section 3.5.3 we saw how Harris (2001a) defined magnification, blur and the ray state at the retina for distant objects. We take a different approach to Harris (2001b) to define magnification, blur and the ray state at the retina for finite distances and these definitions are derived in Section 5.2.2.

The use of a pinhole immediately in front of the eye forms a large role in the experiments for chromatic properties of eyes, particularly chromatic properties dependent on object or image and aperture positions. For this reason we simplify this special situation for magnification of an object at a finite distance in Section 5.2.4.

5.2.1 Relationships between the types of magnification

In Section 3.3.2, we looked at the four special types of systems resulting from equating each of the fundamental properties in turn to zero. Then, in Section 3.5.1, we looked at the three types of magnification defined for Gaussian systems. We now observe that there are distinct similarities in the definitions between two of these systems. Transverse and angular magnification are related to the transference through their being defined in the same way as two of the special systems, that is the conjugate and afocal systems. Also, in a similar way to the relationship that we saw between these two magnifications in Section 3.5.1, the two types of magnification are inversely related to each other through the symplectic equation.

Transverse magnification

Where we have a conjugate system $B = 0$ such that an object at the entrance plane is positioned as height from the optical axis y_0, the point image

will form on the exit plane at position *y*. Equation 3.5.1 is the same as Equation 3.3.2 and *A* represents transverse magnification in a conjugate system. Therefore

$$A = M_{\mathrm{t}} \tag{5.2.1}$$

as long as $B = 0$. This equation is true for all Gaussian systems, both thin and thick, provided the object is at the entrance plane. Should the object be elsewhere, then *A* magnifies the ray height and Equation 5.2.1 does not apply.

Angular magnification

The equation for angular magnification, Equation 3.5.3 is the same equation as Equation 3.3.3. We can therefore state that

$$D = M_{\alpha}. \tag{5.2.2}$$

This is true of all afocal systems $C = 0$ and provided the object point is distant.

Relationships between the magnifications

Equation 3.5.4 gave us the relationship between angular and transverse magnification as the one being the inverse of the other. To confirm this, from the symplectic Equation 3.2.24, and substituting $B = 0$, we can see that

$$AD = 1. \tag{5.2.3}$$

The same is true if we substitute $C = 0$ into the symplectic equation. Substituting Equations 5.2.1 and 2 into Equation 5.2.3, we obtain Equation 3.5.4.

5.2.2 Summary of magnification, blur and ray state at the retina

Equations 3.5.7 and 8 define the magnification, blur and ray state at the retina. We recall that $\boldsymbol{\rho}_{\mathrm{R}} = \begin{pmatrix} y_{\mathrm{R}} & \alpha_{\mathrm{R}} \end{pmatrix}^{\mathrm{T}}$ defines the state of the ray at the retina. However, instead of α_{R} we are interested in the unreduced inclination at the retina a_{R}, and indeed elsewhere in the system. Therefore we define

$$\mathbf{r}_{\mathrm{R}} = \begin{pmatrix} y_{\mathrm{R}} \\ a_{\mathrm{R}} \end{pmatrix} \tag{5.2.4}$$

for the purposes of defining chromatic properties dependent on object and aperture positions. Equations 3.5.7 and 8 become

$$A_{\mathrm{E}} A_{\mathrm{A}}^{-1} y_{\mathrm{P}} + B_{\mathrm{B}} A_{\mathrm{A}}^{-1} n_0 a_{\mathrm{K}} = y_{\mathrm{R}} \tag{5.2.5}$$

and

$$n^{-1}C_{\mathrm{E}}A_{\mathrm{A}}^{-1}y_{\mathrm{P}} + n^{-1}D_{\mathrm{B}}A_{\mathrm{A}}^{-1}n_0 a_{\mathrm{K}} = a_{\mathrm{R}} \tag{5.2.6}$$

where n is the refractive index of the vitreous humour.

We write these two equations in the form

$$\mathbf{V}_{\mathrm{E}}\mathbf{v}_{\mathrm{E}} = \mathbf{r}_{\mathrm{R}} \tag{5.2.7}$$

where

$$\mathbf{V}_{\mathrm{E}} = \begin{pmatrix} W_{\mathrm{E}} & X_{\mathrm{E}} \\ Y_{\mathrm{E}} & Z_{\mathrm{E}} \end{pmatrix} = \begin{pmatrix} A_{\mathrm{E}}A_{\mathrm{A}}^{-1} & B_{\mathrm{B}}A_{\mathrm{A}}^{-1}n_0 \\ n^{-1}C_{\mathrm{E}}A_{\mathrm{A}}^{-1} & n^{-1}D_{\mathrm{B}}A_{\mathrm{A}}^{-1}n_0 \end{pmatrix}, \tag{5.2.8}$$

is the distance coefficient matrix and with subscript E for eye and

$$\mathbf{v}_{\mathrm{E}} = \begin{pmatrix} y_{\mathrm{P}} \\ a_{\mathrm{K}} \end{pmatrix}. \tag{5.2.9}$$

Harris (2001a) names each of the coefficients according to their characters and properties. W_{E} is the distance image blur coefficient, X_{E} is the distance image size coefficient, Y_{E} is the distance directional spread coefficient, and Z_{E} is the distance directional coefficient. While we have defined the coefficients slightly differently with regard to the refractive indices, the meaning conveyed is the same.

5.2.3 Magnification, blur and ray state at the retina for object points at finite distances

To calculate the magnification and blur at the retinal plane for a system where the object point is at a finite distance we take a different approach to Harris (2001b). We define the system of the eye, as shown in Figure 5.2.1, as having the entrance plane T_{K} immediately upstream of the tear layer on the cornea and the exit plane T_{R} immediately in front of the retina. The eye naturally divides into two subsystems at the plane of the pupil T_{P} which also acts as a limiting aperture. We divide our system, which represents the eye, into two subsystems, anterior, with subscript A and posterior, with subscript B. Immediately upstream of the eye is the homogenous gap of width $-z_{\mathrm{O}}$ measured from the corneal plane T_{K} to the object plane T_{O}, which represents the finite working distance. The object is

located at the entrance plane T_O and is positioned at a transverse distance of y_O with respect to the longitudinal axis Z.

We are interested in solving for the state of the ray $\boldsymbol{\rho}_R$ at the retina in terms of its transverse position in the pupil y_P and the transverse position of the object y_O, instead of the incident inclination of the ray at the cornea α_K which we used for the system with a distant object in Section 3.5.3. The advantage of defining the system this way is that we can either use the pupil as our partitioning plane or we can use any limiting aperture within an optical device through which the eye is looking, including a pinhole in front of the eye. The formulae we derive are general and we will show how they simplify further still when using a pinhole immediately in front of the eye. We noted earlier (Section 3.5.3) that the position of the centre of the pupil does vary slightly with changes in diameter, however, the use of a pinhole allows us to manipulate y_P to a much greater extent. In this case y_P is the distance from the longitudinal axis to the centre of the pinhole at the corneal-plane T_K. The near system and symbolism is introduced in Figure 5.2.1.

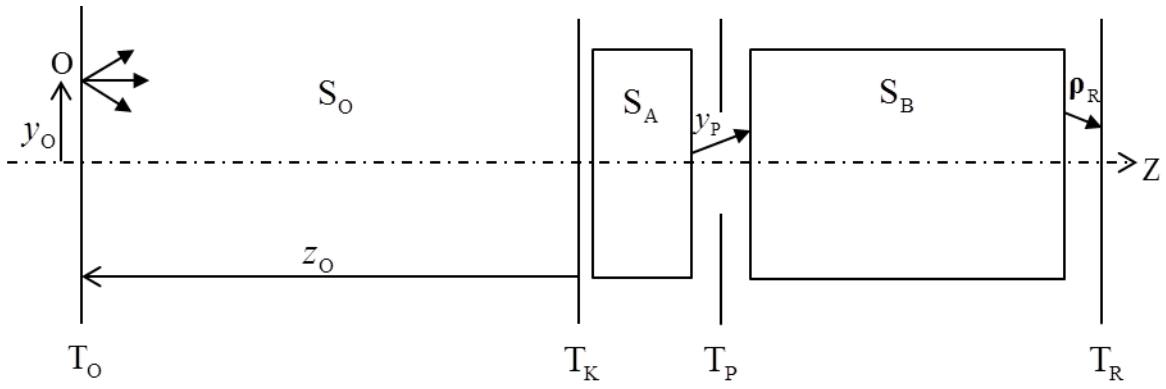

Figure 5.2.1 The Gaussian system of the eye S_E is partitioned into two subsystems by a pupillary plane T_P and consists of an anterior subsystem S_A and posterior subsystem S_B which are juxtaposed. The object plane is located at position $z_O < 0$ measured from the cornea. The width of S_O is $-z_O$.

The system of the eye S_E is made up of the anterior S_A and posterior S_B subsystems to obtain the transference:

$$\mathbf{S}_E = \mathbf{S}_B\mathbf{S}_A = \begin{pmatrix} A_B & B_B \\ C_B & D_B \end{pmatrix}\begin{pmatrix} A_A & B_A \\ C_A & D_A \end{pmatrix} = \begin{pmatrix} A_BA_A + B_BC_A & A_BB_A + B_BD_A \\ C_BA_A + D_BC_A & C_BB_A + D_BD_A \end{pmatrix} = \begin{pmatrix} A_E & B_E \\ C_E & D_E \end{pmatrix} \tag{5.2.10}$$

and for the compound systems of homogenous gap S_O upstream from the eye and either anterior subsystem S_A or eye S_E the transferences are:

$$\mathbf{S}_{OA} = \mathbf{S}_A\mathbf{S}_O = \begin{pmatrix} A_A & B_A \\ C_A & D_A \end{pmatrix}\begin{pmatrix} 1 & -\zeta_O \\ 0 & 1 \end{pmatrix} = \begin{pmatrix} A_A & -A_A\zeta_O + B_A \\ C_A & -C_A\zeta_O + D_A \end{pmatrix} = \begin{pmatrix} A_{OA} & B_{OA} \\ C_{OA} & D_{OA} \end{pmatrix}, \tag{5.2.11}$$

$$\mathbf{S}_{OE} = \mathbf{S}_B\mathbf{S}_{OA} = \begin{pmatrix} A_B & B_B \\ C_B & D_B \end{pmatrix}\begin{pmatrix} A_{OA} & B_{OA} \\ C_{OA} & D_{OA} \end{pmatrix}$$

$$= \begin{pmatrix} A_BA_{OA} + B_BC_{OA} & A_BB_{OA} + B_BD_{OA} \\ C_BA_{OA} + D_BC_{OA} & C_BB_{OA} + D_BD_{OA} \end{pmatrix} = \begin{pmatrix} A_{OE} & B_{OE} \\ C_{OE} & D_{OE} \end{pmatrix} \tag{5.2.12}$$

and

$$\mathbf{S}_{OE} = \mathbf{S}_E\mathbf{S}_O = \begin{pmatrix} A_E & B_E \\ C_E & D_E \end{pmatrix}\begin{pmatrix} 1 & -\zeta_O \\ 0 & 1 \end{pmatrix} = \begin{pmatrix} A_E & -A_E\zeta_O + B_E \\ C_E & -C_E\zeta_O + D_E \end{pmatrix} = \begin{pmatrix} A_{OE} & B_{OE} \\ C_{OE} & D_{OE} \end{pmatrix}. \tag{5.2.13}$$

A ray is traced from the object across the homogenous gap and through the anterior system to its ray state at the pupil to obtain

$$\mathbf{S}_{OA}\boldsymbol{\rho}_O = \boldsymbol{\rho}_P \tag{5.2.14}$$

and

$$A_{OA}y_O + B_{OA}\alpha_O = y_P \tag{5.2.15}$$

$$C_{OA}y_O + D_{OA}\,\alpha_O = \alpha_P. \tag{5.2.16}$$

Similarly from the pupillary plane to the retinal plane

$$\mathbf{S}_B\boldsymbol{\rho}_P = \boldsymbol{\rho}_R \tag{5.2.17}$$

and

$$A_By_P + B_B\alpha_P = y_R \tag{5.2.18}$$

$$C_By_P + D_B\alpha_P = \alpha_R. \tag{5.2.19}$$

Equation 5.2.15 is solved for α_O,

$$\alpha_{\mathrm{O}} = B_{\mathrm{OA}}^{-1} y_{\mathrm{P}} - B_{\mathrm{OA}}^{-1} A_{\mathrm{OA}} y_{\mathrm{O}} \tag{5.2.20}$$

and substituted into Equation 5.2.16 to obtain

$$\alpha_{\mathrm{P}} = C_{\mathrm{OA}} y_{\mathrm{O}} + D_{\mathrm{OA}} B_{\mathrm{OA}}^{-1} y_{\mathrm{P}} - D_{\mathrm{OA}} B_{\mathrm{OA}}^{-1} A_{\mathrm{OA}} y_{\mathrm{O}} . \tag{5.2.21}$$

From Equations 5.2.21 and 5.2.18 we obtain

$$y_{\mathrm{R}} = \left(A_{\mathrm{B}} + B_{\mathrm{B}} D_{\mathrm{OA}} B_{\mathrm{OA}}^{-1}\right) y_{\mathrm{P}} + \left(B_{\mathrm{B}} C_{\mathrm{OA}} - B_{\mathrm{B}} D_{\mathrm{OA}} B_{\mathrm{OA}}^{-1} A_{\mathrm{OA}}\right) y_{\mathrm{O}} .$$

Manipulating, we obtain

$$y_{\mathrm{R}} = \left(A_{\mathrm{B}} B_{\mathrm{OA}} + B_{\mathrm{B}} D_{\mathrm{OA}}\right) B_{\mathrm{OA}}^{-1} y_{\mathrm{P}} + B_{\mathrm{B}} \left(C_{\mathrm{OA}} - D_{\mathrm{OA}} B_{\mathrm{OA}}^{-1} A_{\mathrm{OA}}\right) y_{\mathrm{O}} .$$

From B_{OE}, Equation 5.2.12 and the third Schur complement (Equation 3.2.22) we obtain

$$y_{\mathrm{R}} = B_{\mathrm{OE}} B_{\mathrm{OA}}^{-1} y_{\mathrm{P}} - B_{\mathrm{B}} B_{\mathrm{OA}}^{-1} y_{\mathrm{O}} .$$

We make use here of the Schur compliment instead of the simpler unit determinant because of the generalisation we undertake in Section 5.2.5. Substituting equalities from Equations 5.2.11 and 13 into our equation we obtain

$$y_{\mathrm{R}} = \left(B_{\mathrm{E}} - A_{\mathrm{E}} \zeta_{\mathrm{O}}\right)\left(B_{\mathrm{A}} - A_{\mathrm{A}} \zeta_{\mathrm{O}}\right)^{-1} y_{\mathrm{P}} + B_{\mathrm{B}} \left(A_{\mathrm{A}} \zeta_{\mathrm{O}} - B_{\mathrm{A}}\right)^{-1} y_{\mathrm{O}} , \tag{5.2.22}$$

the transverse position of the ray at the retina.

Substituting from Equation 5.2.21 into Equation 5.2.19 to get rid of α_{P}, we obtain

$$\alpha_{\mathrm{R}} = \left(C_{\mathrm{B}} + D_{\mathrm{B}} D_{\mathrm{OA}} B_{\mathrm{OA}}^{-1}\right) y_{\mathrm{P}} + \left(D_{\mathrm{B}} C_{\mathrm{OA}} - D_{\mathrm{B}} D_{\mathrm{OA}} B_{\mathrm{OA}}^{-1} A_{\mathrm{A}}\right) y_{\mathrm{O}}$$

and manipulating,

$$\alpha_{\mathrm{R}} = \left(C_{\mathrm{B}} B_{\mathrm{OA}} + D_{\mathrm{B}} D_{\mathrm{OA}}\right) B_{\mathrm{OA}}^{-1} y_{\mathrm{P}} + D_{\mathrm{B}} \left(C_{\mathrm{OA}} - D_{\mathrm{OA}} B_{\mathrm{OA}}^{-1} A_{\mathrm{OA}}\right) y_{\mathrm{O}} .$$

From the equality for D_{OE} in Equation 5.2.12 and the third Schur complement (Equation 3.2.22) we obtain

$$\alpha_{\mathrm{R}} = D_{\mathrm{OE}} B_{\mathrm{OA}}^{-1} y_{\mathrm{P}} - D_{\mathrm{B}} B_{\mathrm{OA}}^{-1} y_{\mathrm{O}} .$$

Substituting equalities from Equation 5.2.11 and 13 into our equation we obtain

$$\alpha_{\mathrm{R}} = \left(D_{\mathrm{E}} - C_{\mathrm{E}} \zeta_{\mathrm{O}}\right)\left(B_{\mathrm{A}} - A_{\mathrm{A}} \zeta_{\mathrm{O}}\right)^{-1} y_{\mathrm{P}} + D_{\mathrm{B}} \left(A_{\mathrm{A}} \zeta_{\mathrm{O}} - B_{\mathrm{A}}\right)^{-1} y_{\mathrm{O}} , \tag{5.2.23}$$

the reduced inclination at the retina of the ray from the object. However, the unreduced inclination at the retina is required and so Equation 5.2.23 is rewritten

$$a_{\mathrm{R}} = \left(D_{\mathrm{E}} - C_{\mathrm{E}} \zeta_{\mathrm{O}}\right)\left(nB_{\mathrm{A}} - nA_{\mathrm{A}} \zeta_{\mathrm{O}}\right)^{-1} y_{\mathrm{P}} + D_{\mathrm{B}} \left(nA_{\mathrm{A}} \zeta_{\mathrm{O}} - nB_{\mathrm{A}}\right)^{-1} y_{\mathrm{O}} . \tag{5.2.24}$$

Equations 5.2.22 and 24 represent the physical (unreduced) state of the ray at the retinal plane for the ray from the object point at a finite working distance z_{O}. The equations are general and any ray could be chosen, including, for example, a chief ray or a marginal ray. This solution is summarized, in a similar layout to how we presented Harris's formulae in Equations 5.2.7 to 9, in terms of the system S_{OE} as defined in Equations 5.2.12 and 13 as

$$\mathbf{V}_{\mathrm{OE}}\mathbf{v}_{\mathrm{OE}} = \mathbf{r}_{\mathrm{R}} \tag{5.2.25}$$

where

$$\mathbf{V}_{\mathrm{OE}} = \begin{pmatrix} W_{\mathrm{OE}} & X_{\mathrm{OE}} \\ Y_{\mathrm{OE}} & Z_{\mathrm{OE}} \end{pmatrix} = \begin{pmatrix} \left(B_{\mathrm{E}} - A_{\mathrm{E}}\zeta_{\mathrm{O}}\right)\left(B_{\mathrm{A}} - A_{\mathrm{A}}\zeta_{\mathrm{O}}\right)^{-1} & B_{\mathrm{B}}\left(A_{\mathrm{A}}\zeta_{\mathrm{O}} - B_{\mathrm{A}}\right)^{-1} \\ \left(D_{\mathrm{E}} - C_{\mathrm{E}}\zeta_{\mathrm{O}}\right)\left(nB_{\mathrm{A}} - nA_{\mathrm{A}}\zeta_{\mathrm{O}}\right)^{-1} & D_{\mathrm{B}}\left(nA_{\mathrm{A}}\zeta_{\mathrm{O}} - nB_{\mathrm{A}}\right)^{-1} \end{pmatrix} \tag{5.2.26}$$

is the near coefficient matrix for system S_{OE} where the object point is at a finite working distance z_{O} from the eye, $\mathbf{r}_{\mathrm{R}}$ is defined by Equation 5.2.4 and

$$\mathbf{v}_{\mathrm{OE}} = \begin{pmatrix} y_{\mathrm{P}} \\ y_{\mathrm{O}} \end{pmatrix} \tag{5.2.27}$$

is an input vector for the system S_{OE}, from the object point at y_{O}, through the pupil at position y_{P}, to the retina. The entries in the top row of the near coefficient matrix $\mathbf{V}_{\mathrm{OE}}$ are unitless while the bottom row has units of inverse length. Multiplying Equation 5.2.25 out we obtain

$$W_{\mathrm{OE}}y_{\mathrm{P}} + X_{\mathrm{OE}}y_{\mathrm{O}} = y_{\mathrm{R}} \tag{5.2.28}$$

and

$$Y_{\mathrm{OE}}y_{\mathrm{P}} + Z_{\mathrm{OE}}y_{\mathrm{O}} = a_{\mathrm{R}}\,. \tag{5.2.29}$$

The near coefficient matrix exists provided $\left(B_{\mathrm{A}} - A_{\mathrm{A}}\zeta_{\mathrm{O}}\right)^{-1}$ exists. The coefficient matrix does not exist when $B_{\mathrm{A}} - A_{\mathrm{A}}\zeta_{\mathrm{O}} = 0$, which would imply that $B_{\mathrm{OA}} = 0$. In other words the coefficient matrix exists provided the object and iridial planes are not conjugate.

We note that the disjugacy B and divarication D appear to play a significant role in the magnification and blur of the system. Together the coefficient matrix $\mathbf{V}_{\mathrm{OE}}$ and input vector $\mathbf{v}_{\mathrm{OE}}$ define the position and unreduced

inclination of the pencil of rays at the retina for the system from an object at a finite distance. W_{OE} is the near image blur coefficient, X_{OE} is the near image size coefficient, Y_{OE} is the near directional spread coefficient, and Z_{OE} is the near directional coefficient.

Similar to our interpretation for distant objects, we can interpret Equation 5.2.28 for a system consisting of an eye and an object point at a finite distance upstream. If we wish to obtain the size Δy_R of the image at the exit plane corresponding to an object of size Δy_O for a Gaussian system, we follow the rays from the object through the same position through the pupil such that $y_{P1} = y_{P2}$ we obtain

$$y_{R2} - y_{R1} = W_{OE}(y_{P2} - y_{P1}) + X_{OE}(y_{O2} - y_{O1})$$

which simplifies to

$$\Delta y_R = X_{OE} \Delta y_O . \tag{5.2.30}$$

Equation 5.2.30 is linear in Δy_O and we consider the near image size coefficient, X_{OE} to be the transverse magnification of system S_{OE}.

For a single object point y_O, and a pupil of diameter Δy_P the size of the blur circle on the exit plane (from Equation 5.2.28) is

$$\Delta y_R = W_{OE} \Delta y_P . \tag{5.2.31}$$

The size of the blur circle is dependent on the size of the pupil and the near image blur coefficient W_{OE}. We can think of W_{OE} as a sort of blur-magnification.

One can interpret Equation 5.2.29 in a similar fashion for the angular spread of the rays at the retina Δa_R from an object of size Δy_O. For a Gaussian system, we follow the rays from the object through the same position in the pupil such that $y_{P1} = y_{P2}$ we obtain

$$\Delta a_R = Z_{OE} \Delta y_O \tag{5.2.32}$$

where Z_{OE} is the near directional coefficient. To obtain the angular spread of the blur across the retina produced from a single object point, we see that $\Delta y_O = 0$ and that the blur spread is a function of pupil size Δy_P

$$\Delta a_R = Y_{OE} \Delta y_P \tag{5.2.33}$$

where Y_{OE} is the near directional spread coefficient

The difference in inclinations of the rays reaching the retina has implications for the Stiles-Crawford effect (Smith and Atchison, 1997: 308; Atchison & Smith, 2000: 124-127; Stiles, 1939).

5.2.4 Eye with pinhole

Object at a finite distance

When a pinhole is held immediately in front of the cornea, the system and subsystems simplify. The plane of the pinhole is the partitioning plane, however, the system upstream of the pinhole is merely the homogenous gap of system S_O and the posterior system is that of the eye, S_E. The transference of the anterior subsystem S_A becomes the identity matrix and posterior subsystem S_B becomes S_E, the eye. The transverse position of the pinhole is the distance y_P from the optical axis and we assume that the pupil is sufficiently dilated to accommodate the chief ray through the pinhole. The near coefficient matrix $\mathbf{V}_{OE}$ therefore simplifies to

$$\mathbf{V}_{OE}^{P} = \begin{pmatrix} W_{OE}^{P} & X_{OE}^{P} \\ Y_{OE}^{P} & Z_{OE}^{P} \end{pmatrix} = \begin{pmatrix} A_E - B_E\zeta_O^{-1} & B_E\zeta_O^{-1} \\ n^{-1}\left(C_E - D_E\zeta_O^{-1}\right) & n^{-1}D_E\zeta_O^{-1} \end{pmatrix} \tag{5.2.34}$$

with the superscript P representing the specialisation for a pinhole in front of the eye. Equations 5.2.28 and 29 become

$$y_R = W_{OE}^{P} y_P + X_{OE}^{P} y_O \tag{5.2.35}$$

and

$$a_R = Y_{OE}^{P} y_P + Z_{OE}^{P} y_O . \tag{5.2.36}$$

Equations 5.2.28 and 29 still hold and are general for an eye with an object point at a finite distance, both with and without a pinhole. Equations 5.2.35 and 36 are the same as Equations 5.2.28 and 29 with the four coefficients merely simplifying, as shown in Equation 5.2.34, when a pinhole is placed in front of the eye. For this reason we shall refer to Equations 5.2.28 and 29 in all further discussions, and merely substitute from $\mathbf{V}_{OE}^{P}$ when appropriate.

Distant object

Similarly, for a distant object the coefficient matrix in Equation 5.2.8 simplifies to

$$\mathbf{V}_{\mathrm{E}}^{\mathrm{P}} = \begin{pmatrix} W_{\mathrm{E}}^{\mathrm{P}} & X_{\mathrm{E}}^{\mathrm{P}} \\ Y_{\mathrm{E}}^{\mathrm{P}} & Z_{\mathrm{E}}^{\mathrm{P}} \end{pmatrix} = \begin{pmatrix} A_{\mathrm{E}} & B_{\mathrm{E}} n_0 \\ n^{-1} C_{\mathrm{E}} & n^{-1} D_{\mathrm{E}} n_0 \end{pmatrix} \tag{5.2.37}$$

while Equation 5.2.9 remains unchanged. Equation 5.2.7 holds for the pinhole and the coefficients from Equation 5.2.37 may be substituted, when appropriate.

5.2.5 Generalizing to linear optics

In this section we have retained the order of multiplication and avoided division in an effort to allow the equations to generalize to linear optics for systems that have astigmatic elements. In Section 5.2.1 we can indeed generalize transverse and angular magnification to astigmatic systems. The equations in Sections 5.2.2 and 3 generalize, however we need to include a transpose which comes about from the symplectic equations (Equations 3.2.17 to 19) and the Schur compliments (Equations 3.2.20 to 23). We provide the linear generalizations below, the proofs following the format given in Section 5.2.3. Equation 5.2.8 becomes

$$\mathbf{V}_{\mathrm{E}} = \begin{pmatrix} \mathbf{W}_{\mathrm{E}} & \mathbf{X}_{\mathrm{E}} \\ \mathbf{Y}_{\mathrm{E}} & \mathbf{Z}_{\mathrm{E}} \end{pmatrix} = \begin{pmatrix} \mathbf{A}_{\mathrm{E}} \mathbf{A}_{\mathrm{A}}^{-1} & \mathbf{B}_{\mathrm{B}} \mathbf{A}_{\mathrm{A}}^{-\mathrm{T}} n_0 \\ n^{-1} \mathbf{C}_{\mathrm{E}} \mathbf{A}_{\mathrm{A}}^{-1} & n^{-1} \mathbf{D}_{\mathrm{B}} \mathbf{A}_{\mathrm{A}}^{-\mathrm{T}} n_0 \end{pmatrix} \tag{5.2.38}$$

and Equation 5.2.26 becomes

$$\mathbf{V}_{\mathrm{OE}} = \begin{pmatrix} \mathbf{W}_{\mathrm{OE}} & \mathbf{X}_{\mathrm{OE}} \\ \mathbf{Y}_{\mathrm{OE}} & \mathbf{Z}_{\mathrm{OE}} \end{pmatrix} = \begin{pmatrix} \left(\mathbf{B}_{\mathrm{E}} - \mathbf{A}_{\mathrm{E}} \zeta_{\mathrm{O}}\right)\left(\mathbf{B}_{\mathrm{A}} - \mathbf{A}_{\mathrm{A}} \zeta_{\mathrm{O}}\right)^{-1} & \mathbf{B}_{\mathrm{B}} \left(\mathbf{A}_{\mathrm{A}} \zeta_{\mathrm{O}} - \mathbf{B}_{\mathrm{A}}\right)^{-\mathrm{T}} \\ \left(\mathbf{D}_{\mathrm{E}} - \mathbf{C}_{\mathrm{E}} \zeta_{\mathrm{O}}\right)\left(n\mathbf{B}_{\mathrm{A}} - n\mathbf{A}_{\mathrm{A}} \zeta_{\mathrm{O}}\right)^{-1} & \mathbf{D}_{\mathrm{B}} \left(n\mathbf{A}_{\mathrm{A}} \zeta_{\mathrm{O}} - n\mathbf{B}_{\mathrm{A}}\right)^{-\mathrm{T}} \end{pmatrix}. \tag{5.2.39}$$

The transposes in the right-hand column of these two matrices fall away when we simplify for the situation of a pinhole in front of the eye and so the equations in Section 5.2.4 readily generalize to linear optics to include eyes with astigmatic elements.

5.3 Measurements in object space

From the literature review in Chapter 2, we saw how chromatic difference in position and chromatic difference in magnification are defined in physiological

optics. More specifically, we saw that when these measurements are taken experimentally, that the chromatic difference in object position occurs in object space and alignment is assumed at a position on the retina. Because such measurements are made in the clinical environment, we shall consider the scenario for finite distances only. Pinholes also feature often in such experiments.

The objective in this section is to derive formulae for the transverse position of an object point and the inclination of the ray incident onto the eye or pinhole when the position in the pupil or pinhole and the position at the retinal plane are known. Ultimately we keep the goal of deriving formulae for the chromatic difference in position or magnification in mind. These formulae will form the basis of the derivations for chromatic difference in position and magnification in Chapter 7.

5.3.1 Transverse position of an object point at a finite distance

We will start by deriving the formula for the transverse position of an object point at a finite distance upstream of the eye. We turn our attention to the system of the eye partitioned into anterior and posterior subsystems and object at finite distance upstream of the system illustrated in Figure 5.2.1 which we used in the previous section.

Because the system S_{OE} is the same as that described in Figure 5.2.1, with applicable subsystems S_{O}, S_{A}, S_{B} and combinations thereof, the equations that define S_{OE} and its subsystems, given by Equations 5.2.10 to 19, apply. Solving Equation 5.2.18 for α_{P} we obtain

$$\alpha_{\mathrm{P}} = B_{\mathrm{B}}^{-1} y_{\mathrm{R}} - B_{\mathrm{B}}^{-1} A_{\mathrm{B}} y_{\mathrm{P}} . \tag{5.3.1}$$

Substituting from Equation 5.2.21 into 5.3.1 and rearranging we obtain

$$\left(C_{\mathrm{OA}} - D_{\mathrm{OA}} B_{\mathrm{OA}}^{-1} A_{\mathrm{OA}}\right) y_{\mathrm{O}} = -\left(B_{\mathrm{B}}^{-1} A_{\mathrm{B}} + D_{\mathrm{OA}} B_{\mathrm{OA}}^{-1}\right) y_{\mathrm{P}} + B_{\mathrm{B}}^{-1} y_{\mathrm{R}} . \tag{5.3.2}$$

We make use of the third Schur compliment (Equation 3.2.22) and equalities in Equation 5.2.12 to simplify this equation to

$$-B_{\mathrm{OA}}^{-1} y_{\mathrm{O}} = -B_{\mathrm{B}}^{-1} B_{\mathrm{OE}} B_{\mathrm{OA}}^{-1} y_{\mathrm{P}} + B_{\mathrm{B}}^{-1} y_{\mathrm{R}} .$$

Hence

$$y_{\mathrm{O}} = B_{\mathrm{B}}^{-1} B_{\mathrm{OE}} y_{\mathrm{P}} - B_{\mathrm{OA}} B_{\mathrm{B}}^{-1} y_{\mathrm{R}} .$$

In terms of the distance of the object in front of the eye and the entries of the transferences of the eye, and anterior and posterior subsystems, this is

$$y_{\mathrm{O}} = B_{\mathrm{B}}^{-1}\left(B_{\mathrm{E}} - A_{\mathrm{E}}\zeta_{\mathrm{O}}\right)y_{\mathrm{P}} + \left(A_{\mathrm{A}}\zeta_{\mathrm{O}} - B_{\mathrm{A}}\right)B_{\mathrm{B}}^{-1}y_{\mathrm{R}}\,. \tag{5.3.3}$$

Equation 5.3.3 gives us the transverse position of the object point y_{O} at $\mathrm{T_O}$ of the ray through the pupil at transverse position y_{P} arriving at a position y_{R} on the retina.

Simplification when a pinhole is used

Similar to the scenario in Section 5.2.3, the transverse position of an object point at a finite distance in front of the eye simplifies when a pinhole is positioned immediately upstream of the corneal tear film. Equation 5.3.3 becomes

$$y_{\mathrm{O}} = \left(1 - B_{\mathrm{E}}^{-1}A_{\mathrm{E}}\zeta_{\mathrm{O}}\right)y_{\mathrm{P}} + \zeta_{\mathrm{O}}B_{\mathrm{E}}^{-1}y_{\mathrm{R}}\,. \tag{5.3.4}$$

5.3.2 Incident inclination measured in object space

We again turn our attention to Figure 5.2.1 and accompanying Equations 5.2.10 to 19. We wish to calculate the inclination in object space, a_{O} as a function of the ray, going through the pupil at y_{P} and reaching the retina at transverse position y_{R}. We solve Equation 5.2.15 for y_{O} to obtain

$$y_{\mathrm{O}} = A_{\mathrm{OA}}^{-1}y_{\mathrm{P}} - A_{\mathrm{OA}}^{-1}B_{\mathrm{OA}}\alpha_{\mathrm{O}} \tag{5.3.5}$$

which we substitute into Equation 5.2.16:

$$C_{\mathrm{OA}}A_{\mathrm{OA}}^{-1}y_{\mathrm{P}} - C_{\mathrm{OA}}A_{\mathrm{OA}}^{-1}B_{\mathrm{OA}}\alpha_{\mathrm{O}} + D_{\mathrm{OA}}\alpha_{\mathrm{O}} = \alpha_{\mathrm{P}}\,. \tag{5.3.6}$$

We now substitute from Equation 5.3.1 into Equation 5.3.6, simplify for A_{OA} and C_{OA} from Equation 5.2.11 and rearrange to obtain

$$\left(D_{\mathrm{OA}} - C_{\mathrm{OA}}A_{\mathrm{OA}}^{-1}B_{\mathrm{OA}}\right)\alpha_{\mathrm{O}} = -\left(B_{\mathrm{B}}^{-1}A_{\mathrm{B}} + C_{\mathrm{A}}A_{\mathrm{A}}^{-1}\right)y_{\mathrm{P}} + B_{\mathrm{B}}^{-1}y_{\mathrm{R}}\,. \tag{5.3.7}$$

Substituting the fourth Schur compliment (Equation 3.2.23) and equalities from Equations 5.2.10 into Equation 5.3.7 we obtain

$$A_{\mathrm{A}}^{-1}\alpha_{\mathrm{O}} = -B_{\mathrm{B}}^{-1}A_{\mathrm{E}}A_{\mathrm{A}}^{-1}y_{\mathrm{P}} + B_{\mathrm{B}}^{-1}y_{\mathrm{R}}$$

and, hence,

$$\alpha_{\mathrm{O}} = -B_{\mathrm{B}}^{-1}A_{\mathrm{E}}y_{\mathrm{P}} + A_{\mathrm{A}}B_{\mathrm{B}}^{-1}y_{\mathrm{R}}\,. \tag{5.3.8}$$

While there is an infinity of rays radiating from an object point, this equation singles out the reduced inclination of a single ray from an object point as a function of position in the pupil and at the retina. However, we need to calculate the equation for the unreduced inclination and so Equation 5.3.8 becomes

$$a_{\mathrm{O}} = -\left(n_0 B_{\mathrm{B}}\right)^{-1} A_{\mathrm{E}} y_{\mathrm{P}} + A_{\mathrm{A}} \left(B_{\mathrm{B}} n_0\right)^{-1} y_{\mathrm{R}} . \qquad (5.3.9)$$

Equation 5.3.9 gives the incident inclination of a ray, traversing a specific point in the pupil y_{P}, that will reach the retina at a predetermined transverse position y_{R}. The position through the pupil y_{P} may be chosen to be the chief ray where $y_{\mathrm{P}} = 0$; however the equation is general and any position can be chosen. For obvious reasons, the reduced working distance ζ_{O} and the transverse position y_{O} are both eliminated, implying that a_{O} is a more inclusive parameter to work with than the combination of y_{O} and ζ_{O}.

Simplification when a pinhole is used

The incident inclination from a finite object point to a position at the retina when a pinhole is placed immediately in front of the eye enables us to simplify Equation 5.3.9 to

$$a_{\mathrm{O}} = -\left(n_0 B_{\mathrm{E}}\right)^{-1} A_{\mathrm{E}} y_{\mathrm{P}} + \left(n_0 B_{\mathrm{E}}\right)^{-1} y_{\mathrm{R}} . \qquad (5.3.10)$$

Substituting from Equation 3.4.6 for the corneal-plane refractive compensation F_0 we see that the relationship in Equation 5.3.10 represents

$$a_{\mathrm{O}} = -n_0^{-1} F_0 y_{\mathrm{P}} + \left(n_0 B_{\mathrm{E}}\right)^{-1} y_{\mathrm{R}} . \qquad (5.3.11)$$

We mention in passing that for an emmetropic eye

$$a_{\mathrm{O}} = \left(n_0 B_{\mathrm{E}}\right)^{-1} y_{\mathrm{R}}$$

and the effect of the transverse position of the pinhole y_{P} in front of the emmetropic eye is nullified.

5.3.3 Summary of object space matrix equations with respect to position on the retina

Equations 5.3.3 and 9 are the two matrix equations that determine the incident transverse position and inclination that will result in the ray arriving at

the retina at a specific transverse position. Similarly to Section 3.5.3, we can summarise them as

$$\begin{pmatrix} B_{\mathrm{B}}^{-1}\left(B_{\mathrm{E}}-A_{\mathrm{E}}\zeta_{\mathrm{O}}\right) & \left(A_{\mathrm{A}}\zeta_{\mathrm{O}}-B_{\mathrm{A}}\right)B_{\mathrm{B}}^{-1} \\ -\left(n_0 B_{\mathrm{B}}\right)^{-1}A_{\mathrm{E}} & A_{\mathrm{A}}\left(B_{\mathrm{B}}n_0\right)^{-1} \end{pmatrix}\begin{pmatrix} y_{\mathrm{P}} \\ y_{\mathrm{R}} \end{pmatrix}=\begin{pmatrix} y_{\mathrm{O}} \\ a_{\mathrm{O}} \end{pmatrix} \tag{5.3.12}$$

which we shall abbreviate to

$$\mathbf{V}_{\mathrm{Oy}}\mathbf{v}_{\mathrm{Oy}}=\mathbf{r}_{\mathrm{O}} \tag{5.3.13}$$

where the subscript Oy indicates measurements that are made at a finite distance in front of the eye. $\mathbf{V}_{\mathrm{Oy}}$ is the coefficient matrix defined as

$$\mathbf{V}_{\mathrm{Oy}}=\begin{pmatrix} B_{\mathrm{B}}^{-1}\left(B_{\mathrm{E}}-A_{\mathrm{E}}\zeta_{\mathrm{O}}\right) & \left(A_{\mathrm{A}}\zeta_{\mathrm{O}}-B_{\mathrm{A}}\right)B_{\mathrm{B}}^{-1} \\ -\left(n_0 B_{\mathrm{B}}\right)^{-1}A_{\mathrm{E}} & A_{\mathrm{A}}\left(B_{\mathrm{B}}n_0\right)^{-1} \end{pmatrix}=\begin{pmatrix} W_{\mathrm{Oy}} & X_{\mathrm{Oy}} \\ Y_{\mathrm{Oy}} & Z_{\mathrm{Oy}} \end{pmatrix}, \tag{5.3.14}$$

$$\mathbf{v}_{\mathrm{Oy}}=\begin{pmatrix} y_{\mathrm{P}} \\ y_{\mathrm{R}} \end{pmatrix} \tag{5.3.15}$$

is the input vector and $\mathbf{r}_{\mathrm{O}}$ is the physical (unreduced) ray state at the object transverse plane T_{O} defined as

$$\mathbf{r}_{\mathrm{O}}=\begin{pmatrix} y_{\mathrm{O}} \\ a_{\mathrm{O}} \end{pmatrix}. \tag{5.3.16}$$

From Equation 5.3.12 we summarise Equations 5.3.3 and 9 as

$$y_{\mathrm{O}}=W_{\mathrm{Oy}}y_{\mathrm{P}}+X_{\mathrm{Oy}}y_{\mathrm{R}} \tag{5.3.17}$$

and

$$a_{\mathrm{O}}=Y_{\mathrm{Oy}}y_{\mathrm{P}}+Z_{\mathrm{Oy}}y_{\mathrm{R}}. \tag{5.3.18}$$

Simplification when pinhole is used

Similar to Section 5.2.4, we can summarise Equations 5.3.4 and 10 in the form given in Equation 5.3.14 for a system comprising an eye, given a specific position or inclination of an object point a finite distance upstream of the eye, to obtain the transverse position at the retina when a pinhole is held immediately in front of the corneal tear film. Equation 5.3.12 simplifies to

$$\begin{pmatrix} 1-B_{\mathrm{E}}^{-1}A_{\mathrm{E}}\zeta_{\mathrm{O}} & \zeta_{\mathrm{O}}B_{\mathrm{E}}^{-1} \\ -\left(n_0 B_{\mathrm{E}}\right)^{-1}A_{\mathrm{E}} & \left(n_0 B_{\mathrm{E}}\right)^{-1} \end{pmatrix}\begin{pmatrix} y_{\mathrm{P}} \\ y_{\mathrm{R}} \end{pmatrix}=\begin{pmatrix} y_{\mathrm{O}} \\ a_{\mathrm{O}} \end{pmatrix} \tag{5.3.19}$$

which we summarise as

$$\mathbf{V}_{\mathrm{Oy}}^{\mathrm{P}}\mathbf{v}_{\mathrm{Oy}} = \mathbf{r}_{\mathrm{O}} \tag{5.3.20}$$

and similar to Equation 5.2.34 the coefficient matrix in Equation 5.3.20 is given a superscript P to indicate the use of a pinhole immediately in front of the corneal tear film.

Comment on $\mathbf{V}_{\mathrm{Oy}}$ *and* $\mathbf{V}_{\mathrm{Oy}}^{\mathrm{P}}$

We need to consider for a moment the existence of $\mathbf{V}_{\mathrm{Oy}}$ and $\mathbf{V}_{\mathrm{Oy}}^{\mathrm{P}}$. We can see from Equation 5.3.12 that they exist provided $B_{\mathrm{B}} \neq 0$, or in the case of a pinhole in front of the eye (Equation 5.3.19), where $B_{\mathrm{E}} \neq 0$. The equations hold except in the unlikely situation in which the aperture and the retina are conjugate.

5.3.4 Summary of object space matrix equations with respect to inclination at the retina

When measurements are taken in object space and the corresponding images are perceived to be in alignment by the subject's eye, the physiological optics theory is that the two image points coincide on the retina. That is to say, the rays arrive at the retina at the same transverse position. In the literature review, there was no evidence of any theories that aligned the inclination at the retina from two object points, only the transverse position on the retina. Therefore we conclude that the derivations in object space with respect to transverse position at the retina are considered to be more important than those with respect to inclination at the retina.

Similar to the matrix equations derived in Section 5.3.3 which were obtained with respect to a position at the retinal plane, we can derive equations with respect to the inclination of a ray arriving at the retina. This has implications for the Stiles-Crawford effect. For completeness the summary of these formulae are given in Equations 5.3.21 and 22 below. It is quite possible for two rays of different frequency to arrive at the retina with the same inclination, but may or may not arrive at the same position. The exact implications of this are outside the scope of this dissertation.

The equation for the physical state of a ray $\mathbf{r}_{\mathrm{O}}$ at the object plane in order for that ray traversing the pupil at transverse position y_{P} to arrive at the retina with a certain emergent inclination a_{R} is

$$\begin{pmatrix} (D_{\mathrm{E}} - C_{\mathrm{E}}\zeta_{\mathrm{O}})D_{\mathrm{B}}^{-1} & n(A_{\mathrm{A}}\zeta_{\mathrm{O}} - B_{\mathrm{A}})D_{\mathrm{B}}^{-1} \\ -C_{\mathrm{E}}(D_{\mathrm{B}}n_0)^{-1} & nA_{\mathrm{A}}(D_{\mathrm{B}}n_0)^{-1} \end{pmatrix} \begin{pmatrix} y_{\mathrm{P}} \\ a_{\mathrm{R}} \end{pmatrix} = \begin{pmatrix} y_{\mathrm{O}} \\ a_{\mathrm{O}} \end{pmatrix} \tag{5.3.21}$$

or

$$\mathbf{V}_{\mathrm{Oa}}\mathbf{v}_{\mathrm{Oa}} = \mathbf{r}_{\mathrm{O}}. \tag{5.3.22}$$

Simplification when pinhole is used

Similar to Section 5.2.4 we can summarise for a system comprising an eye, given a specific position or inclination of an object point a finite distance upstream of the eye, to obtain the inclination at the retina when a pinhole is held immediately in front of the corneal tear film. Equation 5.3.21 simplifies to

$$\begin{pmatrix} (D_{\mathrm{E}} - C_{\mathrm{E}}\zeta_{\mathrm{O}})D_{\mathrm{E}}^{-1} & \zeta_{\mathrm{O}}D_{\mathrm{E}}^{-1}n \\ -C_{\mathrm{E}}(D_{\mathrm{E}}n_0)^{-1} & (D_{\mathrm{E}}n_0)^{-1}n \end{pmatrix} \begin{pmatrix} y_{\mathrm{P}} \\ a_{\mathrm{R}} \end{pmatrix} = \begin{pmatrix} y_{\mathrm{O}} \\ a_{\mathrm{O}} \end{pmatrix} \tag{5.3.23}$$

or

$$\mathbf{V}_{\mathrm{Oa}}^{\mathrm{P}}\mathbf{v}_{\mathrm{Oa}} = \mathbf{r}_{\mathrm{O}}. \tag{5.3.24}$$

Comment on $\mathbf{V}_{\mathrm{Oa}}$ *and* $\mathbf{V}_{\mathrm{Oa}}^{\mathrm{P}}$

The relationships derived in Equation 5.3.21 and 23 exist provided $D_B \neq 0$ or $D_E \neq 0$ in the case of a pinhole in front of the system. This would require the system to be entrance-plane focal which seems unlikely in a system comprising an eye and in most eyes D_B and D_E are close to 1.

5.3.5 Generalising to linear optics

The proofs provided in Section 5.3 involve the use of division and Schur compliments whilst at the same time ignoring the order of multiplication and the transpose. Therefore the results cannot be readily generalized to linear optics. However, the resultant generalised coefficient matrices are provided below, without detailed proofs. Equation 5.3.14 becomes

$$\mathbf{V}_{\mathrm{Oy}} = \begin{pmatrix} \left(\mathbf{B}_{\mathrm{A}} - \mathbf{A}_{\mathrm{A}}\zeta_{\mathrm{O}}\right)^{\mathrm{T}}\mathbf{B}_{\mathrm{B}}^{-1}\left(\mathbf{B}_{\mathrm{E}} - \mathbf{A}_{\mathrm{E}}\zeta_{\mathrm{O}}\right)\left(\mathbf{B}_{\mathrm{A}} - \mathbf{A}_{\mathrm{A}}\zeta_{\mathrm{O}}\right)^{-1} & \left(\mathbf{A}_{\mathrm{A}}\zeta_{\mathrm{O}} - \mathbf{B}_{\mathrm{A}}\right)^{\mathrm{T}}\mathbf{B}_{\mathrm{B}}^{-1} \\ -\mathbf{A}_{\mathrm{A}}^{\mathrm{T}}\left(n_0\mathbf{B}_{\mathrm{B}}\right)^{-1}\mathbf{A}_{\mathrm{E}}\mathbf{A}_{\mathrm{A}}^{-1} & \mathbf{A}_{\mathrm{A}}^{\mathrm{T}}\left(\mathbf{B}_{\mathrm{B}}n_0\right)^{-1} \end{pmatrix}$$

$$= \begin{pmatrix} \mathbf{W}_{\mathrm{Oy}} & \mathbf{X}_{\mathrm{Oy}} \\ \mathbf{Y}_{\mathrm{Oy}} & \mathbf{Z}_{\mathrm{Oy}} \end{pmatrix}. \qquad (5.3.25)$$

Equations 5.3.13, 15, 19 and 20 readily generalise to linear optics. Specifically, Equation 5.3.19 becomes

$$\begin{pmatrix} \mathbf{I} - \mathbf{B}_{\mathrm{E}}^{-1}\mathbf{A}_{\mathrm{E}}\zeta_{\mathrm{O}} & \zeta_{\mathrm{O}}\mathbf{B}_{\mathrm{E}}^{-1} \\ -\left(n_0\mathbf{B}_{\mathrm{E}}\right)^{-1}\mathbf{A}_{\mathrm{E}} & \left(n_0\mathbf{B}_{\mathrm{E}}\right)^{-1} \end{pmatrix}\begin{pmatrix} \mathbf{y}_{\mathrm{P}} \\ \mathbf{y}_{\mathrm{R}} \end{pmatrix} = \begin{pmatrix} \mathbf{y}_{\mathrm{O}} \\ \mathbf{a}_{\mathrm{O}} \end{pmatrix}. \qquad (5.3.26)$$

5.4 Cardinal points

The simplification made in ray tracing using the cardinal points relates the conjugal relationship between an object point and its image point but does not reveal what is actually happening inside the system. Linear optics makes no use of cardinal points for its calculations and is true paraxial ray tracing through the system.

5.4.1 Additional relationships among the points

In Section 3.6.3 we looked at the relationships among the cardinal points including the anti-cardinal points. We wish to extend these relationships and attempt to find simpler equations to represent the distances of the points from the entrance and exit plane and between the various points. The symbols used here are consistent with those introduced in Section 3.6.2 and Table 3.6.1.

Starting with the incident anti-cardinal points we find the equation for the distance from the entrance plane to the respective point can simplify further from the equalities given in Equations 3.6.3 and 4 to

$$z_{\bar{\mathrm{N}}0} = n_0C^{-1}D + nC^{-1} = z_{\mathrm{F}0} + nC^{-1}, \qquad (5.4.1)$$

$$z_{\bar{\mathrm{P}}0} = n_0C^{-1}D + n_0C^{-1} = z_{\mathrm{F}0} + n_0C^{-1} \qquad (5.4.2)$$

and similarly the equations for the distance of each emergent anti-cardinal point from the exit plane to the respective anti-cardinal point simplify from Equations 3.6.8 and 9 to

$$z_{\bar{\mathrm{N}}} = -nC^{-1}A - n_0C^{-1} = z_{\mathrm{F}} - n_0C^{-1} \qquad (5.4.3)$$

and

$$z_{\bar{\mathrm{P}}} = -nC^{-1}A - nC^{-1} = z_{\mathrm{F}} - nC^{-1}. \tag{5.4.4}$$

There are a number of relationships among the various cardinal and anti-cardinal points which are presented in summary in Equations 5.4.5 to 11 and corresponding to Figure 5.4.1. For completeness, we include the equalities given in Equations 3.6.13 to 16 and add additional equalities which include those that extend to the anti-cardinal points in Equations 5.4.5 to 8. We retain the symbolism introduced in Table 3.6.1. The equalities are illustrated in Figure 5.4.1 and the corresponding arrow colour is given in brackets for each. The incident equivalent focal length (blue) is therefore

$$f_{0eq} = \mathrm{P}_0\mathrm{F}_0 = \mathrm{FN} = \mathrm{F}_0\bar{\mathrm{P}}_0 = \bar{\mathrm{N}}\mathrm{F} = n_0C^{-1} \tag{5.4.5}$$

and similarly, the emergent equivalent focal length (orange) is

$$f_{eq} = \mathrm{PF} = \mathrm{F}_0\mathrm{N}_0 = \bar{\mathrm{N}}_0\mathrm{F}_0 = \mathrm{F}\bar{\mathrm{P}} = -nC^{-1}. \tag{5.4.6}$$

Pascal's (1950a, b) equalities for "equivalent" radius (green) and "thickness" (red) can be extended to

$$r_{eq} = \mathrm{P}_0\mathrm{N}_0 = \mathrm{PN} = \bar{\mathrm{N}}_0\bar{\mathrm{P}}_0 = \bar{\mathrm{N}}\bar{\mathrm{P}} = (n_0 - n)C^{-1} = f_{0eq} + f_{eq}, \tag{5.4.7}$$

and

$$\mathrm{z}_{eq} = \mathrm{P}_0\mathrm{P} = \mathrm{N}_0\mathrm{N} = z + z_{\mathrm{F}} - z_{\mathrm{F}0} + (n_0 + n)C^{-1} = z + z_{\mathrm{F}} - z_{\mathrm{F}0} + f_{0eq} - f_{eq} \tag{5.4.8}$$

respectively. We now derive some equalities involving the anti-cardinal points (violet)

$$\bar{\mathrm{P}}_0\bar{\mathrm{P}} = \bar{\mathrm{N}}_0\bar{\mathrm{N}} = z + z_{\mathrm{F}} - z_{\mathrm{F}0} - (n + n_0)C^{-1} = z + z_{\mathrm{F}} - z_{\mathrm{F}0} + f_{eq} - f_{0eq}. \tag{5.4.9}$$

From the above equalities we can also see (−2*blue)

$$\bar{\mathrm{P}}_0\mathrm{P}_0 = \mathrm{N}\bar{\mathrm{N}} = -2f_{0eq} \tag{5.4.10}$$

and (2*orange)

$$\bar{\mathrm{N}}_0\mathrm{N}_0 = \mathrm{P}\bar{\mathrm{P}} = 2f_{eq}. \tag{5.4.11}$$

For completeness and to compare to some of the above equalities we note that, while the incident to the emergent focal points (cyan) are not conjugate with each other, the distance from F_0 to F is

$$\mathrm{F}_0\mathrm{F} = z + z_{\mathrm{F}} - z_{\mathrm{F}0}. \tag{5.4.12}$$

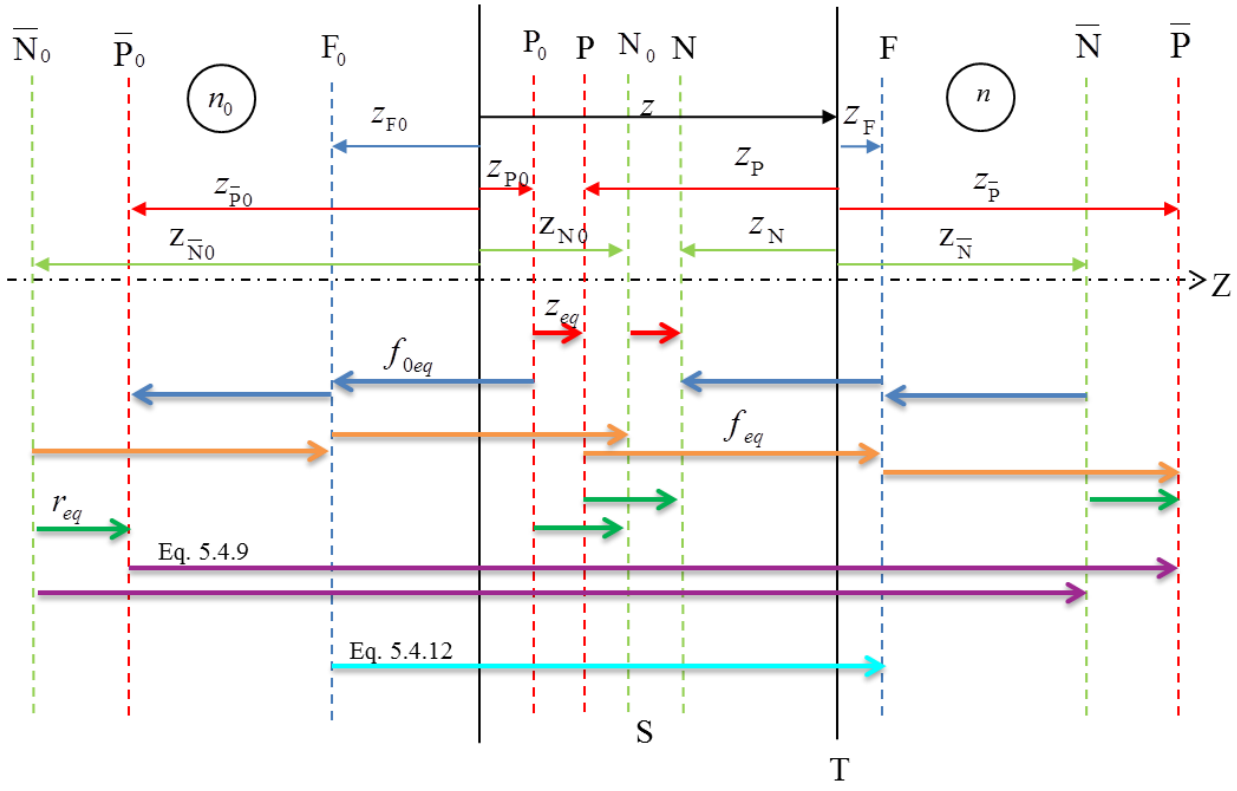

Figure 5.4.1 Cardinal points and their relationships and equalities. General Gaussian system S of length *z* has an entrance plane T_0, an exit plane T and a longitudinal axis Z. Refractive index upstream n_0 is different from *n* downstream. Points are defined as being on the optical axis for a Gaussian system. The distances from the entrance plane to the incident cardinal point and from the exit plane to the emergent cardinal point are shown in the section above the longitudinal axis, with the thin arrows. All the symbols and subscripts are given in Table 3.6.1. The equalities are shown below the longitudinal axis as follows: the equivalent "thickness" z_{eq} (red), incident equivalent focal length f_{0eq} (blue), emergent equivalent length f_{eq} (orange), equivalent radius of curvature r_{eq} (green), Equation 5.4.9 (violet) and Equation 5.4.12 (cyan). Equation 5.4.10 (blue) and 11 (orange) can also be seen from the diagram.

Symmetry points

In Section 3.6.2, we saw that Keating defines symmetry points as the case where lateral magnification is –1. This occurs when the object is at twice the incident equivalent focal length and the image is at twice the emergent equivalent focal length, which we can see from Equations 5.4.10 and 11, respectively. From Figure 5.4.1 this is quite clearly at the position of the incident and emergent anti-principal points.

In order to prove this statement, we need to prove that, firstly, the incident and emergent anti-principal planes are conjugate and secondly, the magnification is –1. We start by obtaining the transference of the compound system from $\overline{\mathrm{P}}_0$ to $\overline{\mathrm{P}}$ as follows

$$\mathbf{S}_{\overline{\mathrm{P}}}\mathbf{S}\mathbf{S}_{\overline{\mathrm{P}}_0} = \begin{pmatrix} 1 & \frac{z_{\overline{\mathrm{P}}}}{n} \\ 0 & 1 \end{pmatrix} \begin{pmatrix} A & B \\ C & D \end{pmatrix} \begin{pmatrix} 1 & \frac{-z_{\overline{\mathrm{P}}_0}}{n_0} \\ 0 & 1 \end{pmatrix}.$$

Substituting from Equations 3.6.4 and 9 we obtain

$$\mathbf{S}_{\overline{\mathrm{P}}}\mathbf{S}\mathbf{S}_{\overline{\mathrm{P}}_0} = \begin{pmatrix} 1 & -\frac{A+1}{C} \\ 0 & 1 \end{pmatrix} \begin{pmatrix} A & B \\ C & D \end{pmatrix} \begin{pmatrix} 1 & -\frac{D+1}{C} \\ 0 & 1 \end{pmatrix}.$$

Multiplying out and substituting from the symplectic equation (Equation 3.2.24) we obtain

$$\mathbf{S}_{\overline{\mathrm{P}}}\mathbf{S}\mathbf{S}_{\overline{\mathrm{P}}_0} = \begin{pmatrix} -1 & 0 \\ C & -1 \end{pmatrix}.$$

From the definition of a conjugate system (Section 3.3.2) we see that this compound system is conjugate and secondly from Equation 5.2.1 we can see that transverse magnification has negative unit magnification ($M_{\mathrm{t}} = A = -1$).

Conjugacy of the anti-nodal planes

Similarly, we can show that the transference of the compound system from the incident to emergent anti-nodal planes is

$$\mathbf{S}_{\overline{\mathrm{N}}}\mathbf{S}\mathbf{S}_{\overline{\mathrm{N}}_0} = \begin{pmatrix} -\frac{n_0}{n} & 0 \\ C & -\frac{n}{n_0} \end{pmatrix},$$

which confirms that the two planes are conjugate and the transverse magnification is $-\frac{n_0}{n}$.

The lengths and directions of each of the incident and emergent cardinal and anti-cardinal points are shown in Figure 5.4.1 in the section above the optical axis. Lengths are given as *z* with subscripts given in Table 3.6.1. Below the

longitudinal axis, the thicker arrows denote the equalities. From Figure 5.4.1, the equalities given in Equations 3.6.13 to 16 and 5.4.5 to 12 can be seen.

5.4.2 Graphical construction, locator lines and anti-cardinal points

In Section 3.6.4 we saw how to obtain the slope and position of the incident and emergent locator lines and to use these to obtain the six cardinal points. We now expand this method to obtain the positions of the four anti-cardinal points. To find the location of the incident anti-cardinal points along the optical axis, one draws a horizontal line at the value for the characteristic X in T_0 (from Table 3.6.1) and where it intersects the incident locator line L_0 one constructs a vertical line to intersect with Z which is the position of the respective incident anti-cardinal point. Similarly, for the emergent anti-cardinal points, one

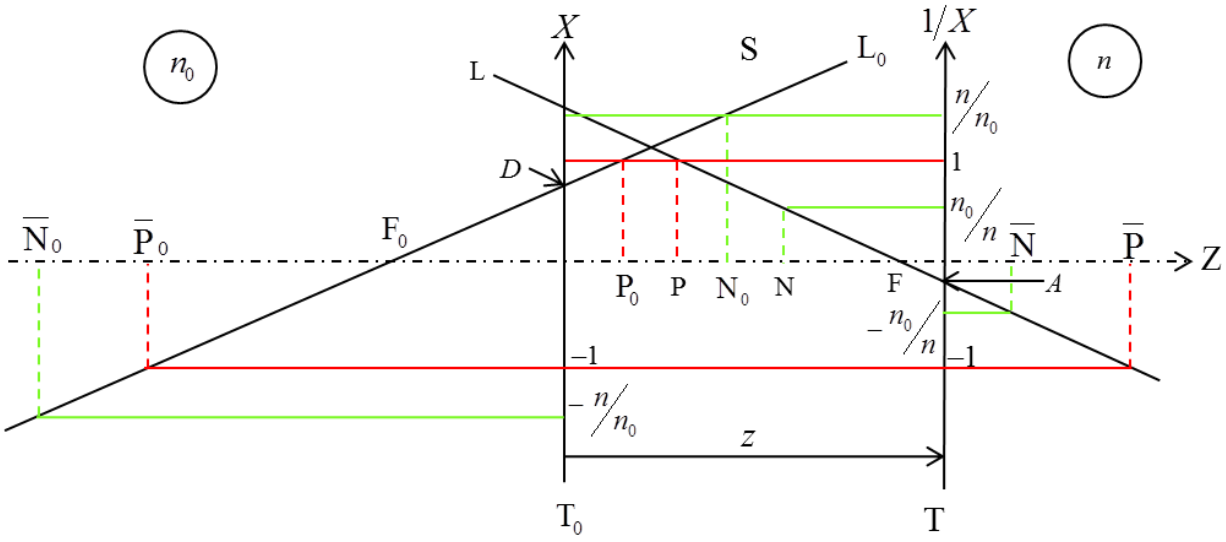

Figure 5.4.2 Graphical representation of a Gaussian optical system showing the locator lines for system S (not to scale). Line L_0 represents Equation 3.6.20 and line L Equation 3.6.21. Axis X is superimposed on entrance plane T_0 and axis $1/X$ on exit plane T, a distance z downstream from T_0. The focal points are on the optical axis Z at intersection with the corresponding locator line. The principal and anti-principal points are shown in red and the nodal and anti-nodal points in green. All symbols are described in Table 3.6.1. All incident points show intersection with the incident locator line and have subscript 0, while the emergent points intersect the emergent locator line L with no subscript.

draws a horizontal line for the value of $\frac{1}{X}$ in T and constructs a vertical line from the intersection with the emergent locator line L to Z.

From Figure 5.4.2 we note that the values of X and $1/X$ are positive for the cardinal points and negative for the anti-cardinal points. The construction is simple enough to be drawn by hand, however the scales on the axes have to be drawn accurately and for a system that includes an eye the scale on the vertical axis needs to be exaggerated. Numerical examples are given in Appendix 1.

5.4.3 Pascal's ring and anti-cardinal points

In Section 3.6.5 we saw how Pascal (1939, 1947, 1950a, b) described a memory scheme as an aid to memorizing the equalities between the six cardinal points. Harris (2011a) extended Pascal's ring and gave the equalities direction and gave proofs for the equalities. Here we extend Pascal's ring further to include the four anti-cardinal points.

In Figure 5.4.1 we see the relationships among the six cardinal points as well as the four anti-cardinal points. In Figure 5.4.3 we see Pascal's ring extended to include the equalities and relationships among the cardinal and anti-cardinal points. We retain Pascal's guideline that distances represented by parallel lines are equal.

The relationships among the cardinal and anti-cardinal points are illustrated in Figure 5.4.3. For example, the four blue arrows represent equal distances given by Equation 5.4.5 each representing $-f_{0eq}$. Equation 5.4.10 shows the equality $\overline{\mathrm{P}}_0\mathrm{P}_0 = \mathrm{N}\overline{\mathrm{N}} = -2f_{0eq}$ for two consecutive blue arrows. Similarly for the orange arrows and f_{eq}. The other colours represent red z_{eq}, green r_{eq} and violet the distance between incident and emergent anti-nodal or anti-principal points. This emphasises what can be seen in Figure 5.4.1. If we consider any one of the green arrows (r_{eq}), we can see that this is equivalent to an orange arrow (f_{eq}) minus a blue arrow ($-f_{0eq}$), which is given in Equation 5.4.7. One final example is to follow the violet arrow from which we can see that this makes up a combination of two orange, one red and two blue arrows. Any

such combination of equalities can be traced by following the arrows in Pascal's ring.

However the power of Pascal's ring lies not only in its use as a memory schema, but also in its ability to show changes in the positions of the points with respect to each other. Because Pascal's ring is not drawn to scale, the movements of the positions of the points are "magnified" and one is able to see how the changes to the system affect the locations of the points.

In order to gain a better understanding of the data, a number of familiar changes in the eye are demonstrated using the Bennett and Rabbetts schematic eye (Rabbetts, 2007: 225). These four numerical examples are given in Appendix 1. The example compares an emmetropic (relaxed) eye with a myopic eye and a hyperopic eye for changes in, firstly, axial length and, secondly, corneal curvature. The third example compares the emmetropic eye to changes due to accommodation and finally a young emmetropic eye is compared to its elderly counterpart. The first two changes are simple changes while the second two are compound changes. Refractive compensation does not form part of this study.

The purpose of the examples is to gain an understanding of the changes in the cardinal and anti-cardinal points arising because of various changes in a system, in particular, using the two models that we have just discussed, graphical construction and Pascal's ring. The examples should facilitate insight into the

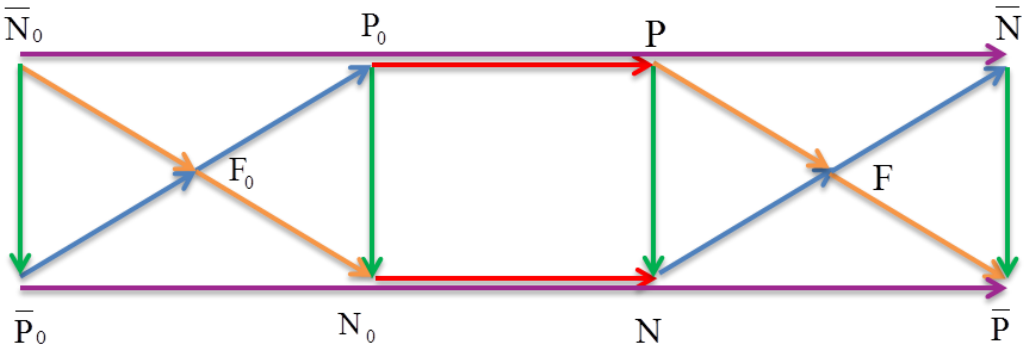

Figure 5.4.3 Pascal's ring showing the equalities and their directions and extended to include the anti-cardinal points. Arrows that are the same colour are equal in length and are either parallel or follow the same direction. The same colour-coding has been maintained as in Figure 5.4.1. Equations 5.4.5 to 12 give the equalities and formulae from the transference. The direction of the blue arrow has been reversed to represent $-f_{0eq}$.

changes in the cardinal points that occur in the eye due to change in the frequency of light, which will be examined in Section 9.1, using the two models.

5.5 Transferences of the two model eyes

The reduced eye is a simple eye and to derive its transference is a simple task because it is the product of only two elementary transferences. The transference of the reduced eye is then obtained using the parameters originally given by Emsley (Section 4.1.3), showing it to be emmetropic. However, we are interested in the dependence of the properties of the two model eyes on the frequency of light and so the transference of the reduced eye is derived as a function of the refractive index of the medium.

Le Grand's eye, on the other hand, is a four-surface eye and its transference is the product of eight elementary transferences. We therefore separate the derivation into anterior and posterior sub-systems, but deriving a single expression for the transference is impractical because the product does not simplify. Similarly, deriving a single expression for the transference for Le Grand's eye as a function of refractive index meets with the same difficulty; there are four media, each with a different refractive index. The transference is calculated for Le Grand's eye using his original parameters and refractive indices and is shown to be emmetropic.

5.5.1 The transference of the reduced eye

To calculate the transference for Emsley's reduced eye, one makes use of Equations 3.2.36 and 37 which we multiply in reverse to obtain the formula for the transference of the reduced eye

$$\mathbf{S}=\begin{pmatrix} 1-\dfrac{z}{n}\left(\dfrac{n-n_0}{r}\right) & \dfrac{z}{n} \\ \dfrac{n-n_0}{-r} & 1 \end{pmatrix}. \qquad (5.5.1)$$

We substitute the values for Emsley's reduced eye given in Section 4.1.3 to obtain the transference of the emmetropic reduced eye

$$\mathbf{S} = \begin{pmatrix} 0 & \frac{50}{3}\,\text{mm} \\ -0.060\,\text{kD} & 1 \end{pmatrix}. \qquad (5.5.2)$$

It is apparent that because $A = 0$ that this is an exit-plane focal system and that the eye is emmetropic with a power of 60 D. Furthermore it has a reduced length of 50/3 mm (or 1/60 m). Divarication *D* is 1 for a reduced eye.

5.5.2 The transference of the reduced eye as a function of refractive index

The variable affected by frequency of light is the refractive index *n*. We substitute the radius of curvature and length of Emsley's reduced eye into Equation 5.5.1 and simplify to obtain the transference for the reduced eye (Evans and Harris, 2011)

$$\mathbf{S} = \begin{pmatrix} \frac{4n_0}{n} - 3 & \frac{200}{9n}\,\text{mm} \\ -\frac{9}{50}(n - n_0)\,\text{kD} & 1 \end{pmatrix} \qquad (5.5.3)$$

where n_0 is the refractive index of air and *n* is the refractive index of the reduced eye. *n* is calculated using Equation 4.4.2. From Equation 5.5.3 we see that dilation *A*, disjugacy *B* and divergence *C* each depend on frequency. The refractive index of the surrounding medium n_0 has an effect only on *A* and *C*. The divarication *D* is constant and equals 1 for all reduced eyes.

5.5.3 The transference of Le Grand's eye

To obtain the transference of Le Grand's eye we substitute from Equations 3.2.36 and 37 as is appropriate and then multiplying in reverse according to Equation 3.2.6. We determine the transference for the anterior and posterior sub-systems and then the transference for the eye itself. The subscripts given correspond to those given in Figure 4.1.2 and Table 4.1.1. Starting with the anterior sub-system (A) we obtain

$$\mathbf{S}_{\text{A}} = \mathbf{S}_{\text{Aq}}\mathbf{S}_{\text{K2}}\mathbf{S}_{\text{K}}\mathbf{S}_{\text{K1}} \qquad (5.5.4)$$

and hence

$$\mathbf{S}_{\mathrm{A}} = \begin{pmatrix} 1 & \frac{z_{\mathrm{Aq}}}{n_{\mathrm{Aq}}} \\ 0 & 1 \end{pmatrix} \begin{pmatrix} 1 & 0 \\ \frac{n_{\mathrm{Aq}} - n_{\mathrm{K}}}{-r_{\mathrm{K2}}} & 1 \end{pmatrix} \begin{pmatrix} 1 & \frac{z_{\mathrm{K}}}{n_{\mathrm{K}}} \\ 0 & 1 \end{pmatrix} \begin{pmatrix} 1 & 0 \\ \frac{n_{\mathrm{K}} - n_0}{-r_{\mathrm{K1}}} & 1 \end{pmatrix}. \tag{5.5.5}$$

Similarly we derive the formula for the posterior sub-system (B)

$$\mathbf{S}_{\mathrm{B}} = \mathbf{S}_{\mathrm{V}}\mathbf{S}_{\mathrm{L2}}\mathbf{S}_{\mathrm{L}}\mathbf{S}_{\mathrm{L1}}, \tag{5.5.6}$$

and

$$\mathbf{S}_{\mathrm{B}} = \begin{pmatrix} 1 & \frac{z_{\mathrm{V}}}{n_{\mathrm{V}}} \\ 0 & 1 \end{pmatrix} \begin{pmatrix} 1 & 0 \\ \frac{n_{\mathrm{V}} - n_{\mathrm{L}}}{-r_{\mathrm{L2}}} & 1 \end{pmatrix} \begin{pmatrix} 1 & \frac{z_{\mathrm{L}}}{n_{\mathrm{L}}} \\ 0 & 1 \end{pmatrix} \begin{pmatrix} 1 & 0 \\ \frac{n_{\mathrm{L}} - n_{\mathrm{Aq}}}{-r_{\mathrm{L1}}} & 1 \end{pmatrix}. \tag{5.5.7}$$

We can now obtain the transference of Le Grand's eye as

$$\mathbf{S} = \mathbf{S}_{\mathrm{B}}\mathbf{S}_{\mathrm{A}}. \tag{5.5.8}$$

This can also be formulated in one step as

$$\mathbf{S} = \mathbf{S}_{\mathrm{V}}\mathbf{S}_{\mathrm{L2}}\mathbf{S}_{\mathrm{L}}\mathbf{S}_{\mathrm{L1}}\mathbf{S}_{\mathrm{Aq}}\mathbf{S}_{\mathrm{K2}}\mathbf{S}_{\mathrm{K}}\mathbf{S}_{\mathrm{K1}}. \tag{5.5.9}$$

This is the general transference of any four-surface schematic eye.

To calculate the transference for Le Grand's eye we substitute the values from Table 4.1.1 into Equation 5.5.9 and then multiplying out we obtain

$$\mathbf{S} = \begin{pmatrix} 0 & 16.6832\ \mathrm{mm} \\ -0.0599\ \mathrm{kD} & 0.9044 \end{pmatrix}. \tag{5.5.10}$$

That $A = 0$ implies an emmetropic eye. Its power is 59.9404D which is the same as given by Le Grand (1945: 48).

5.5.4 The transference of Le Grand's eye as a function of refractive index

Calculating the transference of the Le Grand eye as a function of refractive index is somewhat more complicated and does not simplify like Equation 5.5.3 for the reduced eye. Therefore the transference for each frequency needs to be calculated using Equation 5.5.9 each time.

5.5.5 The refractive indices of the reduced eye and Le Grand's eye for the six reference frequencies

The numerical values for the refractive indices of each of the media for the six reference points are given in tabular form for both the reduced and Le Grand's

Table 5.5.1 **S**ix reference colours, their frequencies υ, vacuum wavelengths λ, refractive indices for the reduced eye using Thibos *et al*'s equation (Equation 4.4.2) and refractive indices for the four media for the Le Grand eye using the Villegas *et al* equations (Equation 4.4.3).

			Refractive Index				
Colour	υ	λ	Thibos	Villegas *et al* equations			
	THz	nm	*et al*	Cornea	Aqueous	Lens	Vitreous
Red	430	697.2	1.3302	1.3729	1.3325	1.4161	1.3327
Orange	494	606.9	1.3325	1.3757	1.3354	1.4191	1.3351
Yellow	558	537.3	1.3350	1.3786	1.3382	1.4225	1.3376
Green	622	482.0	1.3380	1.3817	1.3411	1.4261	1.3404
Blue	686	437.0	1.3416	1.3849	1.3442	1.4300	1.3433
Violet	750	399.7	1.3458	1.3883	1.3474	1.4339	1.3464

eyes in Table 5.5.1. The frequencies and corresponding wavelengths are given for each of the six reference points.

5.6 The Cayley transformed transference for Gaussian systems

In Section 3.7.2 we were introduced to a number of versions of the Cayley transform. In order to choose the right one (or more) for our purposes, we need to be clear about what those purposes and subsequent requirements are. The Cayley transform was introduced as a method to obtain the average of a number of optical systems. The primary interest in the ophthalmic optics literature is its statistical usefulness. Our interest in this study is different; we wish to obtain a vector space to illustrate the dependence of the Gaussian eye on the frequency of light. Hamiltonian matrices belong to the Lie algebra $\mathsf{sp}(n;\mathbb{R})$ which defines a linear space, while symplectic matrices of the Lie group $\mathsf{Sp}(n;\mathbb{R})$ do not. The Cayley transform will allow us to graphically represent the dependence of the eye on the frequency of light.

Returning our attention to the different versions of the Cayley transform in the literature we need to narrow down our choice to the Cayley transform that applies to the symplectic Hamiltonian mapping. Sanyal (2001: 60, 70-71) states that the Cayley transform map relates to Hamiltonian and symplectic matrices the

same way that it relates skew-symmetric matrices to orthogonal matrices, with the exception that the Hamiltonian and symplectic matrices need to be of the order $2n \times 2n$. This implies that any of the Cayley transforms given in Equations 3.7.10 to 13 can be used as a mapping between the Lie group $\mathsf{Sp}(n;\mathbb{R})$ and its Lie algebra $\mathsf{sp}(n;\mathbb{R})$. However, we need to ensure that if we start with a transference **S** and map it into Hamiltonian space ($\hat{\mathbf{S}}$) and then back again, the symplectic matrix returned needs to be the same matrix as **S** that we started out with. We also wish to consider more favourably the Cayley transform that is most likely to exist for transferences of the eye. Finally, it is convenient, as Bernstein (2009:208-209), Tsiotras, Junkins and Schaub (1997) and Sanyal (2001: 72) suggest, that the Cayley transform be its own functional inverse.

Let us start with existence. For Equations 3.7.10, 11 and 13 the inverse exists where the inverse of $\mathbf{I}+\mathbf{S}$ exists. For Equation 3.7.12 the requirement is that the inverse of $\mathbf{I}-\mathbf{S}$ must exist, where **S** is the transference of a system. Because it is conceivable that a transference may be the identity matrix, or approach the identity matrix, we will exclude Equation 3.7.12 as potentially problematic. It is foreseeable that the inverse of $(\mathbf{I}+\mathbf{S})$ should exist for transferences of eyes. The requirement for the Cayley transform of a Hamiltonian matrix to exist is similar and requires that the inverse of $(\mathbf{I}+\hat{\mathbf{S}})$ exists where $\hat{\mathbf{S}}$ is a Hamiltonian matrix.

For each version of the Cayley transform given in Equations 3.7.10 to 13 there exists an inverse. In the case of Equations 3.7.10 and 11, we see that the Cayley transform is its own functional inverse. The same is claimed of Equation 3.7.13. However, let us take a closer look at Equations 3.7.10 and 13 and derive inverses for both of them.

From the definition of the Cayley transform, given in Equation 3.7.10, we derive the inverse transform. Starting with Equation 3.7.10 and changing the symbolism to that for the transference **S** and Hamiltonian transformed transference $\hat{\mathbf{S}}$ we have

$$\hat{\mathbf{S}} = (\mathbf{S}-\mathbf{I})(\mathbf{S}+\mathbf{I})^{-1}. \tag{5.6.1}$$

Solving for **S** we obtain

$$\mathbf{S} = \left(\mathbf{I} - \hat{\mathbf{S}}\right)^{-1}\left(\mathbf{I} + \hat{\mathbf{S}}\right) \tag{5.6.2}$$

which is the inverse given in Equation 3.7.12 and different from the one given in Equation 3.7.11. Similarly, the inverse of Equation 3.7.12 is 3.7.10.

Repeating this procedure to obtain the inverse of the Cayley transform given in Equation 3.7.13, we obtain

$$\hat{\mathbf{S}} = (\mathbf{I} - \mathbf{S})(\mathbf{I} + \mathbf{S})^{-1}. \tag{5.6.3}$$

Solving for **S** we obtain

$$\mathbf{S} = \left(\mathbf{I} + \hat{\mathbf{S}}\right)^{-1}\left(\mathbf{I} - \hat{\mathbf{S}}\right)$$

and because of commutativity,

$$\mathbf{S} = \left(\mathbf{I} - \hat{\mathbf{S}}\right)\left(\mathbf{I} + \hat{\mathbf{S}}\right)^{-1} \tag{5.6.4}$$

which is its own functional inverse.

Commutativity is simple to show. Multiplication shows the following to be true:

$$(\mathbf{I} + \mathbf{A})(\mathbf{I} - \mathbf{A}) = (\mathbf{I} - \mathbf{A})(\mathbf{I} + \mathbf{A}).$$

Hence

$$(\mathbf{I} - \mathbf{A})^{-1}(\mathbf{I} + \mathbf{A}) = (\mathbf{I} + \mathbf{A})(\mathbf{I} - \mathbf{A})^{-1}$$

provided the inverse exists. Hence $(\mathbf{I} - \mathbf{A})^{-1}$ and $\mathbf{I} + \mathbf{A}$ commute.

We return to the issue of which Cayley transform and inverse combination will return the original transference. All of the Cayley transforms given in Equations 3.7.10 to 13 can potentially be done by hand with just a handheld calculator for a Gaussian system. Retaining the symbolism above, we denote the 2×2 (symplectic) transference as **S** and the 2×2 (Hamiltonian) Cayley transformed transference as $\hat{\mathbf{S}}$. Starting with Equation 3.7.10 and expanding we get

$$\hat{\mathbf{S}} = \left(\begin{pmatrix} A & B \\ C & D \end{pmatrix} - \begin{pmatrix} 1 & 0 \\ 0 & 1 \end{pmatrix}\right)\left(\begin{pmatrix} A & B \\ C & D \end{pmatrix} + \begin{pmatrix} 1 & 0 \\ 0 & 1 \end{pmatrix}\right)^{-1}$$

simplifying and using the symplectic equation we obtain

$$\hat{\mathbf{S}} = \begin{pmatrix} A-D & 2B \\ 2C & D-A \end{pmatrix}\frac{1}{2+A+D} \tag{5.6.5}$$

or

$$\hat{\mathbf{S}} = \begin{pmatrix} A-D & 2B \\ 2C & D-A \end{pmatrix} \frac{1}{2+\mathrm{tr}\mathbf{S}} \tag{5.6.6}$$

giving us the Cayley transformed transference of a Gaussian system in terms of the fundamental properties of the Gaussian transference. This transformed transference exists provided $\mathrm{tr}\mathbf{S} \neq -2$, which is unlikely for a reasonable eye. It is, however, clearly a Hamiltonian matrix.

Similarly, we can simplify Equation 3.7.13 to obtain

$$\hat{\mathbf{S}} = \begin{pmatrix} A-D & 2B \\ 2C & D-A \end{pmatrix} \frac{-1}{2+\mathrm{tr}\mathbf{S}}, \tag{5.6.7}$$

the negative equivalent of Equation 5.6.6 and clearly also Hamiltonian.

Similarly, the Cayley transform given by Equation 3.7.12 simplifies for a Gaussian system to

$$\hat{\mathbf{S}} = \begin{pmatrix} A-D & 2B \\ 2C & D-A \end{pmatrix} \frac{1}{2-A-D} \tag{5.6.8}$$

or

$$\hat{\mathbf{S}} = \begin{pmatrix} A-D & 2B \\ 2C & D-A \end{pmatrix} \frac{1}{2-\mathrm{tr}\mathbf{S}} \tag{5.6.9}$$

which is also Hamiltonian. This transformed transference exists provided $\mathrm{tr}\mathbf{S} \neq 2$ which is a possibility. The entries within the matrix are the same for Equations 5.6.6, 7 and 9, but in each case they are multiplied by a different constant, giving different values for each of the three transformed transferences.

From Equations 5.6.6, 7 and 9 we see that the units are the same as for a transference and that the entries along the diagonal are the negative equivalent of each other as shown in Equation 3.7.8. This gives us three independent entries and enables us to create a three-dimensional graph of the Hamiltonian space represented by the Cayley Transform.

We derive an equation for the transference **S** as a function of the coefficients of the transformed transference $\hat{\mathbf{S}}$. We start with the definition of the inverse of the Cayley transform, given in Equation 3.7.12 and substitute the transformed coefficients into it from the Gaussian simplification of Equation 3.7.7,

$$\mathbf{S}=\left(\begin{pmatrix}1&0\\0&1\end{pmatrix}+\begin{pmatrix}\hat{A}&\hat{B}\\\hat{C}&\hat{D}\end{pmatrix}\right)\left(\begin{pmatrix}1&0\\0&1\end{pmatrix}-\begin{pmatrix}\hat{A}&\hat{B}\\\hat{C}&\hat{D}\end{pmatrix}\right)^{-1}$$

$$\mathbf{S}=\begin{pmatrix}1+\hat{A}-\hat{D}-\hat{A}\hat{D}+\hat{B}\hat{C} & 2\hat{B}\\ 2\hat{C} & \hat{C}\hat{B}+1+\hat{D}-\hat{A}-\hat{A}\hat{D}\end{pmatrix}\frac{1}{1-\hat{A}-\hat{D}+\hat{A}\hat{D}-\hat{C}\hat{B}}$$

and substituting the Gaussian simplification of Equation 3.7.8, $\hat{A}=-\hat{D}$ into this equation we can simplify further to obtain

$$\mathbf{S}=\begin{pmatrix}1+2\hat{A}-\hat{A}\hat{D}+\hat{B}\hat{C} & 2\hat{B}\\ 2\hat{C} & 1+2\hat{D}-\hat{A}\hat{D}+\hat{C}\hat{B}\end{pmatrix}\frac{1}{1+\hat{A}\hat{D}-\hat{C}\hat{B}}$$

$$\mathbf{S}=\frac{2}{1+\hat{A}\hat{D}-\hat{C}\hat{B}}\begin{pmatrix}\hat{A}+1 & \hat{B}\\ \hat{C} & \hat{D}+1\end{pmatrix}-\mathbf{I} \tag{5.6.10}$$

$$\mathbf{S}=\frac{2\left(\hat{\mathbf{S}}+\mathbf{I}\right)}{1+\det\hat{\mathbf{S}}}-\mathbf{I} \tag{5.6.11}$$

which is the equation for the transference in terms of the Cayley transformed transference.

Using the same methodology of substituting the entries from Equation 3.7.7 into the Cayley transform given by Equation 3.7.13, we obtain

$$\mathbf{S}=\frac{2\left(\mathbf{I}-\hat{\mathbf{S}}\right)}{1+\det\hat{\mathbf{S}}}-\mathbf{I} \tag{5.6.12}$$

for the transference in terms of the transformed transference for Equation 3.7.13.

Similarly Equations 3.7.10 and 11 simplify and we obtain

$$\mathbf{S}=\frac{2\left(\hat{\mathbf{S}}-\mathbf{I}\right)}{1+\det\hat{\mathbf{S}}}+\mathbf{I} \tag{5.6.13}$$

Which is the same regardless of whether we use the first or second equality, due to the commutativity of the Cayley transform.

We now have three formulae for the transformed transference in terms of the entries of the Gaussian transference and three formulae for the transference in terms of the entries of the transformed transference. We return to our initial requirement for the choice of Cayley transform and inverse Cayley transform; that is, that when a transference is transformed into Hamiltonian space and then the transformed transference is transformed back to a symplectic matrix, then the

same transference must be returned. To do this, we substitute Equation 5.6.7 into Equation 3.7.13 and obtain

$$\mathbf{S}=\begin{pmatrix} A & B \\ C & D \end{pmatrix},$$

the transference in its original values and with the original order. Similarly if we substitute Equation 5.6.12 into Equation 3.7.13 we obtain the transformed transference $\hat{\mathbf{S}}$ in its original values and with original order. This indicates to us that the Cayley transform given in Equation 3.7.13 is its own functional inverse and is the most suitable transform to use, along with the simplifications for Gaussian systems. We will use Equation 5.6.7 for mapping from the symplectic transference to the Hamiltonian matrix and Equation 5.6.12 to map from a Hamiltonian matrix back to its symplectic transference.

Let us consider, for completeness, other versions of the Cayley transform and respective functional inverses that meet our criteria for returning the transference in its original form when transformed into Hamiltonian space and then transformed back to a symplectic transference. If we consider the possibility of Equation 3.7.10 being its own functional inverse (given in Equation 3.7.11) then we should follow the same procedure we did above for Equation 3.7.13. However we find that the transformed transference maps back to

$$\mathbf{S}=\begin{pmatrix} -D & B \\ C & -A \end{pmatrix} \tag{5.6.14}$$

which is a symplectic matrix, but not the original transference. It is the negative inverse of the transference. Similarly the transformed transference maps back to

$$\hat{\mathbf{S}}=\begin{pmatrix} \hat{A} & \hat{B} \\ \hat{C} & \hat{D} \end{pmatrix}\frac{1}{\det\hat{\mathbf{S}}} \tag{5.6.15}$$

which is a Hamiltonian matrix, but not the original Hamiltonian matrix that was started with. We therefore can conclude that, for the 2×2 symplectic – Hamiltonian mapping, Equation 3.7.10 (and 11) is not its own functional inverse. However, we note that applying Equation 3.7.12 as an inverse to Equation 3.7.10 does return the original transference and will fulfil our requirements of returning a transference. However this option requires a different equation to map in each direction whereas Equation 3.7.13 is its own functional inverse and therefore only

one equation transforms a transference to a transformed transference and conversely the transformed transference maps to the original transference. It has the added requirement of having the inverse exist for the transferences of all reasonable eyes. Equation 3.7.13 can be considered more general and convenient and is therefore our Cayley transform of choice. Equation 3.7.13 is expressed in the notation used for transferences as

$$\hat{\mathbf{S}} = (\mathbf{I} - \mathbf{S})(\mathbf{I} + \mathbf{S})^{-1} \tag{5.6.16}$$

and

$$\mathbf{S} = (\mathbf{I} - \hat{\mathbf{S}})(\mathbf{I} + \hat{\mathbf{S}})^{-1}. \tag{5.6.17}$$

5.6.1 The Cayley transformed transference for the reduced eye

We are now in a position to obtain a formula for the transformed transference of the reduced eye as a function of frequency. In Section 5.5.2 we looked at the reduced eye as a function of the refractive index (*n*). Equation 5.5.3 gives the transference of the reduced eye with the refractive indices as the only unknowns. Equating the refractive index of air to be $n_0 = 1$, we substitute the values of A, B, C and D from Equation 5.5.3 into Equation 5.6.7 to obtain

$$\hat{\mathbf{S}} = \begin{pmatrix} n-1 & \dfrac{-100}{9}\,\text{mm} \\ \dfrac{9}{100}\left(n^2 - n\right)\text{kD} & 1-n \end{pmatrix}. \tag{5.6.18}$$

Equation 5.6.18 is the Cayley transformed transference for the reduced eye. The units are the same as for a transference. Of interest is that the refractive indices in $\hat{B}$ cancel out and $\hat{B}$ is a constant and coincidentally it is the negative inverse of the constant obtained in $\hat{C}$. $\hat{A}, \hat{C}$ and $\hat{D}$ are all functions of *n*.

5.6.2 The Cayley transformed transference for Le Grand's eye

Because of the problem we had in Section 5.5.4, that there are too many elementary transferences, we have the same restriction on deriving a transformed transference for Le Grand's eye as a function of refractive index.

5.7 Summary

This chapter provides us with a collection of derived properties of the Gaussian system from the transference, which along with the basis for linear optics and derivations in Chapter 3, brings to completeness the derivations we will need for this dissertation. We now have all the necessary formulae to define chromatic aberration in the eye using linear optics. We also are in a position to derive equations from the transference and the ray traversing the Gaussian system for the chromatic properties defined in the physiological optics literature as studied in Chapter 2.

The equations obtained in Sections 5.1 and 5.2 generalise to linear optics. In Section 5.3 the coefficient matrix defining the ray state in object space that maps to an image point at a selected position on the retina was given for astigmatic systems, although it did not generalise readily from Gaussian optics. Whilst Harris (2010b, e) gives formulae to obtain the position of cardinal points and structures for linear systems in general it is not obvious how the locator lines (Harris, 2011b) and Pascal's ring (Harris, 2011a) might generalize for linear systems. In Section 5.5, the transferences for the two model eyes belong clearly within the framework of Gaussian optics. So too, in Section 5.6, the derivations for the transformed Cayley transference in terms of the fundamental properties belong within the framework of Gaussian optics.

6 DEFINITIONS OF LONGITUDINAL AND TRANSVERSE CHROMATIC ABERRATION

In Chapter 2 we saw that many authors refer to chromatic difference of power, magnification, position or refractive error as chromatic aberration. Formulae to derive these properties from the transference of a Gaussian system will be derived in Chapter 7 to allow these definitions to be applied to more complex model eyes. However, there is a clear need for a general definition of chromatic aberration that makes allowance for astigmatic elements that may be tilted or decentred. This chapter defines chromatic aberration for Gaussian optical systems.

6.1 Defining chromatic aberration

To define longitudinal and transverse chromatic aberration we start with the classical definition, which is restricted to homocentric systems with stigmatic elements. However, we do so by defining chromatic aberration in general for systems with astigmatic and heterocentric elements and then simplifying for Gaussian systems.

6.1.1 Homocentric systems with stigmatic elements

In Section 2.2.1 and Figure 2.2.1 we saw how the first-order chromatic aberrations are defined within the limits of Gaussian optics as the distance between the projections of two focus points for two different wavelengths in the directions parallel and perpendicular to the optical axis as longitudinal and transverse chromatic aberration respectively. In this definition the distances between points are unsigned. The definition holds for optical systems with stigmatic elements. This definition is the starting point for the definition that will be used in this study.

In this study we use the definition by Harris and Evans (2012) and take the distances between image points to be signed. This is shown in Figure 6.1.1 where the longitudinal chromatic aberration δz and transverse chromatic aberration δy are shown in the positive sense as having direction from the red to the blue image

points, in addition to magnitude. In Figure 6.1.1, the object O corresponds to red and blue images $\mathrm{I_r}$ and $\mathrm{I_b}$ respectively.

Figure 6.1.1 shows the definitions of longitudinal and transverse chromatic aberration in Gaussian optics and represents the point of departure for the definition given by Harris and Evans (2012) for astigmatic heterocentric systems. It differs from Figure 2.2.1 in that it has signed distances. System S is Gaussian and consists of any number of centred refracting surfaces with stigmatic elements, but which are not shown. This implies that they are invariant under rotation about the common axis Z, which is therefore also the optical axis. S has entrance plane $\mathrm{T_0}$ and exit plane T and refractive indices n_0 upstream and n downstream of S. Object point O has longitudinal position z_O and transverse position y_O. In Figure 6.1.1 these positions are drawn such that $z_\mathrm{O} < 0$ and $y_\mathrm{O} > 0$.

The position of image point I depends on the frequency ν of light. For this purpose we look at two frequencies on opposite ends of the visible light spectrum, namely red ν_r and blue ν_b. The corresponding images for these two frequencies are red image $\mathrm{I_r}$ and blue image $\mathrm{I_b}$. The corresponding longitudinal positions are

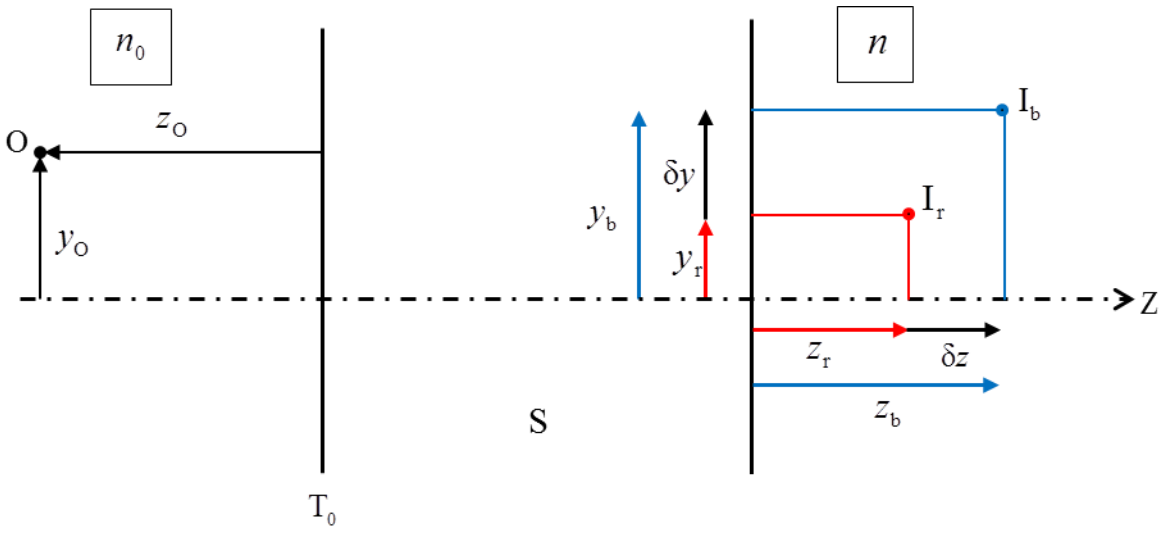

Figure 6.1.1 Longitudinal δz and transverse δy chromatic aberration in a homocentric system with stigmatic elements.

z_r and z_b and transverse positions y_r and y_b. In Figure 6.1.1, all image positions and directions are drawn in the positive sense, however, in a usual system such as the eye $z_r > z_b$.

Subscripts r and b will be used throughout this chapter. They denote two frequencies usually near opposite ends of the visible light spectrum, however, any two frequencies could be chosen. We call them 'red' and 'blue' for convenience. On the visible light spectrum, the blue is the higher frequency and the red is the lower frequency. Therefore the blue photons have a higher energy than the red photons which seems to suggest that we should subtract a lower energy from the higher energy. For this reason we chose to subtract red from blue in all chromatic aberration formulae. However, the formulae derived are general for any chosen frequencies. In Chapters 9 and 10 two frequencies are chosen for illustrative purposes.

We note that Figure 6.1.1 is a two-dimensional diagram and that the optical axis Z, object O and both the image points I_r and I_b lie in the same plane, that of the page. This is because system S is homocentric and has only stigmatic elements within it. Furthermore, a distinction is drawn between incident refractive indices n_{0r} and n_{0b} and emergent refractive indices n_r and n_b.

We define longitudinal (or axial) chromatic aberration as (Harris and Evans, 2012)

$$\delta z = z_b - z_r \tag{6.1.1}$$

and transverse (or lateral) chromatic aberration as

$$\delta y = y_b - y_r . \tag{6.1.2}$$

For convenience, the context of the system is implied when referring to the properties of a system. The chromatic aberration will also depend on the position of a point in object space, O. In Figure 6.1.1 this position is denoted by longitudinal position z_O and transverse position y_O.

For any system S, the chromatic aberration is not unique and usually there will exist an infinity of longitudinal and transverse chromatic aberrations. The chromatic aberration of a system is unique only when the object position is

specified. In other words, chromatic aberration depends on z_O and y_O. As will be shown, longitudinal chromatic aberration is dependent on z_O and transverse chromatic aberration on y_O. Chromatic aberration does not exist for the system in isolation. It is a measurement of a phenomenon of the images formed and for this reason is a property of the object point and the system.

From these definitions, longitudinal δz and transverse δy chromatic aberration are lengths measured orthogonally to each other and represented here by scalars. From Figure 6.1.1 one is tempted to draw an arrow from I_r to I_b, to represent chromatic aberration holistically as a vector with longitudinal and transverse chromatic aberration as components. However, when we make allowance for astigmatism one finds that the two aberrations are fundamentally different and cannot be combined into a single vector (Harris and Evans, 2012). We therefore refrain from representing chromatic aberration as a vector here as well.

6.1.2 Heterocentric systems with stigmatic elements

A heterocentric system is one in which the refracting elements are not all centred on a common optical axis. Elements may be decentred or tilted. We retain the stigmatic elements, however, the longitudinal axis is no longer an optical axis and we need to consider a three-dimensional representation as shown in Figure 6.1.2. In Figure 6.1.2, system S contains refracting surfaces which may be decentred. It may also contain prisms and surfaces which are tilted. Also shown in Figure 6.1.2 are the transverse planes containing the object point O at T_O, the red image I_r at T_r and the blue image I_b at T_b. The object O corresponds to red and blue images I_r and I_b respectively.

From Figure 6.1.2 it becomes clear that the definition of longitudinal chromatic aberration δz in the case of homocentric systems with stigmatic elements can be applied to heterocentric systems, Equation 6.1.1 remains unchanged and δz remains a scalar measurement of length between the red and blue transverse planes. Also from Figure 6.1.2, we can see that this is not the case

for transverse chromatic aberration $\delta\mathbf{y}$. Starting at the object plane T_O we see that the position of object point O is now defined as a vector

$$\mathbf{y}_O = \begin{pmatrix} y_{O1} \\ y_{O2} \end{pmatrix} \tag{6.1.3}$$

with horizontal and vertical components.

Similarly we note that the transverse positions of the red I_r and blue I_b image points are represented by $\mathbf{y}_r$ and $\mathbf{y}_b$ each with horizontal and vertical components. In order to obtain the transverse chromatic aberration, we project the red image point I_r onto the blue transverse plane T_b. The projection is along the longitudinal axis. $\Delta\mathbf{y}$ is represented as the vector from the red to the blue image points and defines transverse chromatic aberration as

$$\delta\mathbf{y} = \mathbf{y}_b - \mathbf{y}_r . \tag{6.1.4}$$

At this point we have transverse chromatic aberration, a vector, and longitudinal chromatic aberration, a scalar. Although one is a scalar and the other a vector, one is still tempted to combine them as a holistic concept of three components.

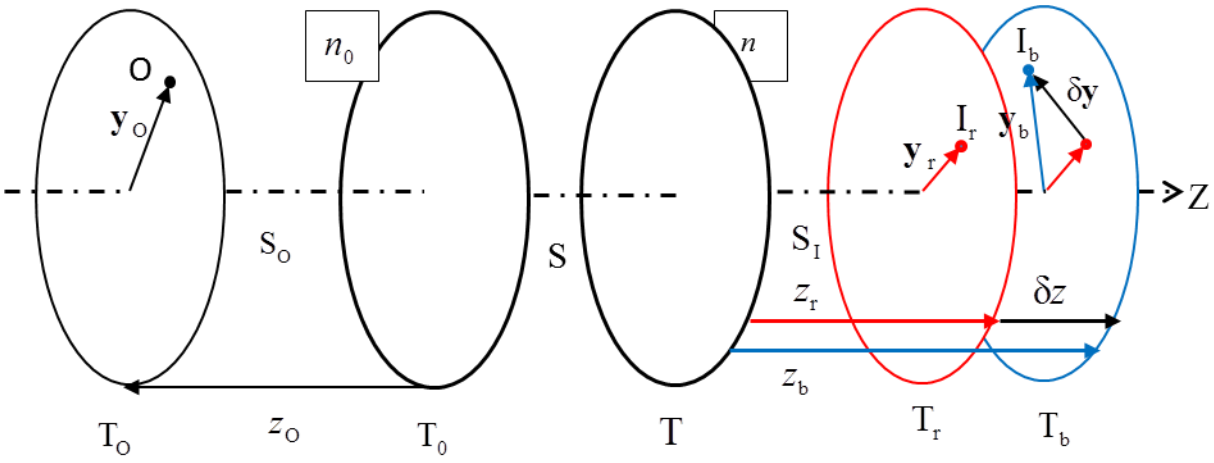

Figure 6.1.2 Longitudinal and transverse chromatic aberration in a heterocentric system with stigmatic elements.

6.1.3 Heterocentric astigmatic systems

We turn now to the general system in which elements may be decentred and astigmatic (Harris and Evans, 2012). System S consists of any number of elements which may be astigmatic, decentred, tilted or prismatic. The longitudinal axis Z is usually not an optical axis. In an astigmatic system image points $\mathrm{I_r}$ and $\mathrm{I_b}$ become fuzzy as shown in Figure 6.1.3. Each image point dissociates longitudinally into two orthogonal image lines and each fuzzy image becomes that of the interval of Sturm, which will be referred to simply as the image structure. The red and blue transverse image planes are no longer planes, but a fuzzy zone the width of the interval of Sturm and denoted by dotted lines in Figure 6.1.3. The system is drawn with the red and blue image zones separate, however, these may overlap. An additional problem arises when defining longitudinal chromatic aberration in that the orientations of the two sets of image lines may not match. That is to say, the first red image line may not be parallel to the first blue image line. There is a relative rotation that occurs between the red and then the blue image structures that must be considered. Additionally, the width of the interval of Sturm is not necessarily the same for each colour.

How now does one define longitudinal chromatic aberration? Intuitively one may wish to calculate a scalar distance between the two image structures by calculating the distance between the planes of the two circles of least confusion. However, the circle of least confusion is not an image point and this does not fully represent what is happening in the system. Each image structure is represented by a 2×2 symmetric vergence matrix and therefore a scalar distance does not make any sense. The definition needs to account for the fact that the two fuzzy image structures differ in position, orientation and degree of fuzziness. Therefore the definition needs to include at least three numbers to represent it completely.

The fuzzy image structure is a representation of light, so we turn our attention to vergence. In the absence of astigmatism the red pencil of light would have reduced vergence

$$L_{\mathrm{r}} = \frac{n_{\mathrm{r}}}{z_{\mathrm{r}}} \tag{6.1.5}$$

at exit plane T, where z_r is the longitudinal distance from exit plane T to transverse red image plane T_r, as shown in Figure 6.1.1. Hence

$$z_r = \frac{n_r}{L_r} \tag{6.1.6}$$

and similarly for the blue vergence and longitudinal distance. In the presence of astigmatism the generalisation of the scalar reduced vergence L is the reduced vergence $\mathbf{L}$, a symmetric matrix as defined in Section 3.8. The unit of vergence is reciprocal length. $\mathbf{L}_r$ is the reduced vergence at the exit plane T of system S of the red astigmatic pencil defined by object O and $\mathbf{L}_b$ is the same for the blue pencil.

From Equation 6.1.6, Harris and Evans (2012) generalize and define

$$\mathbf{Z} = \mathbf{L}^{-1} n . \tag{6.1.7}$$

$\mathbf{Z}$ is symmetric and has the unit length. Because the right-hand side of the equation is multiplied by n, $\mathbf{Z}$ represents the actual distance rather than the reduced distance. It can be regarded as the generalized position of the fuzzy image structure relative to the exit plane T.

Generalizing Equation 6.1.1, we see that

$$\delta\mathbf{Z} = \mathbf{Z}_b - \mathbf{Z}_r \tag{6.1.8}$$

represents the longitudinal chromatic aberration of a heterocentric astigmatic system S for object point O on the longitudinal axis. $\delta\mathbf{Z}$ characterises the longitudinal difference of the two fuzzy image points completely (Harris and Evans, 2012). By this definition longitudinal chromatic aberration becomes the 2×2 symmetric matrix $\delta\mathbf{Z}$ and can be characterised by three independent numbers.

From Equation 6.1.5, we see that the reduced vergence (both scalar L and matrix $\mathbf{L}$) is dependent on the longitudinal position z_O of object point O and system S and is independent of the transverse position y_O of O. Therefore, provided z_O of the object O and system S remain unchanged, decentration of the object point and elements of the system have no effect on the longitudinal positions and nature of the fuzzy image structures and we can take Equation 6.1.8 to be the definition of longitudinal chromatic aberration $\delta\mathbf{Z}$ of a heterocentric

astigmatic system for an object point at any specified position. The longitudinal chromatic aberration is more difficult to represent pictorially. In Figure 6.1.3 $\mathbf{Z}_r$ is shown as two red lines representing the two image line foci, orthogonal to each other. A line is drawn between them, parallel to the longitudinal axis. And similarly for the blue fuzzy image structure. The longitudinal chromatic aberration of system S for object O is $\delta\mathbf{Z}$. $\delta\mathbf{Z}$ is a 2×2 distance matrix and cannot be represented by a vector arrow on the diagram.

In contrast, the transverse chromatic aberration is the vector $\delta\mathbf{y}$, shown in Figure 6.1.3, from $\mathbf{y}_r$ to $\mathbf{y}_b$. Vectors $\mathbf{y}_r$ and $\mathbf{y}_b$ are drawn from the longitudinal axis Z to an axis, parallel to Z, between the two orthogonal image lines within the transverse plane for red and blue, respectively. It is not drawn to the circle of least confusion. The vector for $\mathbf{y}_r$ can be projected onto the blue image plane and the transverse chromatic aberration is vector $\delta\mathbf{y}$. The effect of decentring an object point and system elements is to cause transverse displacement of the fuzzy images I_r and I_b of object point O in the heterocentric astigmatic system S. Equation 6.1.4 defines the transverse chromatic aberration $\delta\mathbf{y}$ of S for O.

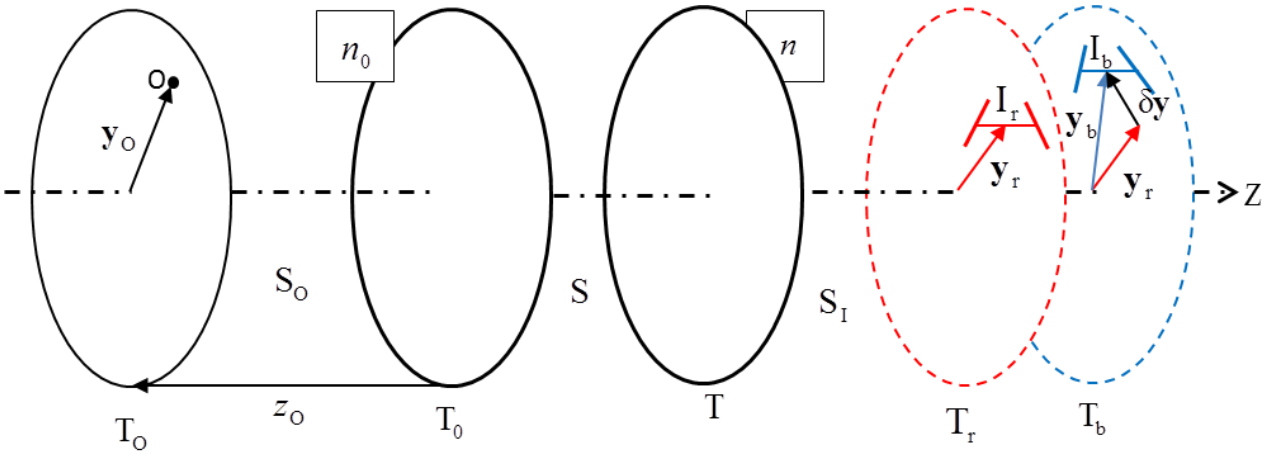

Figure 6.1.3 Longitudinal $\delta\mathbf{Z}$ and transverse $\delta\mathbf{y}$ chromatic aberration in a heterocentric system with astigmatic elements.

6.1.4 Chromatic aberration in general

Equations 6.1.4 and 8 are generalisations from Equations 6.1.2 and 1 to optical systems in general of the definitions for systems whose elements are stigmatic and centred on an optical axis. Equation 6.1.4 defines transverse chromatic aberration $\delta\mathbf{y}$ and Equation 6.1.8 longitudinal chromatic aberration $\delta\mathbf{Z}$ in general. $\delta\mathbf{y}$ is a two dimensional vector and $\delta\mathbf{Z}$ is a 2×2 symmetric matrix. The fact that transverse and longitudinal chromatic aberration are different in mathematical character shows that the two types of aberration are fundamentally different in nature and cannot be meaningfully combined into a single unified concept of chromatic aberration.

These general equations hold and indeed simplify for homocentric systems with stigmatic elements in particular. In such systems the transverse chromatic aberration $\delta\mathbf{y}$ becomes a scalar quantity δy and sketched in a single plane, that of the page. Δy is one component of $\delta\mathbf{y}$ with the other component being zero and perpendicular to the page. The longitudinal chromatic aberration $\delta\mathbf{Z}$ also becomes a scalar quantity represented as a scalar multiple of the identity matrix such that $\delta\mathbf{Z}=\mathbf{I}\delta z$, where $\mathbf{I}$ is the 2×2 identity matrix, and the image is a point. The image too is represented as simply in the plane of the page, as shown in Figure 6.1.1.

Equations 6.1.1 and 8 define longitudinal chromatic aberration and Equations 6.1.2 and 4 define transverse chromatic aberration in Gaussian and linear systems respectively. We now turn our attention to quantifying longitudinal and transverse chromatic aberration in Gaussian systems.

6.2 Quantifying chromatic aberration in Gaussian systems

In order to calculate the longitudinal and transverse chromatic aberration we need to consider the optical system which is represented by the system's ray transference, where the transference is a function of the frequency of light (Evans and Harris, 2011). This 2×2 transference was defined for a Gaussian system in Equation 3.2.38.

6.2.1 Vergence across a Gaussian system derived from the transference

The reduced vergence at an entrance plane T_0 of system S is L_0, given by Equation 3.8.1, for an object O at a longitudinal distance z_O from T_0. Following from this, the reduced vergence at the exit plane T of S for O is given by Equation 3.8.6 for light emerging from a linear system and which reduces to

$$L = (DL_0 - C)(A - BL_0)^{-1} \tag{6.2.1}$$

through a Gaussian system. Substituting Equation 3.8.1 into Equation 6.2.1 we find

$$L = \left(D\frac{n_0}{z_\mathrm{O}} - C \right)\left(A - B\frac{n_0}{z_\mathrm{O}} \right)^{-1} \tag{6.2.2}$$

or

$$L = \left(D - C\frac{z_\mathrm{O}}{n_0} \right)\left(A\frac{z_\mathrm{O}}{n_0} - B \right)^{-1}. \tag{6.2.3}$$

From Equations 6.2.2 and 3 we note that there are two special cases to consider. Firstly where $z_\mathrm{O} \to \infty$ Equation 6.2.2 simplifies to

$$L = -CA^{-1} \tag{6.2.4}$$

and where $z_\mathrm{O} = 0$ Equation 6.2.3 simplifies to

$$L = -DB^{-1}. \tag{6.2.5}$$

Equation 6.2.4 is the same as Equation 3.4.11 and represents the back-vertex power of the system. In order to calculate the red and blue vergences L_r and L_b at T, one can simply add the appropriate subscript to all the parameters of any of Equations 6.2.1 to 5, with the exception of z_O. Because the transference is a function of the frequency of light, a transference will need to be calculated for each of red and blue, $\mathbf{S}_\mathrm{r}$ and $\mathbf{S}_\mathrm{b}$, using the formulae discussed in Section 5.5.

6.2.2 Transference of a compound system: object at finite distance

We now look at the system more carefully to obtain the transference of not just system S, but of the compound system from the object plane to the image plane. From Figure 6.1.1 we see that the system upstream of system S is S_O and is

the homogenous gap of finite length $-z_{\mathrm{O}}$. The minus sign is needed because O is upstream of S.

The transference of a homogenous gap is defined by Equation 3.2.36 where ζ is the reduced distance defined in Equation 3.2.8. In the same way we consider the system $\mathrm{S_I}$, downstream of system S, of length *z*, from the exit plane T of system S, up to the plane of an image line $\mathrm{T_I}$, corresponding to object O, of an image point.

To obtain the transference of the compound system $\mathrm{S_C}$ we start with

$$\mathbf{S}_{\mathrm{C}} = \mathbf{S}_{\mathrm{I}}\mathbf{S}\mathbf{S}_{\mathrm{O}} \tag{6.2.6}$$

then substitute for the individual transferences,

$$\mathbf{S}_{\mathrm{C}} = \begin{pmatrix} 1 & \frac{z}{n} \\ 0 & 1 \end{pmatrix} \begin{pmatrix} A & B \\ C & D \end{pmatrix} \begin{pmatrix} 1 & \frac{-z_{\mathrm{O}}}{n_0} \\ 0 & 1 \end{pmatrix}. \tag{6.2.7}$$

Hence

$$\mathbf{S}_{\mathrm{C}} = \begin{pmatrix} A + C\frac{z}{n} & B + D\frac{z}{n} - \left(A + C\frac{z}{n}\right)\frac{z_{\mathrm{O}}}{n_0} \\ C & D - C\frac{z_{\mathrm{O}}}{n_0} \end{pmatrix}. \tag{6.2.8}$$

From Equation 3.2.40 and the top row of Equation 6.2.8, we see that a ray from object O at transverse position y_{O} on the entrance plane $\mathrm{T_O}$ arrives at the transverse image plane $\mathrm{T_I}$ with transverse position

$$y = \left(A + C\frac{z}{n}\right)y_{\mathrm{O}} + \left(B + D\frac{z}{n} - \left(A + C\frac{z}{n}\right)\frac{z_{\mathrm{O}}}{n_0}\right)n_0 a_{\mathrm{O}}. \tag{6.2.9}$$

From Section 3.3.2, we recognise this as a conjugate system and therefore we set $B + D\frac{z}{n} - \left(A + C\frac{z}{n}\right)\frac{z_{\mathrm{O}}}{n_0} = 0$, effectively nullifying any effect of a_{O}. Hence Equation 6.2.9 simplifies to

$$y = \left(A + C\frac{z}{n}\right)y_{\mathrm{O}}. \tag{6.2.10}$$

which gives us the transverse position of a point *y* at the image plane $\mathrm{T_I}$. Equation 6.2.10 can be written for red and blue image points which would then give y_b and y_r corresponding to an object point at a finite distance .

6.2.3 Transference of a compound system: distant object

We now define the transference of a compound system where the object point is at an infinite distance. Because $z_\mathrm{O} \to \infty$ we rather define our system as starting at $\mathrm{T_0}$ and make use of the incident inclination a_0 of the rays at entrance plane $\mathrm{T_0}$.

We therefore define our system as the compound system from $\mathrm{T_0}$ to $\mathrm{T_I}$, consisting of S and $\mathrm{S_I}$. The transference of $\mathrm{S_C}$ is

$$\mathbf{S}_\mathrm{C} = \mathbf{S}_\mathrm{I}\mathbf{S} \tag{6.2.11}$$

and, hence,

$$\mathbf{S}_\mathrm{C} = \begin{pmatrix} 1 & \frac{z}{n} \\ 0 & 1 \end{pmatrix} \begin{pmatrix} A & B \\ C & D \end{pmatrix} \tag{6.2.12}$$

or

$$\mathbf{S}_\mathrm{C} = \begin{pmatrix} A + C\frac{z}{n} & B + D\frac{z}{n} \\ C & D \end{pmatrix}. \tag{6.2.13}$$

Substituting from the top row of Equation 6.2.13 into Equation 3.2.40 we find that the ray will arrive in $\mathrm{T_I}$ at transverse position

$$y = \left(A + C\frac{z}{n} \right) y_\mathrm{O} + \left(B + D\frac{z}{n} \right) n_0 a_\mathrm{O} \tag{6.2.14}$$

and because the system is exit-plane focal, we have $A + C\frac{z}{n} = 0$ which nullifies any effect of y_O and therefore Equation 6.2.14 simplifies to

$$y = \left(B + D\frac{z}{n} \right) n_0 a_\mathrm{O}. \tag{6.2.15}$$

y is the transverse position on the image plane $\mathrm{T_I}$ corresponding to a point image for a system with an object at an infinite distance. Equation 6.2.15 can be written

for red and blue image points which would then give y_b and y_r for a distant object point.

6.2.4 Transverse chromatic aberration in a Gaussian system

The transverse chromatic aberration was defined in Equation 6.1.2 as $\delta y = y_b - y_r$ for Gaussian systems. Substituting from Equation 6.2.10 we obtain

$$\delta y = y_O\left[\left(A_b + C_b\frac{z_b}{n_b}\right) - \left(A_r + C_r\frac{z_r}{n_r}\right)\right]$$

$$\delta y = y_O\delta\left(A + C\frac{z}{n}\right) \tag{6.2.16}$$

similarly, for an object point at a finite distance and substituting from Equation 6.2.15 into Equation 6.1.2 we obtain

$$\delta y = a_O\delta\left(\left(B + D\frac{z}{n}\right)n_0\right) \tag{6.2.17}$$

for systems when the object point is distant ($z_O \to \infty$).

6.3 Calculation routines for longitudinal and transverse chromatic aberration

1. Calculate $\mathbf{S}_r$ and $\mathbf{S}_b$ the transferences of system S for red and blue light.
2. Calculate the reduced vergence *L* for each of red and blue light.
    i. For a finite object point O with longitudinal position z_O use Equation 6.2.3.
    ii. For a distant object where $z_O \to \infty$, use Equation 6.2.4.
3. Calculate the longitudinal position *z* of the image point for each frequency using Equation 6.1.6.

6.3.1 Calculation routine for longitudinal chromatic aberration

4. Calculate the longitudinal chromatic aberration δz from Equation 6.1.1.

6.3.2 Steps for calculating transverse chromatic aberration

- *For an object point at a finite distance of longitudinal position* z_O *upstream of the system:*

Following from steps 1, 2.i and 3.

4. For each of red and blue calculate $A + C\frac{z}{n}$.
5. Calculate $\delta\left(A + C\frac{z}{n}\right)$.
6. Calculate the transverse chromatic aberration δy using Equation 6.2.16.

- *For an object point at a distance where* $z_O \to \infty$ *upstream of the system:*

Following from steps 1, 2.ii and 3.

4. For each of red and blue calculate $\left(B + D\frac{z}{n}\right)n_0$.
5. Calculate $\delta\left(\left(B + D\frac{z}{n}\right)n_0\right)$.
6. Calculate the transverse chromatic aberration using Equation 6.2.17.

Numerical examples of longitudinal and transverse chromatic aberration for the reduced eye and Le Grand's eye are given in Section 10.1.

6.4 Comments on chromatic aberration

In this chapter we considered the definition for chromatic aberration. Firstly, we looked at the familiar definition given in the literature as the first order chromatic aberrations within the limits of Gaussian optics as the distance between the projections of two focus points for two different frequencies in the directions parallel and perpendicular to the optical axis as longitudinal and transverse chromatic aberration respectively and illustrated in Figure 6.1.1. From this figure it appears logical to draw an arrow between image points I_r and I_b, thereby representing both longitudinal and transverse chromatic aberration holistically as one vectorial chromatic aberration. This, however, would be incorrect. In order to understand why that is so we looked at the generalisation of this definition in heterocentric astigmatic systems and saw that the two aberrations have fundamentally different mathematical characters: longitudinal chromatic

aberration is represented by a 2×2 symmetric matrix $\delta\mathbf{Z}$ whereas transverse chromatic aberration is represented by a vector $\delta\mathbf{y}$. The fact that transverse and longitudinal chromatic aberration have different mathematical character shows that the two types of aberration are fundamentally different in nature and cannot be meaningfully combined into a single unified concept of chromatic aberration.

For any system S the chromatic aberrations are not unique and usually there will exist an infinity of longitudinal and transverse chromatic aberrations. The chromatic aberrations of a system are unique only when the object position is specified. In other words, chromatic aberration is dependent on z_{O} and y_{O}.

We noted that chromatic aberration does not exist for the system in isolation. It is a measurement of a phenomenon of the images formed and for this reason is a result of the system and the location of the object point. From Equations 6.1.1 and 6 and 6.2.2, 3 and 4, longitudinal chromatic aberration is dependent on longitudinal position z_{O} of the object point O and is independent of transverse position y_{O}. Transverse chromatic aberration is defined in Equation 6.1.2 and from Equations 6.2.16 and 17 we see that it is a linear function of the object's transverse position y_{O} in the case of the objects at finite distances and its direction a_{O} in the case of a distant object.

Chromatic aberrations are first-order phenomena and occur in the paraxial region. For this reason, Harris and Evans (2012) express reservations over the use of the word aberration in the context of chromatic aberrations.

The definitions and formulae given in this section are not specific to the eye, but are applicable to systems in general. When applying the definitions to the visual system one needs to be clear how the definitions are being used. Firstly, for an eye or a model eye the entrance plane would be immediately in front of the tear film and the exit plane immediately in front of the retina. Secondly, the position of the longitudinal axis needs to be specified. Thirdly, the location of the object point needs to be given. Finally, the two frequencies of light, ν_{r} and ν_{b}, need to be specified.

7 Quantifying chromatic properties

Longitudinal and transverse chromatic aberration was defined in general for Gaussian optical systems in Chapter 6. In Chapter 2 we reviewed the physiological optics definitions and experimental approaches to measure chromatic effects in the eye and calculate them in model eyes. Most of these approaches define chromatic differences in Gaussian model eyes, usually the reduced eye or modifications thereof. Measurements are done experimentally and calculated within the framework of Gaussian systems. In order to differentiate between the definitions defined in classical and physiological optics, the term "chromatic aberration" will be reserved for the definition given in Chapter 6 and the definitions given in the physiological optics, in this chapter, will be termed "chromatic properties of the eye".

In this section we consider chromatic properties of the eye in two categories: in Section 7.1 we define those that are properties of the eye alone, the independent chromatic properties of the eye, and in Section 7.2 we define the chromatic properties of the eye that are dependent on the object (or image) and aperture positions. Because these definitions are specific to eyes or model eyes, we deem the system of the eye to be from the entrance plane immediately in front of the cornea to the exit plane immediately in front of the retina.

For all the derivations that follow one needs to obtain two transferences, $\mathbf{S}_{\mathrm{r}}$, the transference for the red frequency and $\mathbf{S}_{\mathrm{b}}$, the transference for the blue frequency. In all the formulae below, the fundamental properties are taken from the two transferences with subscripts (or superscripts) r and b corresponding to the respective transference.

7.1 Independent chromatic properties of the eye

In Section 2.3.1 we saw that chromatic difference in power and chromatic difference in refractive compensation are usually categorised as longitudinal chromatic aberration which is in conflict with the definition for longitudinal chromatic aberration given in Chapter 6. In this section we will obtain formulae for the chromatic difference of power, refractive compensation and ametropia.

These chromatic properties of the eye are independent of the aperture, object and image, but depend on the frequencies chosen for red and blue.

7.1.1 Chromatic difference in power

Using Equation 3.4.3 we obtain the power F of the eye from the transference for a particular frequency of light. The chromatic difference in power is defined as

$$\delta F = F_{\mathrm{b}} - F_{\mathrm{r}} \tag{7.1.1}$$

and substituting from Equation 3.4.3 we obtain the chromatic difference in power from the transferences (Evans and Harris, 2011)

$$\delta F = -(C_{\mathrm{b}} - C_{\mathrm{r}})\,. \tag{7.1.2}$$

7.1.2 Chromatic difference in refractive compensation

We use Equation 3.4.6 to obtain the corneal-plane refractive compensation F_0 for an eye from the transference. The chromatic difference in refractive compensation is defined as

$$\delta F_0 = F_{0\mathrm{b}} - F_{0\mathrm{r}}\,. \tag{7.1.3}$$

Hence, from Equation 3.4.6 the chromatic difference in corneal-plane refractive compensation is (Evans & Harris, 2011)

$$\delta F_0 = B_{\mathrm{b}}^{-1} A_{\mathrm{b}} - B_{\mathrm{r}}^{-1} A_{\mathrm{r}}\,. \tag{7.1.4}$$

7.1.3 Chromatic difference in ametropia

The term ametropia is often used to refer to refractive compensation, however the term is used here as defined in Section 3.3.1.We read the ametropia A directly from the transference for each chosen frequency of light. The chromatic difference in ametropia across a specified spectrum of visible light is obtained directly from the transferences and therefore (Evans & Harris, 2011)

$$\delta A = A_{\mathrm{b}} - A_{\mathrm{r}}\,. \tag{7.1.5}$$

7.1.4 Chromatic properties for Emsley's reduced eye

In Section 4.1.3 we saw that the advantage of the reduced eye is its simplicity. It is a Gaussian system, has one refracting surface and there are only two refractive indices. We assume that Emsley's eye is in air and that $n_0 = 1$. What this implies is that we can derive very simple formulae for the chromatic difference of power, refractive compensation, and ametropia for the reduced eye. (Evans and Harris, 2011)

The parameter of the reduced eye that varies with frequency is the refractive index. We define the chromatic difference of refractive index for the reduced eye as

$$\delta n = n_{\mathrm{b}} - n_{\mathrm{r}}. \tag{7.1.6}$$

The refractive index for the reduced eye as a function of wavelength was given in Equation 4.4.2, from which we obtain (Evans & Harris, 2011)

$$\delta n = b\left(\frac{1}{\lambda_{\mathrm{b}} - c} - \frac{1}{\lambda_{\mathrm{r}} - c}\right) \tag{7.1.7}$$

where *b* and *c* are the constants given immediately after Equation 4.4.2. For the frequencies 430 THz and 750 THz, $\delta n = 0.015\,542$ for Emsley's reduced eye.

Chromatic difference in power for Emsley's reduced eye

From Equations 5.5.1 and 7.1.2 and the parameters for Emsley's reduced eye given in Section 4.1.3 for the radius of curvature *r* of the refracting surface and the length *z* of the reduced eye we obtain (Evans & Harris, 2011)

$$\delta F = (180\,\mathrm{D})\delta n, \tag{7.1.8}$$

the chromatic difference in power of Emsley's reduced eye, where δn is calculated according to Equation 7.1.7.

Chromatic difference in corneal-plane refractive compensation for Emsley's reduced eye

From Equations 5.5.1 and 7.1.4 and the parameters for the reduced eye given in Section 4.1.3 we obtain the chromatic difference in corneal-plane refractive compensation (Evans & Harris, 2011)

$$\delta F_0 = (-135\ \mathrm{D})\delta n\,. \tag{7.1.9}$$

Chromatic difference in ametropia for Emsley's reduced eye

From Equations 5.5.1 and Equation 7.1.5 and the parameters for the reduced eye we obtain the chromatic difference in ametropia (Evans & Harris, 2011)

$$\delta A = 4\left(\frac{1}{n_{\mathrm{b}}} - \frac{1}{n_{\mathrm{r}}}\right). \tag{7.1.10}$$

The formulae, given in Equations 7.1.7 to 10, are specific to the reduced eye and make use of the parameters of Emsley's reduced eye in the form of rational numbers. They are not general, but emphasise the simplicity of the reduced eye. Equations 7.1.7 to 10 enable us to very quickly obtain the chromatic difference in refractive index, power, refractive compensation or ametropia for any two chosen frequencies.

Generalizing to linear optics

Equations 7.1.1 to 5 readily generalize to linear systems. Equations 7.1.8 to 10 pertain to the reduced eye which is a Gaussian system.

7.2 Chromatic properties of the eye dependent on object and aperture positions

In Section 2.3.2 we saw that the two chromatic properties usually defined as transverse chromatic aberration are chromatic difference in position and chromatic difference in magnification. They are measured in object space and calculated in both image and object space for model eyes. Our purpose in this section is to derive formulae from the transference for the chromatic properties that are dependent on object and aperture positions for Gaussian eyes.

When we derive formulae for chromatic properties dependent on object and aperture positions we are interested in what is happening at the retina, that is, in image space. If we take into account that the light rays of different frequencies focus at different longitudinal positions, systems where the object and image are in conjugation, such as those discussed in Sections 3.3.2 and 3.5.1, are seldom

useful. Instead, we trace the chief ray from an object point projected onto the retina to locate the image position and magnification at the retinal plane and ignore the amount of blur at the retina. Chromatic difference in position is a commonly used term in the literature and is defined, in Section 2.3.2, as the difference in angular spread or difference in inclination of the red and blue reference rays in either image or object space. We will look at the chromatic difference in transverse position in both image δy_{R} and object space δy_{O} and the chromatic difference in inclination, again in both image δa_{R} and object space δa_{O}.

Unlike the independent chromatic properties of the eye, the chromatic properties discussed in this section are functions of the state of the rays at the retina. Changes in the position of object point and changes to the position of the limiting aperture will influence the state of the rays at the retina.

A ray incident onto the eye undergoes chromatic dispersion and reaches the retina resembling a little rainbow dispersed across the retina (Thibos *et al*, 1991). We concentrate on the two frequencies chosen for the particular study, usually representing the end points of the visual spectrum (as chosen for any specific study) and calculate the difference in position between them. Figure 7.2.1 shows the chromatic difference in position δy_{R} of the blue and red rays at the retina.

We retain the generality of the formulae by including the refractive index of the medium upstream of the eye as dependent on frequency. This is applicable, for example, for an eye submerged in water. Furthermore, equations are written such that they can, as far as possible, generalise to linear optics for centred systems with astigmatic elements. Where equations do not readily generalise, the general linear equation is provided.

7.2.1 Chromatic difference in coefficient matrices

In Section 5.2.2 we defined the distant coefficient matrix $\mathbf{V}_{\mathrm{E}}$. The matrix coefficients $\mathbf{V}_{\mathrm{E}}$ and $\mathbf{V}_{\mathrm{OE}}$ for eyes and either a distant or finite distance object point respectively are dependent on frequency and therefore there will be a blue

and a red matrix coefficient for each object distance. We now define the chromatic difference in distance coefficient matrices

$$\delta\mathbf{V}_{\mathrm{E}} = \mathbf{V}_{\mathrm{E}}^{\mathrm{b}} - \mathbf{V}_{\mathrm{E}}^{\mathrm{r}} = \begin{pmatrix} \delta W_{\mathrm{E}} & \delta X_{\mathrm{E}} \\ \delta Y_{\mathrm{E}} & \delta Z_{\mathrm{E}} \end{pmatrix} \tag{7.2.1}$$

where δW_{E} is the chromatic difference in distance image blur coefficient, δX_{E} is the chromatic difference in distance image size coefficient, δY_{E} is the chromatic difference in distance directional spread coefficient and δZ_{E} is the chromatic difference in distance directional coefficient.

Similarly, we can define the chromatic difference in near coefficient matrices $\delta\mathbf{V}_{\mathrm{OE}}$ and each of the respective simplifications for when a pinhole is in front of the eye, namely $\delta\mathbf{V}_{\mathrm{E}}^{\mathrm{P}}$ and $\delta\mathbf{V}_{\mathrm{OE}}^{\mathrm{P}}$. Also, we can define the chromatic difference in object space coefficient matrix with respect to position at the retina $\delta\mathbf{V}_{\mathrm{Oy}}$ and with respect to the inclination at the retina $\delta\mathbf{V}_{\mathrm{Oa}}$ and the simplifications when a pinhole is used, $\delta\mathbf{V}_{\mathrm{Oy}}^{\mathrm{P}}$ and $\delta\mathbf{V}_{\mathrm{Oa}}^{\mathrm{P}}$.

7.2.2 Chromatic difference in image positions at the retina

In Figure 7.2.1 we see a pencil of rays of inclination a_{K} incident onto the eye at the entrance plane T_{K}. We choose to follow only one ray from this pencil. For convenience, we choose the chief ray, however any ray could be chosen, for example a marginal ray. Because of dispersion we will have a chief ray for each frequency of which we choose to follow the red and blue chief rays. Because refraction and dispersion start at the entrance plane, but the limiting aperture T_{P} is downstream of the entrance plane, there will be a different incident ray for each frequency. In other words $y_{\mathrm{K}}^{\mathrm{b}} \neq y_{\mathrm{K}}^{\mathrm{r}}$. Similarly, the inclination of the red and blue chief rays will be different through the centre of the pupil, that is, $a_{\mathrm{P}}^{\mathrm{b}} \neq a_{\mathrm{P}}^{\mathrm{r}}$. The red and blue chief rays are shown in Figure 7.2.1 to illustrate this.

We start with Equations 5.2.7 to 9 for an eye and distant object point and Equations 5.2.25 to 27 for an eye and an object point at a finite distance in order to obtain the position and inclination of the ray at the retina.

We define the chromatic difference in position at the retina as

$$\delta y_{\mathrm{R}} = y_{\mathrm{R}}^{\mathrm{b}} - y_{\mathrm{R}}^{\mathrm{r}}. \tag{7.2.2}$$

Substituting from Equations 5.2.5 and 8 into this equation we obtain

$$\delta y_{\mathrm{R}} = W_{\mathrm{E}}^{\mathrm{b}} y_{\mathrm{P}} - W_{\mathrm{E}}^{\mathrm{r}} y_{\mathrm{P}} + X_{\mathrm{E}}^{\mathrm{b}} a_{\mathrm{K}} - X_{\mathrm{E}}^{\mathrm{r}} a_{\mathrm{K}}$$

which we rewrite as

$$\delta y_{\mathrm{R}} = (\delta W_{\mathrm{E}}) y_{\mathrm{P}} + (\delta X_{\mathrm{E}}) a_{\mathrm{K}} \tag{7.2.3}$$

where δW_{E} is the chromatic difference in the distance image blur coefficients and δX_{E} is the chromatic difference in the distance image size coefficients as defined in Equation 7.2.1. The incident pencil of rays has inclination a_{K} and both the red and blue rays go through the same position in the pupil, that is $y_{\mathrm{P}}^{\mathrm{r}} = y_{\mathrm{P}}^{\mathrm{b}}$. Similarly, from Equation 5.2.28, for eyes with an object point at a finite distance we obtain

$$\delta y_{\mathrm{R}} = (\delta W_{\mathrm{OE}}) y_{\mathrm{P}} + (\delta X_{\mathrm{OE}}) y_{\mathrm{O}}. \tag{7.2.4}$$

If the model eye has its pupil centred on the optical axis, then tracing the chief rays such that $y_{\mathrm{P}} = 0$, Equations 7.2.3 and 4 simplify to

$$\delta y_{\mathrm{R}} = (\delta X_{\mathrm{E}}) a_{\mathrm{K}} \tag{7.2.5}$$

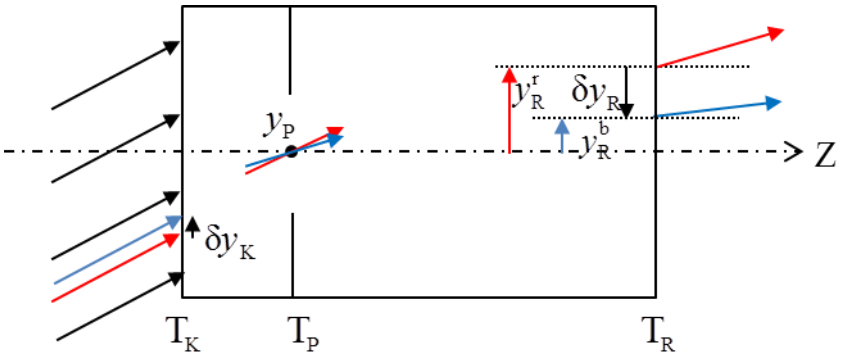

Figure 7.2.1 Chromatic difference in image position is shown as δy_{R}. Rays, all with the same incident inclination a_{K}, enter the eye and traverse a selected position through the pupil, y_{P} and are traced to the retina. The chief ray is illustrated and represents the centre of the blur circle at the retina. At the retina the two rays representing the blue and red light are shown. Chromatic difference in image position is the difference in position on the retina of these two rays, δy_{R}. The red and blue chief rays will follow different paths as illustrated. All measurements are taken at the respective transverse plane. Inclinations and positions are exaggerated for clarity.
for a distant object point and

$$\delta y_{\mathrm{R}} = \left(\delta X_{\mathrm{OE}}\right) y_{\mathrm{O}} \tag{7.2.6}$$

for an object point at a finite distance. Equations 7.2.5 and 6 are both linear equations. From this we can see that the chromatic difference in position for an eye has a linear dependence on incident inclination for distant objects and on object position for finite objects.

We consider distant objects first. In Equation 7.2.5 δX_{E} is a constant for that eye and represents a magnification by the eye. The chromatic difference in position is then linearly dependent on the inclination of the incident light. In Section 5.2.2 we defined the system (subscript E) for the distant object scenario as consisting of just the eye while in Section 5.2.3 we define the system for the near object scenario (subscript OE) to include the eye and working distance. Similarly, at near δX_{OE} represents a constant, provided z_{O} remains unchanged. While the actual value of δX_{OE} will be different to δX_{E} this eye too shows us that chromatic difference in position is linearly dependent on the position of the object. Because z_{O} is incorporated into the coefficient matrix $\delta \mathbf{V}_{\mathrm{OE}}$, δX_{OE} will vary with any change in z_{O}. This will be shown for a selection of numerical examples in Chapter 10.

Let us look at Equations 7.2.5 and 6 in terms of the entries of the transferences. Substituting from Equation 5.2.8 and 5.2.26 into Equations 7.2.5 and 6 respectively, we obtain

$$\delta y_{\mathrm{R}} = \left(\delta \frac{B_{\mathrm{B}} n_0}{A_{\mathrm{A}}}\right) a_{\mathrm{K}} \tag{7.2.7}$$

for a distance object and

$$\delta y_{\mathrm{R}} = \left(\delta \frac{B_{\mathrm{B}}}{A_{\mathrm{A}} \zeta_{\mathrm{O}} - B_{\mathrm{A}}}\right) y_{\mathrm{O}} \tag{7.2.8}$$

for an object at a finite distance before S_{E}. These give us the chromatic difference in transverse position at the retina δy_{R}, firstly with a distant object and secondly with an object at a finite distance, in terms of the fundamental properties of the Gaussian model eye.

An underlying implication

Chromatic dispersion starts as the light enters the first refracting surface, that is, the cornea. However, we then follow only the chief ray, defined by y_{P}. This implies that the blue and red rays that traverse the pupil centre are not originating from the same ray incident on the cornea, but rather two incident rays, both with the same inclination, incident at different positions onto the cornea, as illustrated in Figure 7.2.1. This difference in position is probably rather small, but nonetheless worth noting. Starting with Equations 3.2.40 and 3.5.7 we can derive the formulae for δy_{K}, the chromatic difference in position of the two chief rays at the entrance plane to be

$$\delta y_{\mathrm{K}} = \left[\delta\left(\frac{n_0}{A_{\mathrm{E}}}\left(\frac{B_{\mathrm{B}}}{A_{\mathrm{A}}} - B_{\mathrm{E}}\right)\right)\right]a_{\mathrm{K}} + \left[\delta\left(\frac{1}{A_{\mathrm{A}}}\right)\right]y_{\mathrm{P}} \tag{7.2.9}$$

for a distant object and

$$\delta y_{\mathrm{K}} = \left(\delta\frac{B_{\mathrm{A}}}{B_{\mathrm{OA}}}\right)y_{\mathrm{O}} + \left(\delta\frac{\zeta_{\mathrm{O}}}{B_{\mathrm{OA}}}\right)y_{\mathrm{P}} \tag{7.2.10}$$

for an object point at a finite distance from the eye.

Use of pinhole

We return to Equations 7.2.3 and 4 and consider the clinical scenario where a pinhole is held immediately in front of the eye. The limiting aperture is no longer centred on the optical axis and the chromatic difference in position increases in magnitude with increasing decentration of the pinhole and the object. The entries of $\mathbf{V}_{\mathrm{E}}$ and $\mathbf{V}_{\mathrm{OE}}$, given by Equations 5.2.8 and 26, simplify for the pinhole in front of the eye and therefore Equations 7.2.3 and 4 become

$$\delta y_{\mathrm{R}} = \left(\delta W_{\mathrm{E}}^{\mathrm{P}}\right)y_{\mathrm{P}} + \left(\delta X_{\mathrm{E}}^{\mathrm{P}}\right)a_{\mathrm{K}} \tag{7.2.11}$$

and

$$\delta y_{\mathrm{R}} = \left(\delta W_{\mathrm{OE}}^{\mathrm{P}}\right)y_{\mathrm{P}} + \left(\delta X_{\mathrm{OE}}^{\mathrm{P}}\right)y_{\mathrm{O}} \tag{7.2.12}$$

where the coefficients for $\mathbf{V}_{\mathrm{E}}^{\mathrm{P}}$ and $\mathbf{V}_{\mathrm{OE}}^{\mathrm{P}}$ are given in Equations 5.2.37 and 5.2.34 respectively. In terms of the entries of the transferences Equations 7.2.11 and 12 simplify to become

$$\delta y_{\mathrm{R}} = (\delta A_{\mathrm{E}})y_{\mathrm{P}} + (\delta(B_{\mathrm{E}} n_0))a_{\mathrm{K}} \tag{7.2.13}$$

and

$$\delta y_{\mathrm{R}} = (\delta(A_{\mathrm{E}} - B_{\mathrm{E}}\zeta_{\mathrm{O}}^{-1}))y_{\mathrm{P}} + (\delta(B_{\mathrm{E}}\zeta_{\mathrm{O}}^{-1}))y_{\mathrm{O}}. \tag{7.2.14}$$

Equations 7.2.11 and 12 are the specialised versions of Equations 7.2.3 and 4 which indicate substitution of the coefficients from $\mathbf{V}_{\mathrm{E}}^{\mathrm{P}}$ and $\mathbf{V}_{\mathrm{OE}}^{\mathrm{P}}$ respectively for the special situation of a pinhole placed in front of the eye. The conclusions that we can draw from the four equations are similar: the chromatic difference in position will increase in magnitude firstly for distant objects with the increase in incident inclination, secondly, for object points at a finite distance with increase in transverse displacement of the object point from the axis and finally with increased transverse displacement of the pinhole or position of the ray through the pupil from the optical axis. These conclusions are consistent with the findings in the literature, discussed in Chapter 2.

7.2.3 Chromatic difference in inclination at the retina

In Section 7.2.2 we defined, quite literally, the chromatic difference in image position at the retina. However, in Chapter 2 it was shown that a number of studies treat the chromatic difference in image position as the difference in inclination between the red and blue dispersed rays from a single object point. Here we define chromatic difference in inclination at the retina as the difference in emergent inclination of the two coloured reference rays, dispersed by the eye, from a particular object point, that is to say δa_{R}. This definition is general and defined with centred astigmatic eyes in mind. In an astigmatic eye the nodal structure is not a point and in a multi-surface eye the nodal structure differs in position with frequency and is unlikely to make a pivotal point. Similarly, the entrance pupil is merely an image of the pupil viewed through the cornea. The first refracting surface is a fixed physical structure (with an infinity of optical axes) but is not suitable because the rays do not necessarily coincide at this point. The definition, therefore, measures the difference in inclination of the emergent chromatic rays without concern for where or even if these two rays intersect.

We define the chromatic difference of inclination at the retina as

$$\delta a_{\mathrm{R}} = a_{\mathrm{R}}^{\mathrm{b}} - a_{\mathrm{R}}^{\mathrm{r}} \tag{7.2.15}$$

where $a_{\mathrm{R}}^{\mathrm{b}}$ and $a_{\mathrm{R}}^{\mathrm{r}}$ are the (unreduced) inclinations of the blue and red chief rays at the retina. From Equations 5.2.7 and 29 we obtain the difference in emergent reduced inclination from an eye

$$\delta a_{\mathrm{R}} = (\delta Y_{\mathrm{E}}) y_{\mathrm{P}} + (\delta Z_{\mathrm{E}}) a_{\mathrm{K}} \tag{7.2.16}$$

for a distant object point and

$$\delta a_{\mathrm{R}} = (\delta Y_{\mathrm{OE}}) y_{\mathrm{P}} + (\delta Z_{\mathrm{OE}}) y_{\mathrm{O}} \tag{7.2.17}$$

for a finite-distance object point. For model eyes with a centred pupil this simplifies to

$$\delta a_{\mathrm{R}} = (\delta Z_{\mathrm{E}}) a_{\mathrm{K}} \tag{7.2.18}$$

and

$$\delta a_{\mathrm{R}} = (\delta Z_{\mathrm{OE}}) y_{\mathrm{O}} \tag{7.2.19}$$

for distant and finite object points respectively. Equation 7.2.18, solved for δZ_{E}, resembles Equation 2.3.8 which Thibos, Bradley and Zhang (1991) and Zhang, Thibos and Bradley (1991) define as the chromatic difference in magnification.

The Gaussian eye and a distant object point are shown in Figure 7.2.2. This is an extension of Figure 7.2.1 and the paths of the rays at emergence at the retinal plane are shown. The point where they intersect is unimportant and may, for example, be upstream from the lens which implies that the diagram does not show the actual ray path but merely a projection of the rays inside the eye. In Gaussian eyes, we can envision an intersection, however this may not coincide with the optical axis and is also not necessarily going to intersect with the pupil centre, a refracting surface or any of the cardinal points. This is shown in Figure 7.2.2. It will depend on the complexity of the schematic eye being modelled.

For a Gaussian eye, the red and blue non-parallel rays intersect at some position in the plane of the eye to create a chromatic difference in inclination. However, it is foreseeable that in a three-dimensional linear system with heterocentric astigmatic elements that the red and blue rays are skew rays that may not intersect. It is possible that they may swirl past each other and never coincide. Investigating this is, however, outside the scope of this dissertation.

Use of a pinhole

Let us consider the situation where there is a pinhole held immediately before the corneal plane. Equations 7.2.16 and 17 still hold, however we substitute the relevant coefficients from $\delta\mathbf{V}_{\mathrm{E}}^{\mathrm{P}}$ and $\delta\mathbf{V}_{\mathrm{OE}}^{\mathrm{P}}$ instead of $\delta\mathbf{V}_{\mathrm{E}}$ and $\delta\mathbf{V}_{\mathrm{OE}}$. Two simplifications we will consider are when the light originates firstly from a distant object point and parallel to the optical axis that is $a_{\mathrm{K}}=0$ and secondly from an axial object point, where $y_{\mathrm{O}}=0$. Equations 7.2.16 and 17 simplify to

$$\delta a_{\mathrm{R}}=\left(\delta Y_{\mathrm{E}}^{\mathrm{P}}\right)y_{\mathrm{P}} \tag{7.2.20}$$

and

$$\delta a_{\mathrm{R}}=\left(\delta Y_{\mathrm{OE}}^{\mathrm{P}}\right)y_{\mathrm{P}} \tag{7.2.21}$$

respectively. $Y_{\mathrm{E}}^{\mathrm{P}}$ and $Y_{\mathrm{OE}}^{\mathrm{P}}$ are defined by Equations 5.2.37 and 34. In terms of the entries of the transference, Equations 7.2.20 and 21 simplify to

$$\delta a_{\mathrm{R}}=\left(\delta\left(C_{\mathrm{E}}n^{-1}\right)\right)y_{\mathrm{P}}$$

and

$$\delta a_{\mathrm{R}}=\left(\delta\left(n^{-1}\left(C_{\mathrm{E}}-D_{\mathrm{E}}\zeta_{\mathrm{O}}^{-1}\right)\right)\right)y_{\mathrm{P}},$$

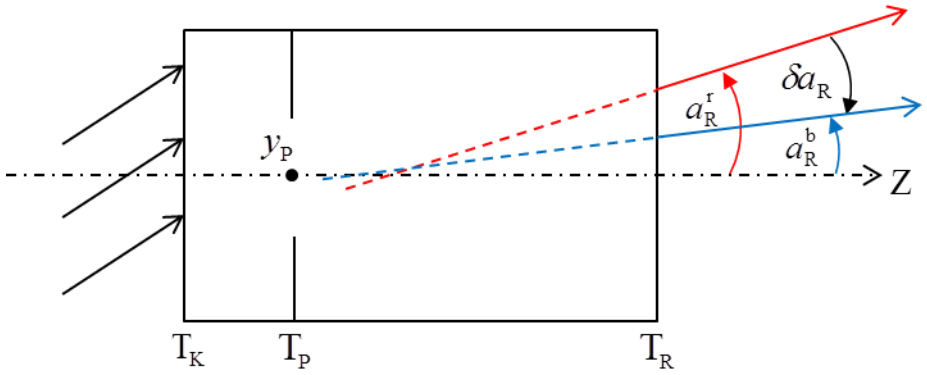

Figure 7.2.2 A Gaussian eye and a pencil of rays from a distant object showing chromatic difference in inclination between the two dispersed rays. The pivotal point is the where the projection of the two rays intersect to create an angle. It may or may not coincide with any reference structure, including the longitudinal axis. Inclinations in the diagram are exaggerated for clarity.

respectively. These are both linear equations showing that, when a pinhole is held immediately in front of the eye, the chromatic difference in inclination at the retina is dependent on the position of the pinhole from the optical axis.

Now from Equations 7.2.16 and 17 we can see that chromatic properties increase with increased transverse displacement of the object point from the optical axis and also with increased transverse displacement of the pinhole from the optical axis. This is consistent with conclusions discussed in Chapter 2.

In summary

Equations 7.2.3 and 16 can be summarised as

$$\delta\mathbf{V}_{\mathrm{E}}\mathbf{v}_{\mathrm{E}} = \delta\mathbf{r}_{\mathrm{R}} \tag{7.2.22}$$

where $\delta\mathbf{V}_{\mathrm{E}}$ is defined by Equation 7.2.1, $\mathbf{v}_{\mathrm{E}}$ by Equation 5.2.9 and $\delta\mathbf{r}_{\mathrm{R}}$ as

$$\delta\mathbf{r}_{\mathrm{R}} = \begin{pmatrix} \delta y_{\mathrm{R}} \\ \delta a_{\mathrm{R}} \end{pmatrix} \tag{7.2.23}$$

giving us δy_{R} the chromatic difference in transverse image position at the retina and δa_{R} chromatic difference in inclination at the retina for a distant object.

Similarly, we can summarise Equations 7.2.4 and 17 as

$$\delta\mathbf{V}_{\mathrm{OE}}\mathbf{v}_{\mathrm{OE}} = \delta\mathbf{r}_{\mathrm{R}} \tag{7.2.24}$$

where $\delta\mathbf{V}_{\mathrm{OE}}$ is defined in Section 7.2.1, $\mathbf{v}_{\mathrm{OE}}$ by Equation 5.2.27 and $\delta\mathbf{r}_{\mathrm{R}}$ by Equation 7.2.23.

In the same way, we can summarise δy_{R} and δa_{R} using a pinhole in front of the eye as

$$\delta\mathbf{V}_{\mathrm{E}}^{\mathrm{P}}\mathbf{v}_{\mathrm{E}} = \delta\mathbf{r}_{\mathrm{R}} \tag{7.2.25}$$

for a distant object and for an object point at a finite distance from the eye as

$$\delta\mathbf{V}_{\mathrm{OE}}^{\mathrm{P}}\mathbf{v}_{\mathrm{OE}} = \delta\mathbf{r}_{\mathrm{R}}\,. \tag{7.2.26}$$

Generalizing to linear optics

The chromatic difference in transverse image position at the retina (Equations 7.2.2 to 6), the chromatic difference in inclination at the retina (Equations 7.2.15 to 19) and their summary (Equations 7.2.22 to 24) readily generalize to linear optics, provided one substitutes from Equations 5.2.38 and 39 when obtaining the chromatic difference in coefficient matrices (Equation 7.2.1). The equations for the scenario when a pinhole is placed immediately in front of the eye for chromatic difference in transverse image position at the retina

(Equations 7.2.11 to 14), the chromatic difference in inclination at the retina (Equations 7.2.20 to 21) and the summary (Equations 7.2.25 and 26) also readily generalize to linear optics. The equations for the underlying implication of chromatic difference in corneal position when the rays originate from the same object point can be rewritten to be general as

$$\delta\mathbf{y}_{\mathrm{K}} = \delta\left(\mathbf{A}_{\mathrm{E}}^{-1}\left(\mathbf{X}_{\mathrm{E}} - n_0\mathbf{B}_{\mathrm{E}}\right)\right)\mathbf{a}_{\mathrm{K}} + \delta\left(\mathbf{A}_{\mathrm{E}}^{-1}\mathbf{W}_{\mathrm{E}}\right)\mathbf{y}_{\mathrm{P}}$$

for a distant object and

$$\delta\mathbf{y}_{\mathrm{K}} = \delta\left(\left(\zeta_{\mathrm{O}}\mathbf{A}_{\mathrm{E}} + n_{\mathrm{O}}^{-1}\mathbf{X}_{\mathrm{E}} - \mathbf{B}_{\mathrm{E}}\right)^{-1}\left(n_{\mathrm{O}}^{-1}\mathbf{X}_{\mathrm{E}} - \mathbf{B}_{\mathrm{E}}\right)\right)\mathbf{y}_{\mathrm{O}} + \delta\left(\left(\zeta_{\mathrm{O}}\mathbf{A}_{\mathrm{E}} + n_{\mathrm{O}}^{-1}\mathbf{X}_{\mathrm{E}} - \mathbf{B}_{\mathrm{E}}\right)^{-1}\left(\zeta_{\mathrm{O}}\mathbf{W}_{\mathrm{E}}\right)\right)\mathbf{y}_{\mathrm{P}}$$

for an object at a finite distance where $\mathbf{X}_{\mathrm{E}}$ and $\mathbf{W}_{\mathrm{E}}$ are given in Equation 5.2.38.

7.3 Chromatic properties of the eye dependent on object size or angular spread

The terminology used in the literature is *chromatic difference in magnification.* Let us start by trying to understand what this term means. Magnification was defined in Section 3.5.1 as a ratio of either the image to object size or the ratio of image's reduced inclination to the object's reduced inclination. In Sections 3.5.3 and 5.2 the magnification is defined for specific circumstances in terms of coefficients, which are also ratios. What meaning, then, can we give to a difference between ratios?

In Chapter 2 we saw that there are a number of different approaches to defining chromatic difference in magnification. Simonet and Campbell (1990) define chromatic difference in magnification as the difference in image sizes at the retina (Equation 2.3.7), but the measurement is given in seconds of arc. Similarly, we firstly define the chromatic difference in image size at the retina, and, secondly, we obtain the chromatic difference in angular spread across the retina.

Thibos, Bradley and Zhang (1991) and Zhang, Thibos and Bradley (1991) define chromatic difference in magnification as the ratio of the difference in angle between the red and blue chief rays to the angle of eccentricity subtended by the object point (Equation 2.3.8). However, is this a difference in magnification or the magnification of differences? They give their resultant chromatic difference in magnification as a percentage. Similarly, we take this definition of magnification

and compare both the magnification of image sizes and the magnification of angular spread between the blue and red images. We will see that the issue of blur is not ignored, but rather is nullified by the definition.

7.3.1 Chromatic difference in image size

In order to obtain the chromatic difference in image size $\delta(\Delta y_{\mathrm{R}})$ we first need to calculate the size of each of the blue and red images from Equation 5.2.5 and then calculate the difference in size between them. For a distant object, the size of the blue image will be

$$\Delta y_{\mathrm{R}}^{\mathrm{b}} = W_{\mathrm{E}}^{\mathrm{b}} y_{\mathrm{P2}} - W_{\mathrm{E}}^{\mathrm{b}} y_{\mathrm{P1}} + X_{\mathrm{E}}^{\mathrm{b}} a_{\mathrm{K2}} - X_{\mathrm{E}}^{\mathrm{b}} a_{\mathrm{K1}}. \tag{7.3.1}$$

The position in the pupil or pinhole is the same for both rays, that is $y_{\mathrm{P1}} = y_{\mathrm{P2}}$ and therefore this simplifies to

$$\Delta y_{\mathrm{R}}^{\mathrm{b}} = X_{\mathrm{E}}^{\mathrm{b}} \Delta a_{\mathrm{K}} \tag{7.3.2}$$

and similarly for the red image. The angle subtended by the distant object is

$$\Delta a_{\mathrm{K}} = a_{\mathrm{K2}} - a_{\mathrm{K1}}. \tag{7.3.3}$$

The chromatic difference in image size is

$$\delta(\Delta y_{\mathrm{R}}) = \Delta y_{\mathrm{R}}^{\mathrm{b}} - \Delta y_{\mathrm{R}}^{\mathrm{r}} = X_{\mathrm{E}}^{\mathrm{b}} \Delta a_{\mathrm{K}} - X_{\mathrm{E}}^{\mathrm{r}} \Delta a_{\mathrm{K}} = (\delta X_{\mathrm{E}})(\Delta a_{\mathrm{K}}) \tag{7.3.4}$$

where $\Delta y_{\mathrm{R}}^{\mathrm{b}}$ is the size of the blue image at the retina and likewise $\Delta y_{\mathrm{R}}^{\mathrm{r}}$ is the size of the red image at the retina, as indicated in Figure 7.3.1. We use the symbolisms Δ to represent a size (difference in position) or angle subtended (difference in inclination) and δ to represent a chromatic difference in, for example, position, size, inclination or angular spread.

The size of the blue image at the retina from an object at a finite distance is

$$\Delta y_{\mathrm{R}}^{\mathrm{b}} = W_{\mathrm{OE}}^{\mathrm{b}} y_{\mathrm{P2}} - W_{\mathrm{OE}}^{\mathrm{b}} y_{\mathrm{P1}} + X_{\mathrm{OE}}^{\mathrm{b}} y_{\mathrm{O2}} - X_{\mathrm{OE}}^{\mathrm{b}} y_{\mathrm{O1}} \tag{7.3.5}$$

but

$$y_{\mathrm{P1}} = y_{\mathrm{P2}} \tag{7.3.6}$$

therefore

$$\Delta y_{\mathrm{R}}^{\mathrm{b}} = X_{\mathrm{OE}}^{\mathrm{b}} \Delta y_{\mathrm{O}}. \tag{7.3.7}$$

and similarly for the size of the red image at the retina. X^{b}_{OE} is the near image size coefficient and represents a magnification of the object to the blue image. It is similar to Equation 3.5.1 which represents a transverse magnification. For near the chromatic difference in image size will be

$$\delta(\Delta y_R) = \Delta y^{b}_{R} - \Delta y^{r}_{R} = X^{b}_{OE}\Delta y_O - X^{r}_{OE}\Delta y_O = (\delta X_{OE})(\Delta y_O) \qquad (7.3.8)$$

where Δy_O is the length of the object at the object plane T_O.

The result indicates that δX_E, the chromatic difference in distance image size coefficients and δX_{OE}, the chromatic difference in near image size coefficients, represent constants and therefore the actual size of the image will depend on the size of the object (for distant objects this is represented by the change in incident inclination of the rays) and not on any transverse displacement of the pupil (or pinhole). We can conclude that δX_E and δX_{OE} represent a chromatic difference in image size magnification by the system of either a distant

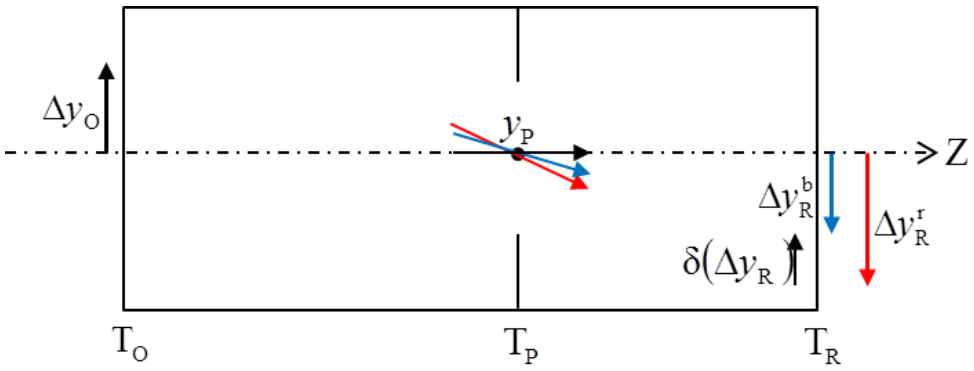

Figure 7.3.1 Chromatic difference in image size $\delta(\Delta y_R)$ in a Gaussian system S_{OE} with the object at a finite distance from the eye S_E. The size of the object is shown at the entrance plane as Δy_O. Rays from the two endpoints of the object enter the eye and are illustrated traversing the pupil, but don't necessarily have to traverse the pupil centre. The two rays are dispersed through the eye and result in a blue and a red image at the retina. One or both images may be blurred, however it is their size magnification that we are interested in. The chromatic difference in magnification is shown as the difference in size of the two coloured images. The figure is drawn for the simpler situation of an axial based object. All objects and images are measured at the respective transverse planes, and are drawn separately for clarity.

or near object. Figure 7.3.1 shows chromatic difference in image size for near for a Gaussian system and axial object, however, it is not necessary for an object to be axial, Equations 7.3.4 and 8 apply to non-axial objects of size Δy_{O}.

7.3.2 Chromatic difference in angular spread at the retina

The chromatic difference in angular spread at the retina $\delta(\Delta a_{\mathrm{R}})$ is obtained in a similar way to the chromatic difference in image size. From Equation 5.2.6 we can define the angular spread of the blue image on the retina as

$$\Delta a_{\mathrm{R}}^{\mathrm{b}} = Y_{\mathrm{E}}^{\mathrm{b}} y_{\mathrm{P2}} - Y_{\mathrm{E}}^{\mathrm{b}} y_{\mathrm{P1}} + Z_{\mathrm{E}}^{\mathrm{b}} a_{\mathrm{K2}} - Z_{\mathrm{E}}^{\mathrm{b}} a_{\mathrm{K1}}. \tag{7.3.9}$$

Equation 7.3.6 applies and so Equation 7.3.9 simplifies to

$$\Delta a_{\mathrm{R}}^{\mathrm{b}} = Z_{\mathrm{E}}^{\mathrm{b}} \Delta a_{\mathrm{K}} \tag{7.3.10}$$

and similarly for the angular spread of the red image across the retina. $Z_{\mathrm{E}}^{\mathrm{b}}$ is the distance directional coefficient and represents a magnification of the angular spread of the incident rays to the blue emergent rays. For an axial object, Equation 7.3.10 is similar to Equation 3.5.3, the angular magnification of image to object. To calculate the chromatic difference in angular spread between the red and blue images across the retina from an object with angular spread of Δa_{K}, we obtain

$$\delta(\Delta a_{\mathrm{R}}) = \Delta a_{\mathrm{R}}^{\mathrm{b}} - \Delta a_{\mathrm{R}}^{\mathrm{r}} = Z_{\mathrm{E}}^{\mathrm{b}} \Delta a_{\mathrm{K}} - Z_{\mathrm{E}}^{\mathrm{r}} \Delta a_{\mathrm{K}} = (\delta Z_{\mathrm{E}})(\Delta a_{\mathrm{K}}). \tag{7.3.11}$$

Similarly, the chromatic difference in angular spread for an object with size Δy_{O} at a finite distance is

$$\delta(\Delta a_{\mathrm{R}}) = (\delta Z_{\mathrm{OE}})(\Delta y_{\mathrm{O}}). \tag{7.3.12}$$

δZ_{E} is the chromatic difference in distance directional coefficient and δZ_{OE} is the chromatic difference in near directional coefficient, both being constants for any particular chosen system. Equations 7.3.11 and 12 are linear equations with δZ_{E} and δZ_{OE} representing the slope. δZ_{E} magnifies the incident angular spread from the object and, likewise, δZ_{OE} magnifies the object size to obtain the $\delta(\Delta a_{\mathrm{R}})$.

The angular spread Δa_{R} is the difference in inclination of the two rays that subtend the end-points of an image on the retina, that is $\Delta a_{\mathrm{R}} = a_{\mathrm{R2}} - a_{\mathrm{R1}}$. The pivotal point where these two rays (a_{R1} and a_{R2}) meet is not necessarily

represented by a cardinal point, the longitudinal axis or a physical structure. The red and blue images have different sizes and will subtend different Δa_{R}. The pivotal points for the red and blue images will not necessarily coincide. This is a different definition to that defined in the literature by angle *t* in Figures 2.3.3 and 4, however, it does represent the actual rays and as such has implications for the Stiles-Crawford effect.

Chromatic difference in image size and angular spread with a pinhole

We can obtain the chromatic difference in image size and angular spread at the retina when a pinhole is placed immediately in front of the eye using Equations 7.3.4, 8, 11 and 12, and replacing the coefficients with the respective coefficients from $\mathbf{V}_{\mathrm{E}}^{\mathrm{P}}$ (Equation 5.2.37) and $\mathbf{V}_{\mathrm{OE}}^{\mathrm{P}}$ (Equation 5.2.34). The effect of placing a pinhole immediately in front of the eye has the effect of moving the limiting aperture longitudinally. However, the effect of any transverse displacement of the pinhole is nullified, as shown by Equation 7.3.6.

In summary

Equations 7.3.4 and 11 can be summarized as

$$\delta\mathbf{V}_{\mathrm{E}}\Delta\mathbf{v}_{\mathrm{E}} = \delta\Delta\mathbf{r}_{\mathrm{R}} \tag{7.3.13}$$

where $\delta\mathbf{V}_{\mathrm{E}}$ is the chromatic difference in coefficient matrix given in Equation 7.2.1,

$$\Delta\mathbf{v}_{\mathrm{E}} = \begin{pmatrix} \Delta y_{\mathrm{P}} \\ \Delta a_{\mathrm{K}} \end{pmatrix} \tag{7.3.14}$$

where $\Delta y_{\mathrm{P}} = 0$ and Δa_{K} is the angular spread indicating the distant object size, and

$$\delta\Delta\mathbf{r}_{\mathrm{R}} = \delta\begin{pmatrix} \Delta y_{\mathrm{R}} \\ \Delta a_{\mathrm{R}} \end{pmatrix} \tag{7.3.15}$$

is the chromatic difference in image sizes $\delta\Delta y_{\mathrm{R}}$ or chromatic difference in angular spread $\delta\Delta a_{\mathrm{R}}$ at the retina.

Similarly, we summarize Equations 7.3.8 and 12 as

$$\delta\mathbf{V}_{\mathrm{OE}}\Delta\mathbf{v}_{\mathrm{OE}} = \delta\Delta\mathbf{r}_{\mathrm{R}} \tag{7.3.16}$$

where

$$\Delta\mathbf{v}_{\mathrm{OE}} = \begin{pmatrix} \Delta y_{\mathrm{P}} \\ \Delta y_{\mathrm{O}} \end{pmatrix}, \tag{7.3.17}$$

$\Delta y_{\mathrm{P}} = 0$ and Δy_{O} is the object size. When placing a pinhole immediately in front of the eye, we substitute $\delta\mathbf{V}_{\mathrm{E}}^{\mathrm{P}}$ for $\delta\mathbf{V}_{\mathrm{E}}$ and $\delta\mathbf{V}_{\mathrm{OE}}^{\mathrm{P}}$ for $\delta\mathbf{V}_{\mathrm{OE}}$ in Equations 7.3.13 and 16 respectively.

Generalizing to linear optics

The chromatic difference in image size (Equations 7.3.1 to 8) and the chromatic difference in angular spread (Equations 7.3.9 to 12) as well as the respective summary (Equations 7.3.13 to 17) readily generalize to linear optics, provided one substitutes from Equations 5.2.38 and 39 when obtaining the chromatic difference in coefficient matrices (Equation 7.2.1).

7.3.3 Retinal chromatic image size magnification

In this section we adopt the method described by Thibos *et al* (1991) and Zhang *et al* (1991) of defining chromatic difference in magnification (Equation 2.3.8) as a ratio. We first investigate the retinal chromatic image size magnification and then the retinal chromatic angular spread magnification. The retinal chromatic image size magnification is defined as the magnification of the size of the red image to obtain the size of the blue image at the retina as

$$M_{\mathrm{yR}}\ \Delta y_{\mathrm{R}}^{\mathrm{r}} = \Delta y_{\mathrm{R}}^{\mathrm{b}} \tag{7.3.18}$$

where $\Delta y_{\mathrm{R}}^{\mathrm{b}}$ and $\Delta y_{\mathrm{R}}^{\mathrm{r}}$ are the blue and red retinal image sizes defined by Equation 7.3.2. Substituting from Equation 7.3.2 into 7.3.18 we obtain

$$M_{\mathrm{yR}} X_{\mathrm{E}}^{\mathrm{r}} \Delta a_{\mathrm{K}} = X_{\mathrm{E}}^{\mathrm{b}} \Delta a_{\mathrm{K}}$$

which simplifies to

$$M_{\mathrm{yR}} X_{\mathrm{E}}^{\mathrm{r}} = X_{\mathrm{E}}^{\mathrm{b}} \tag{7.3.19}$$

for a distant object. Substituting from Equation 7.3.7 into 7.3.18 we obtain

$$M_{\mathrm{yR}} X_{\mathrm{OE}}^{\mathrm{r}} \Delta y_{\mathrm{O}} = X_{\mathrm{OE}}^{\mathrm{b}} \Delta y_{\mathrm{O}}$$

which simplifies to

$$M_{\mathrm{yR}} X^{\mathrm{r}}_{\mathrm{OE}} = X^{\mathrm{b}}_{\mathrm{OE}} \tag{7.3.20}$$

for an object at a finite distance. Taking the magnification a step further, we can substitute the elements of the transferences, as defined in Equations 5.2.8 and 26 into 7.3.19 and 20 to obtain

$$M_{\mathrm{yR}} B^{\mathrm{r}}_{\mathrm{B}} A^{\mathrm{b}}_{\mathrm{A}} n^{\mathrm{r}}_0 = B^{\mathrm{b}}_{\mathrm{B}} A^{\mathrm{r}}_{\mathrm{A}} n^{\mathrm{b}}_0 \tag{7.3.21}$$

and

$$M_{\mathrm{yR}} B^{\mathrm{r}}_{\mathrm{B}} \left(A^{\mathrm{b}}_{\mathrm{A}} \zeta^{\mathrm{b}}_{\mathrm{O}} - B^{\mathrm{b}}_{\mathrm{A}} \right) = B^{\mathrm{b}}_{\mathrm{B}} \left(A^{\mathrm{r}}_{\mathrm{A}} \zeta^{\mathrm{r}}_{\mathrm{O}} - B^{\mathrm{r}}_{\mathrm{A}} \right) \tag{7.3.22}$$

respectively. From Equations 7.3.19 to 22 we can conclude that the retinal chromatic size magnification will be a fixed ratio for the system and does not depend on object size or transverse position.

7.3.4 Retinal chromatic angular spread magnification

The second approach to retinal chromatic magnifications makes use of the angular spread, obtaining the magnification of the red to blue angular spreads of the emergent chief rays reaching the retina from an object. We therefore define the retinal chromatic angular spread magnification as

$$M_{a\mathrm{R}} \Delta a^{\mathrm{r}}_{\mathrm{R}} = \Delta a^{\mathrm{b}}_{\mathrm{R}} \tag{7.3.23}$$

where $\Delta a^{\mathrm{b}}_{\mathrm{R}}$ and $\Delta a^{\mathrm{r}}_{\mathrm{R}}$ are the angular spread across the retina for the blue and red images. We define the blue angular spread at the retina, $\Delta a^{\mathrm{b}}_{\mathrm{R}}$ as

$$\Delta a^{\mathrm{b}}_{\mathrm{R}} = Y^{\mathrm{b}}_{\mathrm{E}} y_{\mathrm{P2}} - Y^{\mathrm{b}}_{\mathrm{E}} y_{\mathrm{P1}} + Z^{\mathrm{b}}_{\mathrm{E}} a_{\mathrm{K2}} - Z^{\mathrm{b}}_{\mathrm{E}} a_{\mathrm{K1}} \tag{7.3.24}$$

however, the two rays traverse the same position through the pupil and therefore

$$\Delta a^{\mathrm{b}}_{\mathrm{R}} = Z^{\mathrm{b}}_{\mathrm{E}} \Delta a_{\mathrm{K}} \tag{7.3.25}$$

and similarly for the angular spread of the red image at the retina. The angular spread of a blue image at the retina from an object at a finite distance is

$$\Delta a^{\mathrm{b}}_{\mathrm{R}} = Z^{\mathrm{b}}_{\mathrm{OE}} \Delta y_{\mathrm{O}} . \tag{7.3.26}$$

Substituting from Equations 7.3.25 and 26 in turn into Equation 7.3.23 we obtain

$$M_{a\mathrm{R}} Z^{\mathrm{r}}_{\mathrm{E}} \Delta a_{\mathrm{K}} = Z^{\mathrm{b}}_{\mathrm{E}} \Delta a_{\mathrm{K}}$$

which simplifies to

$$M_{a\mathrm{R}} Z^{\mathrm{r}}_{\mathrm{E}} = Z^{\mathrm{b}}_{\mathrm{E}} \tag{7.3.27}$$

for a distant object and

$$M_{aR} Z^{r}_{OE} \Delta y_O = Z^{b}_{OE} \Delta y_O$$

which in turn simplifies to

$$M_{aR} Z^{r}_{OE} = Z^{b}_{OE} \tag{7.3.28}$$

for an object at a finite distance, respectively. We now substitute from Equations 5.2.8 and 26 into the above equations respectively to obtain

$$M_{aR} D^{r}_{B} A^{b}_{A} n^{r}_{0} n^{b} = D^{b}_{B} A^{r}_{A} n^{b}_{0} n^{r} \tag{7.3.29}$$

for distance objects and

$$M_{aR} D^{r}_{B} \left(A^{b}_{A} \zeta^{b}_{O} - B^{b}_{A} \right) n^{b} = D^{b}_{B} \left(A^{r}_{A} \zeta^{r}_{O} - B^{r}_{A} \right) n^{r} \tag{7.3.30}$$

for objects at a finite distance. Again we can conclude that the retinal chromatic angular spread magnification is not dependent on the object's size or transverse position.

Comparing Equation 7.3.21 to 7.3.29 and 7.3.22 to 7.3.30 we see that the only variable that is different in the two pairs of equations is the ratio $\frac{B^{b}_{B}}{B^{r}_{B}}$ for retinal chromatic size magnification versus $\frac{D^{b}_{B} n^{r}}{D^{r}_{B} n^{b}}$ for the retinal chromatic angular spread magnification. We will do numerical examples in Chapter 10 to see how these ratios affect our ultimate result.

Retinal chromatic magnifications with a pinhole

We have seen that, when comparing image sizes of the red and blue images on the retina, the effect of transverse displacement of a pinhole y_P in front of the eye is nullified, however, the effect of displacing the longitudinal position of the limiting aperture will have an effect on the coefficients and hence on the magnifications. For each of Equations 7.3.19, 20, 27 and 28, we replace the respective coefficient with those from $\mathbf{V}^{P}_{E}$ (Equation 5.2.37) and $\mathbf{V}^{P}_{OE}$ (Equation 5.2.34), the distance and near coefficient matrices for a Gaussian eye with a pinhole immediately in front of it.

Generalizing to linear optics

The Equations in Section 7.3 have been written and derived such that they readily generalize to linear optics. The proof is beyond the scope of this dissertation.

7.4 Chromatic properties of the eye dependent on image and aperture positions

The derivations in Sections 7.2 and 3 apply in image space. However, experimental measurements and analyses are done in object space. In Section 2.3.2 we learnt that experiments make use of a target at a finite distance, a Vernier scale to measure the induced chromatic effect and a pinhole or Maxwellian view which controls and varies the position of the ray entering the eye (Thibos *et al*, 1990, 1992; Simonet and Campbell, 1990). The pinhole has the added benefit of eliminating any refractive compensation needed without the use of spectacle lenses which could add chromatic properties to the experiment (Thibos *et al*, 1990).

7.4.1 Chromatic difference in object position

Consider an eye and two coloured object points at different positions in object space. The two objects appear to be lined up on the retina as shown in Figure 7.4.1 where $y_{\mathrm{R}}^{\mathrm{b}} = y_{\mathrm{R}}^{\mathrm{r}}$. The superimposed points may or may not be at the fovea, and the emergent inclination need not be the same for the red and blue rays. Because such experiments are conducted in the clinical environment, we shall derive formulae for the near scenario only.

From Figure 7.4.1 we can see that while there are two object points of different frequencies at positions $y_{\mathrm{O}}^{\mathrm{b}}$ and $y_{\mathrm{O}}^{\mathrm{r}}$, we have a common transverse position through the pupil y_{P} for the chosen ray path for each frequency. The two rays arrive at a common point on the retina y_{R} where it should appear to the eye as being one object point; that is the two image points of differing frequencies are superimposed.

We wish to obtain the chromatic distance between the two object points, δy_{O}. From Equation 5.3.17 we obtain

$$\delta y_{\mathrm{O}} = \left(\delta W_{\mathrm{Oy}}\right) y_{\mathrm{P}} + \left(\delta X_{\mathrm{Oy}}\right) y_{\mathrm{R}} \tag{7.4.1}$$

where

$$\delta y_{\mathrm{O}} = y_{\mathrm{O}}^{\mathrm{b}} - y_{\mathrm{O}}^{\mathrm{r}} \tag{7.4.2}$$

is the distance between the red and blue object points at the object plane. δW_{Oy} is the chromatic difference in near object blur coefficient and δX_{Oy} is the chromatic difference in near object size coefficient, both with respect to the position of the image at the retina. Equation 7.4.1 gives us the chromatic difference in position for two object points of different frequencies in object space. This is comparable to the clinical or experimental scenario described in Section 2.3.2. It is a simple matter to choose the position of the fovea as y_{R}, where applicable. For the scenario where there is no pinhole and the pupil is centred on the optical axis such that $y_{\mathrm{P}} = 0$, we obtain the linear relationship

$$\delta y_{\mathrm{O}} = \left(\delta X_{\mathrm{Oy}}\right) y_{\mathrm{R}}. \tag{7.4.3}$$

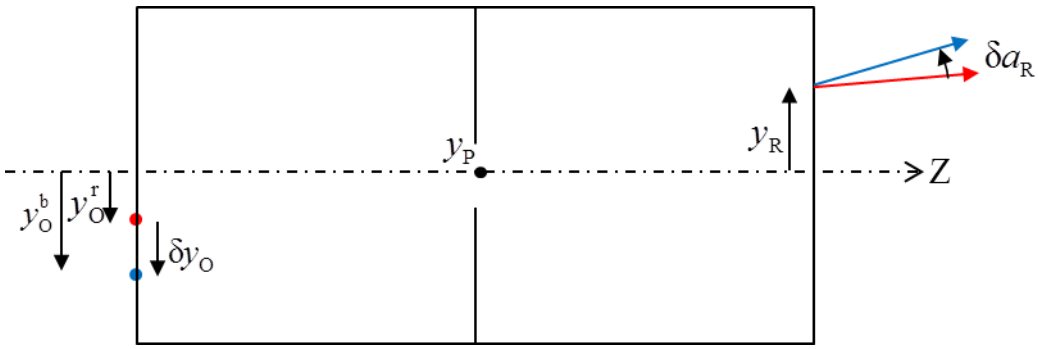

Figure 7.4.1 Chromatic difference in object position. A Gaussian system S_{OE} at near. The object consists of two separated point targets of different frequencies and at different transverse positions. The emergent rays coincide positionally at the retinal plane. The figure is general and the dividing plane may represent either a pupil or a pinhole. All measurements are taken at the respective transverse planes, but these are separated in the diagram for clarity.

For two chosen frequencies and a set working distance, δX_{Oy} will be a constant representing a magnification. Any increase in the magnitude of y_{R} will result in an increase in the separation of the red and blue object points δy_{O}. When fixation is set at the fovea it is possible to obtain the position of the fovea, $y_{\mathrm{R}} = \delta y_{\mathrm{O}} / \left(\delta X_{\mathrm{Oy}}\right)$ (from Equation 7.4.3), for a centred pupil.

Including the use of a pinhole

On the other hand, the preferred experimental procedure is to place a pinhole in front of the eye, immediately in front of the entrance plane or corneal plane and keep the position of the image on the retina constant. Equation 7.4.1 still applies, except that we can substitute the coefficients from the simpler $\delta \mathbf{V}_{\mathrm{Oy}}^{\mathrm{P}}$ such that

$$\delta y_{\mathrm{O}} = \left(\delta W_{\mathrm{Oy}}^{\mathrm{P}}\right) y_{\mathrm{P}} + \left(\delta X_{\mathrm{Oy}}^{\mathrm{P}}\right) y_{\mathrm{R}} . \tag{7.4.4}$$

Substituting from Equation 5.3.19 and then from Equation 3.4.6 we obtain

$$\delta y_{\mathrm{O}} = \left(\delta\left(1 - B_{\mathrm{E}}^{-1} A_{\mathrm{E}} \zeta_{\mathrm{O}}\right)\right) y_{\mathrm{P}} + \left(\delta\left(B_{\mathrm{E}}^{-1} \zeta_{\mathrm{O}}\right)\right) y_{\mathrm{R}} = \left(\delta\left(1 - F_0 \zeta_{\mathrm{O}}\right)\right) y_{\mathrm{P}} + \left(\delta\left(B_{\mathrm{E}}^{-1} \zeta_{\mathrm{O}}\right)\right) y_{\mathrm{R}} \tag{7.4.5}$$

where F_0 is the refractive compensation for the eye at the specified frequency.

For a model eye the fovea coincides with the optical axis at $y_{\mathrm{R}} = 0$ simplifying Equations 7.4.4 and 5 even further. However, the fovea is usually not on the optical axis, but does represent a constant for y_{R}. This means that Equation 7.4.4 is the equation for a straight line with $\left(\delta X_{\mathrm{Oy}}^{\mathrm{P}}\right) y_{\mathrm{R}}$ being a constant and $\left(\delta W_{\mathrm{Oy}}^{\mathrm{P}}\right)$ giving the slope of the straight line. From Equation 7.4.5 we can see that the separation of the two object points is directly proportional to the displacement of the pinhole from the optical axis and the constant of proportionality is related to the chromatic difference in refractive compensation and working distance.

7.4.2 Chromatic difference in inclination in object space

We again turn our attention to Figure 7.4.1, to obtain the chromatic difference in inclination in object space of each of the red and blue chief rays that will ultimately both reach the retina at the same point. When the aperture plane is

that of the pinhole, then these two rays will meet and create a point of intersection at the centre of the pinhole. However, when the aperture plane is the eye's pupil, then the rays will undergo refraction before reaching the pupil and, in Gaussian optics, the straight line projections of the two rays will meet at some other point, which may or may not be on the optical axis.

Figure 2.3.3(b) shows the definition of chromatic difference in position as the angle *t* between the incident chief rays for the blue and red targets. With this in mind we will derive equations to solve for δa_{O}.

In order to obtain the angle between the red and blue chief rays from a red and a blue object point, respectively, on the object plane which coincide at a single point on the retina we can obtain, from Equation 5.3.18, an equation for chromatic difference in inclination in object space

$$\delta a_{\mathrm{O}} = \left(\delta Y_{\mathrm{Oy}}\right) y_{\mathrm{P}} + \left(\delta Z_{\mathrm{Oy}}\right) y_{\mathrm{R}} . \qquad (7.4.6)$$

For a model eye with a centred pupil and no pinhole, we can equate $y_{\mathrm{P}} = 0$ and Equation 7.4.6 simplifies to

$$\delta a_{\mathrm{O}} = \left(\delta Z_{\mathrm{Oy}}\right) y_{\mathrm{R}} \qquad (7.4.7)$$

from which we can see the linear relationship that the angle between the two rays of differing frequencies increases with increasing transverse position on the retinal plane from the optical axis.

Including the use of a pinhole

In Section 2.3.2 we saw that the angular difference between the two incident rays which vary with displacement of a pinhole from the optical axis and create a single image at the retina is referred to by Thibos *et al* (1990) as induced transverse chromatic aberration. This is specifically achieved by the use of a pinhole immediately in front of the eye and held at varying transverse distances from the model eye's optical axis, that is, where y_{P} is not necessarily zero. Equation 7.4.6 is general and still applies, with substitution of the coefficients from $\delta \mathbf{V}_{\mathrm{Oy}}^{\mathrm{P}}$ for the pinhole situation. For simplicity, we again allow the retinal image to coincide with the eye's longitudinal axis, that is at $y_{\mathrm{R}} = 0$. This is

consistent with the assumption that in model eyes the fovea coincides with the optical axis. Equation 7.4.6 therefore simplifies to

$$\delta a_{\mathrm{O}} = \left(\delta Y_{\mathrm{Oy}}^{\mathrm{P}}\right) y_{\mathrm{P}}. \tag{7.4.8}$$

Substituting from Equations 5.3.19 and 3.4.6 we obtain

$$\delta a_{\mathrm{O}} = \left(\delta\left(-\left(n_0 B_{\mathrm{E}}\right)^{-1} A_{\mathrm{E}}\right)\right) y_{\mathrm{P}} = \left(\delta\left(-n_0^{-1} F_0\right)\right) y_{\mathrm{P}}. \tag{7.4.9}$$

Unsurprising, this equation, like Equation 7.4.7, gives us a linear relationship between the angular spread from the red to the blue object points at incidence onto the pinhole, the chromatic difference in refractive compensation and the displacement of the pinhole from the optical axis. It resembles Equation 2.3.5 which Thibos *et al* (1990) define as induced transverse chromatic aberration.

Simonet and Campbell (1990) also describe a relationship resembling Equations 2.3.5 and 7.4.9 to measure the transverse chromatic aberration, however, in their equation *h* is defined at the pupillary plane whereas Thibos *et al* (1990) and Equation 7.4.9 are defined for a pinhole at the corneal plane. However, $\delta Y_{\mathrm{Oy}}^{\mathrm{P}} \neq \delta Y_{\mathrm{Oy}}$ which may explain the discrepancy in results described by Simonet and Campbell between their indirect derivation (using Equation 2.3.5) and direct measurements (obtained experimentally) and defined by Equation 7.4.6. Exploring this further is beyond the scope of this dissertation.

In summary

Equations 7.4.1 and 6 can be summarized as

$$\delta\mathbf{V}_{\mathrm{Oy}}\mathbf{v}_{\mathrm{Oy}} = \delta\mathbf{r}_{\mathrm{O}} \tag{7.4.10}$$

where $\delta\mathbf{V}_{\mathrm{Oy}}$ is defined in Section 7.2.1, $\mathbf{v}_{\mathrm{Oy}}$ is given by Equation 5.3.15 and

$$\delta\mathbf{r}_{\mathrm{O}} = \begin{pmatrix} \delta y_{\mathrm{O}} \\ \delta a_{\mathrm{O}} \end{pmatrix}. \tag{7.4.11}$$

δy_{O} defines the chromatic difference in transverse object position and δa_{O} is the chromatic difference in inclination in object space.

Similarly the scenario of placing a pinhole immediately in front of the eye can be summarized as

$$\delta\mathbf{V}_{\mathrm{Oy}}^{\mathrm{P}}\mathbf{v}_{\mathrm{Oy}} = \delta\mathbf{r}_{\mathrm{O}} \tag{7.4.12}$$

where $\delta\mathbf{V}_{\mathrm{Oy}}^{\mathrm{P}}$ is defined by Equation 5.3.19.

From Equations 7.4.10 and 12 we can see that chromatic difference in position and inclination in object space is a function of both transverse displacement of the retinal image from the optical axis and transverse displacement of the pinhole from the optical axis.

An underlying implication

We return to the experimental setup with the pinhole as the limiting aperture and underlying assumptions as shown in Figure 7.4.1. The experiments theorise that the two different chromatic images are superimposed at the retina and perceived as one. This implies $y_{\mathrm{R}}^{\mathrm{b}} = y_{\mathrm{R}}^{\mathrm{r}}$. However, it is quite possible that the inclination at the retina of the two chromatic rays is not the same. This has implications for the Stiles-Crawford effect. We derive an equation to obtain the chromatic difference in inclination of these two rays at the retina, δa_{R}. The red and blue chief rays are traversing the pupil through the same position. We therefore start at the plane of the aperture. From Equation 5.2.18 and 19 and equating for α_{P}, simplifying, solving for a_{R} and then taking the chromatic difference we obtain

$$\delta a_{\mathrm{R}} = \left(\delta\left(-nB_{\mathrm{B}}\right)^{-1}\right)y_{\mathrm{P}} + \left(\delta\left(D_{\mathrm{B}}\left(B_{\mathrm{B}}n\right)^{-1}\right)\right)y_{\mathrm{R}} \qquad (7.4.13)$$

which is the chromatic difference in inclination at the retina when two rays from separated objects of differing frequencies are superimposed at the retina.

Generalizing to linear optics

Equations 7.4.1 to 12 readily generalize to linear optics provided we substitute from Equation 5.3.25 for $\mathbf{V}_{\mathrm{Oy}}$ and from Equation 5.3.26 for $\mathbf{V}_{\mathrm{Oy}}^{\mathrm{P}}$. For Equation 7.4.13 we need to include a transpose to obtain

$$\delta\mathbf{a}_{\mathrm{R}} = \left(\delta\left(-n\mathbf{B}_{\mathrm{B}}^{\mathrm{T}}\right)^{-1}\right)\mathbf{y}_{\mathrm{P}} + \left(\delta\left(\mathbf{D}_{\mathrm{B}}\left(\mathbf{B}_{\mathrm{B}}n\right)^{-1}\right)\right)\mathbf{y}_{\mathrm{R}}\,. \qquad (7.4.14)$$

7.5 Chromatic properties of the eye dependent on object size or angular spread

In Section 2.3.2 we saw that experiments are designed to measure chromatic difference in position of a red and a blue object point in object space. When working in object space experimentally, we are working with single red and blue object points rather than objects with size, according to the current literature. Chromatic difference in image size and angular spread are calculated in image space using ray tracing based on the experimental data for objects with size. It is conceivable that an experiment could be devised to compare the sizes of a red and a blue object to appear to be the same size in image space.

7.5.1 Chromatic difference in object size

The approach to obtaining the chromatic difference in object size is similar to that for the retinal chromatic difference in image size. Substituting from Equation 5.3.17, the size of the blue object is

$$\Delta y_{\mathrm{O}}^{\mathrm{b}} = W_{\mathrm{Oy}}^{\mathrm{b}} y_{\mathrm{P2}}^{\mathrm{b}} - W_{\mathrm{Oy}}^{\mathrm{b}} y_{\mathrm{P1}}^{\mathrm{b}} + X_{\mathrm{Oy}}^{\mathrm{b}} y_{\mathrm{R2}}^{\mathrm{b}} - X_{\mathrm{Oy}}^{\mathrm{b}} y_{\mathrm{R1}}^{\mathrm{b}} \tag{7.5.1}$$

where the blue rays all go through the same position in the pupil such that

$$y_{\mathrm{P2}}^{\mathrm{b}} = y_{\mathrm{P1}}^{\mathrm{b}}. \tag{7.5.2}$$

Equation 7.5.1 simplifies to obtain

$$\Delta y_{\mathrm{O}}^{\mathrm{b}} = X_{\mathrm{Oy}}^{\mathrm{b}} \left(\Delta y_{\mathrm{R}}^{\mathrm{b}} \right), \tag{7.5.3}$$

the blue object size, where

$$\Delta y_{\mathrm{R}}^{\mathrm{b}} = y_{\mathrm{R2}}^{\mathrm{b}} - y_{\mathrm{R1}}^{\mathrm{b}} \tag{7.5.4}$$

is the size of the blue image at the retina. The size of the red object is obtained in a similar fashion. The chromatic difference in object size is obtained when the red and blue images at the retina appear to have the same size, such that

$$\Delta y_{\mathrm{R}}^{\mathrm{b}} = \Delta y_{\mathrm{R}}^{\mathrm{r}}. \tag{7.5.5}$$

The chromatic difference in object size is

$$\delta\left(\Delta y_{\mathrm{O}}\right) = \Delta y_{\mathrm{O}}^{\mathrm{b}} - \Delta y_{\mathrm{O}}^{\mathrm{r}} = X_{\mathrm{Oy}}^{\mathrm{b}} \left(\Delta y_{\mathrm{R}}^{\mathrm{b}} \right) - X_{\mathrm{Oy}}^{\mathrm{r}} \left(\Delta y_{\mathrm{R}}^{\mathrm{r}} \right) = \delta X_{\mathrm{Oy}} \left(\Delta y_{\mathrm{R}} \right) \tag{7.5.6}$$

where δX_{Oy} is described in Section 7.2.1

7.5.2 Chromatic difference in object angular spread

The angular spread of the blue object $\Delta a_{\mathrm{O}}^{\mathrm{b}}$ is obtained from Equation 5.3.18 to be

$$\Delta a_{\mathrm{O}}^{\mathrm{b}} = Y_{\mathrm{Oy}}^{\mathrm{b}} y_{\mathrm{P2}}^{\mathrm{b}} - Y_{\mathrm{Oy}}^{\mathrm{b}} y_{\mathrm{P1}}^{\mathrm{b}} + Z_{\mathrm{Oy}}^{\mathrm{b}} y_{\mathrm{R2}}^{\mathrm{b}} - Z_{\mathrm{Oy}}^{\mathrm{b}} y_{\mathrm{R1}}^{\mathrm{b}}. \tag{7.5.7}$$

Equation 7.5.2 applies and so Equation 7.5.7 simplifies to obtain the angular spread from the blue object,

$$\Delta a_{\mathrm{O}}^{\mathrm{b}} = Z_{\mathrm{Oy}}^{\mathrm{b}} \left(\Delta y_{\mathrm{R}}^{\mathrm{b}} \right) \tag{7.5.8}$$

where the size of the blue retinal image $\Delta y_{\mathrm{R}}^{\mathrm{b}}$ is defined by Equation 7.5.4. Similarly, we obtain the red object angular spread. The chromatic difference in object angular spread is

$$\delta\left(\Delta a_{\mathrm{O}}\right) = \Delta a_{\mathrm{O}}^{\mathrm{b}} - \Delta a_{\mathrm{O}}^{\mathrm{r}} = Z_{\mathrm{Oy}}^{\mathrm{b}} \left(\Delta y_{\mathrm{R}}^{\mathrm{b}} \right) - Z_{\mathrm{Oy}}^{\mathrm{r}} \left(\Delta y_{\mathrm{R}}^{\mathrm{r}} \right) = \delta Z_{\mathrm{Oy}} \left(\Delta y_{\mathrm{R}} \right) \tag{7.5.9}$$

where δX_{Oy} is described in Section 7.2.1.

Summary of chromatic differences in object space

Equations 7.5.6 and 9 can be summarized as

$$\delta \mathbf{V}_{\mathrm{Oy}} \, \Delta \mathbf{v}_{\mathrm{Oy}} = \delta\left(\Delta \mathbf{r}_{\mathrm{O}}\right) \tag{7.5.10}$$

where $\delta \mathbf{V}_{\mathrm{Oy}}$ is described in Section 7.2.1,

$$\delta\left(\Delta \mathbf{r}_{\mathrm{O}}\right) = \delta \begin{pmatrix} \Delta y_{\mathrm{O}} \\ \Delta a_{\mathrm{O}} \end{pmatrix} \tag{7.5.11}$$

is the chromatic difference in object size and angular spread vector and

$$\Delta \mathbf{v}_{\mathrm{Oy}} = \begin{pmatrix} \Delta y_{\mathrm{P}} \\ \Delta y_{\mathrm{R}} \end{pmatrix} \tag{7.5.12}$$

where $\Delta y_{\mathrm{P}} = 0$.

7.5.3 Chromatic object size magnification

Similar to Section 7.3.3, we can obtain the magnification of the size of the red to blue objects when the red and blue images appear to have the same size to the subject. We define the chromatic object size magnification as

$$M_{\mathrm{yO}} \, \Delta y_{\mathrm{O}}^{\mathrm{r}} = \Delta y_{\mathrm{O}}^{\mathrm{b}}. \tag{7.5.13}$$

Substituting from Equation 7.5.3 for the blue and red object sizes we obtain

$$M_{\mathrm{yO}} X^{\mathrm{r}}_{\mathrm{Oy}}\left(\Delta y^{\mathrm{r}}_{\mathrm{R}}\right) = X^{\mathrm{b}}_{\mathrm{Oy}}\left(\Delta y^{\mathrm{b}}_{\mathrm{R}}\right). \tag{7.5.14}$$

The red and blue images at the retina are the same size and so Equation 7.5.5 applies and Equation 7.5.14 simplifies to

$$M_{\mathrm{yO}} X^{\mathrm{r}}_{\mathrm{Oy}} = X^{\mathrm{b}}_{\mathrm{Oy}}. \tag{7.5.15}$$

7.5.4 Chromatic object angular spread magnification

The magnification of the angular spread of the red to blue incident rays, from the red and blue objects is defined as

$$M_{\mathrm{aO}}\ \Delta a^{\mathrm{r}}_{\mathrm{O}} = \Delta a^{\mathrm{b}}_{\mathrm{O}}. \tag{7.5.16}$$

Substituting from Equation 7.5.8 we obtain

$$M_{\mathrm{aO}}\ Z^{\mathrm{r}}_{\mathrm{Oy}}\left(\Delta y^{\mathrm{r}}_{\mathrm{R}}\right) = Z^{\mathrm{b}}_{\mathrm{Oy}}\left(\Delta y^{\mathrm{b}}_{\mathrm{R}}\right) \tag{7.5.17}$$

and because of Equation 7.5.5 this simplifies to

$$M_{\mathrm{aO}}\ Z^{\mathrm{r}}_{\mathrm{Oy}} = Z^{\mathrm{b}}_{\mathrm{Oy}}. \tag{7.5.18}$$

Including the use of a pinhole

We can see from Equations 7.5.6 and 9 that the transverse position of the rays through the pupil is nullified. When a pinhole is placed immediately in front of the eye its transverse displacement will have no effect on the chromatic difference in object size or angular spread or the chromatic object size or angular spread magnifications, however, the longitudinal displacement of bringing the limiting aperture forward will have an effect. The coefficients in Equations 7.5.6, 9, 15 and 18 are replaced with those from $\mathbf{V}^{\mathrm{P}}_{\mathrm{Oy}}$ (Equation 5.3.19).

Generalizing to linear optics

The equations in Section 7.5 have all been written and derived such that they readily generalized to linear optics. The proofs are beyond the scope of this dissertation.

7.6 Comment on the use of the corneal pinhole inlay

In this section the use of the pinhole is implied in the experimental sense. However, the Acufocus Kamra corneal inlay is an intrastromal pinhole that is placed in the cornea at a depth of $170\,\mu\text{m}$ (Seyeddain, Riha, Hohensinn, Nix, Dexl and Grabner, 2010). The pinhole inlay is 3.8 mm in diameter and has a pinhole in its centre of 1.6 mm in diameter. Its effect is similar to that of moving the limiting aperture from the pupil to the corneal plane. Surgeons and researchers go to great lengths to ensure that the transverse placement of the pinhole inlay is correct, so as to avoid induced aberrations. Research is ongoing into establishing where the correct position is to place the inlay. According to Tabernero and Artal (2011), just a 0.5 mm transverse offset can significantly reduce the retinal image quality and overall vision. Numerical examples in Chapter 10 will illustrate the effect of a misplaced inlay is on the object and aperture-dependent chromatic properties at the retina.

7.7 Summary of equations for chromatic properties

Table 7.7.1 Summary of the independent chromatic properties of the eye. The equation is given as a definition and in terms of the entries of the transferences.

Independent Chromatic Properties		
Chromatic property	**Equation**	**Eq. no.**
Chromatic difference in power	$\delta F = F_{\text{b}} - F_{\text{r}} = -\left(C_{\text{b}} - C_{\text{r}}\right)$	7.1.1 & 2
Chromatic difference in refractive compensation	$\delta F_0 = F_{0\text{b}} - F_{0\text{r}} = \dfrac{A_{\text{b}}}{B_{\text{b}}} - \dfrac{A_{\text{r}}}{B_{\text{r}}}$	7.1.3 & 4
Chromatic difference in ametropia	$\delta A = A_{\text{b}} - A_{\text{r}}$	7.1.5

Table 7.7.2 Summary of the chromatic properties of the eye dependent on object and aperture positions. The table is in a set of four sections each giving the equations for an object at distance and a finite distance. The final column gives the equation number for the respective equations. Only the general derivations are given.

Dependent Chromatic Properties			
Chromatic property	**Equation at distance**	**Equation for finite distance**	**Eq. no.**
Coefficient matrix	$\mathbf{V}_{\mathrm{E}}=\begin{pmatrix} W_{\mathrm{E}} & X_{\mathrm{E}} \\ Y_{\mathrm{E}} & Z_{\mathrm{E}} \end{pmatrix}$ $=\begin{pmatrix} A_{\mathrm{E}}A_{\mathrm{A}}^{-1} & B_{\mathrm{B}}A_{\mathrm{A}}^{-1}n_0 \\ n^{-1}C_{\mathrm{E}}A_{\mathrm{A}}^{-1} & n^{-1}D_{\mathrm{B}}A_{\mathrm{A}}^{-1}n_0 \end{pmatrix}$	$\mathbf{V}_{\mathrm{OE}}=\begin{pmatrix} W_{\mathrm{OE}} & X_{\mathrm{OE}} \\ Y_{\mathrm{OE}} & Z_{\mathrm{OE}} \end{pmatrix}$ $=\begin{pmatrix} (B_{\mathrm{E}}-A_{\mathrm{E}}\zeta_{\mathrm{O}})(B_{\mathrm{A}}-A_{\mathrm{A}}\zeta_{\mathrm{O}})^{-1} & B_{\mathrm{B}}(A_{\mathrm{A}}\zeta_{\mathrm{O}}-B_{\mathrm{A}})^{-1} \\ (D_{\mathrm{E}}-C_{\mathrm{E}}\zeta_{\mathrm{O}})(nB_{\mathrm{A}}-A_{\mathrm{A}}\zeta_{\mathrm{O}})^{-1} & D_{\mathrm{B}}(A_{\mathrm{A}}\zeta_{\mathrm{O}}-nB_{\mathrm{A}})^{-1} \end{pmatrix}$	5.2.8 & 5.2.26
Chromatic difference in image position and inclination at the retina			
Chromatic difference in image position	$\delta y_{\mathrm{R}}=(\delta W_{\mathrm{E}})y_{\mathrm{P}}+(\delta X_{\mathrm{E}})a_{\mathrm{K}}$	$\delta y_{\mathrm{R}}=(\delta W_{\mathrm{OE}})y_{\mathrm{P}}+(\delta X_{\mathrm{OE}})y_{\mathrm{O}}$	7.2.3 & 4
Chromatic difference in inclination	$\delta a_{\mathrm{R}}=(\delta Y_{\mathrm{E}})y_{\mathrm{P}}+(\delta Z_{\mathrm{E}})a_{\mathrm{K}}$	$\delta a_{\mathrm{R}}=(\delta Y_{\mathrm{OE}})y_{\mathrm{P}}+(\delta Z_{\mathrm{OE}})y_{\mathrm{O}}$	7.2.16 & 17
Chromatic difference in image size and angular spread at the retina			
Chromatic difference in image size	$\delta(\Delta y_{\mathrm{R}})=(\delta X_{\mathrm{E}})(\Delta a_{\mathrm{K}})$	$\delta(\Delta y_{\mathrm{R}})=(\delta X_{\mathrm{OE}})(\Delta y_{\mathrm{O}})$	7.3.4 & 8
Chromatic difference in image angular spread	$\delta(\Delta a_{\mathrm{R}})=(\delta Z_{\mathrm{E}})(\Delta a_{\mathrm{K}})$	$\delta(\Delta a_{\mathrm{R}})=(\delta Z_{\mathrm{OE}})(\Delta y_{\mathrm{O}})$	7.3.11 & 12
Chromatic magnification			
Retinal chromatic image size magnification	$M_{\mathrm{yR}}X_{\mathrm{E}}^{\mathrm{r}}=X_{\mathrm{E}}^{\mathrm{b}}$	$M_{\mathrm{yR}}X_{\mathrm{OE}}^{\mathrm{r}}=X_{\mathrm{OE}}^{\mathrm{b}}$	7.3.19 & 20
Retinal chromatic angular spread magnification	$M_{\mathrm{aR}}Z_{\mathrm{E}}^{\mathrm{r}}=Z_{\mathrm{E}}^{\mathrm{b}}$	$M_{\mathrm{aR}}Z_{\mathrm{OE}}^{\mathrm{r}}=Z_{\mathrm{OE}}^{\mathrm{b}}$	7.3.27 & 28

Table 7.7.3 Summary of the chromatic properties of the eye dependent on image and aperture positions. The table gives the equations for an object at a finite distance. The final column gives the equation number for the respective equations. Only the general derivations are given.

Chromatic Properties in Object Space	**-for finite distances-**	
Coefficient matrix	$\mathbf{V}_{\mathrm{Oy}} = \begin{pmatrix} W_{\mathrm{Oy}} & X_{\mathrm{Oy}} \\ Y_{\mathrm{Oy}} & Z_{\mathrm{Oy}} \end{pmatrix} = \begin{pmatrix} B_{\mathrm{B}}^{-1}\left(B_{\mathrm{E}} - A_{\mathrm{E}}\zeta_{\mathrm{O}}\right) & \left(A_{\mathrm{A}}\zeta_{\mathrm{O}} - B_{\mathrm{A}}\right)B_{\mathrm{B}}^{-1} \\ -\left(n_0 B_{\mathrm{B}}\right)^{-1} A_{\mathrm{E}} & A_{\mathrm{A}}\left(B_{\mathrm{B}} n_0\right)^{-1} \end{pmatrix}$	5.3.14
Chromatic difference in object position	$\delta y_{\mathrm{O}} = \left(\delta W_{\mathrm{Oy}}\right) y_{\mathrm{P}} + \left(\delta X_{\mathrm{Oy}}\right) y_{\mathrm{R}}$	7.4.1
Chromatic difference in inclination in object space	$\delta a_{\mathrm{O}} = \left(\delta Y_{\mathrm{Oy}}\right) y_{\mathrm{P}} + \left(\delta Z_{\mathrm{Oy}}\right) y_{\mathrm{R}}$	7.4.6
Chromatic difference in object size	$\delta\left(\Delta y_{\mathrm{O}}\right) = \delta X_{\mathrm{Oy}}\left(\Delta y_{\mathrm{R}}\right)$	7.5.6
Chromatic difference in object angular spread	$\delta\left(\Delta a_{\mathrm{O}}\right) = \delta Z_{\mathrm{Oy}}\left(\Delta y_{\mathrm{R}}\right)$	7.5.9
Chromatic object size magnification	$M_{\mathrm{yO}} X_{\mathrm{Oy}}^{\mathrm{r}} = X_{\mathrm{Oy}}^{\mathrm{b}}$	7.5.15
Chromatic object angular spread magnification	$M_{\mathrm{aO}} Z_{\mathrm{Oy}}^{\mathrm{r}} = Z_{\mathrm{Oy}}^{\mathrm{b}}$	7.5.18

Table 7.7.4 Summary of the coefficient matrices for an eye with a pinhole immediately in front of the eye for either an object at distance or an object at a finite distance.

Coefficient matrices for an eye with pinhole		
Equation at distance	**Equation for finite distance**	**Eq. no.**
$\mathbf{V}_{\mathrm{E}}^{\mathrm{P}} = \begin{pmatrix} W_{\mathrm{E}}^{\mathrm{P}} & X_{\mathrm{E}}^{\mathrm{P}} \\ Y_{\mathrm{E}}^{\mathrm{P}} & Z_{\mathrm{E}}^{\mathrm{P}} \end{pmatrix} = \begin{pmatrix} A_{\mathrm{E}} & B_{\mathrm{E}} n_0 \\ n^{-1} C_{\mathrm{E}} & n^{-1} D_{\mathrm{E}} n_0 \end{pmatrix}$	$\mathbf{V}_{\mathrm{OE}}^{\mathrm{P}} = \begin{pmatrix} W_{\mathrm{OE}}^{\mathrm{P}} & X_{\mathrm{OE}}^{\mathrm{P}} \\ Y_{\mathrm{OE}}^{\mathrm{P}} & Z_{\mathrm{OE}}^{\mathrm{P}} \end{pmatrix} = \begin{pmatrix} A_{\mathrm{E}} - B_{\mathrm{E}}\zeta_{\mathrm{O}}^{-1} & B_{\mathrm{E}}\zeta_{\mathrm{O}}^{-1} \\ n^{-1}\left(C_{\mathrm{E}} - D_{\mathrm{E}}\zeta_{\mathrm{O}}^{-1}\right) & n^{-1} D_{\mathrm{E}}\zeta_{\mathrm{O}}^{-1} \end{pmatrix}$	5.2.37 & 34
—	$\mathbf{V}_{\mathrm{Oy}}^{\mathrm{P}} = \begin{pmatrix} W_{\mathrm{Oy}}^{\mathrm{P}} & X_{\mathrm{Oy}}^{\mathrm{P}} \\ Y_{\mathrm{Oy}}^{\mathrm{P}} & Z_{\mathrm{Oy}}^{\mathrm{P}} \end{pmatrix} = \begin{pmatrix} 1 - B_{\mathrm{E}}^{-1} A_{\mathrm{E}}\zeta_{\mathrm{O}} & B_{\mathrm{E}}^{-1}\zeta_{\mathrm{O}} \\ -\left(n_0 B_{\mathrm{E}}\right)^{-1} A_{\mathrm{E}} & \left(n_0 B_{\mathrm{E}}\right)^{-1} \end{pmatrix}$	5.3.19

Table 7.7.5 Summary of the equations for the chromatic difference in corneal position of the two chief rays, for a single object point either at distance or at a finite distance and for the chromatic difference in inclination of two chief rays that emerge at the same position on the retina, from two separated object points at a finite distance.

Underlying implications			
Chromatic difference in corneal position	$\delta y_{\mathrm{K}} = \left[\delta\left(\frac{n_0}{A_{\mathrm{E}}}\left(\frac{B_{\mathrm{B}}}{A_{\mathrm{A}}} - B_{\mathrm{E}}\right)\right)\right] a_{\mathrm{K}} + \left[\delta\left(\frac{1}{A_{\mathrm{A}}}\right)\right] y_{\mathrm{P}}$	$\delta y_{\mathrm{K}} = \left(\delta\frac{B_{\mathrm{A}}}{B_{\mathrm{OA}}}\right) y_{\mathrm{O}} - \left(\delta\frac{\zeta_{\mathrm{O}}}{B_{\mathrm{OA}}}\right) y_{\mathrm{P}}$	7.2.9 & 10
Chromatic difference in inclination at retina	—	$\delta a_{\mathrm{R}} = \left(\delta\left(-nB_{\mathrm{B}}\right)^{-1}\right) y_{\mathrm{P}} - \left(\delta\left(D_{\mathrm{B}}\left(B_{\mathrm{B}}n\right)^{-1}\right)\right) y_{\mathrm{R}}$	7.4.13

7.8 Discussion

In this section we unpacked and derived equations to enable us to calculate chromatic properties from the transferences. Contrary to the definition of chromatic aberration in Chapter 6 which distinguished between longitudinal and transverse chromatic aberration, chromatic properties are categorised as firstly those chromatic properties that are independent of object, image and aperture positions and secondly the chromatic properties of the eye that are dependent on the object (or image) and aperture positions.

The derivations of the chromatic properties have in certain instances confirmed what we intuitively suspected and in other instances gave us new insight into the definitions. We saw that the independent chromatic properties of the eye are derived from the fundamental properties of the red and blue transferences alone and are not the direct property of light, nor object and image positions. The result is that one obtains, as a result, a single value for each of chromatic difference in power, refractive compensation and ametropia for the eye.

In contrast, the derivations for chromatic properties of the eye and object and aperture positions are dependent on light, relying on ray tracing, and therefore vary with changes in both longitudinal and transverse object position and longitudinal and transverse aperture position. We derived formulae for chromatic

difference in position, firstly for chromatic difference in transverse image position and secondly for chromatic difference in inclination at the retina.

An interesting underlying implication is that even when one chooses a pencil of rays, all having the same incident inclination, and then selects the chief ray through the centre of the pupil, that there is a red ray and blue ray at incidence, separated at the cornea by a distance δy_K. The two rays reaching the retina do not originate from the exact same multi-chromatic ray.

After taking a close look at chromatic difference in magnification we determined that what is being measured in the literature is not a chromatic difference but rather a chromatic magnification. Nonetheless, we derived equations for chromatic difference in image size on the retina and chromatic difference in angular spread which turn out to be independent of transverse displacement of the pupil or pinhole. More appropriately, we derived formulae for the chromatic image size magnification and chromatic image angular spread magnification.

Finally, we take a look at the experimental situation where two coloured object points are positioned a distance apart such that the two coloured images are superimposed at the same point on the retina. We were able to derive equations for the chromatic difference in object position and chromatic difference in object inclination of these two coloured object points.

The underlying implication of the experimental situation is that while the red and blue rays reach the retina at the same position, there is a difference in inclination between these two rays upon reaching the retina. This has possible implications for the Stiles-Crawford effect, but further investigation is beyond the scope of this dissertation.

It is conceivable that an experiment could be set up to compare the sizes of a red and a blue object to appear to be the same size to the subject. The chromatic difference in object size and object angular spread were defined in object space. The chromatic object size magnification and chromatic object angular spread magnification were defined in object space.

All the derivations for the dependent chromatic properties of the eye are amenable to placing a pinhole immediately in front of the eye. In each case the general equations still hold and the coefficients simplify.

8 Chromatic dependence of the transference and transformed transferences on frequency

In this chapter the dependence of each of the four fundamental properties of two model eyes is calculated as a function of frequency with the refractive index of air assumed constant. We then compare the effect on the fundamental properties of the two model eyes when the refractive index of air is treated as a function of frequency. For comparison, the dependence of the fundamental properties on wavelength is displayed graphically. Finally, we consider the two model eyes submerged in water.

The four fundamental properties, each dependent on the frequency of light, are displayed graphically and turn out to be very nearly linear. A linear equation for each fundamental property as a function of frequency is obtained. It turns out that one can utilise this equation to obtain the transference as an approximate function of frequency.

We then turn our attention to the two transformed transferences that were introduced in Section 3.7.1 and 2. These are displayed graphically as a function of frequency using three-dimensional graphs. This enables us to study the fundamental and derived properties, their relationships to each other and their dependence on frequency.

Each of the entries of the transformed transference also displays a nearly linear dependence on the frequency of light. These transformed spaces allow us to derive a formula for a transference, necessarily symplectic, as a function of frequency.

8.1 Transference as a function of frequency

The transference and its fundamental properties are dependent on the frequency of light. In order to study this we first equate the refractive index of air to 1, the usual assumption in optometry. For illustrative purposes, we then examine the effect on the fundamental properties of treating the refractive index of air as a function of frequency. We use Cauchy's formula for that purpose. For comparison, we also consider the dependence of the transference on wavelength.

Finally, we take a look at the more unusual situation of the eye submerged in water.

Each of the graphs in this section shows four sub-graphs, one for each of the fundamental properties as a function of frequency, across the spectrum from 430 to 750 THz. Two graphs in Section 8.1.3 will be in terms of wavelength, but across the same spectrum and with the same six coloured reference points. For the graphs, values are calculated for every 1 THz, that is for 321 points across the spectrum. However, in the tables only the values for the six reference points are given.

We make use of the SI units and prefixes for time, picosecond (ps) which is 10^{-12} s, and its inverse, the derived unit for frequency, teraHertz (THz) which is 10^{12} s^{-1}.

8.1.1 The transference as a function of frequency with $n_0 = 1$

The reduced eye

The transferences of the reduced eye as a function of the frequency of light are given for the six reference frequencies in Table 8.1.1 with the refractive index of air (n_0) equated to 1. The transferences for the reduced eye as a function of frequency are calculated according to Equation 5.5.1 with $n_0 = 1$ and the refractive index *n* calculated according to Equation 4.4.2. The disjugacy *B* is given in millimetres (mm) and the divergence *C* in corresponding units, kilodioptres ($\mathrm{kD} = \mathrm{mm}^{-1}$).

Figure 8.1.1 represents each of the fundamental properties of the reduced eye as a function of frequency. The six coloured reference points described in Section 4.2 are shown by means of coloured diamonds. The coloured diamonds represent five equally spaced intervals (64 THz) of frequency.

In Figure 8.1.1, the axis scales have been chosen to exaggerate curvature. The range of the scale for each sub-graph indicates the chromatic difference in each fundamental property. The dilation *A* ranges from 0.0070 to -0.0277 which represents a chromatic difference in ametropia of –0.0347. The chromatic

Table 8.1.1 Transferences of the reduced eye and Le Grand's eye for six reference frequencies ν (in THz), calculated with $n_0 = 1$.

Colour	ν	Reduced eye	Le Grand's eye
Red	430	$\begin{pmatrix} 0.0070 & 16.7055\,\text{mm} \\ -0.0594\,\text{kD} & 1 \end{pmatrix}$	$\begin{pmatrix} 0.0078 & 16.7276\,\text{mm} \\ -0.0594\,\text{kD} & 0.9044 \end{pmatrix}$
Orange	494	$\begin{pmatrix} 0.0020 & 16.6775\,\text{mm} \\ -0.0598\,\text{kD} & 1 \end{pmatrix}$	$\begin{pmatrix} 0.0024 & 16.6912\,\text{mm} \\ -0.0598\,\text{kD} & 0.9041 \end{pmatrix}$
Yellow	558	$\begin{pmatrix} -0.0038 & 16.6455\,\text{mm} \\ -0.0603\,\text{kD} & 1 \end{pmatrix}$	$\begin{pmatrix} -0.0037 & 16.6494\,\text{mm} \\ -0.0603\,\text{kD} & 0.9034 \end{pmatrix}$
Green	622	$\begin{pmatrix} -0.0105 & 16.6082\,\text{mm} \\ -0.0608\,\text{kD} & 1 \end{pmatrix}$	$\begin{pmatrix} -0.0102 & 16.6029\,\text{mm} \\ -0.0608\,\text{kD} & 0.9026 \end{pmatrix}$
Blue	686	$\begin{pmatrix} -0.0184 & 16.5646\,\text{mm} \\ -0.0615\,\text{kD} & 1 \end{pmatrix}$	$\begin{pmatrix} -0.0170 & 16.5545\,\text{mm} \\ -0.0613\,\text{kD} & 0.9018 \end{pmatrix}$
Violet	750	$\begin{pmatrix} -0.0277 & 16.5126\,\text{mm} \\ -0.0622\,\text{kD} & 1 \end{pmatrix}$	$\begin{pmatrix} -0.0237 & 16.5065\,\text{mm} \\ -0.0619\,\text{kD} & 0.9011 \end{pmatrix}$

difference for disjugacy B is –0.1929 mm and for divergence C it is $-0.0028\,\text{kD}$, or –2.7975 D. For divarication D the chromatic difference is zero.

In Figure 8.1.1, the dashed lines represent the least squares straight line fitted to the data for the reduced eye. Each of A, B and C present as curves in each sub-graph. D is a straight line at 1 as required by Equation 5.5.1. Because the curves in the sub-graphs of Figure 8.1.1 are nearly straight lines, Equations 8.1.1 to 4 below can be thought of as approximations of the dependence of each fundamental property on frequency. The equations for the four dashed straight lines are

$$A = \left(-1.0691\times10^{-4}\,\text{ps}\right)\nu + 0.05494 \tag{8.1.1}$$

$$B = \left(-5.9394\times10^{-4}\,\text{mm ps}\right)\nu + 16.9719\,\text{mm} \tag{8.1.2}$$

$$C = \left(-8.6047\times10^{-6}\,\text{kD ps}\right)\nu - 0.05558\,\text{kD} \tag{8.1.3}$$

$$D = 1 \tag{8.1.4}$$

where ν is measured in THz and the units of each constant is given. The set of equations can be reconstituted into a transference such that

$$\mathbf{S} = \begin{pmatrix} a_1 & b_1 \\ c_1 & d_1 \end{pmatrix} \nu + \begin{pmatrix} a_2 & b_2 \\ c_2 & d_2 \end{pmatrix} \tag{8.1.5}$$

where the constants for the reduced eye are given in Table 8.1.2.

The set of four equations given for the straight line of each fundamental property is an approximation of the value of each fundamental property for any particular frequency. Strictly speaking, because of symplecticity, it is not correct to determine **S** by obtaining expressions for the fundamental properties independently as done in Equation 8.1.5. However, det**S** has a mean of 1.000 024 and a standard deviation of 4.0×10^{-5} across the spectrum which would seem to be sufficiently close to the required 1 for most purposes. We will explore this further in Section 8.2 when we look at mapping transformations into Hamiltonian space.

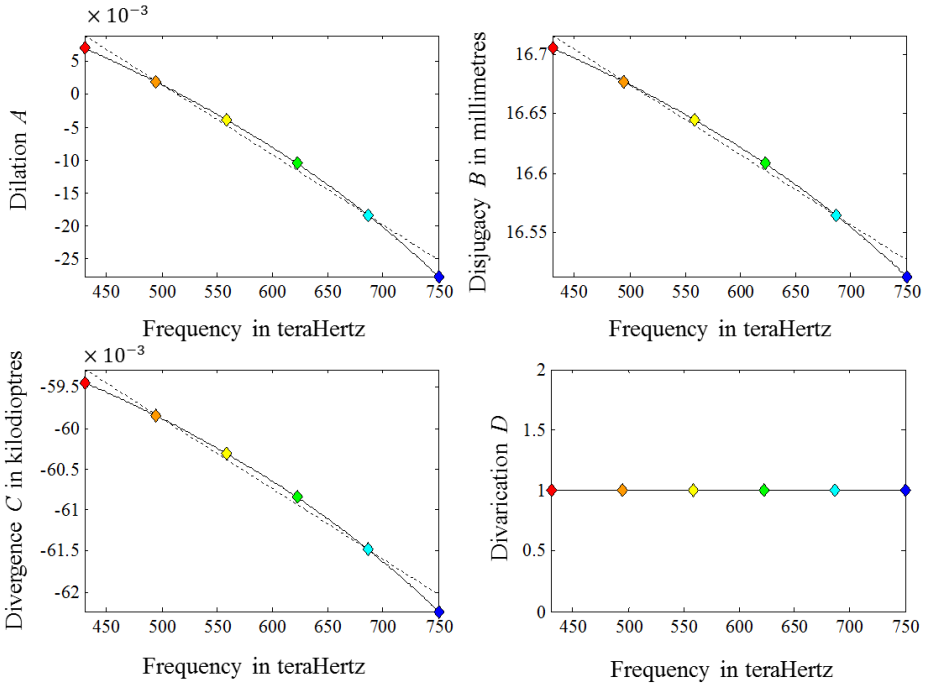

Figure 8.1.1 Fundamental properties of the reduced eye as functions of frequency ν. The refractive index of air is equated to 1. The four sub-graphs are for dilation *A*, disjugacy *B*, divergence *C* and divarication *D*. The six coloured diamonds represent the frequencies listed in Table 4.2.1, red, orange, yellow, green, blue and violet and are evenly spread at 64 THz apart. The dashed lines represent the least squares straight line. Each of *A*, *B* and *C* present as curves, while *D* is a horizontal straight line at 1.

Table 8.1.2 The constants for the reduced eye in air for Equation 8.1.5. The units are picoseconds (ps), millimetres (mm) and kilodioptres (kD).

$a_1 = -1.0691\times10^{-4}$ ps	$a_2 = 0.05494$
$b_1 = -5.9394\times10^{-4}$ mm ps	$b_2 = 16.9719$ mm
$c_1 = -8.6047\times10^{-6}$ kD ps	$c_2 = -0.05558$ kD
$d_1 = 0$ ps	$d_2 = 1$

Le Grand's eye

Similarly we look at the fundamental optical properties for Le Grand's four-surface eye. The transferences were calculated according to Equations 5.5.4 to 8 and the refractive indices given by Equation 4.4.3 with constants listed in Table 4.4.2. The transferences for the six coloured reference frequencies are given in Table 8.1.1.

The range along the vertical axis for each fundamental property shows the range along the spectrum, or chromatic difference. The chromatic difference of dilation or ametropia is –0.0315. The chromatic difference of disjugacy is

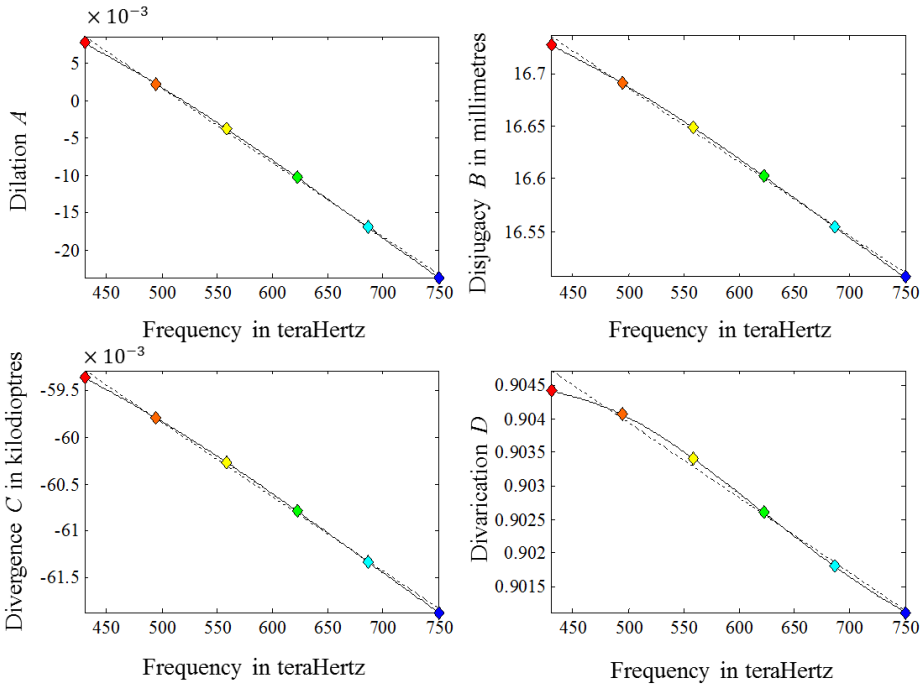

Figure 8.1.2 Fundamental properties of Le Grand's eye as a function of frequency ν. $n_0 = 1$.

Table 8.1.3 The constants for Le Grand's eye in air for Equation 8.1.5.

$a_1 = -0.9973\times10^{-4}$ ps	$a_2 = 0.05156$
$b_1 = -7.0345\times10^{-4}$ mm ps	$b_2 = 17.0382$ mm
$c_1 = -7.9756\times10^{-6}$ kD ps	$c_2 = -0.05581$ kD
$d_1 = -1.1515\times10^{-5}$ ps	$d_2 = 0.9095$

-0.2211 mm and for divergence it is –0.0025 kD or –2.5158 D. The chromatic difference of divarication is –0.0033 which is a very small range from 0.9044 to 0.9011.

From Figure 8.1.2 we can see that the curve is nearly linear. Because of this linearity, the dependence of the four fundamental properties of Le Grand's eye on the frequency of light can be approximated by Equation 8.1.5. The constants for Le Grand's eye for Equation 8.1.5 are given in Table 8.1.3. In contrast to Figure 8.1.1 *D* is no longer a horizontal straight line at 1 but is close to a straight line at $D = 0.9$, approximately.

Table 8.1.4 gives examples of transferences calculated by means of Equation 8.1.5 and constants given in Tables 8.1.2 and 3. Obtaining the approximate transference **S** for each frequency in the spectrum for Le Grand's eye from Equation 8.1.5, the average value for det**S** is $0.999\,35$ and the standard deviation is 3.5×10^{-5}. As for the reduced eye, this is probably sufficiently close to 1 for most purposes.

Comparison of the two model eyes

The graphs of the fundamental properties versus frequency for the reduced eye and Le Grand's eye, are superimposed in Figure 8.1.3. By means of Figure 8.1.3 we can compare the fundamental properties of the reduced eye (in blue) and Le Grand eye (in black). The six reference points are included and are circular for the reduced eye and diamond shaped for the Le Grand eye. For the dilation *A*, disjugacy *B* and divergence *C* we see that the dependence of each fundamental property on frequency is similar for the two model eyes. They are closest in the central part of the spectrum. The divarication *D*, constant at 1 for the reduced eye,

Table 8.1.4 Transferences of the reduced eye and Le Grand's eye for the six reference frequencies (in THz), calculated by means of Equation 8.1.5 and the constants in Tables 8.1.2 and 3 with $n_0 = 1$.

Colour	ν	Reduced eye	Le Grand's eye
Red	430	$\begin{pmatrix} 0.008656 & 16.7148\text{ mm} \\ -0.05930\text{ kD} & 1 \end{pmatrix}$	$\begin{pmatrix} 0.008457 & 16.7336\text{ mm} \\ -0.05930\text{ kD} & 0.9046 \end{pmatrix}$
Orange	494	$\begin{pmatrix} 0.001760 & 16.6764\text{ mm} \\ -0.05986\text{ kD} & 1 \end{pmatrix}$	$\begin{pmatrix} 0.002117 & 16.6890\text{ mm} \\ -0.05981\text{ kD} & 0.9039 \end{pmatrix}$
Yellow	558	$\begin{pmatrix} -0.005135 & 16.6381\text{ mm} \\ -0.06042\text{ kD} & 1 \end{pmatrix}$	$\begin{pmatrix} -0.004223 & 16.6443\text{ mm} \\ -0.06031\text{ kD} & 0.9032 \end{pmatrix}$
Green	622	$\begin{pmatrix} -0.01203 & 16.5998\text{ mm} \\ -0.06097\text{ kD} & 1 \end{pmatrix}$	$\begin{pmatrix} -0.01056 & 16.5997\text{ mm} \\ -0.06082\text{ kD} & 0.9026 \end{pmatrix}$
Blue	686	$\begin{pmatrix} -0.01893 & 16.5615\text{ mm} \\ -0.06153\text{ kD} & 1 \end{pmatrix}$	$\begin{pmatrix} -0.01690 & 16.5551\text{ mm} \\ -0.06133\text{ kD} & 0.9019 \end{pmatrix}$
Violet	750	$\begin{pmatrix} -0.02582 & 16.5232\text{ mm} \\ -0.06208\text{ kD} & 1 \end{pmatrix}$	$\begin{pmatrix} -0.02324 & 16.5104\text{ mm} \\ -0.06183\text{ kD} & 0.9012 \end{pmatrix}$

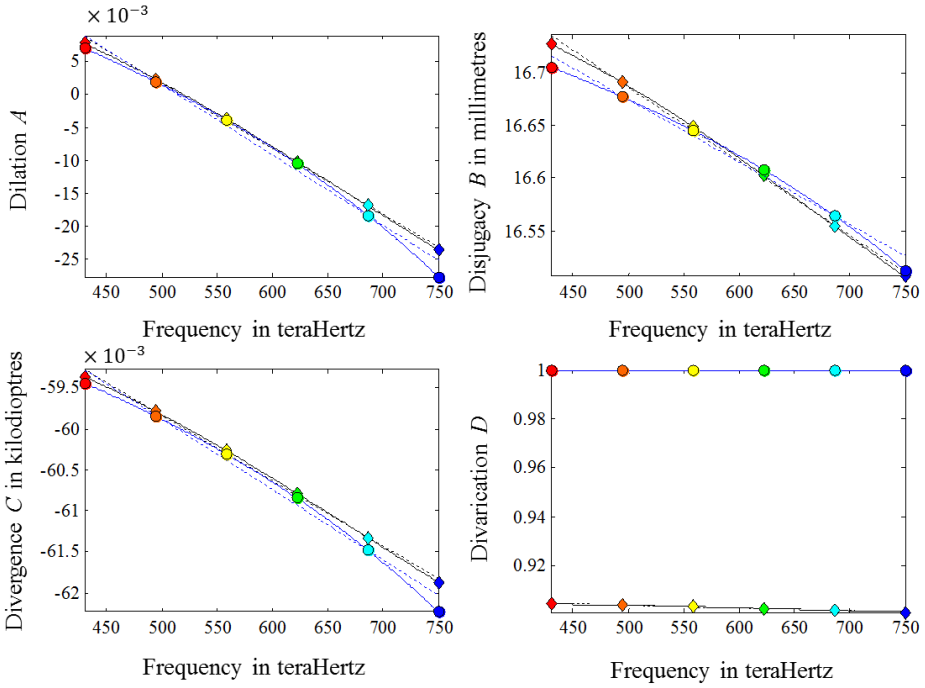

Figure 8.1.3 Fundamental properties of the reduced eye (blue line and circles) and Le Grand's eye (black line and diamonds) versus frequency ν superimposed. The least squares straight lines are also shown.

becomes weakly dependent on frequency at about 0.9 for Le Grand's eye. It is also interesting to note that the curves for Le Grand's eye more closely approximate straight lines than do the curves for the reduced eye.

8.1.2 Transference as a function of frequency using Cauchy's formula for the refractive index of air

For most purposes the index of refraction of air n_0 is taken as 1. Here we examine the effects on the transferences of allowing n_0 to depend on frequency according to Cauchy's dispersion formula (Equation 4.4.4). The effects are shown in Figures 8.1.4 and 5 for the reduced and Le Grand's eyes respectively. The blue line is for n_0 according to Cauchy's formula and the black line is for $n_0 = 1$. The transferences for the six reference frequencies, with n_0 calculated by means of Cauchy's formula, are given in Table 8.1.6 for the reduced and Le Grand's eyes.

The reduced eye

From Equation 5.5.1 for the reduced eye we see that n_0 has no effect on the disjugacy *B* and the divarication *D*. The only fundamental properties that are affected are the dilation *A* and the divergence *C*. This can also be seen in Figure 8.1.4. The effect of setting n_0 equal to 1, and not allowing for dependence of n_0 on ν, is to decrease *A* by about $0.000\,83$ and *C* by about $0.000\,05$ kD across the spectrum. The effect, therefore, would appear to be negligible and the use of $n_0 = 1$ justifiable.

Least-square straight lines fitted to the curves in Figure 8.1.4 lead to the approximate expression for transference **S** in terms of ν given by Equation 8.1.5 with constants given in Table 8.1.5.

Table 8.1.5 Constants for the expressions in Equation 8.1.5 for dilation *A* and divergence *C* for the reduced eye where n_0 is given by Cauchy's formula.

$a_1 = -1.0688 \times 10^{-4}$ ps	$a_2 = 0.05575$
$c_1 = -8.6012 \times 10^{-6}$ kD ps	$c_2 = -0.05553$ kD

Table 8.1.6 Transferences for the reduced eye and Le Grand's eye for the six reference frequencies in THz, calculated for n_0 given by Cauchy's formula.

Colour	ν	Reduced eye	Le Grand's eye
Red	430	$\begin{pmatrix} 0.0078 & 16.7055\text{ mm} \\ -0.0594\text{ kD} & 1 \end{pmatrix}$	$\begin{pmatrix} 0.0084 & 16.7276\text{ mm} \\ -0.0593\text{ kD} & 0.9044 \end{pmatrix}$
Orange	494	$\begin{pmatrix} 0.0028 & 16.6775\text{ mm} \\ -0.0598\text{ kD} & 1 \end{pmatrix}$	$\begin{pmatrix} 0.0029 & 16.6912\text{ mm} \\ -0.0598\text{ kD} & 0.9041 \end{pmatrix}$
Yellow	558	$\begin{pmatrix} -0.0030 & 16.6455\text{ mm} \\ -0.0603\text{ kD} & 1 \end{pmatrix}$	$\begin{pmatrix} -0.0031 & 16.6494\text{ mm} \\ -0.0602\text{ kD} & 0.9034 \end{pmatrix}$
Green	622	$\begin{pmatrix} -0.0097 & 16.6082\text{ mm} \\ -0.0608\text{ kD} & 1 \end{pmatrix}$	$\begin{pmatrix} -0.0096 & 16.6029\text{ mm} \\ -0.0608\text{ kD} & 0.9026 \end{pmatrix}$
Blue	686	$\begin{pmatrix} -0.0175 & 16.5646\text{ mm} \\ -0.0615\text{ kD} & 1 \end{pmatrix}$	$\begin{pmatrix} -0.0164 & 16.5545\text{ mm} \\ -0.0613\text{ kD} & 0.9018 \end{pmatrix}$
Violet	750	$\begin{pmatrix} -0.0269 & 16.5126\text{ mm} \\ -0.0622\text{ kD} & 1 \end{pmatrix}$	$\begin{pmatrix} -0.0231 & 16.5065\text{mm} \\ -0.0618\text{ kD} & 0.9011 \end{pmatrix}$

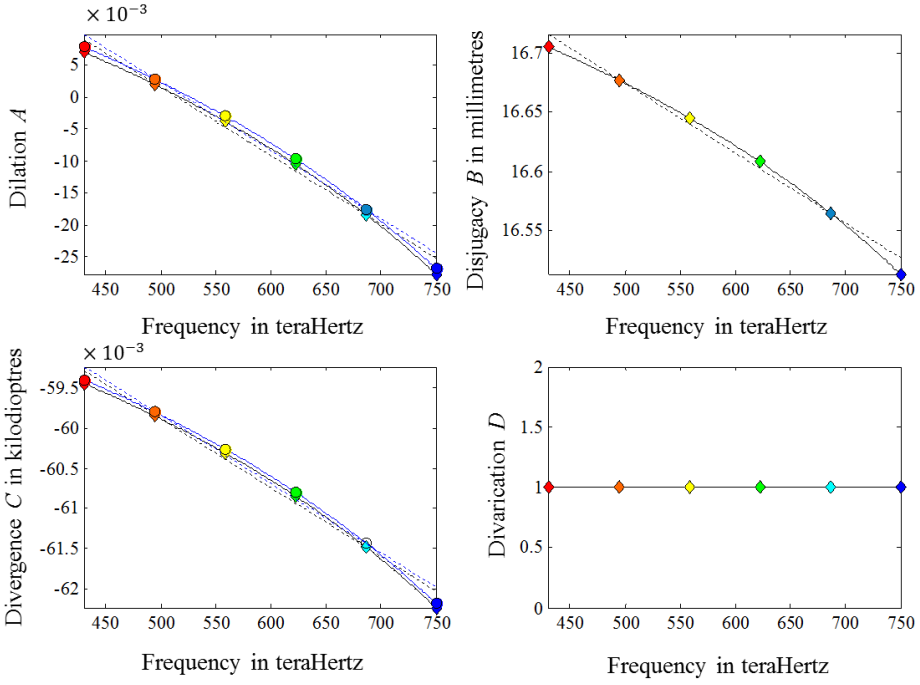

Figure 8.1.4 Fundamental properties of the reduced eye as functions of frequency. The black lines and diamond shaped reference points are for $n_0 = 1$ and the blue lines and circular reference points for n_0 given by Cauchy's formula. For B and D the curves coincide.

Le Grand's eye

Figure 8.1.5 shows the fundamental properties of Le Grand's eye as functions of frequency. The black line is calculated with $n_0 = 1$ and the blue line is calculated with n_0 as a function of frequency according to Cauchy's dispersion formula given by Equation 4.4.4. The results are similar to those in Figure 8.1.4 for the reduced eye in that only the dilation *A* and divergence *C* are affected.

To see why only *A* and *C* are affected by using Cauchy's formula for n_0, let us examine the effect of the refractive index of the surrounding medium on Le Grand's eye. From Equations 5.5.5 and 7 we observe that the only elementary transference containing n_0 is $\mathbf{S}_{\mathrm{K1}}$. The meaning of the subscripts is given in Table 4.1.1. Let us write the transference of the eye as

$$\mathbf{S} = \mathbf{S}_{\mathrm{R}}\mathbf{S}_{\mathrm{K1}} \tag{8.1.6}$$

where

$$\mathbf{S}_{\mathrm{R}} = \mathbf{S}_{\mathrm{V}}\mathbf{S}_{\mathrm{L2}}\mathbf{S}_{\mathrm{L}}\mathbf{S}_{\mathrm{L1}}\mathbf{S}_{\mathrm{Aq}}\mathbf{S}_{\mathrm{K2}}\mathbf{S}_{\mathrm{K}}. \tag{8.1.7}$$

We now substitute for $\mathbf{S}_{\mathrm{K1}}$ from Equation 5.5.5 to obtain

$$\mathbf{S} = \begin{pmatrix} A_{\mathrm{R}} & \mathrm{B}_{\mathrm{R}} \\ C_{\mathrm{R}} & D_{\mathrm{R}} \end{pmatrix} \begin{pmatrix} 1 & 0 \\ \dfrac{n_{\mathrm{K}} - n_0}{-r_{\mathrm{K1}}} & 1 \end{pmatrix} = \begin{pmatrix} A_{\mathrm{R}} - \mathrm{B}_{\mathrm{R}}\left(\dfrac{n_{\mathrm{K}} - n_0}{r_{\mathrm{K1}}}\right) & \mathrm{B}_{\mathrm{R}} \\ C_{\mathrm{R}}\left(\dfrac{n_{\mathrm{K}} - n_0}{-r_{\mathrm{K1}}}\right) & D_{\mathrm{R}} \end{pmatrix} \tag{8.1.8}$$

which shows that, for Le Grand's eye, the only fundamental properties affected by n_0 are the dilation *A* and divergence *C*.

In Figure 8.1.5 the lines for $n_0 = 1$ and for n_0 calculated according to Cauchy's formula, are very close together and appear to be approximately parallel in sub-graphs *A* and *C*. Sub-graphs *B* and *D* are indeed superimposed, as implied by Equation 8.1.8. The formulae for the least-squares straight lines for Le Grand's eye shown in Figure 8.1.5 for *A* and *C* using Cauchy's formula for n_0 as functions of frequency can be obtained from Equation 8.1.5 with the constants given in Table 8.1.7 and transferences given in Table 8.1.6. Comparing the straight lines for $n_0 = 1$ with the straight lines using Cauchy's dispersion formula we observe

Table 8.1.7 The constants for dilation *A* and divergence *C* for Le Grand's eye for the straight line equations in Equation 8.1.5 where the refractive index is calculated according to Cauchy's formula.

$a_1 = -0.9969 \times 10^{-4}$ ps	$a_2 = 0.05214$
$c_1 = -7.9733 \times 10^{-6}$ kD ps	$c_2 = -0.05582$ kD

that the two straight lines (a_1 and c_1) are very nearly parallel and the in positions (a_2 and c_2) change slightly.

Table 8.1.8 shows the difference between the two lines for both model eyes for each of the six reference frequencies. The mean and standard deviation are calculated for every 1 THz across the spectrum. Visual inspection of both Table 8.1.8 and Figure 8.1.5 indicates that the two curves for *A* and *C* are very nearly parallel and are very close together. Because the lines are nearly parallel, any chromatic difference calculations will be negligibly influenced by the choice of refractive index for air.

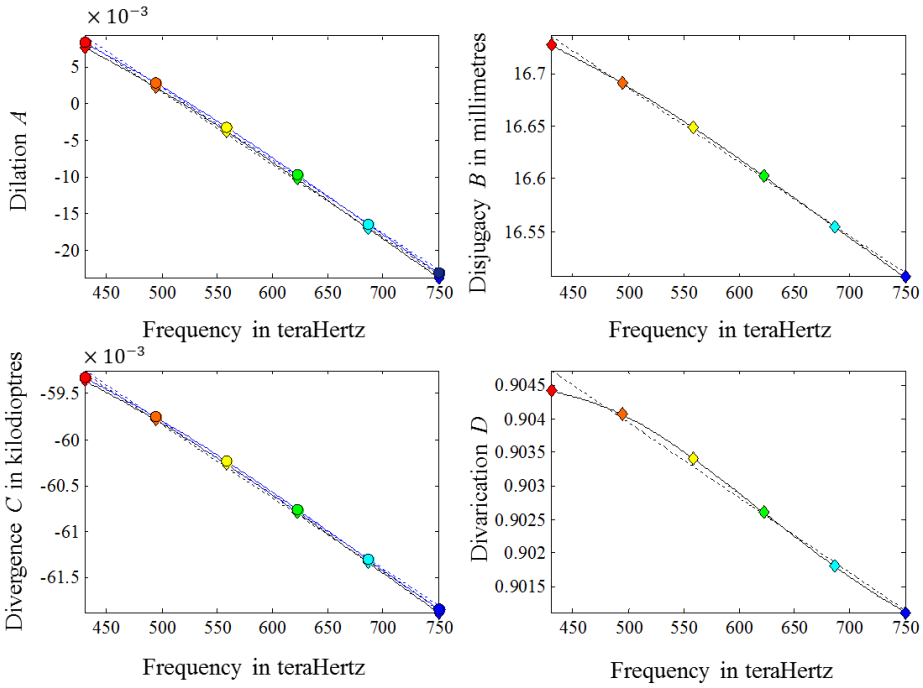

Figure 8.1.5 Fundamental properties of Le Grand's eye as functions of frequency. The black line and diamond shaped reference points are for $n_0 = 1$ and the blue line and circular reference points are for n_0 calculated by means of Cauchy's formula. The two lines for *B* and *D* are superimposed. For *A* and *C* the blue line is displaced upwards.

Table 8.1.8 The differences in each of the fundamental properties between the transference calculated using $n_0 = 1$ and using n_0 according to Cauchy's formula. The numbers indicate the difference (vertical distance) from the black to the blue line in the graphs in Figures 8.1.4 and 5. The mean and standard deviation are obtained for 321 frequencies across the visible spectrum.

Colour	ν in THz	Reduced eye				Le Grand eye			
		ΔA	ΔB in mm	ΔC in kD	ΔD	ΔA	ΔB in mm	ΔC in kD	ΔD
		$\times 10^{-3}$		$\times 10^{-3}$		$\times 10^{-3}$		$\times 10^{-3}$	
Red	430	0.8279	0	0.04956	0	0.5904	0	0.03192	0
Orange	494	0.8293	0	0.04972	0	0.5911	0	0.03202	0
Yellow	558	0.8309	0	0.04992	0	0.5920	0	0.03212	0
Green	622	0.8328	0	0.05015	0	0.5930	0	0.03224	0
Blue	686	0.8350	0	0.05041	0	0.5944	0	0.03238	0
Violet	750	0.8374	0	0.05071	0	0.5962	0	0.03255	0
Mean:		0.8321	0	0.05006	0	0.5927	0	0.03220	0
Standard deviation:		0.002775	0	0.000334	0	0.001629	0	0.01778	0

Discussion

Here we have examined whether the dispersive effect of air plays a significant role in the overall dispersion through the system ultimately reaching the exit plane, or retina. Figures 8.1.4 and 5 compare the eye in air, firstly, with $n_0 = 1$ and secondly, with the refractive index as a function of frequency calculated using Cauchy's formula. The disjugacy *B* and divarication *D* are not affected. Only the dilation *A* and divergence *C* are affected.

Table 8.1.8 shows the difference in each of the fundamental properties when the transference is calculated using $n_0 = 1$ and when using Cauchy's formula. The standard deviation shows how close to being parallel the two lines are and therefore gives an indication of the effect of dispersion, while the mean indicates how accurate the constant for n_0 is and the difference between the two lines. From the graphs and numerical values of the tables in this section, we conclude that because the two lines in each graph are very nearly parallel, the

amount of dispersion occurring in air is insignificant and the refractive index of air can be taken to be 1.

8.1.3 Dependence of the fundamental properties on vacuum wavelength

The fundamental properties of the reduced eye and Le Grand's eye as functions of vacuum wavelength λ are represented in Figures 8.1.6 and 7, respectively. In each graph the visible spectrum used is the same as used throughout this dissertation, that is, frequency from 430 to 750 THz, except that it is converted to vacuum wavelength using Equation 4.3.1 and given in Table 4.2.1. Figures 8.1.6 and 7 depart considerably more from straight lines than the corresponding figures (Figures 8.1.1 and 2) in terms of frequency ν.

The reduced eye

When we compare to the fundamental properties of the reduced eye as a function of vacuum wavelength (Figure 8.1.6) to frequency (Figure 8.1.1), we see that, as expected, the divarication *D* is a constant of 1, but that the other three properties are significantly more curved.

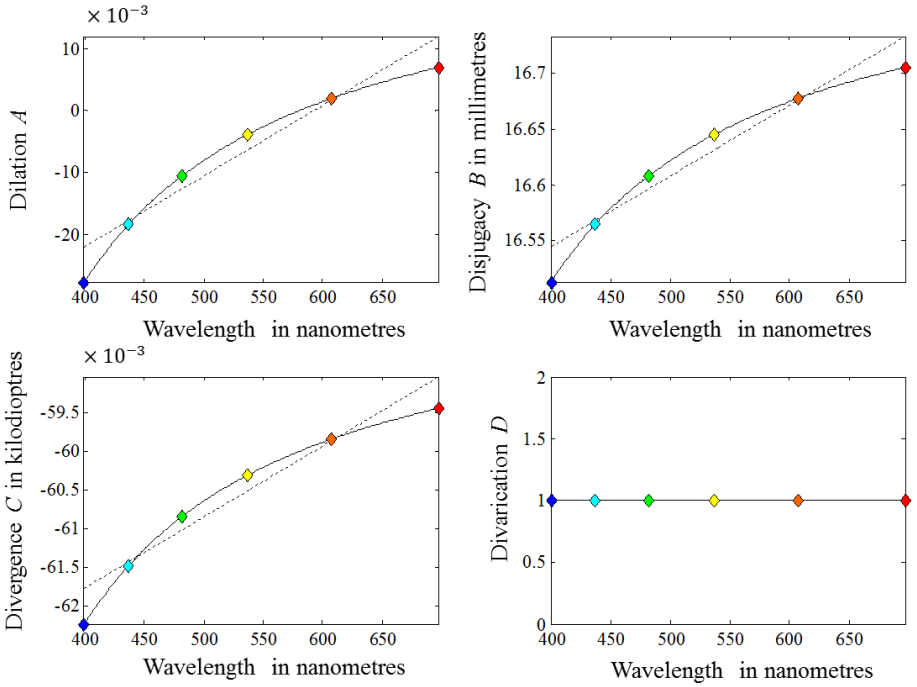

Figure 8.1.6 Fundamental properties of the reduced eye as functions of vacuum wavelength λ with $n_0 = 1$.

Le Grand's eye

Figure 8.1.7, shows the fundamental properties of Le Grand's eye as functions of vacuum wavelength λ. Again the curves depart more from straight lines than for the fundamental properties as functions of frequency ν. The four-surface eye of Le Grand shows less curvature than the single-surface reduced eye, with the exception of the divarication *D*.

Comparing the transferences of the reduced eye and Le Grand's eye

Figure 8.1.8 plots the results of Figures 8.1.6 and 7 together. The behaviour of the fundamental properties versus vacuum wavelength λ is similar for the reduced and Le Grand's eyes, especially in the central region of the spectrum. For both model eyes, the curves of the fundamental properties versus frequency ν are closer to straight lines than the corresponding curves for vacuum wavelength. This provides additional justification for using frequency instead of the more commonly-used wavelength.

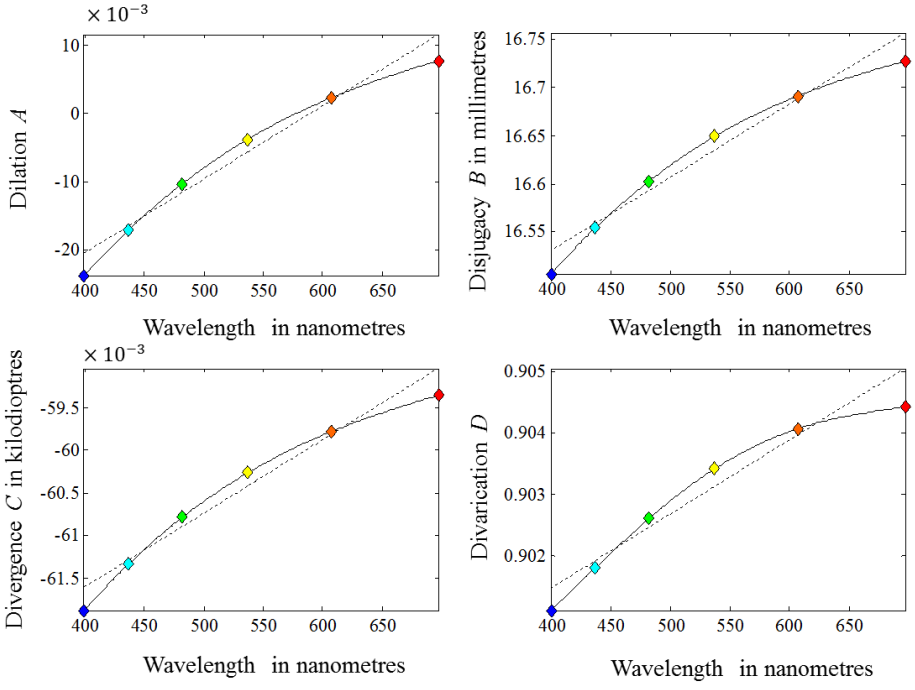

Figure 8.1.7 Fundamental properties of Le Grand's eye as a function of vacuum wavelength λ with $n_0 = 1$. The wavelengths of the six reference points are given in Table 4.2.1. Compared with the graphs for the fundamental properties as functions of frequency, these curves further depart from straight lines.

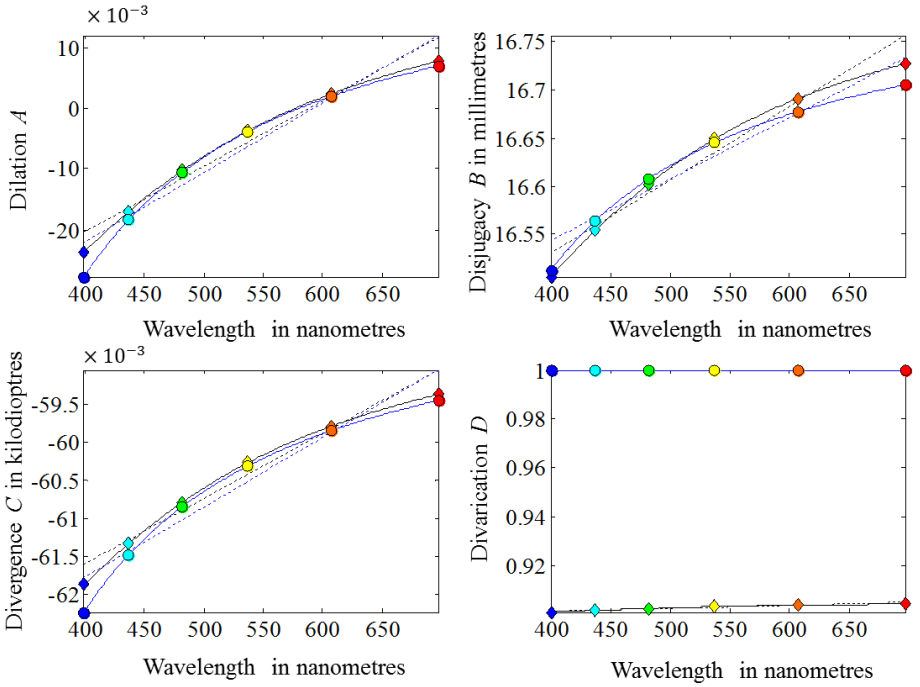

Figure 8.1.8 Dependence of the four fundamental properties of the reduced eye (blue line with circles) and Le Grand's eye (black line with diamonds) on vacuum wavelength.

8.1.4 Transference of the eye submerged in water as a function of frequency with Cornu's formula used for the refractive index of water

The formulae for the dependence of the transference of the reduced eye (Equation 5.5.3) and Le Grand's eye (Equations 5.5.5, 7 and 8) on the refractive indices and hence on the frequency of light include the possibility of n_0 also being dependent on frequency, including media other than air. In Section 8.1.1 we studied the two model eyes in air with the refractive index of air taken as 1. In Section 8.1.2 we compared the effect of the refractive index of air treated as a function of frequency. However, Equations 5.5.1 and 5.5.4 to 9 will hold for the eye in any medium. As an example of the model eye in a medium other than air, we calculate the effect on the fundamental properties of each model eye if the eye is submerged in water. Figure 8.1.9 allows comparison of the fundamental properties of the reduced eye (blue line and circles) and Le Grand's eye (black line and diamonds) as functions of frequency ν when the eye is submerged in water.

In Figure 8.1.9, the refractive index of water is calculated according to Cornu's formula, given as Equation 4.4.1. It is shown in Section 8.1.2 that the

refractive index of the medium upstream of any eye only affects the dilation *A* and divergence *C*. When the eyes are submerged in water the effect on *A* and *C* is still close to straight lines for each model eye; however there is a clear difference in position of the curves of the reduced and Le Grand's eyes. We recall that in Figure 8.1.3 we compared the graphs for the reduced eye and Le Grand's eye on the same set of sub-graphs and that the lines for the eyes were similar, often touching or running parallel. In Figure 8.1.9 we see that this is less so. The lines are similar in slope, but differ in position for *A* and *C* when the eyes are submerged in water.

The constants for the least-squares straight lines for *A* and *C* (Equation 8.1.5) for the reduced and Le Grand's eyes are given in Table 8.1.9. The curves for disjugacy *B* and divarication *C* are the same as in Figures 8.1.1 and 2. We saw from Equations 5.5.1 and 8.1.8 that only *A* and *C* are affected by the change in refractive index upstream of the system.

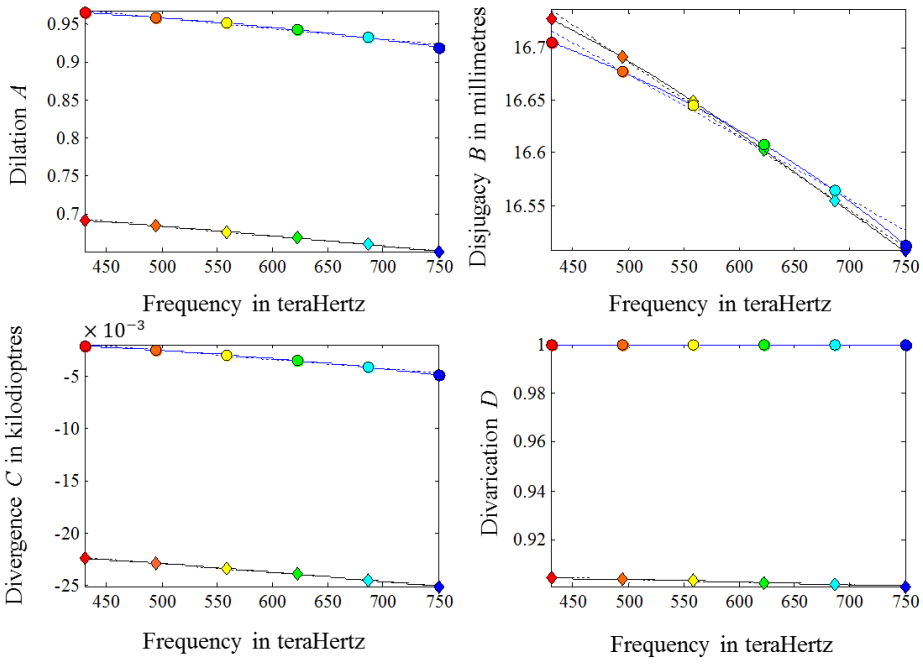

Figure 8.1.9 Dependence of the fundamental properties of the reduced eye (blue line and circles) and Le Grand's eye (black line and diamonds) on frequency ν when the eye is submerged in water. The disjugacy *B* and divarication *D* are, unsurprisingly, the same as for the eyes in air, or any other medium, however the dilation *A* and divergence *C* differ considerably, not only between the two eyes, but also from the eye in air.

Table 8.1.9 Constants for Equation 8.1.5 for *A* and *C* for the reduced and Le Grand's eyes submerged in water. The refractive index of water is calculated using Cornu's formula (Equation 4.4.1).

The Reduced Eye	
$a_1 = -1.4089\times10^{-4}$ ps	$a_2 = 1.0279$
$c_1 = -8.6007\times10^{-6}$ kD ps	$c_2 = 1.7475\times10^{-3}$ kD
Le Grand's Eye	
$a_1 = -1.2838\times10^{-4}$ ps	$a_2 = 0.7472$
$c_1 = -8.4280\times10^{-6}$ kD ps	$c_2 = -0.01871$ kD

Table 8.1.10 The transferences for the reduced eye and for Le Grand's eye submerged in water for the six reference frequencies (in THz), calculated equating the refractive index of water according to Cornu's formula (Equation 4.4.1).

Colour	ν	Reduced eye	Le Grand's eye
Red	430	$\begin{pmatrix} 0.9647 & 16.7055\text{ mm} \\ -0.002114\text{ kD} & 1 \end{pmatrix}$	$\begin{pmatrix} 0.6908 & 16.7276\text{ mm} \\ -0.02243\text{ kD} & 0.9044 \end{pmatrix}$
Orange	494	$\begin{pmatrix} 0.9581 & 16.6775\text{ mm} \\ -0.002515\text{ kD} & 1 \end{pmatrix}$	$\begin{pmatrix} 0.6840 & 16.6912\text{ mm} \\ -0.02287\text{ kD} & 0.9041 \end{pmatrix}$
Yellow	558	$\begin{pmatrix} 0.9504 & 16.6455\text{ mm} \\ -0.002977\text{ kD} & 1 \end{pmatrix}$	$\begin{pmatrix} 0.6761 & 16.6494\text{ mm} \\ -0.02337\text{ kD} & 0.9034 \end{pmatrix}$
Green	622	$\begin{pmatrix} 0.9416 & 16.6082\text{ mm} \\ -0.003515\text{ kD} & 1 \end{pmatrix}$	$\begin{pmatrix} 0.6677 & 16.6029\text{ mm} \\ -0.02393\text{ kD} & 0.9026 \end{pmatrix}$
Blue	686	$\begin{pmatrix} 0.9313 & 16.5646\text{ mm} \\ -0.004150\text{ kD} & 1 \end{pmatrix}$	$\begin{pmatrix} 0.6590 & 16.5545\text{ mm} \\ -0.02451\text{ kD} & 0.9018 \end{pmatrix}$
Violet	750	$\begin{pmatrix} 0.9189 & 16.5126\text{ mm} \\ -0.004910\text{ kD} & 1 \end{pmatrix}$	$\begin{pmatrix} 0.6503 & 16.5065\text{ mm} \\ -0.02508\text{ kD} & 0.9011 \end{pmatrix}$

Constants a_2 and c_2 (Table 8.1.9) for *A* and *C* for the two model eyes are very different, confirming the difference in the vertical position shown in Figure 8.1.9. The slopes (a_1 and c_1) are similar to those for the model eyes in air (Tables 8.1.2 and 3). The transferences for the six reference frequencies for the two eyes submerged in water are given in Table 8.1.10.

Submerging the eye in water has the effect of increasing *A* and *C*. Because the power of the system is the negative of the divergence (Equation 3.4.3), submerging the eye in water has the well-known effect of decreasing and, hence, partly neutralising the power of the eye.

8.1.5 Discussion

In conclusion, we saw how the fundamental properties of the reduced and Le Grand model eyes depend on the frequency of light. We compared the two model eyes in air when the refractive index is equated to the constant of 1 and when it is given by Cauchy's formula and saw firstly, that only the dilation *A* and divergence *C* are affected by the refractive index of the surrounding media, and secondly, that the effect is small and affects the vertical position of the graph. This provides justification for using $n_0 = 1$, as is often done in practice.

We then studied the fundamental properties as a function of vacuum wavelength. We observed that the curves depart further from straight lines than do those with frequency ν as independent variable. We conclude, in addition to the reasons discussed in Section 4.3, that it is preferable to study chromatic properties as functions of ν rather than λ.

Finally we considered the effect on the fundamental properties when the model eyes are submerged in water. Again, only the dilation *A* and divergence *C* are affected. There were two noticeable differences in the graphs. Firstly, in Figure 8.1.9, the curves for *A* and *C* differ in vertical position, but the slopes are similar. Secondly, when we compare the respective model eye (Figure 8.1.9) to the same eye in air (Figure 8.1.3) for *A* and *C*, we again see a significant change in position of the curve, but a similar slope. We know that the effect of submerging any eye in water is to tend to neutralise the refractive effect of the corneal surface. As a result the power *F* is decreased and, hence, the divergence *C* is increased. The ametropia *A* is increased and consequently, because of Equation 3.4.6, there is a need for an increased power of the refractive compensation F_0.

In this section we have seen that the fundamental properties of the two model eyes are dependent on frequency. The dependence curves for the fundamental properties of the two model eyes were roughly similar but differed

due to the underlying differences in design of the two eyes. The dependence is very nearly linear and we obtained a linear expression for the dependence of each fundamental property on frequency. When these expressions are used, the estimated transference is approximately symplectic.

8.2 The transformed transferences

In Section 3.7, we introduced transformed transferences and characteristic matrices. Transformed transferences are members of Hamiltonian space whereas each characteristic matrix represents a combination of derived properties of the system. In this section we look at transformed transferences and then examine characteristic matrices in Chapter 9.

Here we consider the logarithmic and Cayley transforms introduced in Section 3.7, both of which are Hamiltonian. Our interest in these transformed transferences, for the purpose of this dissertation, lies not in calculating an average transference (as done elsewhere; Harris, 2004b; 2005; Harris and Cardoso, 2006) but rather is two-fold. Firstly we wish to study the nature of the transformed matrix itself and how it depends on the frequency of light. An advantage is that, for a Gaussian system, one can represent a transference in three-dimensional linear space. Secondly, we utilise the mathematical properties of the Hamiltonian and symplectic matrices to obtain a formula for transferences as functions of frequency. The advantage is that the transferences one obtains are strictly symplectic which contrasts with the transferences obtained above (Equation 8.1.5) which are approximately symplectic.

In Section 5.6 we saw that the Cayley transform can be represented as a simple equation (Equations 5.6.6, 7 and 9) as a function of the entries of the transference. In contrast, a logarithmic transform makes use of an infinite series (Cardoso, 2005) therefore, because of its simple form, the Cayley transform gives greater insight. For this reason we spend some time unpacking the Cayley transform in Section 8.2.1. We take a brief look at the logarithmic transform in Section 8.2.2

8.2.1 The Cayley transformed transference

The Cayley transform is defined by Equation 3.7.13, and simplified for Gaussian systems to Equation 5.6.7. We use the caret (^) to denote transformed qualities. For example $\hat{\mathbf{S}}$ is the transformed **S** and $\hat{A}$ is the transformed *A*. Hamiltonian matrices are defined by Equation 3.7.4 and the resulting equality given by Equation 3.7.6. For a Gaussian system this simplifies to

$$\hat{A} = -\hat{D}. \tag{8.2.1}$$

Hence there are only three independent variables, $\hat{A}$, (or $\hat{D}$), $\hat{B}$ and $\hat{C}$, and therefore $\hat{\mathbf{S}}$ can be plotted on a three-dimensional graph. We recall that the Cayley transform of a symplectic matrix is Hamiltonian and, therefore, Equation 8.2.1 applies to a Gaussian system.

We now consider the dependence of the Cayley transformed transference $\hat{\mathbf{S}}$ on the frequency ν of light. The dependence of the individual entries is shown in Figures 8.2.1 and 4 for the reduced eye and Le Grand's eyes respectively. The relationship between the three independent entries of the transformed transference can be shown on a three-dimensional graph. This is shown in Figure 8.2.3 for the reduced eye and Figure 8.2.6 for Le Grand's eye. The six reference frequencies, as defined in Table 4.2.1, are used to define the frequency at six points, evenly spaced at every 64 THz.

Because Hamiltonian matrices define a vector space we are able to represent the transformed transference, dependent on ν, in the space. The meaning of each axis in Hamiltonian space is outside the scope of this dissertation. The Hamiltonian spaces generated by the logarithmic and Cayley transforms differ. Equation 5.6.7 begins to give some interpretation of what Hamiltonian space represents. We recall that there is an infinity of transforms between symplectic and Hamiltonian matrices; in this study we consider just two, the logarithmic transform (Equation 3.7.2) and the Cayley transform defined by Equation 3.7.13.

We now take a closer look at the formulae derived in Section 5.6. Firstly, Equation 5.6.7 is the formula for the transformed transference as a function of the fundamental properties of the system. This equation gives us some insight into the

meaning of the three independent entries of the Cayley transformed transference. We see that the transformed transference is multiplied by a constant that includes only the entries on the diagonal, that is, *A* and *D*. Within the matrix, the diagonal entries are the difference between the diagonal entries of the transference, while the two off-diagonal entries are the same as for the transference, each multiplied by 2. This gives us a transformed transference that is an interesting mix of the fundamental properties.

The reduced eye

Equation 5.6.18 gives the transformed transference for the reduced eye. Because we have worked with rational numbers all along, we find some interesting simplifications and the transformed transference for the reduced eye turns out to be a simple matrix dependent on the refractive index and therefore on the frequency of light. $\hat{B}$ turns out to be a constant because the refractive indices cancel out. The result of this Cayley transformed transference for the reduced eye is shown graphically for each entry of the matrix in Figure 8.2.1 as functions of frequency.

In Figure 8.2.1 the dashed red straight lines obtained using the least squares method represent the entries of the Cayley transformed transference as functions of frequency. These three straight line equations are represented as a matrix in Equation 8.2.3, with constants given in Table 8.2.1 for the reduced eye. Calculating a matrix from Equation 8.2.3 for any particular frequency results in a Hamiltonian matrix. This in turn, using the Cayley transform, Equation 8.2.2, maps to a transference. Equations 8.2.2 and 3 together give us the formula for the approximation of the transference for the reduced eye as a function of frequency. The equation to map the transference from the transformed transference (originally given in Equation 5.6.12) is

$$\mathbf{S} = \frac{2\left(\mathbf{I} - \hat{\mathbf{S}}\right)}{1 + \det \hat{\mathbf{S}}} - \mathbf{I} \tag{8.2.2}$$

where

$$\hat{\mathbf{S}} = \begin{pmatrix} \hat{a}_1 & \hat{b}_1 \\ \hat{c}_1 & -\hat{a}_1 \end{pmatrix} v + \begin{pmatrix} \hat{a}_2 & \hat{b}_2 \\ \hat{c}_2 & -\hat{a}_2 \end{pmatrix}. \tag{8.2.3}$$

Table 8.2.1 The constants for the reduced eye in air for Equation 8.2.3. The units are picoseconds (ps), millimetres (mm) and kilodioptres (kD).

$\hat{a}_1 = 4.7804\times10^{-5}$ ps	$\hat{a}_2 = 0.3088$
$\hat{b}_1 = 0$ mm ps	$\hat{b}_2 = -11.1111$ mm
$\hat{c}_1 = 7.2055\times10^{-6}$ kD ps	$\hat{c}_2 = 3.6298\times10^{-2}$ kD

Frequency (ν) is in teraHertz $(10^{12}\ \mathrm{s}^{-1})$ and the constants for Equation 8.2.3 are given in Table 8.2.1 for the reduced eye in air.

Equations 8.2.3 and 2 hold for any Gaussian eye, however, because of the changes in structure, that is, the exact parameters of the refracting surfaces, number of refracting surfaces, width of homogenous gaps and formulae of the refractive indices of the media, we can expect different constants for each model eye. Using the methodology above, it is simple for MATLAB® to generate the constants for any Gaussian eye coded into the Matfile.

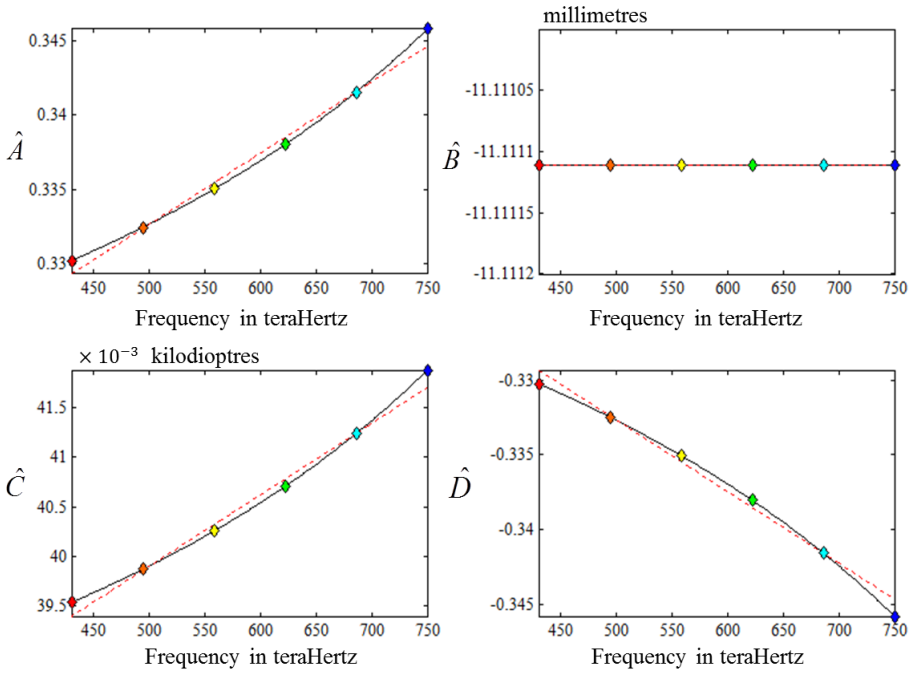

Figure 8.2.1 Entries of the Cayley transformed transference for the reduced eye as functions of frequency. The solid lines represent the entries as functions of frequency and the red dashed lines the fitted least squares straight lines.

The transferences of the reduced eye, obtained using Equations 8.2.2 and 3 are all symplectic matrices to the level of the accuracy of MATLAB®. The graphs for the fundamental properties of the reduced eye in air as a function of frequency are given in Figure 8.2.2. The solid black lines with coloured diamond shaped reference points represent the actual transference of the reduced eye dependent on frequency, and are the same curved lines we saw in Figure 8.1.1. The red lines represent the lines obtained using Equations 8.2.2 and 3 with constants given in Table 8.2.1. The dashed lines representing the least squares straight lines from Figure 8.1.1 are superimposed with the red lines for dilation *A*, disjugacy *B* and divergence *C* and with the black line for divarication *D* and are therefore suppressed to unclutter the figure. Where previously the dashed straight lines created from the least squares of the fundamental properties did not produce transferences that were exactly symplectic, we now have the red lines for each of the fundamental properties representing symplectic transferences. In Hamiltonian space, these red lines are the straight lines produced from the least squares formulation of the entries of the transformed transferences shown by the dashed red lines in Figure 8.2.1.

The relationship between the three independent entries of the Cayley transformed transference for the reduced eye where $n_0 = 1$ are plotted on a three-dimensional graph showing how these properties change with frequency. In Figure 8.2.3, we see how the relationship is a straight line. From Equation 8.2.3 and Table 8.2.1 we have

$\hat{A} = \hat{a}_1 \nu + \hat{a}_2$,

$\hat{B} = \hat{b}_2$

and

$\hat{C} = \hat{c}_1 \nu + \hat{c}_2$.

Manipulating, we obtain

$$\hat{C} = \frac{\hat{c}_1}{\hat{a}_1} \hat{A} + \frac{\hat{a}_1 \hat{c}_2 - \hat{c}_1 \hat{a}_2}{\hat{a}_1},$$

the equation of a straight line.

The derivation of Equation 8.2.2 and the graphs in this section give us some insight into the Hamiltonian space. We have utilised the properties of the Hamiltonian space to derive approximate equations for a transference of the reduced eye as a function of any chosen frequency of light, that is symplectic with determinant exactly 1. Furthermore, Equation 8.2.3 has the advantage of having less constants – six instead of the eight needed for Equation 8.1.5.

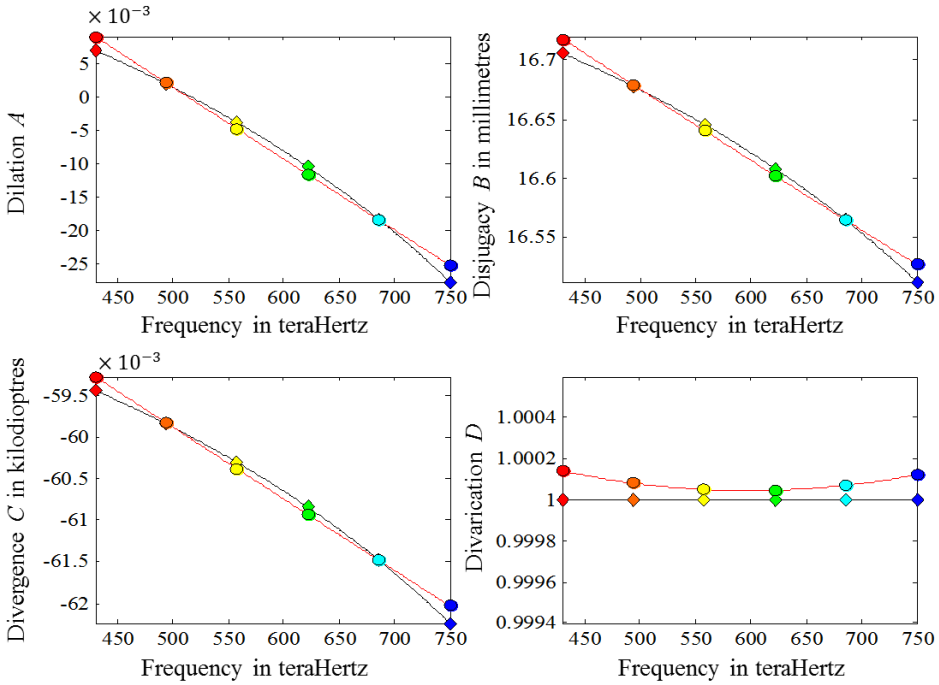

Figure 8.2.2 Fundamental properties of the transference of the reduced eye as functions of frequency. The black lines and diamond reference points represent the dependence as shown in Figure 8.1.1 while the red lines represent the dependence of the reduced eye on frequency according to the formulae and constants given in Equations 8.2.2 and 3 and Table 8.2.1. The least squares straight lines (shown with black dashed lines in Figure 8.1.1) appear superimposed with the red lines for dilation *A*, disjugacy *B* and divergence *C* and have been suppressed.

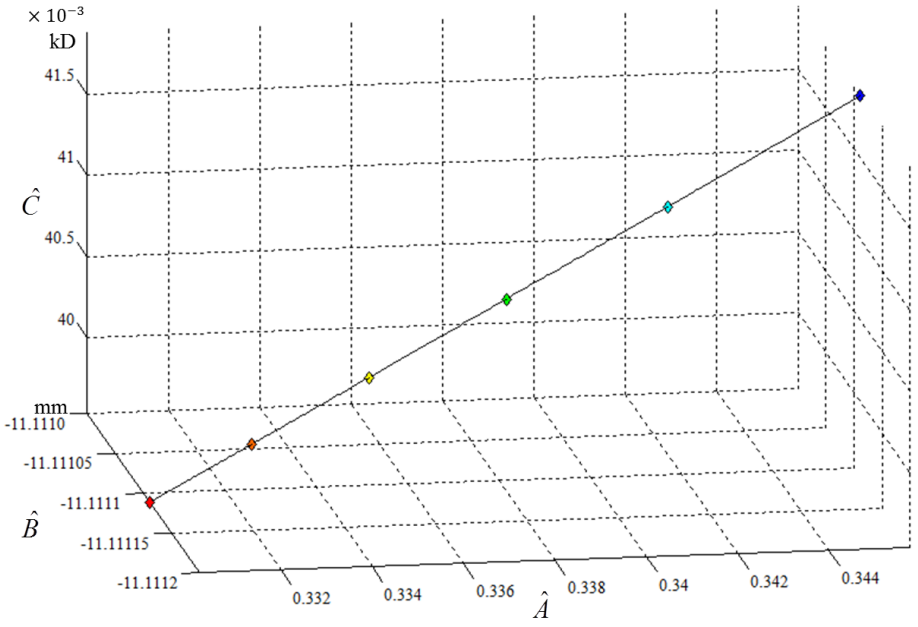

Figure 8.2.3 Three-dimensional graph of the Cayley transformed transference of the reduced eye with $n_0 = 1$ showing change with frequency. The azimuth is -9° and elevation 23°.

Le Grand's eye

In Figure 8.2.4 the individual entries of the Cayley transformed transference for the Le Grand eye are graphed as a function of frequency and in Figure 8.2.6 the three independent entries are graphed in three-dimensions.

If we compare the graphs for the dependence of the transformed transference on the frequency of light for Le Grand's eye (Figure 8.2.4) to that of the reduced eye (Figure 8.2.1) we see strong similarities for $\hat{A}$, $\hat{C}$ and $\hat{D}$, however Le Grand's eye has a curve for $\hat{B}$ whereas the reduced eye has a straight line. However, the scale along the vertical-axis for $\hat{B}$ for Le Grand's eye, indicates that the chromatic difference is small (0.01485 mm) and that the solid lines representing the transformed transference as a function of frequency are very near to linear for each entry.

Similar to the reduced eye, the equations for the dashed red straight lines in Figure 8.2.4 are obtainable using MATLAB®, giving us the constants for Le Grand's eye and given in Table 8.2.2. These constants are substituted into

Table 8.2.2 The constants for Equation 8.2.3 for Le Grand's eye in air.

$\hat{a}_1 = 4.2626\times10^{-5}$ ps	$\hat{a}_2 = 0.2892$
$\hat{b}_1 = 4.6331\times10^{-5}$ mm ps	$\hat{b}_2 = -11.5087$ mm
$\hat{c}_1 = 7.1114\times10^{-6}$ kD ps	$\hat{c}_2 = 3.7630\times10^{-2}$ kD

Equation 8.2.3 to obtain the Cayley transformed transference for each frequency and then into Equation 8.2.2 to obtain the transference for the frequency. The matrix obtained from Equation 8.2.3, by definition, is Hamiltonian and in turn, when transformed using the Cayley transform (Equation 8.2.2), maps to a symplectic matrix. Checking this for every frequency in the visible light spectrum we find that every transference obtained this way has unit determinant and is indeed symplectic.

Equations 8.2.2 and 3 represent a linear approximation to obtain the transference as a function of the frequency of light for any chosen frequency in the visible spectrum. In addition, the calculation can be done with a handheld

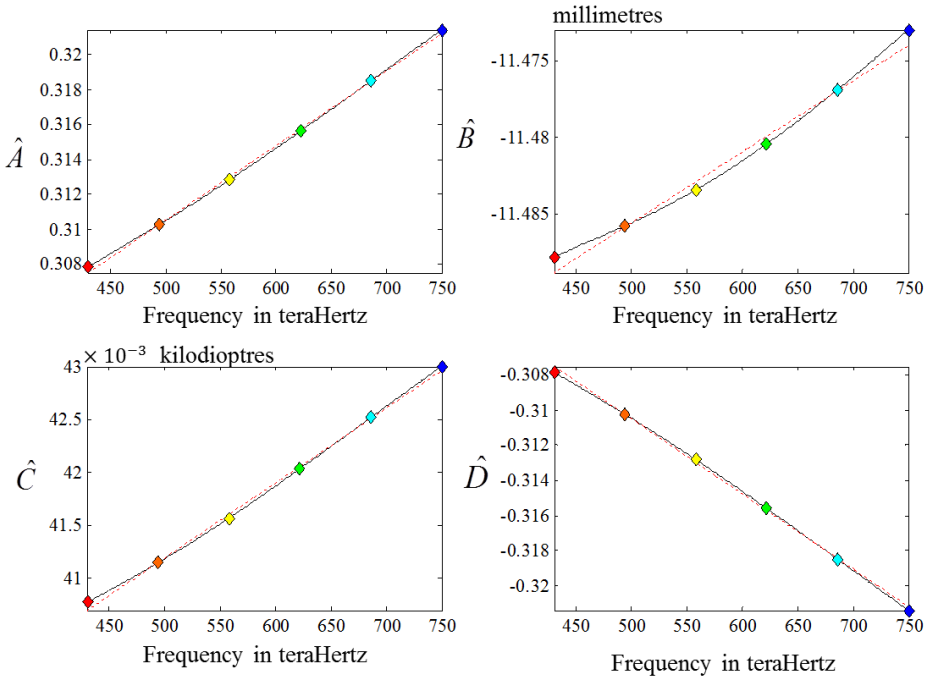

Figure 8.2.4 The entries of the Cayley transformed transference as a function of frequency for the Le Grand eye. The red dashed lines represent the least-squares straight lines for each entry in Hamiltonian space.

calculator in two steps, compared to the far lengthier process of obtaining a refractive index for each medium and then multiplying eight transferences to obtain a transference for the Le Grand eye for a chosen frequency, such as that used to produce the curves in Figure 8.1.2. Deriving the formulae for the transforms enables us to gain some insight into the transformed space and fundamental properties.

The fundamental properties of the transferences for Le Grand's eye obtained from Equations 8.2.3 and 2 are plotted in red in Figure 8.2.5 as functions of the frequency of light. For comparative purposes, we include the lines for the transferences obtained in Figure 8.1.2 in black.

In order to gain some insight into the relationship between the entries of the transformed transference, we plot the Cayley transformed transference for each frequency on a three-dimensional graph in Hamiltonian space. This is shown in Figure 8.2.6, firstly with the azimuth and elevation oriented in order to maximise any curvature along the line plotted and secondly oriented so as to attempt to look along the blue line and superimpose the six coloured diamonds to establish if there is any curvature present on the line. The straight line produced by Equation 8.2.3 is given in red in Figure 8.2.6(a). For the reduced eye we deduced that the line was straight, however, for the Le Grand eye, we see in Figure 8.2.6(b) that there is a small amount of curvature present.

The relationship between each of the fundamental properties and its dependence on frequency of light is nearly linear and similarly the relationship between the entries of the transformed transference and its dependence on the frequency of light are also nearly linear. This applies to both the reduced and Le Grand model eyes. This is in part due to the nature of the frequency of light and the eye being approximately a ball of water. We know from Section 4.3, that the refractive index of water, according to Cornu's equation, is approximately proportional to frequency. The chromatic aberration of the eye is due to the chromatic dispersion of the ocular media, which are mostly water and does not differ much between individuals (Smith, 1995).

Because of the linear relationships, the Cayley transform has enabled us to derive a set of linear equations for the dependence of each of the fundamental

properties on the frequency of light that gives a good approximation of the transference as a function of the frequency of light and given by Equations 8.2.2 and 3. Because we have derived simple equations in terms of the fundamental properties or entries of the transformed transference we have been able to gain some insight into the relationship of the fundamental properties and Hamiltonian space. The numerical transformed transferences for the Cayley transforms of the reduced and Le Grand's eyes, obtained using Equations 8.2.3 and 2, are given in Table 8.2.3.

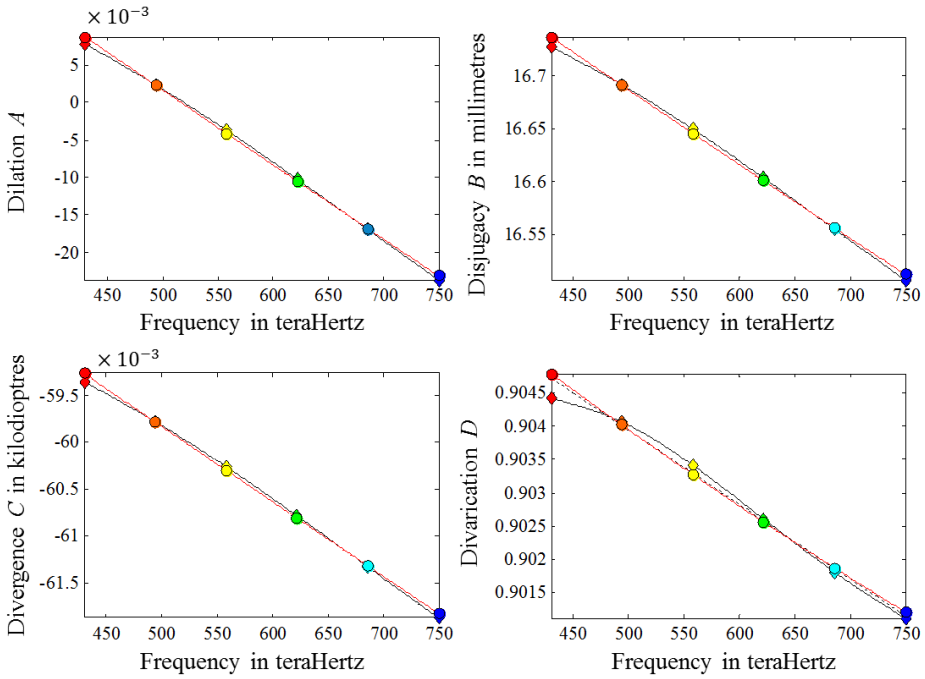

Figure 8.2.5 Fundamental properties of Le Grand's eye as a function of frequency of light. The solid black lines and diamond reference points represent the dependence as shown in Figure 8.1.2 while the red lines represent the dependence of Le Grand's eye on frequency according to the formula and constants given in Equation 8.2.2 and 3 and Table 8.2.2. The least squares straight lines (shown with black dashed lines in Figure 8.1.2) appear superimposed with the red lines for dilation *A*, disjugacy *B* and divergence *C* and have been suppressed. The dashed black least squares line for divarication *D* is shown and can be seen to be very close to the red line.

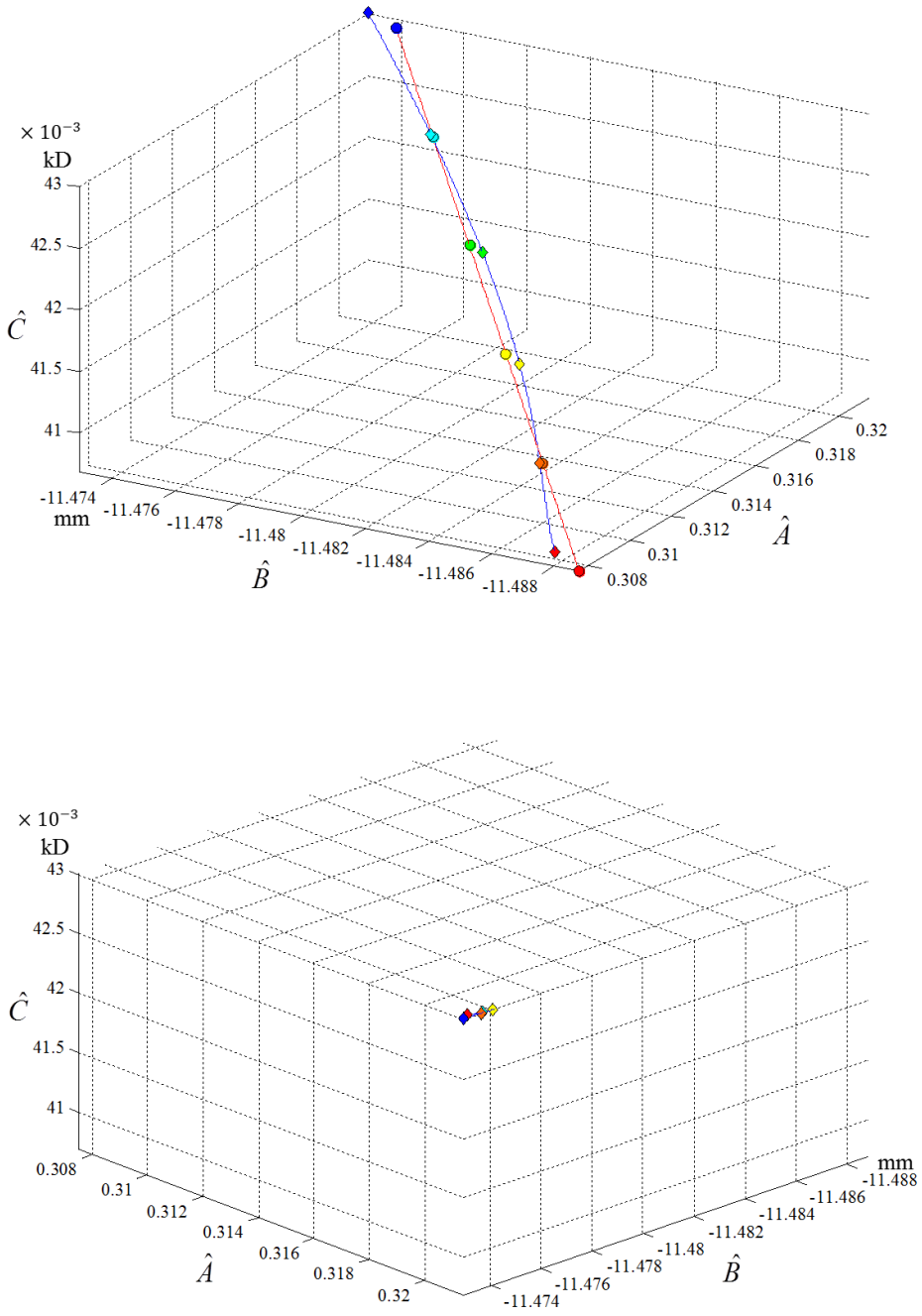

Figure 8.2.6 Three-dimensional graph of the Hamiltonian space of the Cayley transformed transference of Le Grand's eye showing change with frequency with $n_0 = 1$. In **(a)** the azimuth (-60°) and elevation (35°) show a gentle curve along the blue line with diamond markers, representing the transformed transference. The red straight line with circular markers represents the least squares straight line given by Equation 8.2.3. In **(b)** the azimuth (-46.5°) and elevation (-36°) are oriented so as to line up the red and blue diamonds. It is clear from the position of the remaining diamonds that the line is not completely straight, However, in this position the red line creates a single point, but has been suppressed to unclutter the figure.

Table 8.2.3 The numerical values for the Cayley transformed transferences for the six reference frequencies in THz for the reduced and Le Grand's eyes obtained using Equations 8.2.3 and 2 and constants from Tables 8.2.1 and 2.

ν	Colour	Reduced eye	Le Grand's eye
430	Red	$\begin{pmatrix} 0.3302 & -11.1111\,\text{mm} \\ 0.0395\,\text{kD} & -0.3302 \end{pmatrix}$	$\begin{pmatrix} 0.3079 & -11.4878\,\text{mm} \\ 0.0408\,\text{kD} & -0.3079 \end{pmatrix}$
494	Orange	$\begin{pmatrix} 0.3325 & -11.1111\,\text{mm} \\ 0.0399\,\text{kD} & -0.3325 \end{pmatrix}$	$\begin{pmatrix} 0.3102 & -11.4858\,\text{mm} \\ 0.0411\,\text{kD} & -0.3102 \end{pmatrix}$
558	Yellow	$\begin{pmatrix} 0.3350 & -11.1111\,\text{mm} \\ 0.0403\,\text{kD} & -0.3350 \end{pmatrix}$	$\begin{pmatrix} 0.3128 & -11.4834\,\text{mm} \\ 0.0416\,\text{kD} & -0.3128 \end{pmatrix}$
622	Green	$\begin{pmatrix} 0.3380 & -11.1111\,\text{mm} \\ 0.0407\,\text{kD} & -0.3380 \end{pmatrix}$	$\begin{pmatrix} 0.3156 & -11.4804\,\text{mm} \\ 0.0420\,\text{kD} & -0.3156 \end{pmatrix}$
686	Blue	$\begin{pmatrix} 0.3416 & -11.1111\,\text{mm} \\ 0.0412\,\text{kD} & -0.3416 \end{pmatrix}$	$\begin{pmatrix} 0.3185 & -11.4769\,\text{mm} \\ 0.0425\,\text{kD} & -0.3185 \end{pmatrix}$
750	Violet	$\begin{pmatrix} 0.3458 & -11.1111\,\text{mm} \\ 0.0419\,\text{kD} & -0.3458 \end{pmatrix}$	$\begin{pmatrix} 0.3214 & -11.4730\,\text{mm} \\ 0.0430\,\text{kD} & -0.3214 \end{pmatrix}$

8.2.2 The logarithmic-transformed transference

The logarithm of the transference was introduced in Section 3.7.1 and defined by Equation 3.7.2. We denote the transforms, as for Cayley transforms, by means of a caret (^).

The dependence of the logarithmic transformed transference on frequency of light is similar to the Cayley transformed transference in that the logarithmic transformed transference is Hamiltonian and there are three independent entries which show the dependence on frequency of light. The units are the same as the Cayley transformed transference. The dependence of the individual entries of the transformed transference as a function of frequency is given in Figures 8.2.7 and 9 for the reduced and Le Grand's eyes respectively. The relationship represented by Equation 8.2.1 is clear in the graph. The relationship between the dependencies of the three independent entries on the frequency of light on a three-dimensional graph is shown in Figure 8.2.8 for the reduced eye and Figure 8.2.10 for Le Grand's eye.

Table 8.2.4 gives the numerical values of the transformed transferences for six reference frequencies for each of the reduced and Le Grand's eyes with $n_0 = 1$. From the numerical values in the table and the lines in each of the figures, we see that, while the Cayley transform and the logarithmic transform are both Hamiltonian, they each define very different regions within the three-dimensional spaces.

The constants in Equation 8.2.3 for the least-squares straight lines in Figures 8.2.7 and 9 for the logarithmic transform of the reduced eye and Le Grand's eye are given in Table 8.2.5. Using them we obtain a transference dependent on frequency.

From Section 3.7.1 we define the transference **S** obtained from the logarithmic transform $\hat{\mathbf{S}}$ as

$$\mathbf{S} = \exp \hat{\mathbf{S}} \tag{8.2.4}$$

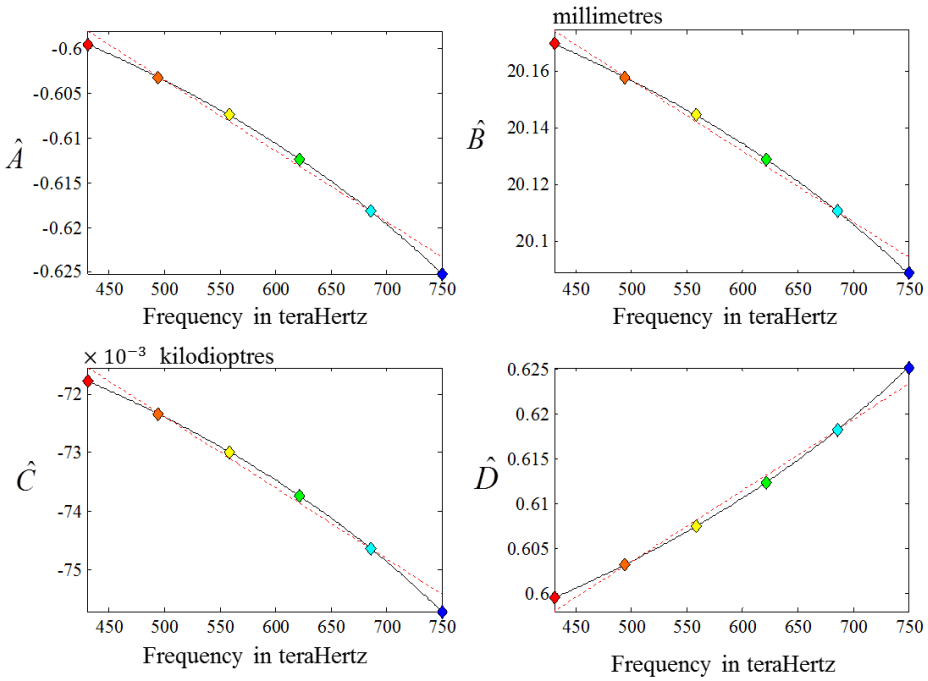

Figure 8.2.7 The entries of the logarithmic transformed transference of the reduced eye as a function of frequency. $\hat{A}$ and $\hat{D}$ are unitless and $\hat{A} = -\hat{D}$, while $\hat{B}$ is in millimetres and $\hat{C}$ is in units of kilodioptres. The red dashed lines represent the least-squares straight line for each entry.

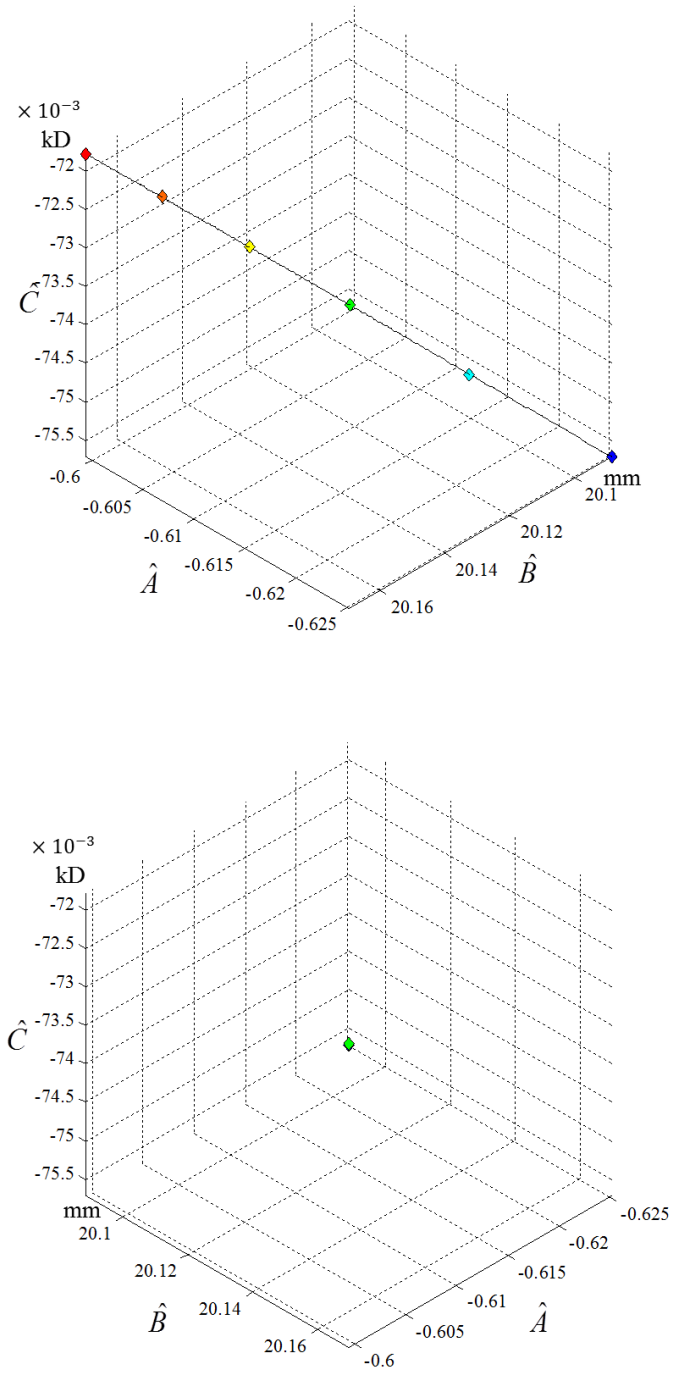

Figure 8.2.8 Three-dimensional graph of the logarithmic transformed transference of the reduced eye showing change with frequency. In **(a)** we see the graph with the azimuth 225° and elevation 35.2° oriented so as to exaggerate any possible curvature. In **(b)** the azimuth 135° and elevation 35.2° are oriented so that we are looking along the line and the coloured diamonds are superimposed on each other showing that the line is straight.

Table 8.2.4 Logarithmic transformed transferences $\hat{\mathbf{S}}$ for six reference frequencies (in THz) for the reduced and Le Grand's eyes.

ν	Colour	Reduced eye	Le Grand's eye
430	Red	$\begin{pmatrix} -0.5995 & 20.1696\text{ mm} \\ -0.0718\text{ kD} & 0.5995 \end{pmatrix}$	$\begin{pmatrix} -0.5527 & 20.6232\text{ mm} \\ -0.0732\text{ kD} & 0.5527 \end{pmatrix}$
494	Orange	$\begin{pmatrix} -0.6032 & 20.1579\text{ mm} \\ -0.0723\text{ kD} & 0.6032 \end{pmatrix}$	$\begin{pmatrix} -0.5566 & 20.6052\text{ mm} \\ -0.0738\text{ kD} & 0.5566 \end{pmatrix}$
558	Yellow	$\begin{pmatrix} -0.6074 & 20.1444\text{ mm} \\ -0.0730\text{ kD} & 0.6074 \end{pmatrix}$	$\begin{pmatrix} -0.5608 & 20.5845\text{ mm} \\ -0.0745\text{ kD} & 0.5608 \end{pmatrix}$
622	Green	$\begin{pmatrix} -0.6124 & 20.1288\text{ mm} \\ -0.0737\text{ kD} & 0.6124 \end{pmatrix}$	$\begin{pmatrix} -0.5652 & 20.5610\text{ mm} \\ -0.0753\text{ kD} & 0.5652 \end{pmatrix}$
686	Blue	$\begin{pmatrix} -0.6182 & 20.1105\text{ mm} \\ -0.0746\text{ kD} & 0.6182 \end{pmatrix}$	$\begin{pmatrix} -0.5699 & 20.5360\text{ mm} \\ -0.0761\text{ kD} & 0.5699 \end{pmatrix}$
750	Violet	$\begin{pmatrix} -0.6252 & 20.0886\text{ mm} \\ -0.0757\text{ kD} & 0.6252 \end{pmatrix}$	$\begin{pmatrix} -0.5746 & 20.5107\text{ mm} \\ -0.0769\text{ kD} & 0.5746 \end{pmatrix}$

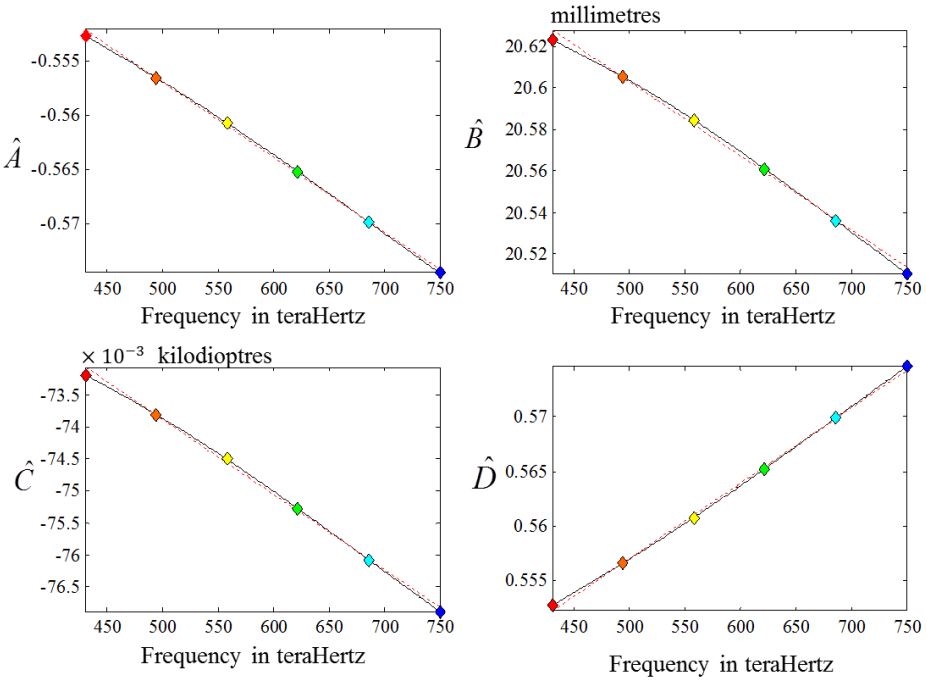

Figure 8.2.9 Entries of the logarithmic transformed transference of Le Grand's eye showing change with frequency. The curves for each entry of the transformed transference are almost linear. The red dashed lines represent the least-squares straight line.

Table 8.2.5 The constants for Equation 8.2.3 for the logarithmic transformed transference $\hat{\mathbf{S}}$ as a function of the frequency of light for the reduced eye and Le Grand's eye.

The Reduced Eye	
$\hat{a}_1 = -7.9053\times10^{-5}$ ps	$\hat{a}_2 = -0.5640$
$\hat{b}_1 = -2.4909\times10^{-4}$ mm ps	$\hat{b}_2 = 20.2813$ mm
$\hat{c}_1 = -1.2145\times10^{-5}$ kD ps	$\hat{c}_2 = -6.6312\times10^{-2}$ kD
Le Grand's Eye	
$\hat{a}_1 = -6.8870\times10^{-5}$ ps	$\hat{a}_2 = -0.5226$
$\hat{b}_1 = -3.5673\times10^{-4}$ mm ps	$\hat{b}_2 = 20.7813$ mm
$\hat{c}_1 = -1.1743\times10^{-5}$ kD ps	$\hat{c}_2 = -6.8009\times10^{-2}$ kD

and substituting from Equation 8.2.3 into this equation we obtain

$$\mathbf{S} = \exp\left(\begin{pmatrix} \hat{a}_1 & \hat{b}_1 \\ \hat{c}_1 & -\hat{a}_1 \end{pmatrix} v + \begin{pmatrix} \hat{a}_2 & \hat{b}_2 \\ \hat{c}_2 & -\hat{a}_2 \end{pmatrix}\right) \tag{8.2.5}$$

the equation for the transference as an approximate dependence on any chosen frequency of light, and which is symplectic. Equation 8.2.5 needs an appropriate software programme such as MATLAB® to execute the principal matrix exponent (*expm*).

The relationship between the three independent entries of the logarithmic transformed transference for Le Grand's eye as a function of frequency is shown by the blue line and diamond markers in Figure 8.2.10(a). By comparison, the red line and circular markers show the relationship obtained from Equation 8.2.5, also for Le Grand's eye. When the blue line is oriented so as to look along the line in Figure 8.2.10 (b), we see that the line is very slightly curved. The red line is straight and is suppressed to unclutter the figure.

In Figures 8.2.11 and 12 the black line with diamonds indicates the dependence of the fundamental properties as functions of frequency and matches the curves in Figures 8.1.1 and 2 for the two model eyes. The red line with circles shows the approximate dependence of the fundamental properties on frequency as calculated using Equation 8.2.5.

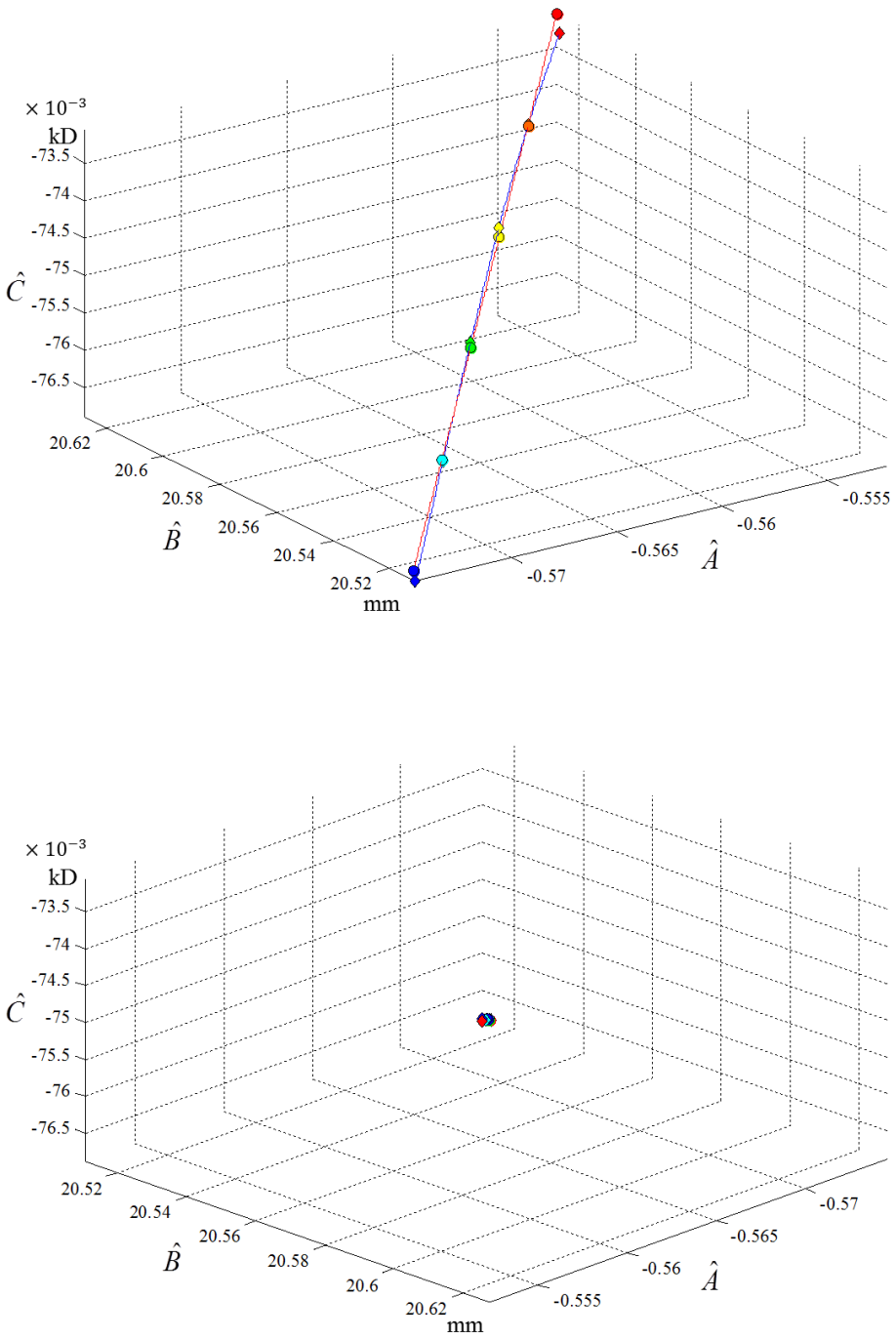

Figure 8.2.10 Three-dimensional graph of the Hamiltonian space of the logarithmic transformed transference of Le Grand's eye showing change with frequency. In **(a)** the azimuth (325°) and elevation (35°) are oriented so as to exaggerate the very slight curve in the line. The blue line and diamond markers show the transformed transference and the red line and circular markers indicate the approximate transformed transference according to Equation 8.2.5. In **(b)** the azimuth (134.5°) and elevation (35.5°) are oriented so as to attempt to line up the coloured diamonds and look along the blue line. This is not completely possible and we note a very slight curvature to the line.

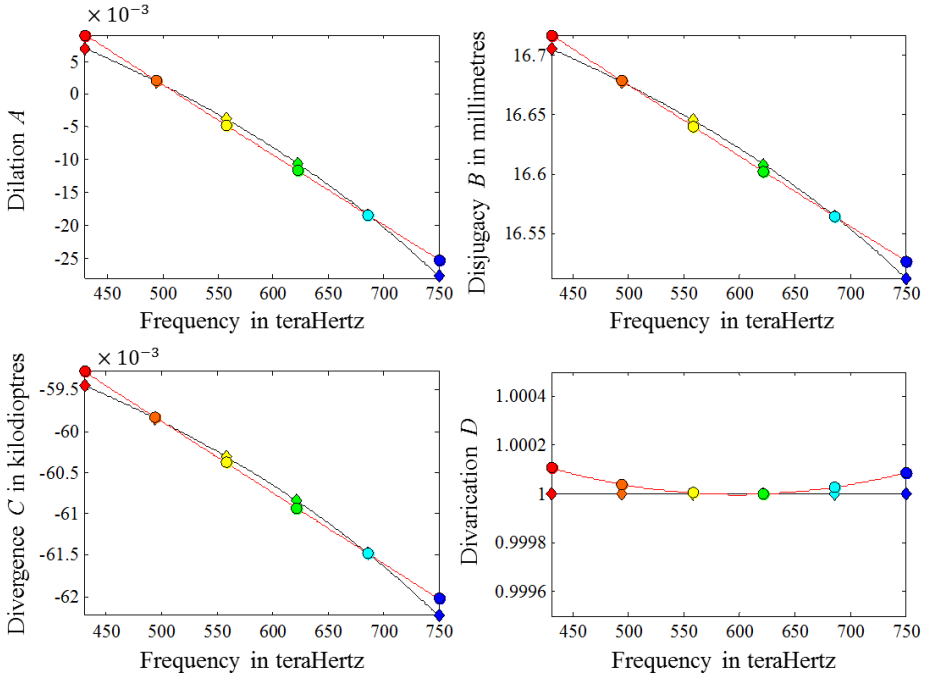

Figure 8.2.11 Fundamental properties of the reduced eye as functions of frequency. The black line and diamond reference points show the transference as an exact function of frequency and the red lines and circular reference points show the approximate transference calculated from the exponential of the linear dependence of the logarithmic transformed transference (Equation 8.2.5). The dashed straight lines seen in Figure 8.1.1 are superimposed on the red lines for dilation *A*, disjugacy *B* and divergence *C* and have been supressed. For divarication *D* it is the straight line at 1.

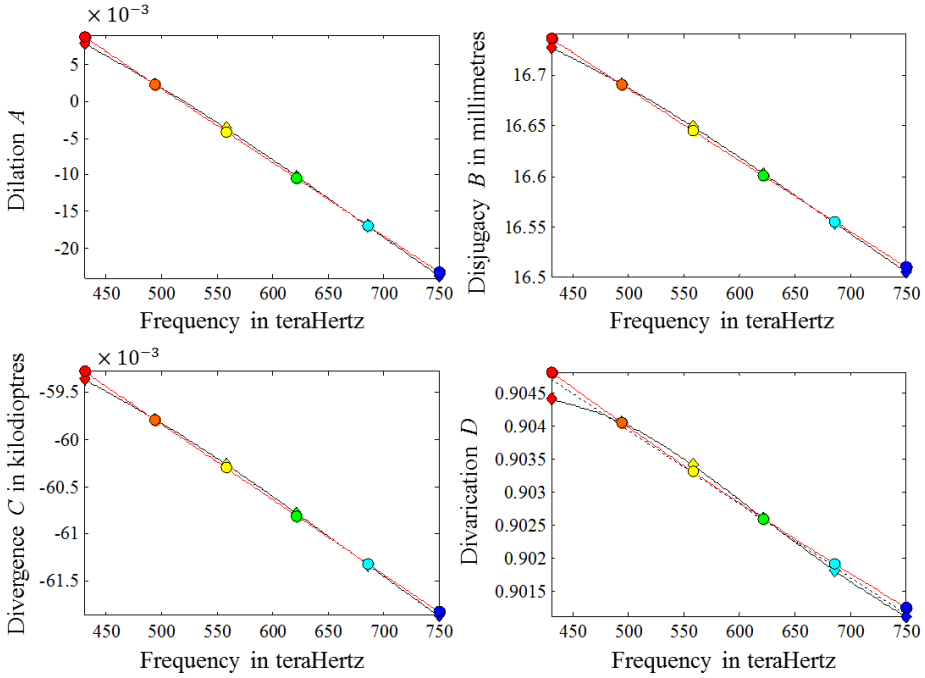

Figure 8.2.12 The fundamental properties of Le Grand's eye as functions of frequency.

The transference for any chosen frequency of light, obtained using the linear approximation given in Equation 8.2.5 and constants in Table 8.2.5 has unit determinant and is symplectic

8.3 Discussion

This chapter has looked at the dependence of the transference on the frequency of light. In Section 8.1, we saw that this relationship for each of the fundamental properties is very close to linear. We obtained an equation for each fundamental property using the least squares method for the straight line, Equation 8.1.5 (shown by a black dashed straight line on each sub-graph). Once combined, the fundamental properties for any particular frequency create an estimated transference whose determinant is approximately 1.

In Section 8.2, we looked at the transformed transference in Hamiltonian vector space. In particular we considered the Cayley and the logarithmic transforms. Because the 2×2 Hamiltonian matrix has three independent entries we were able to visualise the relationship between the entries in three-dimensional vector space. For the reduced eye the relationship is linear and for Le Grand's eye it is nearly perfectly linear. However, when the entries of the transference or transformed transference are looked at independently, Le Grand's eye appears to be closer to linear.

We looked at the dependence of the individual entries of the transformed transference $\hat{\mathbf{S}}$ on the frequency of light and noted, similar to the fundamental properties of the transference **S**, that the entries of $\hat{\mathbf{S}}$ are nearly linear. We obtained equations for the least-squares straight line for each of the three independent entries of the Cayley transformed transference (Equation 8.2.3). When transformed back to a symplectic matrix using Equation 8.2.2, it turns out that we have a matrix for every frequency with a determinant of exactly 1. These two equations are significant because we now have a formula for the straight line approximation giving us the dependence of the fundamental properties and hence the Gaussian transference which is symplectic and therefore the transference of an optical system. The constants are given for Equation 8.2.3 for the reduced eye (Table 8.2.1) and Le Grand's eye (Table 8.2.2).

The formula for the linear dependence of the transference on the frequency of light is based on the Cayley transform. This allows us to create simple equations that are possible to calculate using a handheld calculator. We also derived constants for Equation 8.2.3 for the straight lines of the logarithmic transformed transferences (Table 8.2.5), however Equation 8.2.4 shows that to transform this equation from Hamiltonian space to a symplectic matrix would require the principal matrix exponential which requires sophisticated software such as MATLAB®. Because of this, the Cayley transform gives greater insight.

9 Chromatic dependence of derived properties

Sections 3.4 and 5.1 looked at some familiar optical properties derived from the transference, including power, entrance- and exit-plane refractive compensation, and front- and back-vertex power. Then, Sections 3.6 and 5.4 looked at the cardinal and anti-cardinal points and ways to represent the relationships among the points using graphical construction and Pascal's ring. The distances from the system to the points are also properties of the system that can be derived from the transference. Here we study the dependence of these derived properties on frequency.

Section 3.7.3 introduced the four characteristic matrices. These transformed transferences are not Hamiltonian matrices, but each in its own right creates a vector space enabling us to do certain calculations in these vector spaces. However, unlike the Cayley and Logarithmic transformed transferences, the point **P** and angle **Q** characteristics are dimensionally uniform. Because each characteristic matrix is symmetric in Gaussian optics, it comprises three independent entries which can be graphed in three-dimensions. The dependence of the entries of each of the four characteristic matrices on the frequency of light will be graphed in Section 9.3 below.

9.1 Cardinal and anti-cardinal points

Sections 3.6 and 5.4 looked at the cardinal and anti-cardinal points of systems in general. We now look at how the frequency of light affects the positions and spread of the various points in the reduced and Le Grand's eyes. We start by obtaining the incident and emergent cardinal and anti-cardinal points for the six reference frequencies for each eye. These are given in Tables 9.1.1 to 4. We include the chromatic difference in positions, mean and standard deviation for each cardinal and anti-cardinal point in the tables. The chromatic difference in positions is calculated as

$$\delta z_Q = z_Q^{\mathrm{b}} - z_Q^{\mathrm{r}} \tag{9.1.1}$$

where Q represents any of the cardinal or anti-cardinal points and b and r represent the blue and red frequencies respectively. Longitudinal positions, *z*, are

Table 9.1.1 The positions of the incident cardinal points of the reduced eye for the six reference points, the chromatic difference in positions, mean and standard deviation across the spectrum 430 to 750 THz. Longitudinal positions *z* are relative to entrance plane T_0 and subscripts are defined in Table 3.6.1.

Colour	Freq THz	$z_{\overline{N}0}$ mm	$z_{\overline{P}0}$ mm	z_{F0} mm	z_{P0} mm	z_{N0} mm
Red	430	–39.2018	–33.6463	–16.8231	0	5.5556
Orange	494	–38.9761	–33.4206	–16.7103	0	5.5556
Yellow	558	–38.7198	–33.1643	–16.5821	0	5.5556
Green	622	–38.4263	–32.8708	–16.4354	0	5.5556
Blue	686	–38.0868	–32.5312	–16.2656	0	5.5556
Violet	750	–37.6895	–32.1340	–16.0670	0	5.5556
Chromatic difference		1.5123	1.5123	0.7562	0	0
Mean		–38.5343	–32.9788	–16.4894	0	5.5556
Standard deviation		0.4343	0.4343	0.2172	0	0

Table 9.1.2 Positions of the emergent cardinal and anti-cardinal points of the reduced eye as a function of frequency for the six reference points. The longitudinal positions *z* are given in millimetres from the exit plane T which is 22.2222 mm downstream of the entrance plane. The chromatic difference in position between the red and blue emergent points, the mean and standard deviation across the spectrum are given. Subscripts are defined in Table 3.6.1.

Colour	ν THz	z_P mm	z_N mm	z_F mm	$z_{\overline{N}}$ mm	$z_{\overline{P}}$ mm
Red	430	–22.2222	–16.6667	0.1565	16.9796	22.5352
Orange	494	–22.2222	–16.6667	0.0436	16.7539	22.3095
Yellow	558	–22.2222	–16.6667	–0.0845	16.4976	22.0532
Green	622	–22.2222	–16.6667	–0.2313	16.2041	21.7596
Blue	686	–22.2222	–16.6667	–0.4011	15.8646	21.4201
Violet	750	–22.2222	–16.6667	–0.5997	15.4673	21.0229
Chromatic difference		0	0	–0.7562	–1.5123	–1.5123
Mean		–22.2222	–16.6667	–0.1773	16.3121	21.8676
Standard deviation		0	0	0.2172	0.4343	0.4343

relative to the corresponding transverse plane. Consistent with Section 4.2 the frequency of red is taken to be 430 THz and blue to be

Table 9.1.3 The positions of the incident cardinal and anti-cardinal points of Le Grand's eye as a function of frequency for six reference frequencies. Positions are relative to the entrance plane.

Colour	Freq THz	$z_{\overline{\mathrm{N}}0}$ mm	$z_{\overline{\mathrm{P}}0}$ mm	$z_{\mathrm{F}0}$ mm	$z_{\mathrm{P}0}$ mm	$z_{\mathrm{N}0}$ mm
Red	430	–37.6878	–32.0833	–15.2365	1.6103	7.2148
Orange	494	–37.4540	–31.8489	–15.1221	1.6048	7.2098
Yellow	558	–37.1882	–31.5854	–14.8489	1.6028	7.2056
Green	622	–36.9000	–31.3001	–14.8489	1.6022	7.2022
Blue	686	–36.6078	–31.0094	–14.7042	1.6010	7.1994
Violet	750	–36.3241	–30.7255	–14.5637	1.5637	7.1967
Chromatic difference		1.3638	1.3578	0.6728	–0.0122	–0.0182
Mean		–37.0320	–31.4304	–14.9137	1.6029	7.2045
Standard deviation		0.4032	0.4006	0.1990	0.0027	0.0052

Table 9.1.4 Positions of the emergent cardinal and anti-cardinal points for Le Grand's eye as a function of frequency for six reference frequencies. The distances are relative to the exit plane, which is 24.1965 mm downstream from the entrance plane.

Colour	Freq THz	z_{P} mm	z_{N} mm	z_{F} mm	$z_{\overline{\mathrm{N}}}$ mm	$z_{\overline{\mathrm{P}}}$ mm
Red	430	–22.2758	–16.6712	0.1756	17.0223	22.6269
Orange	494	–22.2793	–16.6742	0.0526	16.7795	22.3845
Yellow	558	–22.2788	–16.6760	–0.0819	16.5122	22.1150
Green	622	–22.2765	–16.6765	–0.2254	16.2258	21.8258
Blue	686	–22.2750	–16.6766	–0.3714	15.9338	21.5322
Violet	750	–22.2754	–16.6766	–0.3714	15.9338	21.5322
Chromatic difference		0.0004	–0.0056	–0.6906	–1.3756	–1.38105
Mean		–22.2771	–16.6755	–0.1588	16.3578	21.9594
Standard deviation		0.0017	0.0015	0.2028	0.4044	0.4070

750 THz, the end-points of the spectrum. The mean and standard deviation are calculated across the spectrum from 430 to 750 THz at every 1 THz.

The reduced eye

Tables 9.1.1 and 2 show that the incident P_0 and emergent P principal points of the reduced eye both coincide with the entrance plane (or cornea) T_0 and the incident N_0 and emergent N nodal points both coincide with each other at the centre of curvature which is 5.5556 mm downstream of the entrance plane. This implies that P_0, P, N_0 and N are independent of frequency in the reduced eye and remain single point structures. On the other hand, the incident F_0 and emergent F and anti-cardinal points $\overline{P}_0$, $\overline{P}$, $\overline{N}_0$ and $\overline{N}$ depend on frequency and are therefore not point structures, but spread out like little rainbows into fuzzy zones rather than points. Furthermore, the magnitude of the chromatic difference in position of each of the anti-cardinal points is the same for the reduced eye, that is, $\left|\delta z_{\overline{Q}}\right| = 1.5123\,\text{mm}$.

Le Grand's eye

Tables 9.1.3 and 4 show that all ten of the cardinal and anti-cardinal points for Le Grand's eye depend on frequency and each is a fuzzy zone like a little rainbow. This is represented by both the chromatic difference and standard deviation. Because the points are mathematical concepts they will not actually be visible as a rainbow, with the exception of F. The statistical data at the bottom of each table shows that the fuzzy spread is greater for the anti-cardinal points than for the cardinal points. The P_0's and P's demonstrate the least spread, with the fuzzy spread increasing with each point as it moves further away from the P_0's and P's.

9.1.1 Graphical construction

The data given in Tables 9.1.1 to 4 is displayed visually using graphical construction as introduced in Sections 3.6.4 and 5.4.2. For this we construct the locator lines and points for the red and blue transferences for each of the reduced and Le Grand's eyes. In order to prevent the graph from being too cluttered, only the locator lines for the transferences representing the red (430 THz) and blue (750 THz) frequencies will be displayed. The positions of the ten cardinal and anti-cardinal points are shown.

Graphical construction of the reduced eye

Figure 9.1.1 shows the graphical construction for the reduced eye showing the locator lines for the red and blue transferences and the ten cardinal and anti-cardinal points. In Figure 9.1.1 the black horizontal line represents the optical axis Z, positioned at $X = 0$. The two vertical black lines represent the entrance plane T_0 at $z = 0$ and the exit plane T a distance z downstream from T_0 at $z = \frac{200}{9}\,\mathrm{mm}$, which is the length of the reduced eye. The locator lines L_0 and L for the reduced eye are drawn in red (430 THz) and blue (750 THz). From Section 3.6.4, the slope of the incident locator lines L_0 is given by $\frac{-C}{n_0}$. For the reduced eye in air, the refractive index of air is constant, 1, however, we know that C depends on frequency, and therefore the slope of L_0 also varies with frequency. The slope of the emergent locator line L is given by $\frac{C}{n}$. Both C and n depend on frequency and hence so does the slope of L. The slope of the blue locator line is steeper in magnitude than that of the red line for both L_0 and L.

In Figure 9.1.1 F_0 and F are positioned at the point of intersection between the respective locator line L_0 and L and the optical axis Z. The F_0's show that the blue F_0 is closer to the eye than the red F_0. More applicably, for F, the blue F is before the exit-plane T or retina and the red F is behind the retina. While the result is not surprising, the locator lines visibly illustrate this.

Locator line diagrams were described in Section 3.6.2. In Figure 9.1.1 horizontal lines are drawn in green at $X=1$ and $X=-1$ and vertical lines extended to the longitudinal axis for P_0 and P in green for the red points and cyan for the blue points. P_0 and P are coincident with T_0 for the reduced eye and only the cyan line is visible in the diagram. The red and blue anti-principal points $\overline{P}_0$ and $\overline{P}$ are distinct. P_0 and P simplify as follows: for z_{P0} for the reduced eye $D=1$ (from Equation 5.5.1), regardless of frequency. Substituting $D=1$ and $X=1$ for P_0 from Table 3.6.1 into Equation 3.6.1, it simplifies to 0 making z_{P0} coincident with the entrance plane for all frequencies. For z_P, by substituting $X=1$ and A and C from Equation 5.5.1 into Equation 3.6.2, z_P simplifies to $-z$. Because z is the length of the reduced eye, P is also coincident with T_0 for all frequencies. This is illustrated in Figure 9.1.1 where all four locator lines cross at the entrance-plane at both $X=1$ and $\frac{1}{X}=1$, shown by the uppermost green horizontal line.

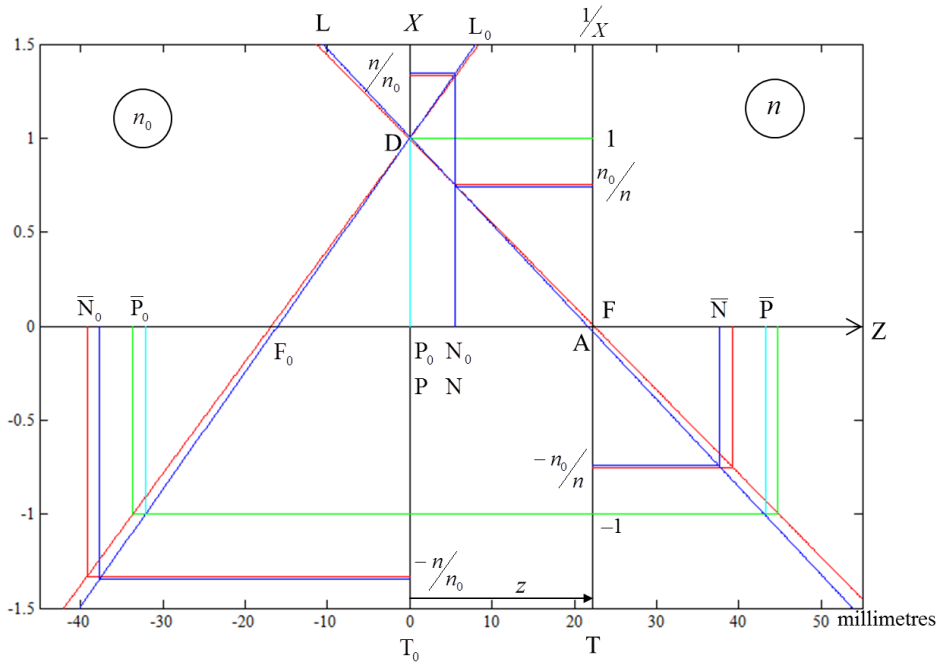

Figure 9.1.1 The graphical construction for the reduced eye showing the locator lines for the red and blue transferences and the ten cardinal and anti-cardinal points.

The nodal and anti-nodal points are indicated in Figure 9.1.1 with horizontal lines at $\pm\frac{n}{n_0}$ for N_0 and $\overline{\mathrm{N}}_0$ and $\pm\frac{n_0}{n}$ for N and $\overline{\mathrm{N}}$ in red and blue respectively. Because the indices depend on frequency, we obtain different positions for the red and blue horizontal lines. In turn vertical lines are extended to indicate the position of the nodal points on the longitudinal axis. For the reduced eye N_0 and N coincide, however $\overline{\mathrm{N}}_0$ and $\overline{\mathrm{N}}$ are distinct. The coincidence of N_0 and N is found in Equation 5.5.1; substituting *C*, *D* and *X* into Equation 3.6.1, z_{N0} simplifies to *r*, the radius of curvature of the corneal refracting surface. Therefore z_{N0} is independent of refractive indices, n_0 and *n*, and, hence, frequency ν. This is seen in Figure 9.1.1 by the single blue line dropping to the position for N_0. Similarly, substituting for *X*, and *A* and *C* from Equation 5.5.1 into Equation 3.6.2 and simplifying, we obtain the position for N as $z_{\mathrm{N}} = r - z$ with respect to T. This places N at position *r* with respect to T_0 for all frequencies. N is therefore independent of frequency and coincident with N_0.

Simplifications of anti-cardinal points for the reduced eye

We now turn our attention to the anti-cardinal points of the reduced eye, starting with $\overline{\mathrm{P}}_0$ and $\overline{\mathrm{P}}$. We know that the horizontal line to find the position of the points on the locator lines needs to be drawn at $X = -1$, shown by the lower green horizontal line in Figure 9.1.1. From the figure and from Equations 5.5.1 and 3.6.1 and 2, we see that $\overline{\mathrm{P}}_0$ and $\overline{\mathrm{P}}$ depend on frequency. Similarly, $\overline{\mathrm{N}}_0$ and $\overline{\mathrm{N}}$ are also dependent on frequency. $\overline{\mathrm{N}}_0$ and $\overline{\mathrm{N}}$ for the reduced eye are equidistant from the entrance-plane, albeit in opposite directions. From Tables 9.1.1 and 2 we see that each of the anti-cardinal points is equidistant between the red and blue positions (chromatic difference); this is shown algebraically for $\overline{\mathrm{P}}_0$, $\overline{\mathrm{P}}$, $\overline{\mathrm{N}}_0$ and $\overline{\mathrm{N}}$ below.

Most of the simplifications that occur for the reduced eye above and in Figure 9.1.1 stem from the transference and the fact that $D = 1$ for all

transferences of the reduced eye, regardless of the frequency. Let us look at this in more detail. Firstly, $\overline{\mathrm{N}}_0$ and $\overline{\mathrm{N}}$ are equidistant from T_0, in opposite directions. Starting with Equation 3.6.3, we substitute the values for *C* and *D* from Equation 5.5.1 and $n_0 = 1$ to obtain

$$z_{\overline{\mathrm{N}}0} = -\frac{n+1}{n-1}r \tag{9.1.2}$$

for the position of $\overline{\mathrm{N}}_0$ of the reduced eye and

$$z_{\overline{\mathrm{N}}} = \frac{n+1}{n-1}r - z \tag{9.1.3}$$

for the position of $\overline{\mathrm{N}}$ of the reduced eye. Because the emergent points are defined as the distance from the exit-plane, we expect that the incident and emergent formulae will differ by the length of the reduced eye, *z*. From Equations 9.1.2 and 3, we see that $\overline{\mathrm{N}}_0$ and $\overline{\mathrm{N}}$ are equidistant from T_0, $\overline{\mathrm{N}}_0$ being upstream and $\overline{\mathrm{N}}$ downstream of T_0.

Similar equations derived for $\overline{\mathrm{P}}_0$ and $\overline{\mathrm{P}}$, from T_0 and T respectively, turn out to be

$$z_{\overline{\mathrm{P}}0} = \frac{-2r}{n-1} \tag{9.1.4}$$

for the distance of $\overline{\mathrm{P}}_0$ from T_0, and

$$z_{\overline{\mathrm{P}}} = \frac{2nr}{n-1} - z \tag{9.1.5}$$

for the distance of $\overline{\mathrm{P}}$ from T. These are clearly not equidistant from T_0 and confirms what we deduce from Figure 9.1.1.

Secondly, we examine the result in Tables 9.1.1 and 2 that the magnitude of the distance between the red and blue anti-cardinal points in the reduced eye is the same for all four anti-cardinal points. Starting with the chromatic difference between points defined in Equation 9.1.1 and substituting in turn the equations derived for each of the anti-cardinal points in Equations 9.1.2 to 5, we obtain the chromatic difference in position of $\overline{\mathrm{P}}_0$

$$\delta z_{\overline{\mathrm{P}}0} = z^b_{\overline{\mathrm{P}}0} - z^r_{\overline{\mathrm{P}}0} = \frac{2r(n_b - n_r)}{(n_b - 1)(n_r - 1)}. \tag{9.1.6}$$

The equation for $\delta z_{\bar{N}0}$, the chromatic difference in distance between the red and blue $\bar{N}_0$'s is equal to Equation 9.1.6. The chromatic difference in position of $\bar{P}$ and $\bar{N}$ are equal in magnitude, but the negative of the incident equation. That is to say

$$\delta z_{\bar{N}0} = \delta z_{\bar{P}0} = -\delta z_{\bar{N}} = -\delta z_{\bar{P}}. \qquad (9.1.7)$$

The negative value found in the chromatic difference of the emergent anti-cardinal points indicates that the positions of the red and blue anti-cardinal points are switched compared to the incident points. The equalities derived in Equations 9.1.2 to 7 only apply to the reduced eye and cannot be generalised to other eyes.

We conclude that while the reduced eye is well suited to the study of most chromatic properties, it is not suitable for studying cardinal points and, in particular, not suitable for studying the dependence of the cardinal points on frequency.

Graphical construction of Le Grand's eye

Let's us, therefore, consider a more complex Gaussian eye, that of Le Grand's four-surface eye. From Table 8.1.1 and Section 8.1.1 we already know that all four fundamental properties depend on the frequency of the light traversing the system. Figure 9.1.2 shows the graphical construction of the locator lines for Le grand's eye for the red (430 THz) and blue (750 THz) frequencies.

The optical axis Z, entrance-plane T_0 and exit-plane T are the same as in Figure 9.1.1. It is apparent that Le Grand's eye does not simplify to the extent that the reduced eye does. We start with the incident locator lines L_0, the slope of which, from the equation for the slope given above and from Figure 9.1.2, depend on frequency. The slope of L_0 is 0.05936 kD for the red line and 0.06187 kD for the blue line. Unsurprisingly, the intersection of L_0 with Z shows that the blue F_0 is in closer proximity to the eye than the red F_0. L_0 intersects the entrance-plane at position *D*. From the transferences listed in Table 8.1.1 we know that the entries for *D* depend on frequency and therefore the two L_0s cross T_0 at different

positions. The values for *D* are, however, very close and it is difficult to see the separation on Figure 9.1.2. The red and blue L_0 s cross at

$$z_{Q0} = \frac{D_b - D_r}{C_b - C_r} \tag{9.1.8}$$

which is 1.32 mm downstream of T_0.

The emergent locator lines L intersect T at *A*. From Section 3.3.1, we know that a positive value for *A* implies hyperopia and a negative value, myopia. This is visible in Figure 9.1.2, where the red L indicates a positive value for *A* and intersects Z behind T or the retina and the blue L shows a negative value for *A* and intersects Z with F before the retina. The red and blue L's intersect at position

$$z_Q = \frac{A_b - A_r}{\frac{C_r}{n_r} - \frac{C_b}{n_b}} \tag{9.1.9}$$

which is –22.4474 mm from T, or 1.7491 mm from T_0. The position of intersection of the incident red and blue L_0 's does not coincide with the same for L's, nor does either intersection coincide with the position of either P_0 's or P's. The slopes of the L's are –0.04454 kD for the red line and –0.04596 kD for the

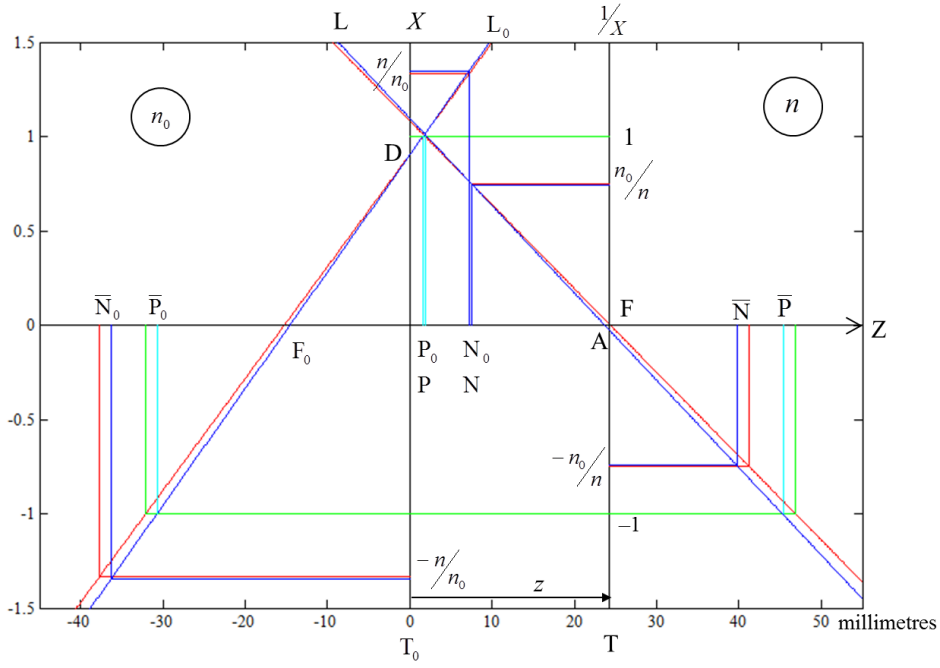

Figure 9.1.2 The graphical construction for Le Grand's eye showing the locator lines for the red and blue transferences and the ten cardinal and anti-cardinal points.

blue line. Because the difference in slope of the L_0's and L's is so slight, it is difficult to distinguish the point of intersection of the red and blue lines in Figure 9.1.2.

In Figure 9.1.2 the principal and anti-principal horizontal lines are drawn in green at 1 or –1 respectively and vertical lines extended to Z in green for the red points and cyan for the blue points. The P_0's and P's are separate, and do not coincide with T_0. The red and blue P_0's and P's are also distinct, but too close to be discernible in the diagram. The cyan lines appear superimposed over the green lines and from the diagram it appears that each of P_0 and P is the same for the red and blue lines. However, if we look at the values given in Tables 9.1.3 and 4, we see that the red and blue transferences have different values for the P_0's and P's and therefore the P_0's and P's depend on frequency. The $\overline{P}_0$'s and $\overline{P}$'s are distinct.

In Figure 9.1.2 the nodal and anti-nodal points are indicated with horizontal lines at $\pm\frac{n}{n_0}$ at N_0 and $\overline{N}_0$ and $\pm\frac{n_0}{n}$ for N and $\overline{N}$ in red and blue respectively. Because the indices depend on frequency, we obtain different positions for the horizontal lines. For Le Grand's eye the N_0's and N's are distinct and the red and blue points are also distinct, but too close to be distinguishable in the diagram. For clarity, we see from Tables 9.1.3 and 4 that the red and blue N_0's and N's are distinct and therefore the N_0's and N's depend on frequency, implying that the N_0's and N's are not points, but rather fuzzy nodal zones. The $\overline{N}_0$'s and $\overline{N}$'s are distinct for red and blue.

Unlike the reduced eye, the chromatic difference in position between each of the four anti-cardinal points for Le Grand's eye is different for all four points.

Summary

We have illustrated how the principal and nodal points for the reduced eye are independent of frequency and that P_0 and P are positioned at the entrance plane while N_0 and N are positioned at the centre of curvature of the single

refracting surface. For the reduced eye, F_0, F and the anti-cardinal points depend on frequency and the chromatic difference in distance between the red and blue position of each of the anti-cardinal points is the same, but the sequence is different for incidence and emergence.

On the other hand, for the four-surface Le Grand eye, all six cardinal and four anti-cardinal points depend on frequency and are distinct from each other, implying that these cardinal points are not points but fuzzy zones.

9.1.2 Pascal's ring

In the previous section, we looked at the positions and changes among the various cardinal and anti-cardinal points. Tables 9.1.1 to 4 gave numerical values and we were able to see which points were dependent on frequency. The graphical constructions given in Figure 9.1.1 for the reduced eye and Figure 9.1.2 for Le Grand's eye showed the relationships between the positions of the points, however, certain points are so close together as to be indiscernible in the figures. Pascal's ring was introduced in Section 3.6.5 and expanded on in Section 5.4.3 and while the ring is not drawn to scale, it does show the relationships among the points and the directions of the changes. Pascal's ring emphasises which points are dependent, or, in the case of the reduced eye, independent, of frequency.

Pascal's ring for the reduced eye

Pascal's ring for the reduced eye as a function of frequency is shown in Figure 9.1.3. For clarity, we compare the rings for only the red and blue cardinal points. From the graphical construction of the reduced eye in Figure 9.1.1, there is no separation of principal planes nor nodal points and so for Pascal's ring the central square fuses to become a single vertical line. As expected, the blue focal points are both closer to the eye than the red focal points and this is represented in Pascal's ring. When we consider the Pascal's ring in Figure 9.1.3 and the extended Pascal's ring in Figure 9.1.4 we see that, for the reduced eye, the blue ring contracts towards the principal-nodal line. The width, between the focal points, is narrower for the blue than for the red ring structure. The vertical height of both red and blue structures is equal.

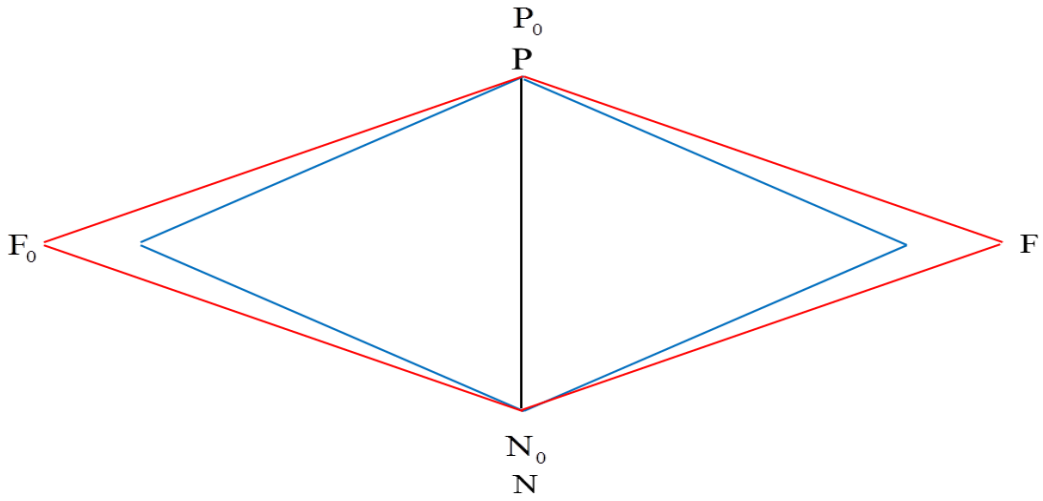

Figure 9.1.3 Pascal's ring for the reduced eye for the red and blue cardinal points. The vertical black line is common to both frequencies.

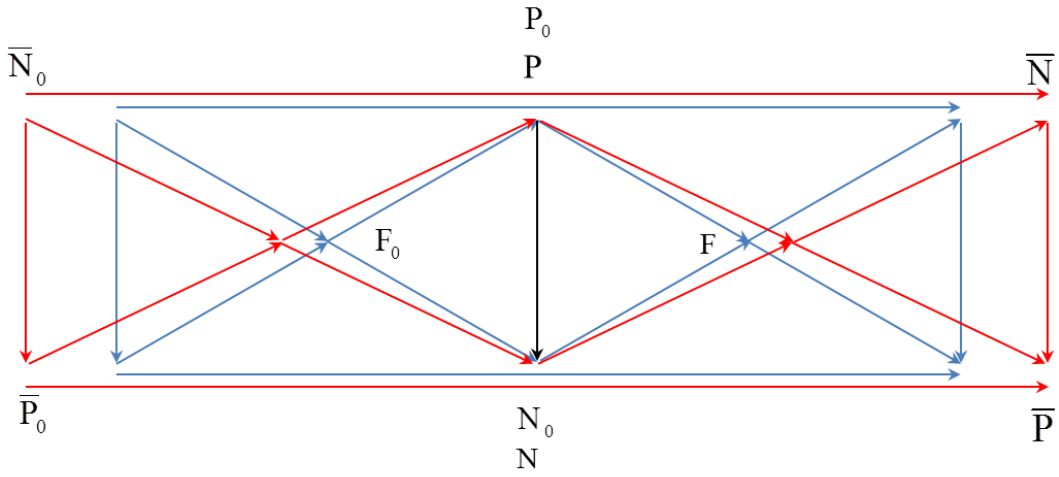

Figure 9.1.4 Extended Pascal's ring for the reduced eye showing the addition of anti-cardinal points and directions of all relationships.

Pascal's ring for Le Grand's eye

The reduced eye has both advantages and disadvantages that come hand in hand with the simplest model eye available. In order to highlight some of the disadvantages of the simplification, let us take a look at Pascal's ring for the four-surface Le Grand eye. Pascal's ring is shown in Figure 9.1.5 and the extended Pascal's ring in Figure 9.1.6.

Pascal's ring is shown in Figure 9.1.5 for Le Grand's eye for the set of six cardinal points for the red and blue frequencies derived from the transferences. The blue ring is narrower than the red ring for the distance between F_0 and F, which matches what we found in the graphical construction in Figure 9.1.2. The blue inner square is wider and shorter than the red inner square. This width

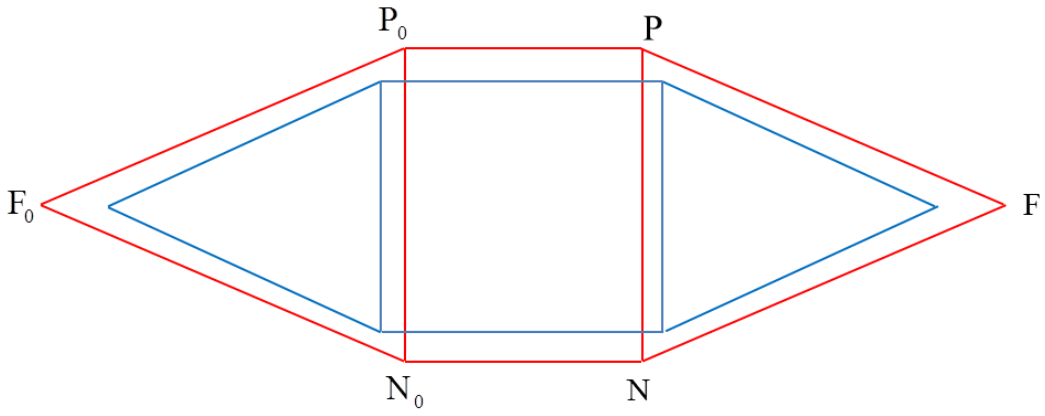

Figure 9.1.5 Pascal's ring for Le Grand's eye showing rings for the red and blue frequencies.

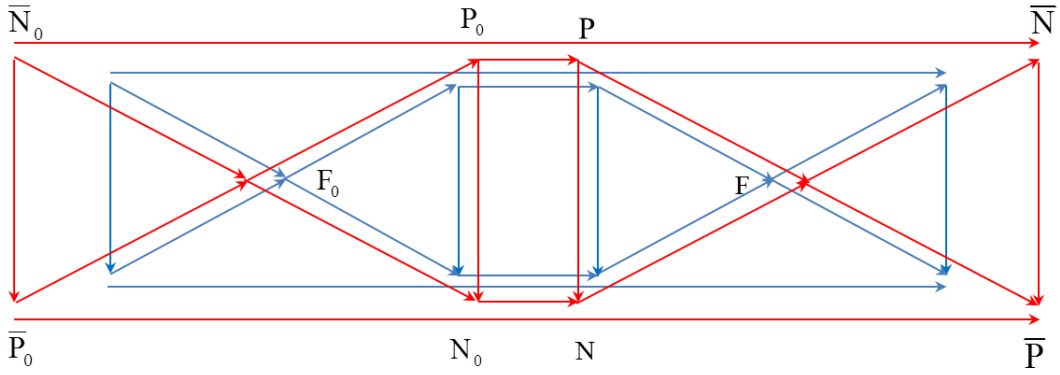

Figure 9.1.6 Extended Pascal's ring of Le Grand's eye for red and blue frequencies, showing the cardinal and anti-cardinal points and the directions of the relationships.

represents the distance between P_0 and P, which Pascal called the "thickness" (Pascal, 1950a), and also between N_0 and N. While the difference is too small to be evident in the graphical construction, from Tables 9.1.3 and 4 we calculate the width of the square to be 0.3230 mm for the blue "thickness" and 0.3105 mm for the red. This represents a chromatic difference of 0.0126 mm between the red and blue "thicknesses". The height of the square represents the distance between P_0 and N_0 or between P and N. The blue P and N are positioned closer together than the red P and N. From Tables 9.1.3 and 4 we calculate the distance from P to N to be 5.5986 mm for blue and 5.6046 mm for red. This represents a chromatic difference of -0.0060 mm which is not discernible in Figure 9.1.2.

The equivalent incident focal length f_{0eq} is represented by the distance from P_0 to F_0 and is equal to the distance from F to N. For the blue f_{0eq} this is a distance of $-16.1618\,\text{mm}$ and for the red f_{0eq} this is $-16.8468\,\text{mm}$, giving us a chromatic difference of $0.6850\,\text{mm}$. f_{eq} is the length from P to F and is equal to the length from F_0 to N_0. This is a distance of 21.7604 mm for the blue f_{eq} and 22.4513 mm for the red f_{eq}, giving us a chromatic difference of –0.6910 mm. These are very small differences and not obvious from Figure 9.1.2, but do indicate that the positions of, and relationships among the cardinal points of Le Grand's eye are all dependent on frequency. When we compare f_{0eq} and f_{eq} it becomes obvious why we cannot draw Pascal's ring to scale. The distortion created by the unequal f_{0eq} and f_{eq} would create a shape that resembles a lightning bolt at best, or one that would not join up at all.

In Figure 9.1.6 we observe that the blue extended Pascal's ring appears to be contracted compared to the red ring. It becomes obvious that, despite the rings not being drawn to scale, the chromatic difference in position of the anti-cardinal points is greater than the same for the cardinal points.

Conclusion

From Pascal's ring we see which points depend on frequency and which are independent of frequency. The reduced eye clearly shows that the principal and nodal points are independent of frequency, but that the focal points and the anti-cardinal points do depend on frequency. Pascal's ring for Le Grand's eye shows clearly that all six cardinal and four anti-cardinal points do depend on frequency. In addition the ring shows the direction of chromatic differences of each point.

9.2 Derived properties as a function of frequency

In Sections 3.4 and 5.1 we looked at a selection of derived properties, including power, entrance- and exit-plane refractive compensation and front- and back-vertex power. For each of these derived properties, we graph its dependence on the frequency of light. Although certain derived properties, such as exit-plane refractive compensation, apply to systems in general and have little application to the eye, we will include them because they have application to the characteristic matrices that will be discussed in Section 9.3.

9.2.1 Power

Power of a system is the simplest derived property, given by Equation 3.4.3. From the simplicity of the definition, we see that the dependence will be similar to that in Section 8.1.1 for each of the *C* sub-graphs. We therefore look at the dependence of power on the frequency of light only briefly.

Figure 9.2.1 shows the dependence of power of the system on the frequency of light for the reduced eye (blue with circles) and Le Grand's eye (black with diamonds). The curves represent the actual values calculated from the transference as a function of frequency and the dotted-dashed lines represent the power approximated from the linear dependence on the frequency of light (Equations 8.2.2 and 3).

The numerical values for the powers at the six reference points are given in Table 9.2.1. In addition the chromatic difference in power is given for the actual and approximate power values, represented by the dashed lines in Figure

Table 9.2.1 The power of the reduced and Le Grand's eyes at six reference frequencies, and their comparative values according to the formula for the symplectic straight line dependence on the frequency of light derived in the previous chapter (Equations 8.2.2 and 3).

Frequency THz	Colour	Reduced eye		Le Grand's eye	
		Actual D	Approximate D	Actual D	Approximate D
430	Red	59.4419	59.2756	59.3586	59.2736
494	Orange	59.8434	59.8299	59.7841	59.7877
558	Yellow	60.3058	60.6825	60.2625	60.2999
622	Green	60.8444	60.9335	60.7860	60.8104
686	Blue	61.4794	61.4828	61.3301	61.3192
750	Violet	62.2394	62.0304	61.8744	61.8263
Chromatic difference in power		2.7975	2.7548	2.5158	2.5526

9.2.1, for the reduced and Le Grand eyes. The values in the column labelled "approximate" have been obtained using Equations 8.2.2 and 3.

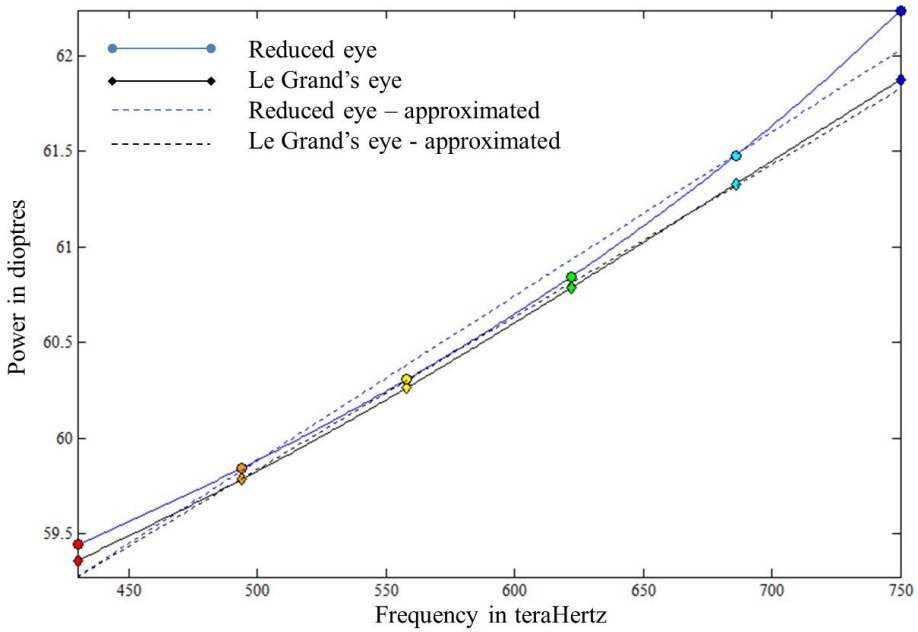

Figure 9.2.1 The dependence of power of the model eyes on the frequency of light. The corresponding dot-dashed lines in blue and black respectively show the straight line relationship according to Equations 8.2.2 and 3.

The values for the actual and approximate powers given in Table 9.2.1 compare well. Additionally, the values for chromatic difference in power compare favourably to published values (Section 2.3.1). These vary according to the frequencies chosen for red and blue ends of the spectrum.

9.2.2 Corneal-plane and exit-plane refractive compensation

The formulae for entrance-plane and exit-plane refractive compensation are given by Equations 3.4.6 and 5.1.3 respectively. While both of these formulae are general for all systems, entrance-plane refractive compensation for an eye is the equivalent of corneal-plane refractive compensation, however, exit-plane refractive compensation is not of conventional optometric interest. However, because the formula is related to the fourth entry for the point characteristic matrix, we will include exit-plane refractive compensation in our discussion. The dependence of the entrance- and exit-plane refractive compensations on frequency are shown in Figures 9.2.2 and 3, respectively.

Figure 9.2.2 shows that the corneal-plane refractive compensation is similar for the reduced and Le Grand's eyes. The reduced eye shows a more curved dependence than Le Grand's eye, which reflects the underlying structure of the two model eyes and the formulae for the refractive indices of the media. The values obtained using the actual transferences dependent on frequency are very similar to the approximated values obtained using the linear symplectic calculated transferences. The values for six reference frequencies are given in Table 9.2.2 for the refractive compensation of the two eyes and compared with the values obtained using Equations 8.2.2 and 3.

The exit-plane refractive compensation in Figure 9.2.3 shows almost six dioptres difference between the lines for the two eyes while the chromatic difference between the red and blue frequencies is far less for each eye compared with the corneal-plane refractive compensation. The dotted-dashed straight line is almost indistinguishable from the solid curved line for Le Grand's eye. From Table 9.2.3 we see that the chromatic difference in exit-plane refractive compensation is 0.69 D for the reduced eye and 0.52 D for Le Grand's eye.

Table 9.2.2 The entrance-plane refractive compensation of the reduced and Le Grand's eyes at six reference frequencies, and their comparative values according to the formula for the symplectic straight line dependence on the frequency of light derived in the previous chapter (Equations 8.2.2 and 3).

Frequency THz	Colour	Reduced eye		Le Grand's eye	
		Actual D	Approximate D	Actual D	Approximate D
430	Red	0.4185	0.5412	0.4674	0.5250
494	Orange	0.1175	0.1264	0.1412	0.1387
558	Yellow	–0.2294	–0.2876	–0.2216	–0.2470
622	Green	–0.6333	–0.7007	–1.6155	–0.6322
686	Blue	–1.1095	–1.1130	–1.0243	–1.0169
750	Violet	–1.6796	–1.5245	–1.4338	–1.4009
Chromatic difference in entrance-plane refractive compensation		–2.0981	–2.0657	–1.9013	–1.9260

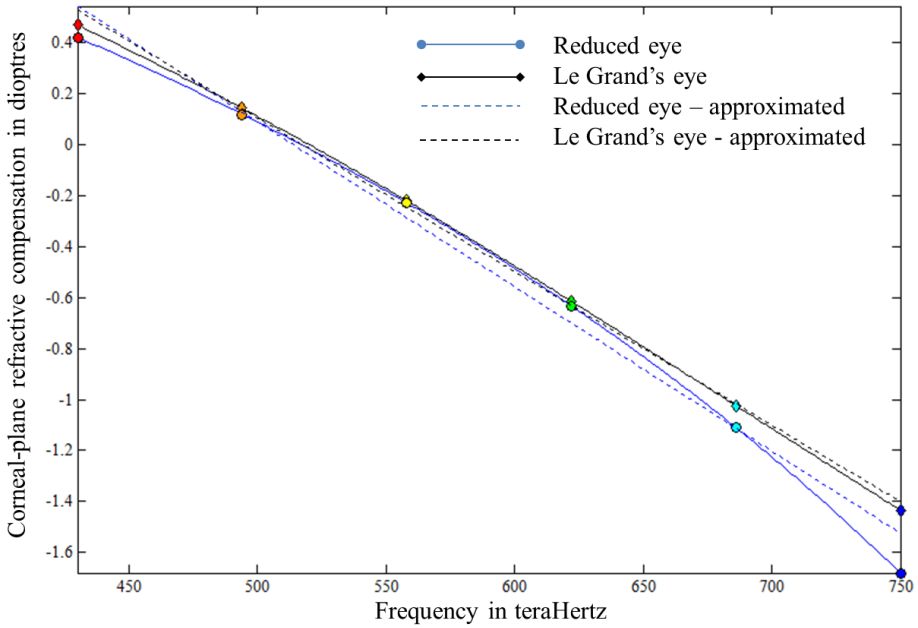

Figure 9.2.2 The dependence of the entrance-plane refractive compensation of the reduced and Le Grand's eyes on the frequency of light. The entrance-plane refractive compensation approximated from Equations 8.2.2 and 3 for the linear symplectic dependence transference is indicated by the straight dotted-dashed lines in corresponding colours.

Table 9.2.3 The exit-plane refractive compensation of the reduced and Le Grand model eyes at the six reference frequencies, and their comparative values according to the formula for the symplectic straight line dependence on the frequency of light derived in the previous chapter (Equations 8.2.2 and 3).

Frequency THz	Colour	Reduced eye		Le Grand's eye	
		Actual D	Approximate D	Actual D	Approximate D
430	Red	59.8605	59.8253	54.0673	54.05699
494	Orange	59.9608	59.9612	54.1638	54.1624
558	Yellow	60.0765	60.0980	54.2611	54.2658
622	Green	60.2111	60.2355	54.3644	54.3699
686	Blue	60.3698	60.3739	54.4751	54.4749
750	Violet	60.5599	60.5131	54.5920	54.5807
Chromatic difference in exit-plane refractive compensation		0.6994	0.6878	0.5247	0.5208

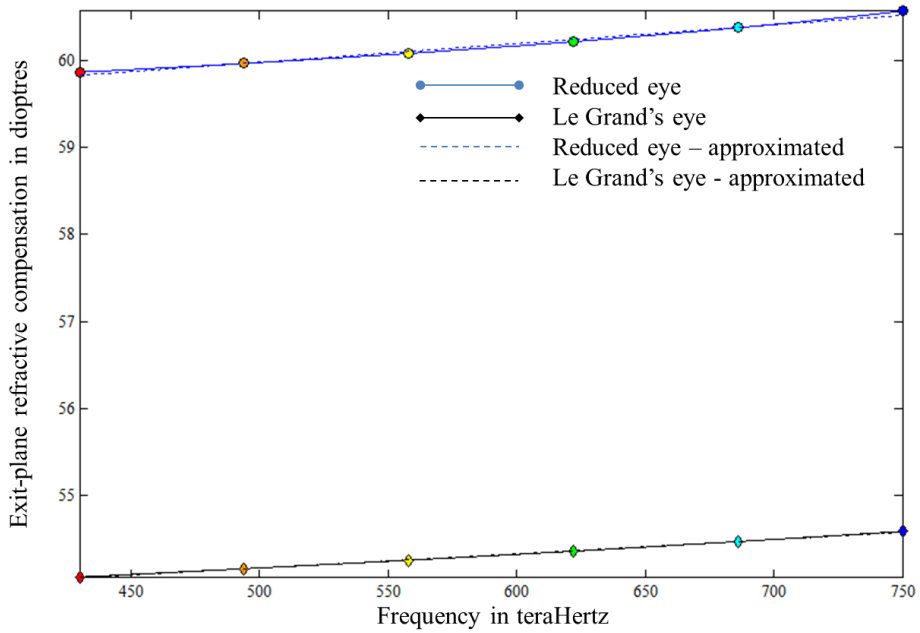

Figure 9.2.3 The dependence of the exit-plane refractive compensation of the reduced eye and Le Grand's eye on the frequency of light. The approximate exit-plane refractive compensation obtained from Equations 8.2.2 and 3 for the linear symplectic dependence transference is indicated by the straight dotted-dashed lines in corresponding colours.

9.2.3 Front- and back-vertex power

The formulae for front- and back-vertex power of systems in general, derived from the transference, were given in Equations 3.4.16 and 11, respectively. From the definition, back-vertex power measures the vergence at emergence from the system when incident vergence is zero. For an eye, including a model eye, this measures the vergence at the retinal-plane. Because light focuses at or close to the retina, we expect the back-vertex power to approach infinity. This is seen in Figure 9.2.4. The formula for back-vertex power is found in the first entry of the first mixed characteristic matrix **M** (Equation 3.7.23).

In Figure 9.2.4 we see the vergence initially increasing rapidly as we move from the red markers to the orange markers and asymptotes to infinity. The back-vertex power between 430 and 517 THz is positive. The vertical lines indicate a jump from infinity to minus infinity and show the frequency at which each eye forms a focal point (image). This is 517 THz for the reduced eye and 520THz for Le Grand's eye. The vergence then, again increasing as we move from yellow through green and blue to violet, asymptotes from minus infinity and eventually asymptotes to the zero dioptre vergence line in the ultra-violet range. The back-vertex powers of six reference frequencies are given in Table 9.2.4 for the two model eyes, compared with the values obtained using Equations 8.2.2 and 3.

Front-vertex-power defines the vergence at the entrance plane required for light to emerge with zero vergence. This is plausible for systems in general, but makes little sense for the eye. It may have an application for the reversed eye, however this is beyond the scope of this dissertation. Nonetheless, because the formula for front-vertex power is the negative of the fourth entry of the second mixed characteristic matrix **N** (Equation 3.7.24) we shall include it here. The dependence of the front-vertex power on frequency is shown in Figure 9.2.5. The dependence is very nearly linear for the two model eyes.

From Table 9.2.5 and Figure 9.2.5 we see that there is approximately a 6 D difference between the two model eyes. The chromatic difference in front-vertex power is 2.80 D for the reduced eye and 3.09 D for Le Grand's eye.

Table 9.2.4 Back-vertex power of the reduced and Le Grand's model eyes for six coloured reference points. The columns are separated into actual values and those approximated using Equations 8.2.2 and 3.

Frequency THz	Colour	Reduced eye		Le Grand's eye	
		Actual D	Approximate D	Actual D	Approximate D
430	Red	8 501	6 551	7 591	6 745
494	Orange	30 548	28 382	25 373	25 824
558	Yellow	–15 795	–12 618	–16 336	–14 664
622	Green	–5 786	–5 238	–5 948	–5 794
686	Blue	–3 345	–3 335	–3 617	–3 642
750	Violet	–2 244	–2 462	–2 614	–2 673

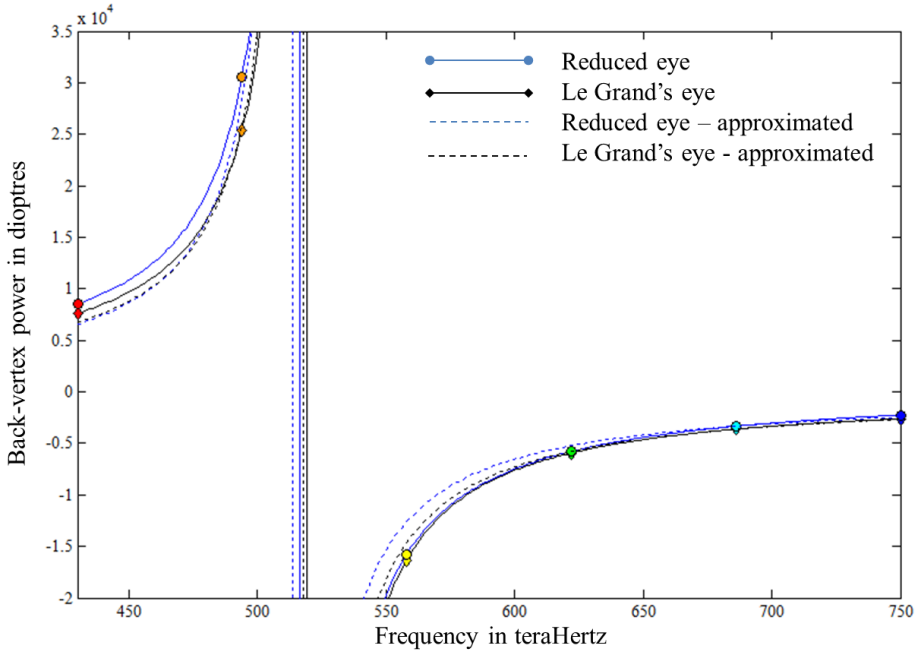

Figure 9.2.4 Back-vertex power of the two model eyes as a function of frequency. The corresponding dashed lines are approximated according to Equations 8.2.2 and 3 for the linear relationship of the transference's dependency on frequency. The vertical axis has been restricted to [–20 000 D 35 000 D] in order to include all six reference points and to discern the individual curves, which approach ± infinity dioptres.

Table 9.2.5 Front-vertex power of the reduced and Le Grand's model eyes for the six coloured reference points. Chromatic difference of front-vertex power is given. The columns are separated into actual values and those approximated using Equations 8.2.2 and 3.

Frequency THz	Colour	Reduced eye		Le Grand's eye	
		Actual D	Approximate D	Actual D	Approximate D
430	Red	59.4419	59.2671	65.6319	65.5111
494	Orange	59.8434	59.8250	66.1284	66.1355
558	Yellow	60.3058	60.0380	66.7053	66.7570
622	Green	60.8444	60.9031	67.3450	67.3755
686	Blue	61.4794	61.1478	68.0077	67.9910
750	Violet	62.2394	62.2023	68.6638	68.6035
Chromatic difference in front-vertex power		2.7975	2.7556	3.0320	3.0924

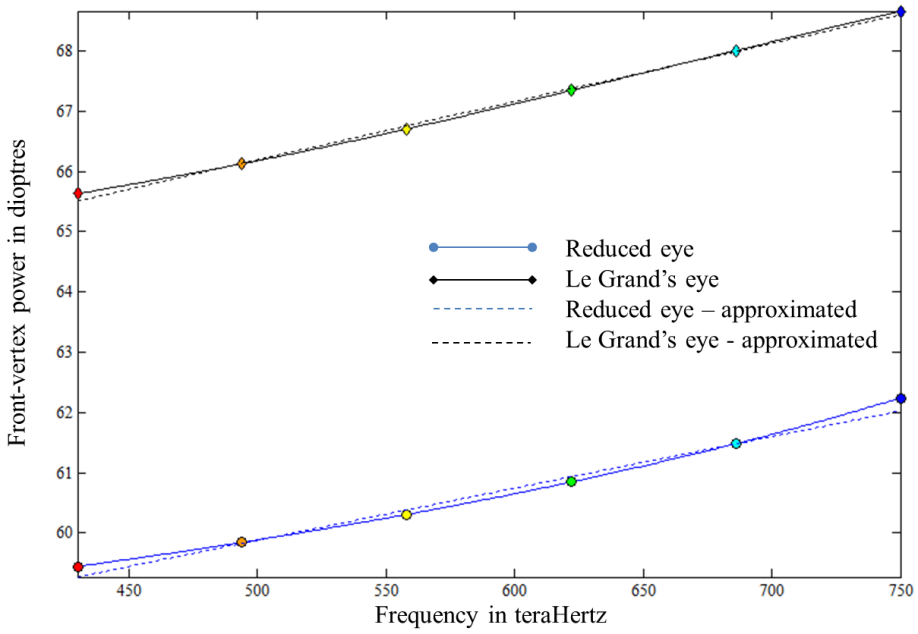

Figure 9.2.5 Front-vertex power of the two model eyes as a function of frequency. The solid lines represent the actual values from the transference while the dotted-dashed lines are approximated from the linearly transformed transferences according to Equation 8.2.2.

9.3 Characteristic matrices

The four characteristic matrices were introduced in Section 3.7.3; they are symmetric and represent familiar derived properties in relationship to each other. Our interest lies in the fact that each of the characteristic matrices is symmetric and therefore can be represented in a three-dimensional vector space. Of these characteristic matrices, the point characteristic **P** and the angle characteristic **Q** appear to be the most promising for our objective because they each have the same units throughout. **P** has units of inverse length and **Q** units of length. It is the uniformity of units of the point- and angle-characteristics that holds appeal for our purposes. **M** and **N** each have mixed units, however there are some interesting relationships among the entries of each of the four characteristic matrices and many of the familiar properties of systems.

Equations 3.7.15, 16, 18 and 19 give the four characteristic matrices in terms of varying combinations of incident or emergent transverse positions or reduced inclinations. In each case, two knowns map to two unknowns. Then the entries of the four characteristic matrices are defined in terms of the fundamental properties of the Gaussian transference in Equations 3.7.21, 22, 23 and 24.

What becomes apparent in Section 3.7.3 is that for each characteristic matrix there are issues of singularity that limit the usefulness of each matrix for particular situations. It further implies that the choice of any two of y_0, y, α_0 or α does not necessarily fix the other two (Harris and van Gool, 2004).

9.3.1 Point characteristic

As is apparent from Equation 3.7.21, the point characteristic exists provided the disjugacy is not zero, or does not approach zero. This would be problematic in a conjugate or thin system, however we foresee no problem in a model eye. As pointed out in Section 3.7.3, the first entry represents the corneal-plane refractive compensation (F_0) given by Equation 3.4.6 and the second and third entries are the negative inverse of disjugacy ($-B^{-1}$). The fourth entry is the exit-plane refractive compensation (F_C) of the system (Equation 5.1.3). This is of interest for systems in general, but apparently holds little practical meaning for the

Table 9.3.1 The point characteristic matrices **P** for the reduced and Le Grand's eyes for six reference frequencies.

Frequency		Point characteristic **P** in dioptres	
THz	Colour	Reduced eye	Le Grand's eye
430	Red	$\begin{pmatrix} 0.4185 & -59.8605 \\ -59.8605 & 59.8605 \end{pmatrix}$	$\begin{pmatrix} 0.4674 & -59.7814 \\ -59.7814 & 54.0673 \end{pmatrix}$
494	Orange	$\begin{pmatrix} 0.1175 & -59.9608 \\ -59.9608 & 59.9608 \end{pmatrix}$	$\begin{pmatrix} 0.1412 & -59.9117 \\ -59.9117 & 54.1638 \end{pmatrix}$
558	Yellow	$\begin{pmatrix} -0.2294 & -60.0765 \\ -60.0765 & 60.0765 \end{pmatrix}$	$\begin{pmatrix} -0.2216 & -60.0623 \\ -60.0623 & 54.2611 \end{pmatrix}$
622	Green	$\begin{pmatrix} -0.6333 & -60.2111 \\ -60.2111 & 60.2111 \end{pmatrix}$	$\begin{pmatrix} -0.6155 & -60.2304 \\ -60.2304 & 54.3644 \end{pmatrix}$
686	Blue	$\begin{pmatrix} -1.1095 & -60.3698 \\ -60.3698 & 60.3698 \end{pmatrix}$	$\begin{pmatrix} -1.0243 & -60.4064 \\ -60.4064 & 54.4751 \end{pmatrix}$
750	Violet	$\begin{pmatrix} -1.6796 & -60.5599 \\ -60.5599 & 60.5599 \end{pmatrix}$	$\begin{pmatrix} -1.4338 & -60.5824 \\ -60.5824 & 54.5920 \end{pmatrix}$

eye. The divergence of the system does not play a role. We summarise the entries of the point characteristic matrix as

$$\mathbf{P} = \begin{pmatrix} F_0 & -\mathrm{B}^{-1} \\ -\mathrm{B}^{-1} & F_\mathrm{C} \end{pmatrix}.$$

The entrance- and exit-plane refractive compensation, dependent on frequency, was shown for the two model eyes in Figures 9.2.2 and 3. The dependence of B on frequency is shown in Figure 8.1.3. The dependence of $-B^{-1}$ resembles a nearly straight line, similar to that shown in Figure 8.1.3. The chromatic difference in $-B^{-1}$ is –0.6994 D and –0.8010 D for the reduced and Le Grand's eyes, respectively. In Figure 9.3.1, we represent the point characteristic of the reduced eye in a three-dimensional vector space. The axes are labelled according to the derived property that each represents and the units are dioptres. Unsurprisingly the relationship is perfectly linear and is seen when the azimuth and elevation are oriented such that all the diamonds line up behind each other perfectly. We note that the coloured reference points, which are evenly spread at

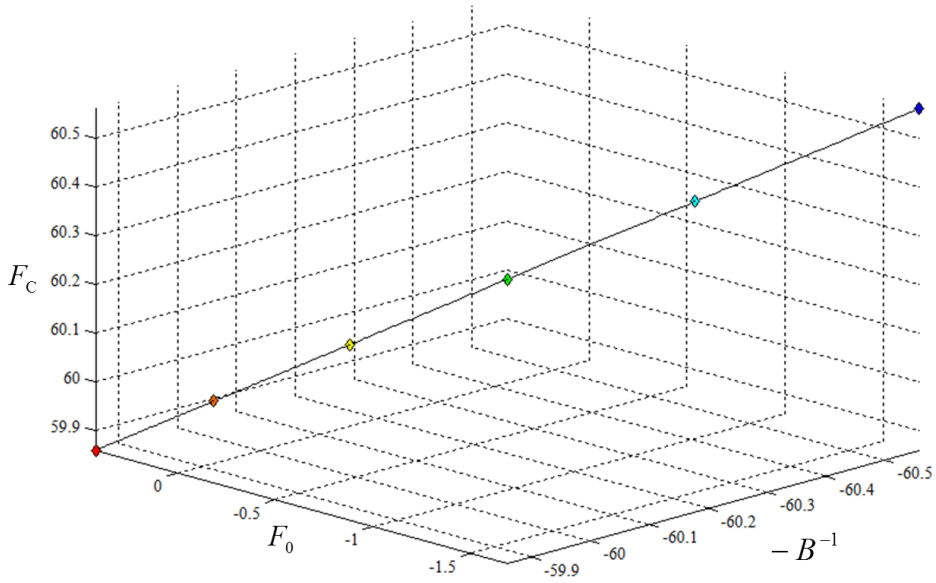

Figure 9.3.1 The three independent entries of **P** the point characteristic for the reduced eye. Units are dioptres.

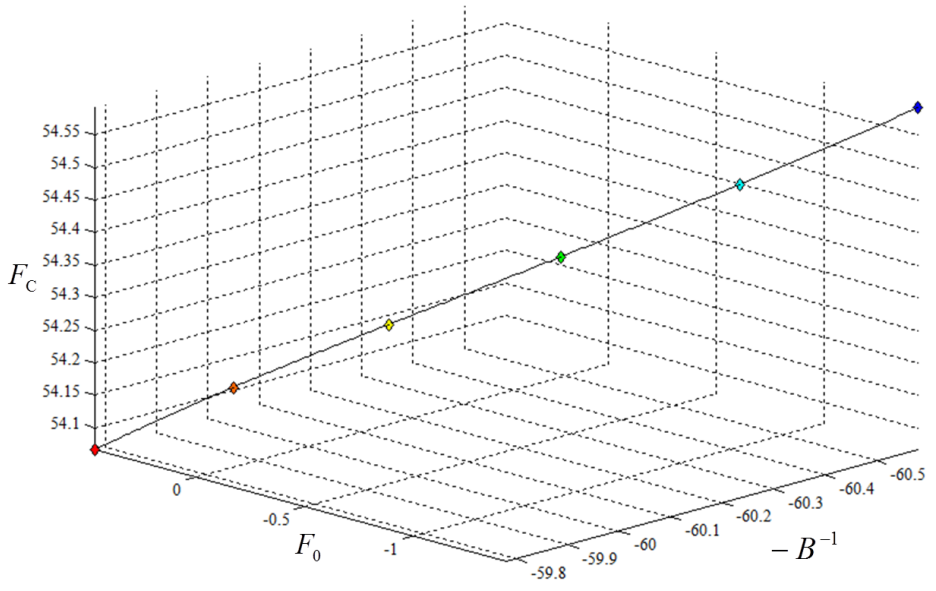

Figure 9.3.2 The three independent entries of **P** the point characteristic as a function of frequency for the Le Grand eye. The line is slightly curved. Units are dioptres.

The three independent entries of **P** for Le Grand's eye are illustrated in every 64 THz, appear to be closer together on the red end of the spectrum compared to the blue end of the spectrum. Figure 9.3.2 and show a slightly curved line. The point characteristic matrices of the two model eyes are given in Table 9.3.1 for six reference frequencies.

9.3.2 Angle characteristic

The angle characteristic **Q** (Equation 3.7.22) exists provided the divergence *C* is not zero. This would be a problem for an afocal system; however this poses no problem for an eye or model eye. Of interest is the relationship of the diagonal elements to the negative inverse of front- (F_{fv}) and back-vertex power (F_{bv}), as given in Equations 3.4.16 and 11. The dependencies of F_{fv} and F_{bv} on frequency are displayed graphically in Figures 9.2.4 and 5. Also related, are the incident (z_{F0}) and emergent focal lengths (z_{F}) (Equations 3.6.5 and 12). The relationships of the focal lengths to the system were discussed in Sections 3.6 and 5.4 and their dependence on frequency displayed graphically in Section 9.1. However all the entries are in units of length and, similar to **P**, make the axes comparable once graphed.

Down the diagonal, the first entry is $-F_{\mathrm{fv}}^{-1}$ and the last entry is $-F_{\mathrm{bv}}^{-1}$. There is also a relationship between the first entry and incident focal length in that

$$C^{-1}D = \frac{1}{n_0} z_{\mathrm{F0}} \tag{9.3.1}$$

and between the fourth entry and the emergent focal length as

$$C^{-1}A = -\frac{1}{n} z_{\mathrm{F}}. \tag{9.3.2}$$

The off-diagonal entries represent the inverse of divergence and are related to the incident and emergent equivalent focal lengths as

$$\frac{1}{C} = \frac{1}{n_0} f_{0eq} = -\frac{1}{n} f_{eq}. \tag{9.3.3}$$

These relationships can be summarised as

$$\mathbf{Q} = \begin{pmatrix} -F_{\mathrm{fv}}^{-1} & n_0^{-1} f_{0\mathrm{eq}} \\ -\mathrm{n}^{-1} f_{\mathrm{eq}} & -F_{\mathrm{bv}}^{-1} \end{pmatrix}$$

or

$$\mathbf{Q} = \begin{pmatrix} n_0^{-1} z_{\mathrm{F0}} & n_0^{-1} f_{0\mathrm{eq}} \\ -\mathrm{n}^{-1} f_{\mathrm{eq}} & -n^{-1} z_{\mathrm{F}} \end{pmatrix}.$$

We saw from Section 9.1 that all of these focal lengths depend on the frequency of light. These relationships are shown in Figure 9.3.3 for the reduced eye and Figure 9.3.4 for Le Grand's eye as a function of frequency. Unsurprisingly, the relationships, as for **P**, form a straight line for the reduced eye and a nearly straight line for Le Grand's eye. **Q** is given for six reference frequencies in Table 9.3.2.

As per the point characteristic, the relationships among the independent entries of **Q** is linear. Furthermore, the spacing between the six reference frequencies is more spread out at the blue end of the spectrum. While the differences between the red and blue angle characteristic matrices are similar for the two model eyes, the actual positions are slightly different. This can be seen by comparing the numerical values in the angle characteristic matrices given in Table 9.3.2.

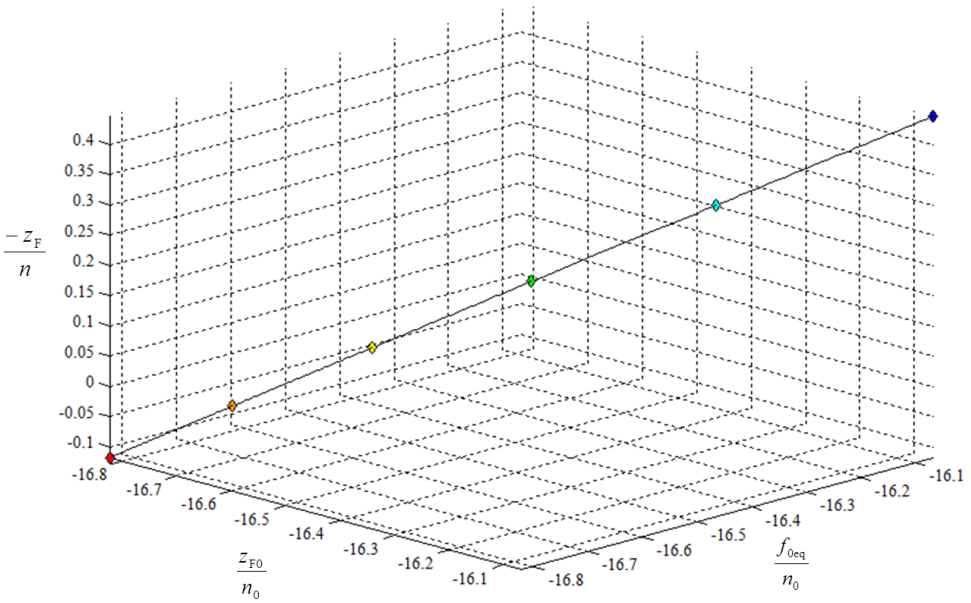

Figure 9.3.3 The angle characteristic **Q** of the reduced eye. Units are millimetres.

Table 9.3.2 The angle characteristic matrices **Q** for the six reference frequencies for the reduced eye and Le Grand's eye.

Frequency		Angle characteristic **Q** in millimetres	
THz	Colour	Reduced eye	Le Grand's eye
430	Red	$\begin{pmatrix} -16.8231 & -16.8231 \\ -16.8231 & -0.1176 \end{pmatrix}$	$\begin{pmatrix} -15.2365 & -16.8468 \\ -16.8468 & -0.1317 \end{pmatrix}$
494	Orange	$\begin{pmatrix} -16.7103 & -16.7103 \\ -16.7103 & -0.0327 \end{pmatrix}$	$\begin{pmatrix} -15.1221 & -16.7269 \\ -16.7269 & -0.03941 \end{pmatrix}$
558	Yellow	$\begin{pmatrix} -16.5821 & -16.5821 \\ -16.5821 & 0.0633 \end{pmatrix}$	$\begin{pmatrix} -14.9913 & -16.5941 \\ -16.5941 & 0.0612 \end{pmatrix}$
622	Green	$\begin{pmatrix} -16.4354 & -16.4354 \\ -16.4354 & 0.1729 \end{pmatrix}$	$\begin{pmatrix} -14.8489 & -16.4511 \\ -16.4511 & 0.1681 \end{pmatrix}$
686	Blue	$\begin{pmatrix} -16.2656 & -16.2656 \\ -16.2656 & 0.2989 \end{pmatrix}$	$\begin{pmatrix} -14.7042 & -16.3052 \\ -16.3052 & 0.2765 \end{pmatrix}$
750	Violet	$\begin{pmatrix} -16.0670 & -16.0670 \\ -16.0670 & 0.4456 \end{pmatrix}$	$\begin{pmatrix} -14.5637 & -16.1618 \\ -16.1618 & 0.3825 \end{pmatrix}$

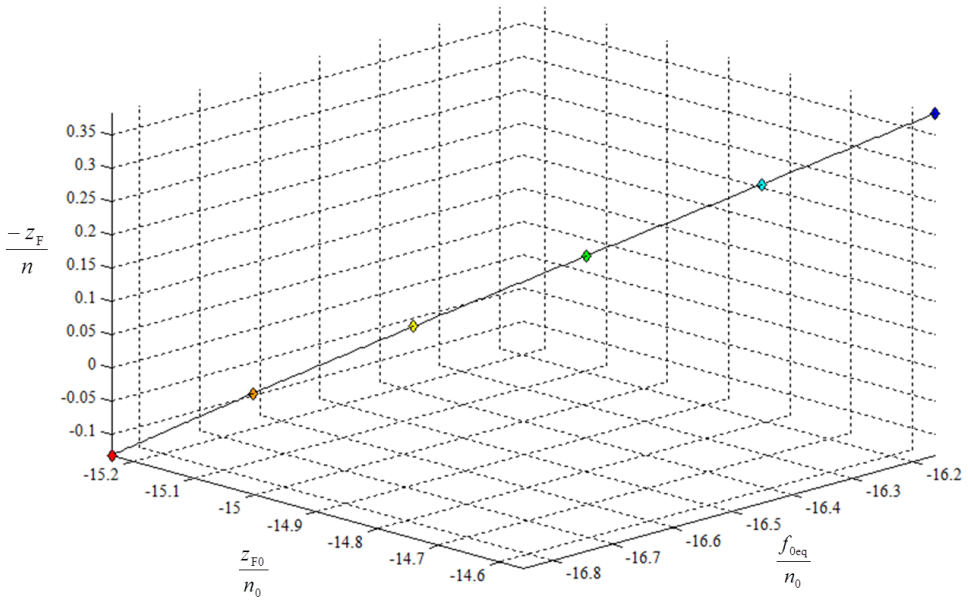

Figure 9.3.4 Angle characteristic **Q** for Le Grand's eye. The units are millimetres.

9.3.3 First mixed characteristic

The first mixed characteristic **M** (Equation 3.7.23) exists provided $D \neq 0$. The entries of **M** is summarised as

$$\mathbf{M} = \begin{pmatrix} F_{\text{fv}} & D^{-1} \\ D^{-1} & F_{\text{C}}^{-1} \end{pmatrix}.$$

The dependence of front-vertex power F_{fv} on the frequency of light was shown in Figure 9.2.5 and the same for exit-plane refractive compensation F_{C} in Figure 9.2.3. From Equation 5.5.1 we see that for a reduced eye $D = 1$, regardless of the frequency ν and for multi-surface eyes D is usually close to 1, but does vary weakly with ν. For systems in general, D will have different values.

In Figures 9.3.5 and 6 we represent **M** on a three-dimensional graph for the reduced eye and Le Grand's eye. For the reduced eye we see that the line is perfectly straight, however Le Grand's eye produces a visible S-shaped curve. F_{fv} has a chromatic difference of 2.7974 D for the reduced eye and 3.0320 D for Le Grand's eye.

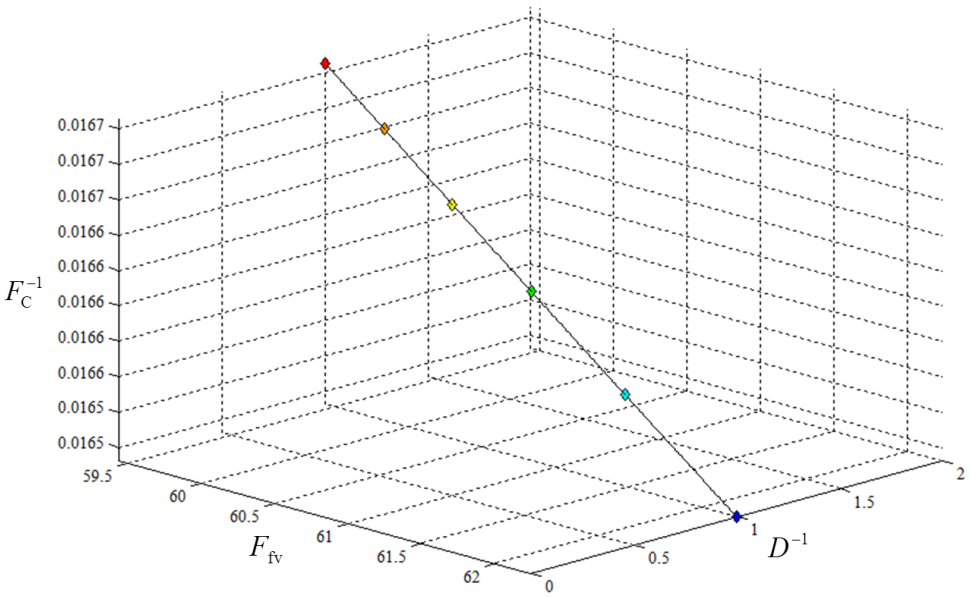

Figure 9.3.5 The first mixed characteristic **M** of the reduced eye. The vertical axis represents F_{C}^{-1} in meters, the middle axis represents F_{fv}, the front vertex power, in dioptres and the right-hand axis represents D^{-1}, which is 1 for all frequencies.

Table 9.3.3 The First mixed characteristic matrix **M** for the six reference frequencies for the reduced eye and Le Grand's eye.

Frequency		First mixed characteristic **M**	
THz	Colour	Reduced eye	Le Grand's eye
430	Red	$\begin{pmatrix} 59.4419\ \text{D} & 1 \\ 1 & 0.01671\ \text{m} \end{pmatrix}$	$\begin{pmatrix} 65.6319\ \text{D} & 1.1057 \\ 1.1057 & 0.01850\ \text{m} \end{pmatrix}$
494	Orange	$\begin{pmatrix} 59.8434\ \text{D} & 1 \\ 1 & 0.01668\ \text{m} \end{pmatrix}$	$\begin{pmatrix} 66.1284\ \text{D} & 1.1061 \\ 1.1061 & 0.01846\ \text{m} \end{pmatrix}$
558	Yellow	$\begin{pmatrix} 60.3058\ \text{D} & 1 \\ 1 & 0.01665\ \text{m} \end{pmatrix}$	$\begin{pmatrix} 66.7053\ \text{D} & 1.1069 \\ 1.1069 & 0.016843\ \text{m} \end{pmatrix}$
622	Green	$\begin{pmatrix} 60.8444\ \text{D} & 1 \\ 1 & 0.01661\ \text{m} \end{pmatrix}$	$\begin{pmatrix} 67.3450\ \text{D} & 1.1079 \\ 1.1079 & 0.01840\ \text{m} \end{pmatrix}$
686	Blue	$\begin{pmatrix} 61.4794\ \text{D} & 1 \\ 1 & 0.01657\ \text{m} \end{pmatrix}$	$\begin{pmatrix} 68.0077\ \text{D} & 1.1089 \\ 1.1089 & 0.01836\ \text{m} \end{pmatrix}$
750	Violet	$\begin{pmatrix} 62.2319\ \text{D} & 1 \\ 1 & 0.01651\ \text{m} \end{pmatrix}$	$\begin{pmatrix} 68.6638\ \text{D} & 1.1097 \\ 11097 & 0.01832\ \text{m} \end{pmatrix}$

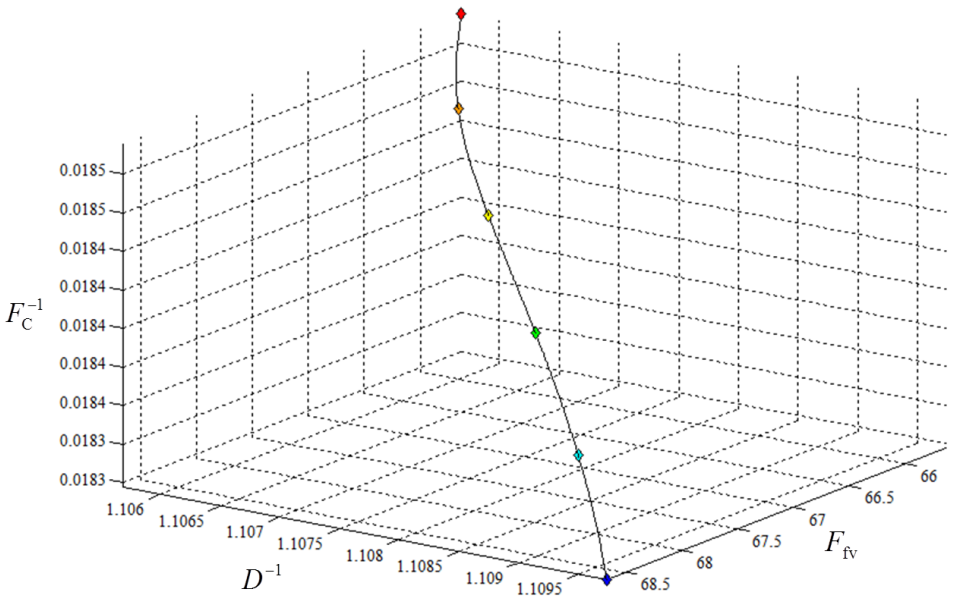

Figure 9.3.6 The first mixed characteristic **M** of the Le Grand eye. The vertical axis represents F_C^{-1} in meters, the right-hand axis represents F_{fv} in dioptres and the middle axis represents D^{-1}.

9.3.4 Second mixed characteristic

The second mixed characteristic **N** (Equation 3.7.24) exists provided the dilation *A* is not zero. For the model eye as a function of frequency, we see *A* approaching zero as we reach the reference frequency, usually in the yellow band, the exact frequency will differ for each model eye and is given in Section 9.2.3 for the reduced eye and Le Grand's eye. It is also dependent on n_0. The problems arising when *A* approaches zero are seen in Figure 9.2.4 where the back-vertex power is graphed as a function of frequency. We see that where *A* approaches zero, back-vertex power approaches infinity, indicating a focal point (or image point) on the exit plane or retina and the curves of the graph extend off the scale.

The entries of **N** are summarised as

$$\mathbf{N} = \begin{pmatrix} -F_0^{-1} & A^{-1} \\ A^{-1} & -F_{\text{bv}} \end{pmatrix}.$$

The dependence of entrance-plane refractive compensation F_0 (Equation 3.4.6) on frequency is shown in Figure 9.2.2 and similarly for back-vertex power F_{bv} (Equation 3.4.11) in Figure 9.2.4. Figures 9.3.7 and 8 show **N** for the reduced eye and Le Grand's eye are graphed, respectively.

We anticipated a problem in calculating **N** for eyes where $A = 0$ or where *A* approaches 0. The axes limits were adjusted to include the orange (494 THz) and yellow (558 THz) points and ignore the values at infinity. The result is that all six reference points are distinct, however, they are no longer sequenced according to their frequencies and instead the sequence is orange, red, then violet, blue, green and yellow. The line does not stop at orange or yellow, but continues to infinity or negative infinity. With infinity (or emmetropia) lying between 494 and 558 THz we conclude that the model eyes' reference frequencies for emmetropia lie between these two frequencies.

Table 9.3.4 The second mixed characteristic matrices **N** for the six reference frequencies for the reduced eye and Le Grand's eye.

Frequency		Second mixed characteristic **N**	
THz	Colour	Reduced eye	Le Grand's eye
430	Red	$\begin{pmatrix} -2.3892\ \text{m} & 143.0200 \\ 143.0200 & -8501.3857\ \text{D} \end{pmatrix}$	$\begin{pmatrix} -2.1393\ \text{m} & 127.8910 \\ 127.8910 & -7591.4352\ \text{D} \end{pmatrix}$
494	Orange	$\begin{pmatrix} -8.5134\ \text{m} & 510.4690 \\ 510.4690 & -30548.1908\ \text{D} \end{pmatrix}$	$\begin{pmatrix} -7.0841\ \text{m} & 424.4182 \\ 424.4182 & -25373.4668\ \text{D} \end{pmatrix}$
558	Yellow	$\begin{pmatrix} 4.3596\ \text{m} & -261.9085 \\ -261.9085 & 15794.6100\ \text{D} \end{pmatrix}$	$\begin{pmatrix} 4.5133\ \text{m} & -271.0772 \\ -271.0772 & 16335.78153\ \text{D} \end{pmatrix}$
622	Green	$\begin{pmatrix} 1.5791\ \text{m} & -95.0799 \\ -95.0799 & 5785.0746\ \text{D} \end{pmatrix}$	$\begin{pmatrix} 1.6246\ \text{m} & -97.8500 \\ -97.8500 & 5947.9146\ \text{D} \end{pmatrix}$
686	Blue	$\begin{pmatrix} 0.9013\ \text{m} & -54.4098 \\ -54.4098 & 3345.0822\ \text{D} \end{pmatrix}$	$\begin{pmatrix} 0.9763\ \text{m} & -58.9759 \\ -58.9759 & 3616.9941\ \text{D} \end{pmatrix}$
750	Violet	$\begin{pmatrix} 0.5954\ \text{m} & -36.0568 \\ -36.0568 & 2244.1573\ \text{D} \end{pmatrix}$	$\begin{pmatrix} 0.6974\ \text{m} & -42.2520 \\ -42.2520 & 2614.3169\ \text{D} \end{pmatrix}$

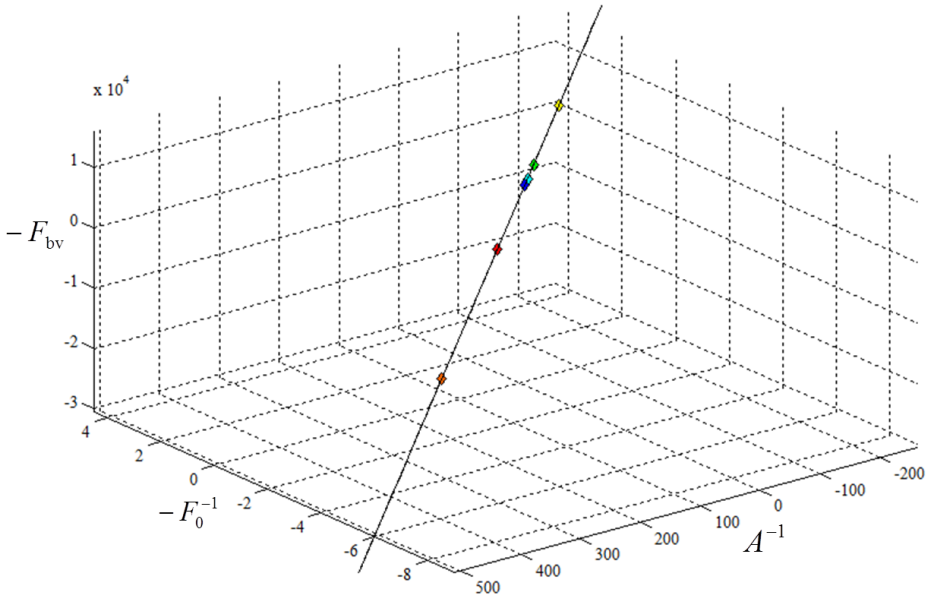

Figure 9.3.7 The second mixed characteristic **N** of the reduced eye. The sequence of the coloured reference points is not in order of frequency.

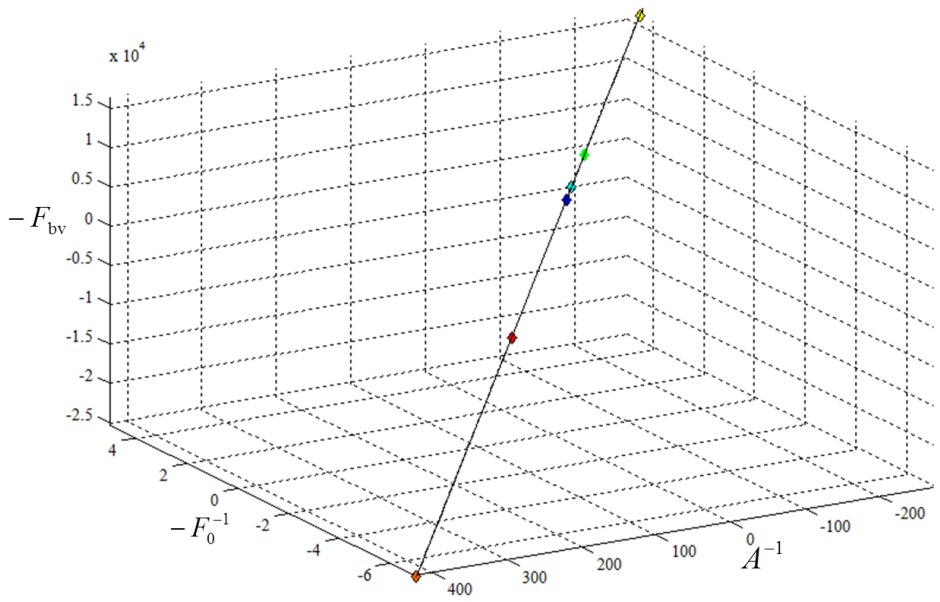

Figure 9.3.8 The second mixed characteristic **N** of Le Grand's eye.

9.4 Discussion

In this chapter we looked at the cardinal and anti-cardinal points of the reduced and Le Grand's eyes and used graphical construction and Pascal's ring methods in an effort to better understand how the cardinal and anti-cardinal points are affected by the frequency of light.

The reduced eye showed that the incident and emergent principal and nodal points are independent of the frequency of light and are not distinct for incidence and emergence. The locations of the focal points and four anti-cardinal points depend on frequency. Interesting relationships arose because of the simplicity of the reduced eye. Firstly, the incident and emergent anti-nodal point pairs are equidistant from the entrance-plane for each frequency, but in opposite directions. Secondly, each of the red and blue pairs of anti-cardinal points are equidistant between the red and blue positions, however the incident anti-cardinal points have the red upstream of the blue points and the emergent anti-cardinal points have the red points downstream of the blue points.

From Le Grand's eye we conclude that the locations of all ten cardinal and anti-cardinal points depend on the frequency of light and their positions are

distinct. In summary, the incident or emergent blue point is always positioned closer to its corresponding entrance- or exit-plane than its paired red point. The frequency-dependent cardinal and anti-cardinal points are more like fuzzy zones than actual points.

We then looked at a selection of optical properties derived from the transference. In particular, we considered power of the system, entrance- and exit-plane refractive compensation and front- and back-vertex power, all of which depend on the frequency of light.

Finally, we explored the characteristic matrices using three-dimensional graphs. Each characteristic matrix has three independent entries which are related in some way to the derived properties and therefore allow us to see the relationships among these properties in three-dimensional space. For the reduced eye all the relationships are linear while for Le Grand's eye the relationships appear nearly perfectly linear for **P**, **Q** and **N**, but has an S-shaped curve for **M**.

10 Numerical examples of chromatic aberration and chromatic properties

The aim of this chapter is to examine the equations derived in Chapters 6 and 7 numerically. The transferences of the reduced and Le Grand's eyes for the red and blue frequencies were given in Table 8.1.1, with $n_0 = 1$ for all frequencies.

In Gaussian systems longitudinal and transverse chromatic aberration are defined by Equations 6.1.1 and 2. Chromatic aberration depends on the longitudinal and transverse position of the object (z_O and y_O) corresponding to longitudinal and transverse image positions (z and y). For a distant object point, the position of the object is defined by its inclination a_O.

In Chapter 7 two categories of chromatic properties of an eye were defined; those independent of and those dependent on the object or image and aperture positions. Three independent chromatic properties of an eye were defined, namely chromatic difference in power δF, refractive compensation δF_0 and ametropia δA.

The chromatic properties of the eye dependent on object and aperture positions depend on both the eye and the longitudinal and transverse object (a_K or z_O and y_O) and aperture (y_P) positions. Chromatic difference in position is defined by chromatic difference in transverse image position at the retina, δy_R and chromatic difference in inclination at the retina, δa_R. Chromatic difference in magnification is defined by the chromatic difference in image size $\delta(\Delta y_R)$ or chromatic difference in angular spread $\delta(\Delta a_R)$. Retinal chromatic size magnification M_{yR} and retinal chromatic angular spread magnification M_{aR} are also defined.

The chromatic properties of the system dependent on image (y_R) and aperture (y_P) positions in object space mimic the experimental situation. The chromatic difference in transverse object position δy_O, chromatic difference in

inclination δa_{O}, chromatic difference in object size $\delta(\Delta y_{\mathrm{O}})$, chromatic difference in angular spread $\delta(\Delta a_{\mathrm{O}})$, chromatic object size ratio M_{yO} and chromatic object angular spread ratio M_{aO} are included.

The chromatic aberration and object or image and aperture-dependent chromatic properties for the two model eyes are illustrated numerically by means of a selection of parameters. Specifically, the numerical examples include a distant object and an object at three illustrative finite distances measured from the entrance plane, namely $z_{\mathrm{O}} = -3$ m, –2 m and –0.5 m. For distant objects, the inclination from an object will be illustrated for $a_{\mathrm{K}} = 0.1$ (radian) and for objects at finite distances, an object of $y_{\mathrm{O}} = 200$ mm in size will be used in the examples. According to the situation, the fovea may be assumed to be centred on the optical axis, or offset $y_{\mathrm{R}} = 1.46$ mm to approximate a visio-optical angle (angle alpha) of 5°.

Finally, we look at the two underlying implications derived in Chapter 7 and resulting from the simplifications that occur when basing chromatic studies on the reduced eye and the use of chief rays.

10.1 Chromatic aberration

In Chapter 6 chromatic aberration was defined for homocentric systems with stigmatic elements, that is, for Gaussian systems in general. It was shown that chromatic aberration is not a property of the system alone, but on the system and the location of the object point.

10.1.1 Longitudinal chromatic aberration

Le Grand's eye

The steps for calculating longitudinal chromatic aberration were given in Section 6.3.1. Equation 6.2.4 defines the vergence exiting the system when incident vergence is from a distant object. For Le Grand's eye the red and blue emergent vergences are

$$L_r = 7.5914 \text{ kD} \qquad (10.1.1)$$

and

$$L_b = -2.6143 \text{ kD} \tag{10.1.2}$$

respectively. Hence from Equation 6.1.6 one obtains

$$z_r = 0.1756 \text{ mm} \tag{10.1.3}$$

and

$$z_b = -0.5150 \text{ mm}, \tag{10.1.4}$$

the positions of red and blue image points from the exit plane. The longitudinal chromatic aberration is (Equation 6.1.1),

$$\delta z = -0.6906 \text{ mm}. \tag{10.1.5}$$

The signed distance of the longitudinal chromatic aberration is from red to blue, and therefore, the direction of δz is from behind the retina to in front of the retina.

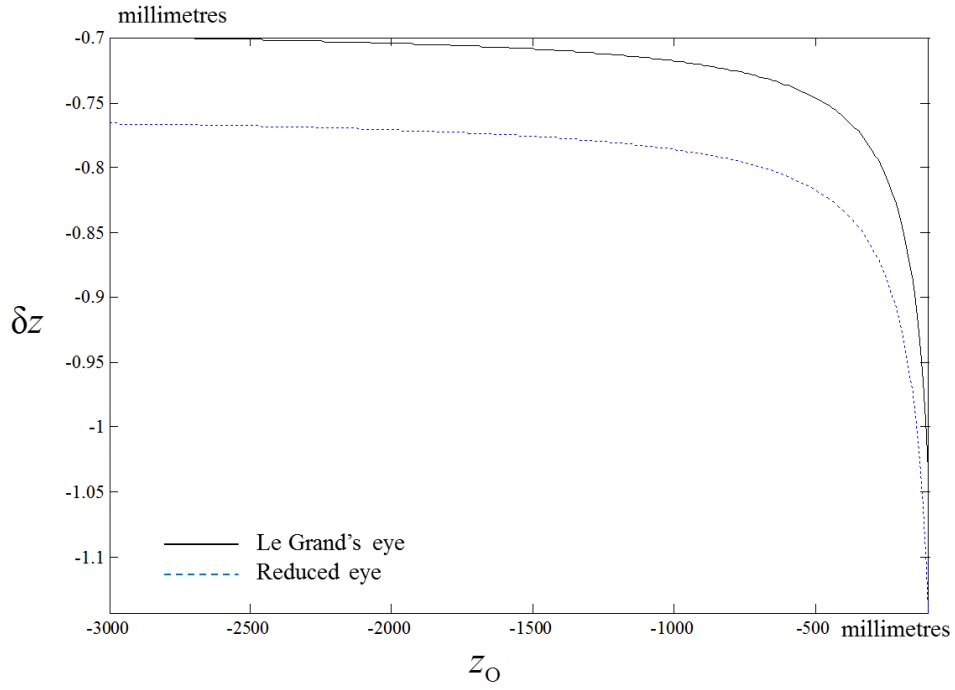

Figure 10.1.1 The longitudinal chromatic aberration δz as a function of object distance z_O for Le Grand's eye in black and the reduced eye in blue. z_O is measured from the cornea to the object point.

Table 10.1.1 Summary, for Le Grand's eye, of the red and blue wavefront vergences (L), image distances (z) from the retina and longitudinal chromatic aberration (δz) at object distances (z_O) of –3, –2 and –0.5 m.

z_O	–3 m	–2 m	–0.5 m
L_r	4.4089 kD	3.6400 kD	1.3943 kD
L_b	–3.3896 kD	–3.9849 kD	6.4280 kD
z_r	0.3023 mm	0.3661 mm	0.9558 mm
z_b	–0.3972 mm	–0.3379 mm	0.2095 mm
δz	–0.6995 mm	–0.7040 mm	–0.7463 mm

Equation 6.2.3 defines the vergence emerging from a system when incident vergence originates from a finite object, as a function of the distance of the object in front of the system (in millimetres). For red vergence this becomes

$$L_r = \frac{0.9044 + 0.05936 z_O}{0.007819 z_O - 16.7276} \tag{10.1.6}$$

and for blue vergence it is

$$L_b = \frac{0.9011 + 0.06187 z_O}{-0.02367 z_O - 16.5065}. \tag{10.1.7}$$

The red and blue emergent vergence L, image distances z and longitudinal chromatic aberration δz for the three illustrative object distances z_O are summarized in Table 10.1.1. From Table 10.1.1 and Figure 10.1.1 we see that as an object approaches the eye, so the magnitude of the longitudinal chromatic aberration increases.

The reduced eye

For the reduced eye we summarize the results for δz in Table 10.1.2. We see from Table 10.1.2 and Figure 10.1.1 that the magnitude of δz increases as the object approaches the eye. The summary in Table 10.1.2 and Figure 10.1.1 both emphasise that as the object point approaches the eye, so the magnitude of the δz increases. From Figure 10.1.1 we see that the changes in δz are similar for the

Table 10.1.2 Summary, for the reduced eye, of the red and blue wavefront vergences (L), image distances from the retina (z) and longitudinal chromatic aberration (δz) at object distances (z_O) distant, –3, –2 and –0.5 m.

z_O	Distant	–3 m	–2 m	–0.5 m
L_r	8.5014 kD	4.7059 kD	3.8412 kD	1.4217 kD
L_b	–2.2442 kD	–2.7848 kD	–3.1698 kD	11.3848 kD
z_r	0.1565 mm	0.2827 mm	0.3463 mm	0.9356 mm
z_b	–0.5997 mm	–0.4833 mm	–0.4246 mm	0.1182 mm
δz	–0.7562 mm	–0.7659 mm	–0.7709 mm	–0.8174 mm

two model eyes, but the magnitude of δz is greater for the reduced eye (blue line) than for Le Grand's eye (black line).

10.1.2 Transverse chromatic aberration

Le Grand's eye

The steps to calculate transverse chromatic aberration (δy) are given in Section 6.3.2. The first three steps have already been calculated above for longitudinal chromatic aberration. δy is dependent on a_O or a combination of z_O and y_O. Starting with a distant object, we continue with step 4 and Equation 6.2.17. Substituting from the red and blue transferences $\mathbf{S}_r$ and $\mathbf{S}_b$ (Table 8.1.1) and from Section 10.1.1 for z_r and z_b (Equations 10.1.3 and 4) we obtain

$$\delta y = a_O(-0.6850 \text{ mm}) \tag{10.1.8}$$

a linear relationship. For the purposes of illustrating δy of a distant object, we substitute $a_O = 0.1$ into Equation 10.1.8 to obtain $\delta y = -0.06850$ mm and the red image point is located superior to the blue image point.

For an object point at a finite distance the position of the object is determined by z_O and y_O. For illustrative purposes, we use the three distances for z_O, and $y_O = 200$ mm as described above. Continuing with step 4 of Section 6.3.2

Table 10.1.3 Summary, for Le Grand's eye, of the transverse chromatic aberration (δy) at working distances of –3, –2 and –0.5 m for an object position (y_O) 200 mm above the longitudinal axis.

z_O	–3 m	–2 m	–0.5 m
δy	0.04614 mm	0.06958 mm	0.2918 mm

to calculate δy for an object at a finite distance and substituting into Equation 6.2.16 we obtain

$$\delta y = y_O(-0.03149 - 0.04595\ \text{kD}\ z_b + 0.04454\ \text{kD}\ z_r) \qquad (10.1.9)$$

as a function of y_O and the respective red z_r and blue z_b image positions, which are, in turn, dependent on z_O and given in Table 10.1.1. The numerical results for δy are given in Table 10.1.3. The dependence of δy on y_O for any chosen z_O will be linear.

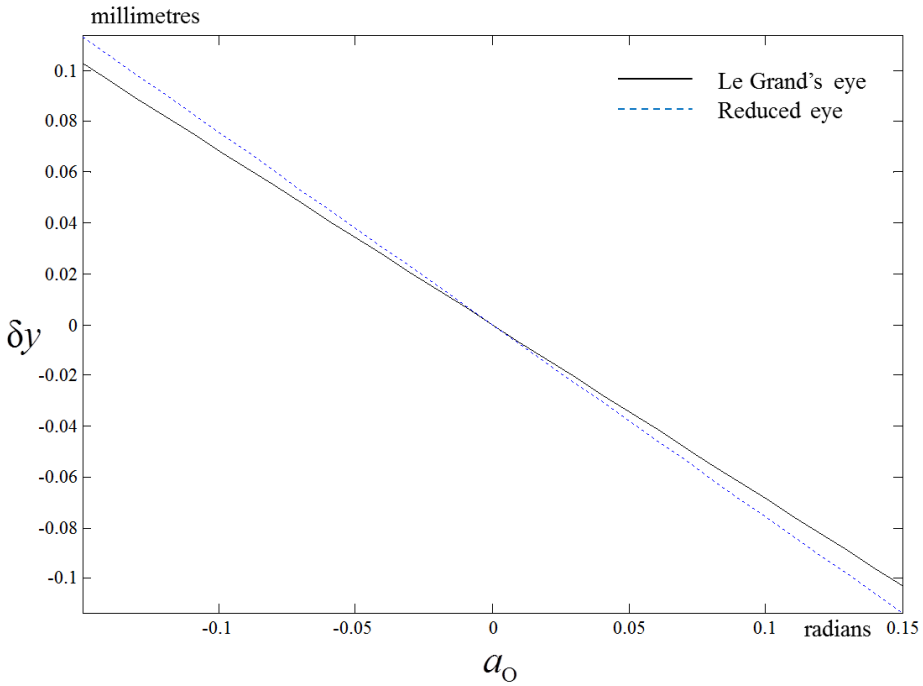

Figure 10.1.2 The dependence of the transverse chromatic aberration δy on the incident inclination a_O for a distant object for Le Grand's eye in black and the reduced eye in blue.

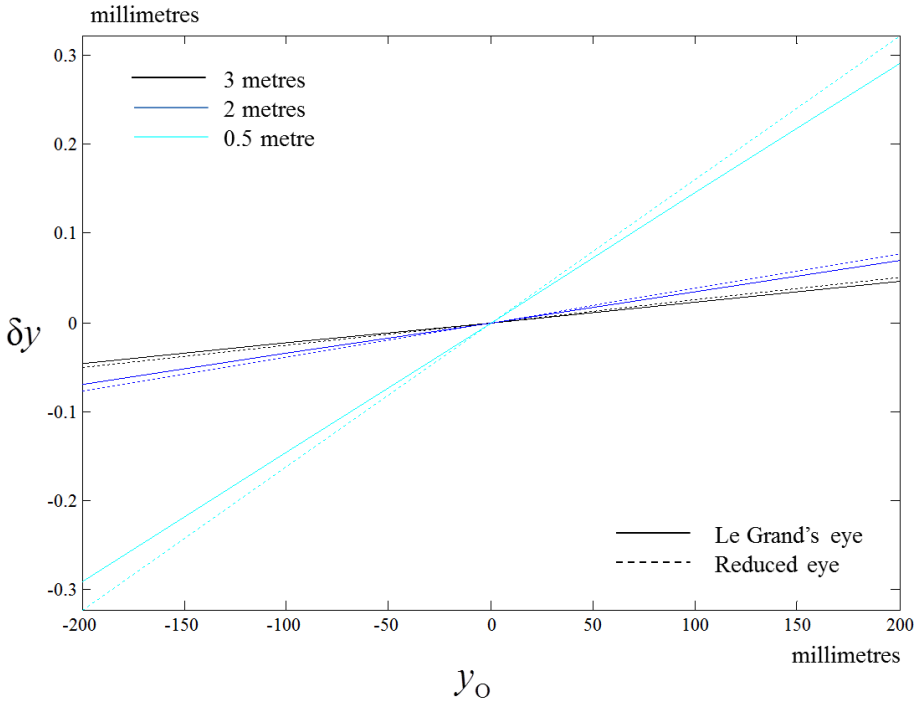

Figure 10.1.3 The transverse chromatic aberration (δy) of Le Grand's eye (solid lines) and the reduced eye (dashed lines) for three longitudinal distances (z_O) as a function of transverse object position y_O. The coloured lines represent the distance of the object from the eye with black being at –3 m, blue at –2 m and cyan at –0.5 m.

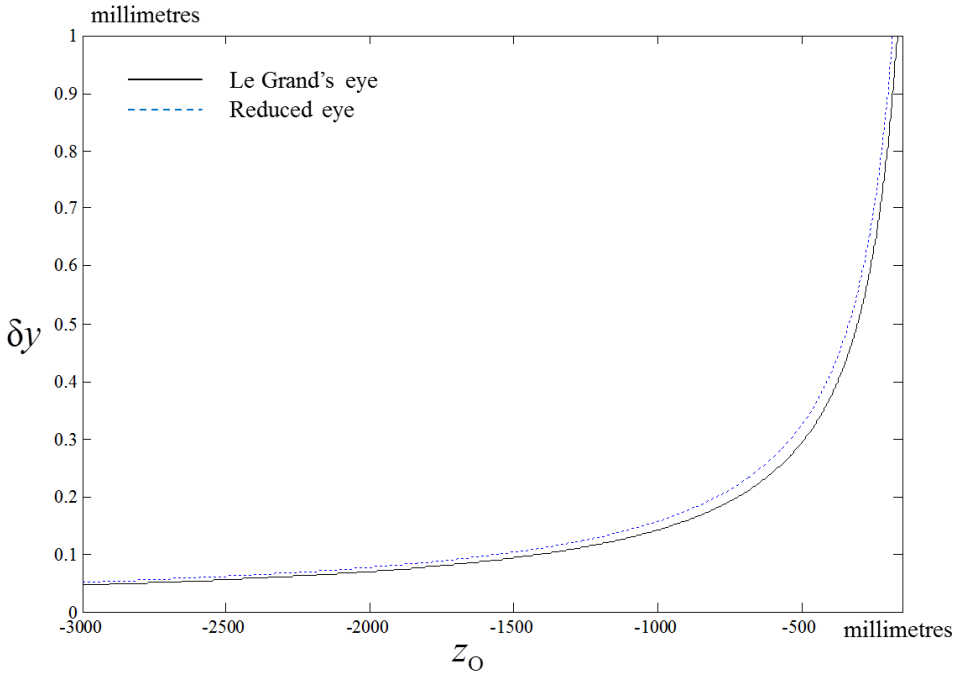

Figure 10.1.4 The transverse chromatic aberration (δy) of Le Grand's eye (black line) and the reduced eye (blue line) as a function of change in z_O for an object at $y_O = 200\,\text{mm}$.

Table 10.1.4 Summary, for the reduced eye, of the transverse chromatic aberration (δy) for a distant object with incident inclination of $a_O = 0.1$ and for an object at finite object distances (z_O) of –3, –2 and –0.5 m with the object at $y_O = 200\,\text{mm}$ above the longitudinal axis.

z_O	Distance	–3 m	–2 m	–0.5 m
δy	–0.07562 mm	0.05097 mm	0.07687 mm	0.3234 mm

The results are unsurprising, as the object approaches the eye, so the incident inclination increases in magnitude. To gain a better understanding, we show the effect of changes in y_O at the three illustrative positions of z_O in Figure 10.1.3. Figure 10.1.4 shows δy as a function of z_O when the object remains at $y_O = 200\,\text{mm}$ above the longitudinal axis.

The reduced eye

Similarly, we obtain the values for δy for the reduced eye for a distant object point and for an object at –3, –2 and –0.5 m from the eye at a distance of 200 mm above the longitudinal axis. The results are summarized in Table 10.1.4.

The conclusion of the effect of transverse chromatic aberration in the reduced eye is similar to that for Le Grand's eye. The relationship between δy and a_O (distant objects) or y_O (objects at a finite distance) at any particular working distance z_O is linear, however $|\delta y|$ for the reduced eye is slightly greater than that for Le Grand's eye.

10.2 Independent chromatic properties of the eye

The chromatic properties of the eye (alone) are defined as functions of the fundamental properties (or derivations thereof) of the red and blue transferences ($\mathbf{S}_r$ and $\mathbf{S}_b$). They are not directly dependent on light and therefore also not on object and image points. The three independent chromatic properties of the eye were defined in Section 7.1 as the chromatic difference in power, δF (Equation 7.1.2), chromatic difference in refractive compensation, δF_0 (Equation 7.1.4) and chromatic difference in ametropia, δA (Equation 7.1.5). The values for the

Table 10.2.1 Independent chromatic properties of Le Grand's and the reduced eyes.

Chromatic difference in:	Le Grand's eye	Reduced eye
Power (δF)	2.5158 D	2.7975 D
Refractive compensation (δF_0)	–1.9013 D	–2.0981 D
Ametropia (δA)	–0.03149	–0.03473

chromatic properties for Le Grand's and the reduced eye are given in Table 10.2.1.

For both model eyes, δF is more than a half dioptre greater in magnitude than δF_0 and therefore the two definitions cannot be interchanged. Also apparent is that the magnitude of all three independent chromatic properties is greater for the reduced eye than for Le grand's eye.

The chromatic difference in refractive compensation has been the subject of numerous experimental measurements and the consensus is that there is very little variation between studies and between subjects (Howarth and Bradley, 1986; Cooper and Pease, 1988; Simonet and Campbell, 1990; Atchison, Smith and Waterworth, 1993; Wald and Griffin, 1947; Bennett and Rabbetts, 2007:292-3; Atchison and Smith, 2000: 184-5). Adjusting for the different wavelengths chosen for each study, the results in Table 10.2.1 compare well to experimental studies.

10.3 Chromatic properties of the eye dependent on object and aperture positions

The chromatic properties dependent on object and aperture positions were defined in Chapter 7. Sections 7.2 and 3 looked at the object and aperture-dependent chromatic properties in image space and Sections 7.4 and 5 looked at the image and aperture-dependent chromatic properties in object space. Definitions for the chromatic properties in image space (subscript R) were derived for both distant objects and objects at finite distances. The definitions for chromatic properties in object space (subscript O) were limited to finite distances to mimic the experimental or clinical situation where these properties are present.

Table 10.3.1 The red and blue coefficient matrices for Le Grand's eye for distant objects, $\mathbf{V}_{\mathrm{E}}$ and objects at the finite distances of –3, –2 and –0.5 m from the eye, $\mathbf{V}_{\mathrm{OE}}$.

		Red	Blue
$\mathbf{V}_{\mathrm{E}}$	Distant	$\begin{pmatrix} 0.008832 & 16.7038\ \mathrm{mm} \\ -0.05031\ \mathrm{kD} & 0.8142 \end{pmatrix}$	$\begin{pmatrix} -0.02685 & 16.5780\ \mathrm{mm} \\ -0.05213\ \mathrm{kD} & 0.8082 \end{pmatrix}$
$\mathbf{V}_{\mathrm{OE}}$	–3 m	$\begin{pmatrix} 0.01511 & -0.005562 \\ -0.05000\ \mathrm{kD} & -0.0002711\ \mathrm{kD} \end{pmatrix}$	$\begin{pmatrix} -0.02059 & -0.005520 \\ -0.05182\ \mathrm{kD} & -0.0002691\ \mathrm{kD} \end{pmatrix}$
$\mathbf{V}_{\mathrm{OE}}$	–2 m	$\begin{pmatrix} 0.01825 & -0.008339 \\ -0.04984\ \mathrm{kD} & -0.0004065\ \mathrm{kD} \end{pmatrix}$	$\begin{pmatrix} -0.01746 & -0.008276 \\ -0.05167\ \mathrm{kD} & -0.0004035\ \mathrm{kD} \end{pmatrix}$
$\mathbf{V}_{\mathrm{OE}}$	–0.5 m	$\begin{pmatrix} 0.04634 & -0.03321 \\ -0.04848\ \mathrm{kD} & -0.001619\ \mathrm{kD} \end{pmatrix}$	$\begin{pmatrix} 0.01054 & -0.03296 \\ -0.05031\ \mathrm{kD} & -0.001607\ \mathrm{kD} \end{pmatrix}$

Table 10.3.2 The red and blue coefficient matrices for the reduced eye for distant objects, $\mathbf{V}_{\mathrm{E}}$ and objects at the finite distances of –3, –2 and –0.5 m from the eye, $\mathbf{V}_{\mathrm{OE}}$.

		Red	Blue
$\mathbf{V}_{\mathrm{E}}$	Distant	$\begin{pmatrix} 0.007650 & 16.6944\ \mathrm{mm} \\ -0.04889\ \mathrm{kD} & 0.8225 \end{pmatrix}$	$\begin{pmatrix} -0.03045 & 16.5562\ \mathrm{mm} \\ -0.05077\ \mathrm{kD} & 0.8157 \end{pmatrix}$
$\mathbf{V}_{\mathrm{OE}}$	–3 m	$\begin{pmatrix} 0.01374 & -0.005562 \\ -0.04859\ \mathrm{kD} & -0.0002740\ \mathrm{kD} \end{pmatrix}$	$\begin{pmatrix} -0.02439 & -0.005516 \\ -0.05047\ \mathrm{kD} & -0.0002718\ \mathrm{kD} \end{pmatrix}$
$\mathbf{V}_{\mathrm{OE}}$	–2 m	$\begin{pmatrix} 0.01678 & -0.008341 \\ -0.04844\ \mathrm{kD} & -0.0004109\ \mathrm{kD} \end{pmatrix}$	$\begin{pmatrix} -0.02137 & -0.008272 \\ -0.05032\ \mathrm{kD} & -0.0004075\ \mathrm{kD} \end{pmatrix}$
$\mathbf{V}_{\mathrm{OE}}$	–0.5 m	$\begin{pmatrix} 0.04407 & -0.03328 \\ -0.04710\ \mathrm{kD} & -0.001640\ \mathrm{kD} \end{pmatrix}$	$\begin{pmatrix} 0.005790 & -0.03301 \\ -0.04898\ \mathrm{kD} & -0.001626\ \mathrm{kD} \end{pmatrix}$

The derivations for chromatic properties dependent on object and aperture positions in image space are all based on the coefficient matrices for distant objects $\mathbf{V}_{\mathrm{E}}$ (Equation 5.2.8) and for objects at a finite distance $\mathbf{V}_{\mathrm{OE}}$ (Equation 5.2.26), both given in the summary in Table 7.7.2. $\mathbf{V}_{\mathrm{OE}}$ is a function of the distance of the object point in front of the eye, z_{O}. Consistent with the three illustrative distances used throughout this chapter, $\mathbf{V}_{\mathrm{OE}}$ is calculated at each

Table 10.3.3 The chromatic difference in red and blue coefficient matrices for Le Grand's and the reduced eye for distant objects, $\delta\mathbf{V}_{\mathrm{E}}$ and objects at the finite distances of –3, –2 and –0.5 m from the eye, $\delta\mathbf{V}_{\mathrm{OE}}$.

		Le Grand's eye	Reduced eye
$\delta\mathbf{V}_{\mathrm{E}}$	Distant	$\begin{pmatrix} -0.03568 & -0.1258\ \mathrm{mm} \\ -0.001822\ \mathrm{kD} & -0.006011 \end{pmatrix}$	$\begin{pmatrix} -0.03810 & -0.1383\ \mathrm{mm} \\ -0.001877\ \mathrm{kD} & -0.006813 \end{pmatrix}$
$\delta\mathbf{V}_{\mathrm{OE}}$	–3 m	$\begin{pmatrix} -0.03570 & 4.1853\times10^{-5} \\ -0.001823\ \mathrm{kD} & 1.9998\times10^{-6}\ \mathrm{kD} \end{pmatrix}$	$\begin{pmatrix} -0.03813 & 4.6047\times10^{-5} \\ -0.001878\ \mathrm{kD} & 2.2687\times10^{-6}\ \mathrm{kD} \end{pmatrix}$
$\delta\mathbf{V}_{\mathrm{OE}}$	–2 m	$\begin{pmatrix} -0.03571 & 6.2720\times10^{-5} \\ -0.001823\ \mathrm{kD} & 2.9968\times10^{-6}\ \mathrm{kD} \end{pmatrix}$	$\begin{pmatrix} -0.03814 & 6.9034\times10^{-5} \\ -0.001879\ \mathrm{kD} & 3.4013\times10^{-6}\ \mathrm{kD} \end{pmatrix}$
$\delta\mathbf{V}_{\mathrm{OE}}$	–0.5 m	$\begin{pmatrix} -0.03580 & 2.4873\times10^{-4} \\ -0.001828\ \mathrm{kD} & 1.1883\times10^{-5}\ \mathrm{kD} \end{pmatrix}$	$\begin{pmatrix} -0.03828 & 2.7484\times10^{-4} \\ -0.001886\ \mathrm{kD} & 1.3541\times10^{-5}\ \mathrm{kD} \end{pmatrix}$

distance for red and blue frequencies. These are summarized for Le Grand's eye in Table 10.3.1 and for the reduced eye in Table 10.3.2. The chromatic difference in coefficient matrices for distant objects $\delta\mathbf{V}_{\mathrm{E}}$ and objects at a finite distance $\delta\mathbf{V}_{\mathrm{OE}}$ as defined by Equation 7.2.1 are given in Table 10.3.3 for both model eyes.

10.3.1 Chromatic difference in transverse image positions at the retina

Le Grand's eye

The chromatic difference in transverse image positions at the retina, δy_{R} is defined by Equation 7.2.3 for an object at distance. Substituting the values from the entries of $\delta\mathbf{V}_{\mathrm{E}}$ we obtain the relationship for δy_{R} for a distant object, given in the first line of Table 10.3.4. From this relationship one can see that δy_{R} is dependent on any decentration of the pupil y_{P} and the incident inclination of the pencil of rays from a distant object, a_{K}. For a centred Gaussian model eye ($y_{\mathrm{P}} = 0$) the relationship simplifies to $\delta y_{\mathrm{R}} = (-0.1258\,\mathrm{mm})\,a_{\mathrm{K}}$. This is illustrated in Figure 7.2.1 and the results shown graphically in Figure 10.3.1. For the illustrative inclination of $a_{\mathrm{K}} = 0.1$ radians we obtain $\delta y_{\mathrm{R}} = -0.01258\,\mathrm{mm}$.

Similarly, we substitute the values from $\delta\mathbf{V}_{\mathrm{OE}}$, given in Table 10.3.3, for the three illustrative object distances z_{O} into Equation 7.2.4 to obtain relationships for the three illustrative finite working distances for Le Grand's eye, summarised in Table 10.3.4. Unsurprisingly, the closer the object is to the eye, so δy_{R} increases, which is seen in Figure 10.3.2

We now substitute the illustrative value of $y_{\mathrm{O}} = 200\,\mathrm{mm}$ for the displacement of the object point from the longitudinal axis at each z_{O} and we obtain δy_{R}, in Table 10.3.4. As expected, from these numerical examples and Figure 10.3.2, we can see that the magnitude of δy_{R} increases as the object approaches the eye for an off-axial object point.

The reduced eye

The results and conclusions for δy_{R} for the reduced eye are similar to Le Grand's eye. The constants for the reduced eye for Equations 7.2.3 and 4 are given in Table 10.3.5.

From Figures 10.3.1 and 2, we see that δy_{R} for the centred reduced eye is slightly greater in magnitude across object points at all distances than for Le

Table 10.3.4 The chromatic difference in image position at the retina, δy_R for Le Grand's eye. The illustrative example is for the centred reduced eye with $a_K = 0.1$ for the distant object point and $y_O = 200$ mm for the three finite distance object points.

Chromatic difference in image position		Illustrative example
Distant object	$\delta y_R = (-0.03568) y_P + (-0.1258\ \text{mm})\, a_K$	$\delta y_R = -0.01258$ mm
–3 m	$\delta y_R = (-0.03570) y_P + (4.1853\times10^{-5}) y_O$	$\delta y_R = 0.008371$ mm
–2 m	$\delta y_R = (-0.03571) y_P + (6.2720\times10^{-5}) y_O$	$\delta y_R = 0.01254$ mm
–0.5m	$\delta y_R = (-0.03580) y_P + (2.4873\times10^{-4}) y_O$	$\delta y_R = 0.04975$ mm

Grand's eye. The reason for this is revealed in Table 10.3.3 where we see that δX_E and δX_{OE} are greater in magnitude for the reduced eye than for Le Grand's eye. Comparing Equations 5.2.8 and 26, we can determine that the discrepancies lie in the underlying structural differences in the two model eyes, that is, number of refracting surfaces and their positions relative to the pupil or limiting aperture.

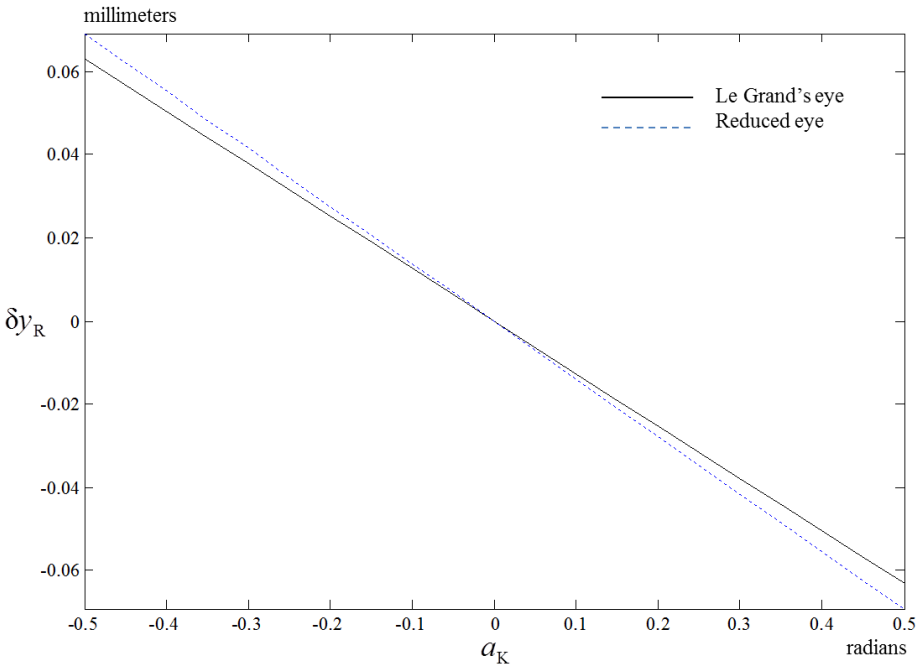

Figure 10.3.1 The chromatic difference in transverse image position at the retina δy_R as a function of incident inclination a_K for Le Grand's eye (solid black line) and reduced eye (dashed blue line) for a distant object point.

Table 10.3.5 The chromatic difference in image position at the retina, δy_{R} for the reduced eye. The illustrative example is for the centred reduced eye with $a_{\mathrm{K}} = 0.1$ for the distant object point and $y_{\mathrm{O}} = 200$ mm for the three finite distance object points.

Chromatic difference in image position		Illustrative example
Distant object	$\delta y_{\mathrm{R}} = (-0.03810) y_{\mathrm{P}} + (-0.1383\ \mathrm{mm}) a_{\mathrm{K}}$	$\delta y_{\mathrm{R}} = -0.01383$ mm
–3 m	$\delta y_{\mathrm{R}} = (-0.03813) y_{\mathrm{P}} + (4.6047 \times 10^{-5}) y_{\mathrm{O}}$	$\delta y_{\mathrm{R}} = 0.009209$ mm
–2 m	$\delta y_{\mathrm{R}} = (-0.03814) y_{\mathrm{P}} + (6.9034 \times 10^{-5}) y_{\mathrm{O}}$	$\delta y_{\mathrm{R}} = 0.01381$ mm
–0.5m	$\delta y_{\mathrm{R}} = (-0.03828) y_{\mathrm{P}} + (2.7484 \times 10^{-4}) y_{\mathrm{O}}$	$\delta y_{\mathrm{R}} = 0.05497$ mm

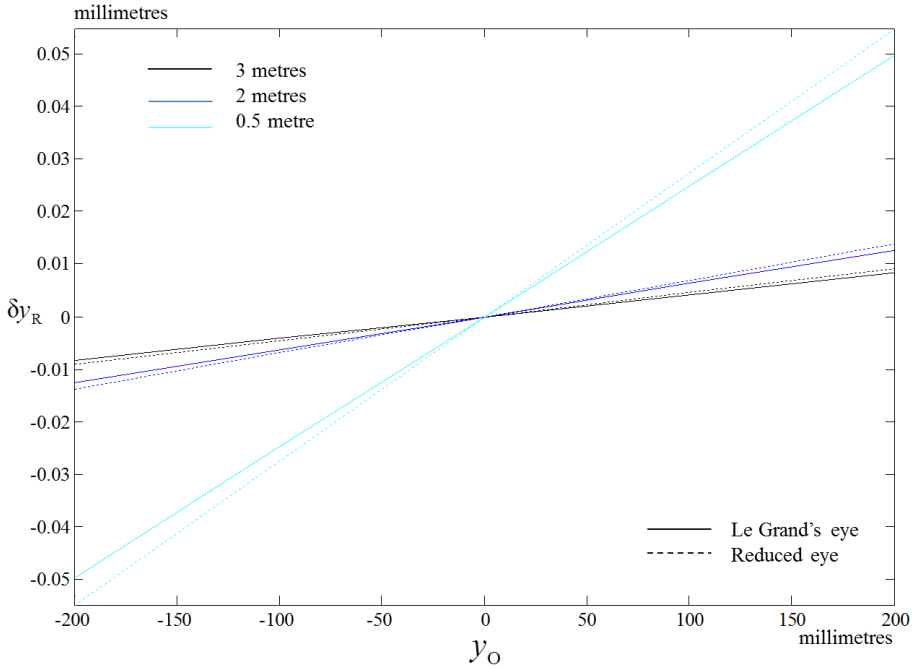

Figure 10.3.2 The chromatic difference in image position at the retina, δy_{R} as a function of transverse displacement of the object point from the longitudinal axis, y_{O} at the three illustrative distances, –3, –2 and –0.5 m for Le Grand's eye (solid lines) and the reduced eye (dashed line).

10.3.2 Chromatic difference in inclination at the retina

Le Grand's eye

Perhaps more insight can be gained from the chromatic difference in inclination at the retina, δa_{R}. Starting with a distant object and substituting from $\delta\mathbf{V}_{\mathrm{E}}$ for Le Grand's eye in Table 10.3.3 into Equation 7.2.16 we obtain a relationship for δa_{R} for a distant object point. This is summarised in Table 10.3.6 and shown in Figure 10.3.3, with the magnitude of a_{K} being magnified slightly more for the reduced eye than for Le Grand's eye.

Similarly, we substitute the respective entries of $\delta\mathbf{V}_{\mathrm{OE}}$ in Table 10.3.3 for the three illustrative z_{O}s in front of the eye into Equation 7.2.17 to obtain relationships at three working distances and summarised in Table 10.3.6. The relationships between δa_{R} and y_{O} are illustrated graphically in Figure 10.3.4.

The illustrative values obtained from Equations 7.2.16 and 17 are summarised in Table 10.3.6. As the object approaches the eye, so the magnitude of the emergent angular spread between the red and blue chief rays increases, as expected. δa_{R} is measured as the emergent inclination from the red ray to the emergent blue ray at the retina. For illustrative purposes, the chief ray has been chosen as $y_{\mathrm{P}} = 0\,\mathrm{mm}$.

The reduced eye

The results and conclusions for δa_{R} for the reduced eye are similar to Le Grand's eye, however the values vary slightly. From Figure 10.3.4, one can see that the magnitude of δa_{R} is consistently slightly greater in magnitude for the reduced eye than for Le Grand's eye. The illustrated values for δa_{R} for the centred reduced eye for a distant object with $a_{\mathrm{K}} = 0.1$ or for an object placed at $y_{\mathrm{O}} = 200\,\mathrm{mm}$ are summarised in Table 10.3.7.

Table 10.3.6 The chromatic difference in inclination at the retina δa_{R} for Le Grand's eye. The illustrative example is for a centred reduced eye and $a_{\mathrm{K}} = 0.1$ for a distant object point or $y_{\mathrm{O}} = 200\ \mathrm{mm}$ for an object point at the three finite distances. δa_{R} is given in radians.

	Chromatic difference in inclination at the retina	Illustrative example
Distant object	$\delta a_{\mathrm{R}} = (-0.001822\ \mathrm{kD})y_{\mathrm{P}} + (-0.006011)a_{\mathrm{K}}$	-6.0110×10^{-4}
–3 m	$\delta a_{\mathrm{R}} = (-0.001823\ \mathrm{kD})y_{\mathrm{P}} + (1.9998\times10^{-6}\ \mathrm{kD})y_{\mathrm{O}}$	3.9996×10^{-4}
–2 m	$\delta a_{\mathrm{R}} = (-0.001823\ \mathrm{kD})y_{\mathrm{P}} + (2.9968\times10^{-6}\ \mathrm{kD})y_{\mathrm{O}}$	5.9936×10^{-4}
–0.5m	$\delta a_{\mathrm{R}} = (-0.001828\ \mathrm{kD})y_{\mathrm{P}} + (1.1883\times10^{-5}\ \mathrm{kD})y_{\mathrm{O}}$	2.3767×10^{-3}

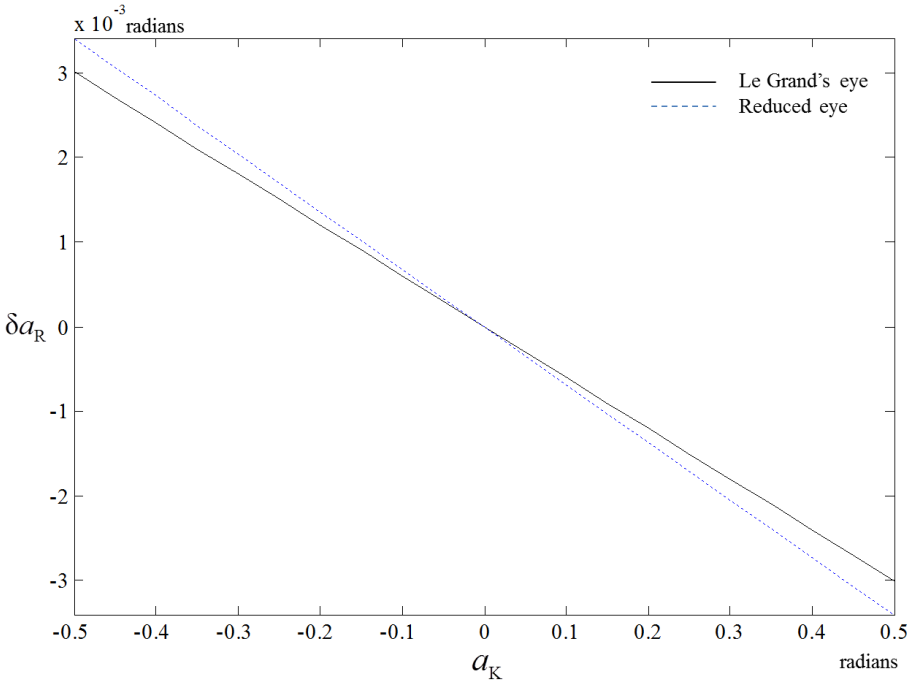

Figure 10.3.3 The chromatic difference in inclination at the retina δa_{R} as a function of incident inclination a_{K} for Le Grand's eye (black line) and the reduced eye (blue line).

Table 10.3.7 The chromatic difference in inclination at the retina δa_{R} for the reduced eye. The illustrative example is for a centred reduced eye and $a_{\mathrm{K}} = 0.1$ for a distant object point or $y_{\mathrm{O}} = 200\ \mathrm{mm}$ for an object point at the three finite distances.

	Chromatic difference in inclination at the retina	Illustrative example
Distant object	$\delta a_{\mathrm{R}} = (-0.001877\ \mathrm{kD})\, y_{\mathrm{P}} + (-0.006813)\, a_{\mathrm{K}}$	-6.8133×10^{-4}
–3 m	$\delta a_{\mathrm{R}} = (-0.001878\ \mathrm{kD})\, y_{\mathrm{P}} + (2.2687\times10^{-6}\ \mathrm{kD})\, y_{\mathrm{O}}$	4.5374×10^{-4}
–2 m	$\delta a_{\mathrm{R}} = (-0.001879\ \mathrm{kD})\, y_{\mathrm{P}} + (3.4013\times10^{-6}\ \mathrm{kD})\, y_{\mathrm{O}}$	6.8025×10^{-4}
–0.5m	$\delta a_{\mathrm{R}} = (-0.001886\ \mathrm{kD})\, y_{\mathrm{P}} + (1.3541\times10^{-5}\ \mathrm{kD})\, y_{\mathrm{O}}$	0.002708

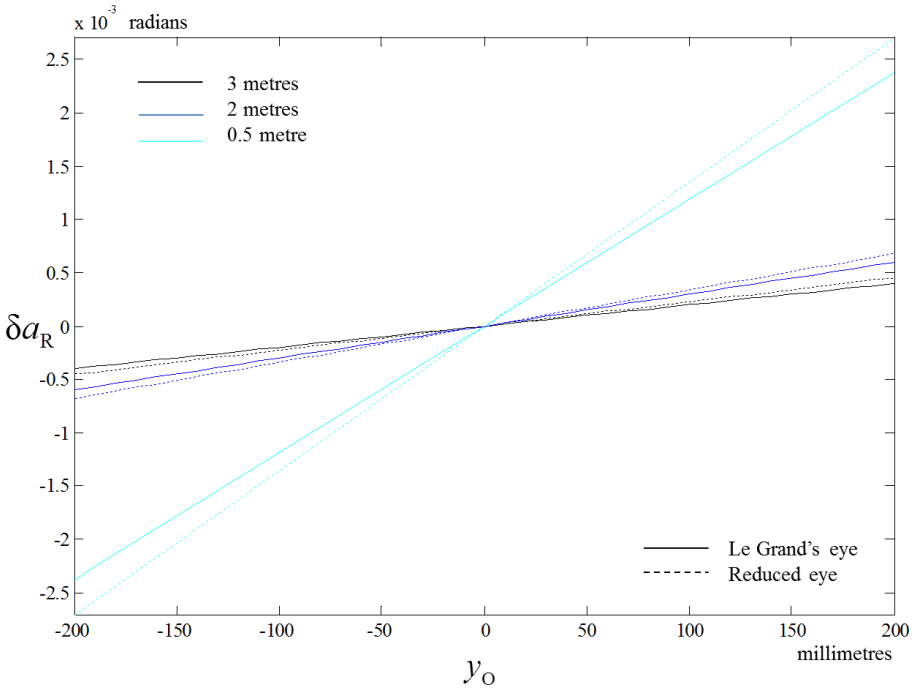

Figure 10.3.4 The chromatic difference in inclination at the retina δa_{R} as a function of transverse displacement of the object point from the longitudinal axis y_{O} at the three illustrative distances of –3, –2 and –0.5m from the eye for Le Grand's eye (solid lines) and the reduced eye (dashed lines).

10.3.3 Chromatic difference in image size

Le Grand's eye

Section 7.3.1 showed that the chromatic difference in image size, $\delta(\Delta y_{\mathrm{R}})$ simplified to a linear relationship between the object and image sizes (Δy_{R}). The size of a distant object is defined by the difference in incident inclination (Δa_{K}) or angular spread and at a finite distance z_{O}, by the object size (Δy_{O}). Substituting the relevant entry from $\delta\mathbf{V}_{\mathrm{E}}$ for Le Grand's eye given in Table 10.3.3 into Equation 7.3.4 for a distant object and from $\delta\mathbf{V}_{\mathrm{OE}}$ in Table 10.3.3 into Equation 7.3.8 we obtain relationships for $\delta(\Delta y_{\mathrm{R}})$ for Le Grand's eye.

For $\delta(\Delta y_{\mathrm{R}})$, the pupil position is nullified (Section 7.3.1) and therefore we obtain the same values as for δy_{R} when the system is assumed to be centred. Therefore the numerical examples for the two model eyes are not repeated. The graphical relationship for a distant object of size $\Delta a_{\mathrm{K}} = 0.1$ will be identical to that shown in Figure 10.3.1 and Figure 10.3.2 for the object of size $\Delta y_{\mathrm{O}} = 200\ \mathrm{mm}$ at finite distances.

The reduced eye

The linear relationships for $\delta(\Delta y_{\mathrm{R}})$ of the reduced eye are summarized in Table 10.3.8. The conclusions drawn are similar to those for Le Grand's eye.

Table 10.3.8 The Chromatic difference in image size at the retina $\delta(\Delta y_{\mathrm{R}})$ for Le Grand's and the reduced eyes.

	Le Grand's eye	Reduced eye
Distant object	$\delta(\Delta y_{\mathrm{R}}) = (-0.1258\ \mathrm{mm})\,\Delta a_{\mathrm{K}}$	$\delta(\Delta y_{\mathrm{R}}) = (-0.1383\ \mathrm{mm})\,\Delta a_{\mathrm{K}}$
–3 m	$\delta(\Delta y_{\mathrm{R}}) = (4.1853\times10^{-5})\,\Delta y_{\mathrm{O}}$	$\delta(\Delta y_{\mathrm{R}}) = (4.6047\times10^{-5})\,\Delta y_{\mathrm{O}}$
–2 m	$\delta(\Delta y_{\mathrm{R}}) = (6.2720\times10^{-5})\,\Delta y_{\mathrm{O}}$	$\delta(\Delta y_{\mathrm{R}}) = (6.9034\times10^{-5})\,\Delta y_{\mathrm{O}}$
–0.5m	$\delta(\Delta y_{\mathrm{R}}) = (2.4873\times10^{-4})\,\Delta y_{\mathrm{O}}$	$\delta(\Delta y_{\mathrm{R}}) = (2.7484\times10^{-4})\,\Delta y_{\mathrm{O}}$

10.3.4 Chromatic difference in angular spread at the retina

Le Grand's eye

Equation 7.3.11 defines the chromatic difference in angular spread across the retina, $\delta(\Delta a_{\mathrm{R}})$, as a linear relationship with the angular spread of the incident rays directed from a distant object. For Le Grand's eye this relationship is given in Table 10.3.9. Equation 7.3.12 defines $\delta(\Delta a_{\mathrm{R}})$ as a linear relationship with the object size Δy_{O} for an object at a finite distance. The values for the $\delta(\Delta a_{\mathrm{R}})$ at the three illustrative distances are given in Table 10.3.9.

Table 10.3.9 The chromatic difference in angular spread across the retina $\delta(\Delta a_{\mathrm{R}})$ for Le Grand's and the reduced eyes.

	Le Grand's eye	Reduced eye
Distant object	$\delta(\Delta a_{\mathrm{R}}) = -0.006011\,\Delta a_{\mathrm{K}}$	$\delta(\Delta a_{\mathrm{R}}) = -0.006813\,\Delta a_{\mathrm{K}}$
–3 m	$\delta(\Delta a_{\mathrm{R}}) = (1.9998\times10^{-6})\,\Delta y_{\mathrm{O}}$	$\delta(\Delta a_{\mathrm{R}}) = (2.2687\times10^{-6})\,\Delta y_{\mathrm{O}}$
–2 m	$\delta(\Delta a_{\mathrm{R}}) = (2.9968\times10^{-6})\,\Delta y_{\mathrm{O}}$	$\delta(\Delta a_{\mathrm{R}}) = (3.4013\times10^{-6})\,\Delta y_{\mathrm{O}}$
–0.5m	$\delta(\Delta a_{\mathrm{R}}) = (1.1883\times10^{-5})\,\Delta y_{\mathrm{O}}$	$\delta(\Delta a_{\mathrm{R}}) = (1.3541\times10^{-5})\,\Delta y_{\mathrm{O}}$

The Reduced eye

The values for the chromatic difference in angular spread across the retina are given in Table 10.3.9 for the reduced eye.

10.3.5 Retinal chromatic magnification

Le Grand's eye

In Sections 7.3.3 and 4 formulae for the retinal chromatic image size magnification M_{yR} and retinal chromatic angular spread magnification $M_{a\mathrm{R}}$ were obtained. These are chromatic magnifications and not chromatic differences and give a magnification of the red compared to the blue image size or angular spread at the retina. The magnification is dependent on the longitudinal distance of the object in front of the eye z_{O}, however, we expect these magnifications to be similar in value. Substituting the relevant values from the red and blue coefficient

matrices $\mathbf{V}_{\mathrm{E}}$ in Table 10.3.1 into Equation 7.3.19 we obtain M_{yR} for a distant object, where $n_0 = 1$ for both the red and blue incident light in air, given in Table 10.3.10. To obtain the retinal chromatic image size magnification for the three illustrative finite object distances in front of Le Grand's eye, we substitute the entries of the red and blue near coefficient matrices $\mathbf{V}_{\mathrm{OE}}$ from Table 10.3.1 into Equation 7.3.20 to obtain the M_{yR} for objects at the three illustrative distances in front of the eye, summarised in Table 10.3.10.

Similarly the retinal chromatic angular spread ratios $M_{a\mathrm{R}}$ are obtained by substituting the relevant entries of $\mathbf{V}_{\mathrm{E}}$ and $\mathbf{V}_{\mathrm{OE}}$ into Equations 7.3.27 and 28. The values are also summarised in Table 10.3.10.

The chromatic magnification of image sizes is 0.75% for distant objects and objects at a finite distance, with the red image being slightly larger than the blue image, which is very much in line with the calculated values in the literature (Thibos *et al*, 1991; Rabbetts, 2007: 291). Similarly, the retinal chromatic angular spread ratio is 0.74% for the objects at a finite distance in front of Le Grand's eye, implying that the red near directional spread is greater than the blue near directional spread.

The reduced eye

The numerical results for the reduced eye are given in Table 10.3.11. Table 10.3.11 indicates that for the reduced eye the retinal chromatic image size magnification is 0.83% regardless of the distance that the object is in front of the reduced eye. The distance and near image size coefficients X_{E} and X_{OE} are greater for red than blue. The retinal chromatic angular spread ratio is also 0.83% and the distance of the object in front of the reduced eye z_{O} plays very little part. The distance and near directional coefficients Z_{E} and Z_{OE} are greater for red than for blue. The object distance plays a negligibly small role.

These results are comparable to those in the literature. Zhang *et al* (1991) and Thibos *et al* (1991) give the magnification calculated using Equation 2.3.9.

Table 10.3.10 The retinal chromatic image size and angular spread magnifications for Le Grand's eye.

Retinal chromatic:	image size ratio	angular spread ratio
Distant object	$M_{yR} = 0.9925$	$M_{aR} = 0.9926$
–3 m	$M_{yR} = 0.9925$	$M_{aR} = 0.9926$
–2 m	$M_{yR} = 0.9925$	$M_{aR} = 0.9926$
–0.5m	$M_{yR} = 0.9925$	$M_{aR} = 0.9927$

Table 10.3.11 The retinal chromatic image size and angular spread magnifications for the reduced eye.

Retinal chromatic:	image size ratio	angular spread ratio
Distant object	$M_{yR} = 0.9917$	$M_{aR} = 0.9917$
–3 m	$M_{yR} = 0.9917$	$M_{aR} = 0.9917$
–2 m	$M_{yR} = 0.9917$	$M_{aR} = 0.9917$
–0.5m	$M_{yR} = 0.9917$	$M_{aR} = 0.9917$

Adjusting for the differences in wavelengths, the results obtained using Equations 7.3.19 and 27 compare well for all the examples given by Zhang *et al*. The same is true when a pinhole is held at a vertex distance of 15 mm and the retinal chromatic image size magnification increases to 4.3% for the reduced eye and 4.1% for Le Grand's eye.

10.4 Chromatic properties dependent on object and aperture positions in an eye – with a pinhole

In Section 5.2.4 we saw that when we introduce a pinhole immediately in front of the eye, Figures 3.5.4 and 5.1.1 simplify; the posterior system S_B is now the eye and the anterior system simplifies to the identity matrix. The coefficient matrix for an object at distance becomes simpler, given by $\mathbf{V}_E^P$ in Equation 5.2.37 and for an object at a finite distance in front of the eye, $\mathbf{V}_{OE}^P$ is given by Equation

5.2.34. The coefficient matrices for Le Grand's and the reduced eye with a pinhole immediately in front are given in Tables 10.4.1 and 2 and the chromatic difference in coefficient matrices with a pinhole in Table 10.4.3.

The methodology for each of the transverse chromatic properties was worked through step by step in Section 10.3. Therefore, in this section, the results are simply given in tabular form and the results discussed, without repeating the methodology.

Table 10.4.1 The red and blue coefficient matrices for Le Grand's eye with a pinhole immediately in front (superscript P) for distant objects (subscript E) and objects at the finite distances of –3, –2 and –0.5 m from the eye (subscript OE).

		Red	Blue
$\mathbf{V}_{\mathrm{E}}^{\mathrm{P}}$	Distant	$\begin{pmatrix} 0.007819 & 16.7276\ \mathrm{mm} \\ -0.04454\ \mathrm{kD} & 0.6786 \end{pmatrix}$	$\begin{pmatrix} -0.02367 & 16.5065\ \mathrm{mm} \\ -0.04596\ \mathrm{kD} & 0.6693 \end{pmatrix}$
$\mathbf{V}_{\mathrm{OE}}^{\mathrm{P}}$	–3 m	$\begin{pmatrix} 0.01340 & -0.005576 \\ -0.04431\ \mathrm{kD} & -2.2622\times10^{-4}\ \mathrm{kD} \end{pmatrix}$	$\begin{pmatrix} -0.01817 & -0.005502 \\ -0.04573\ \mathrm{kD} & -2.2309\times10^{-4}\ \mathrm{kD} \end{pmatrix}$
$\mathbf{V}_{\mathrm{OE}}^{\mathrm{P}}$	–2 m	$\begin{pmatrix} 0.01618 & -0.008364 \\ -0.04420\ \mathrm{kD} & -3.3932\times10^{-4}\ \mathrm{kD} \end{pmatrix}$	$\begin{pmatrix} -0.01541 & -0.008253 \\ -0.04562\ \mathrm{kD} & -3.3464\times10^{-4}\ \mathrm{kD} \end{pmatrix}$
$\mathbf{V}_{\mathrm{OE}}^{\mathrm{P}}$	–0.5 m	$\begin{pmatrix} 0.04127 & -0.03346 \\ -0.04318\ \mathrm{kD} & -1.3573\times10^{-3}\ \mathrm{kD} \end{pmatrix}$	$\begin{pmatrix} 0.009345 & -0.03301 \\ -0.04462\ \mathrm{kD} & -1.3386\times10^{-3}\ \mathrm{kD} \end{pmatrix}$

Table 10.4.2 The red and blue coefficient matrices for the reduced eye with a pinhole immediately in front for distant objects and objects at the finite distances of –3, –2 and –0.5 m.

		Red	Blue
$\mathbf{V}_{\mathrm{E}}^{\mathrm{P}}$	Distant	$\begin{pmatrix} 0.006992 & 16.7055\ \mathrm{mm} \\ -0.04469\ \mathrm{kD} & 0.7517 \end{pmatrix}$	$\begin{pmatrix} -0.02773 & 16.5126\ \mathrm{mm} \\ -0.04625\ \mathrm{kD} & 0.7431 \end{pmatrix}$
$\mathbf{V}_{\mathrm{OE}}^{\mathrm{P}}$	–3 m	$\begin{pmatrix} 0.01256 & -0.005569 \\ -0.04443\ \mathrm{kD} & -2.5058\times10^{-4}\ \mathrm{kD} \end{pmatrix}$	$\begin{pmatrix} -0.02223 & -0.005514 \\ -0.04600\ \mathrm{kD} & -2.4769\times10^{-4}\ \mathrm{kD} \end{pmatrix}$
$\mathbf{V}_{\mathrm{OE}}^{\mathrm{P}}$	–2 m	$\begin{pmatrix} 0.01534 & -0.008353 \\ -0.04431\ \mathrm{kD} & -3.7587\times10^{-4}\ \mathrm{kD} \end{pmatrix}$	$\begin{pmatrix} -0.01948 & -0.008256 \\ -0.04588\ \mathrm{kD} & -3.7153\times10^{-4}\ \mathrm{kD} \end{pmatrix}$
$\mathbf{V}_{\mathrm{OE}}^{\mathrm{P}}$	–0.5 m	$\begin{pmatrix} 0.04040 & -0.03341 \\ -0.04318\ \mathrm{kD} & -1.5035\times10^{-3}\ \mathrm{kD} \end{pmatrix}$	$\begin{pmatrix} 0.005291 & -0.03303 \\ -0.04476\ \mathrm{kD} & -1.4861\times10^{-3}\ \mathrm{kD} \end{pmatrix}$

Table 10.4.3 The chromatic difference between red and blue coefficient matrices for Le Grand's and the reduced eye with a pinhole immediately in front for distant objects and objects at the finite distances of –3, –2 and –0.5 m from the eye.

		Le Grand's eye	Reduced eye
$\delta\mathbf{V}_{\mathrm{E}}^{\mathrm{P}}$	Distant	$\begin{pmatrix} -0.03149 & -0.2212\ \mathrm{mm} \\ -0.001414\ \mathrm{kD} & -9.3691\times10^{-3} \end{pmatrix}$	$\begin{pmatrix} -0.03473 & -0.1929\ \mathrm{mm} \\ -0.001563\ \mathrm{kD} & -0.008682 \end{pmatrix}$
$\delta\mathbf{V}_{\mathrm{OE}}^{\mathrm{P}}$	–3 m	$\begin{pmatrix} -0.03156 & 7.3721\times10^{-5} \\ -0.00417\ \mathrm{kD} & 3.1230\times10^{-6}\ \mathrm{kD} \end{pmatrix}$	$\begin{pmatrix} -0.03479 & 6.4307\times10^{-5} \\ -0.001566\ \mathrm{kD} & 2.8938\times10^{-6}\ \mathrm{kD} \end{pmatrix}$
$\delta\mathbf{V}_{\mathrm{OE}}^{\mathrm{P}}$	–2 m	$\begin{pmatrix} -0.03160 & 1.1058\times10^{-4} \\ -0.001419\ \mathrm{kD} & 4.6845\times10^{-6}\ \mathrm{kD} \end{pmatrix}$	$\begin{pmatrix} -0.03482 & 9.6461\times10^{-5} \\ -0.001567\ \mathrm{kD} & 4.3408\times10^{-6}\ \mathrm{kD} \end{pmatrix}$
$\delta\mathbf{V}_{\mathrm{OE}}^{\mathrm{P}}$	–0.5 m	$\begin{pmatrix} -0.03193 & 4.4233\times10^{-4} \\ -0.001433\ \mathrm{kD} & 1.8738\times10^{-5}\ \mathrm{kD} \end{pmatrix}$	$\begin{pmatrix} -0.03511 & 3.8584\times10^{-4} \\ -0.001580\ \mathrm{kD} & 1.7363\times10^{-5}\ \mathrm{kD} \end{pmatrix}$

10.4.1 Chromatic difference in transverse image positions and inclinations at the retina with pinhole in front of the eye

The chromatic difference in transverse image positions δy_{R} (Equations 7.2.11 and 12) and inclinations δa_{R} (Equations 7.2.20 and 21) at the retina when a pinhole is immediately in front of the eye is given in Table 10.4.4 for Le Grand's eye and Table 10.4.5 for the reduced eye.

To generate numerical examples for the chromatic difference in transverse image positions δy_{R} and inclinations δa_{R} at the retina, we assume that the object is on the longitudinal axis; that is to say $a_{\mathrm{K}} = 0$ or $y_{\mathrm{O}} = 0$. Furthermore, an eye that is cyclopleged will allow for 4 mm of pinhole decentration and we therefore equate $y_{\mathrm{P}} = 4\ \mathrm{mm}$. The values are summarized in Table 10.4.6.

Inspecting the results, in each case there is a very small difference resulting from the change in longitudinal position of the object point from the eye. Additionally, the results obtained for the two eyes are distinct for both δy_{R} and δa_{R}. This is emphasized in Figures 10.4.1 and 2 which give δy_{R} and δa_{R} as a function of transverse displacement of the pinhole y_{P} held immediately in front of the eye.

Table 10.4.4 The chromatic difference in transverse image positions δy_{R} and inclinations δa_{R} at the retina when a pinhole is immediately in front of Le Grand's eye.

	Chromatic difference in transverse image positions	Chromatic difference in inclinations at the retina
Distant	$\delta y_{\mathrm{R}} = (-0.03149) y_{\mathrm{P}} + (-0.2212\ \mathrm{mm}) a_{\mathrm{K}}$	$\delta a_{\mathrm{R}} = (-0.001413\ \mathrm{kD}) y_{\mathrm{P}} + (-0.009369) a_{\mathrm{K}}$
–3 m	$\delta y_{\mathrm{R}} = (-0.03156) y_{\mathrm{P}} + (7.3721\times10^{-5}) y_{\mathrm{O}}$	$\delta a_{\mathrm{R}} = (-0.001417\ \mathrm{kD}) y_{\mathrm{P}} + (3.1230\times10^{-6}\ \mathrm{kD}) y_{\mathrm{O}}$
–2 m	$\delta y_{\mathrm{R}} = (-0.03160) y_{\mathrm{P}} + (1.1058\times10^{-4}) y_{\mathrm{O}}$	$\delta a_{\mathrm{R}} = (-0.001419\ \mathrm{kD}) y_{\mathrm{P}} + (4.6845\times10^{-6}\ \mathrm{kD}) y_{\mathrm{O}}$
–0.5 m	$\delta y_{\mathrm{R}} = (-0.03193) y_{\mathrm{P}} + (4.4233\times10^{-4}) y_{\mathrm{O}}$	$\delta a_{\mathrm{R}} = (-0.001433\ \mathrm{kD}) y_{\mathrm{P}} + (1.8738\times10^{-5}\ \mathrm{kD}) y_{\mathrm{O}}$

Table 10.4.5 The chromatic difference in transverse image positions δy_{R} and inclinations δa_{R} at the retina when a pinhole is immediately in front of the reduced eye.

	Chromatic difference in transverse image positions	Chromatic difference in inclinations at the retina
Distant	$\delta y_{\mathrm{R}} = (-0.03473) y_{\mathrm{P}} + (-0.1929\ \mathrm{mm}) a_{\mathrm{K}}$	$\delta a_{\mathrm{R}} = (-0.001563\ \mathrm{kD}) y_{\mathrm{P}} + (-0.008682) a_{\mathrm{K}}$
–3 m	$\delta y_{\mathrm{R}} = (-0.03479) y_{\mathrm{P}} + (6.4307\times10^{-5}) y_{\mathrm{O}}$	$\delta a_{\mathrm{R}} = (-0.001566\ \mathrm{kD}) y_{\mathrm{P}} + (2.8938\times10^{-6}\ \mathrm{kD}) y_{\mathrm{O}}$
–2 m	$\delta y_{\mathrm{R}} = (-0.03482) y_{\mathrm{P}} + (9.6461\times10^{-5}) y_{\mathrm{O}}$	$\delta a_{\mathrm{R}} = (-0.001567\ \mathrm{kD}) y_{\mathrm{P}} + (4.3408\times10^{-6}\ \mathrm{kD}) y_{\mathrm{O}}$
–0.5 m	$\delta y_{\mathrm{R}} = (-0.03511) y_{\mathrm{P}} + (3.8584\times10^{-4}) y_{\mathrm{O}}$	$\delta a_{\mathrm{R}} = (-0.001580\ \mathrm{kD}) y_{\mathrm{P}} + (1.7363\times10^{-5}\ \mathrm{kD}) y_{\mathrm{O}}$

Table 10.4.6 The values for the chromatic difference in transverse image positions δy_{R} and inclinations δa_{R} at the retina for Le Grand's eye and the reduced eye. The object is on the longitudinal axis and the pinhole in front of the cyclopleged eye is displaced 4 mm from the optical axis.

	Chromatic difference in transverse image positions δy_{R}		Chromatic difference in inclinations δa_{R}	
	Le Grand	Reduced eye	Le Grand	Reduced eye
Distant	–0.1259 mm	–0.1389 mm	–0.005657	–0.006251
–3 m	–0.1262 mm	–0.1392 mm	–0.005670	–0.006262
–2 m	–0.1264 mm	–0.1393 mm	–0.005676	–0.006268
–0.5 m	–0.1277 mm	–0.1404 mm	–0.005732	–0.006320

The relationship obtained for the chromatic difference in inclination at the retina using a pinhole compares well with the theoretically calculated values given by Thibos *et al* (1991).

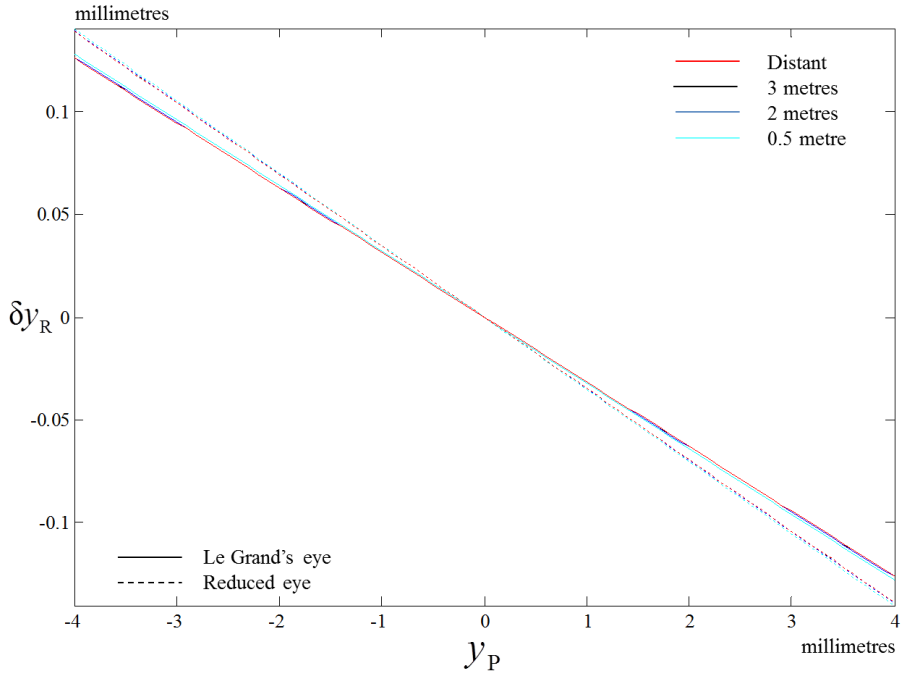

Figure 10.4.1 Chromatic difference in transverse image positions δy_R as a function of displacement of a pinhole y_P immediately in front of the eye. The red, black, blue and cyan lines appear to be superimposed for both the Le Grand and reduced eyes.

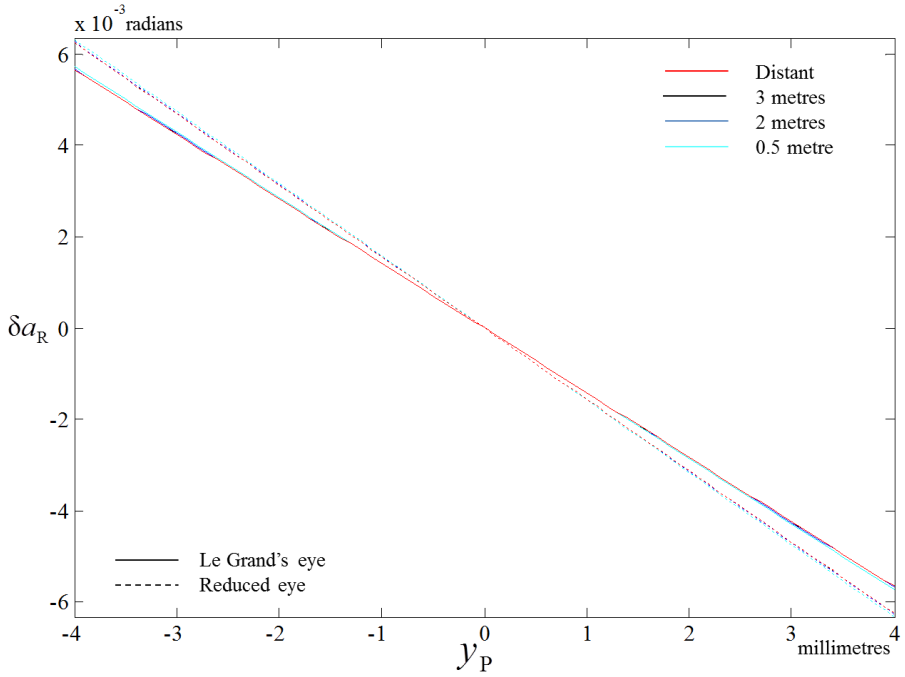

Figure 10.4.2 Chromatic difference in retinal inclinations δa_R as a function of pinhole displacement y_P in front of the eye. The red, black, blue and cyan solid lines representing Le Grand's eye appear to be superimposed and similarly, the red, black, blue and cyan dashed lines representing the reduced eye also appear superimposed.

10.4.2 Chromatic difference in image size, angular spread and chromatic magnifications: with a pinhole

The equations that define the chromatic difference in image size (Equations 7.3.4 and 8), chromatic difference in angular spread (Equations 7.3.11 and 12), retinal chromatic image size magnification (Equations 7.3.19 and 20) and retinal chromatic angular spread magnification (Equations 7.3.27 and 28) are each independent of transverse displacement in the pupil or pinhole planes. However, the longitudinal displacement of the aperture from the plane of the pupil to the plane of the pinhole immediately in front of the cornea will have an effect.

Chromatic difference in image size and angular spread – with a pinhole

The chromatic difference in image size $\delta(\Delta y_{\mathrm{R}})$ when a pinhole is placed immediately in front of the eye is summarized in Tables 10.4.7 and 8 for the two model eyes. It is obvious from Tables 10.4.7 and 8 that the chromatic difference in image sizes and angular spread $\delta(\Delta a_{\mathrm{R}})$ at the retina are all linear equations dependent on the object size.

$\delta(\Delta a_{\mathrm{R}})$ has been defined differently in this study to those definitions in the literature. We saw in Section 2.3.2 that the definitions in the literature differ by the position of the pivotal point used to measure the chromatic difference in angular spread at the retina (for example nodal point, entrance pupil, refracting surface or "cornea"), with adjustments included in the formulae for such differences in choice of pivotal point. In contrast, this study defines the actual difference in the ray inclinations at the retina. For Gaussian eyes these rays will intersect on the Gaussian plane but in astigmatic heterocentric eyes the two rays may not intersect. When comparing the results in this study for the two model eyes to the results in the literature, the results appear similar for the naked centred eye. However, it is when the pinhole is placed away from the eye that the difference in the definitions becomes apparent. This is because the actual point of intersection moves further upstream from those used in the literature. This is an important discrepancy to note. The equations for $\delta(\Delta a_{\mathrm{R}})$ suggest that the chromatic difference in ray inclinations at the retina have implications for the Stiles-Crawford effects that previous definitions have not highlighted.

Table 10.4.7 The chromatic difference in image sizes $\delta(\Delta y_{\mathrm{R}})$ and angular spread $\delta(\Delta a_{\mathrm{R}})$ at the retina when a pinhole is immediately in front of Le Grand's eye.

	Chromatic difference in image sizes at the retina	Chromatic difference in angular spread at the retina
Distant	$\delta(\Delta y_{\mathrm{R}}) = (-0.2212\ \mathrm{mm})\,\Delta a_{\mathrm{K}}$	$\delta(\Delta a_{\mathrm{R}}) = (-0.009369)\,\Delta a_{\mathrm{K}}$
–3 m	$\delta(\Delta y_{\mathrm{R}}) = (7.3721\times10^{-5})\,\Delta y_{\mathrm{O}}$	$\delta(\Delta a_{\mathrm{R}}) = (3.1230\times10^{-6}\ \mathrm{kD})\,\Delta y_{\mathrm{O}}$
–2 m	$\delta(\Delta y_{\mathrm{R}}) = (1.1058\times10^{-4})\,\Delta y_{\mathrm{O}}$	$\delta(\Delta a_{\mathrm{R}}) = (4.6845\times10^{-6}\ \mathrm{kD})\,\Delta y_{\mathrm{O}}$
–0.5 m	$\delta(\Delta y_{\mathrm{R}}) = (4.4233\times10^{-4})\,\Delta y_{\mathrm{O}}$	$\delta(\Delta a_{\mathrm{R}}) = (1.8738\times10^{-5}\ \mathrm{kD})\,\Delta y_{\mathrm{O}}$

Table 10.4.8 The chromatic difference in image size $\delta(\Delta y_{\mathrm{R}})$ and angular spread $\delta(\Delta a_{\mathrm{R}})$ at the retina when a pinhole is immediately in front of the reduced eye.

	Chromatic difference in image sizes at the retina	Chromatic difference in angular spread at the retina
Distant	$\delta(\Delta y_{\mathrm{R}}) = (-0.1929\ \mathrm{mm})\,\Delta a_{\mathrm{K}}$	$\delta(\Delta a_{\mathrm{R}}) = (-0.008682)\,\Delta a_{\mathrm{K}}$
–3 m	$\delta(\Delta y_{\mathrm{R}}) = (6.4307\times10^{-5})\,\Delta y_{\mathrm{O}}$	$\delta(\Delta a_{\mathrm{R}}) = (2.8938\times10^{-6}\ \mathrm{kD})\,\Delta y_{\mathrm{O}}$
–2 m	$\delta(\Delta y_{\mathrm{R}}) = (9.6461\times10^{-5})\,\Delta y_{\mathrm{O}}$	$\delta(\Delta a_{\mathrm{R}}) = (4.3408\times10^{-6}\ \mathrm{kD})\,\Delta y_{\mathrm{O}}$
–0.5 m	$\delta(\Delta y_{\mathrm{R}}) = (3.8584\times10^{-4})\,\Delta y_{\mathrm{O}}$	$\delta(\Delta a_{\mathrm{R}}) = (1.7363\times10^{-5}\ \mathrm{kD})\,\Delta y_{\mathrm{O}}$

Chromatic image size and angular spread magnifications - with a pinhole

The effect of replacing the pupil with a pinhole has a magnifying effect. We substitute from the respective red and blue coefficient matrices $\mathbf{V}_{\mathrm{E}}^{\mathrm{P}}$ and $\mathbf{V}_{\mathrm{OE}}^{\mathrm{P}}$ in Tables 10.4.1 and 2 into Equations 7.3.19, 20, 27 and 28. For Le Grand's eye with a pinhole the retinal chromatic image size magnification is $M_{\mathrm{yR}}^{\mathrm{P}} = 0.9868$ and the retinal chromatic angular spread magnification is $M_{\mathrm{aR}}^{\mathrm{P}} = 0.9862$ for all four illustrative distances. For the reduced eye with a pinhole the retinal chromatic image size magnification, $M_{\mathrm{yR}}^{\mathrm{P}}$ and the retinal chromatic angular spread magnification, $M_{\mathrm{aR}}^{\mathrm{P}}$ are both 0.9885 for all four illustrative distances. This equates to magnifications ranging between 1.1 and 1.4%, and compares well to the values given by Zhang *et al* (1991). These values represent an increased magnification over the naked model eyes.

10.4.3 AcuFocus Kamra corneal pinhole inlay

The AcuFocus Kamra corneal inlay was discussed in Section 7.6 and consists of an intrastromal pinhole inlay. The examples in Section 10.4 have illustrated what the effect of the corneal pinhole inlay are on the visual system. Only the chromatic difference in image position and image inclination are directly dependent on the transverse displacement of the pinhole. A misplaced pinhole inlay of only 0.5 mm can have a significant detrimental effect on the vision of the eye (Tabernero and Artal, 2011).

All the chromatic differences and chromatic magnifications in image space indirectly depend on the longitudinal shift in position of the limiting aperture from the pupillary plane to the corneal plane. Comparison of the equations in Table 10.3.9 with those in Tables 10.4.7 and 8, shows that $\delta(\Delta a_{\mathrm{R}})$ increases when a pinhole is placed at the corneal plane and that this effect is greater for Le Grand's eye than for the reduced eye. When $M_{\mathrm{yR}}^{\mathrm{P}}$ and $M_{\mathrm{aR}}^{\mathrm{P}}$ are compared with M_{yR} and M_{aR} in Tables 10.3.10 and 11 we see that both $M_{\mathrm{yR}}^{\mathrm{P}}$ and $M_{\mathrm{aR}}^{\mathrm{P}}$ increase when a pinhole is placed at the corneal plane and that these chromatic magnification effects are greater in Le Grand's eye than the reduced eye. Additionally, the results for $M_{\mathrm{yR}}^{\mathrm{P}}$ and $M_{\mathrm{aR}}^{\mathrm{P}}$ indicate that the chromatic magnification effects are greater for the retinal inclination than for retinal position. The increase in chromatic magnification will have implications for eyes that have an AcuFocus Kamra corneal pinhole inlay, something that is raised as a concern by Tabernero and Artal (2011).

The corneal pinhole inlay has an outer diameter of 3.8 mm (Seyeddain *et al*, 2010; Tabernero and Artal, 2011). Even with the best centration, a normal pupil, without pharmacological intervention, can dilate wider than the inlay. If we imagine a pencil of rays from an object point, then the effect of rays entering the eye as a full ring around the outer diameter of the inlay will be to create a rainbow-type arc forming a full circle on the retina. For a distant axial object point this will create a chromatic difference in position δy_{R} of $-0.1197\,\mathrm{mm}$ for Le Grand's eye. The red ring will be positioned outer-most and the blue ring will be

the inner-ring. The rainbow-ring will not necessarily be in focus and will be positioned in the peripheral retina.

The rainbow that we see in the sky is part of a full circular-arc, the lower part of which is hidden from view below the horizon. However, the shape of the rainbow is not a bow, but rather a cone shape, the apex of the cone being positioned at the viewer's eye (Lee and Fraser, 2001: 112-113, 322). In effect, the rainbow-ring created in the eye by the outer edge of the pinhole inlay is an image at the retina of a cone of light, with each frequency creating its own cone. The apexes of the cones are unlikely to coincide and the angle between the red and the blue cones is represented by the chromatic difference in image inclination δa_{R} and is -5.3694×10^{-3} (radians) for Le Grand's eye.

10.5 Chromatic properties of the eye dependent on image and aperture positions in object space

Chromatic properties of the eye dependent on image and aperture positions in object space mimic the set-up created in the experimental environment. They differ from the object and aperture dependent chromatic properties of the eye in image space in that the red and blue image points are directed at the same point on the retina and the chromatic separation occurs in object space. The Vernier distance between the red and blue object points is measured when the two points appear to coincide to the subject. Because the use of a pinhole to manipulate and induce transverse chromatic effects features strongly experimentally, we shall include the pinhole alternative in this section. Additionally, because experimental set-ups are conducted at finite distances the study of image- and aperture-dependent chromatic properties in object space shall be limited to finite distances.

The coefficient matrix for the chromatic properties in object space for objects at finite distances ($\mathbf{V}_{\mathrm{Oy}}$) was defined for the eye by Equation 5.3.14 and with a pinhole in front of the eye ($\mathbf{V}^{\mathrm{p}}_{\mathrm{Oy}}$) by Equation 5.3.19. Only the top row is dependent on the longitudinal distance of the object in front of the eye, z_{O}, while the bottom row is independent of object distance in front of the eye. This implies

Table 10.5.1 The red and blue coefficient matrices $\mathbf{V}_{\mathrm{Oy}}$ for image and aperture dependent chromatic properties in object space for Le Grand's eye for objects at the finite distances of 3, 2 and 0.5 metres.

		Red	Blue
$\mathbf{V}_{\mathrm{Oy}}$	–3 m	$\begin{pmatrix} 2.7172 & -179.7819 \\ -5.2871\times10^{-4}\ \mathrm{kD} & 0.05987\ \mathrm{kD} \end{pmatrix}$	$\begin{pmatrix} -3.7289 & -181.1450 \\ 1.6195\times10^{-3}\ \mathrm{kD} & 0.06032\ \mathrm{kD} \end{pmatrix}$
$\mathbf{V}_{\mathrm{Oy}}$	–2 m	$\begin{pmatrix} 2.1885 & -119.9154 \\ -5.2871\times10^{-4}\ \mathrm{kD} & 0.05987\ \mathrm{kD} \end{pmatrix}$	$\begin{pmatrix} -2.1095 & -120.8241 \\ 1.6195\times10^{-3}\ \mathrm{kD} & 0.06032\ \mathrm{kD} \end{pmatrix}$
$\mathbf{V}_{\mathrm{Oy}}$	–0.5 m	$\begin{pmatrix} 1.3954 & -30.1155 \\ -5.2871\times10^{-4}\ \mathrm{kD} & 0.05987\ \mathrm{kD} \end{pmatrix}$	$\begin{pmatrix} 0.3197 & -30.3428 \\ 1.6195\times10^{-3}\ \mathrm{kD} & 0.06032\ \mathrm{kD} \end{pmatrix}$

Table 10.5.2 The red and blue coefficient matrices for image and aperture dependent chromatic properties in object space for the reduced eye for objects at the finite distances of 3, 2 and 0.5 metres.

		Red	Blue
$\mathbf{V}_{\mathrm{Oy}}$	–3 m	$\begin{pmatrix} 2.4696 & -179.7954 \\ -4.5825\times10^{-4}\ \mathrm{kD} & 0.05990\ \mathrm{kD} \end{pmatrix}$	$\begin{pmatrix} -4.4219 & -181.2964 \\ 1.8389\times10^{-3}\ \mathrm{kD} & 0.06040\ \mathrm{kD} \end{pmatrix}$
$\mathbf{V}_{\mathrm{Oy}}$	–2 m	$\begin{pmatrix} 2.0114 & -119.8953 \\ -4.5825\times10^{-4}\ \mathrm{kD} & 0.05990\ \mathrm{kD} \end{pmatrix}$	$\begin{pmatrix} -2.5829 & -120.8959 \\ 1.8389\times10^{-3}\ \mathrm{kD} & 0.06040\ \mathrm{kD} \end{pmatrix}$
$\mathbf{V}_{\mathrm{Oy}}$	–0.5 m	$\begin{pmatrix} 1.3240 & -30.0450 \\ -4.5825\times10^{-4}\ \mathrm{kD} & 0.05990\ \mathrm{kD} \end{pmatrix}$	$\begin{pmatrix} 0.1754 & -30.2951 \\ 1.8389\times10^{-3}\ \mathrm{kD} & 0.06040\ \mathrm{kD} \end{pmatrix}$

Table 10.5.3 The chromatic difference in coefficient matrices for image and aperture dependent chromatic properties in object space for Le Grand's and the reduced eye for objects at the finite distances of 3, 2 and 0.5 metres.

		Le Grand's eye	Reduced eye
$\delta\mathbf{V}_{\mathrm{Oy}}$	–3 m	$\begin{pmatrix} -6.4461 & -1.3630 \\ 2.1482\times10^{-3}\ \mathrm{kD} & 4.5429\times10^{-4}\ \mathrm{kD} \end{pmatrix}$	$\begin{pmatrix} -6.8915 & -1.5010 \\ 2.2972\times10^{-3}\ \mathrm{kD} & 5.0032\times10^{-4}\ \mathrm{kD} \end{pmatrix}$
$\delta\mathbf{V}_{\mathrm{Oy}}$	–2 m	$\begin{pmatrix} -4.2980 & -0.9087 \\ 2.1482\times10^{-3}\ \mathrm{kD} & 4.5429\times10^{-4}\ \mathrm{kD} \end{pmatrix}$	$\begin{pmatrix} -4.5943 & -1.0006 \\ 2.2972\times10^{-3}\ \mathrm{kD} & 5.0032\times10^{-4}\ \mathrm{kD} \end{pmatrix}$
$\delta\mathbf{V}_{\mathrm{Oy}}$	–0.5 m	$\begin{pmatrix} -1.0757 & -0.2273 \\ 2.1482\times10^{-3}\ \mathrm{kD} & 4.5429\times10^{-4}\ \mathrm{kD} \end{pmatrix}$	$\begin{pmatrix} -1.1486 & -0.2502 \\ 2.2972\times10^{-3}\ \mathrm{kD} & 5.0032\times10^{-4}\ \mathrm{kD} \end{pmatrix}$

that the chromatic difference in inclination, δa_{O} (Equation 7.4.6) will be independent of z_{O}.

The red and blue coefficient matrices, $\mathbf{V}_{\mathrm{Oy}}$ for Le Grand's eye are given in Table 10.5.1 and for the reduced eye in Table 10.5.2. The chromatic difference in coefficient matrices $\delta\mathbf{V}_{\mathrm{Oy}}$ is given in Table 10.5.3 for both eyes.

10.5.1 Chromatic difference in object position

The chromatic difference in object position δy_{O} measures the difference in the transverse position from the red object point to the blue object point when the two coloured image points are superimposed on the retina and appear to the subject as a single dichromatic image. The position on the retina y_{R} can be manipulated and may be on the fovea, or some chosen point in the peripheral retina. For model eyes, the fovea is often assumed to be coincidental with the optical axis, thus nullifying the visio-optical angle (angle alpha).

We substitute the relevant entries from $\delta\mathbf{V}_{\mathrm{Oy}}$ in Table 10.5.3 into Equation 7.4.1 to obtain δy_{O} for three illustrative distances of the object from Le Grand's eye. These are given in Table 10.5.4. If we assume that the pupil is centred on the longitudinal axis, then δy_{O} is dependent on the position chosen for the image point to reach the retina, y_{R}. If this is the fovea, then δy_{O} is dependent on the visio-optical angle, the angle between the visual and optical axes (Atchison and Smith, 2000: 30-35; Rabbetts, 2007: 234-235). Because the fovea is static, one obtains a single value for the chosen longitudinal object distance in front of the eye.

If, for example, we assume that the eye is centred $y_{\mathrm{P}} = 0\,\mathrm{mm}$ and that the fovea is 5° from the optical axis, then this equates to an approximate distance of 1.46 mm at the retina for a model eye. Substituting these two illustrative values into the equations in Table 10.5.4, we obtain a chromatic difference in object position, summarized for Le Grand's eye in the right-hand column of Table 10.5.4 and for the reduced eye, the equations and numerical illustrative values are summarized in Table 10.5.5 .

Table 10.5.4 The equations for the chromatic difference in object position δy_O for Le Grand's eye for objects at the finite distances of –3, –2 and –0.5 m. The illustrative values are for a centred reduced eye with transverse retinal displacement of 1.46 mm.

	Chromatic difference in object position	Illustrative values
–3 m	$\delta y_O = (-6.4462)y_P + (-1.3630)y_R$	–1.9900 mm
–2 m	$\delta y_O = (-4.2980)y_P + (-0.9087)y_R$	–1.3267 mm
–0.5 m	$\delta y_O = (-1.0757)y_P + (-0.2273)y_R$	–0.3318 mm

Table 10.5.5 The equations for the chromatic difference in object position δy_O for the reduced eye for objects at the finite distances of –3, –2 and –0.5 m. The illustrative values are for a centred reduced eye with transverse retinal displacement of 1.46 mm.

	Chromatic difference in object position	Illustrative values
–3 m	$\delta y_O = (-6.8915)y_P + (-1.5010)y_R$	–2.1914 mm
–2 m	$\delta y_O = (-4.5943)y_P + (-1.0006)y_R$	–1.4609 mm
–0.5 m	$\delta y_O = (-1.1486)y_P + (-0.02502)y_R$	–0.3652 mm

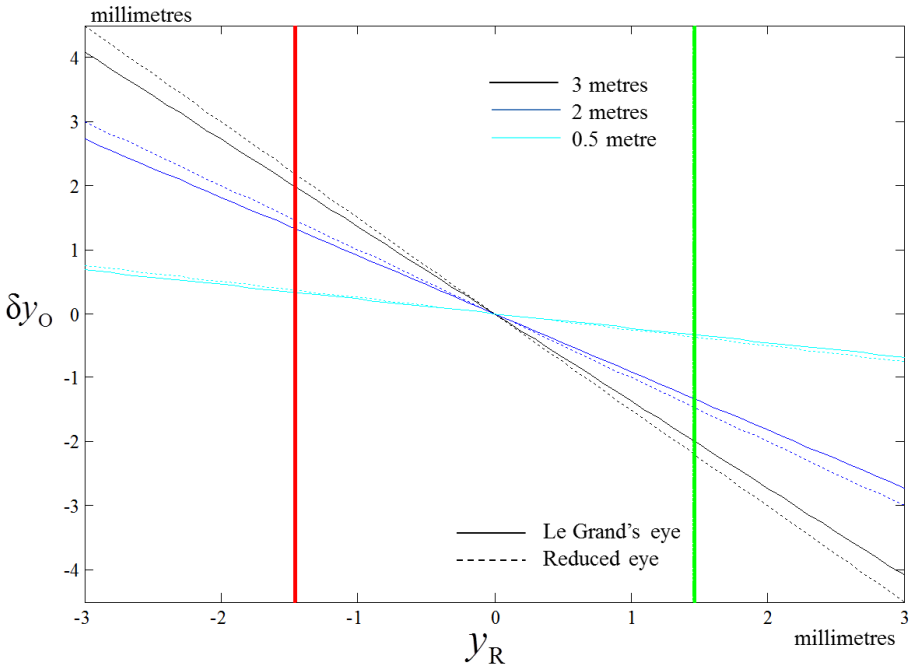

Figure 10.5.1 Chromatic difference in object position δy_O is shown for illustrative working distances of –3 m, –2 m and –0.5 m from the eye. The red and blue images are superimposed at the retina at a chosen position, y_R, with foveal positions shown by the red and green vertical lines for the right and left eyes, respectively.

The chromatic difference in object position δy_O is the Vernier separation from the red object point to the blue object point at illustrative working distances of –3 m, –2 m and –0.5 m. This is indicated in Figure 10.5.1. The red and blue images are superimposed at the retina at a chosen position, y_R. In Figure 10.5.1, the red vertical line indicates the foveal position of the right eye $y_R = -1.46$ mm and the green line indicates the foveal position of the left eye $y_R = 1.46$ mm.

10.5.2 Chromatic difference in inclination in object space

The chromatic difference in inclination in object space δa_O is the angle subtended by the incident rays from the red and blue object points which, after both traversing the same position through the pupil, both reach the retina at the same position so as to appear superimposed to the viewer. The chromatic difference in inclination in object space δa_O utilises the bottom row of $\mathbf{V}_{Oy}$ which

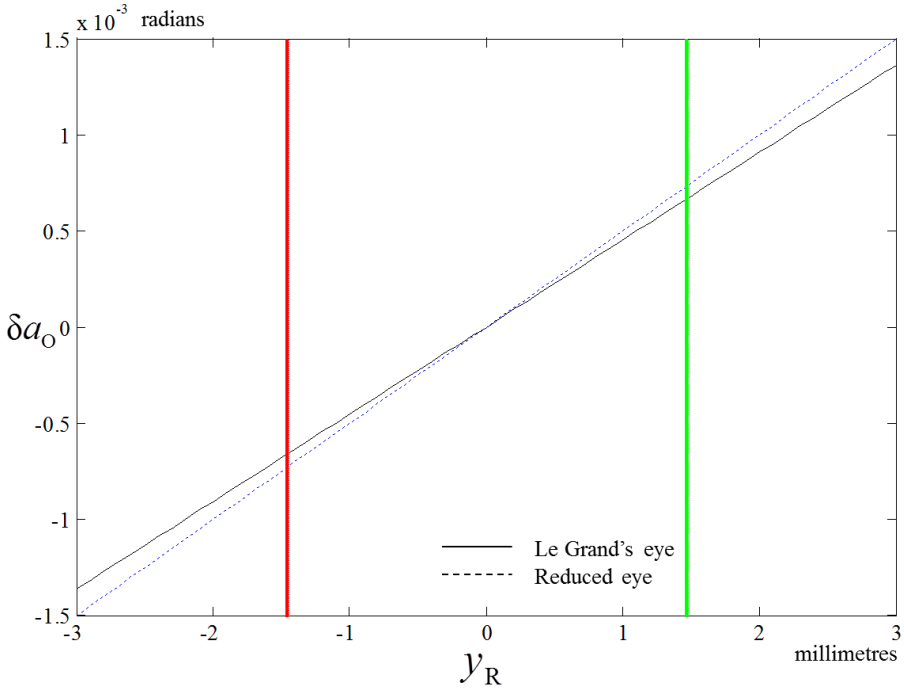

Figure 10.5.2 Chromatic difference in inclination in object space δa_O for Le Grand's eye and the reduced eye as a function of retinal position. δa_O is independent of working distance.

is independent of z_{O}. Substituting the relevant entries from $\mathbf{V}_{\mathrm{Oy}}$ into Equation 7.4.6 we obtain

$$\delta a_{\mathrm{O}} = \left(2.1482\times10^{-3}\ \mathrm{kD}\right) y_{\mathrm{P}} + \left(4.5429\times10^{-4}\ \mathrm{kD}\right) y_{\mathrm{R}} \qquad (10.5.1)$$

for Le Grand's eye and

$$\delta a_{\mathrm{O}} = \left(2.2972\times10^{-3}\ \mathrm{kD}\right) y_{\mathrm{P}} + \left(5.0032\times10^{-4}\ \mathrm{kD}\right) y_{\mathrm{R}} \qquad (10.5.2)$$

for the reduced eye. If we substitute the illustrative values of $y_{\mathrm{P}} = 0$ for a centred system and $y_{\mathrm{R}} = 1.46\ \mathrm{mm}$ for the position of the fovea, then we obtain a chromatic difference in inclination in object space of $\delta a_{\mathrm{O}} = 6.6327\times10^{-4}$ for Le Grand's eye and 7.3047×10^{-4} for the reduced eye.

Figure 10.5.2 illustrates the relationship of δa_{O} as a function of position of the rays reaching the retina. The red vertical line indicates the position of the fovea of the right eye, and the green line indicates the position of the left fovea in schematic eyes that have a 5º visio-optical angle.

10.5.3 Chromatic difference in object size

The results for the chromatic difference in object size $\delta\left(\Delta y_{\mathrm{O}}\right)$ are similar to those in Section 10.5.1 and are given in Table 10.5.6. The relationships are all linear. One can think of the δX_{Oy} as having a magnifying effect on the image size to obtain the chromatic difference in object size.

Table 10.5.6 Chromatic difference in object size for Le Grand's eye and the reduced eye for the three illustrative working distances.

	Le Grand's eye	Reduced eye
–3 m	$\delta(\Delta y_{\mathrm{O}}) = -1.3630\,\Delta y_{\mathrm{R}}$	$\delta(\Delta y_{\mathrm{O}}) = -1.5010\,\Delta y_{\mathrm{R}}$
–2 m	$\delta(\Delta y_{\mathrm{O}}) = -0.9087\,\Delta y_{\mathrm{R}}$	$\delta(\Delta y_{\mathrm{O}}) = -1.0006\,\Delta y_{\mathrm{R}}$
–0.5 m	$\delta(\Delta y_{\mathrm{O}}) = -0.2273\,\Delta y_{\mathrm{R}}$	$\delta(\Delta y_{\mathrm{O}}) = -0.2502\,\Delta y_{\mathrm{R}}$

10.5.4 Chromatic difference in object angular spread

The numerical results for chromatic difference in object angular spread $\delta(\Delta a_{\mathrm{O}})$ are similar to those in Section 10.5.2 for the illustrative examples and are therefore given in Table 10.5.7. Again, the relationships are all linear and because δZ_{Oy} is independent of working distance, we obtain one relationship for each of Le Grand's and the reduced eyes.

Table 10.5.7 Chromatic difference in object angular spread for Le Grand's eye and the reduced eye for the three illustrative working distances.

Le Grand's eye	Reduced eye
$\delta(\Delta a_{\mathrm{O}}) = (4.5429\times10^{-4}\ \mathrm{kD})\,\Delta y_{\mathrm{R}}$	$\delta(\Delta a_{\mathrm{O}}) = (5.0032\times10^{-4}\ \mathrm{kD})\,\Delta y_{\mathrm{R}}$

10.5.5 Chromatic magnification in object space

Le Grand's eye

The chromatic object size magnification M_{yO} (Equation 7.5.15) defines the magnification of the size of the red to blue objects. M_{yO} is 1.0076 for objects at –3 and –2 m and 1.0075 for an object at –0.5m from the eye. The chromatic object angular spread magnification M_{aO} (Equation 7.5.18) defines the magnification of the angular spread subtended by the red object to the angular spread of the blue object where both images appear to be the same size at the retina and is 1.0076. Because the bottom row of $\mathbf{V}_{\mathrm{aO}}$ is independent of z_{O}, M_{aO} is independent of object distance. These both equate to 0.75% magnification where the blue object is larger than the red object. That is $\Delta y_{\mathrm{O}}^{\mathrm{b}} > \Delta y_{\mathrm{O}}^{\mathrm{r}}$ from Equation 7.5.13 and $\Delta a_{\mathrm{O}}^{\mathrm{b}} > \Delta a_{\mathrm{O}}^{\mathrm{r}}$ from Equation 7.5.16.

The reduced eye

For the reduced eye, M_{yO} is 1.0083 for all three illustrative distances and M_{aO} is 1.0084. These equate to 0.83% and 0.84% with the blue object larger than the red object.

10.6 Chromatic properties of the eye dependent on image and aperture positions in object space: with a pinhole

Experimental measurements in object space, as seen in Chapter 2, include the effect of placing a pinhole immediately in front of the eye. The coefficient matrix, $\mathbf{V}_{\mathrm{Oy}}^{\mathrm{P}}$ simplifies to Equation 5.3.19 and is given in Tables 10.6.1 and 2 for Le Grand's eye and the reduced eye respectively. The chromatic difference of the coefficient matrices $\delta\mathbf{V}_{\mathrm{Oy}}^{\mathrm{P}}$ is summarised in Table 10.6.3.

10.6.1 Chromatic difference in object positions: with a pinhole

The chromatic difference in object positions δy_{O} is dependent on image y_{R} and aperture positions y_{P}. The effect of change in aperture position on δy_{O} is direct with respect to y_{P} and indirect in that the longitudinal displacement from the pupil to the corneal plane is incorporated in $\mathbf{V}_{\mathrm{Oy}}^{\mathrm{P}}$. Because the coefficient matrices for the eye with the pinhole $\mathbf{V}_{\mathrm{Oy}}^{\mathrm{P}}$ and measurements in object space are derived from the coefficient matrix for the chromatic properties in object space $\mathbf{V}_{\mathrm{Oy}}$, the bottom row is again independent of z_{O}. The equations for δy_{O} for the three illustrative distances of the object in front of the eye are given in Tables 10.6.4 and 5 for Le Grand's eye and the reduced eye respectively. In the right-hand column of each table is the illustrative value calculated by a 4mm displacement of the pinhole immediately in front of the cyclopleged eye $\left(y_{\mathrm{P}} = 4\ \mathrm{mm}\right)$ and assuming that the image points are both directed at the same point on the retina. The illustrative values are given for an eye with, firstly, the fovea centred on the longitudinal axis $y_{\mathrm{R}} = 0\ \mathrm{mm}$ and, secondly, with the fovea positioned at 1.46 mm to approximate a visio-optical angle of 5°.

Table 10.6.1 The red and blue coefficient matrices for chromatic properties of Le Grand's eye in object space dependent on image and aperture positions for objects at the finite distances of 3, 2 and 0.5 metres, with a pinhole placed immediately in front of the eye.

		Red	Blue
$\mathbf{V}^{\mathrm{P}}_{\mathrm{Oy}}$	–3 m	$\begin{pmatrix} 2.4023 & -179.3441 \\ -4.6744\times10^{-4}\ \mathrm{kD} & 0.05978\ \mathrm{kD} \end{pmatrix}$	$\begin{pmatrix} -3.3015 & -181.7471 \\ 1.4338\times10^{-3}\ \mathrm{kD} & 0.06058\ \mathrm{kD} \end{pmatrix}$
$\mathbf{V}^{\mathrm{P}}_{\mathrm{Oy}}$	–2 m	$\begin{pmatrix} 1.9349 & -119.5628 \\ -4.6744\times10^{-4}\ \mathrm{kD} & 0.05978\ \mathrm{kD} \end{pmatrix}$	$\begin{pmatrix} -1.8677 & -121.1647 \\ 1.4338\times10^{-3}\ \mathrm{kD} & 0.06058\ \mathrm{kD} \end{pmatrix}$
$\mathbf{V}^{\mathrm{P}}_{\mathrm{Oy}}$	–0.5 m	$\begin{pmatrix} 1.2337 & -29.89072 \\ -4.6744\times10^{-4}\ \mathrm{kD} & 0.05978\ \mathrm{kD} \end{pmatrix}$	$\begin{pmatrix} 0.2831 & -30.2912 \\ 1.4338\times10^{-3}\ \mathrm{kD} & 0.06058\ \mathrm{kD} \end{pmatrix}$

Table 10.6.2 The red and blue coefficient matrices for chromatic properties of the reduced eye in object space dependent on image and aperture positions for objects at the finite distances of 3, 2 and 0.5 metres, with a pinhole placed immediately in front of the eye.

		Red	Blue
$\mathbf{V}^{\mathrm{P}}_{\mathrm{Oy}}$	–3 m	$\begin{pmatrix} 2.2556 & -179.5815 \\ -4.1855\times10^{-4}\ \mathrm{kD} & 0.05986\ \mathrm{kD} \end{pmatrix}$	$\begin{pmatrix} -4.0387 & -181.6796 \\ 1.6796\times10^{-3}\ \mathrm{kD} & 0.06056\ \mathrm{kD} \end{pmatrix}$
$\mathbf{V}^{\mathrm{P}}_{\mathrm{Oy}}$	–2 m	$\begin{pmatrix} 1.8371 & -119.7210 \\ -4.1855\times10^{-4}\ \mathrm{kD} & 0.05986\ \mathrm{kD} \end{pmatrix}$	$\begin{pmatrix} -2.3591 & -121.1197 \\ 1.6796\times10^{-3}\ \mathrm{kD} & 0.06056\ \mathrm{kD} \end{pmatrix}$
$\mathbf{V}^{\mathrm{P}}_{\mathrm{Oy}}$	–0.5 m	$\begin{pmatrix} 1.2093 & -29.9302 \\ -4.1855\times10^{-4}\ \mathrm{kD} & 0.05986\ \mathrm{kD} \end{pmatrix}$	$\begin{pmatrix} 0.1602 & -30.2799 \\ 1.6796\times10^{-3}\ \mathrm{kD} & 0.06056\ \mathrm{kD} \end{pmatrix}$

Table 10.6.3 The chromatic difference in coefficient matrices for chromatic properties of the eye in object space dependent on image and aperture positions for Le Grand's and the reduced eye for objects at the finite distances of 3, 2 and 0.5 metres, with a pinhole placed immediately in front of the eye.

		Le Grand's eye	Reduced eye
$\delta\mathbf{V}^{\mathrm{P}}_{\mathrm{Oy}}$	–3 m	$\begin{pmatrix} -5.7038 & -2.4030 \\ 1.9013\times10^{-3}\ \mathrm{kD} & 8.0099\times10^{-4}\ \mathrm{kD} \end{pmatrix}$	$\begin{pmatrix} -6.2943 & -2.0981 \\ 2.0981\times10^{-3}\ \mathrm{kD} & 6.9937\times10^{-4}\ \mathrm{kD} \end{pmatrix}$
$\delta\mathbf{V}^{\mathrm{P}}_{\mathrm{Oy}}$	–2 m	$\begin{pmatrix} -3.8025 & -1.6020 \\ 1.9013\times10^{-3}\ \mathrm{kD} & 8.0099\times10^{-4}\ \mathrm{kD} \end{pmatrix}$	$\begin{pmatrix} -4.1962 & -1.3987 \\ 2.0981\times10^{-3}\ \mathrm{kD} & 6.9937\times10^{-4}\ \mathrm{kD} \end{pmatrix}$
$\delta\mathbf{V}^{\mathrm{P}}_{\mathrm{Oy}}$	–0.5 m	$\begin{pmatrix} -0.9506 & -0.4005 \\ 1.9013\times10^{-3}\ \mathrm{kD} & 8.0099\times10^{-4}\ \mathrm{kD} \end{pmatrix}$	$\begin{pmatrix} -1.0491 & -0.3497 \\ 2.0981\times10^{-3}\ \mathrm{kD} & 6.9937\times10^{-4}\ \mathrm{kD} \end{pmatrix}$

Table 10.6.4 The equations for the chromatic difference in object position δy_O for Le Grand's eye for objects at the finite distances of –3, –2 and –0.5 m from the eye and pinhole displaced by $y_P = 4$ mm.

	Chromatic difference in object position	Illustrative values	
		$y_R = 0$ mm	$y_R = 1.46$ mm
–3 m	$\delta y_O = (-5.7038)y_P + (-2.4030)y_R$	–22.8153 mm	–26.3236 mm
–2 m	$\delta y_O = (-3.8025)y_P + (-1.6020)y_R$	–15.2102 mm	–17.5491 mm
–0.5 m	$\delta y_O = (-0.9506)y_P + (-0.4005)y_R$	–3.8025 mm	–4.3873 mm

Table 10.6.5 The equations for δy_O for the reduced eye for objects at the finite distances of –3, –2 and –0.5 m from the eye. The illustrative values are for an eye with $y_P = 4$ mm and $y_R = 0$ mm or $y_R = 1.46$ mm.

	Chromatic difference in object position	Illustrative values	
		$y_R = 0$ mm	$y_R = 1.46$ mm
–3 m	$\delta y_O = (-6.2943)y_P + (-2.0981)y_R$	–25.1773 mm	–28.2406 mm
–2 m	$\delta y_O = (-4.1962)y_P + (-1.3987)y_R$	–16.7849 mm	–18.8271 mm
–0.5 m	$\delta y_O = (-1.0491)y_P + (-0.3497)y_R$	–4.1962 mm	–4.7068 mm

Figure 10.6.1 gives δy_O as a function of pinhole displacement at the corneal plane for the three illustrative distances from the eye. The image is superimpose on the retina at $y_R = 0$ mm. Not only does δy_O increase as the object points move further away from the eye, but the magnitudes of the illustrative values using a pinhole are greater than those for the eye without the pinhole, given in Section 10.5.1.

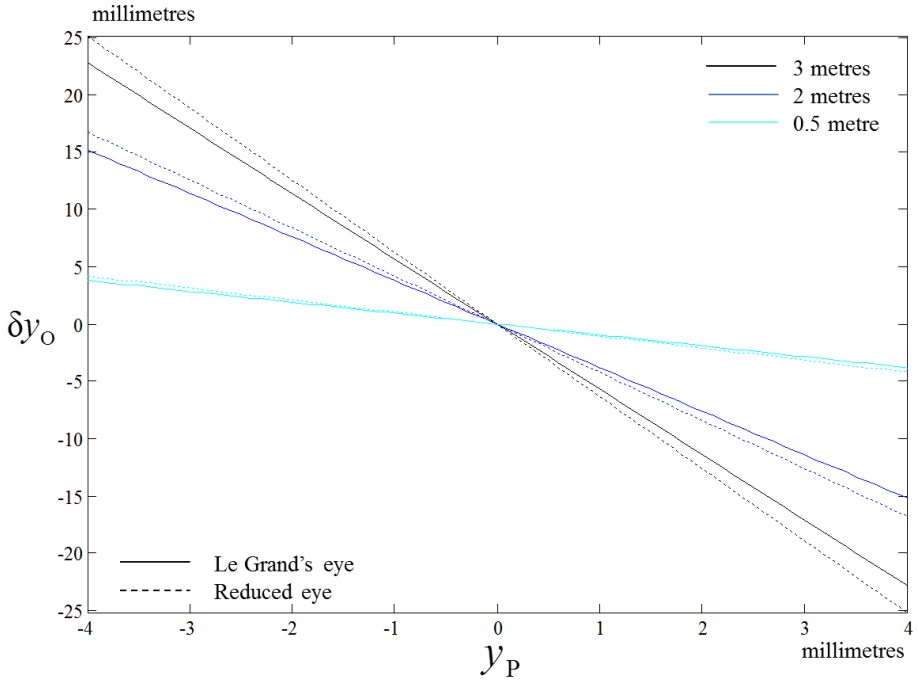

Figure 10.6.1 Chromatic difference in object positions δy_O between the red and blue object points as a function of transverse displacement of the pinhole y_P at three illustrative object distances from the eye, –3 m in black, –2 m in blue and –0.5 m in cyan.

10.6.2 Chromatic difference in inclination in object space: with a pinhole

The chromatic difference in inclination in object space δa_O is dependent on image and aperture positions. δa_O is independent of z_O and therefore we obtain one equation for each model eye. The chromatic difference in inclination in object space is

$$\delta a_O = \left(1.9013\times10^{-3}\ \text{kD}\right)y_P + \left(8.0099\times10^{-4}\ \text{kD}\right)y_R \qquad (10.6.1)$$

for Le Grand's eye and

$$\delta a_O = \left(2.0981\times10^{-3}\ \text{kD}\right)y_P + \left(6.9937\times10^{-4}\ \text{kD}\right)y_R \qquad (10.6.2)$$

for the reduced eye. For the illustrative situation of $y_P = 4\,\text{mm}$ combined with firstly $y_R = 0\,\text{mm}$, then $y_R = 1.46\,\text{mm}$, the chromatic difference in inclination in object space is 7.6051×10^{-3} and 8.7745×10^{-3} respectively for Le Grand's eye and 8.3924×10^{-3} and 9.4135×10^{-3} respectively for the reduced eye. From Equations 10.6.1 and 2 we can see that δa_O is linearly dependent on y_P. For any particular constant distance of the object points from the eye, y_P is "magnified"

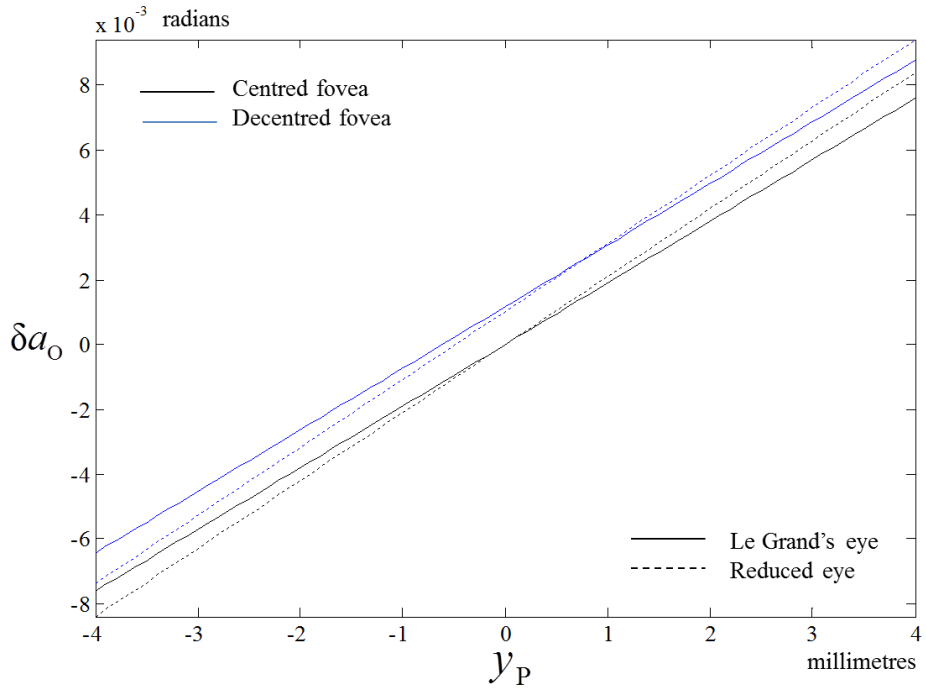

Figure10.6.2 The chromatic difference in inclination in object space δa_{O} as a function of transverse pinhole displacement y_{P} for Le Grand's eye (solid lines) and the reduced eye (dashed lines). The black lines represent the variation in inclination when the fovea is centred on the optical axis $y_{\mathrm{R}} = 0$ and the blue lines represent the fovea some 1.46 mm from the optical axis; that is at $y_{\mathrm{R}} = 1.46\ \mathrm{mm}$ (left eye).

by a constant, δY_{Oy}, the chromatic difference in the near directional spread coefficient and the slope of the line in Figure 10.6.2. If the red and blue image points are superimposed on the fovea, that is to say $y_{\mathrm{R}} = 1.46\ \mathrm{mm}$, then this will merely add a fixed value to the chromatic difference in object inclination which will still vary by y_{P}. This is illustrated graphically in Figure 10.6.2 by the blue lines. Similarly, any point in the peripheral retina can be chosen such that $y_{\mathrm{R}} \neq 0$.

10.6.3 Chromatic difference in object size: with a pinhole

From Equation 7.5.6, we can see that when a pinhole is placed in front of the eye the effect of any transverse displacement is nullified. The only change will be that created by the longitudinal displacement of the pinhole, that is, from the plane of the pupil to the plane immediately in front of the cornea. The effect of

Table 10.6.6 The chromatic difference in object size for the three illustrative distances for Le Grand's eye and the Reduced eye.

	Le Grand's eye	Reduced eye
–3 m	$\delta(\Delta y_{\mathrm{O}}) = -2.4030\ \Delta y_{\mathrm{R}}$	$\delta(\Delta y_{\mathrm{O}}) = -2.0981\ \Delta y_{\mathrm{R}}$
–2 m	$\delta(\Delta y_{\mathrm{O}}) = -1.6020\ \Delta y_{\mathrm{R}}$	$\delta(\Delta y_{\mathrm{O}}) = -1.3987\ \Delta y_{\mathrm{R}}$
–0.5 m	$\delta(\Delta y_{\mathrm{O}}) = -0.4005\ \Delta y_{\mathrm{R}}$	$\delta(\Delta y_{\mathrm{O}}) = -0.3497\ \Delta y_{\mathrm{R}}$

$\delta X_{\mathrm{Oy}}^{\mathrm{P}}$ is to magnify the image size Δy_{R} to obtain the chromatic difference in object size. This is summarized in Table 10.6.6 for the three working distances.

10.6.4 Chromatic difference in object angular spread: with a pinhole

From Equation 7.5.9 we can see that the chromatic difference in object angular spread is also independent of any transverse displacement of the pinhole y_{P}, and the magnification $\delta Z_{\mathrm{Oy}}^{\mathrm{P}}$ differs from δZ_{Oy} for the chromatic difference in object inclination $\delta(\Delta a_{\mathrm{O}})$ due to the longitudinal displacement of the limiting aperture from the pupil to the pinhole plane. Additionally, the bottom row of $\mathbf{V}_{\mathrm{Oy}}^{\mathrm{P}}$ is independent of z_{O} and therefore the chromatic difference in object angular spread $\delta(\Delta a_{\mathrm{O}})$ with a pinhole is also independent of the distance of the object from the eye. $\delta(\Delta a_{\mathrm{O}})$ is given in Table 10.6.7 for the two schematic eyes. When we compare the values for $\delta Z_{\mathrm{Oy}}^{\mathrm{P}}$ in Table 10.6.7 to those for δZ_{Oy} in Table 10.5.7, we see that introducing a pinhole immediately in front of the eye has a magnifying effect. This is more pronounced in Le Grand's eye than for the reduced eye.

Table 10.6.7 The chromatic difference in angular spread for Le Grand's eye and the reduced eye.

Le Grand's eye	Reduced eye
$\delta(\Delta a_{\mathrm{O}}) = (8.0099\times10^{-4}\ \mathrm{kD})\Delta y_{\mathrm{R}}$	$\delta(\Delta a_{\mathrm{O}}) = (6.9937\times10^{-4}\ \mathrm{kD})\Delta y_{\mathrm{R}}$

10.6.5 Chromatic object magnification: with a pinhole

Chromatic object size magnification

In Section 7.5.3 we obtained the chromatic object size magnification M_{yO} (Equation 7.5.15). When a pinhole is placed immediately in front of the eye, we substitute values for $X_{\mathrm{Oy}}^{\mathrm{P}}$ instead of X_{Oy} into Equation 7.5.15. Both M_{yO} and hence $M_{\mathrm{yO}}^{\mathrm{P}}$ are independent of the transverse position of the pinhole, and $M_{\mathrm{yO}}^{\mathrm{P}}$ is influenced only by the longitudinal displacement of the limiting aperture. For Le Grand's eye $M_{\mathrm{yO}}^{\mathrm{P}}$ is 1.0134 and for the reduced eye $M_{\mathrm{yO}}^{\mathrm{P}}$ is 1.0117. Comparing this to the results obtained without the pinhole, the chromatic magnification has increased from 0.75% to 1.3% and 1.2% respectively, nearly double.

Chromatic object angular spread magnification

The chromatic object angular spread magnification with a pinhole immediately in front of the eye $M_{\mathrm{aO}}^{\mathrm{P}}$ is obtained from Equation 7.5.18, substituting values for $Z_{\mathrm{Oy}}^{\mathrm{P}}$. $M_{\mathrm{aO}}^{\mathrm{P}}$, like M_{aO} is independent of any transverse displacement of the pinhole and any magnification is obtained by placing the pinhole in front of the eye, effectively moving the limiting aperture form the pupillary plane to the corneal plane. For Le Grand's eye $M_{\mathrm{aO}}^{\mathrm{P}}$ is 1.0134 and for the reduced eye we have 1.0117, exactly the same results as for $M_{\mathrm{yO}}^{\mathrm{P}}$. The blue object is larger than the red object, that is, $\Delta y_{\mathrm{O}}^{\mathrm{b}} > \Delta y_{\mathrm{O}}^{\mathrm{r}}$ from Equation 7.5.13 and $\Delta a_{\mathrm{O}}^{\mathrm{b}} > \Delta a_{\mathrm{O}}^{\mathrm{r}}$ from Equation 7.5.16.

10.7 Underlying implications

There are two underlying implications which do not appear to be addressed in the literature. Firstly, a chromatic difference in incident position occurs when measuring chromatic difference in position at the retina. The effect is null when a pinhole is introduced in front of the eye. Secondly, there is a chromatic difference in inclination at the retina when measuring the chromatic difference in object positions or inclinations. This effect is null for the reduced

eye. The effects are small and only apparent in eyes with more than one refracting surface and hence, real eyes.

10.7.1 Chromatic difference in incident position

In Section 7.2.2 we defined chromatic difference in image positions at the retina when a pencil of rays is incident at the cornea with inclination a_{K}. We noted that while the red and blue rays both traverse the same transverse position through the pupil, y_{P}, this does not necessarily mean that the red and blue rays originate from the same dichromatic ray that is incident on the eye or cornea. Instead, there are separate red and blue rays, each with incident inclination a_{K} which are refracted and traced through the same position through the limiting aperture y_{P}. This is illustrated in Figure 7.2.1 where we see separate red and blue rays intersecting the cornea, separated by distance δy_{K} and then traversing the pupil through the same point, but with different inclinations.

Equation 7.2.9 enables us to calculate the chromatic difference in corneal position δy_{K}, incident onto the eye, of the red and blue rays from a distance object and Equation 7.2.10 likewise calculates the chromatic difference in incident position δy_{K} for rays originating from an object at a finite distance. Substituting from the red and blue transferences for the anterior and posterior subsystems and the transference for the eye, we obtain a relationship for Le Grand's eye, given in Table 10.7.1. The chromatic difference of incident position δy_{K} is given as an illustrative example for a centred model eye $y_{\mathrm{P}} = 0$ with incident inclination of $a_{\mathrm{K}} = 0.1$, in Table 10.7.1. $\delta y_{\mathrm{K}} = 0.02061\,\mathrm{mm}$ represents a distance of more than 5 000 times the wavelength of the blue ray or almost 3 000 times the wavelength of the red ray.

For the reduced eye with a pupil the equivalent equation for the chromatic difference of incident position δy_{K} for a distant object is given as a relationship in Table 10.7.2. The illustrative value for the reduced eye is also given in Table 10.7.2 for an example where $y_{\mathrm{P}} = 0$ and $a_{\mathrm{K}} = 0.1$.

Table 10.7.1 The chromatic difference in incident position for Le Grand's eye for an object point positioned –3 m, –2 m and –0.5 m from the eye and illustrated with $y_{\mathrm{O}} = 200\ \mathrm{mm}$ and $y_{\mathrm{P}} = 0\ \mathrm{mm}$.

Distance from eye	Chromatic difference in incident position	Illustrative value
Distant object	$\delta y_K = (0.02061\ \mathrm{mm})a_{\mathrm{K}} + 0.004887\, y_{\mathrm{P}}$	0.002061 mm
–3 m	$\delta y_K = -6.8576\times10^{-6}\, y_{\mathrm{O}} - 0.004890\, y_{\mathrm{P}}$	–0.001372 mm
–2 m	$\delta y_K = -1.0276\times10^{-5}\, y_{\mathrm{O}} - 0.004891\, y_{\mathrm{P}}$	–0.002055 mm
–0.5 m	$\delta y_K = -4.0733\times10^{-5}\, y_{\mathrm{O}} - 0.004904\, y_{\mathrm{P}}$	–0.008147 mm

Table 10.7.2 The chromatic difference in incident position for the reduced eye for an object point positioned –3 m, –2 m and –0.5 m from the eye and illustrated with $y_{\mathrm{O}} = 200\ \mathrm{mm}$ and $y_{\mathrm{P}} = 0\ \mathrm{mm}$.

Distance from eye	Chromatic difference in incident position	Illustrative value
Distant object	$\delta y_K = (0.01312\ \mathrm{mm})a_{\mathrm{K}} + 0.003614\, y_{\mathrm{P}}$	0.001312 mm
–3 m	$\delta y_K = -4.3685\times10^{-6}\, y_{\mathrm{O}} - 0.003617\, y_{\mathrm{P}}$	-8.7370×10^{-4} mm
–2 m	$\delta y_K = -6.5493\times10^{-6}\, y_{\mathrm{O}} - 0.003618\, y_{\mathrm{P}}$	–0.001310 mm
–0.5 m	$\delta y_K = -2.6074\times10^{-5}\, y_{\mathrm{O}} - 0.003631\, y_{\mathrm{P}}$	–0.005215mm

For an object at a finite distance, we summarize the three illustrative distances of the object from the eye in Table 10.7.1 for Le Grand's eye and Table 10.7.2 for the reduced eye. The illustrative values are given for an object point that is placed $y_{\mathrm{O}} = 200\ \mathrm{mm}$ above the longitudinal axis and assuming that the eye is centred.

Chromatic difference in incident position with pinhole

When a pinhole is placed in front of the eye the chief ray is the ray traversing the centre of the pinhole, which is placed immediately in front of the eye. Equations 7.2.9 and 10 both simplify to $\delta y_K = (0\ \mathrm{mm})$ and, as expected, there is no chromatic difference in incident position present when a pinhole is placed in front of either model eye.

10.7.2 Chromatic difference in emergent inclination from object space

Equation 7.4.13 was derived to calculate the chromatic difference in inclination of the two rays that traverse, from separated object points through the same position in the pupil or pinhole and arrive at the retina at the same position, that is to say $y_{\mathrm{R}}^{\mathrm{r}} = y_{\mathrm{R}}^{\mathrm{b}}$. For convenience, the chief rays are usually chosen. However, Equation 7.4.13 shows that the two rays are refracted differently and do indeed follow different paths through the system. Although the red and blue rays, by definition, are chosen to both traverse the same position through the aperture, they may not necessarily traverse through this aperture with the same inclination and will not arrive at the retina with the same inclination. This is illustrated in Figure 7.4.1 and has implications for the Stiles-Crawford effects. For Le Grand's eye, the chromatic difference in inclination at the retina will be

$$\delta a_{\mathrm{R}} = \left(-8.2635\times10^{-5}\ \mathrm{kD}\right)y_{\mathrm{P}} + \left(7.3139\times10^{-6}\ \mathrm{kD}\right)y_{\mathrm{R}} \qquad (10.7.1)$$

which is independent of the distance of the object in front of the eye. For a centred model eye ($y_{\mathrm{P}} = 0\ \mathrm{mm}$) with the fovea $y_{\mathrm{R}} = 1.46\ \mathrm{mm}$ from the optical axis, this is a chromatic difference in inclination at the fovea of $\delta a_{\mathrm{R}} = 1.0678\times10^{-5}$. When a pinhole is placed in front of the eye, Equation 7.4.13 becomes

$$\delta a_{\mathrm{R}} = \left(-1.3746\times10^{-4}\ \mathrm{kD}\right)y_{\mathrm{P}} + \left(-2.4013\times10^{-5}\ \mathrm{kD}\right)y_{\mathrm{R}}. \qquad (10.7.2)$$

For a pinhole in front of the cyclopleged Le Grand model eye with transverse displacement of $y_{\mathrm{P}} = 4\ \mathrm{mm}$, the chromatic difference in inclination at the optical axis ($y_{\mathrm{R}} = 0\ \mathrm{mm}$) is $\delta a_{\mathrm{R}} = -5.4984\times10^{-4}$ and at the fovea ($y_{\mathrm{R}} = 1.46\ \mathrm{mm}$) it increases in magnitude to $\delta a_{\mathrm{R}} = -5.8490\times10^{-4}$. However, we note that the direction changes when a pinhole is introduced. When light traverses the pupil, the blue and red rays appear as shown in Figure 7.4.1, however, when a pinhole is introduced the red and blue are swopped. This too has implications for the Stiles-Crawford effects.

The reduced eye, being a much simplified model, has no refractive elements posterior of the "pupil" and therefore Equation 7.4.13 simplifies to

$$\delta a_{\mathrm{R}} = \left(0\ \mathrm{kD}\right)y_{\mathrm{P}} + \left(0\ \mathrm{kD}\right)y_{\mathrm{R}} \qquad (10.7.3)$$

and the reduced eye has zero chromatic difference in inclination at the retina. The same result occurs when a pinhole is placed in front of the reduced eye.

10.8 Summary of dependent chromatic properties

In Sections 10.3 to 10.6 we explored the chromatic properties of Le Grand's and the reduced eye dependent on object or image and aperture position, both with and without a pinhole, for an object at a selection of working distances. All these examples can quickly become overwhelming and confusing, however, it soon becomes clear that all the chromatic difference relationships are linear in nature. The two model eyes tell the same story, however, the slope of the straight line is slightly different each time.

The distant object situation is described in terms of the incident inclination a_{K} however the objects at a finite working distance are described in terms of object position, directly by the object's transverse position y_{O} and indirectly by incorporating the working distance z_{O} into the coefficient matrices, $\mathbf{V}_{\mathrm{OE}}$, $\mathbf{V}_{\mathrm{OE}}^{\mathrm{P}}$, $\mathbf{V}_{\mathrm{yO}}$ and $\mathbf{V}_{\mathrm{yO}}^{\mathrm{P}}$. The combination of y_{O} and z_{O} to describe the object position can be summarily described by the incident inclination a_{K}. The relationship can be simply obtained by $\mathbf{S}_{\mathrm{O}}\boldsymbol{\rho}_{\mathrm{O}} = \boldsymbol{\rho}_{\mathrm{K}}$. Multiplying this out

$$\begin{pmatrix} 1 & -\zeta_{\mathrm{O}} \\ 0 & 1 \end{pmatrix}\begin{pmatrix} y_{\mathrm{O}} \\ \alpha_{\mathrm{O}} \end{pmatrix} = \begin{pmatrix} y_{\mathrm{K}} \\ \alpha_{\mathrm{K}} \end{pmatrix}$$

to obtain

$$\begin{pmatrix} y_{\mathrm{O}} - \zeta_{\mathrm{O}}\alpha_{\mathrm{O}} \\ \alpha_{\mathrm{O}} \end{pmatrix} = \begin{pmatrix} y_{\mathrm{K}} \\ \alpha_{\mathrm{K}} \end{pmatrix}$$

and solving for a_{K} we obtain

$$a_{\mathrm{K}} = \frac{y_{\mathrm{K}} - y_{\mathrm{O}}}{-z_{\mathrm{O}}}. \qquad (10.8.1)$$

From Equation 10.8.1 we can look at the distant object situation and draw conclusions that are general for all systems.

Below we summarise the chromatic properties that are dependent on object or image and apertures position. We divide this summary into three sections, firstly the chromatic difference in image position, inclination, size and angular spread, secondly the chromatic difference in object position, inclination, size and angular spread and finally the chromatic magnifications. For the chromatic differences in image and object space, the two eyes only differ in the

magnitude of the slope and so we will narrow the summary down to only Le Grand's eye.

10.8.1 Chromatic differences in image space

Chromatic difference in image position and inclination

The chromatic difference in image positions δy_{R} and inclinations δa_{R} were summarised by Equation 7.2.22. Substituting for $\delta\mathbf{V}_{\mathrm{E}}$ from Table 10.3.3 into Equation 7.2.22, we obtain

$$\begin{pmatrix} -0.03568 & -0.1258\ \mathrm{mm} \\ -0.001822\ \mathrm{kD} & -0.006011 \end{pmatrix}\begin{pmatrix} y_{\mathrm{P}} \\ a_{\mathrm{K}} \end{pmatrix}=\begin{pmatrix} \delta y_{\mathrm{R}} \\ \delta a_{\mathrm{R}} \end{pmatrix}. \tag{10.8.2}$$

This summarises Figures 10.3.1 and 3, which are very similar. Assuming a centred eye ($y_{\mathrm{P}}=0$), both δy_{R} and δa_{R} have a linear relationship with a_{K} with a negative slope. A decentred pupil will merely add a constant value to δy_{R} and δa_{R}, but the slope will not change.

When a pinhole is placed immediately in front of Le Grand's eye the values in $\delta\mathbf{V}_{\mathrm{E}}$ change due to the longitudinal displacement of the limiting aperture. Equation 10.8.2 becomes

$$\begin{pmatrix} -0.03149 & -0.2212\ \mathrm{mm} \\ -0.001414\ \mathrm{kD} & -9.3691\times10^{-3} \end{pmatrix}\begin{pmatrix} y_{\mathrm{P}} \\ a_{\mathrm{K}} \end{pmatrix}=\begin{pmatrix} \delta y_{\mathrm{R}} \\ \delta a_{\mathrm{R}} \end{pmatrix}. \tag{10.8.3}$$

From Equation 10.8.3 we can see that any increase in incident inclination when a pinhole is placed in front of the eye will magnify the δy_{R} and δa_{R} more than for the naked eye and any transverse movement of the pinhole will very slightly increase the effect on the δy_{R} and δa_{R}. However, the magnitude of y_{P} is potentially far greater for a pinhole than for a pupil. This can be seen in Figures 10.4.1 and 2 where it is evident that the working distance has very little effect for an axial object. The effect of adding a pinhole at the corneal plane is to potentially increase δy_{R} and δa_{R}. This has implications for the AcuFocus Kamra corneal pinhole inlay.

Chromatic difference in image size and angular spread

The chromatic difference in image size $\delta(\Delta y_{\mathrm{R}})$ and angular spread $\delta(\Delta a_{\mathrm{R}})$ were summarised by Equation 7.3.13. Substituting for $\delta\mathbf{V}_{\mathrm{E}}$ from Table 10.3.3 into Equation 7.3.13, we obtain

$$\begin{pmatrix} -0.03568 & -0.1258\ \mathrm{mm} \\ -0.001822\ \mathrm{kD} & -0.006011 \end{pmatrix}\begin{pmatrix} 0 \\ \Delta a_{\mathrm{K}} \end{pmatrix} = \delta\begin{pmatrix} \Delta y_{\mathrm{R}} \\ \Delta a_{\mathrm{R}} \end{pmatrix} \tag{10.8.4}$$

which is very similar to Equation 10.8.2. $\delta(\Delta y_{\mathrm{R}})$ and $\delta(\Delta a_{\mathrm{R}})$ are independent of pupil (or pinhole) position. The relationships are linear, Δa_{K} is magnified by δX_{E} or δZ_{E} to obtain $\delta(\Delta y_{\mathrm{R}})$ and $\delta(\Delta a_{\mathrm{R}})$ respectively.

For a pinhole in front of the eye we obtain

$$\begin{pmatrix} -0.03149 & -0.2212\ \mathrm{mm} \\ -0.001414\ \mathrm{kD} & -9.3691\times10^{-3} \end{pmatrix}\begin{pmatrix} 0 \\ \Delta a_{\mathrm{K}} \end{pmatrix} = \delta\begin{pmatrix} \Delta y_{\mathrm{R}} \\ \Delta a_{\mathrm{R}} \end{pmatrix} \tag{10.8.5}$$

and while the transverse displacement of the pinhole will have no effect on $\delta(\Delta y_{\mathrm{R}})$ and $\delta(\Delta a_{\mathrm{R}})$, the longitudinal change in position of the limiting aperture will create a magnified effect of $\delta(\Delta y_{\mathrm{R}})$ and $\delta(\Delta a_{\mathrm{R}})$, as can be seen by the increase in magnitude of $\delta X_{\mathrm{E}}^{\mathrm{P}}$ and $\delta Z_{\mathrm{E}}^{\mathrm{P}}$ from δX_{E} and δZ_{E} respectively.

10.8.2 Chromatic difference in object space

Chromatic difference in object position and inclination

The object space scenario was derived to mimic the experimental situation and as a result has been limited to finite working distances. The chromatic difference in object position δy_{O} and inclination δa_{O} is summarised by Equation 7.4.10. Substituting for $\delta\mathbf{V}_{\mathrm{Oy}}$ at $z_{\mathrm{O}} = -3\ \mathrm{m}$ from Table 10.5.3 for Le Grand's eye into Equation 7.4.10 we obtain

$$\begin{pmatrix} -6.4461 & -1.3630 \\ 2.1482\times10^{-3}\ \mathrm{kD} & 4.5429\times10^{-4}\ \mathrm{kD} \end{pmatrix}\begin{pmatrix} y_{\mathrm{P}} \\ y_{\mathrm{R}} \end{pmatrix} = \begin{pmatrix} \delta y_{\mathrm{O}} \\ \delta a_{\mathrm{O}} \end{pmatrix}. \tag{10.8.6}$$

Equation 10.8.6 summarises Figures 10.5.1 and 2; the peripheral retina experiences greater magnitudes of chromatic difference in position or inclination than the posterior pole. From Figure 7.4.1 it is easy to see that δy_{O} and δa_{O} will have opposite signs. We recall from Equation 5.3.14 that the bottom row of $\delta\mathbf{V}_{\mathrm{Oy}}$

is independent of working distance z_{O}, making δa_{O} easier to compare across studies.

With a pinhole and substituting $\delta\mathbf{V}_{\mathrm{Oy}}^{\mathrm{P}}$ at $z_{\mathrm{O}} = -3\,\mathrm{m}$ from Table 10.6.3, Equation 7.4.12 becomes

$$\begin{pmatrix} -5.7038 & -2.4030 \\ 1.9013\times10^{-3}\ \mathrm{kD} & 8.0099\times10^{-4}\ \mathrm{kD} \end{pmatrix}\begin{pmatrix} y_{\mathrm{P}} \\ y_{\mathrm{R}} \end{pmatrix} = \begin{pmatrix} \delta y_{\mathrm{O}} \\ \delta a_{\mathrm{O}} \end{pmatrix} \tag{10.8.7}$$

which summarises Figures 10.6.1 and 2. We draw similar conclusions to the image space situation; δy_{O} and δa_{O} will increase in magnitude with an increase in transverse pinhole displacement or with distance at the retina from the posterior pole.

Chromatic difference in object size and angular spread

The chromatic difference in object size $\delta(\Delta y_{\mathrm{O}})$ and angular spread $\delta(\Delta a_{\mathrm{O}})$ is summarised by Equation 7.5.10. Substituting $\delta\mathbf{V}_{\mathrm{Oy}}$ at $z_{\mathrm{O}} = -3\,\mathrm{m}$ from Table 10.5.3 into Equation 7.5.10 we obtain

$$\begin{pmatrix} -6.4461 & -1.3630 \\ 2.1482\times10^{-3}\ \mathrm{kD} & 4.5429\times10^{-4}\ \mathrm{kD} \end{pmatrix}\begin{pmatrix} 0 \\ \Delta y_{\mathrm{R}} \end{pmatrix} = \delta\begin{pmatrix} \Delta y_{\mathrm{O}} \\ \Delta a_{\mathrm{O}} \end{pmatrix} \tag{10.8.8}$$

which, as expected, resembles Equation 10.8.6. Similar to δa_{O}, $\delta(\Delta a_{\mathrm{O}})$ is independent of z_{O}. $\delta(\Delta y_{\mathrm{O}})$ and $\delta(\Delta a_{\mathrm{O}})$ are independent of any pupil decentration y_{P}. It is obvious from Equation 10.8.8 that the relationship between $\delta(\Delta y_{\mathrm{O}})$ or $\delta(\Delta a_{\mathrm{O}})$ and retinal image size Δy_{R} is linear.

Placing a pinhole immediately in front of Le Grand's eye merely changes the values of $\delta\mathbf{V}_{\mathrm{Oy}}$ to those of $\delta\mathbf{V}_{\mathrm{Oy}}^{\mathrm{P}}$ so that Equation 10.8.8 becomes

$$\begin{pmatrix} -5.7038 & -2.4030 \\ 1.9013\times10^{-3}\ \mathrm{kD} & 8.0099\times10^{-4}\ \mathrm{kD} \end{pmatrix}\begin{pmatrix} 0 \\ \Delta y_{\mathrm{R}} \end{pmatrix} = \delta\begin{pmatrix} \Delta y_{\mathrm{O}} \\ \Delta a_{\mathrm{O}} \end{pmatrix} \tag{10.8.9}$$

from which we can see that moving the plane of the limiting aperture from the pupillary plane to immediately in front of the cornea will have a magnifying effect on $\delta(\Delta y_{\mathrm{O}})$ and $\delta(\Delta a_{\mathrm{O}})$, by almost double.

10.8.3 Chromatic magnifications

Obtaining a summarised relationship for the chromatic magnifications is messy and one cannot easily obtain a neat and tidy relationship like those for the chromatic differences (Equations 7.2.22, 7.3.13, 7.4.10 and 7.5.10). However, it is apparent that the influence of working distance on chromatic magnifications is so small as to be ignored. Therefore the magnifications are summarised in Table 10.8.1. We recall that chromatic magnification is independent of transverse pupil or pinhole displacement, but placing a pinhole in front of the eye does have a magnifying effect on the chromatic magnification due to the longitudinal placement of the limiting aperture.

As expected, we see from Table 10.8.1 that in image space the red image is larger than the blue image, or subtends a greater angular spread while in object space the blue object is larger than the red object, or subtends a larger angular spread. It is clear that moving the limiting aperture from the pupillary plane to the cornea increases the chromatic magnification, a result that has implications for the AcuFocus Kamra corneal pinhole inlay.

Table 10.8.1 Chromatic magnifications of Le Grand's eye and the reduced eye, firstly as the naked eye followed by placing a pinhole immediately in front of the eye. The percentages in the last column are included as a guide for comparative purposes only and represent the mean of chromatic magnifications for each eye.

	M_{yR}	M_{aR}	M_{yO}	M_{aO}	as %
Le Grand's eye	0.9925	0.9926	1.0076	1.0076	0.76%
– with pinhole	0.9868	0.9862	1.0134	1.0134	1.34%
Reduced eye	0.9917	0.9917	1.0083	1.0084	0.83%
– with pinhole	0.9885	0.9885	1.0117	1.0117	1.16%

10.9 Summary of dependencies

Nearly all the chromatic effects discussed in this chapter are dependent on up to three different variables, as summarised in Table 10.9.1. In particular the summary highlights which chromatic properties are dependent or independent of object distance z_{O} from the eye. Chromatic aberration, independent chromatic properties and chromatic difference in image size and angular spread are all

Table 10.9.1 Summary of the dependence of the chromatic effects on variable parameters. In particular, chromatic aberrations or properties that are dependent on working distance are indicated by ∘ and those independent of working distance are indicated by •. The dependencies are separated into those with an object at distance and those with an object at a finite distance. Dependencies given in a matrix represent the entries of the respective chromatic difference in coefficients. Additional dependencies are also given.

			Distant object		Finite distance		Eq. no.
			z_O	Additional	z_O	Additional	
Chromatic Aberration							
	Longitudinal	δz	•		∘		6.1.1
	Transverse	δy	•	a_K	∘	y_O	6.1.2
Chromatic Properties							
Independent	δF		•		•		7.1.1
Independent	δF_0		•		•		7.1.3
Independent	δA		•		•		7.1.5
Dependent on object and aperture positions	$\delta \mathbf{V}_E \mathbf{v}_E = \delta \mathbf{r}_R$	$\delta \begin{pmatrix} y_R \\ a_R \end{pmatrix}$	$\begin{pmatrix} • & • \\ • & • \end{pmatrix}$	$\begin{pmatrix} y_P \\ a_K \end{pmatrix}$			7.2.22
Dependent on object and aperture positions	$\delta \mathbf{V}_{OE} \mathbf{v}_{OE} = \delta \mathbf{r}_R$	$\delta \begin{pmatrix} y_R \\ a_R \end{pmatrix}$			$\begin{pmatrix} ∘ & ∘ \\ ∘ & ∘ \end{pmatrix}$	$\begin{pmatrix} y_P \\ y_O \end{pmatrix}$	7.2.24
Dependent on object and aperture positions	$\delta \mathbf{V}_E \Delta \mathbf{v}_E = \delta \Delta \mathbf{r}_R$	$\delta \begin{pmatrix} \Delta y_R \\ \Delta a_R \end{pmatrix}$	$\begin{pmatrix} • & • \\ • & • \end{pmatrix}$	$\begin{pmatrix} • \\ \Delta a_K \end{pmatrix}$			7.3.13
Dependent on object and aperture positions	$\delta \mathbf{V}_{OE} \Delta \mathbf{v}_{OE} = \delta \Delta \mathbf{r}_R$	$\delta \begin{pmatrix} \Delta y_R \\ \Delta a_R \end{pmatrix}$			$\begin{pmatrix} ∘ & ∘ \\ ∘ & ∘ \end{pmatrix}$	$\begin{pmatrix} • \\ \Delta y_O \end{pmatrix}$	7.3.16
Dependent on object and aperture positions	M_{yR}		•		∘		7.3.19 & 20
Dependent on object and aperture positions	M_{aR}		•		∘		7.3.27 & 28
Dependent on image and aperture positions	$\delta \mathbf{V}_{Oy} \mathbf{v}_{Oy} = \delta \mathbf{r}_O$	$\delta \begin{pmatrix} y_O \\ a_O \end{pmatrix}$			$\begin{pmatrix} ∘ & ∘ \\ • & • \end{pmatrix}$	$\begin{pmatrix} y_P \\ y_R \end{pmatrix}$	7.4.10
Dependent on image and aperture positions	$\delta \mathbf{V}_{Oy} \Delta \mathbf{v}_{Oy} = \delta(\Delta \mathbf{r}_O)$	$\delta \begin{pmatrix} \Delta y_O \\ \Delta a_O \end{pmatrix}$			$\begin{pmatrix} ∘ & ∘ \\ • & • \end{pmatrix}$	$\begin{pmatrix} • \\ \Delta y_R \end{pmatrix}$	7.5.10
Dependent on image and aperture positions	M_{yO}				∘		7.5.15
Dependent on image and aperture positions	M_{aO}				•		7.5.18

independent of transverse pupil or pinhole position, y_P. Chromatic aberration is dependent on the conjugate system of object and image positions while the dependent chromatic difference properties depend on object position(s) and position of the centre of the blurred image(s) on the retina. The chromatic

differences in image space are dependent on y_O while those in object space are dependent on y_R. The chromatic magnification for an object at a finite distance is weakly dependent on the working distance and on not on the transverse object and image positions.

10.10 Discussion

The chromatic effects have been explored in this chapter by means of a number of numerical illustrative examples. Two schematic eyes were used in the examples, Le Grand's and the reduced eyes. Where applicable object points were explored at four distances from the eye, that is, for a distant object with $a_K = 0.1$ and at finite distances with of –3, –2 and –0.5m from the eye, each time with $y_O = 0.2$ m. The examples in object space required an image on the retina, and these examples included the three finite distances for the objects from the eye and the image at either $y_R = 0$ mm or $y_R = 1.46$ mm which approximates the position of the fovea at a visio-optical angle of 5º.

From Figure 10.1.1 we saw that the magnitude of δz increases as the object approaches the eye. The relationship is true for both Le Grand's eye and the reduced eye, although the magnitude is generally greater for the reduced eye The magnitude of δy increases as the incident inclination a_O increases, as can be seen from Figures 10.1.2 and 3.

The object or image and aperture-dependent chromatic properties are defined either in image space or object space and each in turn is explored for the naked eye and the eye with a pinhole aperture immediately in front of the eye. The dependence of each of the dependent chromatic properties is summarised in Table 10.9.1.

Finally, two underlying implications arising from the literature are examined. When a pencil of rays is incident on the eye and the red and blue chief rays are traced through the pupil, the incident red and blue rays are distinctly separate by more than 3000 times their wavelength and cannot be assumed to originate from a single dichromatic ray. Furthermore, in the experimental set-up where the red and blue objects are separated in object space and the images are

superimposed at the same position on the retina, the red and blue rays reaching the retina for Le Grand's eye have different inclinations, which may have implications for the Stiles-Crawford effects or other physiological stimulus-response mechanisms that are beyond the scope of this dissertation. The simplified design of the reduced eye nullifies this measurement.

The Stiles-Crawford effects describe the directional sensitivity of the cones. The Stiles-Crawford effects show that the cones are far more sensitive to light that strikes the retina head-on than to light which enters obliquely. The first Stiles-Crawford effect describes how oblique rays appear disproportionately less bright than rays that strike the retina head-on while the second describes that monochromatic rays of different wavelengths appear to have altered hue and saturation when striking the retina obliquely compared to rays striking head-on. The obliquely striking rays produce a different ratio of responses in the three types of cones to a ray that enters head-on. Both Stiles-Crawford effects are produced by directional sensitivity of the cones and may affect object or image and aperture-dependent chromatic properties. (Stiles and Crawford, 1933; Stiles, 1939; Lakshminarayanan, 2009; Westheimer, 2008.)

The chromatic aberrations and object or image and aperture-dependent chromatic properties depend on the transverse and longitudinal position of the object point. The object, image and aperture-dependent chromatic properties are additionally dependent on the longitudinal and transverse displacement of the pupil or pinhole aperture, making their understanding and relationships more complex. The chromatic difference in power, refractive compensation and ametropia are properties of the system alone and are independent of object, image and aperture positions. The object, image and aperture-dependent chromatic properties are defined specially for the eye, while chromatic aberration is defined for systems in general, making chromatic aberration a more general definition.

PART V – CONCLUSION

11 Concluding discussion

11.1 Introduction

We return to the oldest example of chromatic dispersion known to man, the rainbow. We know that the colours are created by chromatic dispersion, but why does the rainbow form a bow shape? The answer lies in the symmetry of the raindrops. Indeed, it is not a bow, but a cone. The bow that we perceive is part of a full circle and the apex of the cone is at the viewer's eye. Each colour forms its own cone, with the red cone outermost and each colour (or frequency) sitting inside the previous cone, with violet being inner-most (Lee and Fraser, 2001:112-113). But this is what is happening in object space.

What happens when an eye looks at a multi-chromatic object point? Is this comparable to the rainbow? Raindrops are spherical and so is the eye. However, in a raindrop as the light enters it is refracted and dispersed, then the light is reflected internally and finally exits the raindrop whilst being refracted and dispersed some more. The rainbow is created by an infinity of rays from the sun being dispersed, refracted and reflected by an infinity of raindrops. In the eye, the light enters and is imaged on the retina after undergoing refraction and dispersion by the eye's structures. (The structure of the eye prevents the light rays from following the same path as they would in a raindrop). So while rainbows and chromatic effects in the eye are both caused by chromatic dispersion, there is a distinct difference between a rainbow and an eye.

11.2 Findings and conclusions

This study is about "The Chromatic Dependence of First-order Optical Properties of the Eye". We saw, in Chapter 3, that the first-order optical properties of the eye can be divided into fundamental properties and derived properties. Therefore the dependence of each of the fundamental properties on frequency and on wavelength is studied. To better understand the relationship between the fundamental properties and their dependence on frequency, we transform the

transference into Hamiltonian space, study the dependence in this linear space and transform the straight line relationships back to a symplectic transference.

Fundamental properties

The chromatic dependence of each of the fundamental properties of the transferences for both the reduced eye and Le Grand's eye as a function of frequency is found to be very nearly linear (Figures 8.1.3). A formula is derived which gives the linear dependence of the transference on the frequency of light. It is given by Equation 8.1.5 where ν is the frequency of light and the constants are given in Tables 8.1.2 and 3 for the reduced eye and Le Grand's eye, respectively. The result of substituting the values into Equation 8.1.5 for any chosen frequency is a transference that is very nearly symplectic with a mean determinant of approximately 1.

When studying the dependence of the fundamental properties on wavelength, the dependence loses it linearity and one cannot derive an equation such as Equation 8.1.5 as a linear function of wavelength with nearly the same level of accuracy (Figure 8.1.8). This confirms what Pease and Barbeito (1989) state, that the linear function of the frequency scale make analysis simpler to compute and understand.

When calculating the refractive index of air as a function of frequency, we see that, firstly, only the dilation (*A*) and divergence (*C*) are affected and that the change in the curve is so slight and so uniform as to be disregarded and the refractive index of air can be equated to 1 (Figures 8.1.4 and 5). Similarly, when the eyes are submerged in water and the dependence of water on the frequency of light is calculated using Cornu's formula, only the dilation and divergence are affected (Figures 8.1.9).

The dependence of each of the entries of the Cayley-transformed transference is graphed as a function of frequency and found to be very nearly linear for both eyes (Figures 8.2.1 and 4). When the three independent entries are graphed on a three-dimensional graph as a function of frequency, we obtain a straight line for the reduced eye and a gently curved line for Le Grand's eye (Figures 8.2.3 and 6). Because of the resultant linearity of each of the entries, a

formula is derived which results in a transference that gives a linear dependence on frequency (Figures 8.2.2 and 5). This is given by Equation 8.2.3 for the Cayley-transformed transference and substituting it into Equation 8.2.2, we obtain the transference with the constants given in Tables 8.2.1 and 2 for the reduced eye and Le Grand's eye in air, respectively. The advantage of Equation 8.2.3 over Equation 8.1.5 is that Equation 8.2.3 has fewer constants and more importantly, is more accurate. Equation 8.2.3 and 2 result in a symplectic transference with a mean determinant of exactly 1 for any chosen frequency.

Similarly, the dependence of the entries of the logarithmic-transformed transference is graphed as a function of frequency and unsurprisingly found to be very nearly linear for both model eyes (Figures 8.2.7 and 9). However, the region that the transformed transference occupies within the Hamiltonian space is different for the Cayley-transformed transference compared to the logarithmic-transformed transference (Figures 8.2.8 and 10). The formula for deriving the transference from the logarithmic-transformed transference as a linear function of frequency is given by Equation 8.2.5 where the constants are given in Table 8.2.5 for the two model eyes (Figures 8.2.11 and 12). The accuracy given by this derivation is similar to that for the Cayley-transformed transference but because of the simplicity of Equation 8.2.2, this is the preferred method.

Derived properties

Next we study the chromatic dependence of a number of derived properties, including cardinal points. Because a relationship between specific derived properties is given by the characteristic matrices, each of these derived properties is studied for its dependence on frequency (Figures 9.2.1 to 5) and the relationship between the entries of each of the symmetric characteristic matrices is displayed as three-dimensional graphs (Figures 9.3.1 to 10). The purpose is two-fold; firstly we wish to understand the dependence of each first-order optical property of the eye on the frequency of light and secondly, we wish to gain a deeper understanding the different linear spaces.

Four characteristic matrices are introduced, each being symmetric and each entry representing a derived property. Five derived properties are of

particular interest and are illustrated graphically for their dependence on the frequency of light. Power F (Equation 3.4.3), entrance- and exit-plane refractive compensation F_0 and F_C (Equations 3.4.6 and 5.1.3) and front-vertex power F_{fv} (Equation 3.4.16) each show a very nearly linear relationship to the frequency of light. Back-vertex power F_{bv}, given by Equation 3.4.11 is representative of vergence at the exit-plane and has a hyperbolic relationship; clearly illustrating which frequency is in focus at the retina. The four characteristic matrices given in Section 3.7.3 represent a linear space and therefore the three independent entries of each characteristic matrix is graphed on a 3-dimensional graph. For the point **P**, angle **Q** and first mixed **M** characteristic matrices the relationship is linear for the reduced eye and nearly linear for Le Grand's eye. The second mixed characteristic matrix **N**, expectedly, was problematic because of the division by *A*, the dilation, which approaches zero for an emmetropic eye.

The dependence of the cardinal and anti-cardinal points on the frequency of light is explored for the two model eyes. For the reduced eye a number of points simplified and we find that the incident and emergent principal and nodal points are independent of frequency. The incident and emergent focal points, anti-principal and anti-nodal points are all dependent on frequency. The chromatic difference between the four red and blue anti-cardinal points all have the same magnitude, the emergent anti-cardinal points having opposite direction to the incident anti-cardinal points (Figures 9.1.1, 3 and 4).

In contrast, for Le Grand's eye we find that all six of the cardinal points and all four of the anti-cardinal points are dependent on frequency and that there is no relationship to the magnitude of the chromatic difference between any of the cardinal or anti-cardinal points (Figures 9.1.2, 5 and 6). This emphasises that while the reduced eye is a convenient simplification, one should be cautious of making conclusions based on the dimensions and mathematics of the reduced eye.

Chromatic aberration and chromatic properties

A study of the chromatic dependence of the first-order optical properties of an eye would be incomplete without a detailed study of chromatic aberration. There are two approaches to defining chromatic aberration, the classical optics

and physiological optics approaches. Both definitions are defined in the literature for Gaussian systems or eyes. In this dissertation we define chromatic aberration for systems in general, that is, systems that may include astigmatic and decentred or tilted elements. Additionally, we define chromatic properties, in line with the physiological optics approach, also generalised for systems with astigmatic elements.

In Gaussian optics longitudinal chromatic aberration is defined as $\delta z = z_{\mathrm{b}} - z_{\mathrm{r}}$, the signed distance from the red image plane to the blue image plane. In an astigmatic system, this is the generalized distance defined as $\delta\mathbf{Z} = \mathbf{Z}_{\mathrm{b}} - \mathbf{Z}_{\mathrm{r}}$ from a matrix representing the red image structure to a matrix representing the blue image structure; each of the red and blue image structures consisting of two orthogonal image line foci, separated by an interval of Sturm. Transverse chromatic aberration is defined as the transverse vector $\delta\mathbf{y} = \mathbf{y}_{\mathrm{b}} - \mathbf{y}_{\mathrm{r}}$, from the transverse position of the red to the blue image structures. In Gaussian optics, it would seem that one could regard longitudinal and transverse chromatic aberration as components of a unified chromatic aberration vector. In linear optics, however, because of their fundamentally different characters (transverse chromatic aberration is a vector and longitudinal chromatic aberration is a matrix) this would not seem possible. Recent research suggests that it may be possible to represent the relationship as a five-dimensional inner-product space (Harris, Evans and van Gool; 2014), however, this is beyond the scope of this dissertation.

The numerical examples give some insight into chromatic aberration, which, because it is based on vergence, is dependent on the object position. Longitudinal chromatic aberration is dependent on the longitudinal object position and transverse chromatic aberration is dependent on both the longitudinal and transverse object position. Longitudinal chromatic aberration increases in magnitude as the object approaches the eye (Figure 10.1.1). Transverse chromatic aberration has a linear dependence on transverse displacement of an object point from the optical axis (Figure 10.1.2 and 3). As the incident inclination increases in magnitude, so the transverse chromatic aberration increases in magnitude (Figure 10.1.4).

The independent chromatic properties of the eye are not dependent on light and therefore not on the object and image positions. They are properties of the system alone and are derived from the fundamental properties of the system. This implies that one will have a single number for each of the definitions with no graph to illustrate any dependence on frequency. The independent chromatic properties of the eye include chromatic difference in power δF, refractive compensation δF_0 and ametropia δA, with derivations obtained from the transference. The results are summarized in Table 10.2.1. Of course, the frequencies chosen for 'red' and 'blue' will influence the results.

Equations are obtained from the transference for the chromatic properties of the eye dependent on the object or image and aperture position. In image space, the chromatic properties dependent on the object and aperture position, derived from the transference, are chromatic difference in transverse image position δy_{R} and inclination at the retina δa_{R}. The chromatic difference in magnification is a misnomer and so we define chromatic difference in image size $\delta(\Delta y_{\mathrm{R}})$ and angular spread $\delta(\Delta a_{\mathrm{R}})$ at the retina. Magnification is a comparative, unitless measure and not defined by a difference. Therefore chromatic magnifications for image size M_{yR} and angular spread M_{aR} are defined and derived from the transference. These formulae allow us to calculate the chromatic properties at the imaging plane, that is to say what is happening in the eye, at the retina. Because the chromatic difference derivations are not dependent on the position of the nodal point or other structures, they measure actual distances and changes in inclination.

Experimental measurements take place in object space and for this reason derivations for chromatic difference in transverse object position δy_{O}, inclination δa_{O}, object size $\delta(\Delta y_{\mathrm{O}})$, object angular spread $\delta(\Delta a_{\mathrm{O}})$, chromatic object size magnification M_{yO} and chromatic object angular spread magnification M_{aO} are included that account for chromatic differences and magnifications in object space. In an experimental situation one manipulates and takes measurements in object space whilst controlling what is happening at the retinal plane. These

equations allow us to compare our theoretical numerical results with published results obtained experimentally, and were found to compare well.

The equations for chromatic properties dependent on object or image and aperture position simplify to account for the effects of introducing a pinhole in front of the eye. δy_{R}, δa_{R}, δy_{O} and δa_{O} are directly dependent on y_{P}, the transverse displacement of the pinhole. However, the longitudinal shift in position of the limiting aperture from the pupillary plane to upstream of the cornea has a magnifying effect and therefore all the chromatic differences and chromatic magnifications are affected by this change. This has implications for both the Stiles-Crawford effect and for the AcuFocus Kamra corneal pinhole inlay.

Table 11.1.1 attempts to simplify the many variations and permutations of the dependent chromatic properties by indicating which variables each chromatic property is dependent on. Any parameter marked ○ has a linear relationship with the chromatic property, that is, magnified by a constant. Where indicated by □, this constant will have its slope affected by the distance of the object in front of the eye. The chromatic properties are symbolized as chromatic difference in transverse image position δy_{R}, inclination δa_{R}, image size $\delta(\Delta y_{\mathrm{R}})$, angular spread $\delta(\Delta a_{\mathrm{R}})$ retinal chromatic image size magnification M_{yR}, retinal chromatic angular spread magnification M_{aR}, chromatic difference in object position δy_{O}, inclination δa_{O}, object size $\delta(\Delta y_{\mathrm{O}})$, object angular spread $\delta(\Delta a_{\mathrm{O}})$, size magnification M_{yO} and object angular spread magnification M_{aO} in object space.

Table 11.1.1 Summary of chromatic properties and their dependencies. Variables marked ○ have a linear dependence on the respective variable. Objects at finite distance which have the slope of the linear dependence affected by the distance of the object in front of the eye are marked □. The table remains unchanged when a pinhole is introduced immediately in front of the eye. Chromatic properties in object space are defined for finite object distances only.

		Distant object		Object at finite distance			
		a_K	y_P	z_O	y_O	y_P	y_R
Image space	δy_R	○	○	□	○	○	
	δa_R	○	○	□	○	○	
	$\delta(\Delta y_R)$	○		□	○		
	$\delta(\Delta a_R)$	○		□	○		
	M_{yR}			□			
	M_{aR}			□			
Object space	δy_O	—		□		○	○
	δa_O	—				○	○
	$\delta(\Delta y_O)$	—		□			○
	$\delta(\Delta a_O)$	—					○
	M_{yO}	—		□			
	M_{aO}	—					

11.3 Limitations in the scope of this dissertation

At the outset it was clear that studying "the chromatic dependence of *all* first-order optical properties of the eye" would have far too large a scope for a Masters dissertation and so a conscious decision was made to limit the scope of the study to firstly Gaussian systems, whilst keeping all derivations as general as possible, and secondly to limit the derived properties to those applicable to the characteristic matrices and appropriate for Gaussian systems. This is a long dissertation and there are numerous topics and derived properties that have been omitted. In particular there are a number of derived properties that would be more appropriately studied as linear systems for their chromatic dependence such as all the axes of the eye. There were a number of issues that were raised during the

study which fell outside the scope of this dissertation, but which warrant further studies. Indeed, this study may give some insight into some of these issues.

There is a need for a complete set of formulae for the refractive indices as a function of frequency for all the media of the eye. The formula used for the refractive index of the reduced eye is based on relatively recent experimental data and is therefore considered to reflect the real eye fairly accurately for most of the properties studied. The refractive indices for Le Grand's eye differed from those for the reduced eye and are based on a combination of refractometer readings and experimental data. More recent refractometer readings are incomplete for the human eye. While these formulae form the basis of all the numerical examples in this dissertation, the derivations based on these formulae are sufficiently general so as to accommodate new formulae that may be available in the future.

In Section 8.2 we made use of the transformed transference. This mapping between the symplectic group and Hamiltonian space enabled us to develop an equation for the straight line dependence of the fundamental properties as a function of frequency and resulting in a symplectic transference with determinant exactly equal to 1. However, what meaning can be given to the entries of the Hamiltonian matrix. What region in the Hamiltonian space would be representative of eyes? Equation 5.6.7 may give us some insight into the meaning of the three-dimensional Hamiltonian space obtained using the Cayley transform and what region within this space is occupied by Gaussian eyes? Would it subsequently be possible to gain insight into what region of the ten-dimensional Hamiltonian space would be representative of real eyes with astigmatic surfaces?

In Gaussian optics it is tempting to represent the longitudinal and transverse chromatic aberration as a single combined chromatic aberration by obtaining a vector from the red to the blue image point. However, in linear optics the longitudinal chromatic aberration is represented by a matrix and the transverse chromatic aberration is a vector and combining the two into a unified chromatic aberration seems improbable. However, recent research indicates that this might be possible using a five-dimensional inner-product space (Harris, Evans and van Gool; 2014). The definition of inner-product space is based on the point and angle

characteristic matrices. How the two are related is beyond the scope of this dissertation and is the topic of further investigation at a later stage.

The definition for chromatic aberration includes astigmatic systems, however, this was not explored further; the scope of the dissertation being purposefully restricted to Gaussian systems. The chromatic properties too were defined for Gaussian systems. Where possible these definitions were generalized to linear optics for astigmatic systems without proof or being explored further. This creates an opportunity for further study of the chromatic properties for systems with astigmatic elements. Indeed, the two eyes studied are not only Gaussian, but emmetropic at a reference frequency. Additional studies into the chromatic properties of myopic, hyperopic, astigmatic, accommodating or even aging eye could be undertaken.

Many of the findings for the chromatic properties have implications for Stiles-Crawford effect. This needs to be explored in more detail.

The chromatic properties dependent on object and aperture position present the formulae necessary to obtain the chromatic properties induced by the placement of a pinhole immediately in front of the eye, or indeed, embedded in the corneal stroma. Further studies need to be done to explore the impact of these findings on the corneal pinhole inlay, such as the Kamra® by AcuFocus.

11.4 Summary of findings

1. The fundamental properties of the reduced and Le Grand's four surface eyes have a nearly perfectly linear dependence on frequency.
2. A formula is derived that gives the linear dependence of the fundamental properties of the transference.
3. Derivations are given for the chromatic aberration of systems in general, including systems with astigmatic and heterocentric elements, such as the eye, and particulated for the Gaussian eye.
4. Longitudinal chromatic aberration depends on the longitudinal position of the object and transverse chromatic aberration is dependent on both the longitudinal and transverse position of the object point.

5. Only the dilation and divergence are dependent on the refractive index upstream of the system. Disjugacy and divarication are independent of the medium upstream of the system.
6. Independent chromatic properties of the eye include:
    - Chromatic difference in power, δF .
    - Chromatic difference in refractive compensation, δF_0 .
    - Chromatic difference in ametropia, δA.
7. A set of formulae is derived for the chromatic properties of the Gaussian eye for
    - Objects at distance and at a finite distance.
    - Image and object space.
    - The special case of a pinhole held immediately in front of the eye.

    Chromatic properties of the eye dependent on object and aperture position include:
    - Chromatic difference in transverse image positions, δy_{R} .
    - Chromatic difference in inclination at the retina, δa_{R} .
    - Chromatic difference in image size, $\delta(\Delta y_{\mathrm{R}})$.
    - Chromatic difference in angular spread at retina, $\delta(\Delta a_{\mathrm{R}})$.
    - Chromatic image size magnification, M_{yR}.
    - Retinal chromatic angular spread magnification, M_{aR} .

    Chromatic properties of the eye dependent on image and aperture position include:
    - Chromatic difference in object position, δy_{O} .
    - Chromatic difference in object inclination, δa_{O} .
    - Chromatic difference in object size, $\delta(\Delta y_{\mathrm{O}})$.
    - Chromatic difference in object angular spread, $\delta(\Delta a_{\mathrm{O}})$.
    - Chromatic object size magnification, M_{yO}.
    - Chromatic object angular spread magnification, M_{aO} .

8. The red and blue chief rays chosen to study the chromatic properties in image space are incident on the entrance-plane of the system a distance of some 5000 times the wavelength of the blue light apart. When the red and blue chief rays from two separated object points coincide at a point on the exit-plane, their emergent inclination is the same for the reduced eye but different for Le Grand's eye.
9. Chromatic aberration and chromatic properties are dependent on:
    - Object position (longitudinal and transverse position, or incident inclination).
    - Frequencies chosen for 'red' and 'blue'.
    - Choice of schematic eye.
    - Formulae used for calculating the refractive indices of the media as a function of frequency.
    - Dependent chromatic properties can additionally be manipulated by introducing a pinhole in front of the eye.
10. Derived properties that are dependent on frequency are:
    - Power (linear).
    - Corneal-plane refractive compensation (linear).
    - Exit-plane refractive compensation (linear).
    - Back-vertex power (hyperbolic).
    - Front-vertex power (linear).
    - All the cardinal and anti-cardinal points for Le Grand's eye.
    - The anti-cardinal and focal points for the reduced eye.
    - All the chromatic properties. When the object distance remains stationary the dependence is linear.
11. The incident and emergent principal and nodal points are independent of frequency for the reduced eye.

11.5 Concluding summary

This dissertation studies the chromatic dependence of first-order optical properties of the eye, investigating both the fundamental and derived properties of the eye as a function of frequency. An equation is obtained that gives the linear dependency of each of the fundamental properties of the model eyes as a function of frequency, giving a transference that is truly symplectic with determinant equal to 1 (Evans and Harris, 2014).

Chromatic aberration is defined for systems in general, that is systems with elements that may be astigmatic and decentred, including the eye. Longitudinal chromatic aberration is defined by a 2×2 matrix and is dependent on the longitudinal position of the object point. Transverse chromatic aberration is defined by a 2×1 vector and is dependent on both the longitudinal and transverse position of the object point (Harris and Evans, 2012).

Chromatic properties are defined as those independent of and those dependent on the image or object and aperture positions. The definitions are derived for the subset of Gaussian eyes, however, the set of equations for astigmatic eyes is provided.

A selection of derived properties including power, corneal-plane and exit-plane refractive compensation, front- and back-vertex power and the cardinal points is investigated for their dependence on frequency. With the exception of the principal and nodal points of the reduced eye, all points investigated are dependent on frequency. The derived properties are related to each other through the characteristic matrices, which each define a linear space.

The transference, being a symplectic matrix, does not define a linear space, but can be mapped to Hamiltonian space which does define a linear space. Two mappings are investigated, namely the Cayley transform and the exponential-logarithmic mapping. The linear dependence of the entries of the Hamiltonian matrix on frequency is obtained. Graphs show the linear dependence on frequency of the individual entries as well as the three-dimensional linear space.

While understanding the meaning of Hamiltonian space and the region occupied by the eye is in its infancy, this study has given us insight into this linear

space. In particular, the Cayley transform derived from the fundamental properties (Equation 5.6.7) can potentially give us a deeper insight into this linear space.

This dissertation has opened the door to the study of the chromatic dependence of the first-order optical properties of the eye. A number of first-order optical properties, both fundamental and derived, have been investigated for their dependence on frequency. All the numerical examples have been purposefully limited to Gaussian eyes to allow insight into the dependence on frequency and chosen variables like object position and pinholes. We have a set of formulae that are not restricted to the reduced, or even schematic eyes. The stage is now set to generalise to systems and eyes with astigmatic and heterocentric elements.

S Afr Optom 2011 **70**(4) 149-155

Dependence of the transference of a reduced eye on frequency of light*

T Evans and WF Harris

Department of Optometry, University of Johannesburg, PO Box 524, Auckland Park, 2006 South Africa

<tevans@uj.ac.za>
<wharris@uj.ac.za>

Received 7 July 2011; revised version accepted 25 October 2011

Abstract

In Gaussian optics the transference is a matrix that is a complete representation of the effects of the system on a ray traversing it. Almost all of the familiar optical properties of the system, such as refractive error and power of the system, can be calculated from the transference. Because of the central importance of the transference it is useful to have some idea of how it depends on the frequency of light. This paper examines the simplest model eye, the reduced eye. The dependence of the transference is calculated in terms of both frequency and wavelength of light and both dependencies are displayed graphically. The principal matrix logarithms are also calculated and displayed graphically. Chromatic difference in refractive compensation, power and ametropia are obtained for the reduced eye from the transferences. (*S Afr Optom* 2011 **70**(4) 149-155)

Key Words: Transference, frequency, wavelength, Emsley's reduced eye, transformed transference, chromatic difference in: refractive compensation, power and ametropia.

Introduction

A transference is a matrix that represents the linear optical properties of an optical system, such as the eye. In Gaussian optics the transference is a complete representation of the effects of the system on a ray traversing it. Most of the optical properties of the system, such as refractive compensation[1], back- and front-vertex power[2], locations of the cardinal points[3, 4] and power of the system[5] can be calculated from the system's transference. Because of the central importance of the transference it is useful to have some idea of how it depends on the frequency of the light traversing it. We take a look at the simplest model eye, the reduced eye.

The dependence of the fundamental first-order properties, calculated in terms of both frequency and wavelength of light, will be represented graphically across the visible light spectrum. Further, the dependence of the transformed transference will be represented graphically. Formulae for the calculation of chromatic difference in corneal-plane refractive-compensation of the reduced eye and chromatic difference in power and ametropia are derived.

Emsley's reduced eye

The advantage of the reduced eye (see Figure 1) is its simplicity. The reduced eye has a single stigmatic refracting surface of radius of curvature r and a homogenous gap of length z. Emsley[6] designed his reduced eye to match certain measurements of the Gullstrand-Emsley schematic eye. He placed specific emphasis on the power of 60 D and chose the refractive index in the reduced eye to be the same as that of water, namely 4/3. He took the index of air to be 1. These numbers imply a radius of curvature r of 50/9 mm (or 1/180 m) and a length z of 200/9 mm (or 1/45

*Based on research towards a higher degree by T Evans under the guidance of Professor WF Harris.

m)[6, 7]. In this paper we will make use of a reduced eye with the same r and z as Emsley's eye and with an index n dependant on the frequency of light.

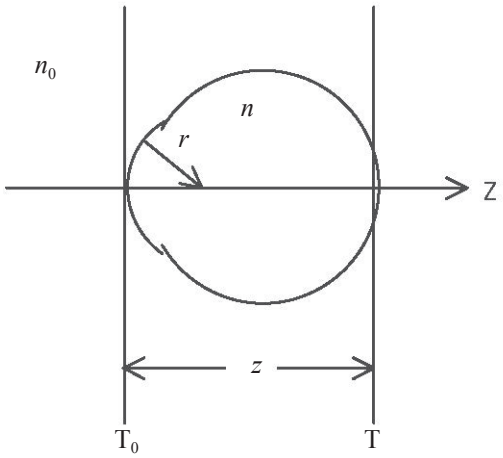

Figure 1. The reduced eye as a defined optical system. The length is z, the radius of curvature of the refracting surface is r, the refractive index outside the system is n_0 and inside the system is n. The optical system has a longitudinal axis, Z and is bound by an entrance plane T_0 immediately in front of the refracting surface and an exit plane T immediately in front of the retinal surface.

Linear optics

An optical system is bound by an entrance plane T_0 and an exit plane T and has a longitudinal axis Z. The transference **T** of a stigmatic, untilted, centred Gaussian optical system is represented by[8]

$$\mathbf{T} = \begin{pmatrix} A & B \\ C & D \end{pmatrix} \tag{1}$$

where A the dilation, B the disjugacy, C the divergence and D the divarication are the fundamental first-order optical properties of the system[1, 8, 9]. The power F is given simply by[5, 8]

$$F = -C\,. \tag{2}$$

When the system is an eye the dilation A can be considered to be the ametropia[8] of the eye. In particular when the eye is emmetropic

$$A = 0\,. \tag{3}$$

The corneal-plane refractive compensation is given by[1, 8]

$$F_0 = B^{-1}A\,. \tag{4}$$

The transferences of the two elementary optical systems[10, 11] are

$$\mathbf{T}_\xi = \begin{pmatrix} 1 & \dfrac{z}{n} \\ 0 & 1 \end{pmatrix} \tag{5}$$

for a homogenous gap and

$$\mathbf{T}_K = \begin{pmatrix} 1 & 0 \\ -\dfrac{n-n_0}{r} & 1 \end{pmatrix} \tag{6}$$

for a refracting surface. To calculate the transference of the reduced eye one multiplies in reverse[12] as follows

$$\mathbf{T} = \mathbf{T}_\xi \mathbf{T}_K\,. \tag{7}$$

Substituting Equations 5 and 6 into Equation 7 and multiplying one obtains

$$\mathbf{T} = \begin{pmatrix} 1-\dfrac{z}{n}\left(\dfrac{n-n_0}{r}\right) & \dfrac{z}{n} \\ -\dfrac{n-n_0}{r} & 1 \end{pmatrix}. \tag{8}$$

Substituting the values for Emsley's reduced eye into Equation 8 one obtains

$$\mathbf{T} = \begin{pmatrix} 0 & \dfrac{50}{3}\ \text{mm} \\ -0.060\ \text{kD} & 1 \end{pmatrix}. \tag{9}$$

It is immediately apparent from Equations 3 and 9 that the eye is emmetropic and has a power of 60 D.

Frequency or wavelength?

The fundamental relationship between frequency (ν) and vacuum wavelength (λ) is given by

$$c_0 = \nu\lambda \tag{10}$$

where light traveling in a vacuum has a speed c_0=299 792 458 m.s^{-1} as defined by the 17th General Conference on Weights and Measures in November 1983. Pease and Barbeito[13] look at the relationship between frequency and wavelength for a number of studies involving chromatic aberration and conclude that results using frequency or wavenumber (the inverse of wavelength) are "nearly perfectly linear"[13, 14] in contrast to those using wavelength. They cite several reasons to support using frequency rather than wavelength (perhaps the most important being that frequency is independent of the medium whereas wavelength is not). These reasons make a compelling argument to study

the dependence of the transference on the frequency of light rather than its dependence on wavelength. We will compare the dependence of the transference on both frequency and wavelength.

Visible light colour spectrum

The spectrum with wavelengths in vacuum is between 400 and 700 nm and represents the range over which human spectral sensitivity varies between 1 and 100%.[14-16] This represents frequencies between 428.3 THz and 749.5 THz, approximately. Six coloured reference points are shown on each of the graphs below. The four colours red-orange, yellow, green and blue represent the peak vacuum wavelengths where each colour is considered "pure"[17] while the deep-red and violet-blue represent the spectral range end-points. The frequencies and wavelengths of the six colours are detailed in Table 1.

Transference as a function of refractive index

The transference of the reduced eye in Equation 8 shows that the variable affected by different frequencies of light is the refractive index n. Entering the radius of curvature and length of Emsley's reduced eye we obtain its transference as a function of the refractive indices:

$$\mathbf{T} = \begin{pmatrix} \dfrac{4n_0}{n} - 3 & \dfrac{200}{9n}\ \text{mm} \\ -\dfrac{9}{50}(n - n_0)\ \text{kD} & 1 \end{pmatrix}. \qquad (11)$$

Refractive index of the Reduced Eye

Thibos *et al*[15] represent the refractive index of the reduced eye as a function of wavelength as follows

$$n = a + \frac{b}{\lambda - c} \qquad (12)$$

where a=1.320535, b=4.685 nm and c=214.102 nm. The formula is based on Cornu's formula for refractive index of water and constants were derived from clinical experimentation on real eyes. Using this formula, Thibos *et al*[15] showed that the refractive index of the body of the reduced eye changes more rapidly with wavelength than a reduced eye filled with water. The predictions for longitudinal chromatic aberration using this formula more closely approximate experimental data than Emsley's reduced eye filled with water. The refractive indices for our six reference points were calculated using Equation 12 and are given in Table 1.

Refractive index of air

The refractive index of air differs only very slightly from that of a vacuum and for most optometric calculations one can put n_0=1. A number of equations, for example Cauchy's dispersion formula[18] and Ciddor's equations[19], are available for calculating the refractive index of air. Cauchy's formula is expressed in terms of wavelength whereas Ciddor's equations are expressed in terms of wavenumber. Cauchy's dispersion formula[18] is

$$(n_0 - 1)10^7 = p + \frac{q}{\lambda^2} + \frac{t}{\lambda^4} \qquad (13)$$

Table 1. The colours of the six reference points and their frequencies, vacuum wavelengths, refractive indices for the reduced eye, ametropias, powers for the reduced eye and refractive compensations are provided. The last row shows the chromatic difference across the spectrum 428.3 to 749.5 THz.

Colour	Frequency in THz	Vacuum wavelength in nm	Refractive index	Ametropia	Power of reduced eye in dioptres	Refractive compensation in dioptres
Deep red	428.27	700	1.3302	0.0071	59.4318	0.4261
Red	475.86	630	1.3318	0.0035	59.7240	0.2070
Yellow	516.88	580	1.3333	0.0000	60.0010	0.0008
Green	576.52	520	1.3359	−0.0057	60.4531	−0.3398
Blue	631.14	475	1.3385	−0.0116	60.9286	−0.6964
Violet-blue	749.48	400	1.3457	−0.0277	62.2327	−1.6745
Chromatic difference in:			Δn = 0.0156	ΔA = −0.0348	ΔF = 2.8008	ΔF_0 = −2.1006

where p=2726.43, q=12.288×10^{6}nm^2 and t=355.5×10^9 nm^4 for dry air at temperature 15°C and pressure 101 kPa.

When Cauchy's dispersion formula is used for n_0 one obtains results that differ insignificantly from those for n_0=1. In particular for dilation the difference is less than 0.00083 across the entire visible light spectrum. For divergence this difference is 0.05 D. This results in a very slight upward shift in the graphs for *A* and *C* in Figure 2, however, the curvatures are unaffected.

Calculation shows that the reduced eye is emmetropic at the frequency 517 THz (580 nm, yellow) when we use n_0=1 but is emmetropic at the frequency 526 THz (570 nm, yellow-green) when the refractive index of air is calculated using Cauchy's formula.

Graphical representation of the fundamental properties

The properties are calculated for frequencies according to Equation 11 with n_0=1 and *n* given by Equation 12. The results of the calculations of each of the fundamental first-order optical properties are given in the accompanying graphs. Figure 2 represents each of the fundamental properties as functions of frequency of light and Figure 3 as functions of wavelength. The six coloured reference points are shown by means of coloured diamonds. The small black dots on Figure 2 represent 10 equally spaced intervals of frequency of approximately 32.1 THz and the crosses on Figure 3 represent 10 equally spaced intervals of 30 nm wavelength.

We note that in Figure 2 the dots are more evenly spaced than the crosses in Figure 3. The dashed line represents the slope of the curve calculated using the least squares method. Each of *A*, *B* and *C* present as curves in both sets of graphs. *D* is a straight line at 1 as required by Equation 11. The curves are closer to straight lines in Figure 2 than in Figure 3; this provides some justification for preferring to think in terms of frequency rather than wavelength of light.

The transferences at the extremes of the visible spectrum (428.3 THz or 700 nm and 749.5 THz or 400 nm), are

$$\mathbf{T}_{428.3\,\mathrm{THz}} = \begin{pmatrix} 0.0071 & 16.7062\ \mathrm{mm} \\ -0.0594\ \mathrm{kD} & 1 \end{pmatrix} \qquad (14)$$

$$\mathbf{T}_{749.5\,\mathrm{THz}} = \begin{pmatrix} -0.0277 & 16.5130\ \mathrm{mm} \\ -0.0622\ \mathrm{kD} & 1 \end{pmatrix}. \qquad (15)$$

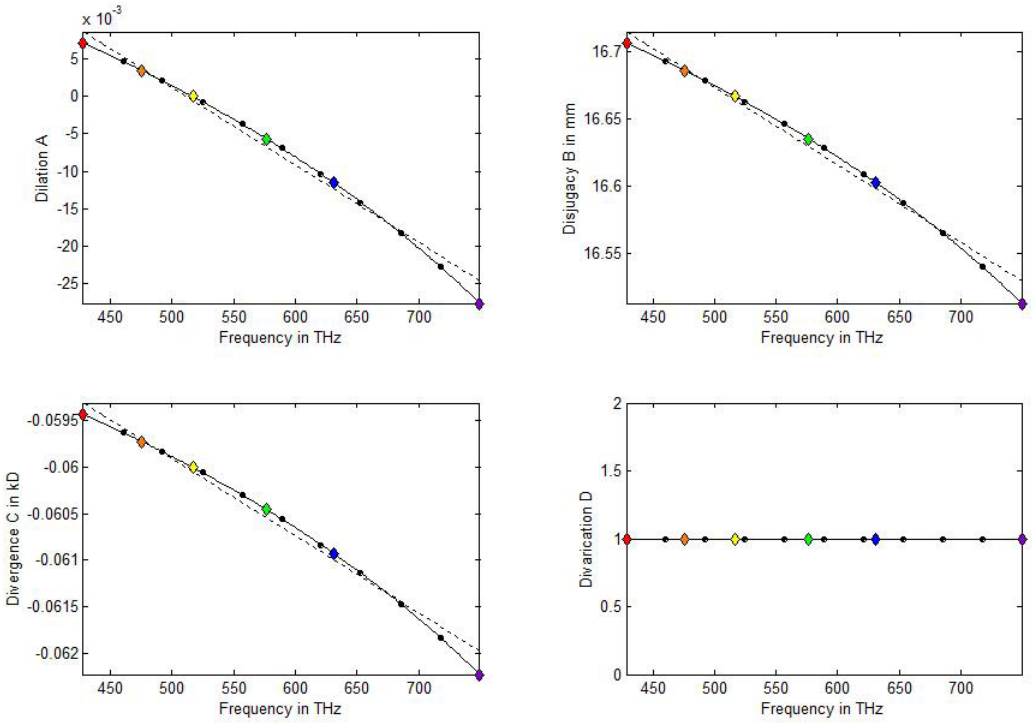

Figure 2. Sub-graphs A, B, C and D represent the four fundamental optical properties of the reduced eye as a function of frequency of light. The six coloured diamonds indicate six reference points as indicated in Table 1. The small black dots represent 10 equal intervals of 32.1 THz each. Each of *A*, *B* and *C* present as curves, while *D* is a horizontal straight line at 1.

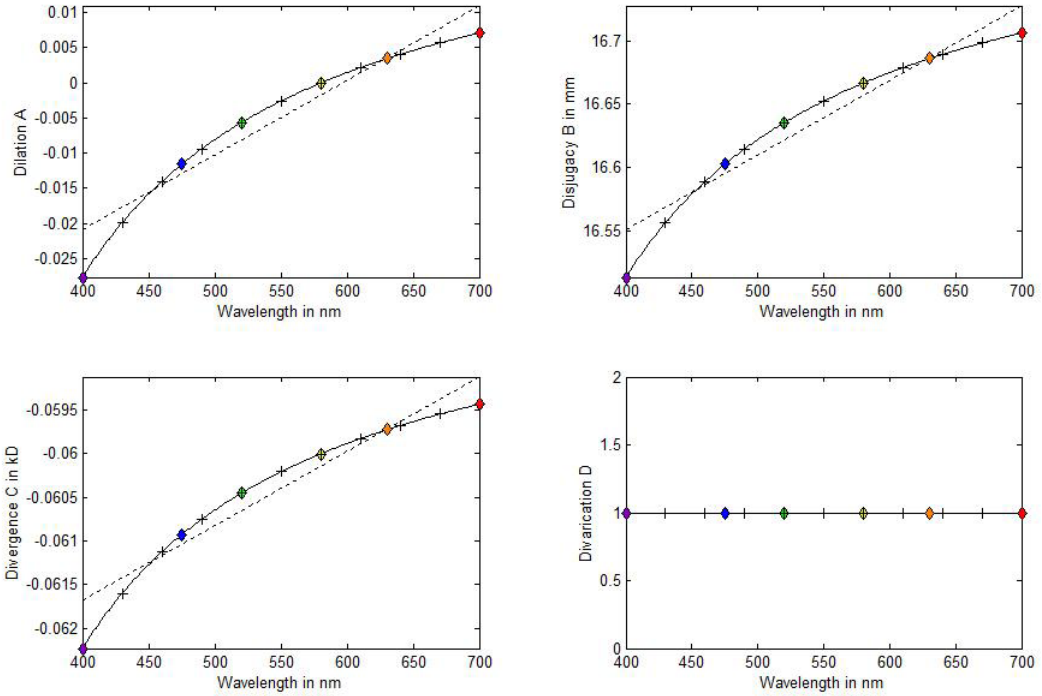

Figure 3. The four fundamental properties of the reduced eye as a function of wavelength. The black crosses represent 10 equal intervals of 30 nm each.

The transformed transference

By taking the principal matrix logarithm we convert each transference T into a Hamiltonian matrix[8, 20]. We represent the transformed matrix[8] by $\hat{\mathbf{T}}$. Thus

$$\hat{\mathbf{T}} = \mathrm{Log}\mathbf{T}. \tag{16}$$

In MATLAB the function used is *logm*. In terms of its entries we write the transformed transference[8] as

$$\hat{\mathbf{T}} = \begin{pmatrix} \hat{A} & \hat{B} \\ \hat{C} & \hat{D} \end{pmatrix}. \tag{17}$$

Because $\hat{\mathbf{T}}$ is Hamiltonian[20],

$$\hat{A} = -\hat{D}. \tag{18}$$

$\hat{\mathbf{T}}$ therefore has only three independent entries. This creates a 3-dimensional vector space which can be plotted on a 3-dimensional graph as done in Figure 4. In the figure $\hat{A}, \hat{B}$ and $\hat{C}$ are along three orthogonal axes, where $\hat{A}$ (and $\hat{D}$) are unitless, $\hat{B}$ is in millimetres and $\hat{C}$ is in kilodioptres. The result is close to a straight line. The small black dots represent 20 equally spaced intervals of frequency of 16.1 THz.

Transforming Equations 14 and 15, we find

$$\hat{\mathbf{T}}_{428.3\,\mathrm{THz}} = \begin{pmatrix} -0.5994 & 20.1699\ \mathrm{mm} \\ -0.0718\ \mathrm{kD} & 0.5994 \end{pmatrix} \tag{19}$$

$$\hat{\mathbf{T}}_{749.5\,\mathrm{THz}} = \begin{pmatrix} -0.6251 & 20.0888\ \mathrm{mm} \\ -0.0757\ \mathrm{kD} & 0.06251 \end{pmatrix}. \tag{20}$$

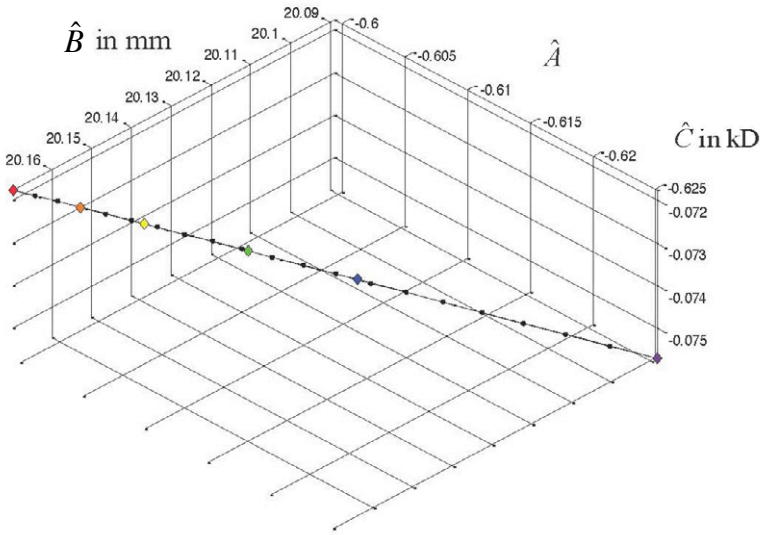

Figure 4. The transformed transference of the reduced eye in Hamiltonian space. The three axes represent $\hat{A}$, $\hat{B}$ and $\hat{C}$. The black dots represent frequencies spaced at intervals of 16.06 THz. The six diamonds represent the six coloured reference points. (The azimuth of 45° and elevation of 125° were chosen to exaggerate any possible curvature.)

Some Derived Properties

We obtain here some derived properties of the reduced eye that are directly and simply obtainable from the transference. Using Equation 2 we calculate the power F of the reduced eye for a particular frequency of light and using Equation 4 we calculate the corneal-plane refractive compensation F_0 for the frequency. We read the ametropia A directly from the transference for the chosen frequency of light. Of greater interest is the chromatic difference in refractive compensation ΔF_0 (known by various terms including longitudinal chromatic aberration[21], chromatic difference of refractive error[21], chromatic difference in refraction[14], and axial chromatic aberration[21]), chromatic difference in power (also known as chromatic difference of equivalent power[14]) and chromatic difference in ametropia across a specified spectrum of visible light to be studied.

Each of these derived properties in chromatic difference between two frequencies or wavelengths can be calculated in two ways: either directly from the two transferences or using the equations below. Equations 21, 23, 24 and 26 are general equations while Equations 22, 25 and 27 apply to the reduced eye.

To calculate the chromatic difference in corneal-plane refractive compensation across a specified spectrum we take values from the two transferences (Equation 1) and substitute them into Equation 4 as follows:

$$\Delta F_0 = B_2^{-1}A_2 - B_1^{-1}A_1 \quad . \tag{21}$$

Now substituting from Equation 8 and also substituting the values for z and r for the reduced eye, we find

$$\Delta F_0 = (-135\ \mathrm{D})\Delta n \tag{22}$$

where Δn simplifies to

$$\Delta n = b\left(\frac{1}{\lambda_2 - c} - \frac{1}{\lambda_1 - c}\right) \tag{23}$$

and b and c are the same constants as for Equation 12.

To calculate chromatic difference in power we similarly take values from the transferences and substitute them into Equation 2 as follows

$$\Delta F = -(C_2 - C_1) \tag{24}$$

and substituting from Equation 8 and then substituting the value for r for the reduced eye we find

$$\Delta F = (180\ \mathrm{D})\Delta n \quad . \tag{25}$$

The chromatic difference in ametropia is derived directly from the transferences and therefore

$$\Delta A = A_2 - A_1 \, . \tag{26}$$

Substituting values for z and r we obtain

$$\Delta A = 4\left(\frac{1}{n_2} - \frac{1}{n_1}\right) \tag{27}$$

where n_1 and n_2 are calculated from Equation 12.

The chromatic difference in corneal-plane refractive compensation of the reduced eye was calculated across the visible light spectrum 428.3 to 749.5 THz and is −2.1006 D (see Table 1). The chromatic difference in power is 2.8 D. The chromatic difference in ametropia is −0.0348.

Conclusion

The transference of the reduced eye depends on the frequency of light. The accuracy of the calculations depends on the formula used to calculate the refractive index as a function of either frequency of light or wavelength. In this article we have used Equation 12.

Results are displayed graphically for the transferences both as a function of frequency and as a function of wavelength. Divarication D is constant while ametropia A, disjugacy B and divergence C exhibit curved lines. The graph for the transformed transference in Hamiltonian space is approximately a straight line.

Chromatic difference in refractive compensation, chromatic difference in power and chromatic difference in ametropia are calculated directly from the transference for the reduced eye.

Acknowledgements

We thank RD van Gool for continued discussions. WF Harris acknowledges support from the National Research Foundation. All calculations and graphs were done using MATLAB.

References

1. Harris WF. Magnification, blur, and ray state at the retina for the general eye with and without a general optical instrument in front of it. 1. Distant objects. *Optom Vis Sci* 2001 **78** 888-900.
2. Harris WF. Back- and front-vertex powers of astigmatic systems. *Optom Vis Sci* 2010 **87** 70-72.
3. Harris WF. Graphical construction of cardinal points from the transference. *S Afr Optom* 2011 **70** 3-13.

4. Harris WF. Pascal's ring, cardinal points, and refractive compensation. *Vision Res* 2011 **51** 1679-1685.
5. Harris WF. Dioptric power: its nature and its representation in three- and four-dimensional space. *Optom Vis Sci* 1997 **74** 349-366.
6. Emsley HH. *Visual Optics*. London: Hatton Press Ltd, 1950 pp 525-527, 543-544.
7. Bennett AG, Rabbetts RB. *Clinical Visual Optics*. London: Butterworth. 1984; p 18.
8. Harris WF. The log-transference and an average Gaussian eye. *S Afr Optom* 2005 **64** 84-88.
9. Harris WF. The four fundamental properties of Gaussian optical systems including the eye. *S Afr Optom* 1999 **58** 69-79.
10. Harris WF. General approach to the sensitivity of the optics of an eye to change in elementary parameters with application to the Gaussian optics of a reduced eye. *S Afr Optom* 2009 **68** 166-174.
11. Harris WF. Symplecticity and relationships among the fundamental properties in linear optics. *S Afr Optom* 2010 **69** 3-13.
12. Harris WF. Stigmatic optical systems. *Optom Vis Sci* 2004 **81** 947-952.
13. Pease PL, Barbeito R. Axial chromatic aberration of the human eye: frequency or wavelength? *Ophthal Physiol Opt* 1989 **9** 215-217.
14. Rabbetts RB. *Bennett and Rabbetts' Clinical Visual Optics*, 4th Ed. Edinburgh: Butterworth Heineman Elsevier, 2007 pp 287-293.
15. Thibos LN, Ye M, Zhang X, Bradley A. The chromatic eye: a new reduced-eye model of ocular chromatic aberration in humans. *Appl Opt* 1992 **31** 3594-3600.
16. Le Grand Y. Light, *Colour and Vision*. Chapman and Hall, London; 1957 pp 72-73.
17. Meyer-Arendt JR. *Introduction to Classical and Modern Optics*. New Jersey: Prentice Hall, 1995 p 5.
18. Hodgson CD. *Handbook of Chemistry and Physics*. Chemical Rubber Publishing Co, Cleveland, 1959 p 2943.
19. Ciddor PE. Refractive index of air: new equations for the visible and near infrared. *Appl Opt* 1996 **35** 1566-1573.
20. Harris WF. Quantitative analysis of transformed ray transferences of optical systems in space of augmented Hamiltonian matrices. *S Afr Optom* 2007 **66** 62-67.
21. Thibos LN, Bradley A, Zhang X. Effect of ocular chromatic aberration on monocular visual performance. *Optom Vis Sci* 1991 **68** 599-607.

APPENDIX to Harris WF & Evans T Chromatic Aberration in Heterocentric Astigmatic Systems Including the Eye Optom Vis Sci 2012;89

The theory is illustrated here for a model eye with four tilted astigmatic refracting surfaces. The optical system is the visual optical system of the eye from immediately in front of the cornea to immediately in front of the retina. The curvatures, tilts, and separations are listed in Table A1. K1 and K2 are the first and second surfaces of the cornea and L1 and L2 are the first and second surfaces of the lens of the eye. K1 has principal meridians at 180° and 90°; the radii of curvature along them are 6.5 and 8 mm respectively. The horizontal and vertical components of tilt of K1 are 0.06 and -0.05 (radians) respectively; the right side of the cornea would be tilted away from and the top towards an observer looking at the eye. We use the equations for refractive index of the cornea, aqueous, lens, and vitreous published by Villegas, Carretero, and Fimia[1]. The index in front of the eye is $n_0 = 1$. We use the vacuum wavelengths 656.3 nm for red and 486.1 nm for blue respectively that have been used by others[2]. In order to show small differences we retain more digits than may be physically meaningful.

TABLE A1.

Principal radii of curvature, separation, and tilt of surfaces of the model eye used in the numerical example.

Surface	Principal radii mm{degr}mm	Separation mm	Tilt
K1	$6.5\{180\}8$		$(0.06 \quad -0.05)^{\mathrm{T}}$
		0.5	
K2	$5.8\{20\}7.2$		$(0.04 \quad 0.06)^{\mathrm{T}}$
		3	
L1	$10.2\{100\}8.7$		$(-0.07 \quad 0.1)^{\mathrm{T}}$
		4	
L2	$-4.5\{70\}-6.5$		$(-0.05 \quad -0.03)^{\mathrm{T}}$
		16.5	

The transferences calculated by the method described elsewhere[3] for red and blue light turn out to be

$$\mathbf{T}_\mathrm{r} = \begin{pmatrix} -0.1513 & -0.0134 & 16.5690 & -0.1292 & -0.3134 \\ -0.0121 & -0.0125 & -0.1290 & 16.3221 & 0.1936 \\ -0.0686 & -0.0012 & 0.9046 & -0.0104 & -0.0176 \\ -0.0011 & -0.0619 & -0.0103 & 0.8840 & 0.0084 \\ 0 & 0 & 0 & 0 & 1 \end{pmatrix} \qquad \text{(A1)}$$

and

$$\mathbf{T}_\mathrm{b} = \begin{pmatrix} -0.1687 & -0.0136 & 16.4641 & -0.1309 & -0.3185 \\ -0.0123 & -0.0279 & -0.1307 & 16.2137 & 0.1957 \\ -0.0700 & -0.0012 & 0.9030 & -0.0106 & -0.0179 \\ -0.0011 & -0.0632 & -0.0105 & 0.8820 & 0.0086 \\ 0 & 0 & 0 & 0 & 1 \end{pmatrix} \qquad \text{(A2)}$$

Entries in the last three columns of the first two rows are in millimetres; entries in the first two columns of the third and fourth rows are in kilodiopters.

Distant Object Point

Consider a distant object point O in a vertical plane containing longitudinal axis Z. Rays from O arrive at the model eye with inclination $\mathbf{a}_\mathrm{O} = \begin{pmatrix} 0 \\ -0.05 \end{pmatrix}$ relative to Z. Details of the calculation are summarized in Table A2. For example, the red blurred image has a near vertical line (it is at about $94.90°$) 2.9567 mm in front of the retina; the other line is 0.2455 mm in front of the retina. (The blue image has a line at $94.87°$, not quite the same as for the red image.) The longitudinal chromatic aberration is $\Delta\mathbf{Z}$ as listed. Its principal structure is -0.3235 mm along $96.96°$ and -0.2884 mm. The horizontal and vertical components of the transverse chromatic aberration are -0.0008 mm and 0.0160 mm respectively.

It may also be of interest to calculate the chromatic difference of refractive compensation for the eye. The refractive compensation is given by[4] $\mathbf{F}_0 = \mathbf{B}^{-1}\mathbf{A}$, a dioptric power matrix. We obtain it from the transferences (Eqs. A1 and A2). In conventional spherocylindrical terms the results are $-0.6958\ -8.5194\times 95.50$ and $-1.6481\ -8.6850\times 95.59$ for red and blue light respectively. The chromatic difference of refractive compensation turns out to be

TABLE A2.

Longitudinal $\Delta\mathbf{Z}$ and transverse $\Delta\mathbf{y}$ chromatic aberration of a model heterocentric astigmatic eye and a distant object point with $\mathbf{a}_O = \begin{pmatrix} 0 \\ -0.05 \end{pmatrix}$.

	red	**blue**
$\mathbf{L}$ (kD) (Eq.11)	$\begin{pmatrix} -0.4874 & 0.4236 \\ 0.4236 & -5.3960 \end{pmatrix}$	$\begin{pmatrix} -0.4270 & 0.1643 \\ 0.1643 & -2.3414 \end{pmatrix}$
$\mathbf{Z}$ (mm) (Eq.4)	$\begin{pmatrix} -2.9369 & -0.2306 \\ -0.2306 & -0.2653 \end{pmatrix}$	$\begin{pmatrix} -3.2258 & -0.2263 \\ -0.2263 & -0.5882 \end{pmatrix}$
z_- (mm)	-2.9567	-3.2451
z_+ (mm)	-0.2455	-0.5960
$\mathbf{v}_+$	$\begin{pmatrix} 0.0853 \\ -0.9964 \end{pmatrix}$	$\begin{pmatrix} 0.0849 \\ -0.9964 \end{pmatrix}$
$\mathbf{V}$ (mm) (Eq. 26)	$\begin{pmatrix} -2.2021 & -0.1729 \\ -0.1729 & -0.1989 \end{pmatrix}$	$\begin{pmatrix} -2.4070 & -0.1689 \\ -0.1689 & -0.4389 \end{pmatrix}$
$(\mathbf{B}+\mathbf{VD})n_0$ (mm)	$\begin{pmatrix} 14.5787 & -0.2592 \\ -0.2833 & 16.1480 \end{pmatrix}$	$\begin{pmatrix} 14.2923 & -0.2545 \\ -0.2785 & 15.8283 \end{pmatrix}$
$\mathbf{e}+\mathbf{V}\boldsymbol{\pi}$ (mm)	$\begin{pmatrix} -0.2762 \\ 0.1950 \end{pmatrix}$	$\begin{pmatrix} -0.2767 \\ 0.1950 \end{pmatrix}$
	$\Delta((\mathbf{B}+\mathbf{VD})n_0) = \begin{pmatrix} -0.2864 & 0.0047 \\ 0.0048 & -0.3197 \end{pmatrix}$ mm	
	$\Delta(\mathbf{e}+\mathbf{V}\boldsymbol{\pi}) = \begin{pmatrix} -0.0006 \\ 0.0000 \end{pmatrix}$ mm	
	$\Delta\mathbf{Z} = \begin{pmatrix} -0.2889 & 0.0042 \\ 0.0042 & -0.3230 \end{pmatrix}$ mm (Eq. 5)	
	$\Delta\mathbf{y} = \begin{pmatrix} -0.0008 \\ 0.0160 \end{pmatrix}$ mm (Eq. 29)	

$\Delta\mathbf{F}_0 = \mathbf{F}_{0b} - \mathbf{F}_{0r} = \begin{pmatrix} -1.1136 & -0.0298 \\ -0.0298 & -0.9565 \end{pmatrix}$ D which is $-0.9510 \quad -0.1680 \times 100.37$ as a spherocylindrical power. It follows from the definitions that there is no simple relationship between chromatic difference of refractive compensation and longitudinal chromatic aberration for a distant object point.

Near Object Point

Table A3 lists the details for the model eye and object point O 400 mm in front of the eye and with transverse position $\mathbf{y}_O = \begin{pmatrix} -30 \\ 30 \end{pmatrix}$ mm relative to longitudinal axis Z. For an observer looking at the eye along Z, with O between the observer and the eye, O is up and to the left. The principal structure of the longitudinal chromatic aberration is -0.3555 mm along $97.25°$ and -0.3139 mm. The principal longitudinal chromatic aberrations are slightly larger in magnitude compared with those for the distant object and the principal meridians have undergone a small anticlockwise rotation. The horizontal and vertical components of the transverse chromatic aberration are -0.0238 mm and 0.0262 mm.

REFERENCES

1. Villegas ER, Carretero L, Fimia A. Le Grand eye for the study of ocular chromatic aberration. Ophthal Physiol Opt 1996; 16: 528-31.
2. Powell I. Lenses for correcting chromatic aberration of the eye. Appl Opt 1981; 20: 4152-5.
3. Harris WF. Transferences of heterocentric astigmatic catadioptric systems including Purkinje systems. Optom Vis Sci 2010; 87: 778-86.
4. Harris WF. A unified paraxial approach to astigmatic optics. Optom Vis Sci 1999; 76: 480-99.

TABLE A3.

Longitudinal $\Delta\mathbf{Z}$ and transverse $\Delta\mathbf{y}$ chromatic aberration of a model heterocentric astigmatic eye and object point with $z_O = -400$ mm and $\mathbf{y}_O = \begin{pmatrix} -30 \\ 30 \end{pmatrix}$ mm.

	red	**blue**
$\mathbf{L}$ (kD) (Eq. 10)	$\begin{pmatrix} -0.5773 & -0.2359 \\ -0.2359 & 1.9984 \end{pmatrix}$	$\begin{pmatrix} -0.4875 & -0.4410 \\ -0.4410 & 4.3566 \end{pmatrix}$
$\mathbf{Z}$ (mm) (Eq. 4)	$\begin{pmatrix} -2.2038 & -0.2601 \\ -0.2601 & 0.6367 \end{pmatrix}$	$\begin{pmatrix} -2.5184 & -0.2549 \\ -0.2549 & 0.2818 \end{pmatrix}$
z_- (mm)	-2.2275	-2.5414
z_+ (mm)	0.6603	0.3048
$\mathbf{v}_+$	$\begin{pmatrix} 0.0904 \\ -0.9959 \end{pmatrix}$	$\begin{pmatrix} 0.0899 \\ -0.9959 \end{pmatrix}$
$\mathbf{V}$ (mm) (Eq. 26)	$\begin{pmatrix} -1.6524 & -0.1950 \\ -0.1950 & 0.4774 \end{pmatrix}$	$\begin{pmatrix} -1.8792 & -0.1902 \\ -0.1902 & 0.2103 \end{pmatrix}$
$\mathbf{A}+\mathbf{VC}$	$\begin{pmatrix} -0.0377 & 0.0007 \\ 0.0008 & -0.0419 \end{pmatrix}$	$\begin{pmatrix} -0.0369 & 0.0007 \\ 0.0008 & -0.0410 \end{pmatrix}$
$\mathbf{e}+\mathbf{V\pi}$ (mm)	$\begin{pmatrix} -0.2860 \\ 0.2011 \end{pmatrix}$	$\begin{pmatrix} -0.2864 \\ 0.2009 \end{pmatrix}$
	$\Delta(\mathbf{A}+\mathbf{VC}) = \begin{pmatrix} 0.0008 & -0.0000 \\ -0.0000 & 0.0009 \end{pmatrix}$	
	$\Delta(\mathbf{e}+\mathbf{V\pi}) = \begin{pmatrix} -0.0004 \\ -0.0001 \end{pmatrix}$ mm	
	$\Delta\mathbf{Z} = \begin{pmatrix} -0.3145 & 0.0052 \\ 0.0052 & -0.3548 \end{pmatrix}$ mm (Eq. 5)	
	$\Delta\mathbf{y} = \begin{pmatrix} -0.0238 \\ 0.0262 \end{pmatrix}$ mm (Eq. 28)	

1040-5488/12/8911-e37/0 VOL. 89, NO. 11, PP. e37–e43
OPTOMETRY AND VISION SCIENCE

TECHNICAL REPORT

Chromatic Aberration in Heterocentric Astigmatic Systems Including the Eye

William F. Harris* and Tanya Evans†

ABSTRACT

Purpose. There is inconsistency in the literature in the definitions of longitudinal and transverse chromatic aberration, and there appear to be no definitions that make allowance for astigmatism and heterocentricity. The purpose is to propose definitions of longitudinal and transverse chromatic aberration that hold for systems which, like the typical eye, may be heterocentric and astigmatic and to develop the associated optics.

Methods. Common definitions of longitudinal and transverse chromatic aberration based on Gaussian optics are generalized naturally in terms of linear optics to accommodate heterocentricity and astigmatism.

Conclusions. The definitions offered here apply to systems in general, including the visual optical system of the eye, and hold for homocentric stigmatic systems in particular. Care is advocated in the use of the terms longitudinal and transverse chromatic aberration.

(Optom Vis Sci 2012;89:e37–e43)

Key Words: longitudinal chromatic aberration, transverse chromatic aberration, astigmatism, heterocentricity, transference, fundamental properties

Definitions in the literature[1–6] of first-order chromatic aberration treat the optical system in question as homocentric and as having refracting elements that are stigmatic. There appear to be no published definitions of longitudinal and transverse chromatic aberration in systems that are heterocentric and astigmatic. The lack of definitions would seem unfortunate in view of the fact that heterocentricity and astigmatism are features of the typical eye. It might also suggest that such definitions may not be easy to come by. This note has the limited objective of proposing definitions and developing the linear optics of longitudinal and transverse chromatic aberration of systems that may be heterocentric and astigmatic. The definitions are natural generalizations of familiar definitions in Gaussian optics. They hold for systems in general and apply to the eye in particular, and they allow one to explore the effects of changes to the eye including those that accompany accommodation and refractive surgery for example.

There is inconsistency in the optometric literature over the use of the term chromatic aberration, particularly, perhaps, in the more clinically oriented literature. This does not facilitate communication within the discipline and between optometry and other disciplines. Greater care needs to be taken over terminology; usage should be as consistent as possible with that of the broader scientific community, and distinct concepts should be assigned distinct names. (We take up these points at the end of this note.) In keeping with these thoughts we take our point of departure to be a definition of chromatic aberration used commonly in the literature of both general optics and optometry.[1–3]

HOMOCENTRIC SYSTEMS WITH STIGMATIC ELEMENTS

Fig. 1 illustrates definitions[1–3] of longitudinal and transverse chromatic aberration. The definitions are in terms of Gaussian optics. System S consists of refracting elements invariant under rotation about, and centered on, a common axis Z, the optical axis of S. None of its refracting surfaces is shown. S has entrance plane T_0 and exit plane T, both transverse to axis Z. The indices of refraction are n_0 and n upstream and downstream, respectively, of S. Object point O has longitudinal position z_O and transverse position y_O. Fig. 1 is drawn with $y_O > 0$ and $z_O < 0$. The location of the image point I depends on the frequency ν of light involved. Consider two particular frequencies ν_r and ν_b. It will be convenient to refer to the light as red and blue, respectively. The red and blue images of O are represented in Fig. 1 as I_r and I_b,

*PhD, FAAO
†BOptom
Department of Optometry, University of Johannesburg, Johannesburg, South Africa.

Supplemental digital content is available for this article. Direct URL citations appear in the printed text and are provided in the HTML and PDF versions of this article on the journal's Web site (*www.optvissci.com*).

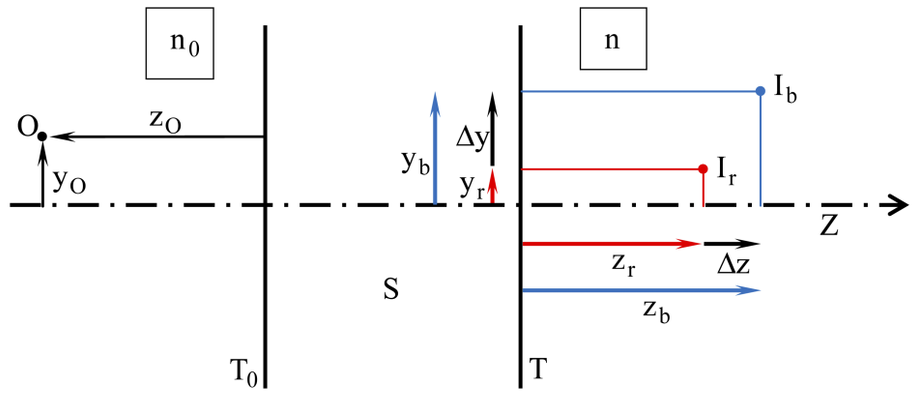

FIGURE 1.

Chromatic aberration in Gaussian optics. S is an optical system with entrance and exit planes T_0 and T, respectively. Z is the optical axis. Corresponding to an object point O are red and blue image points I_r and I_b. By definition, the longitudinal chromatic aberration of S for O is the signed length Δz. The transverse chromatic aberration of S for O is the signed length Δy. Usually $z_r > z_b$ and not as shown here.

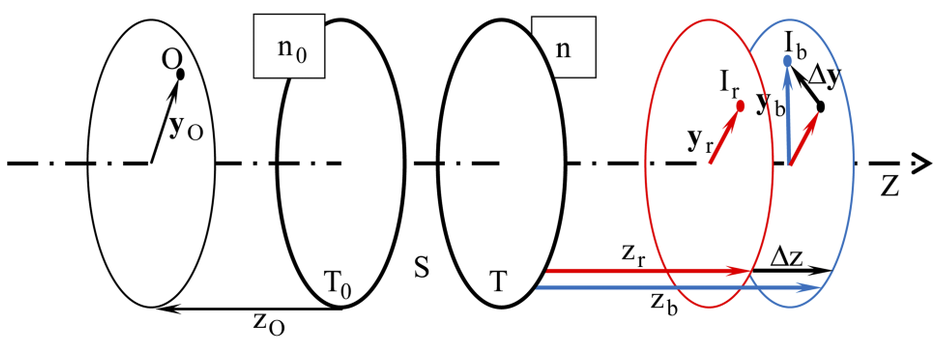

FIGURE 2.

Longitudinal chromatic aberration Δz (a scalar) and transverse chromatic aberration Δy (a vector) of heterocentric stigmatic system S for object point O. Longitudinal axis Z is not an optical axis.

respectively, with longitudinal z_r and z_b and transverse y_r and y_b positions, all being positive in the figure. We need to distinguish the incident n_{0r} and n_{0b} and emergent n_r and n_b indices corresponding to frequencies ν_r and ν_b. By definition

$$\Delta z = z_b - z_r \tag{1}$$

and

$$\Delta y = y_b - y_r \tag{2}$$

are the *longitudinal* (or *axial)* and *transverse* (or *lateral) chromatic aberrations,* respectively.

We note that longitudinal and transverse chromatic aberrations do not depend on the properties of system S alone; they depend on the properties of system S and the property of object point O. Most properties of a system depend on the context or environment of the system, that is, the indices n_0 and n. For convenience, we take reference to properties of a system to imply the context as well. The property of object point O is its position in space. In Fig. 1, it is represented by its longitudinal and transverse positions z_O and y_O. It follows that for a given system S, the chromatic aberration is not unique. There is usually an infinity of longitudinal and transverse chromatic aberrations. The chromatic aberration of the system becomes unique when the location of the object point is specified.

By these definitions, both longitudinal Δz and transverse Δy chromatic aberrations are lengths measured orthogonally and represented by scalars. One is tempted, therefore, to regard the two chromatic aberrations as Cartesian components of a vectorial chromatic aberration and to insert an arrow from I_r to I_b to represent it in Fig. 1. We could then treat chromatic aberration holistically and not have to write separate equations for the two components. We shall find below, however, that the two aspects are fundamentally different and cannot meaningfully be combined in this way.

HETEROCENTRIC SYSTEMS WITH STIGMATIC ELEMENTS

A two-dimensional drawing, like that of Fig. 1, suffices for representing chromatic aberration in the case of homocentric systems free of astigmatism because optical axis Z, object point O, and images I_r and I_b all lie in a common plane; that plane becomes the plane of the paper. However, when homocentricity is relaxed, this is usually no longer the case. In general, for heterocentric systems with stigmatic elements, we need a three-dimensional representation like that attempted in Fig. 2. In Fig. 2, system S contains refracting elements that may be mutually decentered. S may contain prisms and tilted surfaces. Z is no longer an optical axis but merely a longitudinal axis.

It is apparent that the definition for longitudinal chromatic aberration Δz in the case of homocentric systems with stigmatic elements (Eq. 1) can be generalized to heterocentric systems unchanged. This is not the case for transverse chromatic aberration however. Transverse chromatic aberration becomes a two-component vector $\Delta\mathbf{y}$ defined by

$$\Delta\mathbf{y} = \mathbf{y}_b - \mathbf{y}_r \tag{3}$$

where $\mathbf{y}_r$ and $\mathbf{y}_b$ are the transverse position vectors of images I_r and I_b. Transverse chromatic aberration $\Delta\mathbf{y}$ can be decomposed into horizontal and vertical components in the transverse plane if desired.

One still needs to resist any temptation to lump longitudinal and transverse chromatic aberration into a single concept of chromatic aberration that could be represented by an arrow (not shown) in Fig. 2 from I_r to I_b.

HETEROCENTRIC ASTIGMATIC SYSTEMS

We now relax the requirement that the elements of system S of Fig. 2 be stigmatic; the elements of S may be heterocentric and astigmatic. Each image point, I_r and I_b, in Fig. 2 becomes blurred in Fig. 3. One can think of each image point as dissociating longitudinally into a pair of orthogonal image lines. The structure becomes that of the familiar interval of Sturm, its nature and location being dependent on the frequency of the light. We need to allow for the fact that the orientations of the image lines usually do not match; that is, the first image line of the red blurred image is usually not parallel to the first image line of the blue blurred image. How now do we define longitudinal and transverse chromatic aberration?

Let us first consider chromatic aberration in a system with astigmatic elements that are centered on Z. Z then is an optical axis. Suppose, further, that object point O lies on Z. Red image I_r is then centered on Z, and its associated line segments intersect Z. The same holds for blue image I_b. Evidently, there is no transverse chromatic aberration. What chromatic aberration there is longitudinal. But how do we define it? The definition should surely account for the fact that the two blurred images may differ not only in longitudinal position but also in the nature and degree of blur. In other words, longitudinal chromatic aberration would need at least three numbers for its complete quantitative representation.

The images themselves do not suggest an obvious answer. Instead, we shift focus to the pencils of light containing them. In the absence of astigmatism, the red pencil would have reduced vergence $L_r = n_r/z_r$ in exit plane T where z_r is the longitudinal position of the image point relative to T. Turning the equation around, we obtain $z_r = n_r/L_r$. In the presence of astigmatism, the generalization of the scalar reduced vergence L is the matrix reduced vergence $\mathbf{L}$ introduced by Fick[7,8] and, independently, by Keating.[9] $\mathbf{L}$ is a 2×2 symmetric matrix[10] identical in mathematical character to the dioptric power matrix $\mathbf{F}$ described by Fick[7,8] and Long[11] if not by others before them. Its entries have the units of reciprocal length and so can be in diopters. $\mathbf{L}_r$ is the reduced vergence at exit plane T of system S of the red astigmatic pencil defined by O, and $\mathbf{L}_b$ is the same but for the blue pencil.

We define

$$\mathbf{Z} = \mathbf{L}^{-1}\mathrm{n}. \tag{4}$$

$\mathbf{Z}$ is symmetric and has the units of length and can be regarded as a generalized position of the blurred image relative to exit plane T. The eigenvalues of $\mathbf{Z}$ give the longitudinal positions of the image lines, and the eigenvectors define their orientations. (Eigenvalues and eigenvectors are treated in standard texts in linear algebra and have been applied in this context in several articles.[9–11]) (For the moment, we assume that $\mathbf{L}^{-1}$ exists and return to the issue of nonexistence later.) Let the eigenvalues of $\mathbf{Z}$ be z_- and z_+ where $z_- \leq z_+$ and let the corresponding normalized eigenvectors be $\mathbf{v}_-$ and $\mathbf{v}_+$. Then, the first image line has longitudinal position z_- relative to exit plane T and is parallel to the complementary eigenvector $\mathbf{v}_+$, and the second image line has longitudinal position z_+ and is parallel to $\mathbf{v}_-$.

Eq. 1 suggests the definition

$$\Delta\mathbf{Z} = \mathbf{Z}_b - \mathbf{Z}_r \tag{5}$$

for the longitudinal chromatic aberration of a homocentric astigmatic system S for object point O on the optical axis. There is no

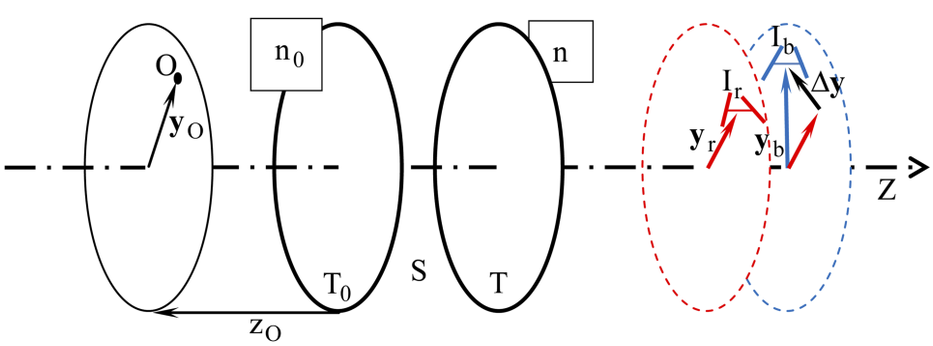

FIGURE 3.

Chromatic aberration of a system S with heterocentric astigmatic elements. Corresponding to object point O are blurred images I_r and I_b, each of which has a pair of longitudinally separated orthogonal image lines shown here by means of short line segments connected by a line segment parallel to Z. Longitudinal chromatic aberration is defined by Eq. 5 in terms of the reduced vergence of light at emergence from S at T. Transverse chromatic aberration is the vector $\Delta\mathbf{y}$. If Z is an optical axis and O is on Z then $\Delta\mathbf{y} = \mathbf{o}$ and I_r and I_b are centered on Z.

transverse chromatic aberration. $\Delta\mathbf{Z}$ characterizes the longitudinal difference of the two images completely. By this definition, longitudinal chromatic aberration becomes the 2×2 symmetric matrix $\Delta\mathbf{Z}$ and, as such, can be characterized by three independent numbers. However, we need to examine it further.

Now reduced vergence (either as scalar L or as matrix $\mathbf{L}$) depends on the relative longitudinal positions of object point and refracting elements and is independent of relative transverse positions. Thus, provided relative longitudinal positions are maintained, decentering the object point and elements of the system has no effect on the longitudinal positions and natures of the blurred images including the longitudinal positions and orientations of the image lines. It follows, therefore, that we can relax the requirement that O and the centers of the elements of S be on axis Z and take Eq. 5 to be the definition of the longitudinal chromatic aberration $\Delta\mathbf{Z}$ of a heterocentric astigmatic system for an object point anywhere.

Because $\Delta\mathbf{Z}$ is 2×2 and symmetric, longitudinal chromatic aberration has two orthogonal principal meridians. They are the meridians within which the longitudinal chromatic aberration is a maximum and a minimum. The maximum and minimum values are the *principal longitudinal chromatic aberrations*. They are the eigenvalues of $\Delta\mathbf{Z}$, and the corresponding principal meridians are the corresponding eigenvectors.

The only effect of relative decentration of object point and system elements is to cause transverse displacement $\mathbf{y}_r$ and $\mathbf{y}_b$ of blurred images I_r and I_b of object point O in heterocentric astigmatic system S. Then, Eq. 3 defines the transverse chromatic difference $\Delta\mathbf{y}$ of the images. We, therefore, call $\Delta\mathbf{y}$ the transverse chromatic aberration of system S for object point O.

CHROMATIC ABERRATION IN GENERAL

Eqs. 3 and 5 represent the generalizations to optical systems in general of the definitions (Eq. 1 and 2) for systems whose refracting elements are all stigmatic and centered on an optical axis. Eq. 3 defines $\Delta\mathbf{y}$ transverse and Eq. 5 $\Delta\mathbf{Z}$ longitudinal chromatic aberration in general; the first is a two-dimensional vector, and the second is a 2×2 symmetric matrix. The essential difference in mathematical character between transverse and longitudinal chromatic aberration highlights the fact that the two types of aberration are fundamentally different in nature and cannot meaningfully be combined into a single unified concept of chromatic aberration.

All this holds in particular for systems whose elements are stigmatic and homocentric. However, in a context in which only such systems are under discussion $\Delta\mathbf{y}$ and $\Delta\mathbf{Z}$ can be reduced to the scalar quantities Δy and Δz and sketched in one plane as in Fig. 1. Then, Δy is one component of $\Delta\mathbf{y}$, the other being zero and perpendicular to the plane of the paper, and Δz is the scalar coefficient in the scalar matrix $\Delta Z = \mathbf{I}\Delta z$, $\mathbf{I}$ being an identity matrix.

QUANTIFYING CHROMATIC ABERRATION

Having defined them, and given the makeup of an optical system, how do we calculate longitudinal and transverse chromatic aberration? Here, we derive general formulae in linear optics. The key is the system's ray transference, which is a function of the frequency of light.[12] For systems that may be heterocentric and astigmatic, the transference is the 5×5 matrix[13,14]

$$\mathbf{T} = \begin{pmatrix} \mathbf{A} & \mathbf{B} & \mathbf{e} \\ \mathbf{C} & \mathbf{D} & \boldsymbol{\pi} \\ \mathbf{o}^{\mathrm{T}} & \mathbf{o}^{\mathrm{T}} & 1 \end{pmatrix}. \quad (6)$$

$\mathbf{A}$, $\mathbf{B}$, $\mathbf{C}$, and $\mathbf{D}$ are 2×2 and $\mathbf{e}$ and $\boldsymbol{\pi}$ are 2×1 submatrices. They are the fundamental properties of the system. $\mathbf{o}^{\mathrm{T}}$ is the matrix transpose of the 2×1 null matrix $\mathbf{o}$. The fifth row of $\mathbf{T}$ is the trivial (0 0 0 0 1). $\mathbf{e}$ and $\boldsymbol{\pi}$ account for the effects of tilt and decentration; each is null if the longitudinal axis is an optical axis.[15]

Longitudinal Chromatic Aberration

If the reduced vergence is $\mathbf{L}_0$ at entrance plane T_0 of system S, then the reduced vergence is[10,16]

$$\mathbf{L} = (\mathbf{D}\mathbf{L}_0 - \mathbf{C})(\mathbf{A} - \mathbf{B}\mathbf{L}_0)^{-1} \quad (7)$$

at the exit plane T of S. For an object point O at longitudinal position z_O relative to T_0

$$\mathbf{L}_0 = \mathbf{I}n_0/z_O. \quad (8)$$

Hence

$$\mathbf{L} = (\mathbf{D}n_0/z_O - \mathbf{C})(\mathbf{A} - \mathbf{B}n_0/z_O)^{-1} \quad (9)$$

or

$$\mathbf{L} = (\mathbf{D} - \mathbf{C}z_O/n_0)(\mathbf{A}z_O/n_0 - \mathbf{B})^{-1} \quad (10)$$

with two special cases,

$$\mathbf{L} = -\mathbf{C}\mathbf{A}^{-1} \quad (11)$$

for $z_O \to \infty$ and

$$\mathbf{L} = -\mathbf{D}\mathbf{B}^{-1} \quad (12)$$

for $z_O = 0$. (Eq. 11 represents the back-vertex power of system S.[17]) Adding subscripts to all the parameters in these equations (except z_O) gives expressions for the red and blue reduced vergences $\mathbf{L}_r$ and $\mathbf{L}_b$ at exit plane T. Substitution into Eq. 5 then gives the longitudinal chromatic aberration $\Delta\mathbf{Z}$ for system S and object point O.

Transverse Chromatic Aberration

Perhaps surprisingly, the problem of calculating the transverse chromatic aberration is more challenging. We first examine object points at finite distances.

Consider the compound system from the transverse plane of O to the transverse plane containing an image line of a blurred image. Let the longitudinal position of the plane of the image line be z relative to exit plane T of system S. The compound system's transference is obtained by multiplying the transferences of the components in reverse order in the usual way.[14] Its top block row turns out to be

$$\left(\mathbf{A} + \mathbf{C}z/n \quad \mathbf{B} + \mathbf{D}z/n \quad -(\mathbf{A} + \mathbf{C}z/n)z_O/n_0 \quad \mathbf{e} + \boldsymbol{\pi}z/n\right). \quad (13)$$

Combining this with the equation for the transverse position at emergence (Eq. 14 of a previous article[14]), we see that a ray of

inclination $\mathbf{a}_O$ at object point O arrives at the transverse plane of the image line with transverse position

$$\mathbf{y} = (\mathbf{A} + \mathbf{C}z/n)\mathbf{y}_O + \Big(\mathbf{B} + \mathbf{D}z/n - (\mathbf{A} + \mathbf{C}z/n)z_O/n_0\Big)n_0\mathbf{a}_O + \mathbf{e} + \boldsymbol{\pi}z/n. \quad (14)$$

In particular for the ray parallel to longitudinal axis Z at O

$$\mathbf{y} = (\mathbf{A} + \mathbf{C}z/n)\mathbf{y}_O + \mathbf{e} + \boldsymbol{\pi}z/n. \quad (15)$$

We write this as

$$\mathbf{y} = \mathbf{A}\mathbf{y}_O + (\mathbf{C}\mathbf{y}_O + \boldsymbol{\pi})z/n + \mathbf{e}. \quad (16)$$

The first image line goes through the point given by Eq. 16 with $z = z_-$ and is parallel to $\mathbf{v}_+$. Hence, we can write a parametric equation for the first image line as

$$\mathbf{y}_- = \mathbf{v}_+k_- + \mathbf{A}\mathbf{y}_O + (\mathbf{C}\mathbf{y}_O + \boldsymbol{\pi})z_-/n + \mathbf{e} \quad (17)$$

for all real scalars k_-. Interchanging the plus and minus signs gives the equation of the second image line. But $\mathbf{v}_+$ is orthogonal to $\mathbf{v}_-$ so we can write the equation for the second image line as

$$\mathbf{y}_+ = \mathbf{E}\mathbf{v}_+k_+ + \mathbf{A}\mathbf{y}_O + (\mathbf{C}\mathbf{y}_O + \boldsymbol{\pi})z_+/n + \mathbf{e} \quad (18)$$

where $\mathbf{E} = \begin{pmatrix} 0 & 1 \\ -1 & 0 \end{pmatrix}$. Subtracting Eq. 17 from Eq. 18 we obtain

$$\mathbf{y}_+ - \mathbf{y}_- = (\mathbf{E}k_+ - \mathbf{I}k_-)\mathbf{v}_+ + \mathbf{c} \quad (19)$$

where

$$\mathbf{c} = (\mathbf{C}\mathbf{y}_O + \boldsymbol{\pi})(z_+ - z_-)/n. \quad (20)$$

Now $\mathbf{y}_+ - \mathbf{y}_-$ is the longitudinal projection of a vector from a point on the first image line to a point on the second. We make this vector parallel to Z, i.e., $\mathbf{y}_+ - \mathbf{y}_- = \mathbf{o}$. Then, in terms of the components of $\mathbf{v}_+$ and $\mathbf{c}$, Eq. 19 becomes

$$\begin{pmatrix} k_- & -k_+ \\ k_+ & k_- \end{pmatrix}\begin{pmatrix} v_{+1} \\ v_{+2} \end{pmatrix} = \begin{pmatrix} c_1 \\ c_2 \end{pmatrix}. \quad (21)$$

Multiplying out, rearranging, and reassembling into matrices we obtain

$$\begin{pmatrix} v_{+2} & -v_{+1} \\ v_{+1} & v_{+2} \end{pmatrix}\begin{pmatrix} k_+ \\ k_- \end{pmatrix} = \begin{pmatrix} -c_1 \\ c_2 \end{pmatrix}. \quad (22)$$

Because $\mathbf{v}_+$ is a unit vector, the 2×2 matrix on the left has unit determinant. Hence

$$\begin{pmatrix} k_+ \\ k_- \end{pmatrix} = \begin{pmatrix} v_{+2} & v_{+1} \\ -v_{+2} & v_{+2} \end{pmatrix}\begin{pmatrix} -c_1 \\ c_2 \end{pmatrix} \quad (23)$$

from which we obtain

$$k_- = \mathbf{v}_+^T\mathbf{c} \quad (24)$$

in particular. Substituting from Eq. 24 into Eq. 17 and rearranging one finds that the transverse position of the image is

$$\mathbf{y} = (\mathbf{A} + \mathbf{V}\mathbf{C})\mathbf{y}_O + \mathbf{e} + \mathbf{V}\boldsymbol{\pi} \quad (25)$$

where $\mathbf{V}$ is the matrix

$$\mathbf{V} = \Big(\mathbf{v}_+\,\mathbf{v}_+^T(z_+ - z_-) + \mathbf{I}z_-\Big)/n. \quad (26)$$

For a distant object point we take the compound system to be system S and the homogeneous gap between S and an image line and apply a similar method to that used above for an object point at a finite distance. We find that, for a distant object point O, the transverse position of the image turns out to be

$$\mathbf{y} = (\mathbf{B} + \mathbf{V}\mathbf{D})n_0\mathbf{a}_O + \mathbf{e} + \mathbf{V}\boldsymbol{\pi} \quad (27)$$

where $\mathbf{a}_O$ is the inclination of the rays from O.

Eqs. 25 to 27 can be written for the red and blue blurred images. Eq. 27 then gives $\mathbf{y}_b$ and $\mathbf{y}_r$ for distant object points and Eq. 25 gives them otherwise. Hence, from Eq. 3, we obtain the transverse chromatic aberration

$$\Delta\mathbf{y} = \Delta(\mathbf{A} + \mathbf{V}\mathbf{C})\mathbf{y}_O + \Delta(\mathbf{e} + \mathbf{V}\boldsymbol{\pi}) \quad (28)$$

for an object point at a finite distance and

$$\Delta\mathbf{y} = \Delta\Big((\mathbf{B} + \mathbf{V}\mathbf{D})n_O\Big)\mathbf{a}_O + \Delta(\mathbf{e} + \mathbf{V}\boldsymbol{\pi}) \quad (29)$$

for a distant object point.

The calculation fails when the reduced vergence $\mathbf{L}$ of either the blue or red light is singular, that is, when an image line is at infinity. However, such cases seem of little practical interest and we consider them no further.

Systems with Stigmatic Elements

In particular, if every element of the system is stigmatic, then $\mathbf{A}$, $\mathbf{B}$, $\mathbf{C}$, and $\mathbf{D}$ are all scalar matrices; that is, $\mathbf{A} = \mathbf{I}A$ where A is a scalar, and similarly for the other three 2×2 fundamental properties. The reduced vergence at emergence is also a scalar matrix, $\mathbf{L} = \mathbf{I}L$, and so is $\mathbf{Z}$ (Eq. 4), $\mathbf{Z} = \mathbf{I}Z$. The eigenvalues of $\mathbf{Z}$ are not distinct: $z_- = z_+ = Z$ is simply the longitudinal position of the image point relative to exit plane T. The longitudinal chromatic aberration is $\Delta\mathbf{Z} = \mathbf{I}\Delta Z$ where ΔZ is the longitudinal position of the blue image point relative to the longitudinal position of the red image point. Eq. 26 reduces to $\mathbf{V} = \mathbf{I}Z/n$ and, finally, Eqs. 28 and 29 become

$$\Delta\mathbf{y} = \Delta(A + ZC/n)\mathbf{y}_O + \Delta(\mathbf{e} + Z\boldsymbol{\pi}/n) \quad (30)$$

and

$$\Delta\mathbf{y} = \Delta\Big((B + ZD/n)n_0\Big)\mathbf{a}_O + \Delta(\mathbf{e} + Z\boldsymbol{\pi}/n). \quad (31)$$

Summary of the Routine for Calculating Longitudinal and Transverse Chromatic Aberration

Suppose we know the transferences of a system S for blue and red light. We can then calculate the longitudinal and transverse chromatic aberrations of the system for a finite object point O with longitudinal position z_O and transverse position $\mathbf{y}_O$. We proceed as follows. We use Eqs. 9 or 10 to determine the reduced vergence $\mathbf{L}$ of blue light from O leaving S. Eq. 4 then gives the generalized longitudinal position $\mathbf{Z}$ of the blue image. We repeat for the red image. The longitudinal chromatic aberration is then $\Delta\mathbf{Z}$ given by Eq. 5. For $\mathbf{Z}$, for blue light, we obtain the eigenvalues z_- and z_+ and the corresponding normalized eigenvectors $\mathbf{v}_-$ and $\mathbf{v}_+$. Eq. 26 gives $\mathbf{V}$. Hence one determines $\mathbf{A} + \mathbf{V}\mathbf{C}$ and $\mathbf{e} + \mathbf{V}\boldsymbol{\pi}$ for the blue light. This is repeated for red light. $\Delta(\mathbf{A} + \mathbf{V}\mathbf{C})$ is calculated by subtraction (blue minus red) and similarly for $\Delta(\mathbf{e} + \mathbf{V}\boldsymbol{\pi})$.

Finally, the transverse chromatic aberration $\Delta\mathbf{y}$ is given by Eq. 28.

If object point O is distant then we need the inclination $\mathbf{a}_O$. The calculation is the same as for a finite object point except that the vergence $\mathbf{L}$ is obtained via Eq. 11, $(\mathbf{B} + \mathbf{VD})n_0$ replaces $\mathbf{A} + \mathbf{VC}$, and Eq. 29 is used instead of Eq. 28.

The Appendix illustrates the calculations for a heterocentric astigmatic model eye with four refracting surfaces (available at http://links.lww.com/OPX/A107).

CONCLUSIONS

For systems with homocentric stigmatic refracting elements definitions of chromatic aberration differ from author to author. Several authors have remarked on the inconsistency and confusion.[18–20] We believe there is a need for authors to take greater care to define terms in general but particularly in the context of chromatic aberration.

Here, we have offered definitions that are natural generalizations of the familiar concepts[1–6] in Gaussian optics; they hold for the special case of systems with homocentric stigmatic elements, and they hold for systems, like the eye, with elements that are heterocentric and astigmatic. We have also derived expressions for longitudinal and transverse chromatic aberration in terms of the fundamental properties of the optical system.

For general systems, which may be heterocentric and astigmatic, we have defined longitudinal chromatic aberration to be the 2×2 symmetric matrix $\Delta\mathbf{Z}$ given by Eq. 5. It depends on the longitudinal position z_O of the object point O but is independent of the transverse position $\mathbf{y}_O$. Its eigenvectors are principal meridians of longitudinal chromatic aberration, and its eigenvalues are the principal longitudinal chromatic aberrations along them.

The transverse chromatic aberration $\Delta\mathbf{y}$, a vector defined by Eq. 3, can be calculated by means of Eqs. 28 or 29. In general, it is an affine function of the object's transverse position $\mathbf{y}_O$ (Eq. 28) in the case of objects at finite distances or of its direction, in effect $\mathbf{a}_O$, (Eq. 29) in the case of distant objects. If the refracting elements of the system are all centered on longitudinal axis Z, then Z is an optical axis, and because $\mathbf{e}$ and $\boldsymbol{\pi}$ are both null,[15] the constant term $\Delta(\mathbf{e} + \mathbf{V}\boldsymbol{\pi})$ in those equations vanishes, and the transverse chromatic aberration becomes linear in $\mathbf{y}_O$ or $\mathbf{a}_O$.

It may be worth mentioning that the principal meridians of the red and blue pencils, leaving the optical system, need not match. This is why one cannot, in general, simply calculate longitudinal chromatic aberration separately in two orthogonal principal meridians. Nevertheless, preliminary calculations (such as those in the Appendix) suggest that, for many practical purposes, it may well be sufficiently accurate to do so.

If the system in question is composed of stigmatic elements arranged homocentrically, then the definitions here reduce to the familiar definitions[1–6] of chromatic aberration in Gaussian optics. This special case has been treated above. We note, however, that stigmatic systems exist with astigmatic elements.[21,22] For them, the special case does not apply, although their longitudinal chromatic aberration $\Delta\mathbf{Z}$ is a scalar matrix.

We are not entirely comfortable with the word aberration in the terms longitudinal and transverse chromatic aberration. It suggests an optical concept beyond first order, whereas here, and in most cases in the literature, the concept is one in first-order optics. However, until a more suitable term is suggested, we believe longitudinal and transverse chromatic aberration be reserved for the concepts defined here.

The definitions proposed here are not specific to the eye. The retina, in particular, is not mentioned in the definitions. When applied to the eye, as to any other system, it is important to be unambiguous about how the definitions are being used. First, it should be clear what the system is whose chromatic aberration is being defined; in particular, the entrance and exit planes T_0 and T should be defined. For the visual optical system of the eye that would most likely have T_0 immediately in front of the tear film on the cornea and T immediately in front of the retina. Second, the location of longitudinal axis Z should be specified in some way. Third, the location of the object point relative to Z should be given. Finally, the two frequencies ν_r and ν_b of the light should be given or understood.

In his or her introduction to optometry, the beginning student often learns to refract with the interval of Sturm and its relation to the retina in mind. What is clear from the analysis here is that there is such an interval for each frequency, that they differ longitudinally and transversely by the longitudinal and transverse chromatic aberration, and that, from a knowledge of the structure of the eye, we are now able to calculate these differences. (A somewhat different perspective on what underlies the routine of refraction is presented elsewhere.[23])

It would seem that the familiar concepts of longitudinal and transverse chromatic aberration, as defined in Gaussian optics,[1–6] are probably less directly useful in the clinical context which may be why a variety of concepts related to them has been devised for use in practice. Confusion arises, however, because many of these concepts are called by the same names. They should, we believe, be assigned suitable distinguishing designations. Our generalization of the concepts in Gaussian optics to allow for heterocentricity and astigmatism may also be of less direct use in the clinical environment. Nevertheless, it has its place in optometric didactics and in the broader understanding of the optics of vision. Furthermore, the theory provides tools for exploring the effects of changes to the eye that accompany accommodation and refractive surgery for example.

APPENDIX

The appendix is available online at http://links.lww.com/OPX/A107.

ACKNOWLEDGMENTS

We thank L. N. Thibos and R. D. van Gool for continuing discussions. WFH gratefully acknowledges a grant from the National Research Foundation of South Africa. TE, a graduate student working with him, acknowledges support from the Medical Research Council of South Africa.

Received January 15, 2012; accepted July 2, 2012.

REFERENCES

1. Born M, Wolf E. Principles of Optics: Electromagnetic Theory of Propagation, Interference and Diffraction of Light, 7th (expanded) ed. Cambridge, UK: Cambridge University Press; 2002.

2. Sharma KK. Optics: Principles and Applications. Amsterdam, The Netherlands: Academic Press; 2006.
3. Smith G, Atchison DA. The Eye and Visual Optical Instruments. Cambridge, UK: Cambridge University Press; 1997.
4. Hofstetter HW, Griffin JR, Berman MS, Everson RW. Dictionary of Visual Science and Related Clinical Terms, 5th ed. Boston, MA: Butterworth-Heinemann; 2000.
5. Millodot M, Laby DM. Dictionary of Ophthalmology. Oxford, UK: Butterworth-Heinemann; 2002.
6. Millodot M. Dictionary of Optometry and Visual Science, 7th ed. Edinburgh, UK: Butterworth-Heinemann Elsevier; 2009.
7. Fick HH. Fortschrittliche Rechnungsarten in der Augenoptik. Der Augenoptiker 1973;(20):55–61.
8. Blendowske R. Hans-Heinrich Fick: early contributions to the theory of astigmatic systems. S Afr Optom 2003;62:105–10.
9. Keating MP. A system matrix for astigmatic optical systems: part I. Introduction and dioptric power relations. Am J Optom Physiol Opt 1981;58:810–9.
10. Harris WF. Wavefronts and their propagation in astigmatic optical systems. Optom Vis Sci 1996;73:606–12.
11. Long WF. A matrix formalism for decentration problems. Am J Optom Physiol Opt 1976;53:27–33.
12. Evans T, Harris WF. Dependence of the transference of a reduced eye on frequency of light. S Afr Optom 2011;70:149–55.
13. Harris WF. Paraxial ray tracing through noncoaxial astigmatic optical systems, and a 5 × 5 augmented system matrix. Optom Vis Sci 1994;71:282–5.
14. Harris WF. Transferences of heterocentric astigmatic catadioptric systems including Purkinje systems. Optom Vis Sci 2010;87:778–86.
15. Harris WF. Optical axes of eyes and other optical systems. Optom Vis Sci 2009;86:537–41.
16. Harris WF. Dioptric power: its nature and its representation in three- and four-dimensional space. Optom Vis Sci 1997;74:349–66.
17. Harris WF. Back- and front-vertex powers of astigmatic systems. Optom Vis Sci 2010;87:70–2.
18. Thibos LN, Bradley A, Still DL, Zhang X, Howarth PA. Theory and measurement of ocular chromatic aberration. Vision Res 1990;30:33–49.
19. Simonet P, Campbell MC. The optical transverse chromatic aberration on the fovea of the human eye. Vision Res 1990;30:187–206.
20. Rabbetts RB. Bennett and Rabbett's Clinical Visual Optics, 4th ed. Edinburgh, UK: Butterworth-Heinemann-Elsevier; 2007.
21. Harris WF. Stigmatic optical systems. Optom Vis Sci 2004;81: 947–52.
22. Harris WF. Proper and improper stigmatic optical systems. Optom Vis Sci 2004;81:953–9.
23. Harris WF. Subjective refraction: the mechanism underlying the routine. Ophthalmic Physiol Opt 2007;27:594–602.

William F. Harris
Department of Optometry,
University of Johannesburg
APK Campus, PO Box 524,
Auckland Park, Johannesburg 2006
South Africa
e-mail: wharris@uj.ac.za

OPO OPHTHALMIC & PHYSIOLOGICAL OPTICS
THE JOURNAL OF THE COLLEGE OF OPTOMETRISTS

Ophthalmic & Physiological Optics ISSN 0275-5408

Line of sight of a heterocentric astigmatic eye

William F Harris, Radboud DHM van Gool and Tanya Evans

Department of Optometry, University of Johannesburg, Johannesburg, South Africa

Citation information: Harris WF, van Gool RDHM & Evans T. Line of sight of a heterocentric astigmatic eye. *Ophthalmic Physiol Opt* 2013, **33**, 57–66. doi: 10.1111/opo.12007

Keywords: astigmatism, corneal sighting centre, heterocentricity, line of sight, sighting axis, transference

Correspondence: William F Harris
E-mail address: wharris@uj.ac.za

Received: 17 July 2012; Accepted: 7 November 2012

Abstract

Background: The line of sight and the corneal sighting centre are important references for clinical work in optometry and ophthalmology. Their locations are not fixed but may vary with displacement of the pupil and other changes in the eye.
Purpose: To derive equations for the dependence of the locations on properties of an eye which may be heterocentric and astigmatic.
Methods: The optical model used is linear optics. It allows for the refracting surfaces of the eye to be astigmatic and tilted or decentred. Because the approach is general it applies not only to the natural eye but also to a pseudophakic eye and to the compound system of eye and any optical instrument in front of it. The analysis begins with the line of sight defined in terms of the foveal chief ray.
Results: Equations are derived for the position and inclination of the line of sight at incidence onto the eye. They allow one to locate the line of sight and corneal sighting centre given the structure (curvatures, tilts, spacings of refracting surfaces) of the eye. The results can be generalized in several ways including application in the case of extra-foveal fixation and when there is a lens or other optical instrument in front of the eye. The calculation is illustrated in the Appendix for a model eye with four separated, astigmatic and tilted refracting surfaces.
Conclusions: The equations allow routine calculation of the line of sight for an eye of known structure and of the eye combined with an optical device such as a spectacle lens. They also allow exploration of the dependence of the line of sight on the location of the centre of the pupil and on other properties in the eye. There is a dependence of the line of sight on the frequency (or vacuum wavelength) of light but this may not be of clinical significance.

Introduction

Among the several axes defined for the eye the line of sight has been described as 'the most important axis from the point of view of visual function, including refraction procedures'.[1] However the line of sight is not fixed for any eye because the centre of the pupil can vary.[1–3] Indeed displacement of the pupil centre is but one of many changes, inside and outside the eye, that may alter the line of sight. Actually, even for a fixed eye, there is strictly no unique line of sight but one for each frequency or vacuum wavelength of light. (These statements will be justified below.) However, how significant are these effects? Despite the importance of the concept the literature seems to have no clear answers. Our purpose here is to develop a framework for finding answers. More particularly we shall make use of the powerful methodology of linear optics to derive an equation for the line of sight as a function of properties of the eye with or without an optical device in front of it.

The methodology used in this note is the same as that used in several recent papers[4–10] to which the reader is referred for more details than are given here. The equations derived below allow one to examine the sensitivity of the line of sight to displacement of the centre of the pupil, to accommodation, to decentration of an intraocular lens, to frequency and so on. Linear optics and the concept of the ray transference allow one to approach the problem in a very general manner; we are not limited to particular models of the eye and can handle eyes with multiple, separated, decentred and nonaligned astigmatic elements. Further-

more, although we shall talk of the eye, the generality of the approach means that the results also apply to compound systems consisting of eye and optical instrument (lens, telescope, etc.) in front of it.

Definition of the line of sight

Like many others[11–16] Alpern[17] defines the line of sight as the line joining the fixation point and the centre of the entrance pupil. It is a line in object space, that is, outside the eye. Implicit in the definitions is that the index of refraction of the medium (usually air but it may be water for example) in object space is uniform and isotropic and, hence, that the line of sight is a straight line. The general direction of the light into the eye assigns it a positive sense. We shall regard the line of sight as infinite; in other words it is the directed straight line segment from fixation point to centre of entrance pupil extended to infinity in both positive and negative senses. It remains a line in object space and allows for the possibility of real and virtual object points. (We shall not consider virtual objects explicitly.)

We mention in passing that the International Organization for Standardization (ISO) defines the line of sight in terms of the entrance and exit pupils and the centre of the fovea.[18] ISO call it the *visual axis* although in the forthcoming edition of the Standard the name has been changed to *line of sight* (personal communication from R. B. Rabbetts).

If the cornea is astigmatic then, strictly speaking, the centre of the entrance pupil is not well defined. The image of the centre of the (actual) pupil in the cornea is not a point but a blurred region consisting of a pair of separated orthogonal lines in the familiar interval of Sturm. The effect is usually sufficiently small to be of no consequence in the clinical environment but it does present problems in optical analyses. Regardless of the degree of astigmatism the problems are overcome if the line of sight is defined in terms of the foveal chief ray[17,19] (the ray through the centres of the pupil and the fovea) instead of the entrance pupil. The Optical Society of America (OSA) defines the line of sight as the foveal chief ray itself.[19] On the other hand, for Alpern the line of sight is that part of the foveal chief ray which can be specified in object space[17]; this has more in common with the definition in terms of entrance pupil. Accordingly, for the purposes of this paper we take the line of sight to be the infinite straight line defined by the portion of the foveal chief ray in object space, that is, the portion incident onto the eye.

The location of the line of sight can be defined by specifying a single point and a direction. A convenient point is the intersection of the line with the first surface of the cornea, the *corneal sighting centre* in Mandell's[20] terminology. Accordingly our primary objective will be to find formulae for the location of the corneal sighting centre and the direction of the line of sight in terms of properties of the eye which can be calculated from knowledge of the structure of the eye.

Locating the line of sight

Figure 1 is a schematic representation of an eye and its line of sight. The only physical structure of the eye actually shown in the figure is the iris (grey). The hole in the iris, not necessarily circular, is the pupil. The pupil lies in transverse plane T_P. Z is a reference longitudinal axis relative to which transverse positions and inclinations are measured. T_K is a transverse plane immediately anterior to the tear film on the cornea and T_R a transverse plane immediately anterior to the retina. The medium immediately anterior to T_K has index of refraction n_0; the indices in the pupil and immediately anterior to the retina are n_P and n_R respectively. The visual optical system of the eye is from T_K to T_R; we represent it as optical system S. T_P partitions S into subsystems S_A and S_B. We call S_A the anterior portion of the eye or simply the anterior eye and similarly for S_B, the posterior portion. Properties of S_A are identified by means of subscript A and similarly for S_B. We call S the eye or the whole eye; properties of S have no subscripts.

In *Figure 1* point P represents the centre of the pupil and point R the centre of the fovea. By definition the foveal chief ray intersects centres P and R; three of its segments are shown, an incident segment, a segment through the pupil and a segment arriving at the fovea. K is the corneal sighting centre. By definition the infinite straight line defined by the incident segment is the line of sight LL.

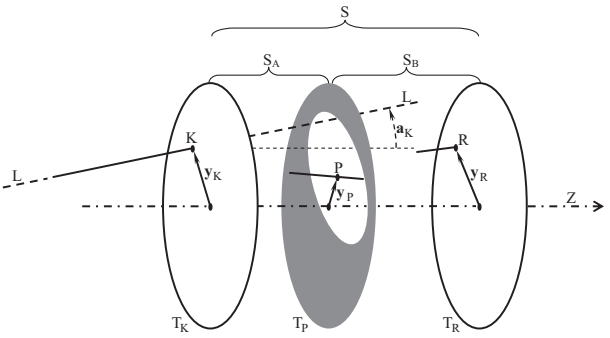

Figure 1. The line of sight or sighting axis LL and the corneal K, pupillary P and retinal R sighting centres (P and R usually being the centres of the pupil and fovea). S is the visual optical system of an eye; it extends from entrance plane T_K, immediately anterior to the corneal tear film, to the exit plane T_R, immediately in front of the retina. The iris and pupil are the only structures of the eye shown explicitly; they define plane T_P which partitions the eye into anterior S_A and posterior S_B portions. Z is the longitudinal axis relative to which transverse positions and inclinations are measured. Three segments of the foveal chief ray or sighting ray are shown: incident onto S at K, in the pupil through P and emergent from S_B at R.

Relative to longitudinal axis Z points K, P and R have transverse positions represented by the vectors $\mathbf{y}_K$, $\mathbf{y}_P$ and $\mathbf{y}_R$ respectively. Each vector is represented by a 2×1 matrix whose top and bottom entries are Cartesian components which we may regard as its horizontal and vertical components respectively; they are in length units.

The line of sight has transverse position $\mathbf{y}_K$ at T_K and inclination $\mathbf{a}_K$. Like $\mathbf{y}_K$, $\mathbf{a}_K$ is 2×1 and its components are the horizontal and vertical components of the inclination; they are in radians and, hence, unitless. $\mathbf{y}_K$ characterizes the location of the corneal sighting centre completely and $\mathbf{y}_K$ and $\mathbf{a}_K$ together completely characterize the line of sight LL. Our objective is to obtain expressions for $\mathbf{y}_K$ and $\mathbf{a}_K$ in terms of other properties of the eye, properties that can be calculated from curvatures, tilts and spacings of refracting elements in the eye and of refractive indices of the media between them.

We represent the inclination of the foveal chief ray at P in the pupil and at R on the retina as $\mathbf{a}_P$ and $\mathbf{a}_R$ respectively. We now apply the basic equations of linear optics across the whole eye (Equations 7, 8 of a previous paper[7] for example). This gives a pair of simultaneous matrix equations in terms of the transverse positions $\mathbf{y}_K$ and $\mathbf{y}_R$ and inclinations $\mathbf{a}_K$ and $\mathbf{a}_R$ of the foveal chief ray at incidence onto the cornea and at the retina:

$$\mathbf{A}\mathbf{y}_K + n_0\mathbf{B}\mathbf{a}_K + \mathbf{e} = \mathbf{y}_R \tag{1}$$

and

$$\mathbf{C}\mathbf{y}_K + n_0\mathbf{D}\mathbf{a}_K + \boldsymbol{\pi} = n_R\mathbf{a}_R. \tag{2}$$

A, **B**, **C**, **D** are 2×2 matrices and **e** and $\boldsymbol{\pi}$ 2×1 matrices; they are submatrices of the ray transference **T** (5×5) of the eye S and represent its fundamental optical properties. **A**, **B** and **e** form the first or top block-row of **T** and **C**, **D** and $\boldsymbol{\pi}$ the second block-row. It is apparent from Equation 1 that **A** is unitless and **B** and **e** have length units and from equation 2 that **C** has reciprocal length units (dioptres, for example) and **D** and $\boldsymbol{\pi}$ no units. Equation 1 written across S_A, the anterior eye, becomes

$$\mathbf{A}_A\mathbf{y}_K + n_0\mathbf{B}_A\mathbf{a}_K + \mathbf{e}_A = \mathbf{y}_P \tag{3}$$

where $\mathbf{A}_A$, $\mathbf{B}_A$ and $\mathbf{e}_A$ are fundamental properties of S_A.

Equations 1 and 3 can be combined into the single matrix equation

$$\mathbf{Q}\begin{pmatrix}\mathbf{y}_K\\ \mathbf{a}_K\end{pmatrix} = \begin{pmatrix}\mathbf{y}_R - \mathbf{e}\\ \mathbf{y}_P - \mathbf{e}_A\end{pmatrix} \tag{4}$$

where $\begin{pmatrix}\mathbf{y}_K\\ \mathbf{a}_K\end{pmatrix}$ is a 4×1 matrix which we call the *incident location* of the line of sight and

$$\mathbf{Q} = \begin{pmatrix}\mathbf{A} & n_0\mathbf{B}\\ \mathbf{A}_A & n_0\mathbf{B}_A\end{pmatrix} \tag{5}$$

is a 4×4 matrix whose top block-row is a property of the whole eye S and whose bottom block-row is a property of the anterior eye S_A. We refer to **Q** as the *coefficient matrix*. The top block-row of the 4×1 matrix on the right of Equation 4 is a property of the whole eye, including the location of the centre of the fovea $\mathbf{y}_R$, and the bottom block-row is a property of the anterior eye including the centre of the pupil $\mathbf{y}_P$.

A line of sight necessarily satisfies Equation 4. Equation 4 is an example of a linear equation, a standard equation in linear algebra. Depending on the coefficient matrix and the matrix on the right of the equation it may have no solution for $\begin{pmatrix}\mathbf{y}_K\\ \mathbf{a}_K\end{pmatrix}$, a unique solution or an infinity of solutions. The conditions on existence and uniqueness, and the set of all solutions when there is more than one solution, have been presented elsewhere.[7,21]

One expects a ray through P and R to be unique. Hence one expects there to be a unique line of sight. Mathematically this means that **Q** should be nonsingular, that is, its determinant should not be zero, in which case one can solve Equation 4 to give the unique solution

$$\begin{pmatrix}\mathbf{y}_K\\ \mathbf{a}_K\end{pmatrix} = \mathbf{Q}^{-1}\begin{pmatrix}\mathbf{y}_R - \mathbf{e}\\ \mathbf{y}_P - \mathbf{e}_A\end{pmatrix}. \tag{6}$$

An exception occurs when P and R happen to be conjugate points; there are then an infinity of lines of sight. It is hard to imagine a situation in which there is no line of sight. It seems safe to disregard such exceptions and take Equation 6 to be the unique solution for the line of sight of an eye. Should they occur, however, one would need to turn to the conditions and expressions presented before.[7,21] We consider them no further here.

We conclude that Equation 6 locates the line of sight in terms of the properties of the eye (represented by **Q**, **e** and $\mathbf{e}_A$) including the locations of the centres of the pupil and fovea $\mathbf{y}_P$ and $\mathbf{y}_R$. It gives the transverse position $\mathbf{y}_K$ and inclination $\mathbf{a}_K$ of the line of sight at incidence onto the cornea, that is, at the corneal sighting centre. For reference below we note from Equation 6 that the incident location $\begin{pmatrix}\mathbf{y}_K\\ \mathbf{a}_K\end{pmatrix}$ of the line of sight is linear in the matrix $\begin{pmatrix}\mathbf{y}_R - \mathbf{e}\\ \mathbf{y}_P - \mathbf{e}_A\end{pmatrix}$.

Because it is a straight line the line of sight intersects the retina in the point with transverse position

$$\mathbf{y}_{KR} = \mathbf{y}_K + z\mathbf{a}_K. \quad (7)$$

z is the length of the eye. This point on the retina provides another way of visualizing the line of sight. It is the transverse position of the image of the centre of the fovea for an observer looking along the line of sight.

Rearranging Equation 2 and substituting from Equation 6 we obtain

$$\mathbf{a}_R = (\,\mathbf{C} \quad n_0\mathbf{D}\,)\mathbf{Q}^{-1}\begin{pmatrix}\mathbf{y}_R - \mathbf{e}\\ \mathbf{y}_P - \mathbf{e}_A\end{pmatrix}/n_R + \boldsymbol{\pi}/n_R, \quad (8)$$

the inclination, relative to longitudinal axis Z, of the foveal chief ray at the fovea explicitly in terms of properties of the eye.

The use of Equations 6, 7 and 8 is illustrated in the Appendix where the line of sight is determined for a model eye with four separated, astigmatic and tilted refracting surfaces. The calculation is performed for two frequencies of light.

Sensitivity to changes in the eye

Coefficient matrix **Q**, defined by Equation 5, depends on fundamental properties **A** and **B** of the whole eye and of the anterior portion of the eye. These fundamental properties in turn depend on curvatures and separations of the refracting surfaces in the eye but they are independent of tilts or decentrations of those surfaces.[8] Thus **Q** is usually affected by changes in curvatures and spacings of the refracting surfaces but not by changes in tilt or decentration. Fundamental property **e**, however, is usually altered by changes in curvatures, spacings, tilts and decentrations. This means that changes in transverse position of the centres of the pupil and fovea, $\mathbf{y}_P$ and $\mathbf{y}_R$, and changes in tilt and decentration of the refracting surfaces in the eye change $\begin{pmatrix}\mathbf{y}_R - \mathbf{e}\\ \mathbf{y}_P - \mathbf{e}_A\end{pmatrix}$ without changing **Q**; the incident location of the line of sight is, therefore, linear in such changes. Relatively simple explicit equations are easily obtained as illustrated below for changes in $\mathbf{y}_P$ and $\mathbf{y}_R$.

Because changes in curvatures and spacings of refracting surfaces may change **Q**, **e** and $\mathbf{e}_A$ one expects from Equation 6 that the sensitivity of the line of sight to such changes should be much more complicated. By making use of the fact that properties **A**, **B** and **e** of a system are particular affine functions of curvatures and spacings of the refracting surfaces[8] one could, if desired, obtain explicit equations for the sensitivity to changes in curvature and separation of refracting surfaces in the eye. However because such equations are probably very messy, differ for each surface and gap and depend on the particular model eye chosen it seems unwarranted to attempt to do so here. Furthermore they are probably of little interest because the change in the line of sight can be determined simply by applying Equation 6 twice, once before and once after a change. (This is illustrated in the Appendix for changes in curvature of the first and third surfaces of the four-surface model eye and in the distance between the second and third surfaces.)

Alternative approaches

Equation 6 represents a direct and relatively simple routine for locating the line of sight of an eye of known optical structure. It is unlikely to present problems in most applications of interest. However it displays little information on relationships and gives little insight. There are a number of different approaches which lead to equations which do not have those disadvantages. Each of these other approaches, however, brings with it additional problems concerning singularity and possible associated computational difficulties. We outline some of them here.

From Equation 1 one can write

$$\mathbf{a}_K = \mathbf{B}^{-1}(\mathbf{y}_R - \mathbf{e} - \mathbf{A}\mathbf{y}_K)/n_0. \quad (9)$$

Substitution into Equation 3 gives an equation in $\mathbf{y}_K$ which can be solved to give

$$\mathbf{y}_K = (\mathbf{A}_A - \mathbf{B}_A\mathbf{F}_0)^{-1}\big(\mathbf{y}_P - \mathbf{B}_A\mathbf{B}^{-1}(\mathbf{y}_R - \mathbf{e}) - \mathbf{e}_A\big), \quad (10)$$

the transverse position of the corneal sighting centre relative to longitudinal axis Z. Here

$$\mathbf{F}_0 = \mathbf{B}^{-1}\mathbf{A} \quad (11)$$

is the corneal-plane refractive compensation of the eye.[22] Equation 9 holds under the assumption that fundamental property **B** of the eye is nonsingular; Equation 10 holds under the assumption that both **B** and $\mathbf{A}_A - \mathbf{B}_A\mathbf{F}_0$ are nonsingular. Substitution from Equation 10 into Equation 9 gives an explicit equation for the inclination $\mathbf{a}_K$ of the line of sight. Together $\mathbf{y}_K$ and $\mathbf{a}_K$ locate the line of sight completely relative to longitudinal axis Z.

We could also find the line of sight by solving Equation 1 for $\mathbf{y}_K$, substituting into Equation 3 and, hence, obtaining expressions for $\mathbf{y}_K$ and $\mathbf{a}_K$. The first step in that approach assumes that **A** is nonsingular. **A** is strictly a measure of the ametropia of the eye[22]; it is singular whenever a distant object point maps to a point (emmetropia) or a line (simple astigmatism or what we might call semi-emmetropia) on the retina. Equations for the line of sight obtained this way would fail, therefore, for such eyes at

least. Furthermore one would anticipate computational problems and uncertainty for eyes that are close to these conditions if not for others.

Yet more equations can be obtained for the line of sight if one begins by solving Equation 3 for $\mathbf{y}_K$ or $\mathbf{a}_K$ and substituting into Equation 1.

Although these equations have limitations arising out of possible singularity they may all have their uses for particular applications. For example suppose the centre of the pupil undergoes a transverse displacement $\Delta\mathbf{y}_P$. Then it follows from Equation 10 that the corneal sighting centre is displaced by

$$\Delta\mathbf{y}_K = (\mathbf{A}_A - \mathbf{B}_A\mathbf{F}_0)^{-1}\Delta\mathbf{y}_P. \qquad (12)$$

Equation 12 shows explicitly that change in the location of the corneal sighting centre, and the incident position of the line of sight, is linear in the transverse displacement of the centre of the pupil, the proportionality matrix being the property $(\mathbf{A}_A - \mathbf{B}_A\mathbf{F}_0)^{-1}$ of the eye. According to Equation 9 transverse displacement of the centre of the pupil has no effect on the inclination of the line of sight. On the other hand both the inclination and the incident position of the line of sight are dependent on the location of the centre of the fovea; from Equations 9 and 10 we obtain a transverse shift in incident position

$$\Delta\mathbf{y}_K = -(\mathbf{A}_A - \mathbf{B}_A\mathbf{F}_0)^{-1}\mathbf{B}_A\mathbf{B}^{-1}\Delta\mathbf{y}_R \qquad (13)$$

and change in inclination

$$\Delta\mathbf{a}_K = \mathbf{B}^{-1}\left(\mathbf{I} + \left(\mathbf{B}\mathbf{B}_A^{-1}\mathbf{A}_A\mathbf{A}^{-1} - \mathbf{I}\right)^{-1}\right)\Delta\mathbf{y}_R/n_0 \qquad (14)$$

of the line of sight corresponding to a transverse displacement $\Delta\mathbf{y}_R$ of the centre of the fovea. (We are not implying that the fovea actually shifts; we could, for example, be comparing the lines of sight of two model eyes identical except for the locations of the centres of their foveas.) $\mathbf{I}$ represents the identity matrix. Both dependences are linear.

The proportionality matrices in Equations 12 to 14 are calculated for the model eye in the Appendix.

In effect Equations 9, 10 and 12–14 all represent special cases of the linearity in $\begin{pmatrix}\mathbf{y}_R - \mathbf{e}\\ \mathbf{y}_P - \mathbf{e}_A\end{pmatrix}$ represented by Equation 6 and discussed above under the heading **Sensitivity to changes in the eye**.

Chromatic dependence

Equation 6 expresses the location of the line of sight in terms of the fundamental properties (more particularly the top block-row fundamental properties) of the whole eye and the anterior eye. However, the fundamental properties are dependent on the frequency of light.[23] Hence we expect there to be a line of sight for each frequency. One can define a chromatic difference for lines of sight by

$$\Delta\begin{pmatrix}\mathbf{y}_K\\ \mathbf{a}_K\end{pmatrix} = \begin{pmatrix}\mathbf{y}_K\\ \mathbf{a}_K\end{pmatrix}^b - \begin{pmatrix}\mathbf{y}_K\\ \mathbf{a}_K\end{pmatrix}^r \qquad (15)$$

where the superscripts b and r denote light of two specified frequencies. In the numerical example in the Appendix the corneal sighting centres for red and blue light are more than two wavelengths apart and the inclinations of the lines of sight differ by a little more than 0.001 radians. These differences are small and may be of little clinical significance.

Generalizations

Although we have talked here of the eye and the centres of the pupil and fovea there is nothing in the mathematics that limits application to the eye as such or that requires the points in the pupil and fovea to be their centres. This means that the results described above can be generalized. We outline three generalizations.

The results apply equally well, for example, to a compound system of eye and lens or other optical instrument in front of the eye. In the analysis above system S then becomes the compound system, and, instead of being immediately anterior to the tear film on the cornea, transverse plane T_K is now immediately anterior to the first surface of the optical instrument. T_R, immediately in front of the retina, is unchanged. T_P is unchanged at the plane of the pupil unless an aperture in the optical instrument becomes the limiting aperture of the compound system in which case T_P is at that limiting aperture. As above, system S_A is from T_K to T_P and S_B is from T_P to T_R. $\mathbf{y}_R$ remains the position vector relative to longitudinal axis Z of the centre of the fovea on the retina. $\mathbf{y}_P$ remains the centre of the pupil or becomes the centre of the limiting aperture if the pupil is not the limiting aperture. The line of sight for the compound system is located by Equation 6 in which $\mathbf{a}_K$ is its inclination at incidence onto the instrument and $\mathbf{y}_K$ is its transverse position on the first surface of the instrument. Instead of being the corneal sighting centre $\mathbf{y}_K$ becomes the sighting centre as it were on the front of the instrument. In the case of a thin spectacle lens $\mathbf{y}_K$ locates the visual point on the lens with respect to longitudinal axis Z. It can also be obtained directly from Equation 10.

In the case of extra-foveal fixation one can interpret $\mathbf{y}_R$ as the transverse position of the centre of visual attention on the retina. The results above then can be applied in physiological and pathological conditions in which fixation is not centred on the centre of the fovea.

There may be circumstances in which one wishes to interpret $\mathbf{y}_P$ as the transverse position relative to Z of a point in the pupil other than the centre. We have in mind here the Stiles-Crawford effect[24] and Tscherning's comment[15] that 'In sighting … the image of the point fixed … has nothing to do with the centre of the pupil'. Or the pupil may be irregular in shape with a centre not easy to define.[3] A line of sight could be located using the results above if $\mathbf{y}_P$ were known.

Concluding remarks

Equation 6 represents the central result of this paper; it locates the line of sight of an eye (natural or pseudophakic) in terms of properties of the eye. It does so by giving the transverse position $\mathbf{y}_K$ at incidence onto the eye and the inclination $\mathbf{a}_K$ of the line of sight, both being relative to longitudinal axis Z. Coefficient matrix $\mathbf{Q}$ in Equation 6 is defined by Equation 5 and depends on the top block-rows of the transferences of the whole eye and the anterior portion of the eye. The transferences can be determined from knowledge of the structure of the eye. (The use of the equations is illustrated in the Appendix for a particular heterocentric astigmatic eye.)

The usual definition of line of sight in terms of the entrance pupil may suggest that the line of sight of an eye depends on the location of the centre of the entrance pupil and is independent of other structures. The analysis here shows that in fact it may vary with change of any structure in the eye; in particular one expects it to vary with accommodation.

Strictly there is a line of sight for each frequency of light. Whether the differences between them are of any significance remains to be seen.

Although we refer here to the eye, with some appropriate reinterpretations (described under **Generalizations**), the analysis has much broader application. It can be applied, for example, to the compound system of eye and any optical instrument in front of the eye. $\mathbf{y}_K$ and $\mathbf{a}_K$, then, given by Equation 6, represent the transverse position and inclination of the line of sight relative to Z at incidence onto the anterior surface of the instrument.

The analysis can also accommodate physiological and pathological conditions in which fixation is not foveal or phenomena such as the Stiles-Crawford effect in which it may be appropriate to use a point in the pupil other than the centre. In situations such as these it seems appropriate to extend Mandell's terminology[20] (corneal sighting centre) to other surfaces. Hence we have *retinal sighting centre*, for example, whose location is given by $\mathbf{y}_R$. Usually it is the centre of the fovea but it is elsewhere in extra-foveal fixation. Similarly $\mathbf{y}_P$ locates the *pupillary sighting centre* which may usually be taken as the centre of the pupil but could be elsewhere. The visual point on a thin spectacle lens would be the *spectacle sighting centre*.

The line of sight was defined above in terms of the foveal chief ray but, when the retinal or pupillary sighting centres are not the centres of the fovea or pupil, then the ray in terms of which the line of sight is defined is not the foveal chief ray. In general one might refer to the ray through the pupillary and retinal sighting centres as the *sighting ray*. Usually one would expect the sighting ray to be the foveal chief ray.

It is possible for Equation 6 for the line of sight to fail. This occurs when matrix $\mathbf{Q}$ is singular. We do not expect that to happen in the case of eyes but it is conceivable when the eye is a component of a compound system. In such cases, depending on the nature of $\mathbf{Q}$ and the matrix on the right of Equation 4, there may be no line of sight or multiple lines of sight. Equation 4 is standard in linear algebra. Conditions of existence and uniqueness of solutions are presented elsewhere.[7,21] When there are multiple solutions the equation for all solutions is also given in those papers.

Alternative equations for the line of sight can be obtained. Examples include Equations 9 and 10. Some give additional insight into relationships and may be useful but all have potential problems associated with singularity.

The equations here allow one to explore the effects of changes both inside and outside the eye, for example when a spectacle lens is placed in front of the eye or there is accommodation or shift in location of the centre of the pupil. The location of the pupil centre, if regarded as the pupillary sighting centre, is represented explicitly as $\mathbf{y}_P$ in Equation 6 and accommodation changes at least the top-block row of $\mathbf{Q}$ in that equation.

The nature of Equation 6 suggests a complicated dependence of the line of sight on changes of curvature and spacings of refracting surfaces within the eye. However, tilts and decentrations of refracting surfaces and the locations of the centres of the pupil and fovea (or pupillary and retinal sighting centres) are exceptional in that changes in them produce linear changes in the line of sight. If there are no other changes Equation 9 shows that a transverse shift of the centre of the pupil has no effect on the inclination of the line of sight; its effect on the incident position of the line of sight is linear (Equation 12). For the model eye treated in the Appendix the corneal sighting centre undergoes a shift approximately 13% larger than the pupillary sighting centre and approximately in the same direction. Equations 13 and 14 show that the incident transverse position and inclination of the line of sight are both linearly sensitive to position of the retinal sighting centre. The sensitivities are calculated for the model eye in the Appendix.

The Appendix also illustrates application of Equation 6 to determine the effect on the line of sight of other particular changes within the eye, including changes of curvature of the first and third surfaces of the eye and separation between the

second and third surfaces. In most of these cases the effects are small and, perhaps, of little significance in many applications. They depend, however, on the particular model eye chosen for the analysis and should not necessarily be regarded as representative of eyes in general. Nevertheless the numbers do suggest that accommodation and other changes in the eye are less significant than displacement of the centre of the pupil. It is also evident that change in curvature, tilt or decentration of the first surface of the eye causes no shift in position of the corneal sighting centre.

The line of sight is based on the incident segment of the sighting ray, the segment external to the eye. However, the Stiles-Crawford phenomenon[24] and what Bradley and Thibos[25] describe as the retina's 'inherent optical axis' suggest that there might be merit in also defining an axis based on the segment of the sighting ray at the retina. We would then distinguish between the *incident* or *external* line of sight of an eye (what we have simply been calling the line of sight) and the eye's *retinal* line of sight. The latter would be the infinite straight line containing the segment of the sighting ray at the retina. The retinal line of sight is located by Equation 8 which gives its inclination, its transverse position at the retina, of course, being the retinal sighting centre.

Ordinarily a lens or other instrument placed in front of a fixed eye changes the incident line of sight but not the retinal line of sight. It is only if an aperture in the instrument becomes limiting that both incident and retinal lines of sight may change.

One expects the pupillary sighting centre to be the centre of the pupil but it may be elsewhere in the pupil. If the structure of the anterior part of the eye and the location of the line of sight are known then the location of the pupillary sighting centre can be calculated by means of Equation 3.

The entrance pupil of an eye is in object space. Thus the traditional definition of line of sight in terms of point of fixation (in object space) and entrance pupil (also in object space) might, at first sight, give the impression that the line of sight of an eye is more a property of object space and less a property of the eye. The equations developed here stress the fact that the line of sight of an eye is a property of the eye alone. In particular it does not depend on a fixation point. Indeed the line of sight exists even if there is no fixation point (in the dark for example). The only provisos are that the index of refraction immediately in front of the eye does not change and that the pupil remains the limiting aperture. (The line of sight changes, for example, if an eye in air submerges in water or a pinhole aperture is placed in front of the eye.) We can think of the eye as having a pointer attached to it at the cornea along the line of sight and directed forward. The act of fixating a point object involves turning the eye so that the pointer points at the object in question.

Line of sight is a term not unique to optometry, ophthalmology and vision science. It is common in several fields, cosmology[26] being but one example. In such fields, in contrast to the term we have been using, the term does not necessarily imply an eye at all. The line of sight is simply a ray from some object in question. If one wishes to see the object then one needs to bring the line of sight of an eye, or of each eye, into coincidence locally with a line of sight of the object. Again 'eye' here may also be interpreted 'compound system of eye and instrument in front of it'.

Partly because two such distinct concepts have the same name we have reservations about the term 'line of sight' for the property of the eye. Implicit in the traditional definition is that the line is straight, but lines are not necessarily straight. 'Axis' seems more appropriate than 'line'; it better suggests a straight line and is more in keeping with the names of other axes of the eye including optical axis, visual axis and achromatic axis. 'Sighting axis' seems a possible alternative to 'line of sight'. An eye would then have corneal, pupillary and retinal sighting centres, a sighting ray and a sighting axis. To see a distant object one would need to turn the eye to bring its sighting axis into coincidence with a line of sight of the object.

We have used here the powerful methodology of linear optics to obtain explicit equations for the location of the line of sight in the case of an eye with multiple separated refracting surfaces that may be heterocentric, tilted and astigmatic. All that is required beyond refractive indices and axial separations is the paraxial geometry of each refracting surface. As with the simpler optical model, Gaussian optics, we need to keep in mind, however, that the theory is paraxial and that accuracy declines with increasing distances and inclinations relative to the longitudinal axis. For greater accuracy we would need to turn to geometrical optics but then we would need the whole geometry of every surface (which we seldom have) and we would usually have to be satisfied with numerical computation. The explicit equations obtained here are, we assert, the best obtainable.

Traditionally the line of sight is defined in terms of the entrance pupil. But, strictly speaking, an entrance pupil is not well defined if the eye has an astigmatic cornea; its centre, as any other point in it, is blurred out as an interval of Sturm. Although this effect may be negligible for clinical purposes it presents a problem for optical analyses including the analysis presented here. By making use of the actual pupil instead the entrance pupil, as one does when defining the line in terms of the foveal chief ray, one avoids the problem. The clinician, however, does not have the luxury of access to the pupil and has to be satisfied with the entrance pupil. Nevertheless, for most purposes, there is no conflict between the two definitions; the clinician and the theoretician are talking about the same thing and merely approaching it with the particular tools that each has at his or her disposal.

Acknowledgements

WF Harris gratefully acknowledges a grant from the National Research Foundation of South Africa. T Evans, a graduate student working with him, acknowledges support from the Medical Research Council of South Africa. We thank Ronald B Rabbetts for helpful comments and Margaret McGovern (Librarian, College of Optometrists, UK) and Kay Hévey (Editorial Assistant, *Optician*) for help with references.

References

1. Atchison DA & Smith G. Optics of the Human Eye. Butterworth-Heinemann: Oxford, 2000; pp. 31–36.
2. Yang Y, Thompson K & Burns SA. Pupil location under mesopic, photopic, and pharmacologically dilated conditions. *Invest Ophthalmol Vis Sci* 2002; 43: 2508–2512.
3. Wyatt HJ. The form of the human pupil. *Vis Res* 1995; 14: 2021–2036.
4. Harris WF. Nodes and nodal points and lines in eyes and other optical systems. *Ophthalmic Physiol Opt* 2010; 30: 24–42.
5. Harris WF. Visual axes in eyes that may be astigmatic and have decentred elements. *Ophthalmic Physiol Opt* 2010; 30: 204–207.
6. Harris WF. Aperture referral in heterocentric astigmatic systems. *Ophthalmic Physiol Opt* 2011; 31: 603–614.
7. Harris WF. Achromatic axes and their linear optics. *Vis Res* 2012; 58: 1–9.
8. Harris WF. Dependence of optical properties of heterocentric astigmatic systems on internal elements, with application to the human eye. *Trans Roy Soc S Afr* 2012; 67: 11–16.
9. Harris WF & Evans T. Chromatic aberration in heterocentric astigmatic systems including the eye. *Optom Vis Sci* 2012; 89: e37–e43.
10. Harris WF. Chief nodal axes of a heterocentric astigmatic eye and the Thibos-Bradley achromatic axis. *Vis Res* 2012; 73: 40–45.
11. Millodot M & Laby DM. Dictionary of Ophthalmology. Butterworth-Heinemann: Oxford, 2002; p. 163.
12. Hofstetter HW, Griffin JR, Berman MS & Everson RW. Dictionary of Visual Science and Related Clinical Terms, 5th edn. Butterworth-Heinemann: Boston, 2000; p. 306.
13. Millodot M. Dictionary of Optometry and Visual Science, 7th edn. Butterworth-Heinemann-Elsevier: Edinburgh, 2009; p. 208.
14. Stidwill D & Fletcher R. Normal Binocular Vision: Theory, Investigation and Practical Aspects. Wiley-Blackwell: Oxford, 2011; p. 4.
15. Tscherning MHE. Physiologic Optics, 2nd edn. The Keystone: Philadelphia, PA, 1904; p. 74.
16. Le Grand Y & El Hage SG. Physiological Optics. Springer-Verlag: Berlin, 1980; p. 72.
17. Alpern M. Specification of the direction of regard. In: Muscular Mechanisms. Vol. 3 of The Eye, (Davson H, editor), 2nd edn, Academic Press: New York, 1969; pp. 5–12.
18. International Organization for Standardization. Ophthalmic Optics Spectacle Lenses Vocabulary, International Standard ISO 13666. ISO: Geneva, 1998; p. 13.
19. Applegate RA, Thibos LN, Bradley A *et al.* Reference axis selection: subcommittee report of the OSA working group to establish standards for measurement and reporting of optical aberrations of the eye. *J Refract Surg* 2000; 16: S656–S658.
20. Mandell RB. Locating the corneal sighting center in videokeratography. *J Refract Surg* 1995; 11: 253–258.
21. Harris WF. Optical axes of eyes and other optical systems. *Optom Vis Sci* 2009; 86: 537–541.
22. Harris WF. A unified paraxial approach to astigmatic optics. *Optom Vis Sci* 1999; 76: 480–499.
23. Evans T & Harris WF. Dependence of the transference of a reduced eye on frequency of light. *S Afr Optom* 2011; 70: 149–155.
24. Stiles WS & Crawford BH. The luminous efficiency of rays entering the eye pupil at different points. *Proc Roy Soc* 1933; 112: 428–450.
25. Bradley A & Thibos LN. Modelling off-axis vision. I: The optical effects of decentering visual targets or the eye's entrance pupil. In: Vision Models for Target Detection and Recognition (E Peli, editor), World Scientific: Singapore, 1995; pp. 313–337.
26. Eggleton P. Evolutionary Processes in Binary and Multiple Stars. Cambridge University Press: Cambridge, 2006; pp. 3, 6, 10, etc.
27. Villegas ER, Carretero L & Fimia A. Le Grand eye for the study of ocular chromatic aberration. *Ophthalmic Physiol Opt* 1996; 16: 528–531.

Appendix

We illustrate application of the theory by locating the line of sight, including the corneal sighting centre, for a particular ametropic heterocentric astigmatic model eye. We also illustrate the effect on the line of sight of changes in frequency of light, transverse position of the centres of the pupil and fovea, curvature of the third and first refracting surfaces and separation of the second and third surfaces.

The model eye has four separated astigmatic and tilted refracting surfaces the details of which are listed in *Table 1*. The principal radii of curvature of the first surface of the cornea (K1) are 5.8 mm along the horizontal and 7 mm along the vertical and the surface has tilts 0.06 in the horizontal (from in front of the eye the right of the surface would appear pushed away relative to the left) and −0.05 in the vertical (the bottom of the surface would appear pushed away relative to the top) all measured at the reference axis Z. The tilts are in radians or, equivalently, no units. The curvatures and tilts of the second surface of the cornea (K2) and the first (L1) and second (L2) surfaces of the lens of the eye should be interpreted similarly. The

Table 1. Principal radii of curvature, separation, and tilt of surfaces (K1 and K2 of the cornea and L1 and L2 of the lens) of the model eye used in the numerical example

Surface	Principal radii, mm{degr}mm	Separation, mm	Tilt
K1	5.8{180} 7		$(0.06\ -0.05)^{\mathrm{T}}$
		0.5	
K2	5{10}6.2		$(0.04\ \ 0.06)^{\mathrm{T}}$
		4	
L1	4.1{20}5		$(-0.07\ 0.1)^{\mathrm{T}}$
		4	
L2	−5{70}−6.2		$(-0.05\ -0.03)^{\mathrm{T}}$
		16	

separation between K1 and K2 is 0.5 mm. The expressions for refractive index as a function of vacuum wavelength published by Villegas *et al.*[27] have been used.

The principal meridians of the refracting surfaces are not aligned. The eye is in air; hence we set $n_0 = 1$. The eye's length is $z = 24.5$ mm. We suppose the centre of the pupil is located 1 mm to the left of axis Z. Hence, taking it to be the pupillary sighting centre, we set $\mathbf{y}_{\mathrm{P}} = \begin{pmatrix} -1 \\ 0 \end{pmatrix}\mathrm{mm}$.

We also suppose that the retinal sighting centre is located 1 mm from Z in the 45° direction. It may be at the centre of the fovea but this makes no difference to the calculation. Thus $\mathbf{y}_{\mathrm{R}} = \begin{pmatrix} \cos 45^\circ \\ \sin 45^\circ \end{pmatrix}\mathrm{mm}$.

The calculation is done for light of frequencies corresponding to the vacuum wavelengths 486.1 ('blue') and 656.3 ('red') nm; the results are summarized in Table 2. **A** is the top left 2 × 2 submatrix of the transference, **B** the top middle 2 × 2 matrix and **e** the top right 2 × 1 submatrix. Below **A**, **B** and **e** in the transference are **C**, **D** and $\boldsymbol{\pi}$ respectively. The coefficient matrices **Q** were calculated using Equation 5. Their determinants turn out to be approximately 205 and 202 mm^2 for red and blue respectively which confirms that the lines of sight exist uniquely and that Equation 6 gives their transverse positions $\mathbf{y}_{\mathrm{K}}$ and inclinations $\mathbf{a}_{\mathrm{K}}$ at incidence on to the eye. The red and blue corneal sighting centres are about 1.3 mm left and 0.2 mm below longitudinal axis Z. The lines of sight slope up and to the right into the eye at about 0.04 radians (4 prism dioptres) away from axis Z. The chromatic difference for the eye of the red and blue lines of sight is (Equation 15)

$$\Delta\begin{pmatrix} \mathbf{y}_{\mathrm{K}} \\ \mathbf{a}_{\mathrm{K}} \end{pmatrix} = \begin{pmatrix} 0.001335\,\mathrm{mm} \\ -0.000432\,\mathrm{nm} \\ -0.00101 \\ -0.00016 \end{pmatrix}.$$

Thus the red and blue corneal sighting centres are a few wavelengths apart. The lines of sight intersect the retina in the point represented by $\mathbf{y}_{\mathrm{KR}}$ calculated by means of Equation 7. The blue and red sighting rays arrive at the retina with inclination $\mathbf{a}_{\mathrm{R}}$ given by Equation 8; here they are identical up to a few tens of microradians.

The last row in *Table 2* lists the proportionality matrix $(\mathbf{A}_{\mathrm{A}} - \mathbf{B}_{\mathrm{A}}\mathbf{F}_0)^{-1}$ of Equation 12. It differs only slightly for red and blue light and is close to the scalar matrix 1.13**I**. In other words a transverse shift of the centre of the pupil causes a shift of the line of sight, and hence of the corneal sighting centre, that is approximately 13% larger in magnitude and in approximately the same transverse direction.

The proportionality matrices in Equations 13 and 14 also turn out to be close to identity matrices, −0.24**I** and $0.057\mathbf{I}\ \mathrm{mm}^{-1}$ respectively. Thus a shift of the retinal sighting centre causes a shift in the corneal sighting centre that is about a quarter in magnitude but in approximately the opposite direction and it causes the inclination of line of sight to change by about 5.7 prism dioptres or 3.3 degrees per millimetre in approximately the same direction.

Repeating the calculation using Equation 6 but with the principal powers of the third surface of the model eye each increased by 1 D we obtain a change in incident location of the line of sight by about $\begin{pmatrix} 0.0033717\,\mathrm{mm} \\ 0.0000003\,\mathrm{mm} \\ -0.0008066 \\ -0.0000008 \end{pmatrix}$. Thus the corneal sighting centre has been shifted by roughly 3 μm approximately to the right and the inclination of the line of sight has increased by about 0.05 degrees approximately to the left.

If instead 1 D is added to each principal power of the first surface Equation 6 shows that the change in incident location of the line of sight is $\begin{pmatrix} 0\ \mathrm{mm} \\ 0\ \mathrm{mm} \\ -0.0012896 \\ -0.0001956 \end{pmatrix}$. Thus the corneal sighting centre is not moved, as is to be expected, while the inclination of the line of sight increases by about 0.08 degrees approximately to the left.

Increasing the distance between the second and third surfaces (the depth of the anterior chamber) by 1 mm the incident location of the line of sight changes by $\begin{pmatrix} -0.0640562\,\mathrm{mm} \\ -0.0437903\,\mathrm{mm} \\ -0.0036075 \\ -0.0020368 \end{pmatrix}$, that is, the incident position shifts about 0.08 mm in the 214-degree direction (left and down) and the incident inclination increases by about 0.24 degrees in the 209-degree direction.

Many of these numbers may well be negligibly small for most purposes. The degree to which they are representative of eyes, however, remains to be examined.

Table 2. Locating the lines of sight for red and blue light for the heterocentic astigmatic model eye defined in Table 1. Lengths are in millimetres and reciprocal lengths in kilodioptres

	Red	**Blue**
Transference of S	$\begin{pmatrix} -0.3718 & -0.0183 & 16.2363 & -0.1309 & -0.3073 \\ -0.0169 & -0.2012 & -0.1303 & 16.1841 & 0.1944 \\ -0.0811 & -0.0014 & 0.8522 & -0.0100 & -0.0165 \\ -0.0013 & -0.0723 & -0.0100 & 0.8459 & 0.0076 \\ 0 & 0 & 0 & 0 & 1 \end{pmatrix}$	$\begin{pmatrix} -0.3914 & -0.0186 & 16.1246 & -0.1321 & -0.3121 \\ -0.0171 & -0.2185 & -0.1315 & 16.0708 & 0.1964 \\ -0.0826 & -0.0014 & 0.8500 & -0.0102 & -0.0168 \\ -0.0013 & -0.0737 & -0.0101 & 0.8435 & 0.0077 \\ 0 & 0 & 0 & 0 & 1 \end{pmatrix}$
Top block-row of the transference of S_A	$\begin{pmatrix} 0.8066 & 0.0008 & 3.3717 & 0.0003 & -0.0708 \\ 0.0008 & 0.8396 & 0.0003 & 3.3701 & 0.0703 \end{pmatrix}$	$\begin{pmatrix} 0.8035 & 0.0008 & 3.3538 & 0.0003 & -0.0719 \\ 0.0008 & 0.8370 & 0.0003 & 3.3522 & 0.0712 \end{pmatrix}$
$\mathbf{Q}$	$\begin{pmatrix} -0.3718 & -0.0183 & 16.2363 & -0.1309 \\ -0.0169 & -0.2012 & -0.1303 & 16.1841 \\ 0.8066 & 0.0008 & 3.3717 & 0.0003 \\ 0.0008 & 0.8396 & 0.0003 & 3.3701 \end{pmatrix}$	$\begin{pmatrix} -0.3914 & -0.0186 & 16.1246 & -0.1321 \\ -0.0171 & -0.2185 & -0.1315 & 16.0708 \\ 0.8035 & 0.0008 & 3.3538 & 0.0003 \\ 0.0008 & 0.8370 & 0.0003 & 3.3522 \end{pmatrix}$
$\begin{pmatrix} \mathbf{y}_R - \mathbf{e} \\ \mathbf{y}_P - \mathbf{e}_A \end{pmatrix}$	$\begin{pmatrix} 1.0144 \\ 0.5127 \\ -0.9292 \\ -0.0703 \end{pmatrix}$	$\begin{pmatrix} 1.0192 \\ 0.5107 \\ -0.9281 \\ -0.0712 \end{pmatrix}$
$\mathbf{y}_K$	$\begin{pmatrix} -1.2896 \\ -0.1956 \end{pmatrix}$	$\begin{pmatrix} -1.2882 \\ -0.1960 \end{pmatrix}$
$\mathbf{a}_K$	$\begin{pmatrix} 0.0330 \\ 0.0282 \end{pmatrix}$	$\begin{pmatrix} 0.0319 \\ 0.0280 \end{pmatrix}$
$\mathbf{y}_{KR}$	$\begin{pmatrix} -0.4821 \\ 0.4944 \end{pmatrix}$	$\begin{pmatrix} -0.5056 \\ 0.4901 \end{pmatrix}$
$\mathbf{a}_R$	$\begin{pmatrix} 0.08712 \\ 0.03518 \end{pmatrix}$	$\begin{pmatrix} 0.08715 \\ 0.03518 \end{pmatrix}$
$(\mathbf{A}_A - \mathbf{B}_A\mathbf{F}_0)^{-1}$	$\begin{pmatrix} 1.1315 & -0.0063 \\ -0.0063 & 1.1345 \end{pmatrix}$	$\begin{pmatrix} 1.1301 & -0.0064 \\ -0.0064 & 1.1331 \end{pmatrix}$

Dependence of the ray transference of model eyes on the frequency of light

Tanya Evans* and William F Harris
Department of Optometry, University of Johannesburg, Johannesburg, South Africa
*Corresponding author: tevans@uj.ac.za

The transference defines the first-order character of an optical system; almost all the system's optical properties can be calculated from it. It is useful, therefore, to have some idea of how it depends on the frequency of light. We examine the dependence for two Gaussian eyes. It turns out to be nearly linear for all four fundamental properties. The result is an equation for the dependence of the transference on frequency which is almost symplectic. We also transform the transference into Hamiltonian space, obtain equations for the least-squares straight line for the three independent transformed properties and map them back to the group of transferences. The result is an equation for the dependence of the transference on frequency which is exactly symplectic and therefore representative of an optical system. The results may approximate those of real eyes and give estimates of the dependence of almost all optical properties on frequency.

Keywords: ray transference; frequency; symplecticity

Introduction

The ray transference is of central importance in linear optics. Nearly all the familiar optical properties of an eye such as power, refractive compensation, magnification and cardinal points can be derived from the transference. It is therefore useful to have some idea of how it depends on the frequency of light. In this presentation we examine the dependence of the transference of the reduced eye [1] and Le Grand's four-surface schematic eye [2] on frequency with the objective of obtaining an equation for the dependence. Consequently, the dependence of the eye's optical properties on frequency, as well as their chromatic difference between two frequencies, can be obtained from the frequency-dependent transference. This forms part of a much larger study. Many of these chromatic properties can be generalised to astigmatic heterocentric eyes.

Method

The underlying method used here is that of first-order optics. We make use of the ray transference which is a complete representation of the first-order effects of an optical system on the rays traversing it [3]. We represent the transference as

$$\mathbf{S} = \begin{pmatrix} A & B \\ C & D \end{pmatrix} \tag{1}$$

where A the dilation, B the disjugacy, C the divergence and D the divarication are the four fundamental properties of the Gaussian system [4].

Being a member of the symplectic group, the transference has unit determinant [4, 5]. Symplectic matrices are closed under multiplication, inversion and transposition but are not closed under

addition nor multiplication by a scalar [4, 5]. This creates problems when doing quantitative analyses on sets of transferences [5]. To overcome this limitation, we make use of the mapping from the symplectic group to the set of Hamiltonian matrices. The set of all Hamiltonian matrices defines a linear (vector) space and is therefore closed under matrix addition and multiplication by a scalar, [4, 5]. This makes the set of Hamiltonian matrices suitable for quantitative analysis including conventional statistical analysis. We explore two mappings. Firstly, the principal matrix logarithm of a symplectic matrix is a Hamiltonian matrix and inversely the matrix exponential of a Hamiltonian matrix is a symplectic matrix. Secondly, the Cayley transform, being its own functional inverse, provides a mapping between symplectic and Hamiltonian matrices. The Cayley transform is defined as [6]

$$\hat{\mathbf{S}} = (\mathbf{I} - \mathbf{S})(\mathbf{I} + \mathbf{S})^{-1} \tag{2}$$

where the caret (^) denotes the Hamiltonian transformed transference.

We are interested in the dependence of the transference on the frequency of light across the visible spectrum, 430 to 750 THz ($\times 10^{12}\mathrm{s}^{-1}$). Frequency is independent of the medium whereas wavelength is not and energy is proportional to frequency, good reasons for studying the dependence of properties on the frequency of light rather than on wavelength [7]. When obtaining the transference, it is the refractive index that is dependent on frequency. We make use of the formula for the refractive index as a function of wavelength developed for the chromatic eye [8] and the formulae for the refractive indices as functions of wavelength for the cornea, aqueous, lens and vitreous developed by Villegas *et al.* [9] based on the polynomial fit of Le Grand's findings [10] for the four-surface schematic eye. Both sets of equations are based on experimental findings. The refractive index of air is approximated by $n_0 = 1$. The transferences were calculated as described elsewhere [11].

Results

In Figure 1 the dependence of the transference on the frequency of light is shown for the reduced eye (blue) and Le Grand's eye (black) and is very nearly linear for each of the fundamental properties. The dashed straight lines shown in the figure are obtained using the least-squares method. The formula for the straight lines as a function of frequency (v) is given by

$$\mathbf{S} = \begin{pmatrix} a_1 & b_1 \\ c_1 & d_1 \end{pmatrix} v + \begin{pmatrix} a_2 & b_2 \\ c_2 & d_2 \end{pmatrix} \tag{3}$$

with constants given in Table 1 for the reduced and Le Grand's eyes. This gives us a good approximation for the transference of a Gaussian eye as a function of frequency.

Transforming the frequency-dependent transferences into Hamiltonian matrices, we are able to obtain the least-squares straight line for each of the three independent entries in Hamiltonian space, which we map back to symplectic matrices. This allows us to obtain an expression for the dependence of the transference on the frequency of light which is exactly symplectic. The least-squares straight line in Hamiltonian space is

$$\hat{\mathbf{S}} = \begin{pmatrix} \hat{a}_1 & \hat{b}_1 \\ \hat{c}_1 & -\hat{a}_1 \end{pmatrix} v + \begin{pmatrix} \hat{a}_2 & \hat{b}_2 \\ \hat{c}_2 & -\hat{a}_2 \end{pmatrix} \tag{4}$$

with the constants for the reduced and Le Grand's eyes given in Table 2 for the Cayley transform and Table 3 for the logarithmic transform. To obtain the transference as a function of frequency one

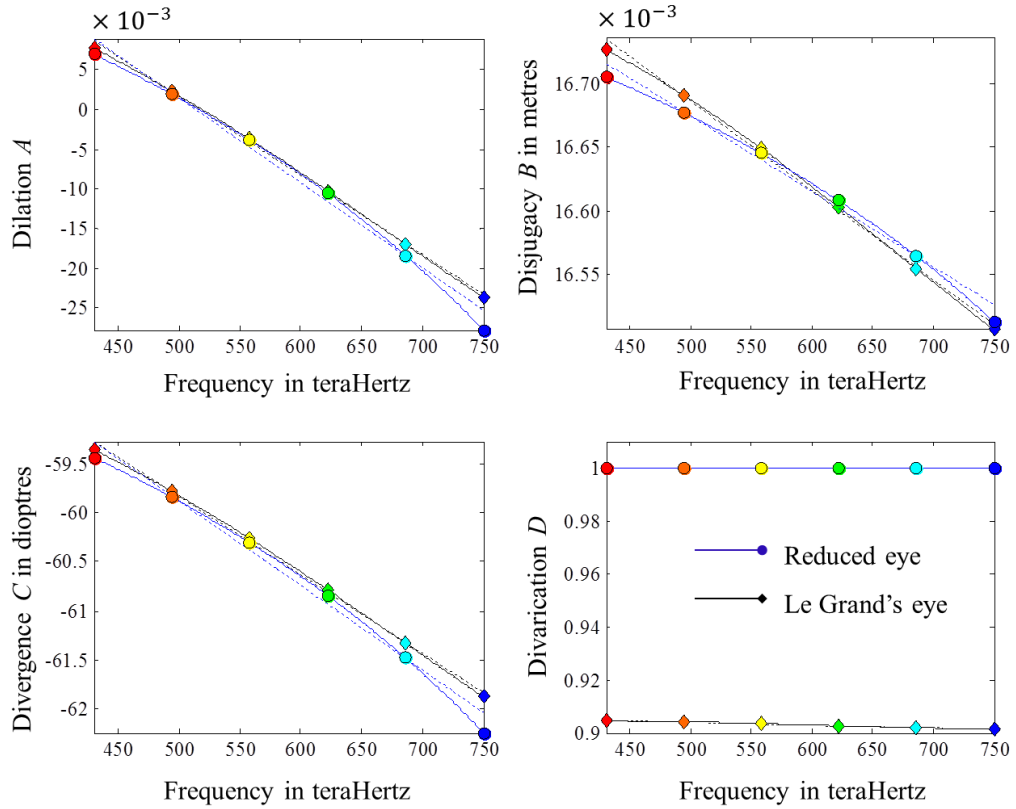

Figure 1. The fundamental properties of the reduced and Le Grand's eyes as functions of frequency. The least squares straight lines (Equation 3) are shown with dashed lines. The coloured markers represent equal spacings of 64 THz ($\times 10^{12}$ s^{-1}) and approximate the colours represented at each frequency.

Table 1. Constants for Equation 3, the units being picoseconds ($\times 10^{-12}$ s), metres and dioptres (m^{-1}).

Reduced eye		Le Grand's eye	
$a_1 = -1.069\times10^{-4}$ ps	$a_2 = 0.0549$	$a_1 = -0.997\times10^{-4}$ ps	$a_2 = 0.0516$
$b_1 = -5.939\times10^{-7}$ m ps	$b_2 = 16.972\times10^{-3}$ m	$b_1 = -7.034\times10^{-7}$ m ps	$b_2 = 17.038\times10^{-3}$ m
$c_1 = -8.605\times10^{-3}$ D ps	$c_2 = -55.579$ D	$c_1 = -7.975\times10^{-3}$ D ps	$c_2 = -55.849$ D
$d_1 = 0$ ps	$d_2 = 1$	$d_1 = -1.115\times10^{-5}$ ps	$d_2 = 0.910$

Table 2. Constants for Equation 4 for the Cayley transform.

Reduced eye		Le Grand's eye	
$\hat{a}_1 = 4.780\times10^{-5}$ ps	$\hat{a}_2 = 0.309$	$\hat{a}_1 = 4.263\times10^{-5}$ ps	$\hat{a}_2 = 0.289$
$\hat{b}_1 = 0$ m ps	$\hat{b}_2 = -11.111\times10^{-3}$ m	$\hat{b}_1 = 4.633\times10^{-8}$ m ps	$\hat{b}_2 = -11.509\times10^{-3}$ m
$\hat{c}_1 = 7.206\times10^{-3}$ D ps	$\hat{c}_2 = 36.298$ D	$\hat{c}_1 = 7.111\times10^{-3}$ D ps	$\hat{c}_2 = 37.630$ D

Table 3. Constants for Equation 4 for the logarithmic transform.

Reduced eye		Le Grand's eye	
$\hat{a}_1 = -7.905\times10^{-5}$ ps	$\hat{a}_2 = -0.564$	$\hat{a}_1 = -6.887\times10^{-5}$ ps	$\hat{a}_2 = -0.523$
$\hat{b}_1 = -2.491\times10^{-7}$ m ps	$\hat{b}_2 = 20.281\times10^{-3}$ m	$\hat{b}_1 = -3.567\times10^{-7}$ m ps	$\hat{b}_2 = 20.781\times10^{-3}$ m
$\hat{c}_1 = -12.145\times10^{-3}$ D ps	$\hat{c}_2 = -66.312$ D	$\hat{c}_1 = -11.743\times10^{-3}$ D ps	$\hat{c}_2 = -68.009$ D

needs to map the transformed transference back to its respective transference using either the Cayley transform (Equation 2) or the matrix exponential. The frequency-dependent transference is easy to obtain using pencil and paper and either the Cayley transform of Equation 2 or, easier still,

$$\mathbf{S} = \frac{2\left(\mathbf{I} - \hat{\mathbf{S}}\right)}{1 + \det \hat{\mathbf{S}}} - \mathbf{I}. \qquad (5)$$

On the other hand, the logarithmic transform requires the use of sophisticated matrix software.

Conclusion

The four fundamental properties of a Gaussian eye are shown to have a very nearly linear dependence on frequency. An equation is obtained for the least-squares straight line dependence of the fundamental properties on frequency, the estimated transference is almost symplectic. A transference, that is, a matrix which is exactly symplectic, is obtained by fitting a straight line in Hamiltonian space, giving the dependence of the transference of a Gaussian eye on the frequency of light across the visible spectrum. These equations allow one to write approximate equations for the dependence of almost all the optical properties of the eye, both fundamental and derived, on frequency.

Acknowledgements

This work is based on research by TE towards a higher degree under the guidance of WFH who gratefully acknowledges support from the National Research Foundation of South Africa.

References

[1] Emsley HH. *Visual Optics.* 4th ed. London: Hatton Press Ltd. 1950; 523-544.

[2] Le Grand Y. *Optique Physiologique. Tome Premier, le Dioptrique de l'Œil et sa Correction*. Paris: Revue d'optique. 1945; 50-51.

[3] Torre, A. Linear Ray and Wave Optics in Phase Space. Amsterdam: Elsevier. 2005; 60.

[4] Harris WF. The log-transference and an average Gaussian eye. *S. Afr. Optom.* 2005; **64**: 84-88.

[5] Harris WF. Symplecticity and relationships among the fundamental properties in linear optics. *S. Afr. Optom.* 2010; **69**: 3-13.

[6] Bernstein DS. *Matrix Mathematics. Theory, Facts, and Formulas.* 2nd ed. Princeton: Princeton University Press. 2009; 208-9, 238-9.

[7] Pease PL, Barbeito R. Axial chromatic aberration of the human eye: frequency or wavelength? *Ophthal. Physiol. Opt.*1989; **9**: 215-217.

[8] Thibos LN, Ye M, Zhang X, Bradley A. The chromatic eye: a new reduced-eye model of ocular chromatic aberration in humans. *Appl. Opt*. 1992; **31**: 3594-3600.

[9] Villegas ER, Carretero L, Fimia A. Le Grand eye for the study of ocular chromatic aberration. *Ophthal. Physiol. Opt*. 1996; **16**: 528-531.

[10] Le Grand Y. *Optique Physiologique. Tome Troisième, L'espace Visuel*. Paris: Revue d'optique. 1956; 9-27.

[11] Guillemin V, Sternberg S. *Symplectic Techniques in Physics.* Cambridge: Cambridge University Press. 1984; 9-27.

Inner-product spaces for quantitative analysis of eyes and other optical systems

William F Harris*, Tanya Evans and Radboud D van Gool
Department of Optometry, University of Johannesburg, Johannesburg, South Africa
*Corresponding author: wharris@uj.ac.za

Because dioptric power matrices of thin systems constitute a (three-dimensional) inner-product space it is possible to define distances and angles in the space and so do quantitative analyses on dioptric power for thin systems. That includes astigmatic corneal powers and refractive errors. The purpose of this paper is to generalize to thick systems. The paper begins with the ray transference of a system. Two 10-dimensional inner-product spaces are devised for the holistic quantitative analysis of the linear optical character of optical systems. One is based on the point characteristic and the other on the angle characteristic; the first has distances with the physical dimension L^{-1} and the second with the physical dimension L. A numerical example calculates the locations, distances from the origin and angles subtended at the origin in the 10-dimensional space for two arbitrary astigmatic eyes.

Keywords: ray transference; inner-product space; linear optics; astigmatism

Introduction

The optical character of a thin system in linear optics can be represented by a symmetric 2×2 matrix **F**, the symmetric dioptric power matrix. The set of all such powers defines a three-dimensional linear (or vector) space, symmetric dioptric power space [1]. Because the matrix has uniform physical dimensionality [2] (each entry has the dimension L^{-1} and is usually measured in dioptres) one can define an inner-product on the space and the space becomes an inner-product space. Because symmetric dioptric power space is an inner-product space we have been able to define distances, angles, orthonormal axes, confidence ellipsoids, *etc.* in the space. This has provided the basis for the quantitative analysis we have done on powers including refractive errors and corneal powers (*e.g.* [3]).

For some years we have sought to extend this type of analysis to thick systems like the eye (*e.g.* [4]). In linear optics the optical character of a system that may be thick or thin is completely characterized by the ray transference (a real 4×4 matrix)

$$\mathbf{S}=\begin{pmatrix}\mathbf{A} & \mathbf{B}\\ \mathbf{C} & \mathbf{D}\end{pmatrix} \tag{1}$$

of the system [5]. In strong contrast to the set of symmetric dioptric powers the set of transferences is neither a linear space nor does it have uniform dimensionality. There is, therefore, no inner-product space that would provide a basis for holistic quantitative analysis of the optical character of thick systems like the eye. The purpose of this paper is to show how inner-product spaces can in

fact be constructed for general optical systems.

Method

The method is based on the transference. The transference **S** (Equation 1) obeys the equation [5]

$$\mathbf{S}^{\mathrm{T}}\mathbf{E}\mathbf{S} = \mathbf{E} \tag{2}$$

where

$$\mathbf{E} = \begin{pmatrix} \mathbf{O} & \mathbf{I} \\ -\mathbf{I} & \mathbf{O} \end{pmatrix} \tag{3}$$

and **I** and **O** are identity and null matrices respectively. Such matrices are called *symplectic* [6]. **A**, **B**, **C** and **D** are 2×2 submatrices of **S** and represent the *fundamental* (linear) optical properties of the system [7]. **B** has the physical dimension L and **C** the physical dimension L^{-1}; the other two fundamental properties are dimensionless. Other optical properties of the system can be obtained from the fundamental properties; for example the power of the system is given by [7]

$$\mathbf{F} = -\mathbf{C} \tag{4}$$

and, for eyes, the corneal-plane refractive compensation (or refractive error) is given by [7]

$$\mathbf{F}_0 = \mathbf{B}^{-1}\mathbf{A}\,. \tag{5}$$

Two matrices related to the transference are the *point characteristic*

$$\mathbf{P} = \begin{pmatrix} \mathbf{B}^{-1}\mathbf{A} & -\mathbf{B}^{-1} \\ -\mathbf{B}^{-\mathrm{T}} & \mathbf{D}\mathbf{B}^{-1} \end{pmatrix} = \begin{pmatrix} \mathbf{U} & \mathbf{V} \\ \mathbf{V}^{\mathrm{T}} & \mathbf{W} \end{pmatrix} \tag{6}$$

and the *angle characteristic*

$$\mathbf{Q} = \begin{pmatrix} \mathbf{C}^{-1}\mathbf{D} & \mathbf{C}^{-1} \\ \mathbf{C}^{-\mathrm{T}} & \mathbf{A}\mathbf{C}^{-1} \end{pmatrix} = \begin{pmatrix} \mathbf{X} & \mathbf{Y} \\ \mathbf{Y}^{\mathrm{T}} & \mathbf{Z} \end{pmatrix}. \tag{7}$$

Elsewhere [8] we use these matrices to calculate average systems.

Results

From **P** and **Q** we construct the 2×6 matrices

$$\mathbf{G} = \begin{pmatrix} \mathbf{U} & \mathbf{V} & \mathbf{W} \end{pmatrix} \tag{8}$$

and

$$\mathbf{H} = \begin{pmatrix} \mathbf{X} & \mathbf{Y} & \mathbf{Z} \end{pmatrix}. \tag{9}$$

It is a consequence of symplecticity (Equation 2) that **U**, **W**, **X** and **Z** are symmetric; **V** and **Y** are general. (Properties of symplectic matrices are summarised elsewhere [9]). The set of all matrices **G** is a linear space and **G** has uniform physical dimensionality (L^{-1}). Similarly matrices **H** define a dimensionally uniform (dimension L) vector space.

G can be expanded as

$$\begin{aligned}\mathbf{G} = {} & U_{\mathbf{I}}(\mathbf{I} \quad \mathbf{O} \quad \mathbf{O}) + U_{\mathbf{J}}(\mathbf{J} \quad \mathbf{O} \quad \mathbf{O}) + U_{\mathbf{K}}(\mathbf{K} \quad \mathbf{O} \quad \mathbf{O}) \\ & + V_{\mathbf{I}}(\mathbf{O} \quad \mathbf{I} \quad \mathbf{O}) + V_{\mathbf{J}}(\mathbf{O} \quad \mathbf{J} \quad \mathbf{O}) + V_{\mathbf{K}}(\mathbf{O} \quad \mathbf{K} \quad \mathbf{O}) + V_{\mathbf{L}}(\mathbf{O} \quad \mathbf{L} \quad \mathbf{O}) \\ & + W_{\mathbf{I}}(\mathbf{O} \quad \mathbf{O} \quad \mathbf{I}) + W_{\mathbf{J}}(\mathbf{O} \quad \mathbf{O} \quad \mathbf{J}) + W_{\mathbf{K}}(\mathbf{O} \quad \mathbf{O} \quad \mathbf{K})\end{aligned} \tag{10}$$

where $\mathbf{J} = \begin{pmatrix} 1 & 0 \\ 0 & -1 \end{pmatrix}$, $\mathbf{K} = \begin{pmatrix} 0 & 1 \\ 1 & 0 \end{pmatrix}$, $\mathbf{L} = \begin{pmatrix} 0 & 1 \\ -1 & 0 \end{pmatrix}$. Also

$$V_{\mathbf{I}} = (v_{11} + v_{22})/2 \qquad V_{\mathbf{J}} = (v_{11} - v_{22})/2 \qquad V_{\mathbf{K}} = (v_{12} + v_{21})/2 \qquad V_{\mathbf{L}} = (v_{12} - v_{21})/2 \tag{11}$$

and similarly for $U_{\mathbf{I}}$ and the other coefficients in Equation 10. We define the coordinate vector

$$\mathbf{g} = (U_{\mathbf{I}} \quad U_{\mathbf{J}} \quad U_{\mathbf{K}} \quad V_{\mathbf{I}} \quad V_{\mathbf{J}} \quad V_{\mathbf{K}} \quad V_{\mathbf{L}} \quad W_{\mathbf{I}} \quad W_{\mathbf{J}} \quad W_{\mathbf{K}})^{\mathrm{T}} \tag{12}$$

relative to the basis

$$\beta = \{(\mathbf{I} \quad \mathbf{O} \quad \mathbf{O}), (\mathbf{J} \quad \mathbf{O} \quad \mathbf{O}), (\mathbf{K} \quad \mathbf{O} \quad \mathbf{O}), \cdots, (\mathbf{O} \quad \mathbf{O} \quad \mathbf{K})\}. \tag{13}$$

Consider two optical systems 1 and 2. Their coordinate vectors are $\mathbf{g}_1$ and $\mathbf{g}_2$. Now we define the inner product of $\mathbf{g}_1$ and $\mathbf{g}_2$ by

$$\langle \mathbf{g}_1, \mathbf{g}_2 \rangle = \mathbf{g}_1^{\mathrm{T}} \mathbf{g}_2. \tag{14}$$

Consequently we have distances (magnitudes) g and angles θ in the space defined by

$$g = \sqrt{\mathbf{g}^{\mathrm{T}} \mathbf{g}} \tag{15}$$

and

$$\cos\theta = \frac{\mathbf{g}_1^{\mathrm{T}} \mathbf{g}_2}{g_1 g_2} \tag{16}$$

respectively.

Thus we have a 10-dimensional inner-product space for quantitative analysis of optical systems in linear optics for which **B** is nonsingular. One can think of distances in the space as powers (*e.g.* dioptres).

For matrices of the form **H** (Equation 9) one can follow a similar approach. It leads to a second 10-dimensional inner-product space. It applies for optical systems for which **C** is nonsingular and distances in the space are lengths (*e.g.* metres).

We illustrate the theory using two optical systems whose transferences have been presented before [8]:

$$\mathbf{S}_1 = \begin{pmatrix} -0.2066 & -0.0031 & 0.0200 & 0.0000 \\ -0.0031 & -0.2240 & 0.0000 & 0.0200 \\ -58.8160 & -0.0853 & 0.8569 & 0.0017 \\ -0.0841 & -59.5090 & 0.0017 & 0.8599 \end{pmatrix}$$

and

$$\mathbf{S}_2 = \begin{pmatrix} -0.1641 & 0.0060 & 0.0197 & 0.0000 \\ 0.0060 & -0.1399 & 0.0000 & 0.0197 \\ -57.9190 & 0.3455 & 0.8670 & 0.0024 \\ 0.3415 & -56.9734 & 0.0024 & 0.8637 \end{pmatrix},$$

the units being dioptres and metres. The coordinate vectors (Equation 12) turn out to be

$$\mathbf{g}_1 = \begin{pmatrix} -10.7650 & 0.4350 & -0.1550 & -50.0000 & 0 & 0 & 0 & 42.9200 & -0.0750 & 0.0850 \end{pmatrix}^{\mathrm{T}} \text{ D}$$

and

$$\mathbf{g}_2 = \begin{pmatrix} -7.7157 & -0.6142 & 0.3046 & -50.7614 & 0 & 0 & 0 & 43.9264 & 0.0838 & 0.1218 \end{pmatrix}^{\mathrm{T}} \text{ D}.$$

These vectors locate the two optical systems relative to the origins of the space. Their distances from the origin are $g_1 = 66.77$ D and $g_2 = 67.57$ D respectively and they subtend an angle $\theta = 2.90°$ at the origin.

Conclusion

We have here constructed two inner-product spaces for the linear optical characters of optical systems. One is based on the point characteristic and the other on the angle characteristic. Both spaces can be used for eyes because they have nonsingular **B** and **C**. We now have the machinery for holistic quantitative analysis of optical systems in general and eyes in particular.

Acknowledgements

WFH gratefully acknowledges support from the National Research Foundation of South Africa.

References

[1] Harris WF. Representation of dioptric power in Euclidean 3-space. *Ophthal. Physiol. Opt.* 1991; **11**: 130-136

[2] Hart GW. Multidimensional Analysis: Algebras and Systems for Science and Engineering. New York: Springer. 1995; 66.

[3] Harris WF. Reduction of artefact in scatter plots of spherocylindrical data. *Ophthal. Physiol. Opt.* 2005; **25**: 13-17.

[4] Harris WF, Cardoso JR. The exponential-mean-log-transference as a possible representation of the optical character of an average eye. *Ophthal. Physiol. Opt.* 2006; **26**: 380-383.

[5] Torre A. Linear Ray and Wave Optics in Phase Space. Amsterdam: Elsevier. 2005; 60, 155.

[6] Guillemin V, Sternberg S. Symplectic Techniques in Physics. Cambridge: Cambridge University Press. 1984; 23 *et seq*.

[7] Harris WF. Dioptric power: its nature and its representation in three- and four-dimensional space. *Optom. Vis. Sci*. 1997; **74**: 349-366.

[8] van Gool R D, Harris WF. The concept of the average eye. *S. Afr. Optom.* 2005; **64**: 38-43.

[9] Harris WF. Symplecticity and relationships among the fundamental properties in linear optics. *S. Afr. Optom.* 2010; **69**: 3-13.

APPENDIX A LIST OF SYMBOLS

Symbol	Meaning	Ch	Sym-bol	Sub-script	Super script
A	Anterior	3		•	
A, **A**	Dilation (scalar, 2×2)	3, 1	•		
a	Angle between visual axis and red chief ray	2	•		
a, **a**	Inclination of the ray relative to Z (scalar, 2×1)	3	•		
Aq	Aqueous / anterior camber	4	•	•	
aO	Of inclinations from two object points	7		•	
aR	Of angular spread at the retina	7		•	
$\hat{A}$, $\hat{B}$, $\hat{C}$, $\hat{D}$, $\hat{\mathbf{A}}$, $\hat{\mathbf{B}}$, $\hat{\mathbf{C}}$, $\hat{\mathbf{D}}$	Entries of the transformed transference $\hat{\mathbf{S}}$ (scalar, 2×2)	3	•		
B	Posterior	3		•	
B, **B**	Disjugacy (scalar, 2×2)	3, 1	•		
b	Angle between visual axis and blue chief ray	2	•		
b	Blue	2		•	•
bv	Back-vertex	3		•	
C	Exit-plane compensation system	5		•	
C	Compound system	6		•	
C, **C**	Divergence (scalar, 2×2)	3, 1	•		
$\mathcal{C}(\mathbf{S})$	The Cayley transform	3	•		
c	Speed of light	4	•		
D	Dioptres	4	•		
D	Fraunhofer line D ($\lambda_D = 589.3\,\text{nm}$)	2		•	
D, **D**	Divarication (scalar, 2×2)	1	•		
det	Determinant	3	•		
E	Eye (with distant object)	3		•	
E	The symplectic unit matrix	3	•		
e	Equivalent	2		•	
e	Euler's number	3	•		
e	Transverse translation (2×1)	3	•		
eq	Equivalent (measured from principal plane)	3		•	
F	Fovea	2	•		
F	Focal point	3	•	•	
F, **F**	Power (scalar, 2×2)	2, 3	•		
f	Focal length (measured from transverse plane T)	3	•		
fn	Front-neutralising	3		•	
fv	Front-vertex	3		•	
G	A matrix Lie Group	3	•		
GL	General linear group	3	•		
$\mathfrak{g}$	The Lie algebra of **G**	3	•		
gl	The Lie algebra of GL	3	•		
H	Hamiltonian matrix	3	•		
H	The symplectic Lie group	3	•		

Symbol	Meaning	Ch	Sym-bol	Sub-script	Super script
h	Transverse displacement of pinhole from visual axis or displacement in entrance pupil of rays with respect to achromatic axis	2	•		
$\mathfrak{h}$	The set of Hamiltonian matrices, the symplectic algebra of **H**	3	•		
I	Image	2	•	•	
I	Identity matrix	3	•		
i	Angle between normal to the surface and the ray	3	•		
K	Cornea (refracting surface)	3	•	•	
K1	Corneal anterior surface	4	•	•	
K2	Corneal posterior surface	4	•	•	
kD	Kilodioptres	5	•		
kPa	KiloPascal	4	•		
L	Lens	4	•	•	
L	Locator line	3	•		
L, **L**	Vergence (scalar, 2×2); reduced wavefront curvature	3	•		
L1	Lens anterior surface	4	•	•	
L2	Lens posterior surface	4	•	•	
M	Magnification	2	•		
M	First mixed characteristic	3	•		
mm	Millimetres	4	•		
N	Nodal point	2, 3	•	•	
$\overline{\text{N}}$	Anti-nodal point	3	•	•	
N	Second mixed characteristic	3	•		
n	Refractive index	2	•		
$n\times n$ or n	Size of a square matrix	3	•		
nm	Nanometres $\left(\times10^{-9}\text{ m}\right)$	4	•		
O	Object or subsystem from object to first surface of eye; Object point or in object space	2, 3	•	•	
O	Null matrix	3	•		
o	Reference	2		•	
o	Null matrix (2×1 or 4×1)	3	•		
OA	Super-system from object, including anterior subsystem	5		•	
Oa	Measurements of inclination made at a finite distance in front of the eye	5		•	
OE	Super-system from object, including eye	5		•	
Oy	In object space, with respect to y, transverse position,				
Oy	Measurements of distance made at a finite distance in front of the eye	5		•	
P	Principal point	3	•	•	
$\overline{\text{P}}$	Anti-principal point	3	•	•	
P	Pupillary	3		•	
P	Pinhole	5			•
P	Point characteristic	3	•		
ppm	Parts per million	4	•		

Symbol	Meaning	Ch	Sym-bol	Sub-script	Super script
ps	Picosecond (10^{-12} s)	8	•		
Q	A cardinal point	3		•	
Q	Angle characteristic	3	•		
R	Retina (imaging surface) or in image space	3	•	•	
R	Ray	3	•		
$\mathbb{R}$	Set of real numbers	3	•		
r	Red	2		•	•
r	Radius of curvature	2	•		
r	State of the ray with unreduced inclination (2×1)	5	•		
S	General system	3, 5	•	•	
S	Transference (4×4 or 2×2)	3	•		
$\hat{\mathbf{S}}$	The transformed transference	3	•		
Sl(2;$\mathbb{R}$)	The group of 2×2 real matrices with determinant 1	3	•		
Sp	Symplectic group (Lie group)	3	•		
sp	Lie algebra (set of Hamiltonian matrices)	3	•		
T	Transverse plane	2	•		
T	Matrix transpose	3			•
T	Augmented transference (5×5)	3	•		
THz	Terahertz $(\times10^{12}\ \mathrm{s}^{-1})$	4	•		
t	Transverse (magnification)	3		•	
t	Transverse chromatic aberration	2	•		
t	All real numbers	3	•		•
tr	Trace	5	•		
V	Vitreous/ Posterior chamber	4	•	•	
V	Coefficient matrix	5	•		
v	Vitreous	2		•	
v	Input vector	5	•		
W, **W**	Image blur coefficient (scalar, 2×2)	5	•		
X, **X**	Image size coefficient (scalar, 2×2)	5	•		
X	Characteristic	3	•		
X	Set of all real matrices	3	•		
Y, **Y**	Directional spread coefficient (scalar, 2×2)	5	•		
y	Transverse position (scalar)	2, 3	•		
y	Transverse position (2×1)	3	•		
yO	Of size or separation distance of the object(s)	7		•	
yR	Of size at the retina	7		•	
Z	Longitudinal axis	2	•		
Z, **Z**	Directional coefficient (scalar, 2×2)	5	•		
Z	Generalised distance (2×2)				
z	Longitudinal position or gap, measured from a transverse plane T	3	•		
z	Axial (magnification)	3		•	
∞	Infinity	3	•		
0	Associated with incidence or upstream	2		•	
(No subscript)	Associated with emergence or downstream	2		•	
α, **α**	Reduced inclination (scalar, 2×1)	3	•		

Symbol	Meaning	Ch	Sym-bol	Sub-script	Super script
α	Angular (magnification)	3		•	
Δ	Physical difference	2	•		
δ	Chromatic difference	2	•		
$\boldsymbol{\delta}$	System vector accounting for prism and decentration of elements of the system (4×1)	3	•		
ε	Eccentricity	2	•		
$\boldsymbol{\gamma}$	Augmented ray state (5×1)	3	•		
$\imath$	Reduced angle between ray and normal	3	•		
λ	Wavelength	2	•		
ν	Frequency	4	•		
$\boldsymbol{\pi}$	Deflectance (2×1)	3	•		
$\boldsymbol{\rho}$	State of the ray at a transverse plane T (4×1 or 2×1)	3	•		
ζ	Reduced distance	3	•		
F_{bv}	Back-vertex power	3	•		
F_C	Exit-plane compensation	5	•		
F_{fv}	Front-vertex power	3	•		
F_0	Refractive compensation	3	•		
M_{aO}	Chromatic object angular spread magnification	7	•		
M_{aR}	Retinal chromatic angular spread magnification	7	•		
M_{yO}	Chromatic object size magnification	7	•		
M_{yR}	Retinal chromatic size magnification	7	•		
c_0	Speed of light in a vacuum	4	•		
n_∞, K, Λ	Constants in Cornu's formula	4	•		
δA	Chromatic difference in ametropia	7	•		
δF	Chromatic difference in power	7	•		
δF_0	Chromatic difference in refractive compensation	7	•		
δa_{O}	Chromatic difference in inclination in object space	7	•		
$\delta(\Delta a_{\mathrm{O}})$	Chromatic difference in object angular spread	7	•		
δa_{R}	Chromatic difference in inclination at the retina	7	•		
$\delta(\Delta a_{\mathrm{R}})$	Chromatic difference in angular spread at the retina	7	•		
δy	Transverse chromatic aberration (scalar)	6	•		
δy_{K}	Chromatic difference in corneal position	7	•		
δy_{O}	Chromatic difference in object position	7	•		
$\delta(\Delta y_{\mathrm{O}})$	Chromatic difference in object size	7	•		
δy_{R}	Chromatic difference in image position	7	•		
$\delta(\Delta y_{\mathrm{R}})$	Chromatic difference in image size	7	•		
δz	Longitudinal chromatic aberration (scalar)	6	•		
δy, $\delta\mathbf{y}$	Transverse chromatic aberration (scalar, 2×1)	6	•		
δz, $\delta\mathbf{Z}$	Longitudinal chromatic aberration (scalar, 2×2)	6	•		
λ_0	Vacuum wavelength	4	•		

APPENDIX B LIST OF FIGURES

APPENDIX C LIST OF TABLES

APPENDIX D PUBLICATIONS

1. EVANS T, Harris WF. Dependence of the transference of a reduced eye on frequency of light. *South African Optometrist* 2011 **70** 149-155.

2. Harris WF, EVANS T. Chromatic aberration in heterocentric astigmatic systems including the eye. *Optometry and Vision Science* 2012 **89** e37-e43.

3. Harris WF, van Gool RDHM, EVANS T. Line of sight of a heterocentric astigmatic eye. *Ophthalmic and Physiological Optics* 2013 **33** 57-66.

4. EVANS, T and Harris, WF. (2014) Dependence of the ray transference of model eyes on the frequency of light. *Proceedings: VII European / I World Meeting in Visual and Physiological Optics VPOptics 2014*. Wrocław University of Technology, Wrocław, 25-27 Aug 2014, ed by DR Iskander and HT Kasprzak. 74-77.

5. Harris WF, EVANS T and van Gool RDHM. (2014) Inner-product spaces for quantitative analysis of eyes and other optical systems. *Proceedings: VII European / I World Meeting in Visual and Physiological Optics*. Wrocław University of Technology, Wrocław, 25-27 Aug 2014, ed by DR Iskander and HT Kasprzak. 116-119.

PART II – LITERATURE REVIEW

In the literature review of the chromatic dependence of the first-order optical properties of the eye we consider three aspects, firstly chromatic aberrations, secondly first-order optical properties, both fundamental and derived, and finally the eye as a Gaussian optical system. For this reason, the literature review is divided into three chapters, each chapter dealing with these three aspects of this dissertation in turn.

In Chapter 2 we take a look at chromatic dispersion which is the basis for chromatic aberration, and how chromatic dispersion is measured for the media of the eye. We then take an in-depth look at the current definitions of chromatic aberration in both the classical and ophthalmic optics literature.

In Chapter 3 we look at the background theory of linear optics. In particular we are interested in Gaussian systems. The transference defines the fundamental properties of the eye and this enables one to trace the state of a ray through a system. A selection of derived properties that are of interest to this study of chromatic effects in the eye will be looked at. Because magnification, cardinal points and vergence form a pivotal role in chromatic aberration studies, we take a close look at how these are defined in the linear optics literature. Finally we take a look at the transformed transference and how this enables us to represent the transference in a three-dimensional space.

Chapter 4 is the final chapter of the literature review and looks at a number of considerations that are needed for this study. Firstly we take a look at the schematic eyes that are available in the literature, choosing Emsley's reduced eye and Le Grand's four-surface eye to base the numerical examples on. Secondly, the visible light spectrum that shall be used in this study is defined. Next, we consider the reasons for using frequency rather than wavelength. Finally, we look at the formulae for the refractive index of the various media as a function of frequency and wavelength.

PART III - DEFINITIONS AND DERIVATIONS

This study of the chromatic dependence of the first-order optical properties of the eye relies mostly on linear optics of systems in general. The background theory of Gaussian and linear optics needed for this study was summarized in Chapter 3. There are, however, formulae that we will need for this dissertation that have not been published in the literature which are derived in Part III.

In Chapter 5 we take a look at derivations for systems and rays that are needed as background equations that are not available in the literature. The chapter consists of an assortment of properties, derived from the transference, that are needed in Chapters 6 and 7. In particular, we shall revisit derived properties, magnification, cardinal points and Cayley's transform. Formulae are derived for the reduced and Le Grand's eyes as a function of refractive index and hence frequency.

In Chapter 6 longitudinal and transverse chromatic aberration are defined for systems in general and then simplified for the Gaussian model eye. The basis of the definition is the classical optics definition of chromatic aberration given in Section 2.2 which is generalized to systems that include astigmatic and decentred elements (Harris and Evans, 2012).

In Chapter 7 a number of formulae for quantifying chromatic properties are derived from the transference. The bases for these derivations are the physiological optics' definitions of the chromatic properties as defined in the literature in Section 2.3. Numerous formulae for chromatic properties both independent of and dependent on the object or image and aperture positions, each with a variety of alternatives, are summarized in tables at the end of the chapter.

Part III concentrates on Gaussian optics and linear optics of systems in general. All the formulae in this part, consisting of three chapters, are derived from the transference with special interest in the effect of frequency on the transference. The properties derived in these three chapters are done so specifically to illustrate and emphasise the effect of frequency on systems in general and the eye. Numerical examples, represented graphically and in tabular form, will be given in Part IV based on the derivations given in Part III.

PART IV – FINDINGS AND DISCUSSIONS

Because of the central importance of the transference it is useful to have some idea of how it depends on the frequency of light. In this part we examine the dependence of the transference of the reduced eye and Le Grand's four-surface schematic eye on frequency for several chromatic properties.

The considerations discussed in Chapter 4 will be applied or explored in the three chapters that make up this part. We will use the refractive index formula for the chromatic eye, developed by Thibos *et al* (1992), to calculate the refractive index of the reduced eye (Section 4.4.2) and the formula of Villegas, Carretero and Fimia (1996) for the refractive indices of Le Grand's complete theoretical eye given by Equation 4.4.3. As discussed in Section 4.2, the visible light spectrum, between the frequencies of 430 and 750 THz and will be used.

In Chapter 8 we examine the dependence of the fundamental properties of the model eyes on the frequency of light. The effect of the refractive index of air as a function of frequency is considered. Also studied are the dependence of the transference on vacuum wavelength and on frequency when the eye is submerged in water. The two transformed transferences will be calculated and displayed graphically both in terms of their individual entries and as three-dimensional graphs. These three-dimensional graphs show how the entries of the Hamiltonian matrix are related and begin to give us some insight into the meaning of Hamiltonian space.

In Chapter 9, various derived properties will be studied as a function of frequency. The effect of frequency on the cardinal points will be calculated and displayed using graphical construction and Pascal's ring methods. The formulae for both the derived properties and the cardinal points were given in Chapter 3 and further formulae derived in Chapter 5. The dependence of the four characteristic matrices on the frequency of light will be studied and the relationships among various derived properties will be explored.

Finally in Chapter 10, chromatic aberration will be calculated numerically and displayed according to changes in the object position. In Chapter 7 we derived the formulae for a variety of chromatic difference properties. These will be

calculated in both object and image space for the two model eyes. Numerical examples are given for all of the chromatic properties given by the equations summarized in Sections 7.4 and 5.

The numerical examples in Chapter 10 and the cardinal points examples in Section 9.1 show the difference between the two end points of the chosen spectrum and do not give us any insight into the dependence of the system on frequency across the visible light spectrum. In contrast to this, the numerical examples of the two model eyes in Chapter 8 and Sections 9.2 and 3 show us the dependence of the system on frequency across the spectrum. Firstly the fundamental properties of the transference, then the entries of the Hamiltonian matrix and finally the derived properties and the characteristic matrices are all studied to understand the dependence of each on the frequencies of light.

REFERENCES

Anton, H and Rorres, C. (2005). *Elementary Linear Algebra. Applications Version*. 9th ed. New Jersey: John Wiley & Sons, Inc.

Aristotle. (1906). *De Sensu and De Memoria*. Text and Translation with Introductory Comment by Ross, GRT. Cambridge: Cambridge University Press.

Aristotle. (1928). *Meteorologica*. Book 3, sections 4 and 5. The works of Aristotle, translated into English, Ross, WD (Ed). Available from: http://etext.lib.virginia.edu/etcbin/toccer-new2?id=AriMete.xml&images=images/modeng&data=/texts/english/modeng/parsed&tag=public&part=3&division=div2 Accessed 24 June 2013.

Arnaud, JA. (1970). Nonorthogonal optical waveguides and resonators. *The Bell System Technical Journal*, **49**: 2311-2348.

Atchison, DA, Smith, G and Waterworth, MD. (1993). Theoretical effect of refractive error and accommodation on longitudinal chromatic aberration of the human eye. *Optometry and Vision Science*, **70**: 716-722.

Atchison, DA and Smith, G. (2000). *Optics of the Human Eye*. Oxford: Butterworth-Heinemann.

Bennett, AG and Rabbetts, RB. (1989). Letter to the Editor (on proposals for new reduced and schematic eyes). *Ophthalmic and Physiological Optics*, **9**: 228-230.

Bernstein, DS. (2005). *Matrix Mathematics. Theory, Facts, and Formulas with Application to Linear Systems Theory*. Princeton: Princeton University Press.

Bernstein, DS. (2009). *Matrix Mathematics. Theory, Facts, and Formulas*. 2nd ed. Princeton: Princeton University Press.

Blendowske, R. (2003). Hans-Heinrich Fick: Early contributions to the theory of astigmatic systems. *South African Optometrist*, **62**: 105-110.

Born, M and Wolf, E. (2002). *Principles of Optics. Electromagnetic Theory of Propagation, Interference and Diffraction of Light.* 7th ed. Cambridge: Cambridge University Press.

Cardoso, JR. (2005). An explicit formula for the matrix logarithm. *South African Optometrist*, **64**: 80-83.

Cardoso, JR and Harris, WF. (2007). Transformations of ray transferences of optical systems to augmented Hamiltonian matrices and the problem of the average system. *South African Optometrist*, **66**: 56-61.

Cayley, A. (1846). Sur quelques propriétés des déterminants gauches. [On some properties of left determinants]. *Journal für die reine und angewandte Mathematik (Crelle).* **32**: 119-123. From The Collected Mathematical Papers of Arthur Cayley, Volume I: 332-336. Cambridge University Press (1897). Obtained from: http://quod.lib.umich.edu/u/umhistmath/abs3153.0001.001/349?didno=ABS3153.0001.001;page=root;rgn=full+text;size=100;view=image Accessed 27 June 2013.

Ciddor, PE. (1996). Refractive index of air: new equations for the visible and near infrared. *Applied Optics*, **35**: 1566-1573.

Cooper, DP and Pease, PL. (1988). Longitudinal chromatic aberration of the human eye and wavelength in focus. *American Journal of Optometry and Physiological Optics*, **65**: 99-107.

Courant, R and Hilbert, D. (1953). *Methods of mathematical physics, Volume I*. New York: Interscience Publishers, Inc.

Dieci, L. (1996). Considerations on computing real logarithms of matrices, Hamiltonian logarithms, and skew-symmetric logarithms. *Linear Algebra and its Applications*, **244**: 35-54.

Dieci, L. (1998). Real Hamiltonian logarithm of a symplectic matrix. *Linear Algebra and its Applications*, **281**: 227-246.

El Hage, SG and Le Grand, Y. (1980). *Physiological Optics*. Berlin: Springer-Verlag.

Emsley, HH. (1950). *Visual Optics*. 4th ed. London: Hatton Press Ltd.

Evans, T and Harris, WF. (2011). Dependence of the transference of a reduced eye on frequency of light. *South African Optometrist*, **70**: 149-155.

EVANS, T and Harris, WF. (2014) Dependence of the ray transference of model eyes on the frequency of light. *Proceedings: VII European / I World Meeting in Visual and Physiological Optics VPOptics 2014*. Wrocław University of Technology, Wrocław, 25-27 Aug 2014, ed by DR Iskander and HT Kasprzak. 74-77.

Fallat, SM and Tsatsomeros MJ. (2002). On the Cayley transform of positivity classes of matrices, *The Electronic Journal of Linear Algebra*, **9**: 190-196.

Fick, HH. (1972). Fortschrittliche Rechnungsarten in der Augenoptik [Progressive calculation methods in optometry]. *Der Augenoptiker*, **12/1972**: 60-63.

Fick, HH. (1973a). Fortschrittliche Rechnungsarten in der Augenoptik [Progressive calculation methods in optometry]. *Der Augenoptiker*, **2/1973**: 45-49.

Fick, HH. (1973b). Fortschrittliche Rechnungsarten in der Augenoptik [Progressive calculation methods in optometry]. *Der Augenoptiker*, **4/1973**: 39-43.

Fick, HH. (1973c). Fortschrittliche Rechnungsarten in der Augenoptik [Progressive calculation methods in optometry]. *Der Augenoptiker*, **10/1973**: 55-61.

Fiori, S. (2011). Solving minimal-distance problems over the manifold of real-symplectic matrices. *Society for Industrial and Applied Mathematics: Journal on Matrix Analysis and Applications*, **32**: 938-968.

Gatinel, D. (2010). Personal communications in preparation for Tshukudu Conference.

Golub, GH and van Loan, CF. (1996). *Matrix Computations*. 3rd ed. Baltimore: The Johns Hopkins University Press.

Guillemin, V and Sternberg, S. (1984). *Symplectic Techniques in Physics*. Cambridge: Cambridge University Press.

Hadjidimos, A and Tzoumas, M. (2008). The principle of extrapolation and the Cayley transform. *Linear Algebra and its Applications*, **429**: 2464-2480.

Hadjidimos, A and Tzoumas, M. (2009). On the optimal complex extrapolation of the complex Cayley transform. *Linear Algebra and its Applications*, **430**: 619-632.

Hall. BC. (2004). Lie Groups, Lie Algebras, and Representations. An Elementary Introduction. New York: Springer.

Harris, WF. (1993). Astigmatic optical systems with separated and prismatic or noncoaxial elements: system matrices and system vectors. *Optometry and Vision Science*, **70**: 545-551.

Harris, WF. (1994). Paraxial ray tracing through noncoaxial astigmatic optical system, and a 5×5 augmented system matrix. *Optometry and Vision Science*, **71**: 282-285.

Harris, WF. (1996a). Ray vector fields, prismatic effect, and thick astigmatic optical systems. *Optometry and Vision Science*, **73**: 418-423.

Harris, WF. (1996b). Wavefronts and their propagation in astigmatic optical systems. *Optometry and Vision Science*, **73**: 606-612.

Harris, WF. (1997). Dioptric power: its nature and its representation in three- and four-dimensional space. *Optometry and Vision Science*, **74**: 349-366.

Harris, WF. (1999a). A unified paraxial approach to astigmatic optics. *Optometry and Vision Science*, **76**: 480-499.

Harris, WF. (1999b). The four fundamental properties of Gaussian optical systems including the eye. *South African Optometrist*, **58**:69-79.

Harris, WF. (2000). Interconverting the matrix and principal-meridional representations of dioptric power and reduced vergence. *Ophthalmic and Physiological Optics*, **20**: 494-500.

Harris, WF. (2001a). Magnification, blur, and the ray state at the retina for the general eye with and without a general optical instrument in front of it: 1. Distant objects. *Optometry and Vision Science*, **78**: 888-900.

Harris, WF. (2001b). Magnification, blur, and ray state at the retina for the general eye with and without a general optical instrument in front of it: 2. Near objects. *Optometry and Vision Science,* **78:** 901-905.

Harris, WF. (2001c). Interconverting the matrix and principal meridional representations of dioptric power in general including powers with nonorthogonal and complex meridians. *Ophthalmic and Physiological Optics*, **21**: 247-252.

Harris, WF. (2002). Symplecticity in visual optics. *South African Optometrist*, **61**: 97-100.

Harris, WF. (2004a). Realizability of optical systems of given linear optical character. *Optometry and Vision Science*, **81**: 807-809.

Harris, WF. (2004b). The average eye. *Ophthalmic and Physiological Optics*, **24**: 580-585.

Harris, WF. (2005). The log-transference and an average Gaussian eye. *South African Optometrist*, **64**: 84-88.

Harris, WF. (2007a). Quantitative analysis of transformed ray transferences of optical systems in a space of augmented Hamiltonian matrices. *South African Optometrist*, **66**: 62-67.

Harris, WF. (2007b). Subjective refraction: the mechanism underlying the routine. *Ophthalmic and Physiological Optics*, **27**: 594-602.

Harris, WF. (2008). The geometric mean transference and the problem if the average eye. *South African Optometrist*, **67**: 48-55.

Harris, WF. (2009). Optical axes of eyes and other optical systems. *Optometry and Vision Science*, **86**: 537-541.

Harris, WF. (2010a). Back- and front-vertex powers of astigmatic systems. *Optometry and Vision Science*, **87**: 70-72.

Harris, WF. (2010b). Cardinal points and generalizations. *Ophthalmic and Physiological Optics*, **30**: 391-401.

Harris, WF. (2010c). Visual axes in eyes that may be astigmatic and have decentred elements. *Ophthalmic and Physiological Optics*, **30**: 204-204.

Harris, WF. (2010d). Symplecticity and relationships among the fundamental properties in linear optics. *South African Optometrist*, **69**: 3-13.

Harris, WF. (2010e). Nodes and nodal points and lines in eyes and other optical systems. *Ophthalmic and Physiological Optics*, **30**: 24-42.

Harris, WF. (2010f). Special rays and structures in general optical systems: generalized magnifications associated with the fundamental properties. *South African Optometrist*, **69**: 51-57.

Harris, WF. (2011a). Pascal's ring, cardinal points, and refractive compensation. *Vision Research*, **51**: 1679-1685.

Harris, WF. (2011b). Graphical construction of cardinal points from the transference. *South African Optometrist*, **70**: 3-13.

Harris, WF. (2011c). Effective corneal patch of an astigmatic heterocentric eye. *Ophthalmic and Physiological Optics*, **31**: 79-90.

Harris, WF. (2012a). Achromatic axes and their linear optics. *Vision Research*, **58**: 1-9.

Harris, WF. (2012b). Chief nodal axes of a heterocentric astigmatic eye and the Thibos-Bradley achromatic axis. *Vision Research*, **73**: 40-45.

Harris, WF. (2012c). Dependence of optical properties of heterocentric astigmatic systems on internal elements, with application to the human eye. *Transactions of the Royal Society of South Africa*, **67**: 11-16.

Harris, WF. (2012d). Aperture referral in dioptric systems with stigmatic elements. *South African Optometrist*, **71**: 3-11.

Harris, WF. (2013a). Pupillary axis of a heterocentric astigmatic eye. *South African Optometrist*, **72**: 3-10.

Harris, WF. (2013b). Yves Le Grand on matrices in optics with. vision: Translation and critical analysis, *South African Optometrist*, **72**: 145-166.

Harris, WF and Cardoso, JR. (2006). The exponential-mean-log-transference as a possible representation of the optical character of an average eye. *Ophthalmic and Physiological Optics*, **26**: 380-383.

Harris, WF and Evans, T. (2012). Chromatic aberration in heterocentric astigmatic systems including the eye. *Optometry and Vision Science*, **89**: e37-e43.

Harris WF, EVANS T and van Gool RDHM. (2014) Inner-product spaces for quantitative analysis of eyes and other optical systems. *Proceedings: VII European / I World Meeting in Visual and Physiological Optics*. Wrocław University of Technology, Wrocław, 25-27 Aug 2014, ed by DR Iskander and HT Kasprzak. 116-119.

Harris, WF and van Gool, RD. (2001). Comparing optical systems, and the concept of the converter system. *Optometry and Vision Science*, **78**: 825-830.

Harris, WF and van Gool, RD. (2004). First-order characteristic matrices of optical systems. *South African Optometrist*, **63**: 142-146.

Harris, WF and van Gool, RD. (2009). Thin lenses of asymmetric power. *South African Optometrist*, **68**: 52-60.

Harris, WF, van Gool, RDHM and Evans T. (2013). Line of sight of a heterocentric astigmatic eye. *Ophthalmic and Physiological Optics*, **33**: 57-66.

Hastings, CS. (1901*). Light; A Consideration of the More Familiar Phenomena of Optics*. New York: Charles Scribner's Sons.

Herzberger, M. (1959). Colour correction in optical systems and a new dispersion formula. *Optica Acta*, **6**: 197-215.

Hodgman, CD (Editor). (1959). *Handbook of Chemistry and Physics*. Cleveland: Chemical Rubber Publishing Co.

Howarth, PA and Bradley, A. (1986). The longitudinal chromatic aberration of the human eye, and its correction. *Vision Research*, **26**: 361-366.

Katz, M. (2002). *Introduction to Geometrical Optics*. Singapore: World Scientific Publishing Co.

Keating, MP. (1980). An easier method to obtain the sphere, cylinder, and axis from an off-axis dioptric power matrix. *American Journal of Optometry and Physiological Optics*, **57**: 734-737.

Keating, MP. (1981a). A system matrix for astigmatic optical systems: I. Introduction and dioptric power relations. *American Journal of Optometry and Physiological Optics*, **58**: 810-819.

Keating, MP. (1981b). A system matrix for astigmatic optical systems: II. Corrected systems including an astigmatic eye. *American Journal of Optometry and Physiological Optics*, **58**: 919-929.

Keating, MP. (1982). Advantages of a block matrix formulation for an astigmatic system. *American Journal of Optometry and Physiological Optics*, **59**: 851-857.

Keating, MP. (1988). *Geometric, Physical, and Visual Optics*. Boston: Butterworth-Heinemann.

Keating, MP. (1997a). Equivalent dioptric power asymmetry relations for thick astigmatic systems. *Optometry and Vision Science*, **74**: 388-392.

Keating, MP. (1997b). Asymmetric dioptric power matrices and corresponding thick lenses. *Optometry and Vision Science*, **74**: 393-396.

Keating, MP. (2002). *Geometric, Physical, and Visual Optics*. 2nd ed. Boston: Butterworth-Heinemann.

Keating, MP, Harris, WF and van Gool, RD. (2002b). Relation between anterior and posterior converter systems. *Optometry and Vision Science*, **79**: 459-461.

Koczorowski, P. (1990). Axial chromatic aberration: linear or power function of wavenumber? *Ophthalmic and Physiological Optics*, **10**: 405-408.

Korsch, D. (1991). *Reflective Optics*. Boston: Academic Press.

Lakshminarayanan, V. (2009). Introduction. *Journal of Modern Optics*, **56**: 2159-2163.

Lee, RL and Fraser, AB. (2001). *The Rainbow Bridge: Rainbows in Art, Myth and Science.* Bellingham: The Pennsylvania State University Press.

Le Grand, Y. (1945). *Optique Physiologique. Tome Premier, le Dioptrique de l'Œil et sa Correction* [Physiological optics. First volume, dioptrics of the eye and its correction]. Paris: Revue d'optique.

Le Grand, Y. (1956). *Optique Physiologique. Tome Troisième, L'espace Visuel* [Physiological optics. Third volume, Visual space]. Paris: Revue d'optique.

Le Grand Y. (1957). *Light, Colour and Vision*. Translated from French by Hunt, RWG, Walsh, JWT and Hunt, FRW. London: Chapman & Hall Ltd.

Long, WF. (1976). A matrix formulation for decentration problems. *American Journal of Optometry and Physiological Optics*, **53**: 27-33.

MacKenzie, GE. (2004). *Linear Optics of the Pseudophakic Eye*. Doctoral thesis. Johannesburg: Rand Afrikaans University.

Mathebula, SD, Rubin, A and Harris, WF. (2007). Quantitative analysis in Hamiltonian space of the transformed ray transferences of a cornea. *South African Optometrist*, **66**: 68-76.

Mathebula, SD and Rubin, A. (2011). Application of optical transferences for ray tracing through the human cornea. *South African Optometrist*, **70**: 156-167.

Meyer-Arendt, JR. (1984). *Introduction to Classical and Modern Optics.* 2nd ed. New-Jersey: Prentice-Hall, Inc.

Newton, I. (1670-1672). *Optica*, Part II, Lecture 11. In *The Optical Papers of Isaac Newton, Volume 1: The Optical Lectures 1670-1672* (1984). Edited by Shapiro, AE. Cambridge: Cambridge University Press.

Pascal, JI. (1939). A memory scheme for the cardinal points. *Archives of Ophthalmology*, **22**: 448-449.

Pascal, JI. (1947). Cardinal points in aphakia. *Archives of Ophthalmology*, **37**: 83-84.

Pascal, JI. (1950a). Role of the cardinal points in the correction of ametropia. *Eye, Ear, Nose and Throat Monthly*, **29**: 24-28.

Pascal, JI. (1950b). The cardinal points in corrected ametropia. *British Journal of Ophthalmology*, **34**: 261-264.

Pease, PL and Barbeito, R. (1989). Axial chromatic aberration of the human eye: frequency or wavelength? *Ophthalmic and Physiological Optics*, **9**: 215-217.

Puzio, RS. (2013). Cayley's parameterization of orthogonal matrices. Available from: http://planetmath.org/cayleysparameterizationoforthogonalmatrices (Accessed 22 June 2013).

Rabbetts, RB. (2007). *Bennett & Rabbetts' Clinical Visual Optics*. 4th ed. London: Butterworth-Heinemann-Elsevier.

Sears, FW, Zemansky, MW and Young, HD. (1987). *University Physics*. 7th ed. Reading, Massachusetts: Addison-Wesley Publishing Company.

Seyeddain, O, Riha, W, Hohensinn, M, Nix, G, Dexl, AK and Grabner, G. (2010). Refractive surgical correction of presbyopia with the AcuFocus small aperture corneal inlay: two-year follow-up. *The Journal of Refractive Surgery*, **26**: 707-715.

Sharma, KK. (2006). *Optics. Principles and Applications*. Boston: Elsevier.

Simonet, P and Campbell, MCW. (1990). The optical transverse chromatic aberration on the fovea of the human eye. *Vision Research*, **30**: 187-206.

Sivak, JG and Mandelman, T. (1982). Chromatic dispersion of the ocular media. *Vision Research*, **22**: 997-1003.

Smith, G. (1993). Calculation of the cardinal points of an optical system. *Ophthalmic and Physiological Optics*, **13**: 327-332.

Smith, G. (1995). Schematic eyes: history, description and applications. *Clinical and Experimental Optometry*, **78**: 176-189.

Smith, G and Atchison, DA. (1997). *The Eye and Visual Optical Instruments*. Cambridge: Cambridge University Press.

Stiles, WS and Crawford, BH. (1933). The luminous efficiency of rays entering the eye pupil at different points. *Proceedings of the Royal Society of London, Series B*, **112**: 428-450.

Stiles, WS. (1939). The directional sensitivity of the retina and the spectral sensitivities of the rods and cones. *Proceedings of the Royal Society of London, Series B*, **127**: 64-105.

Sunyal, AK. (2001). *Geometrical Transformations in Higher Dimensional Euclidean Spaces.* Masters dissertation. College Station: Texas A & M University.

Tabernero, J and Artal P. (2011). Optical modelling of a corneal inlay in real eyes to increase depth of focus: Optimum centration and residual focus. *Journal of Cataract and Refractive Surgery*, **38**: 270-277.

Thibos, LN. (1987). Calculation of the influence of lateral chromatic aberration on image quality across the visual field. *Journal of the Optical Society of America*, **4**: 1673-1680.

Thibos, LN. (2011). Personal communication to Harris, WF, 7 December 2011.

Thibos, LN, Bradley, A, Still, DL, Zhang, X and Howarth, PA. (1990). Theory and measurement of ocular chromatic aberration. *Vision Research*, **30**: 33-49.

Thibos, LN, Bradley, A and Zhang, X. (1991). Effect of ocular chromatic aberration on monocular visual performance. *Optometry and Vision Science*, **68**: 599-607.

Thibos, LN, Ye, M, Zhang, X and Bradley, A. (1992). The chromatic eye: a new reduced-eye model of ocular chromatic aberration in humans. *Applied Optics*, **31**: 3594-3600.

Torre, A. (2005). *Linear Ray and Wave Optics in Phase Space*. Amsterdam: Elsevier.

Tscherning, M. (1904). *Physiologic Optics: Dioptrics of the Eye, Functions of the Retina, Ocular Movements and Binocular Vision*. Translated from French by Weiland, C. 2nd ed. Philedelphia: The Keystone.

Tsiotras, P, Junkins, JL and Schaub, H. (1997). Higher order Cayley transforms with applications to attitude representations. *Journal of Guidance, Control, and Dynamics*, **20**: 528-536.

Van Gool, RD and Harris, WF. (2005). The concept of the average eye. *South African Optometrist*, **64**: 38-43.

Villegas, ER, Carretero, L and Fimia, A. (1996). Le Grand eye for the study of ocular chromatic aberration. *Ophthalmic and Physiological Optics*, **16**: 528-531.

von Helmholtz, H. (1909). *Treatise on Physiological Optics, Volume I*. Translated from the German (2005): Southall, JPC (ed), New York: Dover Phoenix Editions Inc. (Original work published in 1909; Original translation published in 1924).

Wald, G and Griffin, DR. (1947). The change in refractive power of the human eye in dim and bright light. *Journal of the Optical Society of America*, **37**: 321-336.

Waldman, G. (2002). *Introduction to Light: The Physics of Light, Vision, and Color*. New York: Dover Publications Inc.

Walther, A. (1995). *The Ray and Wave Theory of Lenses*. Cambridge: Cambridge University Press.

Waring, GO. (2010). Corneal inlay uses pinhole effect. *Ophthalmology Times*, 35(7). Available from: http://ophthalmologytimes.modernmedicine.com/ophthalmologytimes/news/modernmedicine/modern-medicine-feature-articles/corneal-inlay-uses-pinhole-e (Accessed on: 8 June 2013.)

Watkins, DS. (2004). On Hamiltonian and symplectic Lanczos processes. *Linear Algebra and its Applications*, **385**: 24-45.

Westheimer. G. (2008). Directional sensitivity of the retina: 75 years of Stiles-Crawford effect. *Proceedings of the Royal Society B*, **275**: 2777-2786.

Wilson, MA, Campbell, MCW and Simonet, P. (1992). Change of pupil centration with change of illumination and pupil size. *Optometry and Vision Science*, **69**: 129-136.

Yang, Y, Thompson, K and Burns, SA. (2002). Pupil location under mesopic, photopic and pharmacologically dilated conditions. *Investigative Ophthalmology and Visual Science*, **43**: 2508-2512.

Zhang, X, Bradley, A and Thibos, LN. (1993). Experimental determination of the chromatic difference of magnification of the human eye and the location of the anterior nodal point. *Journal of the Optical Society of America A*, **10**: 213-220.

Zhang, X, Thibos, LN and Bradley, A. (1991). Relation between the chromatic difference of refraction and the chromatic difference of magnification for the reduced eye. *Optometry and Vision Science*, **68**: 456-458.

Zhang, X, Thibos, LN and Bradley, A. (1997). Wavelength-dependent magnification and polychromatic image quality in eyes corrected for longitudinal chromatic aberration. *Optometry and Vision Science*, **74**: 563-569.